

UNITED STATES DEPARTMENT OF THE INTERIOR  
GEOLOGICAL SURVEY

GEOTECHNICAL FRAMEWORK, NORTHEAST GULF OF ALASKA

by

Homa J. Lee  
William C. Schwab

Open File Report 83-499

This report is preliminary and has not been reviewed for conformity with Geological Survey editorial standards and stratigraphic nomenclature.

Any use of trade names is for descriptive purposes only and does not imply endorsement by the United States Geological Survey.

Menlo Park, California

1983

Table of Contents

INTRODUCTION.....	1
SETTING.....	1
Geologic Setting.....	1
Offshore Geologic Hazards.....	2
Morphology of Submarine Slides and Flows.....	3
GEOTECHNICAL APPROACH.....	5
General Methodology.....	5
Cyclic Degradation and Test Type Effects.....	5
Summary of NSP Strength Determination.....	7
Quantitative Evaluation of Offshore Stability.....	8
TEST PROCEDURES.....	9
Shipboard Sampling and Testing.....	9
In Place Testing.....	9
Shore Laboratory Testing.....	10
RESULTS.....	12
Study Areas and Core Locations.....	12
Organization of Laboratory Test Data Presentation.....	12
In Place Test Data.....	13
SYNTHESIS AND DISCUSSION.....	13
Analysis of parameters.....	13
Undrained Strength to Consolidation Stress Ratio for Normal Consolidation, $S_{nc}$ .....	14
Test Type Correction Factor, $A_C$ .....	14
Cyclic Strength Degradation Factor, $A_D$ .....	15
Degree of Consolidation, U, Overconsolidation Ratio, OCR, and Normalized Strength Exponent, $\Lambda_o$ .....	16
Ratio of Submerged to Total Unit Weight, $\gamma'/\gamma$ .....	16
Validity of NSP Approach, Vane Shear Tests and Type (a) Triaxial Tests.....	17
Evaluation of Consolidation State Using Field Strength Results and Gibson's Theory.....	17
Critical Acceleration Calculation.....	18
Regional Variations.....	19
SUMMARY AND CONCLUSIONS.....	20
ACKNOWLEDGEMENTS.....	21
REFERENCES.....	22
APPENDIX A. METHANE IN SEDIMENTS OF THE EASTERN GULF OF ALASKA by Marge Golan-Bac and Keith A. Kvenvolden.....	108
APPENDIX B. RELATIVE IMPORTANCE OF SEISMIC AND STORM WAVE LOADING.....	112
APPENDIX C. INDEX PROPERTY PROFILES.....	115
Copper River Study Area.....	116
Kayak Trough Study Area.....	123
Bering Trough Study Area.....	133
Icy Bay-Malaspina Study Area.....	135
Icy Bay Study Area.....	181
Yakutat Bay Study Area.....	183
Yakutat Study Area.....	188
Alsek River Study Area.....	207
Other.....	224
APPENDIX D. CONSOLIDATION AND TRIAXIAL TEST RESULTS-LAW ENGINEERING AND TESTING COMPANY (1977 Cores).....	230

Table of Contents (continued)

APPENDIX E. CONSOLIDATION AND TRIAXIAL TEST RESULTS-GEOTECHNICAL ENGINEERS, INC. (1977 Cores).....	241
APPENDIX F. CONSOLIDATION AND TRIAXIAL TEST RESULTS-LAW ENGINEERING AND TESTING COMPANY (1980 Cores).....	270
APPENDIX G. CONSOLIDATION AND TRIAXIAL TEST RESULTS-USGS (1980 and 1981 Cores).....	287

## INTRODUCTION

The U.S. Geological Survey began a systematic study of sediment distribution, depositional environments, and shallow structure of the northeast Gulf of Alaska in 1974. The objective of the study was primarily to evaluate seafloor hazards on a regional basis in preparation for possible offshore petroleum development. The study was extended to include an extensive sediment sampling program in 1975 when approximately 400 samples of continental shelf sediments were collected (Carlson and others, 1977). Systematic measurement of geotechnical properties was started in 1977 (Carlson and others, 1978).

Detailed geologic study of seismic reflection records and sediment samples in areas of sediment instability, although valuable for specifying the types and extents of different past hazardous conditions, leave unanswered questions. For example, they often do not specify causes of failures, provide information on the safety of apparently unfailed areas, suggest whether existing slide bodies will fail again or enlarge, or predict the implications of certain earthquake or storm events.

The quantitative methods of geotechnology have the potential for answering some of these questions. A vast amount of previously unpublished geotechnical data, primarily derived from tests on core samples but supplemented with a few in situ tests, has been accumulated on the continental shelf between Montague Island and Cross Sound (Fig. 1). The primary objective of this report is to make these data available with a consistent format. A secondary objective is to provide preliminary quantitative analyses of some of the geologic hazards.

## SETTING

Geologic Setting. Glaciation is the most important process contributing sediment to the northeast Gulf of Alaska continental shelf. In Miocene time, glaciation was restricted to the onshore area but by early to middle Pleistocene, a large ice sheet had spread across the continental shelf (Molnia and Carlson, 1978; Molnia and Sangrey, 1979; Carlson and others, 1982). Today glaciers in the Gulf of Alaska region are restricted to the onshore areas (Fig. 1). As recently as 75 years ago, however, a glacier filled Icy Bay and extended 5 km or 6 km onto the continental shelf (Molnia, 1979).

The complex Quaternary history of the northeast Gulf of Alaska has generated a variety of sedimentary deposits. Four major sedimentary units (Fig. 1) are defined on the basis of seismic reflection and sedimentologic data (Carlson and Molnia, 1975; Molnia and Carlson, 1975, 1980; Carlson and others, 1977, Molnia and Sangrey, 1979; Molnia and Carlson, 1980). These units are: A. Holocene glacial-marine sediment; B. Holocene end moraine deposits; C. Quaternary glacial deposits; and D. Pleistocene and older lithified sedimentary rocks. Holocene end moraine deposits, Quaternary glacial-marine sediment, and Pleistocene and older lithified sedimentary rocks are predominantly dense and hard, reflecting diagenesis or glacial ice loading. These compacted deposits are probably not susceptible to instability on the continental shelf (Lee and Schwab, 1982). Therefore, Geotechnical studies have been directed almost exclusively toward investigating Holocene glacial-marine sediment.

Fine sand and clayey silt of the Holocene glacial-marine unit cover most of the inner shelf, reaching a maximum thickness of about 350 m seaward of the Copper River, about 200 m seaward of Icy Bay (Carlson and Molnia, 1975), and about 260 m seaward of the Alsek River. This sediment is glacially derived from the Gulf of Alaska Tertiary province and bordering rocks of Mesozoic and older age, then fluvially transported to the gulf as rock flour (Molnia and Carlson, 1980). The Mesozoic and older age rocks are highly deformed, locally metamorphosed sedimentary and volcanic rocks that are commonly intruded by igneous plutons, whereas the Tertiary Province is a compound continental margin basin made up almost entirely of terrigenous clastic rocks with minor coal. For a summary of the onshore geology of the Gulf of Alaska the reader is referred to Plafker (1971), Bruns (1979), and Bruns and Plafker (1982).

West of Kayak Island, the Copper River is the primary source of Holocene sediment, carrying a sediment load of  $107 \times 10^9$  kg/yr (Reimnitz, 1966). East of Kayak Island, major sediment sources are streams draining the larger ice fields (Malaspina and Bering Glaciers) and the Alsek River. Accumulation rates of the Holocene glacial-marine unit on the continental shelf range from 0 to 29 mm/yr (Molnia and others, 1980). Accumulation rates of Holocene glacial-marine sediment in coastal embayments are thought to be as high as 2 to 3.75 m/yr (Molnia, 1979).

The largest deposits of sand in the Holocene glacial-marine unit occur along the barrier islands at the mouth of the Copper River, along the nearshore zone both adjacent to and west of the Malaspina Glacier (Carlson and others, 1977), and along the nearshore zone between the Alsek River and Yakutat Bay (Fig. 1). The moderately well sorted, mineralogically immature sand (containing about equal parts of quartz and metamorphic rock fragments) is mostly found in water depths less than 50 m indicating an environment subject to high wave and current energy. Storm waves and longshore currents resuspend the fine silt and clay particles or maintain them in suspension and the Alaska Current transports them offshore and westward (Molnia and Carlson, 1980).

Large deposits of Holocene glacial-marine clayey silt occur seaward of the Copper River and seaward of the Malaspina and Bering Glaciers (Carlson and others, 1977). The mean grain size of Gulf of Alaska Holocene glacial-marine sediment generally decreases with distance from shore and is largely glacial rock flour which is dominated by the silt fraction (Carlson and others, 1977).

Offshore Geologic Hazards. Seafloor geologic hazards in the northeast Gulf of Alaska are summarized by Carlson and Schwab (1982) and have been described by Carlson and others (1975), Carlson and Molnia (1977), Molnia and others (1977), Carlson (1978), and Carlson and others (1980). The hazards include shallow faults, buried channels, gas-charged sediment, and submarine slides and flows.

Active faulting is well documented using conventional geophysical techniques (Bruns 1979; 1982; Bruns and Schwab, 1982; Carlson and Schwab, 1982). Buried channels involve sediment and sedimentary rocks that are too deeply buried to be sampled with conventional coring equipment and therefore have not been studied except with geophysical profiling.

Bubble phase gas charging, although present in the northeastern Gulf of Alaska, is not widespread. Of the hydrocarbon gases, only methane is present in concentrations that may exceed the saturation of interstitial water (Appendix A). Anomalously high concentrations of methane suggesting the presence of bubble phase gas in place and potentially unstable sediment, were found in only two areas: a fault zone southeast of Kayak Island (sample concentration of 14,000  $\mu\text{l/l}$ ), and an area east of Dry Bay (sample concentration of 32,8000  $\mu\text{l/l}$ ). Other locations had significant amounts of methane but the amounts measured in samples were insufficient to indicate that the sediment *in situ* was, indeed, charged with bubble-phase gas. No correlation between the occurrence of seismic reflection anomalies and the presence of gas-charged sediment is apparent, except for the sediment southeast of Kayak Island. The sampling and analytical techniques needed to quantitatively assess gas-charged sediment as a geologic hazard have not been fully developed.

Geotechnical studies have been directed almost exclusively toward investigating slides and flows in the Holocene glacial-marine sediment. Holocene morainal sediments, Quaternary glacial-marine sediment and Pleistocene and older lithified sedimentary rocks are predominantly dense and hard, reflecting diagenesis or glacial ice loading. These compacted deposits are probably not susceptible to sliding on the continental shelf. In contrast, the Holocene glacial marine sediment is weak. In this area of frequent earthquakes and large storm waves, the Holocene glacial marine sediment is susceptible to slope failure under cyclic loading (Lee and Schwab, 1982).

Morphology of Submarine Slides and Flows. Numerous slides and slumps have been identified from seismic profiles of an 8 by 100 km area seaward of the mouth of the Copper River (Hampton and others, 1978; Carlson and Schwab, 1982) (Fig. 4). Some disrupted reflectors on a few of the profiles may indicate the presence of gas-charged sediment (Fig. 5). The disrupted reflectors occur beneath a slope of about  $0.5^\circ$  and appear to outline individual slump "blocks" that range in height from 1 m to 5 m and in length from 0.3 km to 1.0 km. The slump structures appear to be developed to a depth in the sediment of 20 m to 40 m in water depths of 40 m to 125 m.

A spectacular example of a large submarine slide is located in Kayak Trough (Carlson and Molnia, 1977; Molnia and others, 1977; Hampton and others, 1978) (Fig. 4). This slide has a length of 17 km, a maximum width of 12 km, and a maximum thickness of 115 m (estimated volume is approximately  $5.9 \text{ km}^3$ ). The slide occurred on a  $1^\circ$  slope. Seismic profiles over the Kayak Trough slide typically show disrupted internal reflectors and irregular surface morphology. This slide has a fairly well-preserved pull-apart scarp with a relief of about 10 m and a well-developed toe that is 20 m thick about 2 km from the distal end (Fig. 6). Apparently there was enough momentum to carry the toe of the slide past the thalweg of the trough (Carlson and Molnia, 1977).

The largest known slide on the continental shelf east of Kayak Island is the Icy Bay-Malaspina slump (Carlson, 1978), located seaward of the Malaspina Glacier (Slide A, Fig. 7). Here a process of en echelon slumping of Holocene clayey silt is taking place in water depths of 70 m to 150 m on a slope of less than  $0.5^\circ$  (Fig. 8). These slump structures extend over an area of about

$1080 \text{ km}^2$ . The slump blocks are about 0.5 km long and have reliefs of 2 m to 5 m. The slip surfaces extend to a depth of 15 m to 40 m beneath the sea floor. The volume of the entire slump is about  $32 \text{ km}^3$ .

Four smaller slides have been mapped in the nearshore zone east of the Icy Bay-Malaspina slump, all of which begin in water shallower than 100 m (Carlson and others, 1980) (Slide B, Fig. 7). One slide southwest of Yakutat Bay begins on the north wall of Yakutat Sea valley and extends across most of the valley floor. This slide covers an area of  $350 \text{ km}^2$  and incorporates the upper few meters of clayey silt. This slide appears to fit into Varnes (1978) classification as a mudflow that failed due to lateral spreading (Carlson and others, 1980).

The second of the four smaller slides, the Yakutat slide, begins 4 km seaward of the coastline between Yakutat Bay and the Dangerous River. It is about 40 km in width, and about  $260 \text{ km}^2$  in area (Carlson and others, 1980) (Slide C, Fig. 7). The slope of the upper part of the slide is about  $1^\circ$  and decreases to about  $0.5^\circ$  at the seaward edge of the slide. This slide mass is characterized by a series of clayey silt blocks undergoing rotational slump movement. The steplike surfaces of the blocks have a tread length of about 100 m and a riser height of 3 to 4 m (Fig. 9). The slip surfaces extend 10 m below the sea floor and the volume of slumped material is nearly  $3 \text{ km}^3$ .

The third smaller slide is located southeast of the Dangerous River in clayey silt (Carlson and others, 1980) (Slide D, Fig. 7). This slide begins about 2 km offshore in water depths less than 20 m. This area of seafloor instability is thought to be associated with gas-charged sediment interpreted from acoustic anomalies in high resolution seismic profiles, and water column gas plumes visible on side-scan sonographs (Carlson and others, 1980) (Fig. 10).

The fourth of the smaller slides is just seaward of the Alsek River (Alsek River Prodelta) (Slide E, Fig. 7) and has an area of  $150 \text{ km}^2$ . The shoreward edge of the slide is in sand and sandy mud less than 2 km offshore. Water depths are around 35 m and the slope is about  $0.5^\circ$ . This slide is thought to have moved down the headwall of the Alsek Sea Valley ( $1.3^\circ$  slope) possibly as far offshore as the floor of the valley (Slide F, Fig. 7) where it offsets the clayey silt to a depth of 10 m to 20 m (Carlson and others, 1980). A detailed picture of the sea floor in a  $10 \times 2 \text{ km}$  area within the Alsek River prodelta was made by assembling 21 speed corrected, digitally processed, side-scan sonographs (Molnia and Rappeport, 1980). Typical side-scan sonographs of the Alsek River slide are presented in Figures 11, 12, and 13. Molnia and Rappeport (1980) suggest that the principal factor for causing the Alsek Prodelta slope failures is saturation of the sediment by biogenic methane gas. Carlson and others (1980) also mapped this failure as an area of gas-charged sediment.

In addition to the slides and flows in the nearshore zone, other slides have been mapped within the Yakutat and Alsek Sea Valleys (Carlson and others, 1980) (Fig. 7). These slides all appear to be mud flows affecting the upper 10 m to 20 m of clayey silt.

Numerous areas of slides and slumps have been mapped on the continental slope (Fig. 7) (Carlson and others, 1980). Although most of these slides are

immediately seaward of the valleys, sliding appears to be a common mechanism for transporting sediment down the continental slope in the entire Gulf of Alaska (Hampton and others, 1978; Carlson, 1979). Many of these slides are longer than 5 km and occur on slopes with gradients of 3° to 6°. The slides range from discrete mudflows, thinner than 50 m, to complex zones of mass transport several hundred meters thick consisting of multiple slides, such as in the area southeast of Yakobi Sea Valley (Carlson and others 1980; Carlson and Schwab, 1982). The sediment contained in these slides is primarily a pebbly mud that was deposited by glaciers on the shelf during parts of the Pleistocene (Carlson and others, 1980).

#### GEOTECHNICAL APPROACH

General Methodology. The critical sediment geotechnical property measured for use in geologic hazards evaluations is the shearing strength. It must be exceeded by environmental loads for most types of failure to occur. Index properties (grain size, water content, bulk density, Atterberg limits and grain density) are measured as well because they aid in classifying the sediment and can be correlated with both strength parameters and sedimentary processes. Also, they are not strongly affected by coring disturbance. Compression or consolidation properties are measured because the consolidation state (relative degree of compaction) correlates well with relative shearing strength (Ladd and Foott, 1974), and reflects earlier geologic events (for example preloading by glaciers or erosion of overburden).

The usefulness of most of our geotechnical data are limited by the short length of cores (typically 1 m to 10 m) and by core disturbance. Because many failure features have basal shearing planes that are much deeper (50 m or more) than conventional coring devices penetrate, the sediment involved in failure may not have the same properties as that sampled. Coring disturbance, generated by the thick walled samplers that are commonly used, alters the engineering properties of the sampled sediment from the properties of the sediment in place. Both of these limitations, core shortness and disturbance, are serious and capable of greatly reducing the validity of any geotechnical study.

A methodology for partially overcoming these limitations is provided by the normalized soil parameter (NSP) approach (Ladd and Foott, 1974, Mayne, 1980). The NSP approach is based on empirical results that show certain engineering properties of certain sediments to be constant if normalized by appropriate consolidation stresses. For example, in a normally consolidated sediment profile (one in which no removal of sediment or preloading has occurred), the ratio of undrained shearing strength to overburden effective stress is often constant. If this ratio is known, a strength profile can be constructed by multiplying the ratio by values of overburden effective stress (sub-bottom depth times the average submerged density). If the sediment is overconsolidated, that is, if it has been preloaded by glaciers or other sediment that has since been eroded, a different ratio of strength to overburden stress will result. This ratio of strength to overburden stress is constant as long as the degree of overconsolidation, expressed as the overconsolidation ratio (OCR), is constant. The ratio of strength to overburden stress typically varies with the OCR raised to the power  $\Lambda_o$ , where  $\Lambda_o$  is a sediment constant (Mayne, 1980). If the variation of OCR with depth in the sediment column is known, a prediction of the strength variation can be

made. If the sediment is normally or underconsolidated, as the Holocene glacial-marine sediment appears to be in most locations, the value of  $A_o$  is irrelevant.

One advantage of the NSP approach lies in its ability to provide parameters that are independent of consolidation stress and depth in the sediment column. In a sense, therefore, the limitation imposed by short samples is at least partially removed, particularly in large depositional environments where the type of sediment being deposited at a given location is fairly constant over a long period of time (i.e., to a significant depth). The northeast Gulf of Alaska is probably such a large depositional environment. A second advantage of the NSP approach is that normalized parameters can be made somewhat independent of coring disturbance by conducting all strength tests at greatly increased consolidation stresses (Ladd and Foott, 1974). That is, a disturbed sample and a nearly undisturbed sample would produce almost the same normalized strength parameters if both are consolidated (in a triaxial or direct simple shear cell) to a high stress level before testing for shear. Once the normalized strength parameters have been measured at the high stress levels, they can be applied to any stress level including the low level that the sample originally experienced in place.

The NSP approach cannot handle all offshore geotechnical conditions. Ladd and Foott (1974) warn against applying it in cases of naturally cemented clays. Offshore sediments often display "psuedo-overconsolidation"; that is, most aspects (low surface strength, no obvious hiatus, steady increase of strength with depth) point to normal consolidation but consolidation tests indicate a moderate degree of overconsolidation. If "psuedo-overconsolidation" results from a form of interparticle cementation, the NSP approach would predict strengths that are too low.

The presence of significantly different sediment below the level of sampling or the presence of undetermined environmental factors that might alter the consolidation state also cannot be handled by the NSP approach. Bubble phase gas might be an example of the latter. Highly varied or stratified sediment might also produce complications.

Cyclic Strength Degradation and Test Type Effects. Excess pore water pressures that develop during episodes of cyclic loading from earthquakes or storm waves effectively reduce the ability of the sediment to resist shear. This effect on shearing resistance can be expressed as a strength degradation factor,  $A_D$ . If this factor is multiplied by the static shearing strength obtained by the NSP approach, an estimate of the strength remaining in the sediment after dynamic loading will result. The degradation factor,  $A_D$ , varies with the type and magnitude of cyclic loading. If the loading is wave induced and the sediment is fairly pervious, an effective stress approach with allowance for partial pore pressure dissipation may be required for accurate modeling. For this situation a worst case (lower bound of strength) model can be provided by using a strength degradation parameter,  $A_D$  corresponding to no drainage. For earthquakes the duration of cyclic loading is short and a simple, undrained approach can be taken.

Another factor affecting measured sediment strength is the type of strength test performed. A reported value of shearing strength is not independent of test type because of initial consolidation conditions, shearing

rate, stress inhomogeneities, variations in stress orientations and many other potential differences. A parameter that relates the strength corresponding to the mode and rate of stress application that would exist during failure in the field to the strength of the same material measured in a field or laboratory test is needed. In the present studies most strengths were obtained through isotropically consolidated triaxial shear tests. Because field consolidation conditions are typically anisotropic, a correction factor,  $A_c$ , is applied to correct strength values for these consolidation effects.

Summary of NSP Strength Determination. A summary of the normalized soil parameter approach as it has been applied in the northeastern Gulf of Alaska is given by the following equation:

Where  $S_u$  = The undrained shearing strength applicable to the mode of failure under consideration

$\sigma_v'$  = overburden effective stress =  $U\gamma'z$

**U = degree of consolidation**

= 1 for complete normal or over-consolidation

$\gamma'$  = average submerged density

**z = sub-bottom depth**

$A_C$  = Test type correction factor

$A_D$  = Cyclic strength degradation factor

**OCR = Overconsolidation ratio**

$$= \sigma_{\text{mm}}' / \sigma_{\text{uu}}'$$

$\sigma_{\text{um}}'$  = Maximum past effective stress

= A normalized strength exponent that is constant for a given

**sediment** 00

$S_{u-}$  = the ratio of static undrained shearing strength to isotropic

consolidation stress for normally consolidated conditions.

A program that involves a family of triaxial test types has been developed to obtain the parameters needed to evaluate Equation 1. The specific procedures are described under TEST PROCEDURES. Note that all of these properties relate to undrained conditions. For earthquake loading and wave loading of relatively impervious sediment, the undrained assumption is valid. For long term gravitational loading and wave loading of pervious sediment, a drained or partially drained analysis would be required.

Other shearing strength tests have been conducted that do not follow the NSP methodology directly. These include laboratory vane shear, field vane shear and static cone penetration, and certain types of triaxial shearing tests. The field tests were conducted to establish a level of ground truth and provide a basis for judging the quality of subsequent laboratory data. Also, some field penetration tests were conducted in sandy deposits and provide the only reliable geotechnical data for these deposits. Laboratory vane tests were conducted onboard the ship immediately following sample recovery. They typically provide a lower bound estimate of the in place undrained shearing strength (Lee, 1979). The triaxial tests that did not follow the NSP methodology involved samples consolidated to the in situ effective overburden stress or lower. These types of tests typically produce an upper bound estimate of the in place undrained shearing strength (Ladd and Lambe, 1963).

Quantitative Evaluation of Offshore Stability. Some of these geotechnical results can be readily used to evaluate geologic hazards or provide a means of mapping relative stability. The three major offshore downslope driving forces are gravity, earthquake shaking and storm wave loading. By writing a simplified equation for each driving force and setting it equal to the estimated, in place undrained shearing strength, we can determine the level of force needed to achieve failure. For example, it can be shown (Lee and others, 1981) that the approximate shearing stress developed under combined earthquake and gravitational loading is given by the simplified equation:

Where:  $\tau$  = mobilized shearing stress at depth  $z$

$\alpha$  = slope angle

**k** = horizontal pseudo-static earthquake acceleration ( in g's )

$\gamma$  = average total density of sediment (unit weight in air)

This relation was derived from Morgenstern's (1967) infinite-slope pseudo-static, earthquake-influenced slope stability analysis. It is valid only for small slope angles ( $\alpha$  less than about  $10^\circ$ ). The pseudo-static approach assumes that an earthquake can be modeled by a constant horizontal acceleration. The infinite slope approach assumes that the seafloor is smooth and has the same slope over a large area. Failure occurs on a plane parallel to the surface of the slope and movement takes the form of a sliding sheet. At failure the driving force will equal the resisting force. Substituting  $T$  from Equation 2 for  $S_u$  in Equation 1 and solving for  $k$  yields:

The resulting critical acceleration,  $k$ , derived from Equation 3 is the pseudo-static acceleration needed to induce failure given all of the conditions and assumptions present in the derivation. It is a function of sediment and site parameters. Lower values of the critical acceleration would correspond to areas that are more vulnerable to seismically induced sliding, given a uniform degree of seismicity over the region being investigated. The value of this approach is increased if known failures are sampled. Critical accelerations from a known failure area indicate the level of shaking required to cause failure and provide a value by which the significance of other measured critical accelerations can be judged.

A similar approach could be followed to evaluate relative stability with respect to storm wave-induced shearing stresses. However, as shown in Appendix B, the magnitude of peak wave-induced stresses exceeds that of peak earthquake-induced stresses only in relatively shallow water (water depth less than 35 to 76 m). In these depths the sediment is primarily sand which might allow nearly full dissipation of excess pore water pressures during storms. If full dissipation did not occur, a condition similar to liquefaction might develop under certain combinations of density, wave height and permeability (Clukey and others, 1980). This situation is unlikely and not considered in this report. For other conditions, earthquake loading dominates and Equation (3) can serve as the critical equilibrium relation.

## TEST PROCEDURES

Geotechnical testing was conducted in conjunction with four cruises to the Gulf of Alaska: three from the R/V DISCOVERER in 1977, 1980 and 1981 (DC1-77-EG, DC2-80-EG and DC1-81-EG) and one from the R/V SEA SOUNDER in 1977 (S8-77-EG). Many different USGS individuals were involved in planning and conducting these tests in-house, and three outside laboratories conducted additional tests on four separate contracts (Geotechnical Engineers, Incorporated (GEI), 1977 cores, University of California, Berkeley, 1977 cores and Law Engineering Testing Company (LETCO), 1977 cores and 1980 cores). As a result, not all of the procedures followed in determining each property were identical throughout the test program. In the following discussion, major differences in procedure are listed whenever significant.

Shipboard Sampling and Testing. Most core samples were taken with gravity corers weighing between 2 and 10 kNt. A few samples were obtained with piston samplers or a vibratory corer similar to the Alpine Vibracore sampler described by Tirey (1972). All cores were contained within a plastic liner. Once aboard ship the core liners were sectioned into 1 or 1.5 m lengths. At most sites replicate cores were obtained; one was split, described and subsampled on shipboard (stratigraphy-sedimentology core), while the other was sealed with cheesecloth and microcrystalline wax and preserved under refrigeration for shore laboratory testing (geotechnical core). One of the split core sections was subsampled for water content determination.

Most vane shear testing was conducted on split cores sections. A miniature four-bladed vane (typically 1.22 x 1.22 cm) was inserted perpendicular to the split face so that it was at least 1.2 cm below the surface. The vane was rotated by a motor-driven device through a calibrated spring on the 1977 cruises and through a torque cell on the 1980 and 1981 cruises. The top of the torque cell or spring rotated at 90°/minute, a rate relayed directly to the vane by the stiff torque cell. With the more flexible springs, the true vane rotation rate was less than 90°/minute before failure and greater after failure. The peak torque was measured and used to calculate the sample undrained shearing strength (ASTM, 1982 standard D 2573-72).

In Place Testing. In place vane shear and cone penetration tests were conducted during the 1980 cruise. The Multi-purpose in situ testing system (MITS) was leased from Woodward-Clyde Consultants, Plymouth Meeting, PA, and deployed at seven locations in the eastern Gulf of Alaska. The device is a tethered, bottom-supported platform capable of conducting static cone penetration and vane shear tests to a depth of 6 m below the seafloor. The device weighs 27 kNt (2.7 metric tons) in water. The ultimate cone penetration depth at a few locations was limited because of insufficient reaction force. The static cone penetrometer tip has a standard 10 cm<sup>2</sup> base area and a 60° tip angle. The load on the cone was measured by a full-bridge strain gage load cell mounted directly above the cone. The shear vane sensor consisted of a torque cell mounted above the vane blade. The vane was rotated by a pressure compensated electric motor at a rate of 60°/min and the shearing strength was calculated from the same formula as that used for laboratory vane shear measurements. Both the cone and the vane were driven into the seafloor by a sliding drive head coupled to a drill rod. The drive head was moved at 1 m/minute by an electric motor and a chain and sprocket assembly. The sub-

bottom depth to the cone or vane was measured by a 360° potentiometer connected to the sprocket assembly. A tilt indicator mounted on the base sensed the attitude of the frame to determine whether the maximum deadweight reaction was exceeded or if lateral loads on the tether line were pulling the device over. All electrical signals were carried to shipboard recorders through a shielded cable.

The MITS system was deployed from the R/V DISCOVERER from a two-point mooring. Typically the system was assembled in the cone penetrometer mode on its first deployment at a site. After a penetrometer record was obtained, the device was returned to the ship and rigged to perform a vane shear test. The size of vane and torque cell as well as sub-bottom locations for vane shear tests were selected based on the cone penetration resistance. The device was redeployed and the vane was driven in to the predetermined depths. At each depth the vane was rotated to obtain a peak torque and thus a measure of in place undrained shearing strength. At some depths the vane was rotated in the opposite direction (following an initial undisturbed strength determination) to obtain a measure of the remolded strength and the sediment sensitivity.

Shore Laboratory Testing. Water contents were obtained using drying and weighing techniques (ASTM, 1982 standard D2216-80). A correction was made to the weights to account for dried salts (assuming a salinity of 35 ppt).

Atterberg limits were obtained using ASTM standards (D 423-66, D 424-59 and wet preparation technique, D 2217-66) with the exception that the Casagrande grooving tool was used instead of the ASTM tool. Salt corrections identical to those described above were applied to both the liquid and plastic limits. The grain density was obtained using a Beckman air comparison pycnometer at the USGS laboratory and by ASTM Standard D 854-58 for the tests conducted by contractors. Grain size distributions and parameters were obtained using pipette analysis (Carver, 1971) at the USGS and by the hydrometer technique (ASTM Standard D 422-63) at the contractor laboratories.

Consolidation testing followed ASTM Standard D 2435-70 with these exceptions:

- (a) In two early contracts (GEI and LETCO testing of 1977 cores), calculated and plotted void ratios corresponded to the end of a stress increment time period. In later testing the plotted void ratios corresponded to 100% consolidation.
- (b) In all contracted tests the coefficient of consolidation ( $c_v$ ) was calculated using the square root of time method. For the tests conducted at the USGS,  $c_v$  was obtained using the log of time method.
- (c) In the LETCO testing of 1980 samples, about half of the tests were conducted with a pneumatically controlled Anteus consolidometer while the remainder were conducted with a dead weight oedometer.
- (d) Some of the tests conducted by the USGS on 1980 and 1981 samples were performed in a back pressured triaxial cell using the constant rate of strain technique (Wissa and others, 1971).

In all cases the results were used to estimate the maximum past vertical stress,  $\sigma'_{ym}$ , using the Casagrande (1936) construction and to obtain other consolidation parameters.

Static triaxial testing roughly followed the procedures given by Bishop and Henkel (1957). Cylindrical samples (3.6 cm in diameter by about 9 cm in height) were hand-trimmed from larger core sections extruded from the plastic liner. Filter strips were attached and the sample was enclosed in a thin rubber/latex membrane in a triaxial cell. Differential pressures between cell and sample fluids were applied and full drainage was allowed. These consolidation stresses were applied in increments until a final value was reached. In some tests conducted by the USGS and LETCO on 1980 and 1981 samples, final consolidation was set to a level of about four times the maximum past stress. This was followed by a reduction in differential pressure and full drainage. In this way, an induced state of overconsolidation with a known value of OCR was generated. A few samples were consolidated anisotropically with the horizontal consolidation stress equal to about 0.5 times the vertical consolidation stress.

Most samples were sheared without drainage by increasing the axial load at a constant rate of strain, typically 0.03% to 0.16% per hour. Some of the LETCO testing of 1977 cores involved constant rate of stress application. Excess pore water pressures developed in the samples during undrained shear were measured using electronic pressure transducers. Axial loads were measured with strain gage type load cells and axial deformations were obtained with linearly variable differential transformers (LVDT's). Testing was continued until about 20% axial strain was obtained. Stresses and strains were calculated using standard procedures but without membrane or filter strip corrections. The static undrained shearing strength was obtained from the peak axial load measured over the full 20% axial strain range of the test.

Three types of static triaxial tests were performed:

- (a) Consolidation to a stress level less than three times the estimated maximum past stress without rebound.
- (b) Consolidation to a stress level greater than three times the estimated maximum past stress with a subsequent rebound to a lower final consolidation stress. A known induced overconsolidation ratio is obtained.
- (c) Consolidation to a stress level greater than three times the estimated maximum past stress without rebound.

Type (a) tests produce strength values that may be less than, equal to or greater than the in place shearing strength, depending on the details of the consolidation stresses. The approach does not provide parameters that can be used in the NSP approach. The value of this type of test would be in obtaining upper and lower bound values of strength and in studying naturally cemented sediment for which the NSP approach is not applicable.

Type (b) and (c) tests yield strength values for use in the NSP approach. Type (c) is used to obtain the ratio of strength to consolidation stress for normal consolidation,  $S_{nc}$ , while type (b) yields the parameter  $A_o$  required for Equation 1.

Specimens for cyclic triaxial tests were prepared and consolidated in the same way as specimens for static tests (b) and (c) above. Because the static test for each consolidation condition was performed first on an adjacent sample, an estimate of the static strength of the cyclic specimen could be

made. Cyclic stresses less than the estimated static strength were then applied and the number of cycles needed to cause a predetermined one-directional strain was measured. Nearly full stress reversal (tensile and compressive stresses approximately equal) was developed. Loading was sinusoidal with a frequency of 0.1 Hz. The results were graphed on a plot of relative stress level (maximum average one-directional cyclic stress/estimated static strength) versus the log of number of cycles to 20% one-directional strain. A straight line connecting the data points was drawn and the stress level required for failure in 10 cycles was estimated by interpolation or extrapolation. Because 10 cycles is a characteristic number of significant cycles for a major earthquake (Seed and Peacock, 1971), this stress level was used for  $A_D$  in Equations 1 and 3 for earthquake analysis. The parameter  $A_D$  for storm-wave-induced instability would correspond to a larger number of cycles.

## RESULTS

Study Areas and Core Locations. To simplify locating core sample and in place data, the region has been divided into eight study areas. Many of the study areas are associated with the major failure features discussed previously. Proceeding from west to east the eight study areas are (Figure 14):

- (A) Copper River
- (B) Kayak Trough
- (C) Bering Trough
- (D) Icy Bay
- (E) Icy Bay-Malaspina
- (F) Yakutat Bay
- (G) Yakutat
- (H) Alsek River

A ninth category, "other", includes a few sampling and in place stations that fall outside the regular areas.

Core and in place test location maps for each study area are given in Figures 15 through 21. The coordinates for these locations are given in Table 1.

Organization of Laboratory Test Data Presentation. All of the index property data are provided on summary plots in Appendix C. These data include water content, Atterberg limits, vane shear, grain size and grain density. Downcore locations of samples on which consolidation and triaxial tests were performed are also shown. The nature of these tests is indicated by a coded test number. The code for the test numbering system is as follows:

First two letters:

- (a) OE - Oedometer test
- (b) CE - Constant rate of strain (CRS) consolidation test
- (c) TE - Static triaxial test
- (d) TC - or D - Cyclic triaxial test

Trailing characters:

- (a) No trailing characters - test performed by the USGS

- (b) L1 - Test of 1977 core sample by Law Engineering and Testing Company
- (c) G - Test of 1977 sample by Geotechnical Engineers, Incorporated
- (d) B - Test of 1977 sample by University of California, Berkeley
- (e) L2 - Test of 1980 sample by Law Engineering and Testing Company

Critical sediment geotechnical parameters from each test are summarized in Tables 2 (consolidation), 3 (static triaxial) and 4 (cyclic triaxial). Graphical presentations of the results of each test are given in Appendices D (Law Engineering testing of 1977 cores), E (Geotechnical Engineers, Incorporated testing), F (Law Engineering testing at 1980 cores) and G (USGS testing of 1980 and 1981 cores). The appendices are grouped according to the organization performing the test because of a variation in the formats followed in graphically presenting the data. Each appendix is subdivided according to test type (consolidation, static triaxial or cyclic triaxial).

For the consolidation tests, a standard plot of void ratio,  $e$ , versus vertical effective stress,  $\sigma_v'$ , is given. These plots were used to obtain the slopes of the virgin compression and rebound curves ( $C_c$  and  $C_r$ ) and the maximum past stresses,  $\sigma_{vm}'$ , all of which are tabulated in Table 2. For some of the testing organizations, a plot is also given of the calculated coefficient of consolidation,  $c_v$ , versus the vertical effective stress.

For the static triaxial tests, plots are given of the shearing or deviatoric stress,  $q$ , versus the mean normal effective stress,  $p$ . These stress paths provide a definition of the failure envelope and indicate whether sediment behavior is of a collapsing (bend to the left) or dilatative (bend to the right) nature. Also given are plots of shearing or deviatoric stress and pore pressure change versus axial stress.

The cyclic triaxial test plots include shearing stress-axial strain curves (hysteresis loops) and shearing stress-average normal effective stress (stress path) plots for selected cycles. The stress path plots indicate roughly the failure envelope applicable for cyclic loading and the rapidity with which pore pressures develop as a result of cyclic loading. The hysteresis loops indicate damping (proportional to relative area of each loop) and degrading stiffness (proportional to average slope through each loop). For the USGS tests these results are further presented on four additional plots that show pore pressure developed, damping, stiffness (modulus) and peak strain developed as a function of cycle number.

In Place Test Data. The results of in place vane shear testing are given in Figures 22 through 26 and cone penetrometer records appear in Figures 27 through 34. The vane shear results are plots of calculated undrained shearing strength versus sub-bottom depth. The cone results are continuous plots of cone pressure versus depth. Additional information plotted on the figures is discussed in a later section.

#### SYNTHESIS AND DISCUSSION

Analysis of Parameters. A major goal of the geotechnical testing was to provide parameters that could be inserted into Equation 3 so that a stability-related parameter, the critical acceleration,  $k$ , could be calculated. These parameters are:

- (a)  $S_{nc}$  - ratio of uniaxial strength to consolidation stress for normal consolidation
- (b)  $A_C$  - test type correction factor
- (c)  $A_D$  - cyclic strength degradation factor
- (d)  $U$  - degree of consolidation
- (e) OCR - overconsolidation ratio
- (f)  $\Lambda$  - normalized strength exponent
- (g)  $\gamma/\gamma'$  - ratio of submerged unit weight to total unit weight
- (h)  $\alpha$  - slope angle

The next few sections discuss several of these parameters and how they were obtained from the basic engineering properties given in Tables 2 through 4 and in the appendices. Most of these parameters are correlated with sediment water content. In these correlations the water content is used as an index property that is representative of more basic sediment characteristics such as clay mineralogy, grain size and plasticity. The water content is used in place of these other parameters because it is the only parameter that was measured in conjunction with every other test. Also, because more water contents were measured than any other property, correlations can be applied to any location where a water content measurement was made. The influence of in place consolidation on reducing the water content with sub-bottom depth is ignored because of the shortness of the cores and the relative incompressibility of the silty sediment. The significant down-core fluctuations in water content in many of the cores appear to be related to basic lithologic changes.

Undrained Strength to Consolidation Stress Ratio for Normal Consolidation,  $S_{nc}$ . The type (c) tests listed in Table 3 were used to obtain values of  $S_{nc}$ . The criterion used to distinguish type (c) tests was that the final consolidation stress applied in the triaxial cell needed to exceed the natural maximum past stress by at least a factor of 3. Any lower consolidation stresses, in conjunction with disturbance effects, might produce a sample with some characteristics of overconsolidation (Ladd and Foott, 1974). The ratios of strength to overburden pressure for all of the type (c) tests were obtained and are plotted versus water content in Figure 35. The correlation is fairly good, given the scatter typically involved in geotechnical measurements, and shows a trend toward decreasing  $S_{nc}$  with increasing water content. A solid line follows the trend of the tests for which the initial consolidation was isotropic. The tests for which initial consolidation was anisotropic (lateral stress about one-half of the vertical stress) are shown with circled dots. Although a limitation in the number of these points prevents the construction of a line as complete as that for isotropic consolidation, a line with values of  $S_{nc}$  that are 0.8 times the isotropic values seems to fit the data fairly well.

Test Type Correction Factor,  $A_C$ . The factor  $A_C$  ideally should relate strength under laboratory test rate, test mode and consolidation stress conditions to the strength effective in the field under natural loading conditions. Most aspects cannot be considered without a major increase in the scope of investigation. The relation between strength under laboratory consolidation (predominately isotropic) and field consolidation (predominately anisotropic) condition is straightforward and represented by the difference between the two lines in Figures 35. Because a ratio of 0.8 appeared to account for most of the variation, this value will be used for  $A_C$ . The value

is similar to that obtained in an earlier study of sediment from offshore northern California. (Lee and others, 1981).

Cyclic Strength Degradation Factor,  $A_D$ . Results of cyclic triaxial tests on fine grained sediment are typically presented on a plot of cyclic stress level (as a percent of static strength) versus number of cycles to failure (Lee and Focht, 1976). Such a presentation is dependent upon knowledge of a static strength that can be used for normalization. In the University of California, Berkeley tests, the static strength of a third sample cut from the same increment as two cyclic test samples was determined. Normalizing the cyclic stress levels by this static strength is legitimate because the cyclic samples probably would have had the same strength if failed statically. For the USGS and Law Engineering tests, however, a static strength was measured on a sample from the same core but a different depth increment from that of the cyclic tests. One method (Method I) of normalizing the cyclic stress is to divide the cyclic stress level by this measured static strength. In some cores, however, there were lithologic changes downcore and the static and cyclic tests were not run on the same material type. This problem was solved partially by estimating a static strength from the water content and consolidation stress of the cyclic sample and an estimate of the ratio of static strength to consolidation stress from Figure 35. This approach to obtaining the static strength is termed Method II. A third method of handling this problem is to eliminate the need for static strength estimation by evaluating the product  $A_D S_{nc}$  rather than its components. Because  $A_D$  is a cyclic shear stress,  $\tau_c$ , divided by a static strength,  $S_u$ , and  $S_{nc}$  is  $S_u$  divided by a consolidation stress,  $\sigma_{vc}'$ , the product is  $\tau_c / \sigma_{vc}'$ . This ratio can be obtained from a cyclic test alone without any static test results. The use of the ratio  $\tau_c / \sigma_{vc}'$  is termed Method III.

Plots of relative cyclic stress levels versus number of cycles to failure are given in Figures 36 through 48. Separate figures corresponding to the three methods of analysis are given for the USGS/Law Engineering test results. The lines shown in the figures connect two or more cyclic test results and have been extended when necessary to cover the 10 cycles to failure zone. For methods I and II, the relative stress level corresponding to 10 cycles to failure was taken as  $A_D$ . For method III this value was taken as  $A_D S_{nc}$  or  $\tau_c / \sigma_{vc}'$ . Plots of relative stress level for failure in 10 cycles versus representative water content for the three methods of analysis are given in figures 49 through 51. Method II (Figure 50) shows a somewhat closer correlation than Method I (Figure 49); a solid line fit of the data shows an acceptable level of scatter (Figure 50). The trend shows an increase in  $A_D$  with increasing water content. That is, the lower water content coarse silts and sands are more susceptible to cyclic strength degradation than are the higher water content fine silts and clays. The product of the solid line fits for  $S_{nc}$  (Figure 35) and  $A_D$  (Figure 50) yields a solid line fit for  $S_{NC} A_D$  versus water content (Method III, Figure 51).

Some of the University of California, Berkeley, tests were performed with a static bias (Figures 36 through 39). That is, following nearly isotropic consolidation but before cyclic shear, a static shearing stress was applied. The sinusoidal cyclic stress was then applied relative to the static bias. The level of principal stress rotation (alternating compressive and tensile stresses) is reduced as the static bias is increased. Herrmann and Houston

(1976) show that the greater the level of principal stress rotation the greater is the extent of cyclic strength degradation. In cyclic earthquake loading of nearly horizontal sediment deposits, there is considerable rotation of principal stresses with each major cycle of loading (Seed and Peacock, 1971). Therefore, the case of no static bias or full stress rotation is more realistic as well as more conservative. The tests with a significant static bias give an intermediate level of cyclic strength degradation.

Degree of Consolidation,  $U$ , Overconsolidation Ratio (OCR) and Normalized Strength Exponent,  $\Lambda_o$ . A critical concern is evaluating offshore stability is the relative consolidation state of the sediment. Table 2 provides some information on consolidation state in the form of two parameters:  $\sigma_e'$  and  $\sigma_{vm}'/\gamma'z$ . The parameter,  $\sigma_e'$  is the difference between the maximum past stress,  $\sigma_{vm}'$  and the submerged weight per unit area of overlying material,  $\gamma'z$ . The parameter is negative for underconsolidated sediment (not all submerged overburden carried by interparticle stress), zero for normal consolidation and positive for overconsolidation. The ratio  $\sigma_{vm}'/\gamma'z$  is the degree of consolidation,  $U$ , for values of  $\sigma_e'$  less than or equal to zero and the overconsolidation ratio (OCR) for values greater than or equal to zero. As may be seen, scattered values of both parameters were obtained with apparently underconsolidated, normally consolidated and overconsolidated sediment all present. There is little consistency among the values, however, and in only about 10% of the tests is the absolute value of  $\sigma_e'$  greater than 50 kPa. Because of inaccuracies present in the Casagrande procedure and coring disturbance, these small deviations from normal consolidation are probably insignificant. In later sections additional in place data and theoretical information is used to further evaluate the consolidation state of these sediments. Based on Table 2 alone, it appears that the best estimate for both  $U$  and OCR for most of the cores is 1.0 (normal consolidation).

In anticipation of at least some of the cores being overconsolidated, a few static triaxial tests of the type (b) variety (induced overconsolidation ratio) were performed. These were used to obtain estimates of the parameter  $\Lambda_o$  needed for Equations 1 and 3. To obtain  $\Lambda_o$ , one first obtains the ratio of undrained strength to consolidation stress for a specimen that has an induced overconsolidation ratio (OCR known). This ratio is divided by the ratio of strength to consolidation stress for normal consolidation,  $S_{nc}$  to obtain a shear strength that has been normalized twice. Again,  $S_{nc}$  may be obtained from a test on a different sample from the same core or estimated from Figure 35 (if the initial water content of the induced OCR sample is known). These methods are termed I and II, respectively, and are similar to Methods I and II for normalizing cyclic triaxial test data discussed previously. The parameter  $\Lambda_o$  is obtained by dividing the log of the twice normalized shear strength by the log of the induced OCR (Mayne, 1980). Values of  $\Lambda_o$  (by both Methods I and II) and the intermediate parameters required to calculate them are given in Table 5. There is considerable scatter and a few values exceed 1.0 (not physically reasonable; probably indicative of experimental error at some level). Also, there is no correlation between  $\Lambda_o$  and water content. The average value of 0.9 would be appropriate for overconsolidated sediment. However, in the present study, all Holocene glacial-marine silty clays tested appear to be under- or normally consolidated.

Ratio of Submerged to Total Unit Weight,  $\gamma'/\gamma$ . The ratio of submerged to total unit weight can be calculated directly from the water content by

assuming 100% saturation and using the average measured grain density, 2.8 g/cm<sup>3</sup>.

Validity of NSP Approach, Vane Shear Tests and Type (a) Triaxial Tests. One purpose of performing in place strength tests was to provide a ground truth check on values obtained in the laboratory. The locations where both in place vane shear tests were performed and cores were taken for shore geotechnical analysis offer an opportunity to check the quality of laboratory strength determination procedures. Strengths were measured in the laboratory using the miniature vane, type (a) static triaxial tests (consolidation to a low value, often near the estimated in situ overburden stress) and normalized soil property (NSP) oriented tests (types (b) and (c)). These laboratory strength determinations are shown on the same figures as the field vane shear results (Figures 22 through 26). In these comparisons the laboratory vane shear results are consistently lower than the field results. The laboratory values range between about 50 and 80% of the field values. These findings are thus in line with a value of 60% obtained for a low plasticity (PI=15%) southern California sediment (Lee, 1979). The type (a) static triaxial tests consistently yielded strengths 150 to 250% higher than the field values.

The NSP values were obtained by using measured core water contents to obtain ratios of static strength to overburden effective stresses ( $S_{nc}$ ) from Figure 34. The overburden effective stresses were obtained from  $\gamma'z$  (average submerged unit weight times depth) and multiplied by the  $S_{nc}$  estimates to obtain an estimated shear strength profile. An implicit assumption of normal consolidation was made. These estimated shear strength values ranged between about 60% and 140% of the measured field values for the depth range sampled (excluding the upper 1 m). Below the level of sampling, a range of estimated strengths is given, corresponding to the range of water contents measured in the core. In this deeper unsampled sediment the NSP estimated shearing strengths were about 80 to 140% of the field values.

The NSP approach appears to provide the best estimate of the in place shearing strength values while the type (a) static triaxial test (consolidation to a low stress level with no normalization) appears to provide the poorest estimate and has the lowest correlation with the in place results. The simple laboratory vane shear test is nearly as accurate as the NSP approach if measured strengths are multiplied by a correction factor of about 1.7 (1/0.6) to account for disturbance. The laboratory vane test is not suitable for extrapolation below the level of sampling or evaluating cyclic strength degradation, however.

Evaluation of Consolidation State Using Field Strength Results and Gibson's Theory. Laboratory consolidation tests showed little indication of underconsolidation but the results were fairly scattered. Another means of judging consolidation state is to compare field vane strengths with NSP generated strengths. Such a comparison (Figures 22 through 26) shows no indication of overconsolidation except possibly for the upper 3.5 m of field test MV-1. That is, the field strengths do not greatly exceed the NSP strengths calculated by assuming normal consolidation. With field test MV-1 the high field strengths are probably a result of layered sand observed in nearby vibratory cores rather than true overconsolidation.

Field tests MV-4 (Figure 25) and, to a lesser extent MV-5 (Figure 26) suggest that a state of underconsolidation exists in the sediment in the eastern portion of the Icy Bay-Malaspina study area. The field strengths are 60 to 80% of the NSP generated strengths for normal consolidation. Excluding any other errors or opportunities for variability, these values correspond directly to the degree of consolidation.

To further evaluate the potential for underconsolidation in the northeast Gulf of Alaska, we performed a simplified theoretical analysis using the method of Gibson (1958). Gibson modeled a layer of sediment deposited at a steady and continuing sedimentation rate,  $m$ , that began to be deposited at a time,  $t$ , in the past. The degree of consolidation at the base of the sediment column can be predicted (Figure 52) as a function of the dimensionless parameter,  $m^2t/c_v$ , where  $c_v$  is the coefficient of consolidation. The degree of consolidation at shallower levels is somewhat lower.

Values of  $c_v$  were measured in this study but are fairly scattered and inconsistent (Table 2). To reduce the scatter, a simplified correlation between  $c_v$  and liquid limit (Figure 53) from Lambe and Whitman (1969, p. 412) was used along with average liquid limit values for several locations. Sedimentation rates were taken from Figure 3.

By combining the results of Figures 52 and 53, we constructed lines of constant degree of consolidation on a plot of liquid limit versus  $m^2t$  (Figure 54). Using measured results, locations within the eastern Gulf of Alaska were plotted on the same figure. The position of these data points relative to the lines of constant degree of consolidation indicates the theoretical degree of consolidation of the sites. Most of the sites fall to the left of the 90% consolidation line indicating a degree of consolidation approaching 100%. All of the field vane shear tests except MV-4 (eastern Icy Bay-Malaspina study area) correspond to sites that fall in this range. The eastern Icy Bay-Malaspina study area has a theoretical degree of consolidation of about 85%, somewhat greater than the discrepancy between NSP and field strengths (Figures 25 and 26), but in the same range. Therefore, several lines of evidence (field versus NSP strength, theory and consolidation test results) suggest a degree of underconsolidation (60 to 85% of normal consolidation) of the sediment in the eastern Icy Bay-Malaspina study area. As indicated on Figure 54, the eastern portion of the Alsek prodelta study area and Kayak Trough may also display a similar underconsolidation level. Two of the embayments, Icy Bay and Yakutat Bay, appear to be highly underconsolidated, having degrees of consolidation of 30 and near 15%, respectively. The remainder of the Holocene glacial-marine sediment sites appear to be normally consolidated.

Critical Acceleration Calculation. The critical acceleration,  $k$ , is calculated from Equation 3. If we assume normal consolidation ( $U=OCR=1$ ) and horizontal surfaces ( $\alpha=0$ ), then all of the remaining parameters have been obtained as a function of water content in the sections above. Note that with a value of OCR equal to 1.0, the value of  $\Lambda$  is irrelevant. Also, with OCR equal to 1.0, the solution for  $k$  is independent of sub-bottom depth. By combining the best fits of the data using Equation 3, a plot of critical acceleration versus water content can be drawn (Figure 55). The resulting values of the critical acceleration have a broad-based minimum between water contents of 35% and 45%. On either side of this zone the acceleration increases rapidly. The existence of this minimum range indicates that certain

types of sediment found in the eastern Gulf of Alaska are more susceptible to earthquake loading than others. If we assume that each location within the region has the same potential ground shaking intensity and that underconsolidation and slope effects can be ignored initially, then locations that have more of the susceptible material should have failed more often. Within the Icy Bay-Malaspina study area (Figure 56), this appears to be the case. The portion of each core with a water content between 35% and 45% has been calculated and listed by the location of the core. It appears that those cores within the observed failure feature typically have more of the susceptible sediment than do those outside the feature. The correlation is not exact but is consistent. Thus mapping of vulnerable material according to surface core water content may be viable even though the extent of underconsolidation, steepness of slope, variations in seismicity and variations in seismic response have not been considered.

The distribution of susceptible material in the Yakutat study area is shown in Figure 57. The correlation of susceptible material with the slump zone is not as good as for the Icy Bay-Malaspina area. The higher level of underconsolidation in the Icy Bay-Malaspina area may contribute to the greater extent of failure. Also, the boundaries of the Yakutat slump are poorly defined acoustically.

In the Alsek study area (Figure 58), all cores were collected within the failure zone. The majority of samples appear to consist of susceptible sediment.

Regional Variations. Most of the geotechnical properties discussed above have been tied together through a seismic-induced instability analysis. A correlation of parameters with water content has shown some consistent trends and has helped to identify a susceptible sediment type. The water content, in turn, typically increases offshore, although not consistently. Downcore variations in water content are large.

No consistent variations in the correlations of geotechnical parameters with water content were found that could be related to study area. Indeed, the differences between study areas appear to be of the same order as variations within study areas. Some differences in landslide morphology were noted in the geologic framework discussion that cannot be explained by these basic correlations. For example, the multiple, complex flows of the Alsek prodelta contrast with the massive but simple rotational slumps of the Icy Bay-Malaspina study area. One possible explanation of these morphology differences is that fundamental sedimentological parameters contribute to variations in post failure behavior. That is, certain geotechnical properties that correlate well with water content may determine the point of initial failure. Movement after failure may be controlled by other characteristics that are not properly evaluated in triaxial testing.

An example of at least one characteristic that appears to vary consistently among the study areas is plasticity. All of the Atterberg limits measurements, grouped according to geographic area, are plotted on a series of plasticity charts (plasticity index versus liquid limit, Lambe and Whitman, 1969, p. 35) in Figures 59 through 64. Least squares regression fits of each set of data were developed and displayed fairly good correlation coefficients. Figure 65 presents a summary of all of the linear regression

lines. All plot above the "A-line" and fall near or within the zone generally occupied by glacial clay (Lambe, 1951, p. 27). Most sediment classifies as CL ("inorganic clays of low to medium plasticity, gravelly clays, sandy clays, silty clays, lean clays"). The regression lines are nearly parallel to each other and to the "A-line." The continental shelf study areas (Alsek prodelta, Yakutat, Icy Bay-Malaspina, Copper River) show a progressively greater distance from the "A-line" as one progresses toward the west. The Alsek prodelta slide, which has the most unusual morphology, provides data that plot closest to the "A-line." The embayments (Icy Bay, Yakutat Bay) and troughs (Bering, Kayak) show the greatest distance from the "A-line". This behavior probably relates to changes in clay mineral activity. The unusual morphology of the Alsek prodelta slides and flows may relate to these changes in index properties.

#### SUMMARY AND CONCLUSIONS

1. Previous studies have shown the major seafloor geologic hazards in the eastern Gulf of Alaska to be slides and flows, shallow faults, gas charged sediment and buried channels. Excluding shallow faulting, these hazards on the continental shelf are associated with Holocene glacial-marine sediment. This sediment consists primarily of sand and muddy sand in water depth less than 50 m and clayey silt at greater depths. The Holocene glacial-marine sediment is a typical glacial rock flour produced by intense mechanical weathering. Massive failure features have been identified acoustically on slopes of 0.5° to 1.3° on the continental shelf. Sediment volumes of up to 32 km<sup>3</sup> are involved.
2. Both underconsolidation (Hampton and others, 1978; Carlson and others, 1978; Molnia and Sangrey, 1979) and bubble-phase gas charging (Carlson and others, 1980; Hampton and others, 1978; Molnia and Rappeport, 1980) have been suggested as principal causative factors for sediment instability in the region. The present study indicated that both features are present but that their occurrence is uncommon.
3. Cyclic loading by storm waves and particularly earthquakes appears sufficient to cause the observed failure features. Gas charging and underconsolidation may facilitate failure in a few locations. Major wave induced shearing stresses exceed major earthquake induced stresses only in relatively shallow water (less than 35 to 76 m).
4. As noted by Ladd and Foott (1974), the normalized soil parameter (NSP) approach appears capable of partially overcoming the problems of coring disturbance and core shortness in obtaining valid geotechnical properties. This is illustrated in this study by good comparisons between NSP generated strength profiles and those measured with an in place vane shear device. One comparison that is not as good can be explained by underconsolidation predicted by Gibson's (1958) analysis.
5. Laboratory vane shear tests produce shearing strengths that are consistently lower than the field strengths. Triaxial specimens consolidated to near the in place overburden stress produce strengths that are erratically higher to much higher than the field strengths.

6. There is little evidence for overconsolidation in the Holocene glacial-marine sediment tested.

7. Many of the geotechnical parameters correlate well with water content, which is probably representative of more basic sediment characteristics such as clay mineralogy, grain size, and plasticity. According to laboratory tests, sediment with a water content between 35% and 45% is most susceptible to earthquake loading. Cores that contain more of this susceptible material roughly correlate with the locations of failure features.

8. Differences in failure morphology are difficult to relate to advanced geotechnical parameters but may relate to observed variations in plasticity.

#### ACKNOWLEDGEMENTS

These studies were supported by the U.S. Geological Survey and the Bureau of Land Management through an interagency agreement with the National Oceanic and Atmospheric Administration, under which a multiyear program responding to needs of petroleum development of the Alaskan continental shelf is managed by the Outer Continental Shelf Environmental Assessment Program (OCSEAP) office.

We wish to thank Bill Levy, Ed Clukey, Charles Fitts, Dwight Sangrey, Arnold Bouma, Bruce Molnia and Paul Carlson for their effort in acquiring the early geotechnical data presented in this report. We also wish to thank Dan Bright, Pat Spragge, Kris Johnson and Mike Torresan for performing the later geotechnical tests. Finally, we thank Monty Hampton, Bill Winters and Jim Booth for their thoughtful and helpful reviews of this manuscript.

## REFERENCES

- American Society for Testing and Materials (ASTM), 1982, 1982 annual book of ASTM Standards, part 19, Natural Building Stones; Soil and Rock, ASTM, Philadelphia, 710 pp.
- Bea, R.G., 1976, Earthquake criteria for platforms in the Gulf of Alaska: Proceedings of the 8th Offshore Technology Conference, Houston, vol. 2., p. 657-679.
- Beikman, Helen, 1974, Preliminary geologic map of the southeast quadrant of Alaska: U.S. Geological Survey Miscellaneous Field Studies Map MF-612, Scale 1:1,000,000.
- Beikmann, Helen, 1975, Preliminary geologic map of southeastern Alaska: U.S. Geological Survey Miscellaneous Field Studies Map MF-673, Scale 1:1,000,000.
- Bishop, A.W. and Henkel, D.J., 1957, The measurement of soil properties in the triaxial test, Edward Arnold, Ltd, London, 227 p.
- Bruns, T.R., 1979, Late Cenozoic structure of the continental margin, northern Gulf of Alaska, in Sisson, Alexander, ed., The relationship of plate tectonics to Alaskan geology and resources: Alaska Geological Society 1977 Symposium Proceedings, p. I1-I30.
- Bruns, T.R., 1982, Structure and petroleum potential of the continental margin between Cross Sound and Icy Bay, northern Gulf of Alaska: U.S. Geological Survey Open-File Report 82-929, 63 p.
- Bruns, T.R. and Plafker, George, 1982, Geology, structure, and petroleum potential of the southeastern Alaska and northern Gulf of Alaska continental margins, in Bruns, T.R., ed., Hydrocarbon resource report for proposed O.C.S. Lease Sale 88: Southeastern Alaska, Northern Gulf of Alaska, Cook Inlet, and Shelikof Strait, Alaska, p. 11-52.
- Bruns, T.R., and Schwab, W.C., 1982, Structure maps and seismic stratigraphy of the Yakataga segment of the continental margin, northern Gulf of Alaska: U.S. Geological Survey Miscellaneous Field Studies Map MF-1424, 2 sheets and 25 p., scale 1:250,000 (in press).
- Carlson, P.R., 1978, Holocene slump on continental margin off Malaspina Glacier, Gulf of Alaska: American Association of Petroleum Geologists, Bulletin, vol. 62, no. 12, p. 2412-2426.
- Carlson, P.R., 1979, Extensive sliding of continental slope sediments, eastern Gulf of Alaska (abs.): Geol. Soc. of America, Abstracts with Program, vol. 11, p. 398.
- Carlson, P.R., Bruns, T.R., and Molnia, B.F., 1975, Submarine slides and near surface faults, northern Gulf of Alaska: U.S. Geological Survey Open-File Report 75-505, 1 map.

Carlson, P.R., Bruns, T.R., Molnia, B.F., and Schwab, W.C., 1982, Submarine valleys in the northeastern Gulf of Alaska: Characteristics and probable origin: *Marine Geology*, vol. 47, p. 217-242.

Carlson, P.R., Levy, W.P., Molnia, B.F. and Hampson, J.C., 1978, Geotechnical properties of sediments from the continental shelf south of Icy Bay, northeastern Gulf of Alaska: U.S. Geological Survey Open-File Report 78-1071, 29 p.

Carlson, P.R., and Molnia, B.F., 1975, Preliminary isoch map of Holocene sediments, northern Gulf of Alaska: U.S. Geological Survey Open-File Report 75-507.

Carlson, P.R., and Molnia, B.F., 1977, Submarine faults and slides on the continental shelf, northern Gulf of Alaska: *Marine Geotechnology* vol. 2, p. 275-280.

Carlson, P.R., Molnia, B.F., Kittelson, S.C., and Hampson, J.C., Jr., 1977, Distribution of bottom sediments on the continental shelf, northern Gulf of Alaska: U.S. Geological Survey Miscellaneous Field Studies Map MF-876, 2 sheets and 13 p., scale 1:500,000.

Carlson, P. R., Molnia, B. F., and Wheeler, M. C., 1980, Seafloor geologic hazards in O.C.S. lease area 55, eastern Gulf of Alaska: *Proceedings of the 12th Offshore Technology Conference*, Houston, v. 1, p. 563-603.

Carlson, P. R., and Schwab, W. C., 1982, Northern Gulf of Alaska environmental geology, in Bruns, T. R., ed., *Hydrocarbon resource report for proposed OCS lease sale 88: southeastern Alaska, northern Gulf of Alaska, Cook Inlet, and Shelikof Strait, Alaska*: U.S. Geological Survey Open-File Report 82-928, p. 73-86.

Carver, R. E., 1971, *Procedures in sedimentary petrology*: Wiley-Interscience, New York.

Casagrande, Arthur, 1936, The determination of the pre-consolidation load and its practical significance: *Proceedings, 1st International Conference of Soil Mechanics and Foundation Engineering*, p. 60.

Clukey, E. C., Cacchione, D. A., and Nelson, C. H., 1980, Liquefaction potential of the Yukon Prodelta, Bering Sea: *Proceedings of the 12th Annual Offshore Technology Conference*, Houston, vol. 1, p. 315-325.

Gibson, R. E., 1958, The progress of consolidation in a clay layer increasing in thickness with time: *Geotechnique*, vol. 8, p. 71-182.

Hampton, M. A., Bouma, A. H., Carlson, P. R., Molnia, B. F., Clukey, E. C., and Sangrey, D. A., 1978, Quantitative study of slope instability in the Gulf of Alaska: *Proceedings of the 10th Offshore Technology Conference*, Houston, vol. 4, p. 2307-2318

Herrmann, H. G., and Houston, W. N., 1976, Response of seafloor soils to combined static and cyclic loading: *Proceedings of the Eighth Offshore Technology Conference*, paper number OTC 2428.

Ladd, C. C., and Foott, Roger, 1974, New design procedure for stability of soft clays: American Society of Civil Engineers, Journal of the Geotechnical Engineering Division, vol. 100, no. GT7, p. 763-786.

Ladd, C. C., and Lambe, T. W., 1963, The strength of "undisturbed" clay determined from undrained tests: American Society for Testing and Materials, Standard Technical Publication 361, p. 342-371.

Lambe, T. W., 1951, Soil testing for engineers, J. Wiley and Sons, New York, 165 p.

Lambe, T. W. and Whitman, R. V., 1969, Soil Mechanics, J. Wiley and Sons, New York, 533 p.

Lee, H. J., 1979, Offshore soil sampling and geotechnical parameter determination: Proceedings of the 11th annual Offshore Technology conference, paper number OTC 3524.

Lee, H. J., Edwards, B. D., and Field, M. E., 1981, Geotechnical analysis of a submarine slump, Eureka, California: Proceedings of the 13th annual Offshore Technology Conference, paper number OTC 4121.

Lee, H. J., and Schwab, W. C., 1982, Geotechnical investigations related to geologic hazards: northern Gulf of Alaska, in, Bruns, ed, Hydrocarbon resource report for proposed O.C.S. Lease Sale 88: southeastern Alaska, northern Gulf of Alaska, Cook Inlet, and Shelikof Strait, Alaska: U.S. Geological Survey Open-File Report 82-928, p. 87-94.

Lee, K. L., and Focht, J. A., 1976, Strength of clay subjected to cyclic loading: Marine Geotechnology, vol. 1, no. 3, p. 165-186.

Mayne, Paul, 1980, Cam-clay prediction of undrained strength: American Society of Civil Engineers, Journal of the Geotechnical Engineering Division, vol. 106, p. 1219-1242.

Minster, J. B., and Jordon, T. H., 1978, Present day plate motions: Journal of Geophysical Research, vol. 83, no. B11, p. 5331-5354.

Molnia, B. F., 1979, Sedimentation in coastal embayments, northeastern Gulf of Alaska: Proceedings of the 11th Annual Offshore Technology Conference, Houston, vol. 2, p. 665-676.

Molnia, B. F., and Carlson, P. R., 1975, Surface sediment distribution, northern Gulf of Alaska: U.S. Geological Survey Open-File Report 75-505, 1 sheet.

Molnia, B. F., and Carlson, P. R., 1978, Surface sedimentary units of northern Gulf of Alaska continental shelf: American Association of Petroleum Geologists Bulletin, vol. 62, no. 4, p. 633-643.

Molnia, B. F., and Carlson, P. R., 1980, Quaternary sedimentary facies on the continental shelf of the northeastern Gulf of Alaska, in Field, M. E., Bouma, A., and Colburn, I., ed., Quaternary depositional environment of the U.S. Pacific continental margin: Society of Economic Paleontologists and Mineralogists Symposium, Pacific Section, Bakersfield, p. 157-168.

Molnia, B. F., Carlson, P. R., and Bruns, T. R., 1977, Large submarine slide in Kayak Trough, Gulf of Alaska, in Coates, D. R., ed., Landslides: Reviews in Engineering Geology, vol. 3, Geological Society of America, p. 137-148.

Molnia, B. F., Levy, W. P., and Carlson, P. R., 1980, Map showing sedimentation rates in the northeastern Gulf of Alaska: U.S. Geological Survey Miscellaneous field studies Map, MF-1170 1 sheet.

Molnia, B. F., and Rappeport, M. L., 1980, Seafloor mosaic of the Alsek pockmark, slump, and sediment failure area, northeast Gulf of Alaska (Abs.): Geol. Soc. Amer., abstracts with programs, Atlanta, p. 436.

Molnia, B. F., and Sangrey, D. A., 1979, Glacially derived sediments in the Gulf of Alaska; geology and engineering characteristics: Proceedings of the 1979 Offshore Technology Conference, Houston, vol. 1, p. 647-655.

Morgenstern, N. M., 1967, Submarine slumping and the initiation of turbidity currents: in Marine Geotechnique, A. F. Richards (ed.), University of Illinois Press, p. 189-220.

Plafker, George, 1967, Geologic map of the Gulf of Alaska Tertiary province, Alaska: U.S. Geological Survey Miscellaneous Geologic Investigations Map I-484, scale 1:500,000.

Plafker, George, 1971, Pacific margin Tertiary basin, in Future petroleum provinces of North America: American Association of Petroleum Geologists Memoir 15, p. 120-125.

Reimnitz, Erk, 1966, Late Quaternary history and sedimentation of the Copper River delta and vicinity, Alaska: University of California, San Diego, Ph.D. thesis (unpub.), 160 p.

Seed, H. B., and Peacock, W. H., 1971, Procedures for measuring soil liquefaction characteristics: American Society of Civil Engineers, Journal of the Soil Mechanics and Foundation Engineering Division, vol. 97, no. SM8, p. 1099-1119.

Seed, H. B., and Rahman, M. S., 1978, Wave-induced pore pressure in relation to ocean floor stability of cohesionless soils: Marine Geotechnology, vol. 3, no. 2, p. 123-150.

Stephens, C. D., and Page, R. A., 1982, Seismic activity in the northern Gulf of Alaska since 1974, in, Bruns, T. R., Hydrocarbon resource report for proposed O.C.S. Lease Sale 88: Southeastern Alaska, Northern Gulf of Alaska, Cook Inlet, and Shelikof Strait, Alaska, p. 115-121.

Tirey, G. B., 1972, ~~recent~~ Trends in underwater soil sampling methods:  
American Society for Testing and Materials, Standard Technical Publication  
501, p. 42-54.

Varnes, D. J., 1978, Slope movement types and processes, in Schuster, R. L.,  
ed., Landslides, analysis and control: National Research Council,  
Transportation Research Board Special Report 176, p. 12-23.

Wissa, A.E.Z., Christian, J. T., Davis, E. H., and Heiberg, Sigurd, 1971,  
Consolidation at constant rate of strain, American Society of Civil  
Engineers, Journal of the Soil Mechanics and Foundation Division, vol. 97,  
no. SM10, p. 1393-1413.

Table 1. Core and in place test locations organized by study area

Study Area	Cruise	Core or In Place Test Number	Latitude		Longitude	
Copper River	S8-77-EG	4G	60°	15.18' N	145°	45.91' W
		6G	60°	12.94' N	145°	44.87' W
		7G	60°	12.93' N	145°	44.79' W
		8G	60°	10.64' N	145°	45.13' W
		9G	60°	10.64' N	145°	45.13' W
Kayak Trough	S8-77-EG	10G	60°	06.59' N	144°	39.06' W
		11G	60°	06.59' N	144°	39.06' W
		13G	60°	05.12' N	144°	40.44' W
		14G	60°	05.12' N	144°	40.44' W
		15G	60°	00.44' N	144°	34.55' W
		16G	60°	00.93' N	144°	40.16' W
		17G	60°	01.15' N	144°	40.7' W
		18G	59°	56.05' N	144°	39.14' W
		19G	59°	56.22' N	144°	39.24' W
		20G	59°	56.35' N	144°	39.34' W
		21G	59°	56.43' N	144°	38.27' W
Bering Trough	S8-77-EG	34G	59°	56.53' N	143°	32.36' W
		36G	59°	56.64' N	143°	35.75' W
		38G	59°	58.05' N	143°	38.00' W
Icy Bay-Malaspina	S8-77-EG	25G	59°	34.86' N	141°	58.20' W
		26G	59°	45.29' N	141°	57.17' W
		27G	59°	49.38' N	141°	55.61' W
		28G	59°	30.98' N	141°	20.73' W
		29G	59°	31.13' N	141°	20.90' W
		31G	59°	34.30' N	141°	21.04' W
		32G	59°	34.43' N	141°	20.96' W
		33G	59°	37.45' N	141°	20.18' W
		95G	59°	36.60' N	141°	23.40' W
		96G	59°	36.60' N	141°	23.30' W
		173G	59°	38.05' N	141°	22.75' W
		175G	59°	37.25' N	141°	23.35' W
		176G	59°	37.25' N	141°	23.15' W
		178G	59°	36.10' N	141°	23.50' W
		179G	59°	36.00' N	141°	23.40' W
		181G	59°	35.30' N	141°	24.60' W
		182G	59°	35.20' N	141°	24.50' W
		184G	59°	34.40' N	141°	25.30' W
		185G	59°	34.40' N	141°	25.30' W
		187G	59°	33.30' N	141°	25.80' W
		188G	59°	33.30' N	141°	25.80' W
		190G	59°	32.50' N	141°	26.30' W
		191G	59°	32.50' N	141°	26.30' W
		193G	59°	31.20' N	141°	26.6' W
		194G	59°	31.30' N	141°	26.20' W

**Table 1. Core and in place test locations organized by study area (continued)**

Study Area	Cruise	Core or In Place Test Number*	Latitude	Longitude
Icy Bay-Malaspina	DC2-80-EG	196G	59° 36.50' N	141° 19.10' W
		197G	59° 36.50' N	141° 19.10' W
		MP9	59° 36.6' N	141° 23.4' W
		MP10	59° 36.5' N	140° 19.1' W
		MV4	59° 36.6' N	141° 23.4' W
		MV5	59° 36.5' N	140° 19.1' W
		626G3	59° 35.00' N	140° 33.60' W
		627G1	59° 36.30' N	140° 45.20' W
		627G2	59° 36.35' N	140° 44.80' W
	DC1-81-EG	628G2	59° 37.60' N	140° 57.00' W
		628G3	59° 37.50' N	140° 56.90' W
		630A1	59° 41.90' N	141° 20.10' W
		630A2	59° 41.70' N	141° 20.20' W
		632G1	59° 35.50' N	141° 09.50' W
		632G2	59° 35.50' N	141° 09.50' W
		633G1	59° 32.40' N	141° 06.00' W
		633G2	59° 32.40' N	141° 06.00' W
		634G1	59° 30.20' N	141° 00.00' W
		634G2	59° 30.20' N	141° 00.00' W
		635A2	59° 39.81' N	141° 09.15' W
		709B	59° 34.30' N	141° 51.45' W
Icy Bay	DC1-77-EG	709C	59° 34.30' N	141° 51.45' W
		710B	59° 41.50' N	141° 40.50' W
		710C	59° 41.40' N	141° 40.40' W
		711B	59° 42.60' N	141° 39.85' W
		715B	59° 36.45' N	141° 47.45' W
		715C	59° 36.45' N	141° 47.45' W
		717B	59° 39.30' N	141° 42.20' W
		717C	59° 39.30' N	141° 42.20' W
		718B	59° 38.45' N	142° 07.30' W
		719B	59° 42.60' N	142° 01.85' W
		720B	59° 45.65' N	141° 57.85' W
		721C	59° 47.00' N	141° 52.85' W
		721D	59° 48.00' N	141° 52.85' W
Icy Bay	S8-77EG	39G	60° 04.16' N	141° 23.42' W
		40G	60° 03.56' N	141° 22.27' W
		41G	60° 01.71' N	141° 21.06' W
		42G	60° 01.05' N	141° 21.31' W
		43G	59° 56.99' N	141° 26.49' W
		44G	59° 59.03' N	141° 27.94' W
Yakutat Bay	S8-77-EG	45G	59° 52.15' N	139° 41.85' W
		46G	59° 52.21' N	139° 41.81' W
		47G	59° 43.93' N	139° 42.08' W
		48G	59° 38.22' N	139° 47.93' W
Yakutat	DC2-80-EG	61G	59° 28.45' N	139° 48.16' W
		64G	59° 28.23' N	139° 48.83' W

**Table 1. Core and in place test locations organized by study area (continued)**

Study Area	Cruise	Core or In Place Test Number	Latitude		Longitude	
Yakutat	DC2-80-EG	65G	59°	28.22' N	139°	48.97' W
		66G	59°	28.20' N	139°	48.88' W
		69G	59°	28.13' N	139°	49.38' W
		72G	59°	27.83' N	139°	49.59' W
		83G	59°	28.21' N	139°	48.00' W
		84G	59°	28.21' N	139°	48.40' W
		85G	59°	27.71' N	139°	50.06' W
		87G	59°	27.49' N	139°	50.58' W
		88G	59°	27.50' N	139°	50.64' W
		MP4	59°	28.21' N	139°	48.40' W
		MP5	59°	28.63' N	139°	48.14' W
		MV2	59°	28.21' N	139°	48.40' W
		MV3	59°	28.63' N	139°	48.15' W
	DC1-81-EG	616A2	59°	28.80' N	139°	48.10' W
		617G1	59°	22.70' N	139°	48.90' W
		617G2	59°	22.90' N	139°	48.80' W
		618G1	59°	23.19' N	139°	48.45' W
		618G2	59°	23.34' N	139°	48.44' W
		619G1	59°	24.45' N	139°	48.19' W
		620G1	59°	25.59' N	139°	48.09' W
		620G2	59°	26.03' N	139°	48.20' W
		621G1	59°	26.58' N	139°	47.31' W
		621G2	59°	27.04' N	139°	47.34' W
		623A1	59°	28.70' N	139°	49.70' W
		624A1	59°	28.70' N	139°	49.10' W
		624A2	59°	28.70' N	139°	48.70' W
		625A1	59°	28.70' N	139°	47.90' W
		625A2	59°	28.50' N	139°	48.20' W
Alsek River	DC2-80-EG	MC3-22	59°	06.99' N	138°	44.31' W
		23G	59°	06.99' N	138°	44.31' W
		26G	59°	07.09' N	138°	44.19' W
		28G	59°	06.99' N	138°	43.97' W
		29G	59°	06.93' N	138°	43.85' W
		31G	59°	06.89' N	138°	43.72' W
		32G	59°	06.99' N	138°	43.72' W
		35G	59°	06.99' N	138°	43.39' W
		36G	59°	06.94' N	138°	43.44' W
		38G	59°	06.94' N	138°	43.17' W
		43G	59°	06.94' N	138°	43.09' W
		46G	59°	06.91' N	138°	42.85' W
		47G	59°	06.94' N	138°	42.79' W
		49G	59°	06.92' N	138°	42.63' W
		50G	59°	06.92' N	138°	42.67' W
		52G	59°	06.93' N	138°	42.58' W
		55G	59°	06.93' N	138°	42.10' W
		56G	59°	06.88' N	138°	42.11' W
		MP3	59°	07.00' N	138°	44.29' W
		MP6	59°	07.74' N	138°	43.85' W

Table 1. Core and in place test locations organized by study area (continued)

Study Area	Cruise	Core or In Place * Test Number	Latitude	Longitude
Alsek River	DC2-80-EG	MP7	59° 07.74' N	138° 43.85' W
		MV1	59° 07.00' N	138° 44.31' W
	DC1-81-EG	601G2	59° 06.60' N	138° 42.20' W
		602G3	59° 06.18' N	138° 40.25' W
		603G1	59° 06.16' N	138° 39.25' W
		604G3	59° 06.02' N	138° 39.42' W
		604G4	59° 06.09' N	138° 39.57' W
		605G1	59° 05.47' N	138° 38.01' W
		605G2	59° 05.49' N	138° 38.09' W
		606G1	59° 05.50' N	138° 36.80' W
		606G2	59° 05.27' N	138° 37.13' W
		607A1	59° 07.60' N	138° 44.60' W
		607A2	59° 07.50' N	138° 44.60' W
		608A2	59° 06.90' N	138° 45.40' W
		609A1	59° 05.70' N	138° 39.60' W
		610A2	59° 05.50' N	138° 37.70' W
		611G1	59° 04.90' N	138° 38.60' W
		611G2	59° 05.10' N	138° 39.10' W
		G12G1	59° 05.60' N	138° 40.50' W
		G13G2	59° 06.20' N	138° 43.70' W
		G14G2	59° 07.00' N	138° 46.10' W
Other	S8-77-EG	1G	60° 02.21' N	147° 11.28' W
		2G	60° 02.21' N	147° 11.28' W
		23G	59° 50.75' N	144° 24.26' W
		92G	59° 00.15' N	139° 54.03' W
	DC2-80-EG	MP2	59° 18.81' N	139° 18.59' W
		MP8	59° 00.16' N	139° 54.01' W
	DC1-81-EG	615A1	58° 18.80' N	139° 19.20' W
	DC1-77-EG	700B	59° 42.15' N	142° 41.80' W
		704B	59° 55.10' N	142° 31.05' W

Core or test number code

G, B, C, or D - Gravity or piston core

A - Vibratory core

MP - In place cone penetration test

MV - In place vane shear test

Table 2. Consolidation Test Results

Cruise Core #	Depth in Core, z, cm	Test Number	Study Area	$\gamma'z$ , kPa <sup>a</sup>	$\sigma_{vm}'$ , kPa <sup>b</sup>	$\sigma'_e$ , kPa <sup>c</sup>	$\frac{\sigma_{vm}'}{\gamma'z}$	Initial Water Content, w		
								$c_s^d$	$c_s^e$	$c_s^f$
88-77-EG										
1G	80-90	OE1L1	Other	6.5	7	0.5	1.08	0.20	0.015	0.5-2
	230-235	OE2L1	Other	17.8	17	-0.8	0.96	0.15	0.020	0.5-3
4G	90-100	OE1G	Copper River	7	13	6	1.86	0.13	0.027	0.8-4
	190-200	OE2G	Copper River	13	12	-1	0.92	0.20	0.023	1.1-4-4
	310-320	OE3G	Copper River	23	14(?)	-9	0.61	0.25	0.038	2.0-4-1
	400-410	OE4G	Copper River	31	40	9	1.29	0.24	0.020	4.5-5.8
	605-610	OE5G	Copper River	49	29(?)	-20	0.73	0.23	0.032	4.0-5.0
6G	30-40	OE6G	Copper River	3	10	7	3.33	0.41	0.032	0.4-2.5
	100-107	OE7G	Copper River	6	8	2	1.33	0.48	0.053	0.6-2.4
7G	850-860	OE86	Copper River	66	39(?)	-27	0.59	0.36	0.045	2.0-3.3
8G	200-210	OE9G	Copper River	12	11	-1	0.92	0.49	0.061	0.5-1.4
	350-360	OE10G	Copper River	22	20	-2	0.91	0.41	0.041	2.0-3.1
	410-420	OE11G	Copper River	26	26	0	1.00	0.71?	0.105?	1.5-3.3
	660-670	OE12G	Copper River	45	68	23	1.51	0.42	0.062	2.5-3.1
	730-740	OE13G	Copper River	51	56	5	1.10	0.37	0.039	3.8-4.8
	800-810	OE14G	Copper River	58	58	0	1.00	0.30	0.033	3.5-4.8
	860-870	OE15G	Copper River	63	56	-7	0.89	0.33	0.033	3.9-4.9
9G	85-100	OE16G	Copper River	5	11	6	2.20	0.48	0.048	1.0-3.0
	290-300	OE17G	Copper River	20	18	-2	0.90	0.25?	0.034	2.1-4.1
10G	190-200	OE3L1	Kayak Trough	13.9	27	13.1	1.94	0.17	0.015	7-2
11G	115-125	OE4L1	Kayak Trough	-1.8	?	?	0.17	0.02	0.2-2	28.4
	240-250	OE5L1	Kayak Trough	19.8	15	-4.8	0.76	0.15	0.015	2.6-3.5
	390-400	OE6L1	Kayak Trough	31.9	60	28.1	1.88	0.20	0.02	1-3
	545-555	OE7L1	Kayak Trough	44.2	45	0.8	1.02	0.20	0.03	2.5-8
14G	100-110	OE8L1	Kayak Trough	6.3	10	3.7	1.59	0.23	0.02	0.4-1.5
16G	10-15	OE9L1	Kayak Trough	1.1	6	4.9	5.45	0.31	0.015	?
	102-107	OE10L1	Kayak Trough	9.2	12	2.8	1.30	0.13	0.02	1-2.5
	190-195	OE11L1	Kayak Trough	16.9	24	7.1	1.42	0.32	0.03	0.7-1.3
18G	30-40	OE12L1	Kayak Trough	2.2	?	?	?	0.30	0.02	0.2-0.5
	180-190	OE13L1	Kayak Trough	14	7	-7	0.50	0.21	0.03	?
	250-260	OE14L1	Kayak Trough	18.2	44	25.8	2.41	0.24	0.03	1-2.5
19G	65-75	OE15L1	Kayak Trough	4.6	8	3.4	1.74	0.24	0.015	7
	160-170	OE16L1	Kayak Trough	10.9	17	6.1	1.56	0.38	0.04	0.7-1.5
	260-270	OE17L1	Kayak Trough	17.5	15	-2.5	0.86	0.20	0.03	0.5-1.8
21G	280-300	OE18L1	Kayak Trough	13.8	14	0.2	1.01	0.30	0.04	0.5-2.0
	400-410	OE19L1	Kayak Trough	19.3	35	15.7	1.81	0.25	0.02	0.03-2.5
23G	100-110	OE20L1	Other	8.6	11	2.4	1.28	0.09	0.01	1-5
25G	80-90	OE18G	Icy Bay-Malaspina	6	9	3	1.50	0.21	0.026	1.0-3.1
	290-300	OE19G	Icy Bay-Malaspina	21	44	23	2.10	0.40	0.050	0.9-2.6
26G	100-110	OE20G	Icy Bay-Malaspina	9	12	3	1.33	0.17	0.02	2.5-3.3
	200-210	OE21G	Icy Bay-Malaspina	19	14	-5	0.74	0.18	0.029	2.1-4.0
27G	190-200	OE22G	Icy Bay-Malaspina	18	37	19	2.06	0.07	0.010	2.9-5.6
29G	105-115	OE23G	Icy Bay-Malaspina	9	14	5	1.56	0.23	0.021	2.1-4.5
	185-195	OE24G	Icy Bay-Malaspina	16	14	-2	0.88	0.25	0.027	2.0-4.1

Table 2. Consolidation Test Results (continued)

Cruise Core #	Depth in Core, z, cm	Test Number	Study Area	$\gamma'z, \text{kPa}^a$	$\sigma_{\text{vm}}', \text{kPa}^a$	$\sigma_{\text{e}'}, \text{kPa}^a$	$c_{\text{vm}}^{\text{f}}$	$c_{\text{e}}^{\text{f}}$	$c_s^{\text{g}}$ ( $\text{cm}^2/\text{sec}$ ) ( $\times 10^{-3}$ )	Initial Water Content, %
<b>86-77-EG</b>										
29G	290-300	0E25G	Icy Bay-Malaspina	26	20	-6	0.77	0.19	0.020	2.9-4.8
31G	90-100	0E26G	Icy Bay-Malaspina	9	15	6	1.67	0.16	0.019	4.6-6.1
180-190	0E27G	Icy Bay-Malaspina	17	12	-5	0.71	0.17	0.017	2.0-5.5	
273-283	0E28G	Icy Bay-Malaspina	21	26	5	1.24	0.18	0.028	2.1-4.2	
33G	22-30	0E29G	Icy Bay-Malaspina	2	13	11	6.50	0.24	0.025	1.0-5.7
90-100	0E30G	Icy Bay-Malaspina	9	33	24	3.67	0.13	0.019	2.8-6.1	
205-216	0E31G	Icy Bay-Malaspina	19	16	-3	0.84	0.13	0.018	2.7-5.0	
361-371	0E32G	Icy Bay-Malaspina	32	25	-7	0.78	0.21	0.025	2.3-4.9	
500-510	0E33G	Icy Bay-Malaspina	48	25	-23	0.52	0.22	0.029	2.9-4.8	
675-685	0E34G	Icy Bay-Malaspina	62	66	4	1.06	0.18	0.023	2.9-5.3	
790-800	0E35G	Icy Bay-Malaspina	73	35(?)	-38	0.48	0.16	0.024	3.8-5.1	
60-70	0E21L1	Bering Trough	7	6	-1	0.86	0.05	0.008	1-2.5	
34G	27-37	0E22L1	Bering Trough	3	6	3	2.00	0.20	0.020	0.9-1.6
38G	40G	0E36G	Icy Bay	22	12	-8	0.55	0.020	0.23	0.3-2.0
506-516	0E37G	Icy Bay	44	23	-21	0.52	0.43	0.081	1.8-3.2	
110-120	0E38G	Icy Bay	8	8	0	1.00	0.34	0.039	0.3-1.6	
270-280	0E39G	Icy Bay	20	13	-7	0.65	0.29	0.050	1.0-2.8	
47G	100-110	0E23L1	Yakutat Bay	7.7	11	3.3	1.43	0.18	0.020	?
	250-260	0E24L1	Yakutat Bay	18.8	10	-8.8	0.53	0.18	0.025	0.5-3.5
<b>DC2-80-EG</b>										
MC3-22	86-92	0E1L2	Alsek River	7.6	22	14.4	2.89	0.20	0.023	43.0
28G	37-39	CE11	Alsek River	3.8	80	76.2	20.9	0.09	0.014	26.7
35G	10-13	CE7	Alsek River	1.0	19(?)	18.0	19.3	---	---	34.7
40-44	CE8	Alsek River	3.2	47	43.8	14.6	0.22	0.02	---	46.4
68-74	0E2L2	Alsek River	6	22	16	3.67	0.20	0.021	6-17	31.6
43G	4-8	CE4	Alsek River	.5	11(?)	10.5	23.0	0.08	0.01	30.0
38-41	CE5	Alsek River	3.6	17(?)	13.4	4.7	0.09	0.01	---	31.9
46G	4-7	CE10	Alsek River	.5	42	41.5	79.6	0.12	---	35.8
41-44	CE9	Alsek River	3.8	51	47.2	13.5	0.15	0.02	---	36.1
64-77	0E3L2	Alsek River	5.6	30	24.4	5.4	0.16	0.037	2.6-14	41.4
55G	74-80	0E4L2	Alsek River	6.2	28	21.8	4.5	0.27	0.028	5.3-15.6
84G	14-21	0E5L2	Yakutat	1.6	12	11.4	7.5	0.18	0.035	1.5-8
76-84	0E6L2	Yakutat	5.6	20	14.4	3.6	0.22	0.030	---	44.0
200-210	0E7L2	Yakutat	14.4	50	35.6	3.5	0.10	0.016	5.7-23	23.8
87G	146-148	CE26	Yakutat	11.8	50	38.2	4.2	0.17	---	20-80
96G	86-96	0E8L2	Icy Bay-Malaspina	7.4	10	2.6	1.4	0.17	0.053	1.8-15.3
	263-271	0E9L2	Icy Bay-Malaspina	27.0	120	93.0	4.4	0.13	0.015	19-28
354-261	0E10L2	Icy Bay-Malaspina	30.8	31	0.2	1.0	0.17	0.022	1.5-7.9	32.7
374-381	0E11L2	Icy Bay-Malaspina	33.4	40	6.6	1.2	0.14	0.037	3.0-12.3	38.0
181G	33-35	CE3	Icy Bay-Malaspina	2.7	11	9.3	4.1	0.22	---	40.0
116-118	CE1	Icy Bay-Malaspina	9.4	22	12.6	2.3	0.21	---	41.3	
196-198	CE2	Icy Bay-Malaspina	15.8	13	-2.8	0.8	0.26	---	44.0	
190G	30-38	0E12L2	Icy Bay-Malaspina	3.2	70	65.8	21.9	0.16	0.017	19-26
	227-234	0E13L2	Icy Bay-Malaspina	18.8	45	26.2	2.4	0.21	0.028	2.1-9.3

Table 2. Consolidation Test Results (continued)

Cruise Core #	Depth in Core	Test Number	Study Area	$\gamma'z$ , kPa <sup>a</sup>	$\sigma'_v$ , kPa <sup>b</sup>	$\sigma'_e$ , kPa <sup>c</sup>	$\frac{\sigma'_v - \sigma'_e}{\gamma'z}$	$c_e^d$	$c_c^e$	$c_s^f$	$c_g^g$ ( $\text{cm}^2/\text{sec}$ ) ( $\times 10^{-3}$ )	Initial Water Content
DC2-80-EG 190G	281-289	OE14L2	Icy Bay-Malaspina	23.2	50	26.8	2.2	0.21	0.054	2.1-6.7	38.0	
	142-148	OE15L2	Icy Bay-Malaspina	14.2	23	8.8	1.6	0.10	0.031	10.5-34.8	28.6	
	248-255	OE16L2	Icy Bay-Malaspina	25.2	140	114.8	5.6	0.12	0.021	14.7-21.7	25.7	
	435-439	OE17L2	Icy Bay-Malaspina	45.8	120	74.2	2.6	0.11	0.027	8.6-17.8	21.9	
DC1-81-EG 604-G3	142	OE44	Alsek River	11.6	280(?)	268.4	24.1	0.13	0.009	10-30	32.2	
	70	OE46	Alsek River	5.0	70	65	14.0	0.25	0.017	2-11	52.8	
	154	CE25	Alsek River	11.0	50	39	4.5	0.25	---	6-22	46.9	
	198	OE45	Alsek River	16.4	42	25.6	2.6	0.17	0.012	2.5-9	40.2	
618G2	62-64	CB22	Yakutat	5	31	26	6.2	0.25	---	6-55	49.7	
	106-108	OE41	Yakutat	10	250(?)	240	25.0	0.16	0.007	9-12	31.3	
	110-115	CE17	Yakutat	11	14	3	1.3	0.14	0.014	3-40	30.0	
	166-168	CE29	Yakutat	13.4	32	18.6	2.4	0.25	---	5-22	44.8	
190-195	CE18	Yakutat	16.4	22	5.6	1.3	?	---	3-30	39.0		
	71-73	CE23	Yakutat	5.8	28	22	4.3	0.26	---	5-22	43.0	
	152-157	CE33	Yakutat	15.7	570	554	36.3	0.03	---	2000	27.6 sand	
	210-212	CE27	Yakutat	19.5	8.4 to 105	-11 to 85	.4 to 5.4	0.12	---	2-40	33.6	
627G2	26-28	CE16	Icy Bay-Malaspina	2	22	20	11.0	0.21	---	3.5-15	44.2	
	32-34	CB14	Icy Bay-Malaspina	2.6	82	80	31.6	0.21	---	10-25	41.1	
	116-118	CE13	Icy Bay-Malaspina	9.4	28	18.6	3.0	0.27	0.025	4-22	40.1	
	122-124	OE40	Icy Bay-Malaspina	9	15	6	1.7	0.24	0.017	0.9-10	48.1	
630A2	222-224	CE15	Icy Bay-Malaspina	18	28	10	1.6	0.20	---	2-10	38.7	
	210	CE32	Icy Bay-Malaspina	21	1050	1029	49.3	?	---	?	26.2 Sand	
	632G1	CE31	Icy Bay-Malaspina	7	90	83	12.9	0.16	---	5-30	33.9	
	634G2	CE24	Icy Bay-Malaspina	3	12	9	4.0	0.33	---	2-12	56.7	

a - Sediment submerged unit weight times embedment depth, equal to in situ overburden stress for normal- and over-consolidation

b - Maximum past stress obtained by Casagrande technique

c - Difference between  $\sigma'_v$  and  $\gamma'z$ ; negative values correspond to underconsolidation, near zero values to normal consolidation and positive values to overconsolidation

d - This parameter is the overconsolidation ratio for normally or overconsolidated sediment and the degree of consolidation for normally or underconsolidated sediment

e - Slope of the laboratory virgin compression curve

f - Slope of the laboratory rebound curve

g - Coefficient of consolidation for stresses greater than  $\sigma'_v$

Table 3. Static Triaxial Test Results

Cruise Core #	Depth in core, z, cm	Test Number	Study Area	$\gamma_{z,kPa}^a$	$\sigma'_{vm}, kPa^b$	$\sigma'_{vc}, kPa^c$	$\sigma'_{hc}, kPa^d$	Test Type	Induced f OCR	$q_u(Su), g$	$s_u/\sigma_{vc}$	$\phi', ^h$	Initial degrees Water Content, %
88-77-EG 1G	117-130	TE1L1	Other	9.5	9.1	10				16.5	1.65	47.4	
	140-150	TE4L1	Other	11.2	10.7	7				27.5	3.93	44.6	
	163-177	TE2L1	Other	13.1	12.6	20				17	0.85	44.7	
	190-202	TE3L1	Other	15.1	14.5	40				29.5	0.74	42.4	
	202-214	TE7L1	Other	16.0	15.4	50				34.3	0.69	34.3	
	214-225	TE6L1	Other	16.9	16.2	30				25.5	0.85	41.1	
	225-235	TE5L1	Other	17.7	17.0	20				29.7	1.49	38.4	
	210-220	TE1G	Copper River	17.1	14	15				16.5	1.10	42.0	
	220-230	TE2G	Copper River	17.9	14.5	29				21.0	0.72	45.7	
	230-240	TE3G	Copper River	18.7	15.0	59				35.5	0.60	36.0	
4G	240-250	TE4G	Copper River	19.5	15.5	10	5			15.0	1.50	41.6	
	630-640	TE5G	Copper River	50.4	29.5	34				39.5	1.16	39.2	
	640-650	TE6G	Copper River	51.2	30.0	69				53.5	0.78	36.9	
	650-660	TE7G	Copper River	52.0	30.5	139				63.0	0.46	34.5	
	660-670	TE8G	Copper River	52.8	30.5	25	12.5			55.0	2.20	36.0	
	670-680	TE9G	Copper River	53.6	31.0	75				40.5	0.54	40.5	
	680-690	TE10G	Copper River	54.4	31.5	200				93.0	0.47	36.5	
	690-700	TE11G	Copper River	55.2	32.0	125				76.0	0.61	34.8	
	780-790	TE12G	Copper River	60.8	35	40				22	0.55	47.7	
	790-800	TE13G	Copper River	61.5	36	80				39	0.49	46.6	
7G	800-810	TE14G	Copper River	62.3	36	30	15			27	0.90	46.6	
	810-820	TE15G	Copper River	63.1	37	160				73	0.46	34.8	
	820-830	TE16G	Copper River	16.2	11	15				9	0.60	61.3	
	230-240	TE17G	Copper River	16.9	12	30				16	0.53	67.8	
	240-250	TE18G	Copper River	17.6	13	10	5			9	0.90	66.0	
	250-260	TE19G	Copper River	18.3	14	23				23	1.00	63.3	
	260-270	TE20G	Copper River	45.3	49	50				23	0.47	58.4	
	650-660	TE21G	Copper River	46.6	51	90				46	0.51	50.3	
	670-680	TE22G	Copper River	47.3	52	140				51	0.36	53.7	
	790-800	TE23G	Copper River	54.9	62	160				80	0.50	45.4	
8G	810-820	TE24G	Copper River	56.3	64	40				36	0.90	45.7	
	820-830	TE25G	Copper River	57.0	64.5	80				54	0.68	44.3	
	830-840	TE26G	Copper River	57.7	65.5	30	15			41	1.37	---	
	260-270	TE27G	Copper River	18.4	17	30				11.5	0.38	63.3	
	270-280	TE28G	Copper River	19.1	17.5	15				30	0.70	48.7	
	270-280	TE29G	Copper River	19.1	17.5	60				24	0.40	32.4	
	280-290	TE30G	Copper River	19.8	18	10				11	1.10	59.5	
	120-137	TE8L1	Kayak Trough	9.2	17.8	10				6	0.60	46.4	
	137-150	TE9L1	Kayak Trough	10.3	20.0	20				9.5	0.48	45.0	
	150-162	TE10L1	Kayak Trough	11.1	21.5	30				11.5	0.38	49.2	
10G	162-174	TE11L1	Kayak Trough	12.0	23.3	7				14.7	2.10	41.6	
	270-284	TE12L1	Kayak Trough	22.4	27.3	35				21.3	0.61	38.3	
	300-314	TE13L1	Kayak Trough	24.8	30.3	60				50.1	0.84	36.3	
	354-368	TE14L1	Kayak Trough	29.2	35.6	90				38.2	0.42	35.8	
11G	555-568	TE15L1	Kayak Trough	45.4	55.4	120				50.8	0.25	40.3	

Table 3. Static Triaxial Test Results (continued)

Cruise Core #	Depth in core, z, cm	Test Number	Study Area	$\gamma'_{z,kPa}^a$	$\sigma'_{vm,kPa}^b$	$\sigma'_{vc,kPa}^c$	$\sigma'_{hc,kPa}^d$	$S_u/\sigma_{vc}^e$	$\phi_f(S_u)/\phi_kPa^f$	Initial Water Content,
58-77-EG 11G	582-592	TE18L1	Kayak Trough	47.4	57.8	21		0.66	42.1	
	642-655	TE16L1	Kayak Trough	52.4	63.9	60		0.32	35.7	
	662-675	TE15L1	Kayak Trough	54.0	65.9	30		0.56	34.0	
14G	41-54	TE19L1	Kayak Trough	2.9	4.6	10		0.90	70.1	
	54-68	TE20L1	Kayak Trough	3.7	5.9	20		0.24	60.3	
	84-98	TE21L1	Kayak Trough	5.5	8.7	40		0.50	55.5	
16G	120-132	TE22L1	Kayak Trough	11.1	15.2	13		1.00	29.8	
	132-144	TE24L1	Kayak Trough	12.2	16.6	54		0.37	35.1	
	144-156	TE25L1	Kayak Trough	12.9	17.9	7		20	2.86	
	167-180	TE23L1	Kayak Trough	15.3	20.8	20		30	1.50	
19G	80-94	TE26L1	Kayak Trough	5.8	8.0	10		11.5	2.00	
	94-108	TE27L1	Kayak Trough	6.7	9.3	20		4.3	2.13	
	108-122	TE28L1	Kayak Trough	7.6	10.5	40		17.0	2.23	
21G	140-160	TE29L1	Kayak Trough	10.2	14.4	20		11.7	0.59	
	195-210	TE30L1	Kayak Trough	13.7	19.3	35		26.3	0.75	
	210-225	TE31L1	Kayak Trough	14.8	20.9	60		1	0.43	
23G	42-56	TE33L1	Other	4.0	6.4	20		25.8	34.7	
	56-70	TE34L1	Other	5.1	7.5	40		1	2.10	
	70-84	TE35L1	Other	6.3	8.9	7		24	33.5	
	84-108	TE32L1	Other	7.8	11.0	10		1	37	
25G	240-250	TE31G	Icy Bay-Malaspina	18.0	35.5	15		11	1.61	
	260-270	TE32G	Icy Bay-Malaspina	19.5	39	60		1	37.5	
	270-280	TE33G	Icy Bay-Malaspina	20.2	41	10		5	40.5	
	280-290	TE34G	Icy Bay-Malaspina	20.9	43	30		5	34.3	
26G	90-100	TE35G	Icy Bay-Malaspina	8.5	11	10		5	40.5	
	160-170	TE36G	Icy Bay-Malaspina	14.8	13	20		1	34.3	
	170-180	TE37G	Icy Bay-Malaspina	15.7	13	40		5	40.5	
	180-190	TE38G	Icy Bay-Malaspina	16.6	13.5	10		5	34.3	
27G	50-60	TE39G	Icy Bay-Malaspina	4.9	29	10		5	40.5	
	60-70	TE40G	Icy Bay-Malaspina	5.8	30	30		5	34.3	
	80-90	TE41G	Icy Bay-Malaspina	7.6	31	20		5	34.3	
	90-100	TE42G	Icy Bay-Malaspina	8.5	31.5	10		5	34.3	
	140-150	TE43G	Icy Bay-Malaspina	13.0	34	25		5	34.3	
	150-160	TE44G	Icy Bay-Malaspina	13.9	35	15		5	34.3	
	180-190	TE45G	Icy Bay-Malaspina	16.5	36	40		5	34.3	
	135-145	TE46G	Icy Bay-Malaspina	12.1	14	15		5	34.3	
	145-155	TE47G	Icy Bay-Malaspina	13.0	14	25		5	34.3	
	155-165	TE48G	Icy Bay-Malaspina	13.9	14.5	40		5	34.3	
	250-260	TE49G	Icy Bay-Malaspina	22.1	18	15		5	34.3	
	330-340	TE50G	Icy Bay-Malaspina	29.0	21	10		5	34.3	
	340-350	TE51G	Icy Bay-Malaspina	29.9	21.5	60		5	34.3	
31G	350-360	TE52G	Icy Bay-Malaspina	30.8	22	30		5	34.3	
	150-160	TE53G	Icy Bay-Malaspina	14.4	15.5	10		5	34.3	
	160-170	TE54G	Icy Bay-Malaspina	15.4	16	10		5	34.3	
	170-180	TE55G	Icy Bay-Malaspina	16.3	17	20		5	34.3	

Table 3. Static Triaxial Test Results (continued)

Cruise Core #	Depth in core, z, cm	Test Number	Study Area	$\gamma'_{\text{z}}, \text{kPa}$	$\sigma'_{\text{vm}}, \text{kPa}$	$\sigma'_{\text{vc}}, \text{kPa}$	$\sigma'_{\text{hc}}, \text{kPa}$	Test Type	Induced OCR	$q_r(\text{Su}), \text{kPa}$	$s_u/\sigma_{\text{vc}}$	$\phi^{\text{i}}$ , degrees	Initial Water Content, %			
<u>88-77-EG</u>																
31G	190-200	TE56G	Icy Bay-Malaspina	18.2	18	40		a		32.5	0.81	34.				
33G	290-300	TE57G	Icy Bay-Malaspina	27.4	21	10	5	a		18.5	1.85	32.4				
321-331	321-331	TE58G	Icy Bay-Malaspina	30.2	22	10	5	a		13.5	1.35	37.2				
331-341	331-341	TE59G	Icy Bay-Malaspina	31.2	22	15	a	a		10	0.66	31.0				
341-351	341-351	TE60G	Icy Bay-Malaspina	32.1	22.5	30		a		25	0.83	36.0				
351-361	351-361	TE61G	Icy Bay-Malaspina	33.0	23	60		a		46.5	0.78	33.3				
470-480	470-480	TE62G	Icy Bay-Malaspina	44.0	26.5	45		a		30	0.67	37.5				
480-490	480-490	TE63G	Icy Bay-Malaspina	45.0	27	75		a		33	0.44	43.8				
490-500	490-500	TE64G	Icy Bay-Malaspina	45.9	27	98		c	1	41	0.42	30.5	40.0			
36G	46-60	TE37L1	Bering Trough	4.7	---	40		a		39	0.98	37.9				
60-75	60-75	TE36L1	Bering Trough	5.9	---	10		a		13.3	1.33	27.0				
38G	90-110	TE38L1	Bering Trough	9.5	19	10		a		24.5	2.45	25.9				
40G	340-350	TE65G	Icy Bay	23.7	14	40		a		19	0.48	49.3				
42G	350-360	TE66G	Icy Bay	24.4	14.5	80		c	1	26.5	0.33	25.8	51.8			
42G	231-245	TE67G	Icy Bay	17.9	12	20		a		18.5	0.93	41.6				
245-258	245-258	TE68G	Icy Bay	18.9	12	39		c	1	22.5	0.58	30.0	43.1			
258-270	258-270	TE69G	Icy Bay	19.9	12.5	10	5	a		13.5	1.35	42				
47G	133-147	TE41L1	Yakutat Bay	10.3	12.4	50		a		58.8	1.18	42.3				
189-202	189-202	TE39L1	Yakutat Bay	14.4	14.4	20		a		24.0	1.20	42.8				
239-250	239-250	TE40L1	Yakutat Bay	18.0	?	30		a		70.5	1.45	48.6				
<u>DC2-80-EG</u>										13	9.27	35.0				
<u>MC3-22</u>	3-13	TE1L2	Alsek River	0.5	22	1.4		a		58	17.06	25.0				
47-62	47-62	TE6L2	Alsek River	4.8	22	3.4		a		3	124.4	4.51	29.4			
62-76	62-76	TE4L2	Alsek River	6.1	22	27.6		b			159.4	0.48	39.6			
28G	6-14	TE64	Alsek River	0.8	80	328.5	136.8	c	1		227.1	3.99	36.2			
25-34	25-34	TE63	Alsek River	2.6	80	56.9		b	5.7			268.8	0.87	30.5		
26-35	26-35	TE62	Alsek River	2.6	80	310.7		c	1				27.2	9.08	28.7	
31G	4-11	TE65	Alsek River	0.7	60	3		a					215.0	0.96	38.2	
4-11	4-11	TE66	Alsek River	0.7	60	223.2		c	1				146.1	0.58	33.5	
11-19	11-19	TE67	Alsek River	1.4	60	251.2	126.1	c	1				80.8	0.52	36.3	
35G	14-23	TE56	Alsek River	1.6	40	154.8		c	1					80.8	0.52	40.4
18-27	18-27	TE34	Alsek River	1.5	40	24.7		b	6.2					58.4	2.36	40.4
25-32	25-32	TE58	Alsek River	2.3	40	137.6	68.5	c	1					60.3	0.44	34.8
38G	52-64	TE3L2	Alsek River	5.4	22	27.6		b	6					86.1	3.12	31.6
43G	8-17	TE27	Alsek River	1.1	14(?)	6.5		b	5					37.4	5.74	33.9
28-37	28-37	TE61	Alsek River	2.0	14(?)	31.3		a						79.9	2.55	32.5
18-27	18-27	TE35	Alsek River	2.0	14(?)	31.1		a						73.9	2.38	32.9
28-37	28-37	TE59	Alsek River	2.1	45	203.1		c	1					222.4	1.10	31.5
28-37	28-37	TE60	Alsek River	2.0	45	35.7		b	6.2					166.0	4.66	33.9
49G	18-28	TE5L2	Alsek River	2.24	30	169.2	61.93	c	1					89.5	0.53	40.5
46G	18-27	TE2L2	Alsek River	3.19	30	120.6		c	1					87.7	0.73	35.2
84G	21-33	TE11L2	Yakutat	2.45	15	103.4		c	1					64.4	0.62	33.9
63-76	63-76	TE8L2	Yakutat	6.06	20	3.4		b	6					27.8	8.17	35.7

Table 3. Static Triaxial Test Results (continued)

Core #	Depth in core, z, cm	Test Number	Study Area	$\gamma'z, \text{kPa}^a$	$\sigma'_{\text{vm}}, \text{kPa}^b$	$\sigma'_{\text{vc}}, \text{kPa}^c$	$\sigma'_{\text{hc}}, \text{kPa}^d$	Test Type	Induced OCR	$q_f(\text{Su}), \text{g}$	$S_u/\sigma_{\text{vc}}$ , h	$\phi^{i,1}$ , degrees	Initial Water Content, %
DC2-80-EG	100-112	TE71L2	Yukutat	9.26	20	20.7		c	1	14.6	0.70	33.2	
	160-172	TE10L2	Yukutat	15.78	3	1.4		a		34.9	24.93	24.6	
	176-190	TE9L2	Yukutat	17.97	35	17.2		a		78.2	4.54	21.0	
	150-158	TE84	Yukutat	13.04	50	203.1		c	1	122.8	0.61	35.7	38.6
	108-124	TE17L2	Icy Bay-Malaspina	11.17	95(?)	379.3	165.8	c	1	135.8	0.36	37.3	36.4
	155-170	TE12L2	Icy Bay-Malaspina	15.27	30	1.4		a		12.1	8.71	34.4	
	173-183	TE3L2	Icy Bay-Malaspina	16.74	30	35.1		a		30.1	0.85	38.8	
	198-212	TE16L2	Icy Bay-Malaspina	19.28	30	30.3		b	3	61.3	2.02	32.8	
	343-356	TE15L2	Icy Bay-Malaspina	34.51	35	34.8		b	4	70.4	2.02	33.3	
	361-374	TE14L2	Icy Bay-Malaspina	36.11	35	139.9		c	1	71.8	0.51	31.7	
181G	5-15	TE15	Icy Bay-Malaspina	0.84	15	277.7		c	1	131.5	0.47	35.9	
	5-15	TE16	Icy Bay-Malaspina	0.84	15	45.0		b	6.1	105.6	2.35	39.2	
	71-81	TE18	Icy Bay-Malaspina	6.16	15	39.9		c	1	23.7	0.59	39.8	42.2
	71-81	TE19	Icy Bay-Malaspina	6.16	15	5.3		b	7.3	19.0	3.57	41.9	
	100-110	TE20	Icy Bay-Malaspina	8.04	15	39.4	20.3	c	1	17.6	0.45	33.6	46.5
	100-110	TE21	Icy Bay-Malaspina	8.04	15	13.1		b	3	17.4	1.33	46.2	
	120-130	TE22	Icy Bay-Malaspina	11.00	15	0.5		a		8.7	18.49	36.9	
	120-130	TE23	Icy Bay-Malaspina	11.00	15	9.7		a		20.9	2.15	35.7	
	80-94	TE20L2	Icy Bay-Malaspina	7.86	50	48.2		b	6	97.8	2.03	31.9	
	101-114	TE8L2	Icy Bay-Malaspina	10.38	50	62.0		a		36.1	0.58	39.8	38.8
196G	114-125	TE19L2	Icy Bay-Malaspina	11.44	50	96.5		b	3	80.7	0.84	42.6	
	175-188	TE21L2	Icy Bay-Malaspina	17.70	50	230.6	96.4	c	1	82.6	0.36	39.0	41.0
	201-214	TE22L2	Icy Bay-Malaspina	19.74	50	1.4		a		11.0	7.86	39.4	
	214-227	TE23L2	Icy Bay-Malaspina	20.6	50	16.5		a		12.7	0.77	42.2	
	160-173	TE24L2	Icy Bay-Malaspina	17.0	100	165.2	82.8	a		99.3	0.60	32.0	
	234-246	TE28L2	Icy Bay-Malaspina	24.8	100	48.2		a		48.6	1.01	30.7	
	274-286	TE25L2	Icy Bay-Malaspina	29.0	100	172.3		b	3	251.8	1.46	25.9	
	286-298	TE26L2	Icy Bay-Malaspina	30.3	100	1.4		a		42.4	30.29	25.9	
	355-365	TE29L2	Icy Bay-Malaspina	37.6	100	55.1		b	6	184.3	3.34	26.0	
	367-377	TE30L2	Icy Bay-Malaspina	38.8	100	248.1		c	1	265.9	1.07	37.2	24.0
DC1-81-EG	381-400	TE27L2	Icy Bay-Malaspina	42.0	100	320.4		c	1	256.4	0.80	37.2	25.2
	120-127	TE114	Alsek River	11.0	280(?)	293.4		a	1	176.6	0.60	34.7	
	44-52	TE113	Alsek River	4.3	55	222.2		c	1	163.8	0.74	38.1	34.4
	141-149	TE116	Alsek River	11.1	55	0.3		a		8.4	28.07	46.8	
	156-164	TE111	Alsek River	13.6	55	216.1		c	1	127.9	0.59	37.0	38.4
	156-164	TE112	Alsek River	13.6	55	35.3		b	6.2	87.6	2.48	38.4	
	176-184	TE115	Alsek River	14.8	55	227.9	102.9	c	1	114.2	0.50	39.9	40.8
	186-194	TE117	Alsek River	15.4	55	71.3		b	3.1	91.0	1.28	42.0	
	127-132	TE87	Yukutat	10.2	35	184.7		c	1	95.6	0.52	34.2	44.2
	149-158	TE74	Yukutat	11.9	35	0.5		a		157.8	0.68	44.2	
620G2	149-158	TE75	Yukutat	11.9	35	12.1		a		15.6	1.29	46.4	
	90-99	TE82	Yukutat	7.1	28	120.8		c	1	53.2	0.44	32.5	48.3

Table 3. Static Triaxial Test Results (continued)

Cruise Core #	Depth in core, z, cm	Test Number	Study Area	$\gamma'z, \text{kPa}^a$	$\sigma'_{\text{vm}}, \text{kPa}^b$	$\sigma'_{\text{vc}}, \text{kPa}^c$	$\sigma'_{\text{hc}}, \text{kPa}^d$	Test Type	Induced OCR	$q_f(\text{Su}),^g$ kPa	$s_u/\sigma_{\text{vc}}^h$	$\phi'^i$ , degrees Water Content, °
DC1-81-EG												
62AA1	141-150	TE91	Yakutat	14.7	100 $\times$ 500	333.1		c?	1.21	38.0	29.0	
	141-150	TE93 <sup>k</sup>	Yakutat	14.7	100 $\times$ 500	341.5		c?	1.2	440.27?	34.3?	37.0
62SA1	170-180	TE118	Yakutat	18.0	?	293.3		c?	1.2	889.0	3.03	25.3
62TG2	71-78	TE72	Icy Bay-Malaspina	6.0	25	18.6	b	5.5	44.7	2.40	42.2	
	71-78	TE73	Icy Bay-Malaspina	6.0	25	31.0	b	3.1	45.9	1.48	46.4	
	82-90	TE70	Icy Bay-Malaspina	7.0	25	104.7	48.7	c	1	44.4	0.42	42.3
	82-90	TE71	Icy Bay-Malaspina	7.0	25	100.1		c	1	53.2	0.53	40.7
	104-112	TE68	Icy Bay-Malaspina	8.5	25	1.6	a	2.1	1.31		45.1	
	104-112	TE69	Icy Bay-Malaspina	8.5	25	10.4	a	10.4	0.99		43.4	
630A2	220-229	TE89	Icy Bay-Malaspina	23.1	1050	299.9		a		561.98	1.87	24.3
	220-229	TE90 <sup>k</sup>	Icy Bay-Malaspina	23.1	1050	295.5		a		631.95	42.5	25.9
632G1	80-89	TE92	Icy Bay-Malaspina	7.8	90	362.8		c	1	208.4	0.57	32.4
634G2	73-80	TE93	Icy Bay-Malaspina	5.3	12	57.9		c	1	23.9	0.41	33.7

a - Sediment submerged unit weight times sub-bottom depth, equal to in place overburden stress for normal - and over-consolidation

b - Sediment natural maximum past stress, interpolated or extrapolated from adjacent consolidation tests

c - final vertical consolidation stress

d - final horizontal consolidation stress, blank if same as vertical stress

e - Type (a) test has a final vertical consolidation stress less than three times the maximum past stress without rebound. Type (b) test has a maximum triaxial vertical consolidation stress greater than three times the natural maximum past stress. The sample was subsequently rebounded to a lower consolidation stress inducing a known overconsolidation ratio. Type (c) test has a final vertical consolidation stress greater than three times the maximum past stress without rebound.

f - Blank indicates a type (a) test; final level of overconsolidation is unknown. Value greater than 1 indicates a type (b) test: value given is known induced overconsolidation ratio. Value of 1 indicates a type (c) test: sample has been forced to be normally consolidated.

g - maximum shear stress over 15 or 20% strain: assumed equal to undrained shear strength,  $s_u$ .

h - Ratio of undrained shear strength to vertical consolidation stress

i - Effective friction angle assuming no cohesion intercept: given for type (c) or drained tests only

j - Stress control test

k - Drained test

Table 4. Cyclic Triaxial Test Results

Cruise Core #	Depth in Core, z, cm	Test Number	Study Area	$\sigma'_{vc}$ , kPa <sup>a</sup>	$\sigma'_h$ , kPa <sup>b</sup>	Induced OCR	( $q_f$ Static) <sub>I</sub> <sup>c</sup>	( $q_f$ Static) <sub>II</sub> <sup>c</sup>	Static Bias, kPa	Peak Cyclic Stress, kPa	$\tau_c^h$	$\tau_c^g$	$\tau_c^f$	# of Cycles to failure	Strain at failure, %	Water Content	
<b>88-77-EG</b>																	
4G	485	TC1B	Copper River	29.4	29.4	27.0	0.70	18.9	5	39.9							
	485	TC2B	Copper River	34.3	29.4	27.0	1.02	11.9	12	41.5							
	485	TC3B	Copper River	33.3	29.4	36.8	0.76	27.5	11	41.5							
	500	TC4B	Copper River	34.3	29.4	25.0	0.70	15.5	28.0	0.84	403	11					
	500	TC5B	Copper River	34.3	29.4	25.0	0.70	10.5	17.5	0.51	5000	6	42.3				
	500	TC6B	Copper River	33.3	29.4	25.0	0.94	10.8	23.5	0.69	45	12	43.3				
	510	TC7B	Copper River	34.3	29.4	31.9	0.73	13.7	23.3	0.70	4583	8.8	43.3				
	520	TC8B	Copper River	211.8	196.1	1	107.8	8.6	25.5	0.78	5000	7.4	44.3				
	520	TC9B	Copper River	212.7	196.1	1	107.8	3.2	10.7	0.63	0.32	30	-8.8				
	530	TC10B	Copper River	216.7	196.1	1	100.5	42.2	94.5	0.94	0.44	37	12	42.7			
	545	TC11B	Copper River	217.6	196.1	1	92.6	38.0	80.6	0.87	0.37	150	12	40.7			
	555	TC12B	Copper River	217.6	196.1	1	108.8	38.1	74.0	0.68	0.34	935	12	39.3			
	575	TC13B	Copper River	217.6	196.1	1	93.1	37.2	70.8	0.76	0.33	5000	10	40.8			
8G	495	TC14B	Copper River	216.7	196.1	1	100.0	19.0	63.0	0.63	0.29	87	12	41.4			
	530	TC15B	Copper River	215.7	196.1	1	96.1	16.3	53.8	0.56	0.25	500	12	40.8			
	11G	420	Kayak Trough	32.4	29.4	18.1	0.7	11.2	0.62	0.35	71	12	46.7				
	450	TC17B	Kayak Trough	32.4	29.4	24.0	2.4	9.1	0.38	0.28	3994	12	39.6				
	450	TC18B	Kayak Trough	32.4	29.4	24.0	2.4	10.3	0.43	0.32	2679	12	40.6				
	470	TC19B	Kayak Trough	32.4	29.4	19.6	2.0	11.8	0.60	0.36	243	12	42.7				
	470	TC20B	Kayak Trough	32.4	29.4	19.6	2.0	12.5	0.64	0.39	152	12	43.6				
	485	TC21B	Kayak Trough	32.4	29.4	20.6	1.6	14.4	0.70	0.44	74	12	45.0				
	485	TC22B	Kayak Trough	32.4	29.4	20.6	1.6	16.5	0.80	0.51	13	12	44.8				
	515	TC23B	Kayak Trough	32.4	29.4	24.0	8.4	19.7	0.82	0.61	200	12	39.8				
	515	TC24B	Kayak Trough	32.4	29.4	24.0	8.1	20.4	0.85	0.63	15	12	41.9				
	28G	20	TC25B	Icy Bay-Malaspina	32.4	29.4	27.9	0.5	10.3	0.37	0.32	391	12	35.4			
	40	TC26B	Icy Bay-Malaspina	32.4	29.4	20.6	1.4	12.2	0.59	0.38	35	12	40.7				
33G	550	TC27B	Icy Bay-Malaspina	32.4	29.4	26.5	9.0	16.7	0.63	0.51	5000	5.1	33.9				
	550	TC28B	Icy Bay-Malaspina	32.4	29.4	26.5	8.2	20.7	0.78	0.64	175	12	35.6				
	560	TC29B	Icy Bay-Malaspina	33.3	29.4	56.4	18.6	28.2	0.50	0.85	5000	4.3	26.6				
	560	TC30B	Icy Bay-Malaspina	23.3	29.4	56.4	18.6	33.8	0.60	1.02	537	11	26.1				
	585	TC31B	Icy Bay-Malaspina	217.6	196.1	1	98.0	16.7	61.7	0.63	0.28	21	12	33.6			
	600	TC32B	Icy Bay-Malaspina	215.7	196.1	1	103.9	12.5	63.4	0.61	0.29	2	-12	34.3			
	610	TC33B	Icy Bay-Malaspina	217.6	196.1	1	87.7	29.8	78.1	0.89	0.36	55	12	39.6			
	620	TC34B	Icy Bay-Malaspina	217.6	196.1	1	100.5	19.1	68.3	0.68	0.31	29	12	34.8			
	630	TC35B	Icy Bay-Malaspina	216.7	196.1	1	104.4	18.8	60.6	0.58	0.28	500	12	32.6			
<b>DC2-80-EG</b>																	
MC3-22	35-47	TC1L2	Alsek River	27.6	6	84.6	-23.7	0.28		35	-15	28.1					
28G	15-22	TC24	Alsek River	302.6	1	268.9	115.6	0.43		4	-20	31.8					
	15-22	TC25	Alsek River	297.9	1	268.9	21	0.08		0.07	-20	31.8					
	35G	32-39	TC18	Alsek River	160.3	1	80.8	54.9	0.68		7	20	41.2				
	32-39	TC19	Alsek River	154.6	1	80.8	75.8	0.64		0.33	20	20	44.8				
	38G	1-15	TC212	Alsek River	27.6	6	86.4	-38.0	0.44		3	-15	40.7				
	27-38	TC312	Alsek River	120.6	1	88.9	-24.9	0.28		0.21	8	-15	40.9				

Table 4. Cyclic Triaxial Test Results (continued)

Cruise Core #	Depth in Core, z, cm	Test Number	Study Area	$\sigma'_{vc}$ , kPa <sup>a</sup>	$\sigma'_{hc}$ , kPa <sup>b</sup>	Induced <sup>c</sup> ( $q_f$ Static) <sup>d</sup> I (q <sub>f</sub> Static) <sup>e</sup> II Bias, OCR	Peak <sup>f</sup> $\tau_c$ Cyclic Stress, $\tau_c$ , kPa	$\tau_c$ to failure, kPa	# of <sup>k</sup> Strain at Initial Cycles failure, <sup>l</sup> Water Content, %
<b>DC2-80-EG</b>									
38G	40-52	TC4L2	Alsek River	120.6	1	87.4	74.8	-33.2	0.38
43G	27-35	TC20	Alsek River	28.3	1	73.9	43.2	0.59	0.28
	27-55	TC21	Alsek River	27.2	1	73.9	43.2	0.62	0.28
46G	7-15	TC22	Alsek River	196.2	1	222.4	141.3	-42.4	0.30
	7-15	TC23	Alsek River	192.6	1	222.4	138.7	79	0.36
49G	6-17	TC5L2	Alsek River	120.6	1	87.1	71.2	-65.3	0.57
84G	33-48	TC6L2	Yakutat	103.3	1	64.6	108.5	-23.9	0.92
	48-63	TC7L2	Yakutat	103.3	1	64.1	72.3	-31.4	0.22
87G	161-172	TC52	Yakutat	200.9	1	122.8	148.7	-106.3	0.49
87G	161-169	TC53	Yakutat	194.3	1	122.8	147.7	-45.5	0.30
96G	145-155	TC11L2	Icy Bay-Malaspina	34.5	4	70	70	-39.2	0.37
	226-337	TCBL2	Icy Bay-Malaspina	137.8	1	71	107.5	-34.1	0.31
	286-300	TC10L2	Icy Bay-Malaspina	35.1	4	70	70	-16.1	0.30
181G	331-343	TC9L2	Icy Bay-Malaspina	137.8	1	78.7	96.5	-59.8	0.32
61-68	TC30	Icy Bay-Malaspina	30.3	1	23.7	14.5	-25	1.06	0.25
61-68	TC31	Icy Bay-Malaspina	24.2	1	23.7	11.4	-24	1.00	0.23
85-95	TC32	Icy Bay-Malaspina	10.4	3.5	19.0	19.0	-15	0.79	0.23
85-95	TC33	Icy Bay-Malaspina	2.5	14.4	19.0	19.0	-15.9	0.84	0.23
190G	66-80	TC12L2	Icy Bay-Malaspina	151.6	1	88.4	86.4	-61.9	0.62
	80-97	TC13L2	Icy Bay-Malaspina	151.6	1	87.8	87.9	-40.4	0.83
196G	160-175	TC14L2n	Icy Bay-Malaspina	232	96.5	1	89.4	89.6	0.46
	197-213	TC15L2n	Icy Bay-Malaspina	166.5	83.3	1	99.3	41.6	0.46
312-326	TC16L2	Icy Bay-Malaspina	53.4	6	182.1	187.7	-51.0	0.72	0.27
326-340	TC17L2	Icy Bay-Malaspina	53.4	6	187.7	256	-41.3	1.00	0.27
400-414	TC18L2	Icy Bay-Malaspina	320.2	1	257.0	256	-187.6	0.73	0.59
414-428	TC19L2	Icy Bay-Malaspina	320.2	1	255.5	256	-92	0.36	0.29
<b>DC1-8-EG</b>									
604G3	130-137	TC99	Alsek River	297.1	1	176.6	175.3	61.5	0.35
	130-137	D102	Alsek River	290.4	1	176.6	174.2	86.5	0.21
605G2	55-62	TC92	Alsek River	215.9	1	163.8	127.4	-55.7	0.50
	55-62	TC93	Alsek River	204.8	1	163.8	120.8	-84.1	0.34
	166-173	TC87	Alsek River	215.1	1	127.9	133.4	-41.8	0.33
618G2	166-173	TC86	Alsek River	216.3	1	127.9	125.5	-66.5	0.52
	138-145	TC58	Yakutat	184.8	1	95.6	92.4	56.2	0.61
	138-145	TC59	Yakutat	183.9	1	95.6	86.4	44.6	0.47
620G2	100-148	TC46	Yakutat	121.8	1	53.2	67.0	31.0	0.52
	100-108	TC47	Yakutat	117.6	1	53.2	65.9	46.1	0.46
624A1	172-179	TC60	Yakutat	338.9	1	401.3	186.4	206.6	0.87
	172-179	TC61	Yakutat	344.7	1	401.3	186.1	-134.6	0.51
627G2	60-71	TC36	Icy Bay-Malaspina	18.3	5.4	44.7	44.7	21.5	0.48
	60-67	TC37	Icy Bay-Malaspina	17.3	5.7	44.7	34.7	0.78	0.25
93-104	TC34	Icy Bay-Malaspina	100.7	1	53.2	47.3	-39.4	0.74	0.39
93-100	TC35	Icy Bay-Malaspina	99.5	1	53.2	48.8	-26.4	0.50	0.26

Table 4. Cyclic Triaxial Test Results (continued)

Cruise Core #	Depth in Core, z, cm	Test Number	Study Area	$\sigma_{vc}^a$ , kPa	$\sigma_{hc}^b$ , kPa	Induced <sup>c</sup> OCR	( $q_f$ , Static) <sup>d</sup> I	( $q_f$ , Static) <sup>e</sup> II Bias, kPa	Static <sup>f</sup> Cyclic <sup>h</sup> Stress, $\tau_c$ , kPa	Peak <sup>g</sup> Cyclic <sup>h</sup> $\tau_c$ , kPa	$\frac{\tau_i}{\tau_c}$	$\frac{\tau_j}{\tau_c}$	# of <sup>k</sup> Cycles failure, <sup>l</sup> to failure	Strain at <sup>l</sup> Failure <sup>m</sup>
DC1-81-EG 630A2	153-161	TC57	Icy Bay-Malaspina	297.9	1	562	259.2	162.9	0.29	0.63	0.55	>27	-20	29.3
	153-161	TC56	Icy Bay-Malaspina	301.0	1	562	295.0	120.2	0.21	0.41	0.40	>37	-20	27.4
634G2	61-69	TC48	Icy Bay-Malaspina	60.3	1	23.9	25.3	-40.6	1.70	1.60	0.67	2	-20	56.4
	61-68	TC49	Icy Bay-Malaspina	58.1	1	23.9	24.4	-31.8	1.33	1.30	0.55	6	-20	59.0
	72-79	TC54	Icy Bay-Malaspina	61.9	1	23.9	27.9	17.6	0.74	0.63	0.28	158	20	48.9
	73-80	TC55	Icy Bay-Malaspina	59.3	1	23.9	26.7	22.2	0.93	0.83	0.37	37	20	50.3

<sup>a</sup> - Final vertical consolidation stress<sup>b</sup> - Final horizontal consolidation stress, blank if same as vertical stress<sup>c</sup> - Induced OCR defined in Table 3.<sup>d</sup> - Static shear strength obtained from test on sample from the same core (Method I)<sup>e</sup> - Static shear strength obtained from water content, consolidation stress and Figure 35 (Method II)

41

<sup>f</sup> - A static shear stress applied under undrained conditions prior to cyclic testing. The cyclic shear stress is symmetrical about this bias level.<sup>g</sup> - The maximum shear stress level applied during cyclic loading (may include some static bias in addition to cyclic component - negative sign indicates tension)<sup>h</sup> - Ratio of maximum cyclic shear stress to static shearing strength estimated using Method I.<sup>i</sup> - Ratio of maximum cyclic shear stress to static shearing strength estimated using Method II<sup>j</sup> - Ratio of maximum cyclic shear stress to vertical consolidation stress (termed method III)<sup>k</sup> - Number of cycles required to reach strain given in next column<sup>l</sup> - Strain level defined as failure or strain level at which test was halted (if less than 10%)<sup>m</sup> - Reconsolidated sample<sup>n</sup> - Cyclic loading in compression only

Table 5. Calculation of NSP exponent,  $\Lambda_o$ 

Cruise Core #	Depth in Core, z, cm	Test Number	Study Area	Induced <sup>a</sup> OCR	$(S_{nc})_I^b$	$(S_{nc})_{II}^C$	$q_f/\sigma_{vc}^d$	$(\Lambda_o)_I^e$	$(\Lambda_o)_{II}^f$	Initial Water content, <sup>g</sup>
<b>DC2-80-BG</b>										
HC3-22	62-76	TE4L2	Alsek River	3	----	0.86	4.51	----	1.51	29.4
28	25-34	TE63	Alsek River	5.7	0.87	0.62	3.99	0.88	1.07	36.2
35	14-23	TE57	Alsek River	6.2	0.52	0.53	2.36	0.83	0.82	40.4
38	18-28	TE3L2	Alsek River	6	----	0.76	3.12	----	0.79	31.6
43	8-17	TE27	Alsek River	5	----	0.67	5.74	----	1.33	33.9
46	28-37	TE60	Alsek River	6.2	1.10	0.67	4.66	0.82	1.06	33.9
84	63-76	TE8L2	Yakutat	6	0.70	0.63	8.17	1.37	1.43	35.7
96	198-212	TE16L2	Icy Bay-Malaspina	3	0.51	0.72	2.02	1.25	0.74	32.8
	343-356	TE15L2	Icy Bay-Malaspina	4	0.51	0.70	2.02	0.99	0.76	33.3
181	5-15	TE16	Icy Bay-Malaspina	6.1	0.47	0.55	2.35	0.89	0.80	39.2
	71-81	TE19	Icy Bay-Malaspina	7.3	0.47	0.52	3.57	1.02	0.97	41.9
	100-110	TE21	Icy Bay-Malaspina	3	0.47	0.48	1.33	0.95	0.93	46.2
190	80-94	TE20L2	Icy Bay-Malaspina	6	0.58	0.75	2.03	0.70	0.91	31.9
	114-125	TE19L2	Icy Bay-Malaspina	3	0.58	0.50	0.84	0.34	0.47	42.6
196	274-286	TE25L2	Icy Bay-Malaspina	3	0.93	1.06	1.46	0.41	0.29	25.9
	355-365	TE29L2	Icy Bay-Malaspina	6	0.93	1.06	3.34	0.71	0.64	26.0
<b>DC1-81-BG</b>										
605G2	186-194	TE112	Alsek River	3.1	0.59	0.51	1.28	0.68	0.81	42.0
	156-164	TE117	Alsek River	6.2	0.59	0.57	2.48	0.79	0.81	38.4
627G2	71-78	TE72	Icy Bay-Malaspina	5.5	0.53	0.51	2.40	0.89	0.91	42.6
	71-78	TE73	Icy Bay-Malaspina	3.1	0.53	0.47	1.48	0.91	1.01	46.4

<sup>a</sup> - Induced OCR defined in Table 3<sup>b</sup> - Ratio of undrained shear strength,  $S_u'$ , to vertical consolidation stress,  $\sigma_{vc}'$ , for normal consolidation obtained from test on sample from the same core (Method I)<sup>c</sup> - Ratio of undrained shear strength,  $S_u'$ , to vertical consolidation stress,  $\sigma_{vc}'$ , for normal consolidation obtained from initial water content and Figure 35 (Method II)<sup>d</sup> - Ratio of measured undrained shear strength to vertical consolidation stress<sup>e</sup> - The NSP exponent,  $\Lambda_o'$ , calculated using  $S_{nc}$  from Method I.<sup>f</sup> - The NSP exponent,  $\Lambda_o'$ , calculated using  $S_{nc}$  from Method II

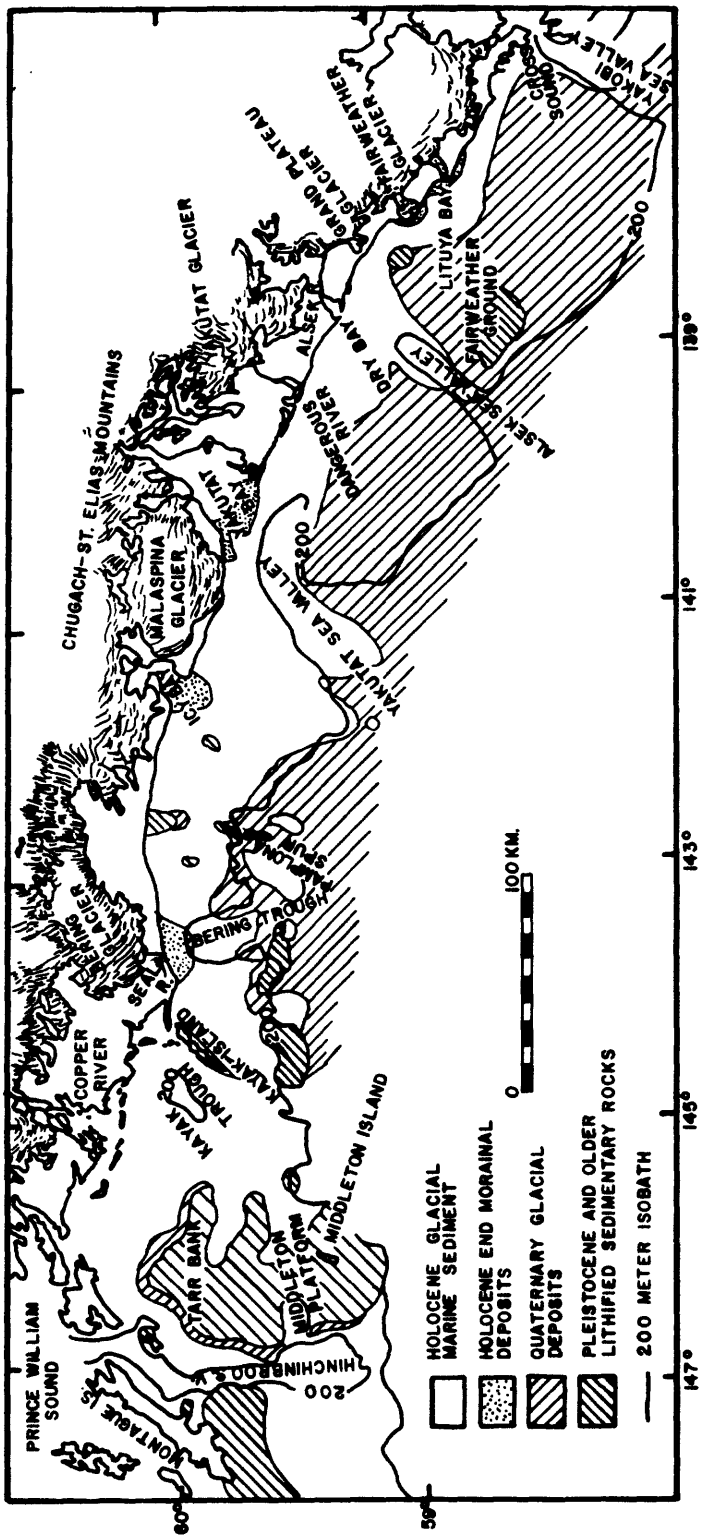


Figure 1. Distribution of four continental shelf surface sedimentary units between Cross Sound and Prince William Sound (Molnia and Carlson, 1980)

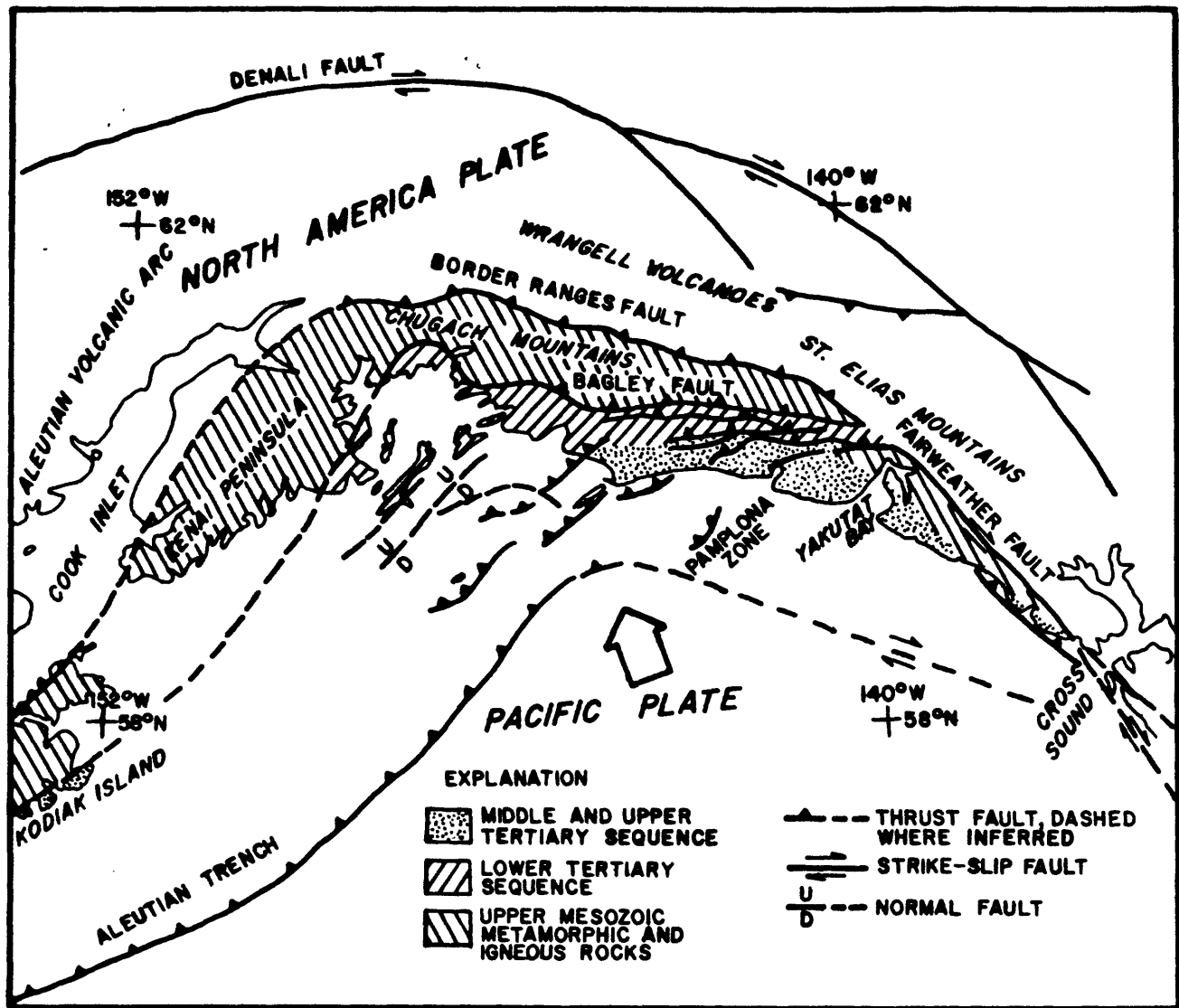


Figure 2. Simplified geologic setting of the northern Gulf of Alaska, showing general trends of Mesozoic and Cenozoic rocks (modified from Bruns, 1979). Onshore geology is from Plafker (1967), and Beikman (1974, 1975). Relative convergence vector between Pacific and North American plates (large arrow) is from Minster and Jordon (1978)

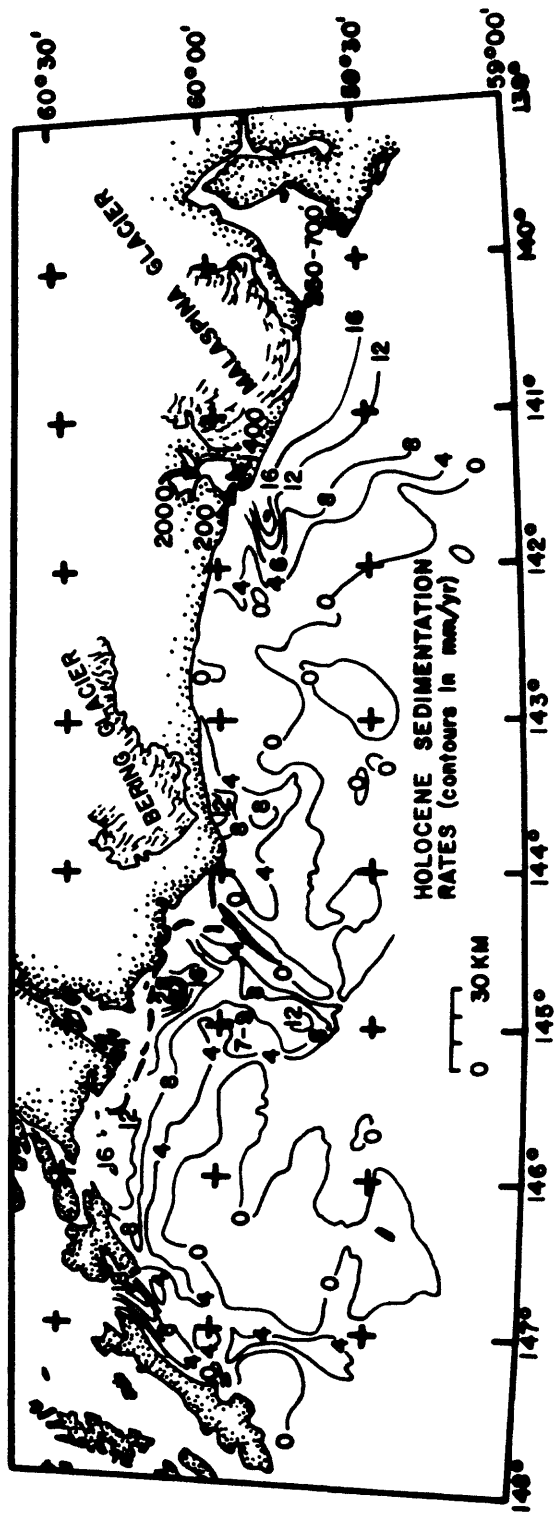


Figure 3. Holocene sedimentation rates (mm/yr) in the northeast Gulf of Alaska (Molnia and Carlson, 1980)

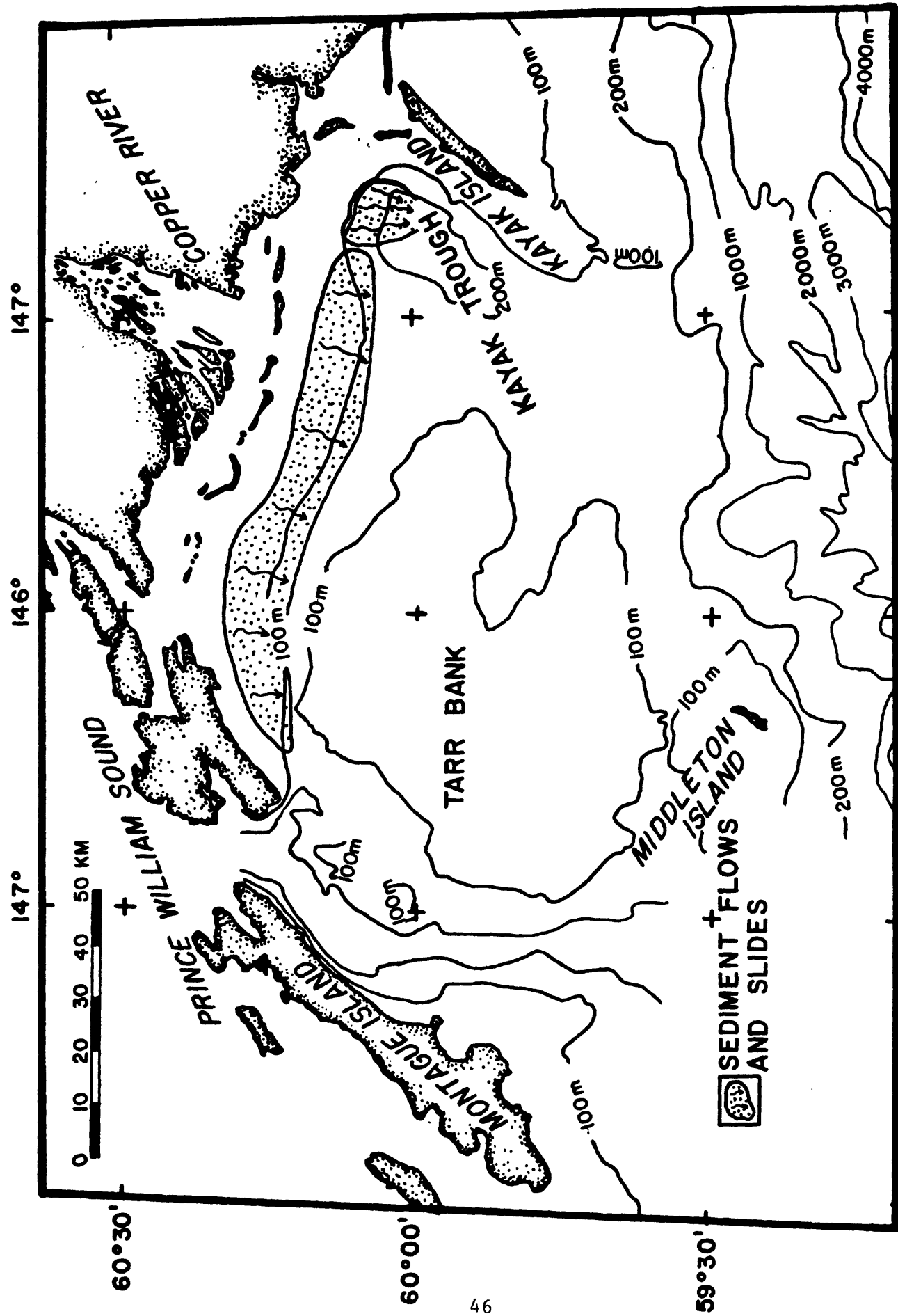


Figure 4. Location map of seafloor flows and slumps west of Kayak Island (Carlson and Schwab, 1982)

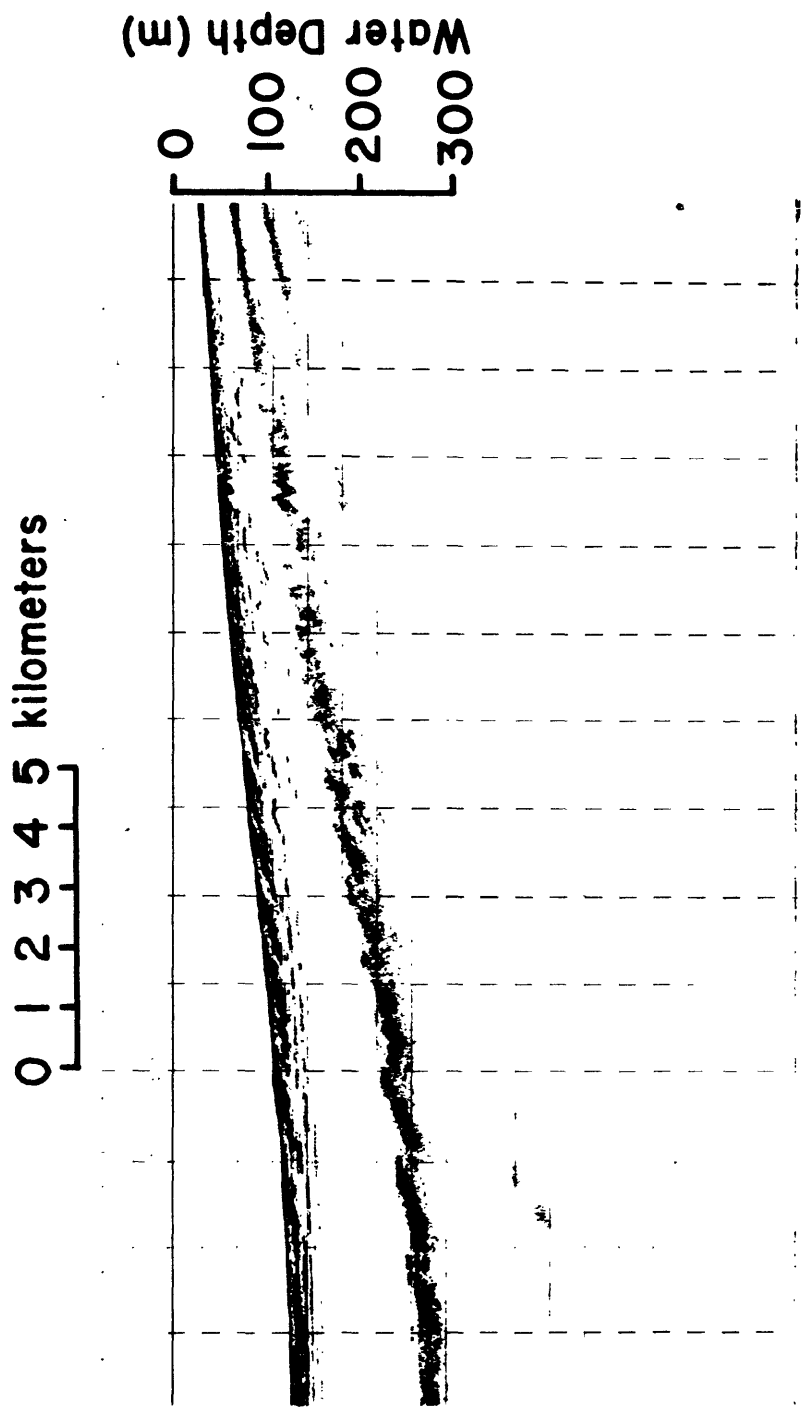


Figure 5. High resolution seismic reflection record of the sediment slide off the Copper River.

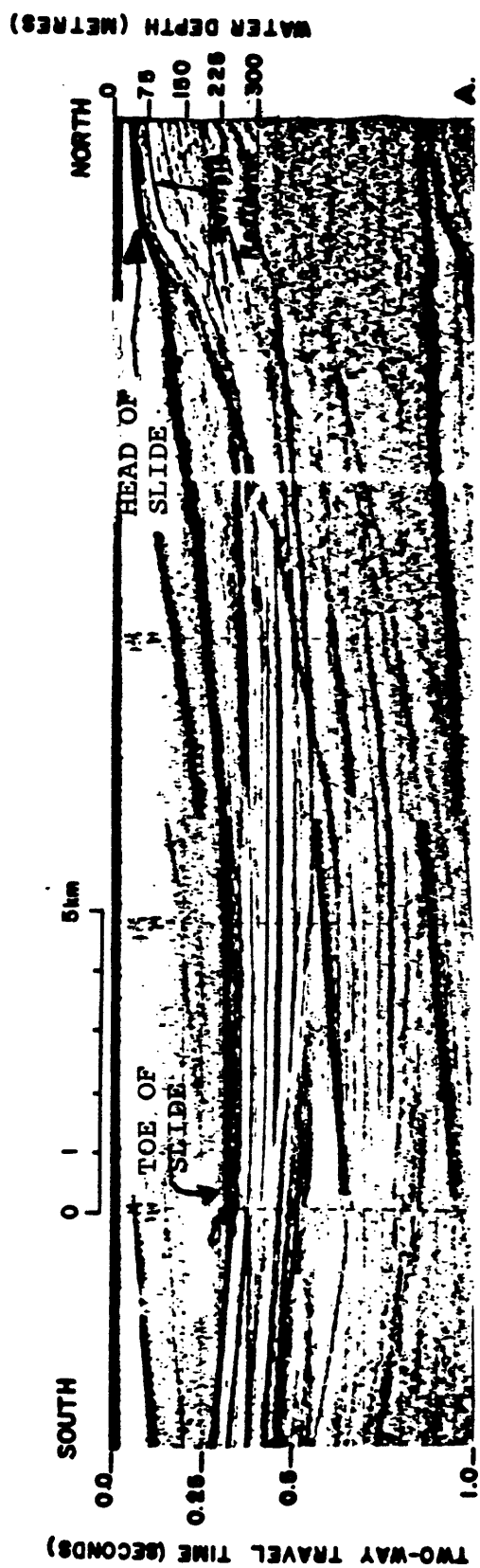


Figure 6. High resolution seismic reflection record of the submarine slide located in Kayak Trough (Hampton and others, 1978).

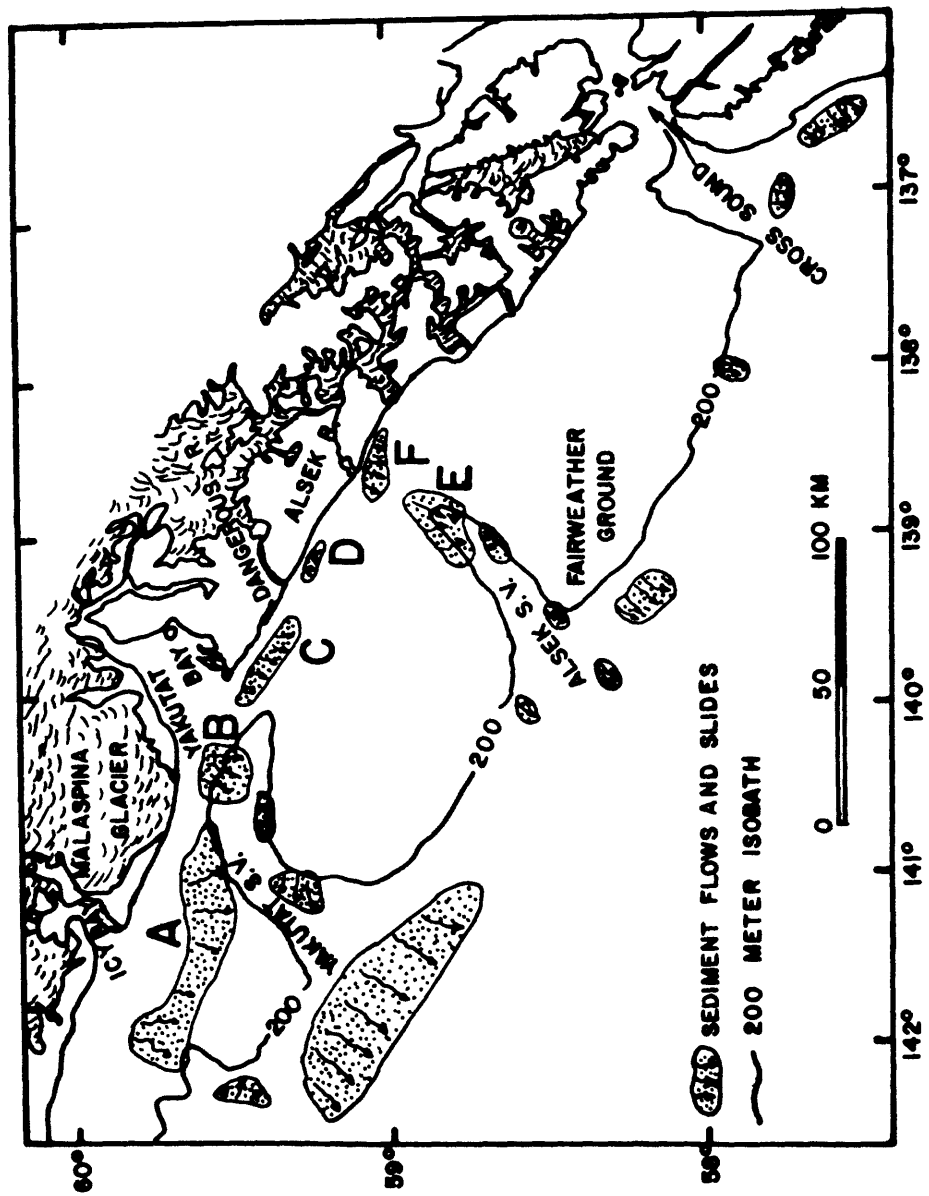


Figure 7. Location map of seafloor geologic hazards east of Icy Bay, Gulf of Alaska (modified from Carlson and others, 1980).

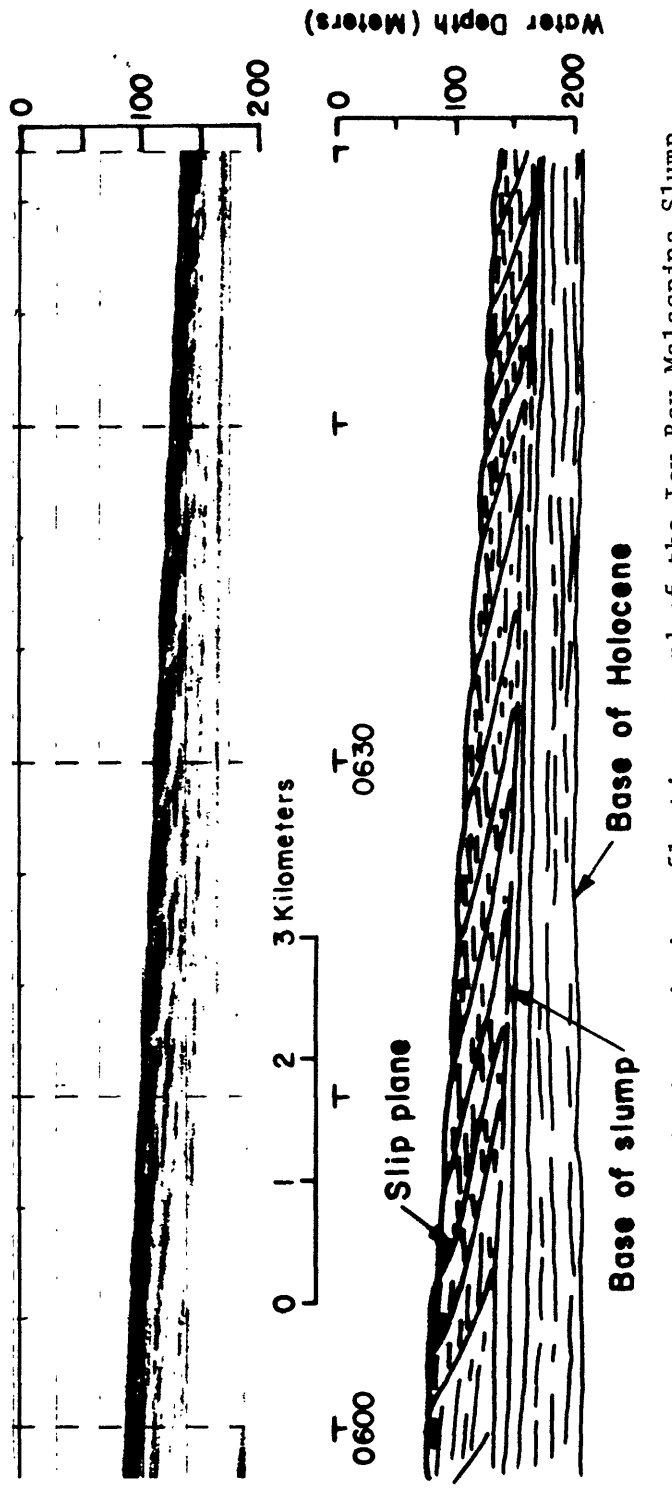


Figure 8. High resolution seismic reflection record of the Icy Bay-Malaspina Slump (Carlson, 1978).

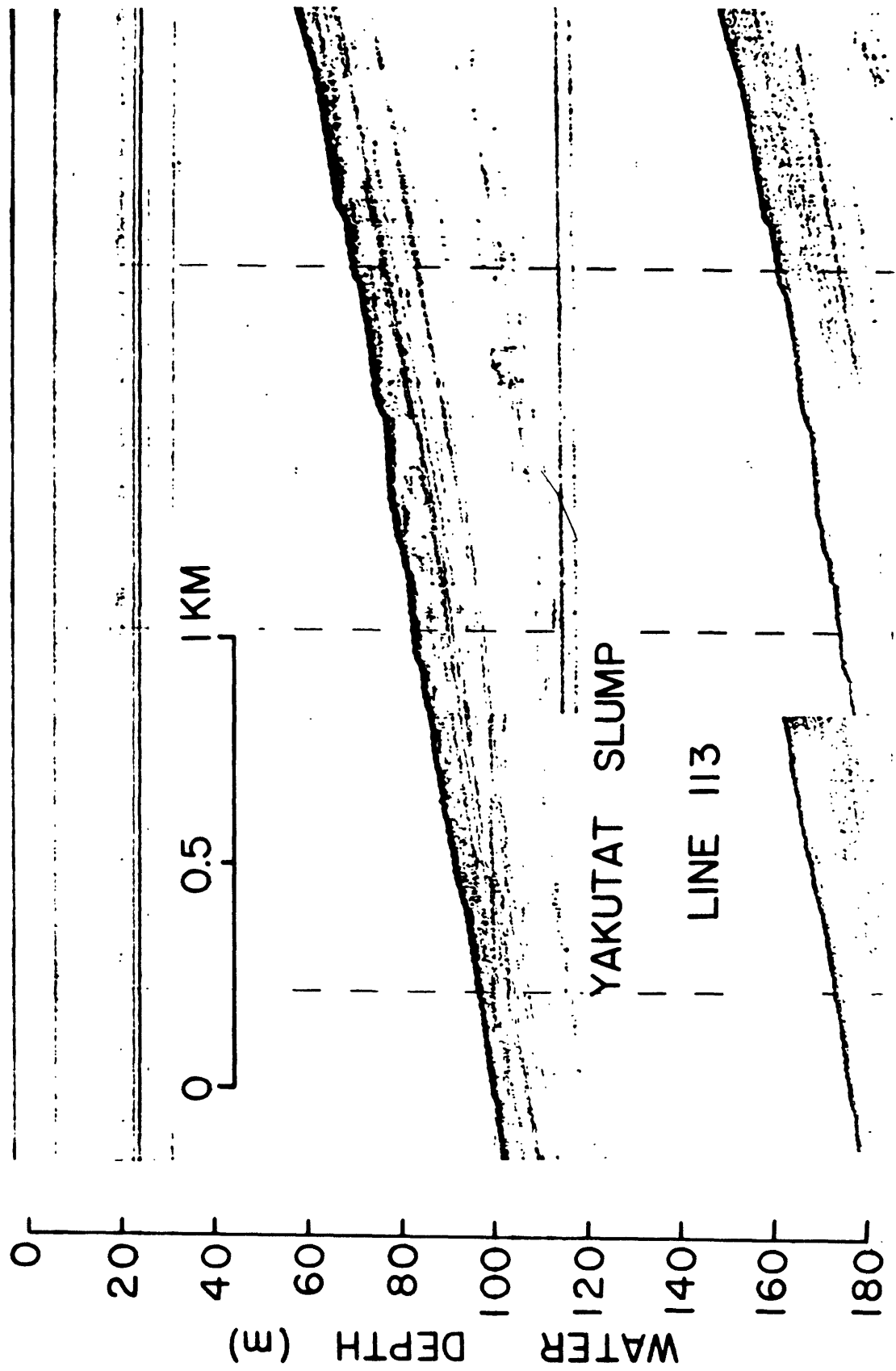


Figure 9. High resolution seismic reflection record of the Yakutat Slump.

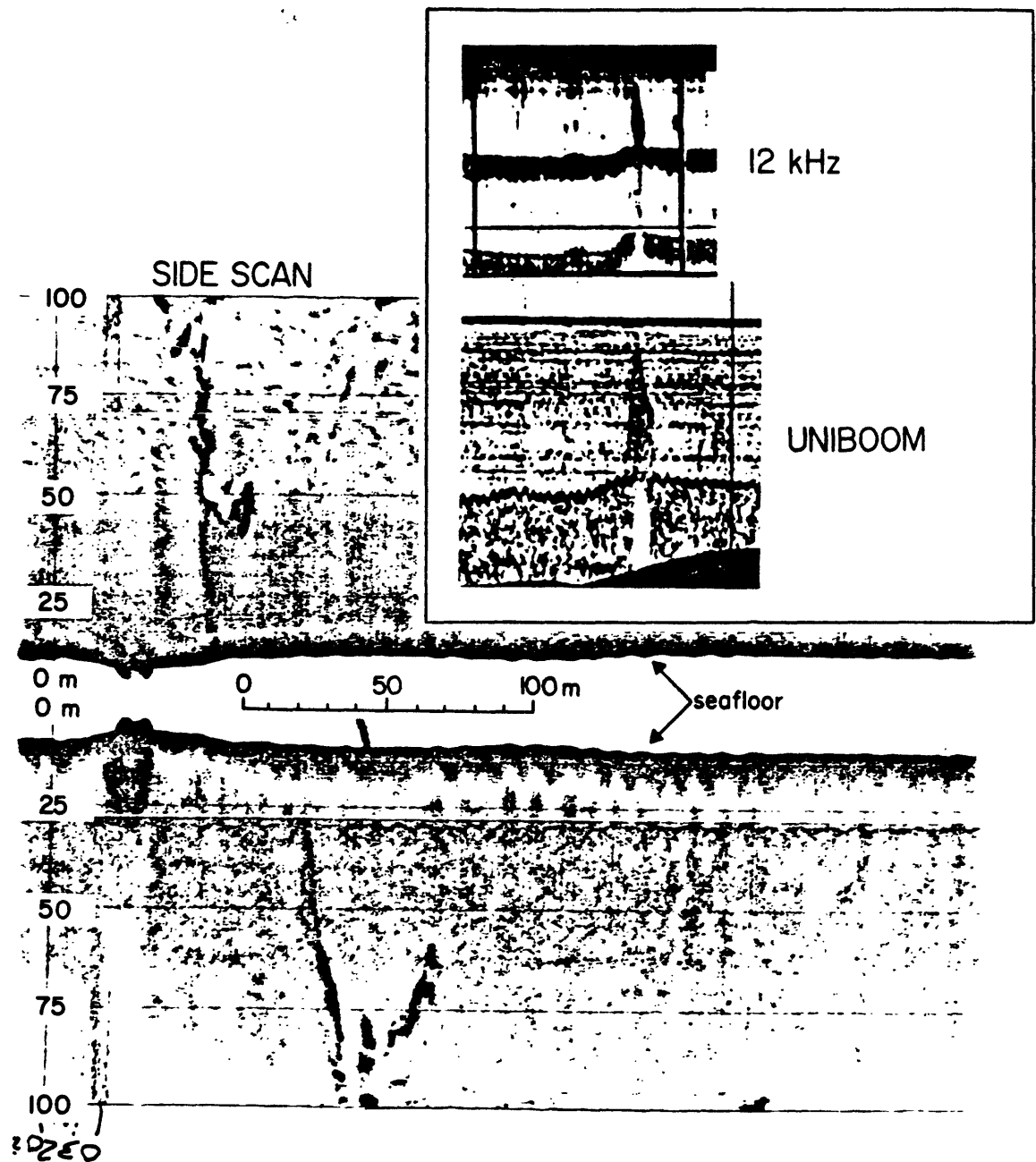


Figure 10. High resolution seismic reflection data and side scan sonographs depicting a water column gas plume southeast of the Dangerous River delta (Carlson and others, 1980).

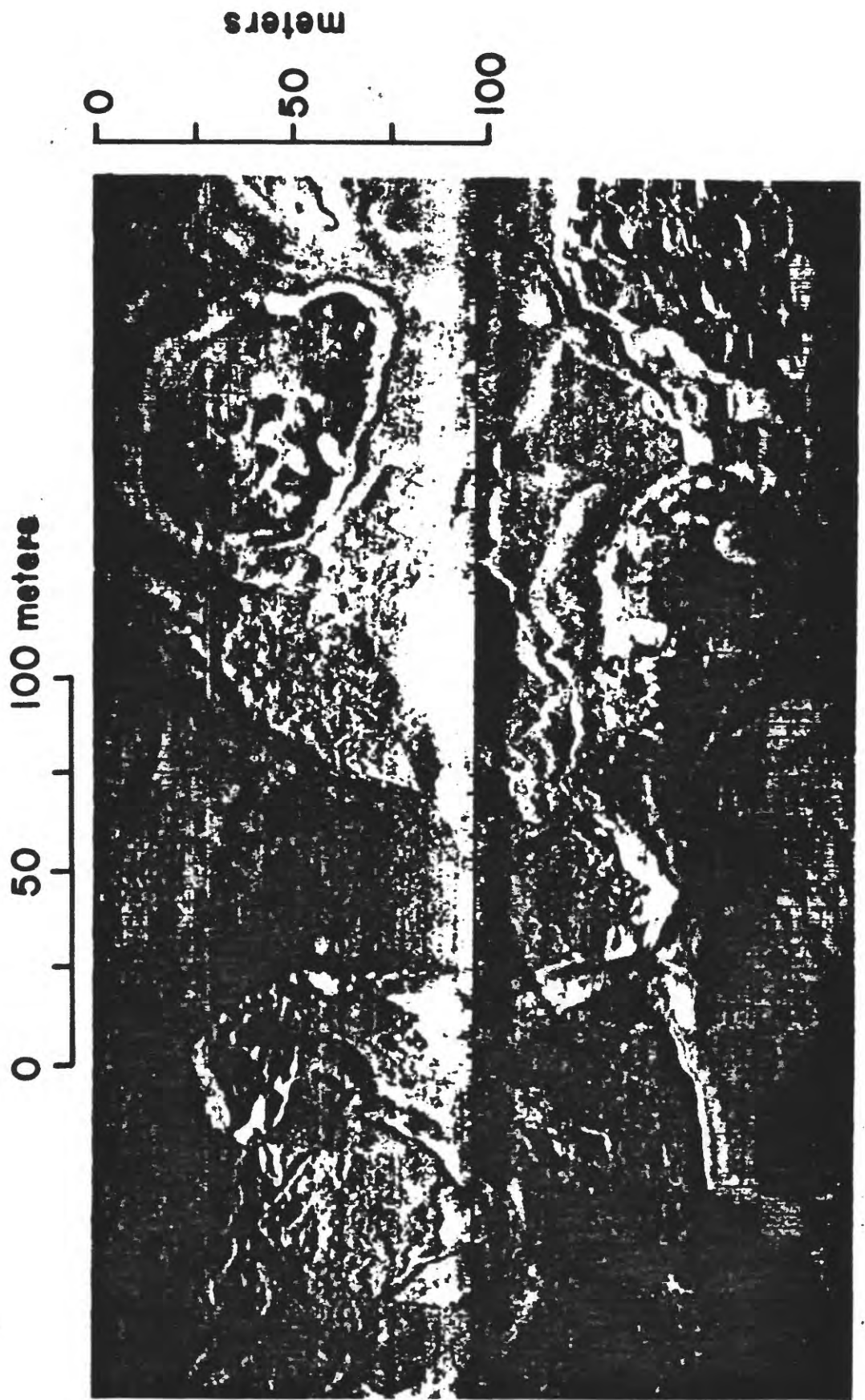


Figure 11. Side scan sonograph example of small slides and linear flows on the Alsek River prodelta (Molnia and Rappoport, 1980). Onshore direction is toward the top of the figure.

0 50 100 meters



Figure 12. Side scan sonograph depicting a massive, lobate slide toe and a series of smaller slide toes on the Alsek River prodelta (Molnia and Rappeport, 1980). Onshore direction is toward the top of the figure.

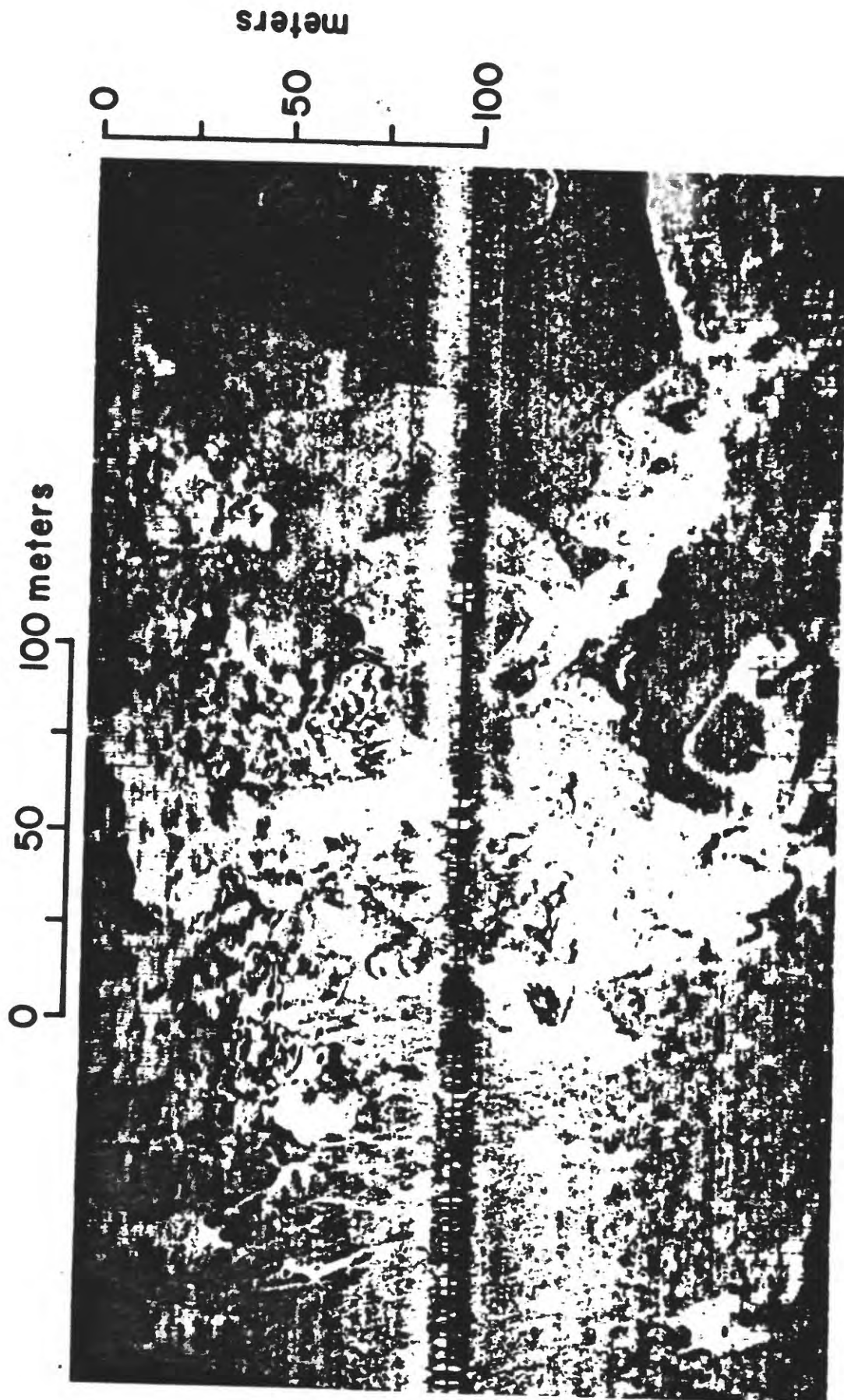


Figure 13. Side scan sonograph depicting multiple flows, slumps and slides on the Alsek River prodelta (Molnia and Rappoport, 1980).

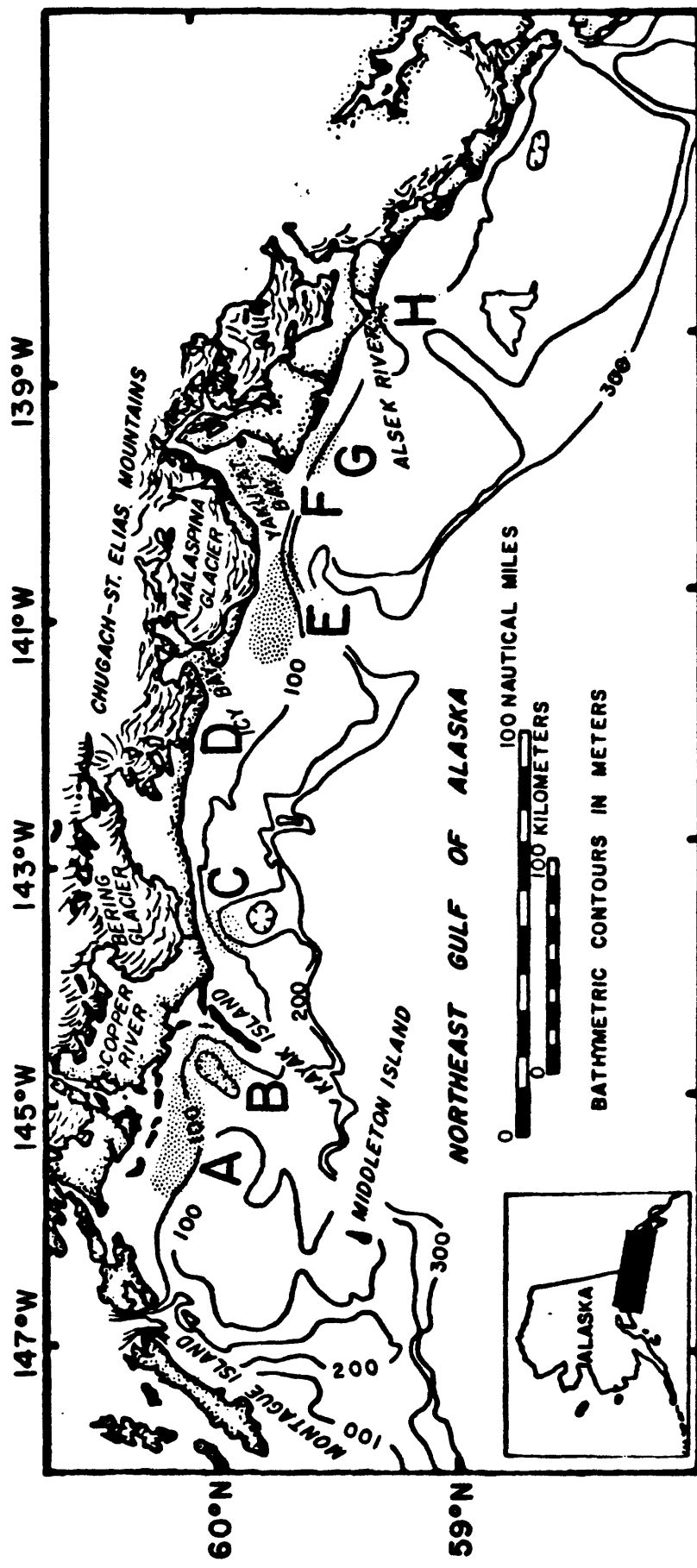


Figure 14. Locations of study areas.

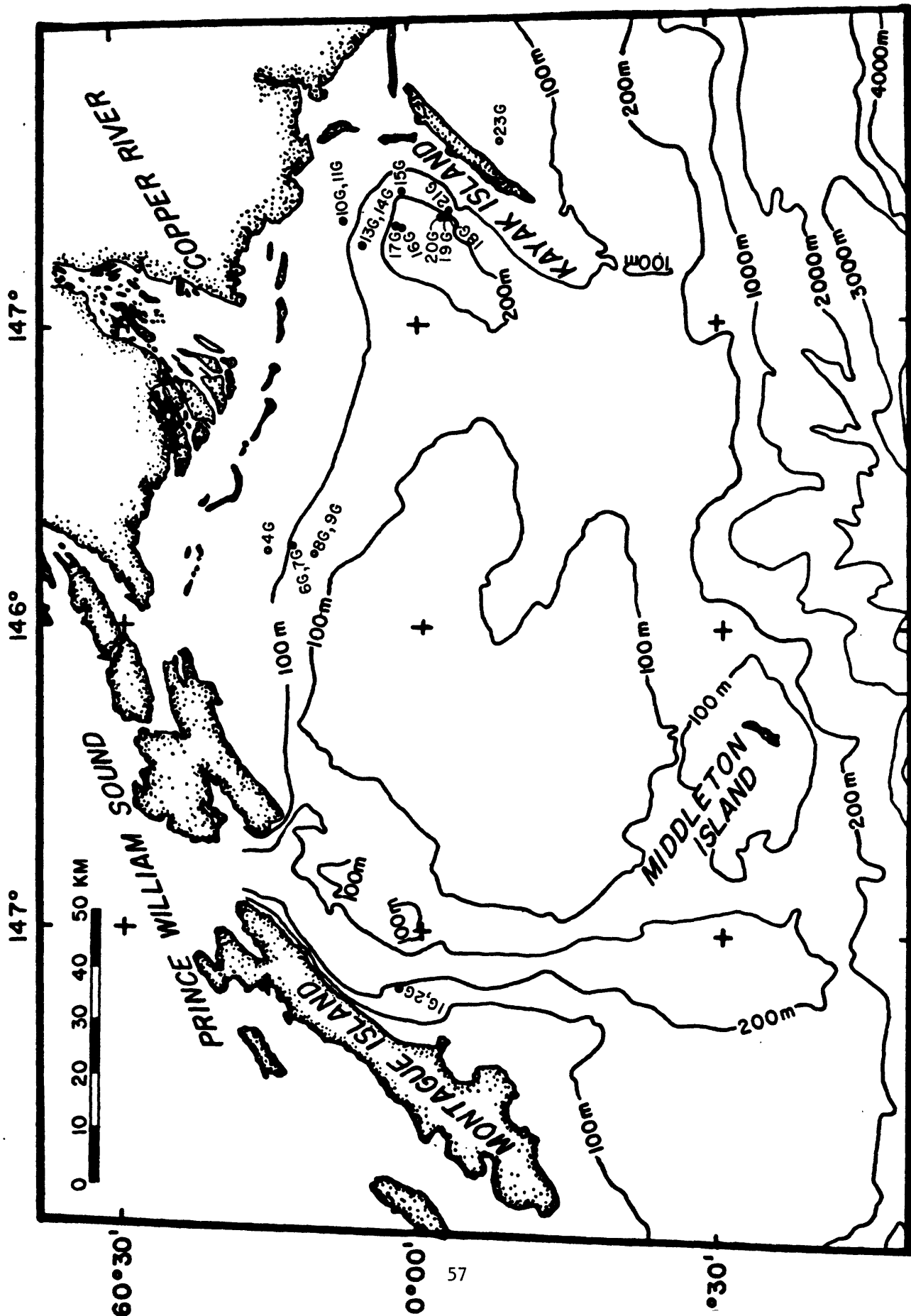


Figure 15. Core locations-Copper River Study Area (group to west) and Kayak Trough Study Area (group to east)

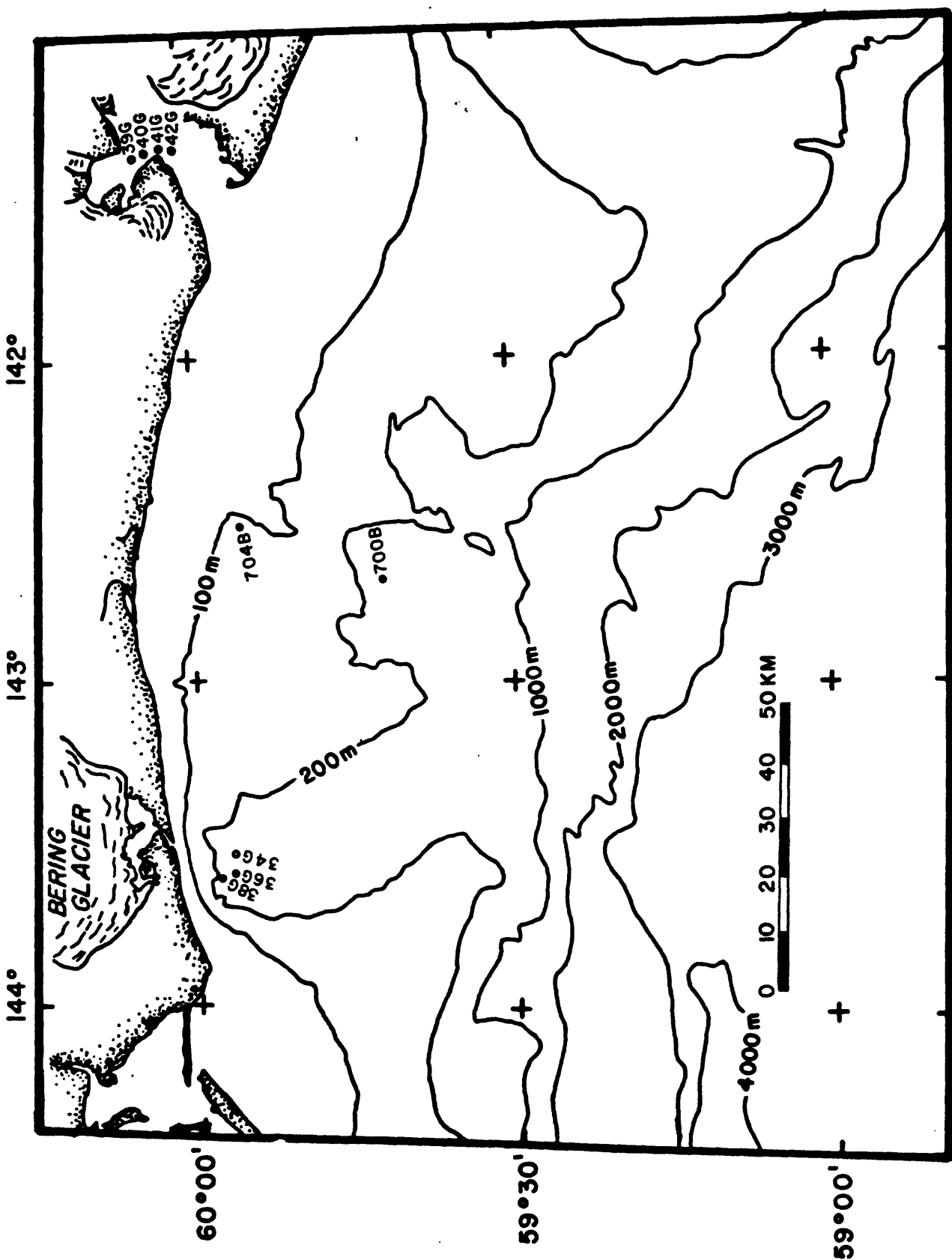


Figure 16. Core locations-Bering Trough and Icy Bay Study Areas.

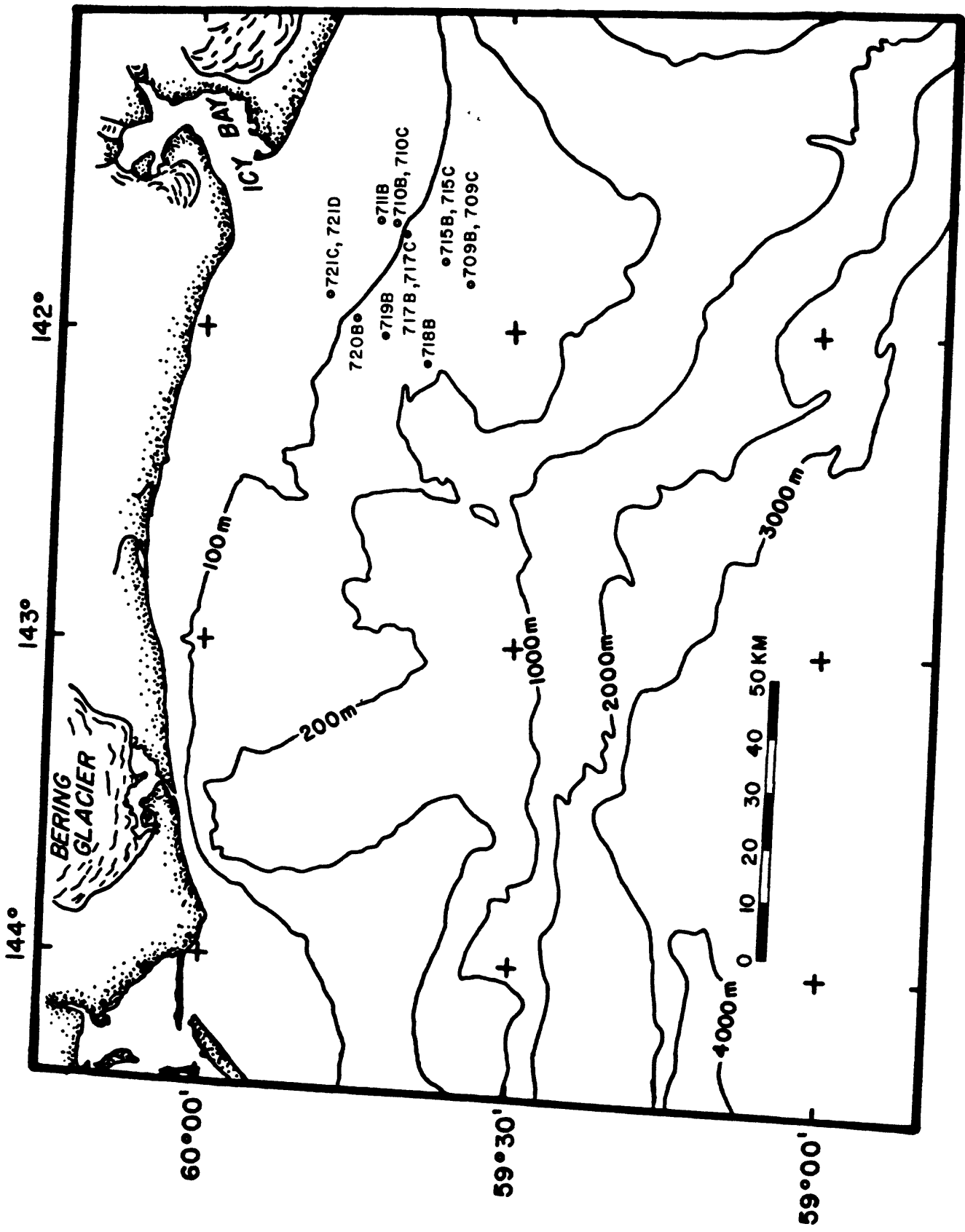


Figure 17. Core locations-Icy Bay-Malaspina Study Area (Cruise DC1-77-EG)

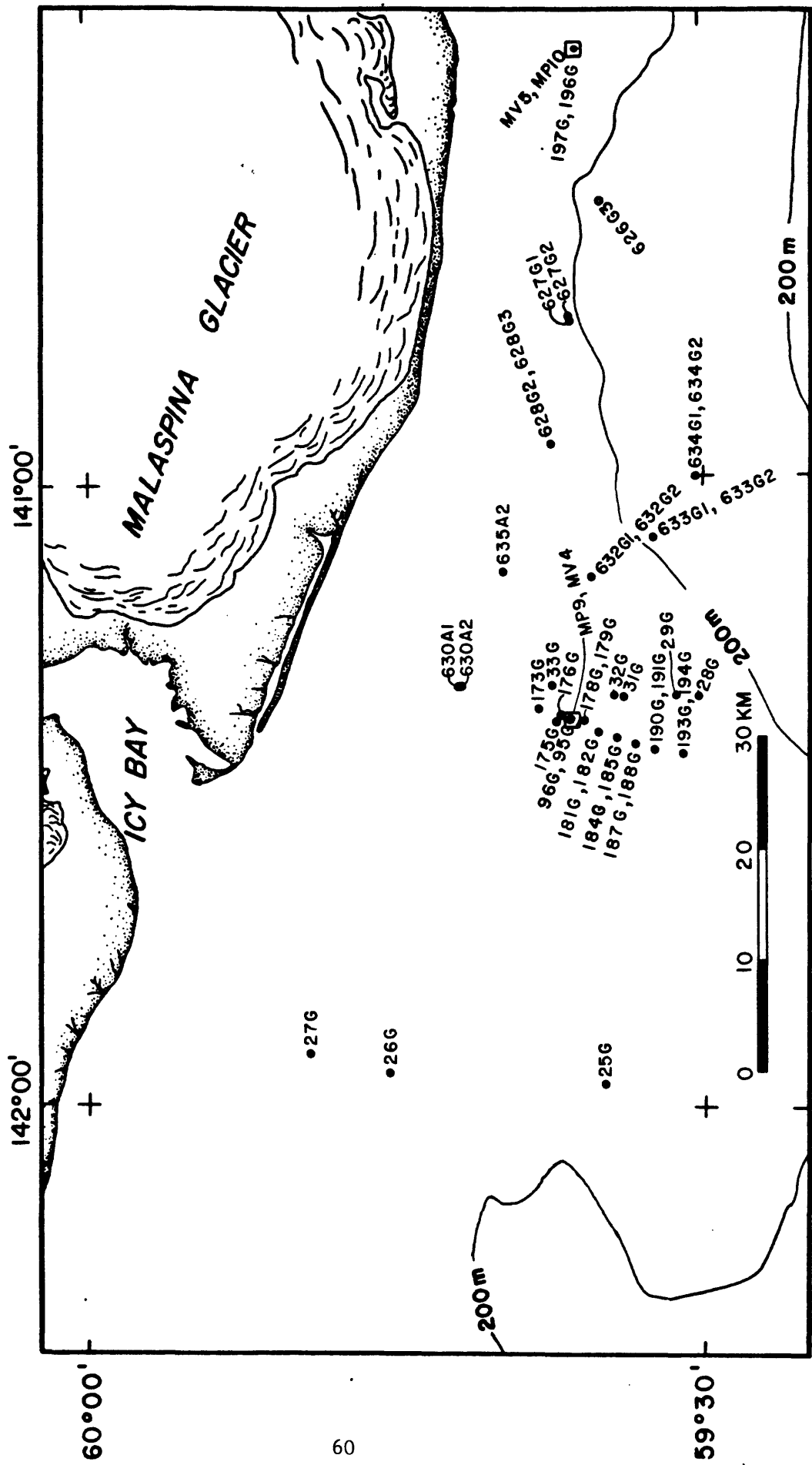


Figure 18. Core and in place test locations-Icy Bay-Malaspina Study Area (Cruises S8-77-EG, DC2-80-EG and DC1-81-EG).

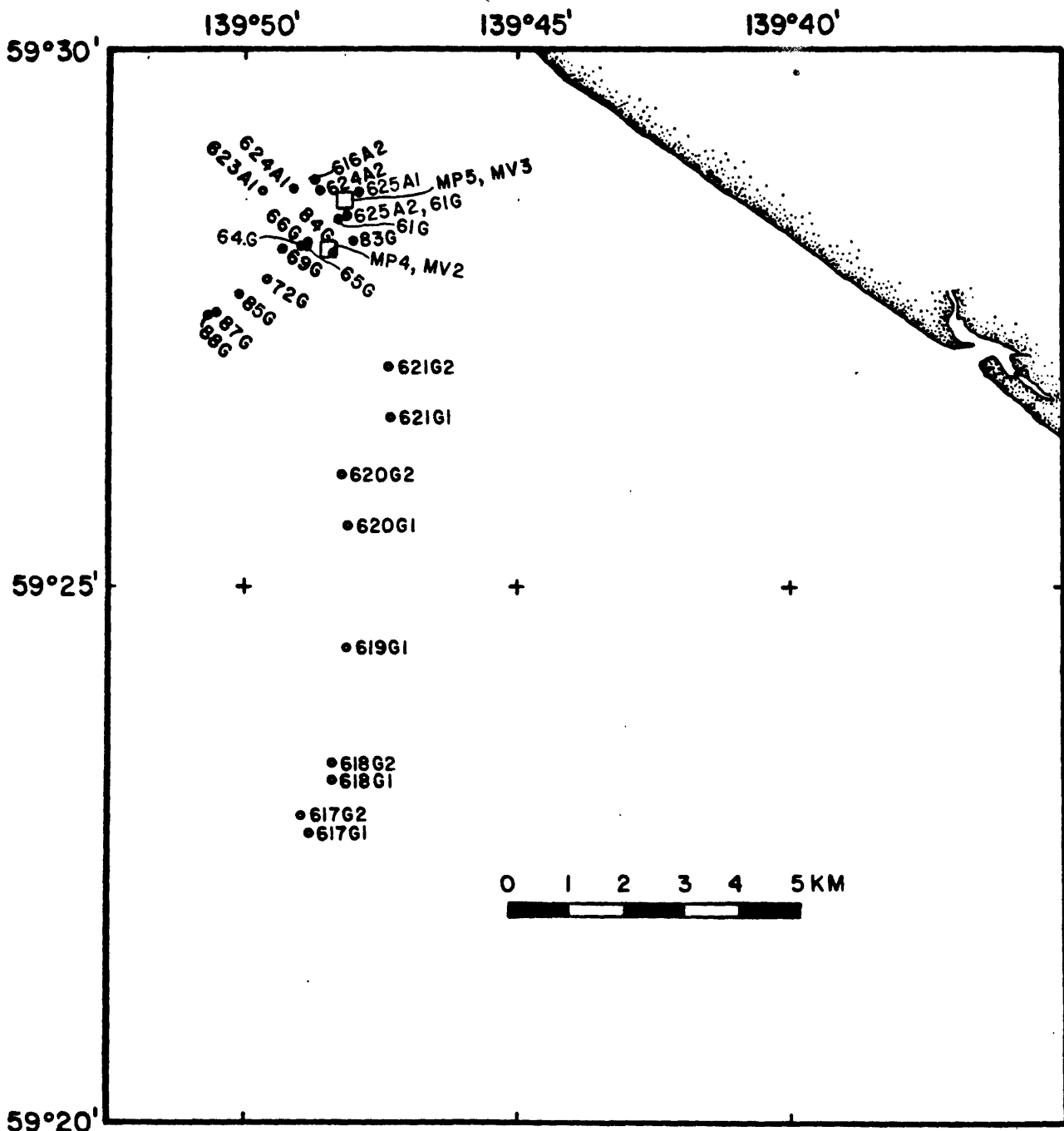


Figure 19. Core and in place test locations-Yakutat Study Area.

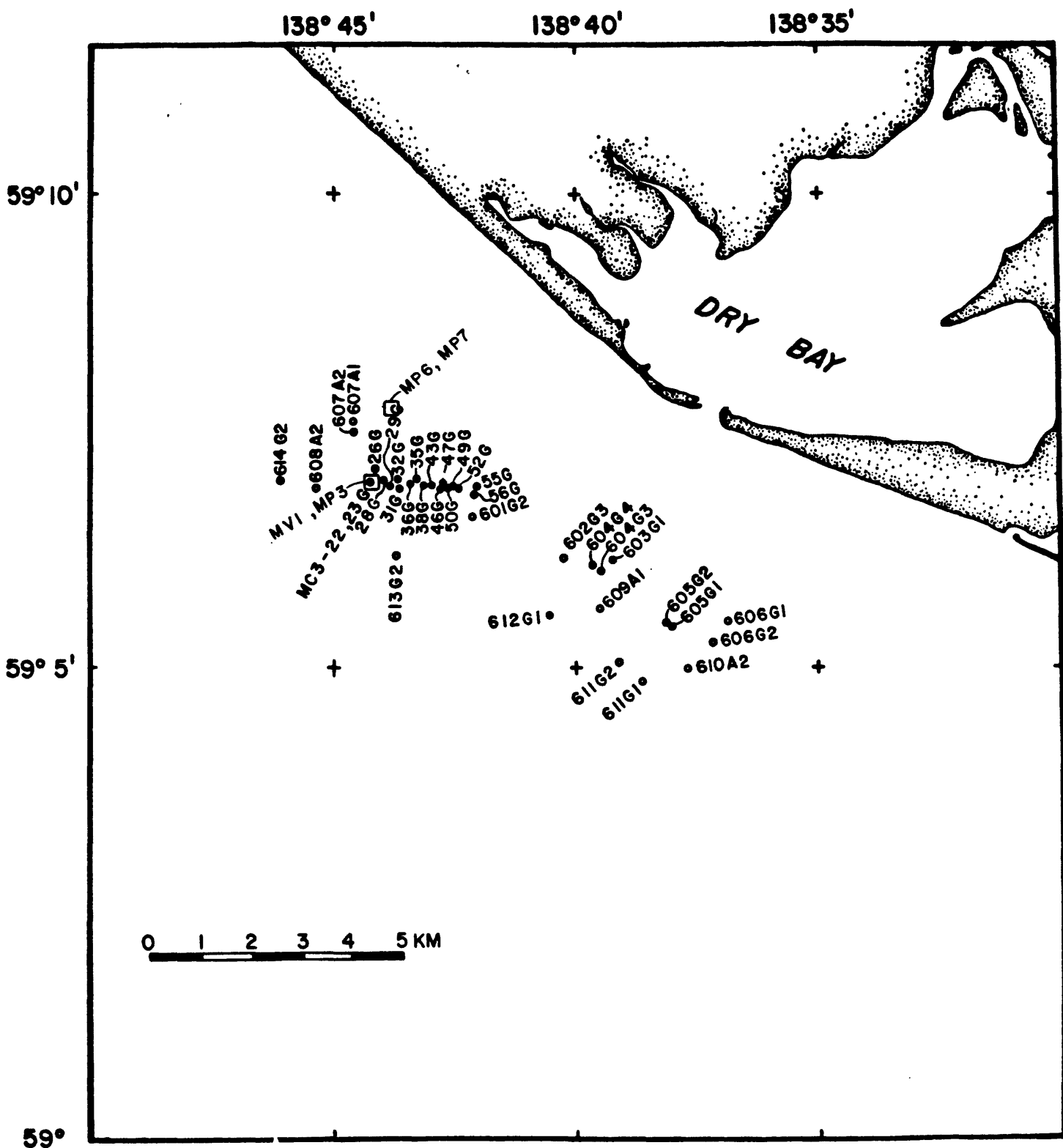


Figure 20. Core and in place test locations-Alsek River Study Area.

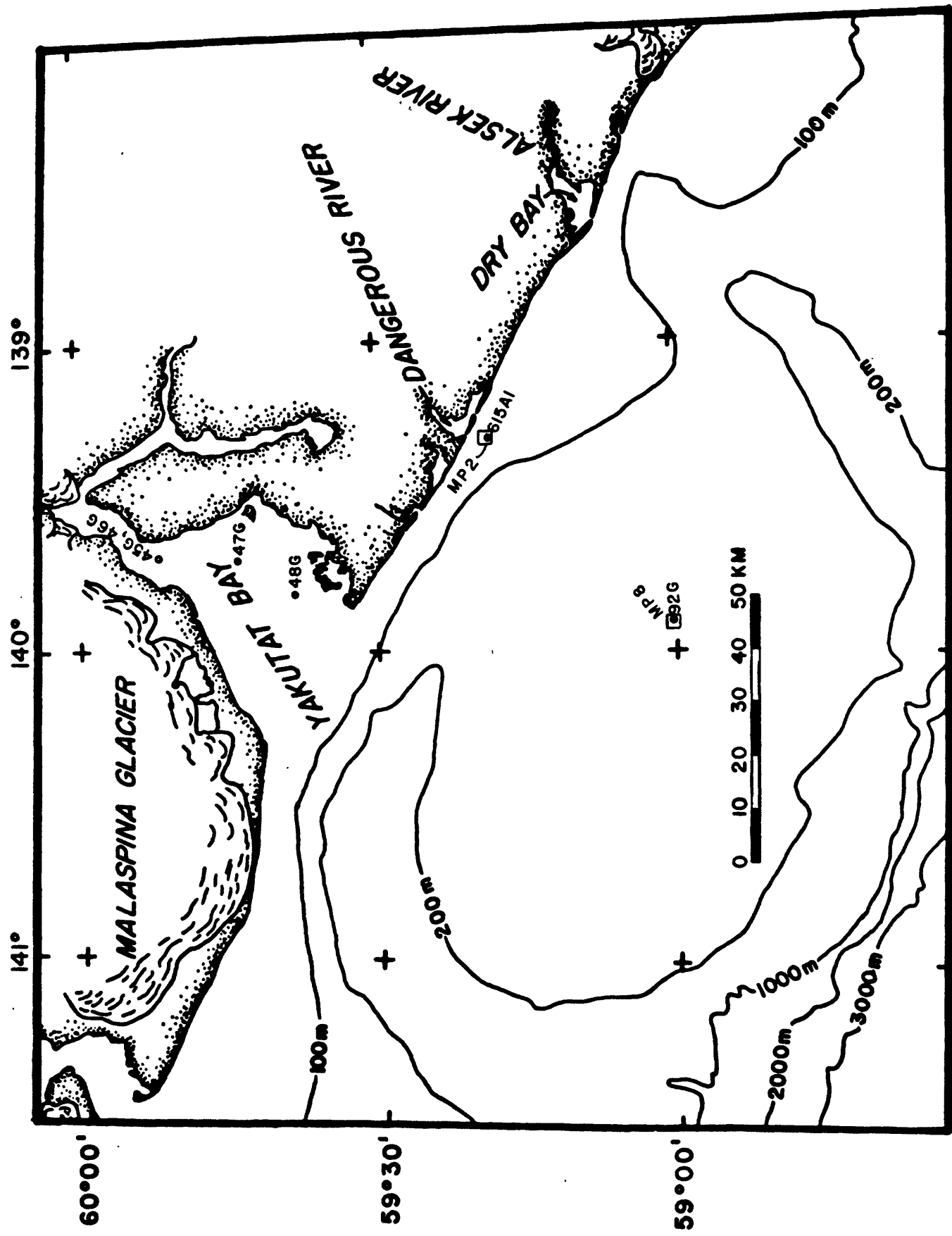


Figure 21. Core locations-Yakutat Bay Study Area and "other".

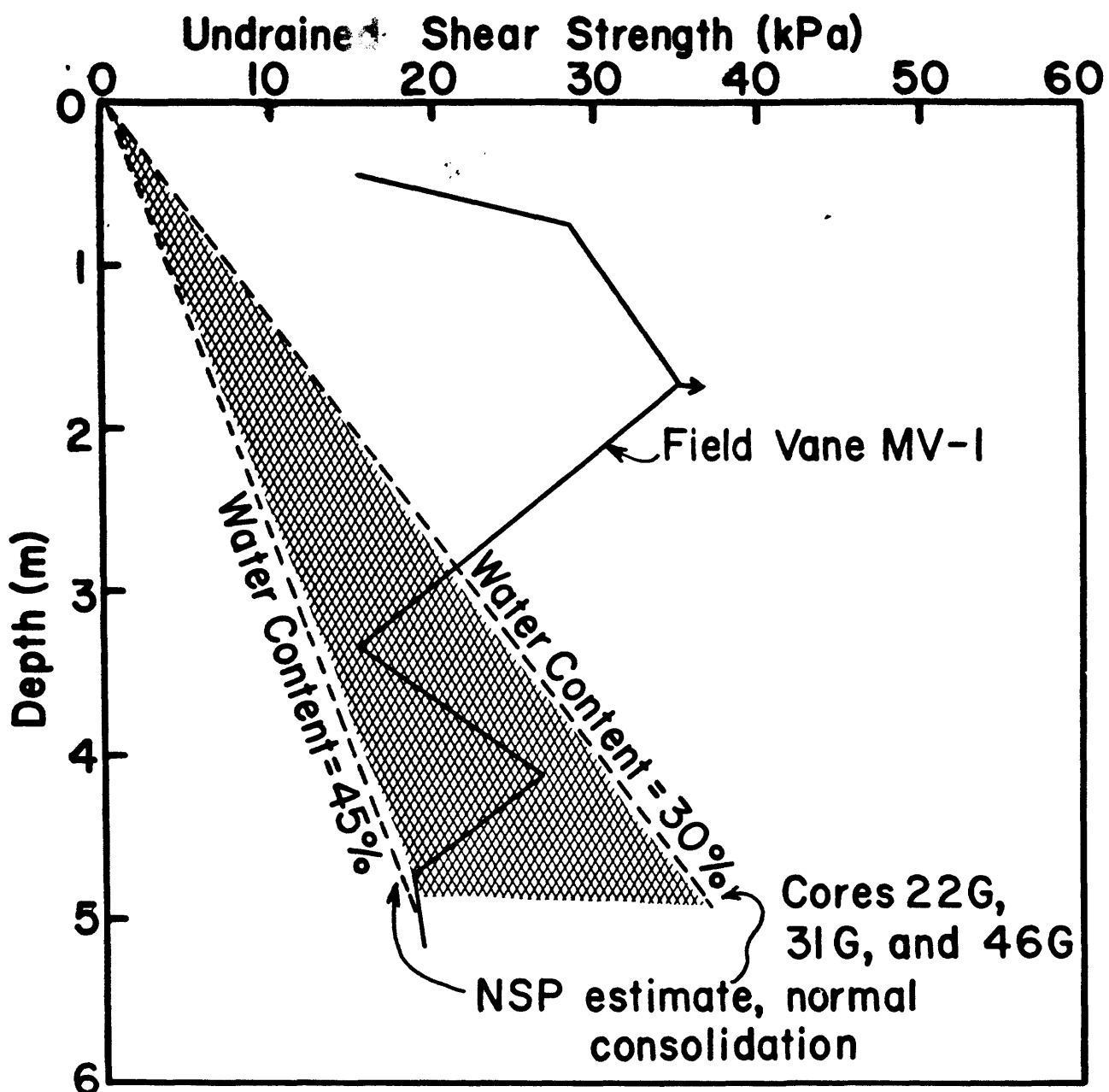


Figure 22. Results of field vane shear test MV-1 (Alsek River Study Area) compared with normalized strength parameter (NSP) estimate of undrained strength from triaxial tests.

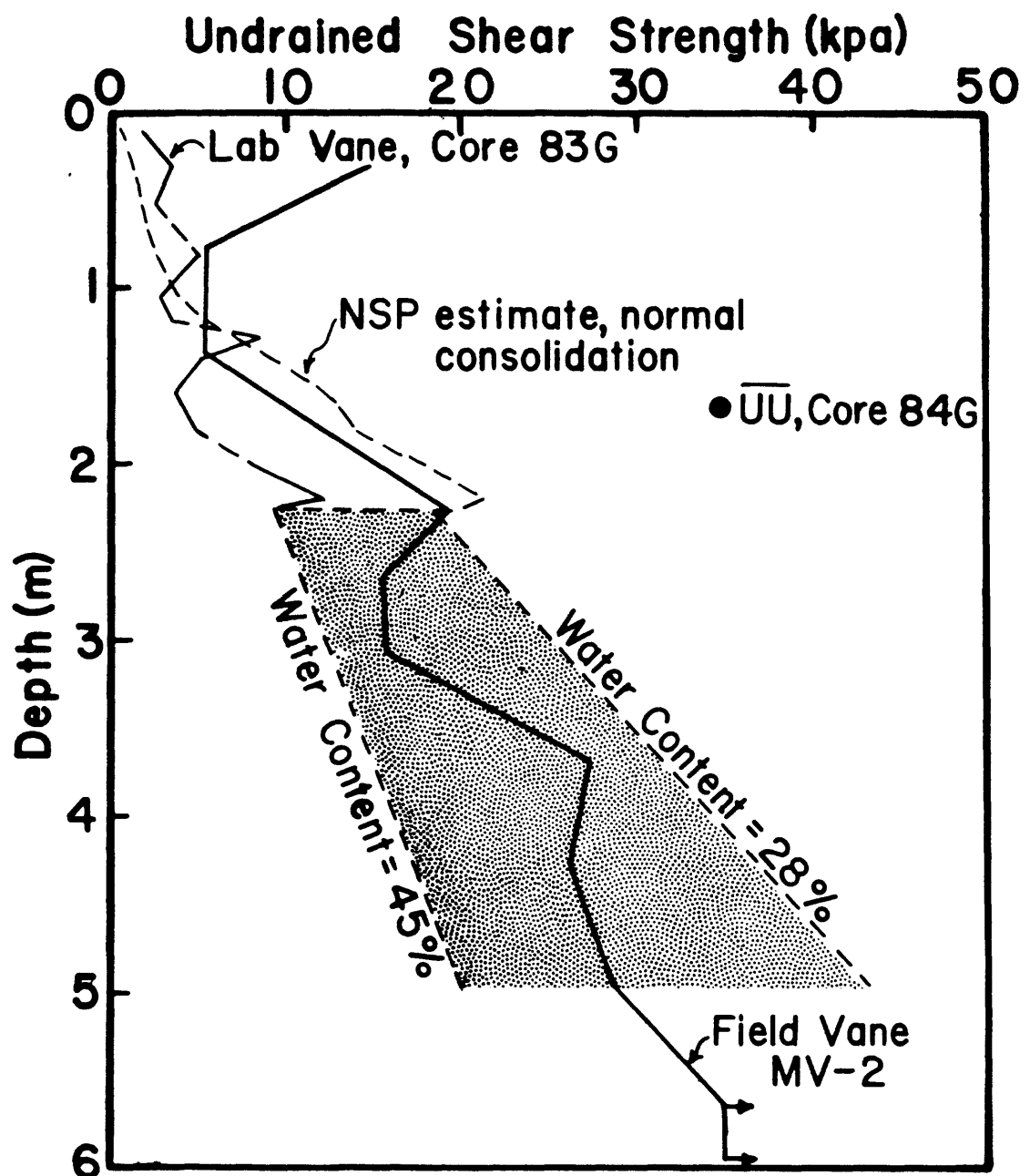


Figure 23. Results of field vane shear test MV-2 (Yakutat Study Area) compared with laboratory vane shear strengths and NSP estimates from triaxial tests. CIU and UU tests represent triaxial tests with consolidation to near the overburden stress and to nearly no stress, respectively.

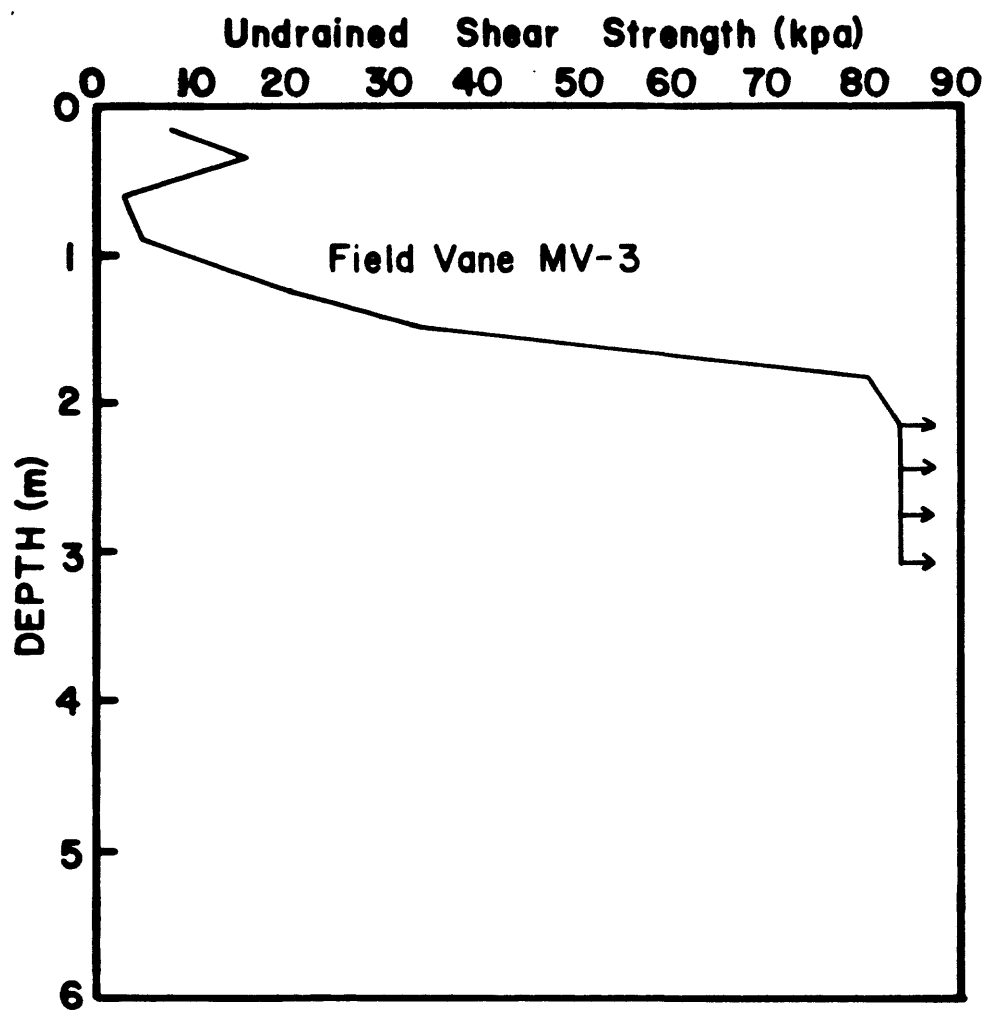


Figure 24. Results of field vane shear test MV-3 (Yakutat Study Area). Arrows indicate locations where the capacity of the field vane torque cell was reached.

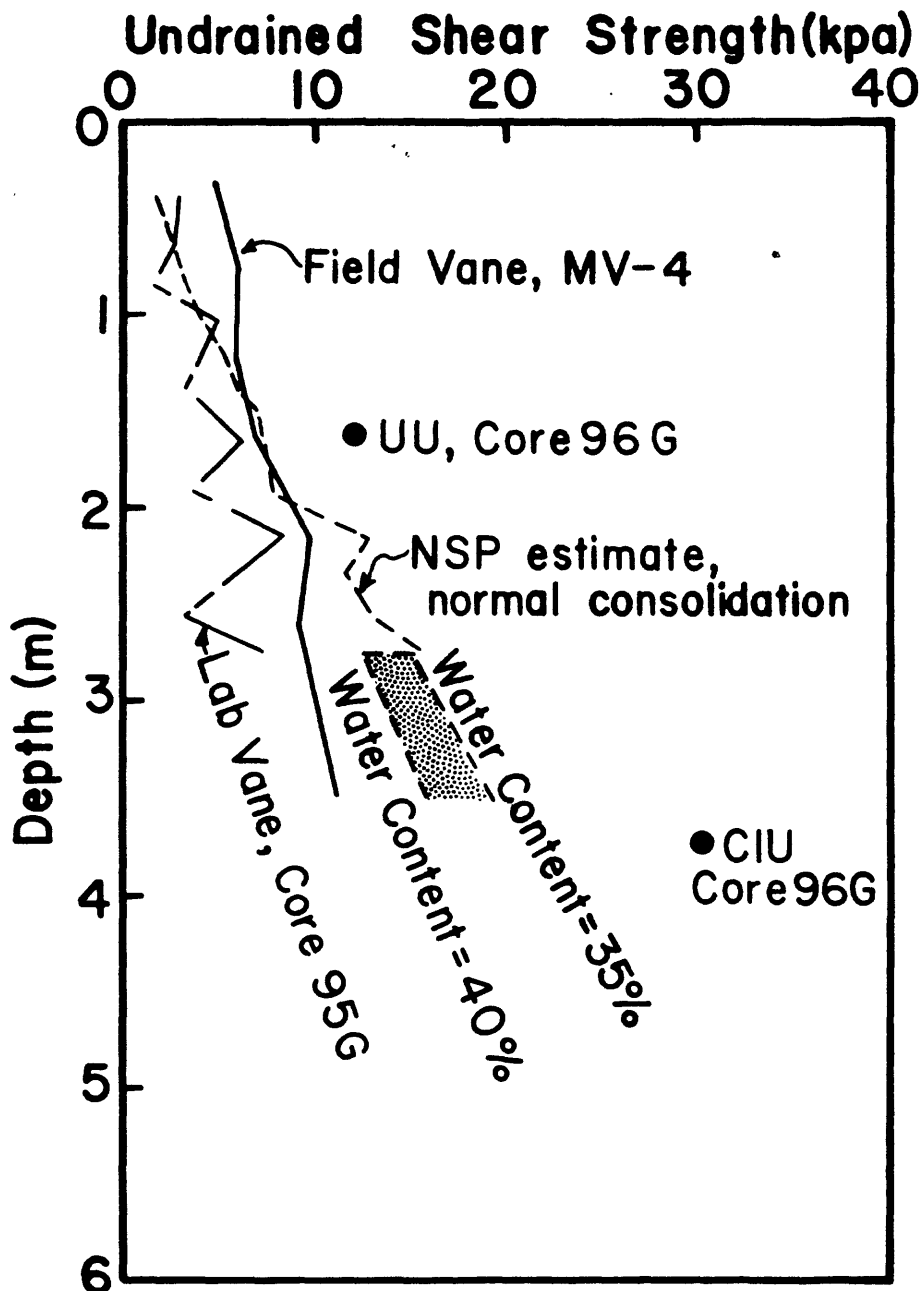


Figure 25. Results of field vane shear test MV-4 (Icy Bay-Malaspina Study Area) compared with laboratory vane shear strengths and NSP estimates from triaxial tests. CIU and UU tests represent triaxial tests consolidated to near the overburden stress and to nearly no stress, respectively.

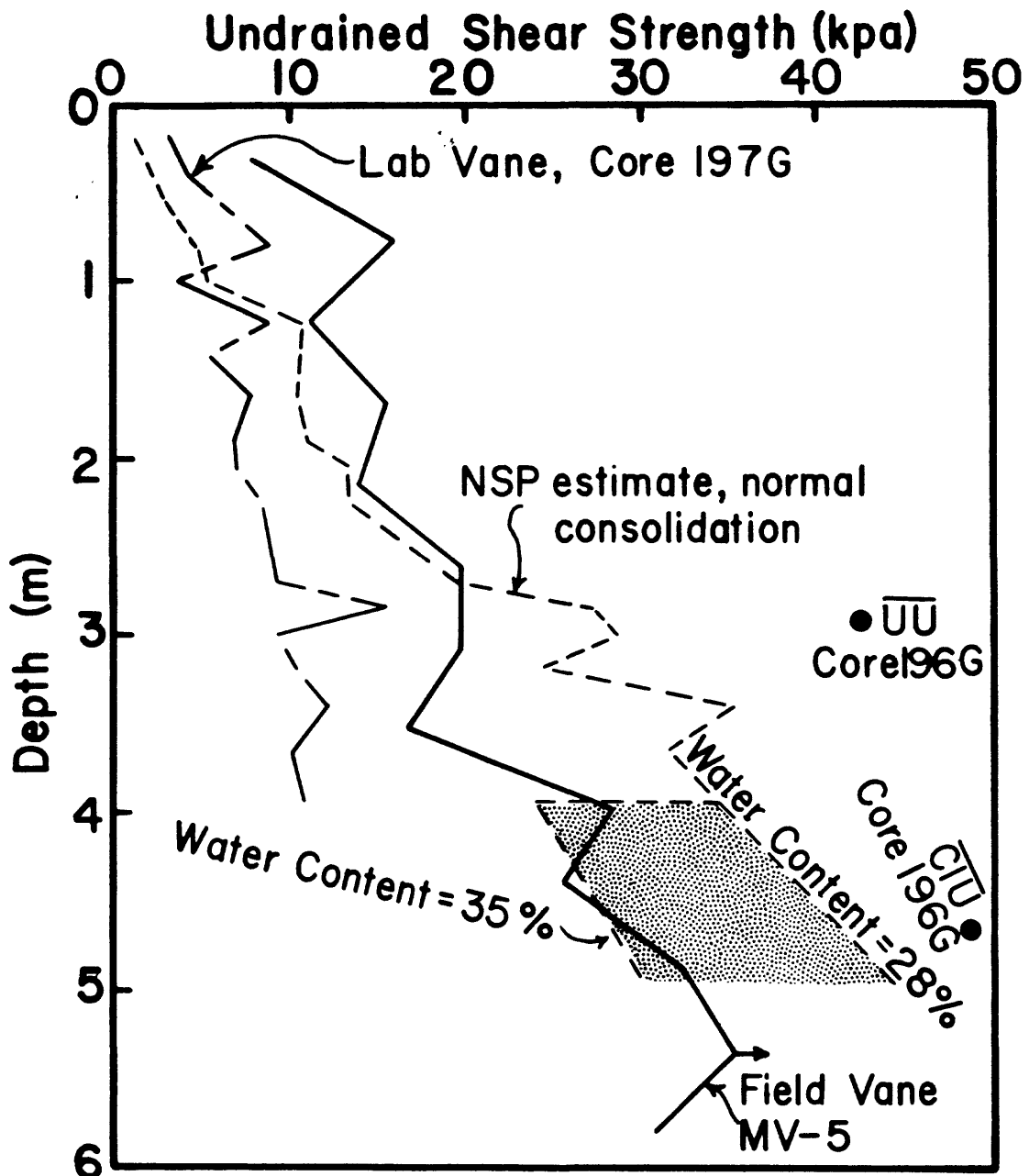


Figure 26. Results of field vane shear test MV-5 (eastern part of Icy Bay-Malaspina Study Area) compared with laboratory vane shear strengths and NSP estimates from triaxial tests. CIU and UU tests represent triaxial tests to near the overburden stress and to nearly no stress, respectively.

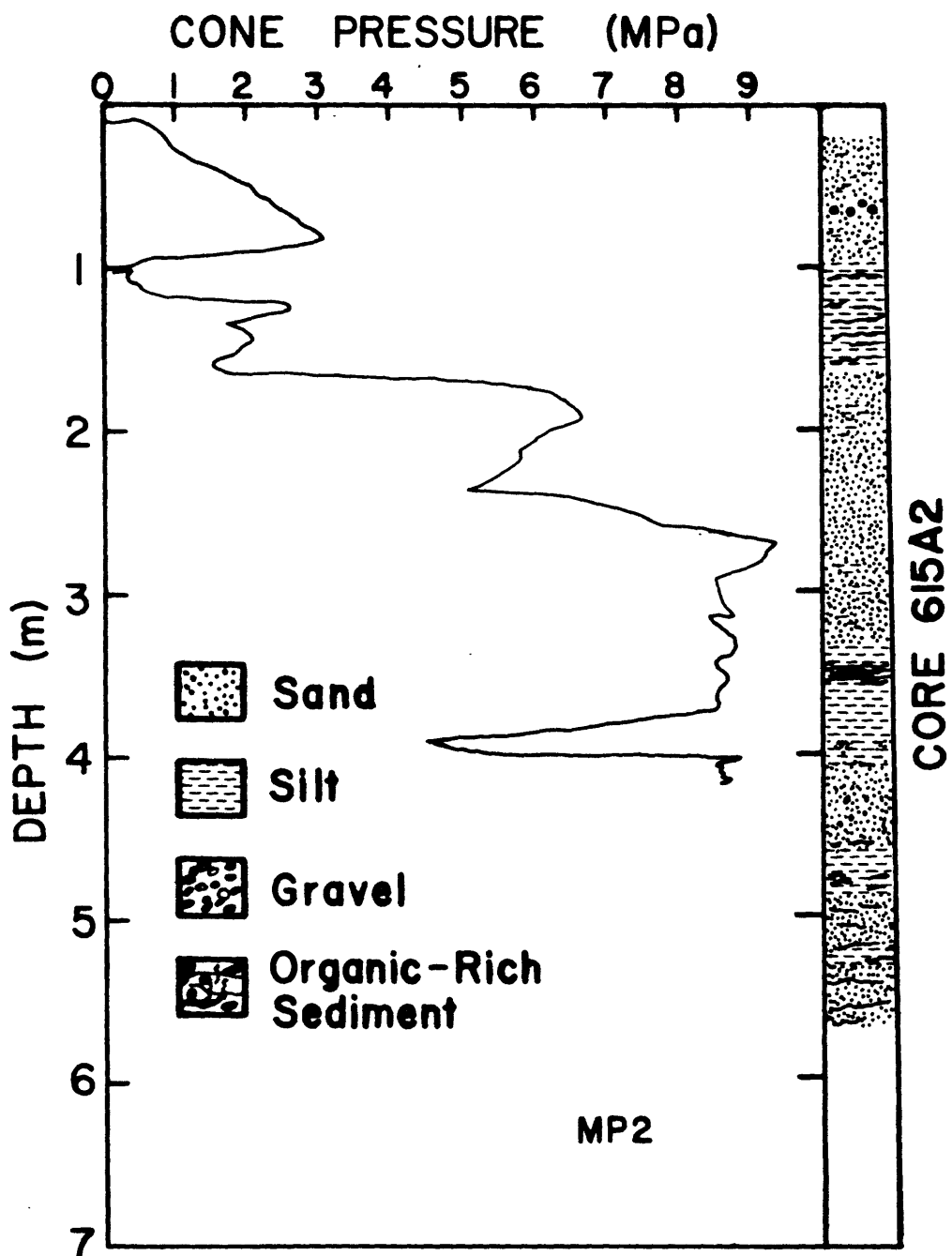


Figure 27. Results of in place cone penetration test MP-2 (off the mouth of the Dangerous River). Stratigraphy of nearby core is given at right.

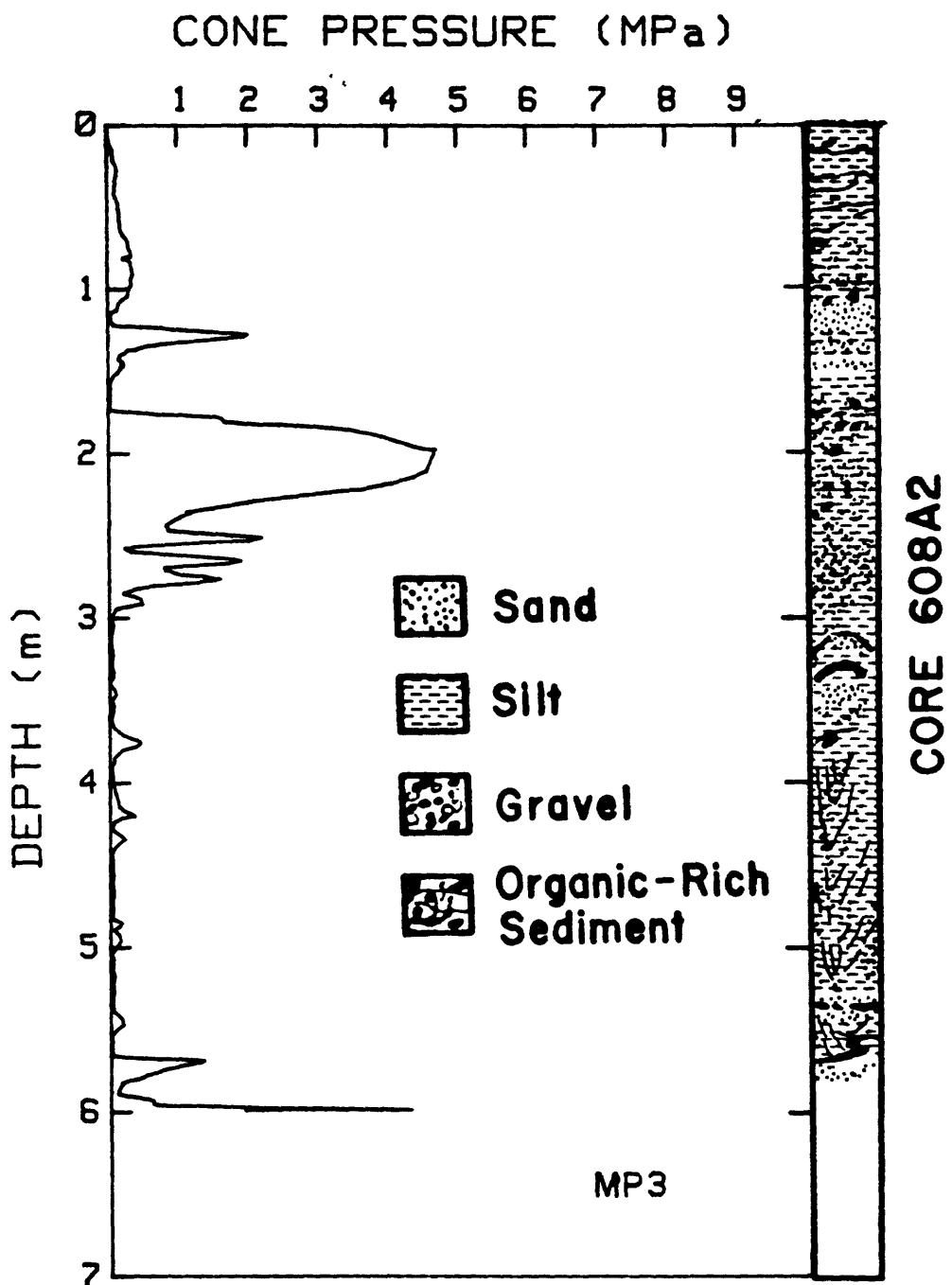


Figure 28. Results of in place cone penetration test MP-3. (Alsek River Study Area). Stratigraphy of nearby core is given at right.

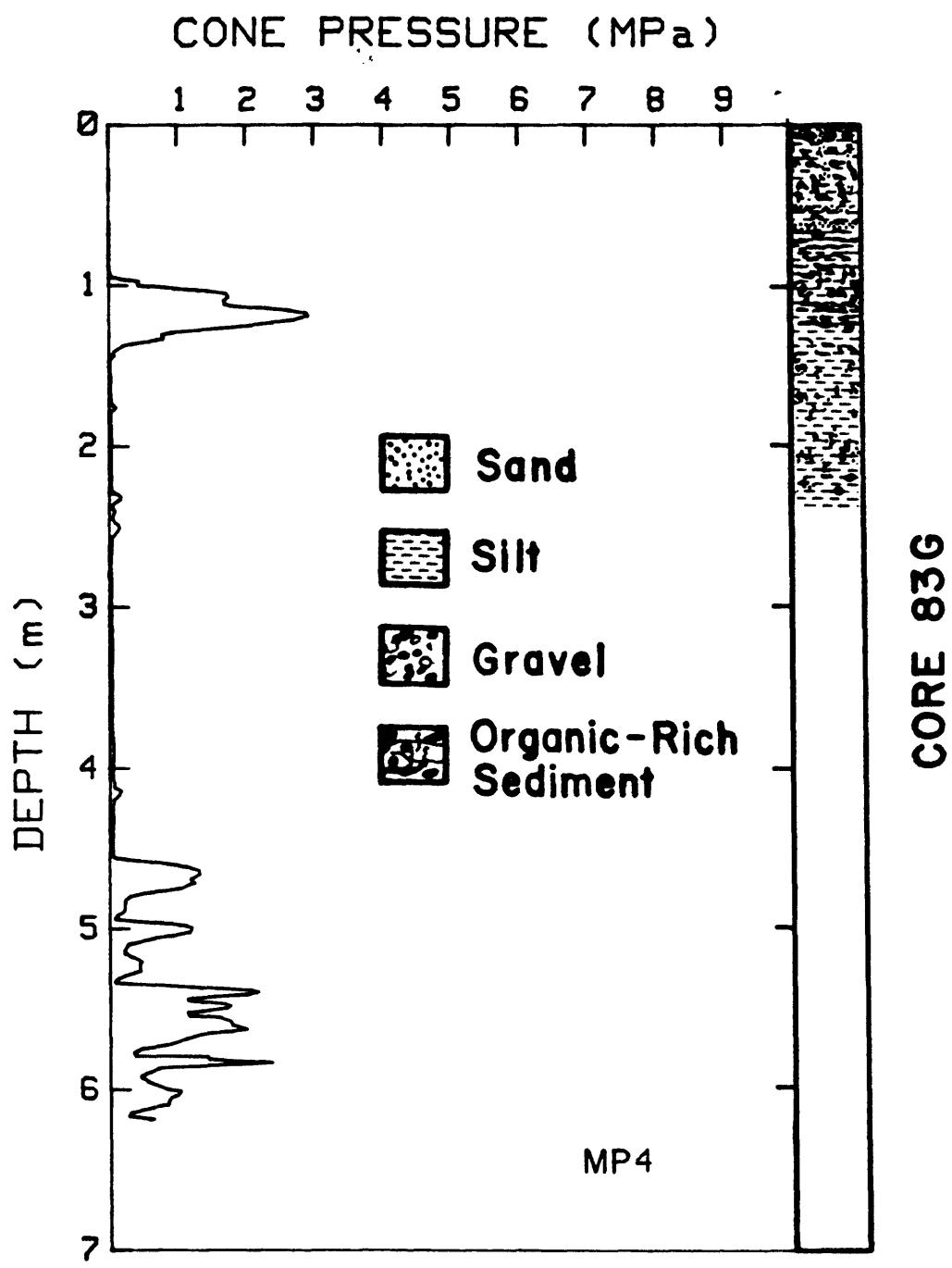


Figure 29. Results of in place cone penetration test MP-4 (Yakutat Study Area). Stratigraphy of nearby core is given at right.

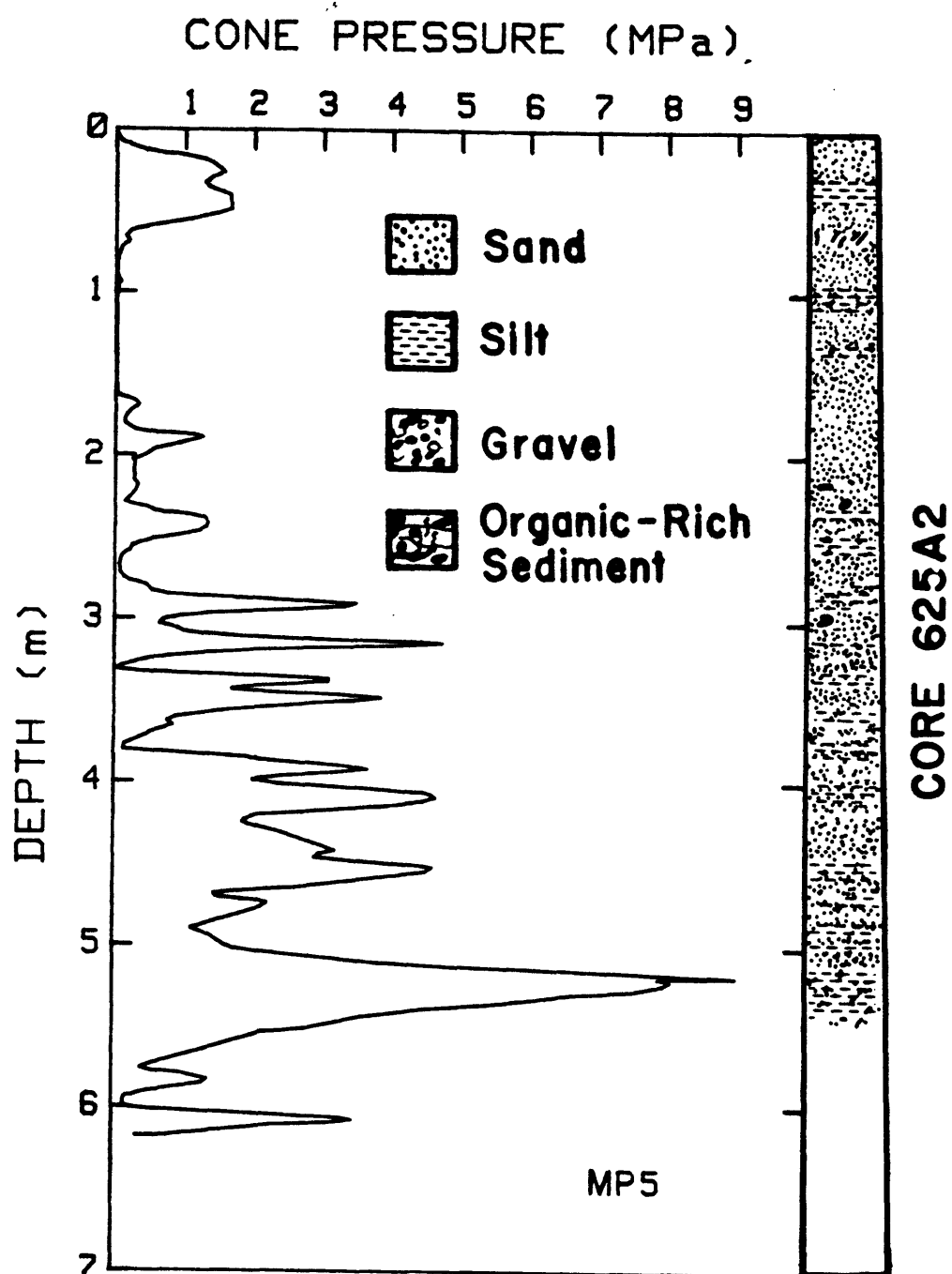


Figure 30. Results of in place cone penetration test MP-5 (Yakutat Study Area). Stratigraphy of nearby core is given at right.

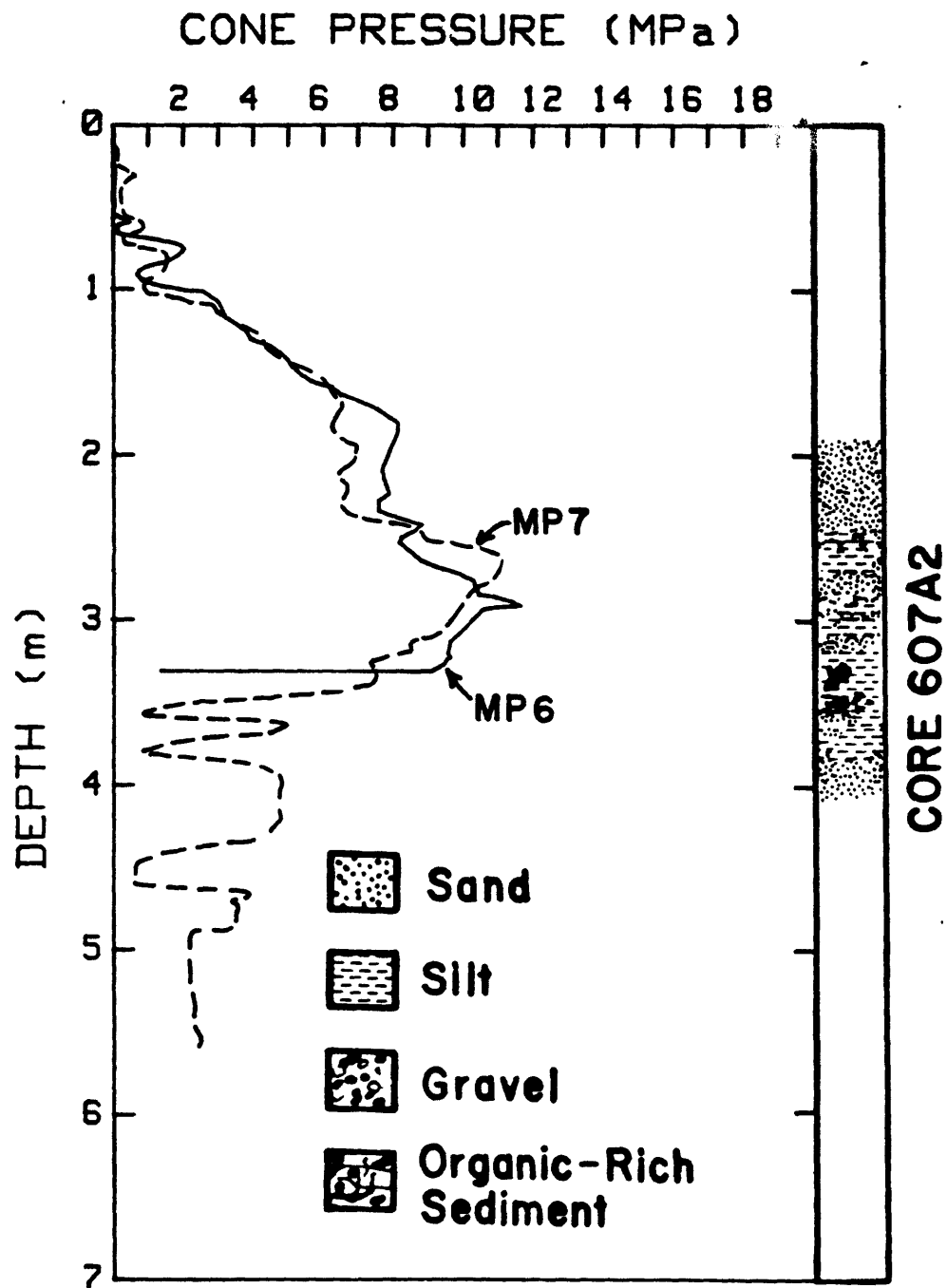


Figure 31. Results of in place cone penetration tests MP-6 and MP-7 (Alsed River Study Area). Stratigraphy of nearby core is given at right.

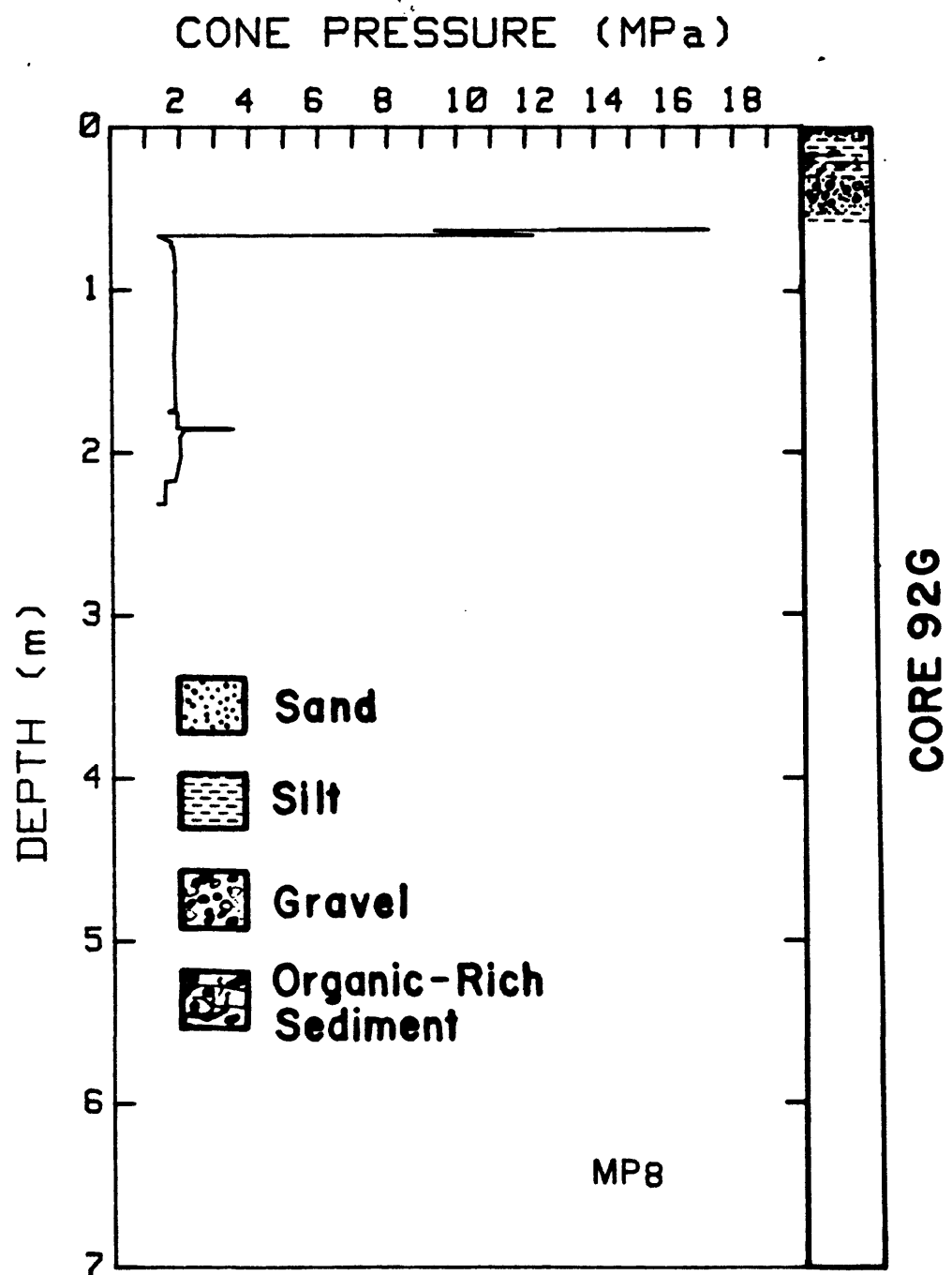


Figure 32. Results of in place cone penetration test MP-8 (Quaternary glacial deposits off Dangerous River Delta). Stratigraphy of nearby core is given at right.

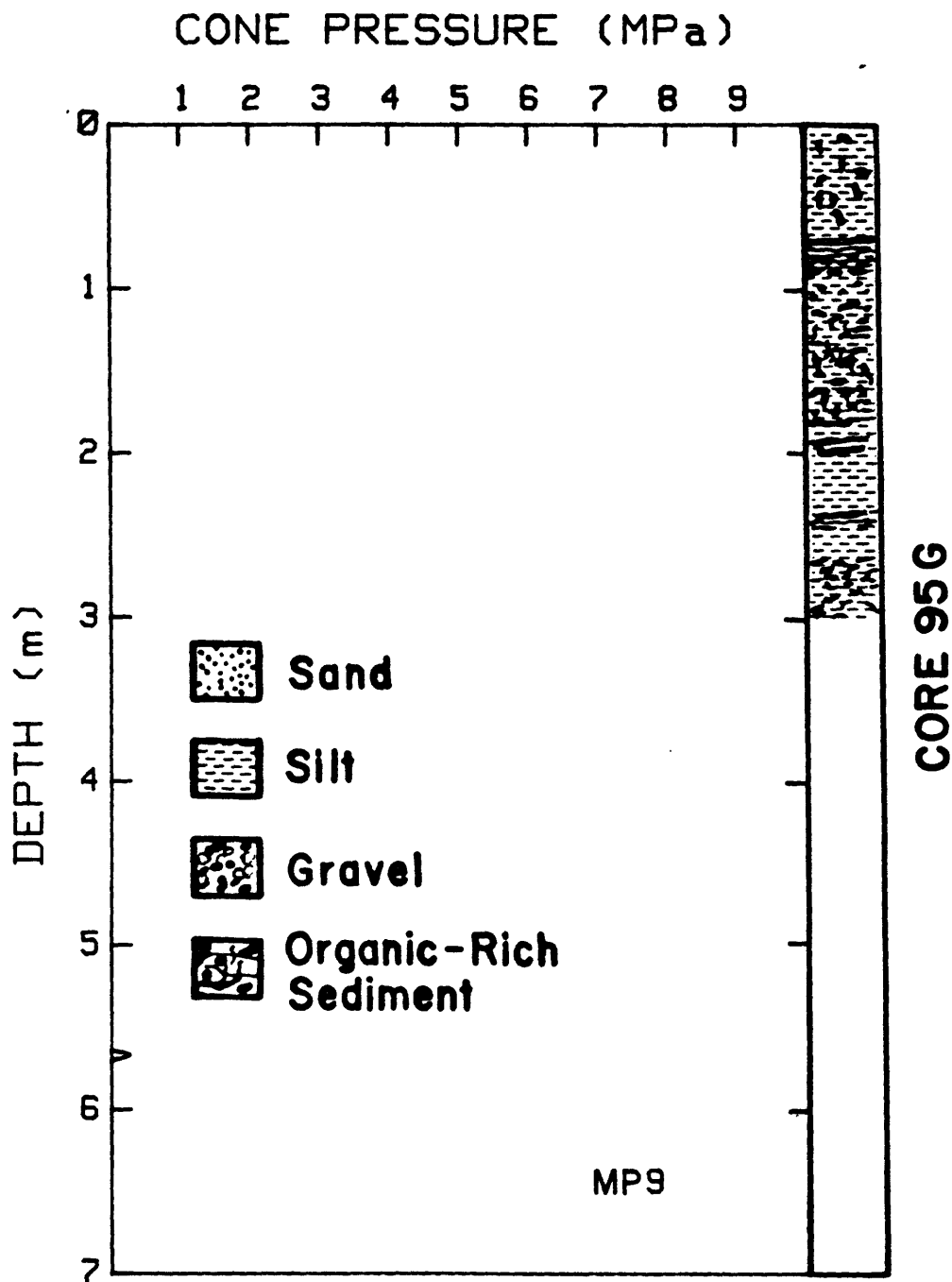


Figure 33. Results of in place cone penetration test MP-9 (Icy Bay-Malaspina Study Area). Stratigraphy of nearby core is given at right.

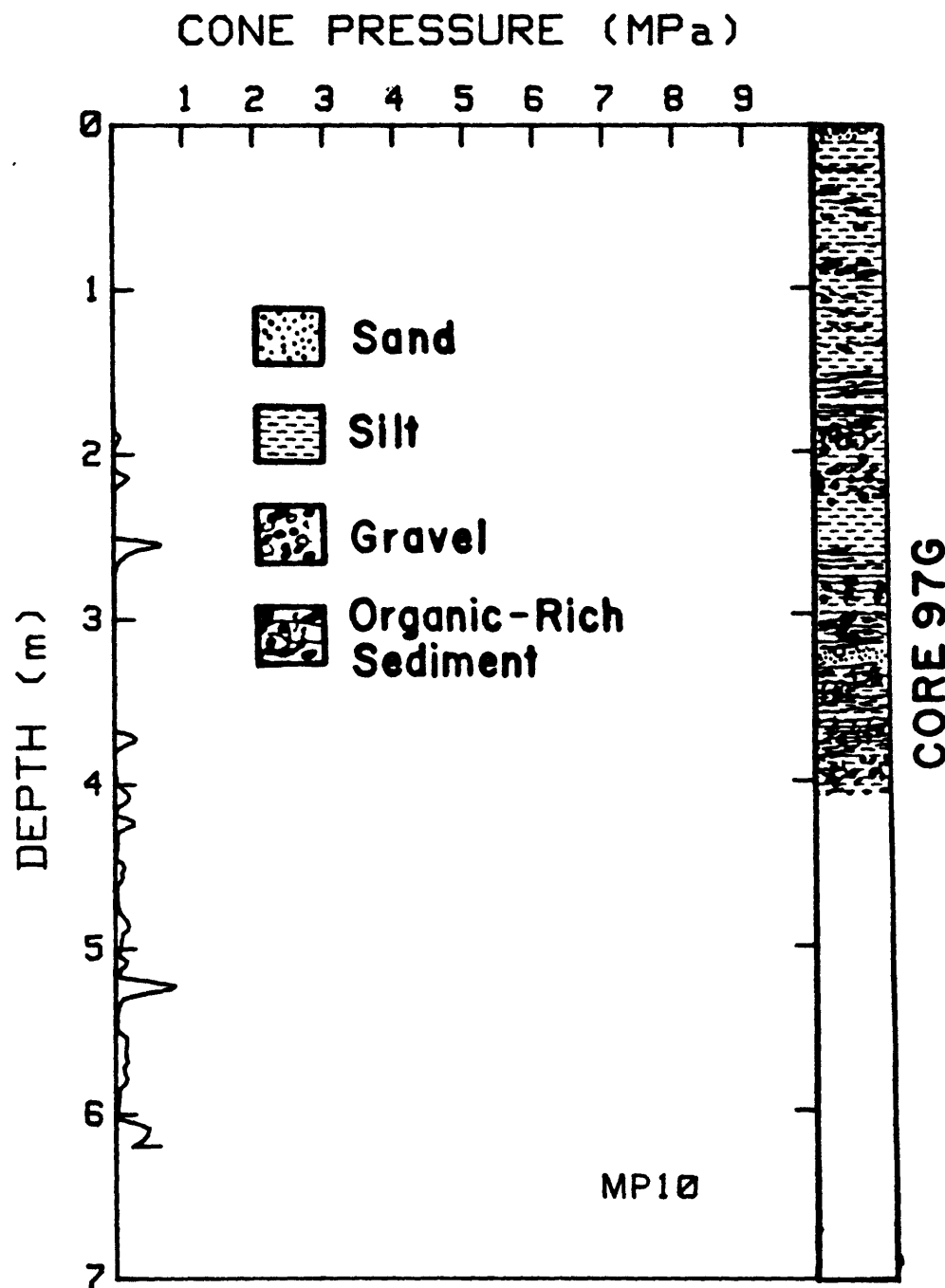


Figure 34. Results of in place cone penetration test MP-10 (eastern part of Icy Bay-Malaspina Study Area). Stratigraphy of nearby core is given at right.

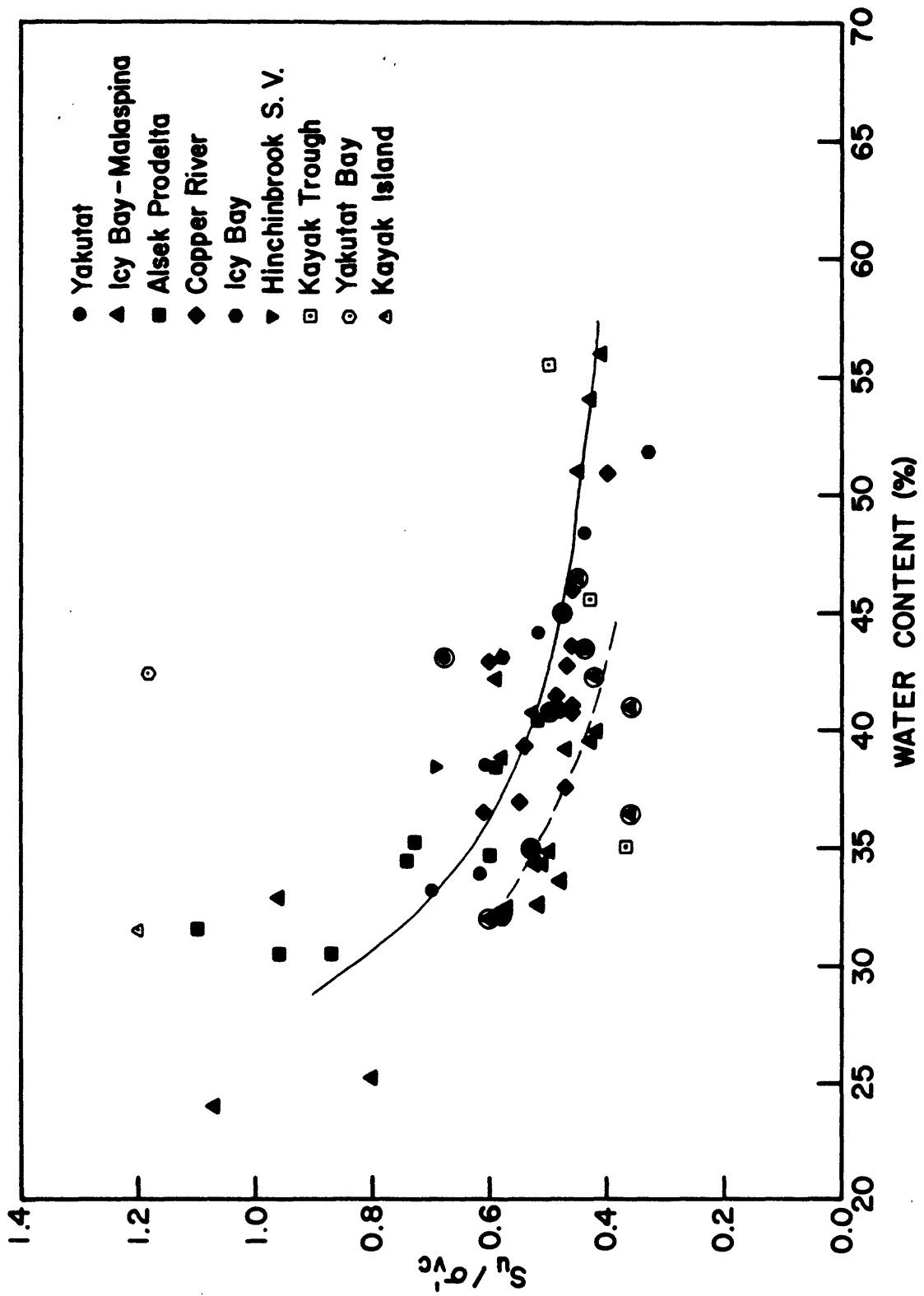


Figure 35. Correlation of ratio of undrained shearing strength,  $S_u$ , to vertical consolidation stress,  $\sigma'_vc$ , with natural water content; all type (c) static triaxial tests. Circled data points represent anisotropic consolidation. Solid line is a fit of the isotropic consolidation data points (uncircled dots). Dashed line represents 0.8 times the solid line and roughly follows anisotropic data points.

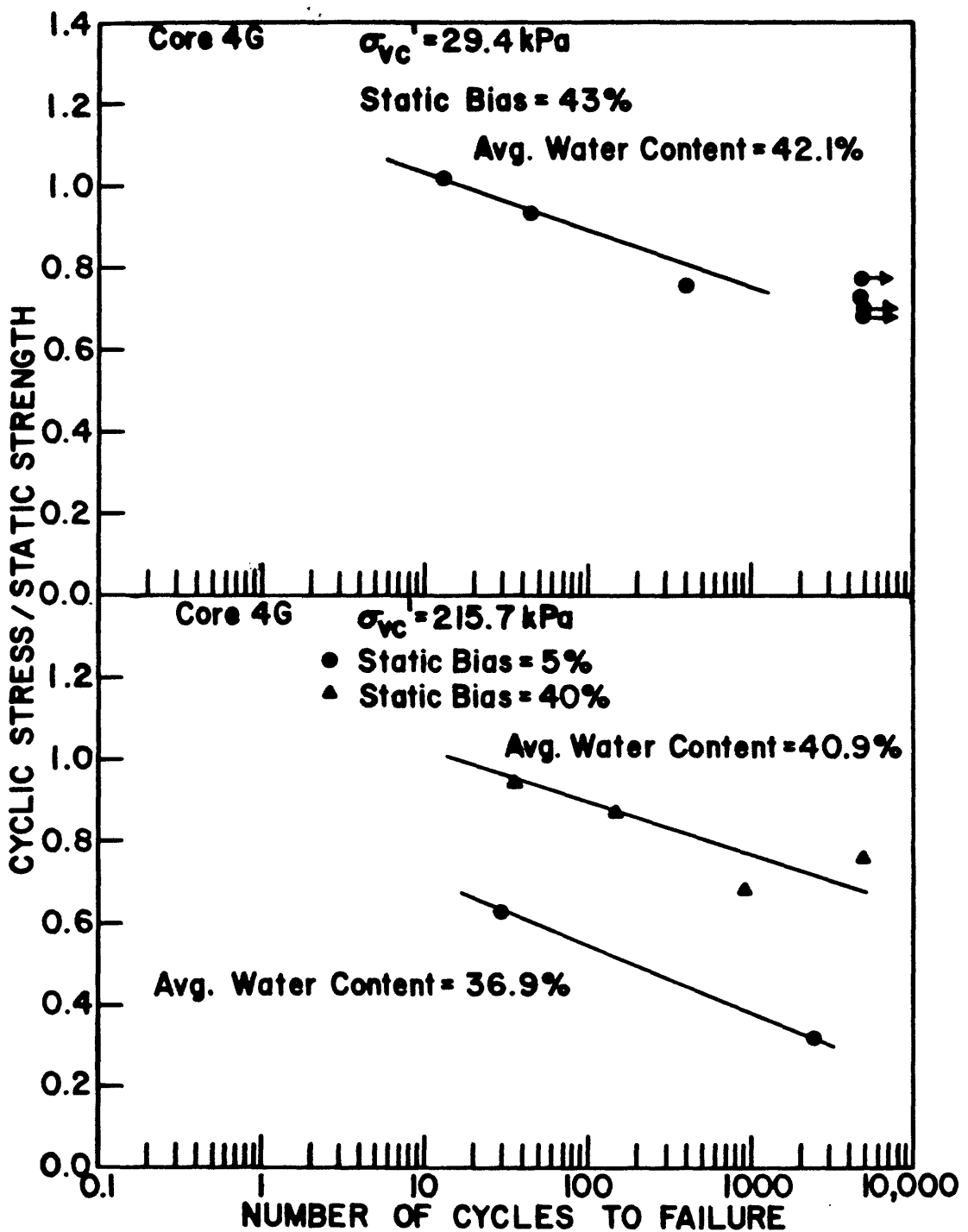


Figure 36. Relative cyclic stress level versus number of cycles to failure: Core 4G (Copper River Study area).

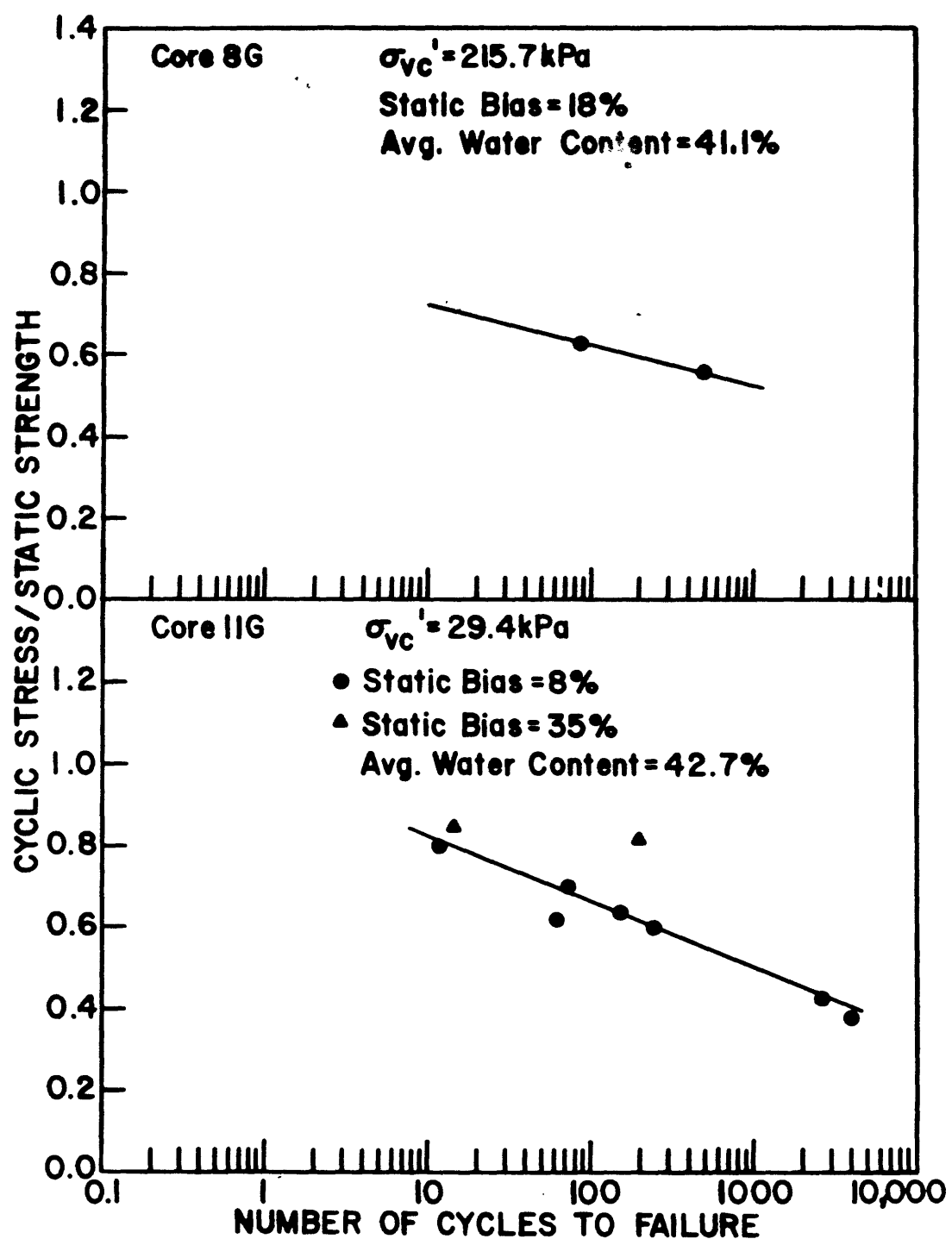


Figure 37. Relative cyclic stress level versus number of cycles to failure: Cores 8G and 11G (Copper River and Kayak Trough Study Areas).

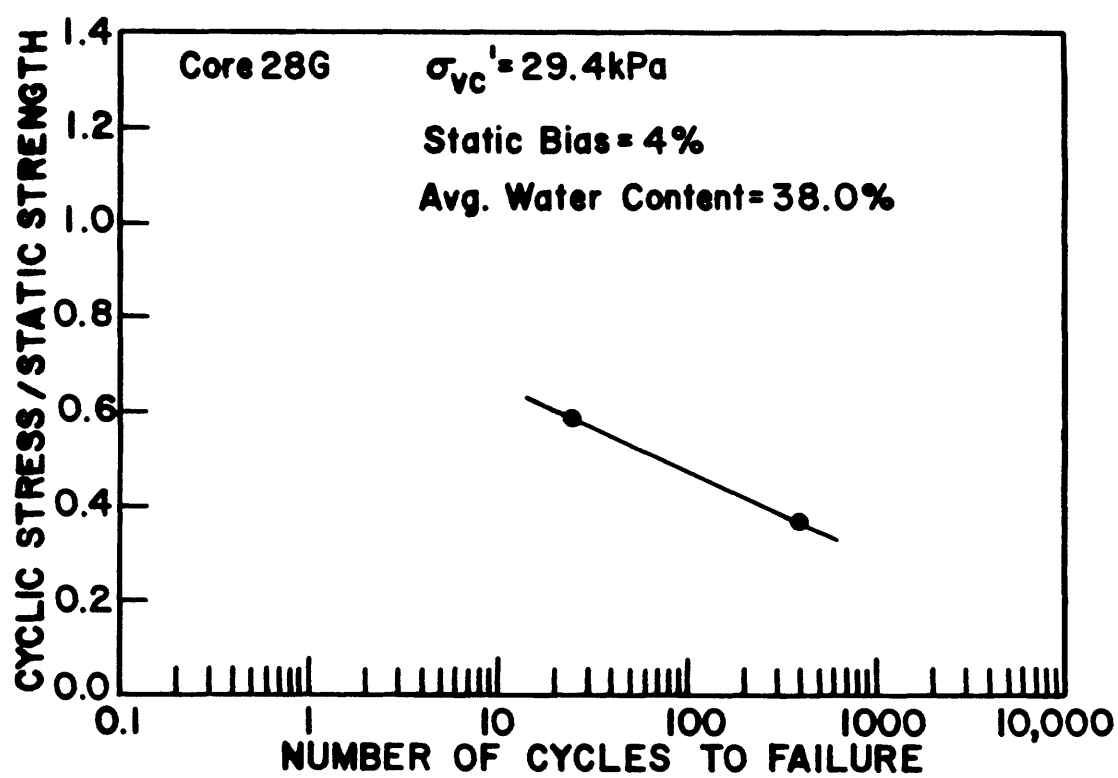


Figure 38. Relative cyclic stress level versus number of cycles to failure: Core 28G (Icy Bay-Malaspina Study Area).

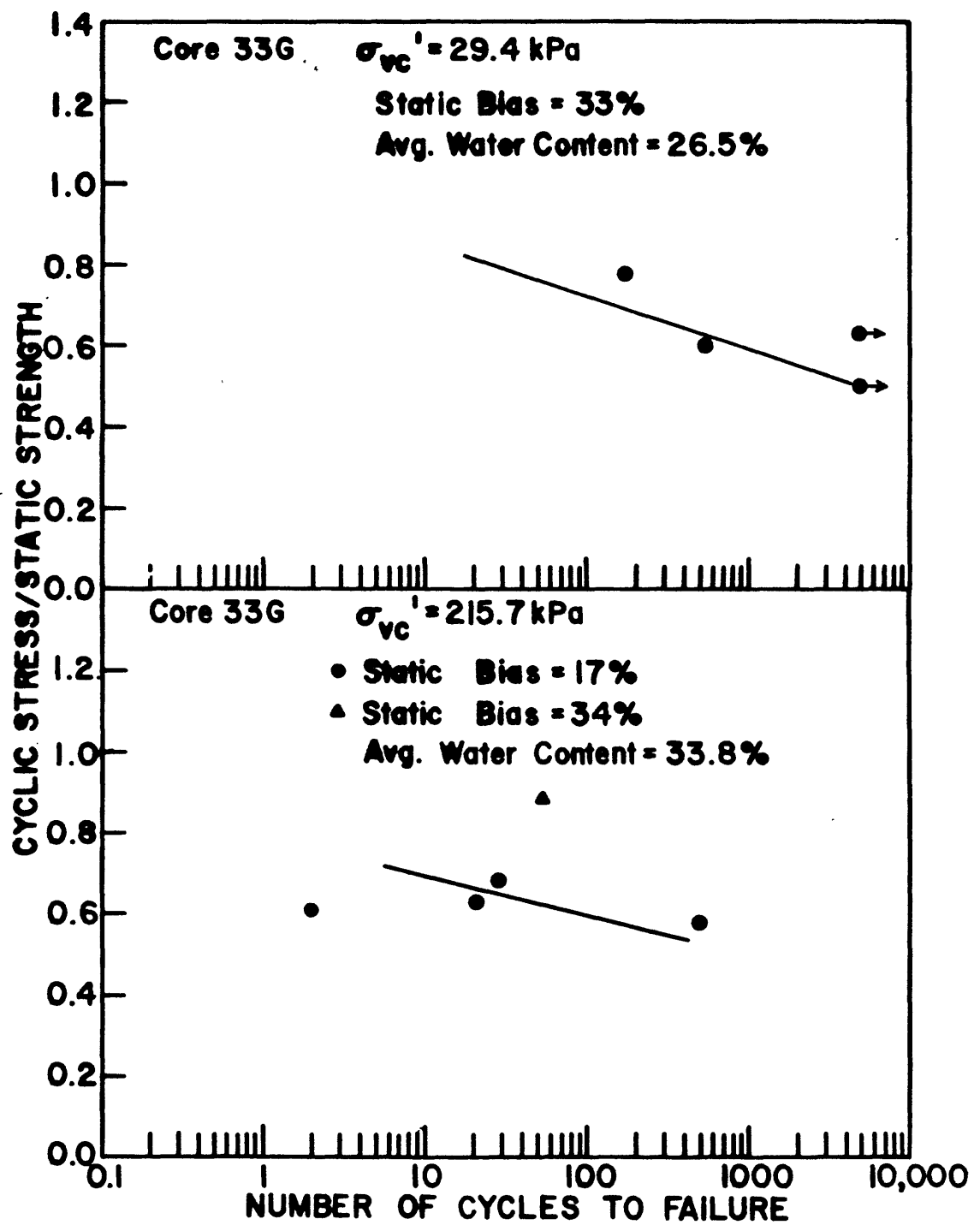


Figure 39. Relative cyclic stress level versus number of cycles to failure: Core 33G (Icy Bay-Malaspina Study Area).

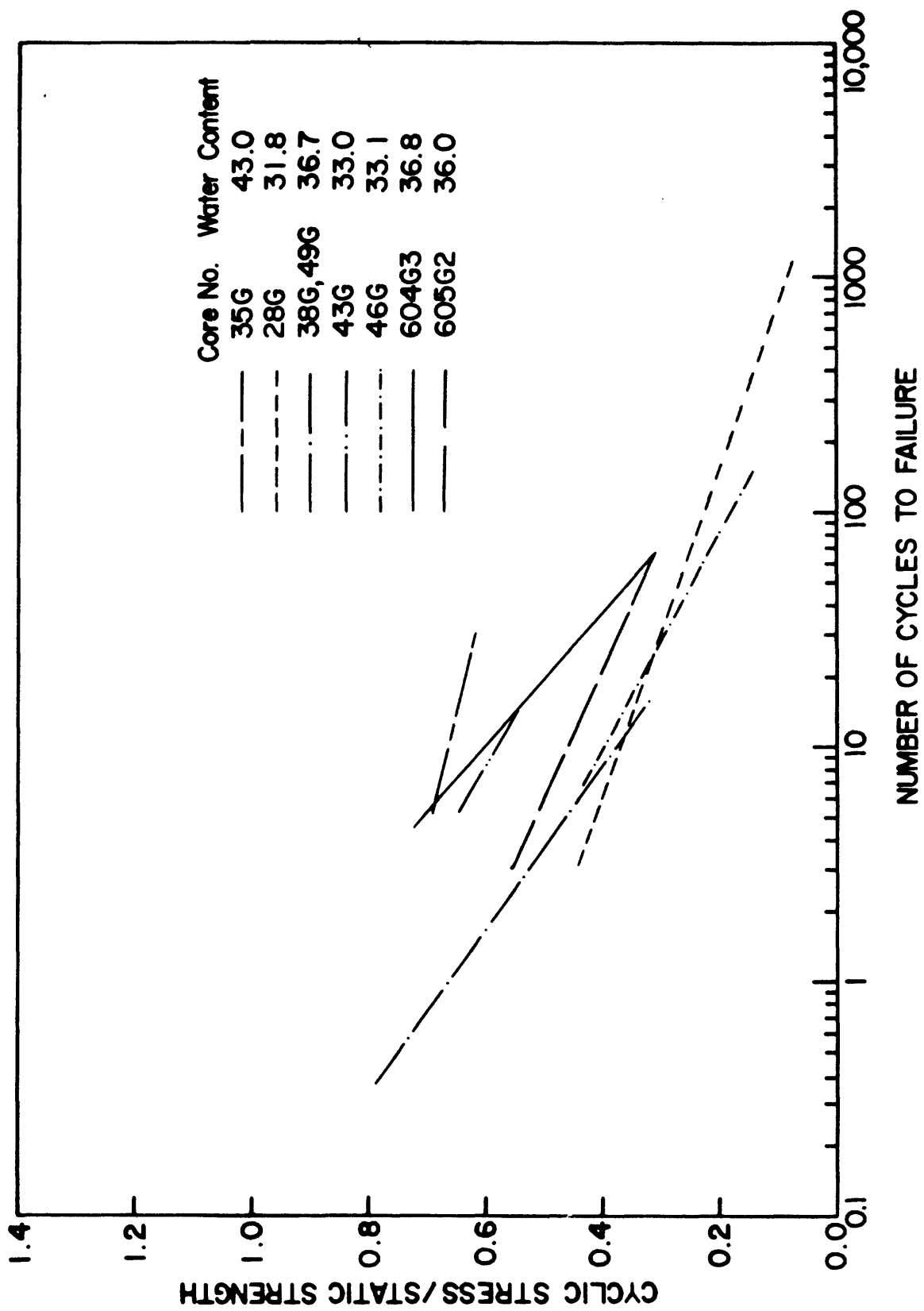
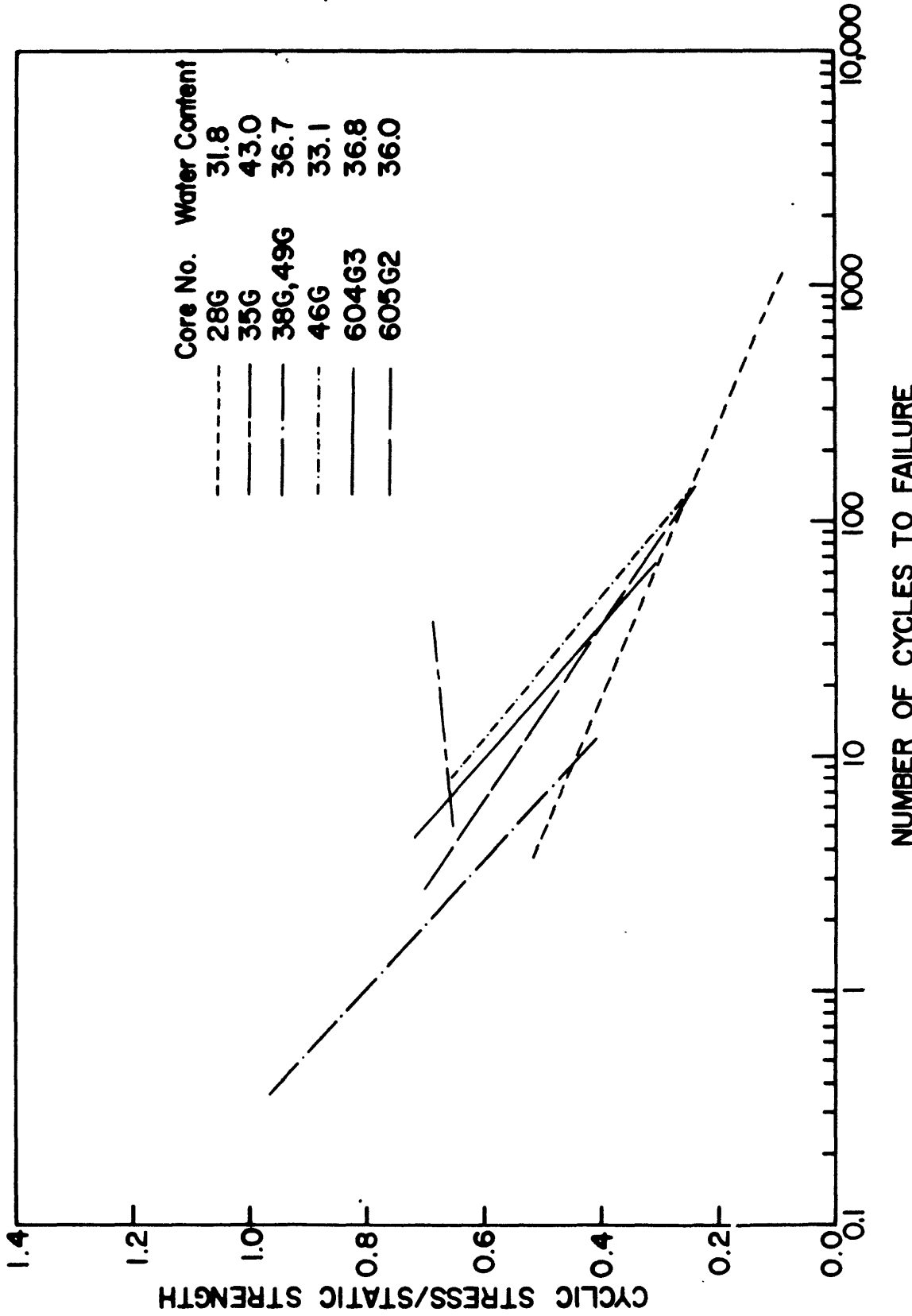


Figure 40. Relative cyclic stress level versus number of cycles to failure: Alsek River Study Area, Method I.



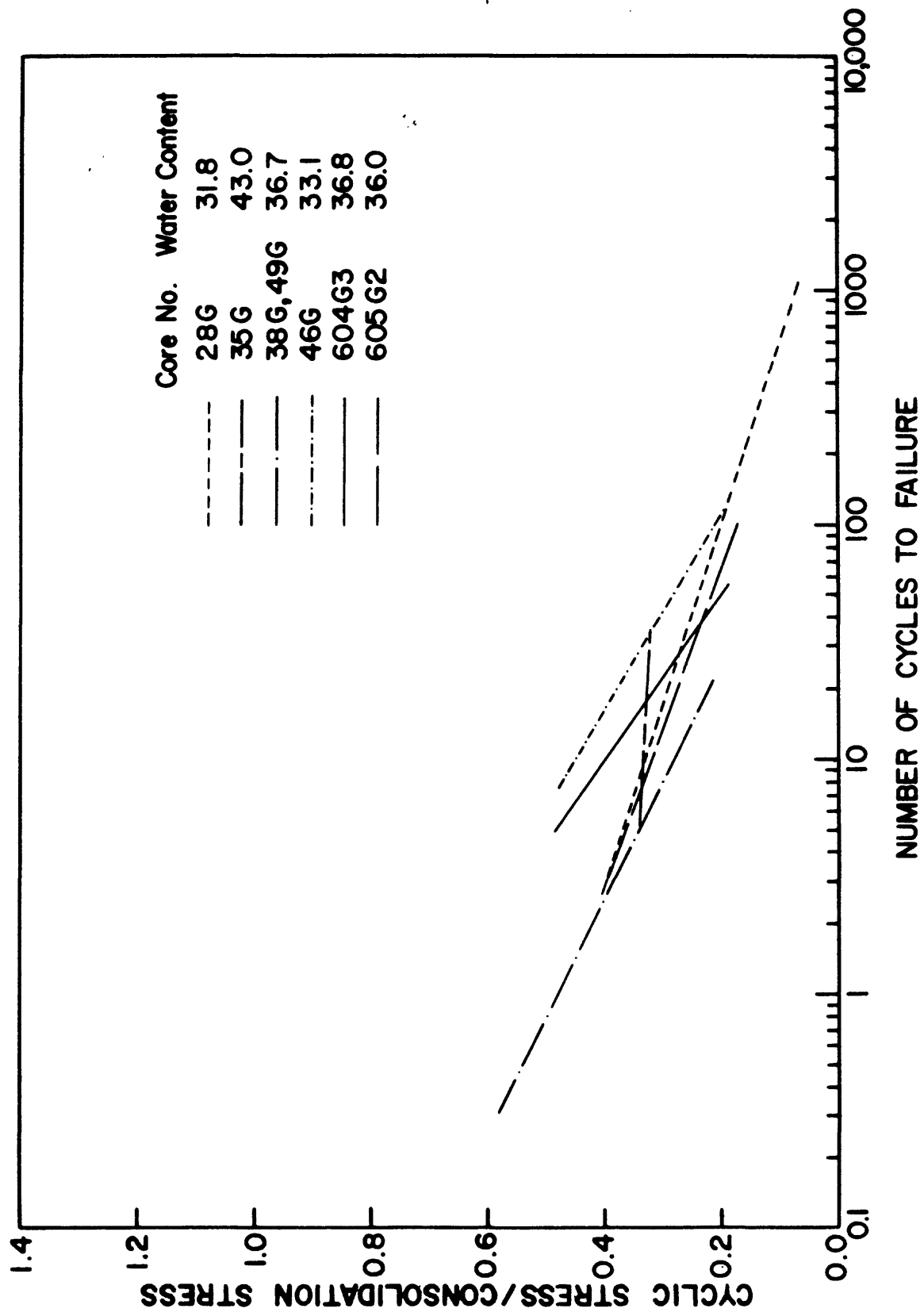


Figure 42. Relative cyclic stress level versus number of cycles to failure: Alsek River Study Area, Method III.

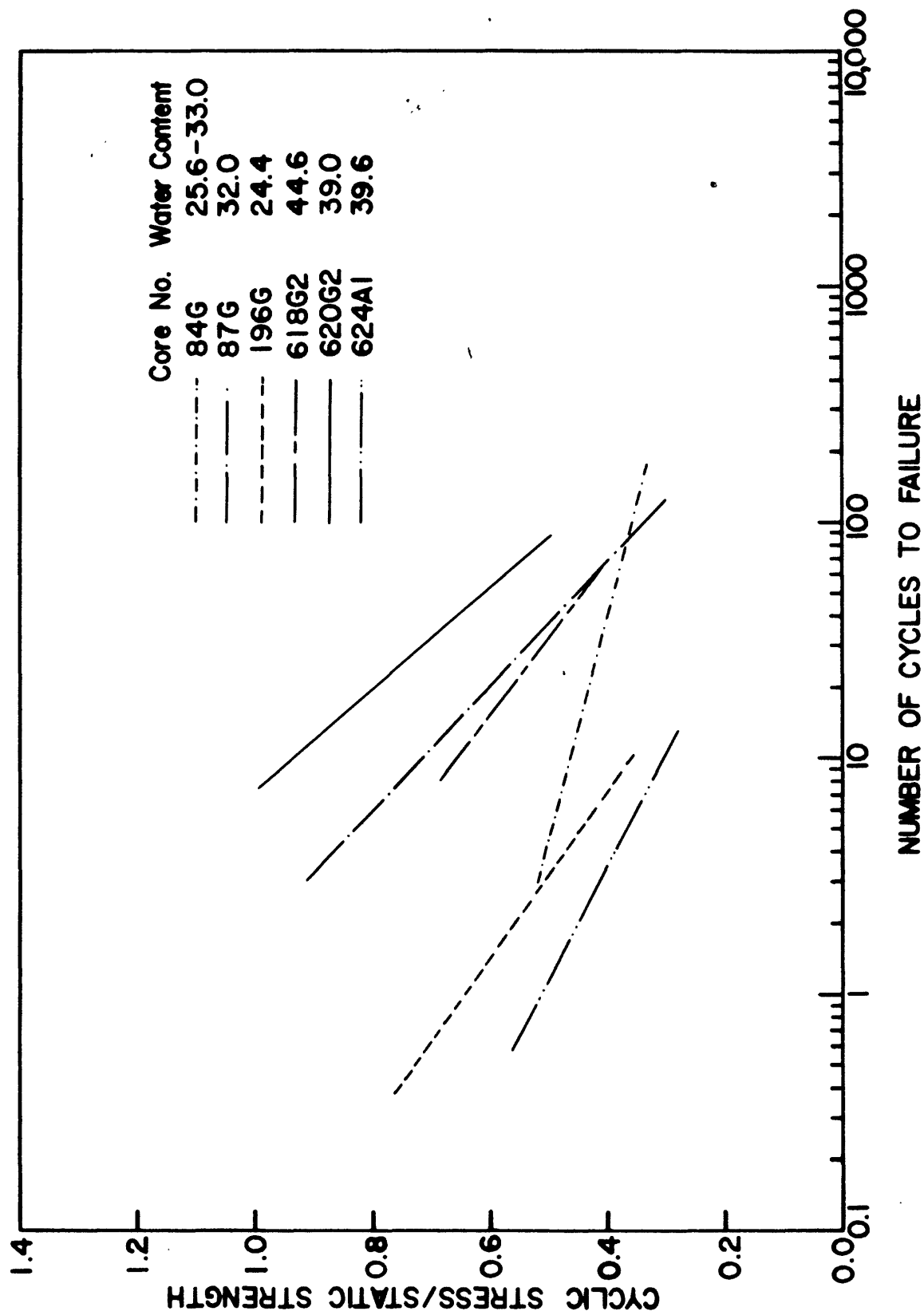


Figure 43. Relative cyclic stress level versus number of cycles to failure: Yakutat Study Area, Method I.

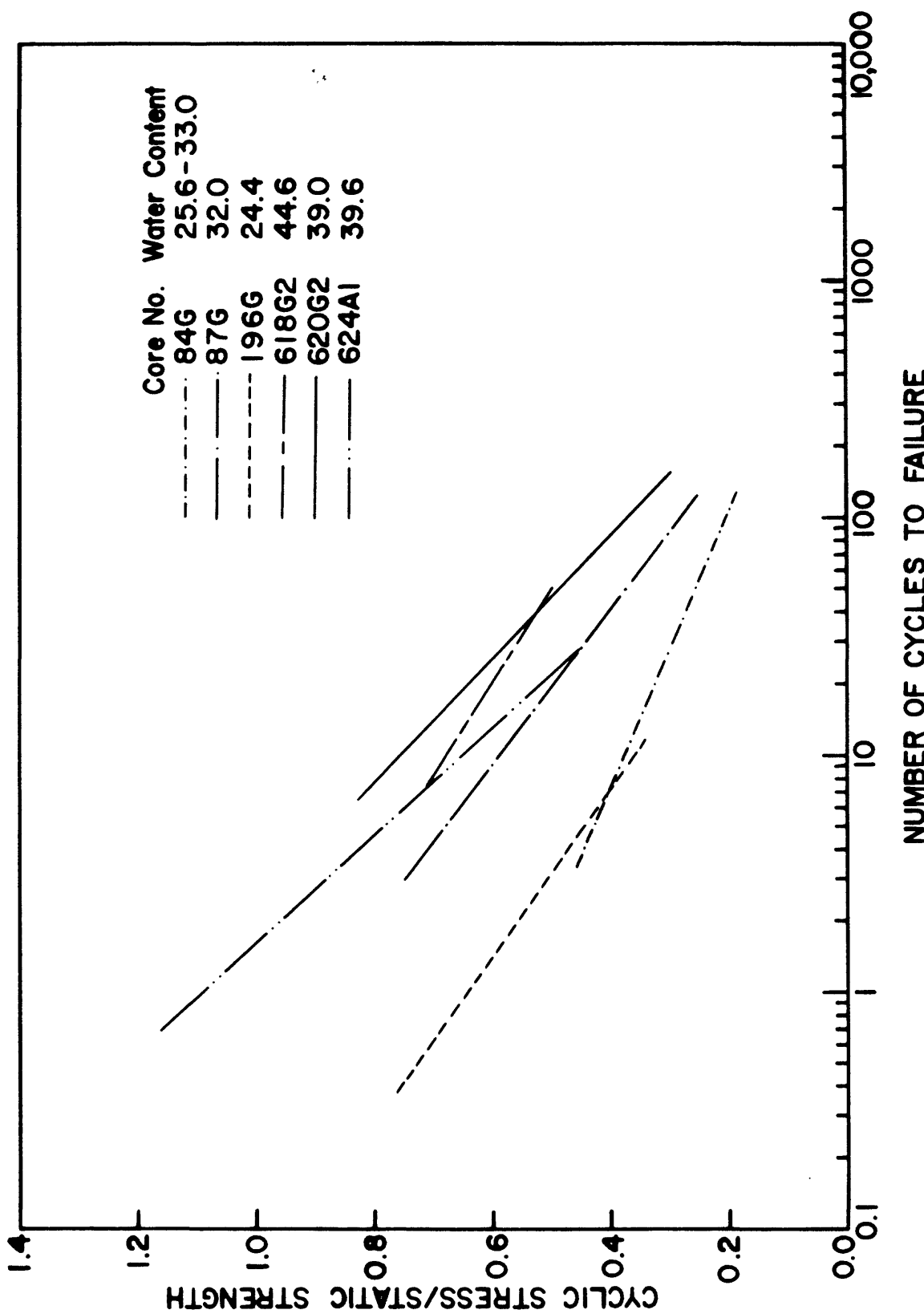


Figure 44. Relative cyclic stress level versus number of cycles to failure: Yakutat Study Area, Method II.

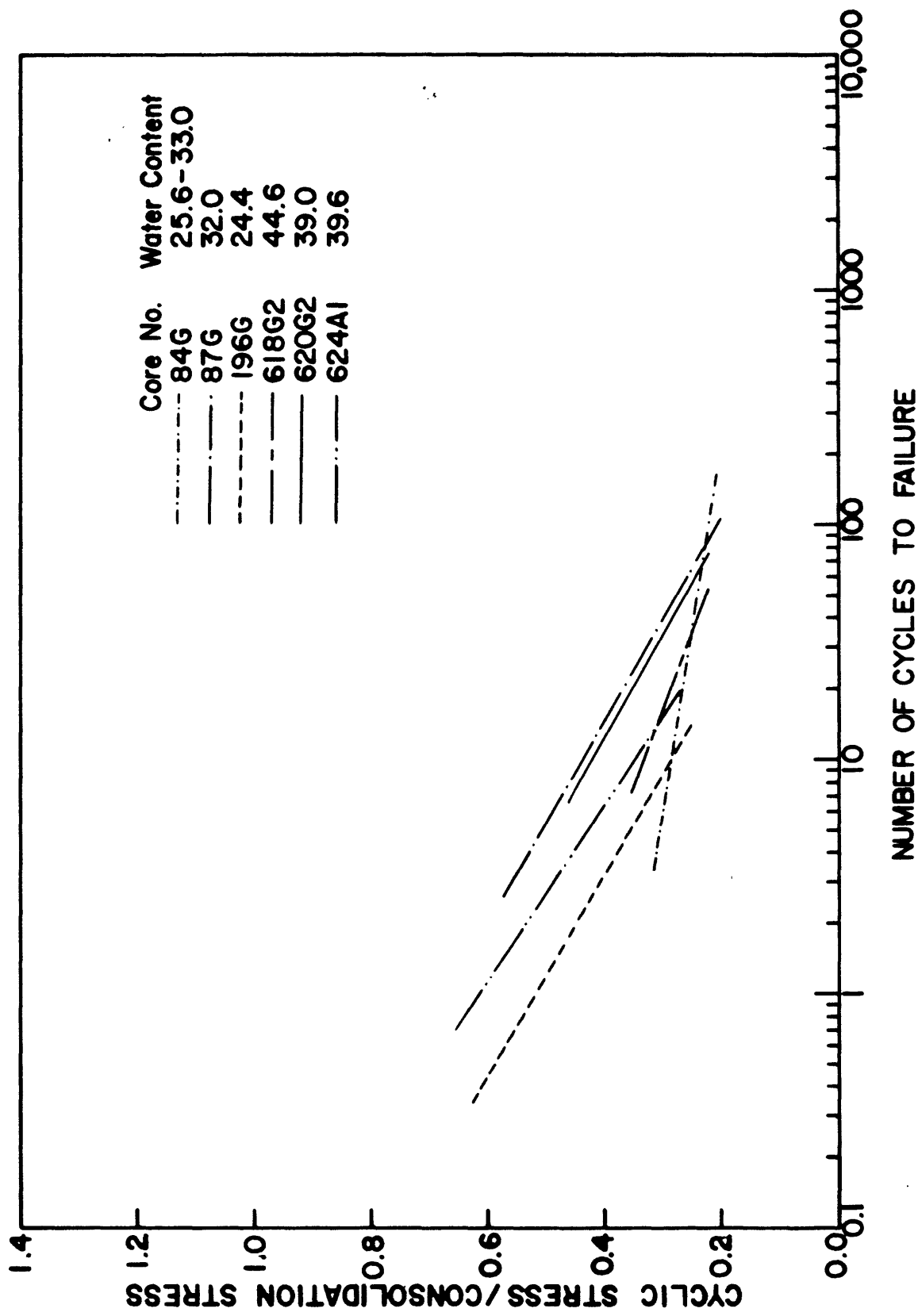


Figure 45. Relative cyclic stress level versus number of cycles to failure: Yakutat Study Area, Method III.

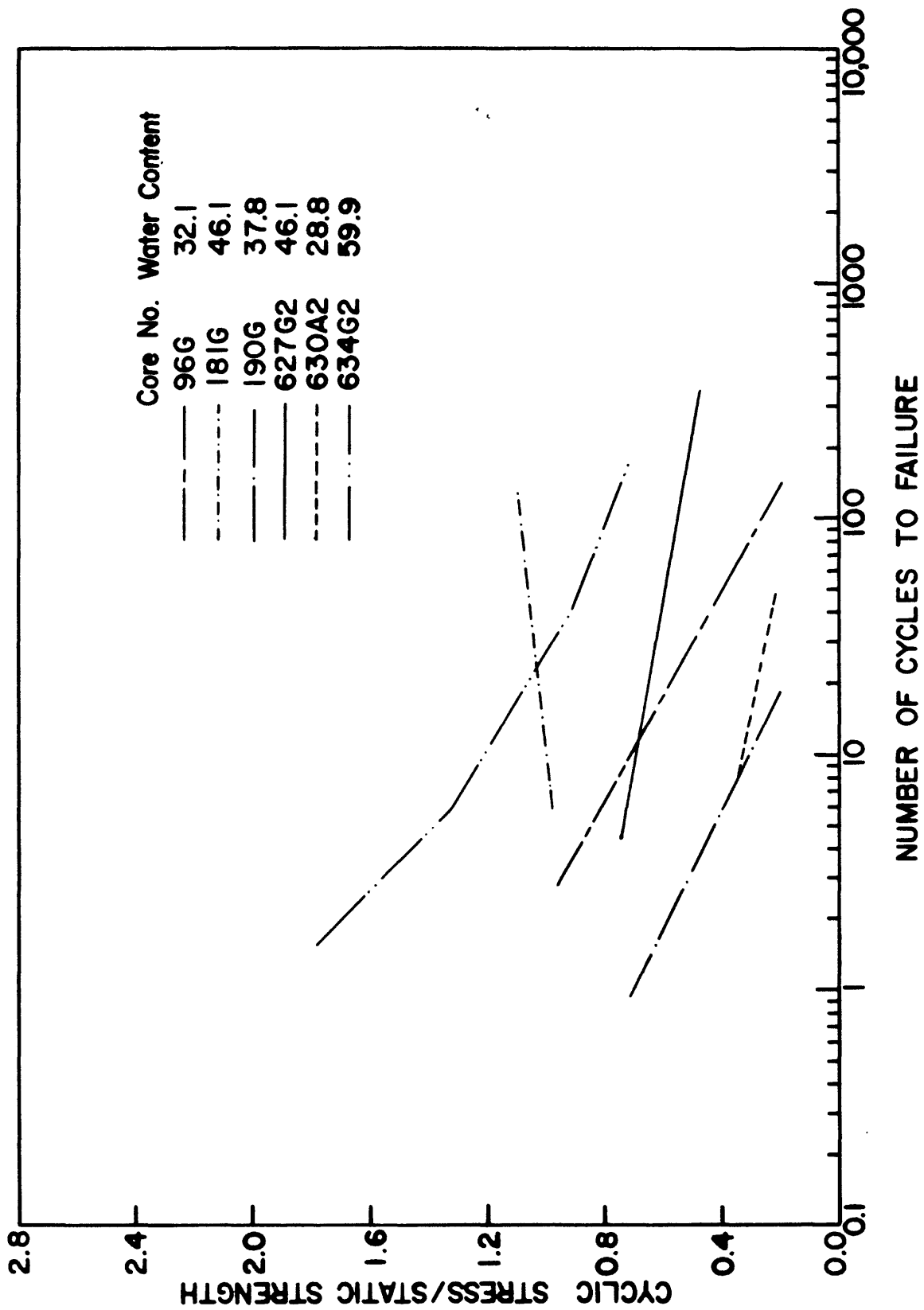


Figure 46. Relative cyclic stress level versus number of cycles to failure: Icy Bay-Malaspina Study Area (USGS testing), Method I.

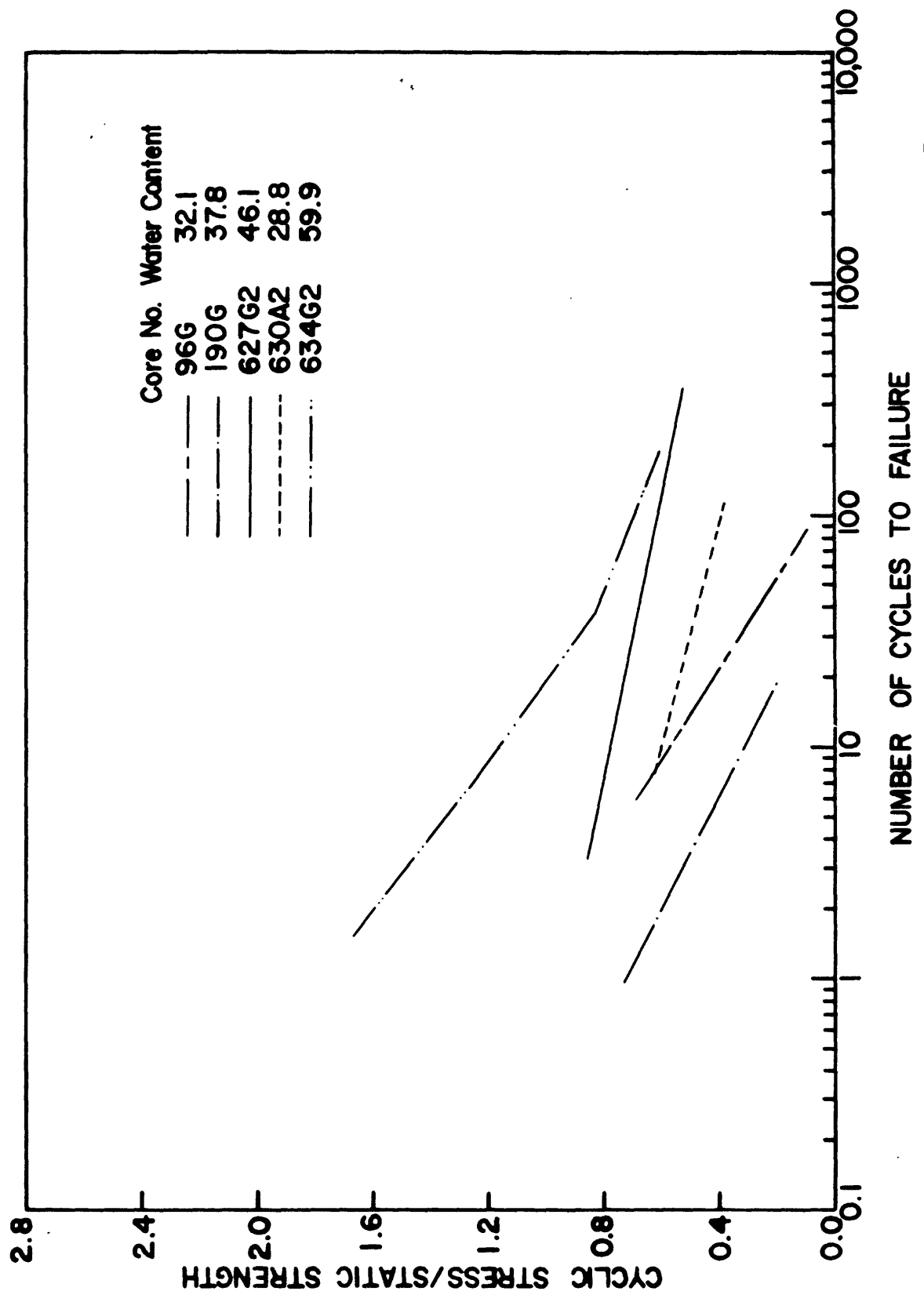


Figure 47. Relative cyclic stress level versus number of cycles to failure: Icy Bay-Malaspina Study Area (USGS testing), Method II.

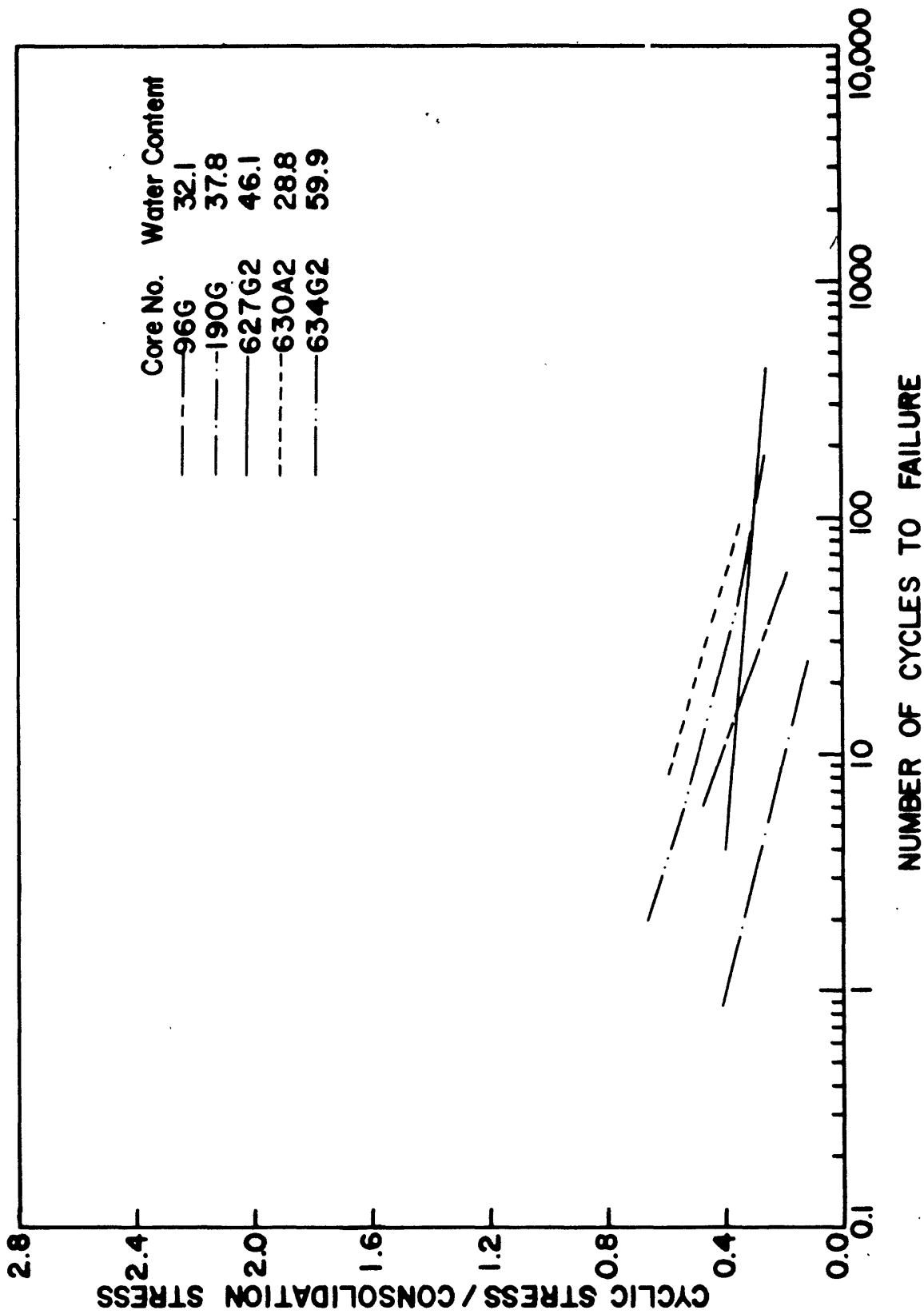


Figure 48. Relative cyclic stress level versus number of cycles to failure: Icy Bay-Malaspina Study Area (USGS testing), Method III.

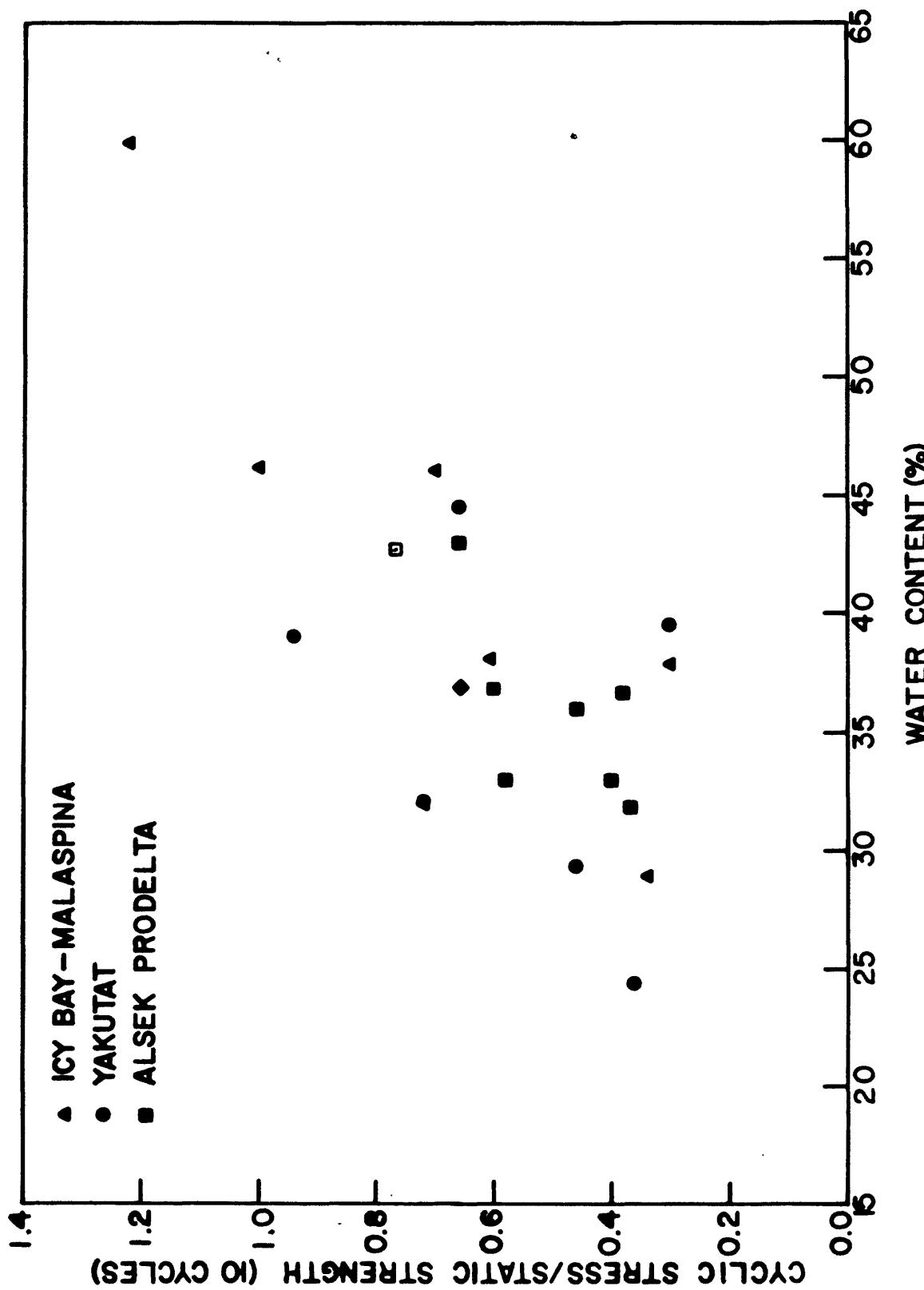


Figure 49. Relative cyclic stress level for failure in 10 cycles versus natural water content. Method I.

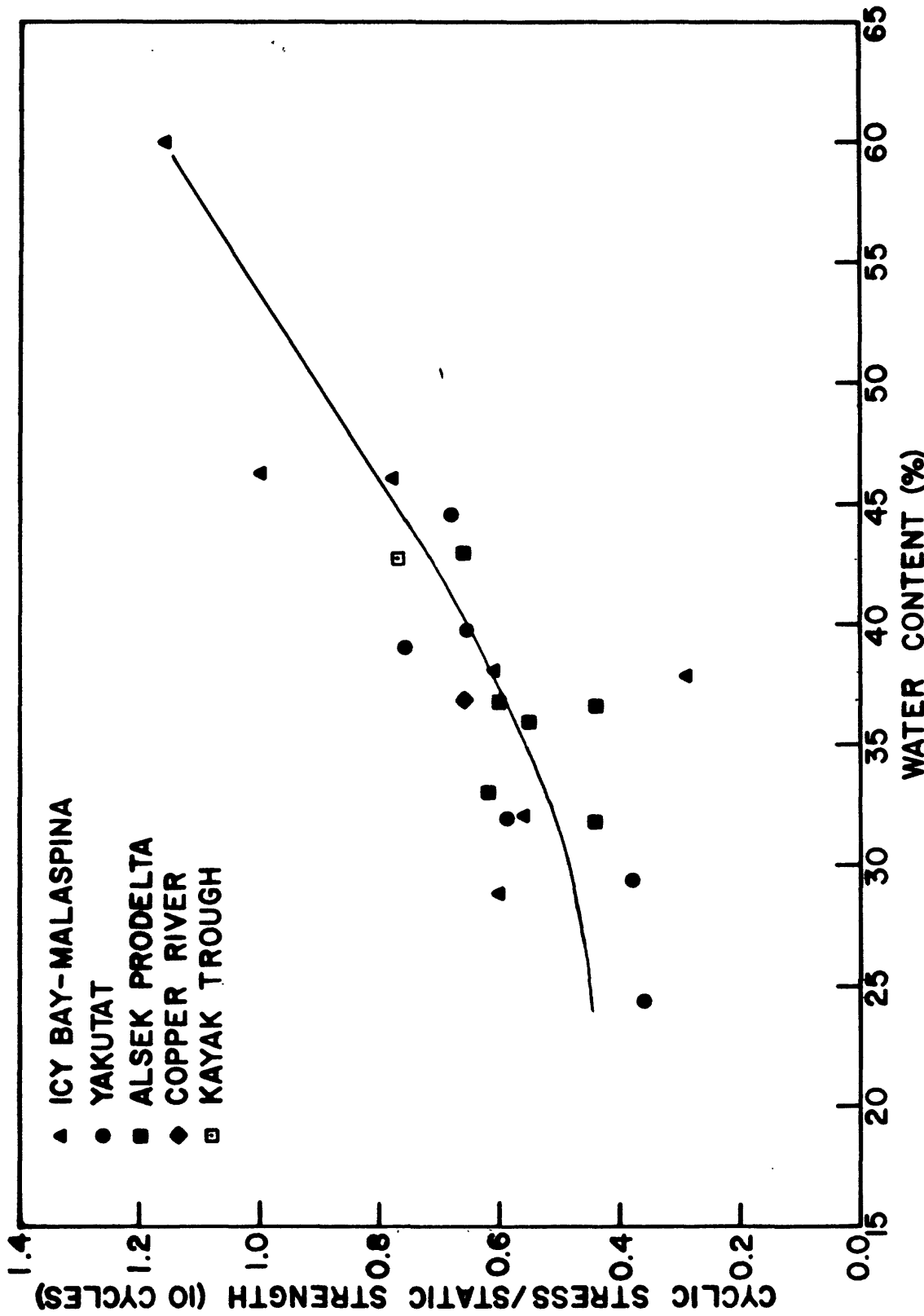


Figure 50. Relative cyclic stress level for failure in 10 cycles versus natural water content, Method II.

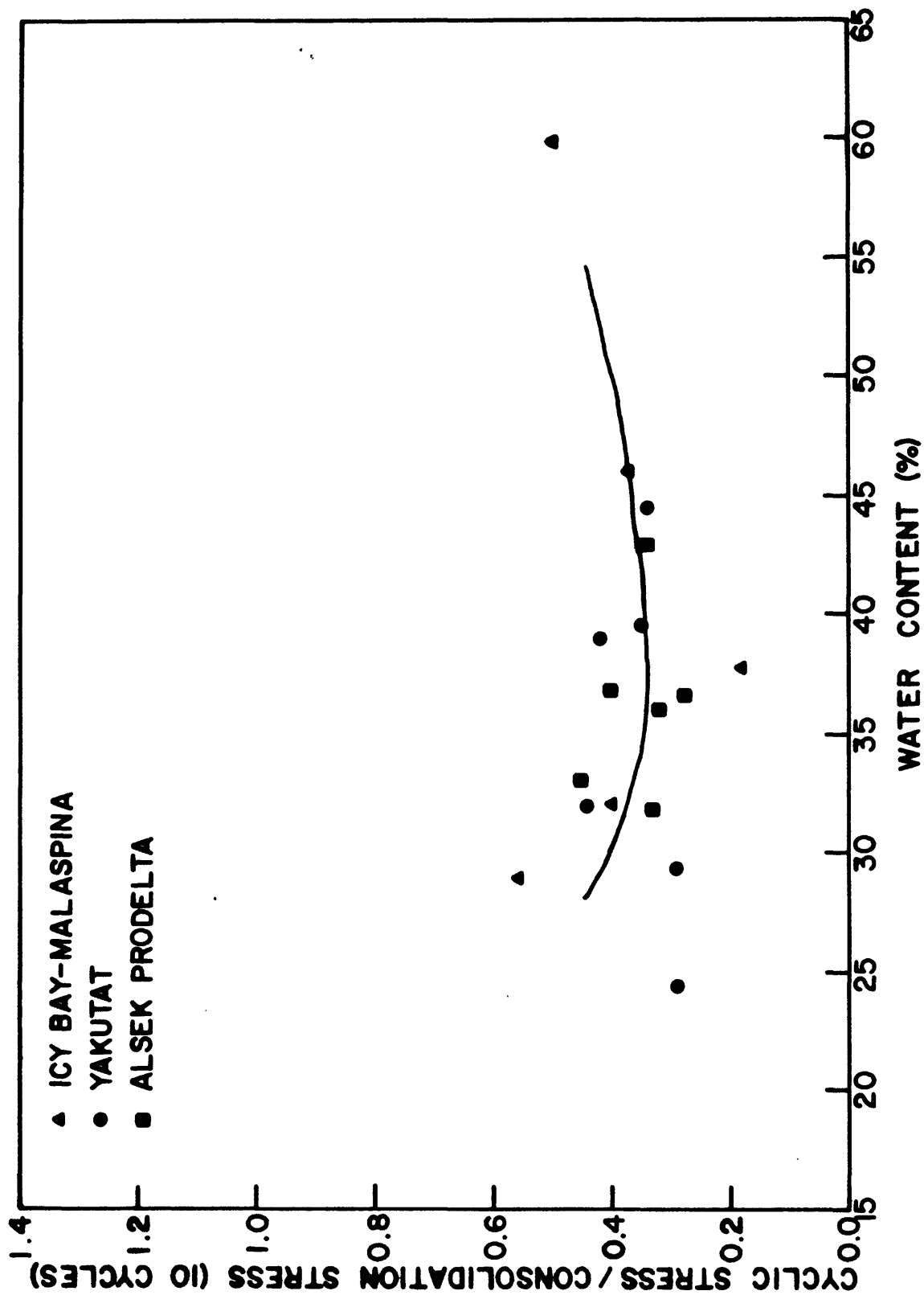


Figure 51. Relative cyclic stress level for failure in 10 cycles versus natural water content, Method III.

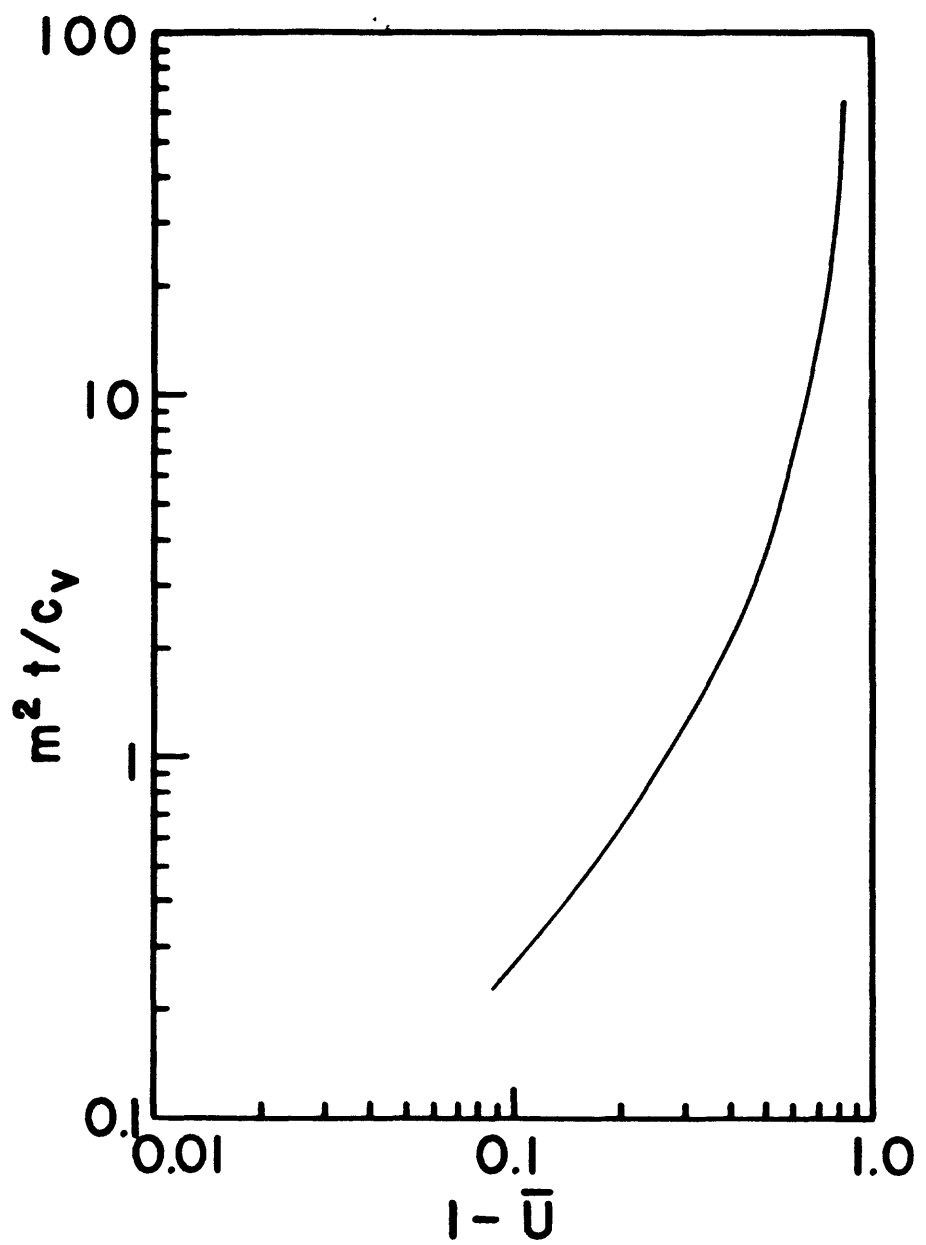


Figure 52. Predicted degree of consolidation ( $U$ ) at the base of a sediment column that has been deposited at a steady rate,  $m$ , for  $t$  years (after Gibson, 1958).

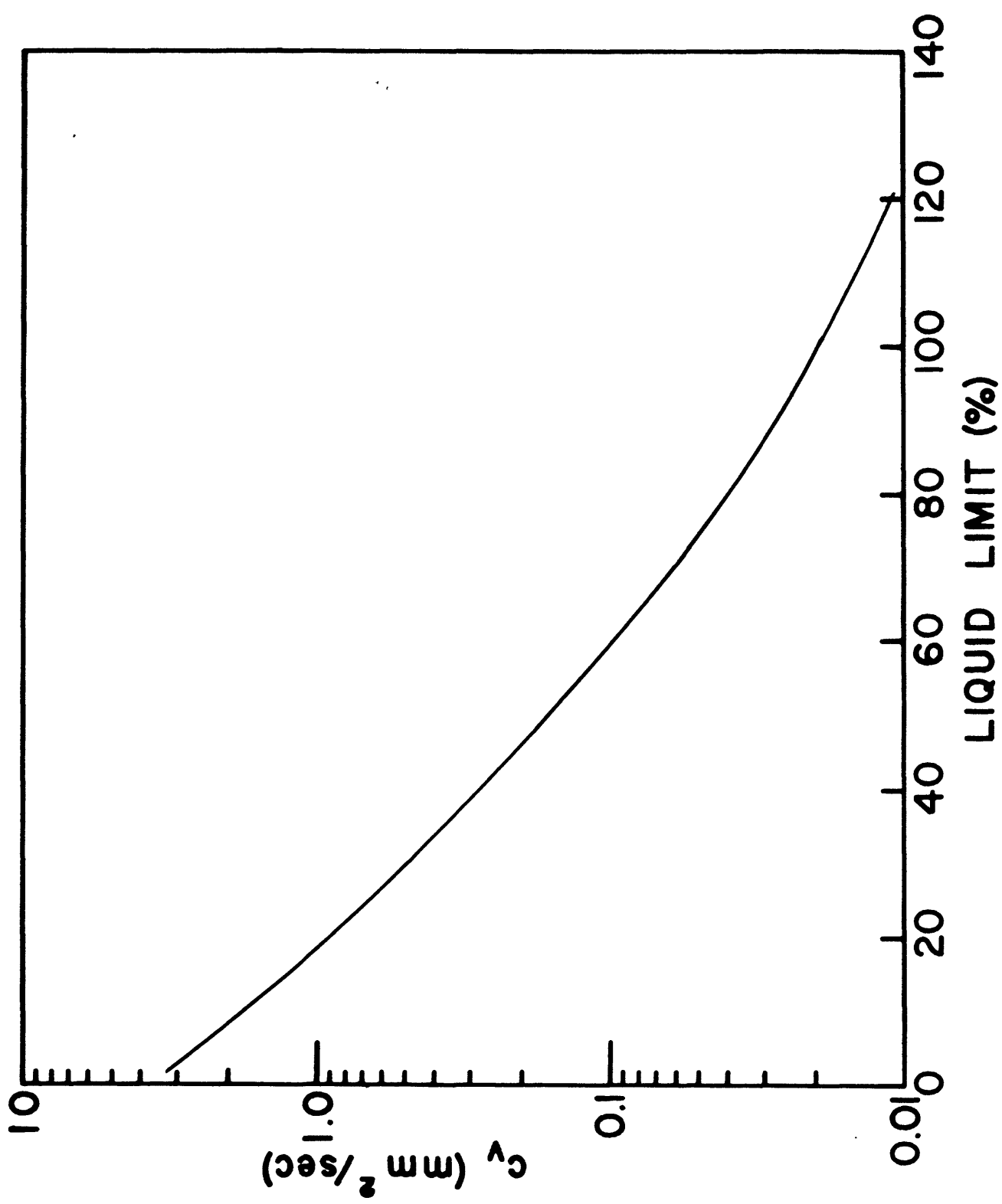


Figure 53. Correlation between coefficient of consolidation ( $c_v$ ) and liquid limit (after Lambe and Whittman, 1969, p. 412).

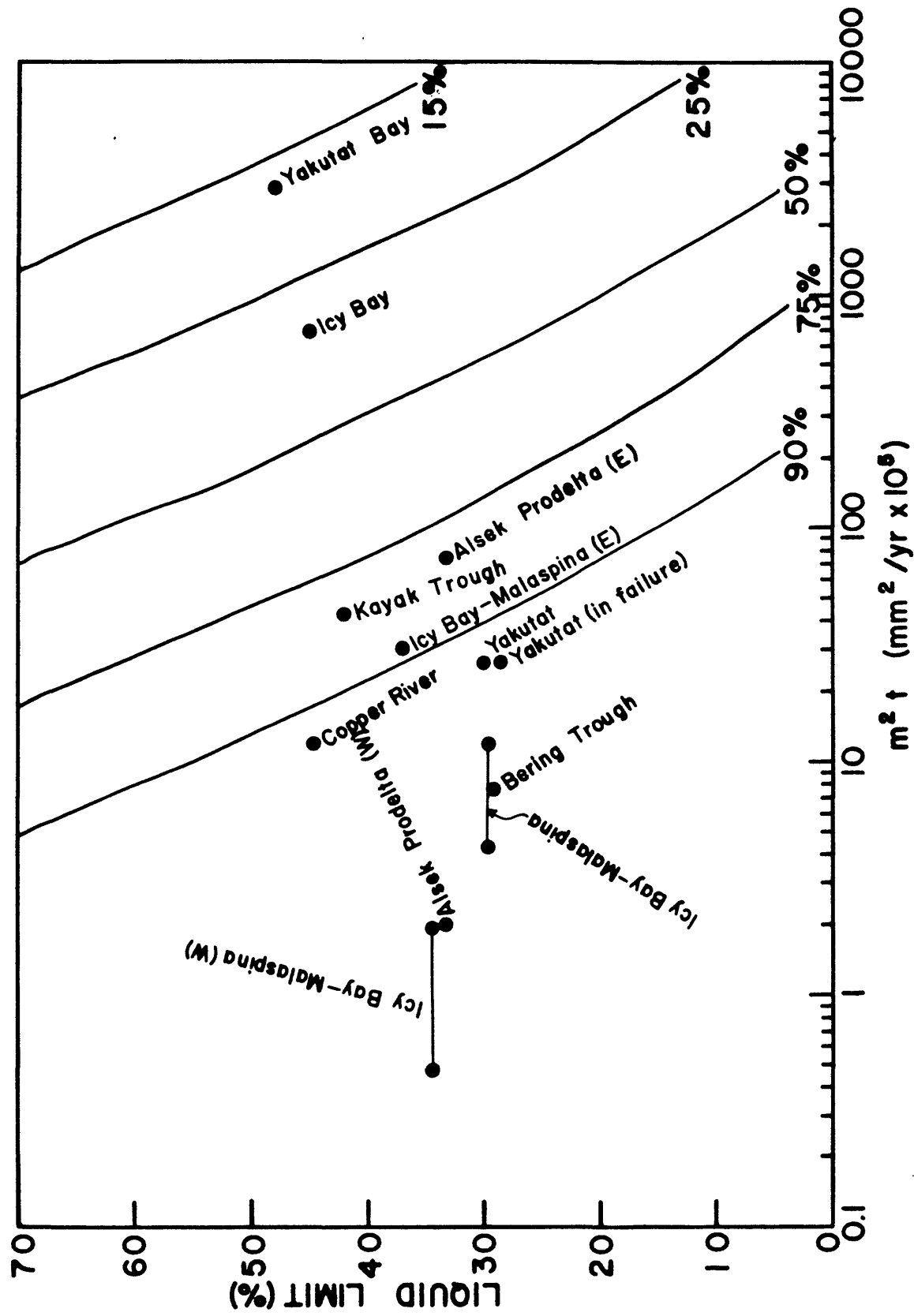


Figure 54. Solid lines represent constant degrees of consolidation,  $U$ , predicted by the Gibson (1958) technique. Selected locations in the eastern Gulf of Alaska for which the required parameters were available are shown as data points. Bars indicate a larger segment over which the sedimentation rate varies.

**Malaspina and Yakutat**

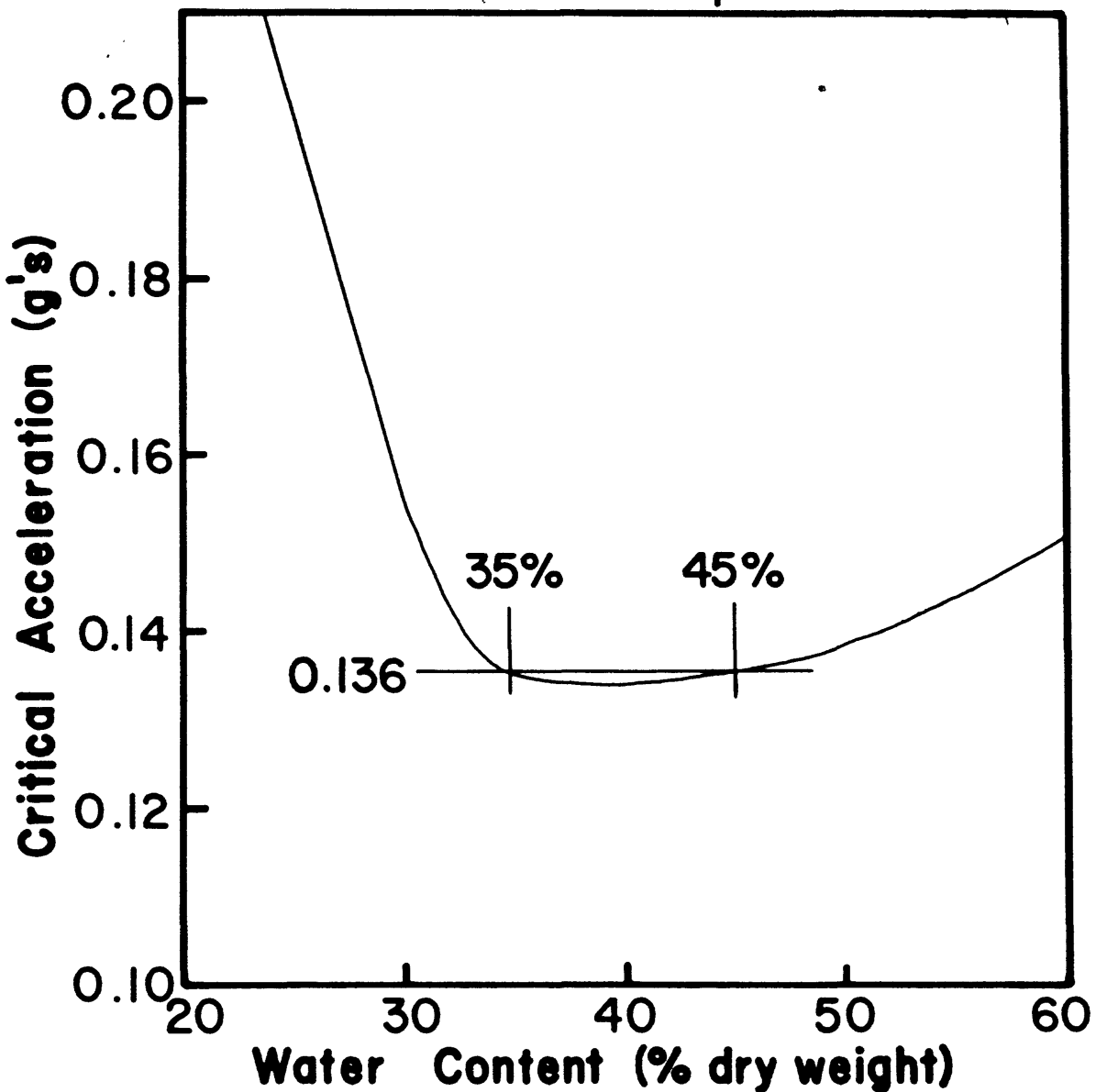


Figure 55. Estimate of critical earthquake acceleration,  $k$ , versus natural water content.

## % Of Core With 35 < Water Content < 45

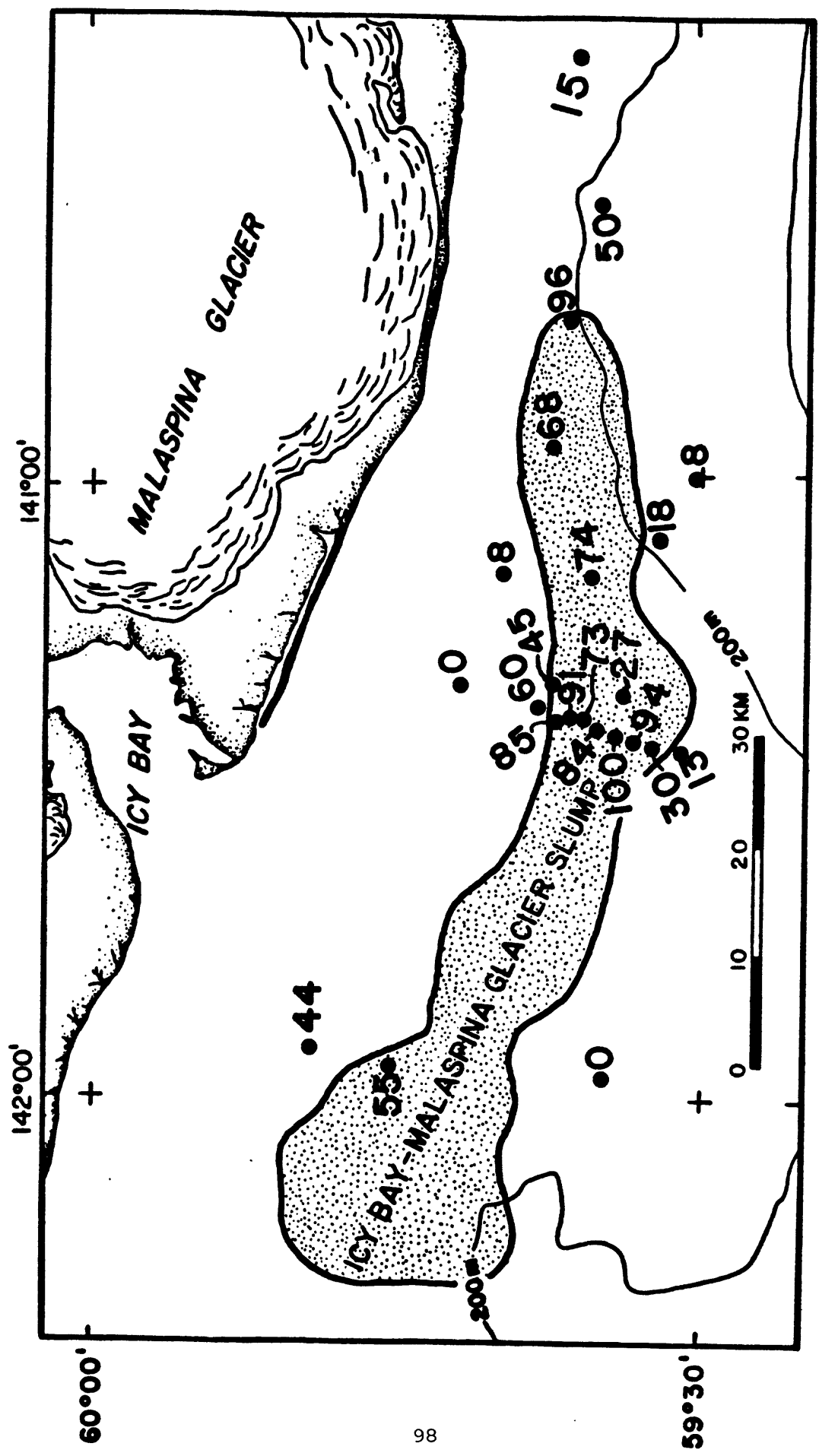
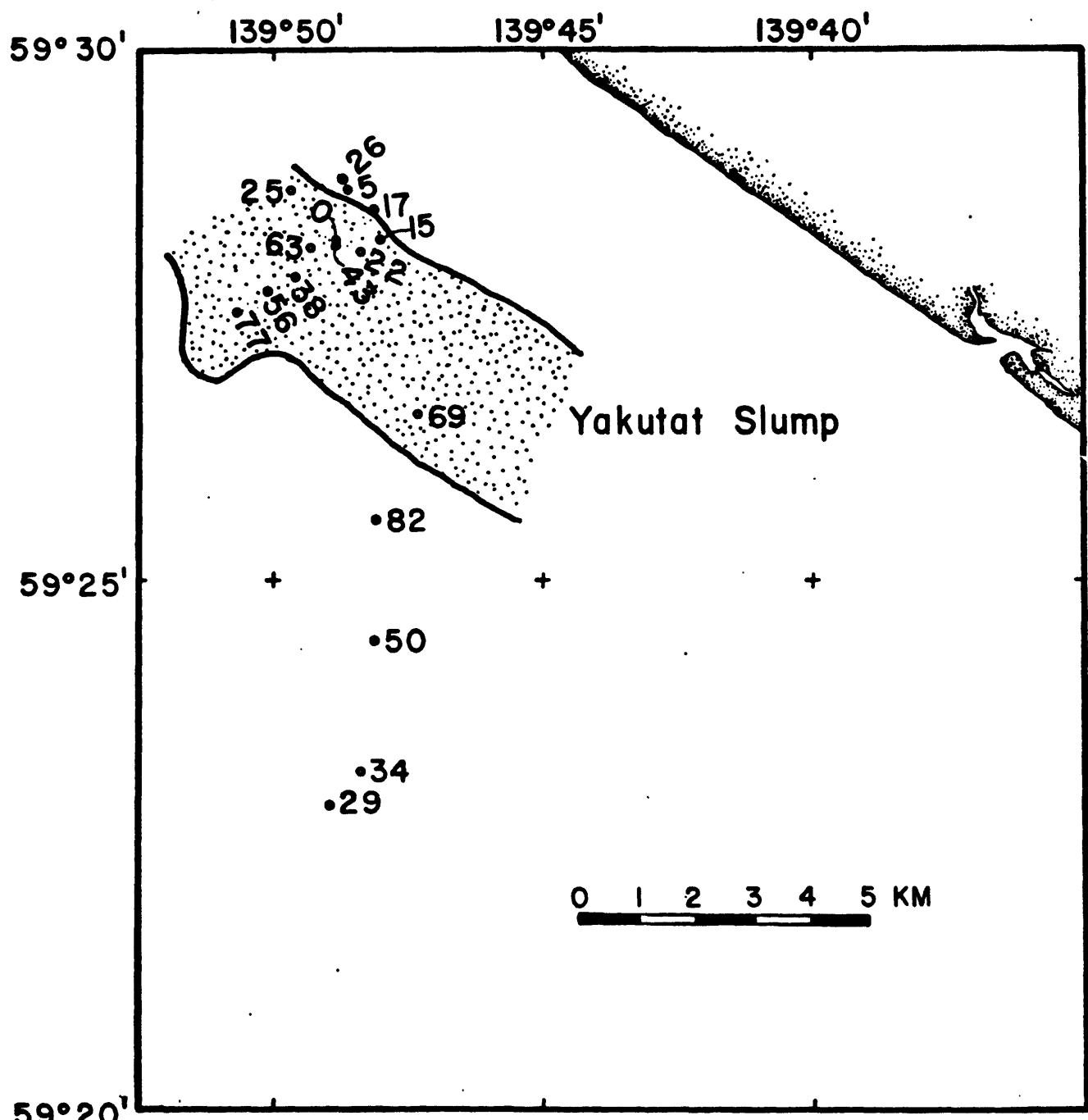


Figure 56. Locations of core samples within the Icy Bay-Malaspina Study Area relative to the observed slump feature. Numbers near the core locations represent the percentage of the core that has a water content in the critical 35% to 45% range.



### % Of Core With $35 < \text{Water Content} < 45$

Figure 57. Locations of core samples within the Yakutat Study Area relative to the observed slump feature. Numbers near the core locations represent the percentage of the core that has a water content in the critical 35% to 45% range.

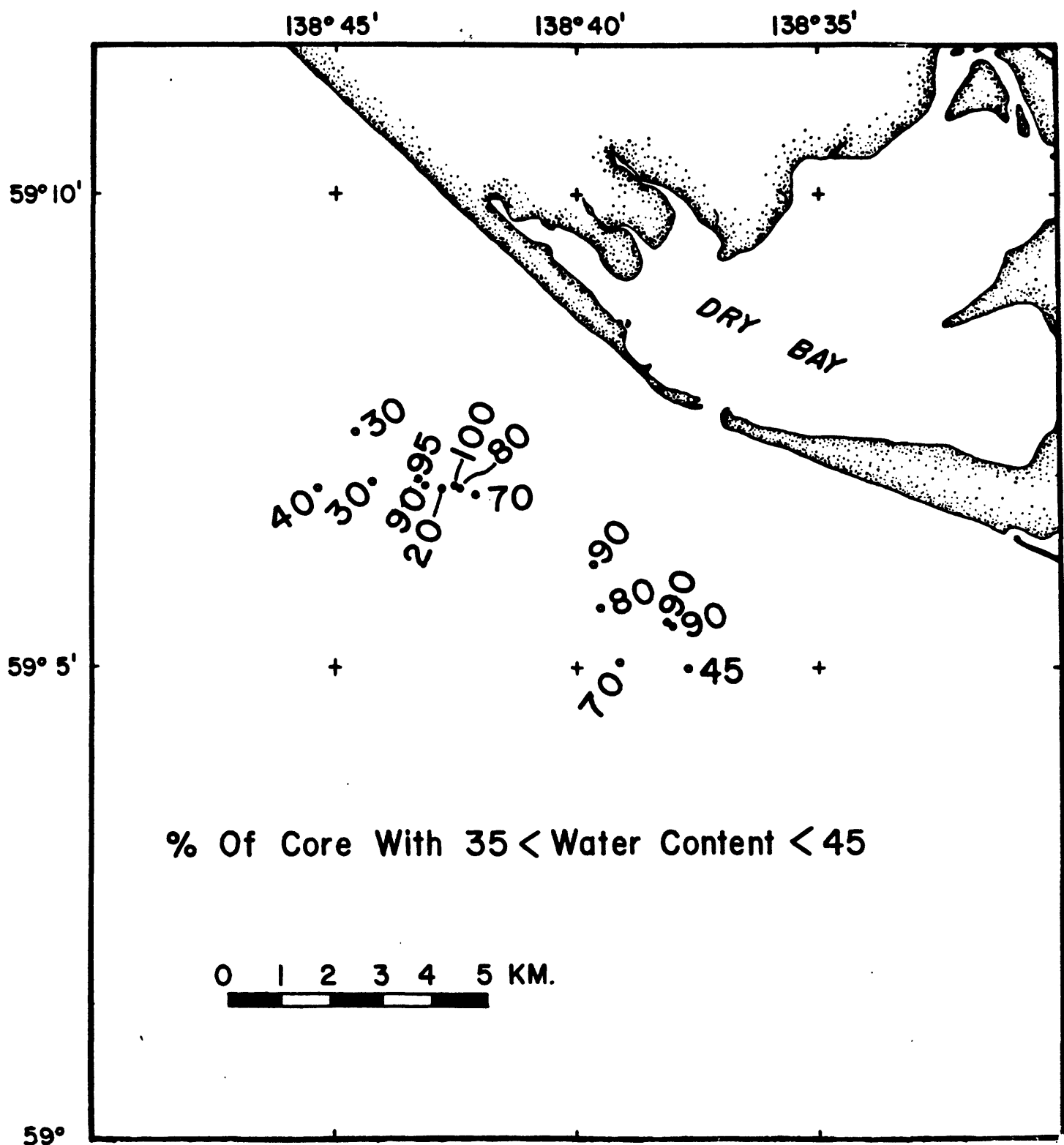


Figure 58. Locations of core samples within the Alsek River Study Area. Numbers near the core locations represent the percentage of the core that has a water content in the critical 35% to 45% range. All cores are thought to be in the failed zone.

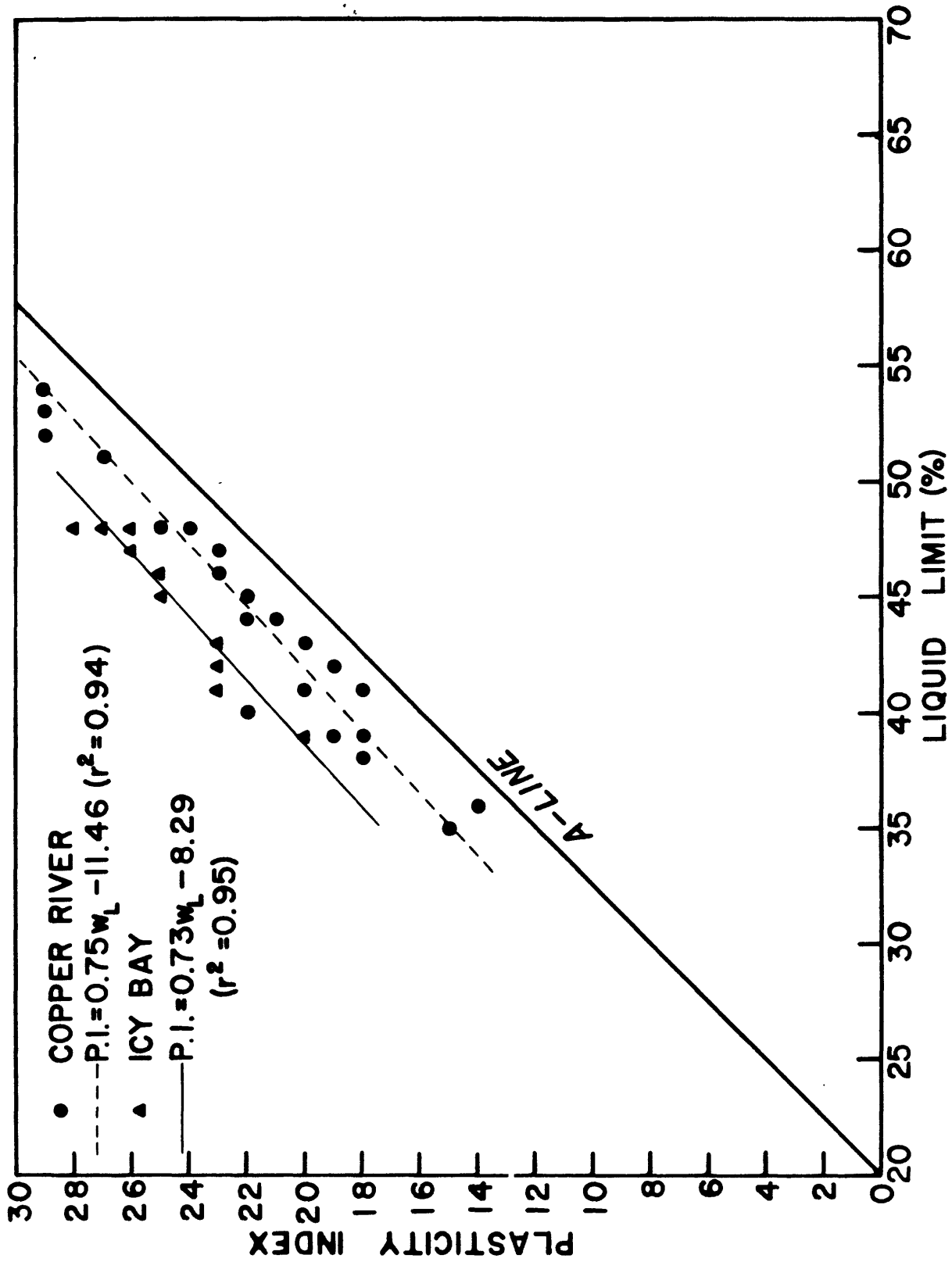


Figure 59. Plasticity chart for Copper River and Icy Bay Study Areas with least squares regression fits of the data.

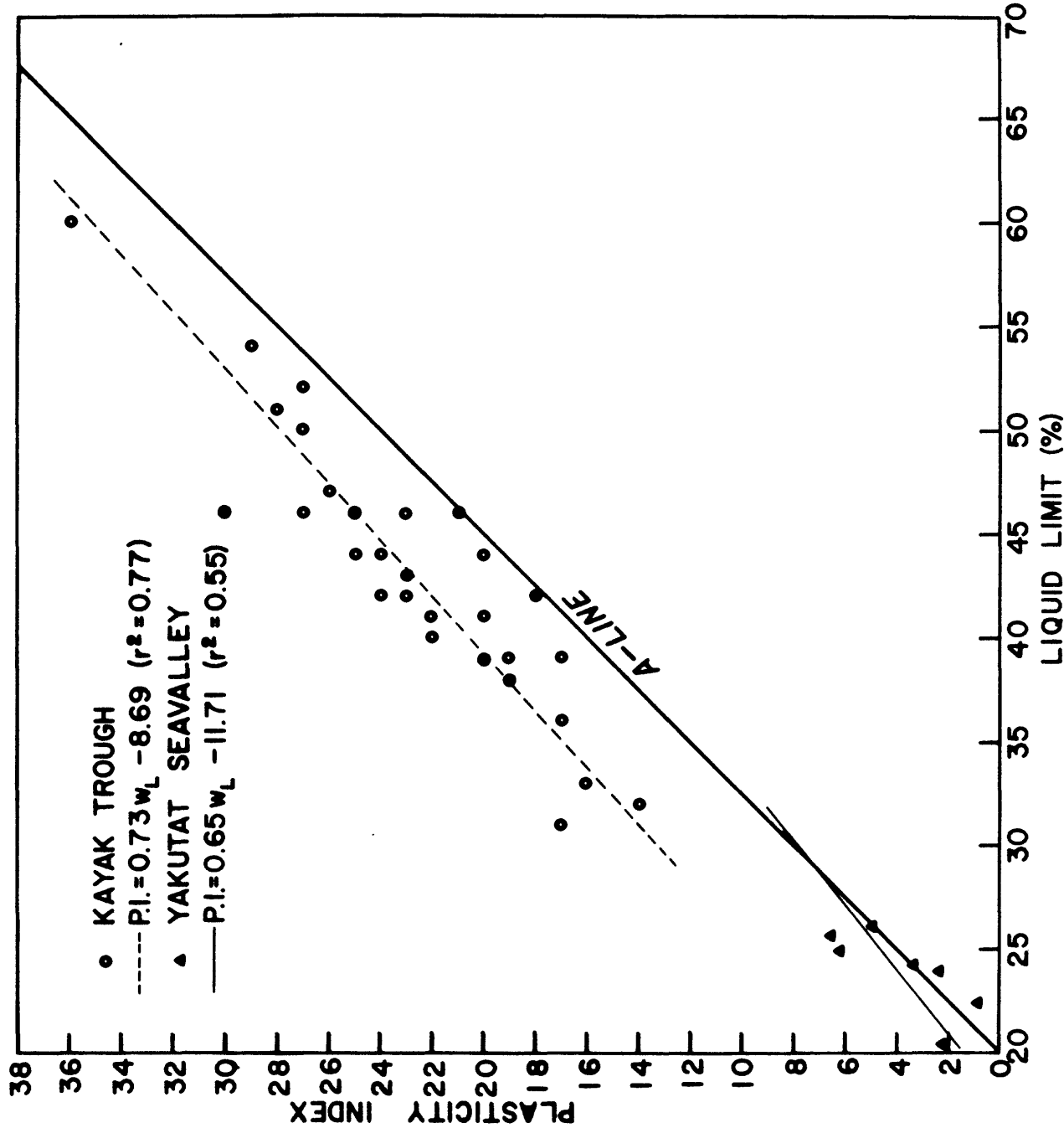


Figure 60. Plasticity chart for Kayak Trough Study Area and Yakutat Sea Valley (SE portion of Icy Bay-Mallaspina Study Area) with least squares regression fits of data.

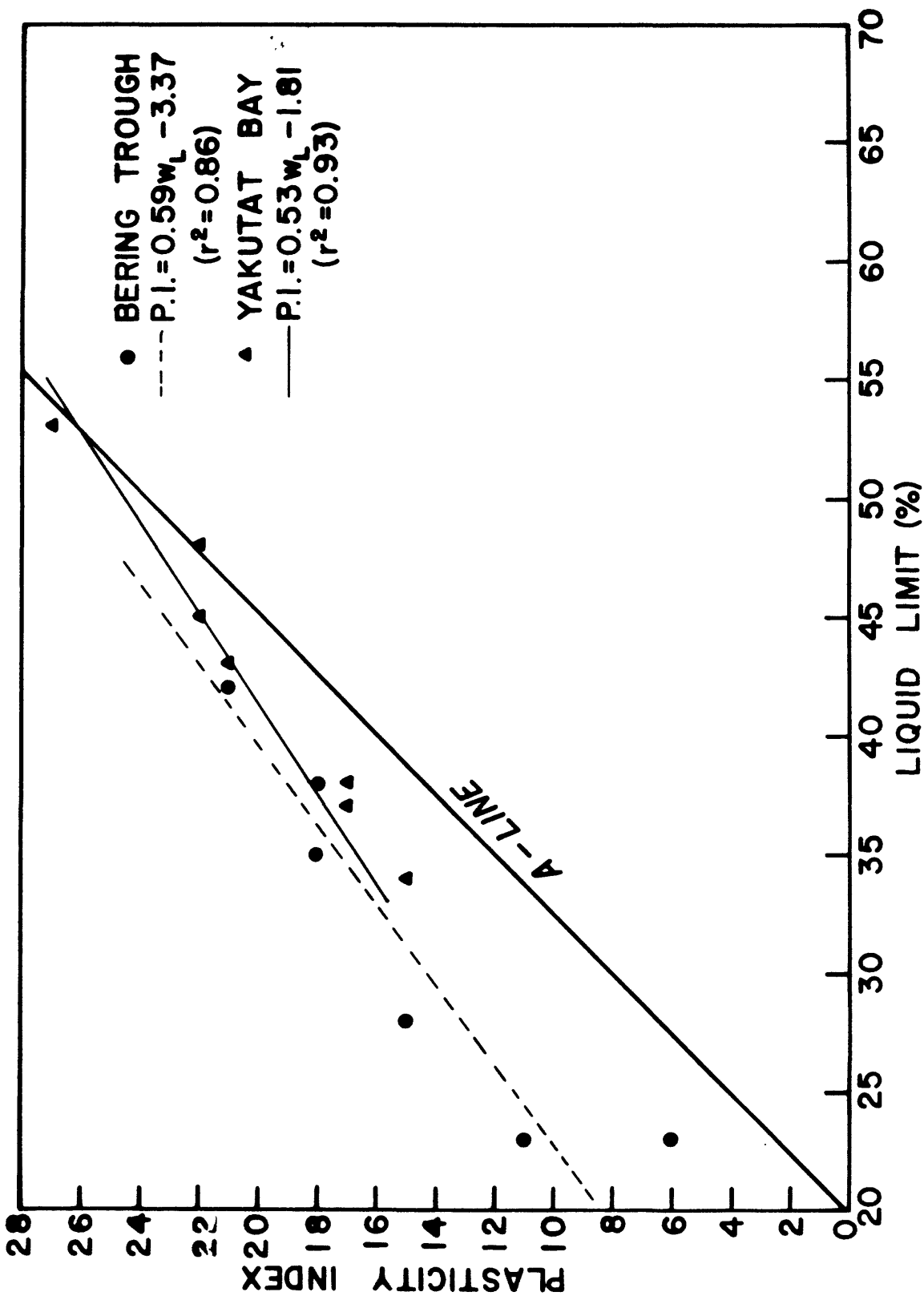


Figure 61. Plasticity chart for Bering Trough and Yakutat Bay Study Areas with least squares regression fits of data.

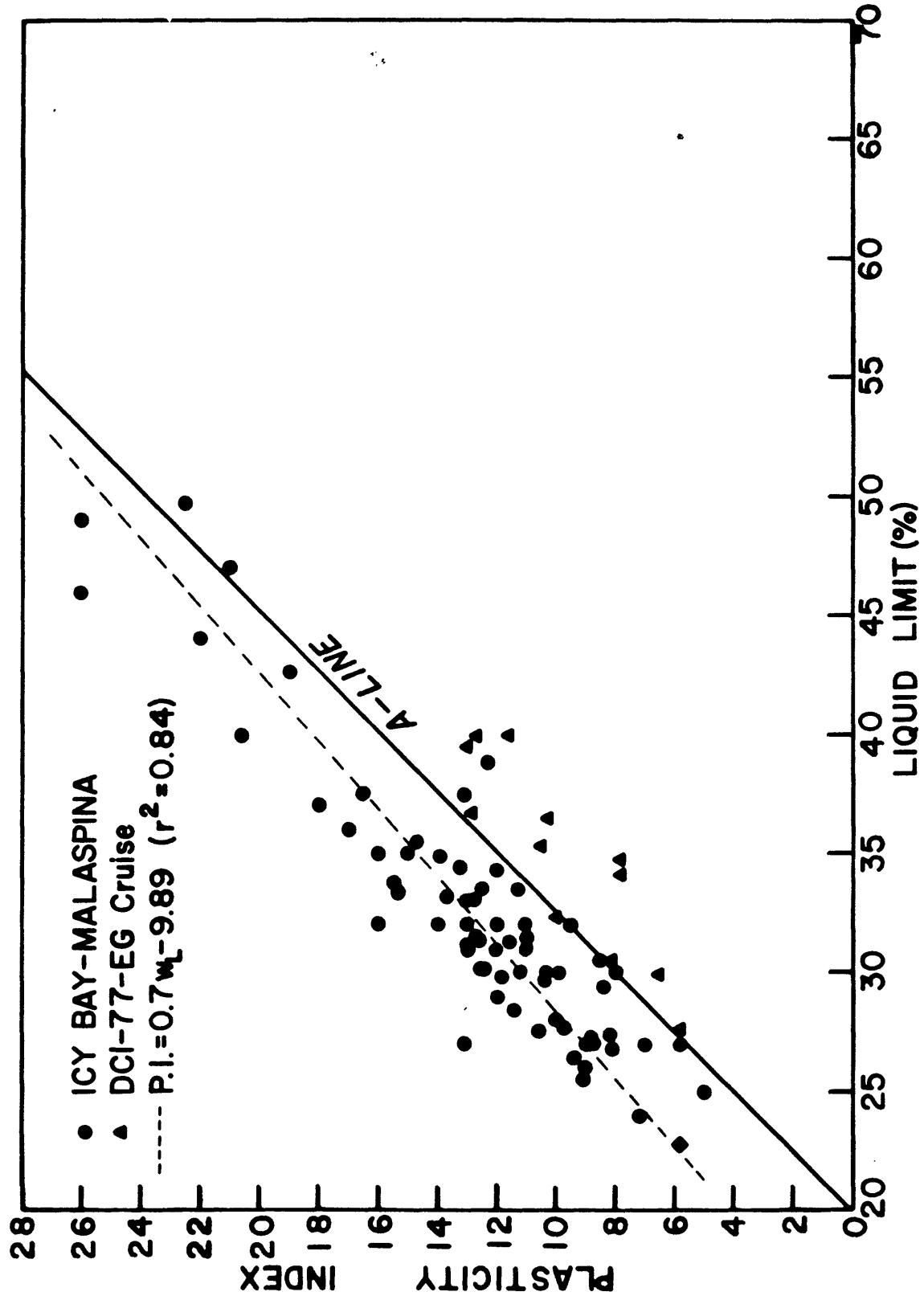


Figure 62. Plasticity chart for Icy Bay-Malaspina Study Area with least squares regression fit of the data (not including Cruise DCI-77-EG data).

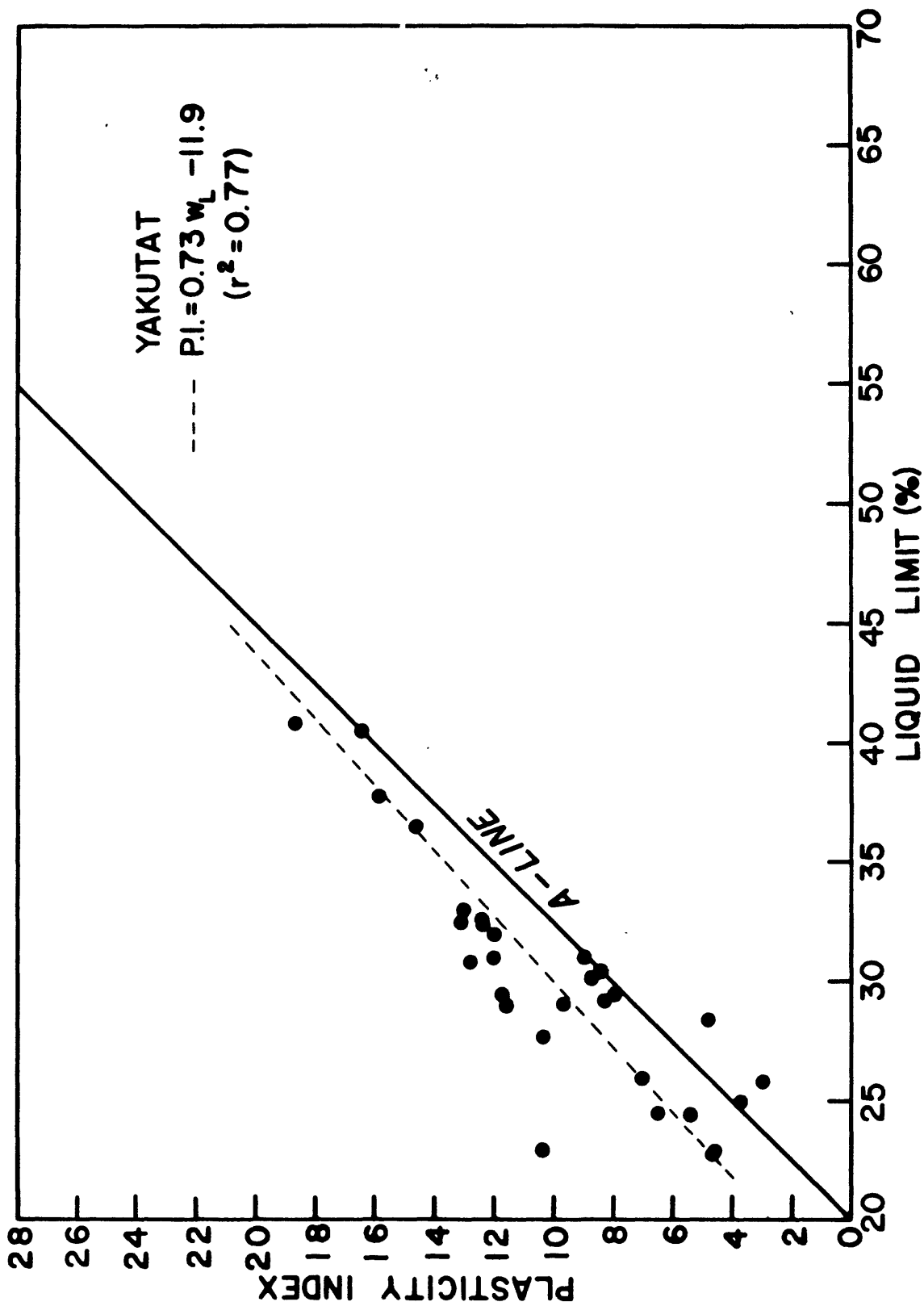


Figure 63. Plasticity chart for Yakutat Study Area with least squares regression fit of data.

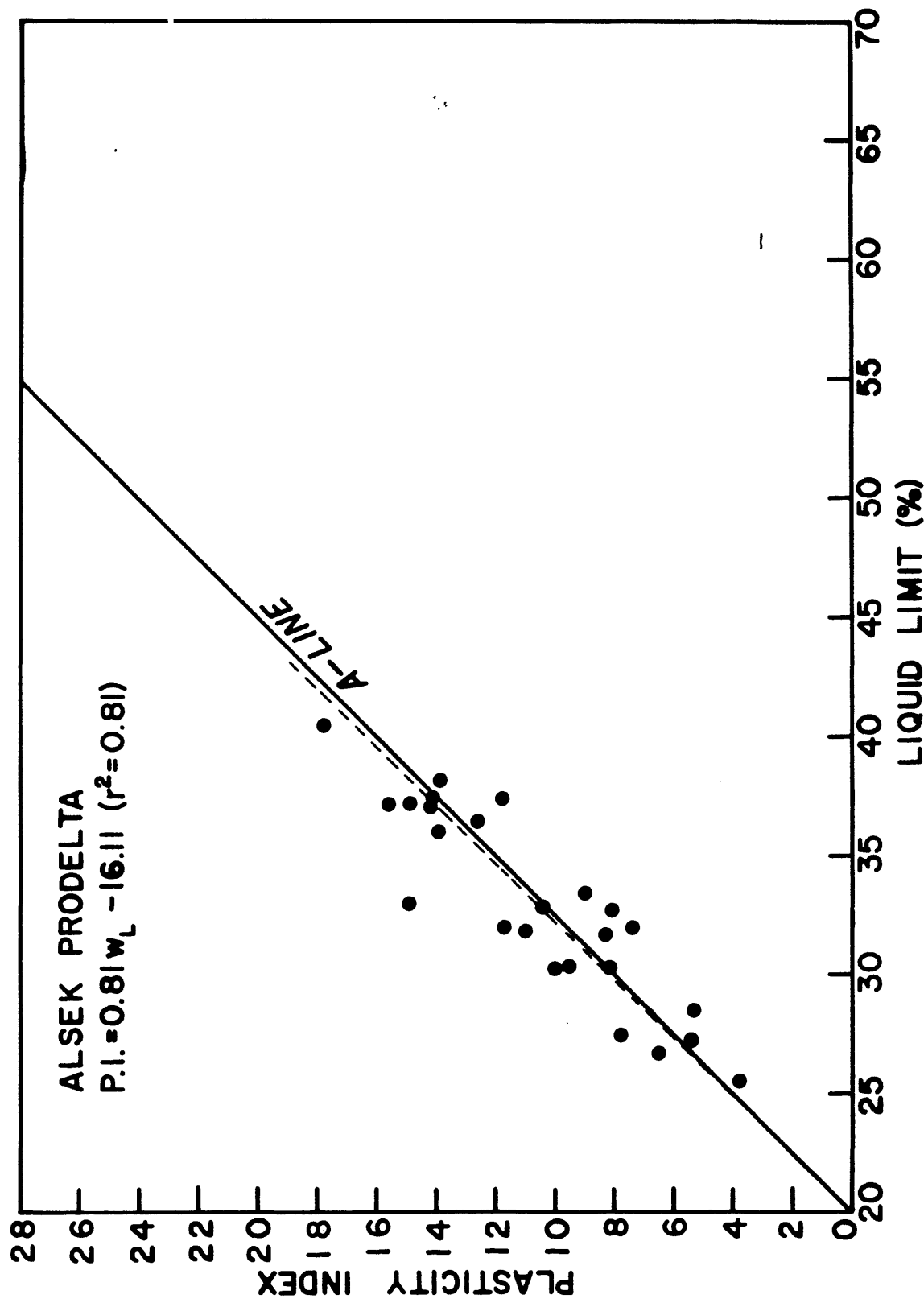


Figure 64. Plasticity chart for Alsek River Study Area with least squares regression fit of data.

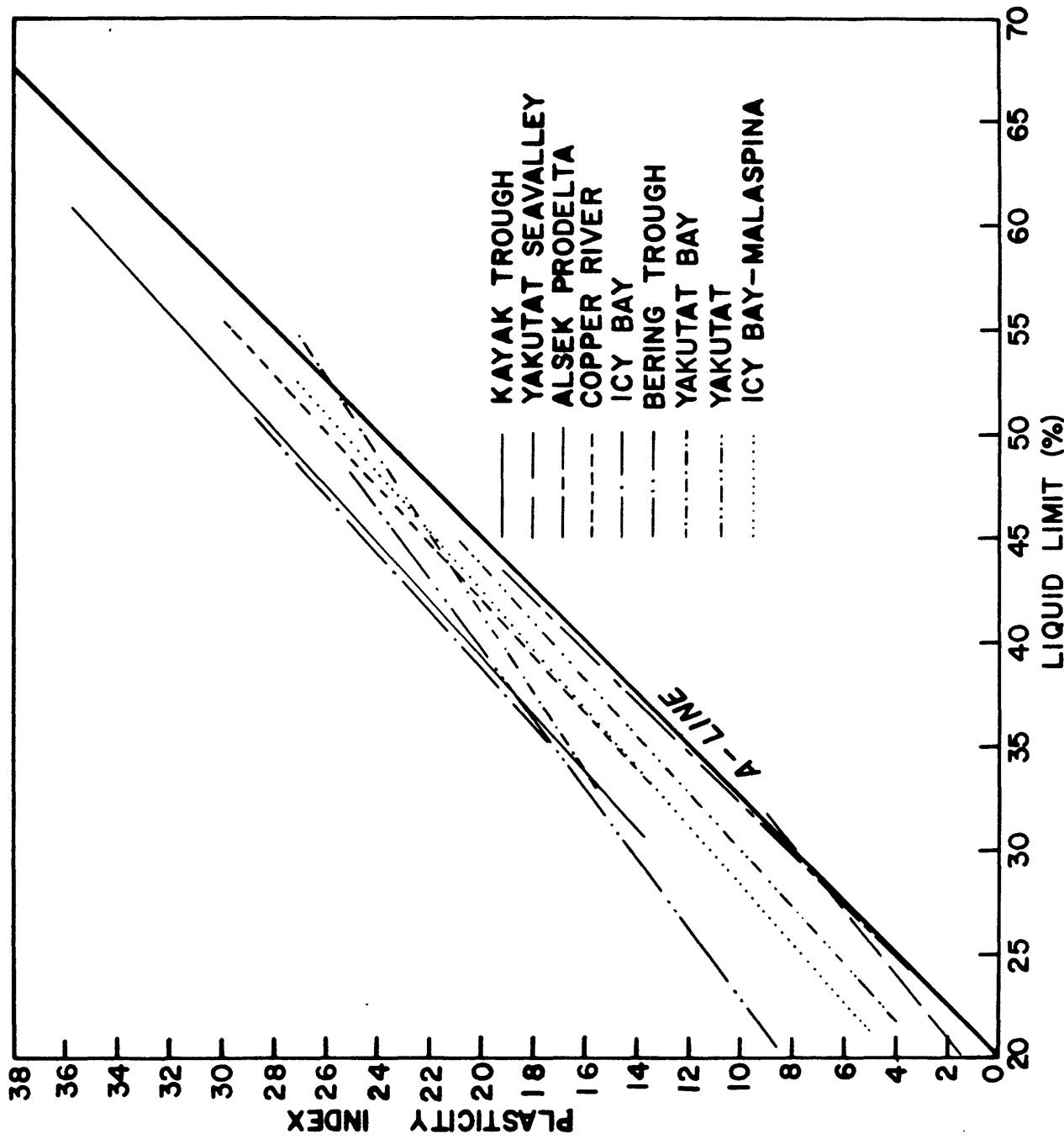


Figure 65. Summary of linear regression fits of plasticity data for the various study areas.

**APPENDIX A**

**METHANE IN SEDIMENTS OF THE EASTERN GULF OF ALASKA**

**by**

**Marge Golan-Bac  
Keith A. Kvenvolden**

Because the presence of interstitial gas may have a significant effect on the stability of sediment, analysis of gas contents can be an important part of an overall hazards evaluation of an area. Accordingly, hydrocarbon gas data from four cruises in the eastern Gulf of Alaska (S1-76-EG, S8-77-EG, S6-78-EG, and S11-79-EG) may be applied to this investigation. Although the gases methane, ethane, ethene, propane, propene, iso-butane, and n-butane were analyzed, this discussion is limited to the concentrations and distributions of methane. It is the only hydrocarbon gas present in concentrations that may exceed its saturation level in the interstitial water.

During the S1-76-EG cruise, 15 samples from 12 stations were taken from Van Veen samples and gravity cores that covered a large area of the eastern Gulf of Alaska, from off the western end of the Copper River Delta to the western end of Palma Bay (geographic locations shown in Fig. 1 of the main text). Methane values ranged from the detection level to approximately 60  $\mu\text{l/l}$  wet sediment. Note that these and other gas concentration values reported in this appendix are sample concentrations. The actual gas concentrations in place are probably higher. The highest concentration was found at Station 665 near the mouth of the Copper River. The next highest concentrations (approximately 30 and 40  $\mu\text{l/l}$ ) were at stations 658 and 659 respectively, east of the southern end of Kayak Island. Discontinuous seismic reflectors and turbid seismic returns were found in this area, suggesting that the sediments are gas-charged. The gas concentrations, although among the highest measured during this cruise, are well below saturation level (which is about 40,000  $\mu\text{l/l}$  at atmospheric pressure): free gas is probably not present in the sediment. During the 1977 cruise, samples taken near these stations measured much higher concentrations of methane as discussed below. At Station 661 in the Kayak Trough Slump the methane concentration was approximately 30  $\mu\text{l/l}$ . All other samples from the 1976 cruise had methane concentrations less than 10  $\mu\text{l/l}$ .

The S8-77-EG cruise concentrated on recovering samples from specific geologic features located in an area from off the east coast of Montague Island to Yakutat Bay. The specific areas involved, from west to east, were: the Hinchenbrook Sea Valley, east of Montague Island; a slump in the Egg Island Trough, southwest of the Copper River Delta; a slump mass in the Kayak Trough, southeast of the Copper River Delta; a zone of faulting southeast of Kayak Island; the Bering trough, off the Bering Glacier; a large slump southwest of Icy Bay; Icy Bay; a slump off the western edge of Malaspina Glacier; Yakutat Bay. Sixty samples from 23 stations were obtained from gravity, piston and hydroplastic cores. Methane values ranged from 0.8 to 19,000  $\mu\text{l/l}$  wet sediment. Most concentrations were equal to or exceeded by a factor of 2 the four highest concentrations measured during the 1976 cruise. Core 14G in the Kayak Trough Slump and Cores 36G and 38G from the Bering Trough had higher concentrations (180, 380, and 180  $\mu\text{l/l}$ , respectively) than other cores in this particular area. The concentrations of methane from these samples were not high enough to indicate gas-charged sediment in place, however. At these stations the sediment may have larger concentrations of methane at depth. Core 23G from the zone of faulting southeast of Kayak Island had anomalously high concentrations of methane. This core was taken in the same area as those cores from stations 658 and 659 from the S1-76-EG cruise. However, the concentrations obtained from Core 23G were 2,100  $\mu\text{l/l}$  at the surface and 14,000  $\mu\text{l/l}$  at the 100 cm depth. The latter concentration

begins to approach the solubility of methane in water at atmospheric conditions. Because these laboratory values represent a lower bound for the in place concentrations, the concentration of methane at this station in place may in fact have reached or exceeded its solubility. These anomalously high methane values correlate with acoustic anomalies attributed to gas-charged sediments; the presence of gas may affect the stability of the sediment southeast of Kayak Island.

The S6-78-EG cruise recovered 17 samples from Van Veen samplers and gravity cores. The area covered included 5 main localities: Icy Bay and a slump off the western edge of the Malaspina Glacier, both areas covered during the S8-79-EG cruise; off the Dangerous River and just east of Dry Bay, both areas which were later covered during the S11-79-EG cruise; and an area beyond the 200 m bathymetric contour situated southwest of Lituya Bay, that was not sampled during any other cruise. These methane values ranged from about 1 to 48  $\mu\text{l/l}$  wet sediment from sediments up to a depth of 296 cm. Core 13A in Icy Bay represents the upper limit of this range and is similar to the concentrations obtained in 1977. Four cores (8A, 8B, 9B, and 12B) from off the western edge of Malaspina Glacier ranged from 21 to 40  $\mu\text{l/l}$  wet sediment, which is also similar to the concentrations obtained in the 1977 cruise. Three cores off the Dangerous River (3, 4, and 5) had low concentrations of methane, averaging 1.4  $\mu\text{l/l}$  wet sediment. The S11-79-EG cruise the next year confirmed these low concentration levels in 4 cores (3, 5, 6, and 26) which averaged 7.0  $\mu\text{l/l}$  wet sediment. Core 1 just east of Dry Bay indicated a very low concentration of methane (1.4  $\mu\text{l/l}$ ) similar to 7 of 8 cores taken in that area on the S11-79-EG cruise. The concentrations averaged 12  $\mu\text{l/l}$  wet sediment. Two cores (10A and 11A) were taken beyond the 200 m bathymetric level southwest of Lituya Bay and averaged 3.0  $\mu\text{l/l}$  wet sediment.

The S11-79-EG cruise concentrated on 3 main localities: off the Dangerous River, off Dry Bay and just east of Dry Bay. Thirty-seven samples were obtained from 17 vibracores and gravity cores. Methane concentrations ranged from just detectable to 33,000  $\mu\text{l/l}$ . In eight cores (1, 2, 11, 16, 20, 21, 26 and 30) the amount of methane was greater than 10 but less than 64  $\mu\text{l/l}$ , a range of values similar to those observed on the S1-76-EG and S6-78-EG cruises. Except for one core the methane concentrations at the other stations were less than 10  $\mu\text{l/l}$ . Core 14 at a site just east of Dry Bay was anomalous. At the 80-90 cm depth interval, the concentration of methane was approximately 32,800  $\mu\text{l/l}$  wet sediment, a value which nearly equals the solubility of methane in the interstitial water at atmospheric conditions. This high concentration of methane may indicate gas-charging which would affect the stability of the sediments.

Anomalously high concentrations of methane suggesting the presence of gas-charged and, therefore, unstable sediments, were found in only two areas: a fault zone southeast of Kayak Island and east of Dry Bay. Sediments from near the mouth of the Copper River, from the Kayak Trough, and from east of Kayak Island had significant amounts of methane, but the amount measured was insufficient to indicate that the sediments in place were, indeed, gas-charged. Deeper sediments in the area may be gas-charged, however. There appears to be no good correlation between the occurrence of seismic anomalies and the possible presence of sampled gas-charged sediment except for the sediment southwest of Kayak Island.

Methane in Sediments of the Eastern Gulf of Alaska-Sample Locations.

<u>Cruise</u>	<u>Sample or station</u>	<u>Latitude</u>	<u>Longitude</u>
S1-76-EG	658B	59°47.19'N	144°28.83'W
	659B	59°49.40'N	144°28.03'W
	661	60°06.20'N	144°40.30'W
	665	60°08.20'N	145°00.00'W
S8-77-EG	14G	60°05.12'N	144°40.44'W
	23G	59°50.75'N	144°24.26'W
	36G	59°56.64'N	143°35.75'W
	38G	59°58.05'N	143°38.00'W
S6-78-EG	1	59°02.70'N	138°22.80'W
	3	59°17.70'N	139°16.60'W
	4	59°17.35'N	139°15.90'W
	5	59°16.95'N	139°14.30'W
	8A	59°36.50'N	140°55.50'W
	8B	59°36.20'N	140°56.00'W
	9B	59°37.40'N	140°55.70'W
	10A	57°55.01'N	138°04.89'W
	11A	57°55.36'N	138°04.19'W
	12B	59°36.80'N	140°55.80'W
	13A	59°55.97'N	141°32.27'W
	1	59°06.08'N	138°42.36'W
	2	59°06.00'N	138°42.17'W
S11-79-EG	3	59°16.33'N	139°12.29'W
	5	59°17.49'N	139°16.10'W
	6	59°17.74'N	139°17.31'W
	11	59°03.53'N	138°25.32'W
	14	59°02.21'N	138°25.50'W
	16	59°05.95'N	138°38.97'W
	20	59°05.81'N	138°42.01'W
	21	59°02.45'N	138°25.38'W
	26	59°17.27'N	139°16.03'W
	30	58°59.84'N	138°43.51'W

**APPENDIX B**

**RELATIVE IMPORTANCE OF SEISMIC AND STORM WAVE LOADING**

The Gulf of Alaska is susceptible to both high seismicity (Stephens and Page, 1982) and large storm waves (Bea, 1976). This appendix provides a brief discussion of the factors influencing cyclic loading dominance and develops a quantitative estimate of the water depth separating storm wave and earthquake control.

One way of separating earthquake and wave control is to determine the water depth at which the shearing stresses developed by peak storm waves equal the shearing stresses developed by a critical earthquake. Modifying Equation (2) from the main text for a horizontal bottom, we obtain:

where  $\tau$  is the shearing stress generated by an earthquake with a critical acceleration,  $k$ .

As shown in the main text, the critical acceleration corresponding to many of the failure features (including the Icy Bay-Malaspina slump in water depths ranging from 75 to 175 m) is 0.136g (Figure 55). Assuming that failures in relative deep water are earthquake induced, this critical value of  $k$  can be used to estimate a representative level of shearing stress developed by major earthquakes in the area. For typical sediment densities ( $\gamma = 1.8 \text{ g/cm}^3$  and  $\gamma' = 0.8 \text{ g/cm}^3$ ), Equation (B-1) yields  $\tau/\sigma_v' = 0.306$  for major earthquakes.

Seed and Rahman (1978) provide the following equation for shearing stresses near the seafloor surface produced by large storm waves:

where  $\gamma_w$ =unit weight of water  
 $d$ =water depth  
 $H$ =wave height  
 $L$ =wave length

The maximum probable storm wave for the area (Bea, 1976) is 37 m, corresponding to a very limited number of waves. For a longer series of waves, we assumed 30 m as a more realistic maximum wave height. Because the solution is fairly independent of wave length, any reasonable choice of wave length is satisfactory. We assumed a representative value of 300 m. Inserting these values into Equation B-2 and solving for the water depth,  $d$ , necessary to produce shearing stresses comparable to those produced by earthquakes ( $\tau/\sigma_v' = 0.306$  from Fig. 35 in the main text) yields a critical water depth of 35 m. Therefore, in water depths shallower than 35 m, major storms would produce shearing stresses greater than major earthquakes would induce. In greater water depths earthquakes would produce the greater stresses.

Equating stress levels does not completely determine the level at which the influence of major earthquakes and waves is equal. Waves produce a much larger number of critical cycles than earthquakes and would cause a greater level of strength degradation under completely undrained conditions. That is, waves might cause the same damage at a lower stress level than that produced

by an earthquake. Judging by the extensive data base of Lee and Focht (1976), the strength degradation factor,  $A_D$ , might be reduced by up to 50% if 1000 cycles were considered rather than 10. Under fully undrained conditions and a major storm with 1000 cycles, the stress level required to cause the same damage as the representative major earthquake for the area would be only one-half as much as that induced by the earthquake. That is, a value of  $\tau/\sigma_v' = (0.5)(0.306) = 0.153$  would be needed. The water depth at which earthquakes and waves would cause the same level of damage would drop to 76 m, as calculated from Equation (B-2).

The 76 m level is the deepest for which storm waves and earthquakes could be equivalent. The water depth at which earthquakes and waves would cause the same level of failure is probably shallower because some drainage of pore pressures during a storm would be expected (Seed and Rahman, 1978). If enough drainage were to occur, the level of equivalence could even be shallower than the 35 m calculated for equivalent stresses. Because the glacial marine sediment is silty and drains fairly easily, the 35 m level is probably a good estimate of the depth of equivalent damage; the depth could drop to as deep as 76 m under special circumstances.

## APPENDIX C. INDEX PROPERTIES

This Appendix presents downcore profiles of all the index property measurements. The profiles are organized by study area ordered from west to east. Within study areas the profiles are ordered by core number. The measurements include laboratory original and remolded vane shear strength, natural water content, liquid and plastic limits, grain density, and grain size (as percent sand, silt, and clay). Also shown are locations of consolidation or triaxial tests. The identification number indicates the type of test and the testing organization. The nature of these tests is indicated by a coded test number. The code for the test numbering system is as follows:

### First two letters:

- (a) OE - Oedometer test
- (b) CE - Constant rate of strain (CRS) consolidation test
- (c) TE - Static triaxial test
- (d) TC - or D - Cyclic triaxial test

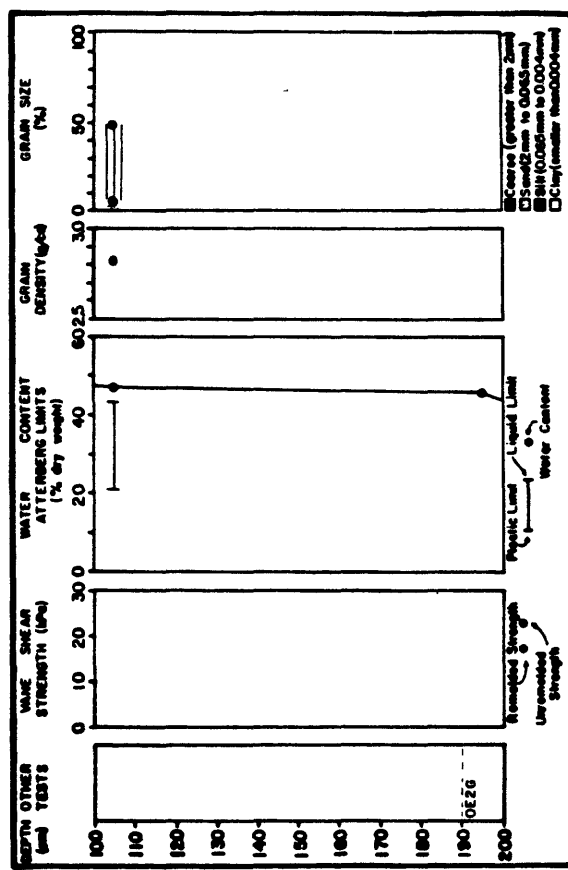
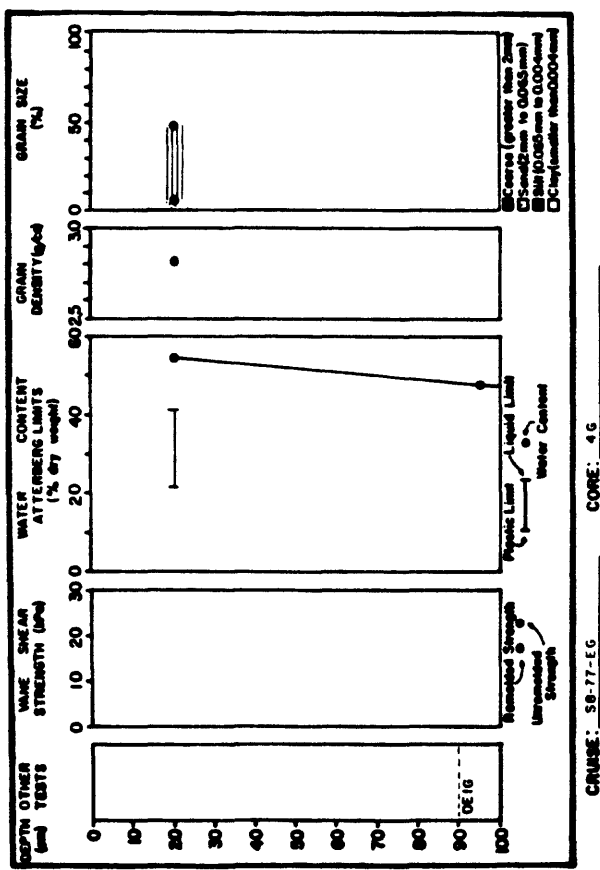
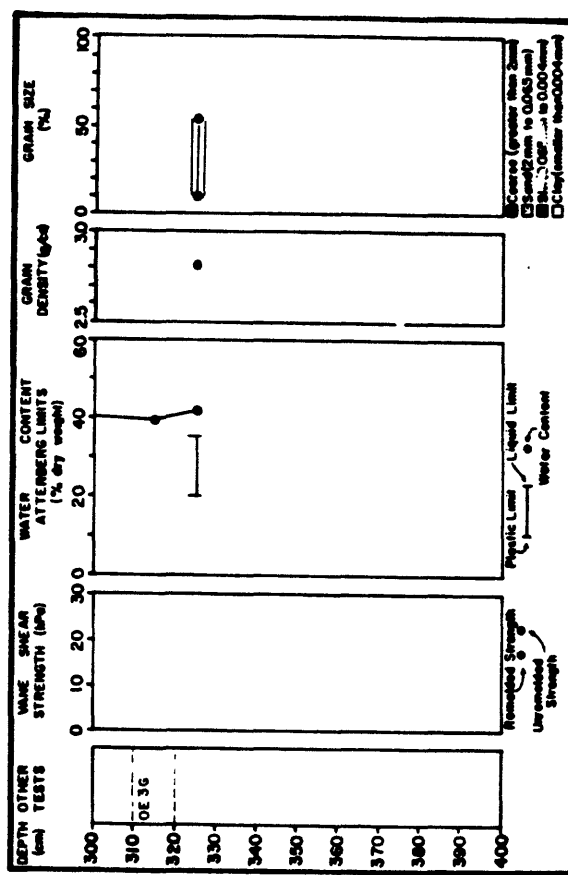
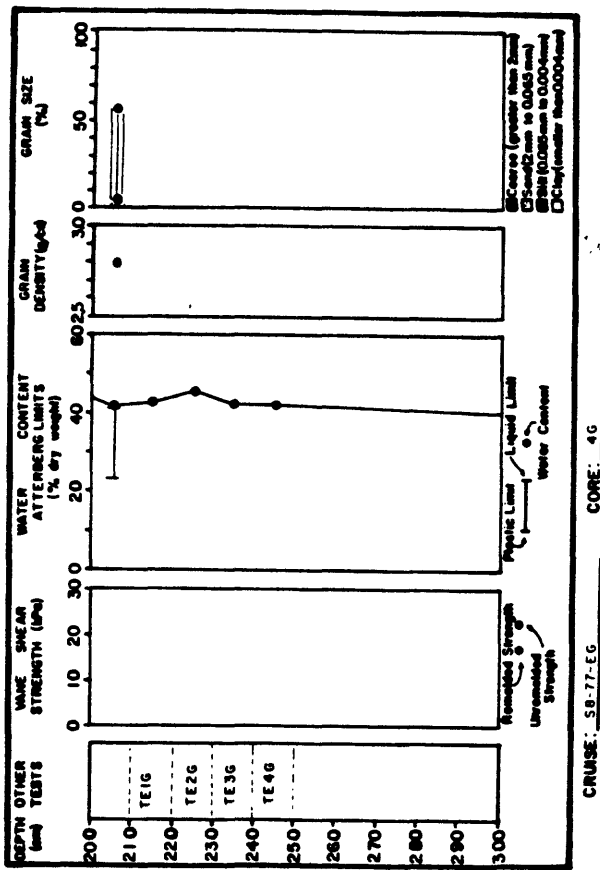
### Trailing characters:

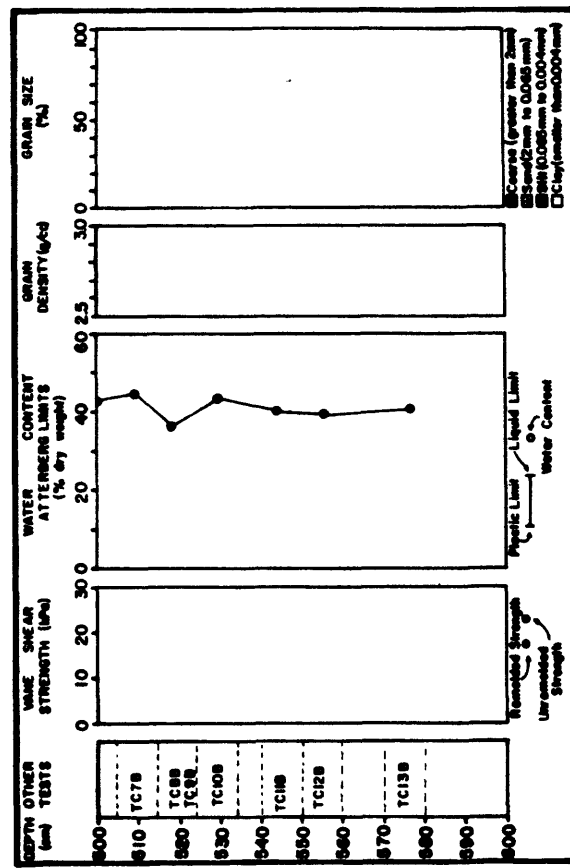
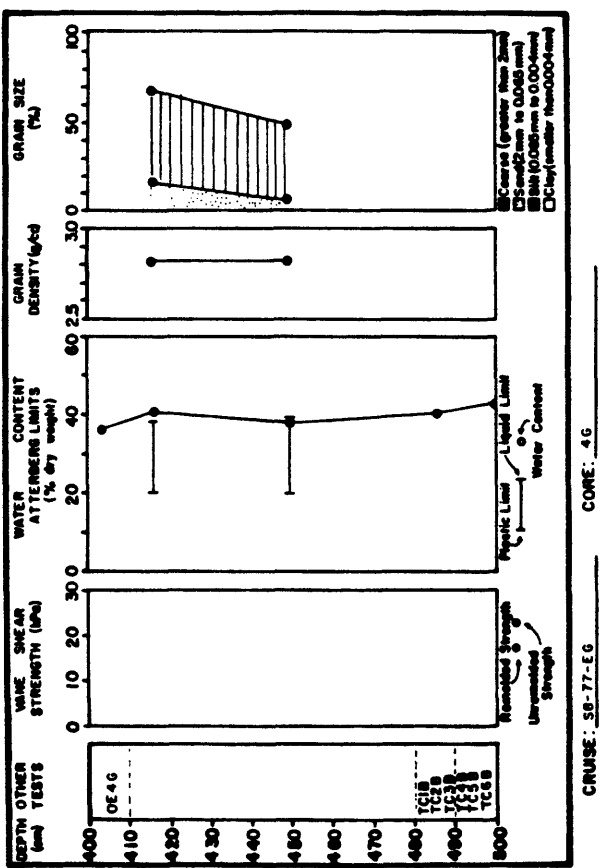
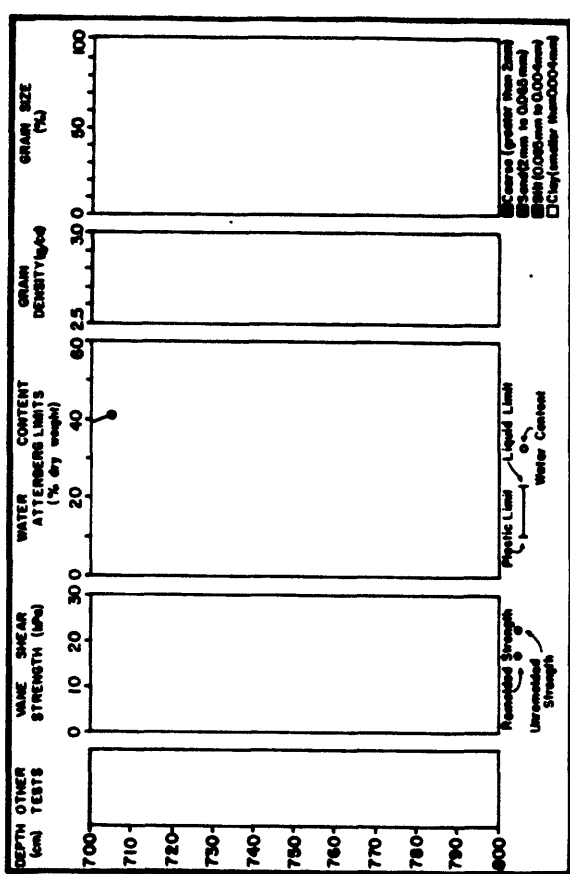
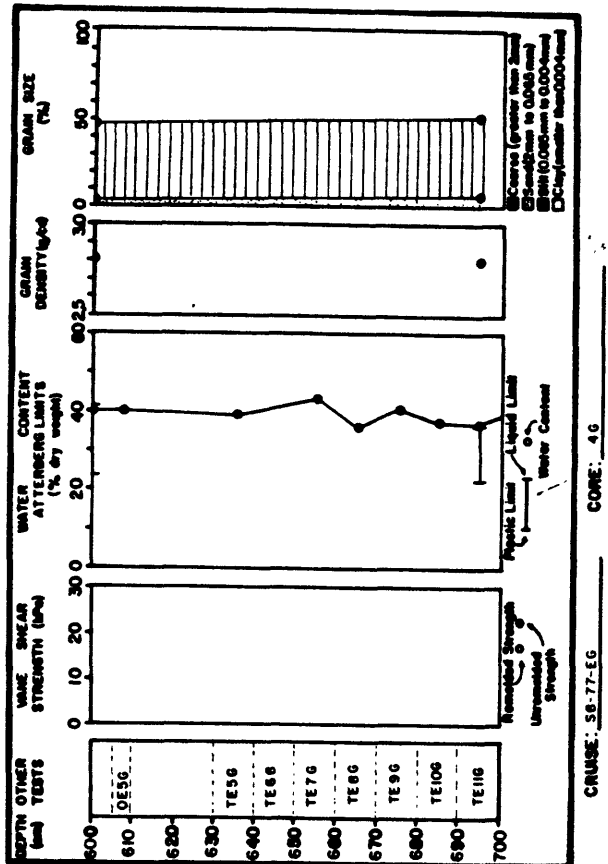
- (a) No trailing characters - test performed by the USGS
- (b) L1 - Test of 1977 core sample by Law Engineering and Testing Company
- (c) G - Test of 1977 sample by Geotechnical Engineers, Incorporated
- (d) B - Test of 1977 sample by University of California, Berkeley
- (e) L2 - Test of 1980 sample by Law Engineering and Testing Company

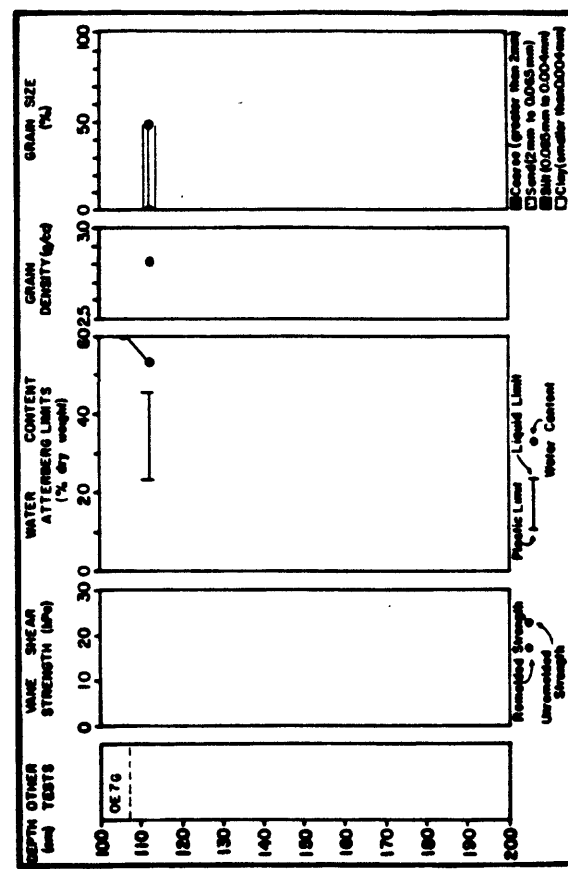
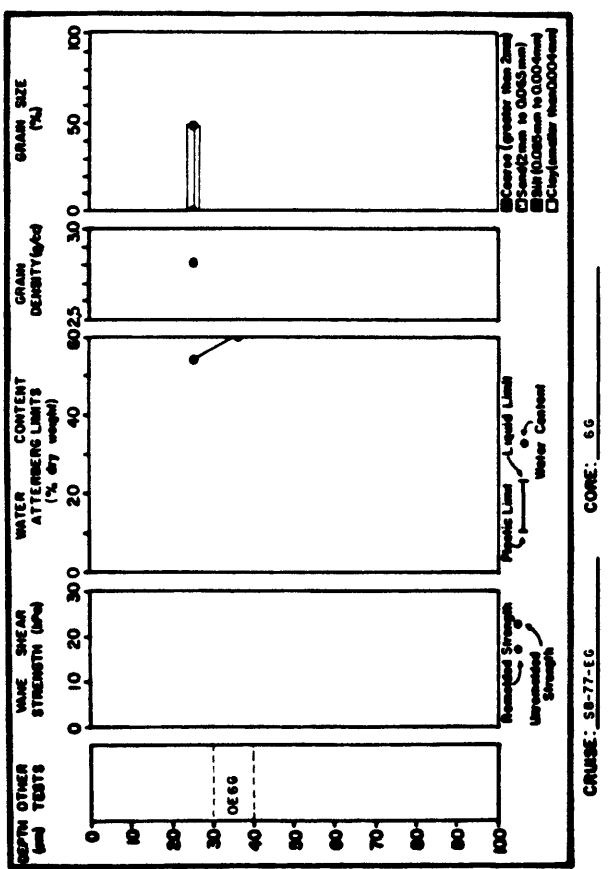
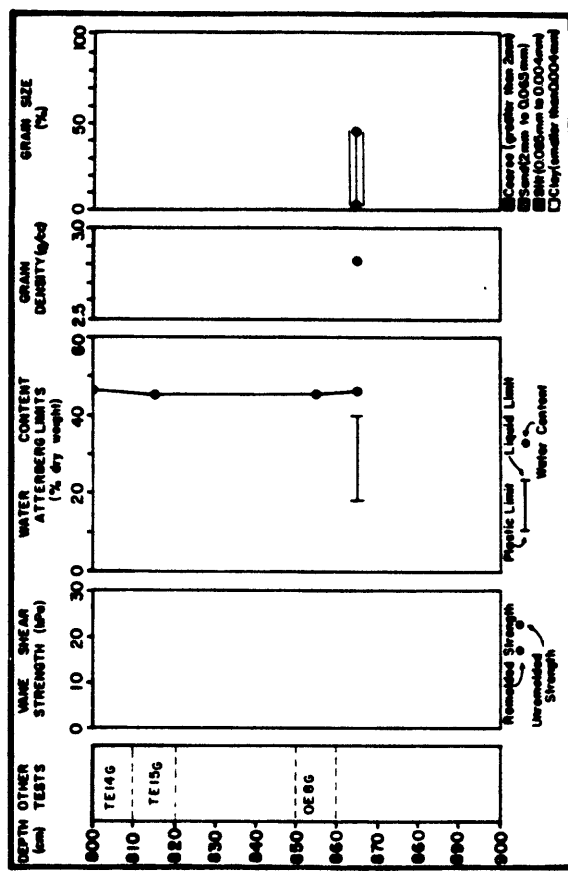
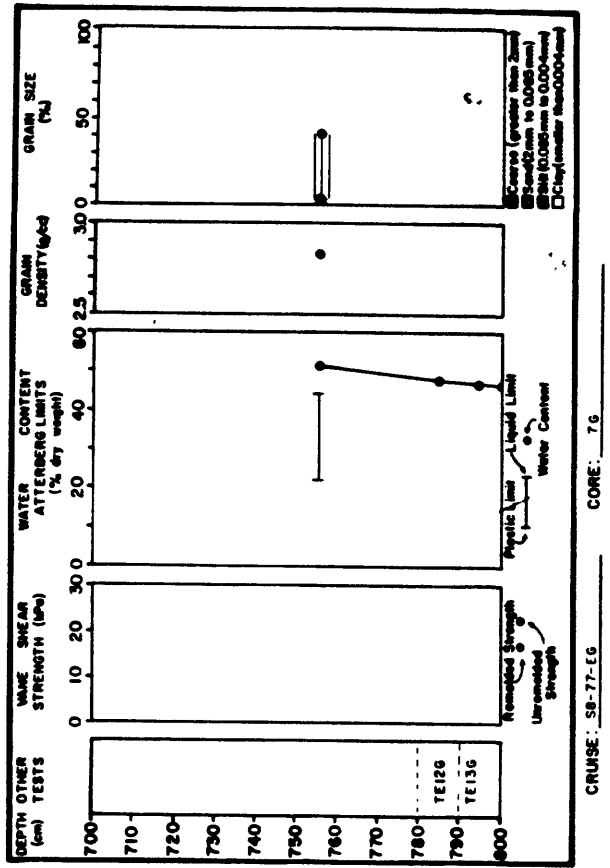
These consolidation and triaxial test results are presented in Appendices D through G and are grouped according to the organization performing the test.

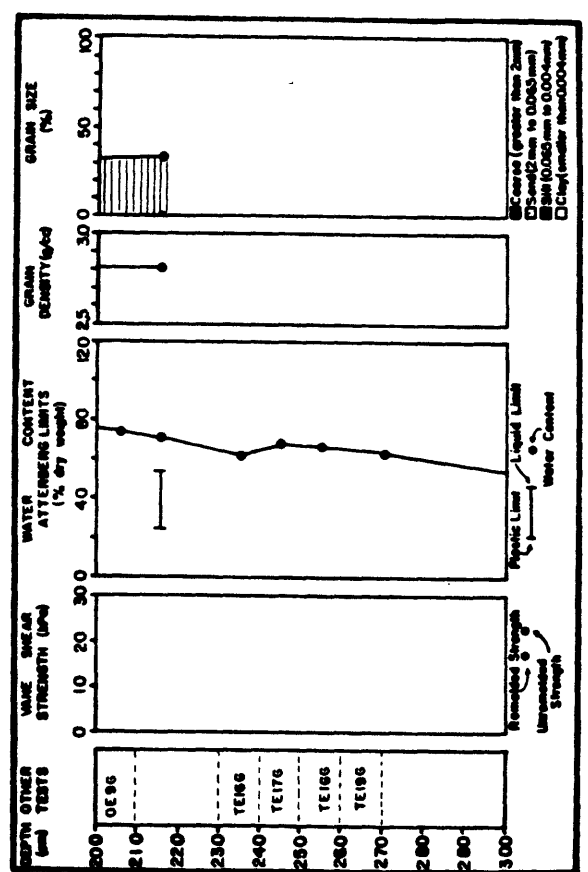
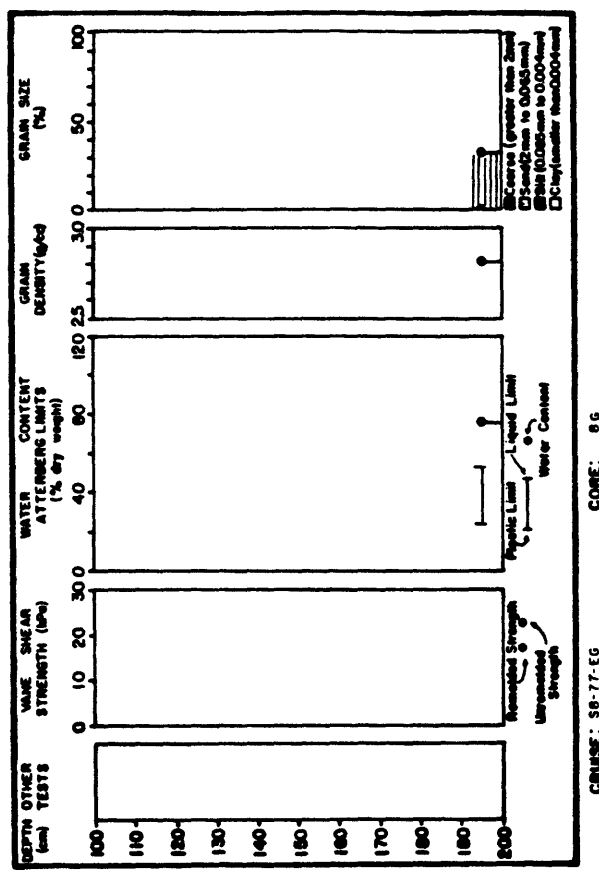
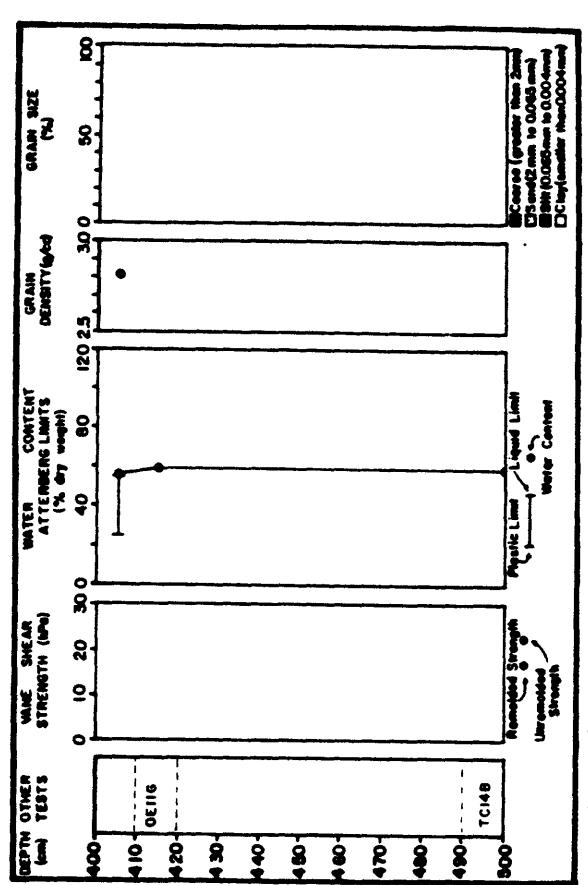
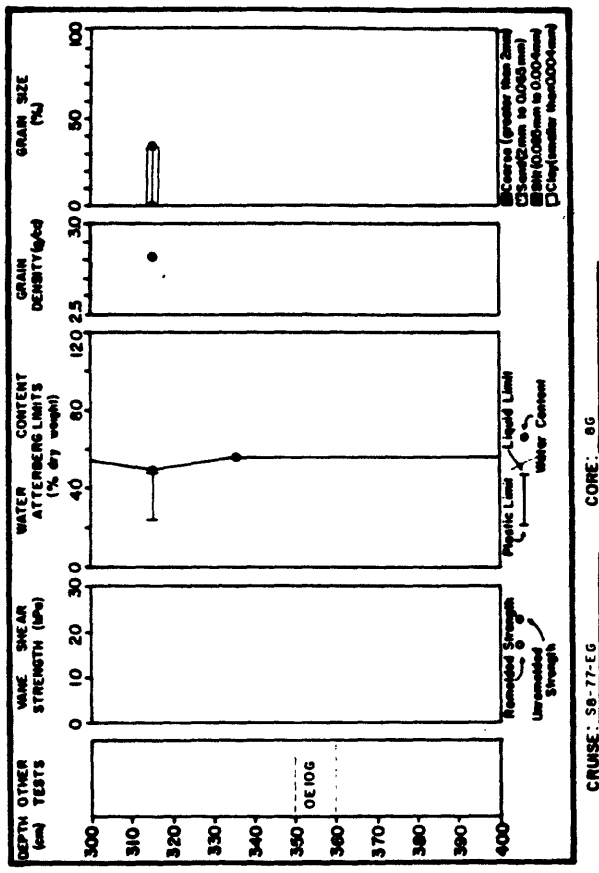
The water contents from Cruise DC1-77-EG (Carlson and others, 1978b) appear to have been calculated incorrectly, possibly through a faulty computer program. The error is indicated in Figure 62 in which the Atterberg limits for DC1-77-EG plot in a distinctly different section of the plasticity chart from that in which the results of tests from other cruises to the same area plot. Because of this discrepancy, water contents from DC1-77-EG were not shown in Figure 56.

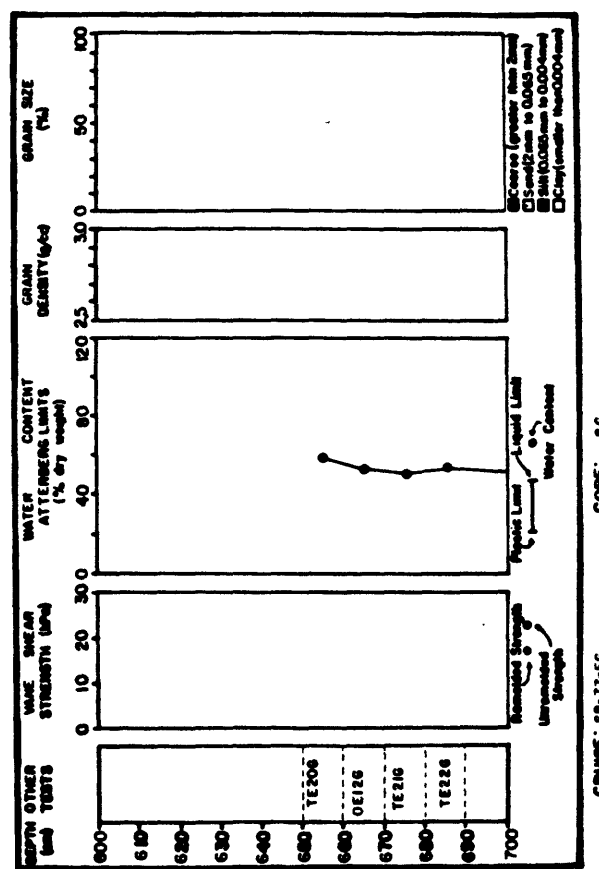
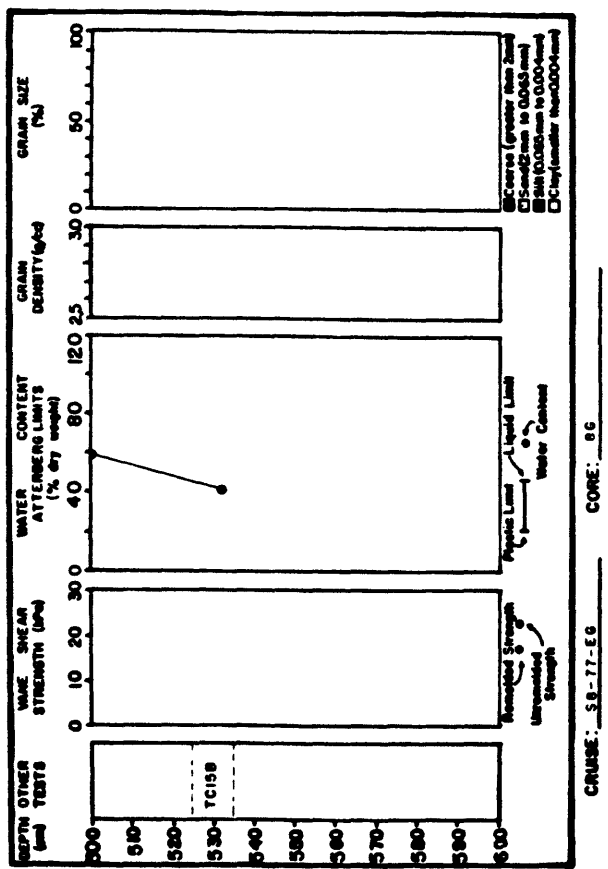
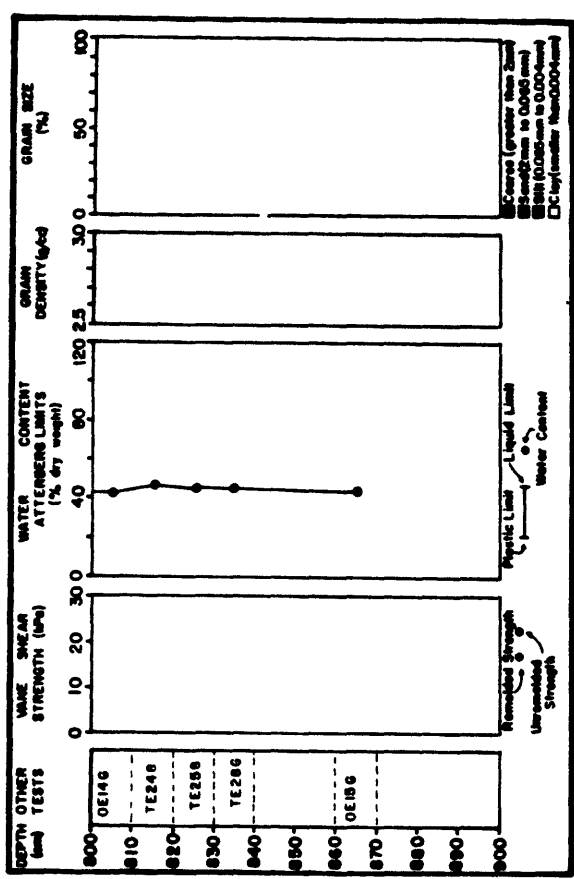
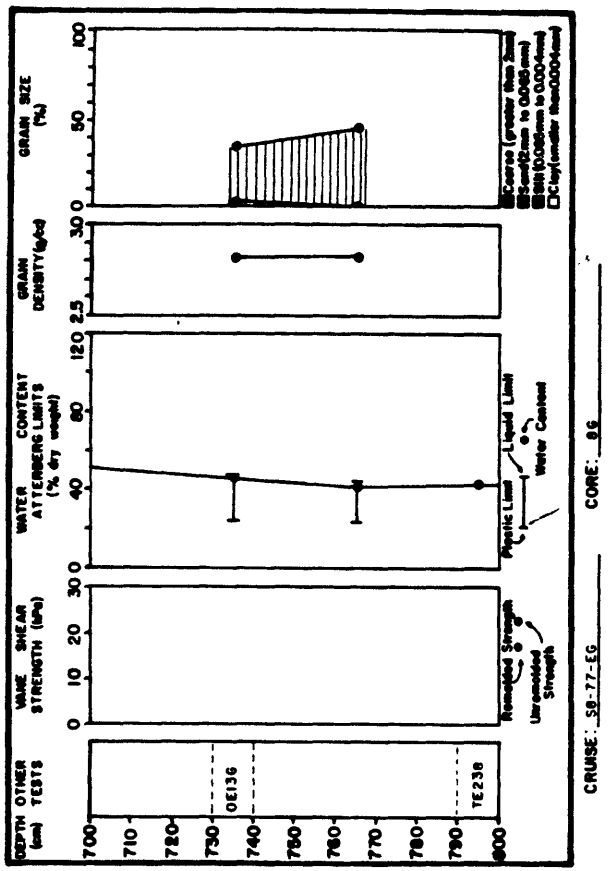
COPPER RIVER STUDY AREA

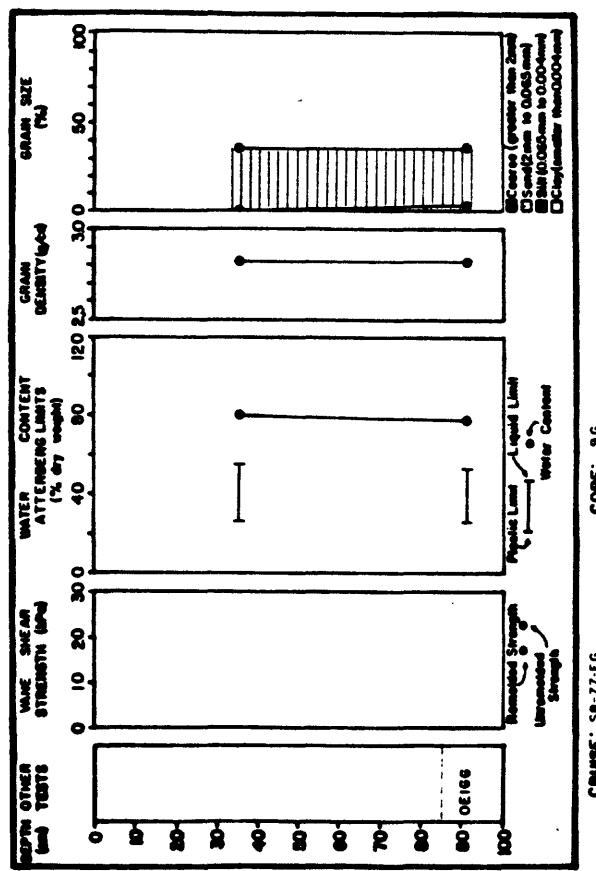
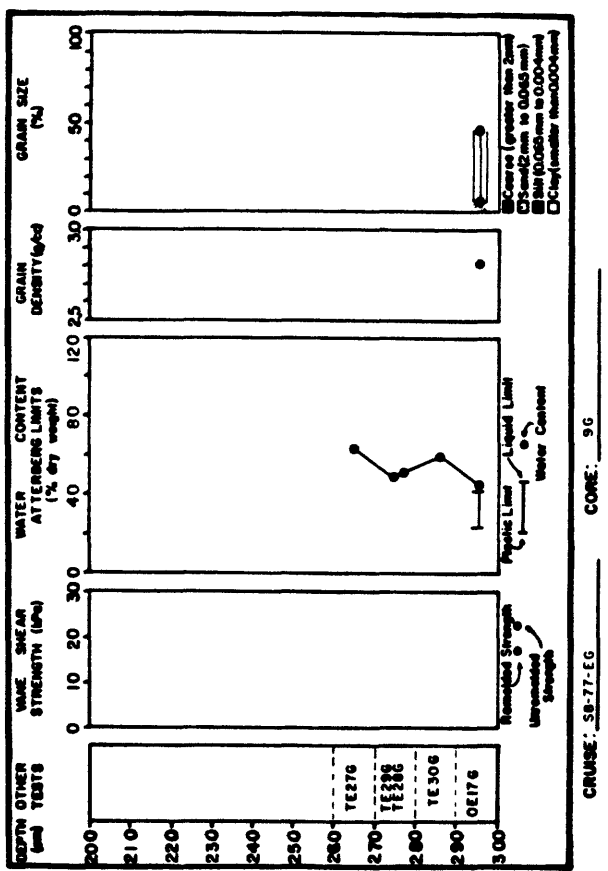




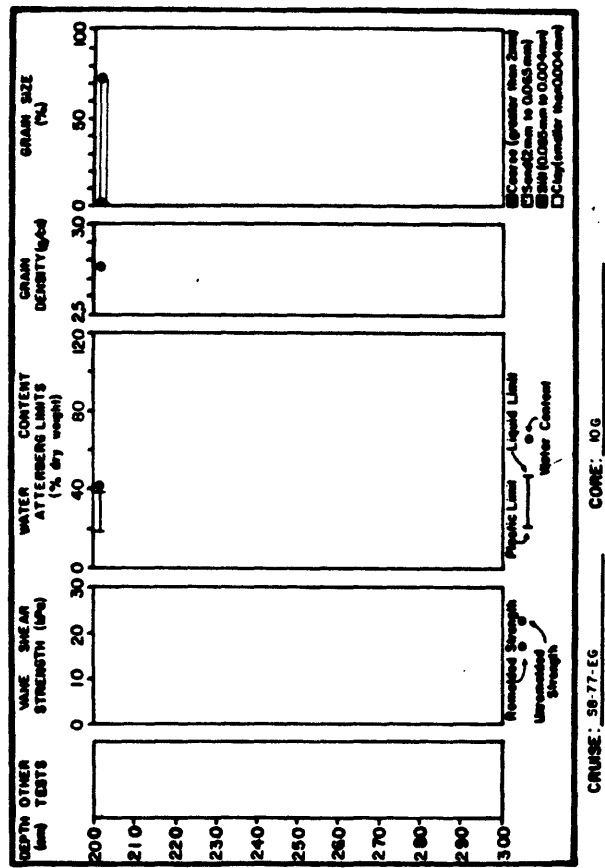




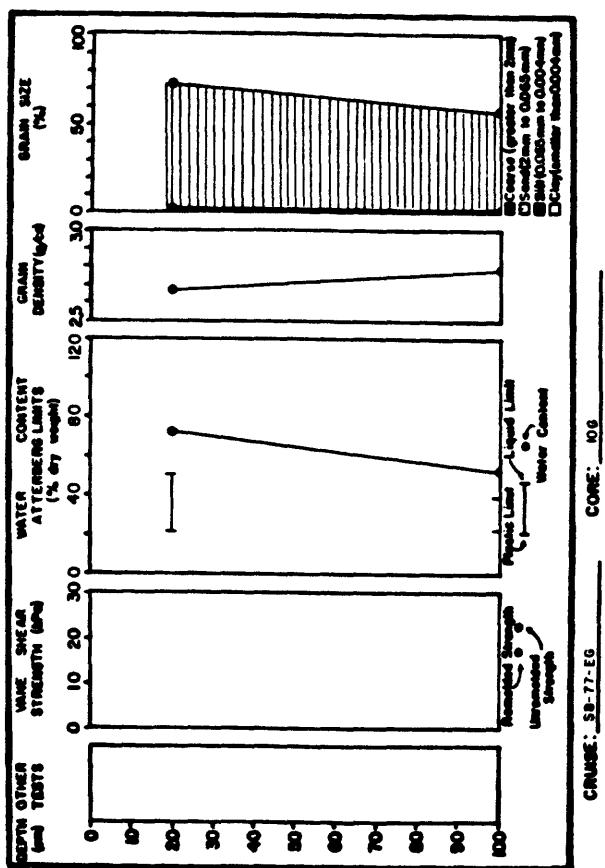




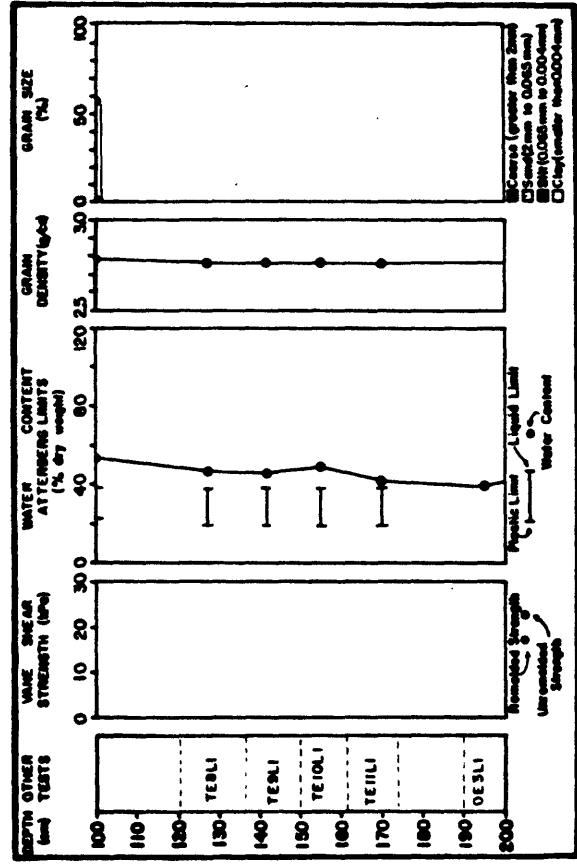
KAYAK TROUGH STUDY AREA



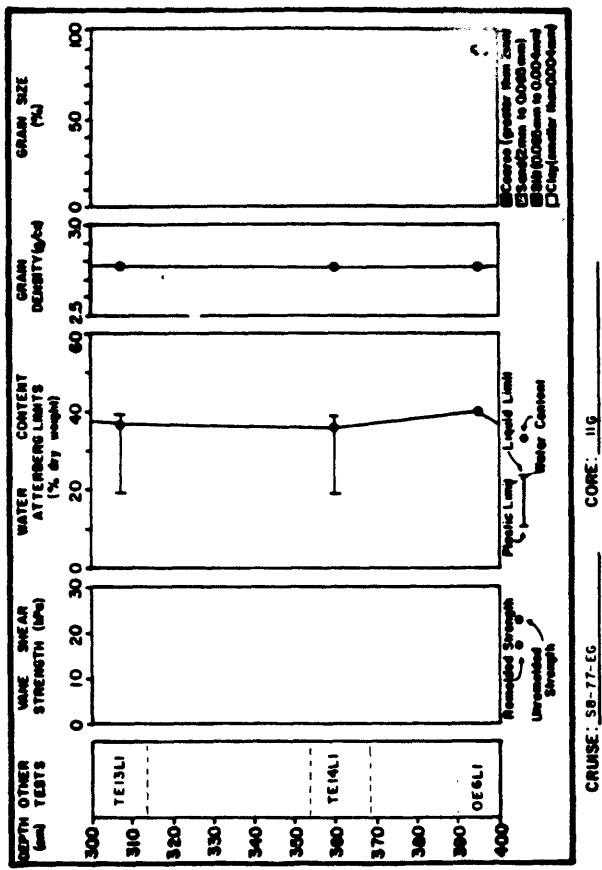
CORE: 50-77-EG



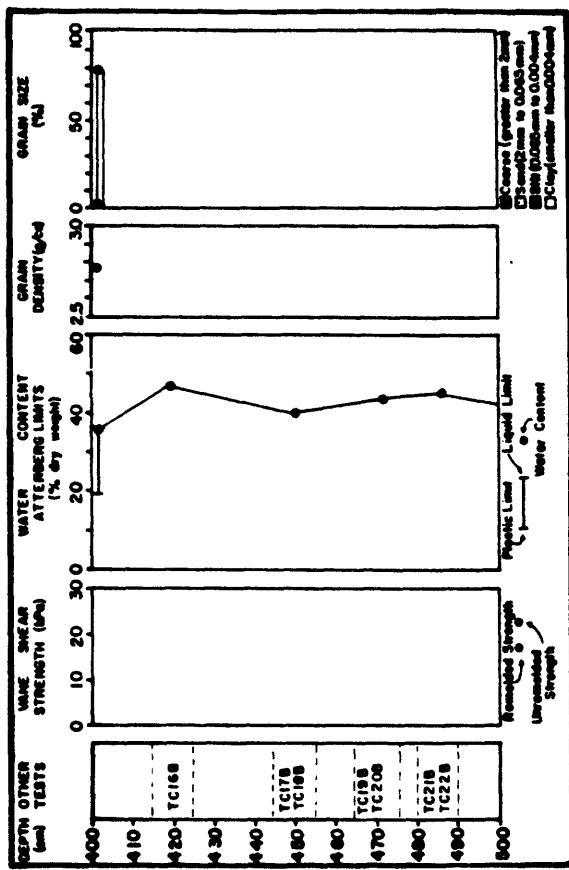
CORE: 50-77-EG



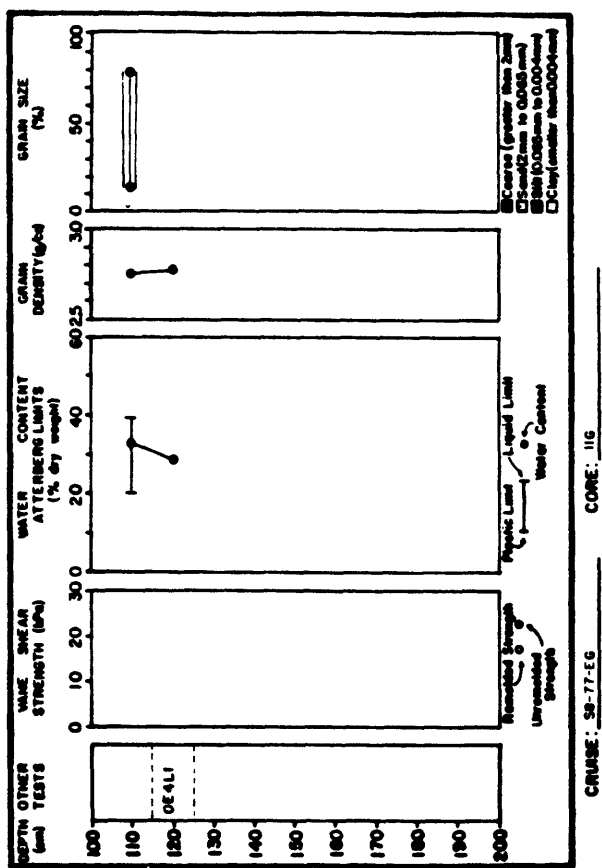
CORE: 50-77-EG



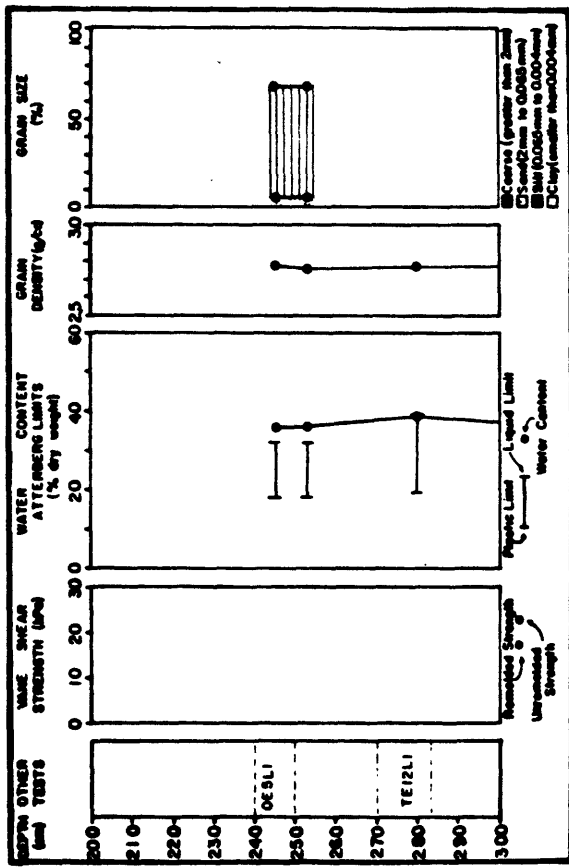
CORE: SB-77-EG



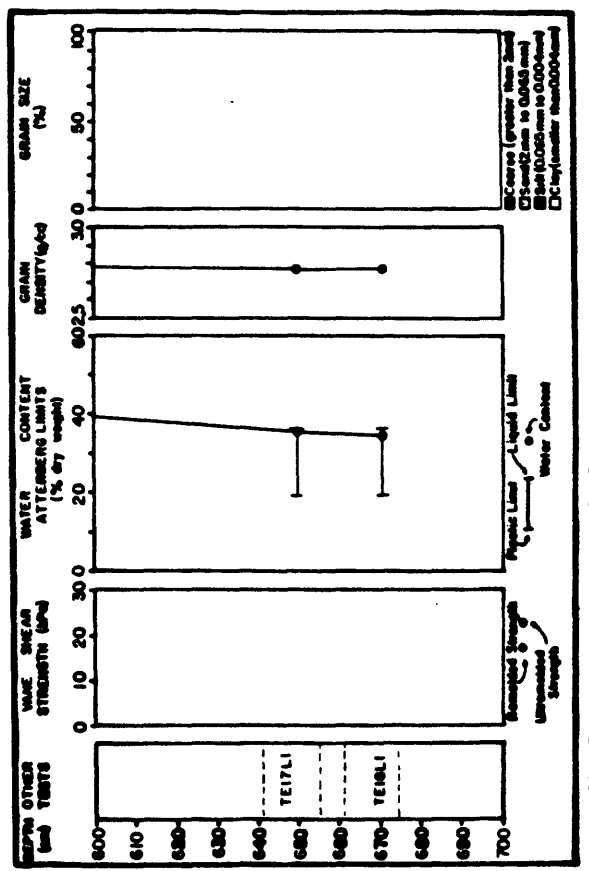
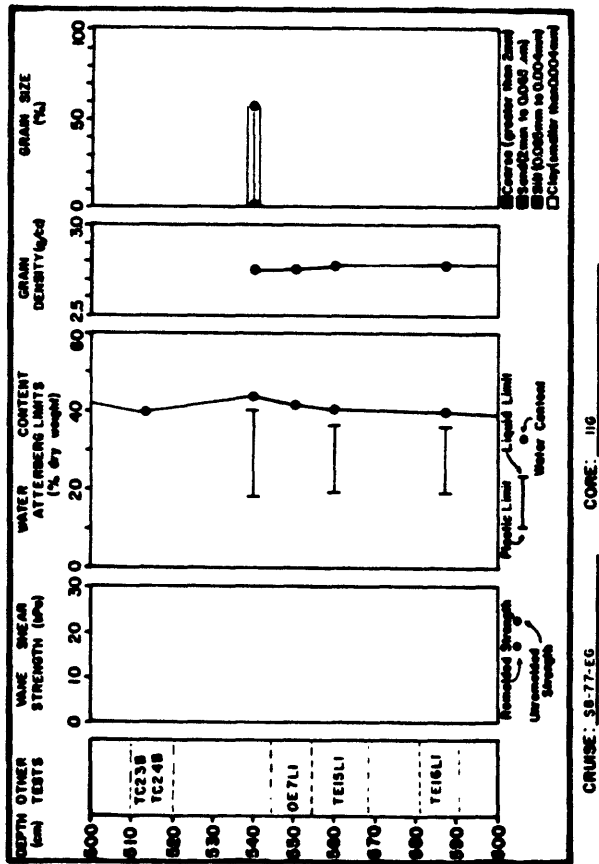
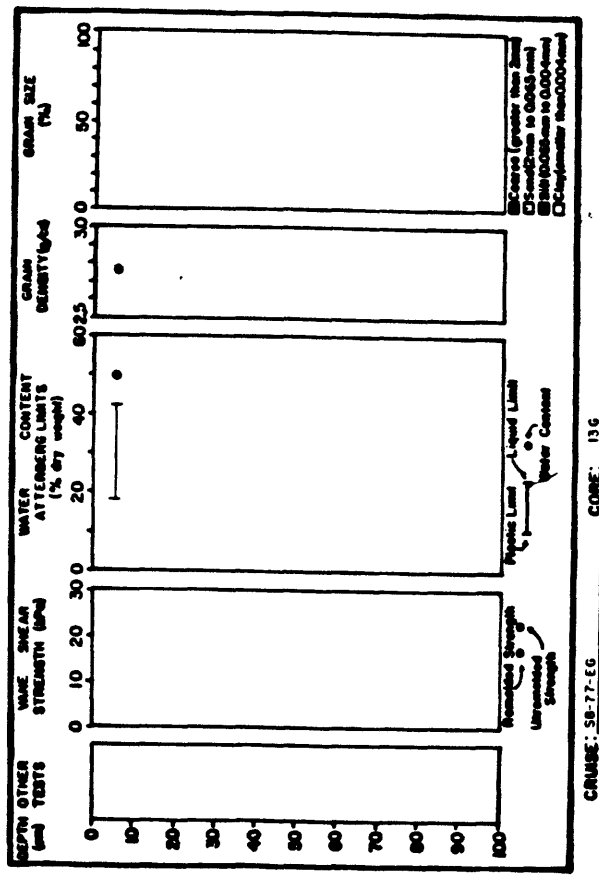
CORE: SB-77-EG

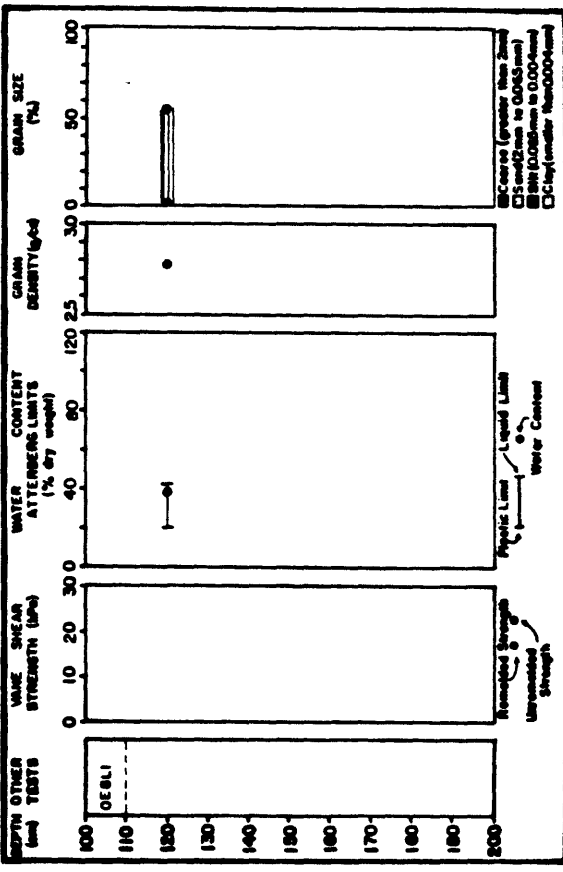
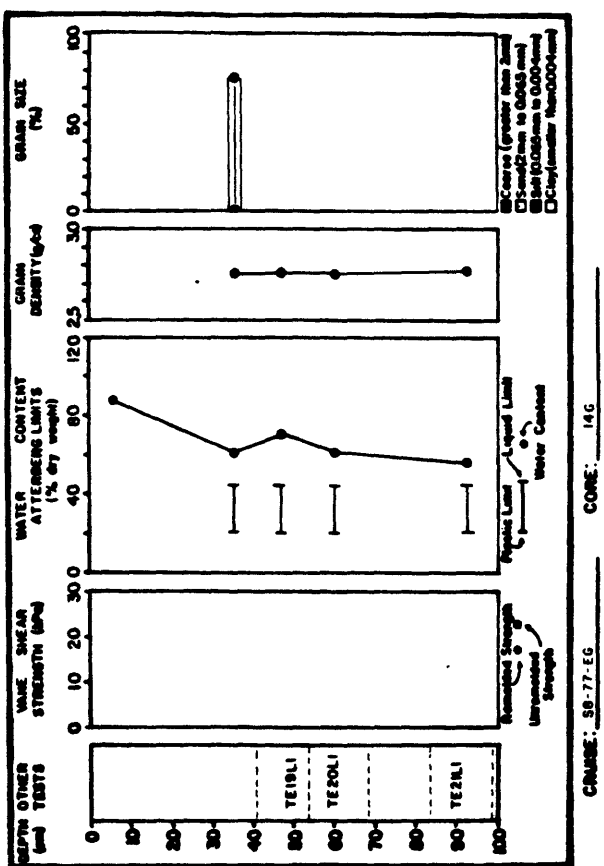
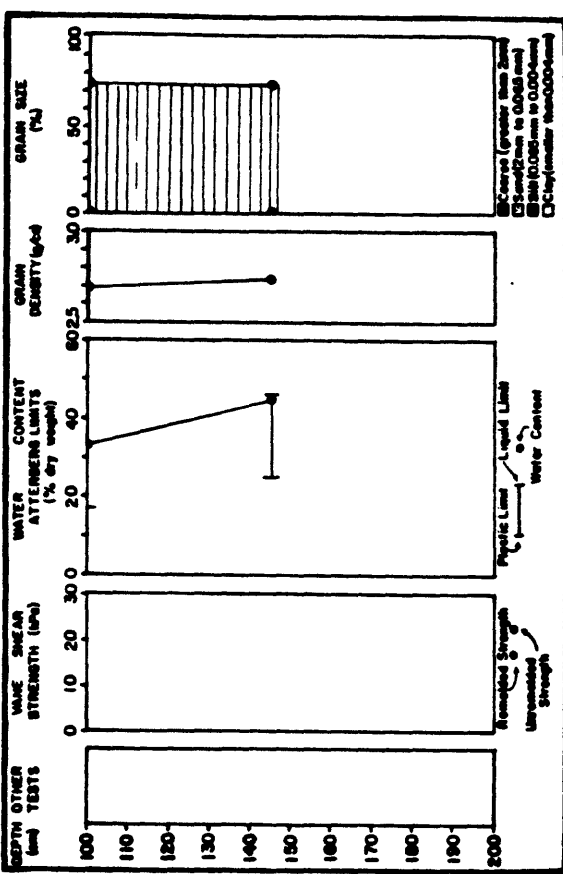
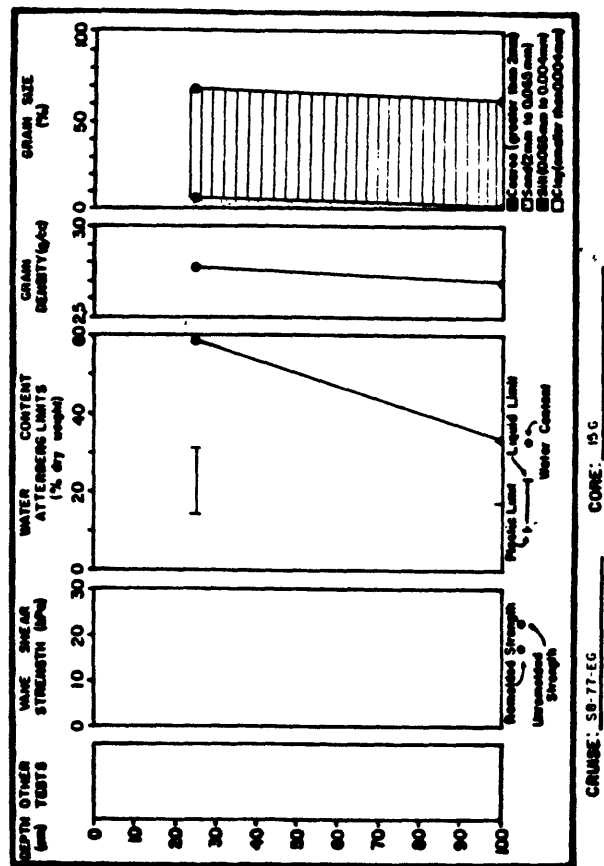


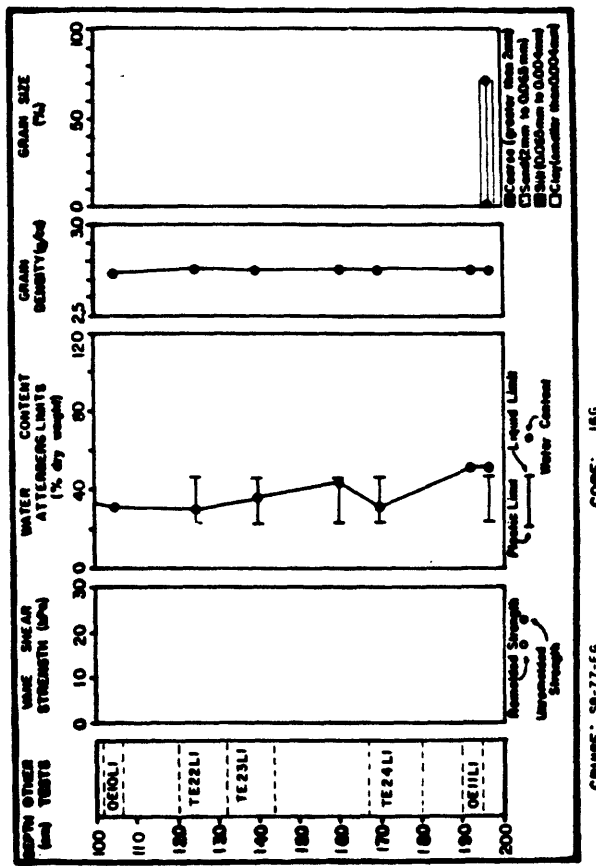
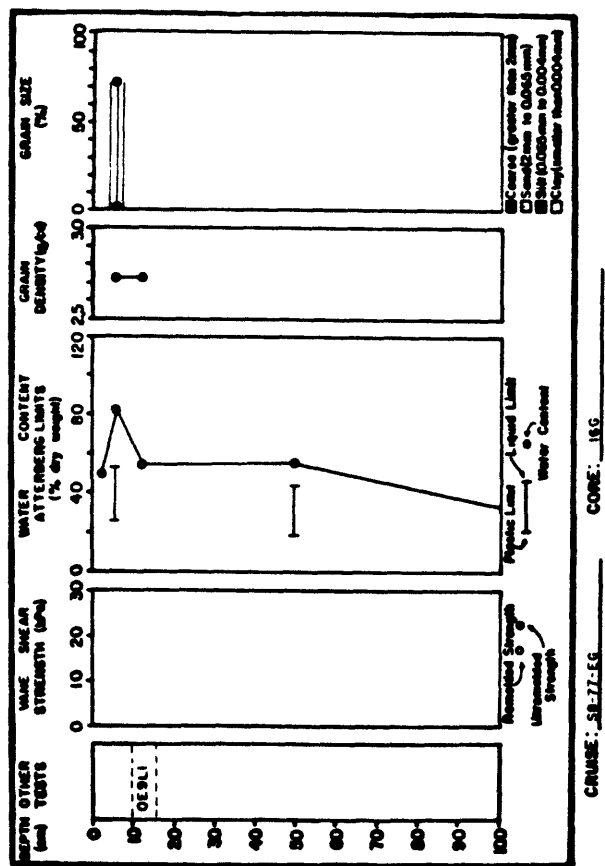
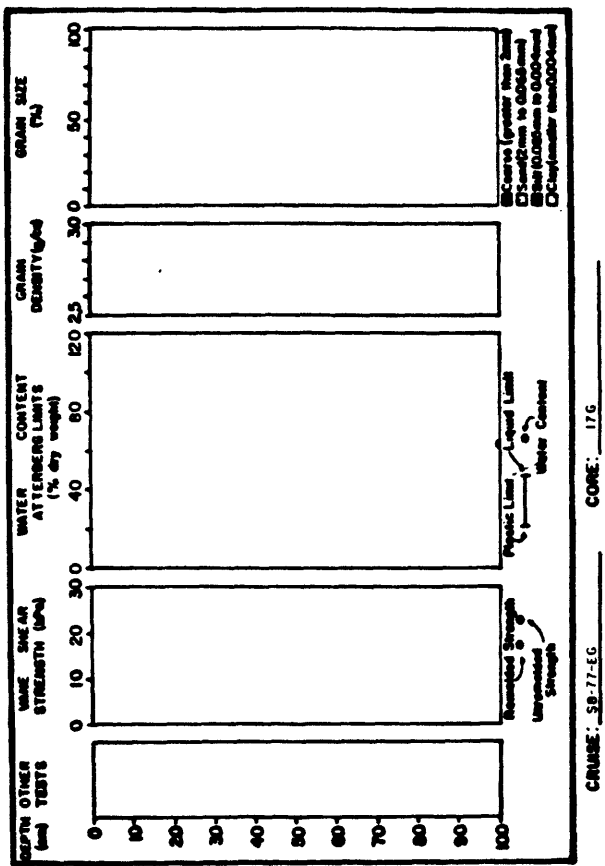
CORE: SB-77-EG

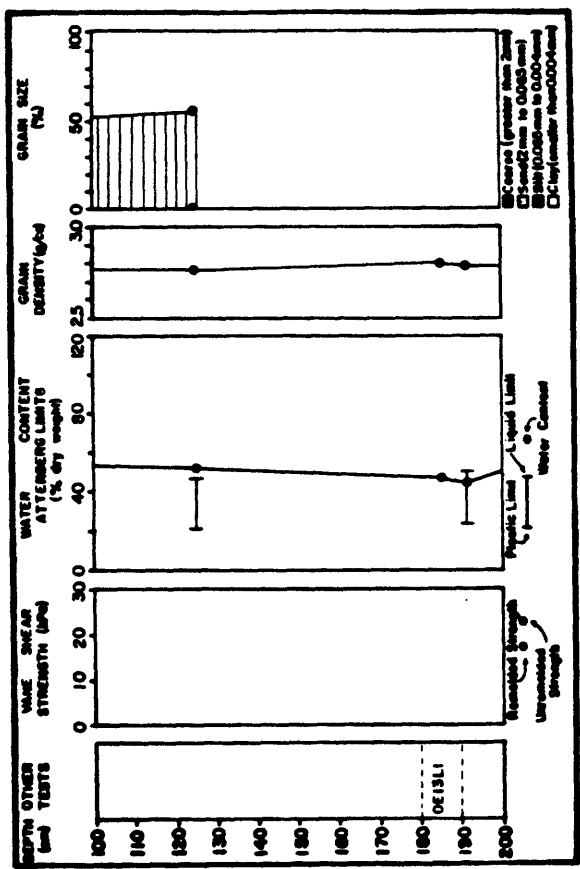
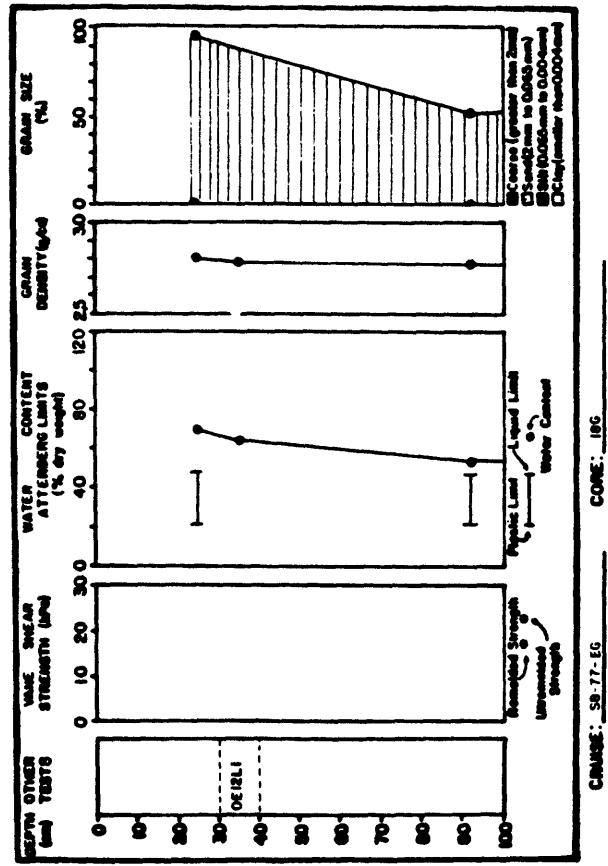
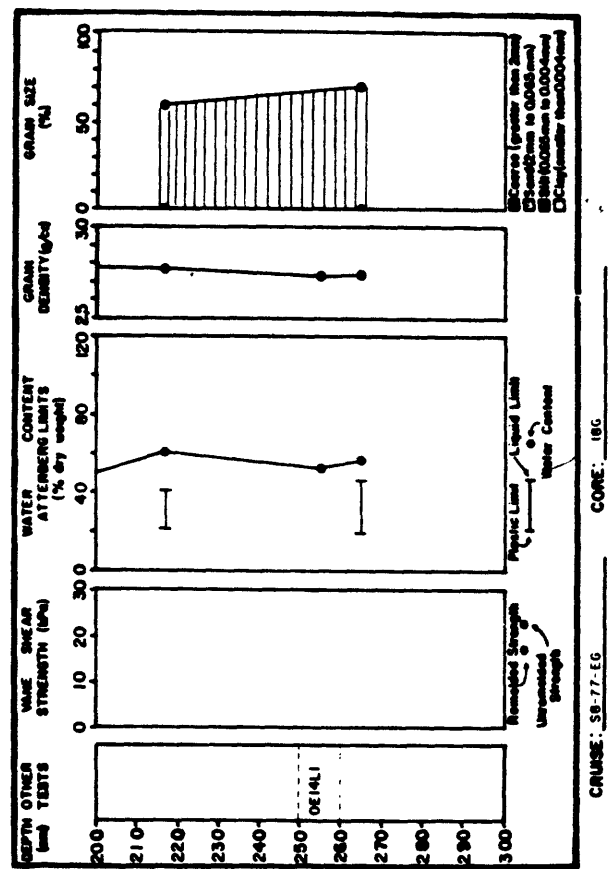


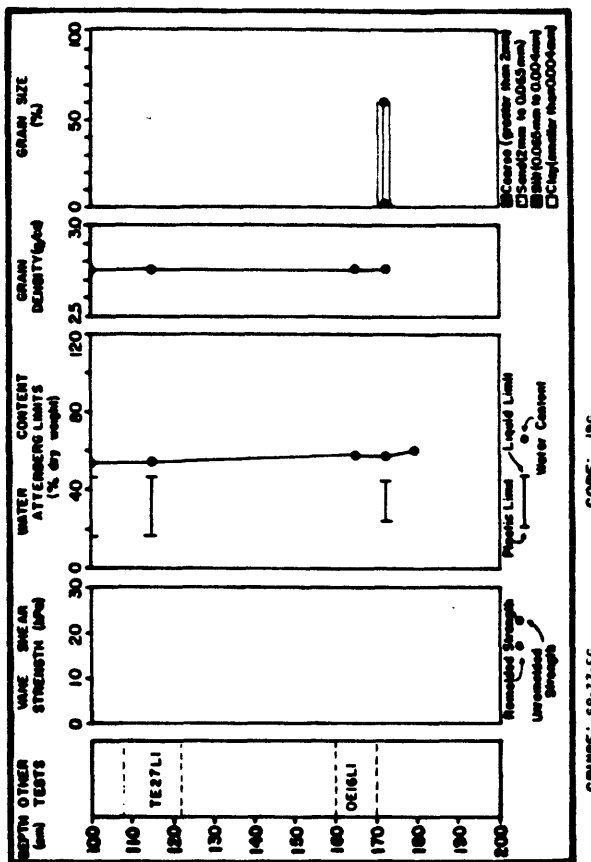
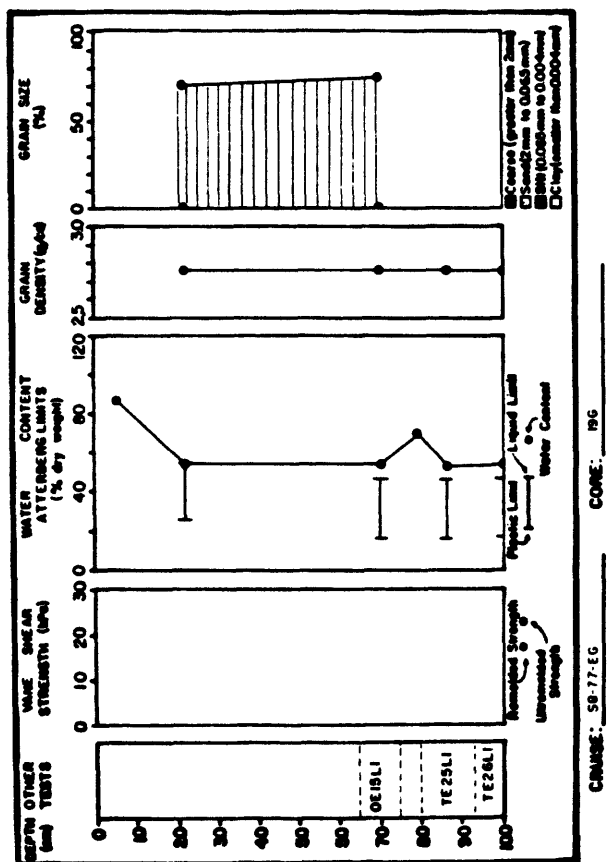
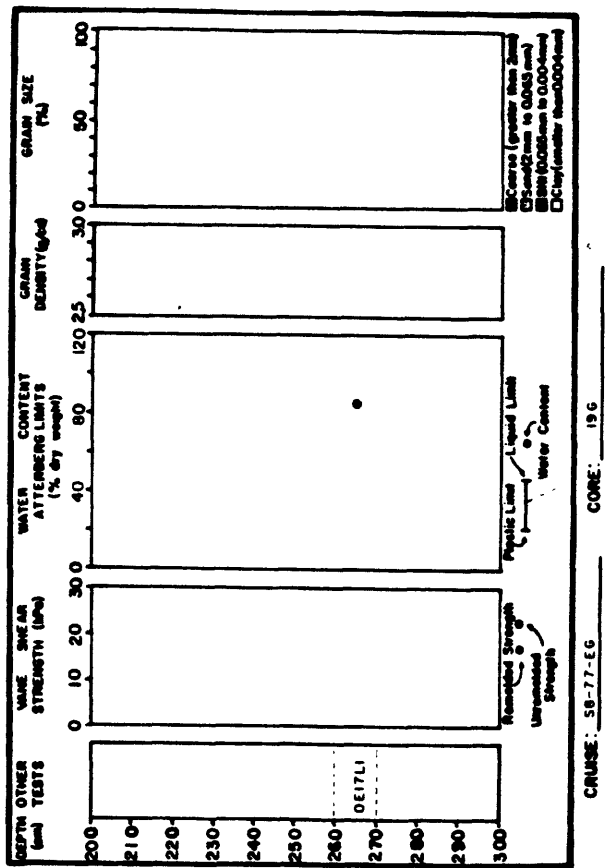
CORE: SB-77-EG

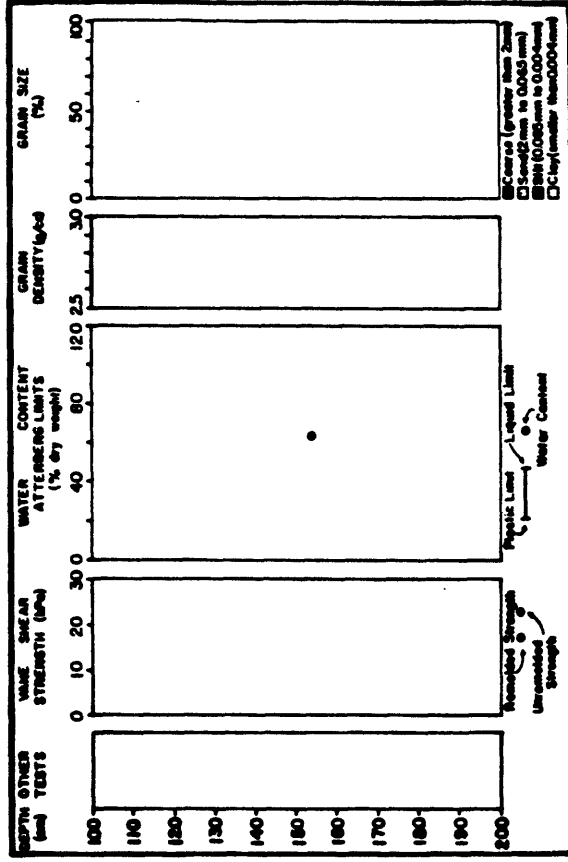
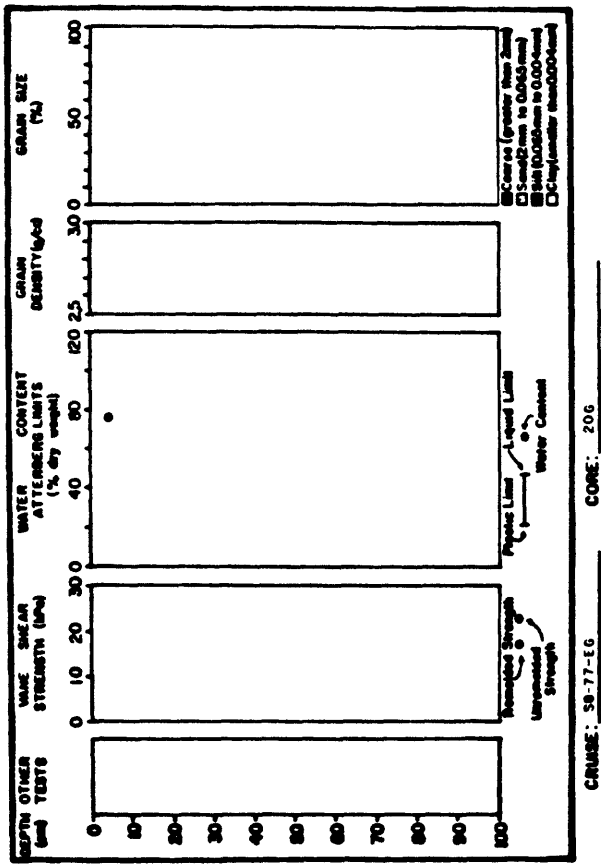


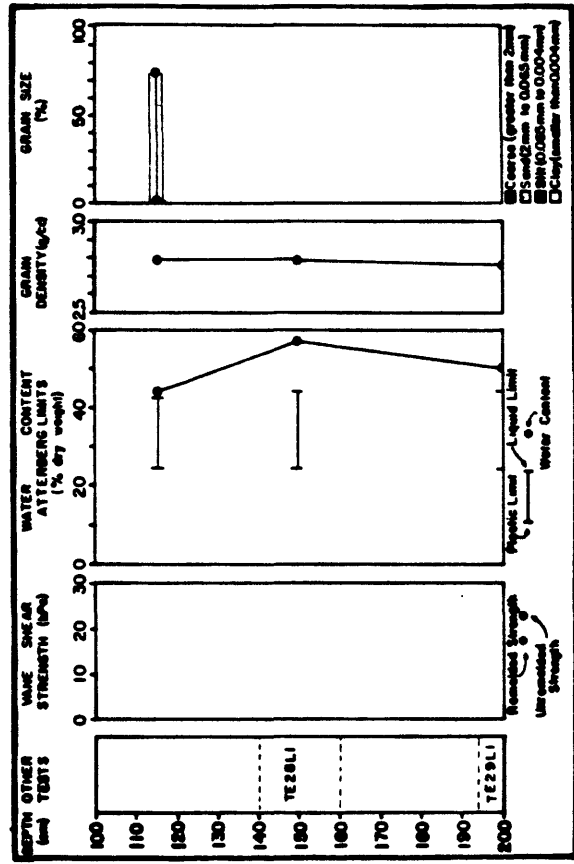
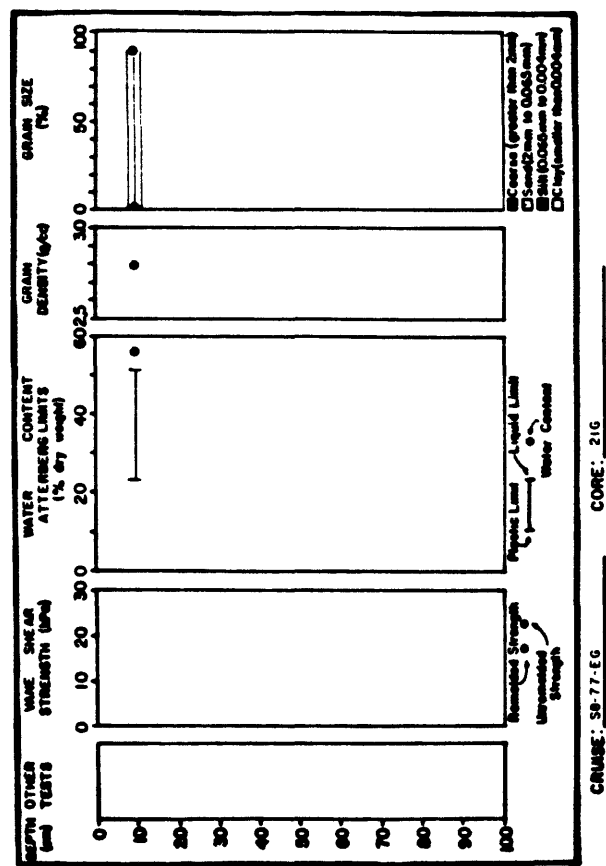
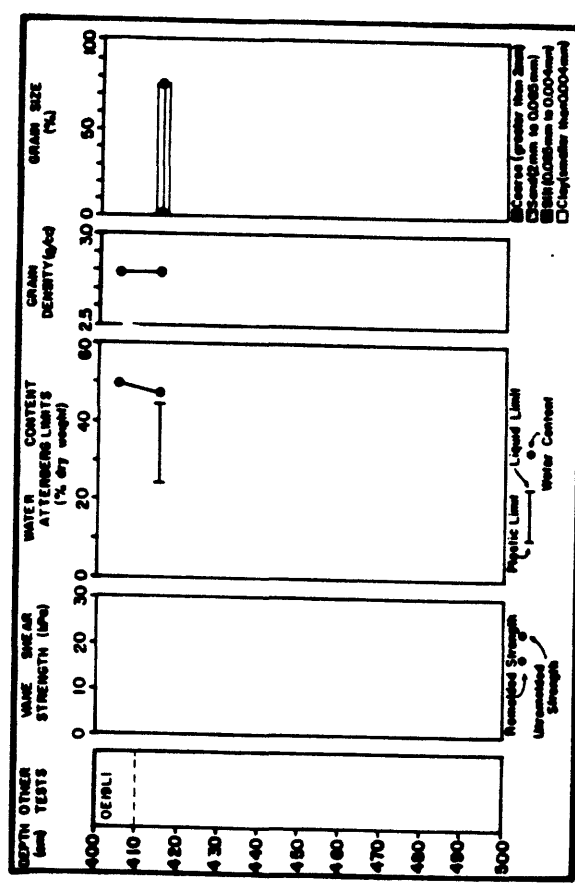
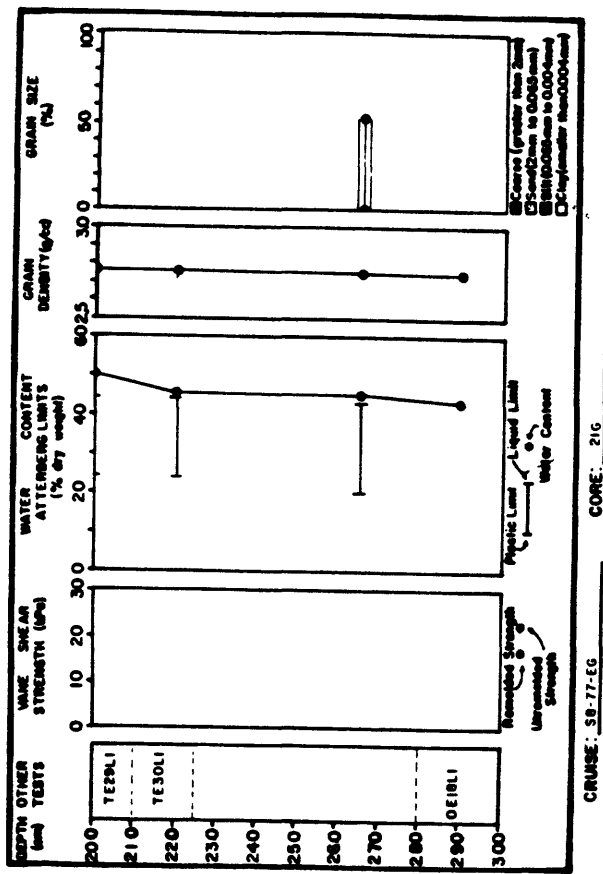




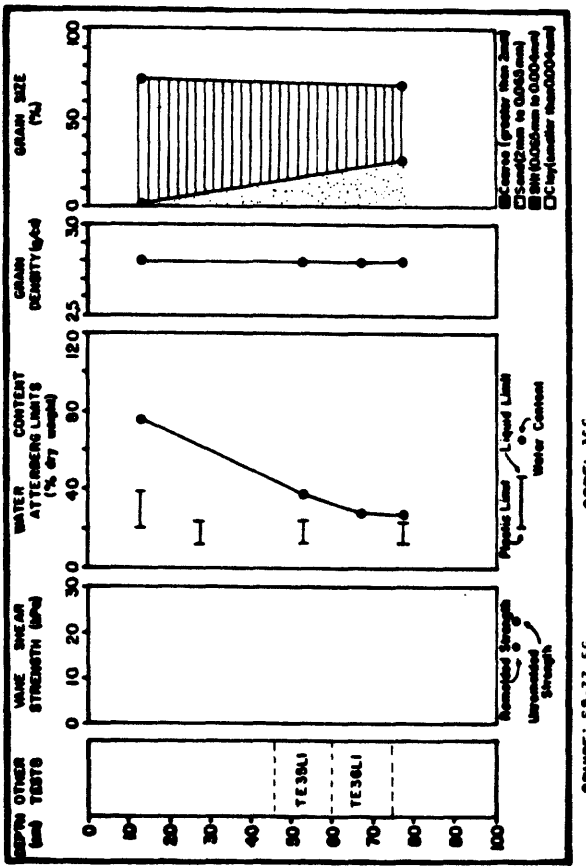
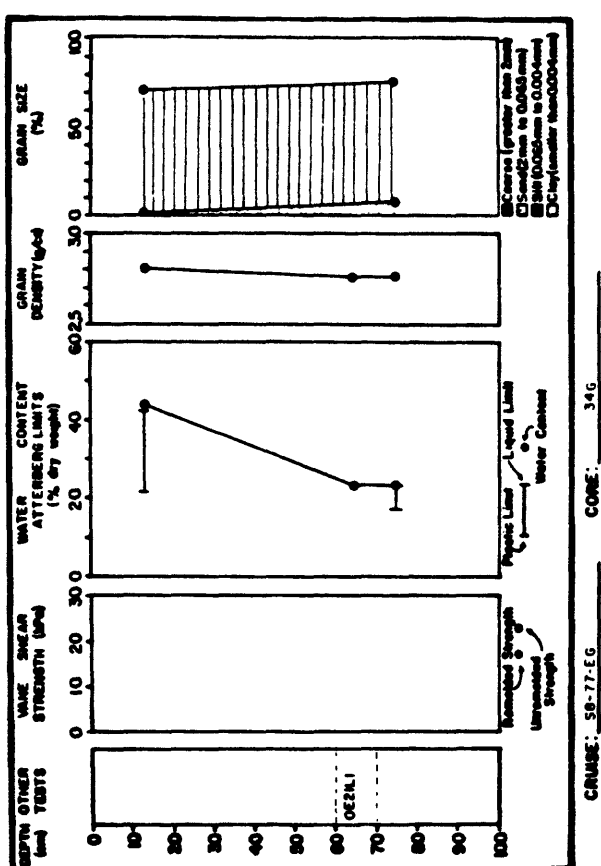
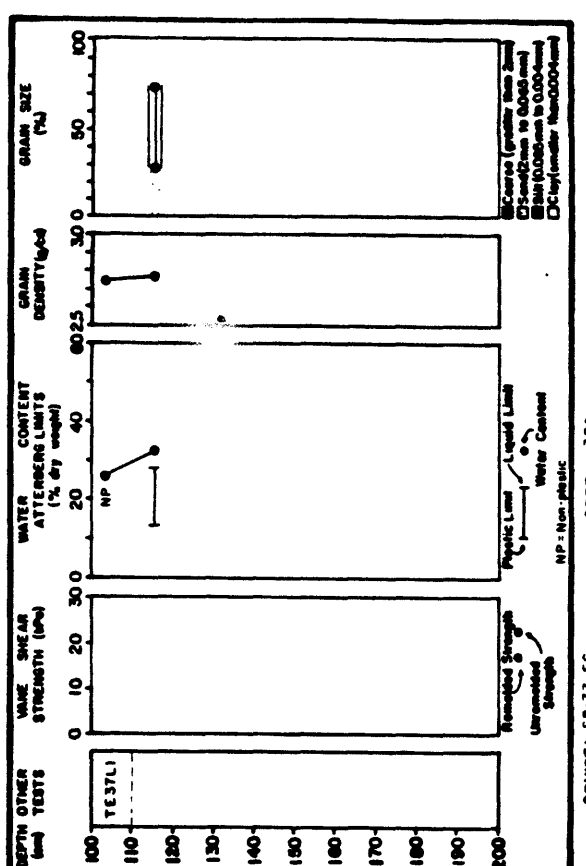
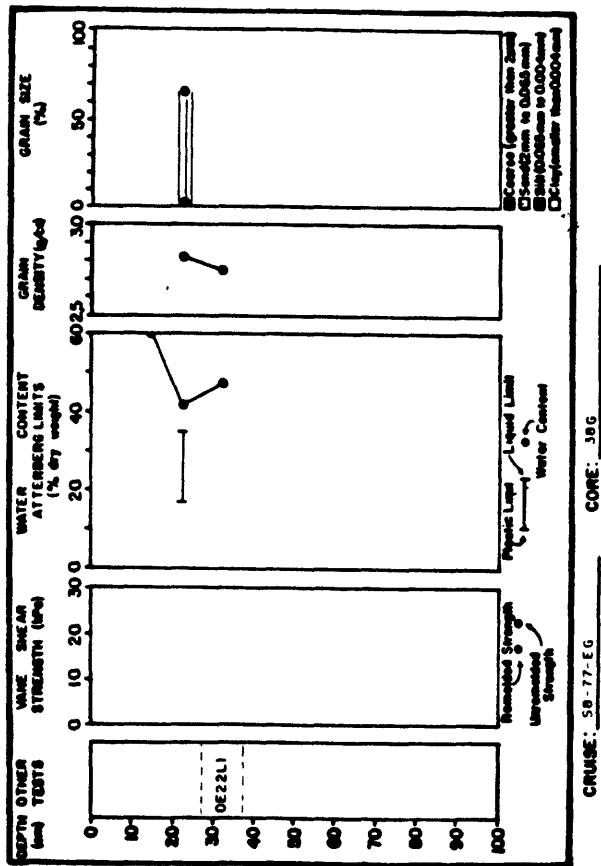




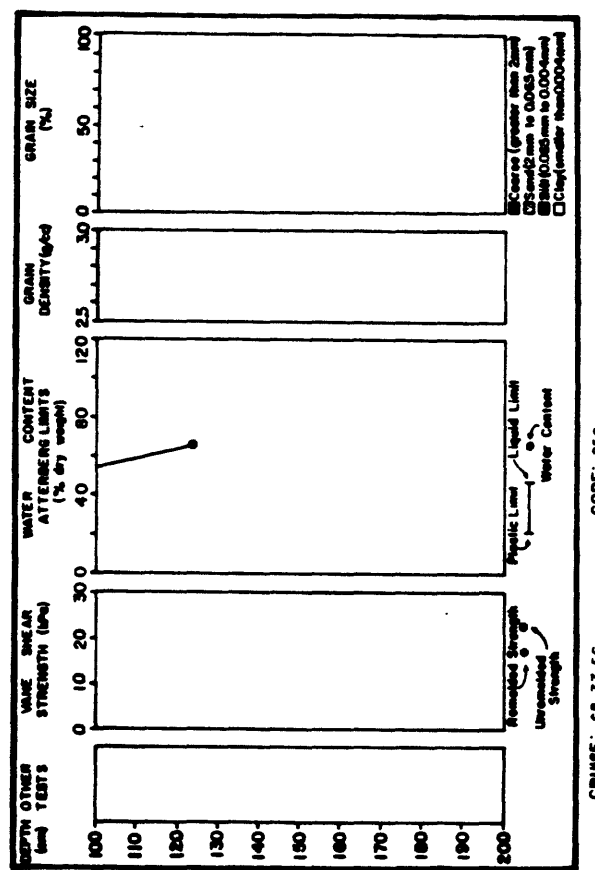
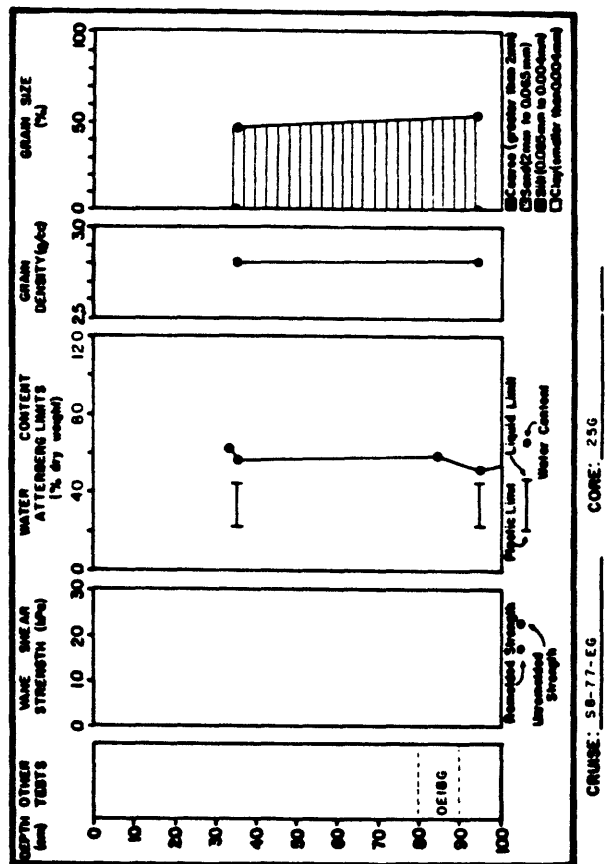
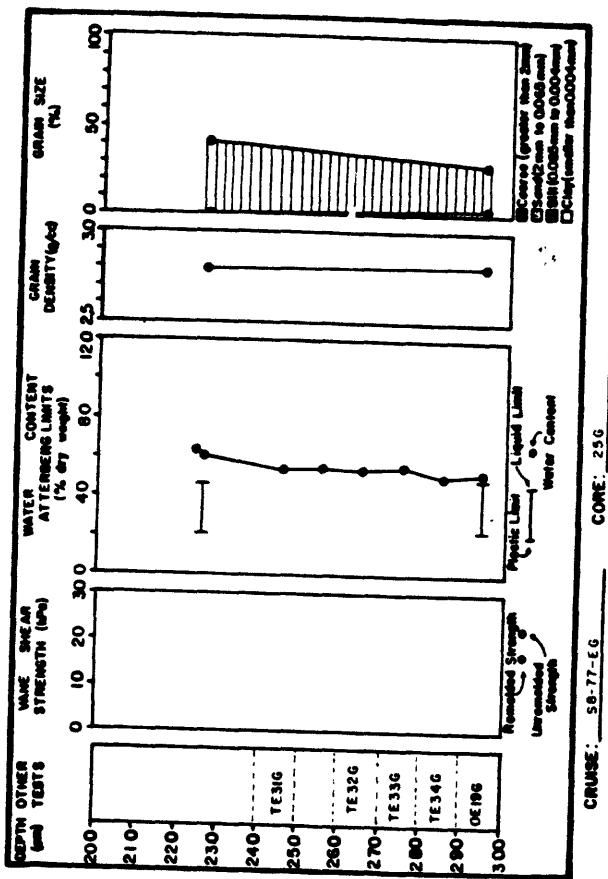


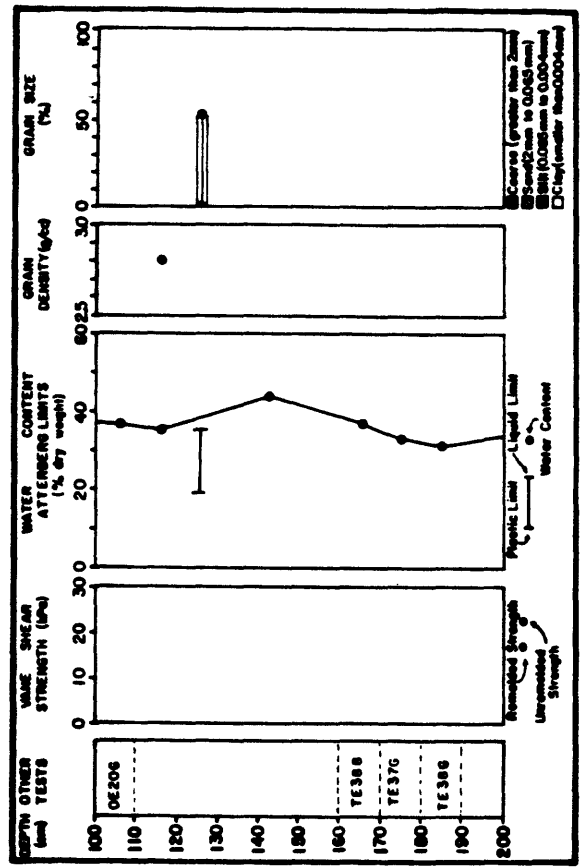
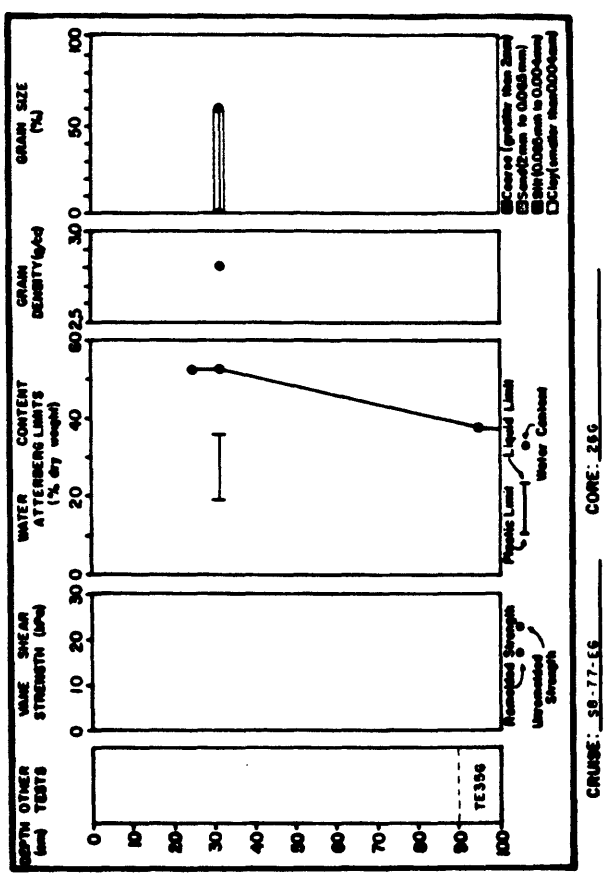
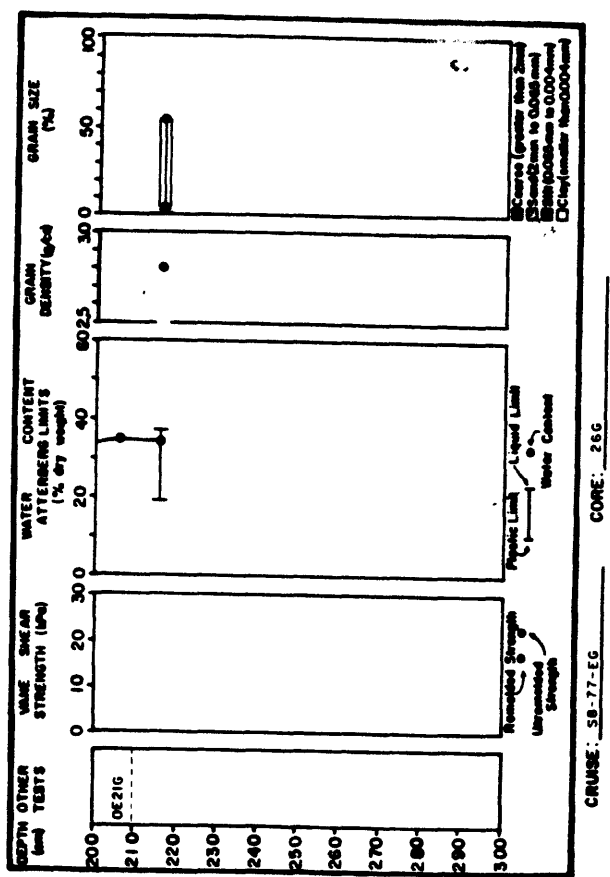


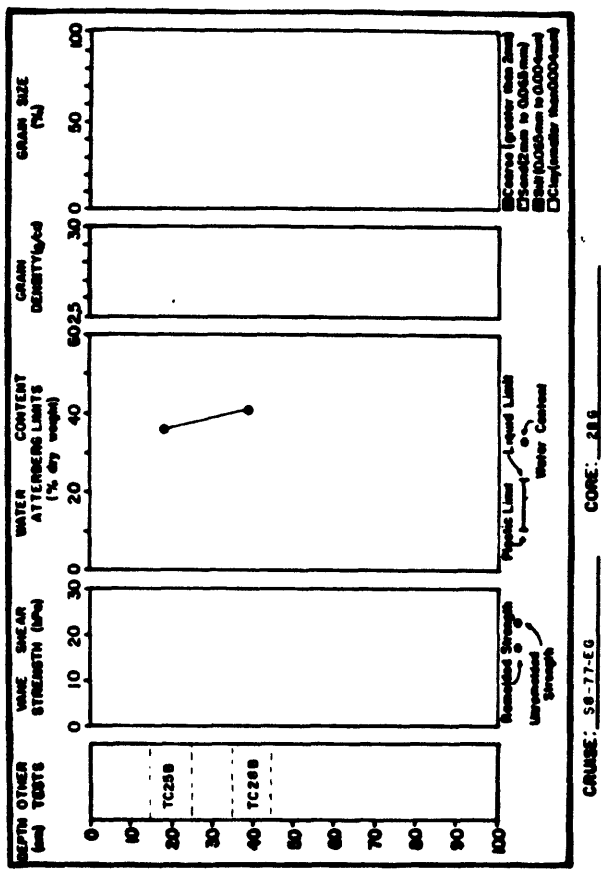
BERING TROUGH STUDY AREA



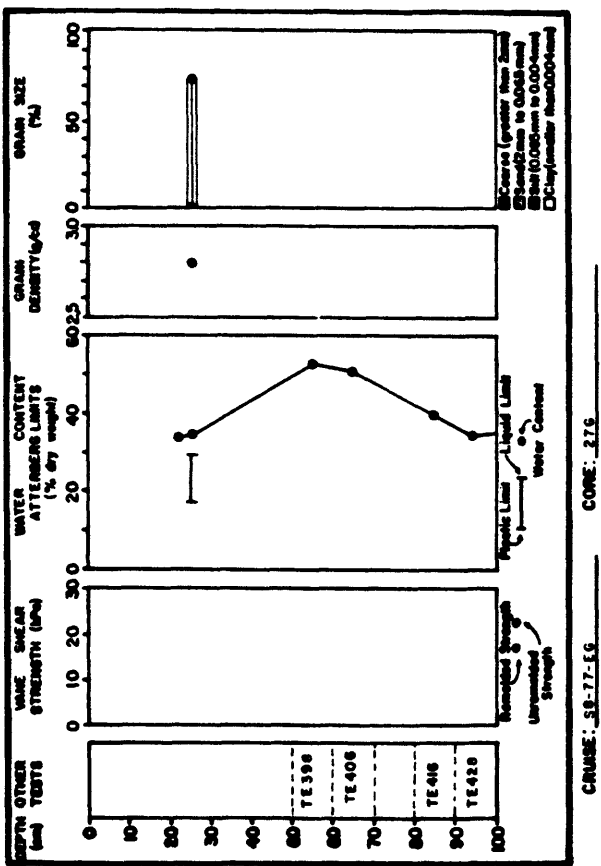
**ICY BAY-MALASPINA STUDY AREA**



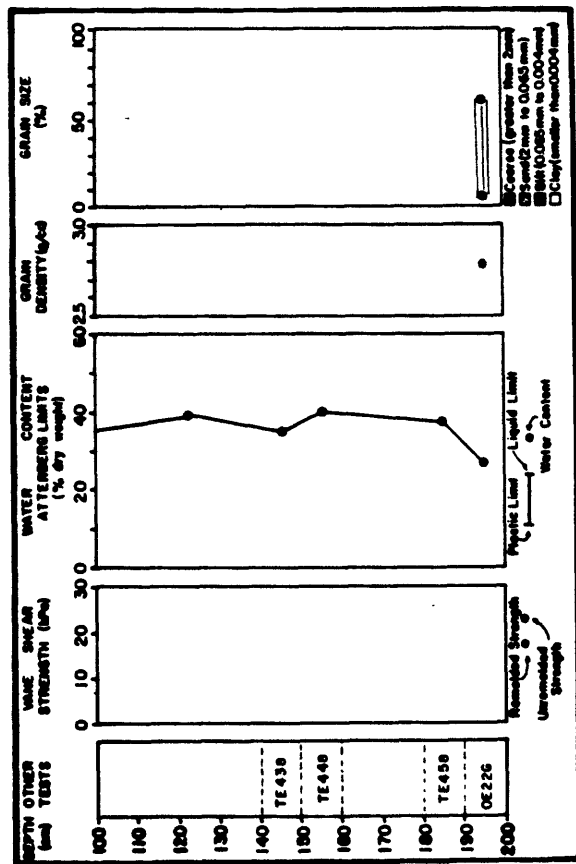




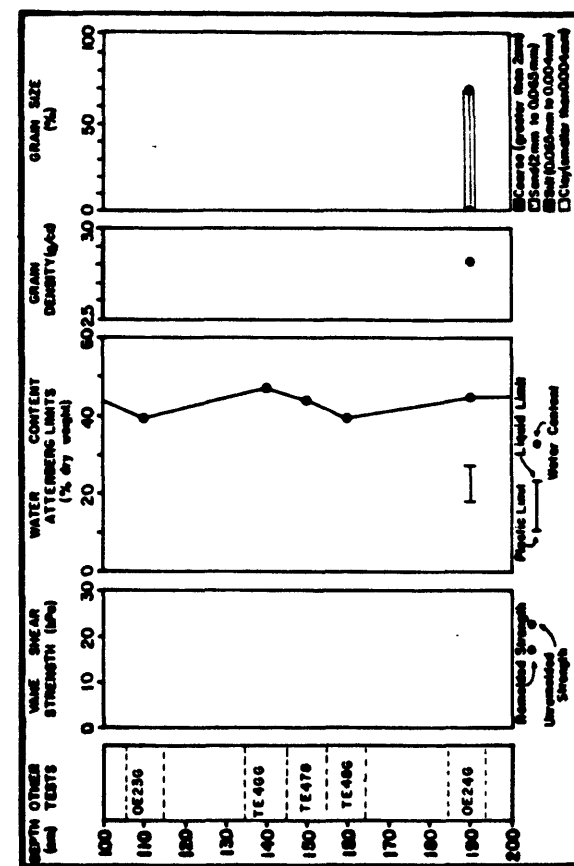
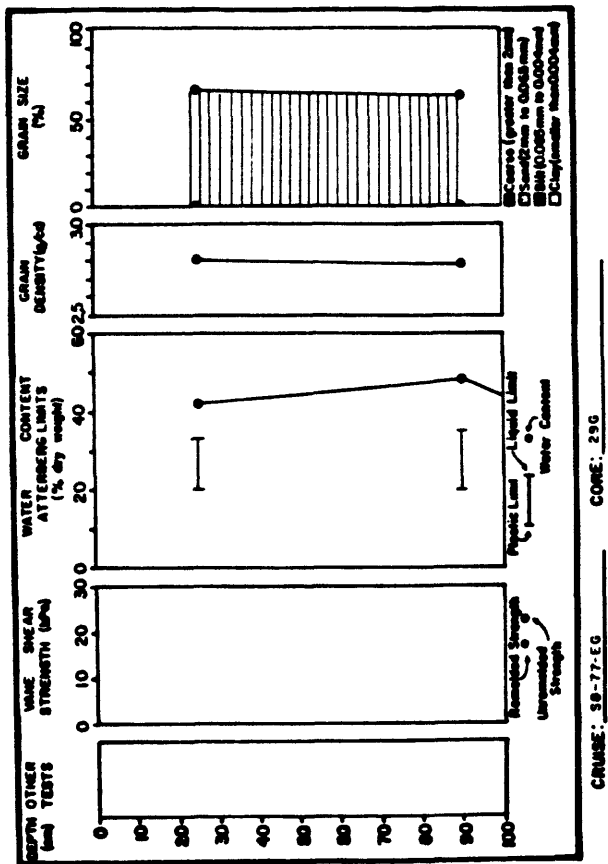
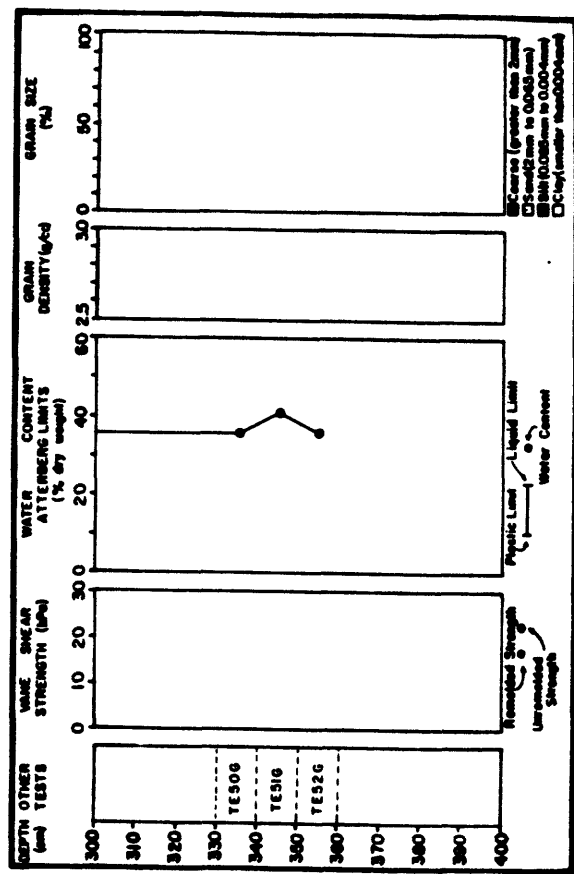
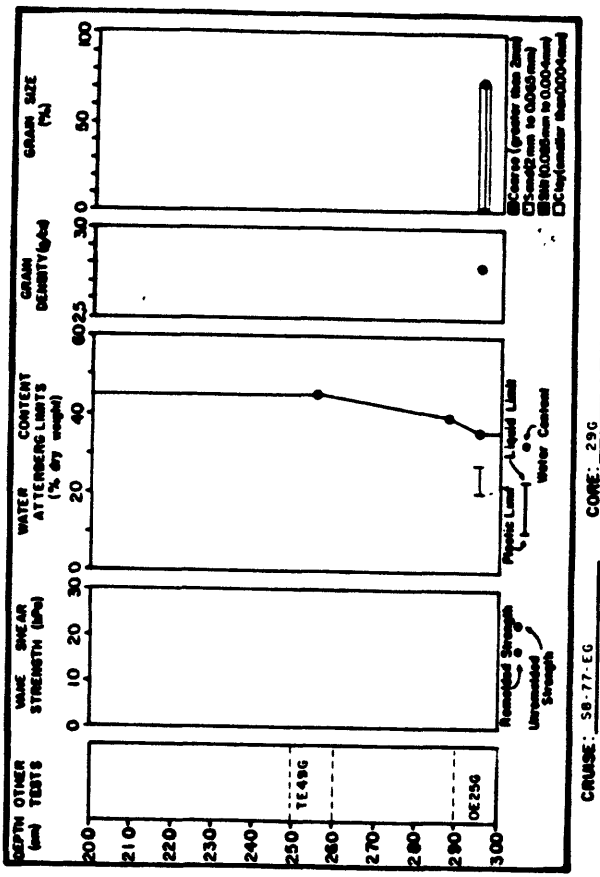
CRUISE: SE-77-EG      CORE: 216

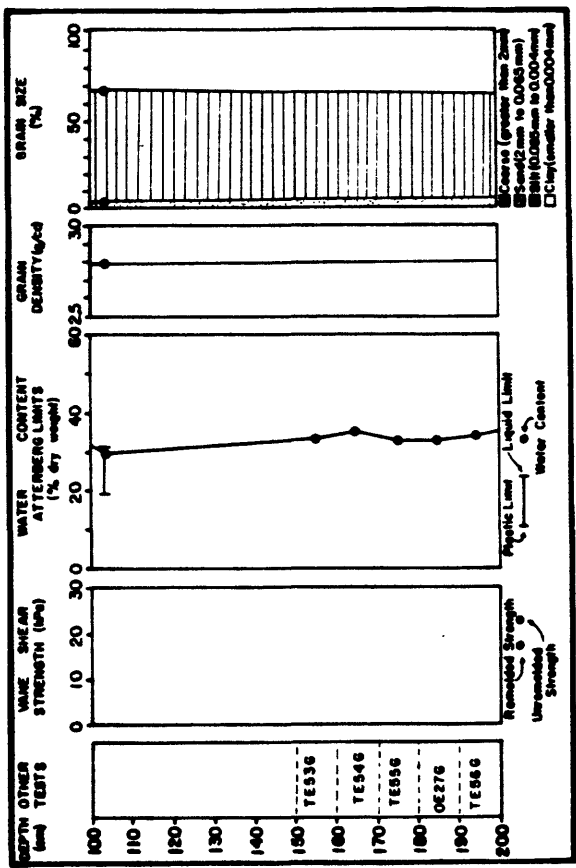
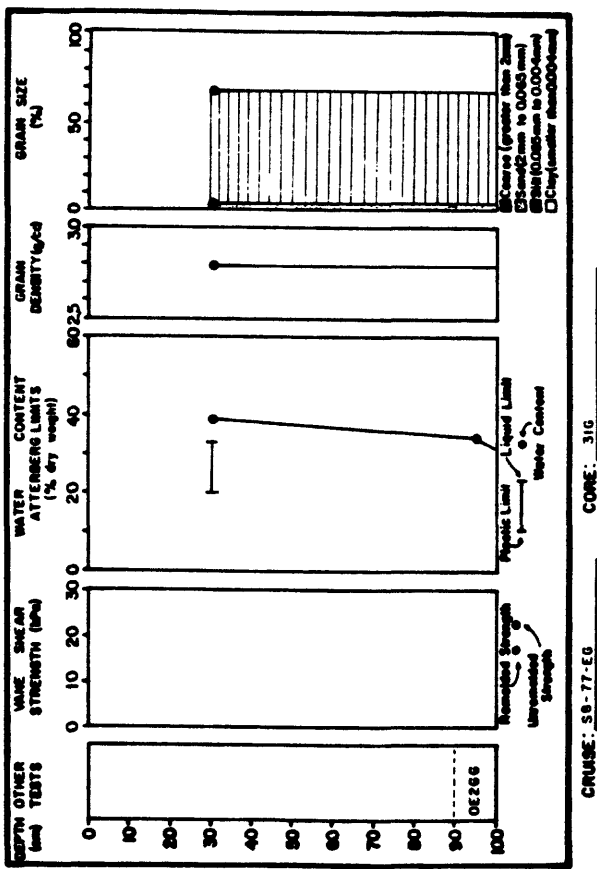
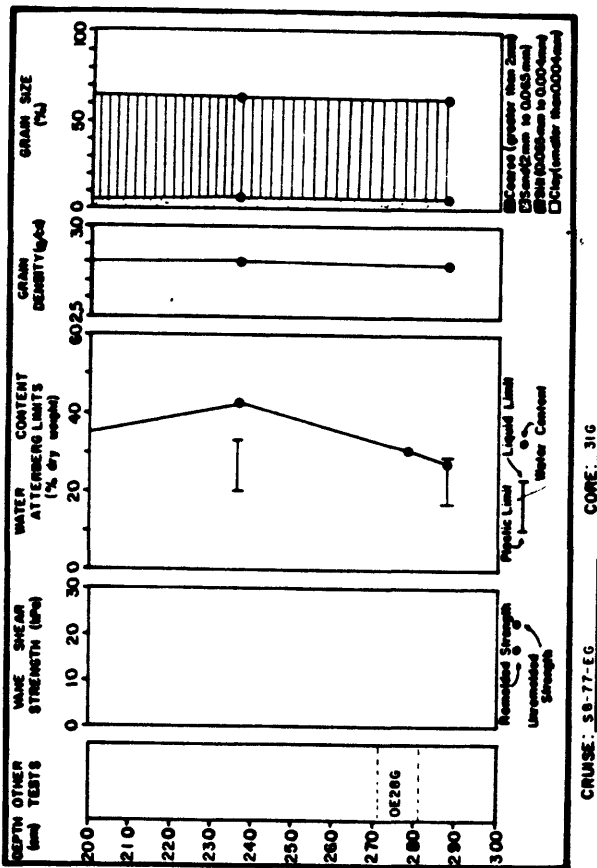


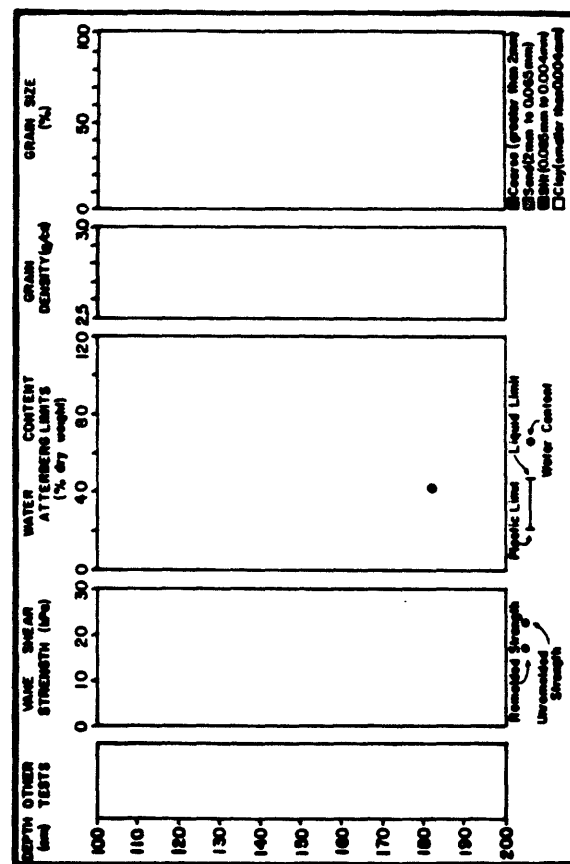
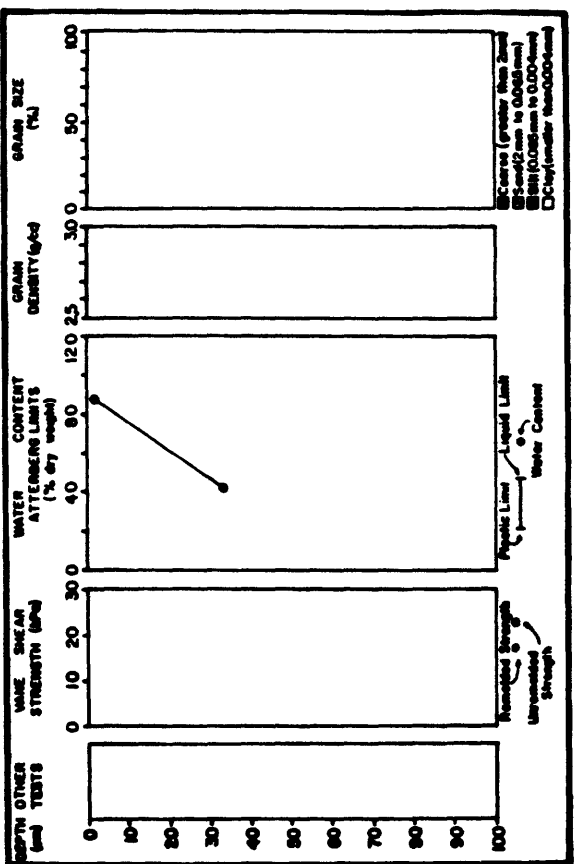
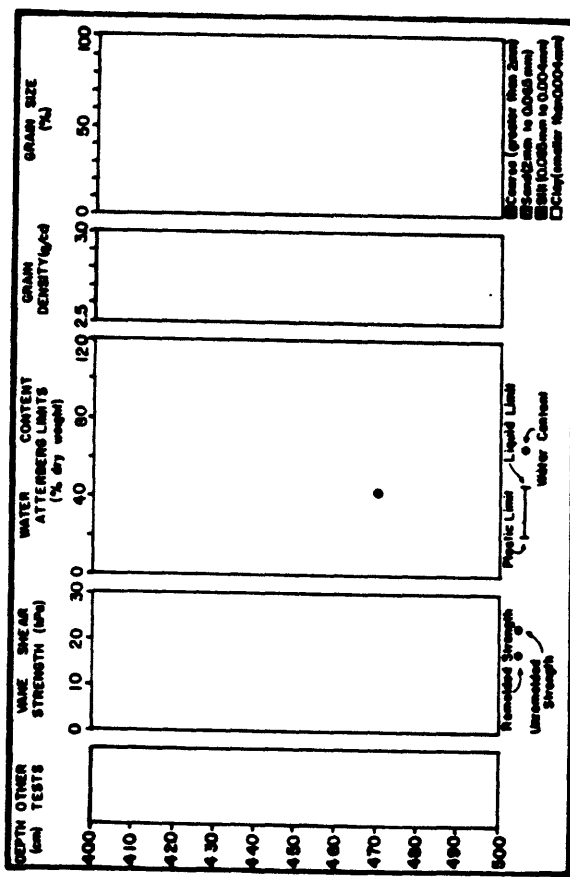
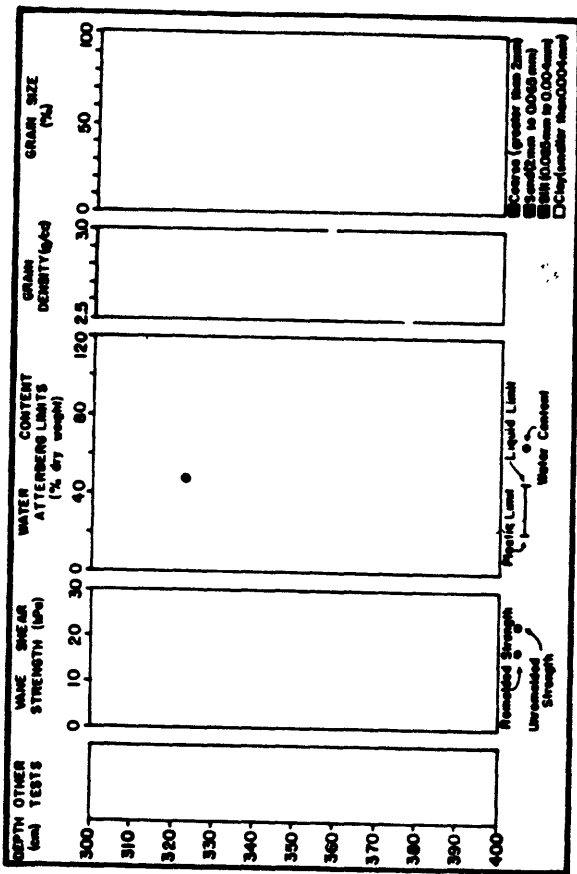
CRUISE: SE-77-EG      CORE: 216

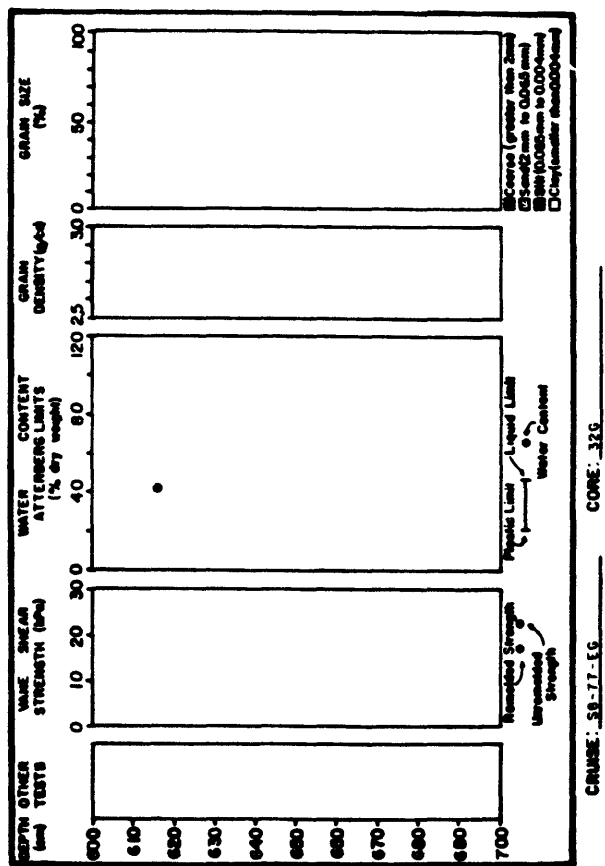


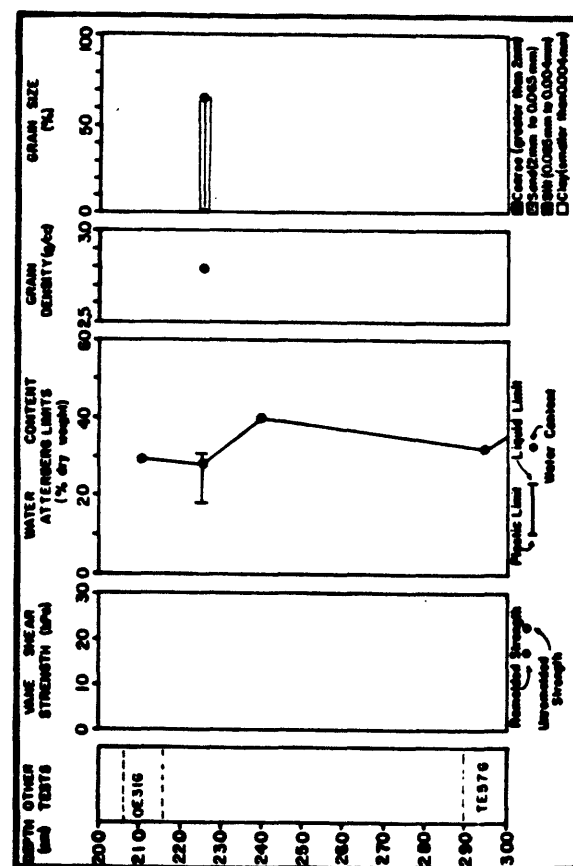
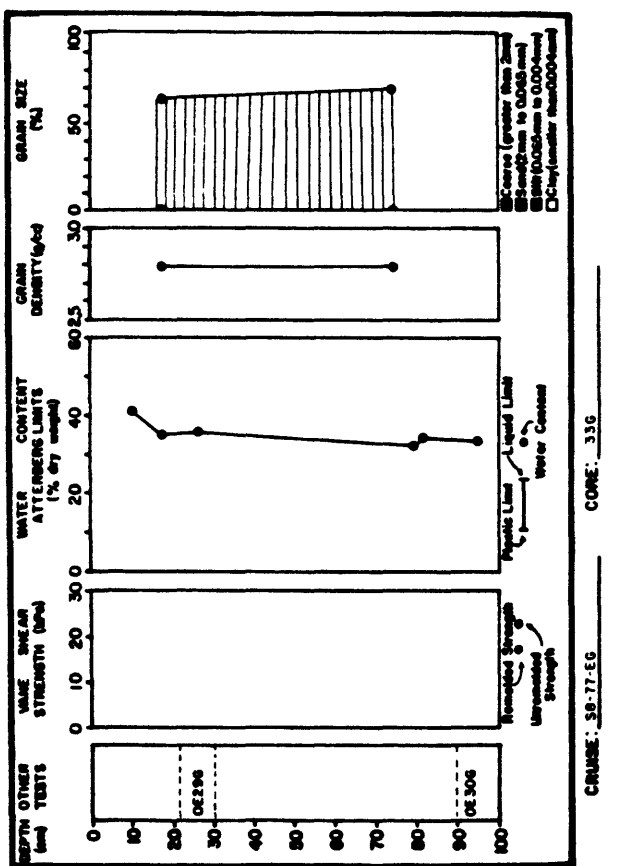
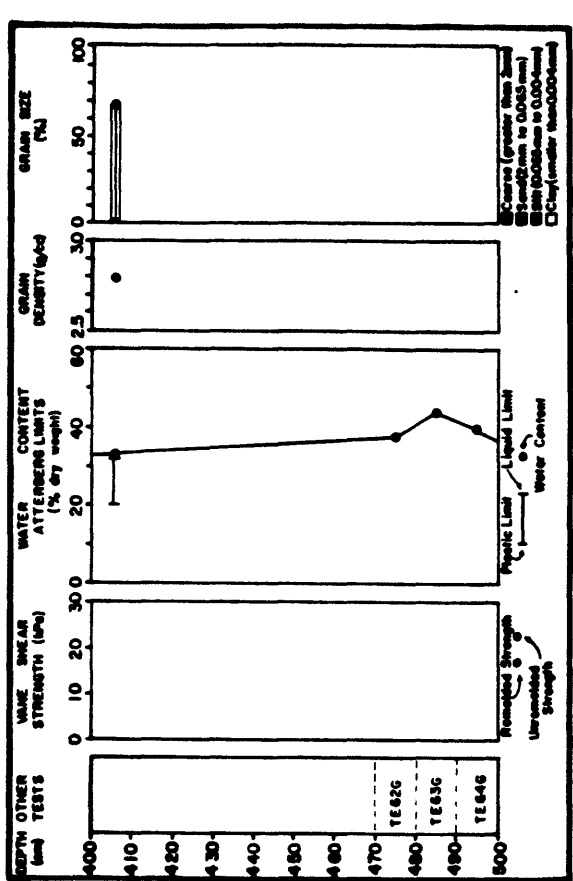
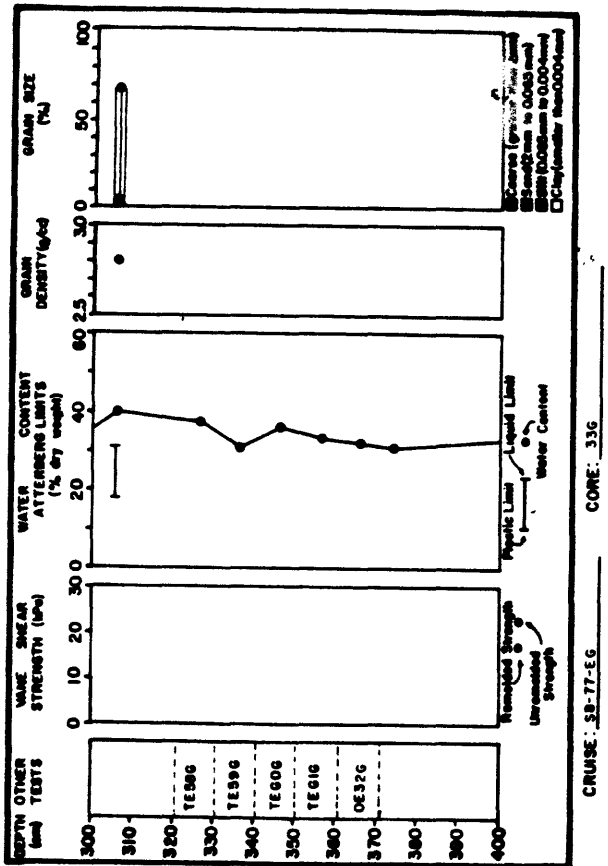
CRUISE: SE-77-EG      CORE: 276

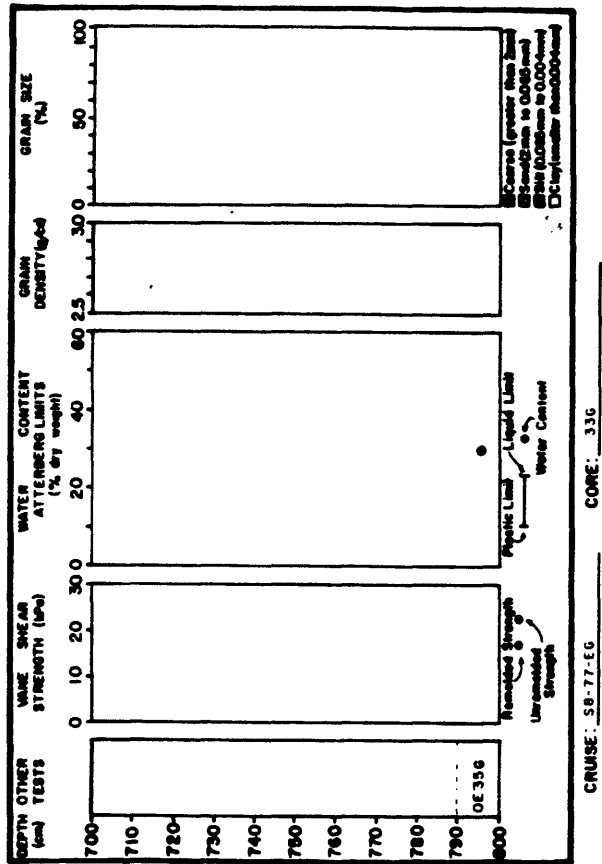




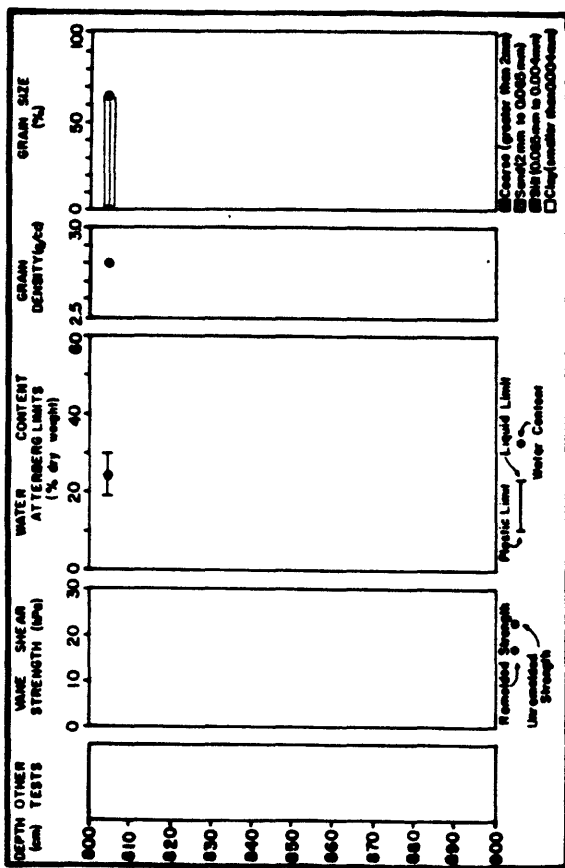




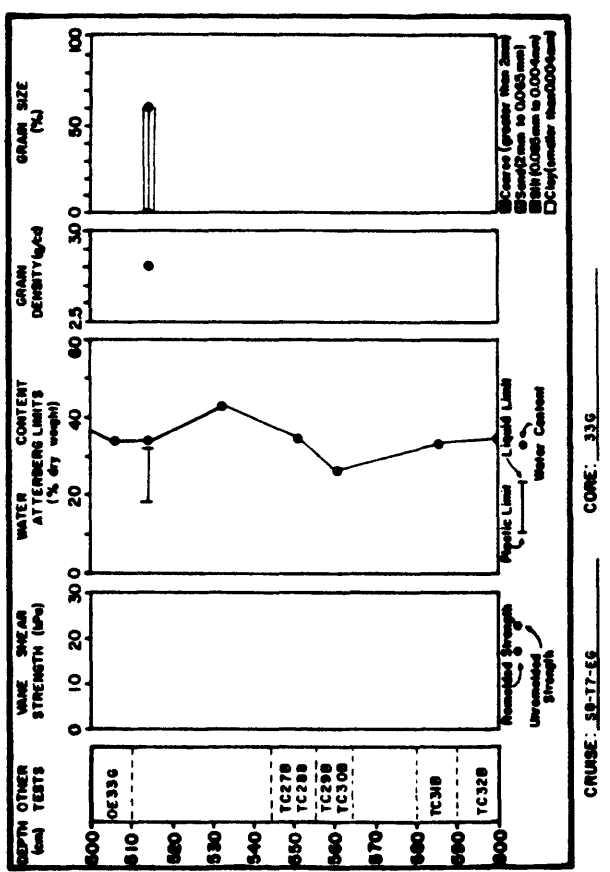




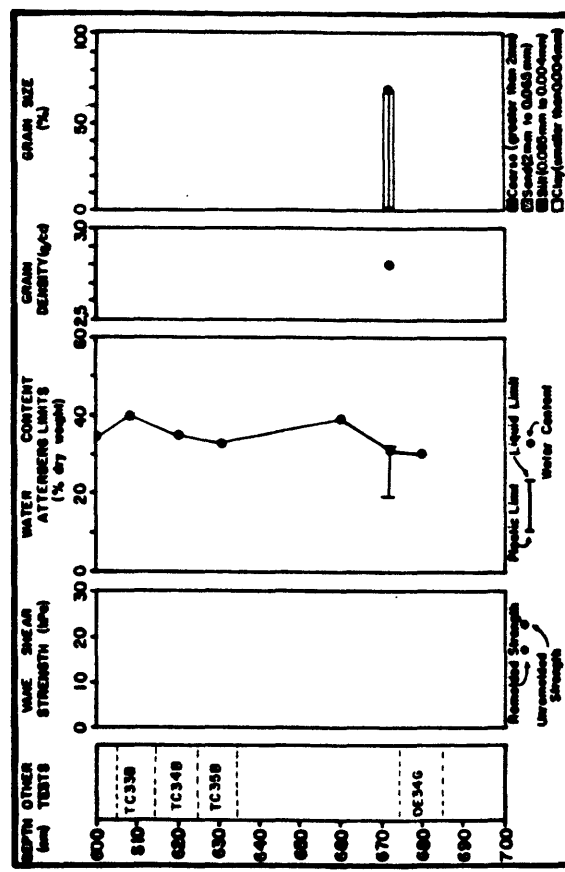
CRUISE: SB-77-EG      CORE: 33G



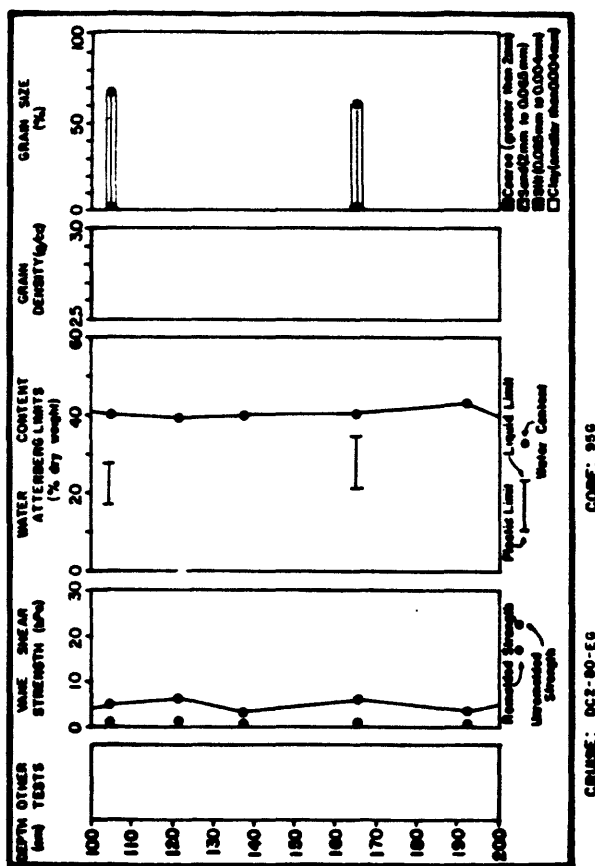
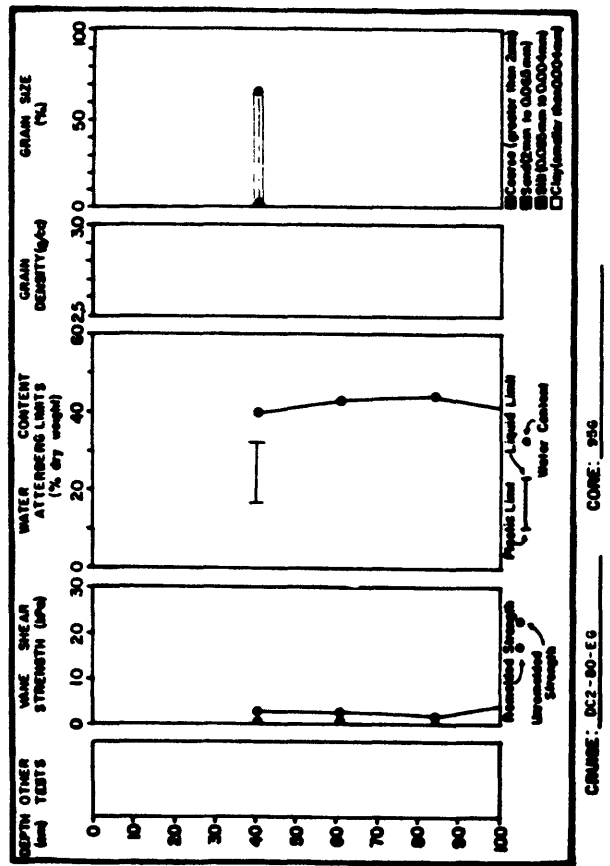
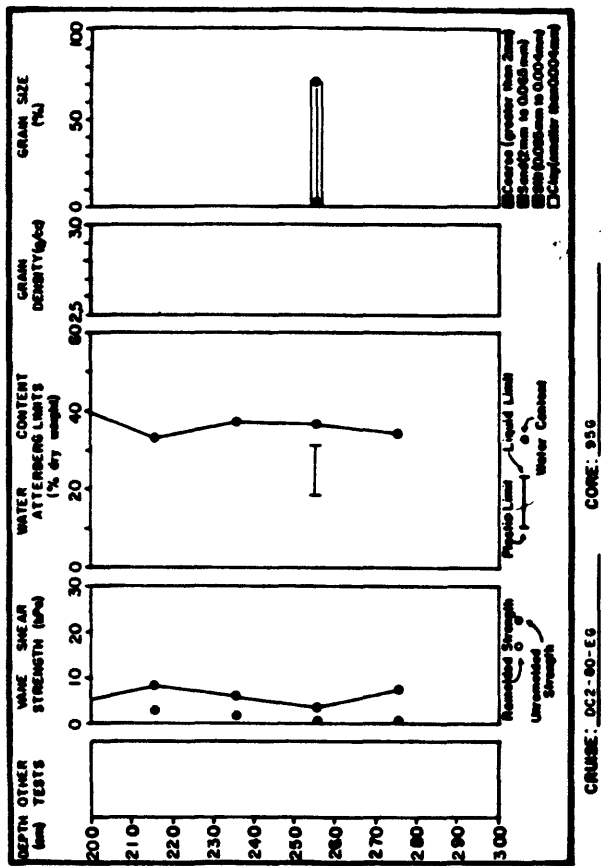
CRUISE: SB-77-EG      CORE: 33G

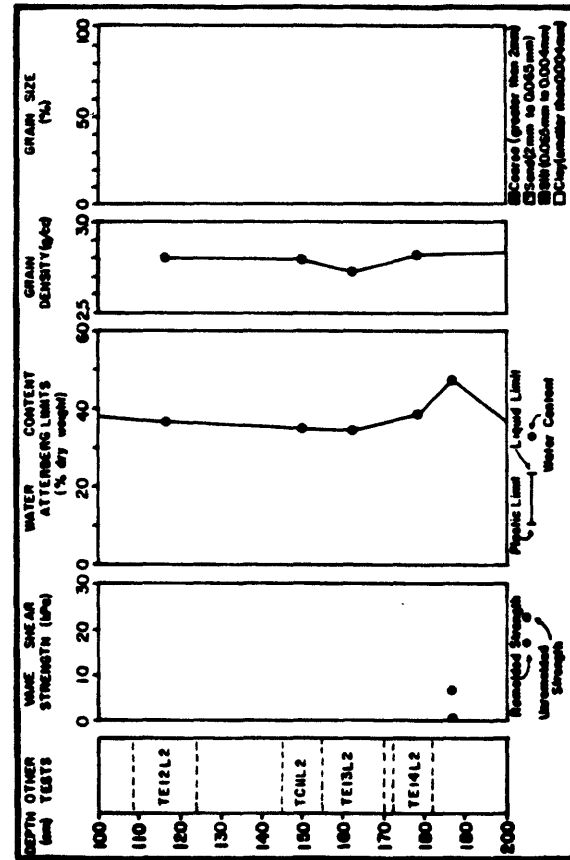
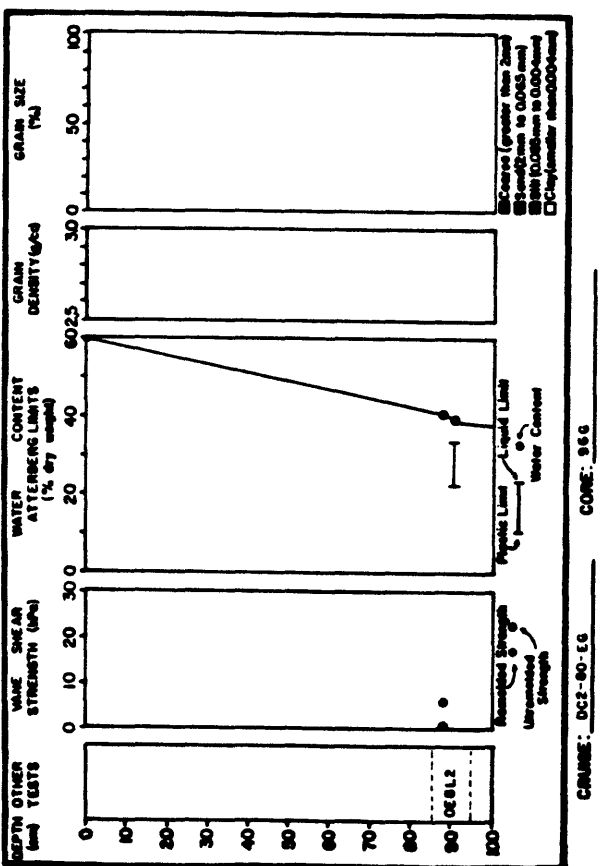
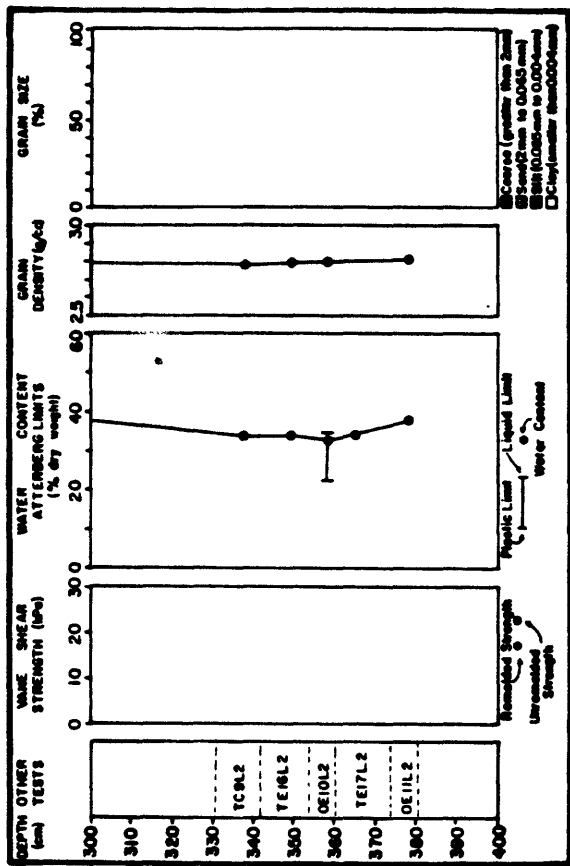
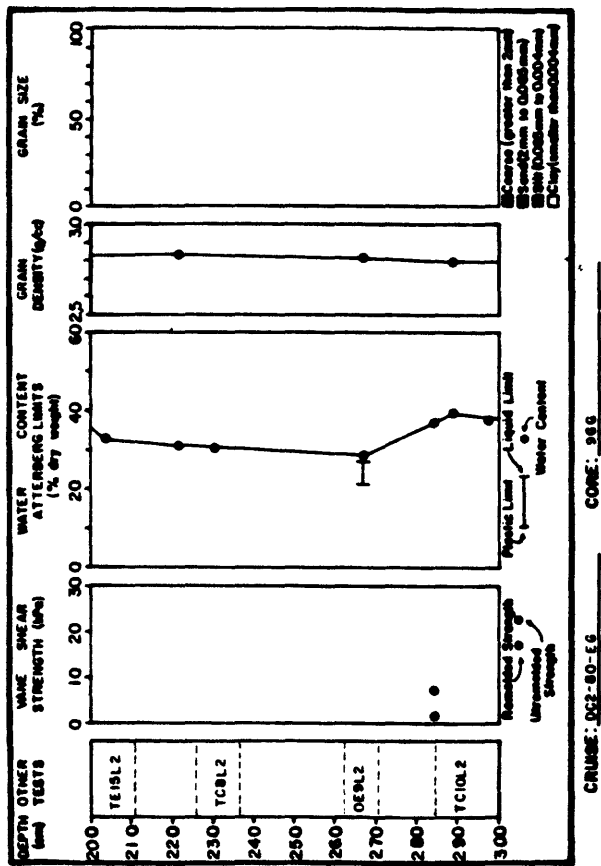


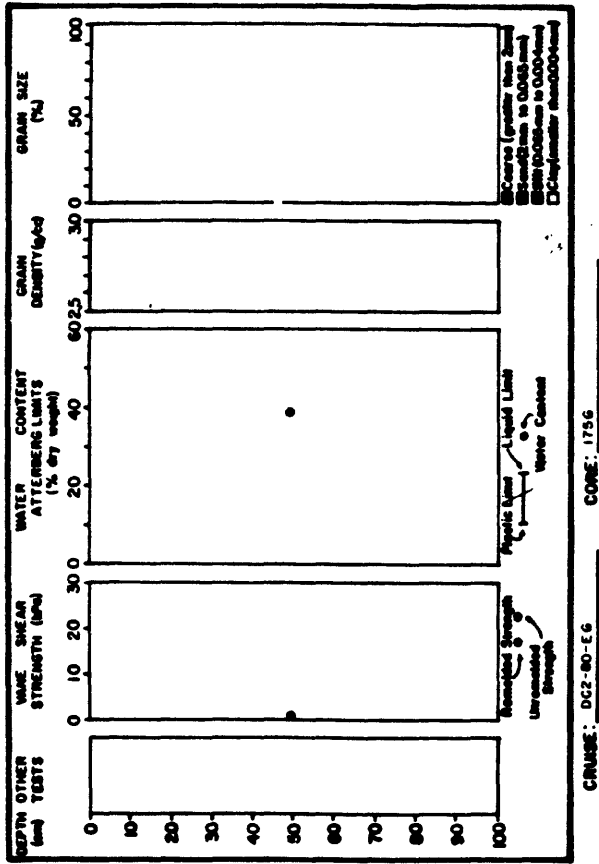
CRUISE: SB-77-EG      CORE: 33G



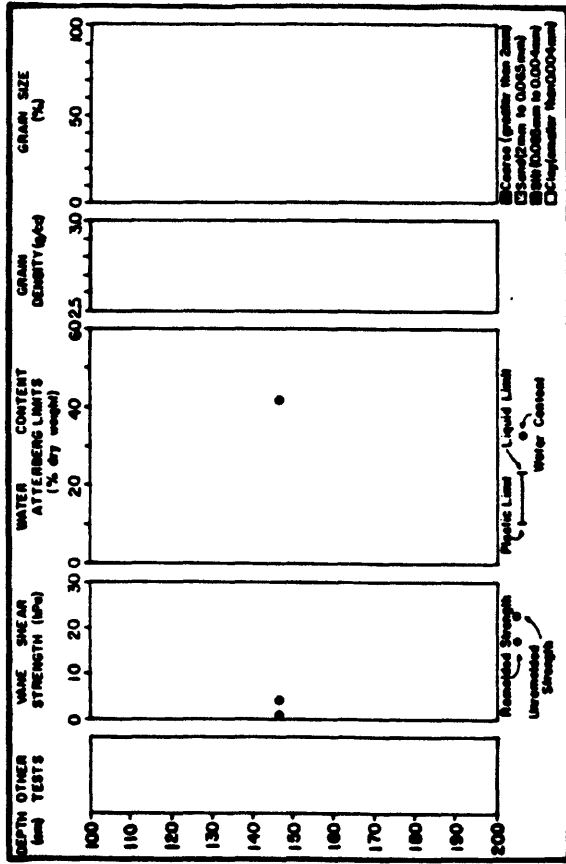
CRUISE: SB-77-EG      CORE: 33G



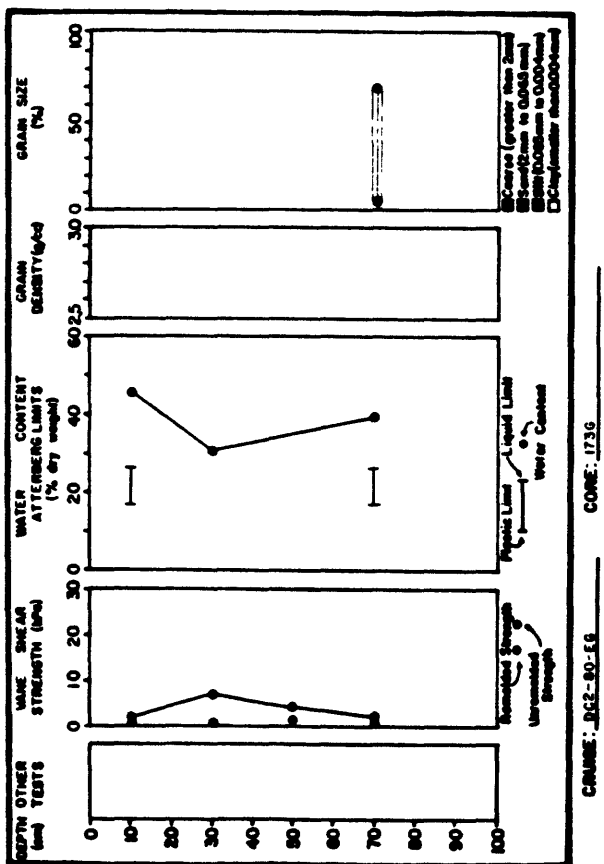




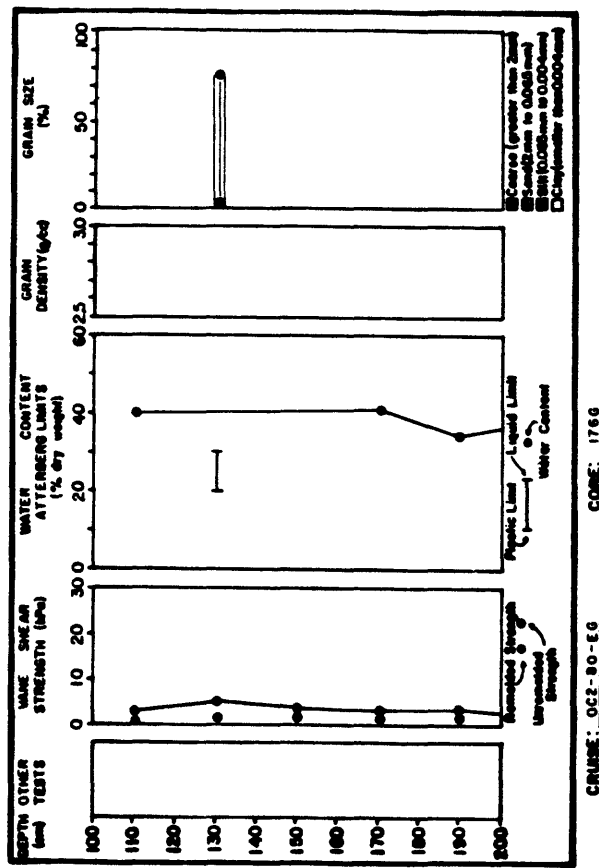
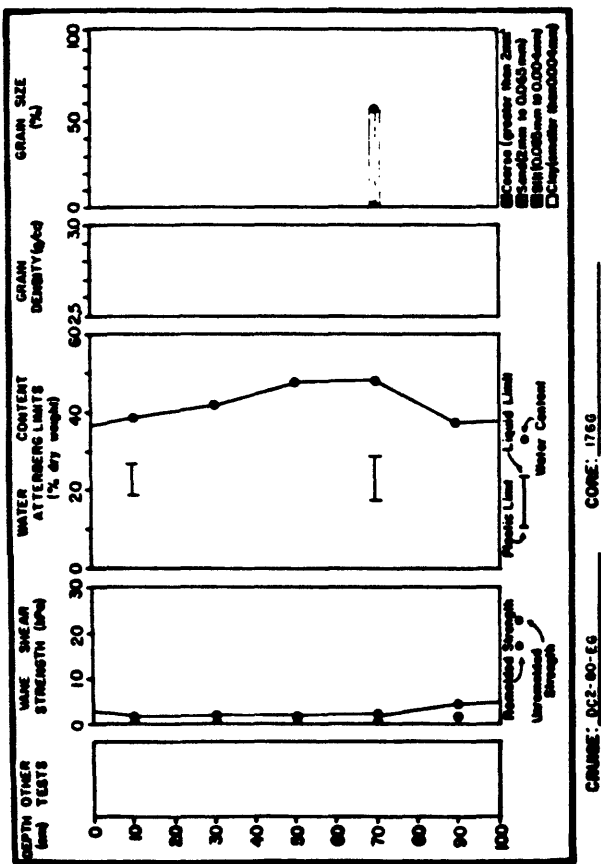
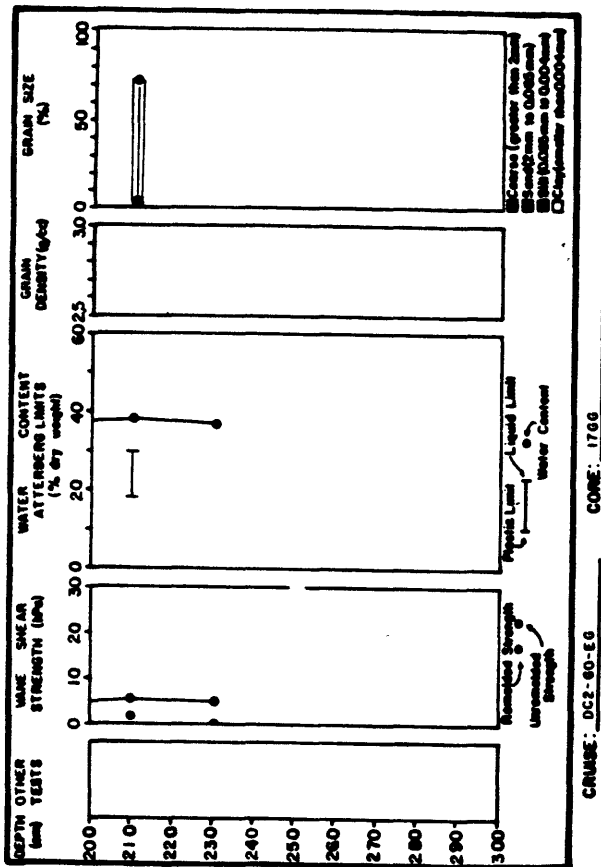
CRUISE: DCC-80-EG CORE: 1756

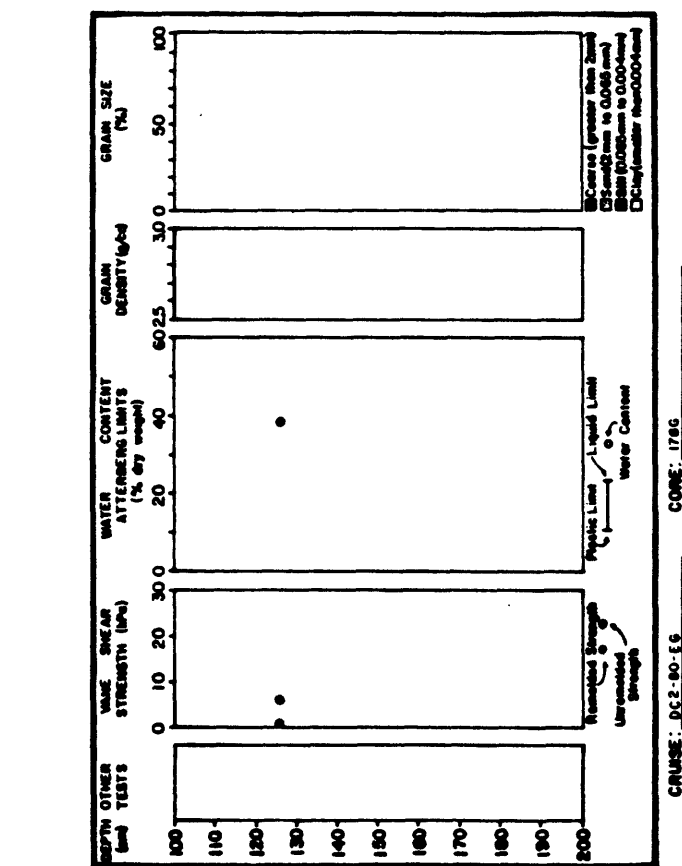
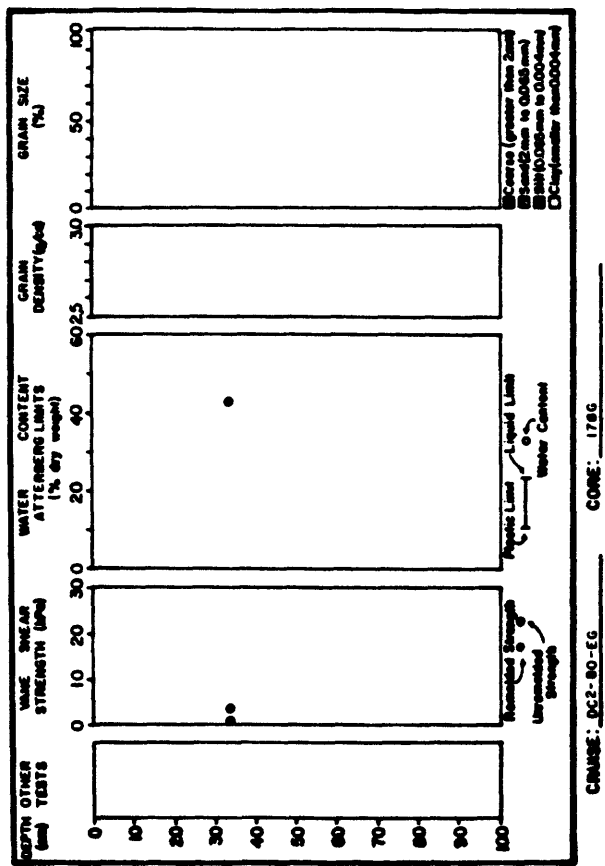


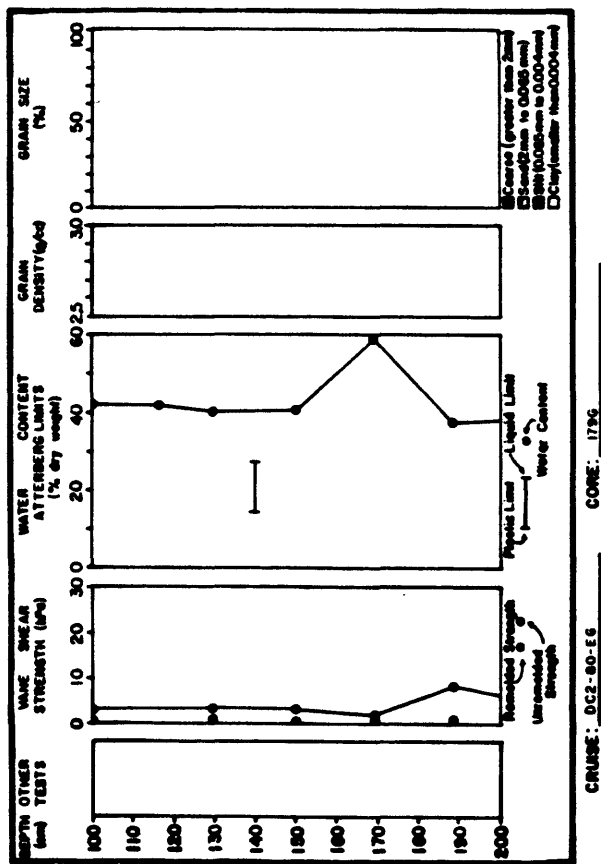
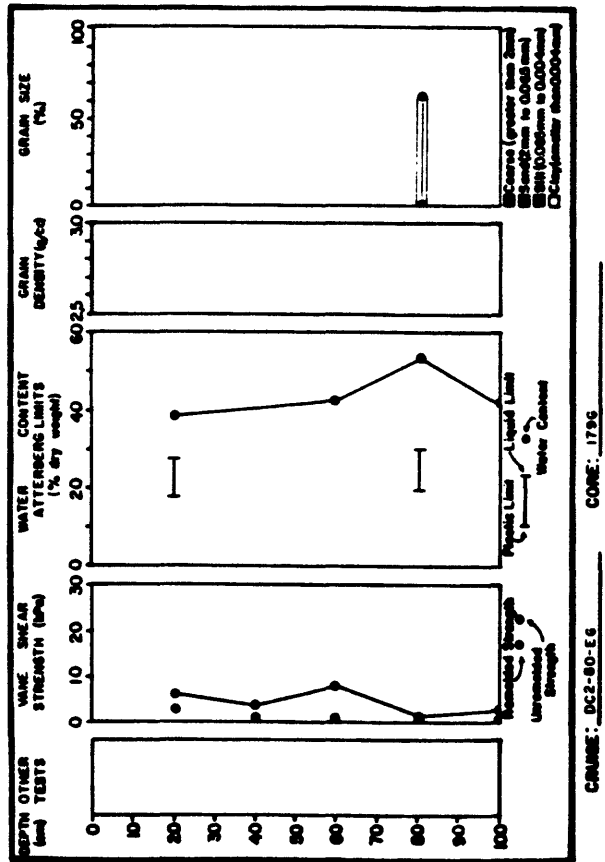
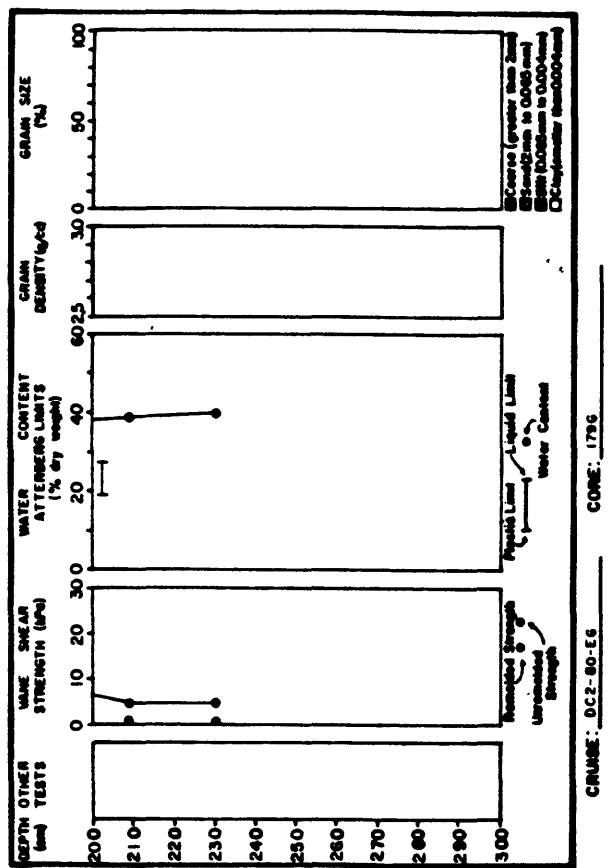
CRUISE: DCC-80-EG CORE: 1756

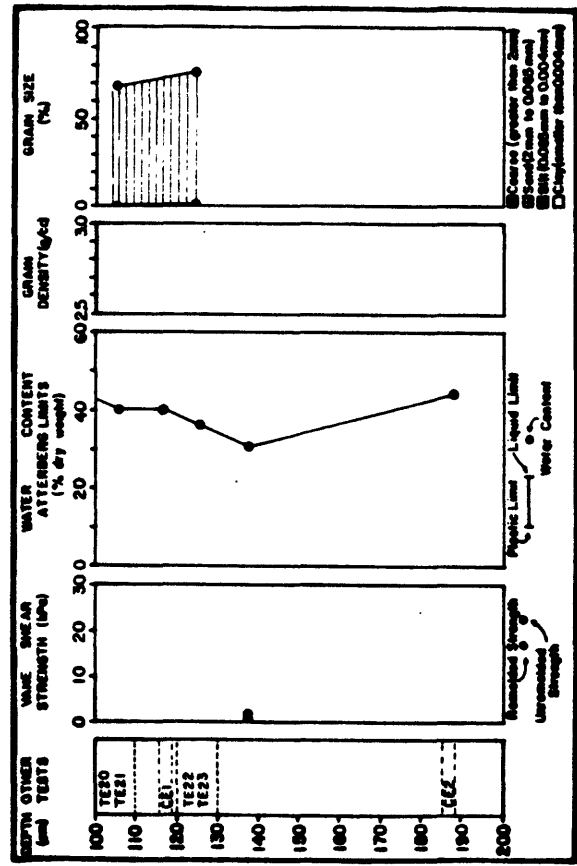
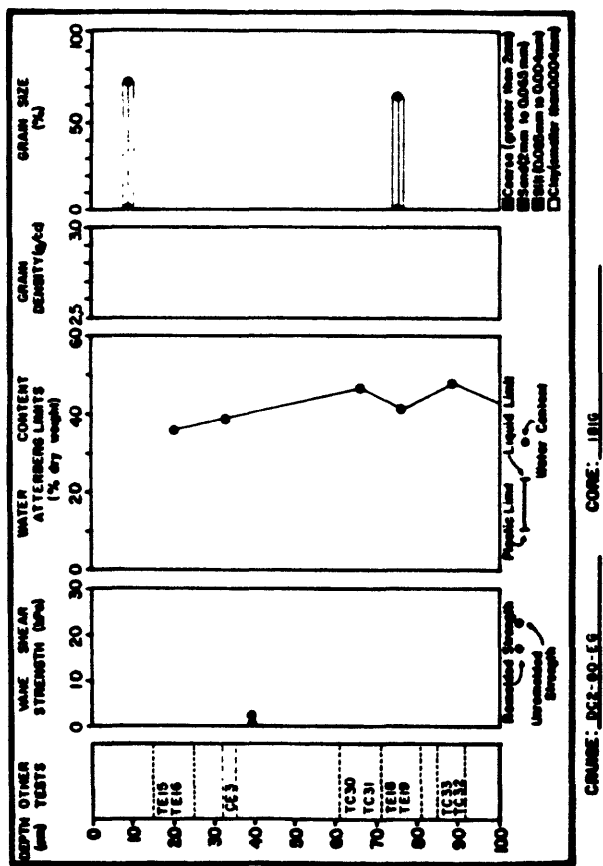


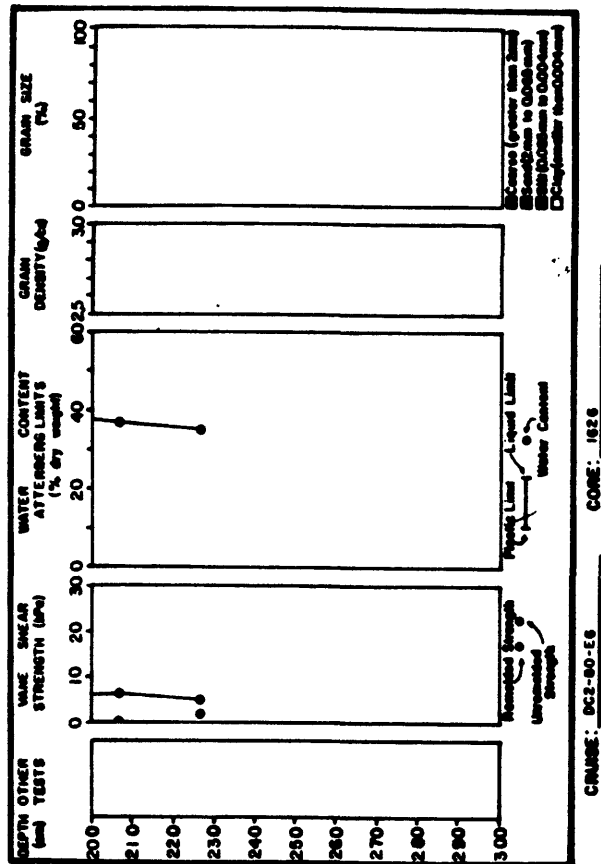
CRUISE: DCC-80-EG CORE: 1756



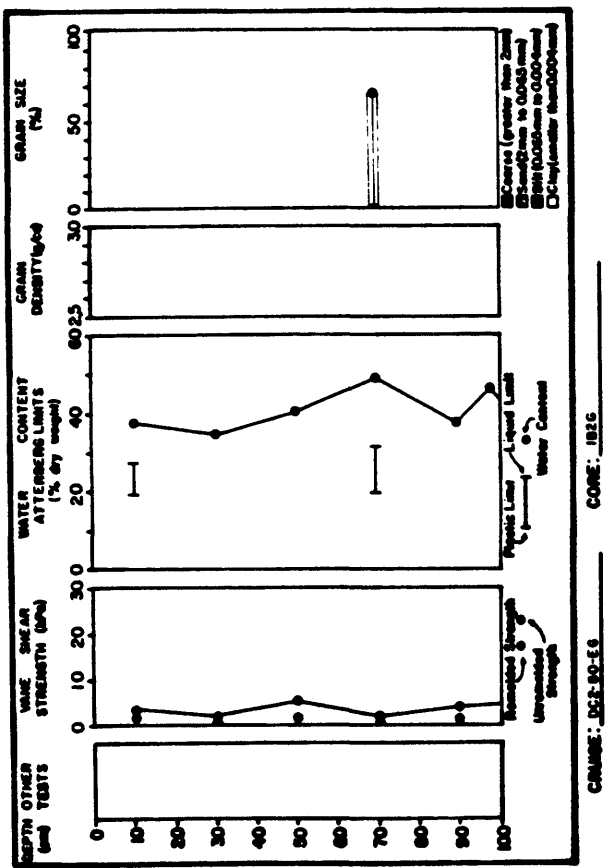




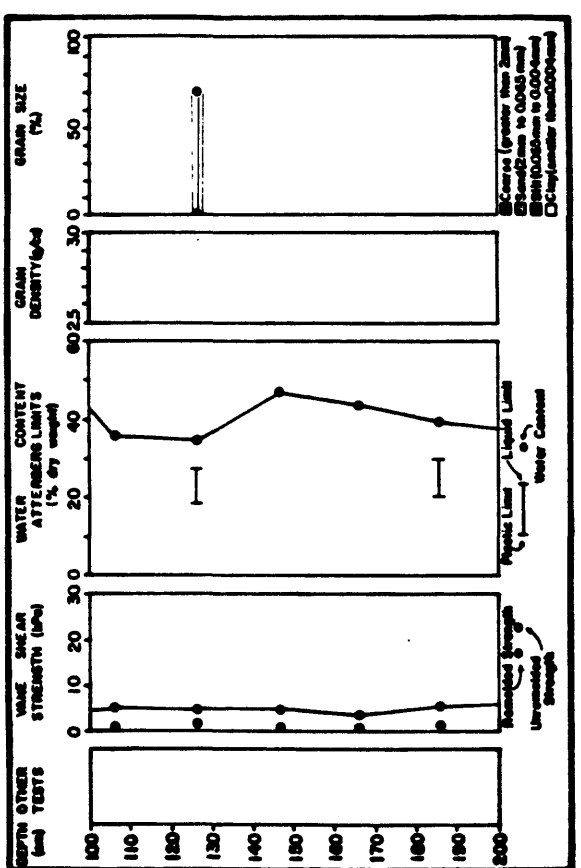




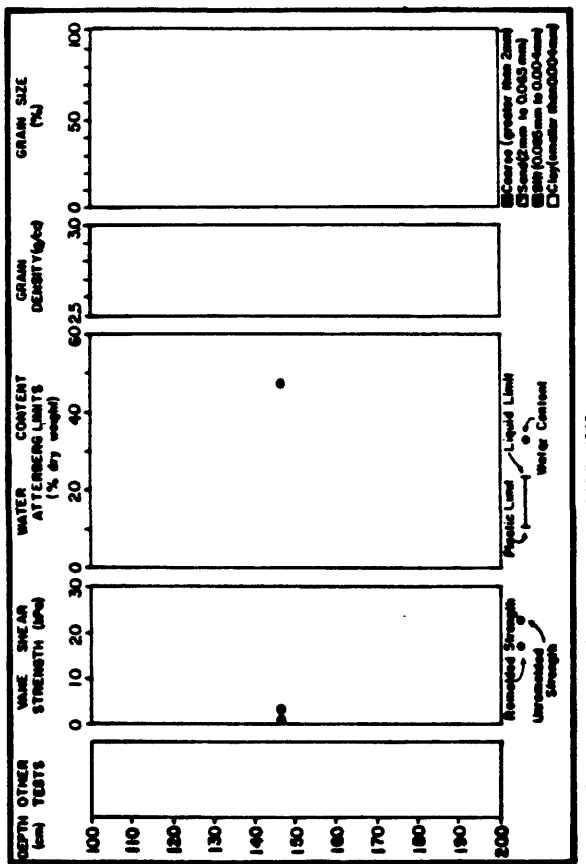
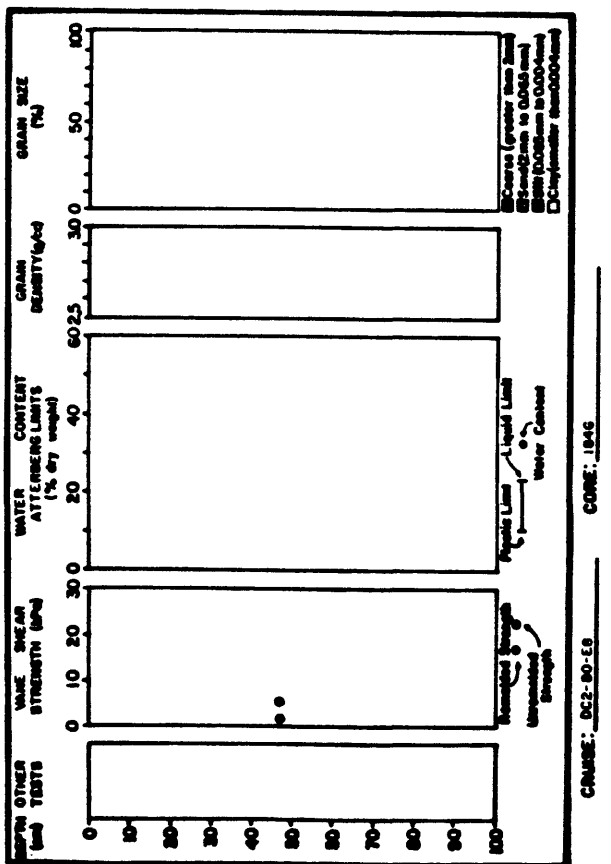
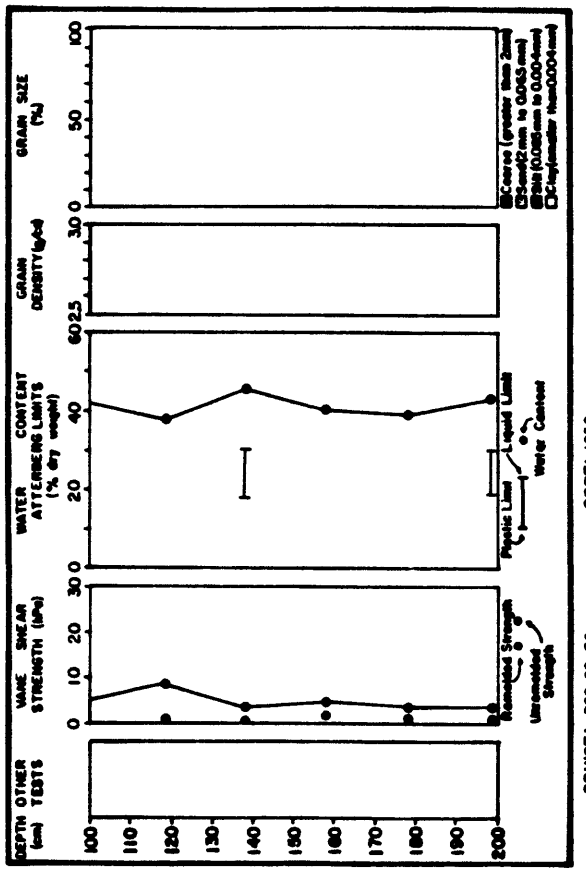
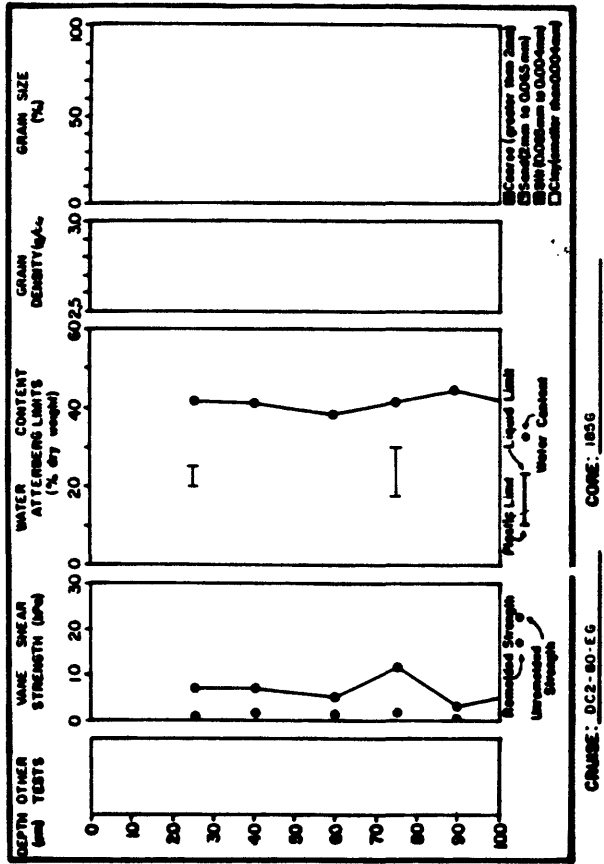
CRUISE: 1626 CORE: 1626-E6

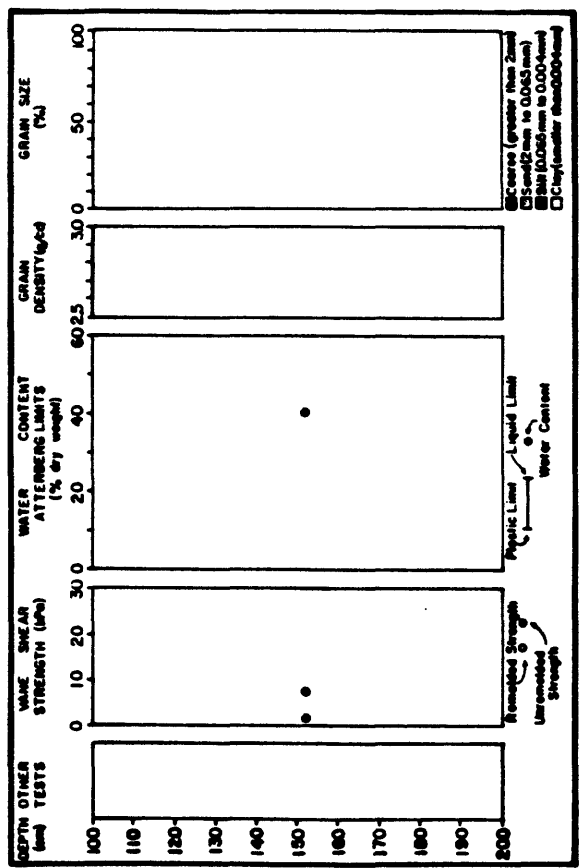
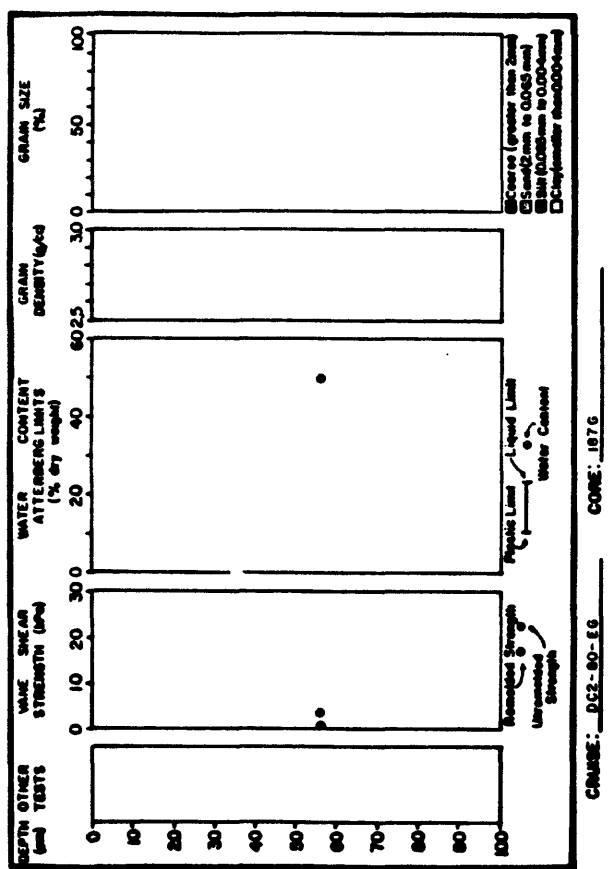


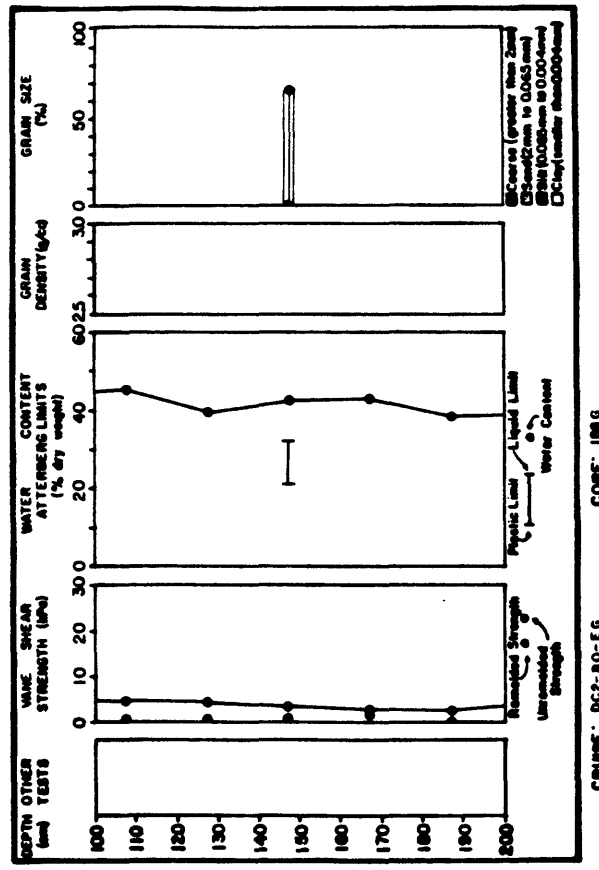
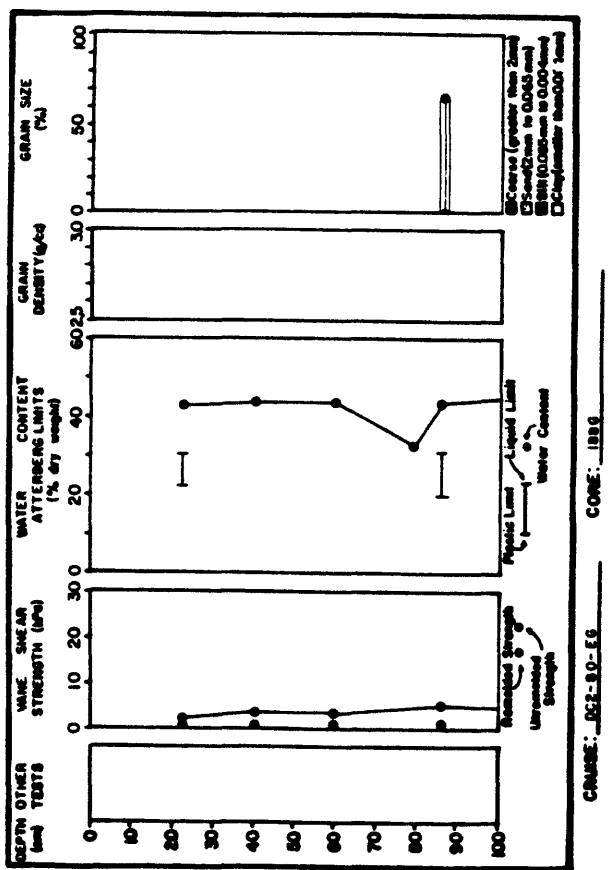
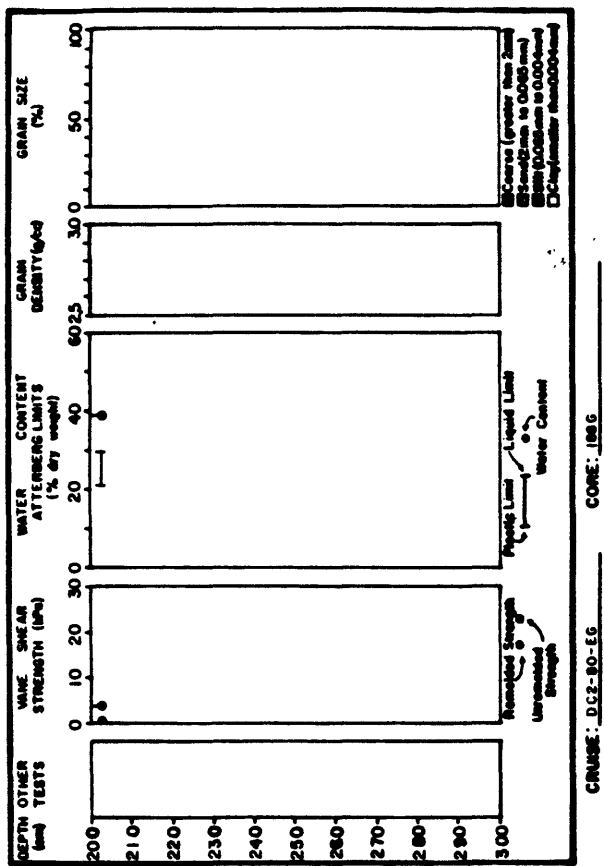
CRUISE: 1626 CORE: 1626-E6

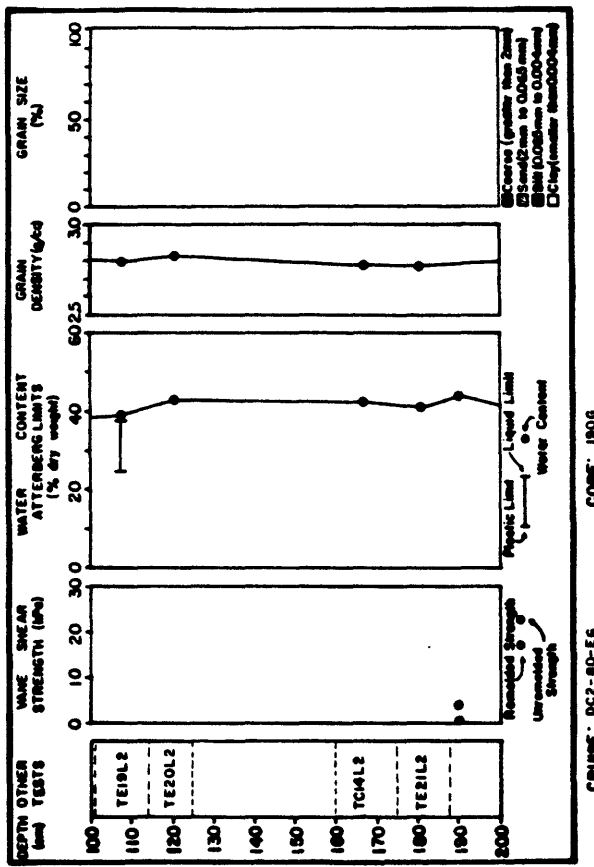
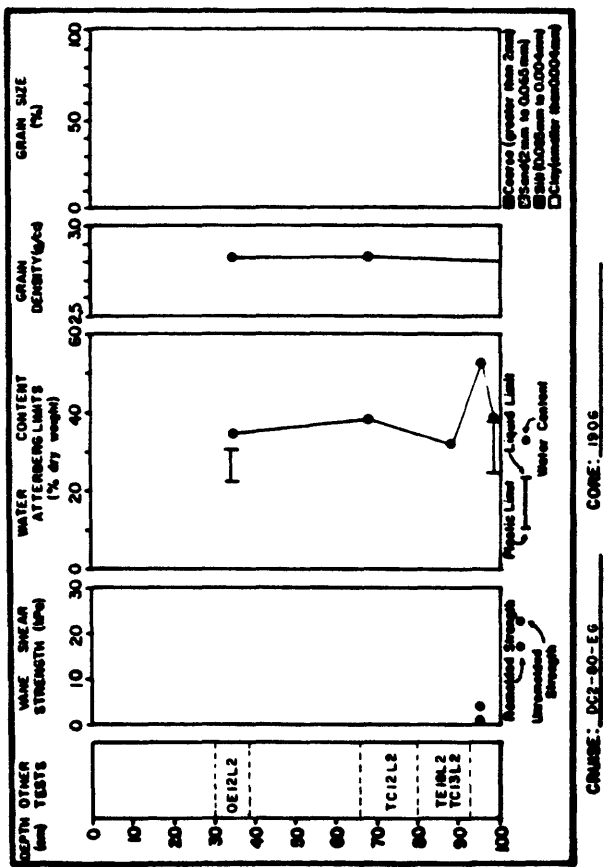
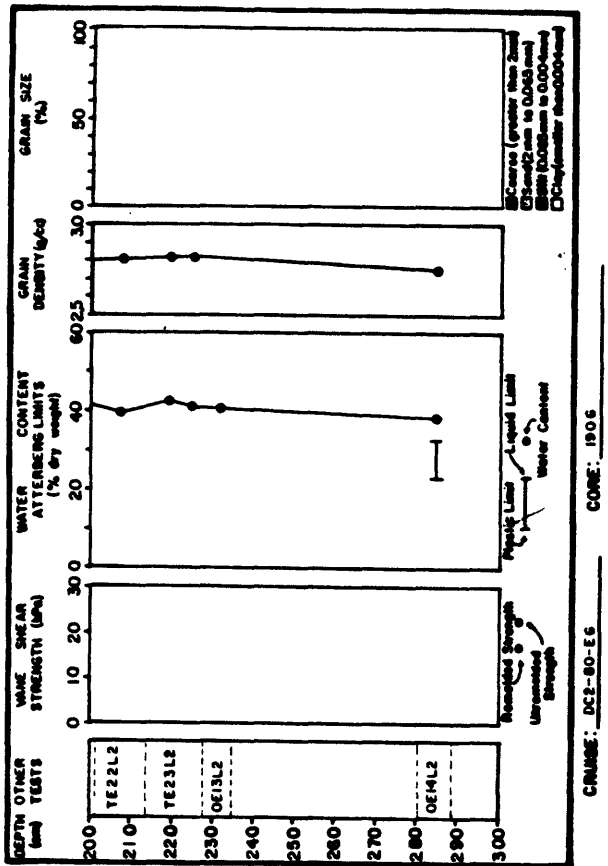


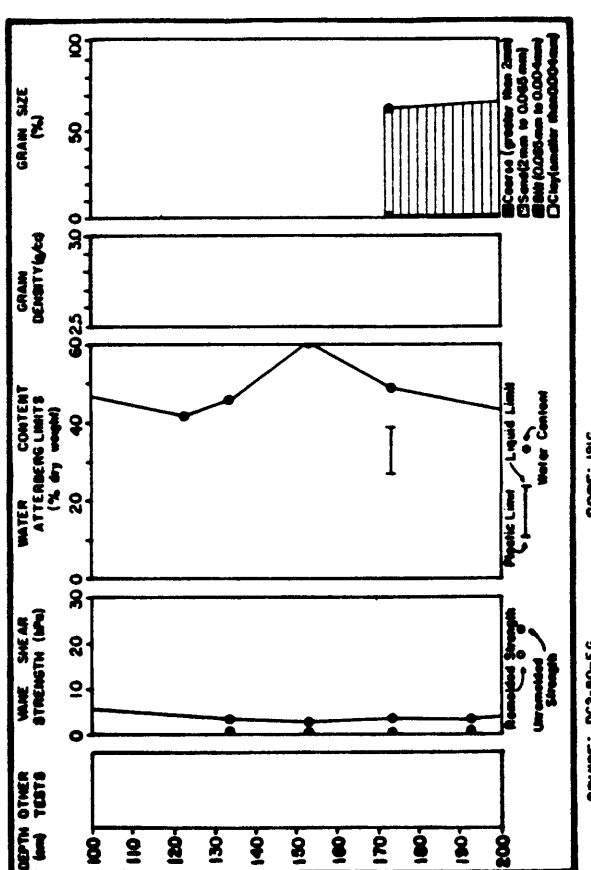
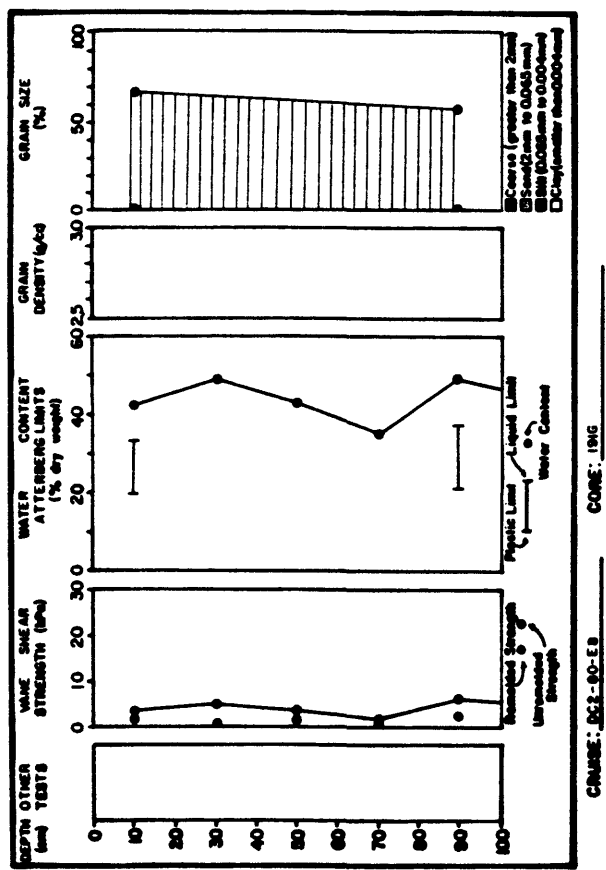
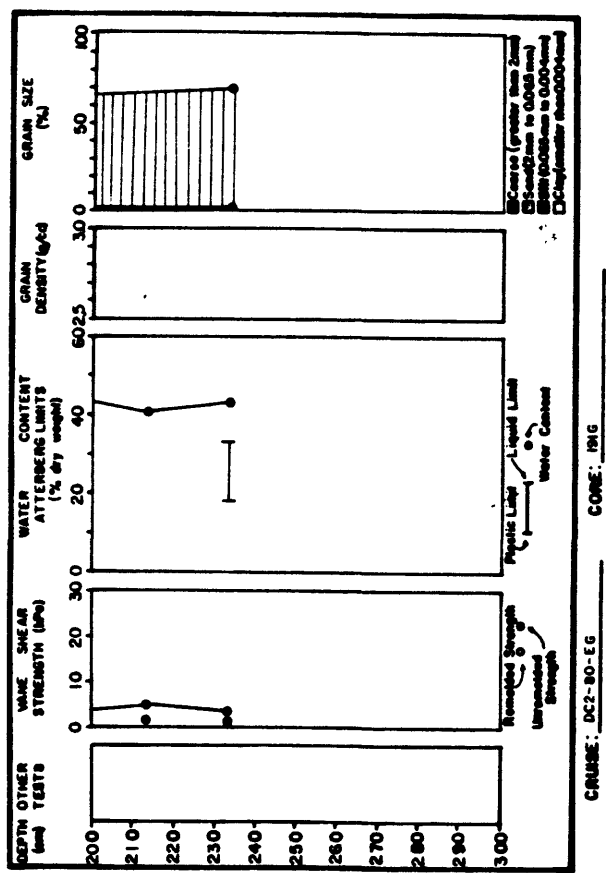
CRUISE: 1626 CORE: 1626-E6

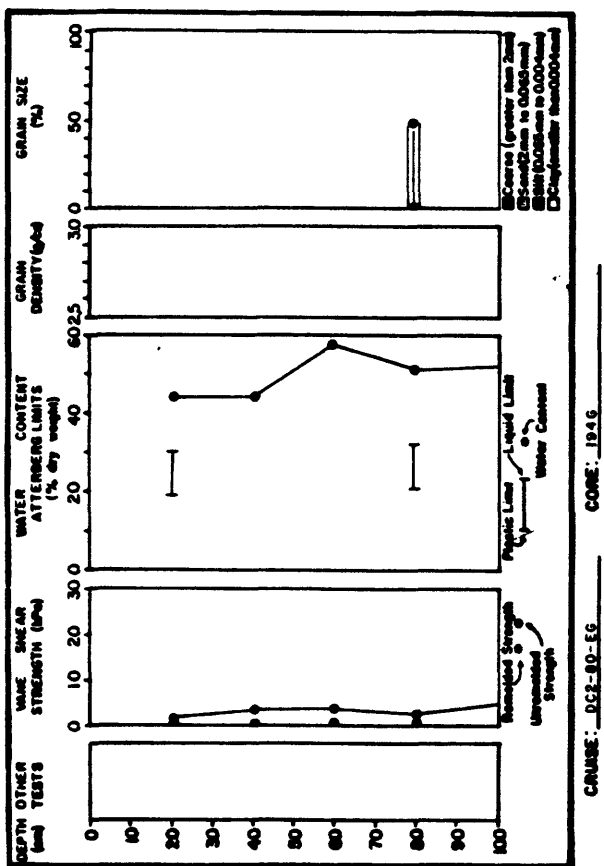




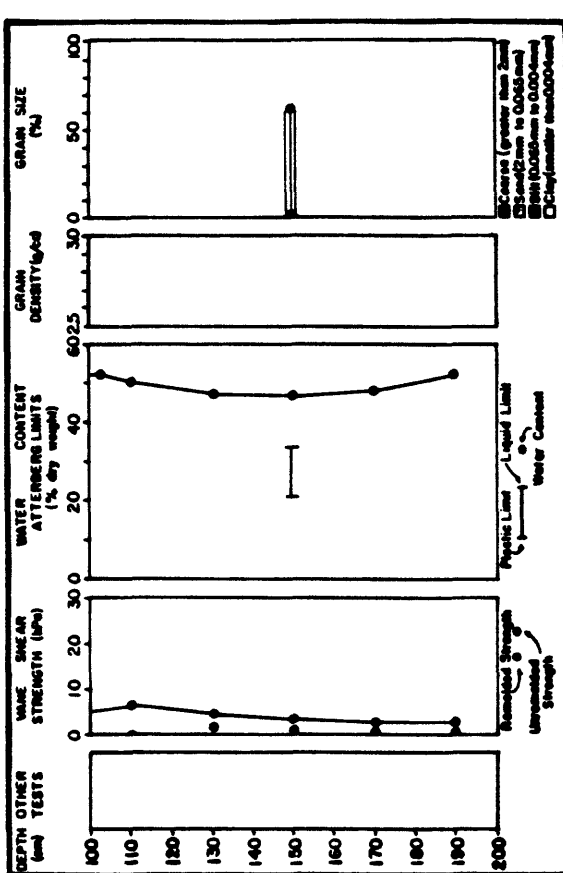




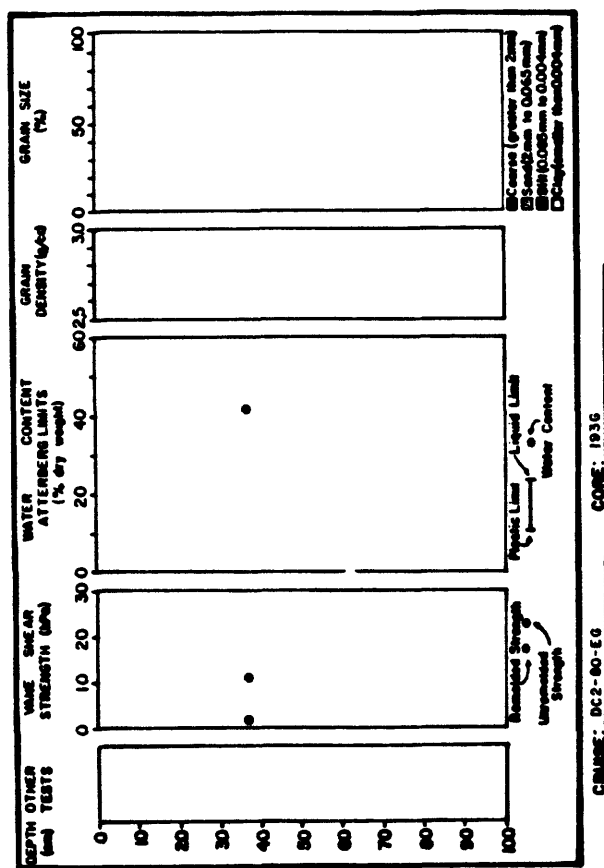




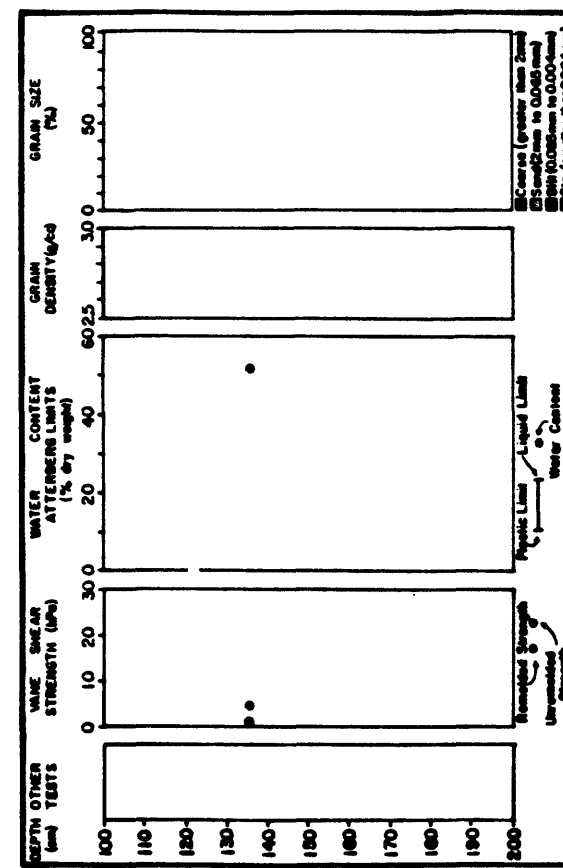
CAUSE : DC2-80-EG CORE: 1946



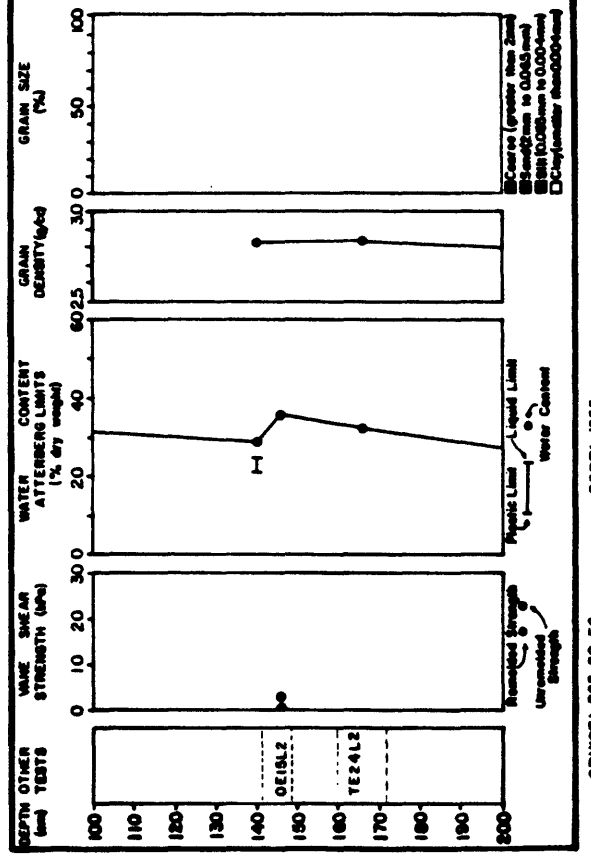
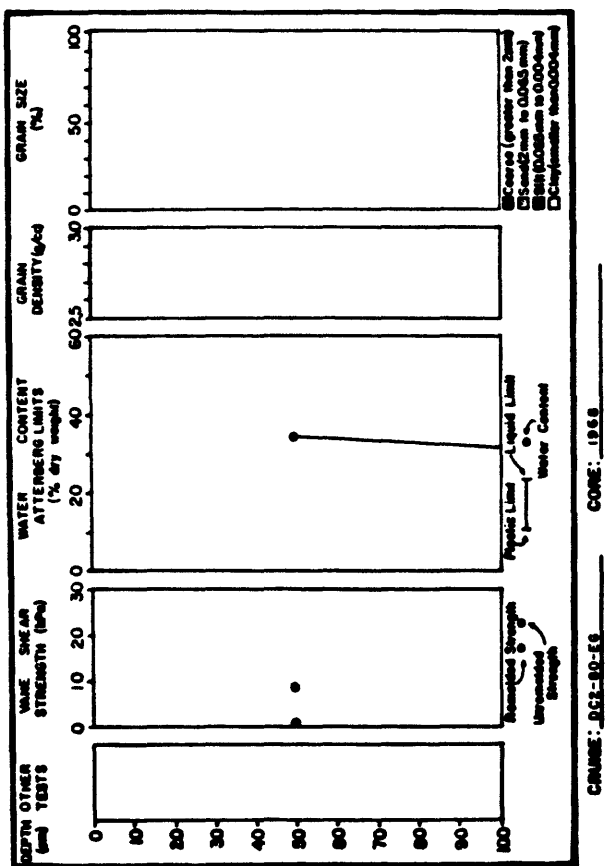
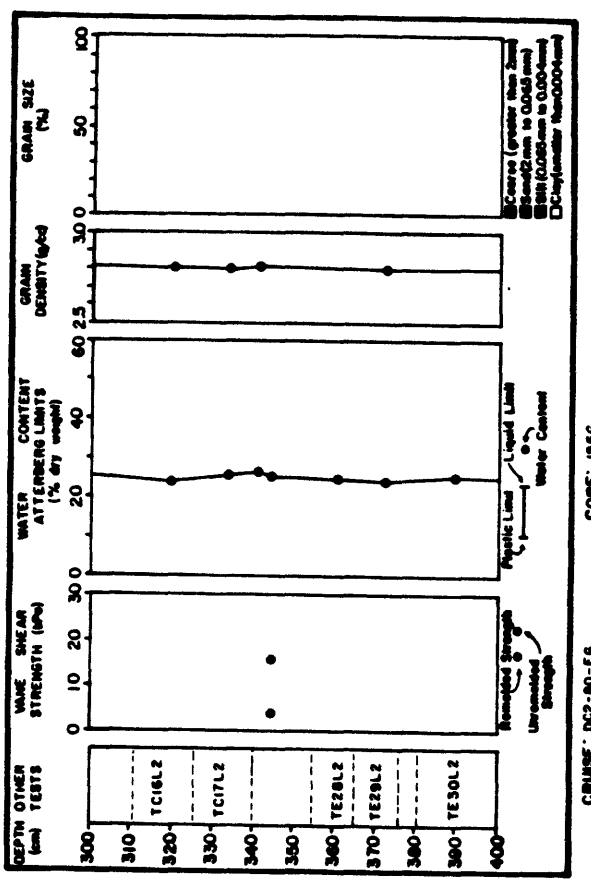
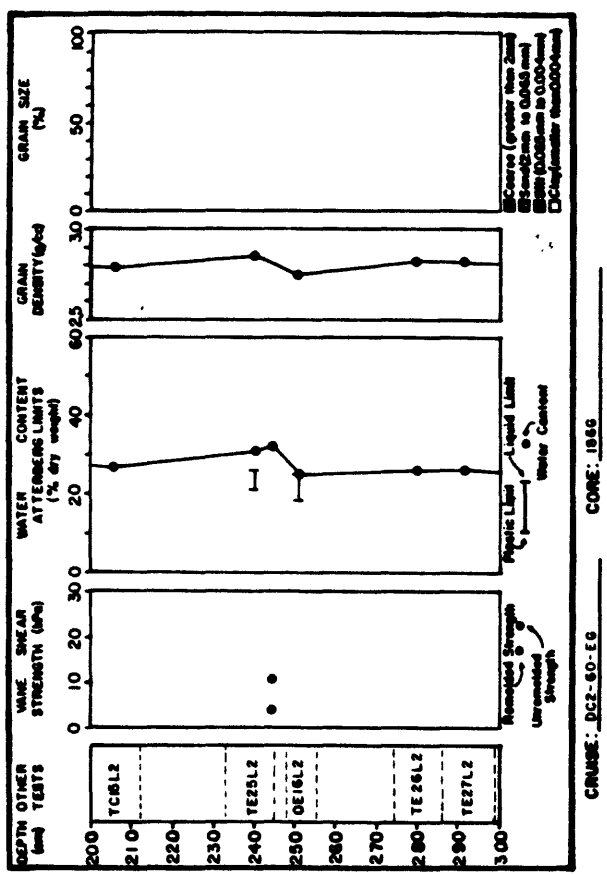
CAUSE : DC2-10-EG CORE: 1946

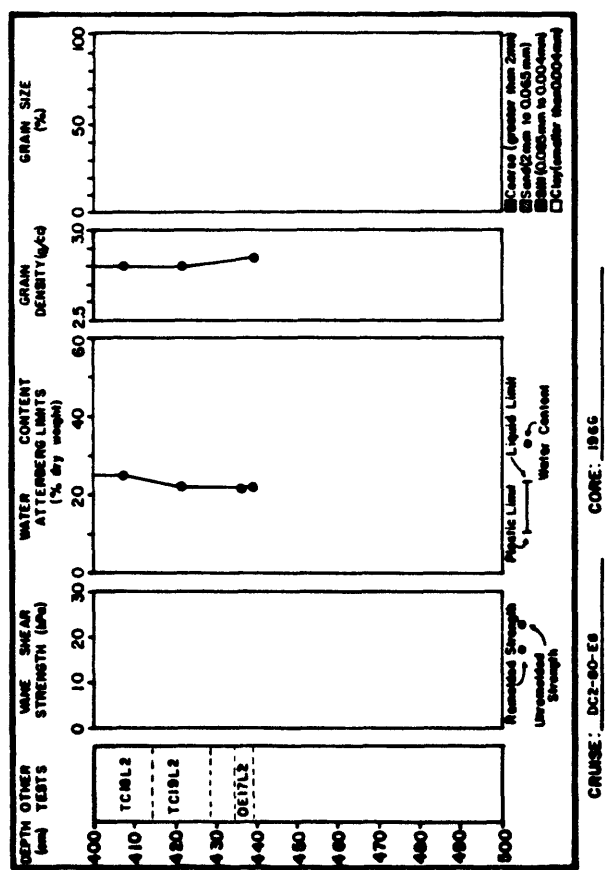


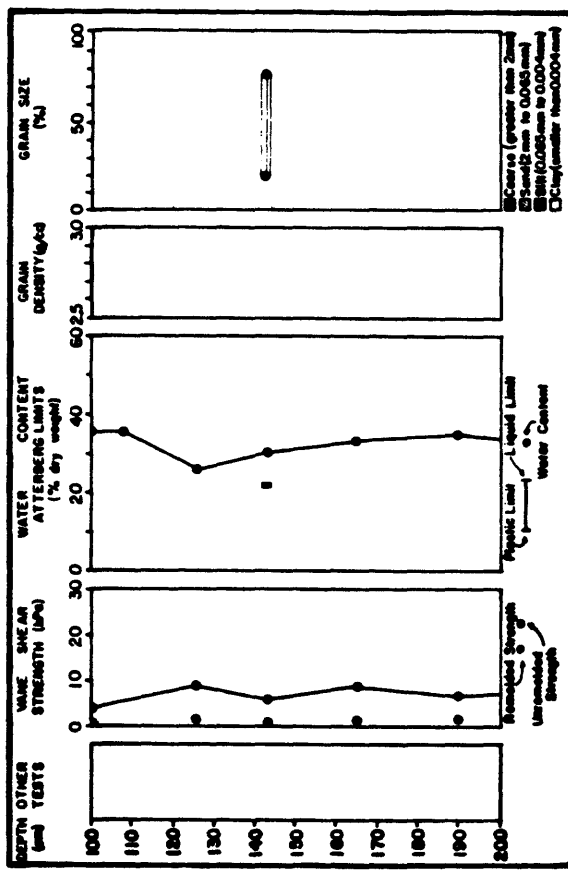
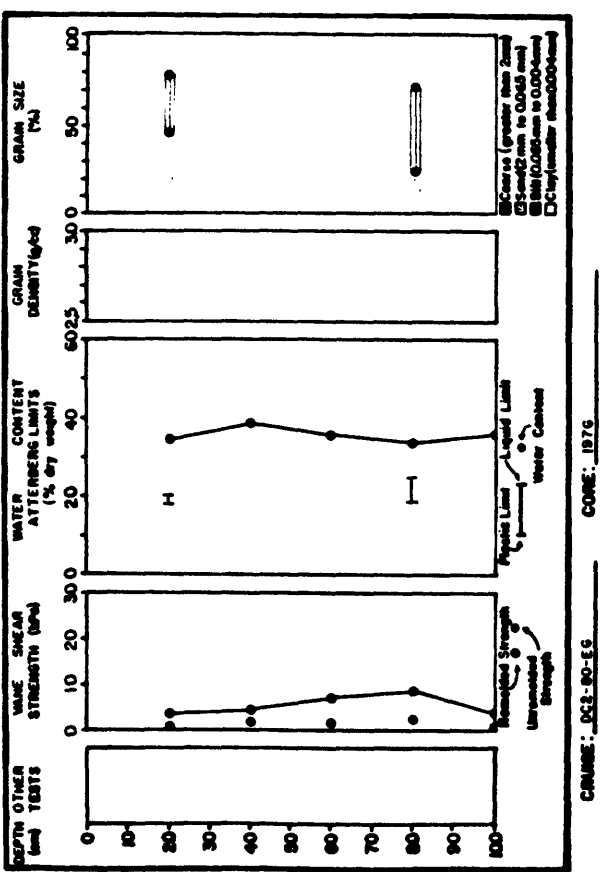
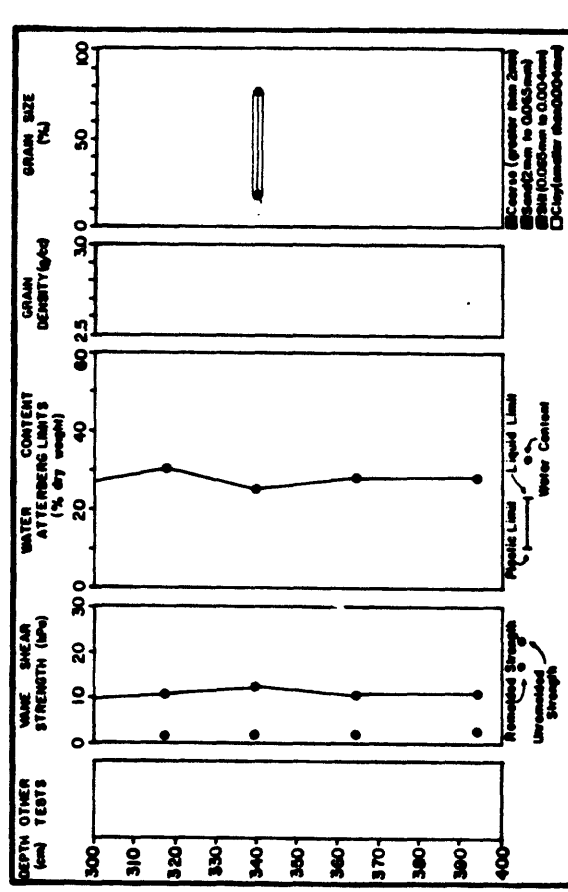
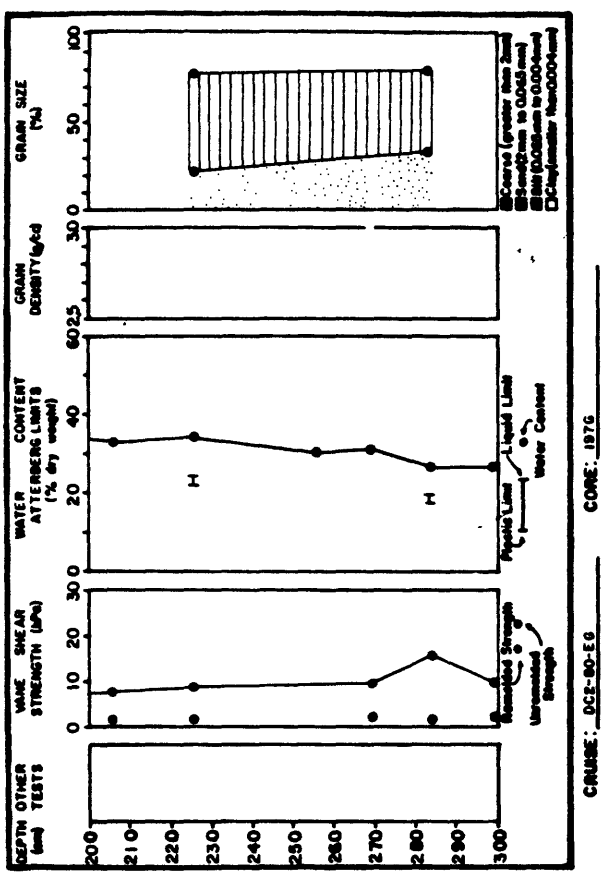
CAUSE : DC2-80-EG CORE: 1936

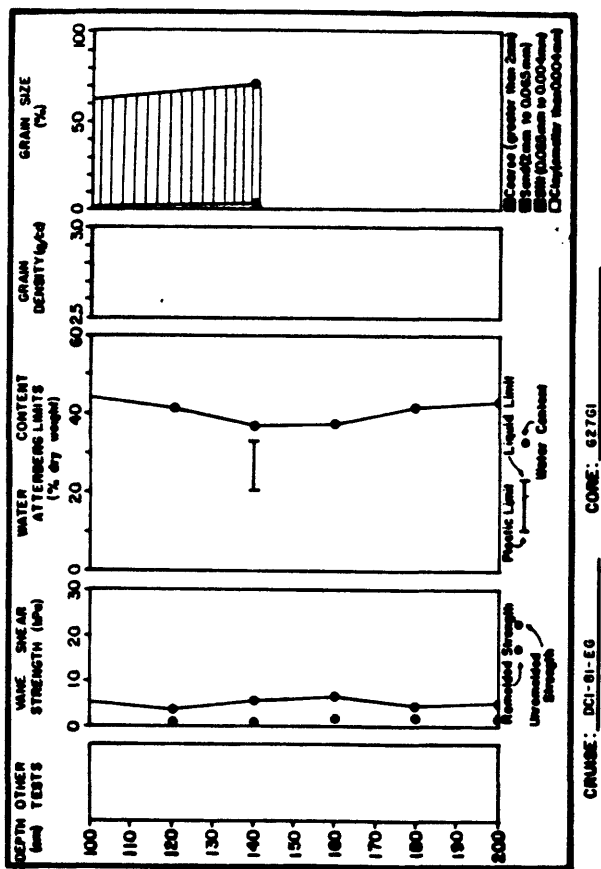


CAUSE : DC2-10-EG CORE: 1936

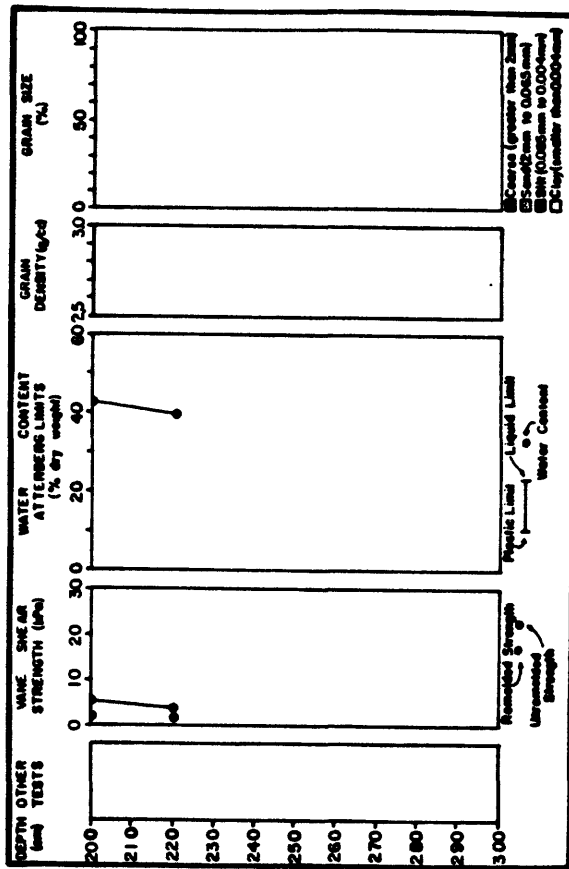




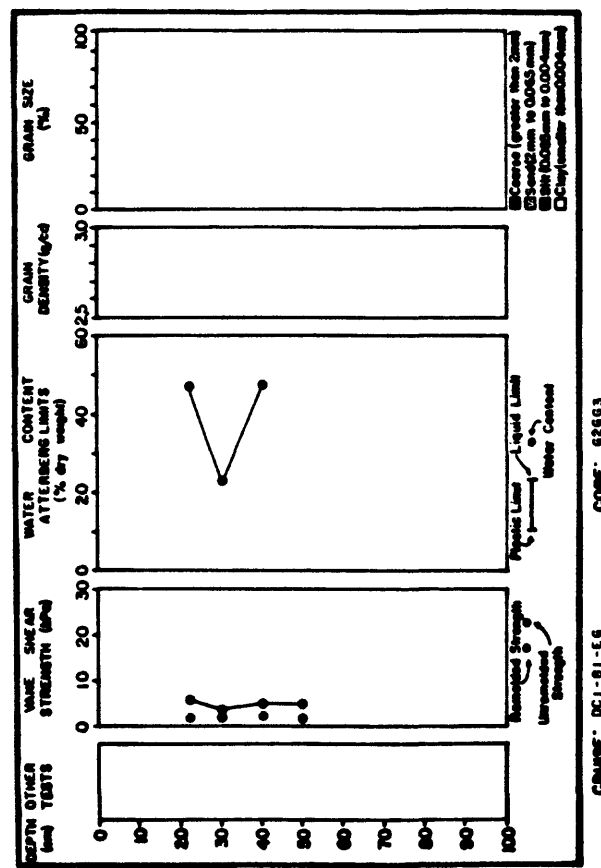




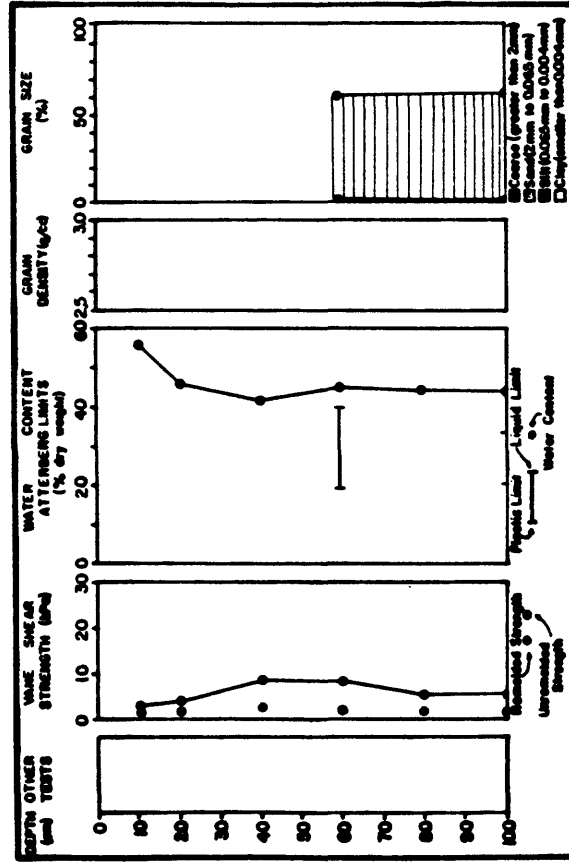
CRUISE: DCI-91-EG      CORE: 627.61



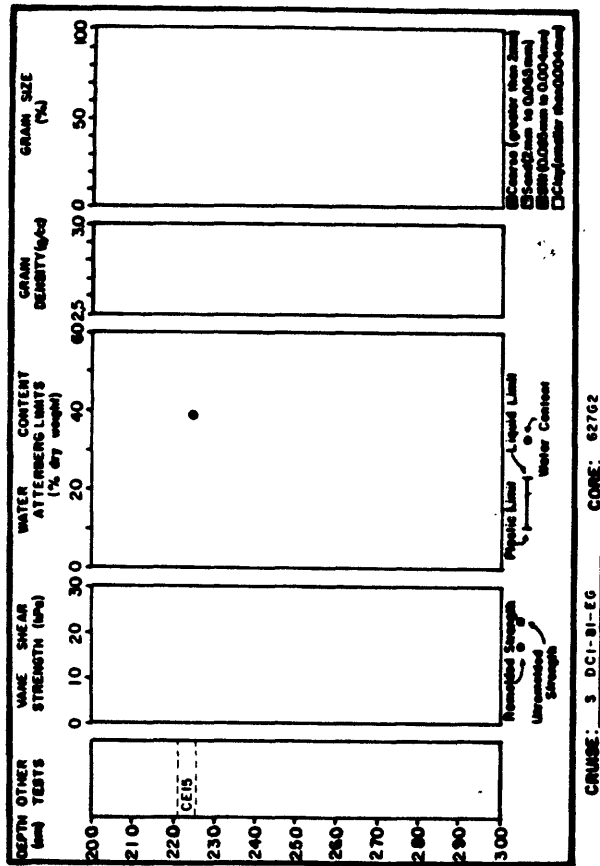
CRUISE: DCI-91-EG      CORE: 627.61



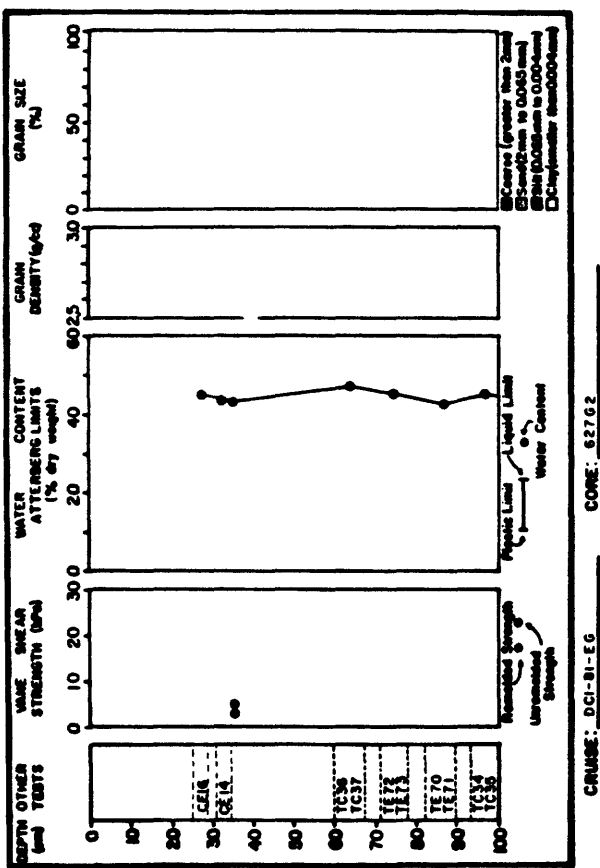
CRUISE: DCI-91-EG      CORE: 626.61



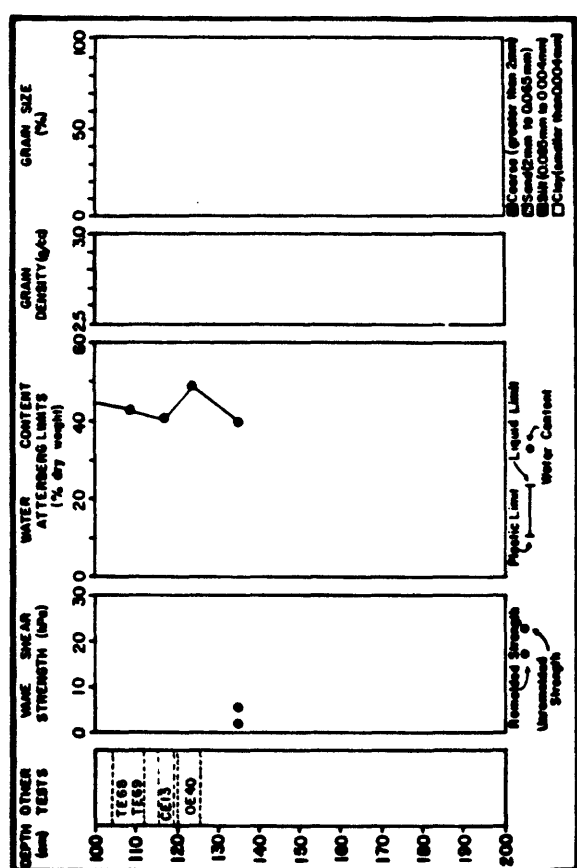
CRUISE: DCI-91-EG      CORE: 626.61



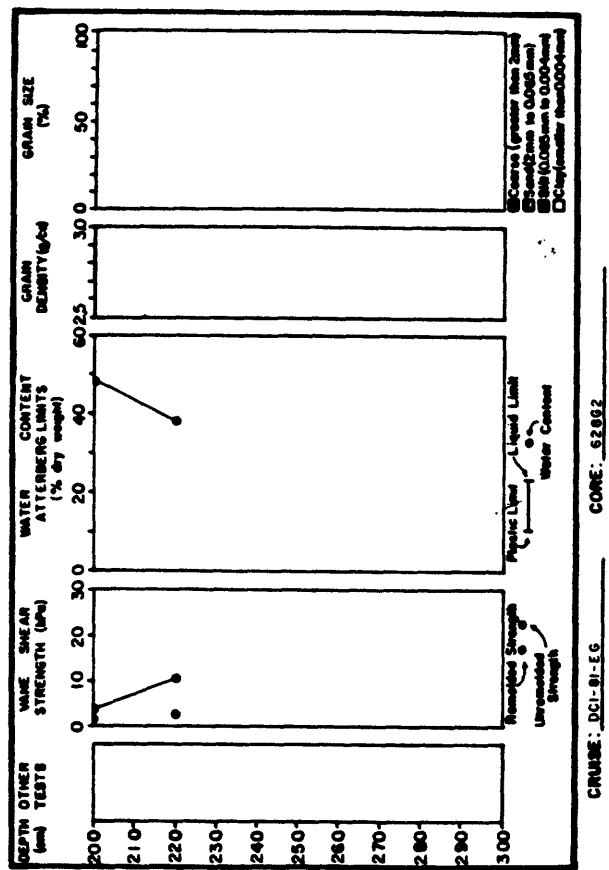
CRUISE: 3 DCI-BI-EG CORE: 627G2



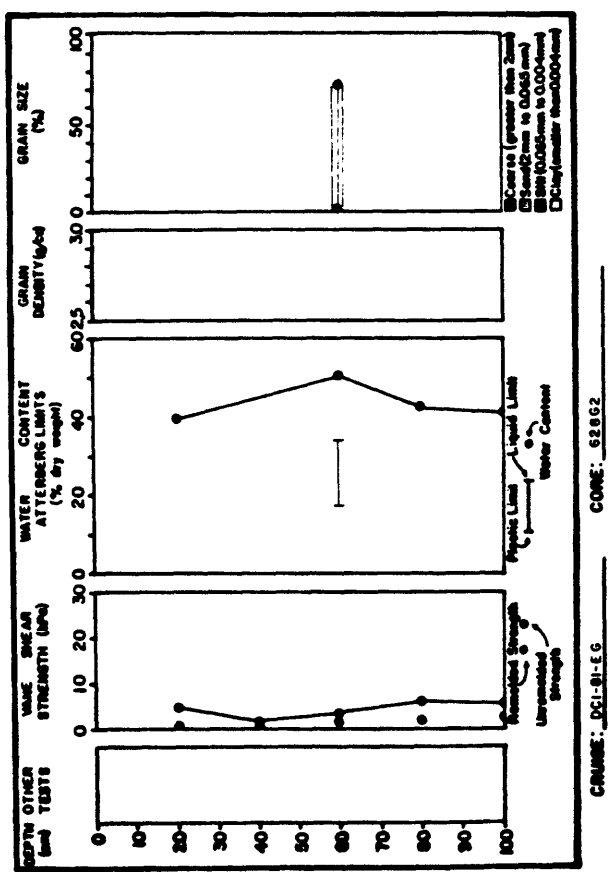
CRUISE: DCI-BI-EG CORE: 627G2



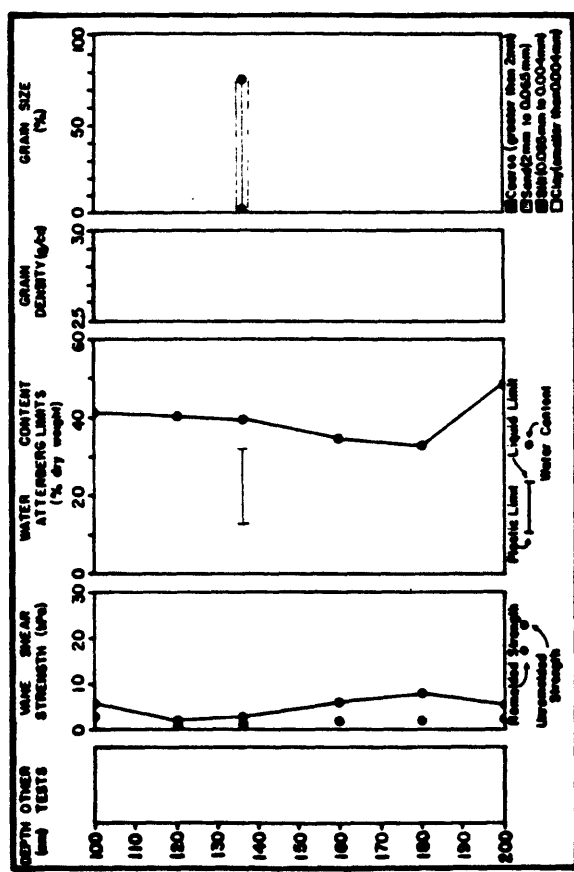
CRUISE: DCI-BI-EG CORE: 627G2



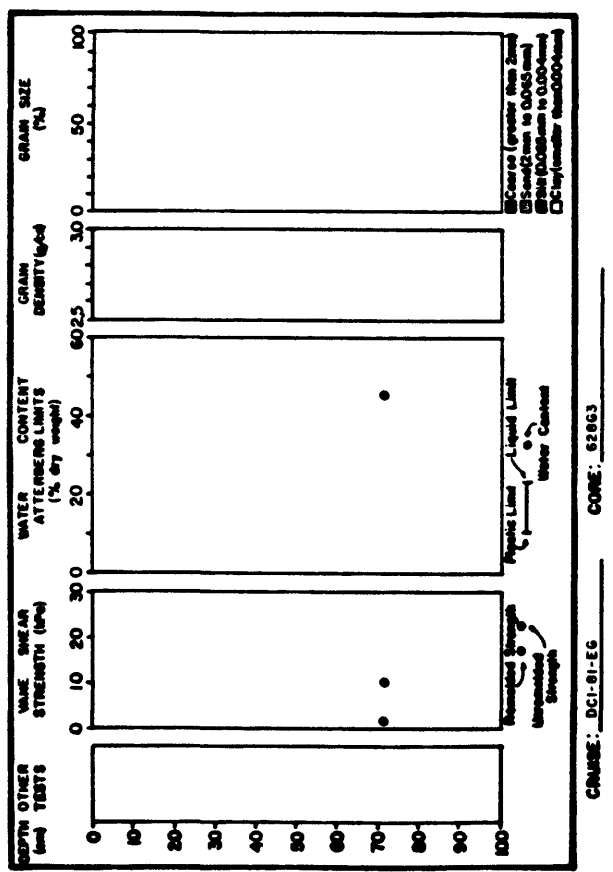
CRUISE: DCI-81-EG      CORE: 62862



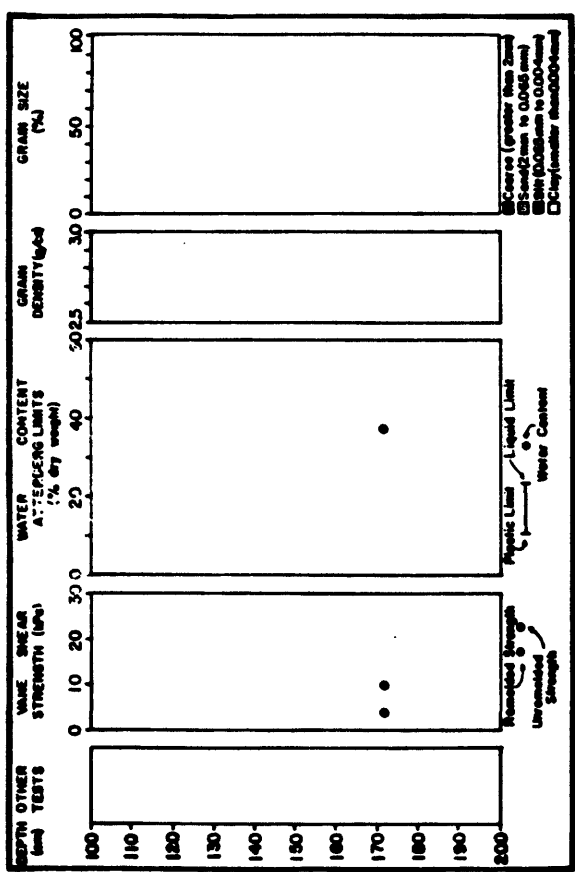
CRUISE: DCI-81-EG      CORE: 62862

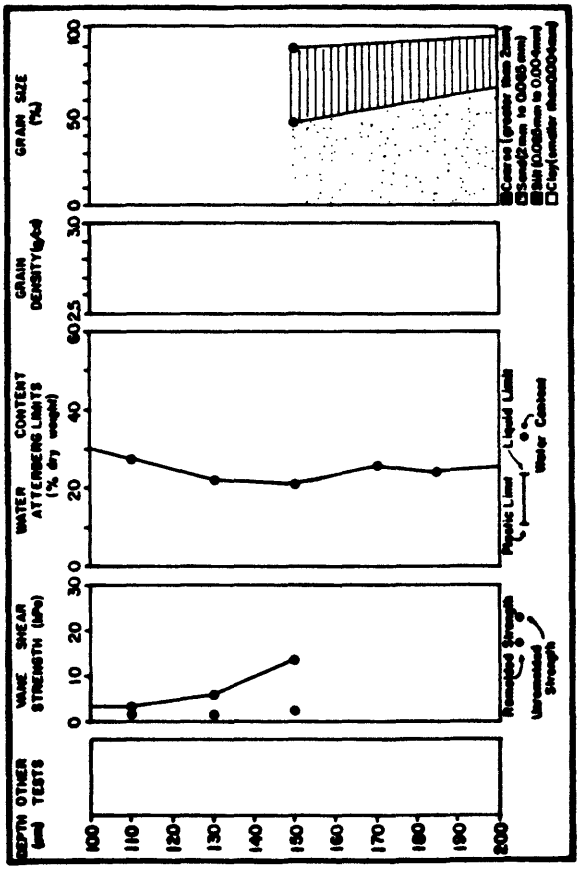
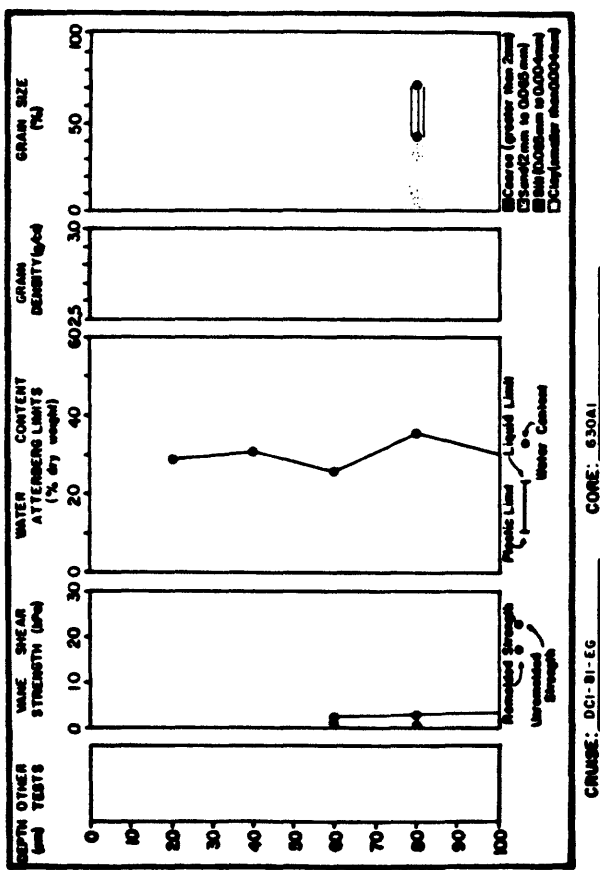
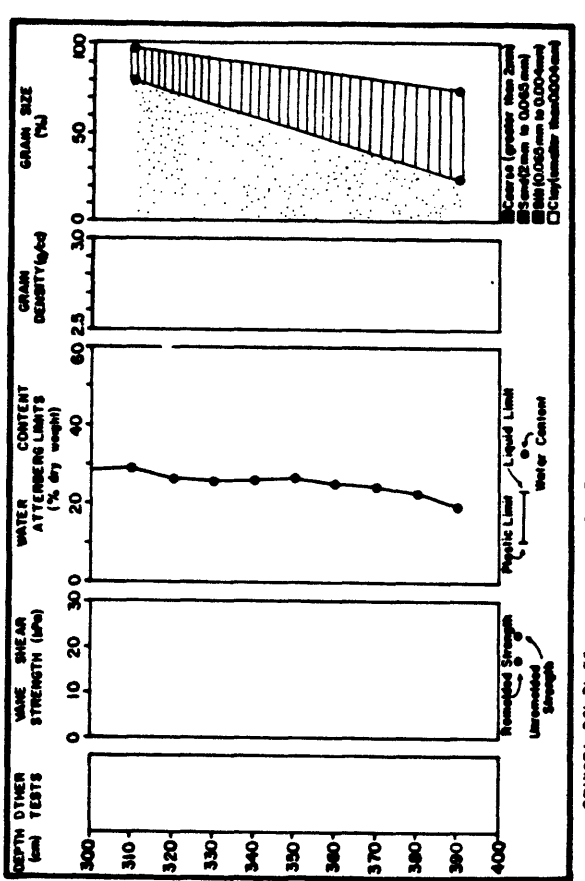
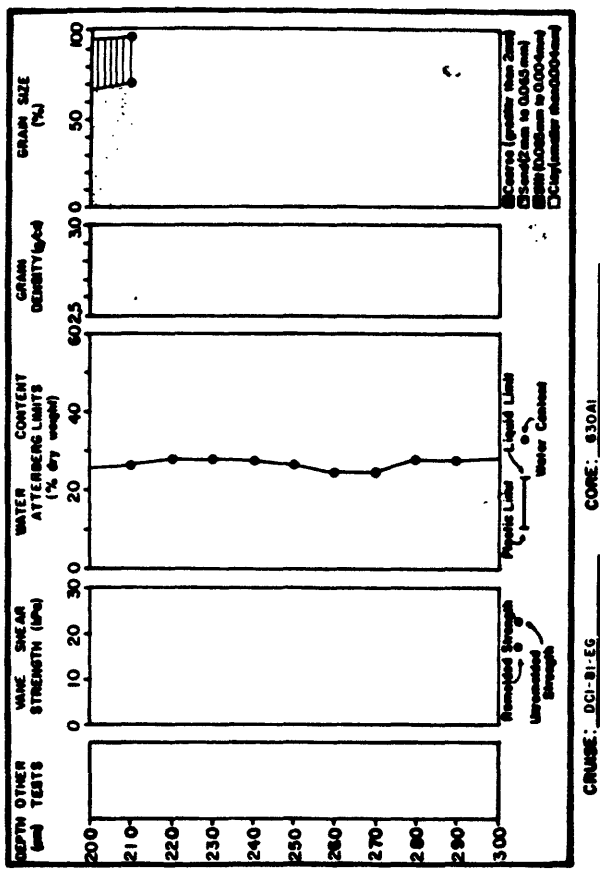


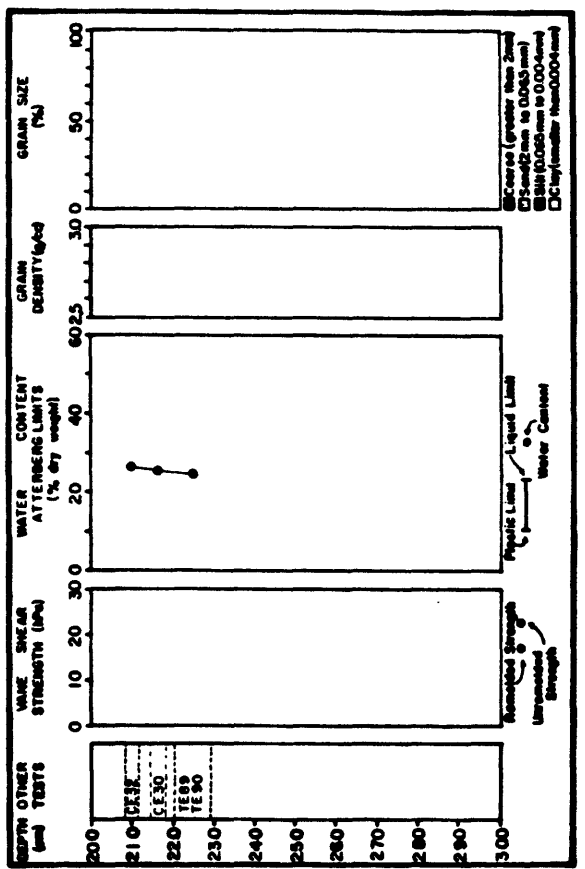
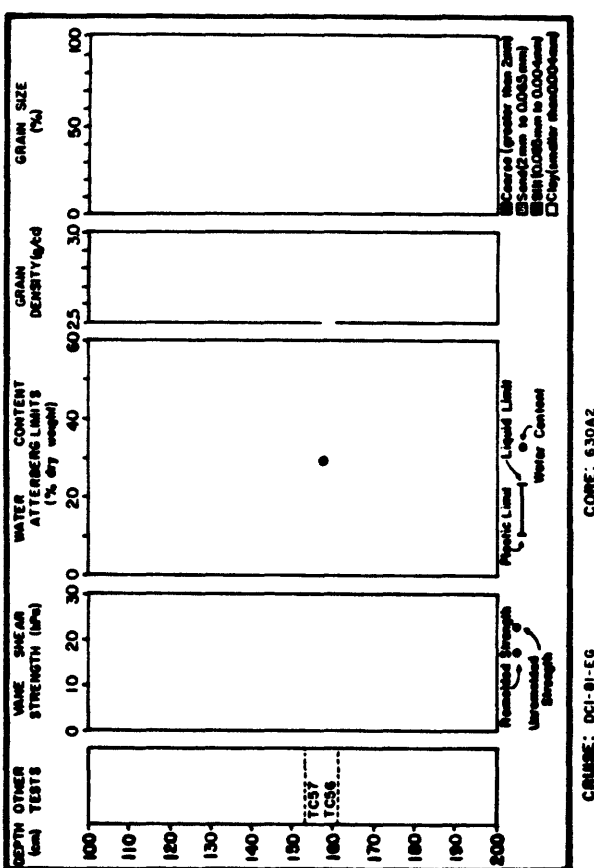
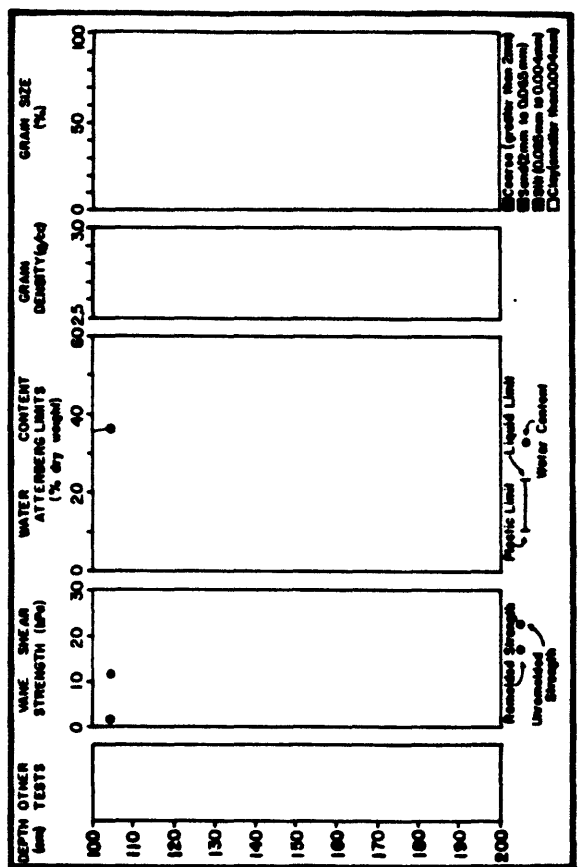
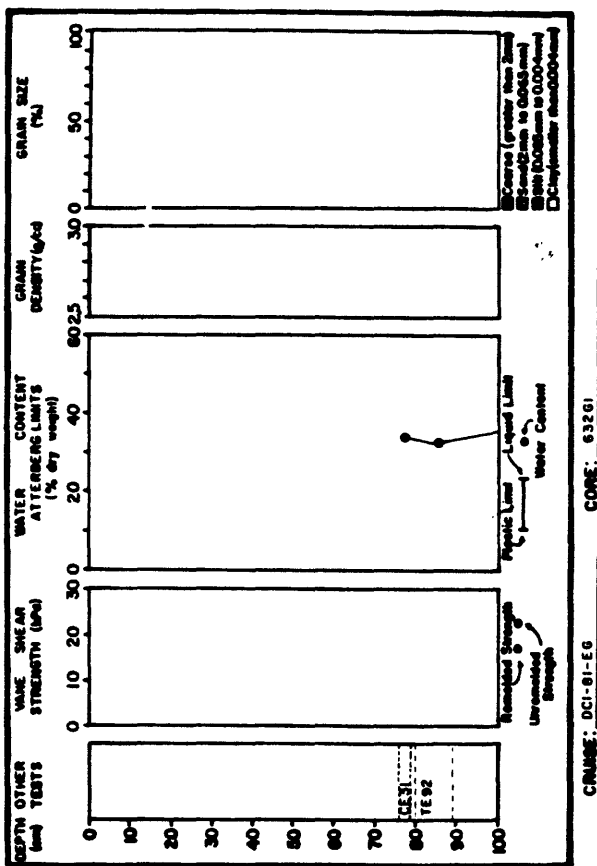
CRUISE: DCI-81-EG      CORE: 62862

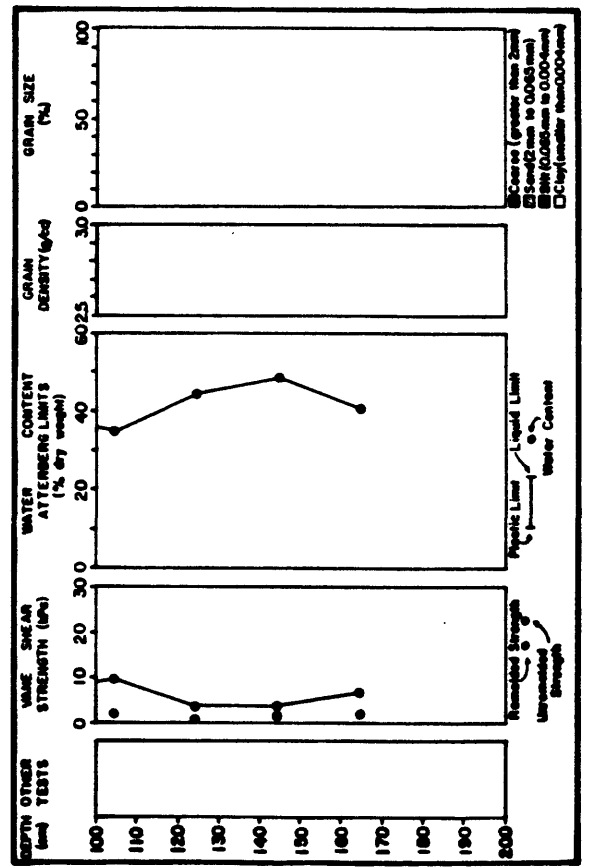
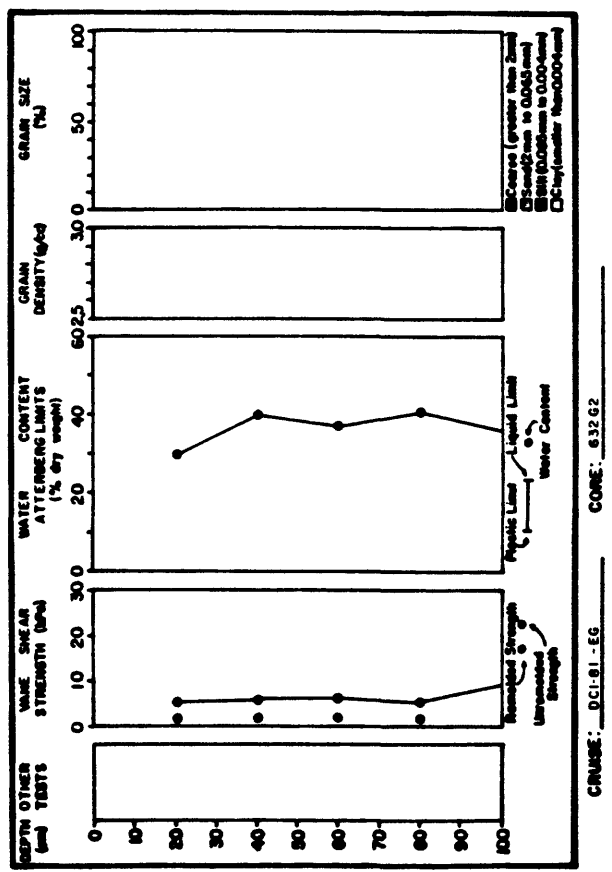


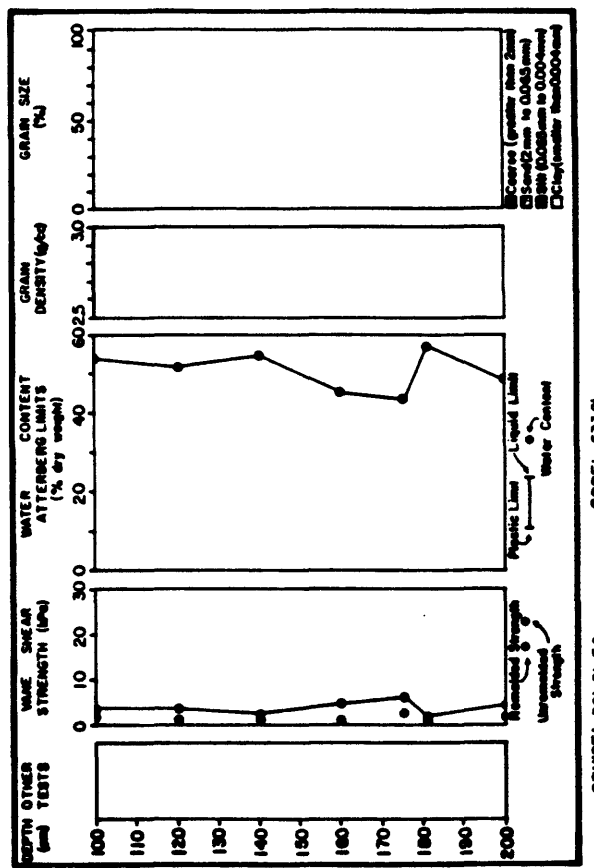
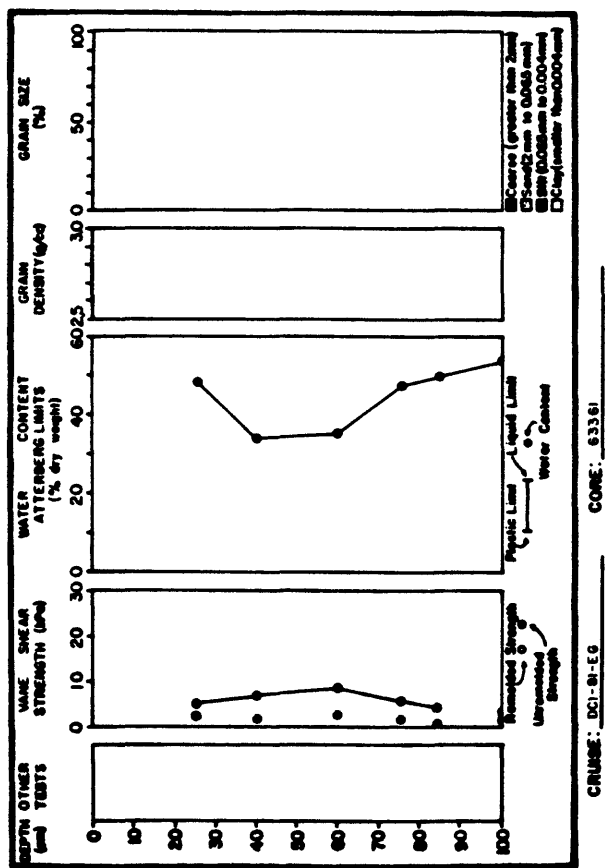
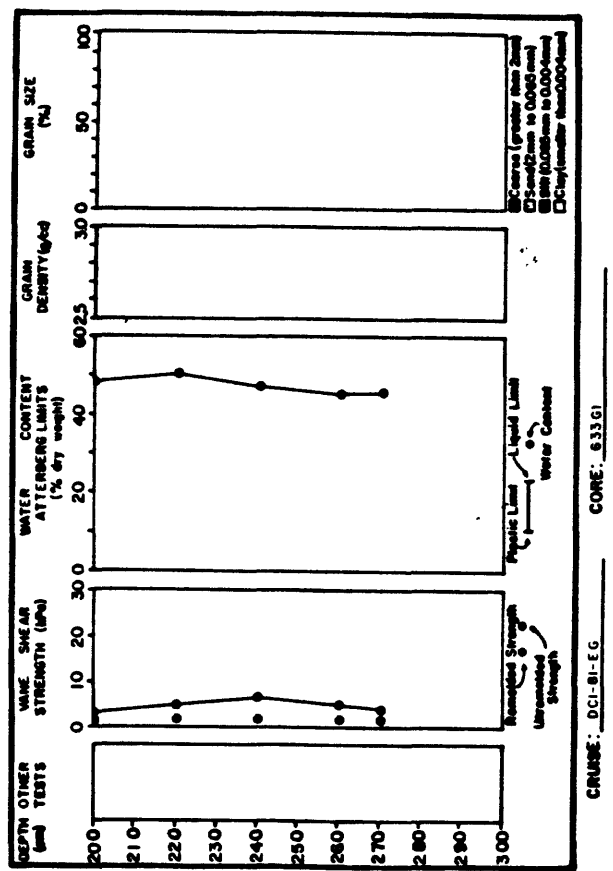
CRUISE: D-1-E6      CORE: 62863

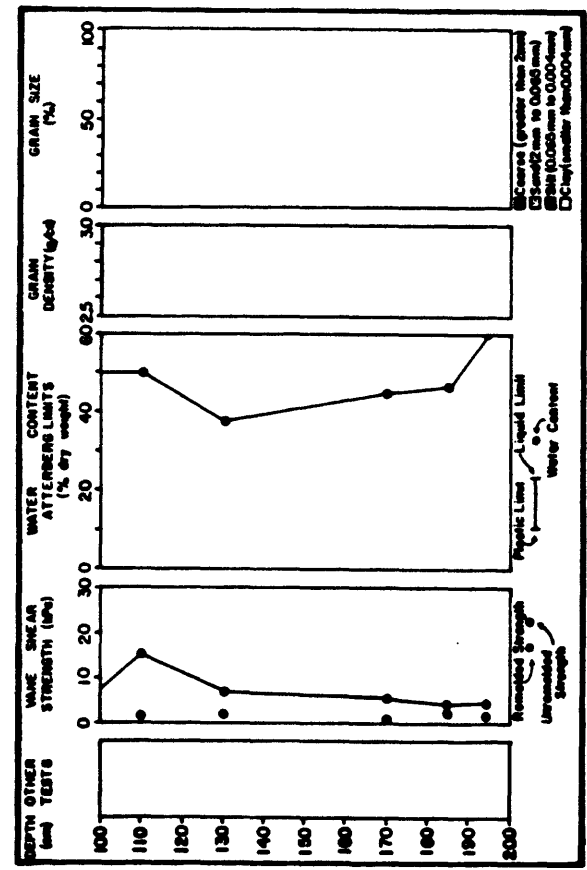
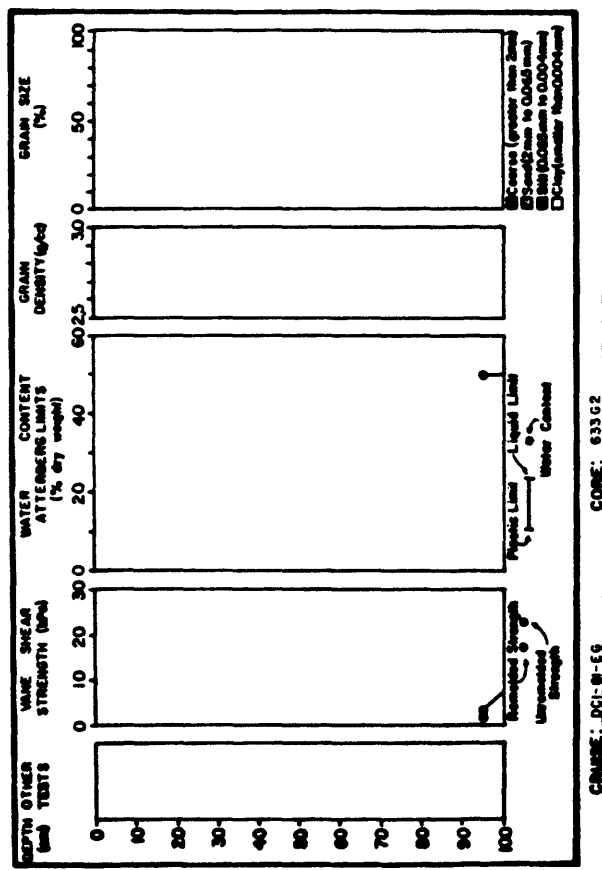


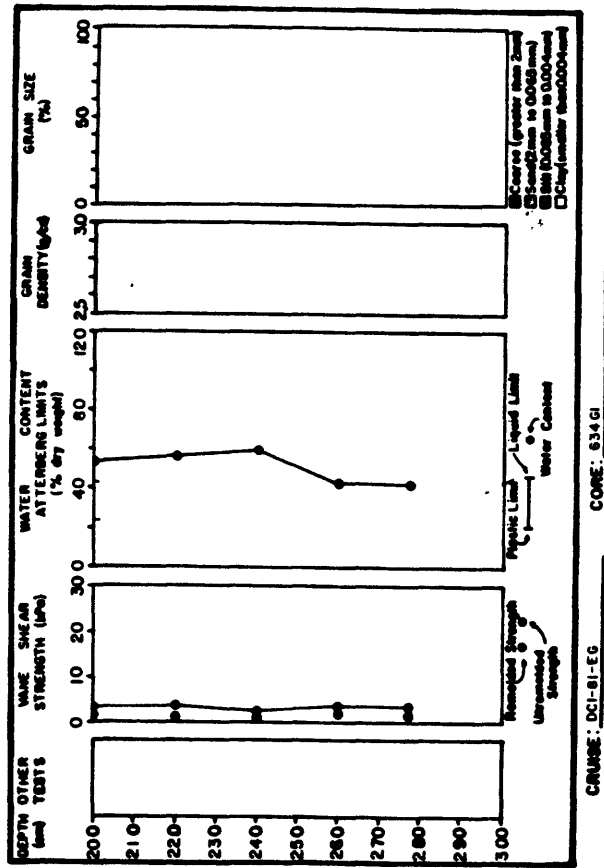




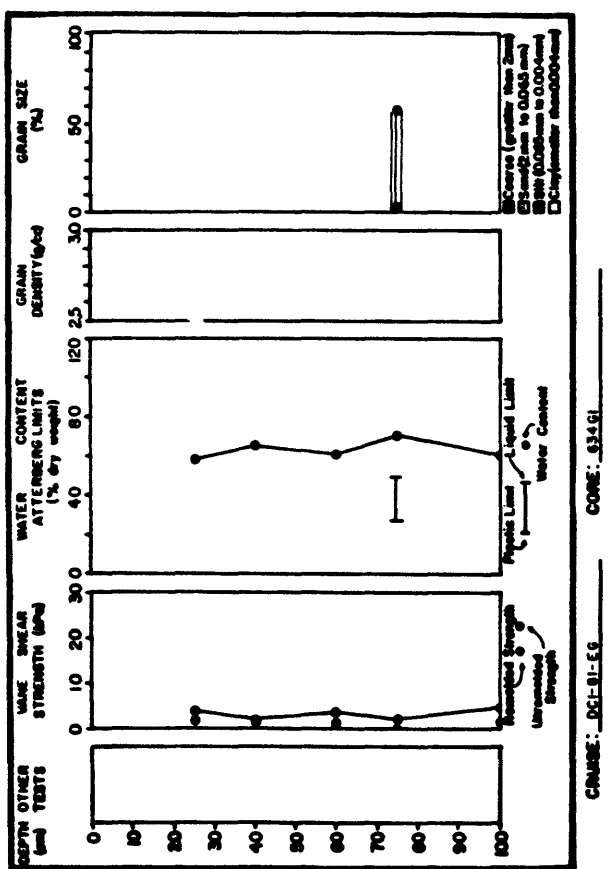




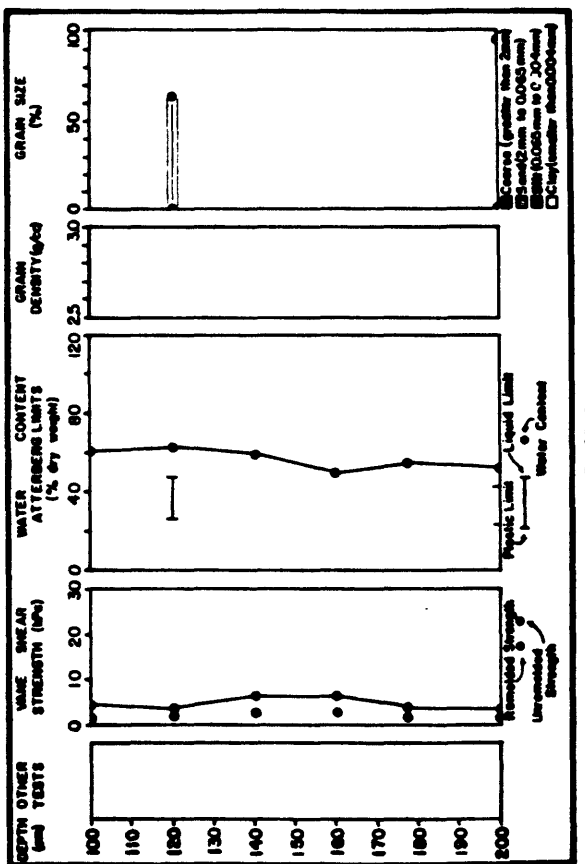




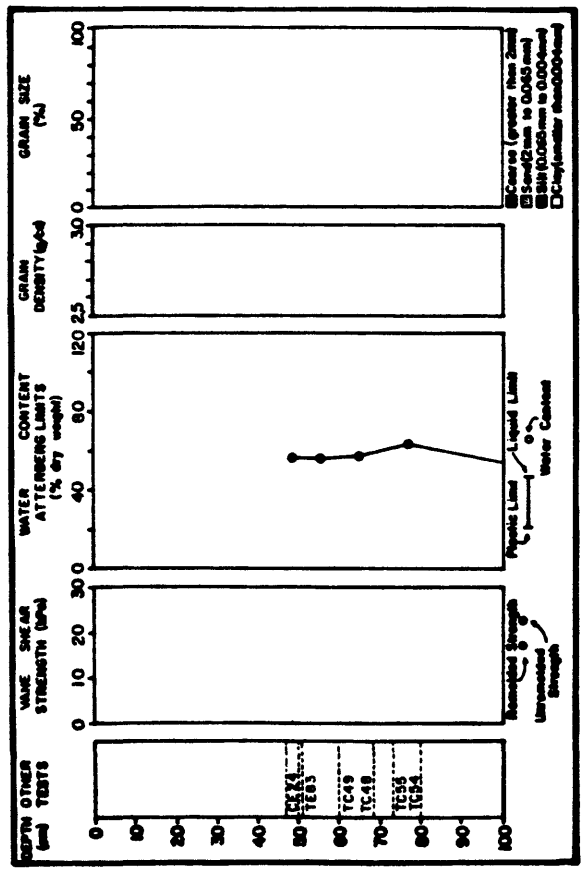
CORE: DCI-81-E6



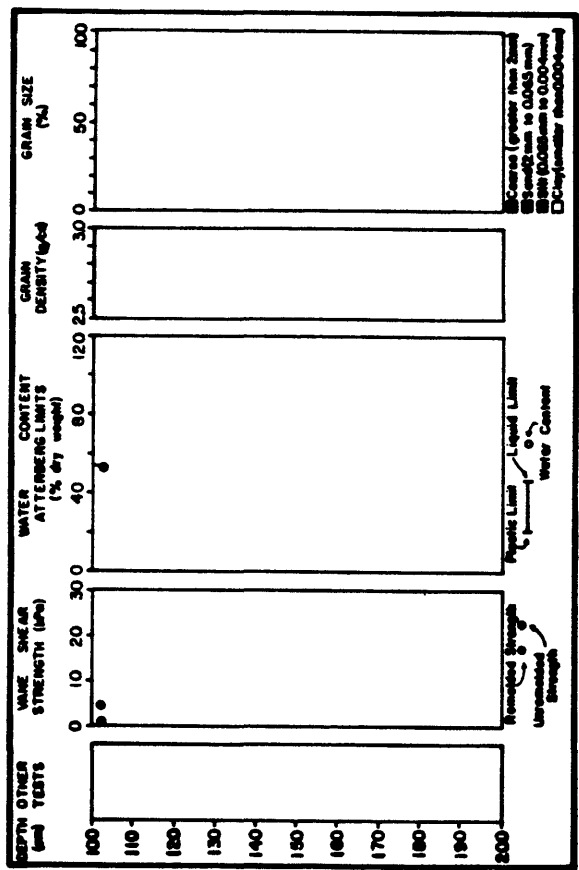
CORE: DCI-81-E6

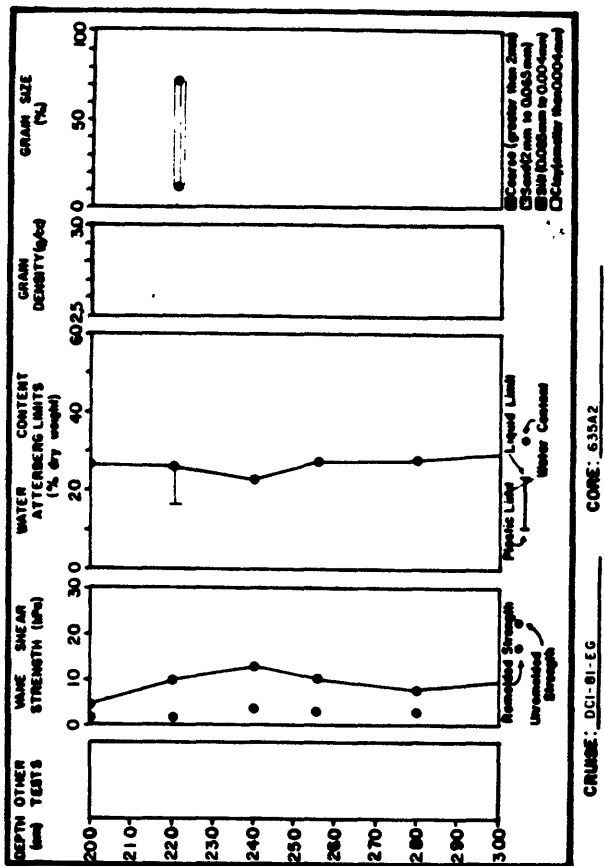


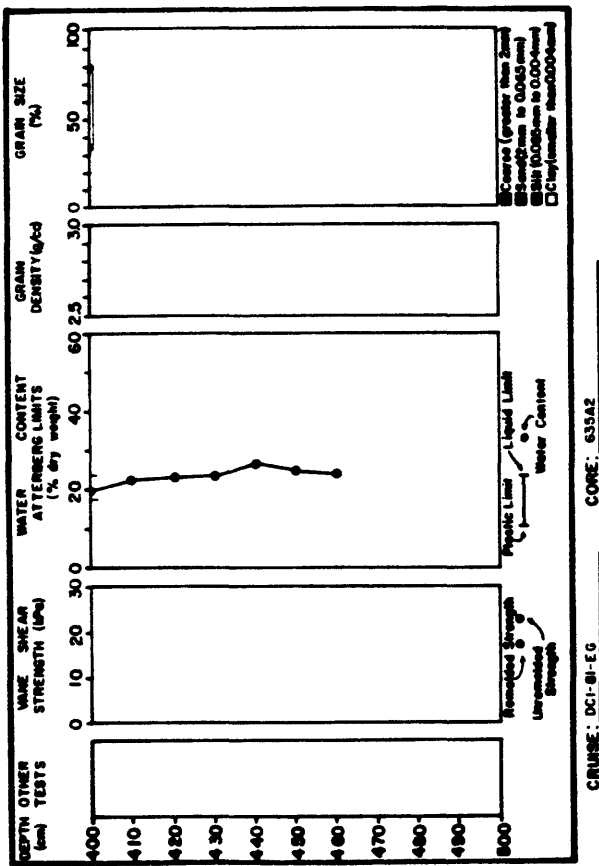
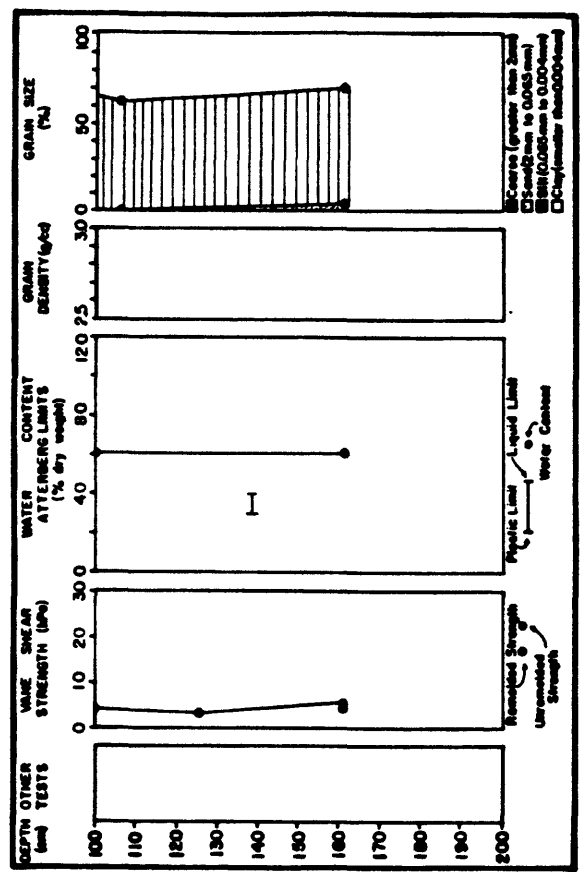
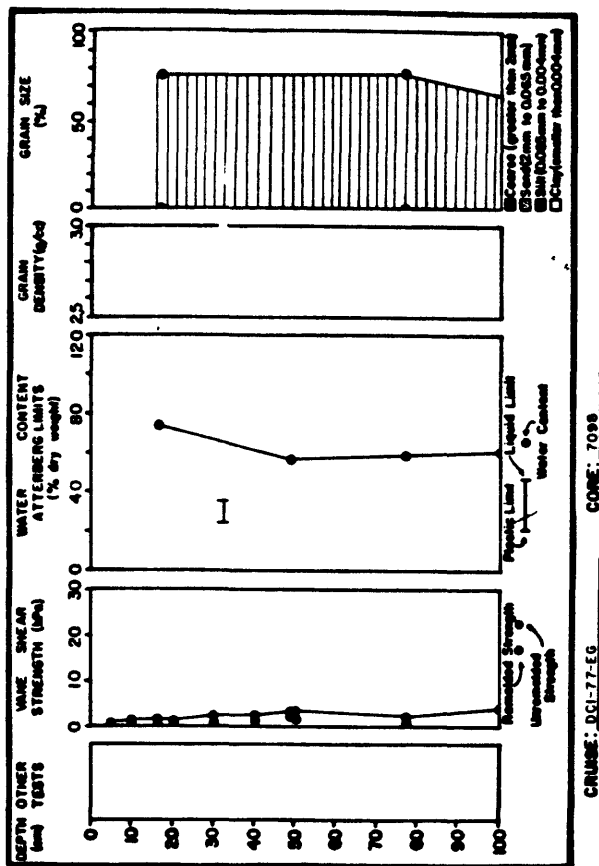
CORE: 83461

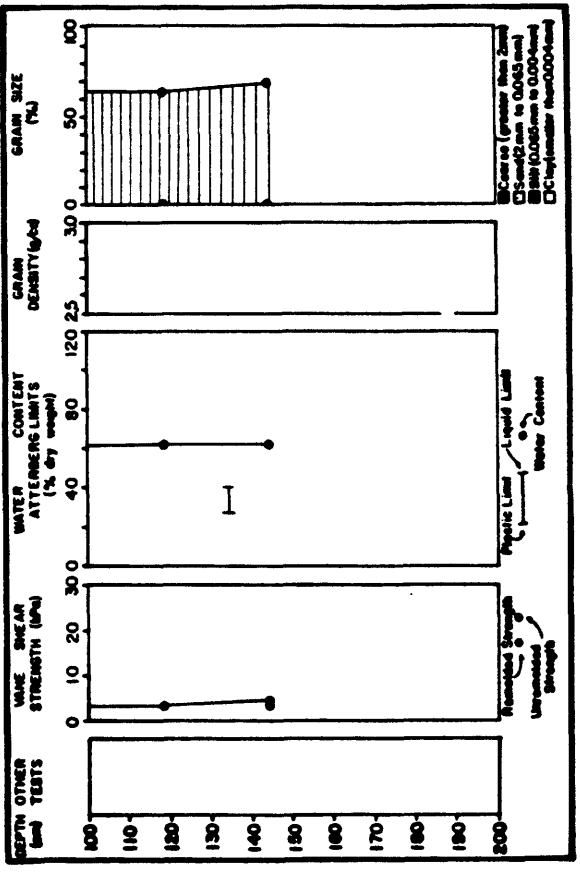
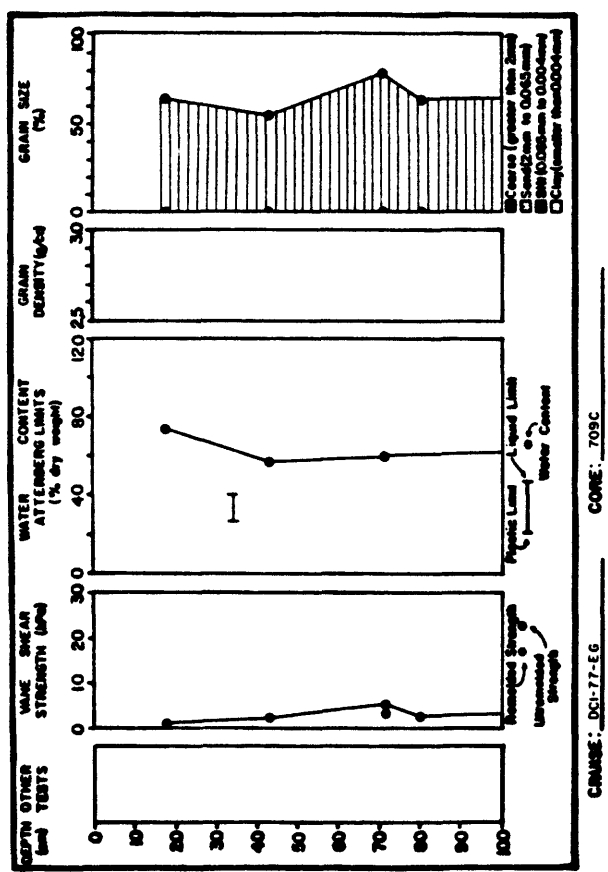
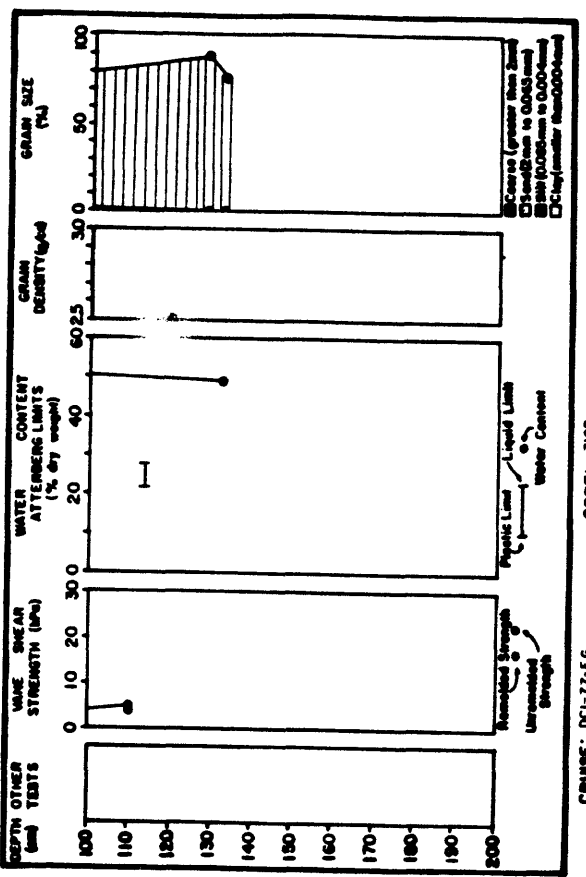
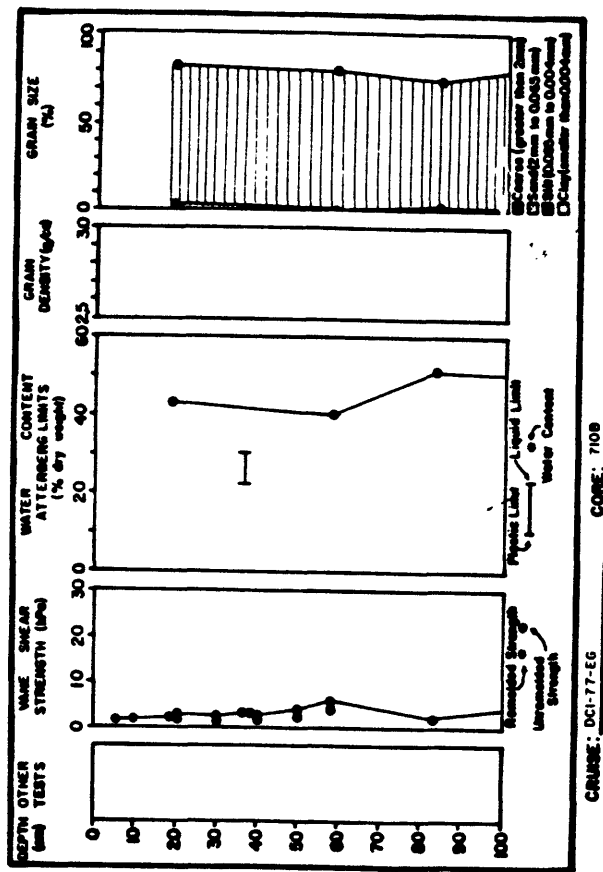


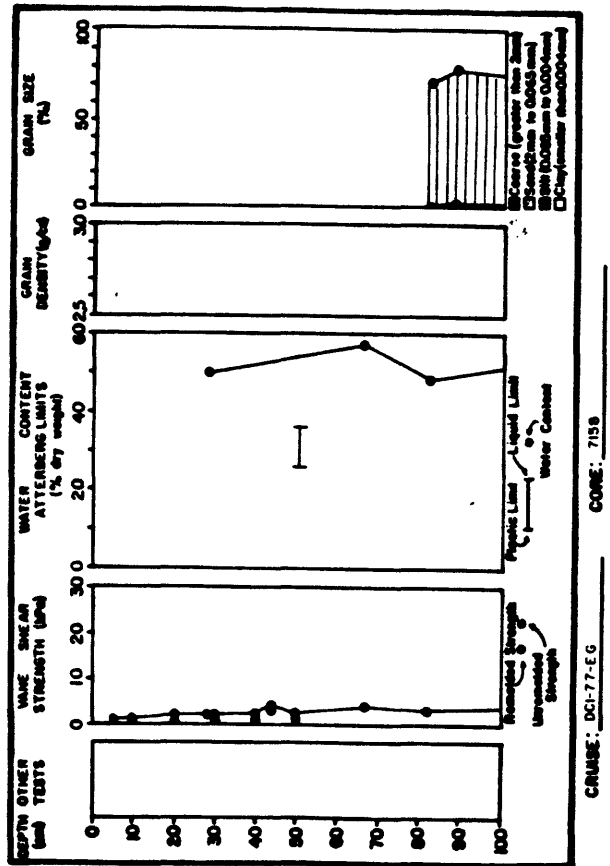
Core: 61-E6



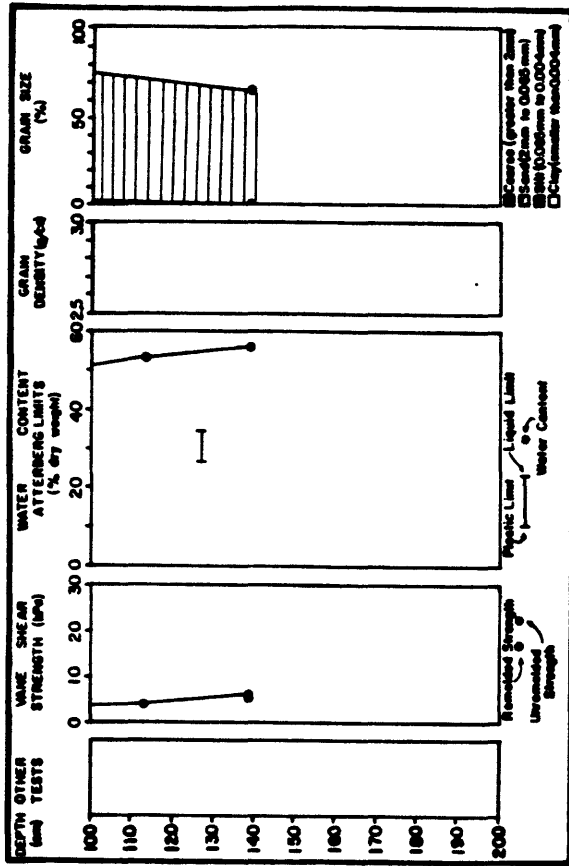




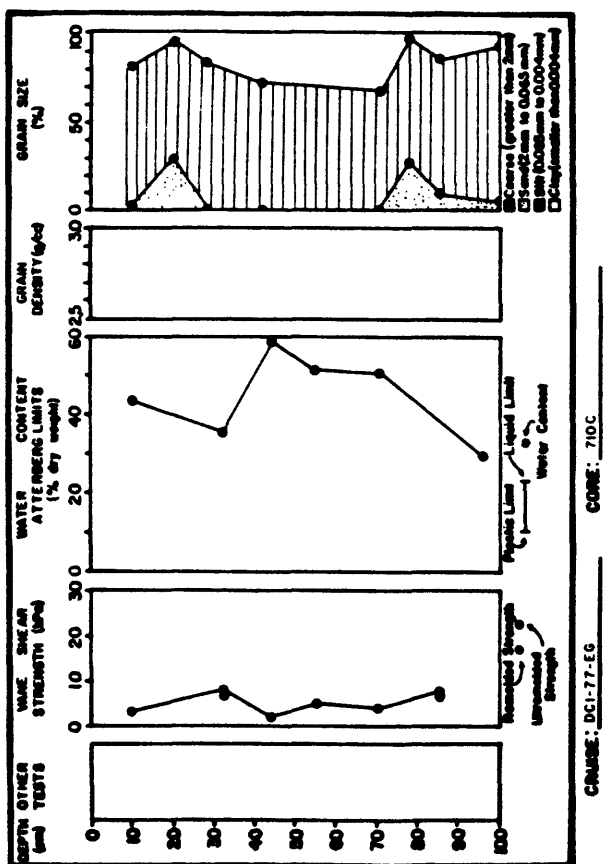




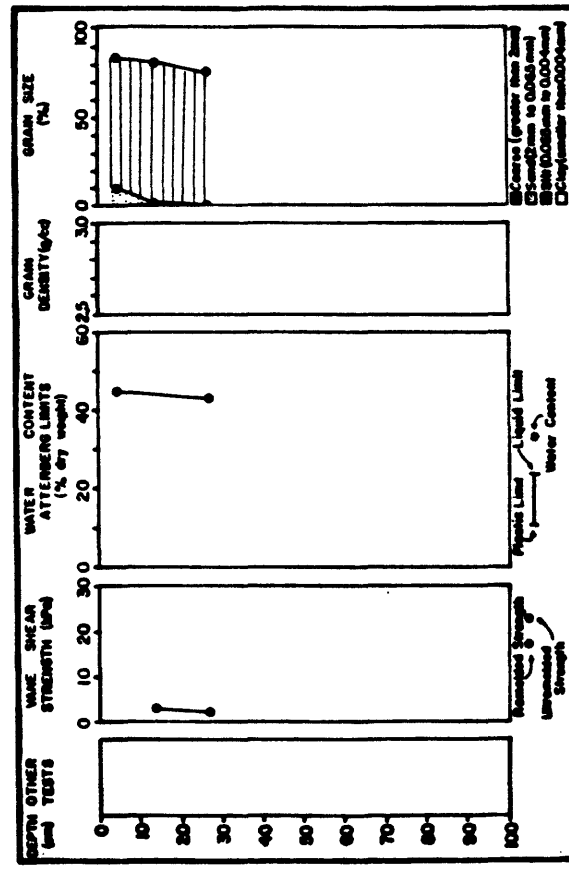
CRUISE: DCI-77-EG CORE: 7158



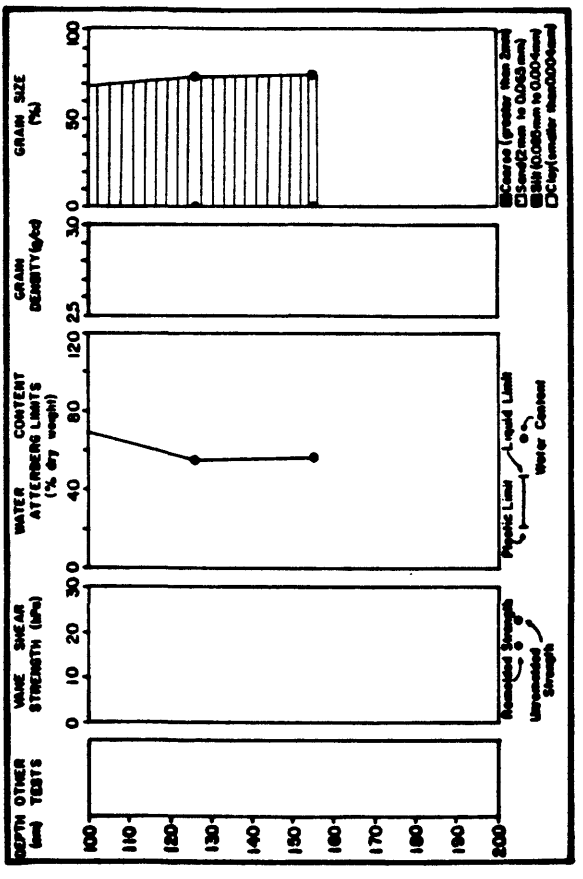
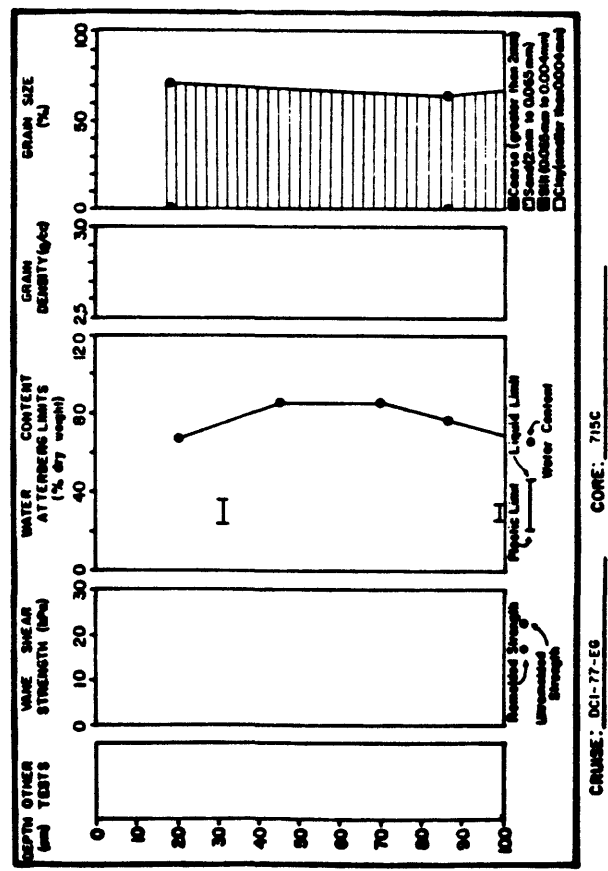
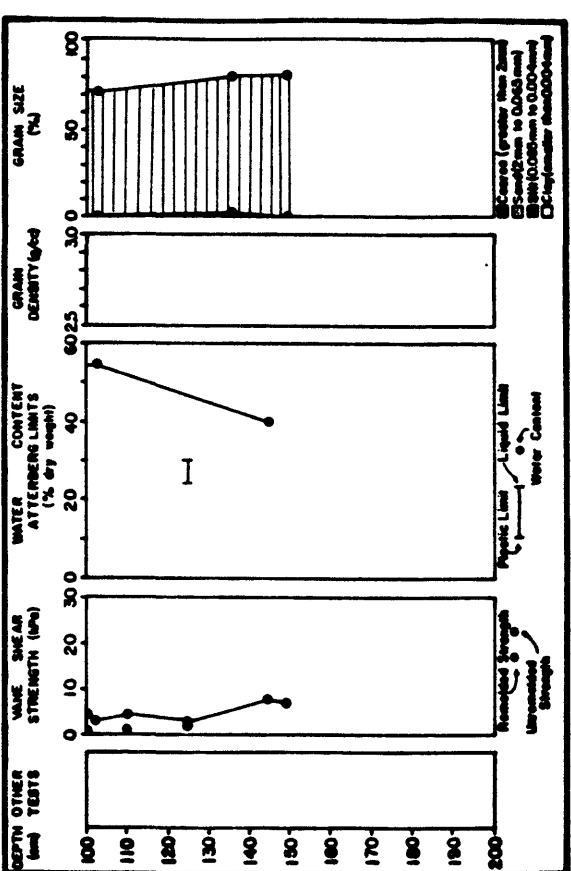
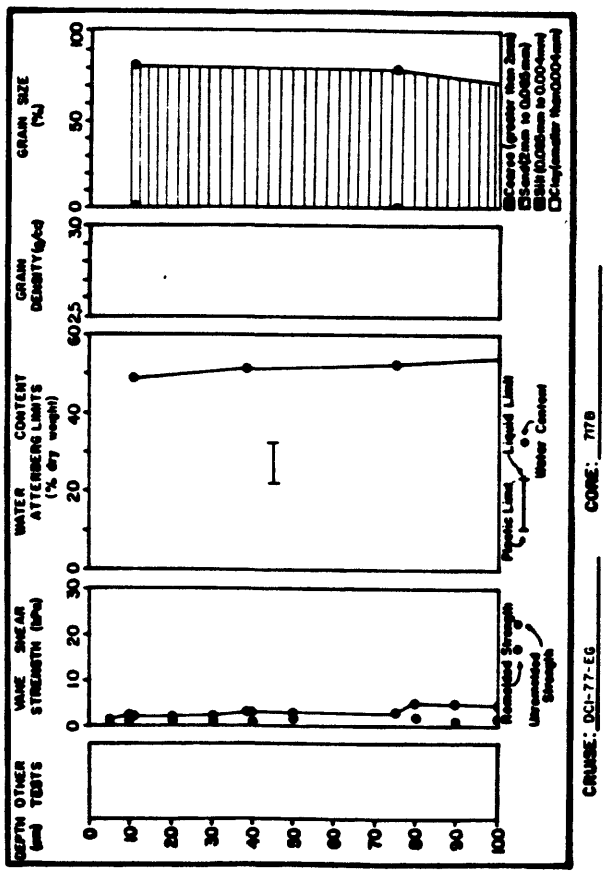
CRUISE: DCI-77-EG CORE: 7158

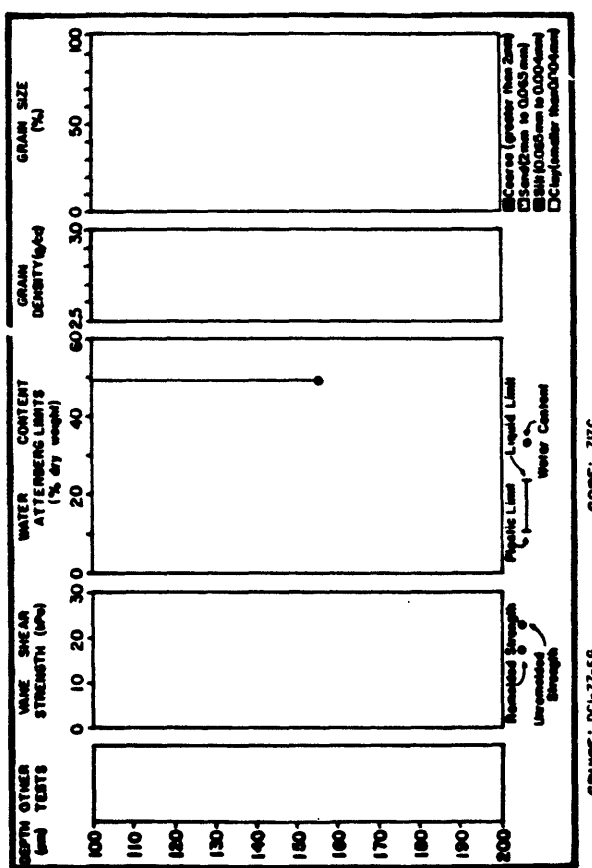
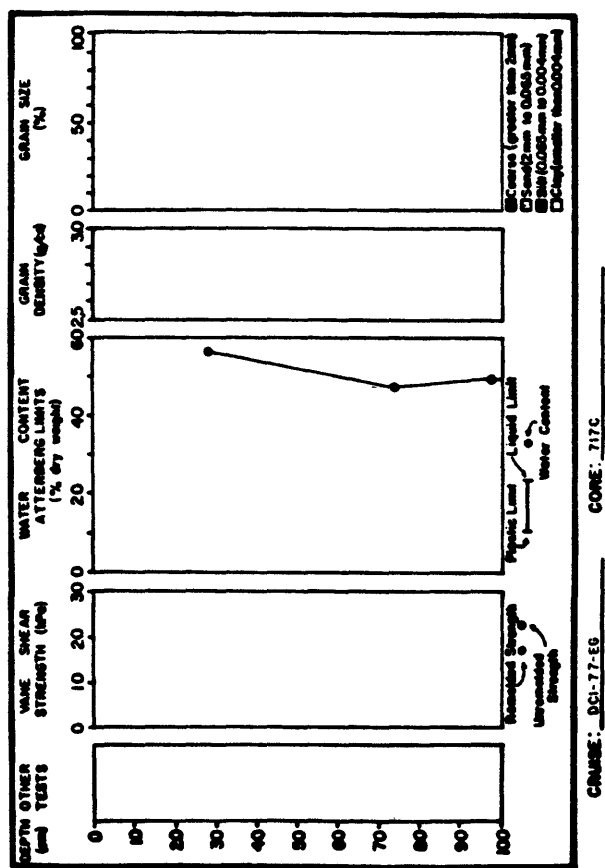
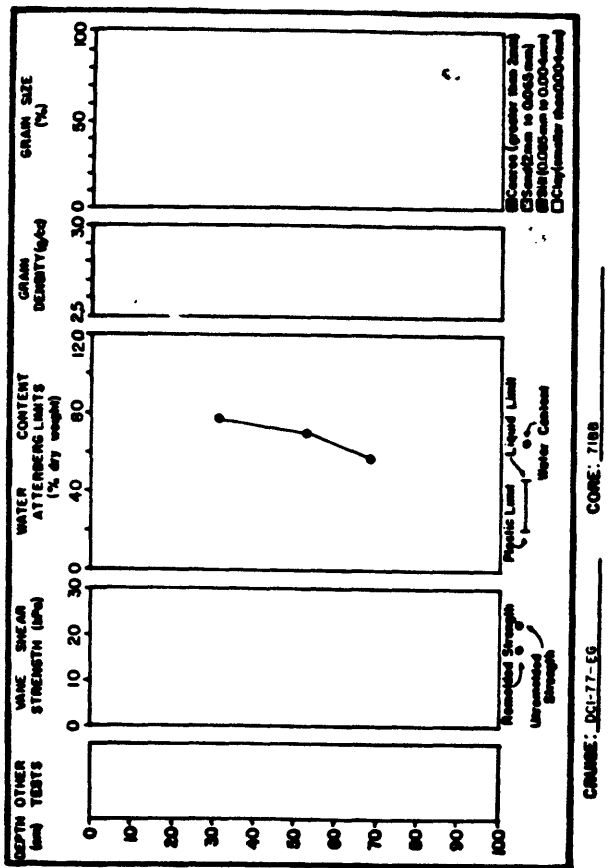


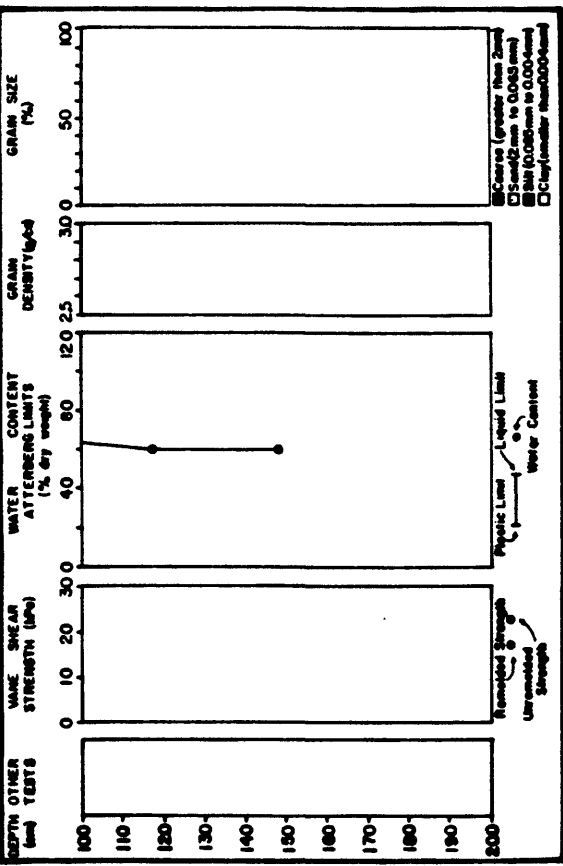
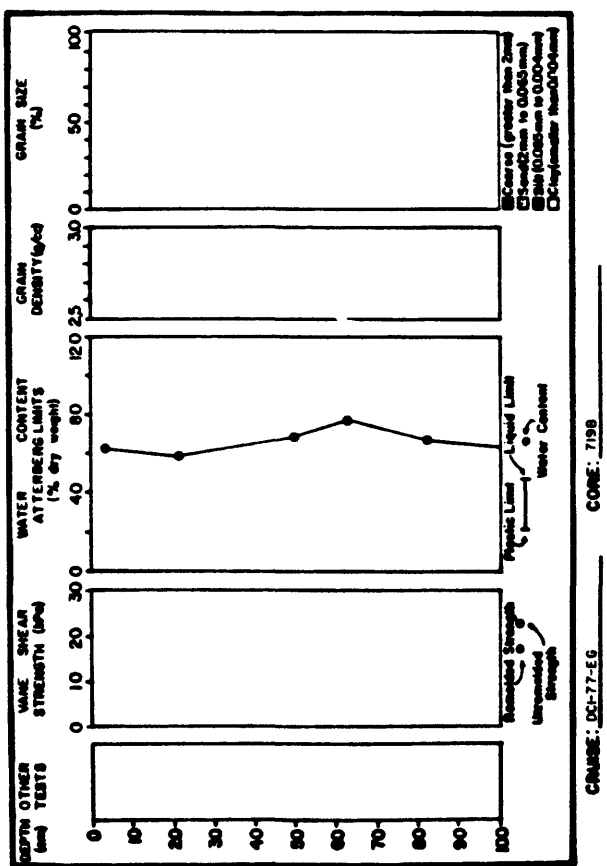
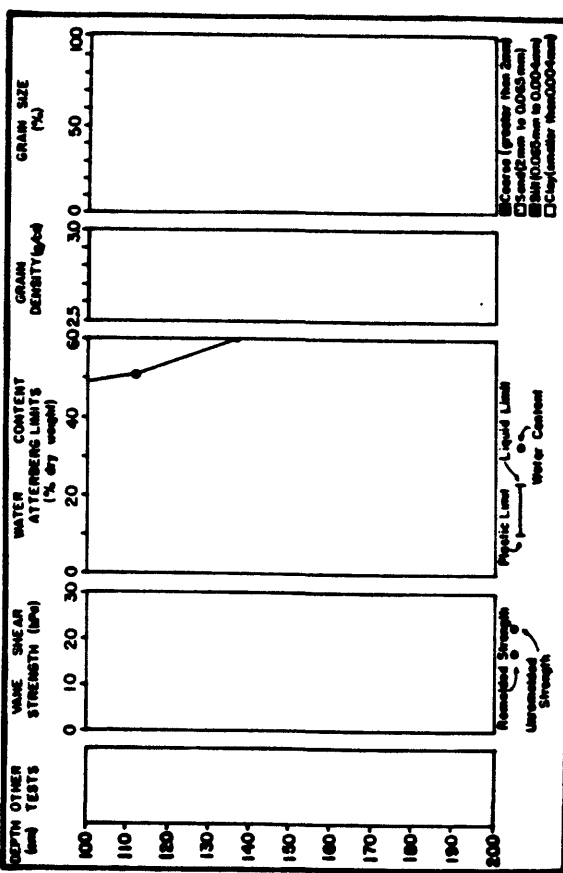
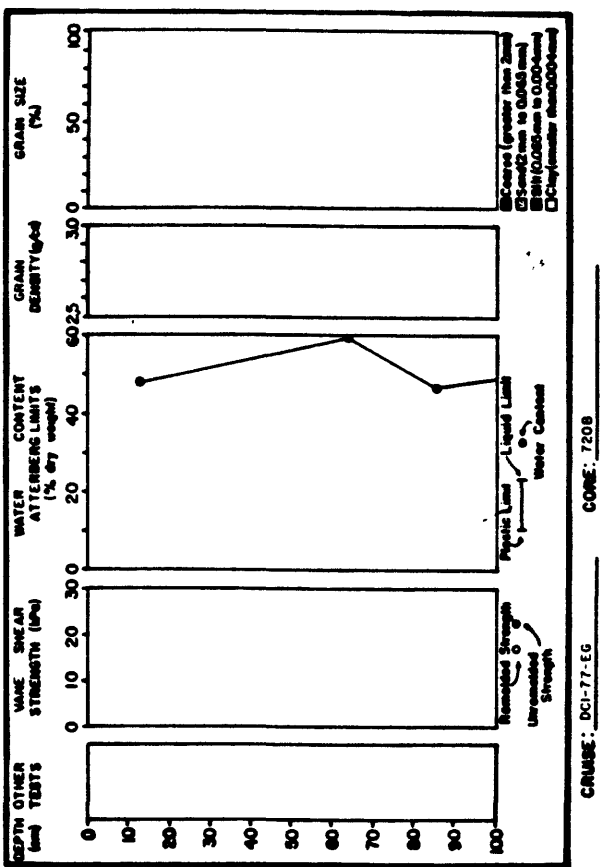
CRUISE: DCI-77-EG CORE: 710C

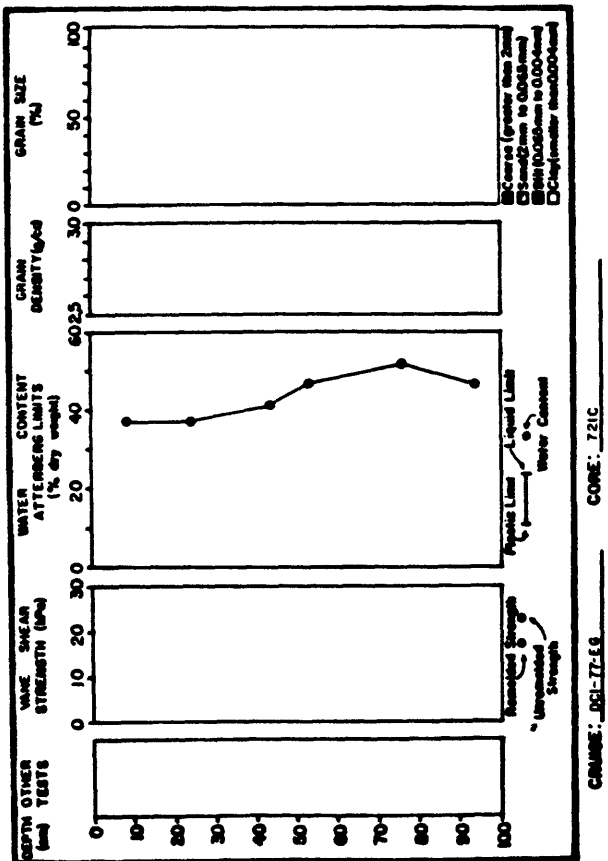
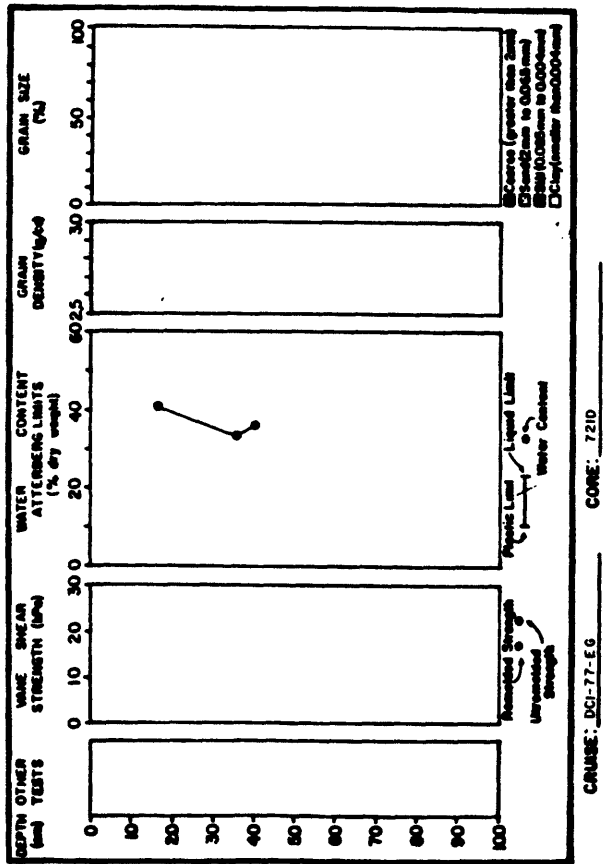


CRUISE: DCI-77-EG CORE: 710C

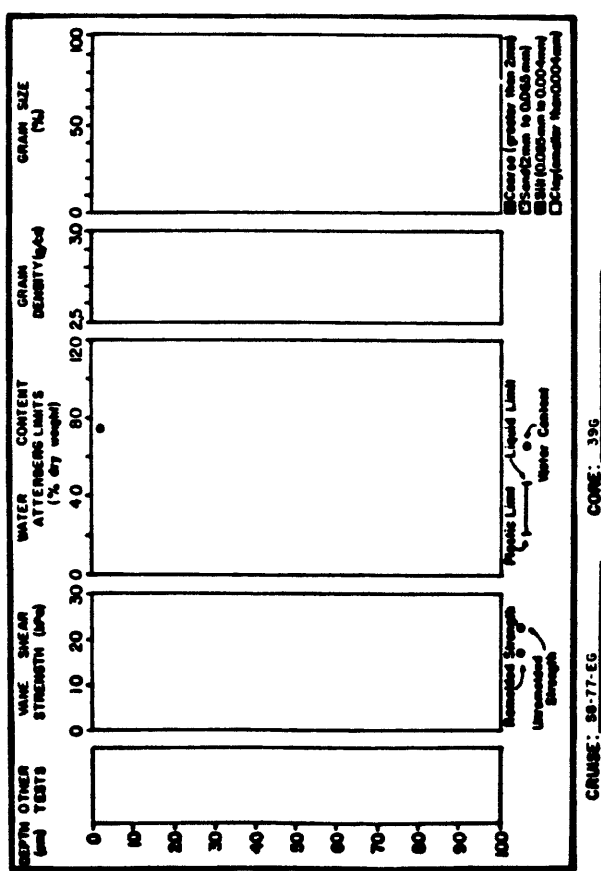
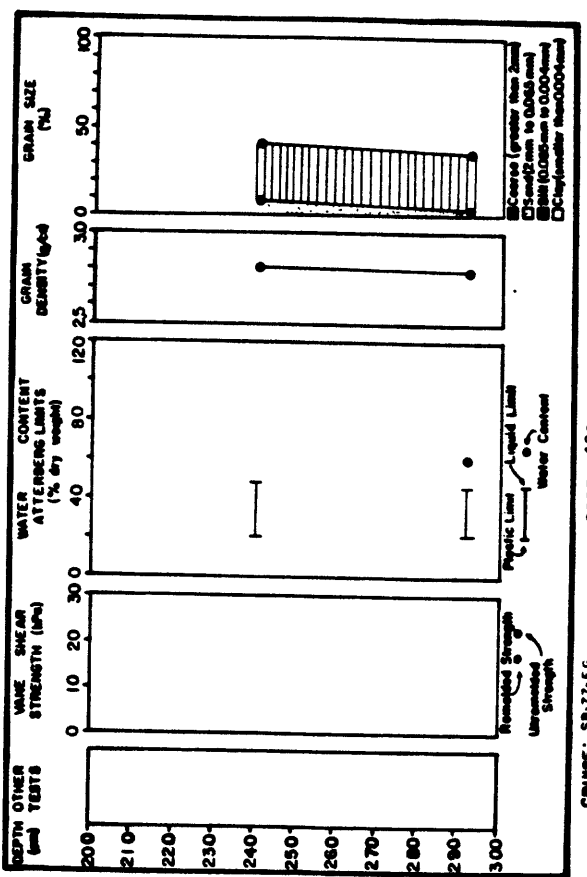
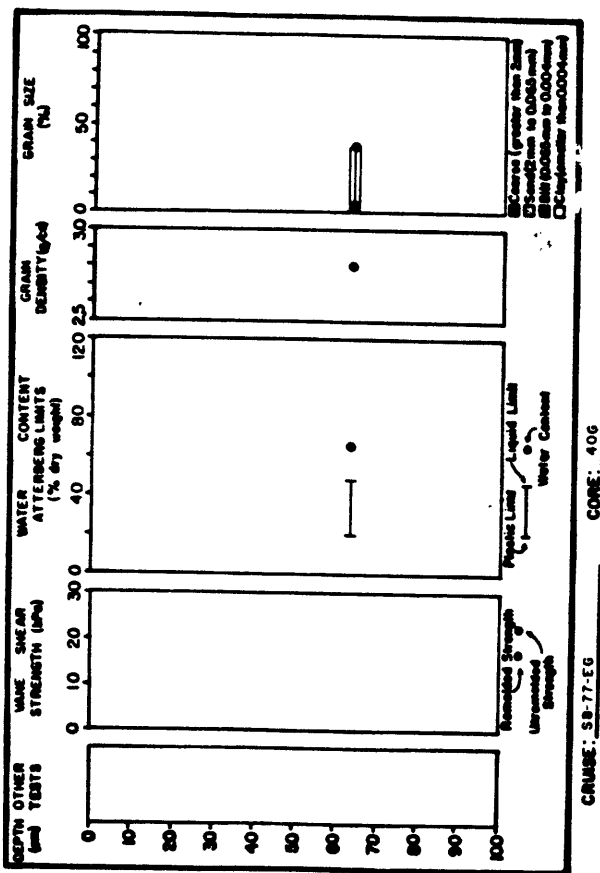


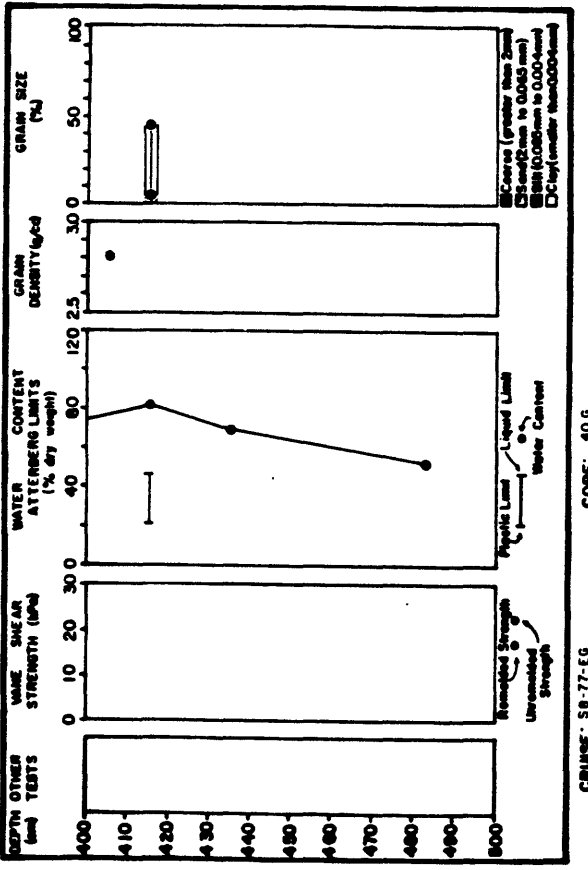
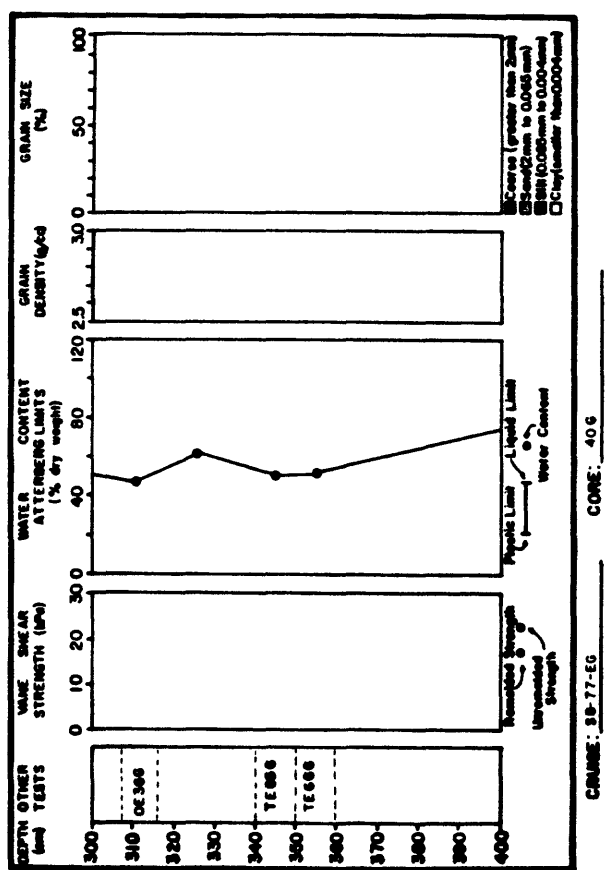
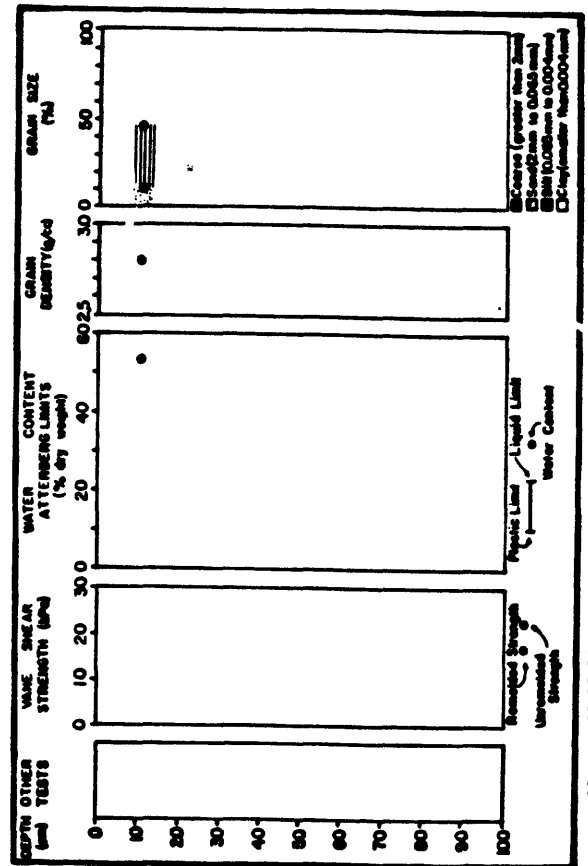
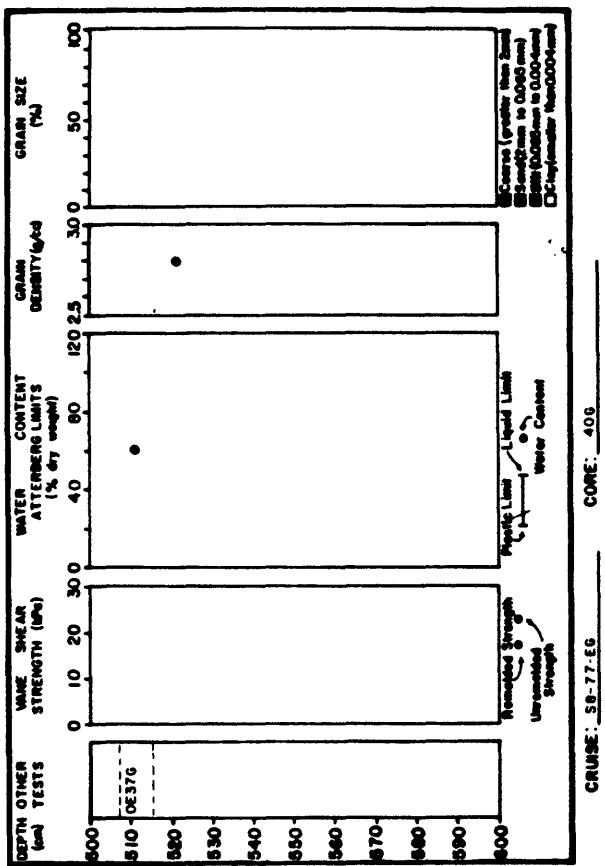


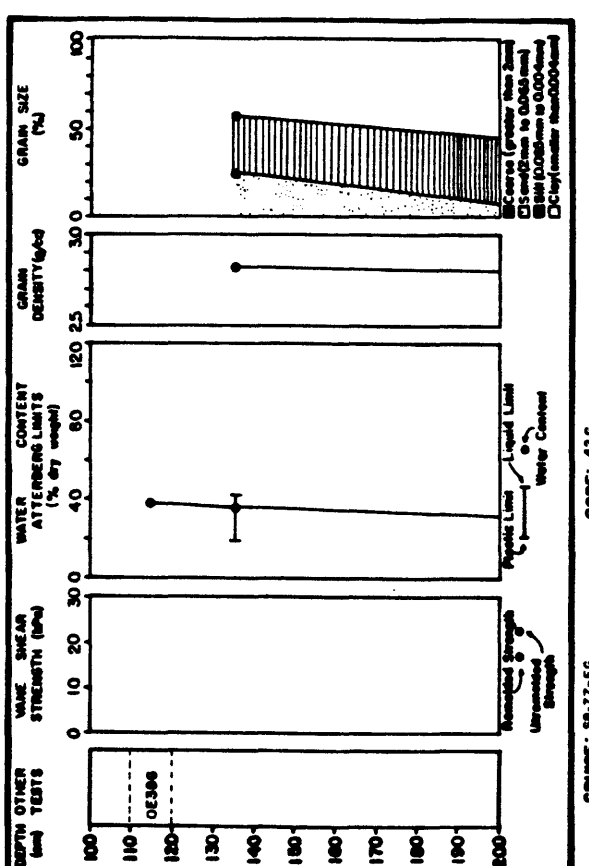
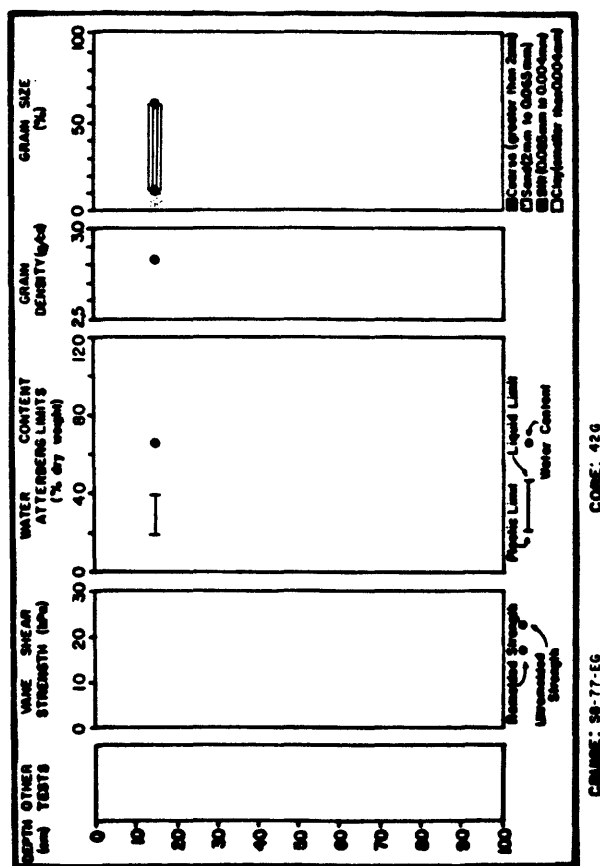
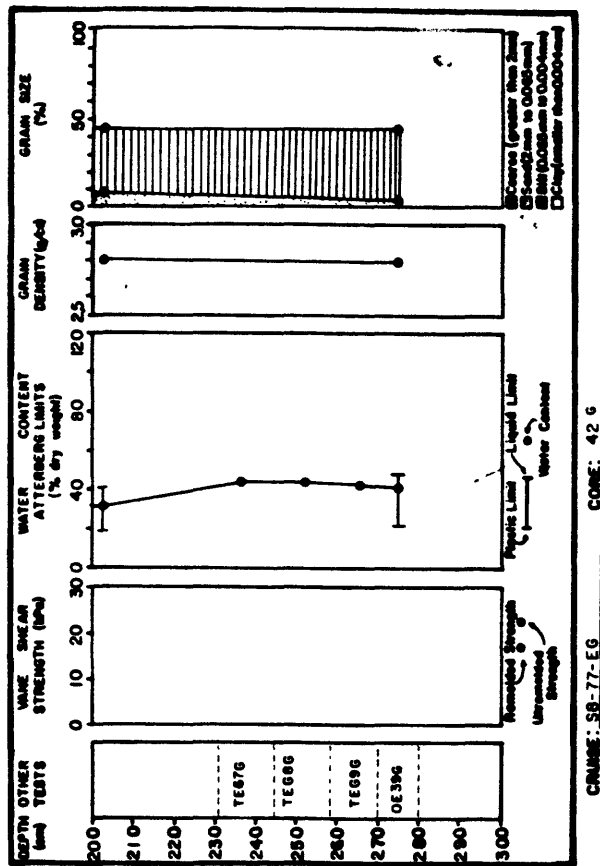




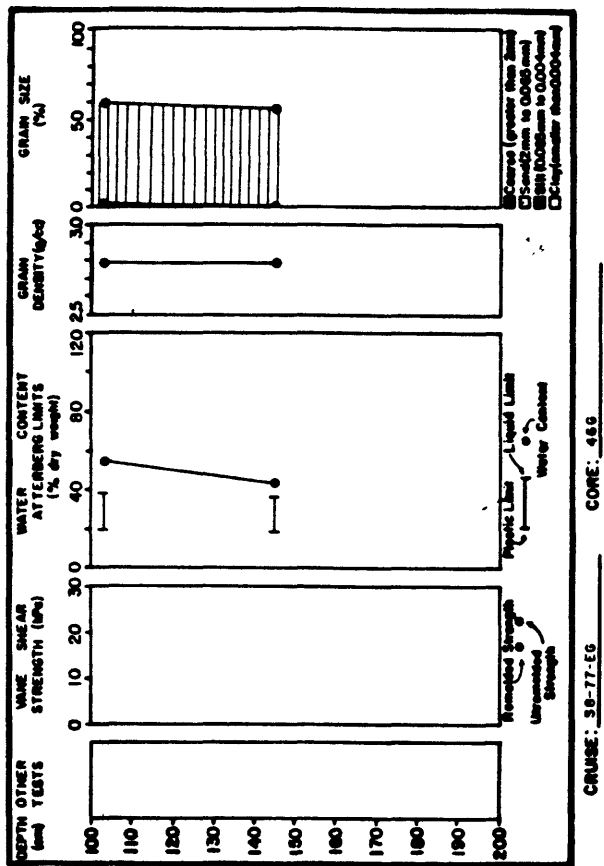
ICY BAY STUDY AREA



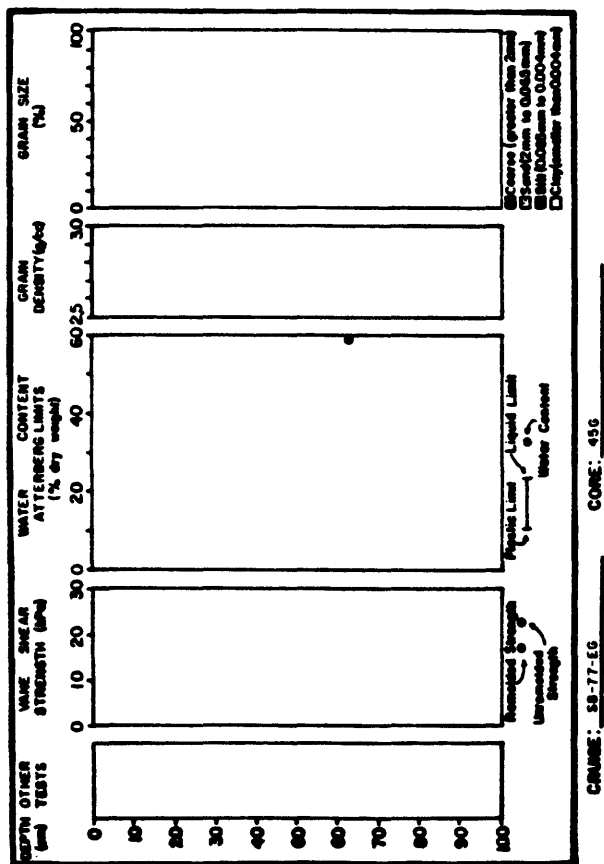




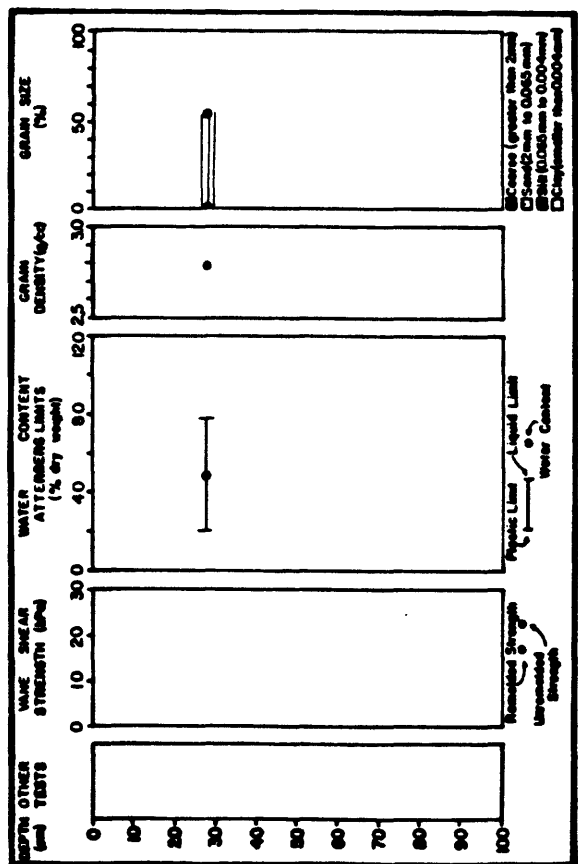
**YAKUTAT BAY STUDY AREA**



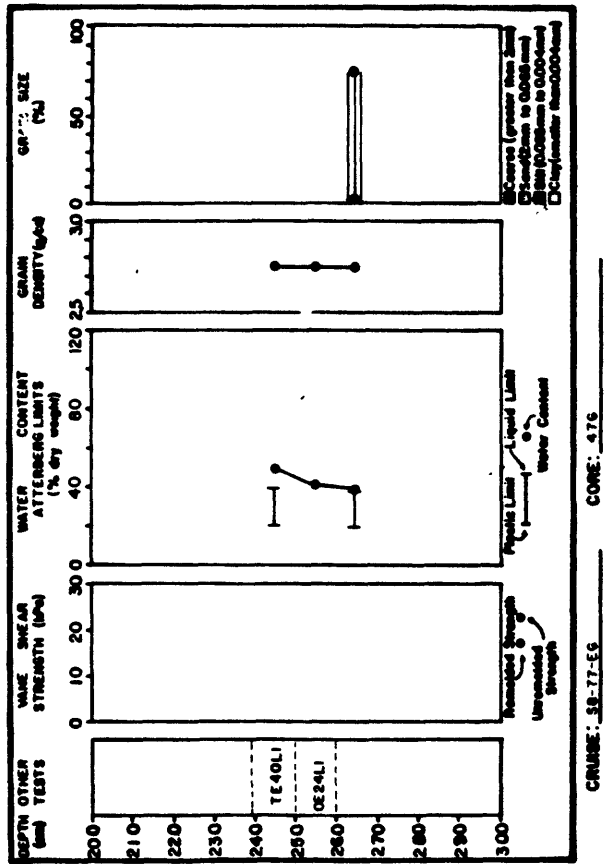
CONE: 58-77-EG



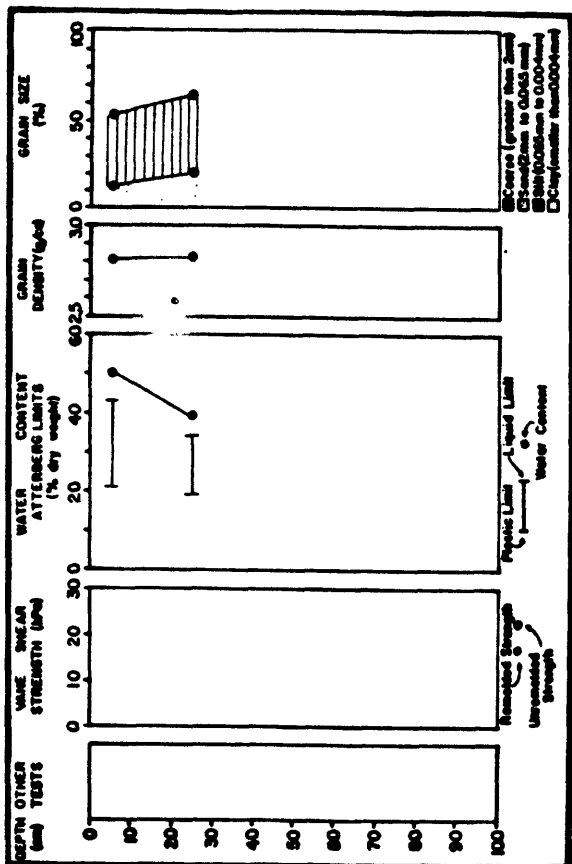
CONE: 58-77-EG



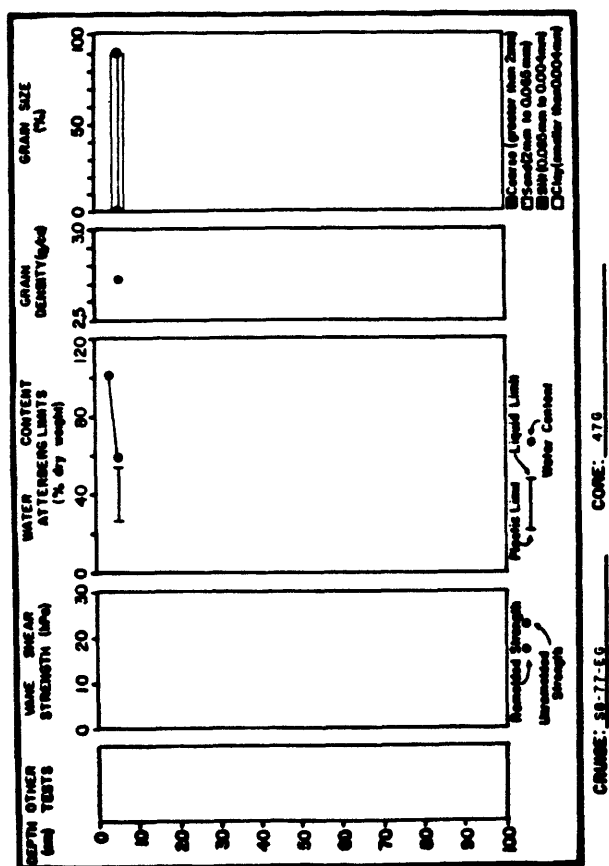
CONE: 45G



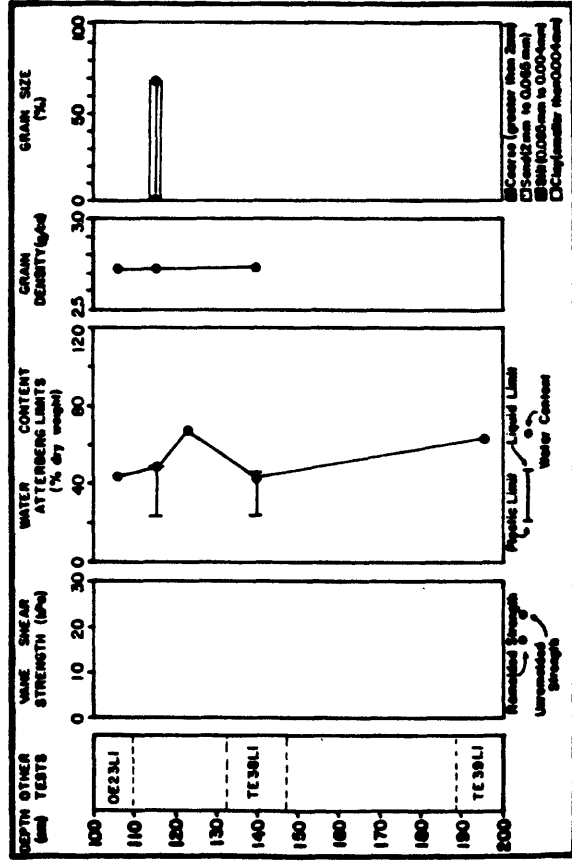
CORE: 476



CORE: 476

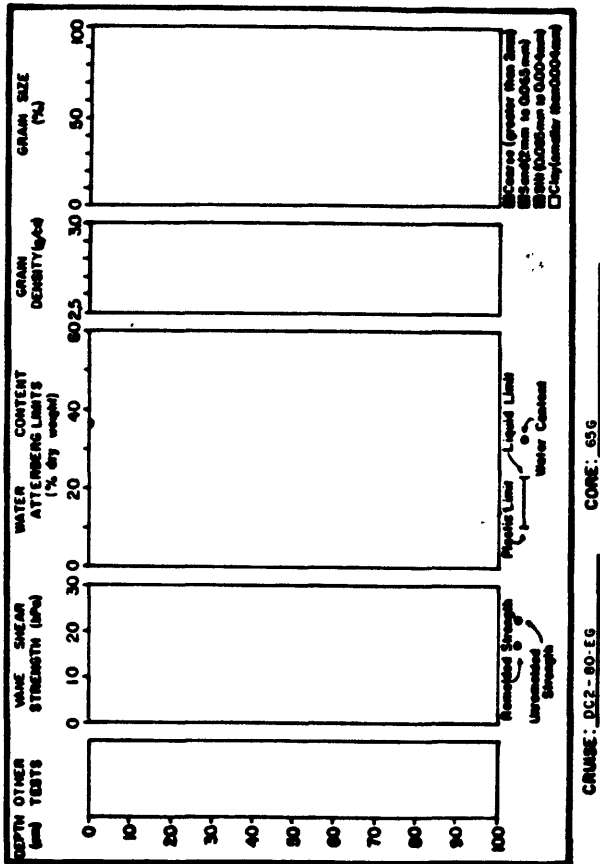


CORE: 476

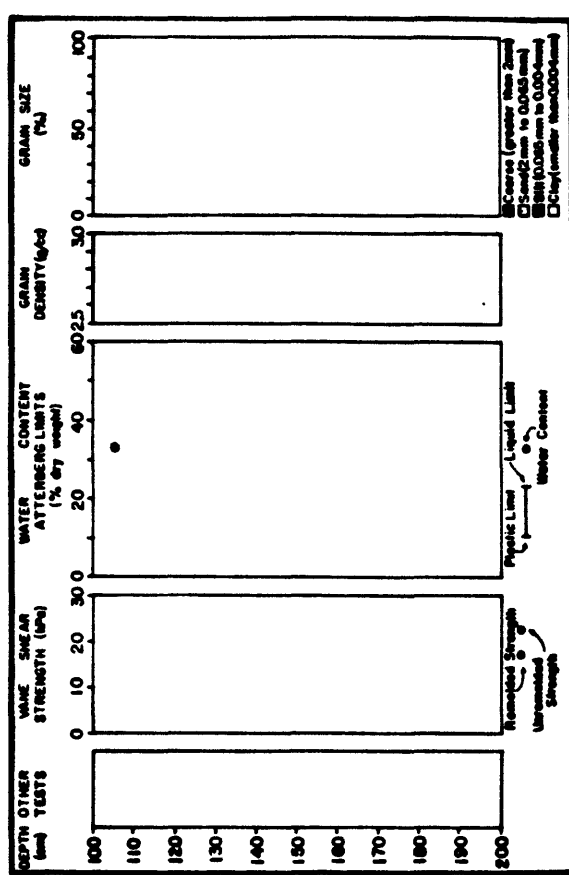


CORE: 476

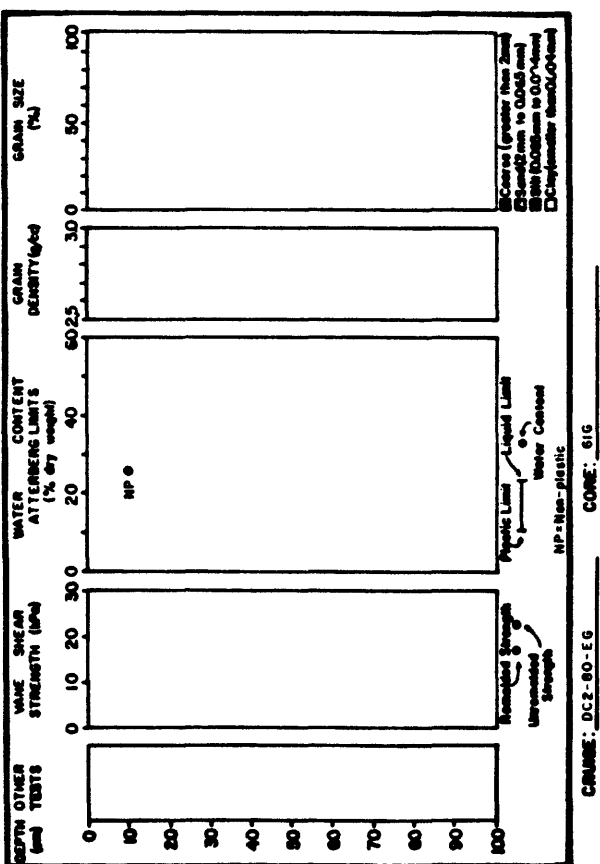
YAKUTAT STUDY AREA



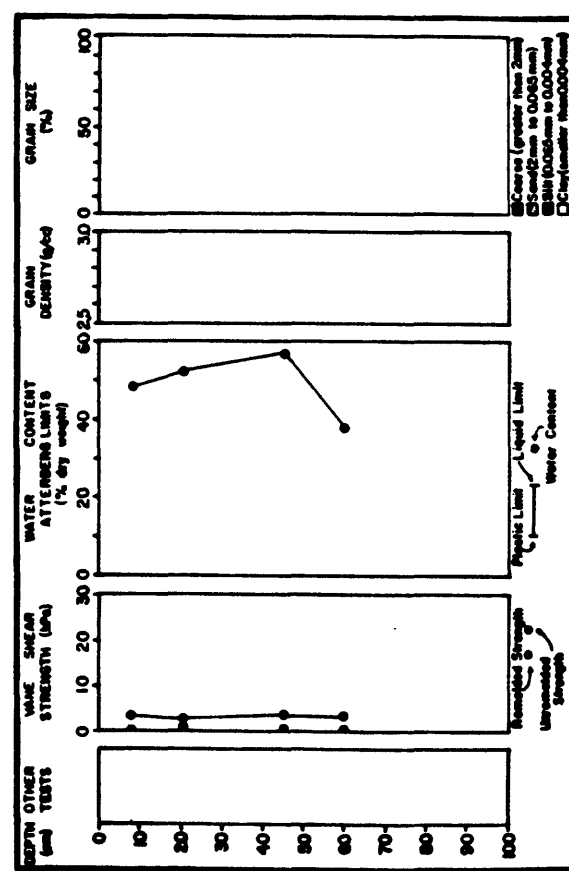
CRUISE: DCE-80-EG      CORE: 65G



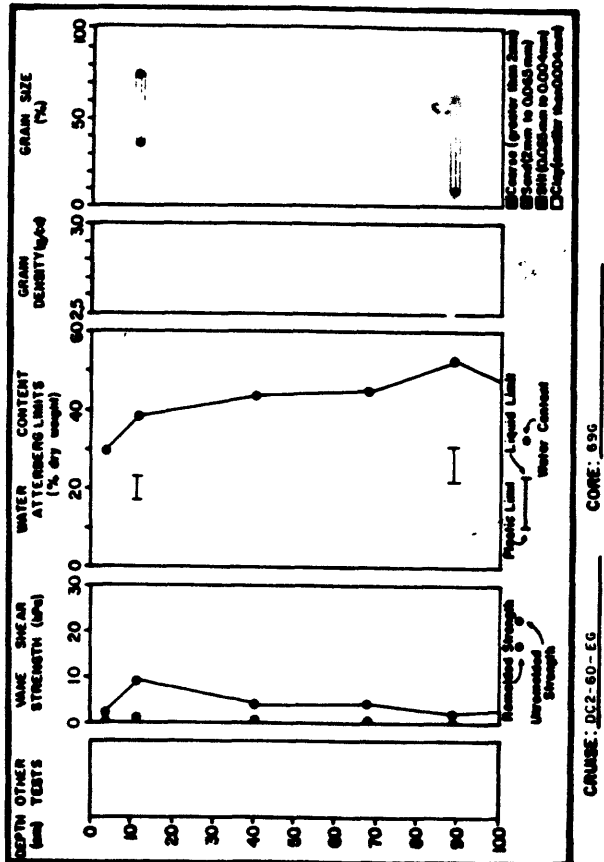
CRUISE: DCE-80-EG      CORE: 65G



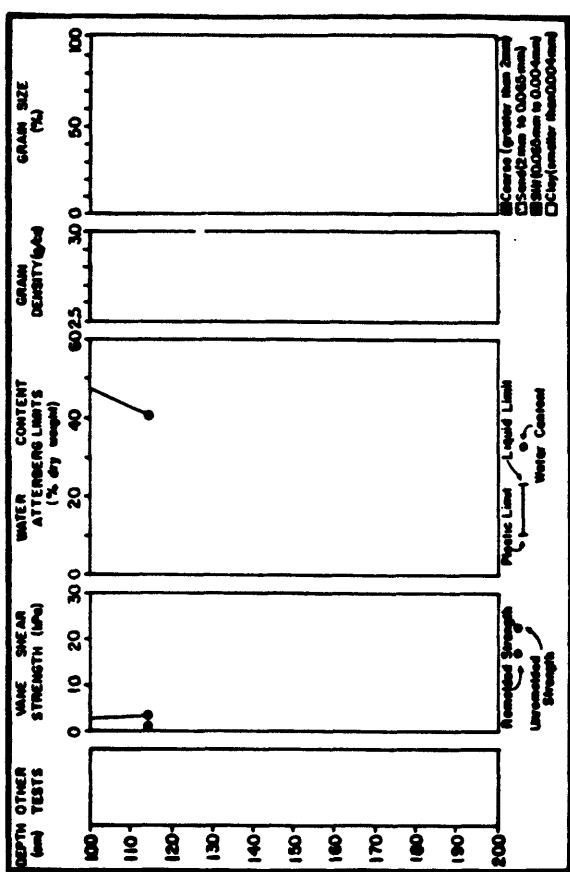
CRUISE: DCE-80-EG      CORE: 61G



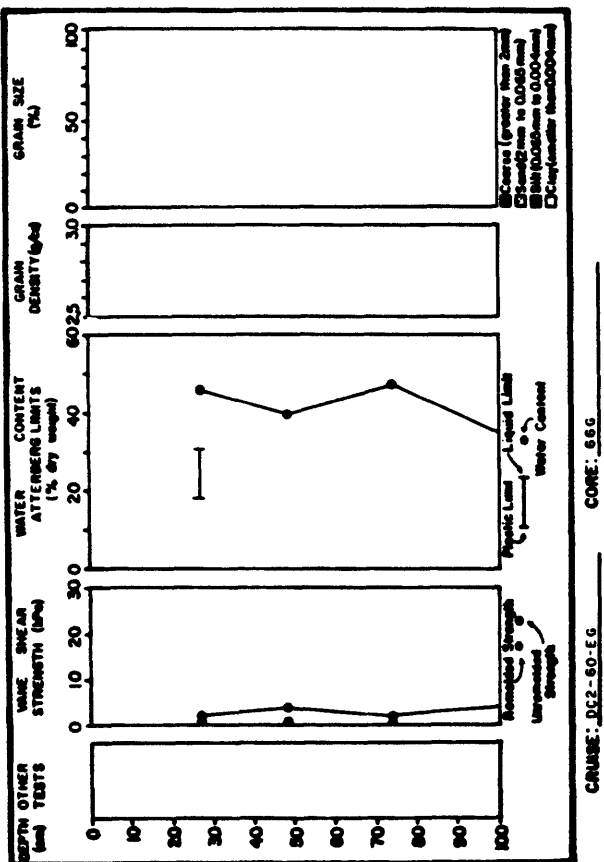
CRUISE: DCE-80-EG      CORE: 64G



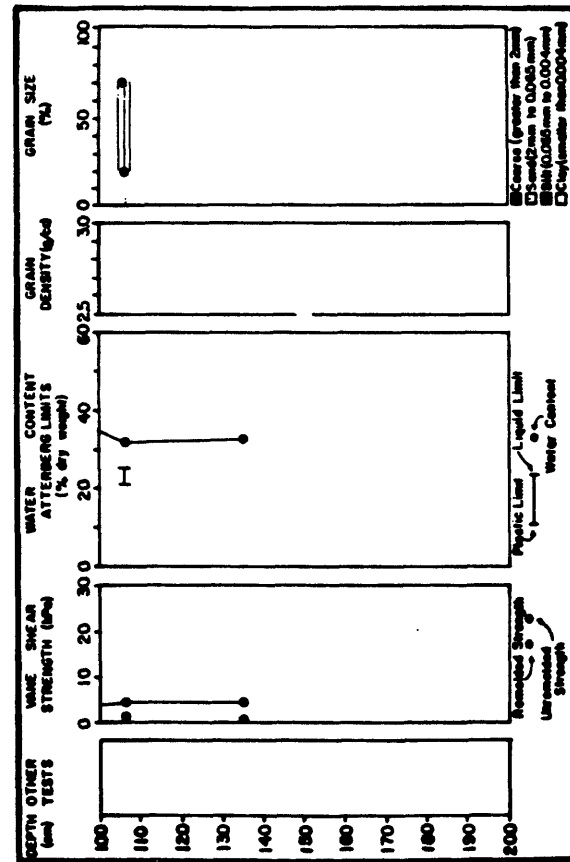
CRUISE: DC2-80-EG CORE: 696



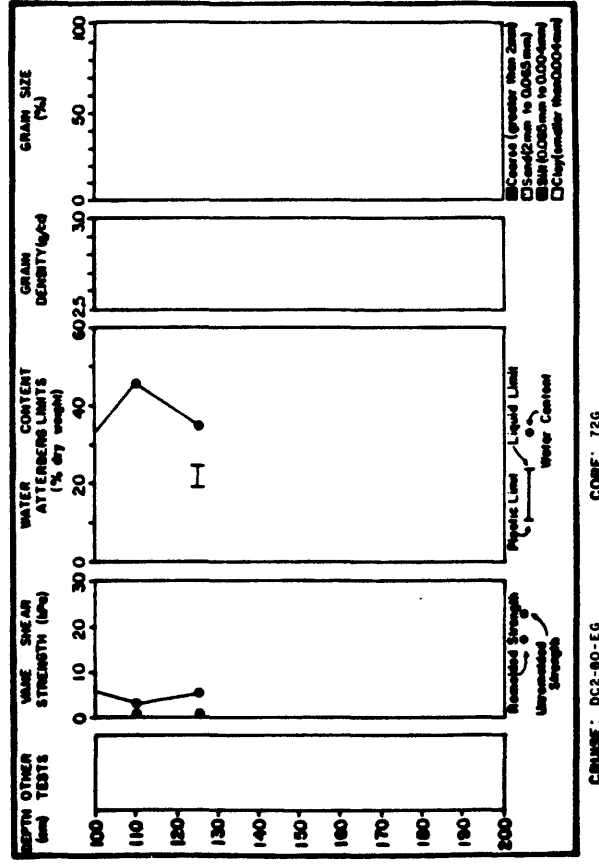
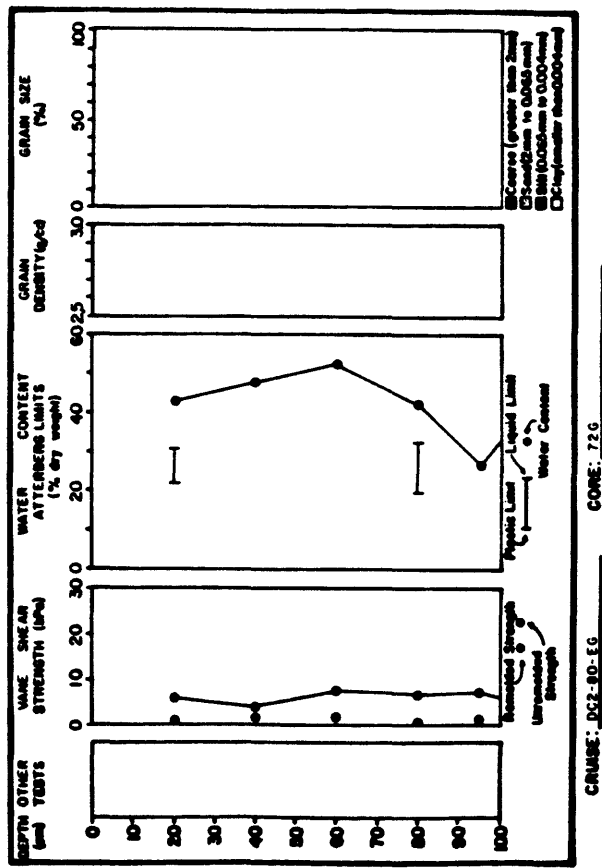
CRUISE: DC2-80-EG CORE: 696

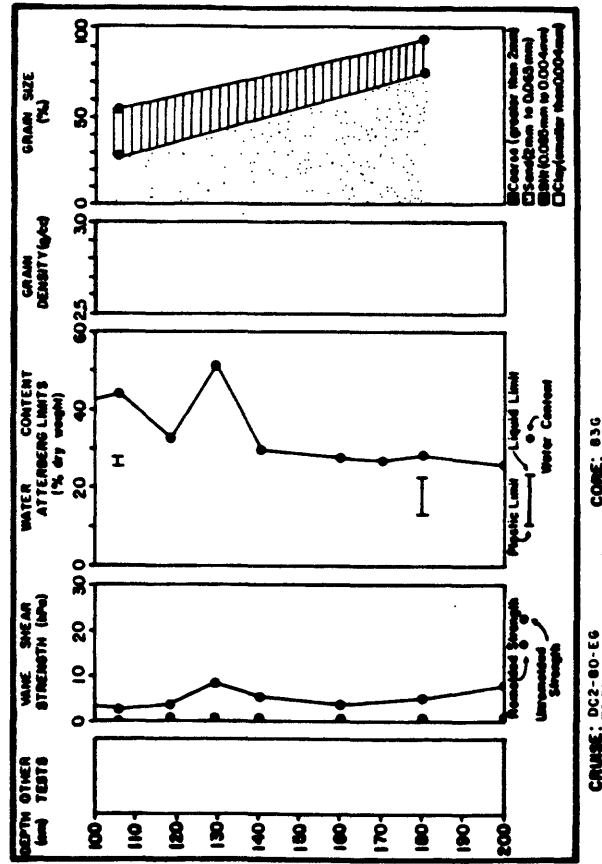
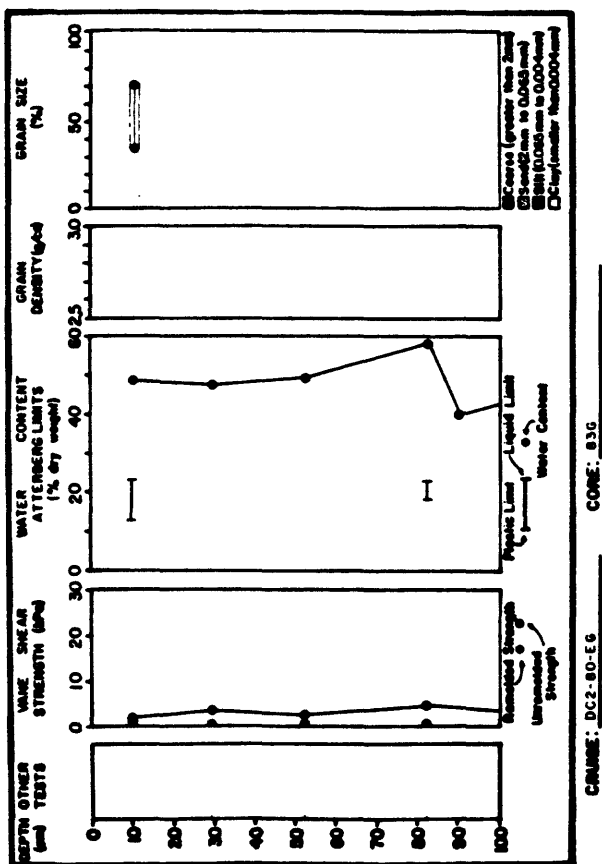
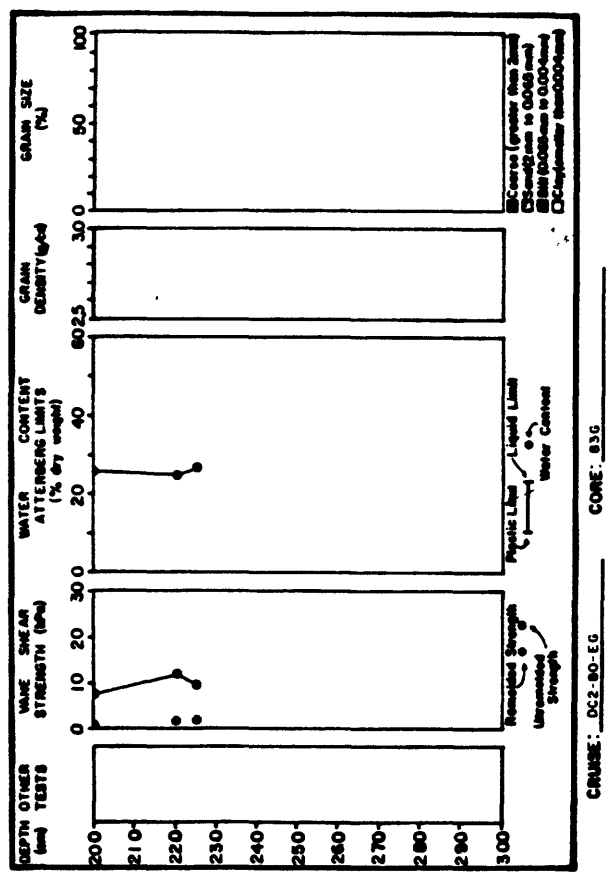


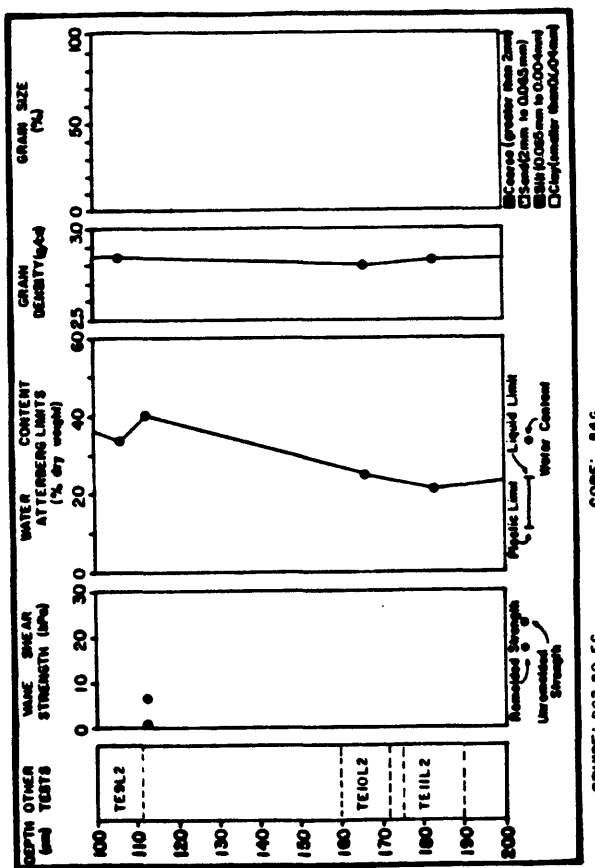
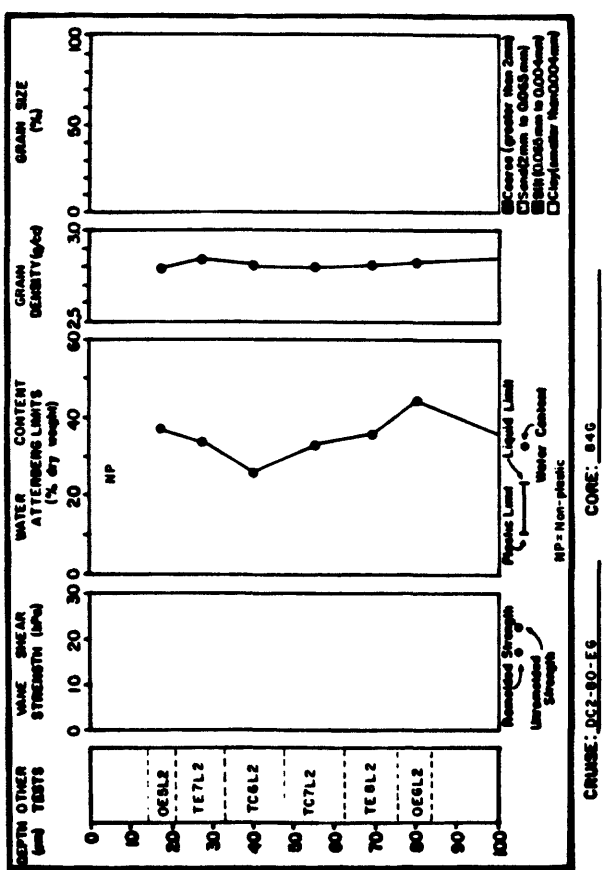
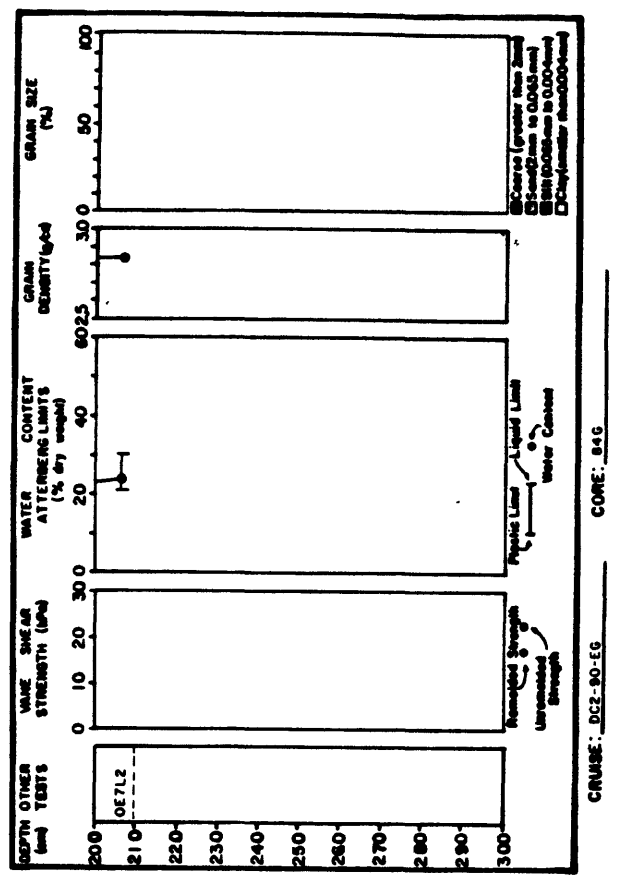
CRUISE: DC2-80-EG CORE: 666

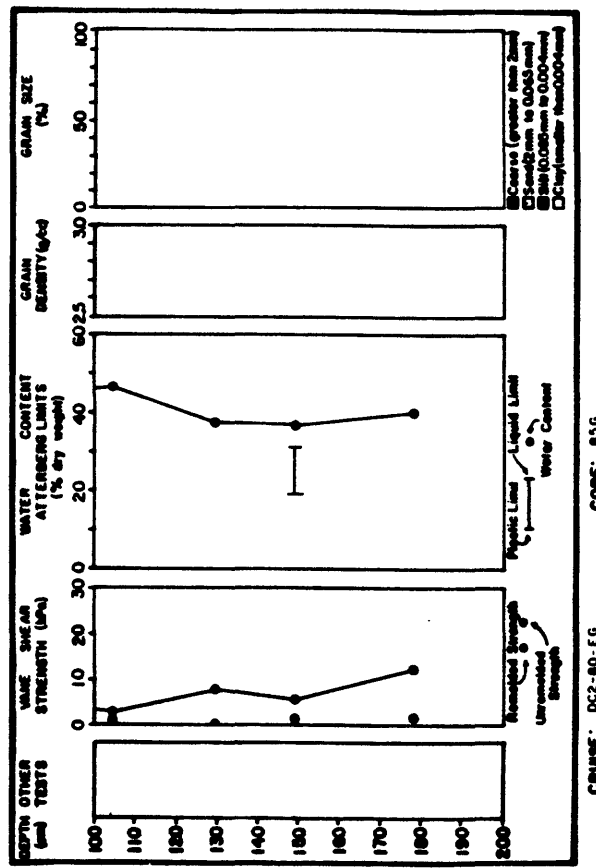
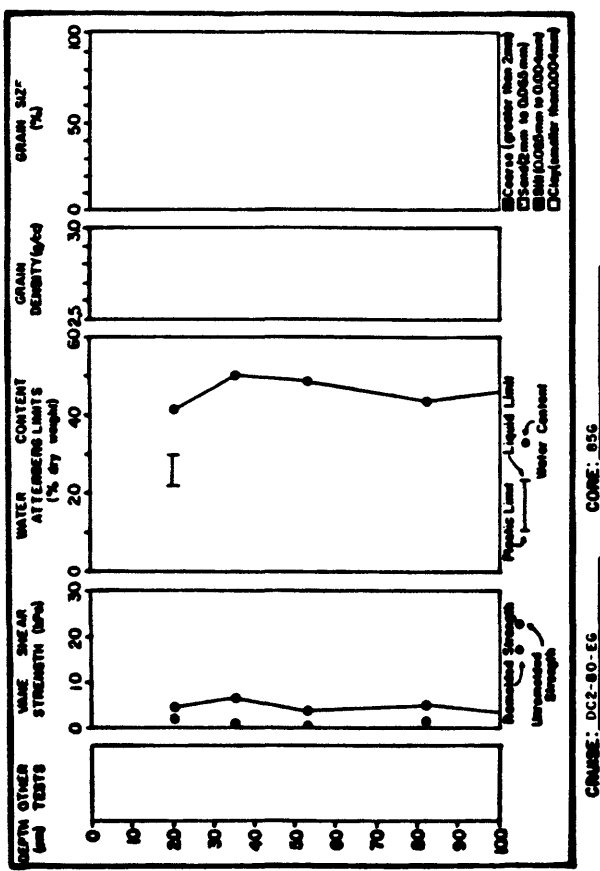
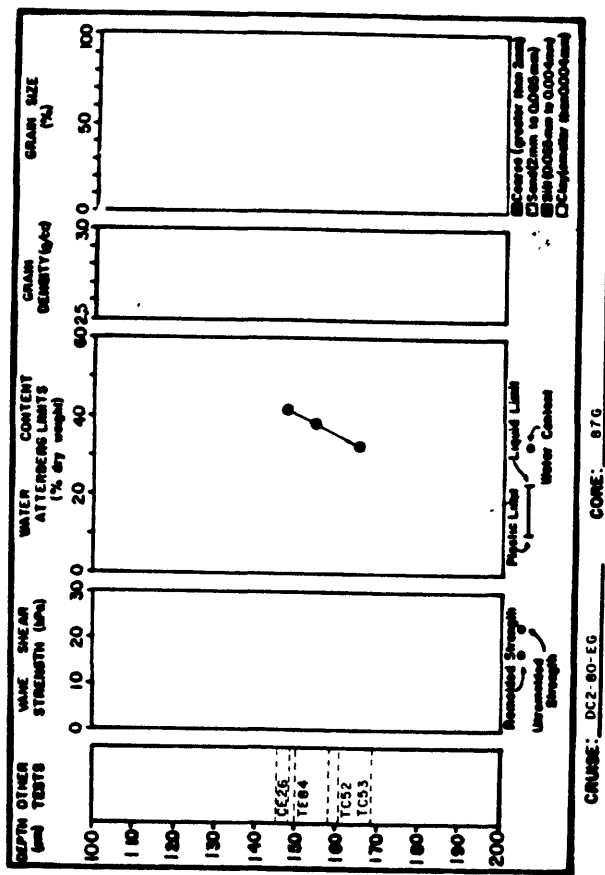


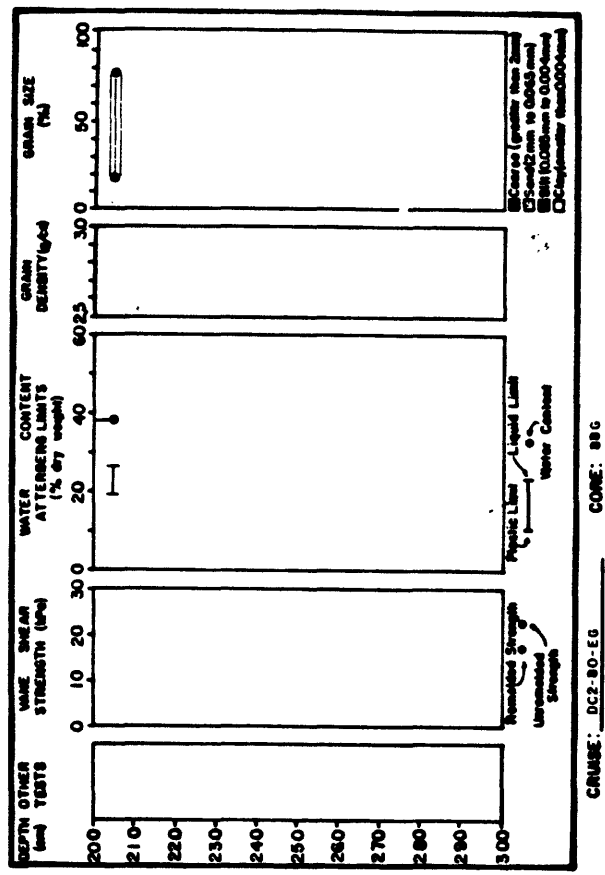
CRUISE: DC2-80-EG CORE: 666



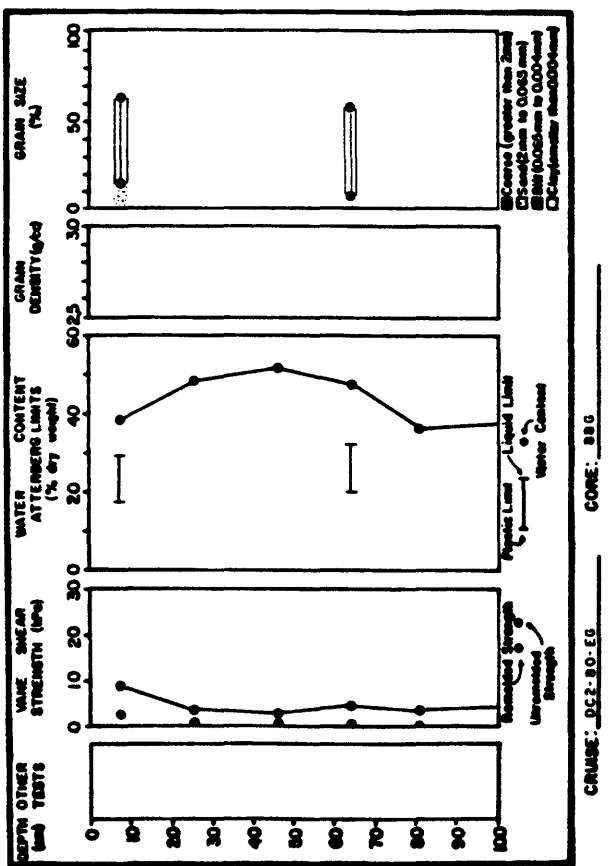




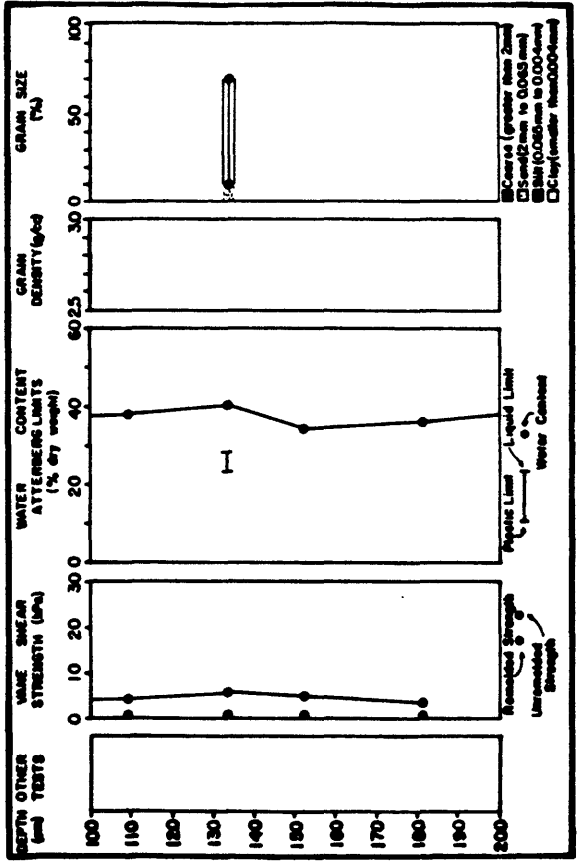




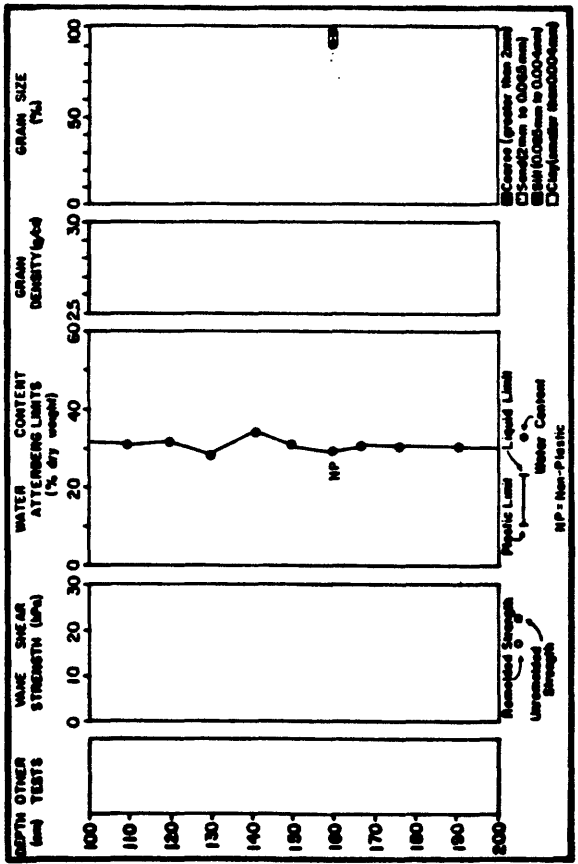
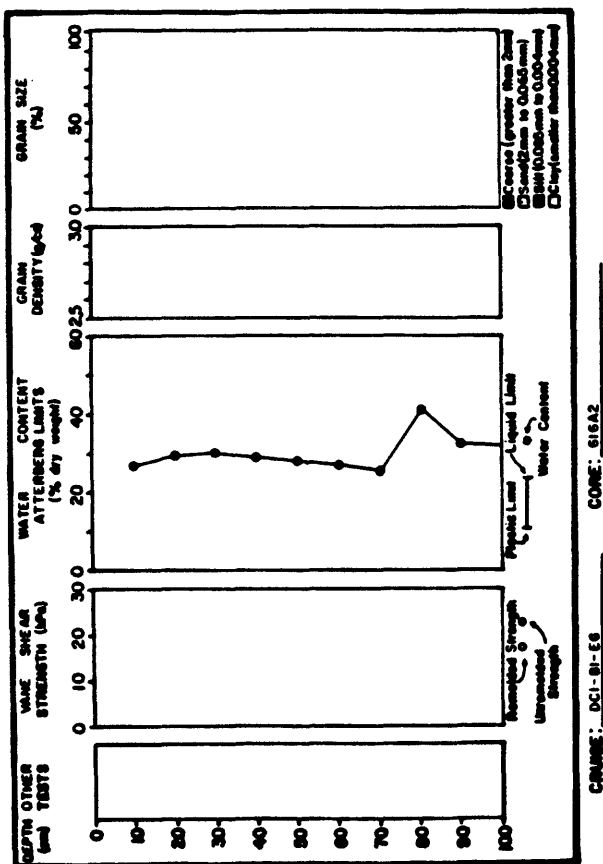
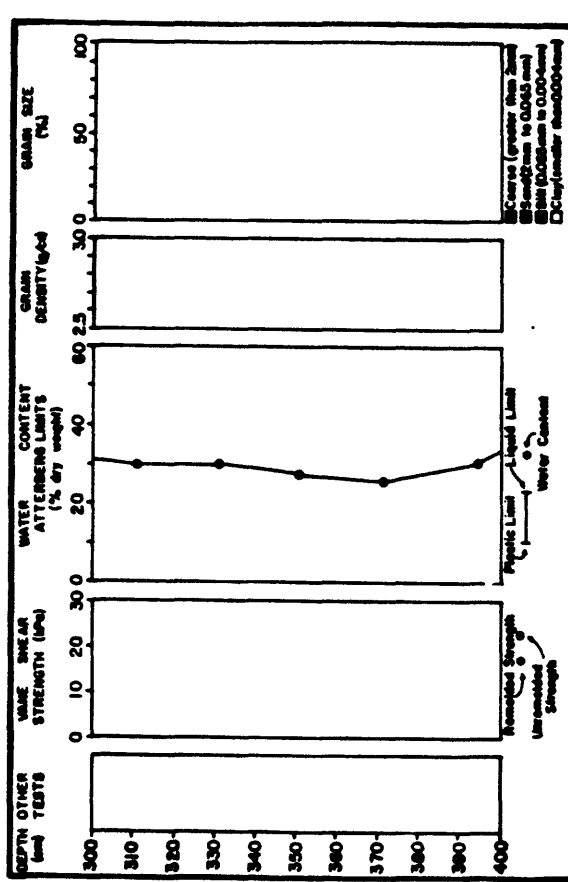
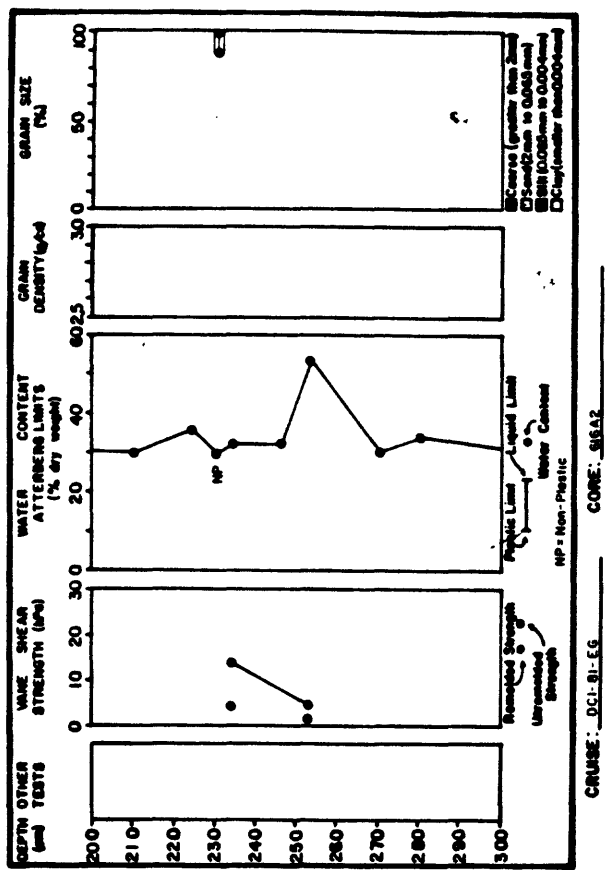
CORE: DC2-90-EG

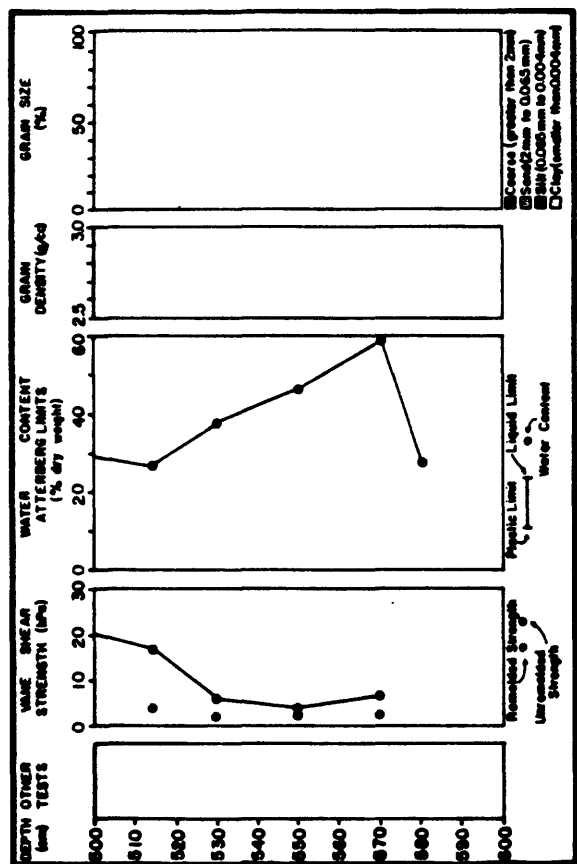
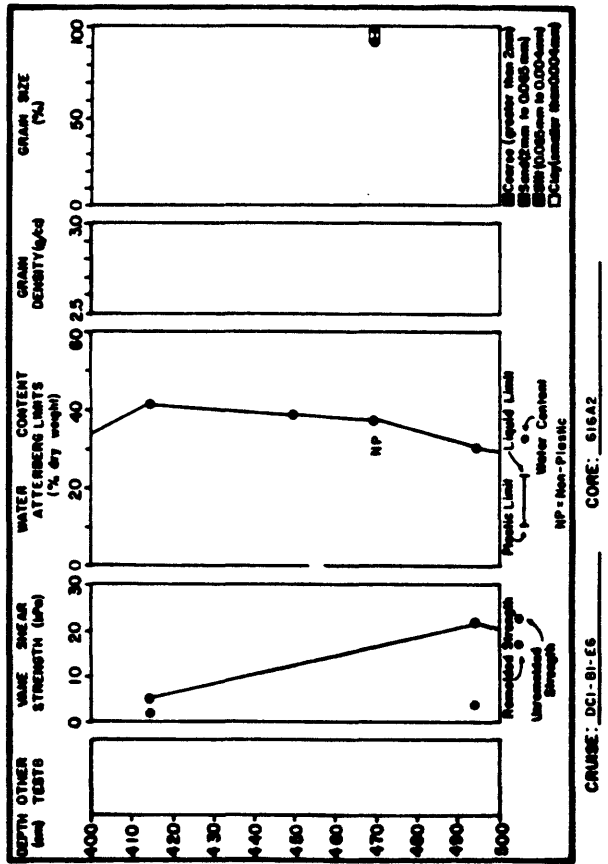
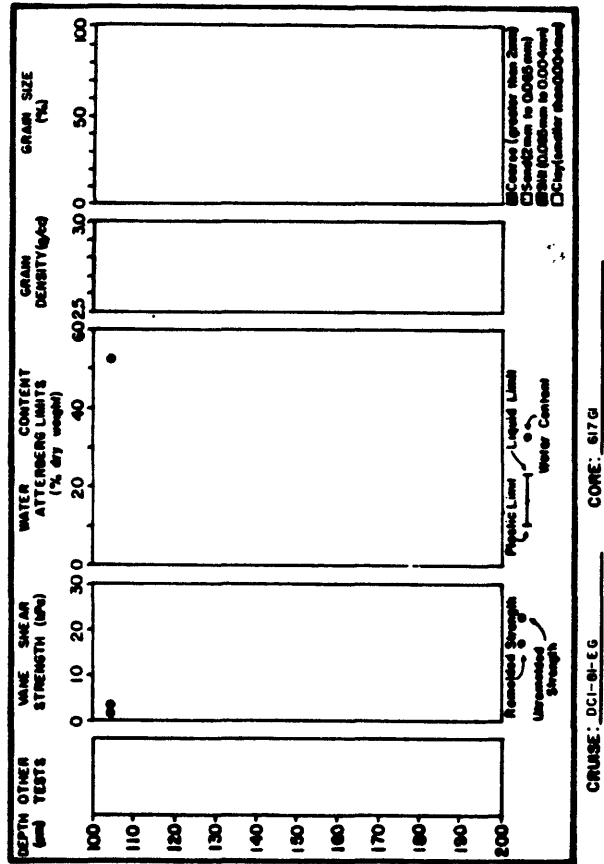


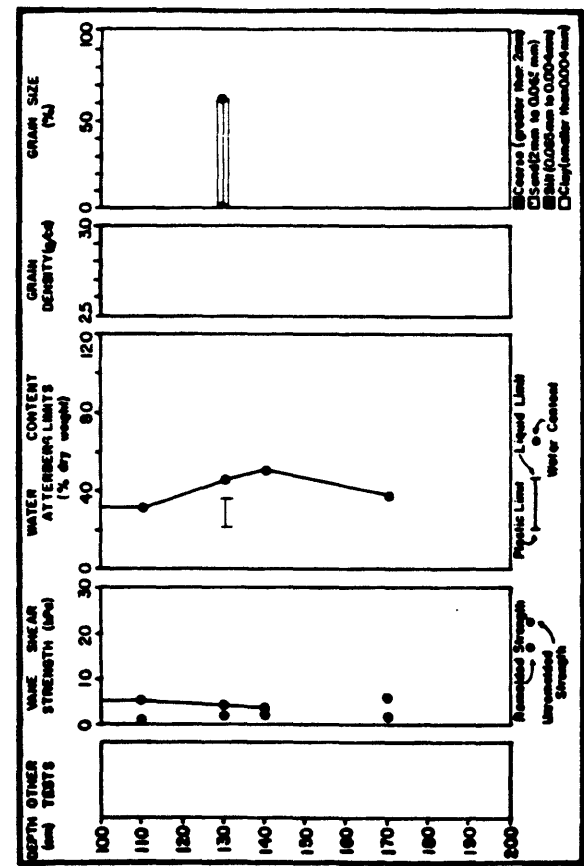
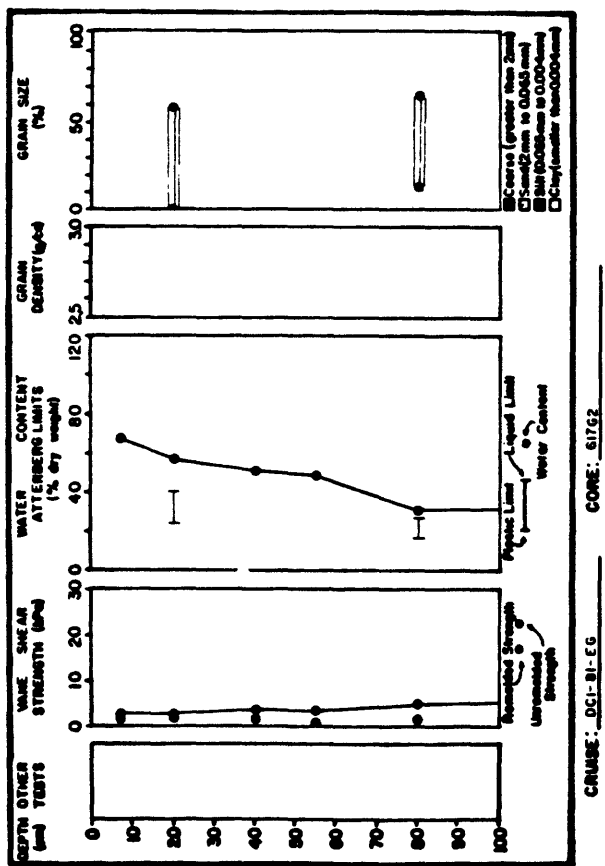
CORE: DC2-90-EG

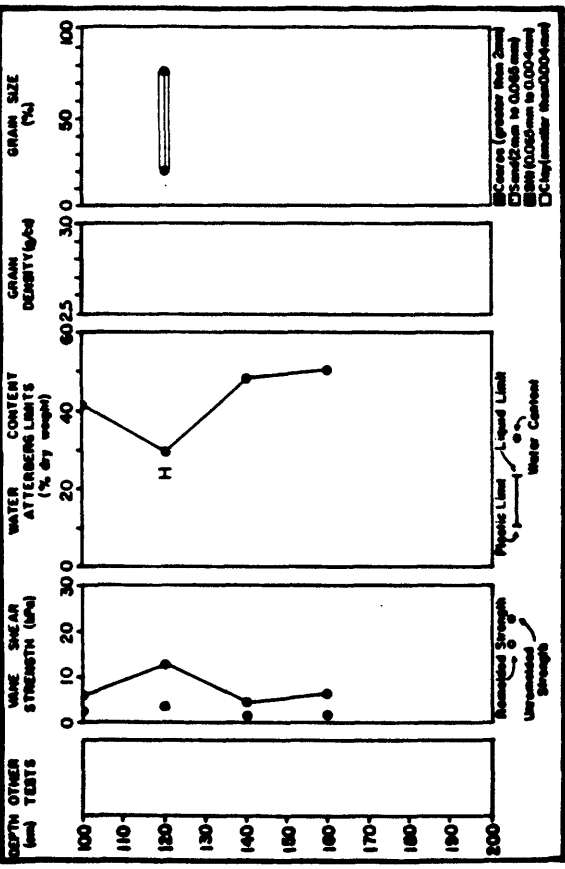
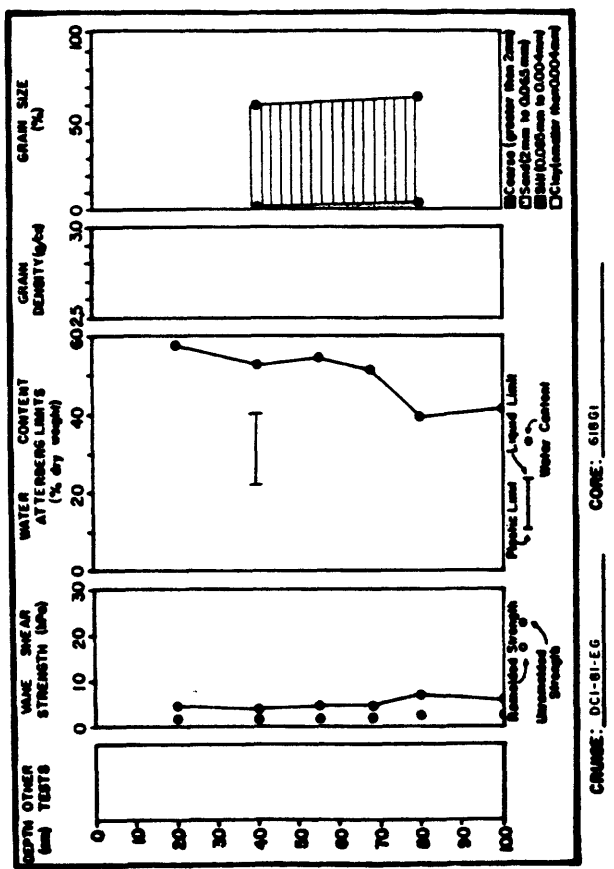
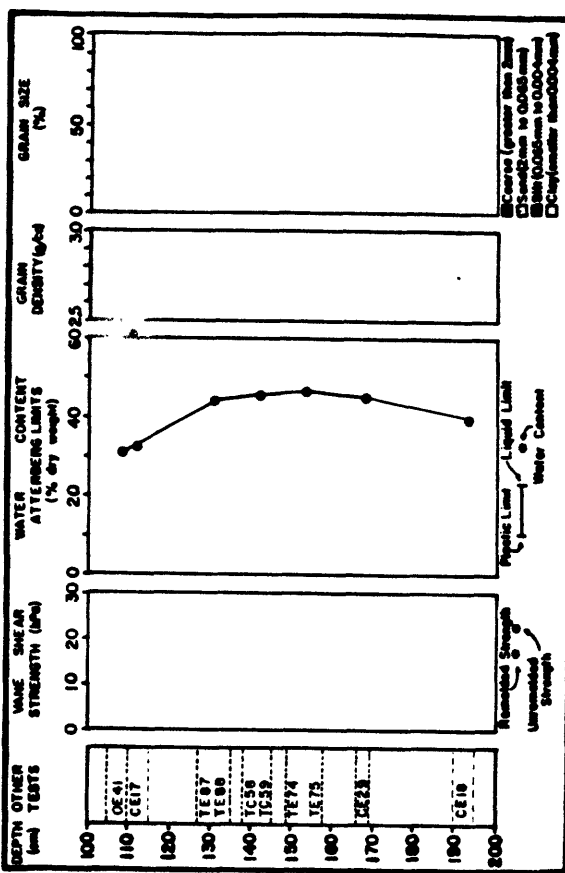
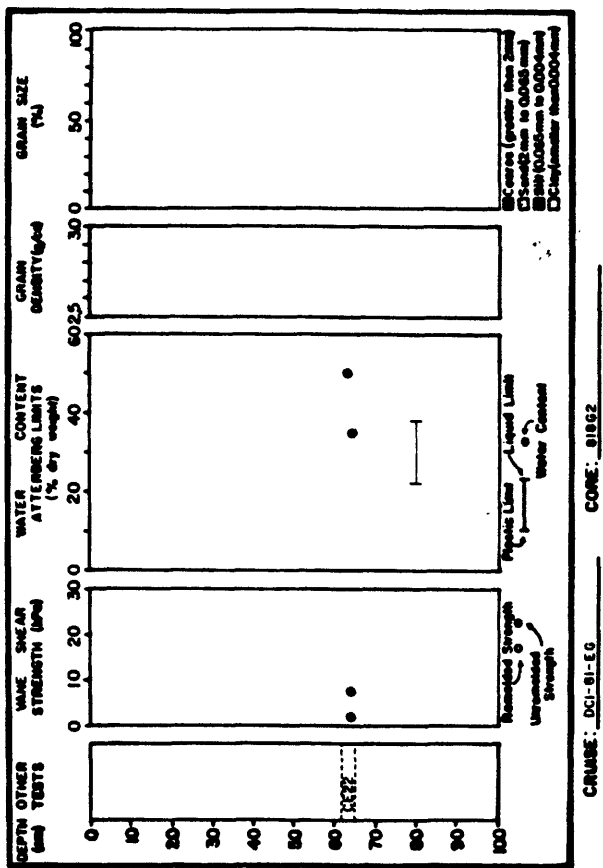


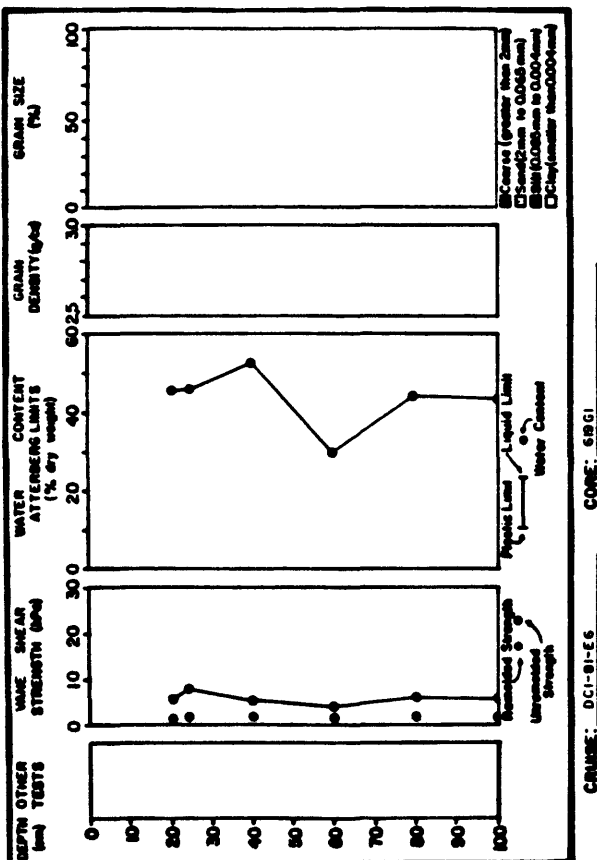
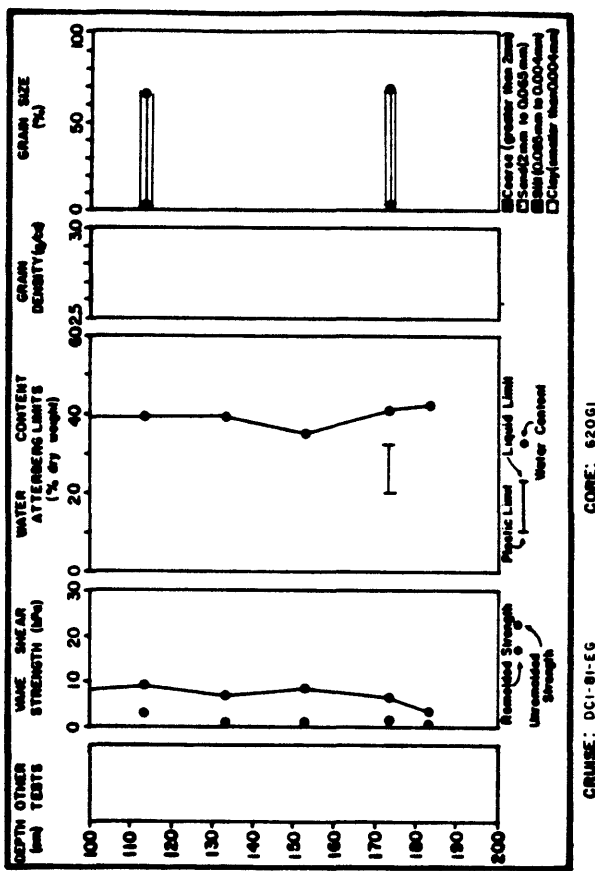
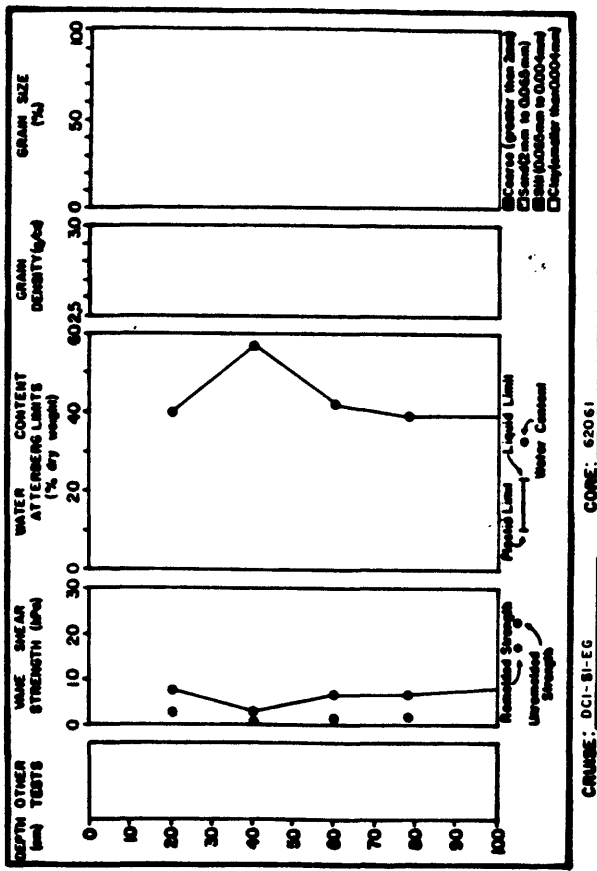
CORE: DC2-90-EG

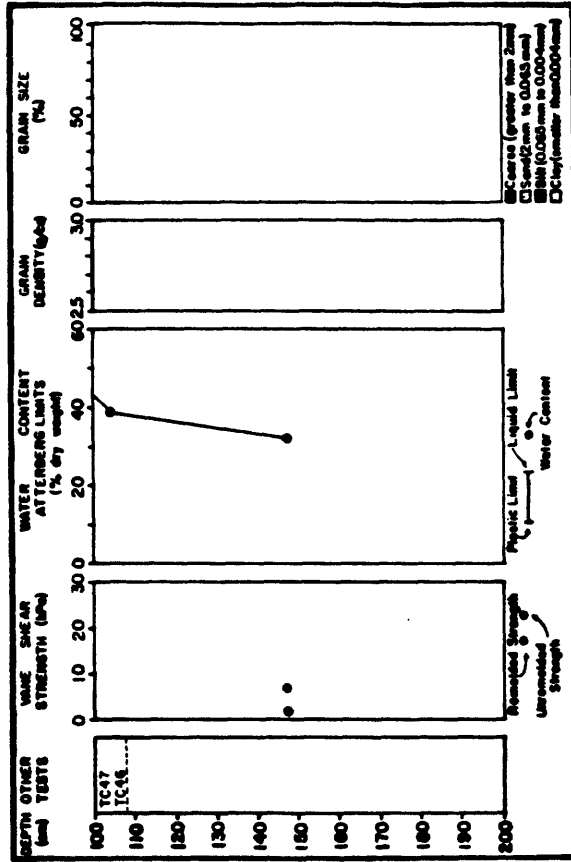
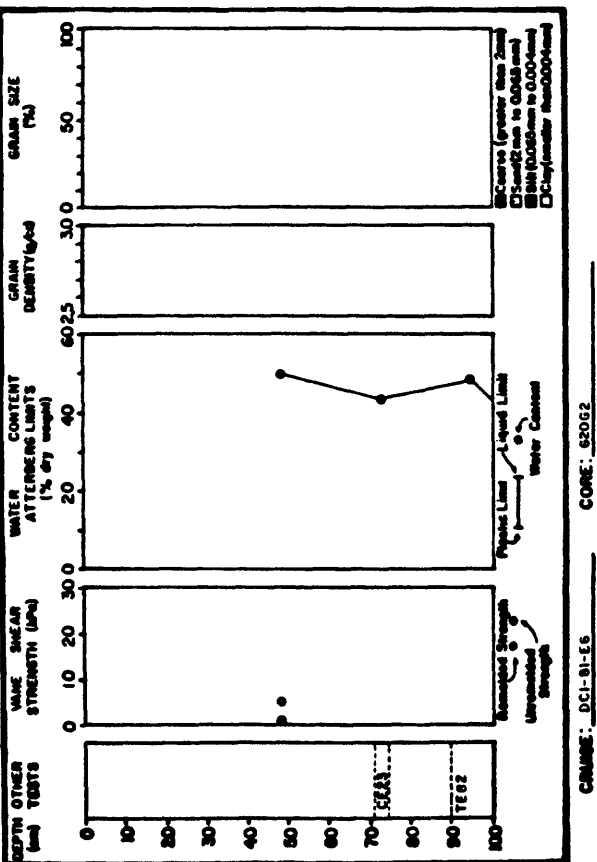
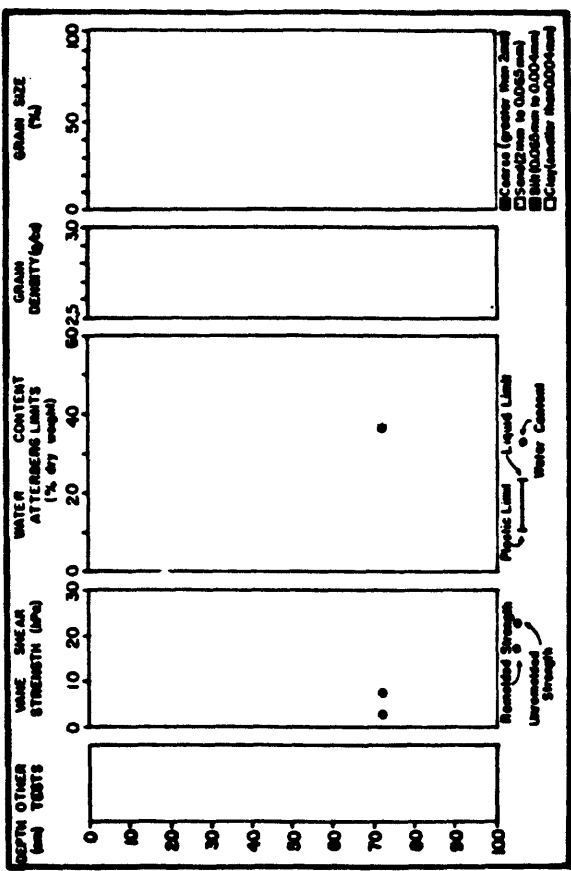
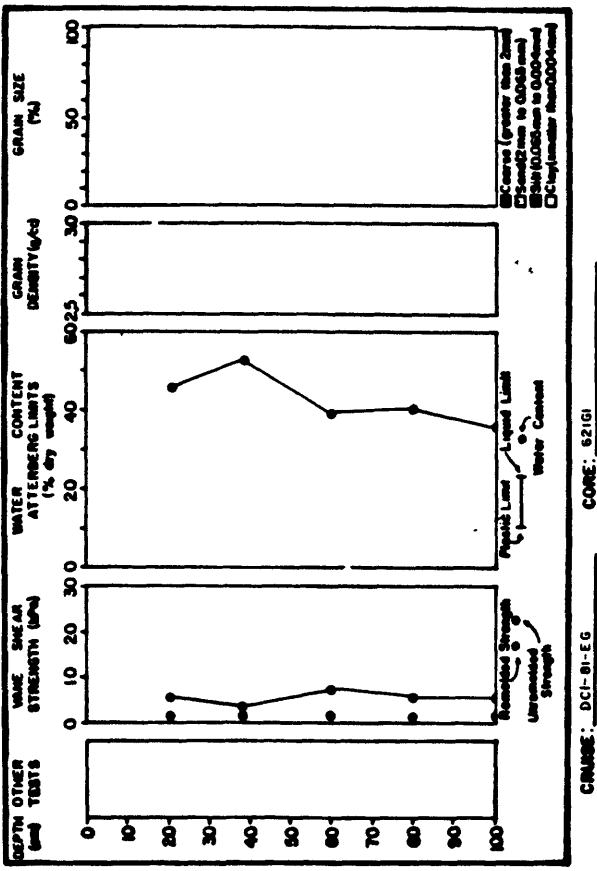


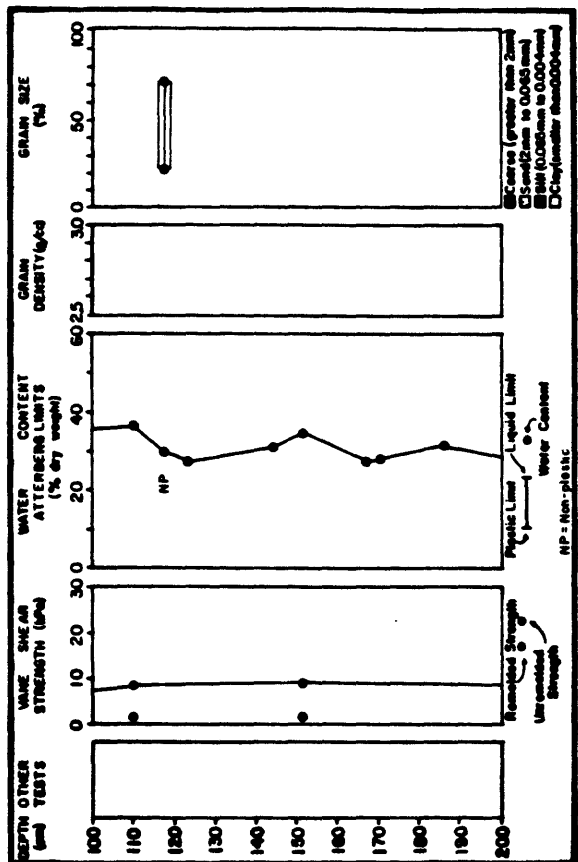
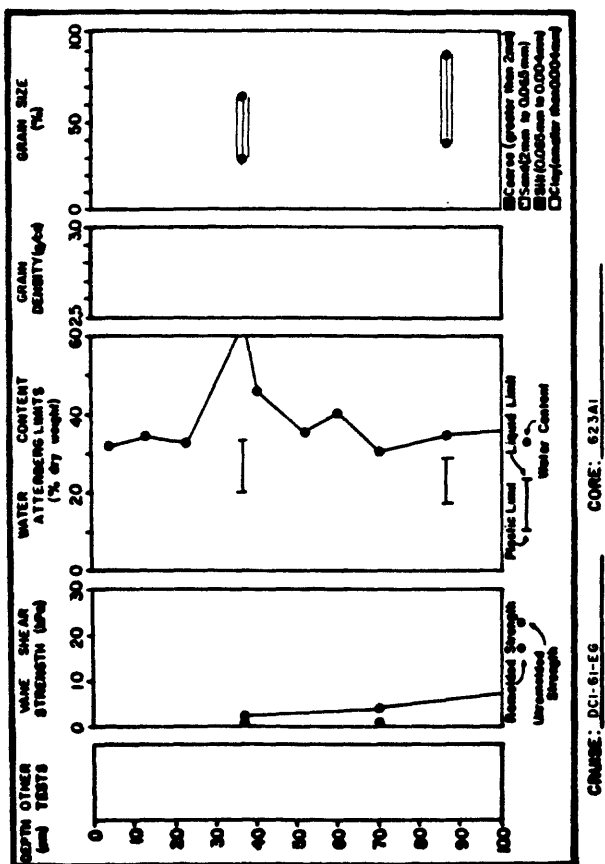
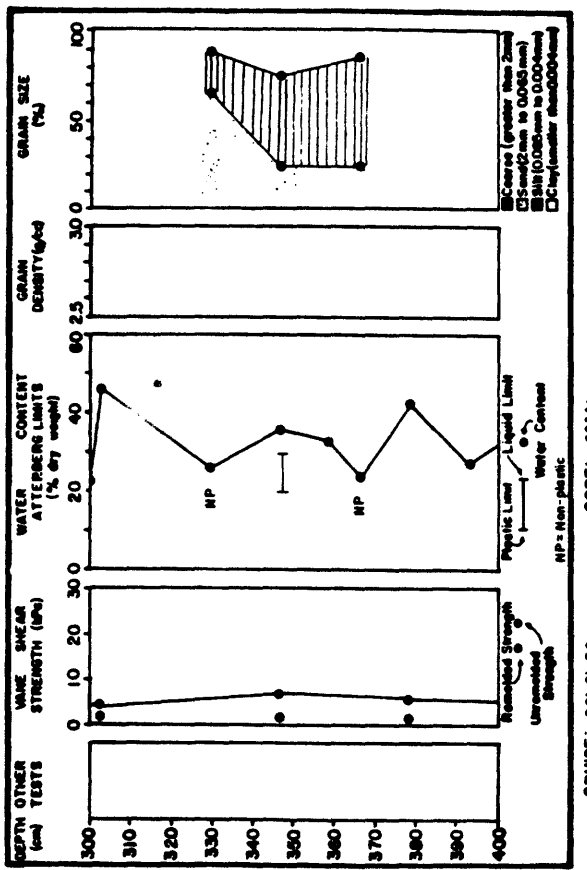
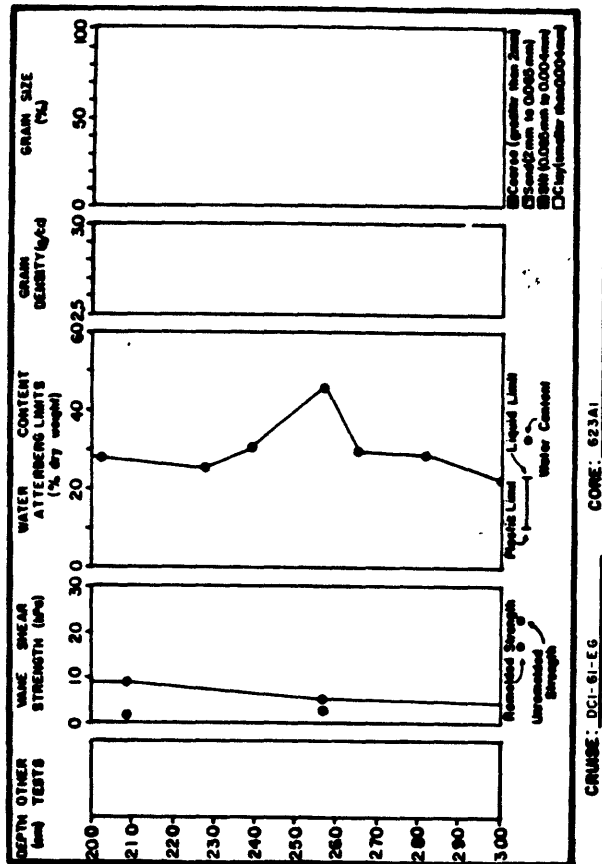


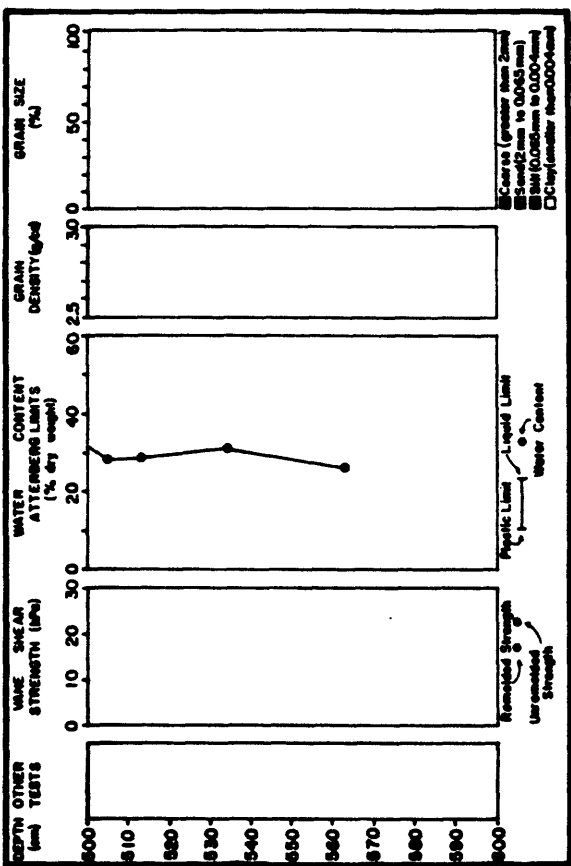
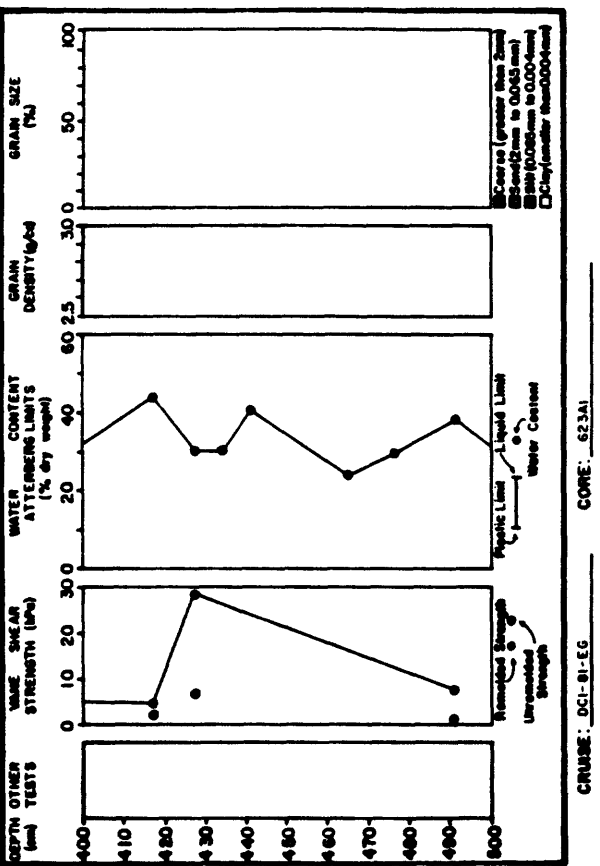
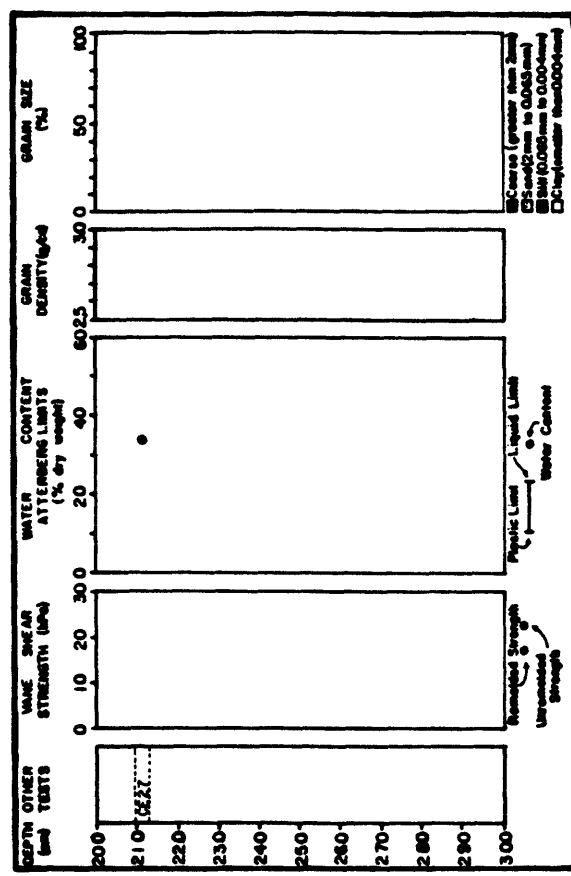
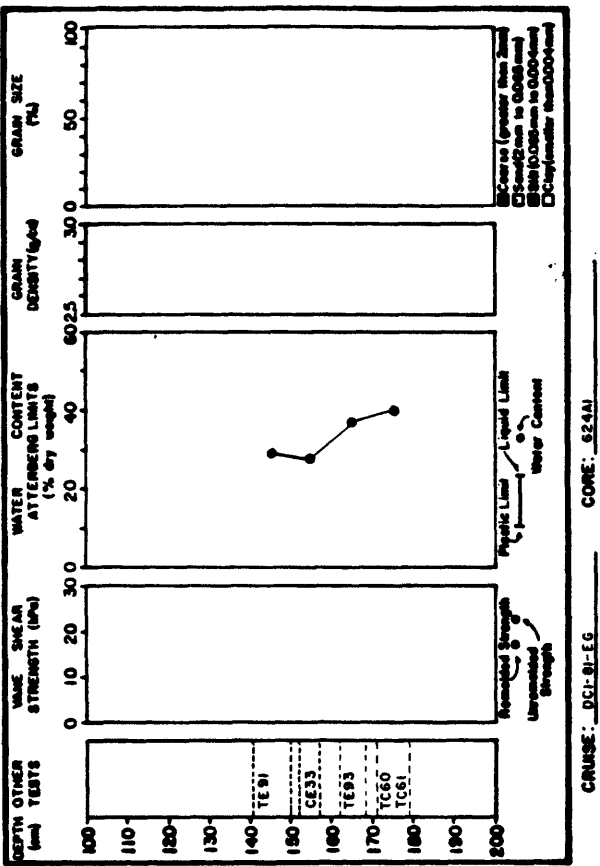


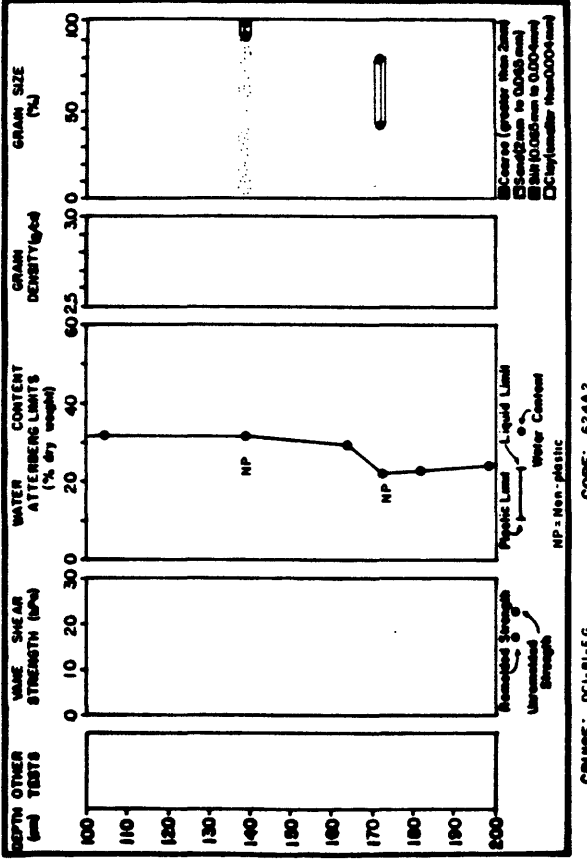
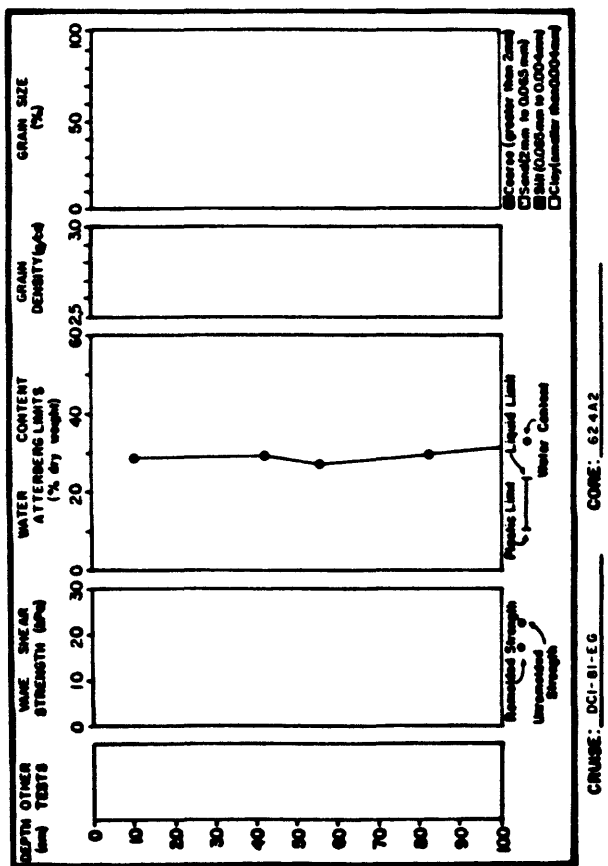
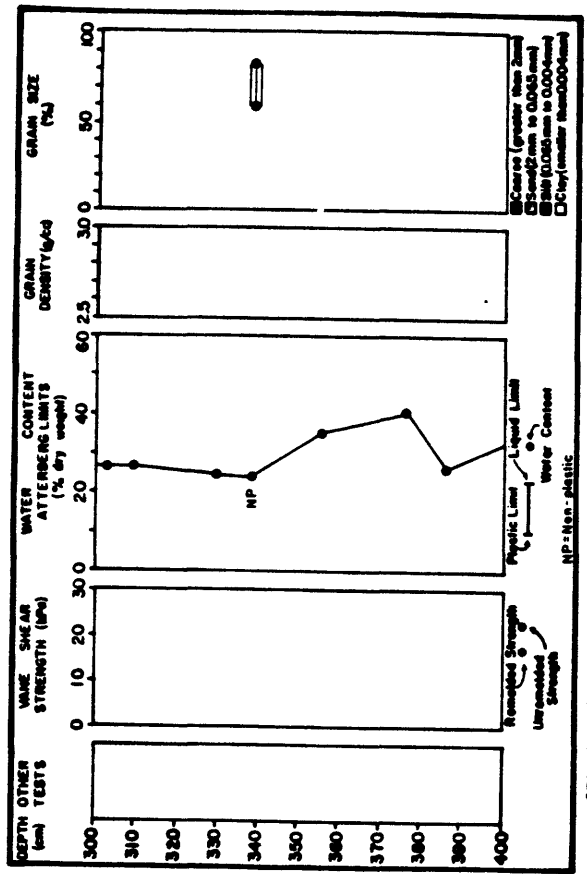
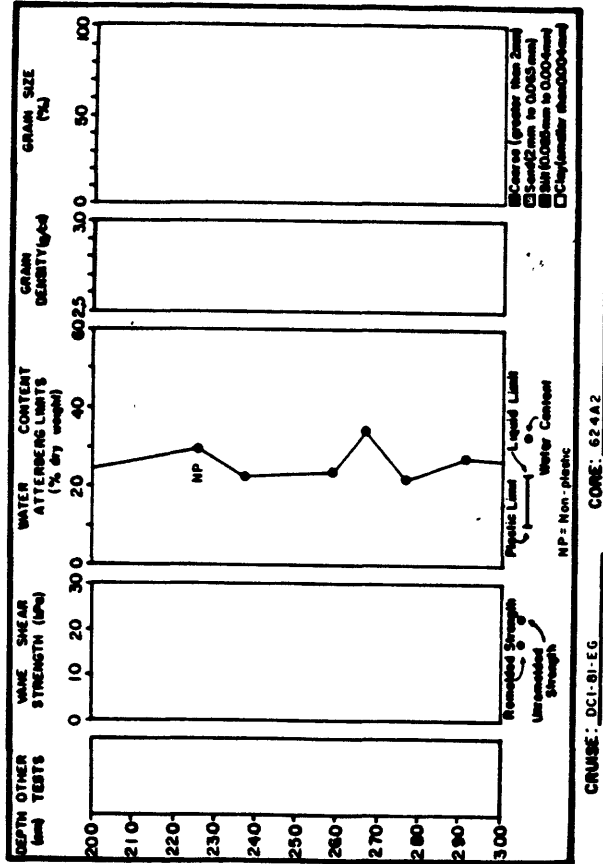


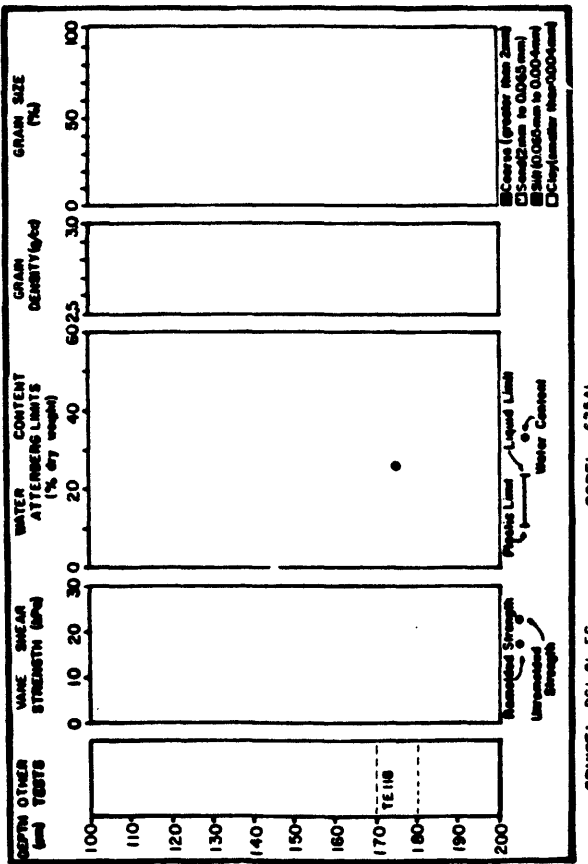
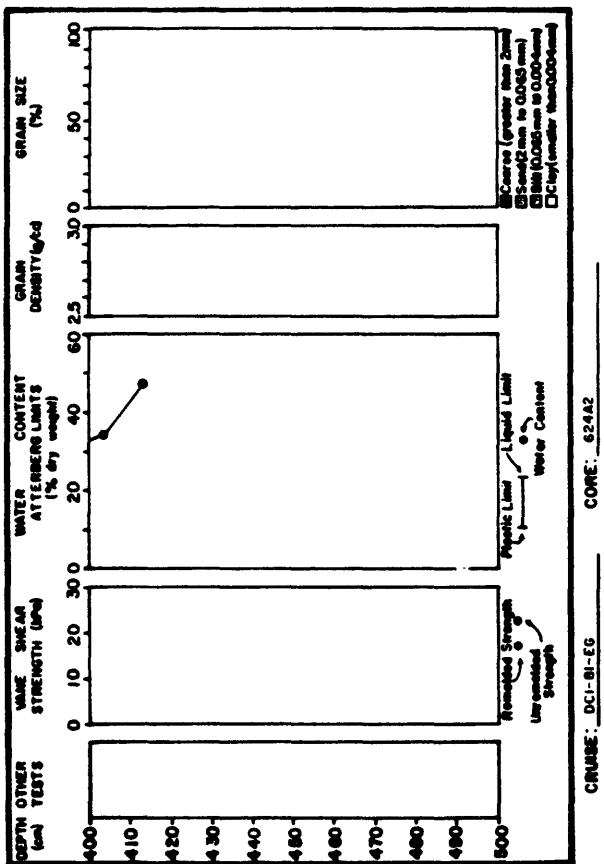
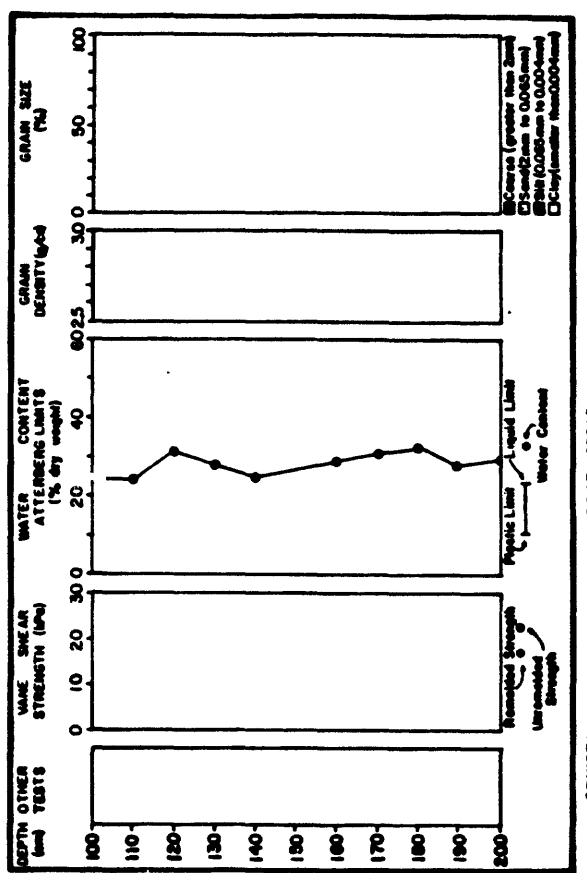
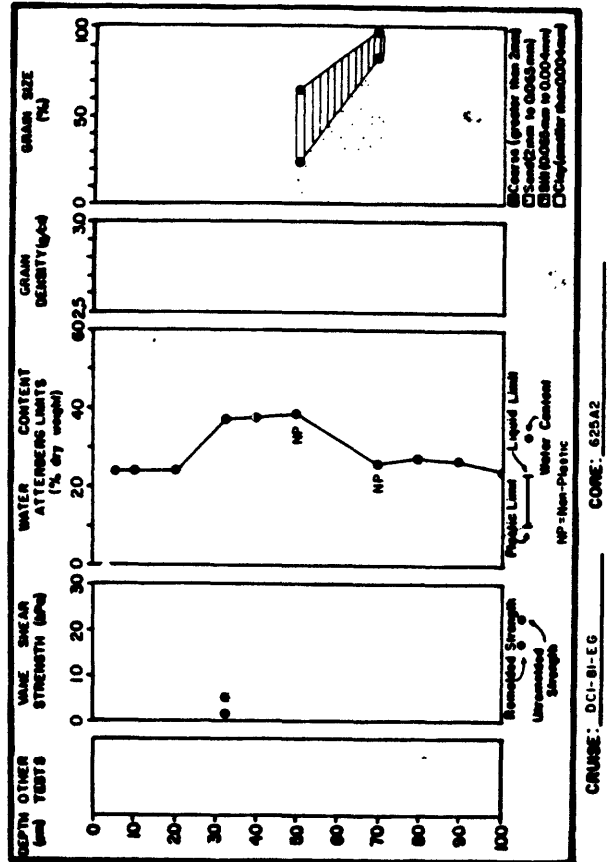


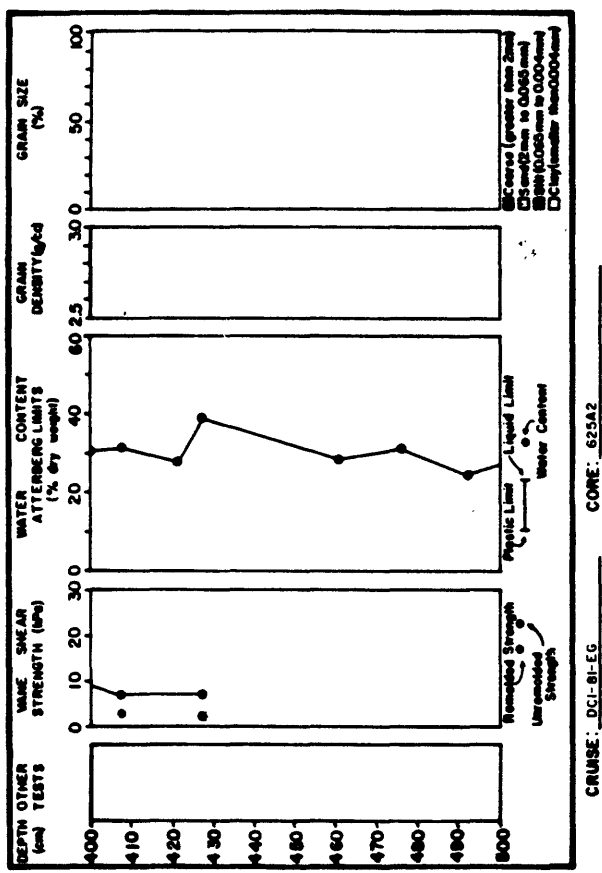




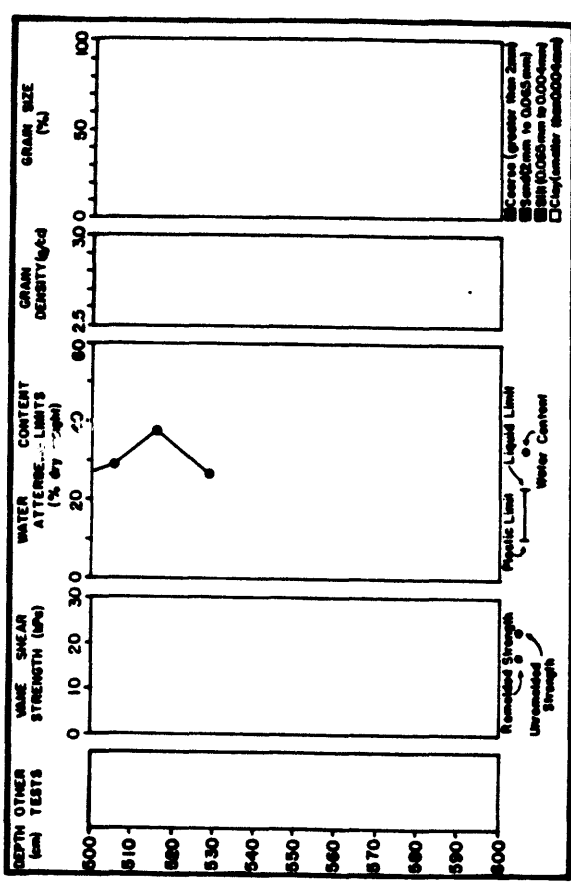




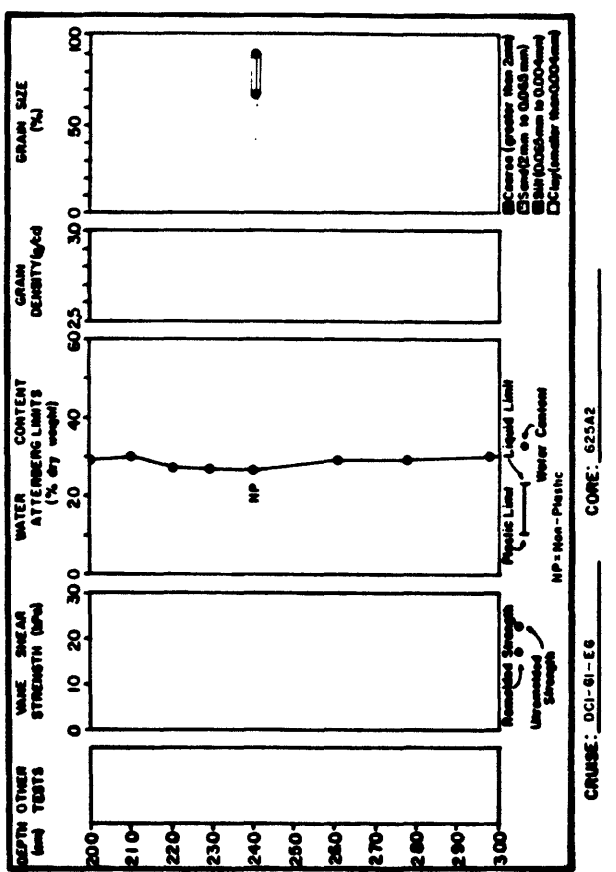




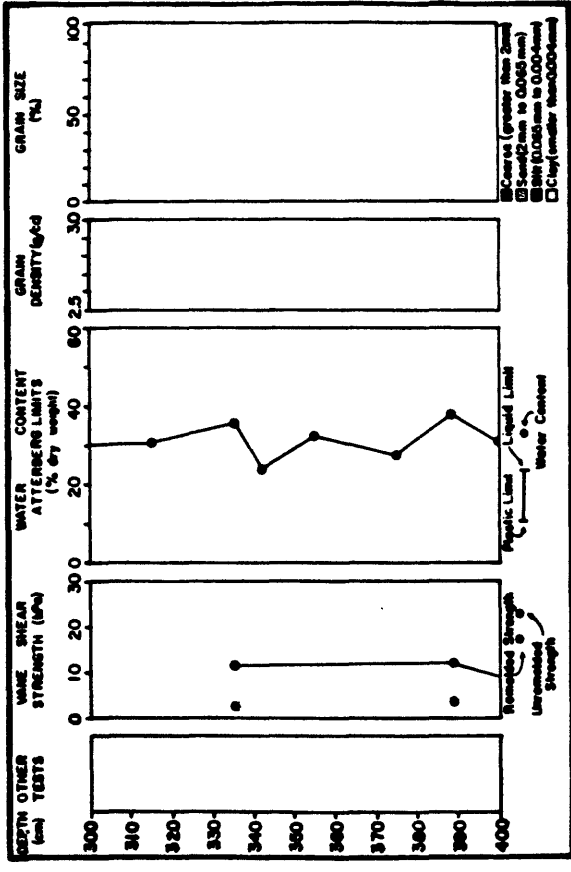
CRUISE: DCI-E-G CORE: 625A2



CRUISE: DCI-E-G CORE: 625A2

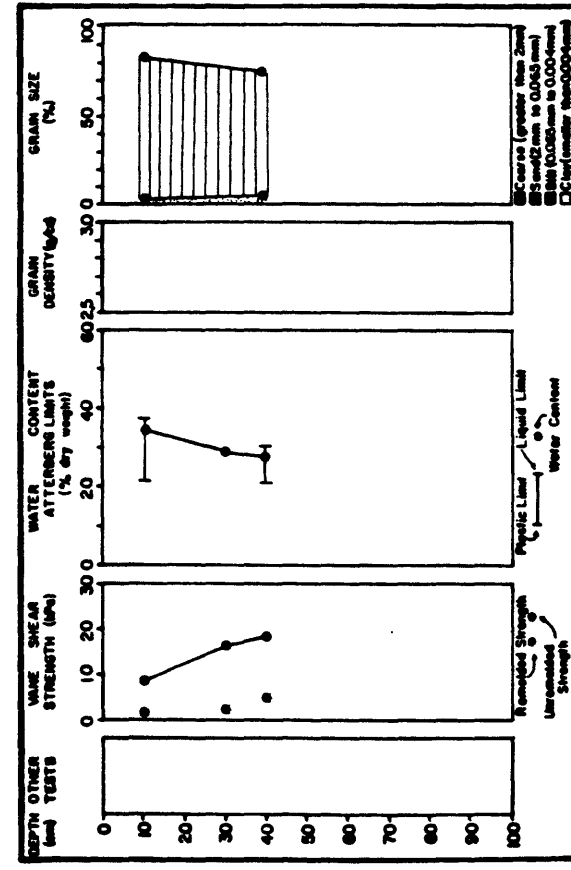
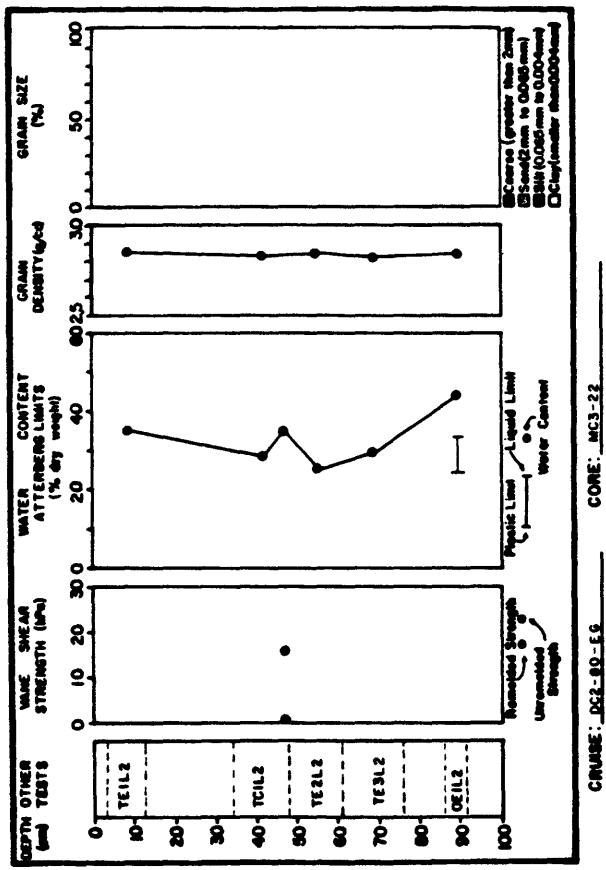
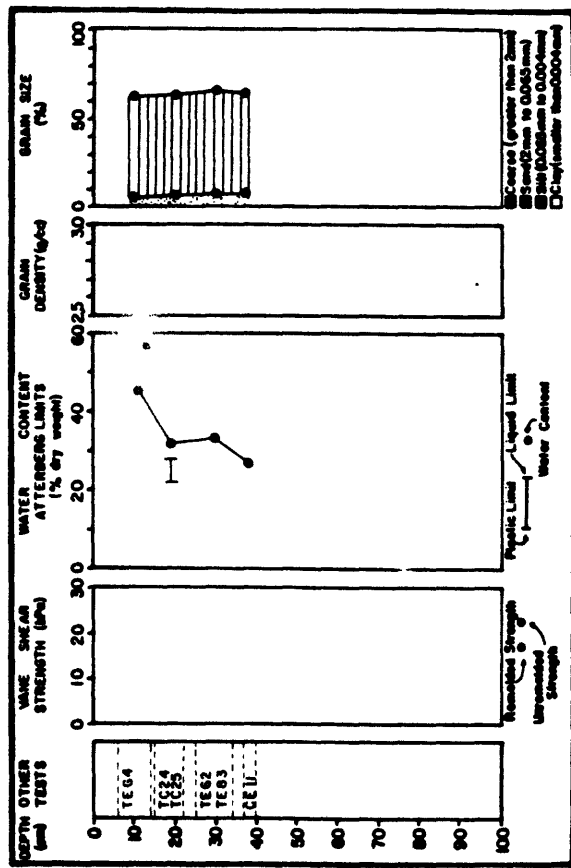
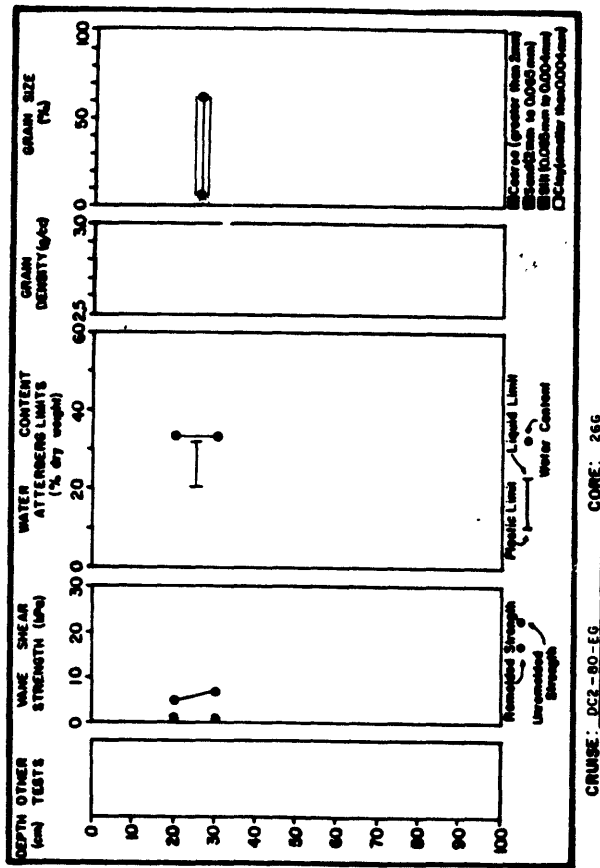


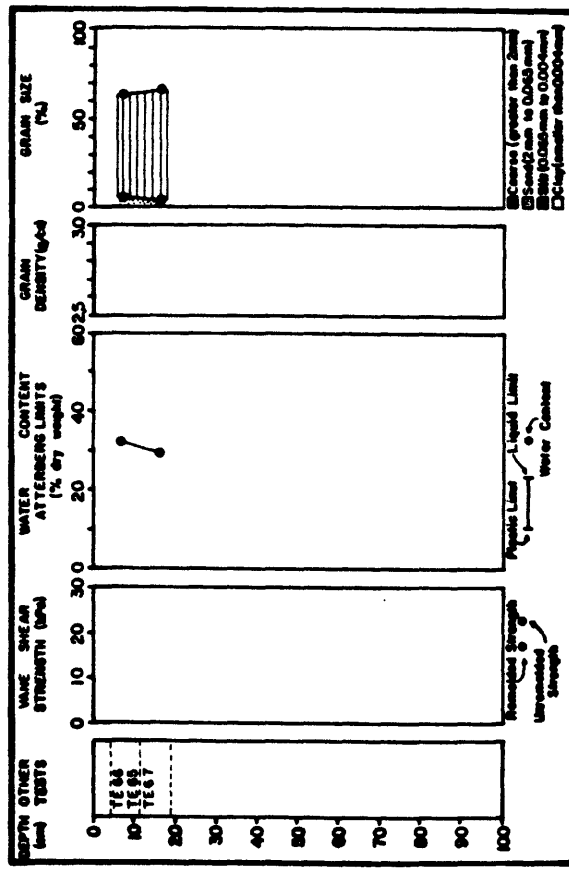
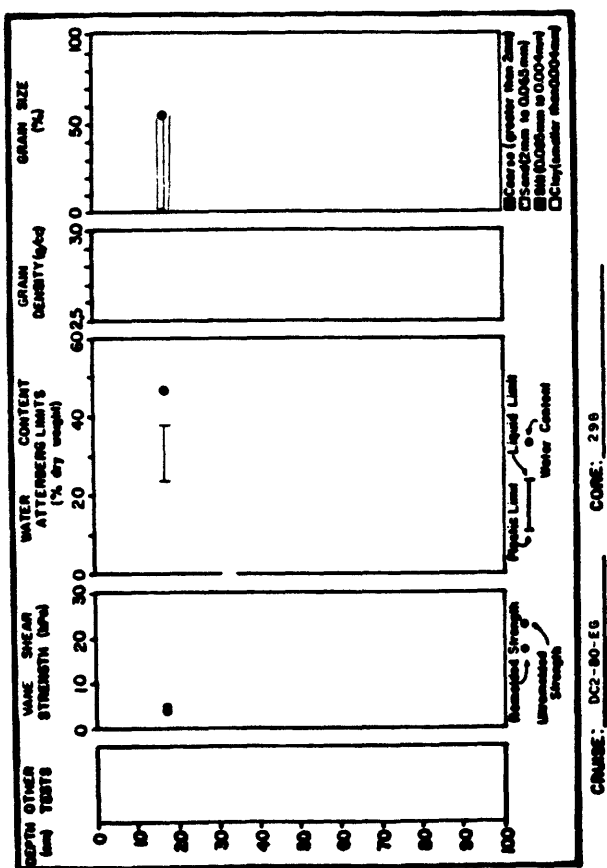
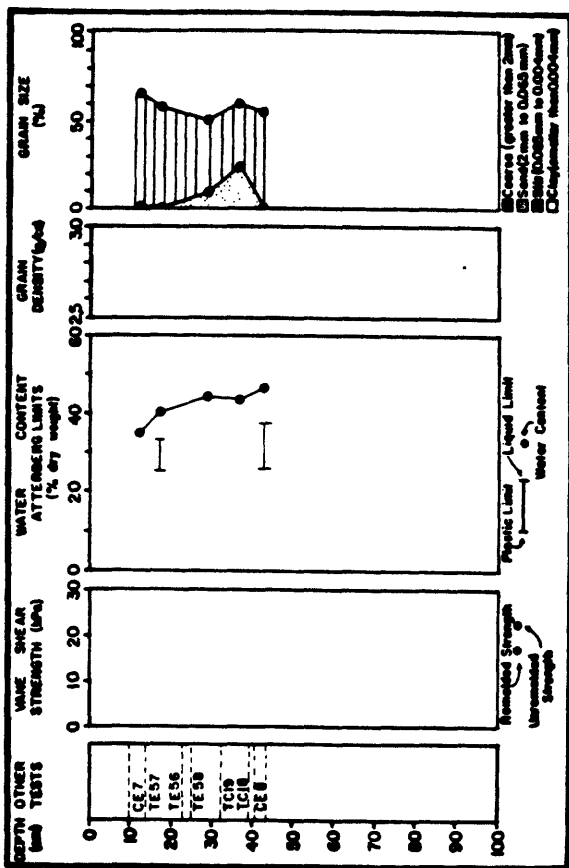
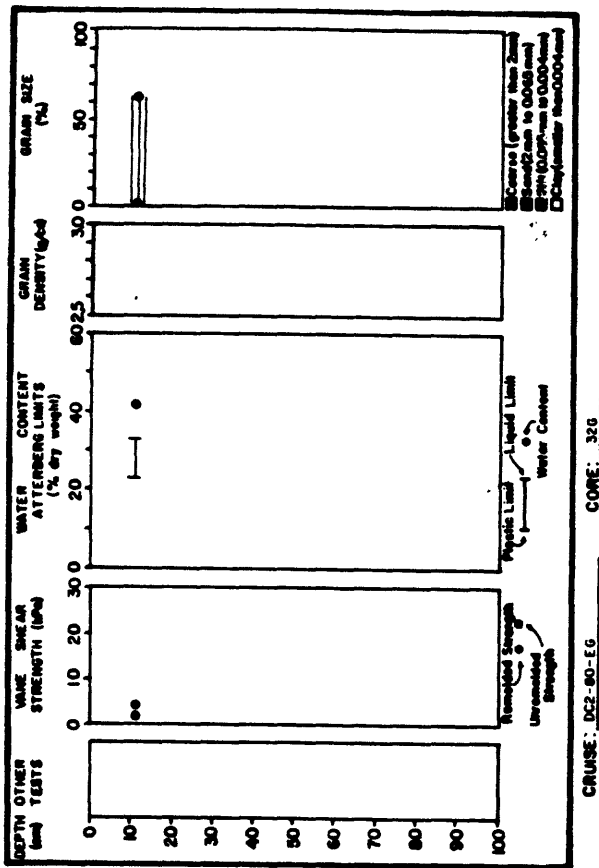
CRUISE: DCI-E-G CORE: 625A2

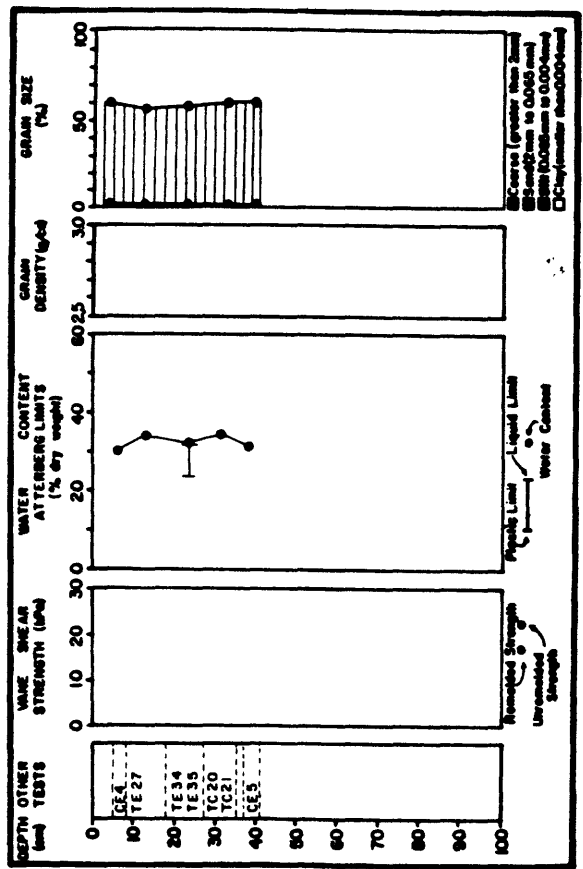


CRUISE: DCI-E-G CORE: 625A2

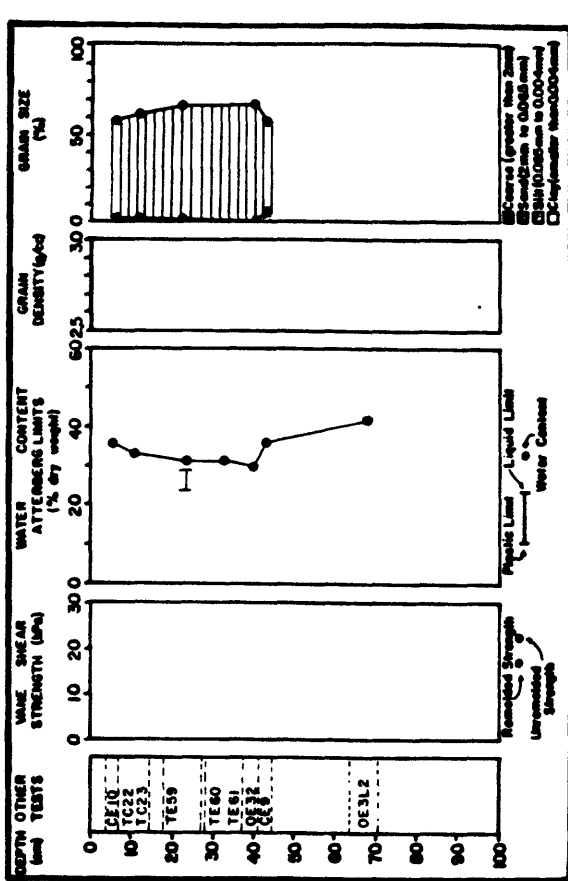
**ALSEK RIVER STUDY AREA**



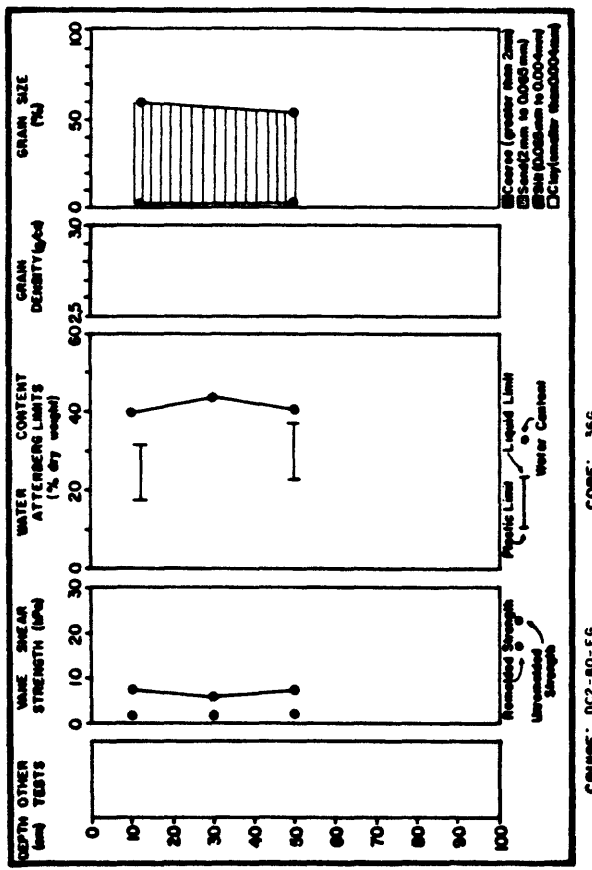




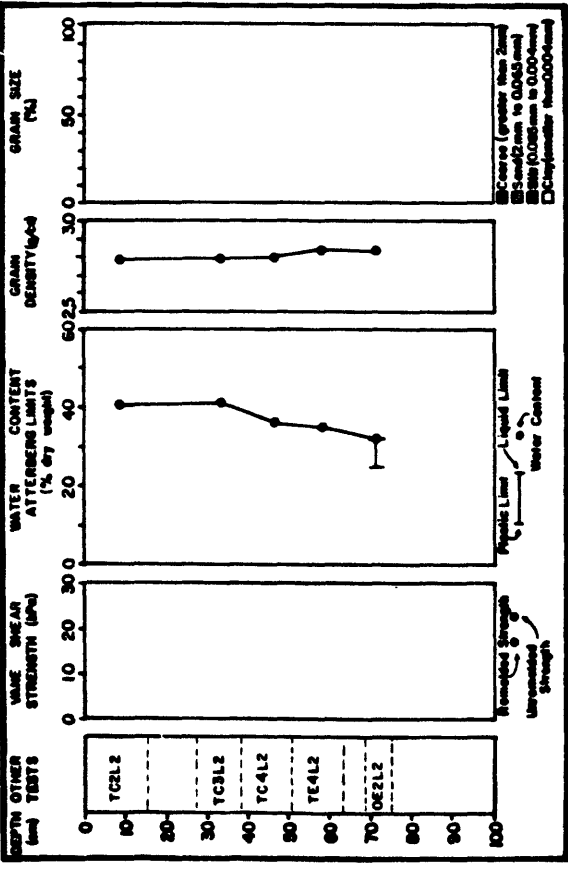
CRUISE: DC2-80-EG    CORE: 436



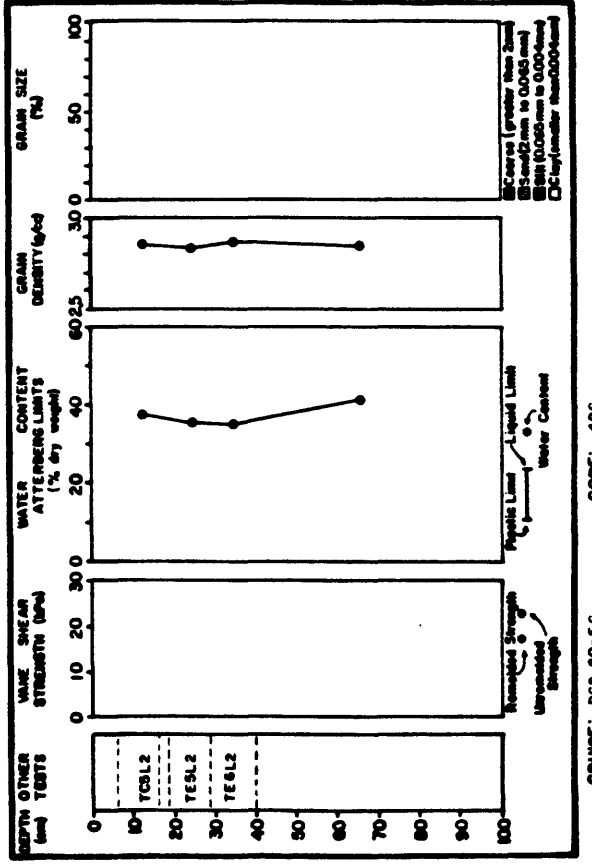
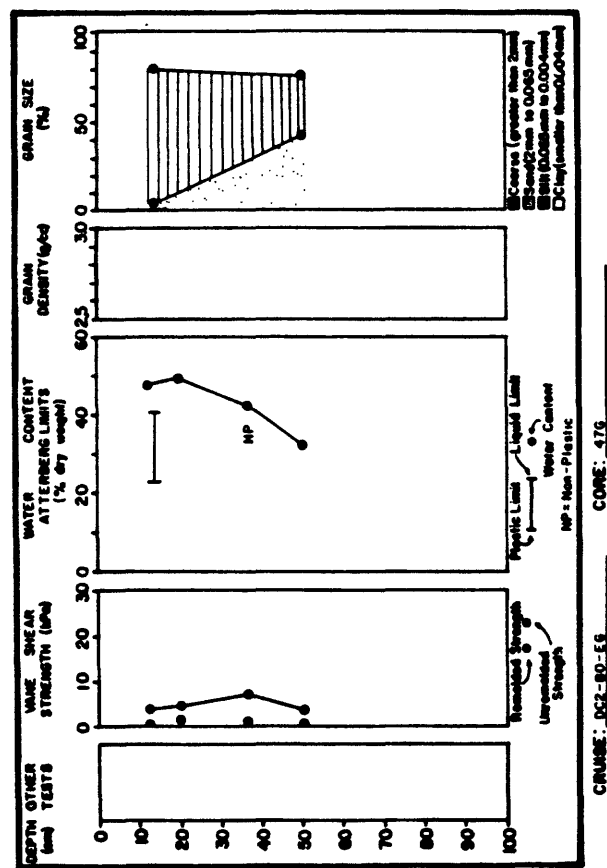
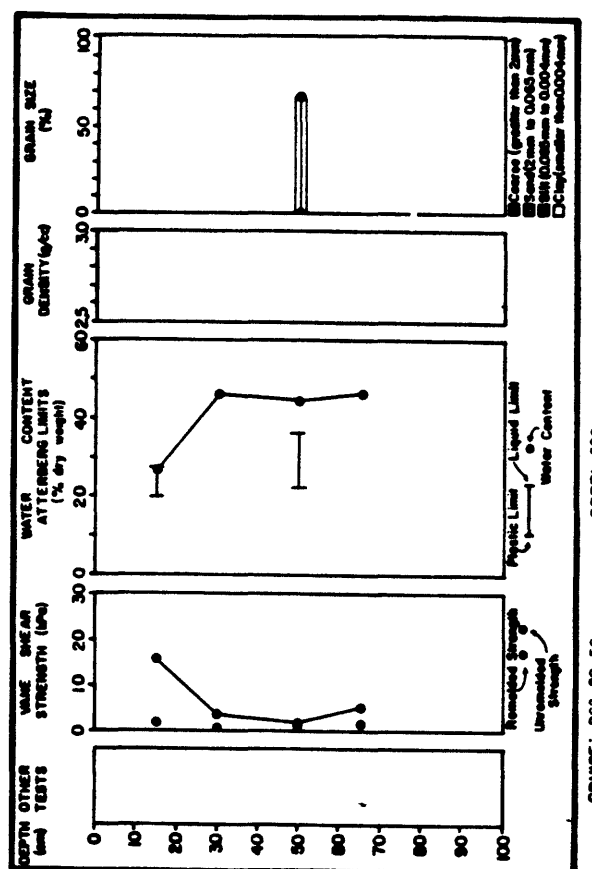
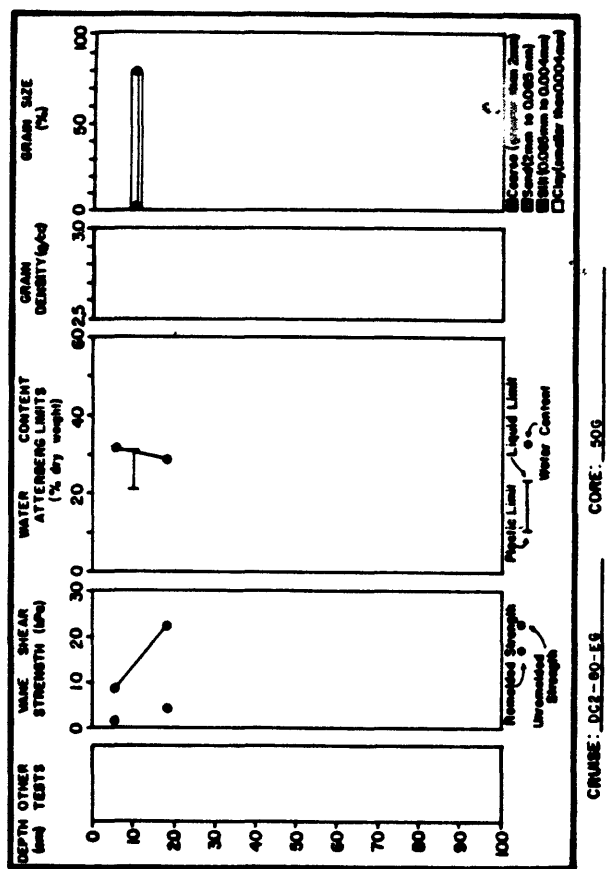
CRUISE: DC2-80-EG    CORE: 436

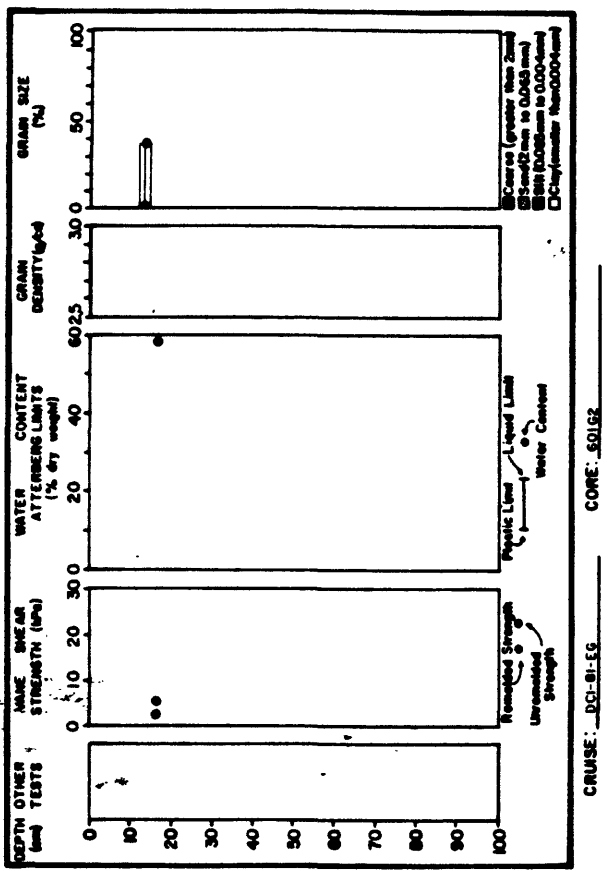


CRUISE: DC2-80-EG    CORE: 366

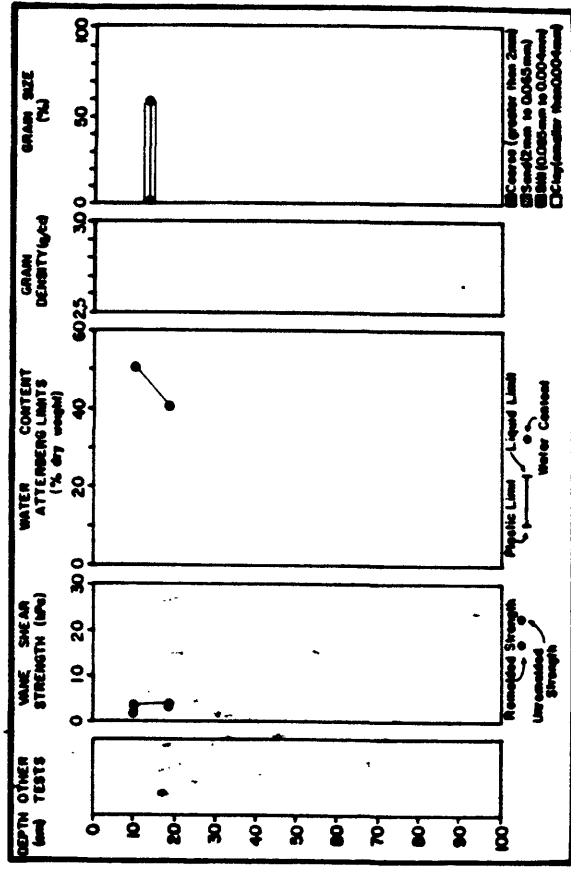


CRUISE: DC2-80-EG    CORE: 366

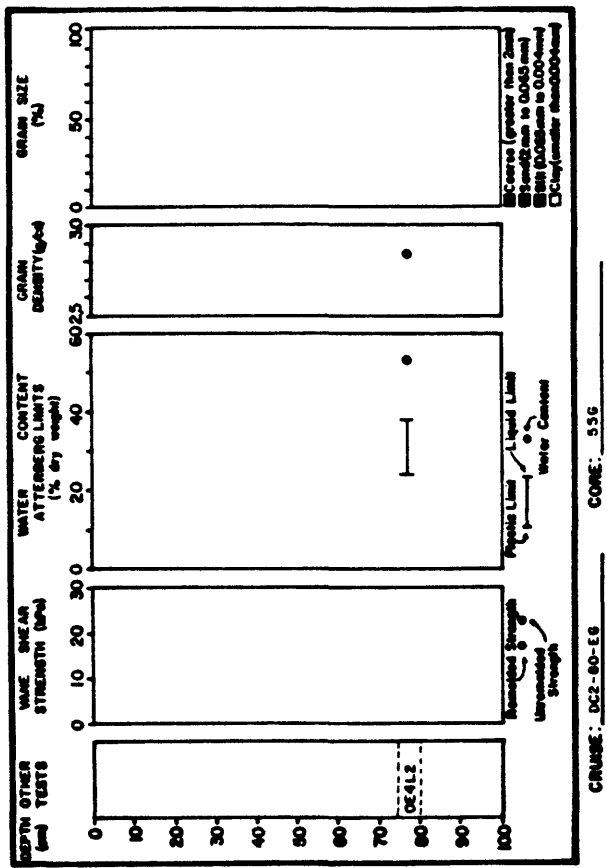




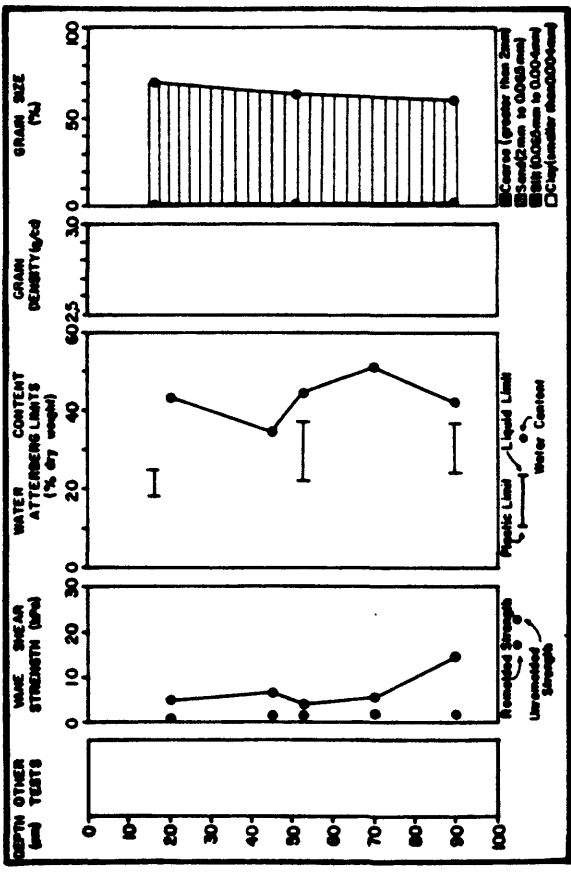
CRUISE: DCI-9-E6 CORE: 6025



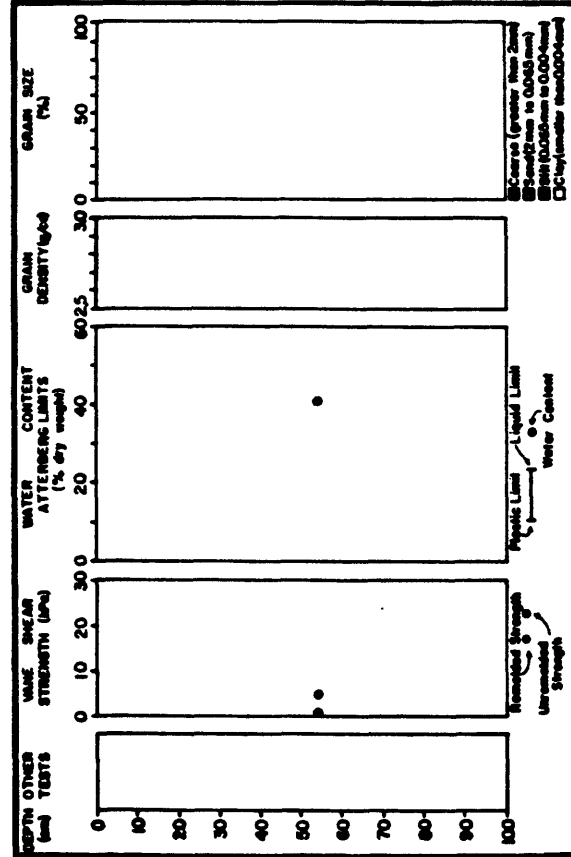
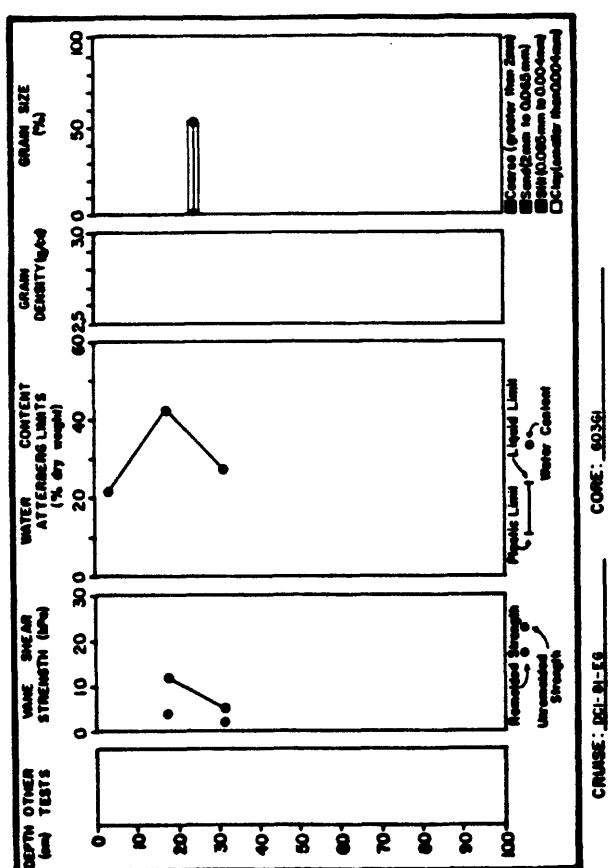
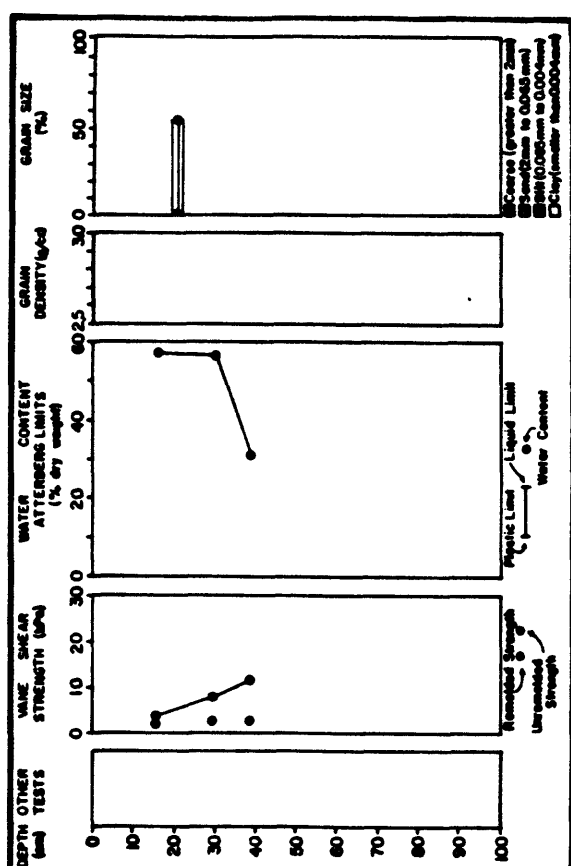
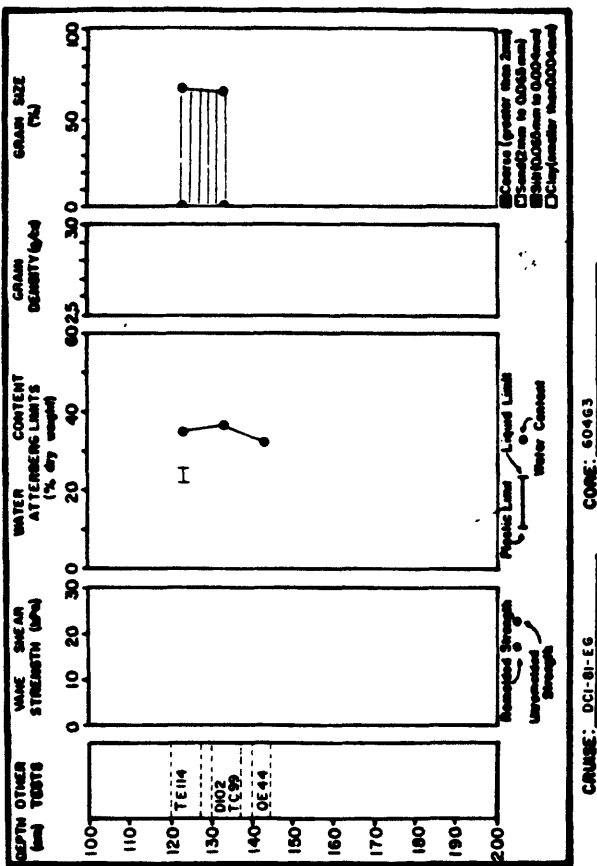
CRUISE: DCI-9-E6 CORE: 6025

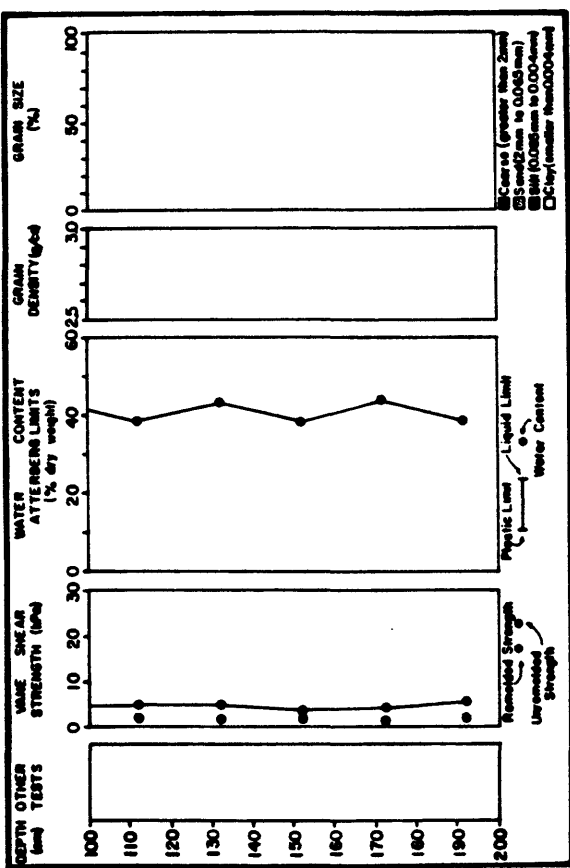
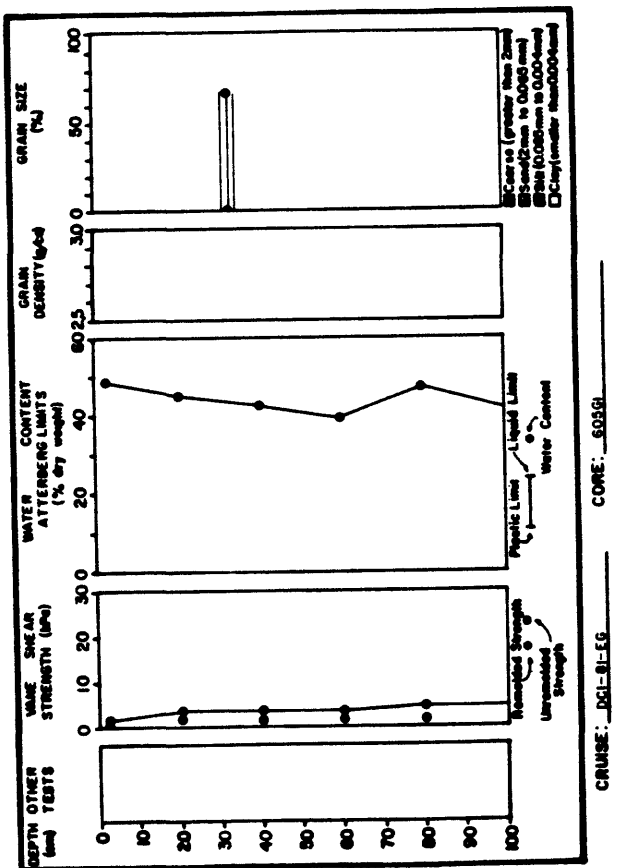
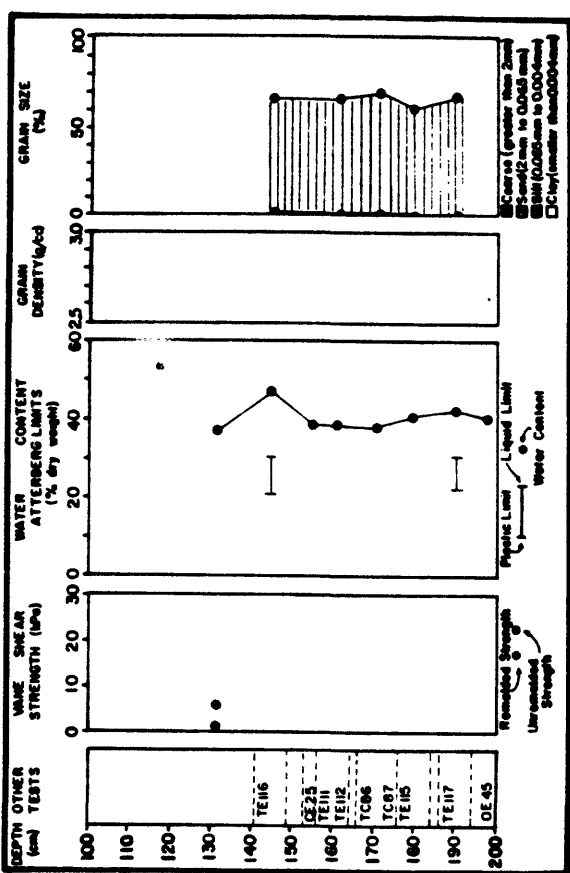
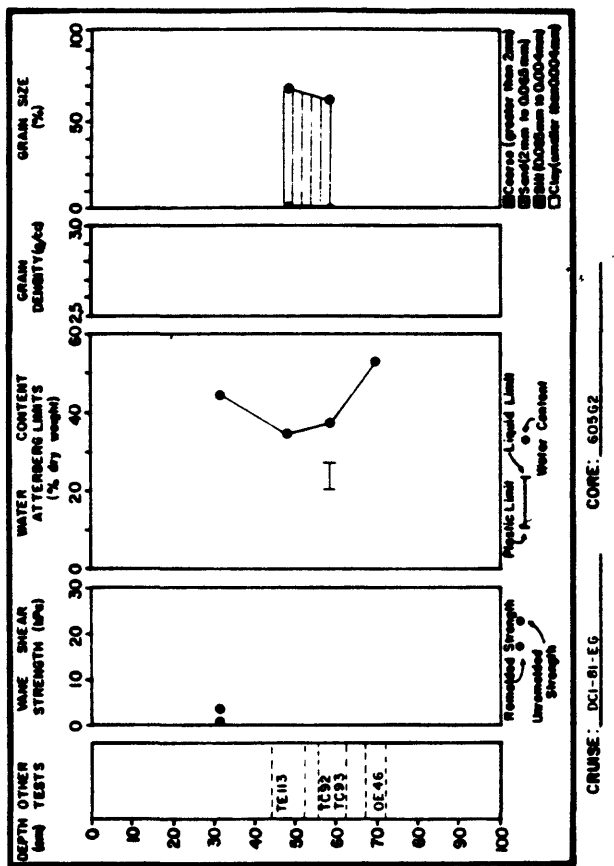


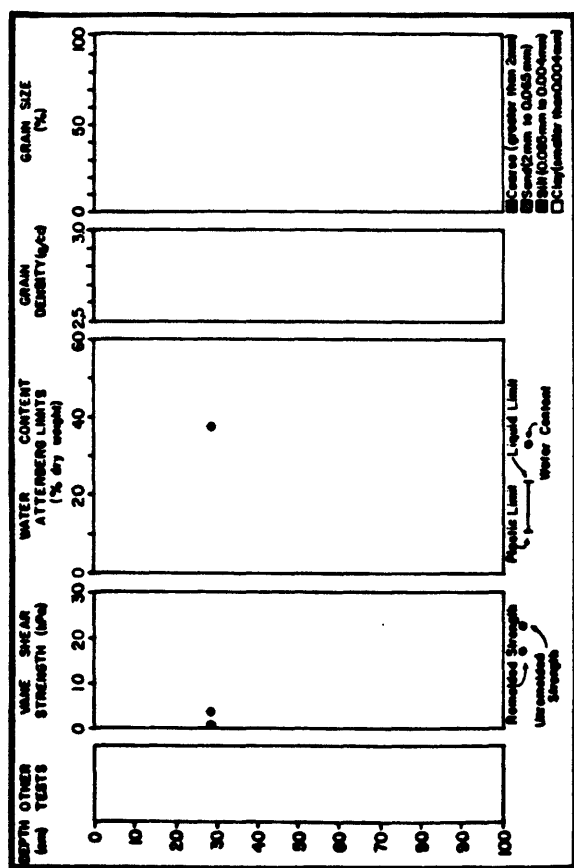
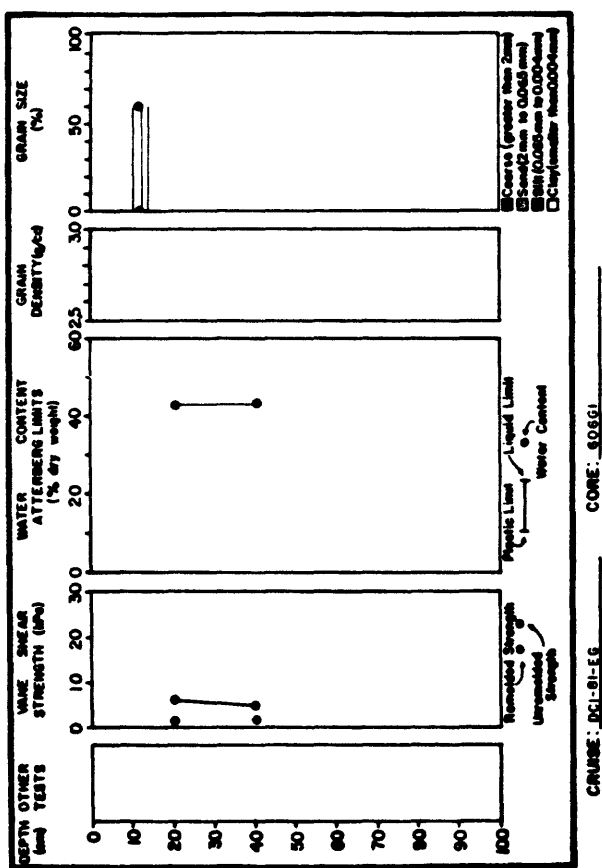
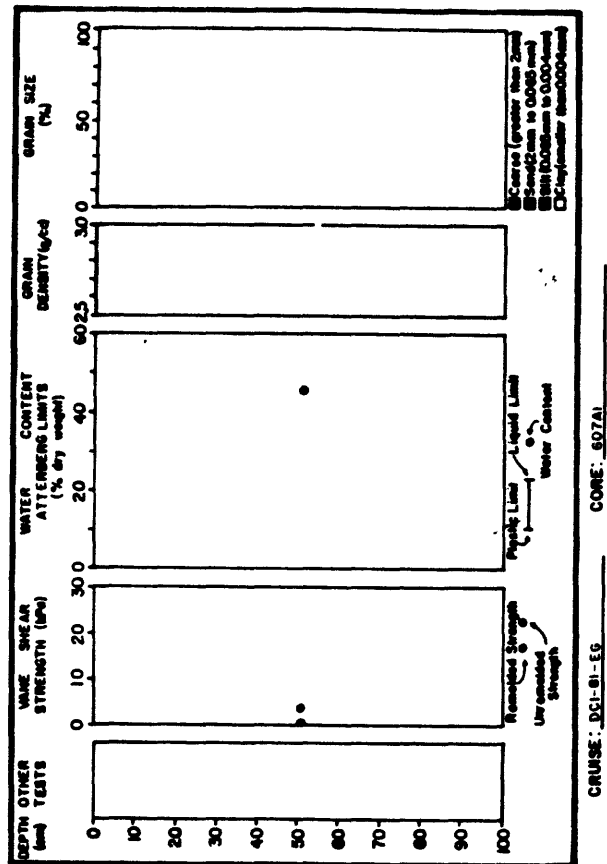
CRUISE: DCI-9-E6 CORE: 6025

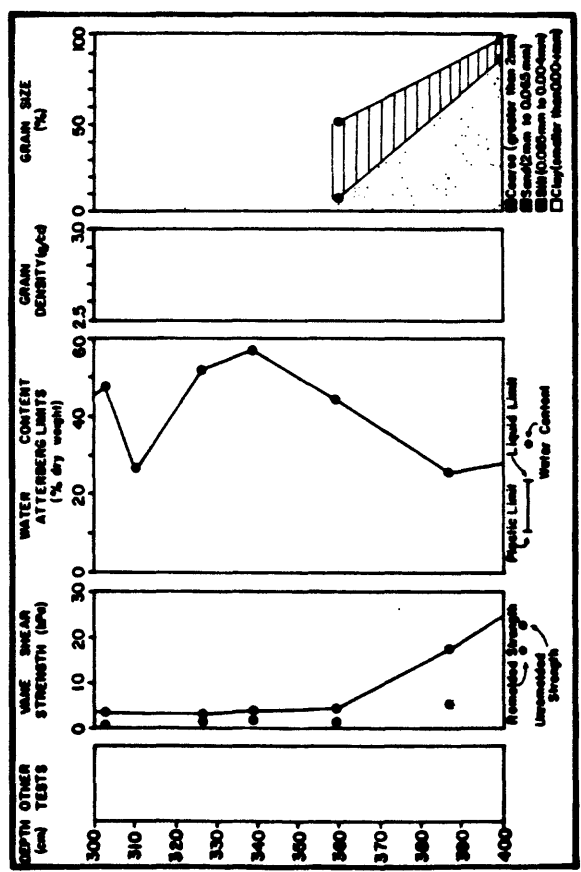
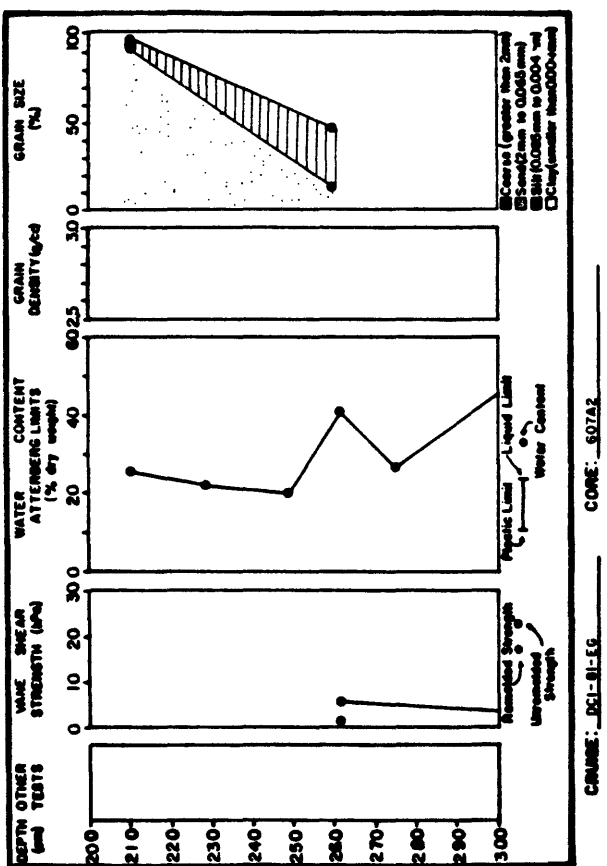
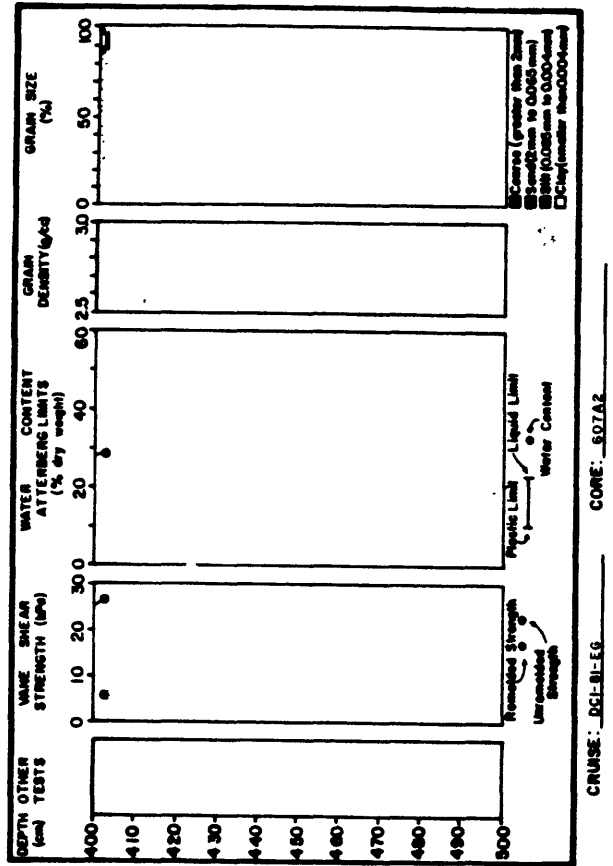


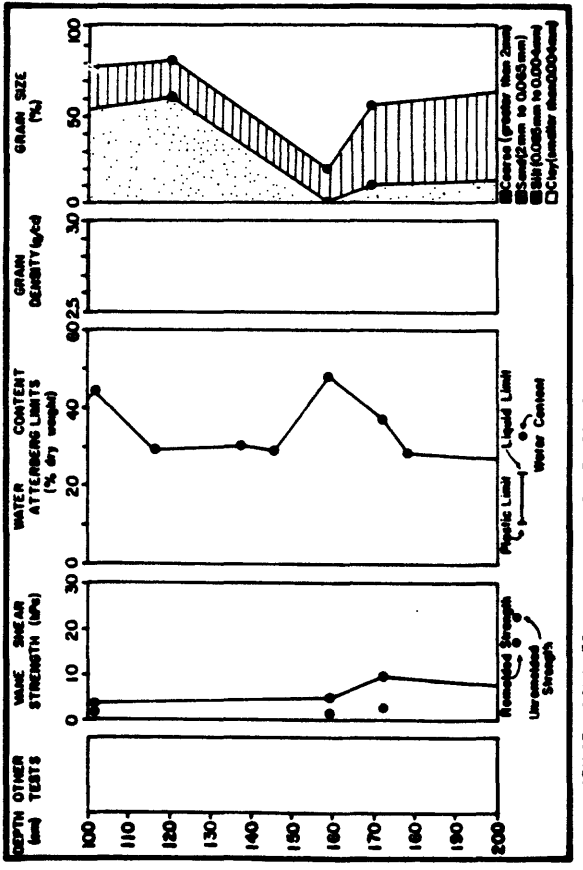
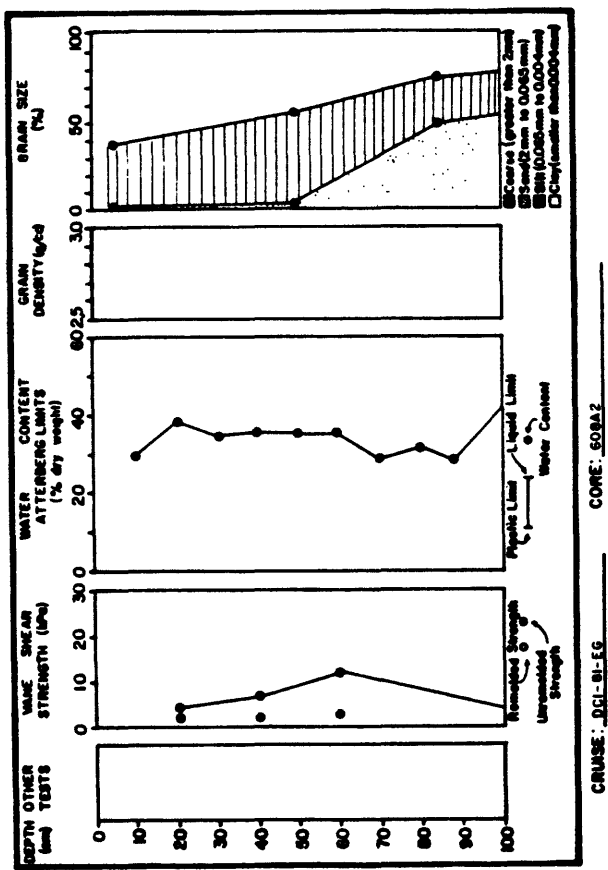
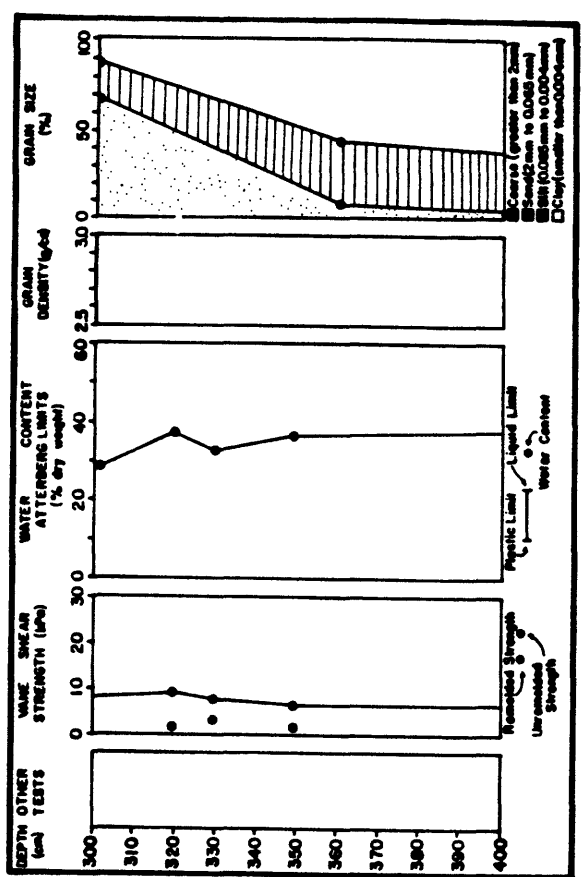
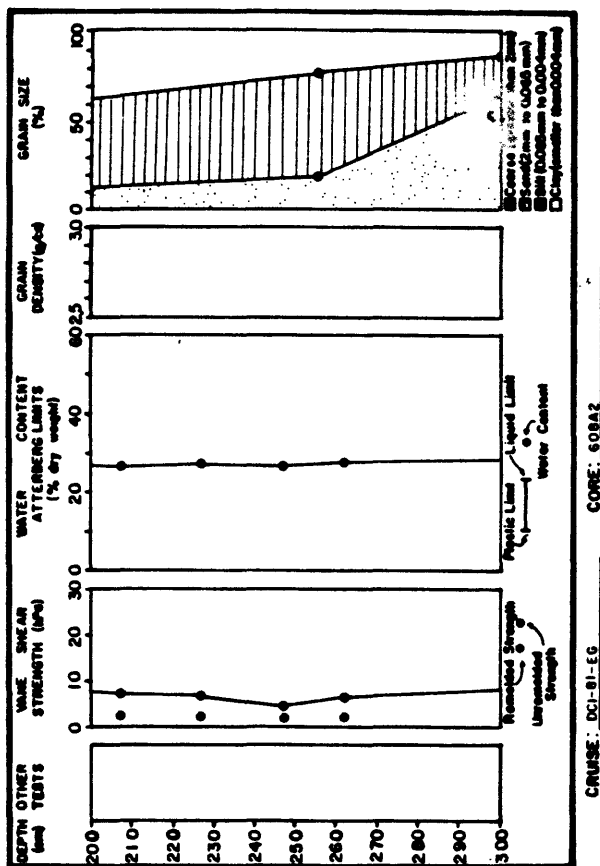
CRUISE: DCI-9-E6 CORE: 6025

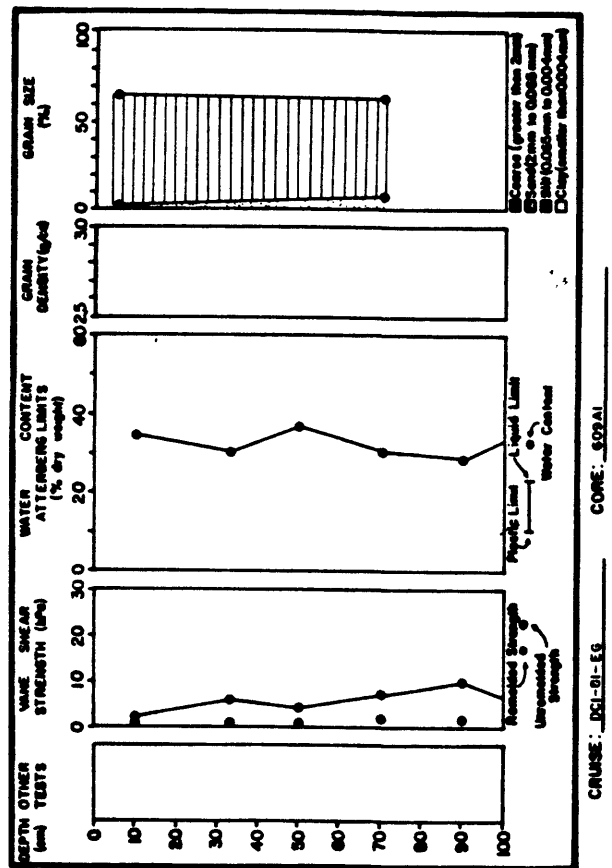




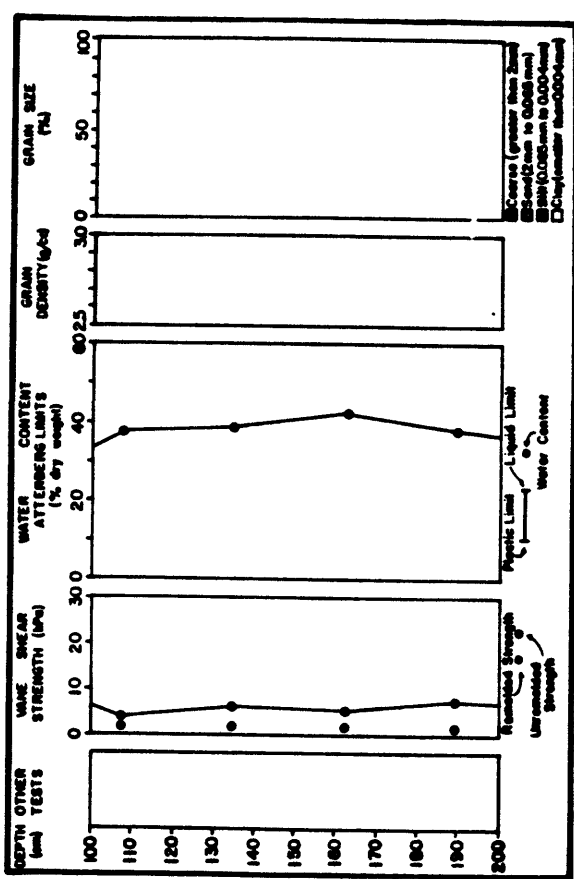




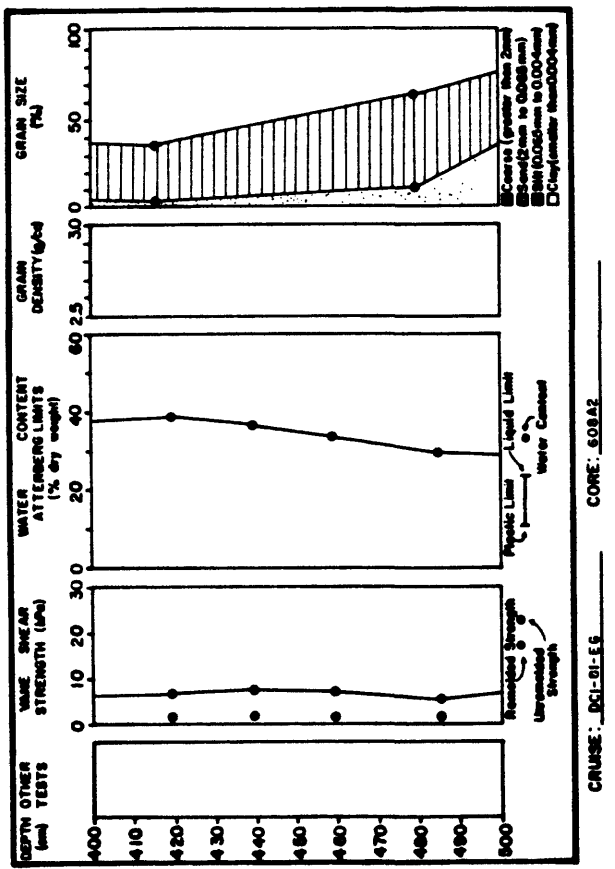




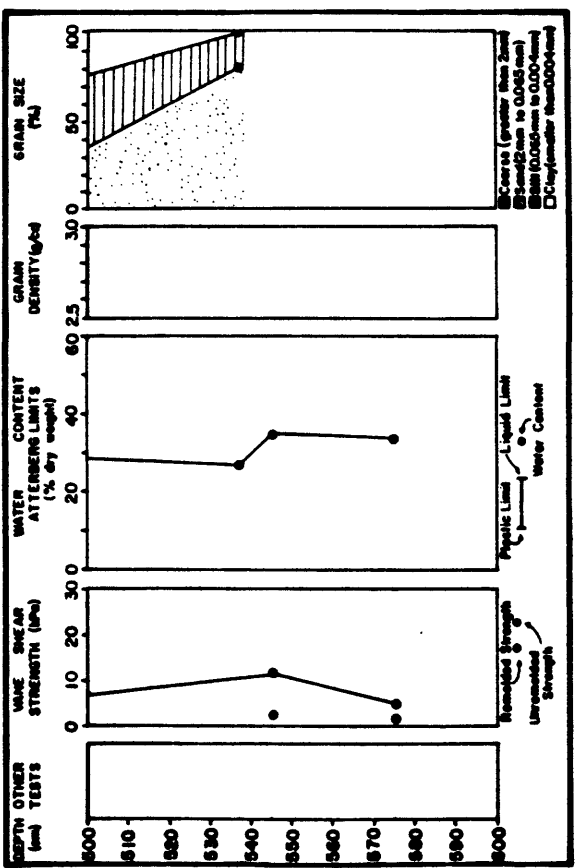
CRUISE: DCI-81-E6 CORE: 600AI



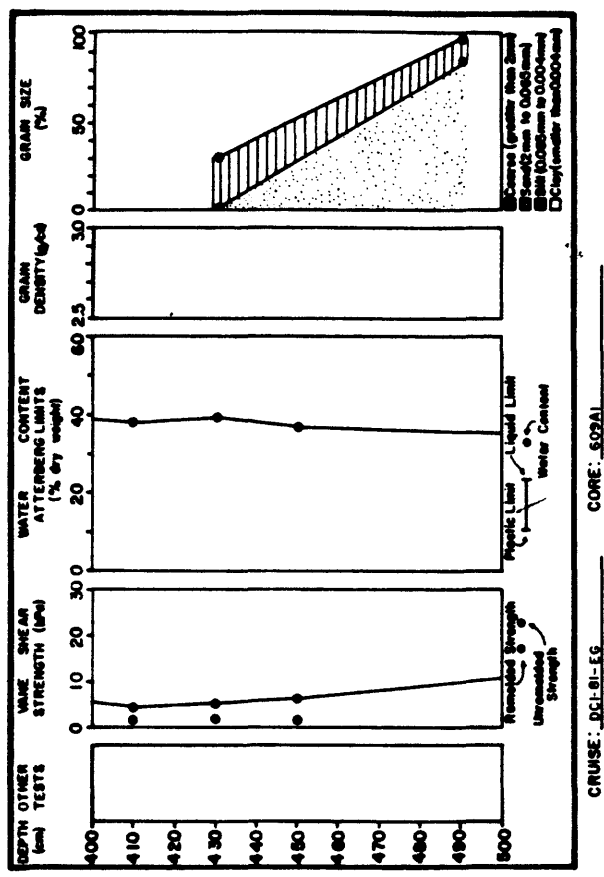
CRUISE: DCI-81-E6 CORE: 500AI



CRUISE: DCI-81-E6 CORE: 400AI

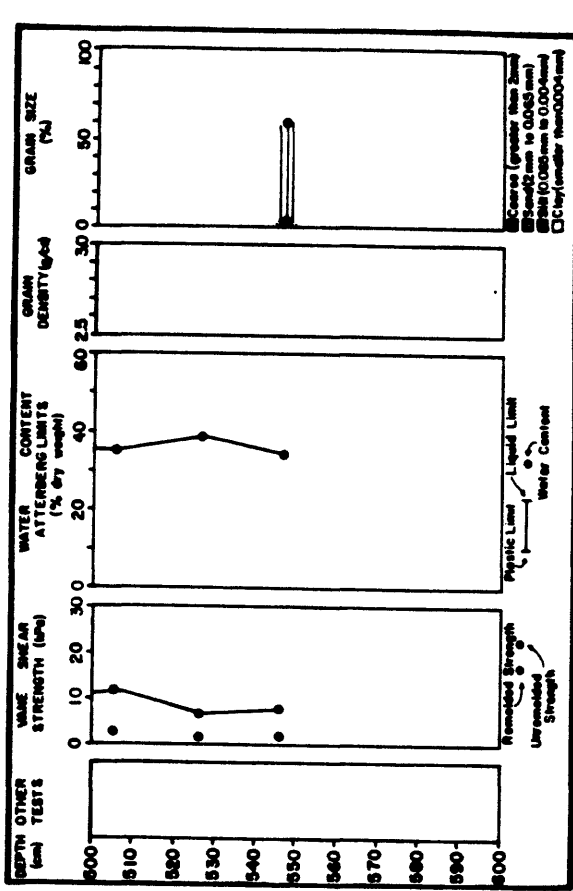


CRUISE: DCI-81-E6 CORE: 300AI

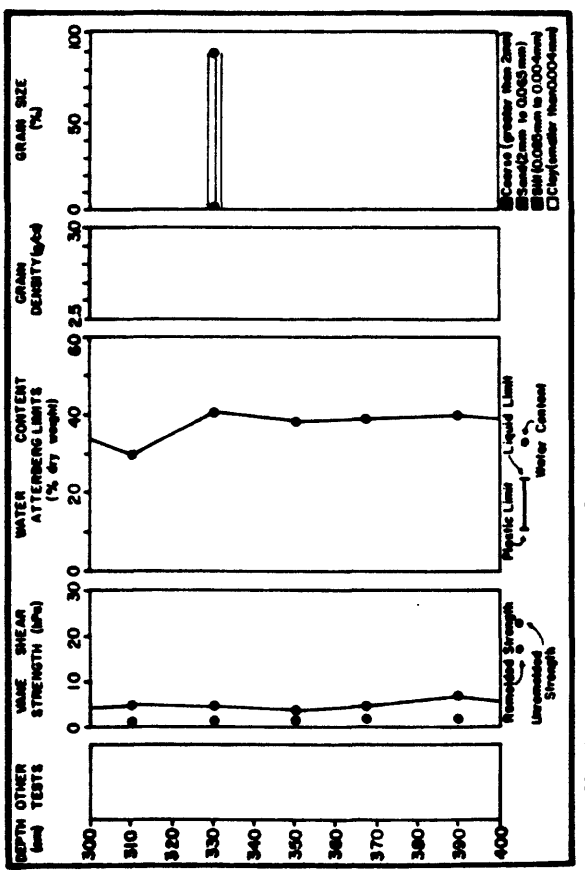


CORE: 602A1

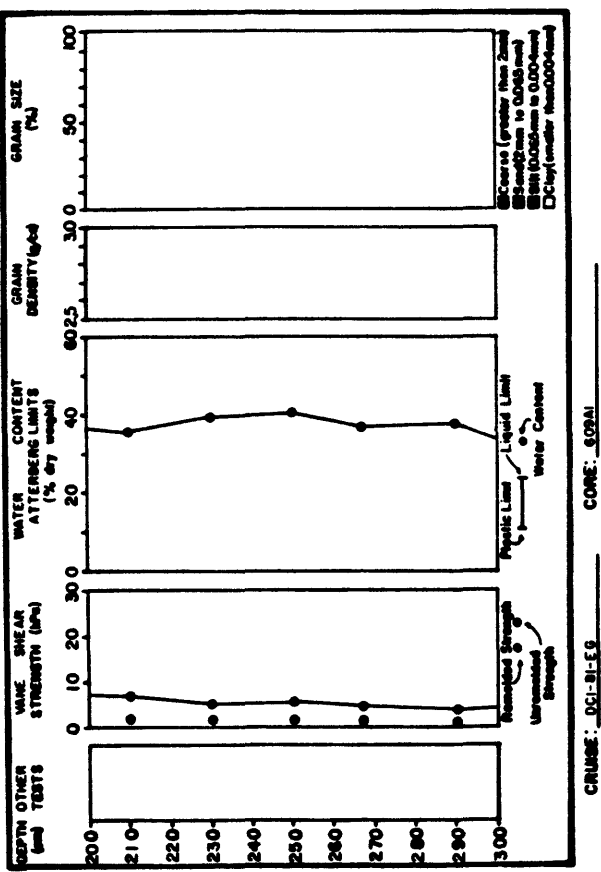
CORE: 602A1



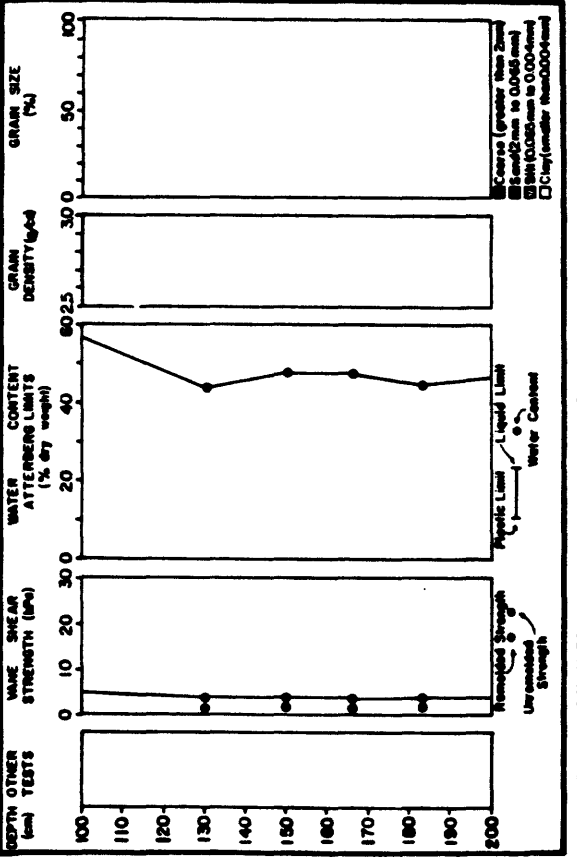
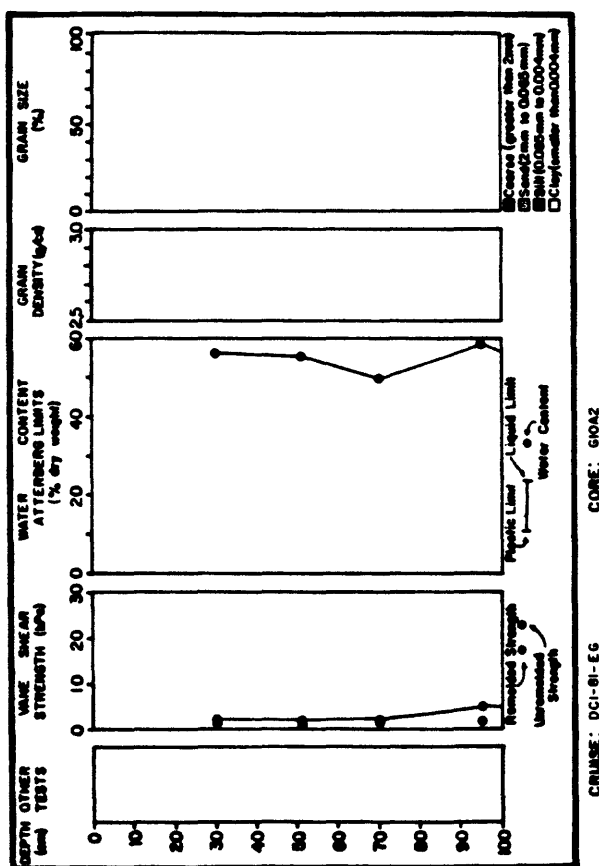
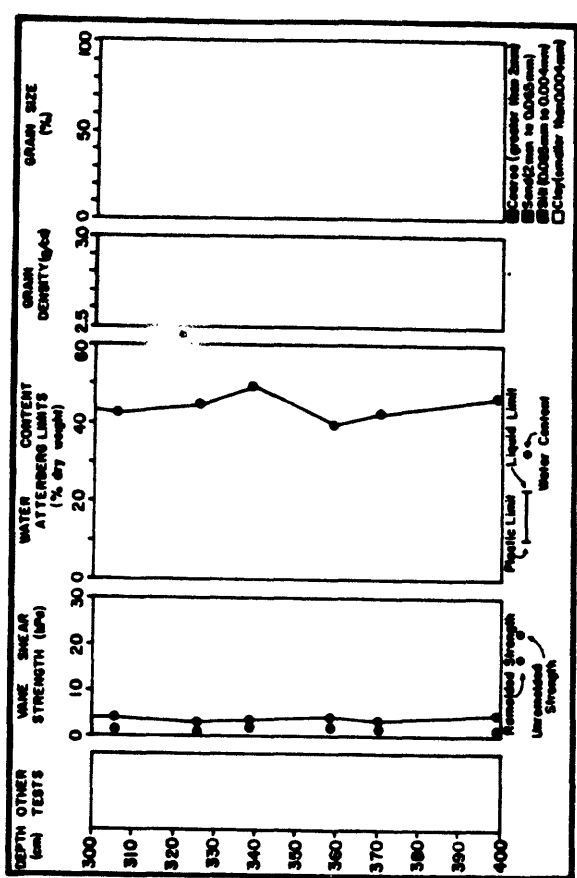
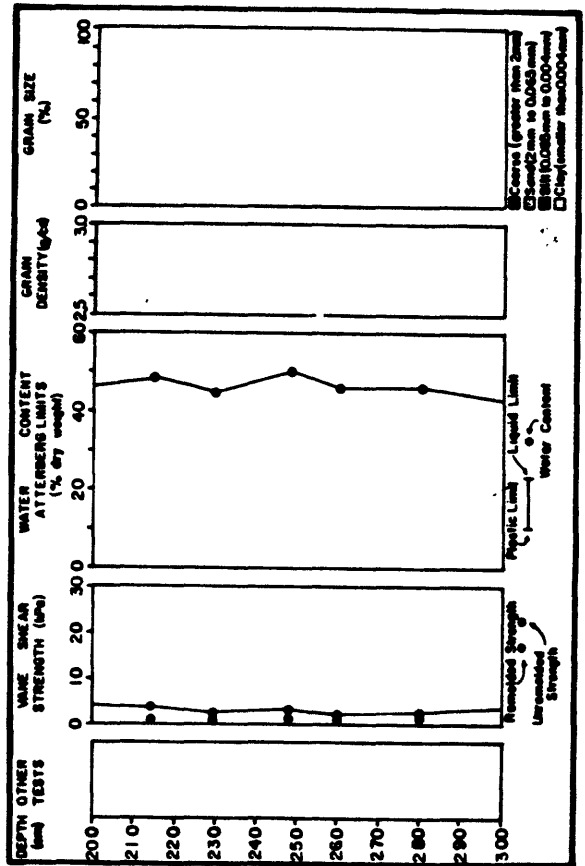
CORE: 602A1

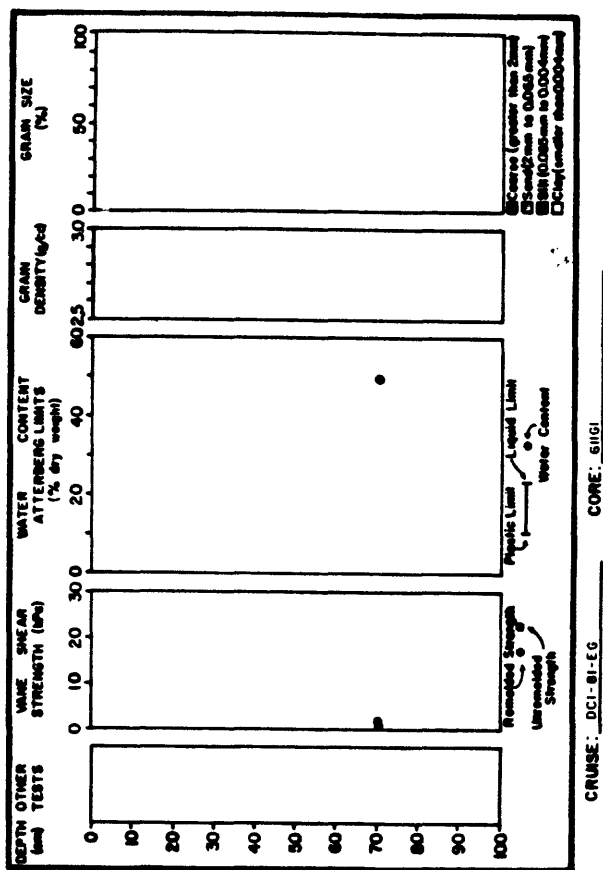


CORE: 602A1

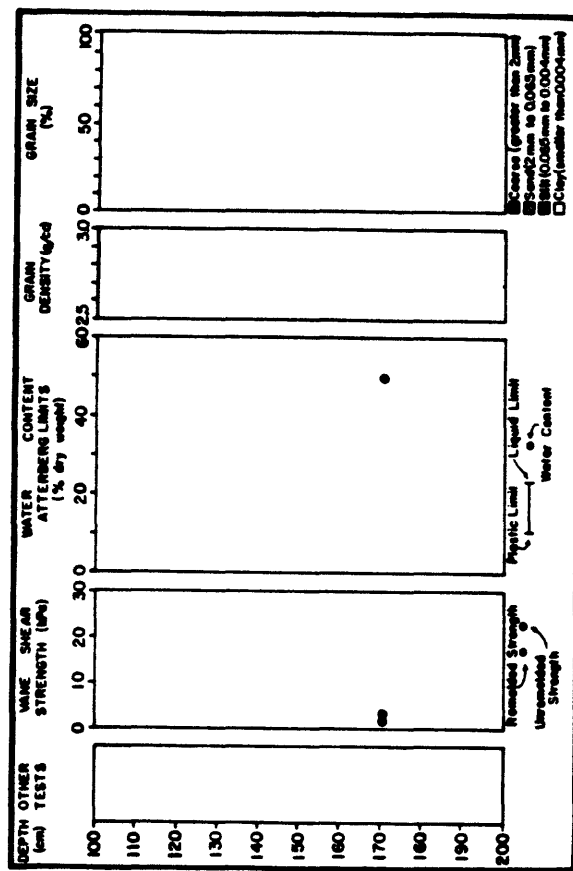


CORE: 602A1

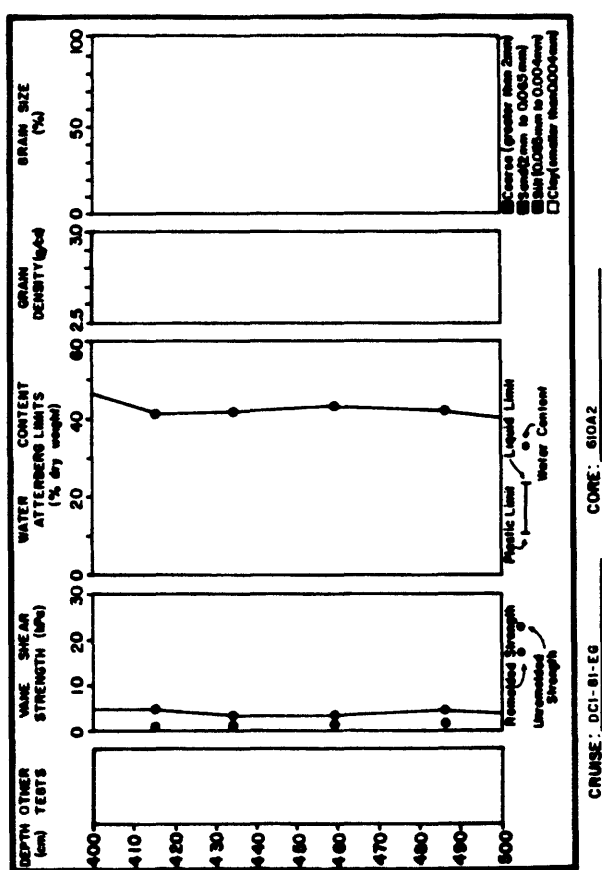




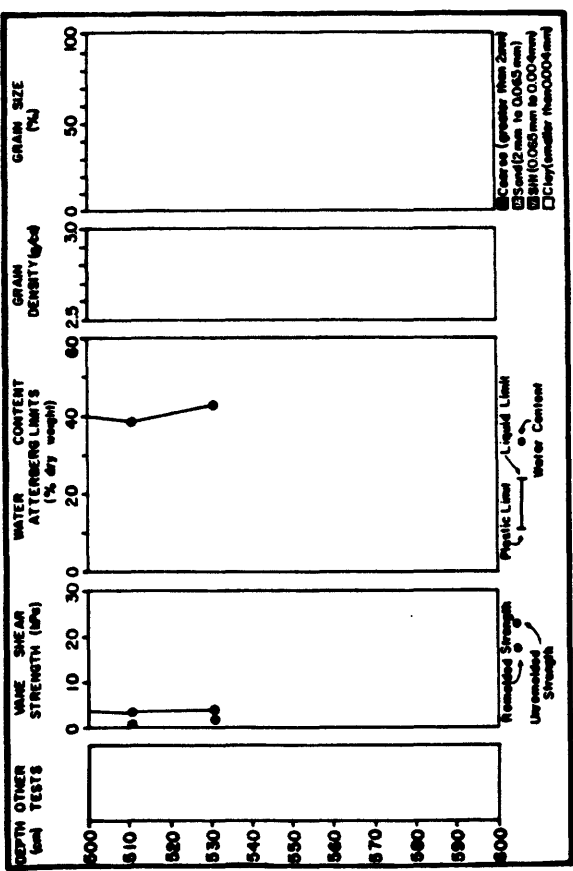
CRUISE: 61GI



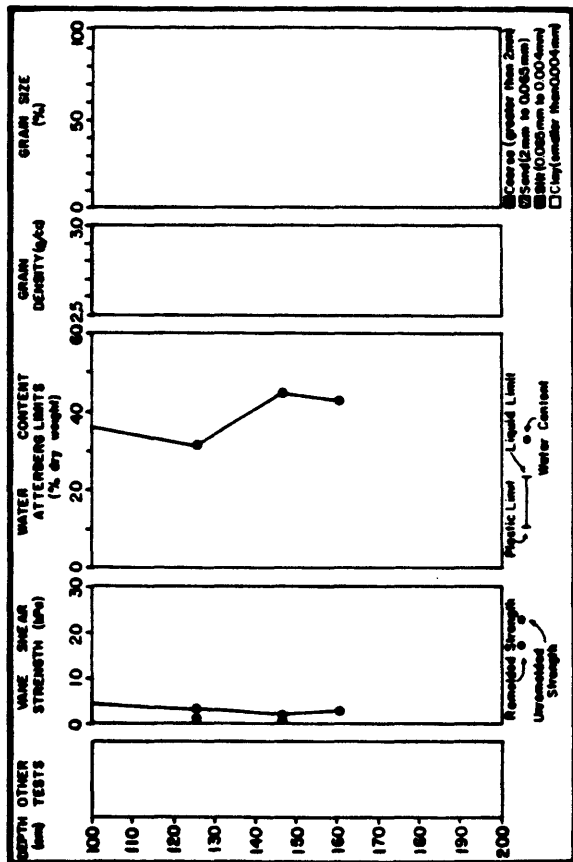
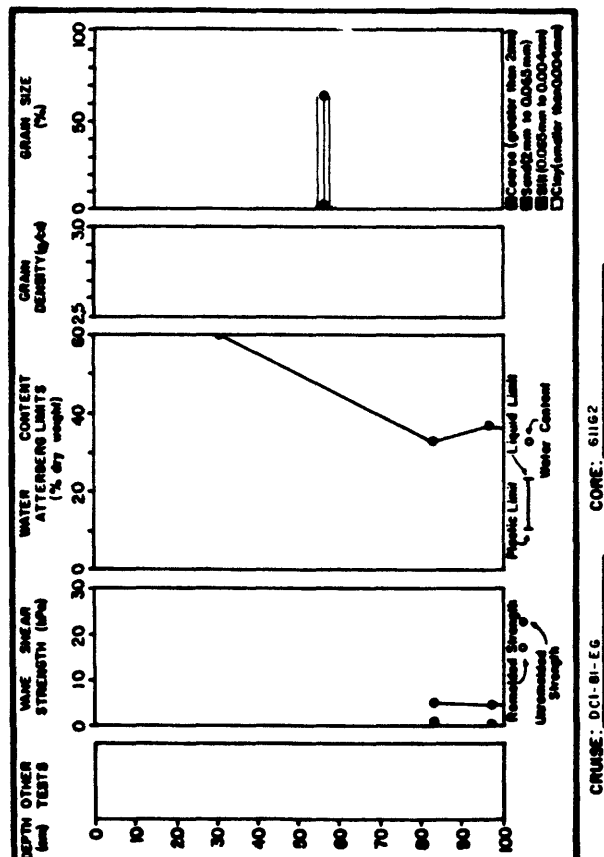
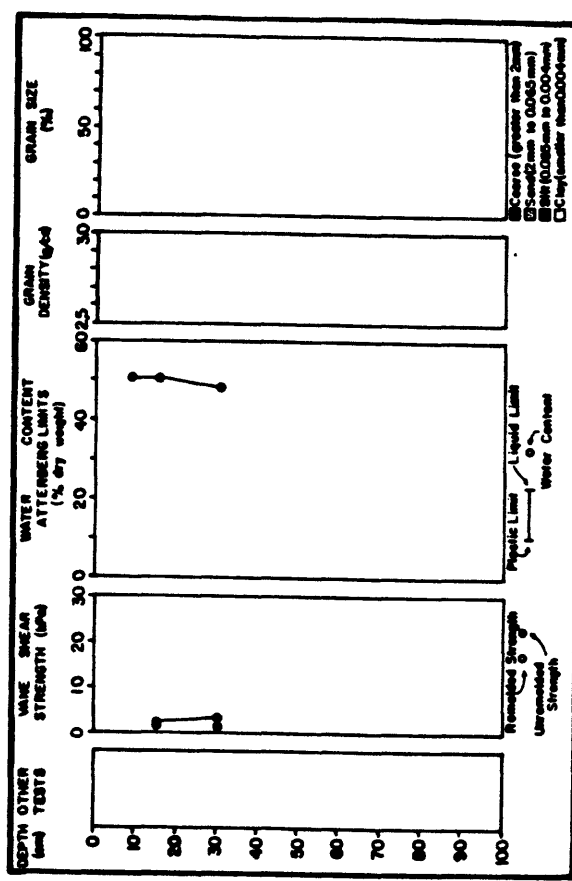
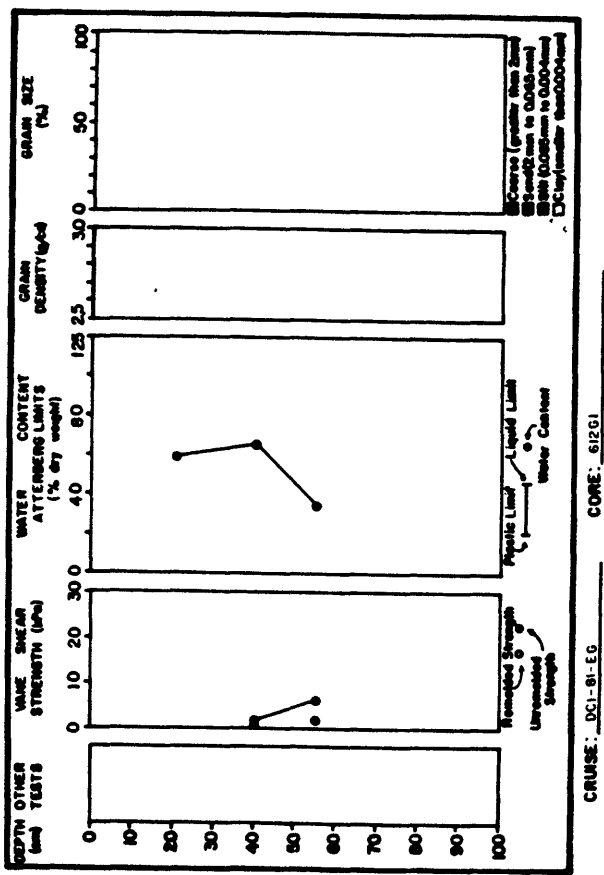
CRUISE: 61GI

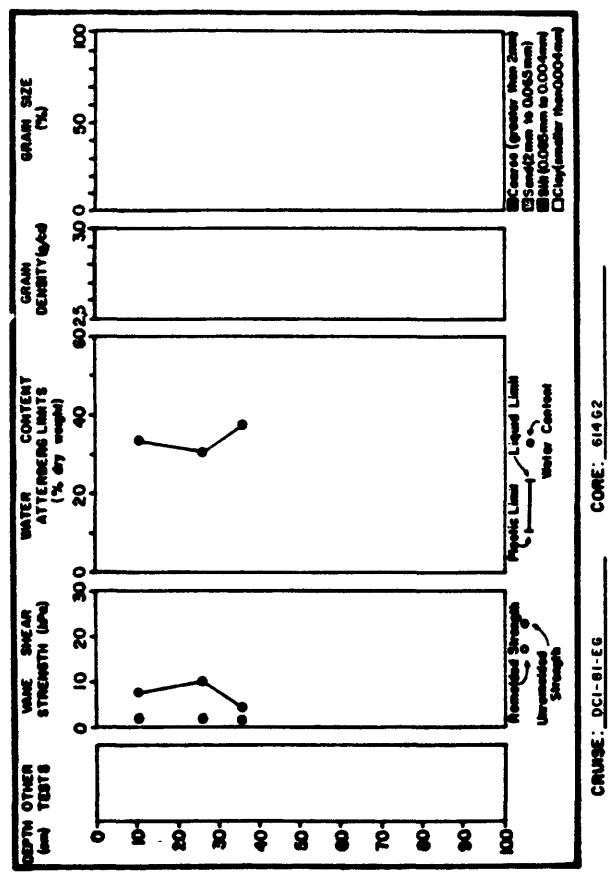


CRUISE: 61GI

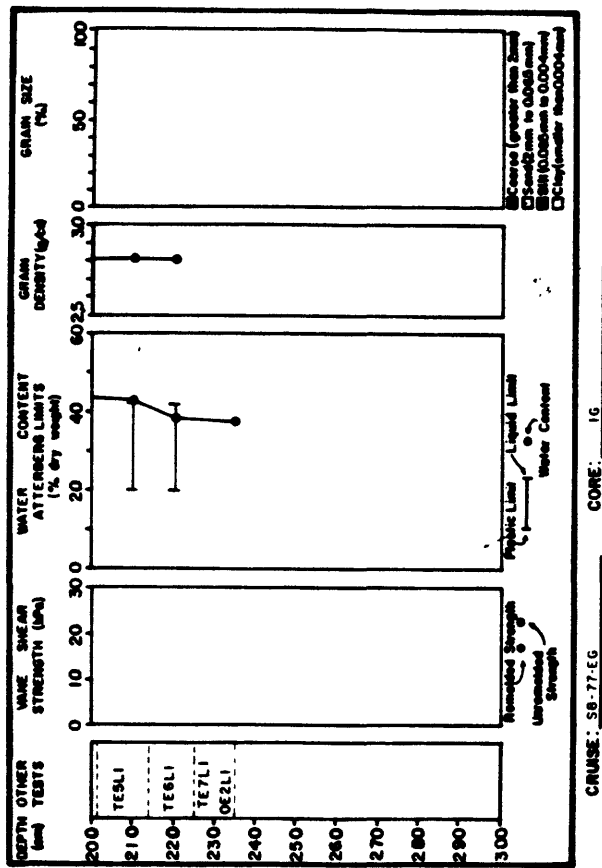


CRUISE: 61GI

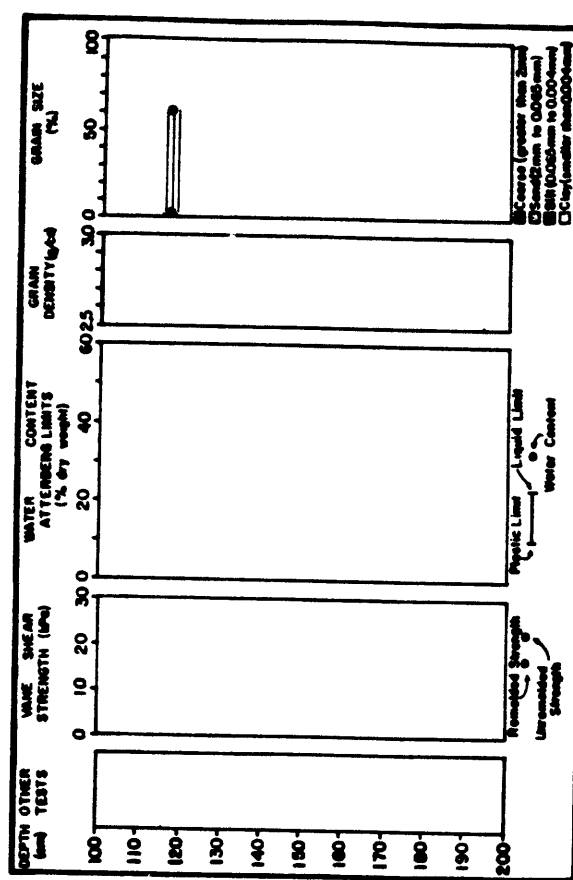




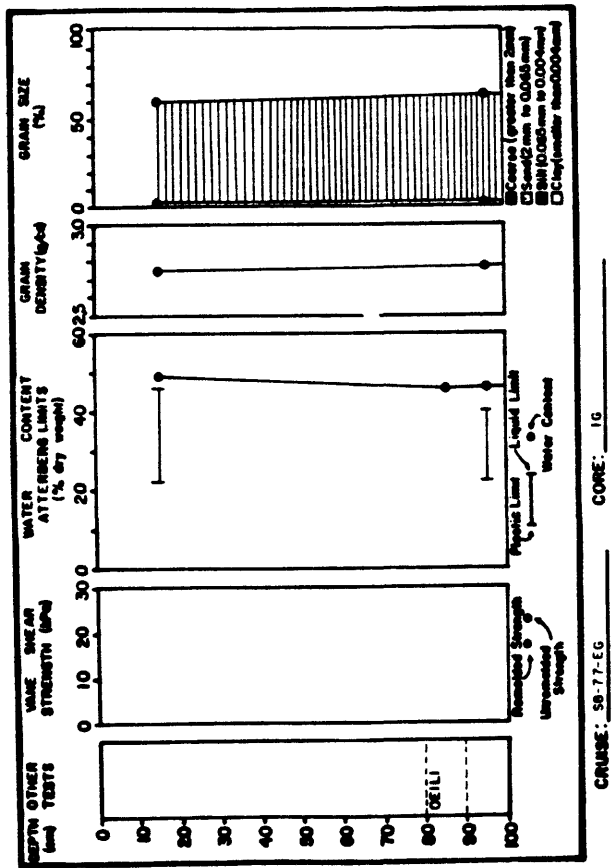
OTHER



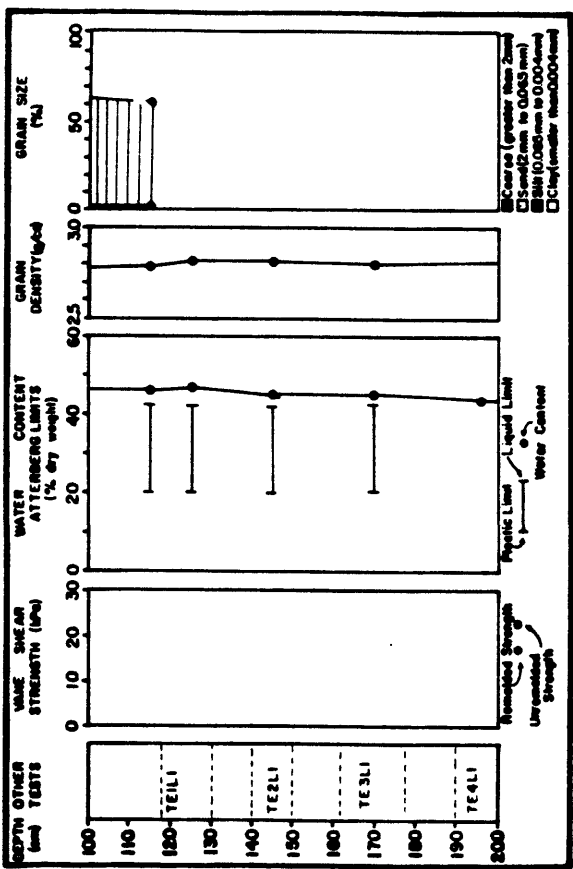
CRUISE: SB-77-EG CORE: 1G



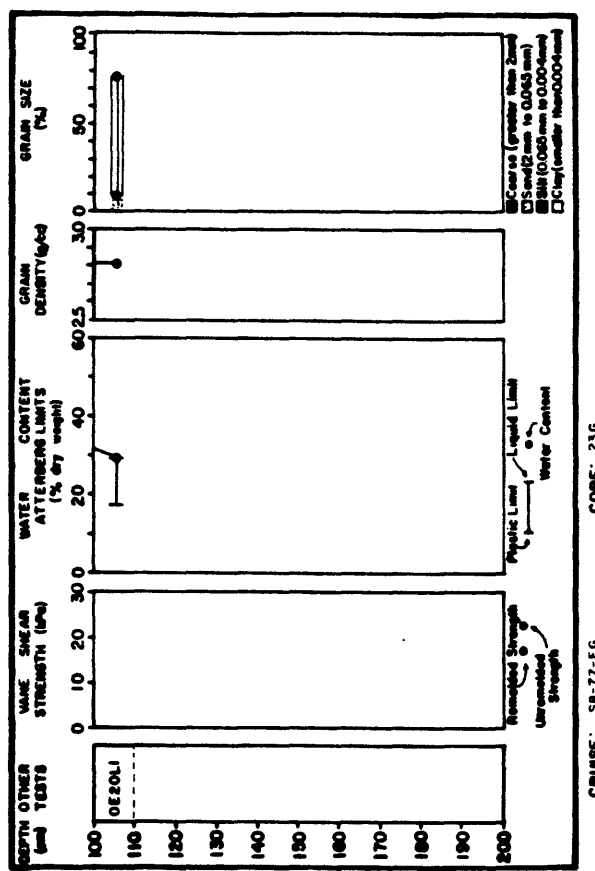
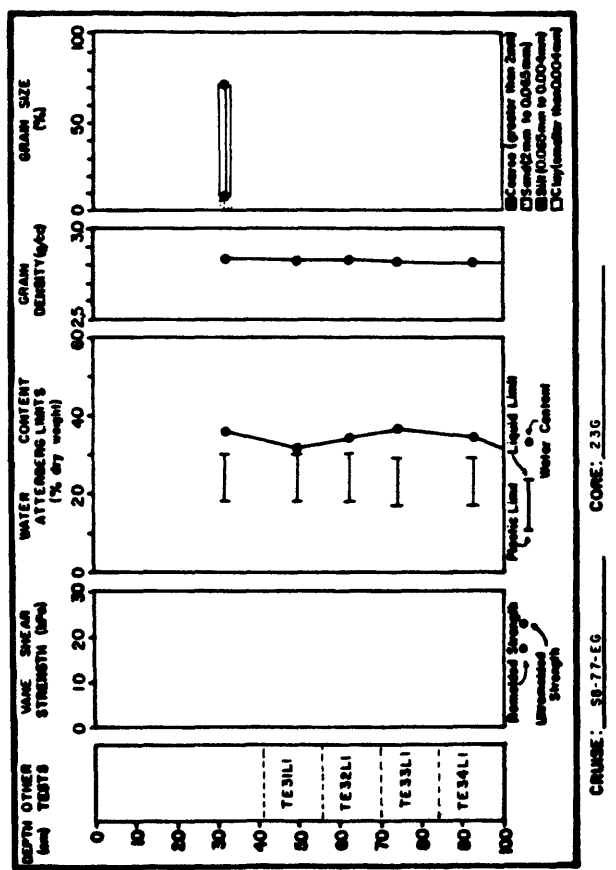
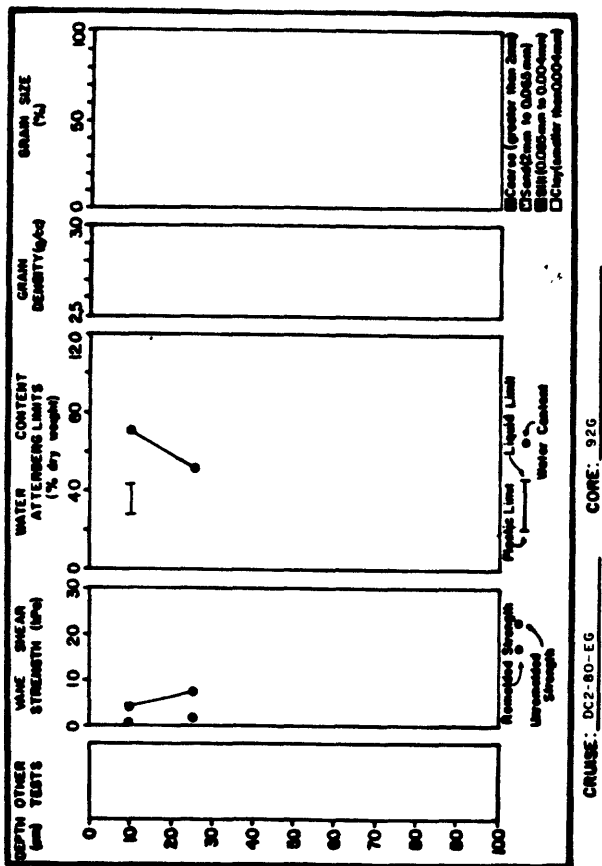
CRUISE: SB-77-EG CORE: 1G

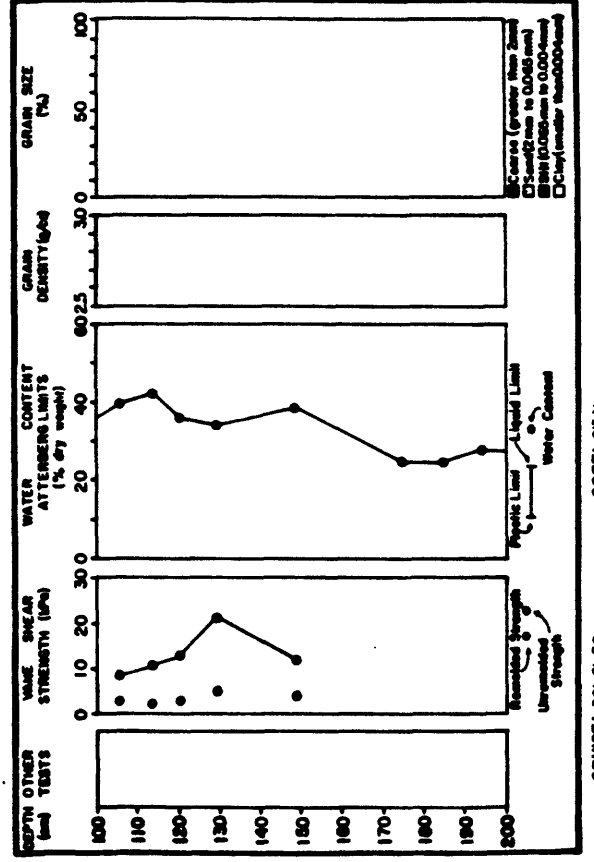
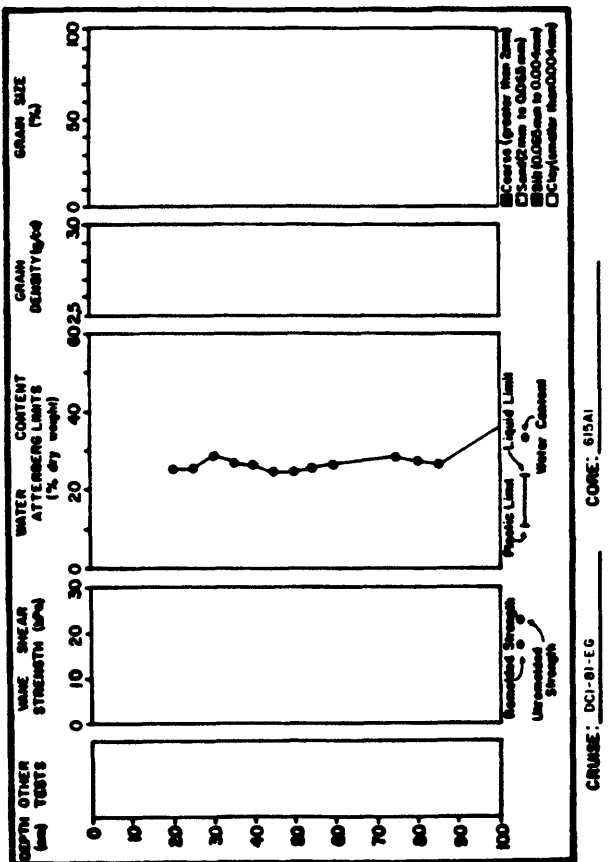
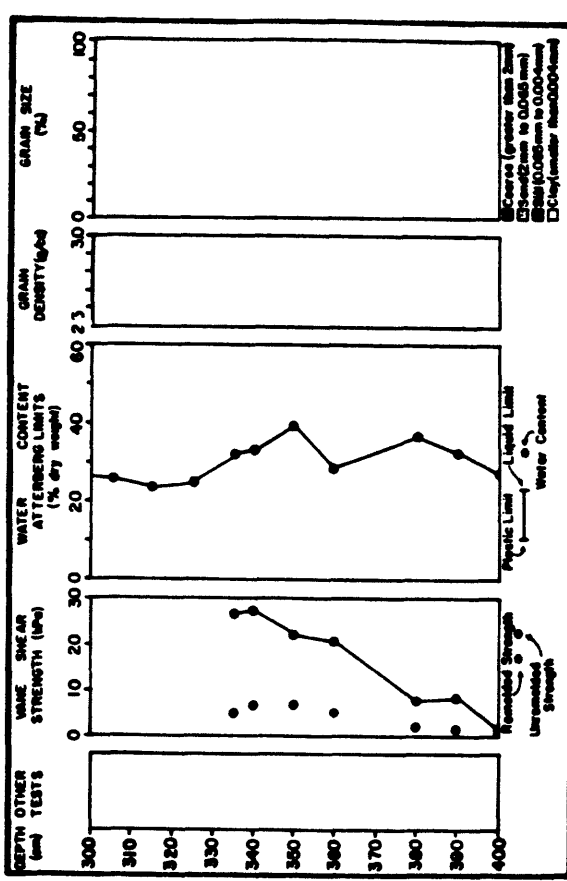
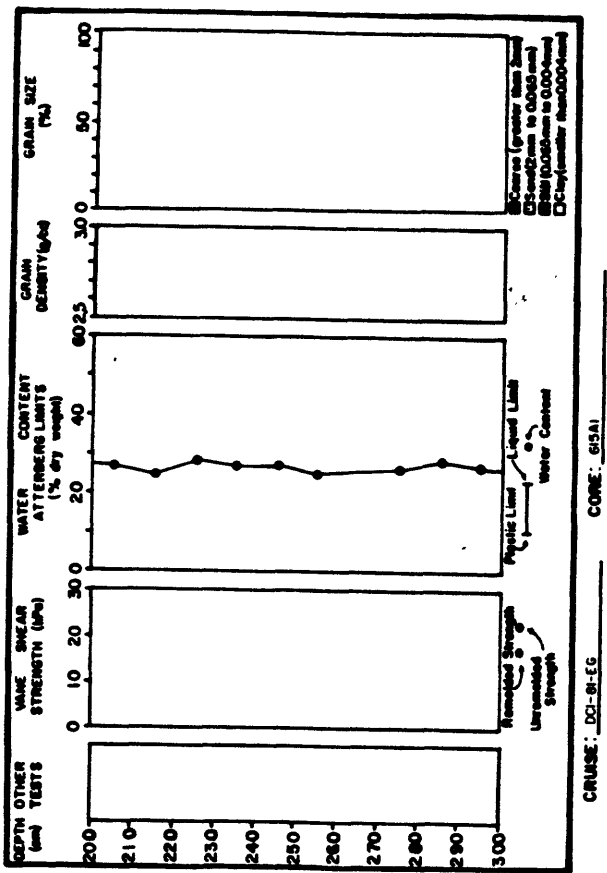


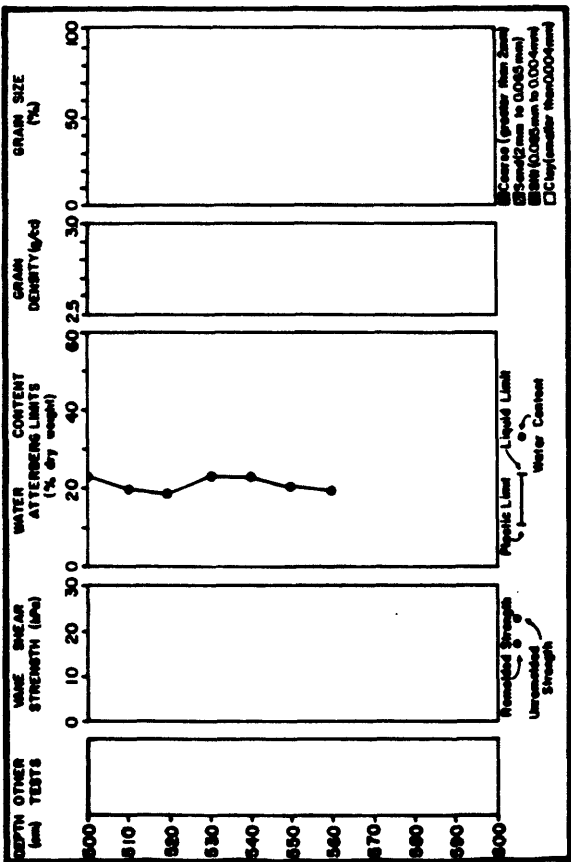
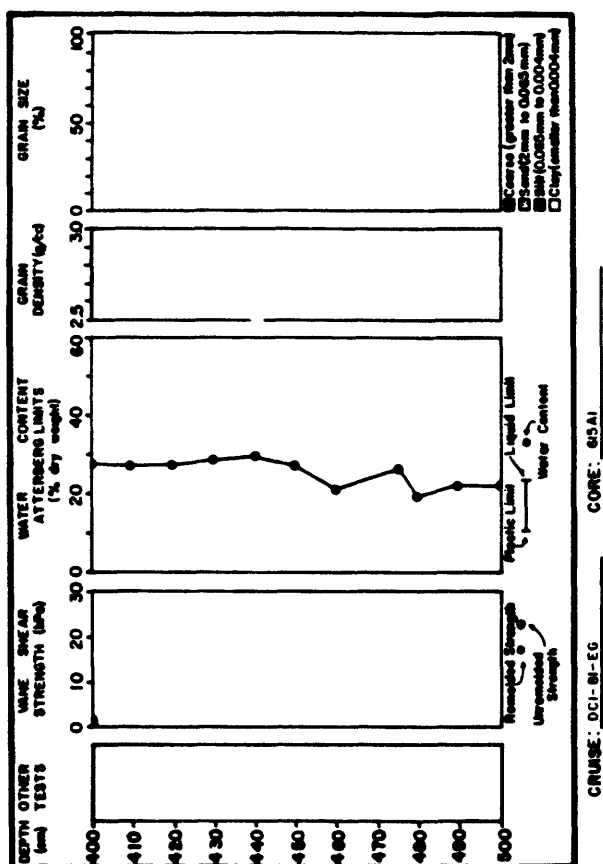
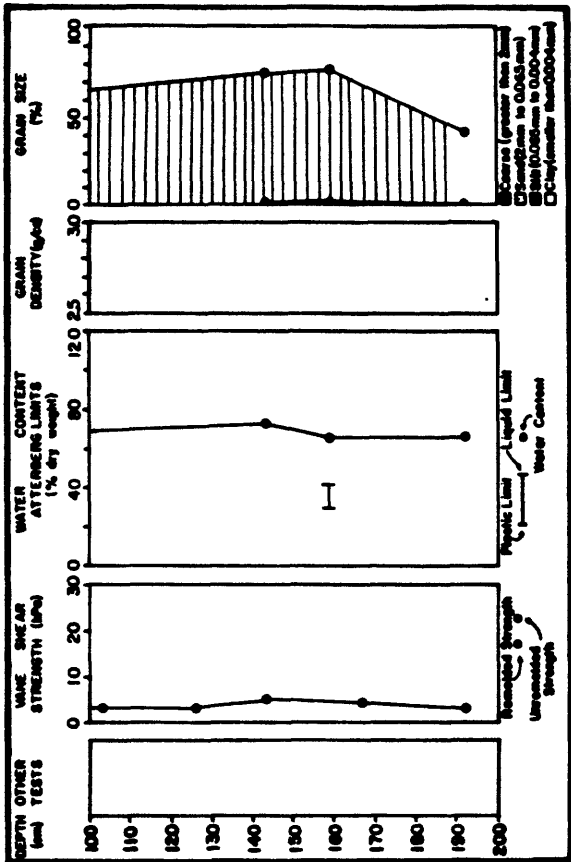
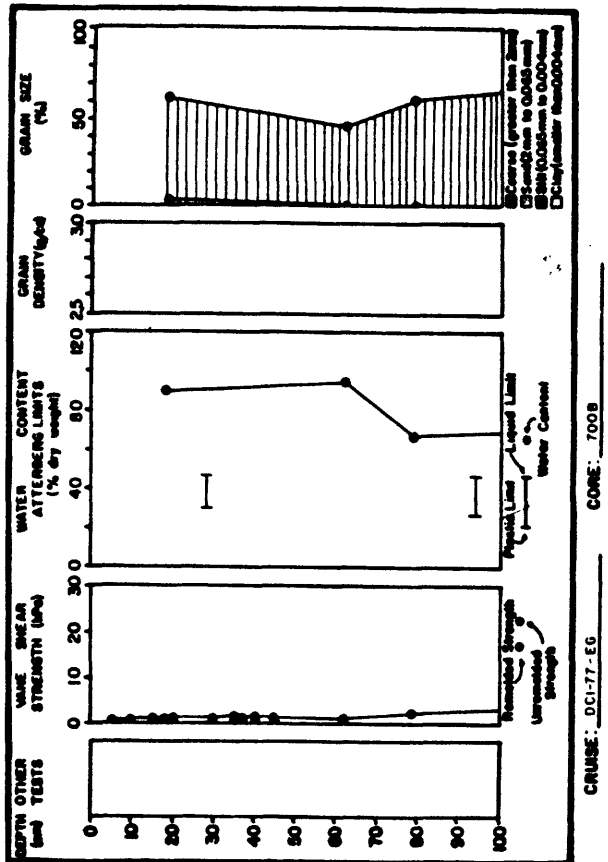
CRUISE: SB-77-EG CORE: 1G

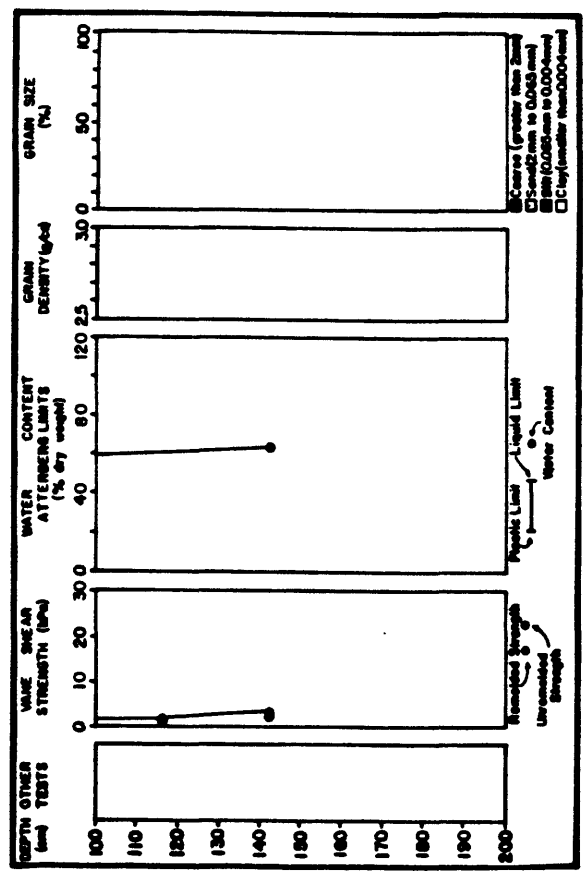
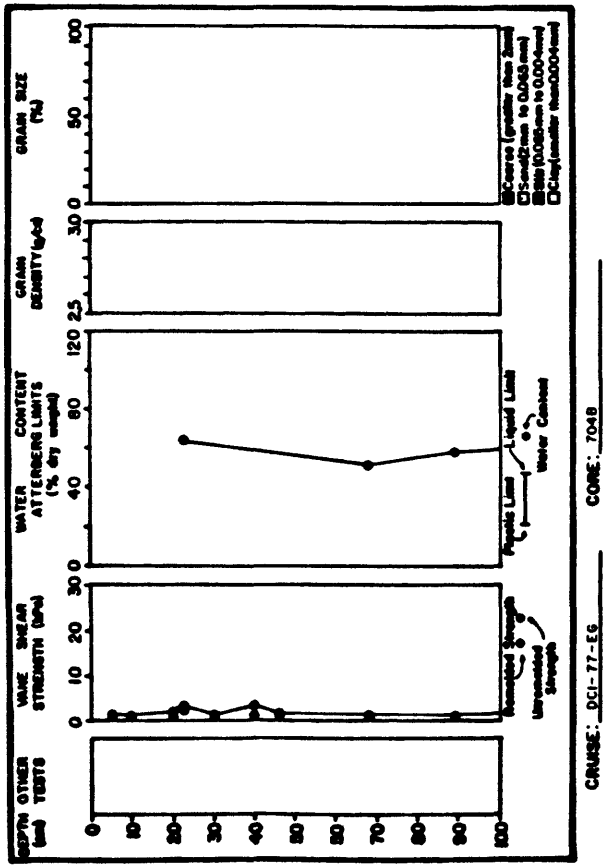


CRUISE: SB-77-EG CORE: 1G









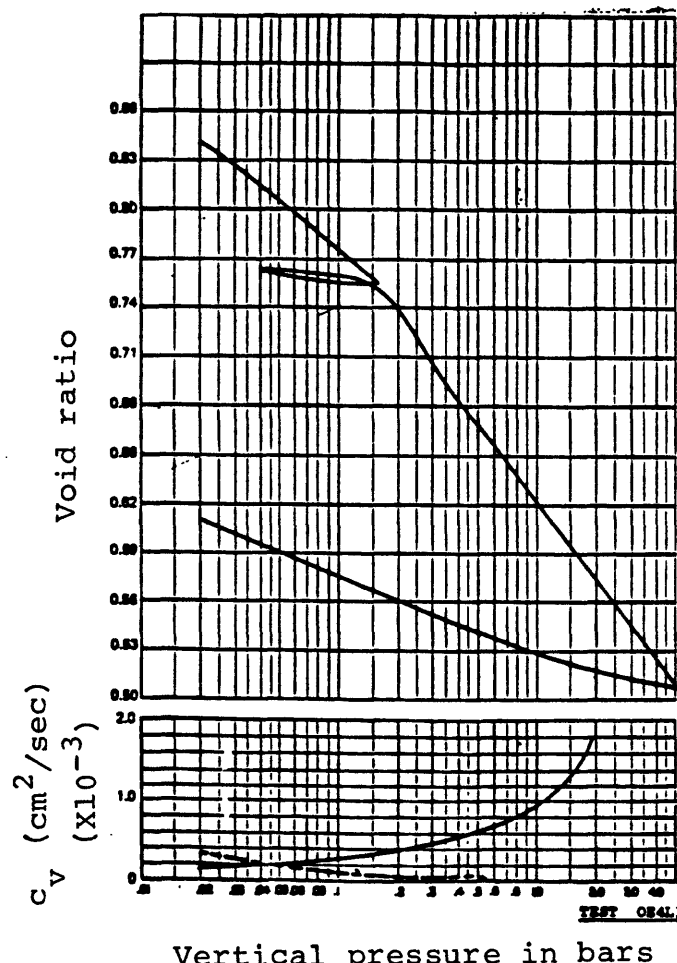
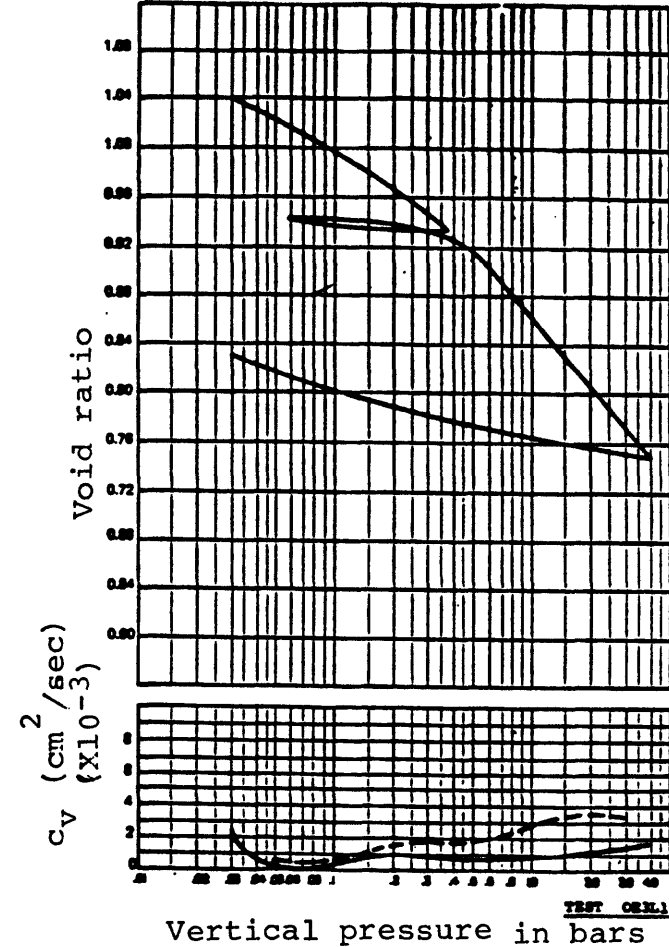
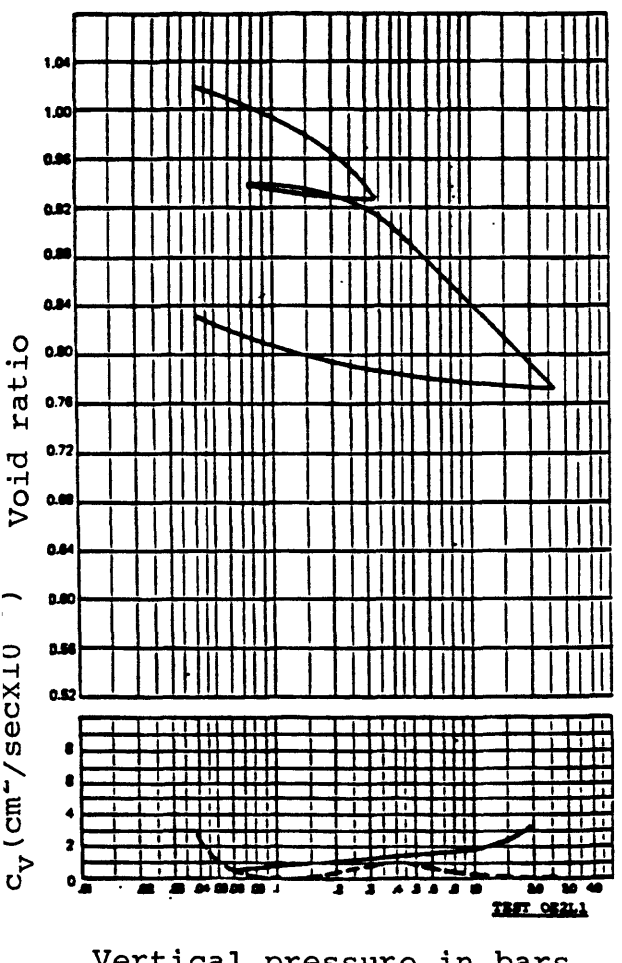
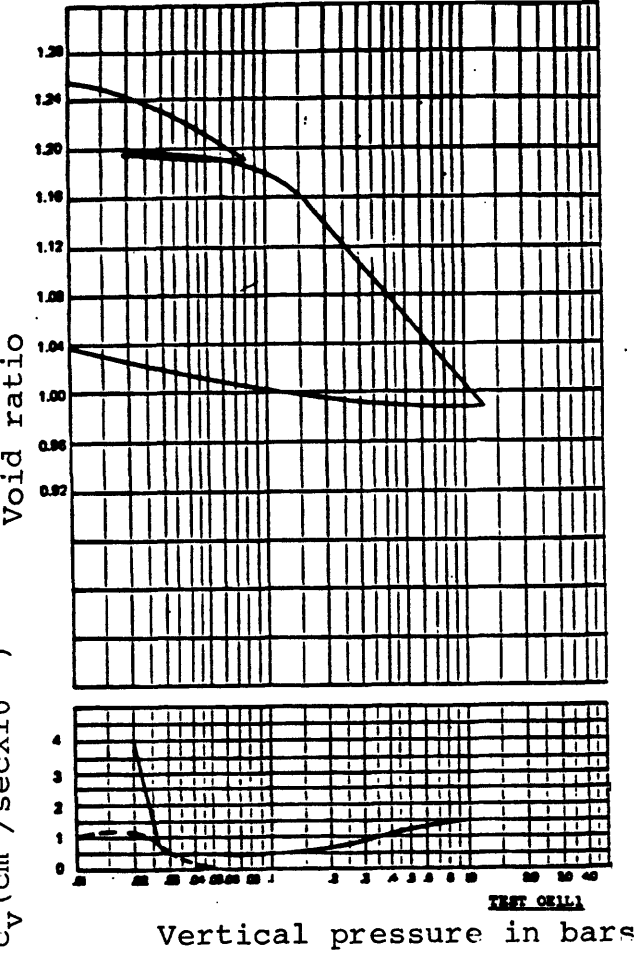
APPENDIX D. CONSOLIDATION AND TRIAXIAL TEST RESULTS-LAW ENGINEERING AND TESTING COMPANY (1977 cores)

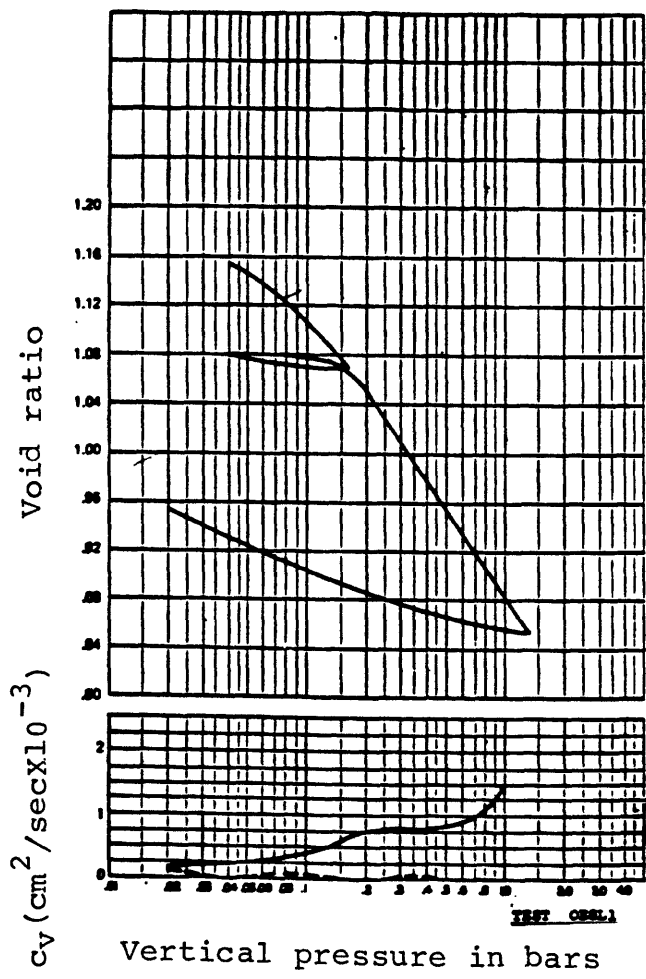
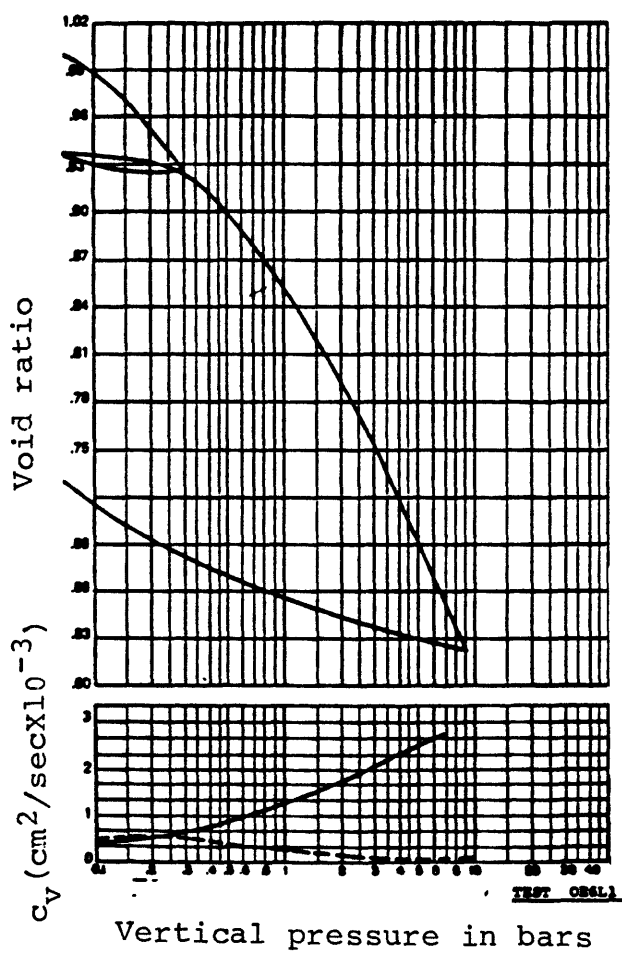
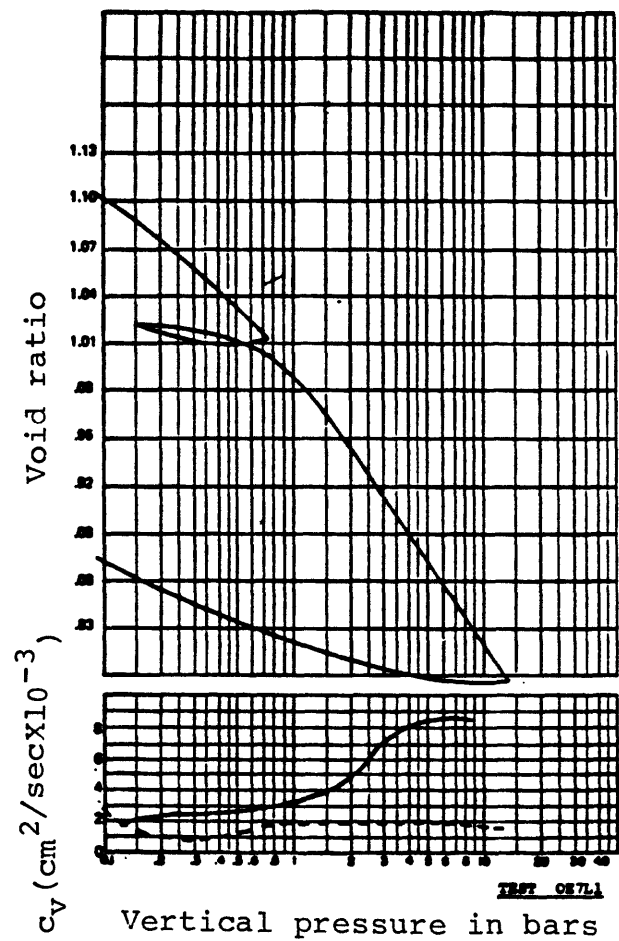
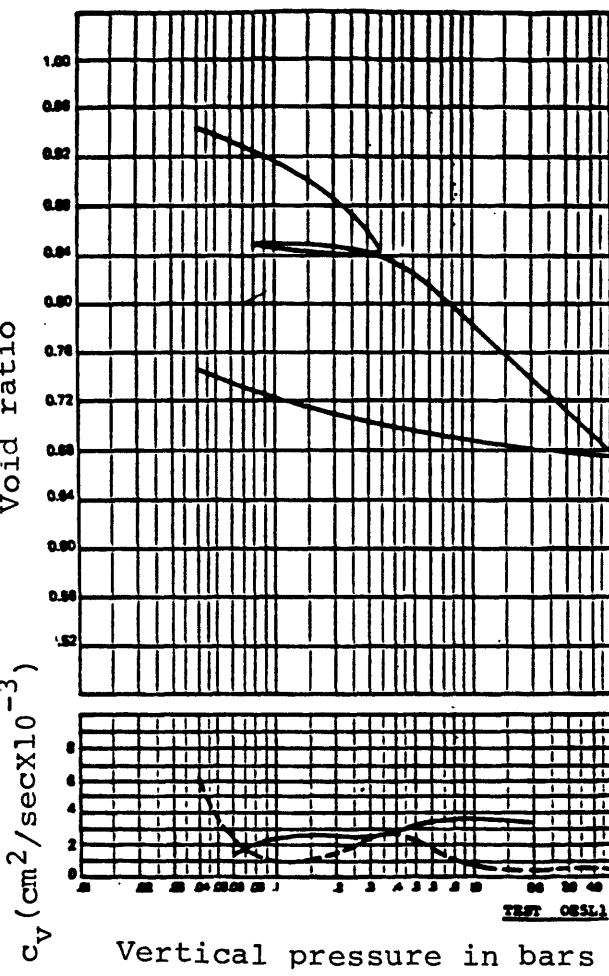
This appendix presents the results of consolidation and static triaxial testing performed by Law Engineering and Testing Company under Contract number 14-08-0001-17356 with the U.S. Geological Survey. Testing was performed under the direction of R.W. Sparrow, P.G. Swanson and R.E. Brown. Core samples were from Cruise S8-77-EG.

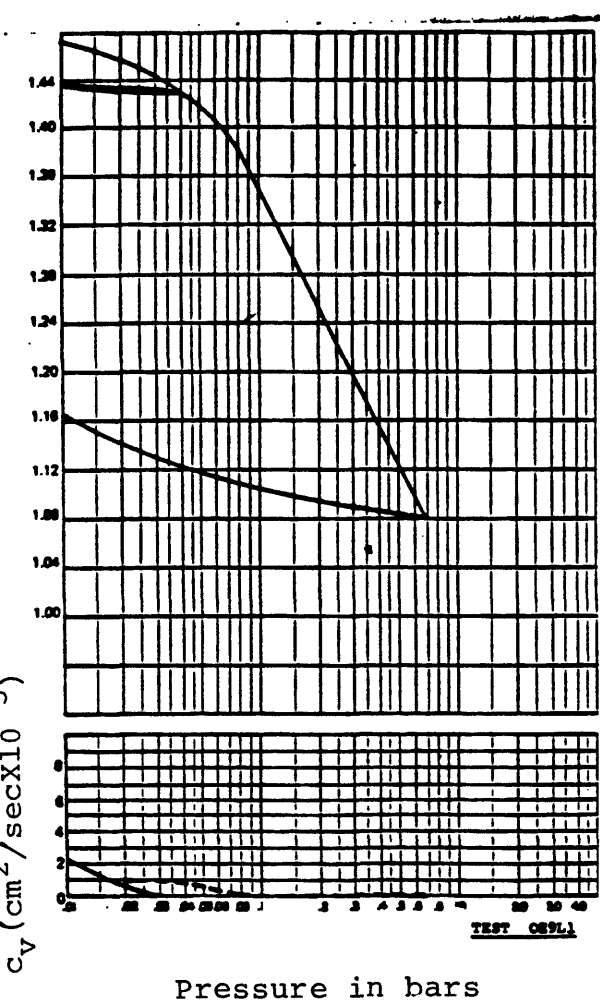
All tests in this group have been assigned a test number with L1 as the last two characters. The consolidation tests (first two characters are OE) are presented first and are ordered by test number. Results from a single test are presented on a page in the form of void ratio and calculated coefficient of consolidation ( $c_v$ ) versus the vertical effective stress given in bars (1 bar=101.3 kPa).

The static triaxial tests (first two characters are TE) are given second and ordered by test number. Results from one to as many as four tests are presented on the same sheet. The uppermost plot is a stress path presented as a plot of deviator stress versus mean normal effective stress. The deviator stress is the vertical effective stress ( $\sigma_v'$ ) minus the horizontal effective stress ( $\sigma_h'$ ). The mean normal effective stress is  $(\sigma_v' + 2\sigma_h')/3$ . Note: This definition is not the same as that used in the stress paths given in Appendices E, F, and G.

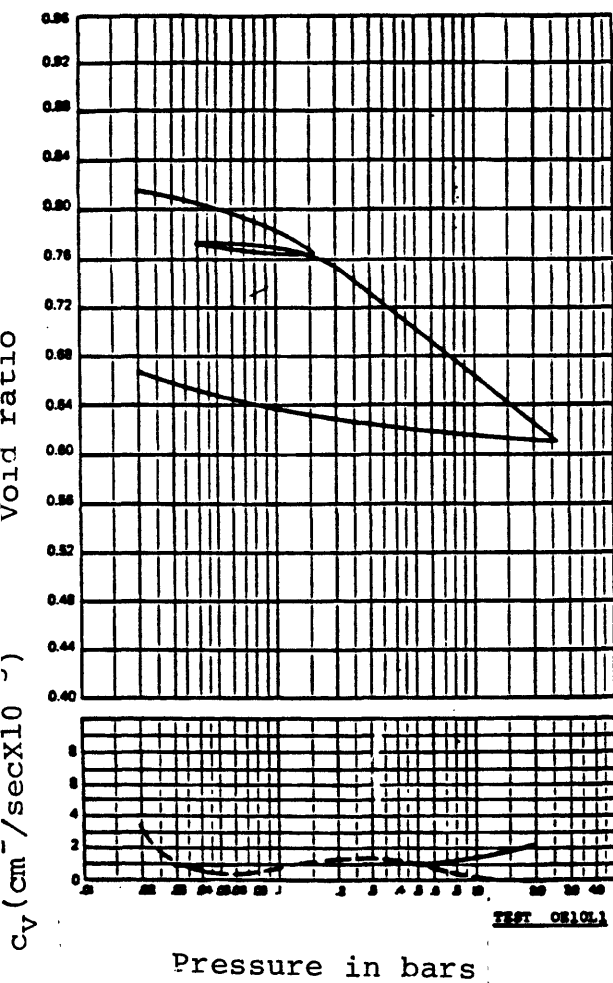
The middle graph is either the deviator stress or  $Q/\sigma_c$  versus the axial strain. The parameter Q is the deviator stress while  $\sigma_c$  is the consolidation stress (or confining pressure). The last graph is the measured excess pore water pressure plotted versus axial strain.



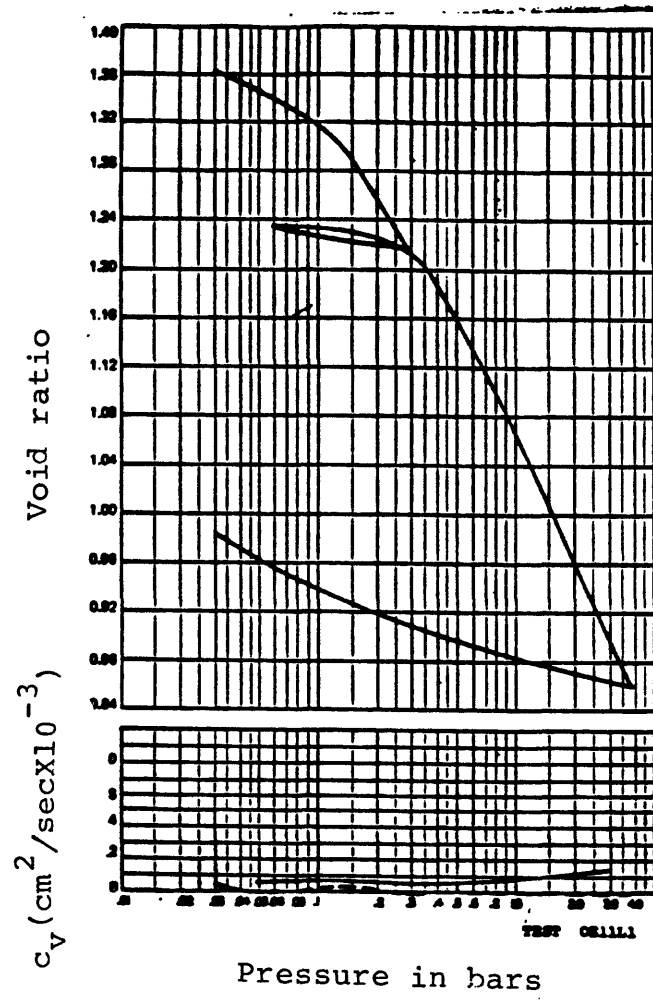




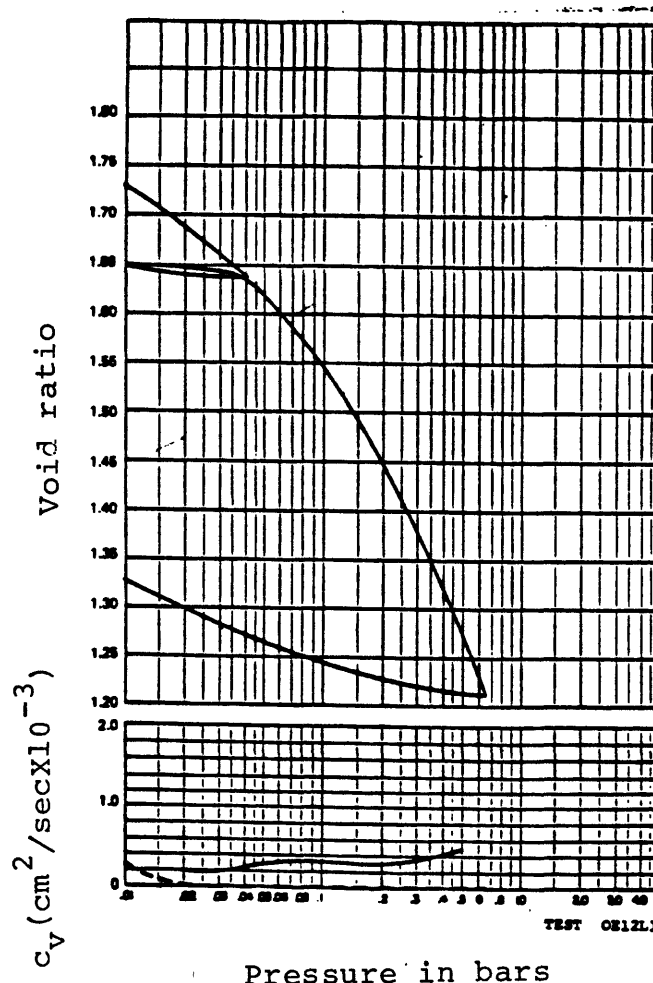
Pressure in bars



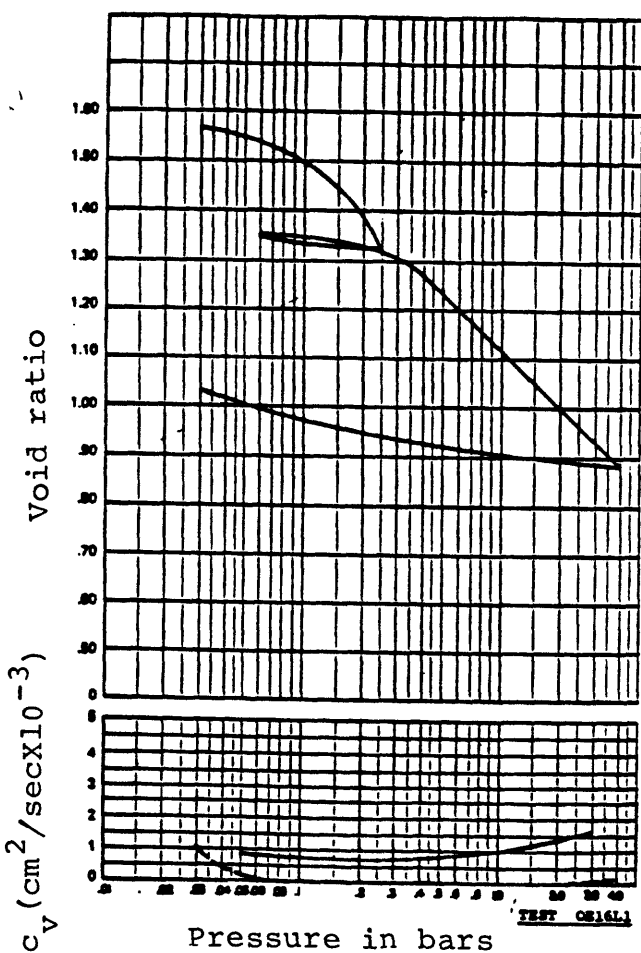
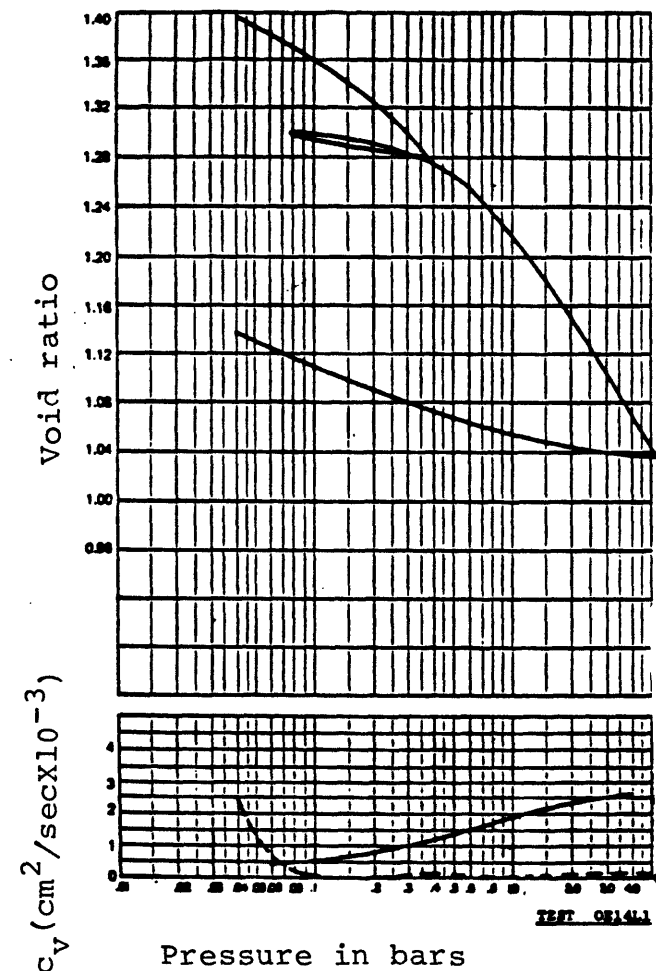
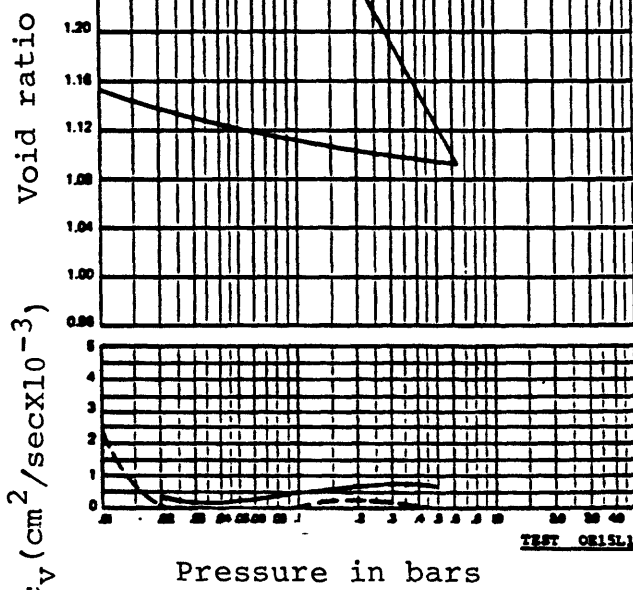
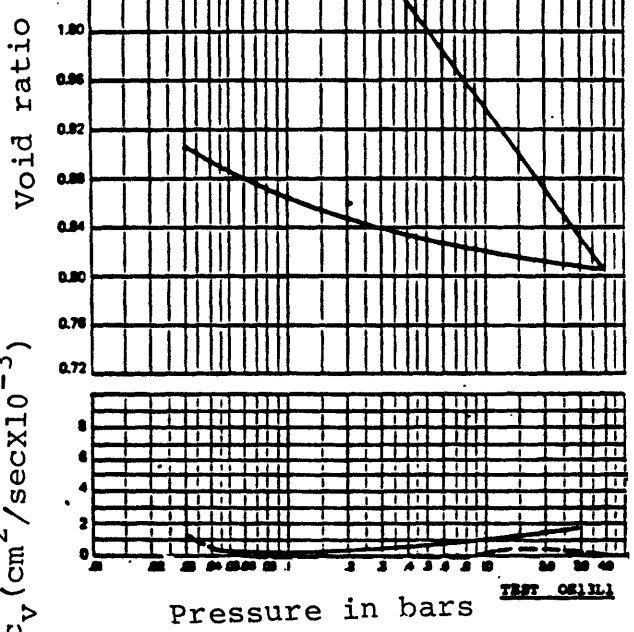
Pressure in bars

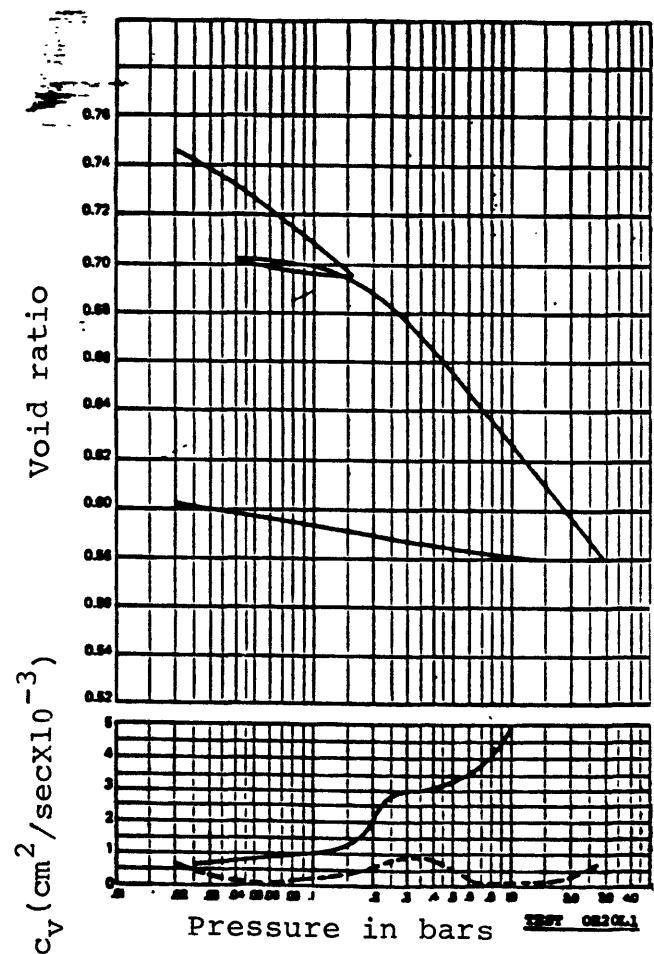
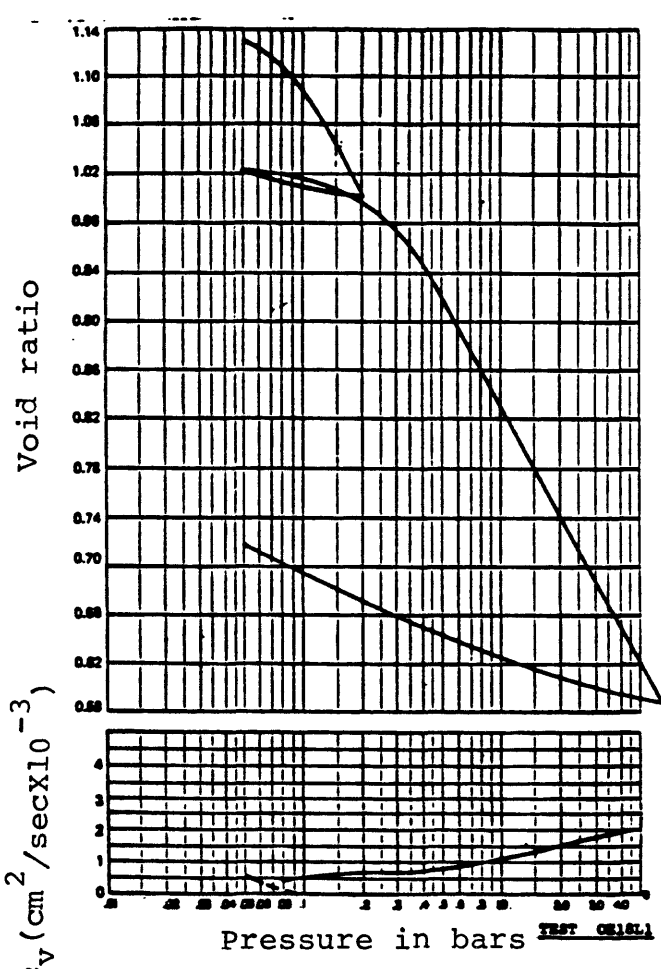
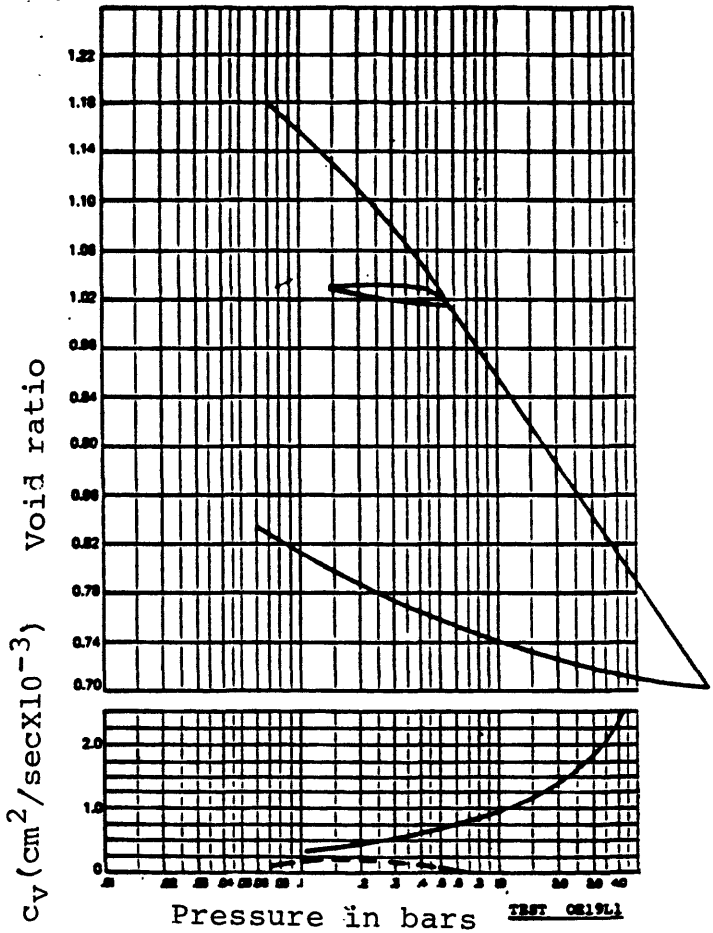
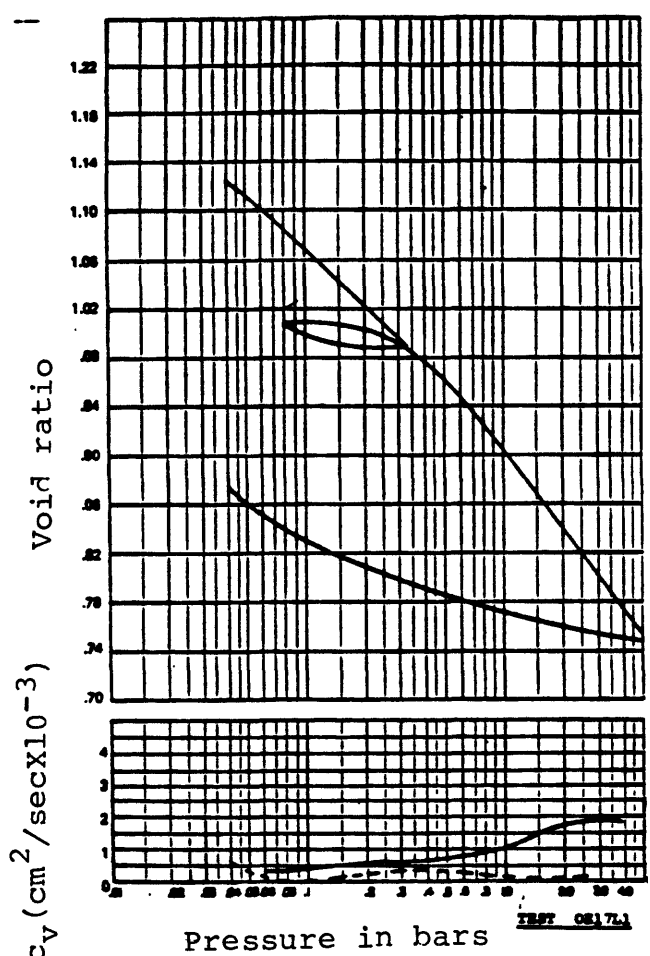


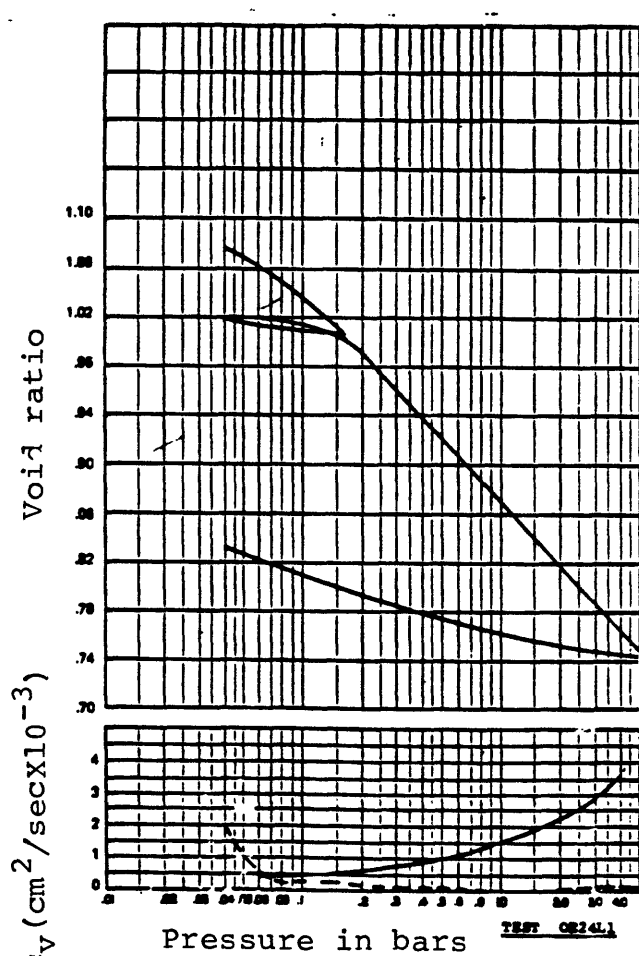
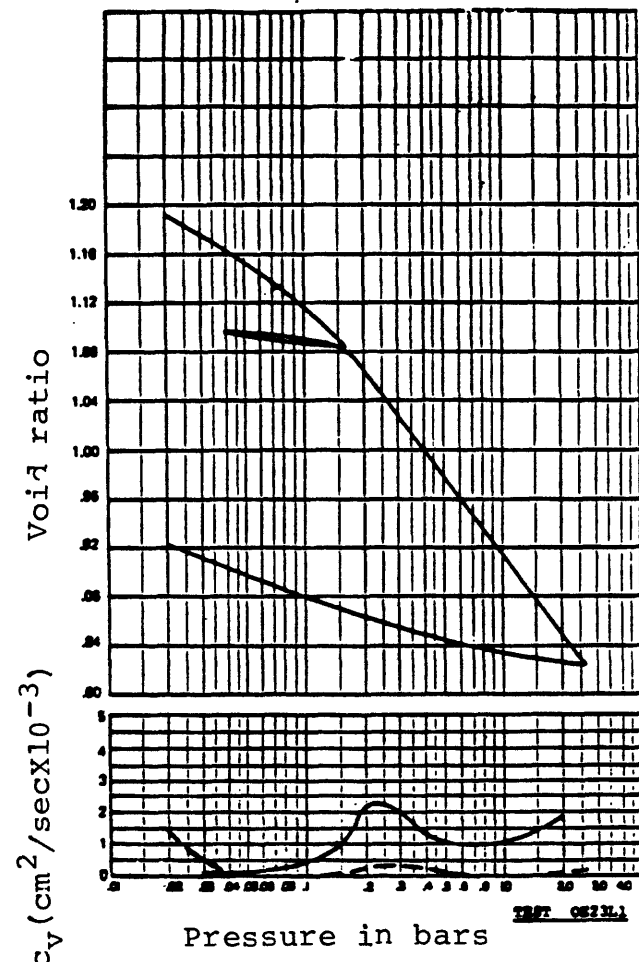
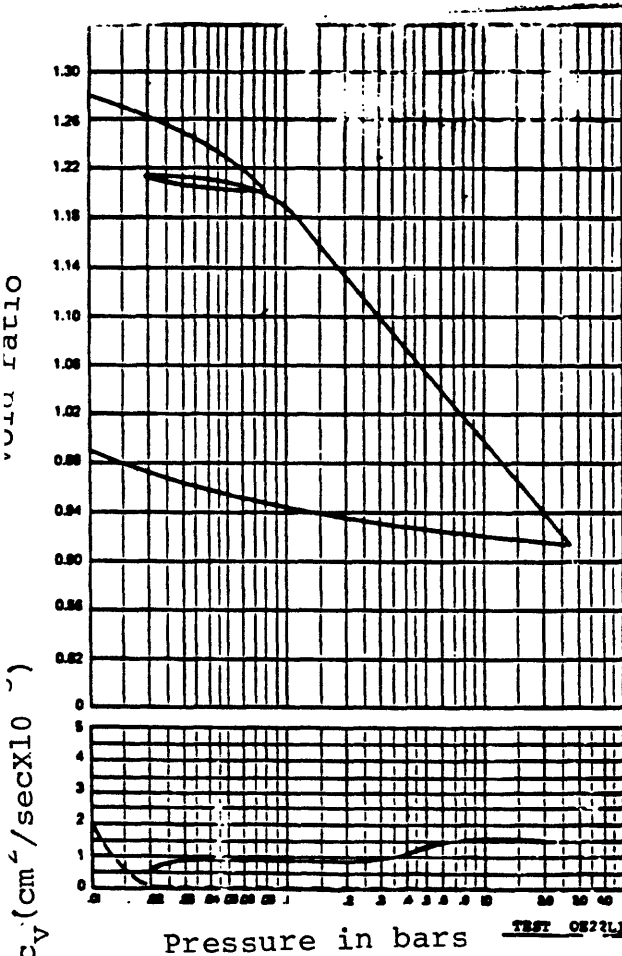
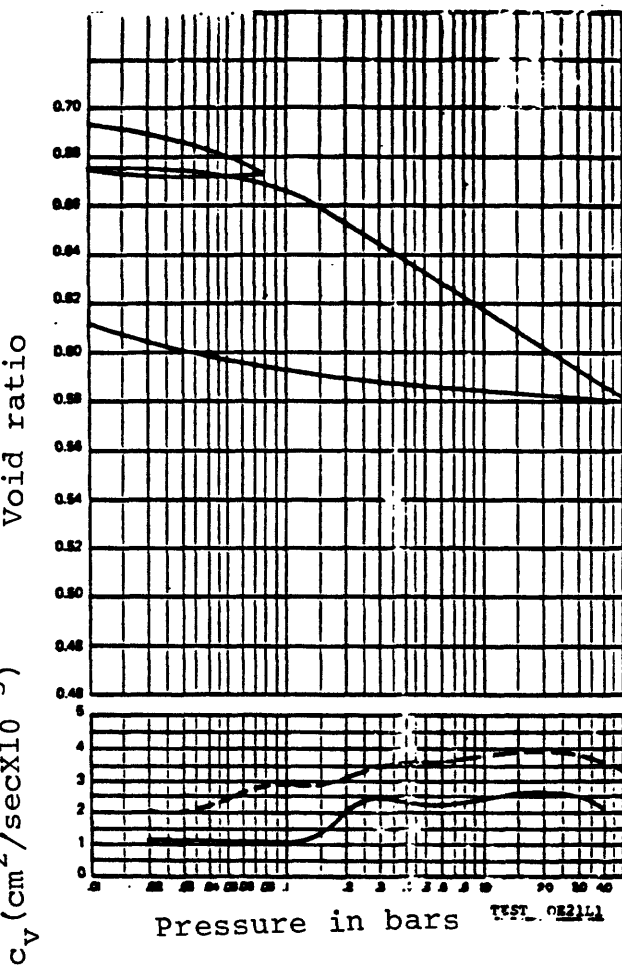
Pressure in bars

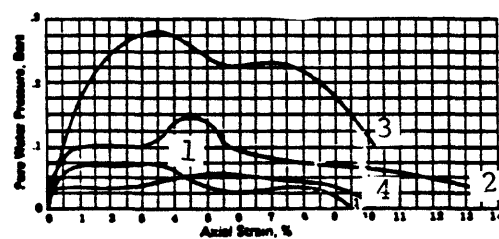
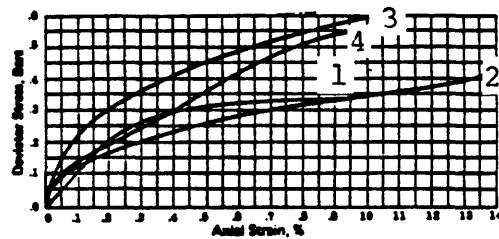
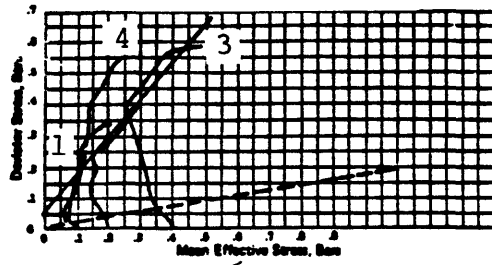


Pressure in bars

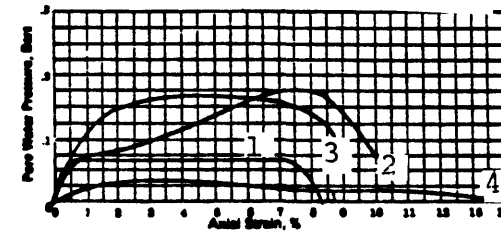
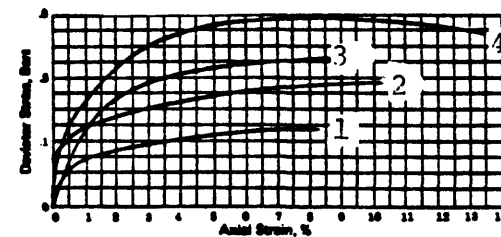
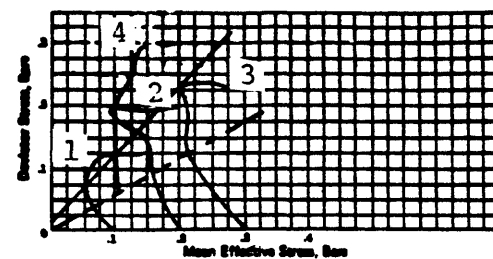




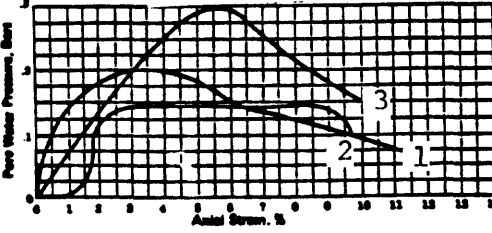
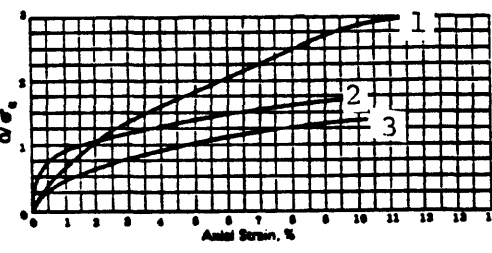
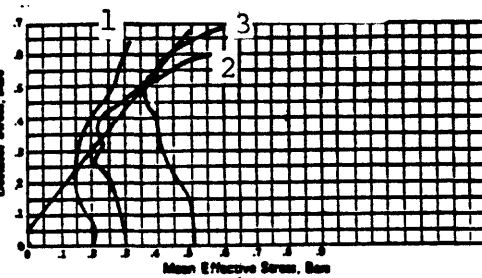




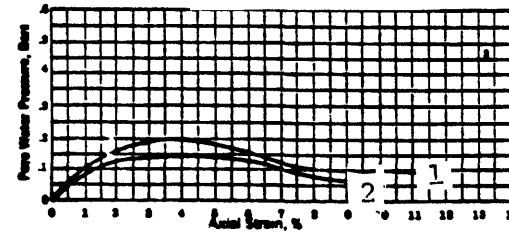
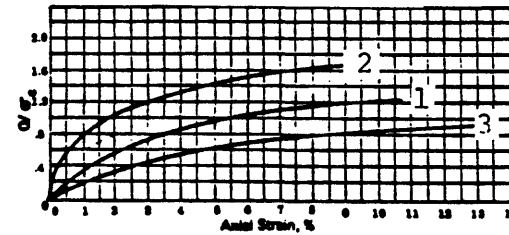
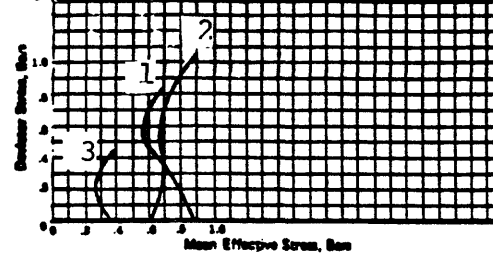
TESTS  
 (1) TE1LL1  
 (2) TE2LL1  
 (3) TE3LL1  
 (4) TE4LL1



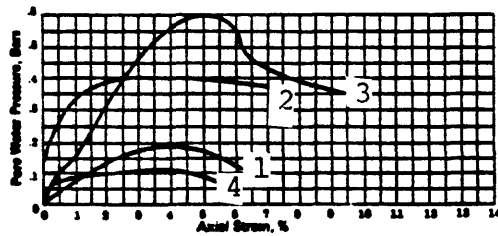
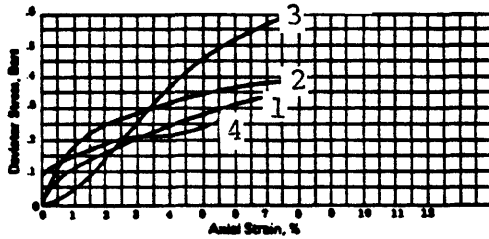
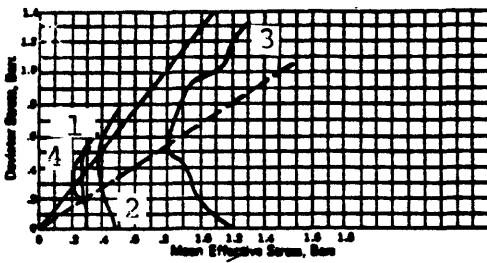
TESTS  
 (1) TE5LL1  
 (2) TE6LL1  
 (3) TE7LL1  
 (4) TE1OL1



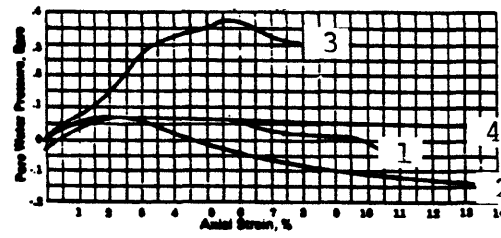
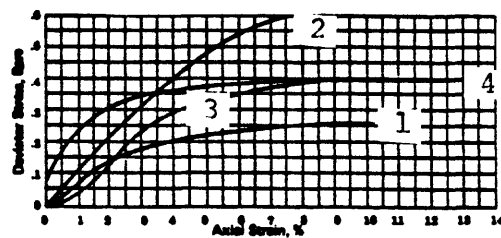
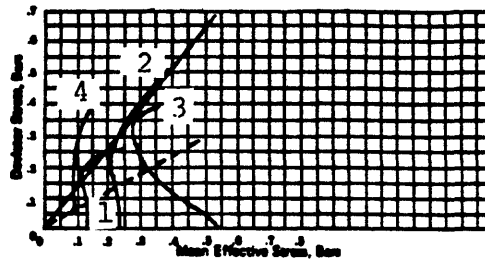
TESTS  
 (1) TE12L1  
 (2) TE13L1  
 (3) TE14L1



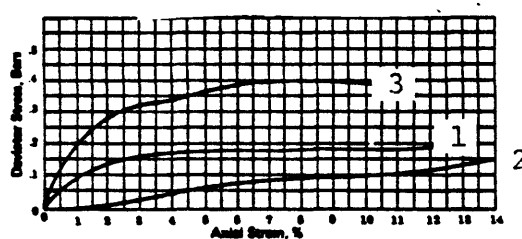
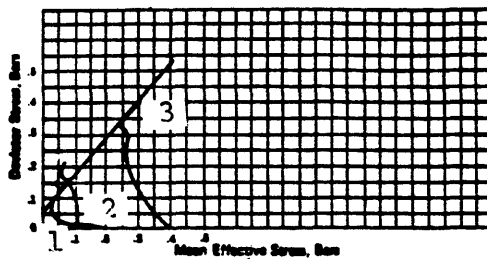
TESTS  
 (1) TE12L1  
 (2) TE13L1  
 (3) TE14L1



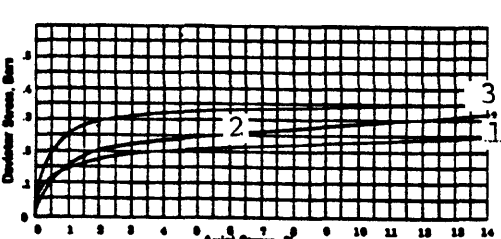
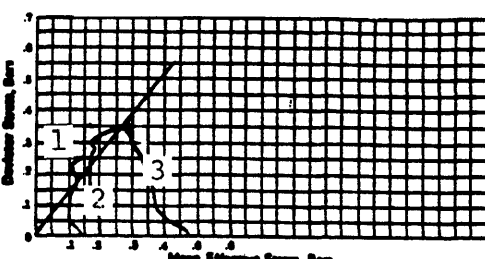
TESTS  
 (1) TE15L1  
 (2) TE16L1  
 (3) TE17L1  
 (4) TE18L1



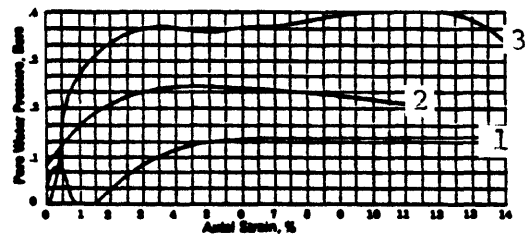
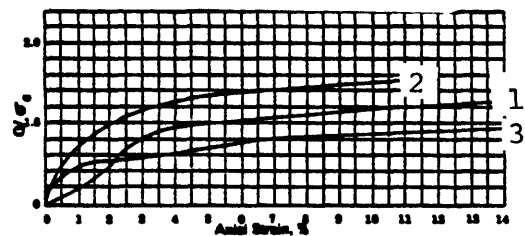
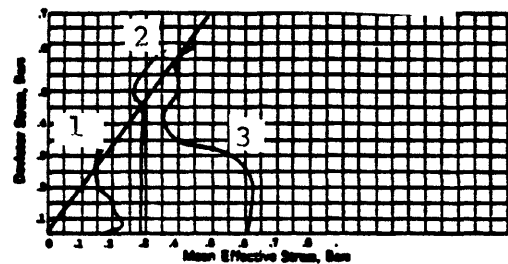
TESTS  
 (1) TE22L1  
 (2) TE23L1  
 (3) TE24L1  
 (4) TE25L1



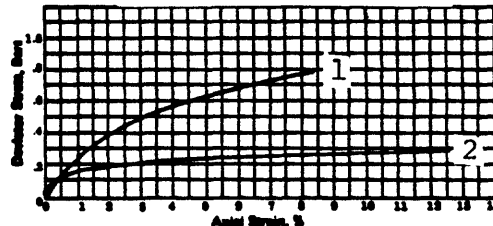
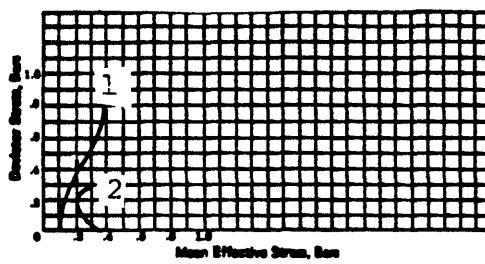
TESTS  
 (1) TE19L1  
 (2) TE20L1  
 (3) TE21L1



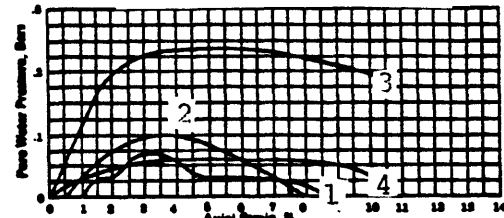
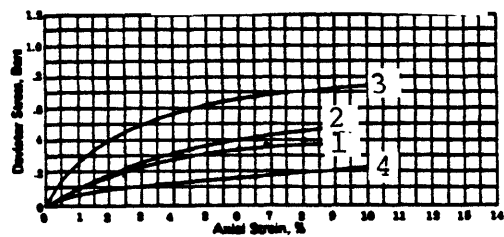
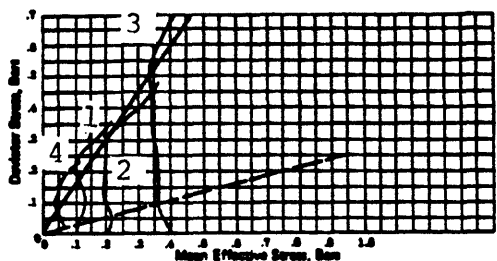
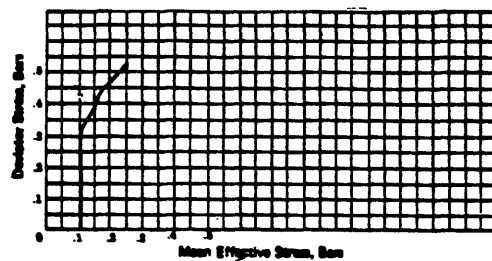
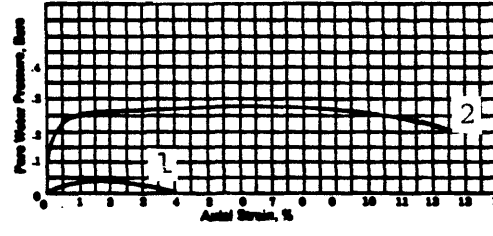
TESTS  
 (1) TE26L1  
 (2) TE27L1  
 (3) TE28L1



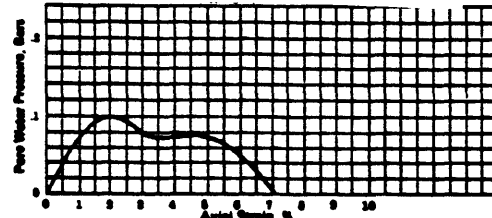
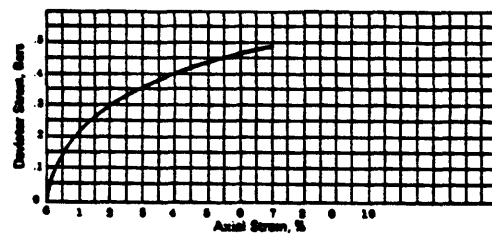
TESTS  
 (1) TE29L1  
 (2) TE30L1  
 (3) TE31L1



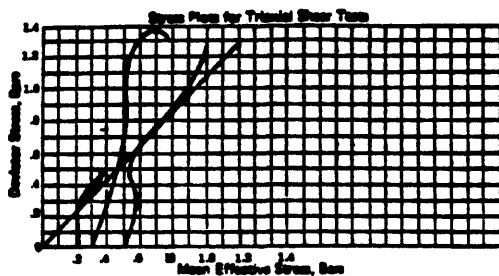
TESTS  
 (1) TE36L1  
 (2) TE37L1



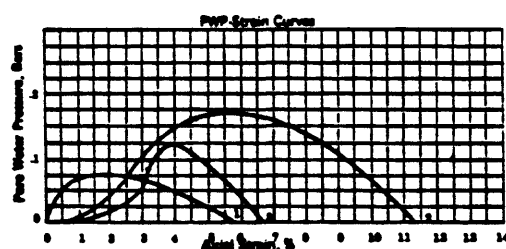
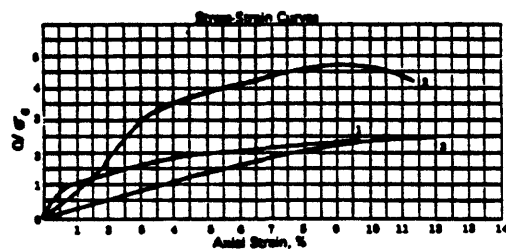
TESTS  
 (1) TE32L1  
 (2) TE33L1  
 (3) TE34L1  
 (4) TE35L1



TEST TE36L1



Cohesion, C \_\_\_\_\_  
Angle of Shear Resistance \_\_\_\_\_



TESTS  
(1) TE39L1  
(2) TE40L1  
(3) TE41L1

Stress Corrected Test

Curve No.	(1)	(2)	(3)	(4)
Confining Pressure Bar	.30	.30	.30	
Initial Length, mm	7.1	8.7	10.3	
Initial Diameter, mm	2.00	2.00	2.10	
Wet Unit Weight, graves	1.80	1.75	1.80	
Moisture Content, %	49.70	49.80	49.70	
Initial Void Ratio	1.17	1.20	1.20	
Initial Percent Saturated	99	98	98	

Consolidated Undrained  
Triaxial Shear Test  
with Pore Pressure Measurements  
CORE 470  
CRUZER 88-77-88  
Date 6-17-78  
Job No. 16-0097

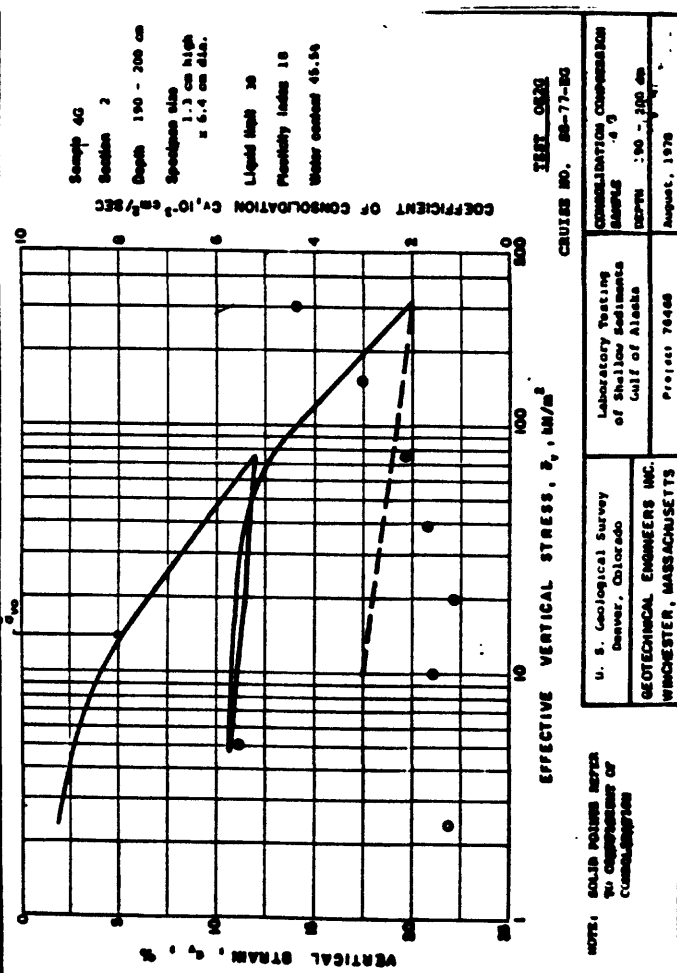
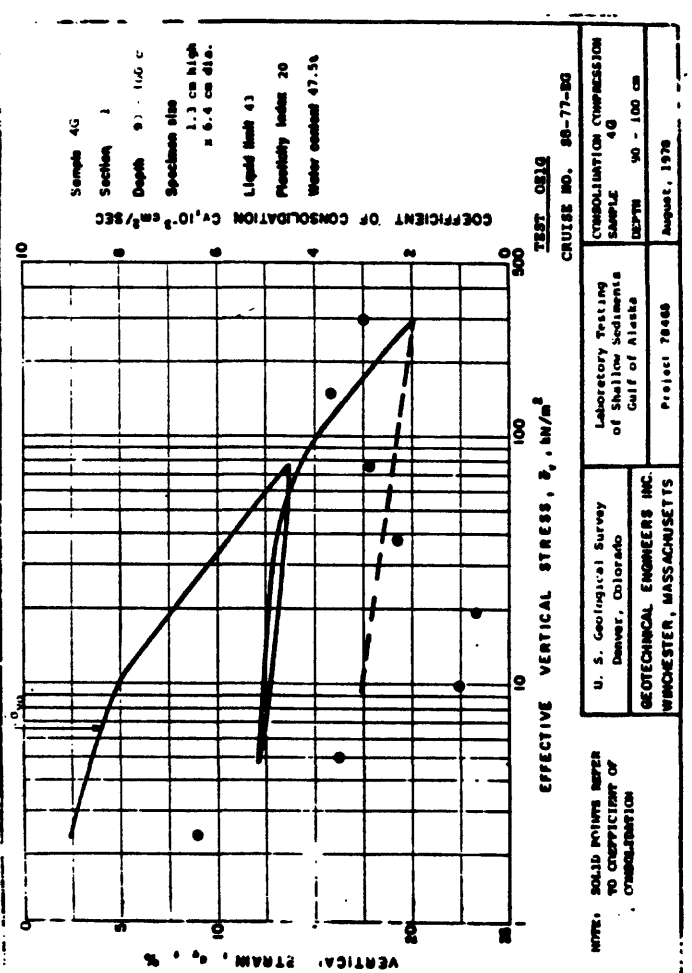
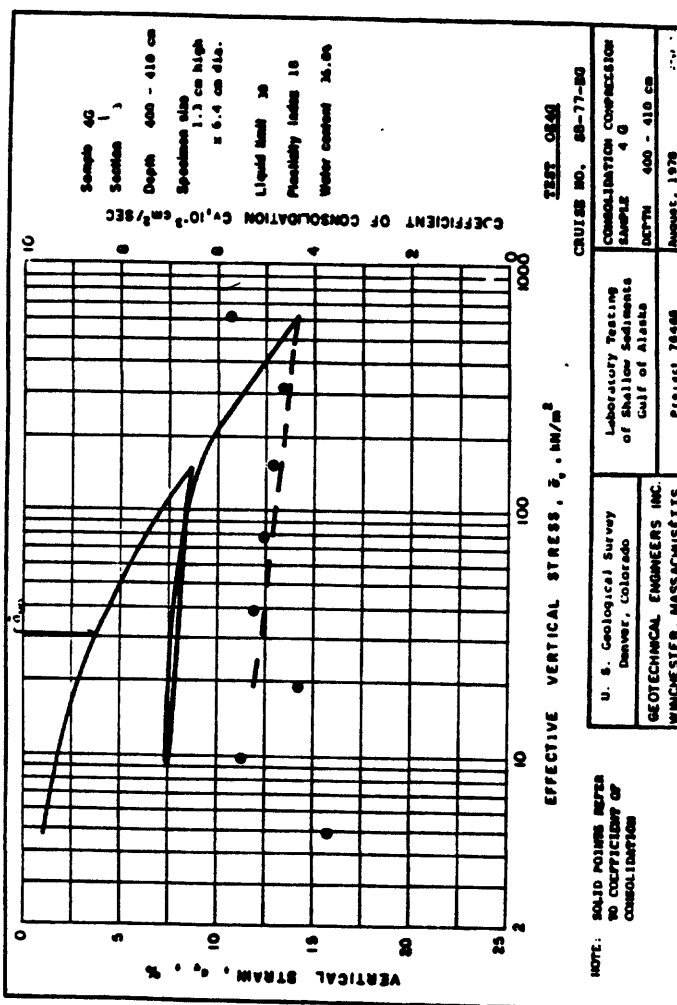
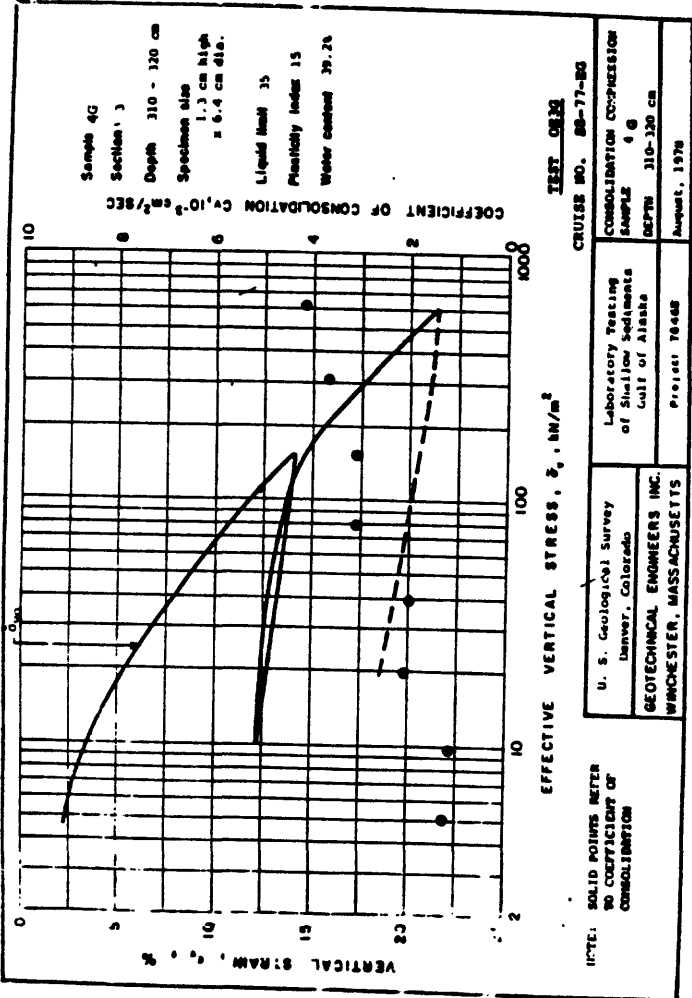
LAW ENGINEERING TESTING COMPANY

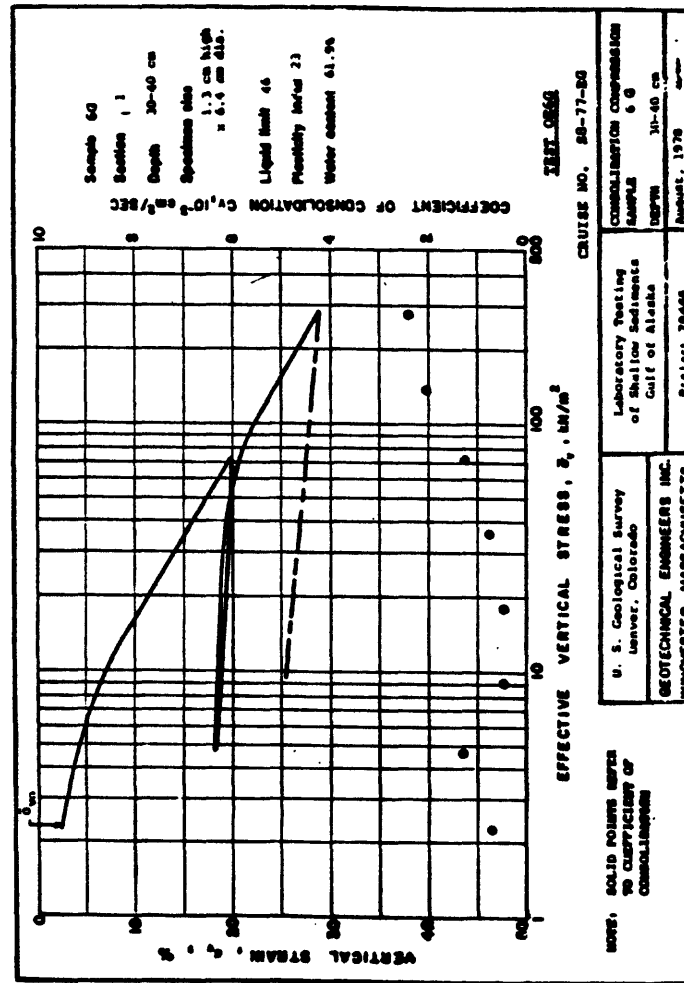
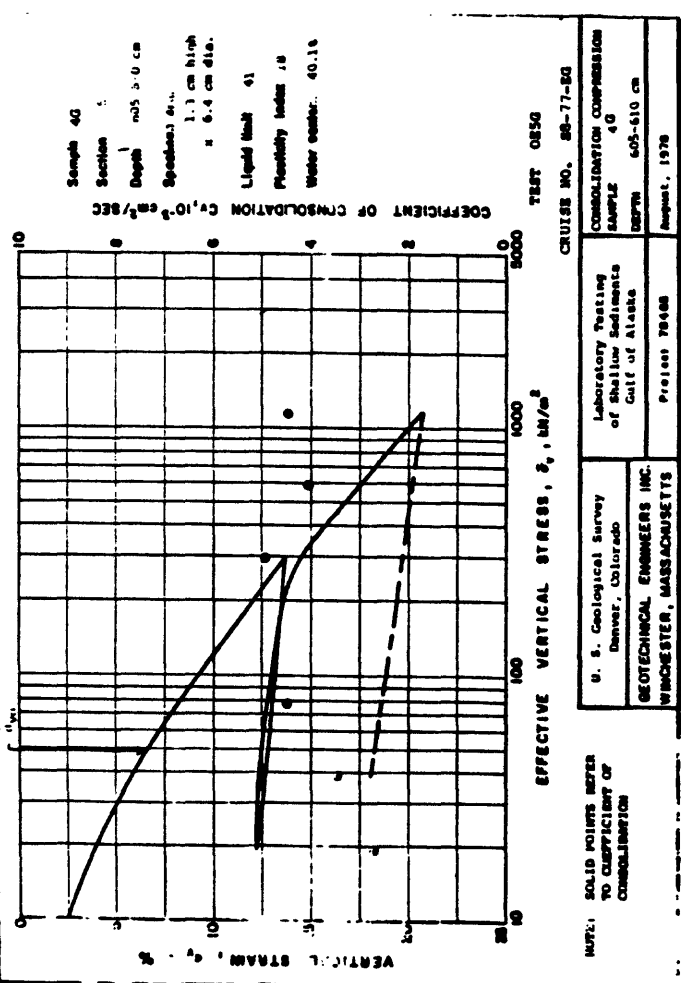
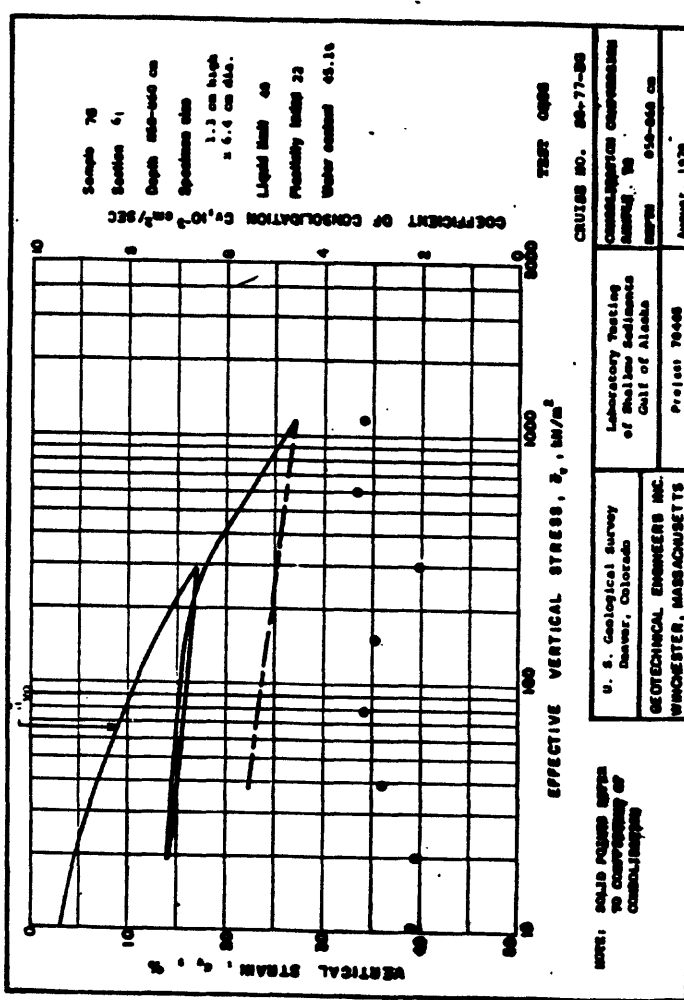
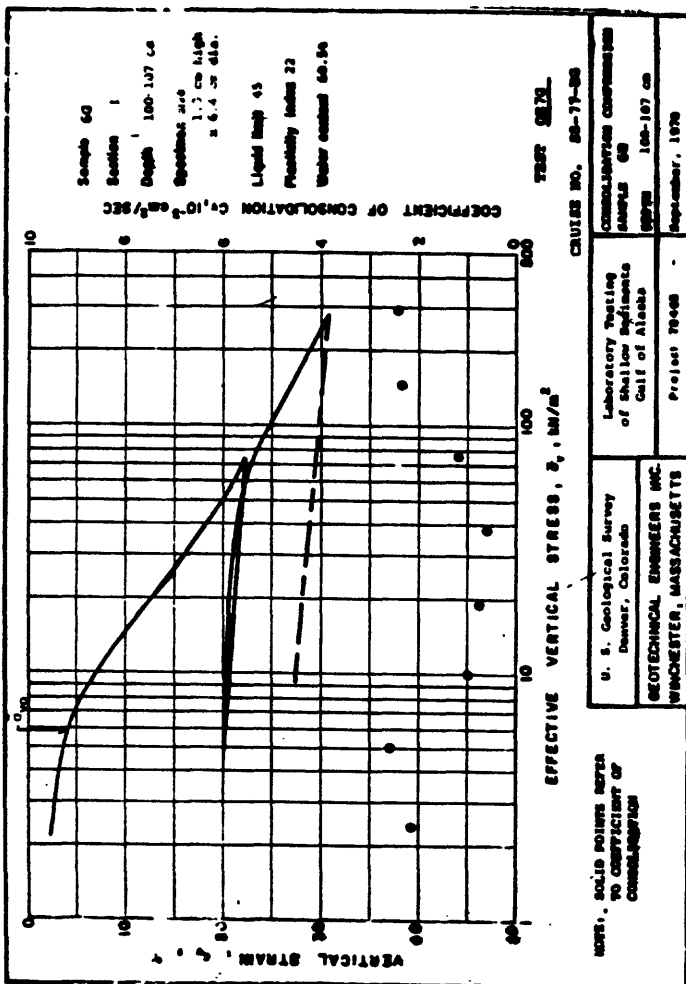
APPENDIX E. CONSOLIDATION AND TRIAXIAL TEST RESULTS-GEOTECHNICAL ENGINEERS,  
INCORPORATED (1977 cores)

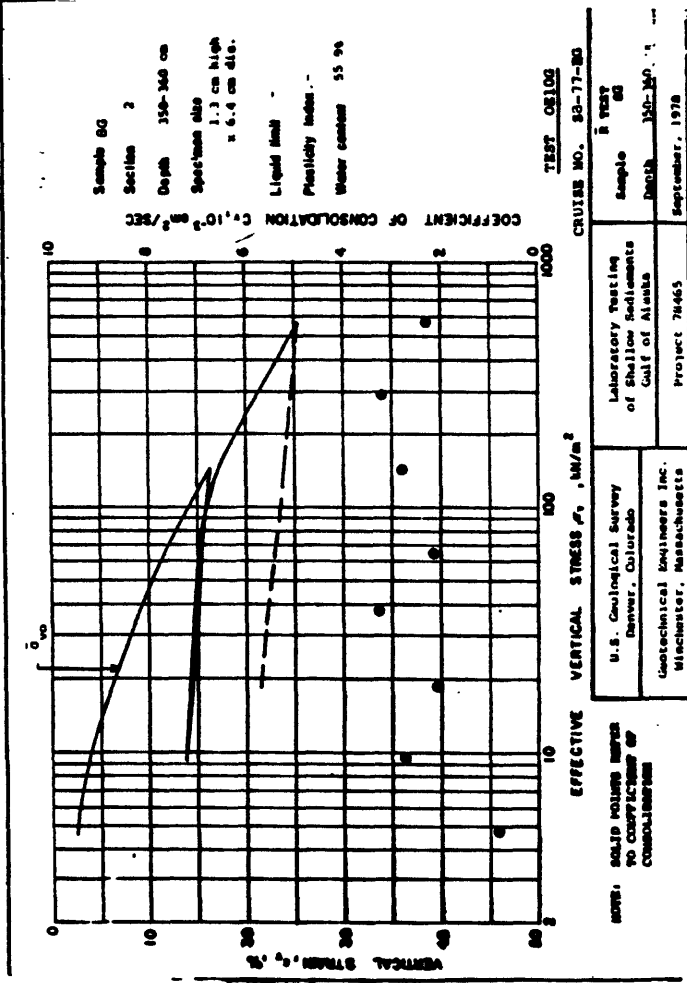
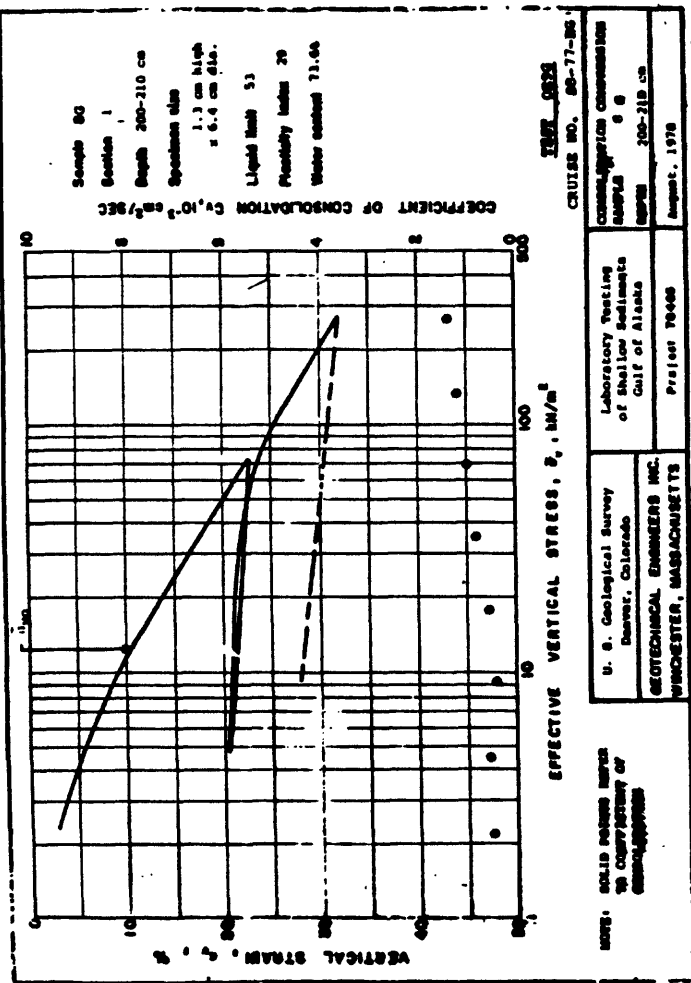
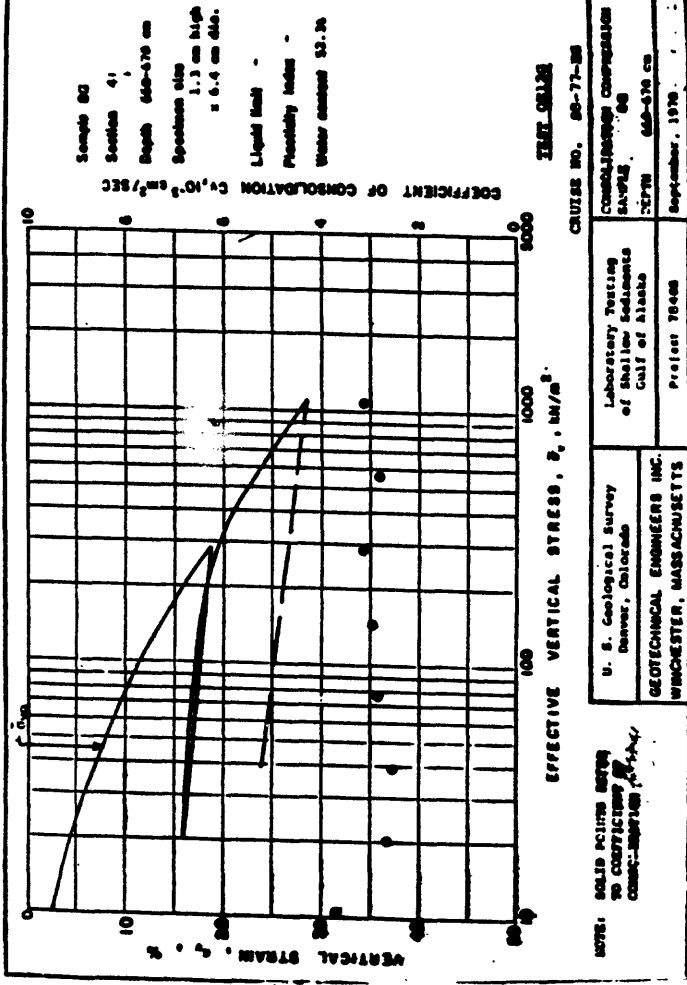
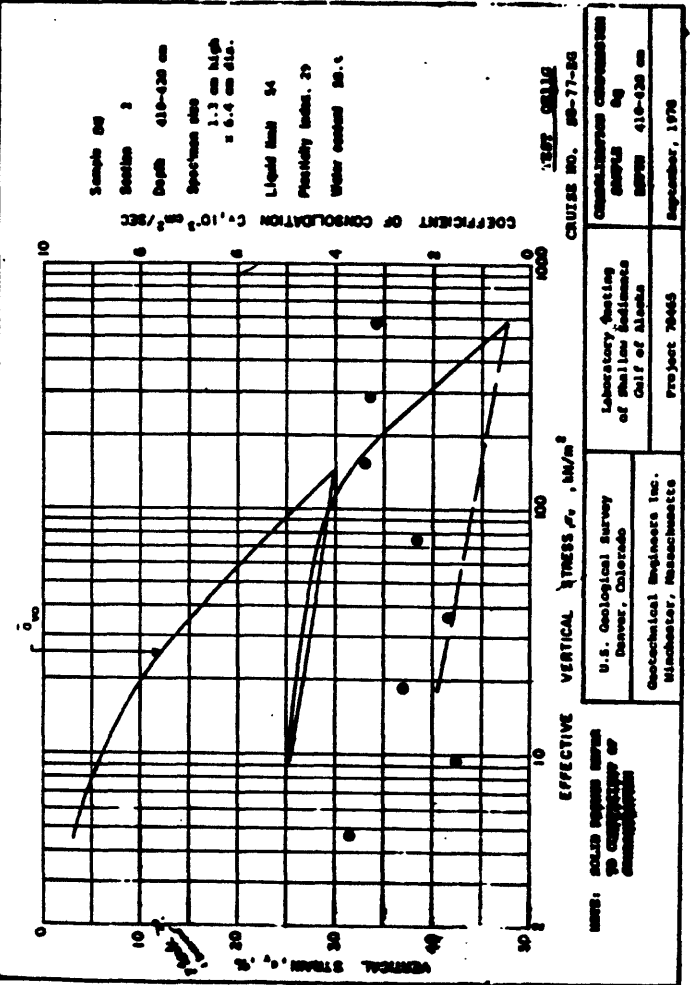
This appendix presents the results of consolidation and static triaxial tests performed by Geotechnical Engineers, Incorporated under Contract number 14-08-0001-17353 with the U.S. Geological Survey. Testing was performed under the direction of K. Dalenberg and D.P. LaGatta. Cores were from Cruise S8-77-EG.

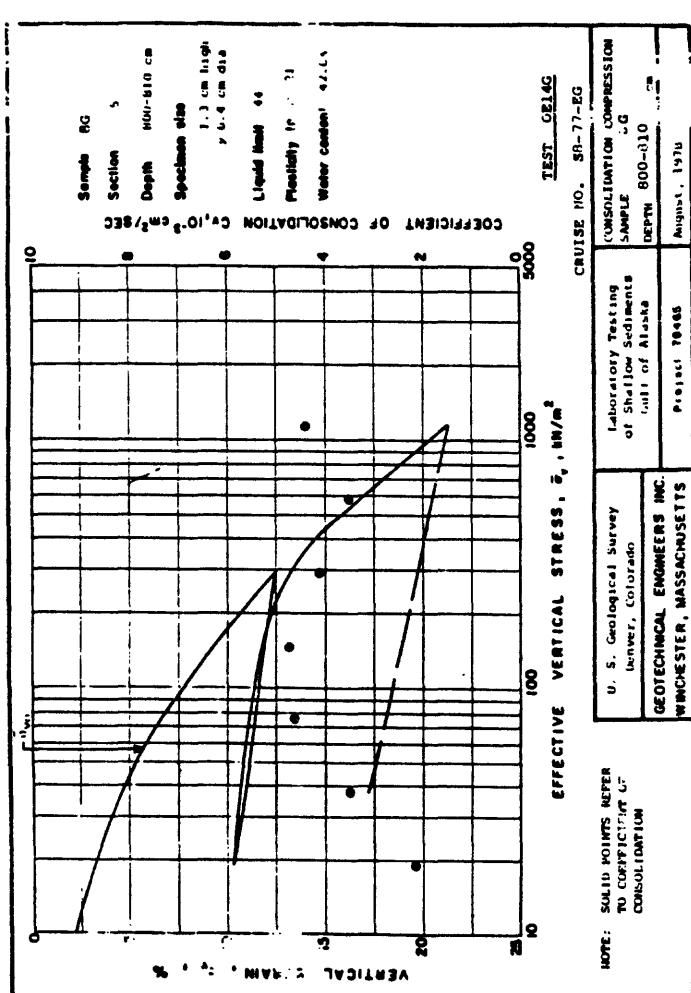
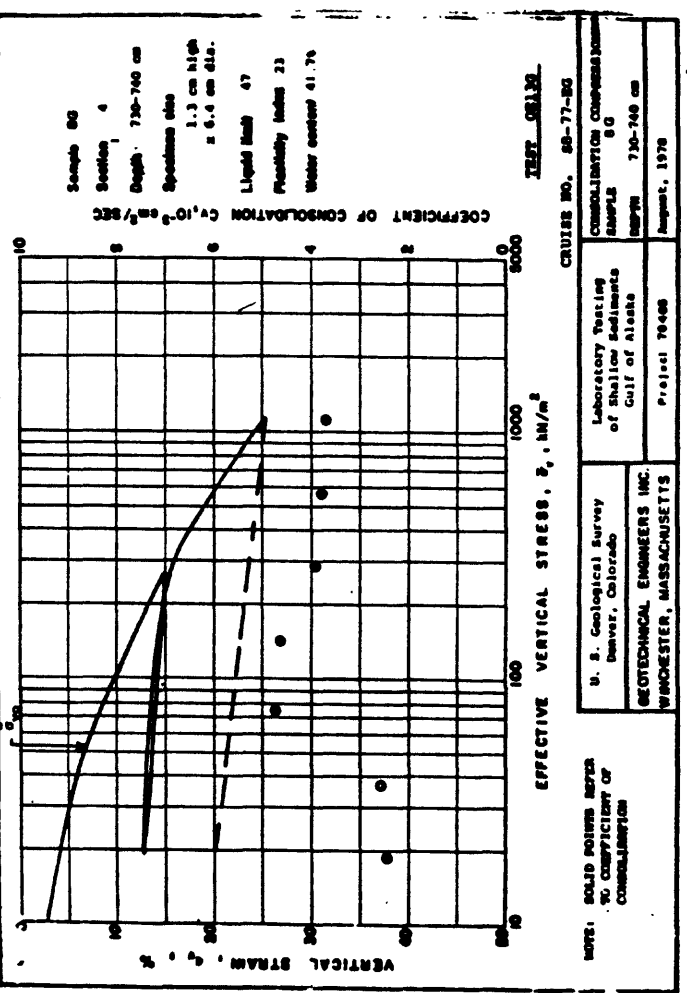
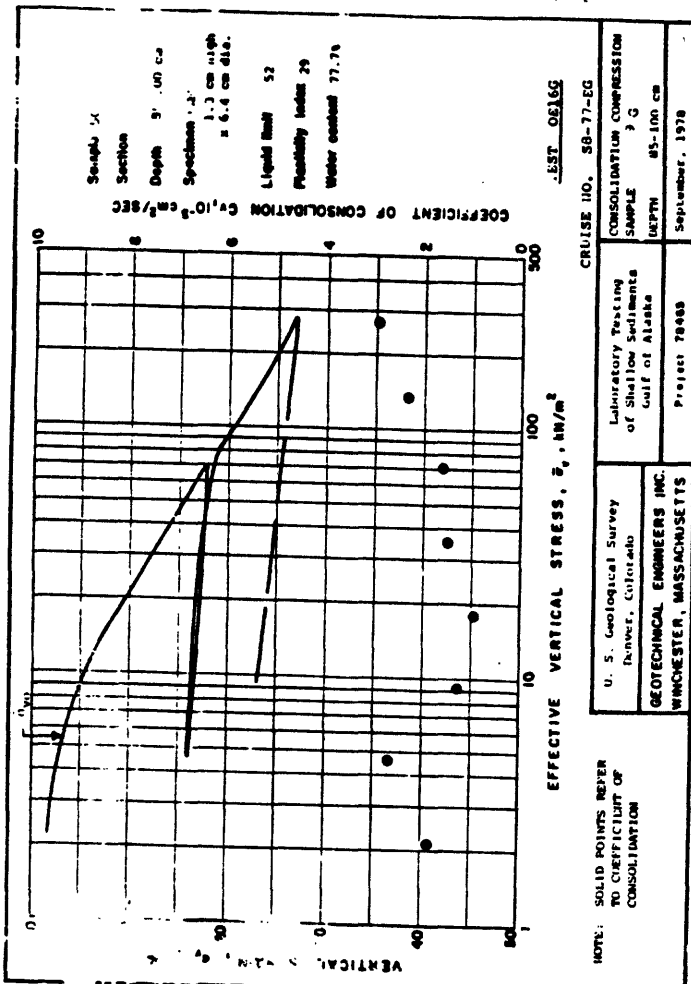
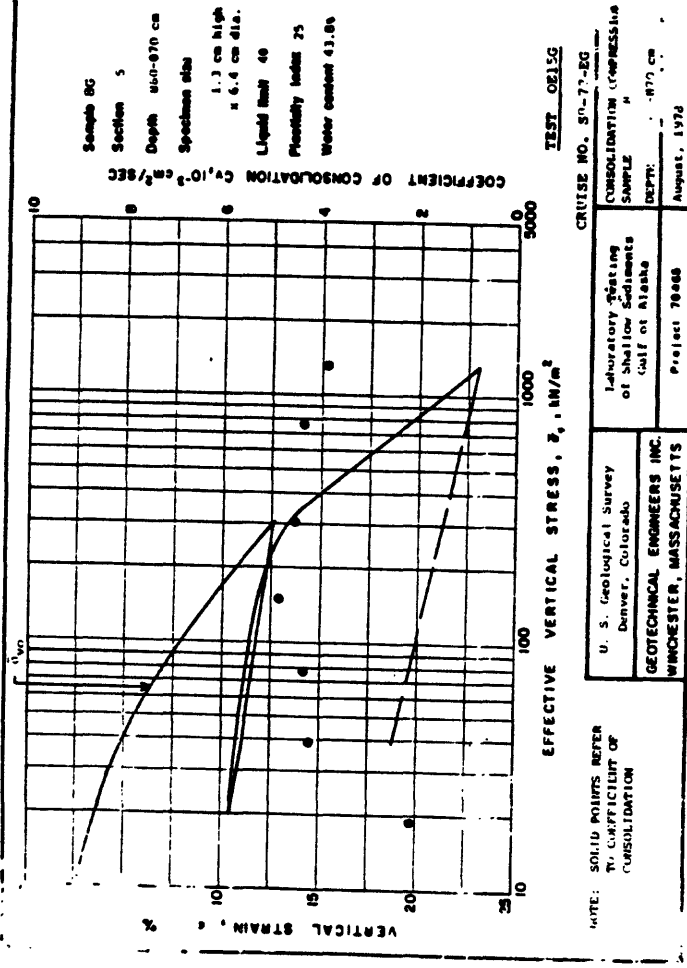
All tests in this group have been assigned a test number with G as the last character. The consolidation tests (first two characters are OE) are presented first and are ordered by test number. Results from a single test are presented on a page in the form of vertical strain and calculated coefficient of consolidation ( $c_v$ ) versus the vertical effective stress in kPa (equivalent to  $\text{kN/m}^2$ ).

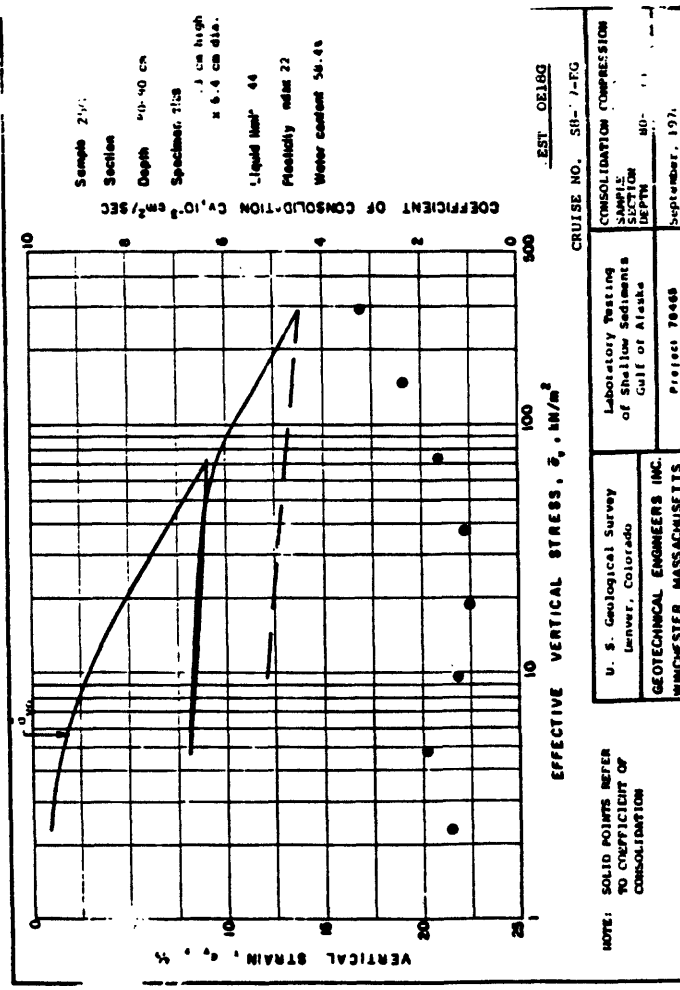
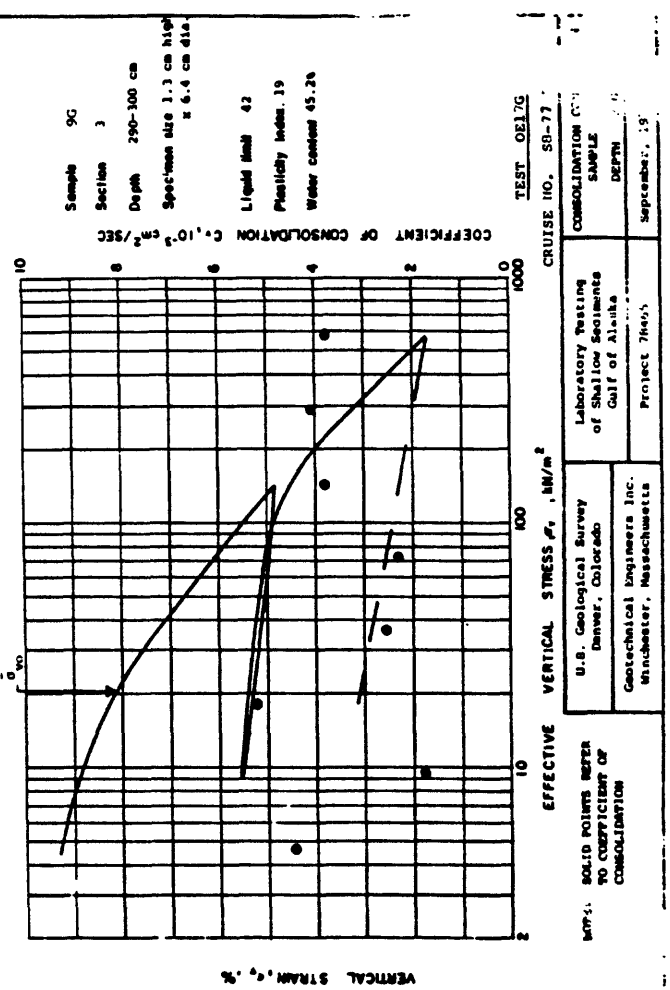
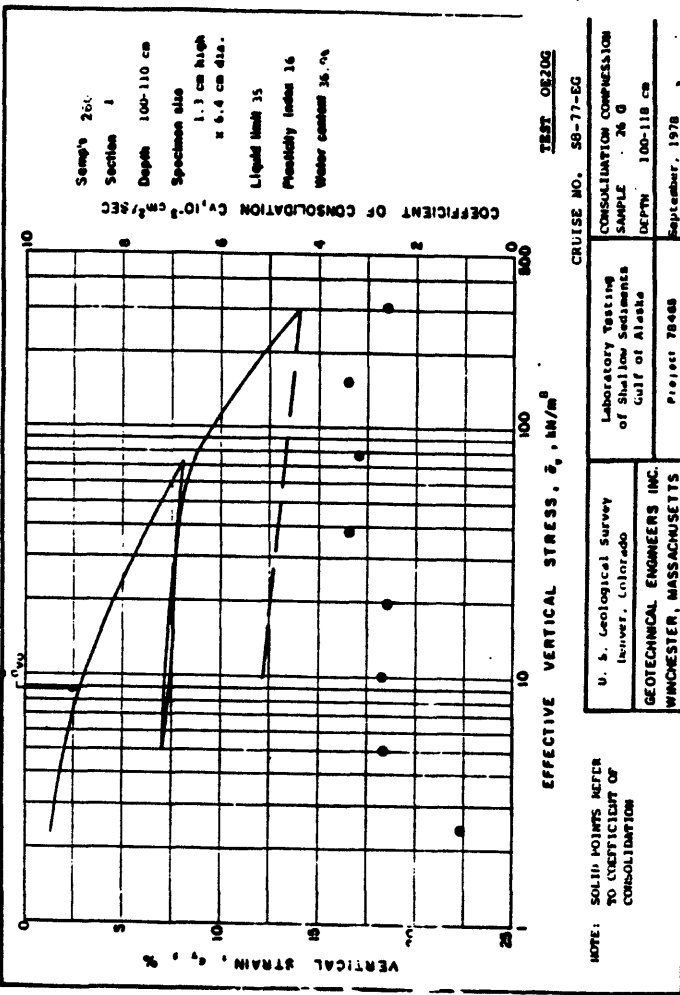
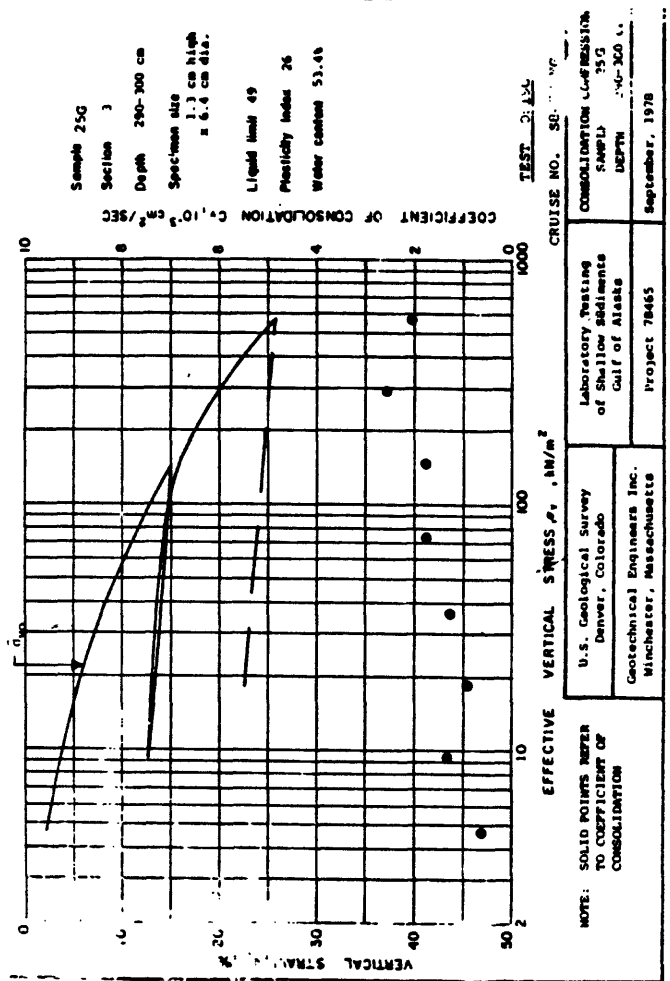
The static triaxial tests (first two characters are TE) are given second and ordered by test number. Results from a single test are given on a single page. The upper left plot is the maximum shearing stress or  $(\sigma_1 - \sigma_3)/2$  versus the axial strain. The upper right plot is a stress path presenting the maximum shearing stress versus the normal effective stress on the plane of maximum shearing stress or  $(\sigma_1' + \sigma_3')/2$ . In Appendices F and G, the stress path plots are defined in the same way but identified as  $q$  versus  $p'$ . The stress path plots of Appendix D are defined differently. The lower left plot is the excess pore water pressure developed during shear ( $u - u_o$ ) versus the axial strain.

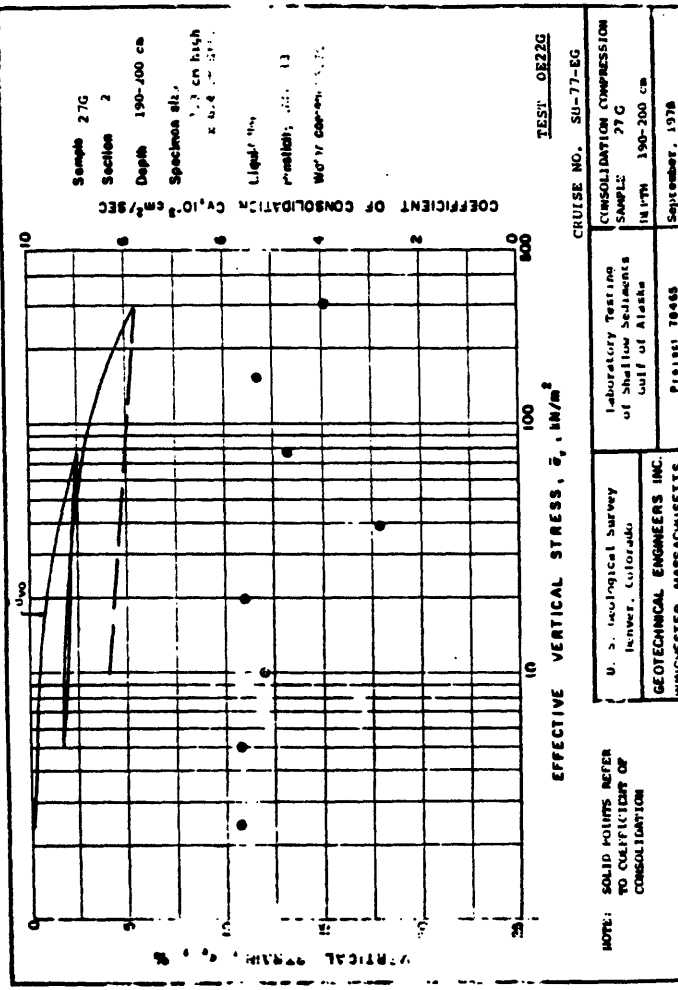
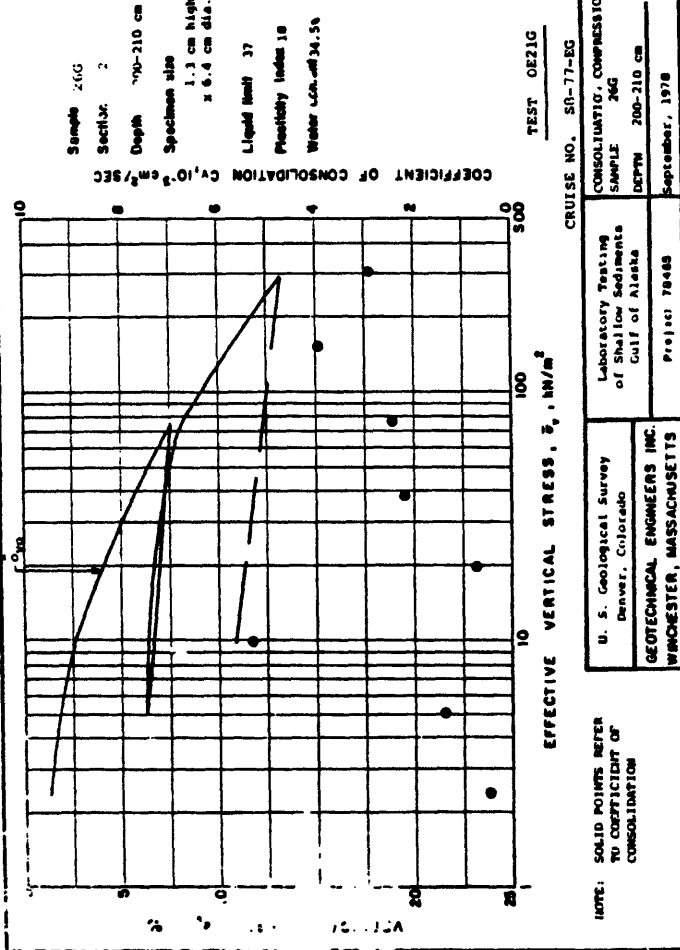
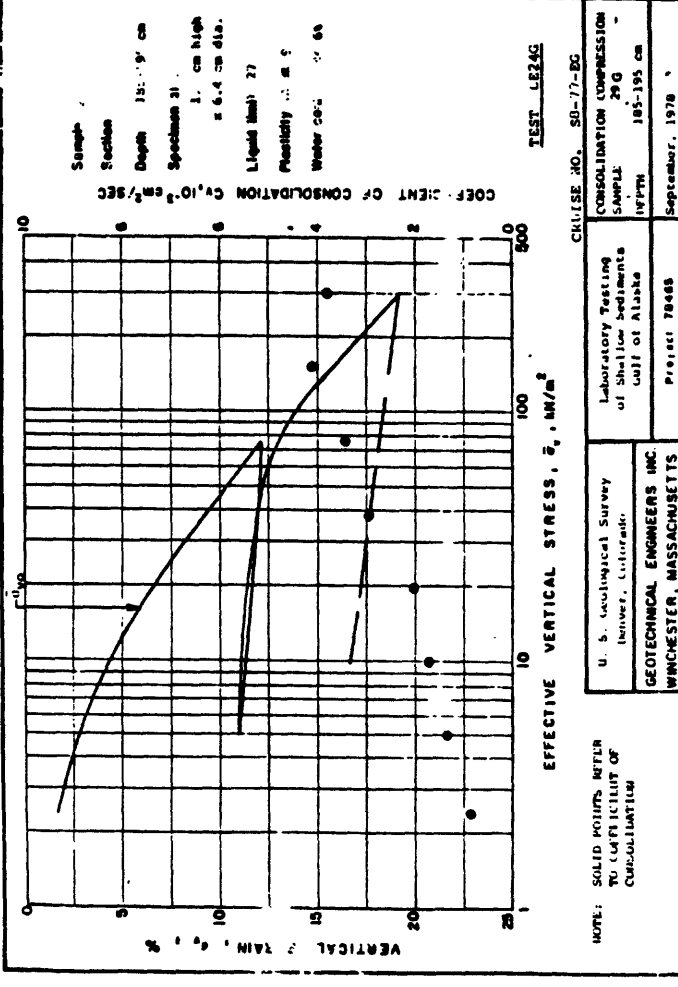
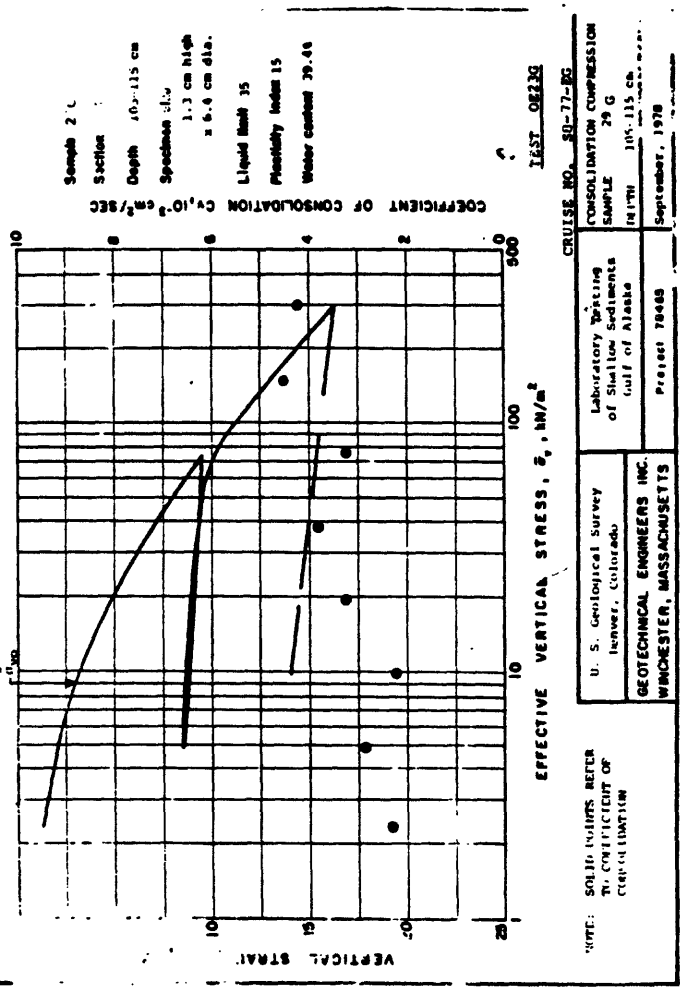


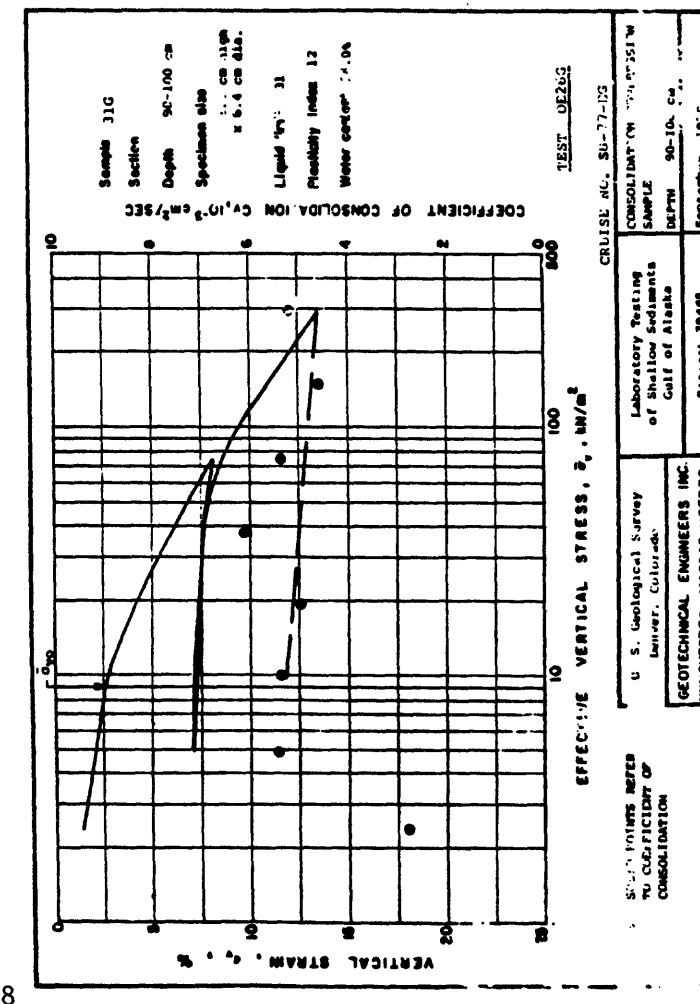
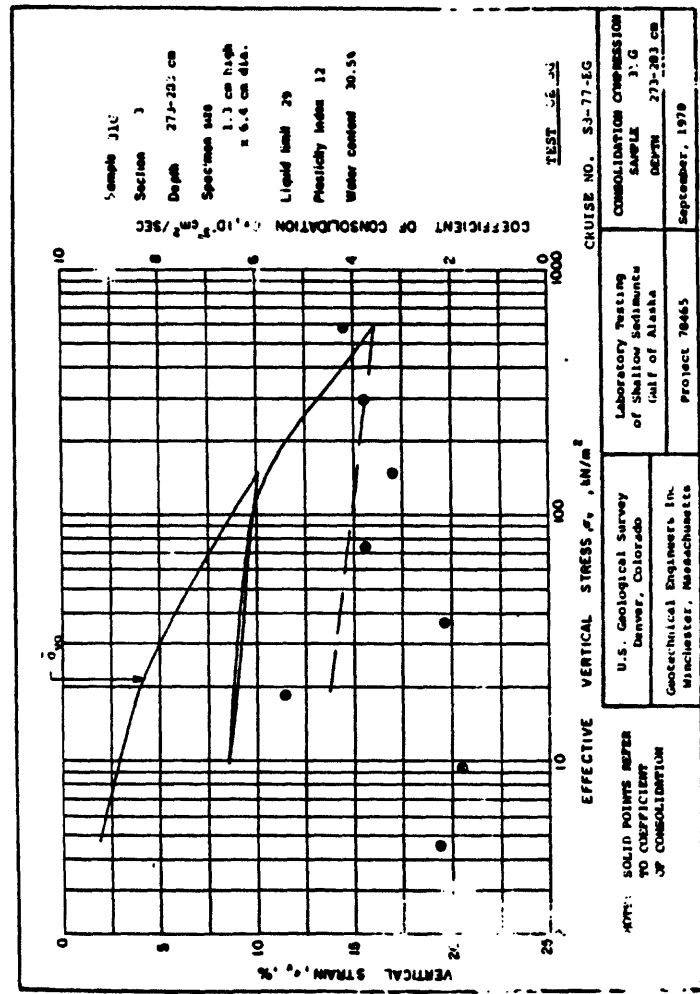
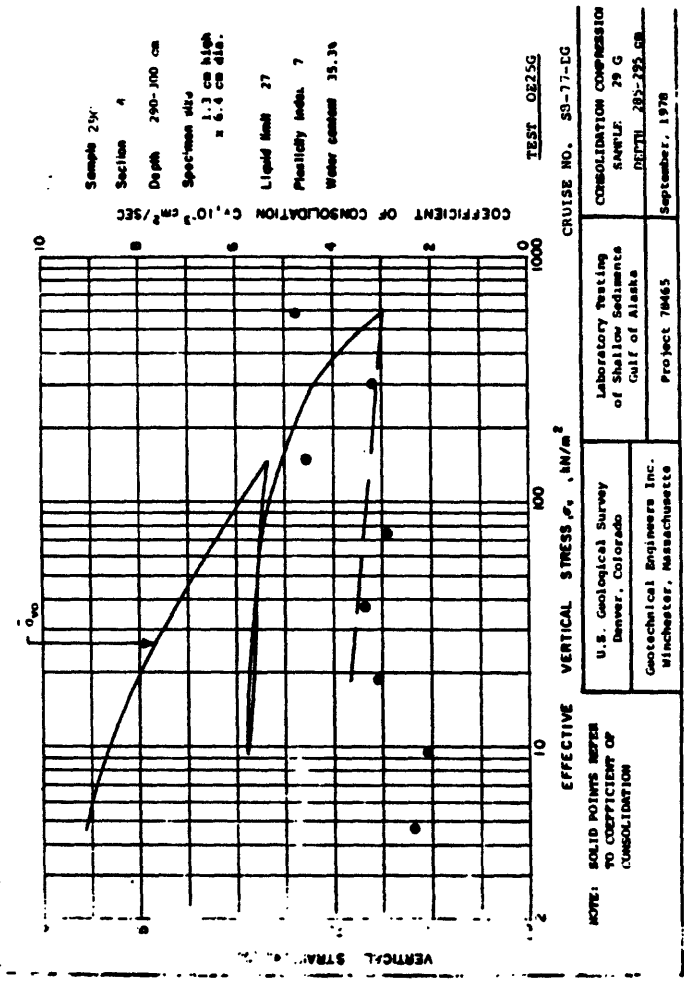
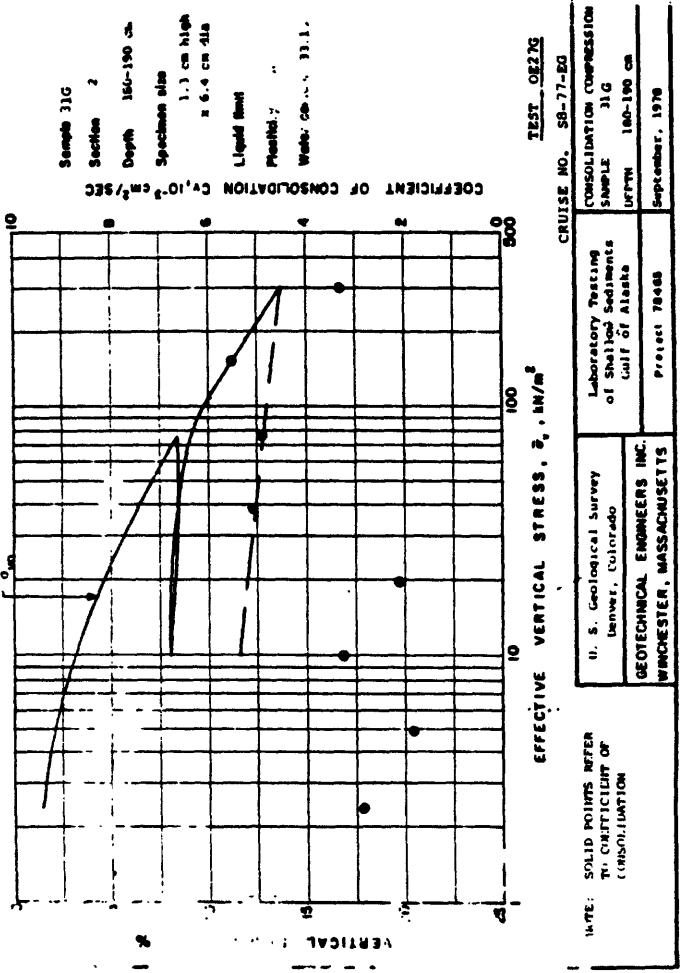


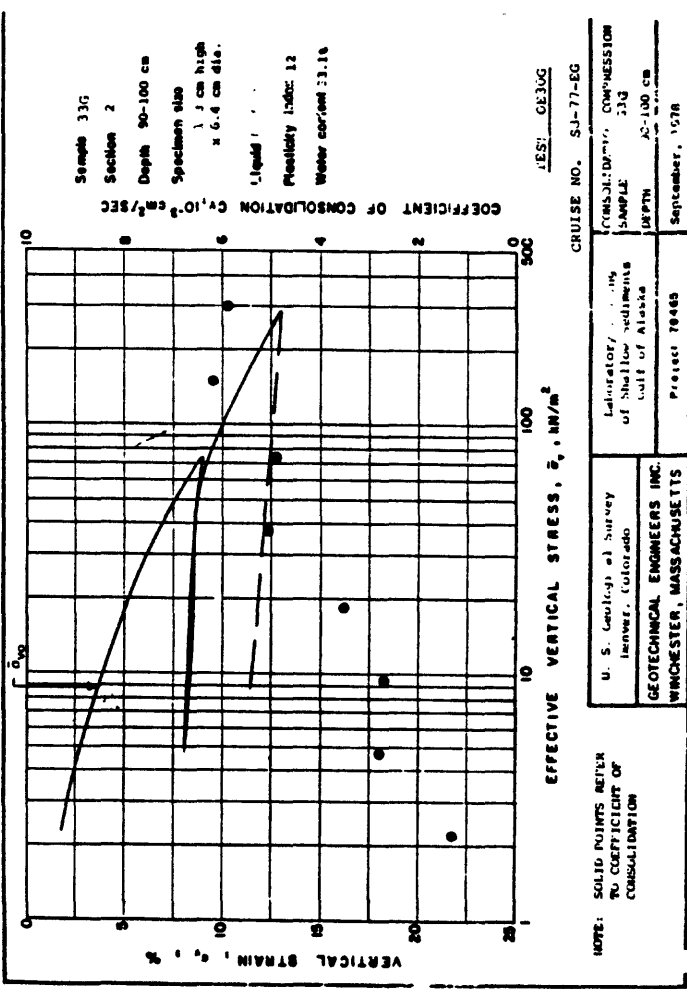
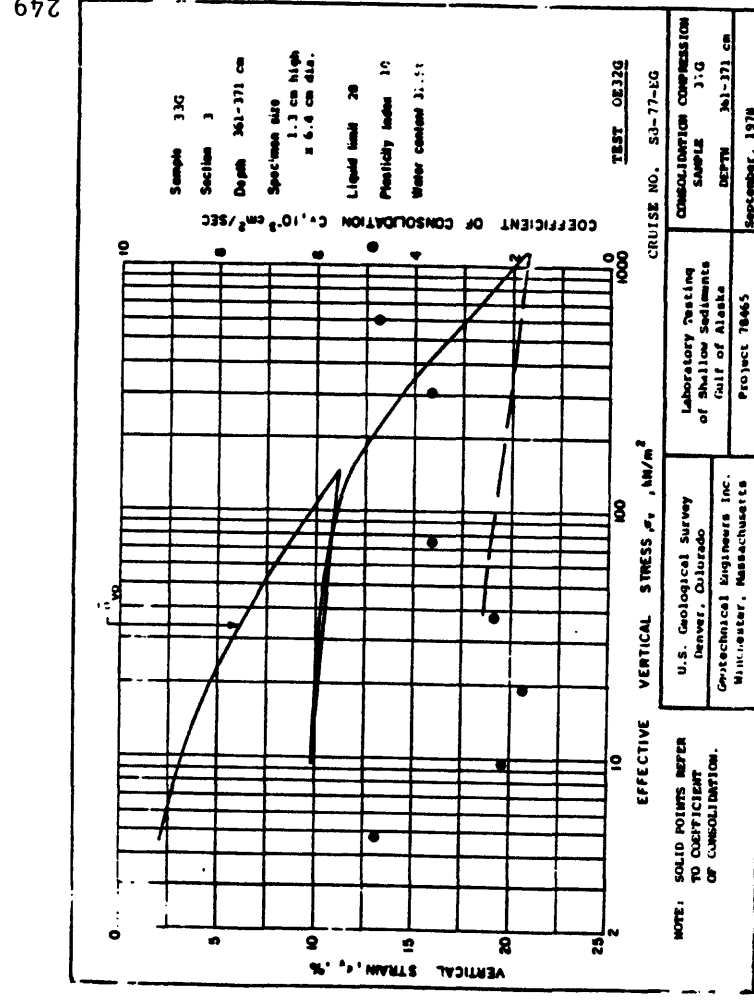
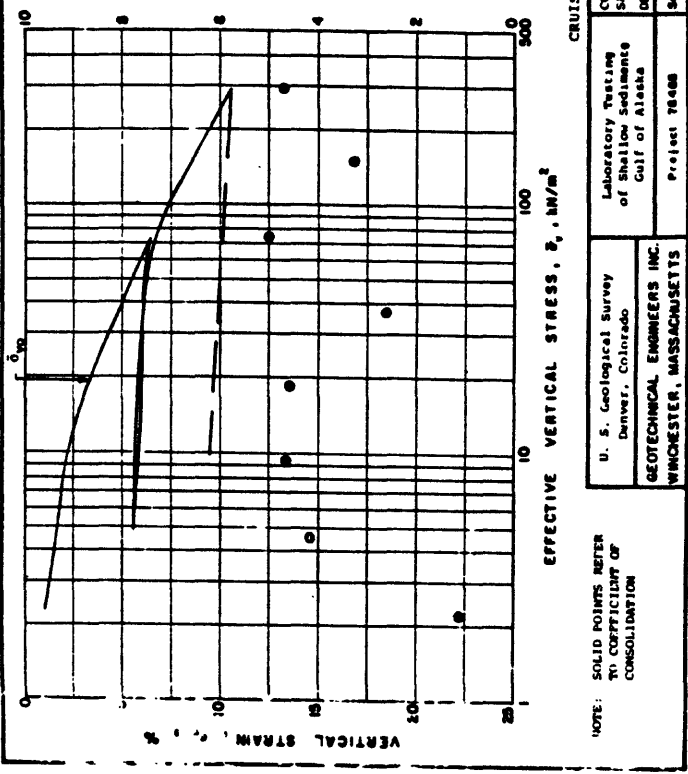
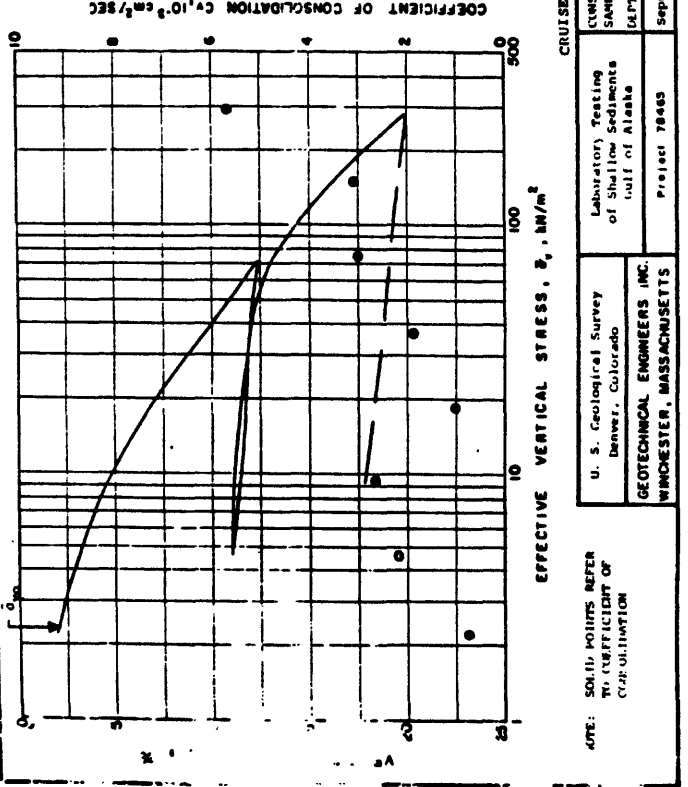


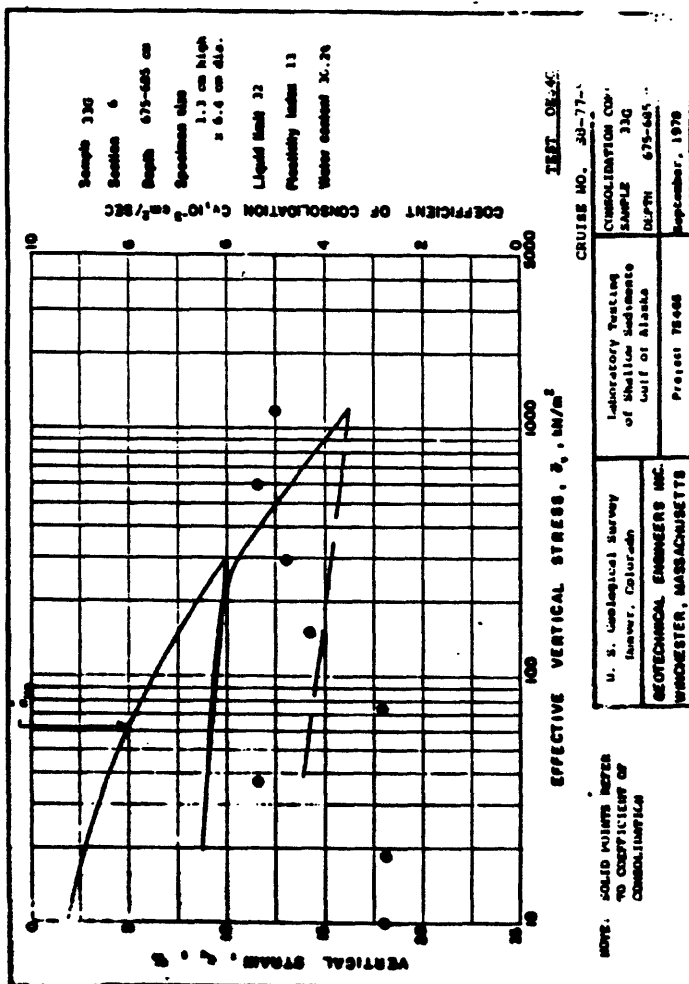
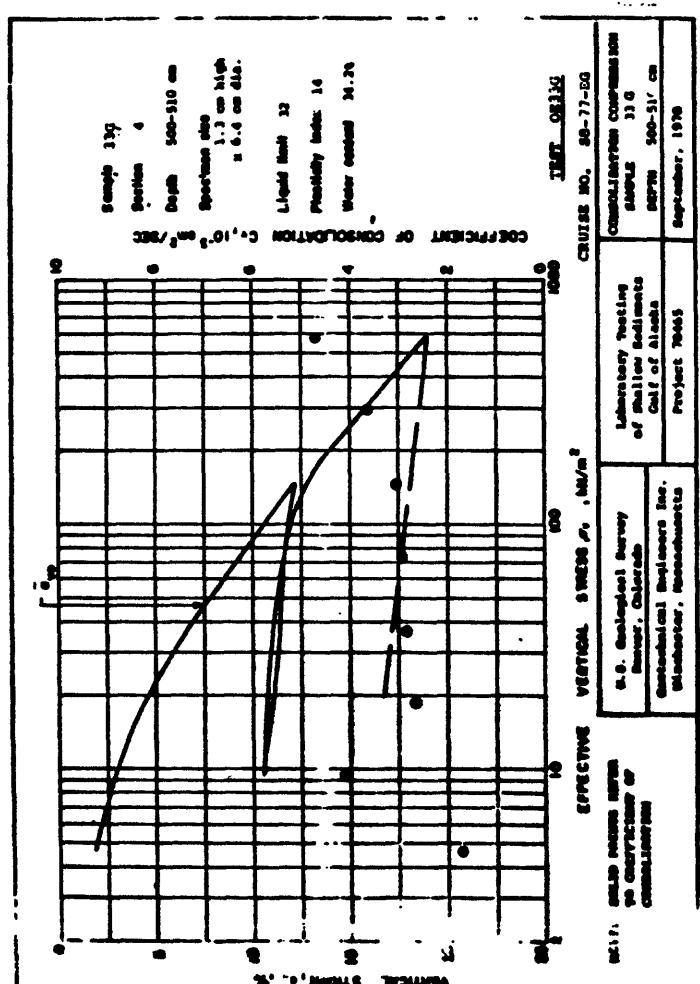
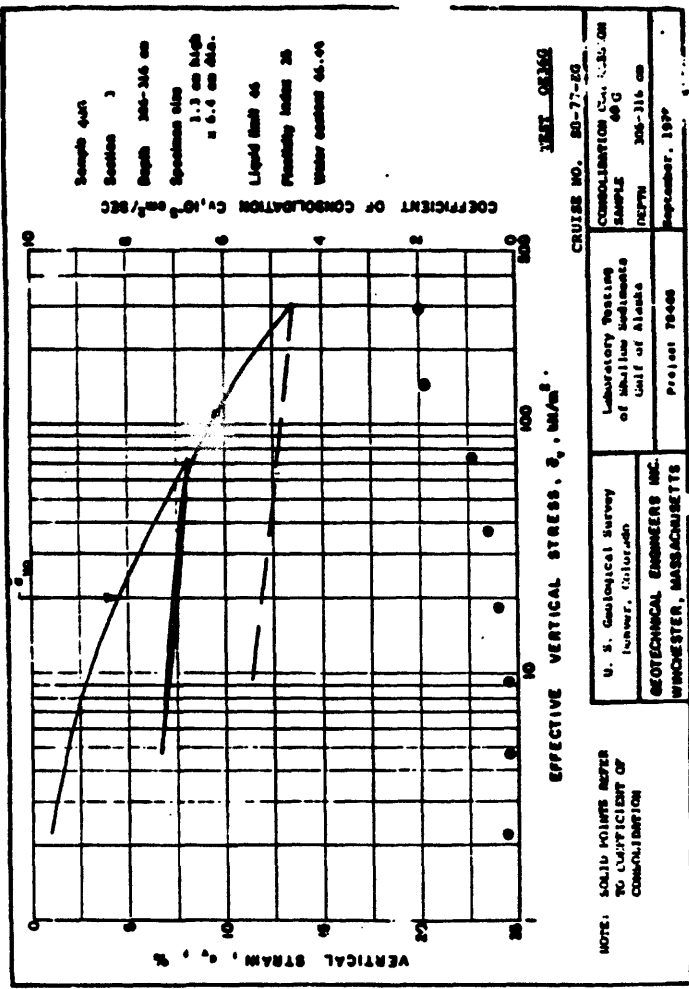
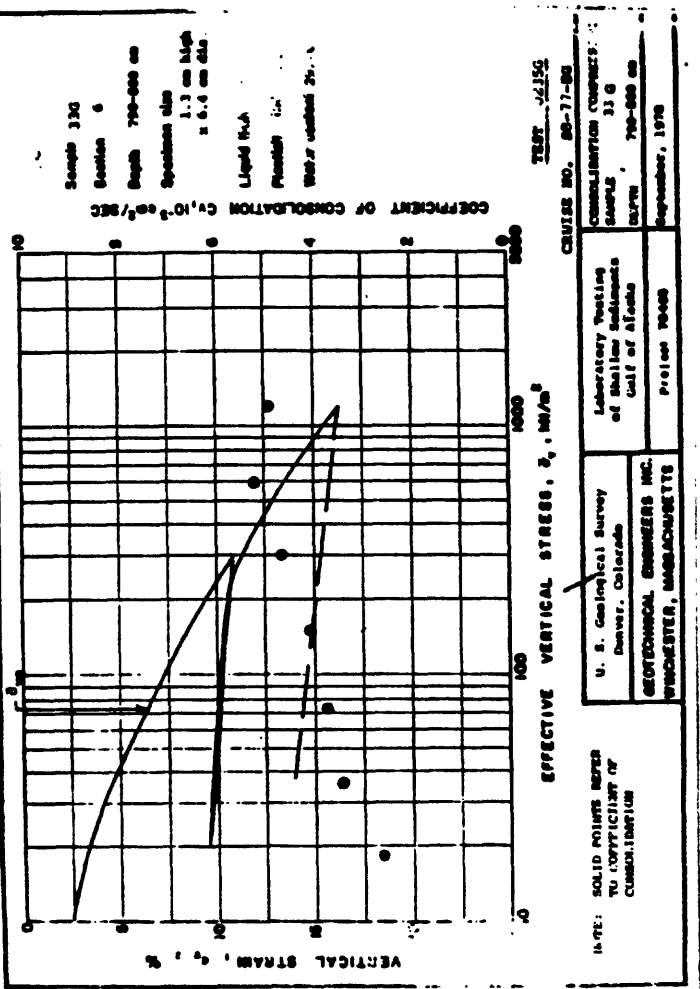


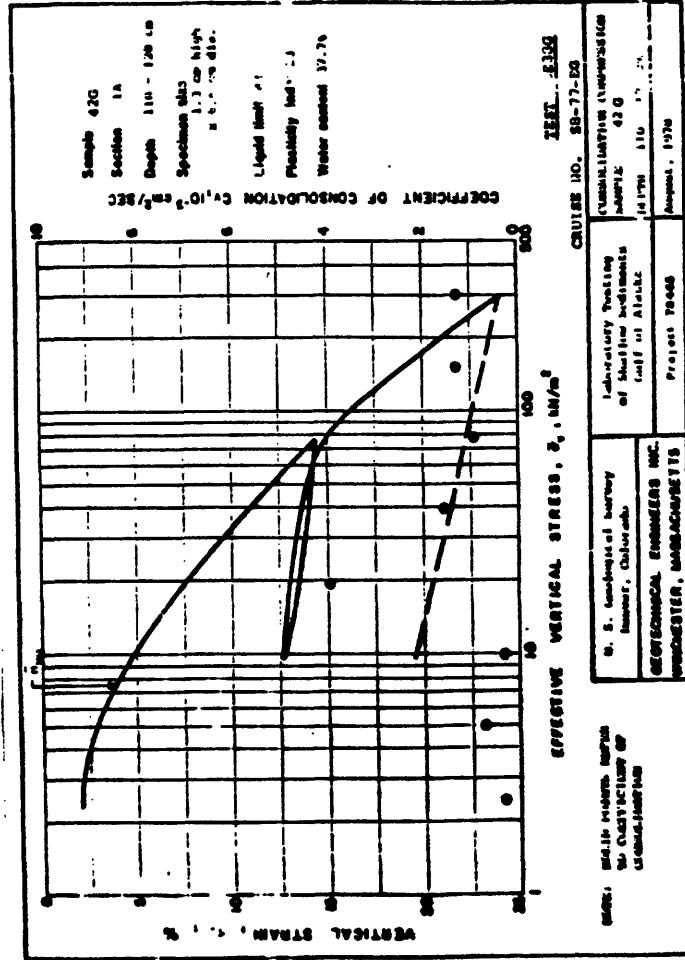
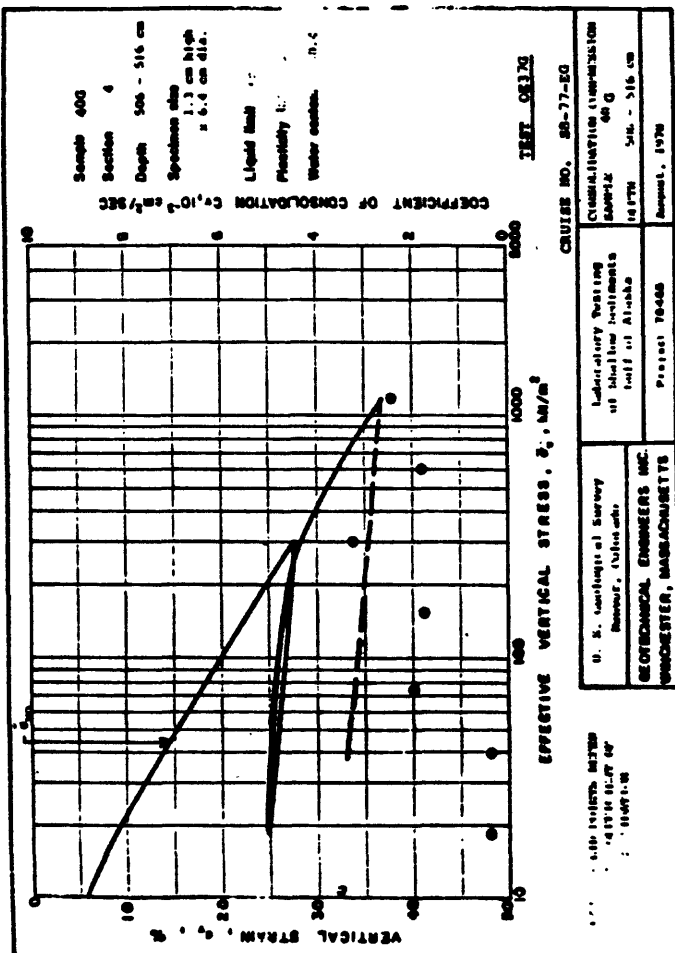
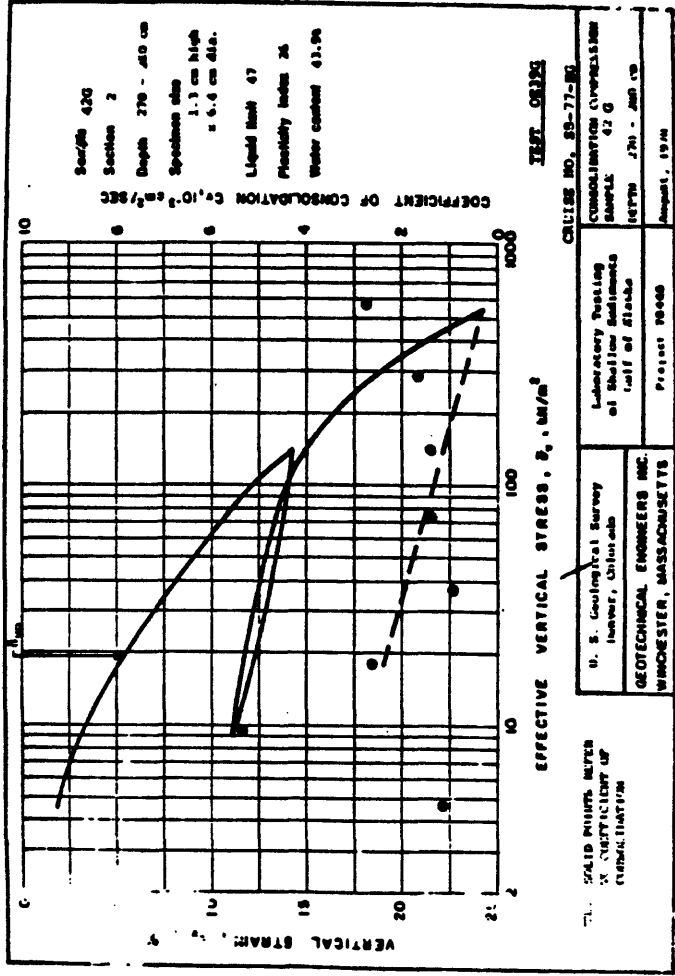


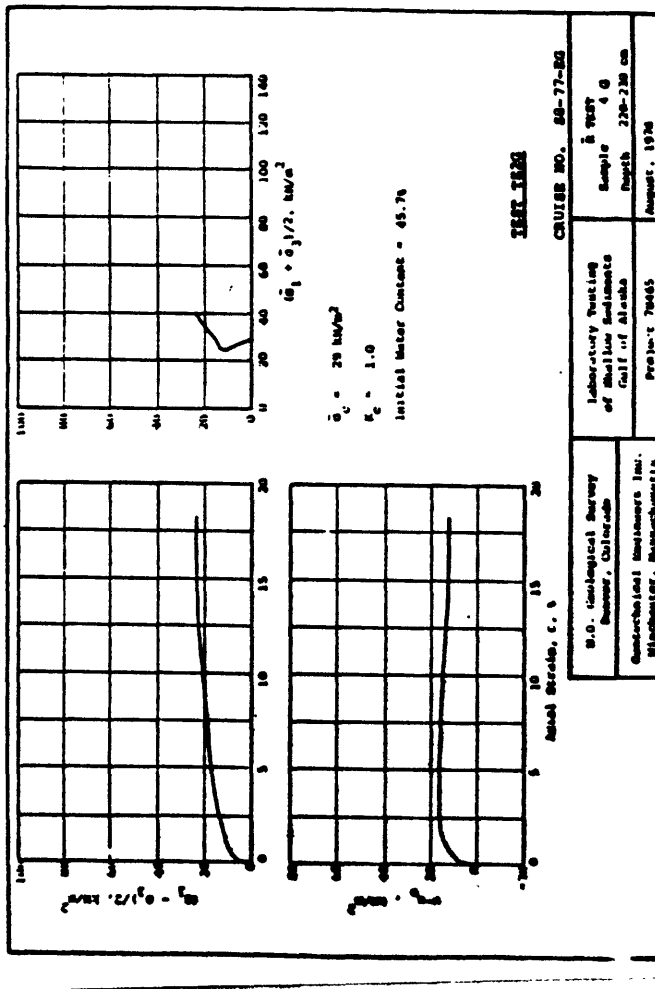
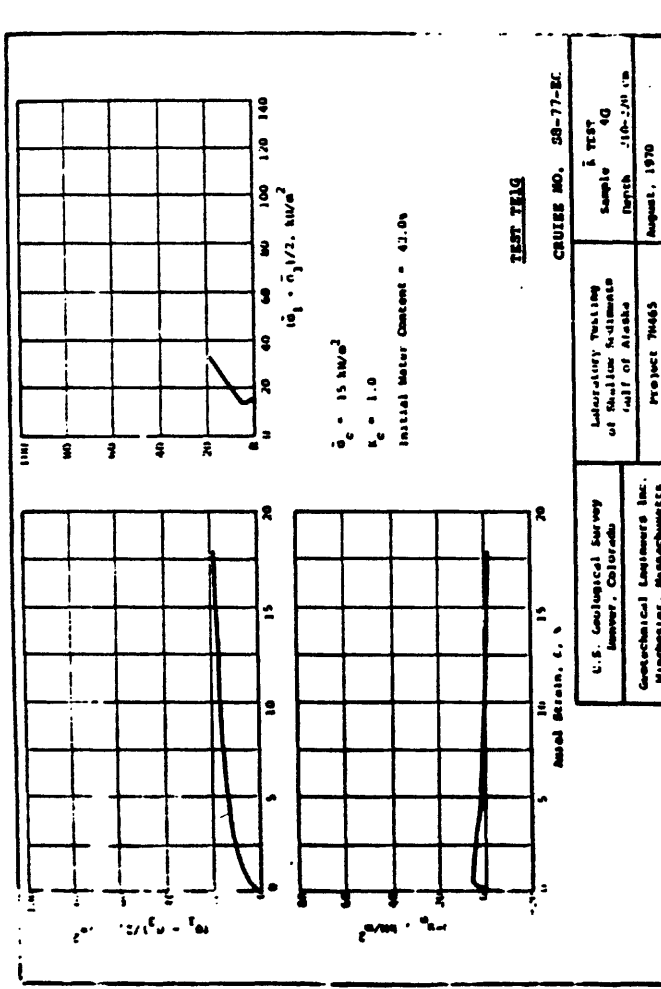
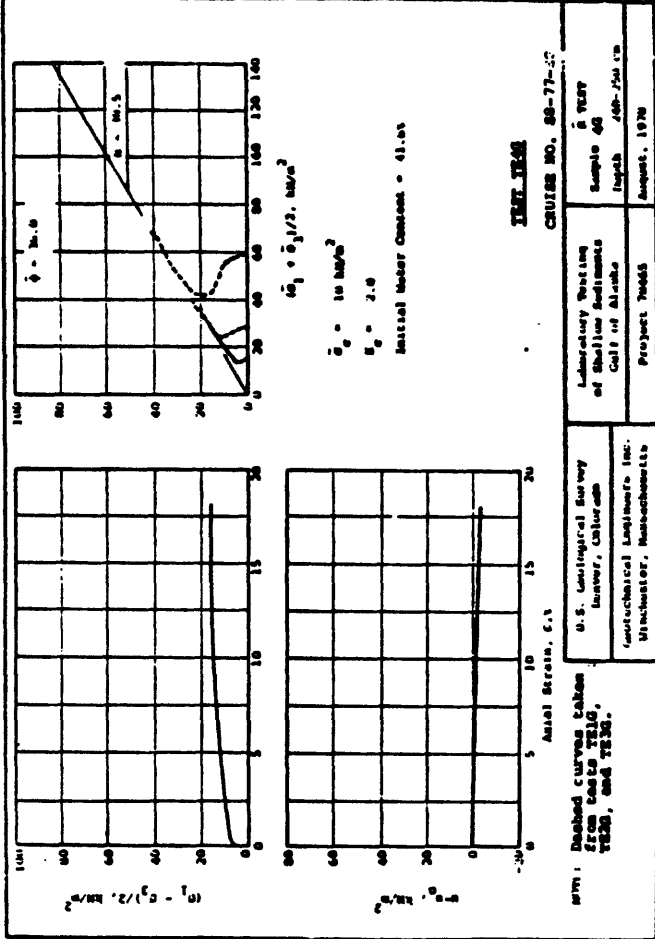
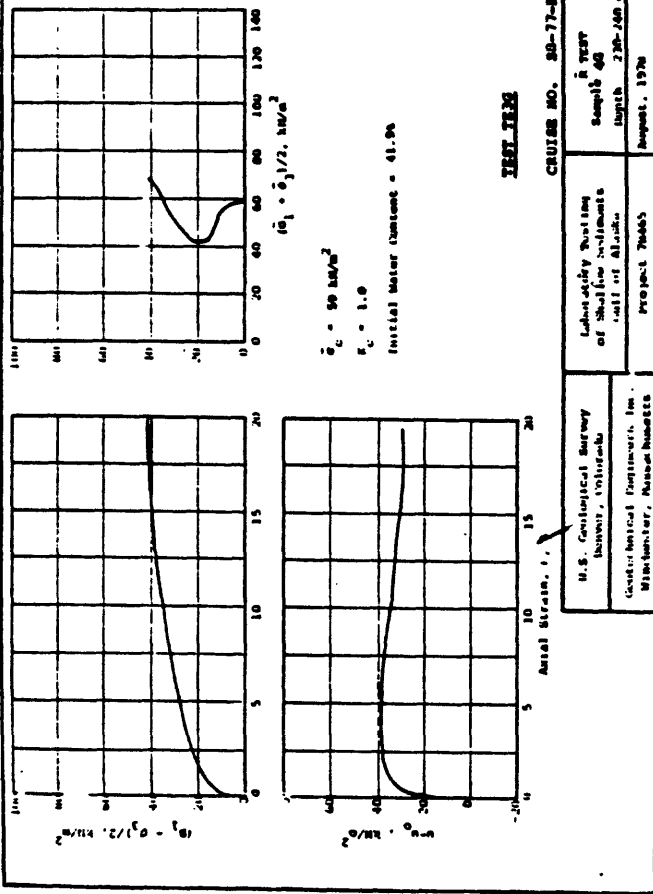


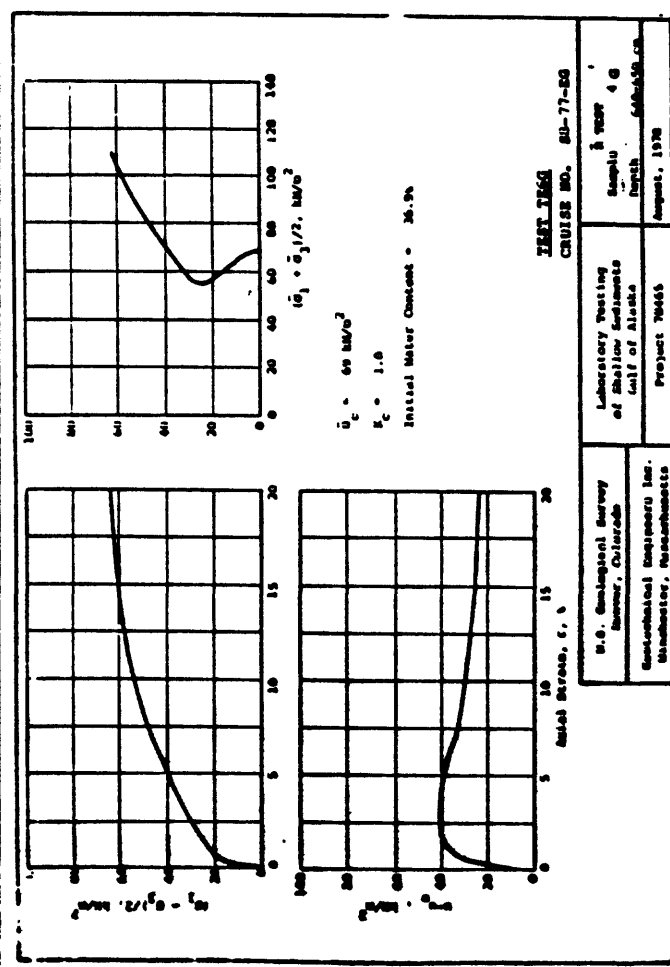
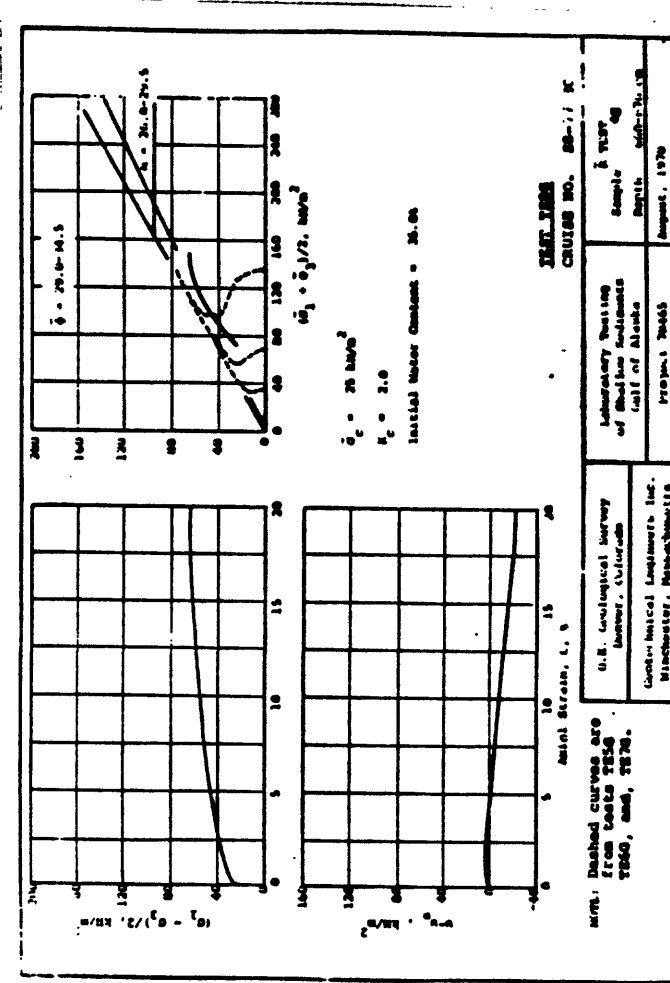
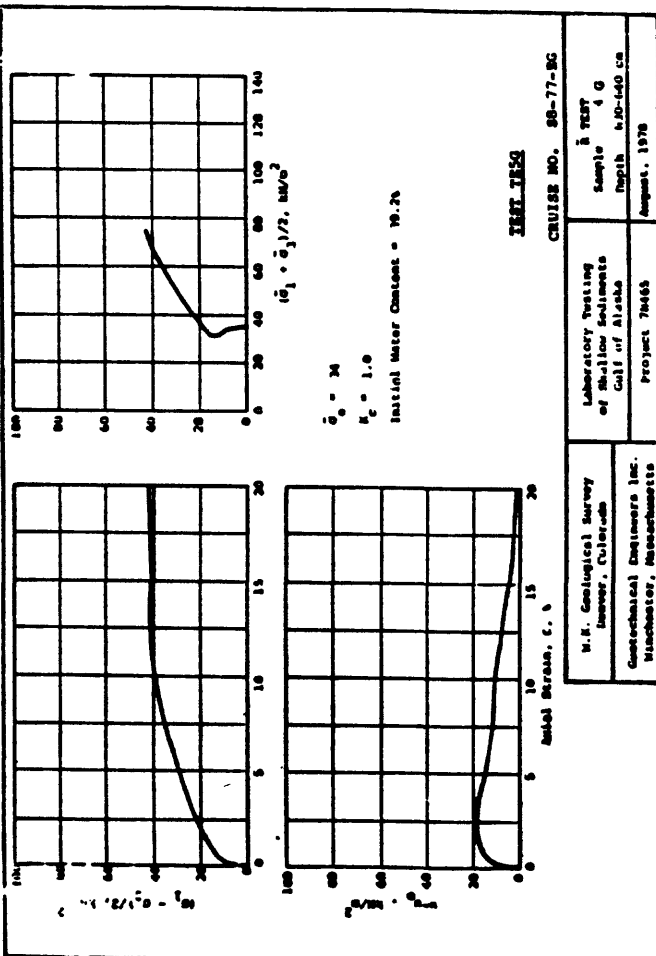
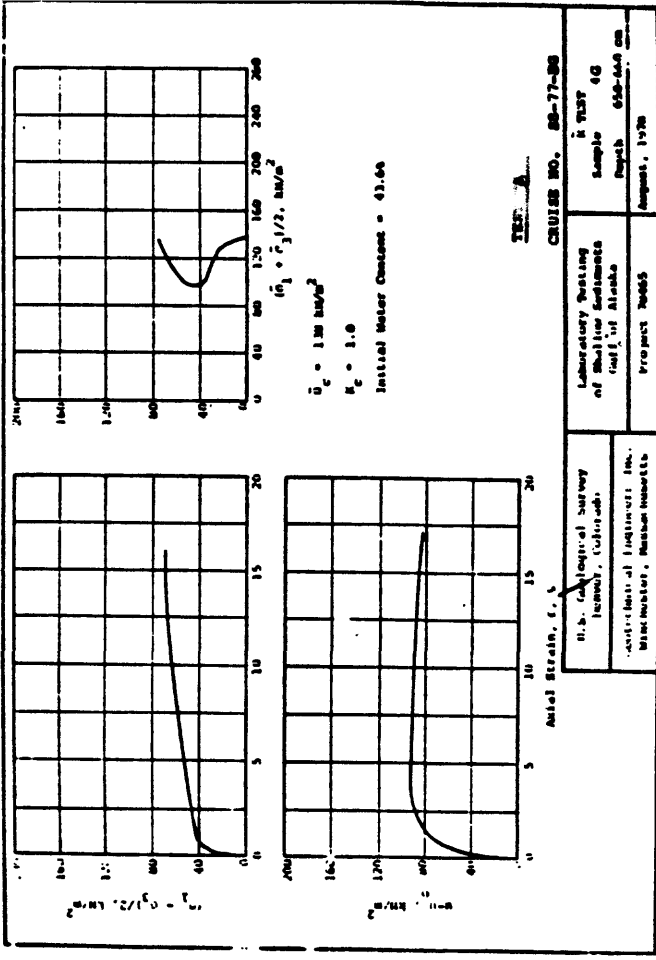


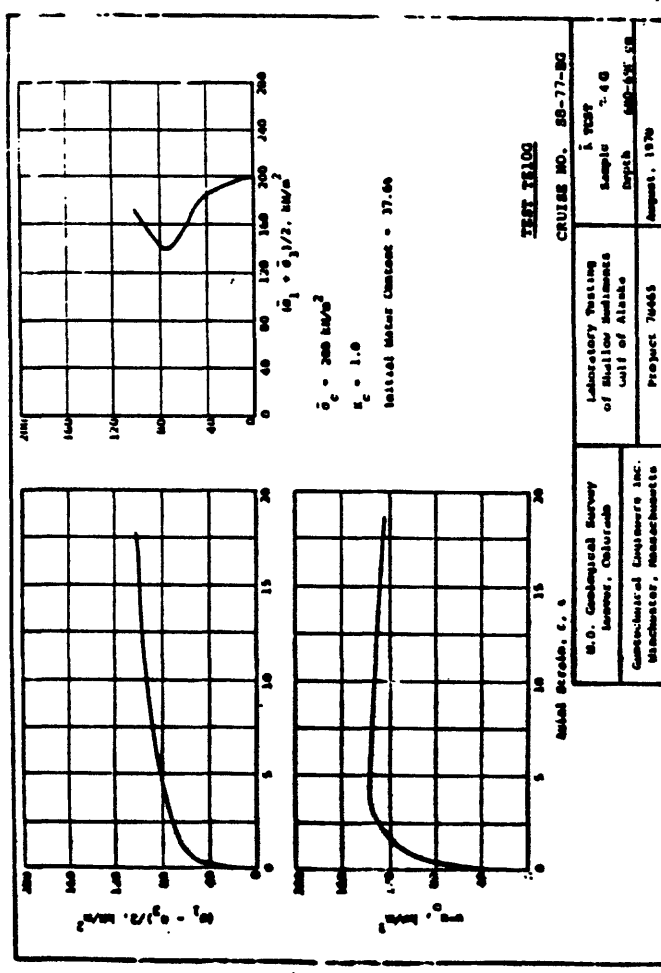
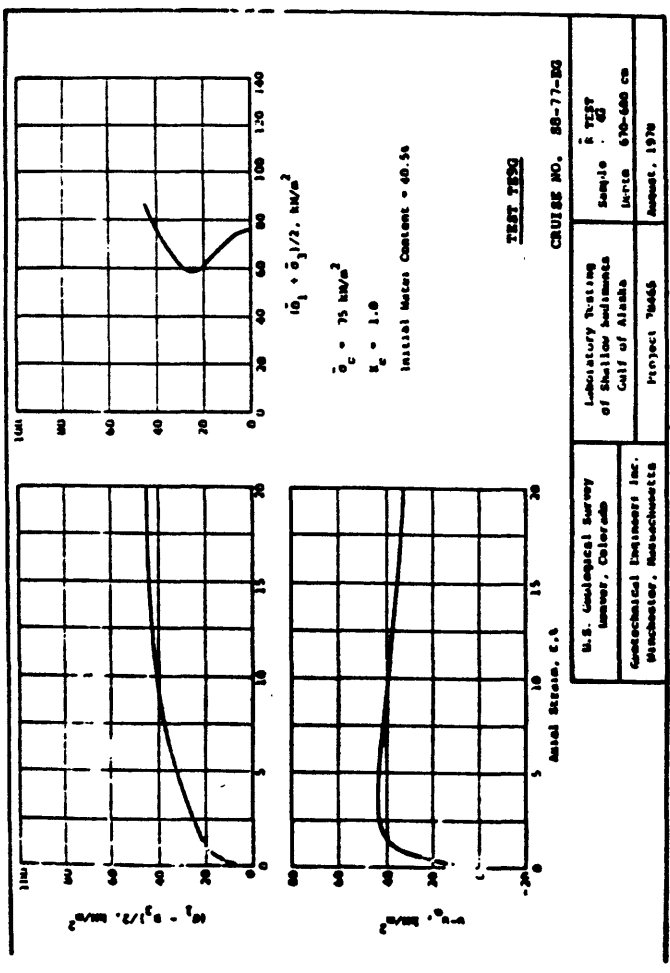
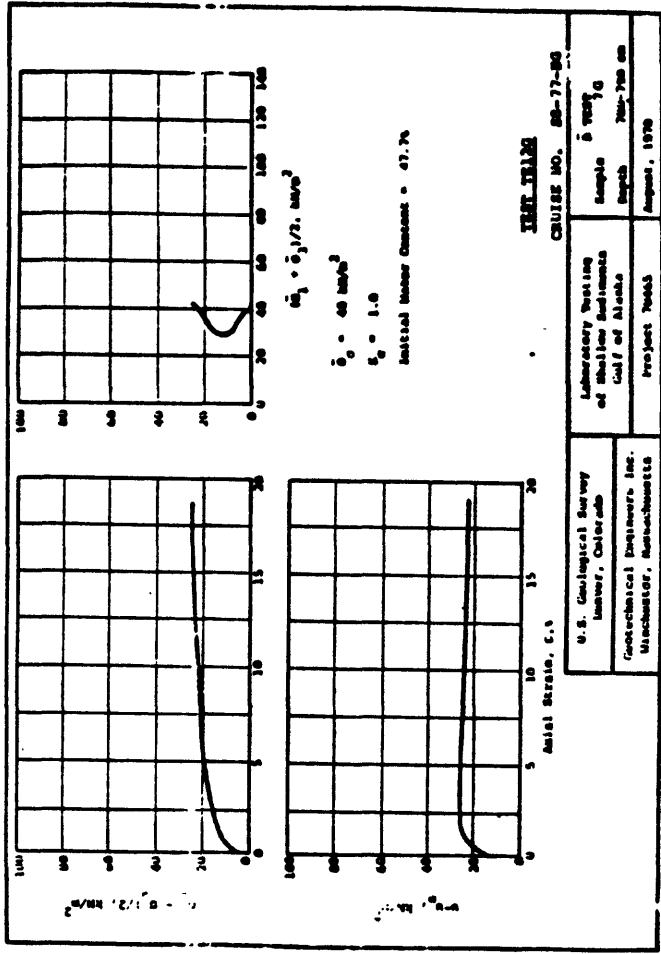
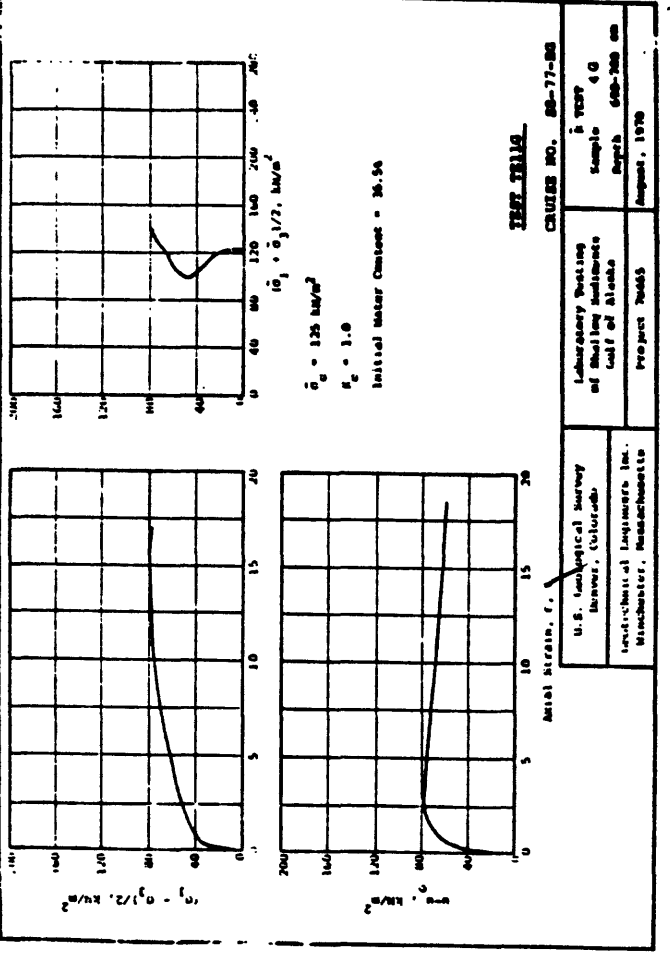


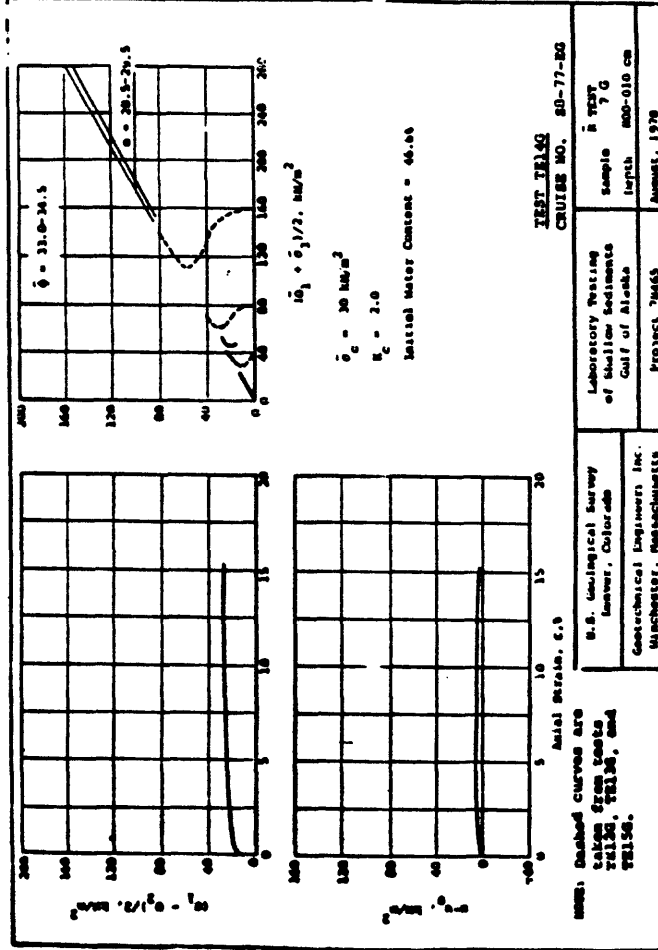
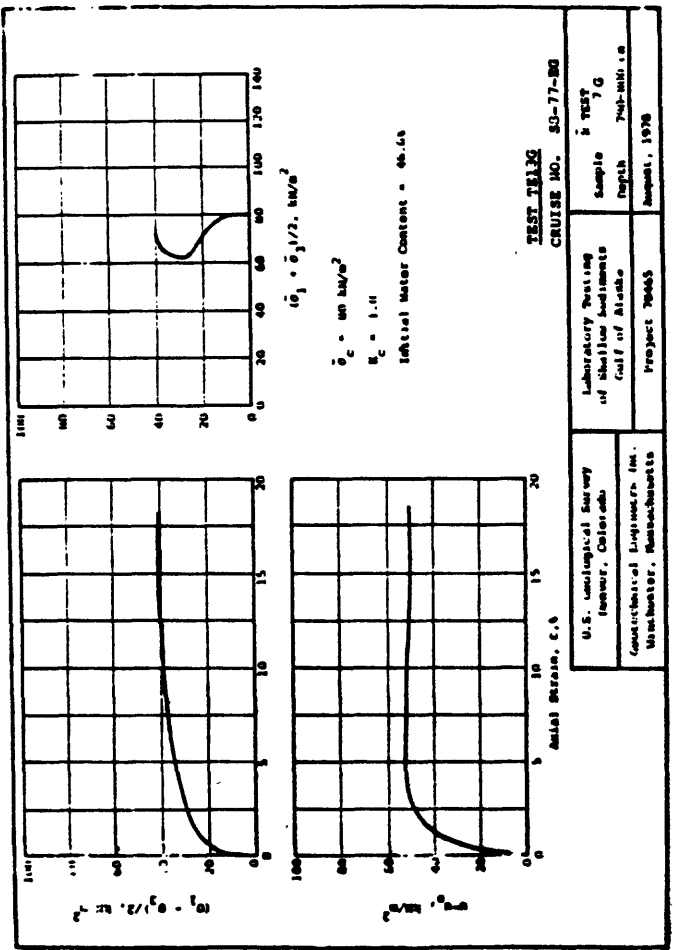
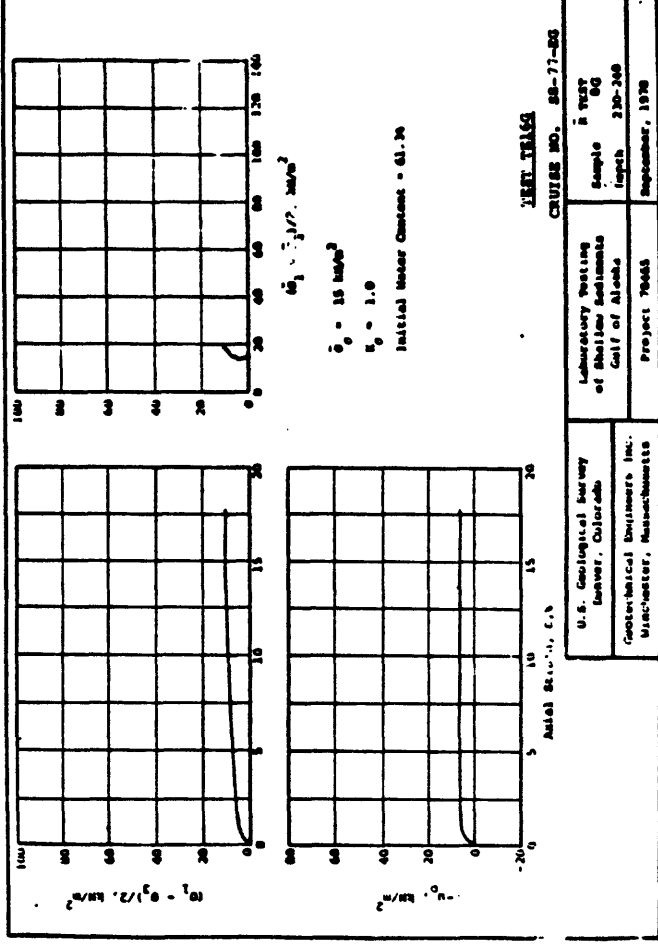
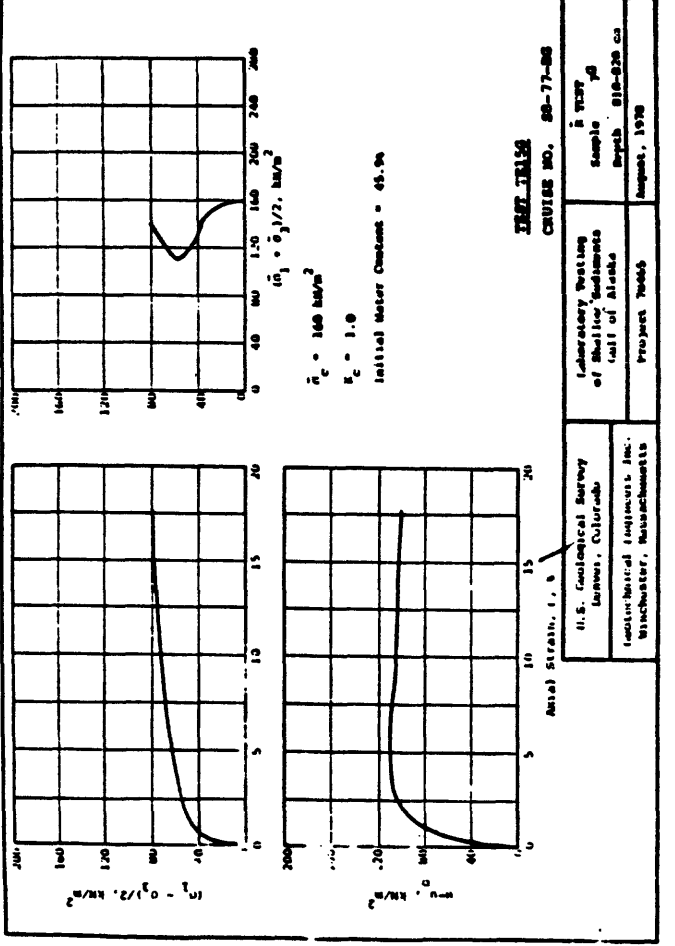


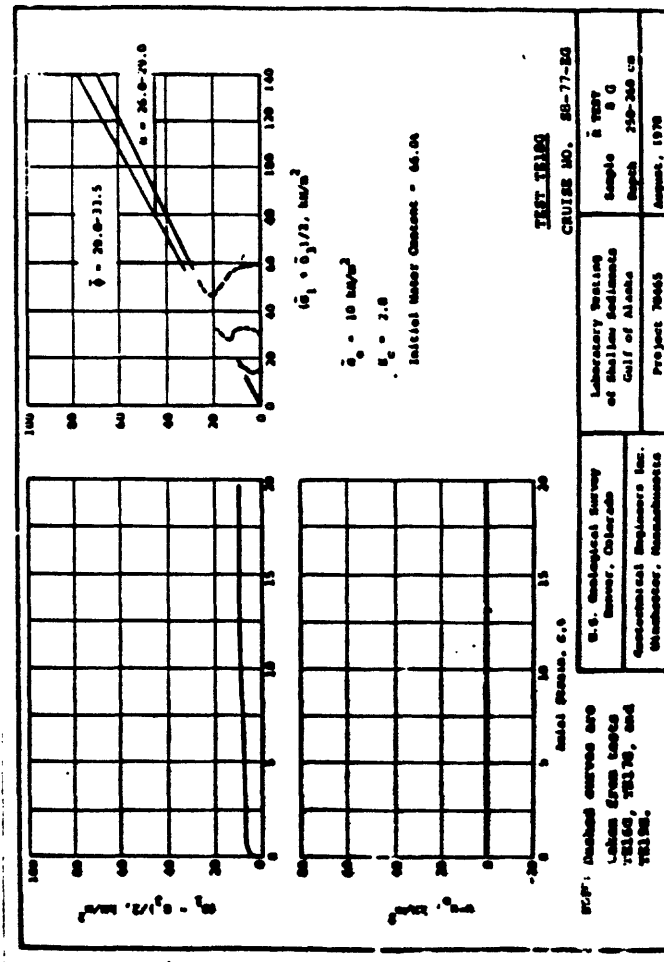
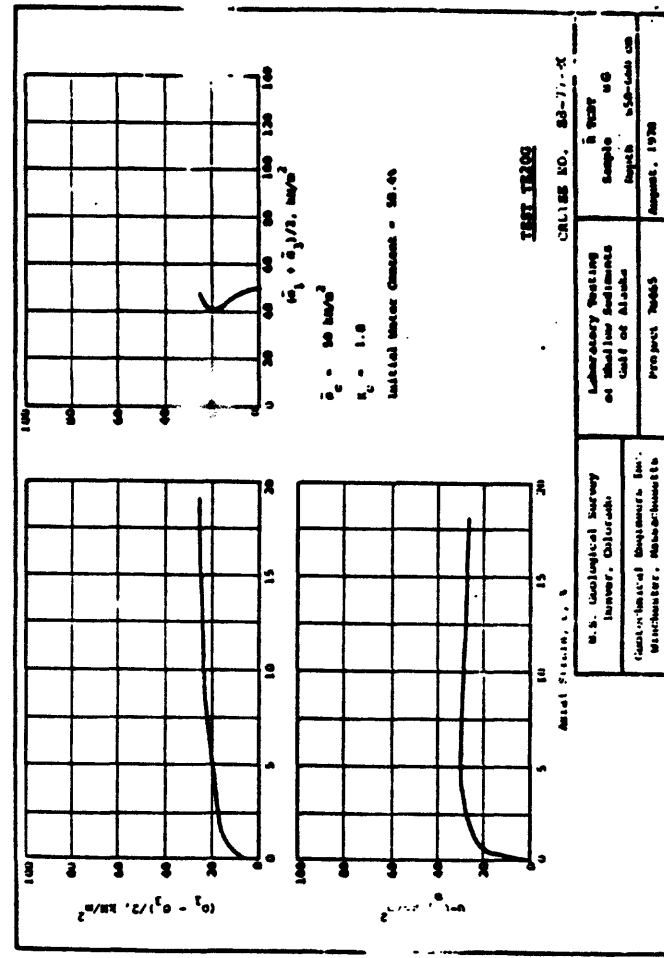
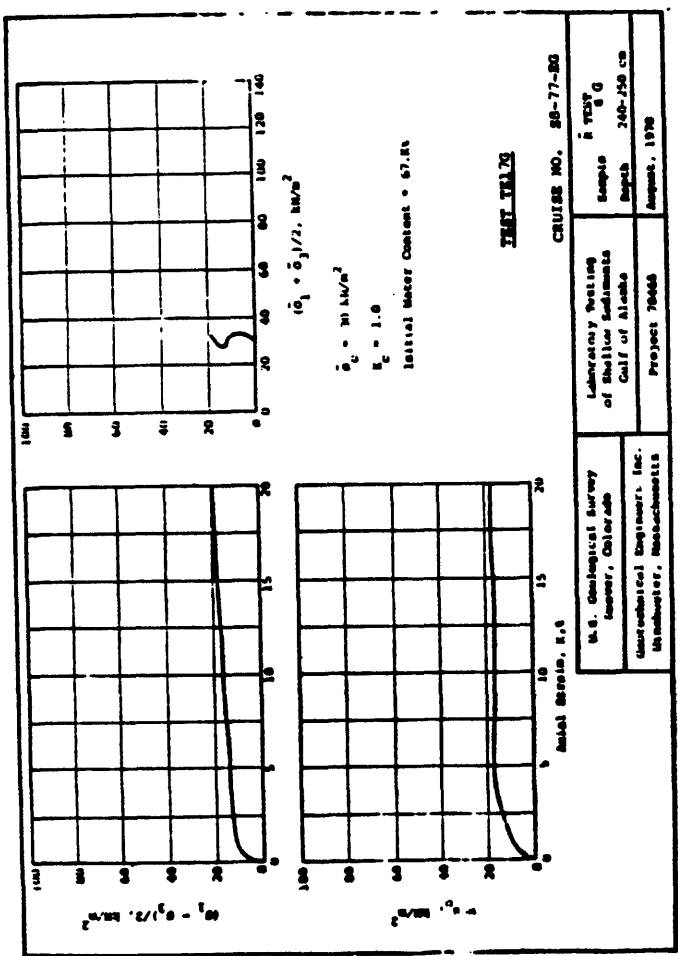
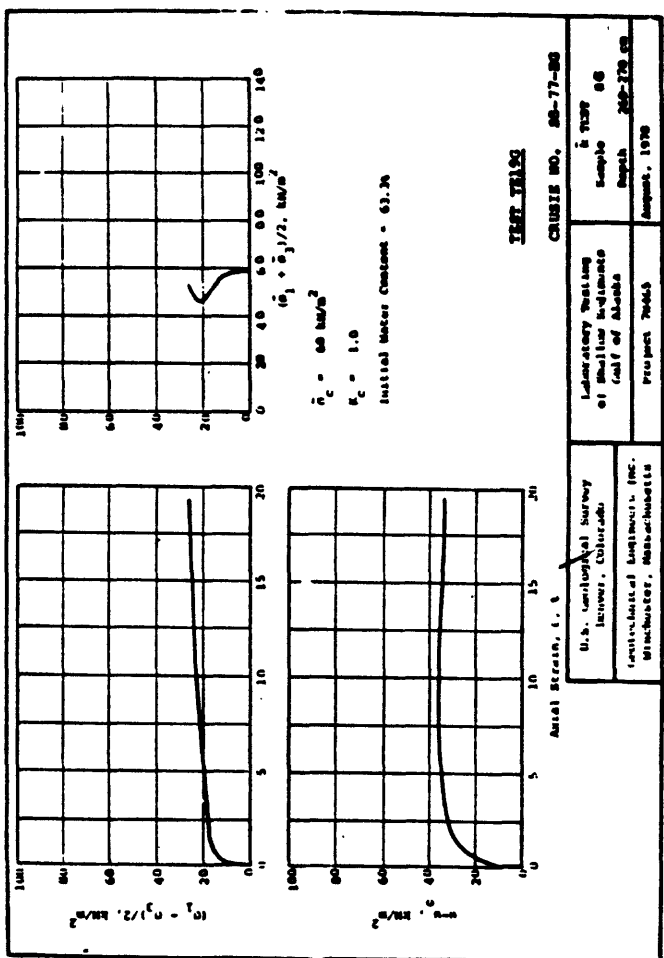


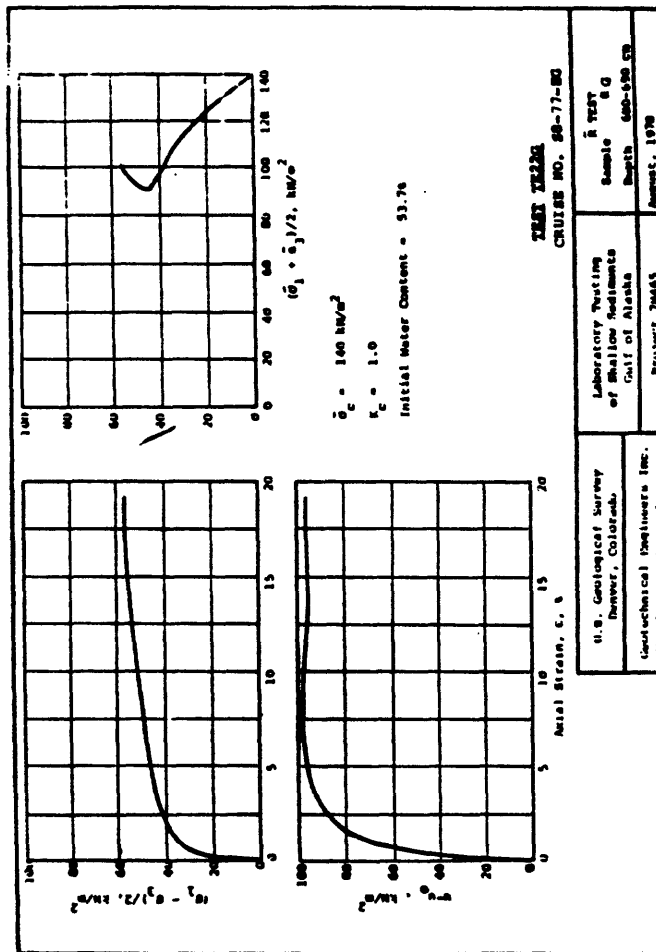
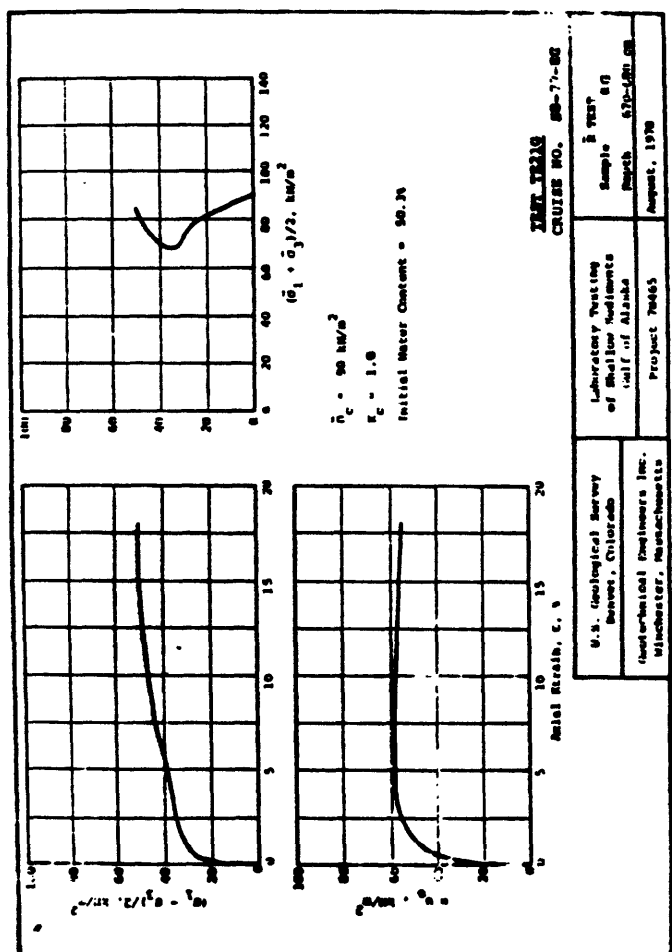
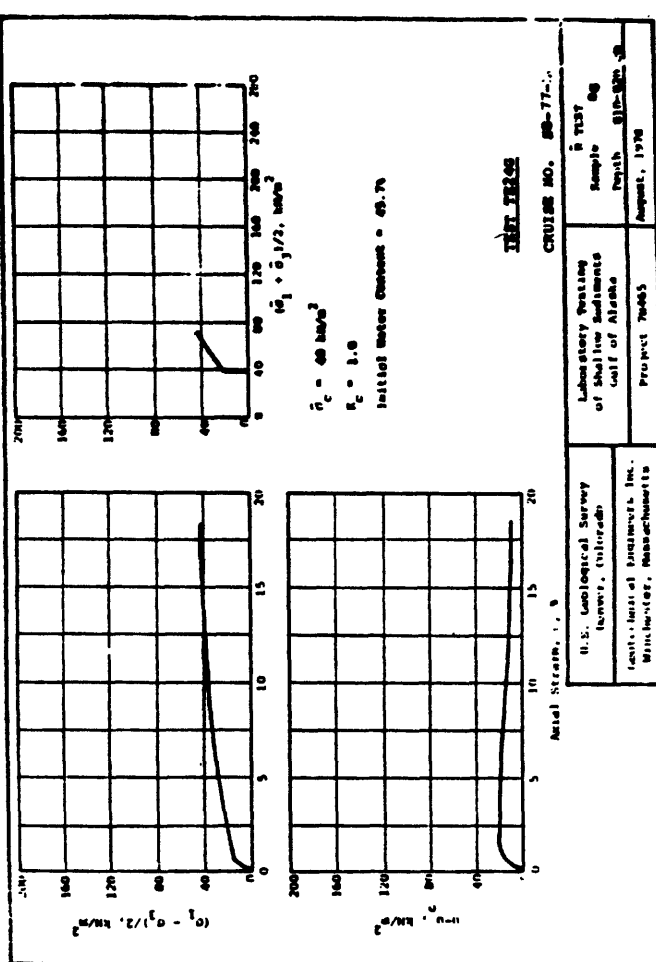
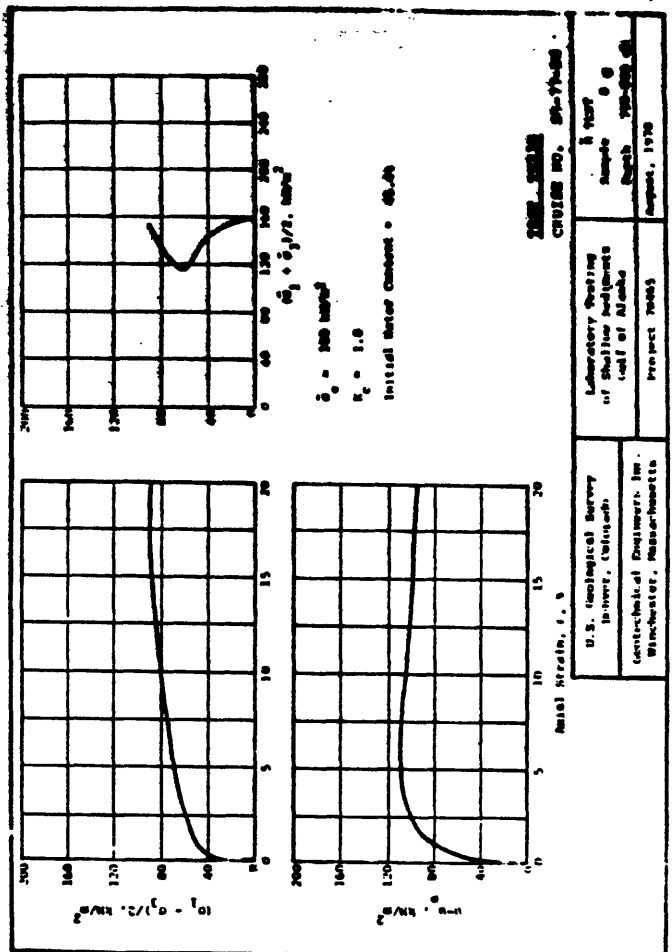


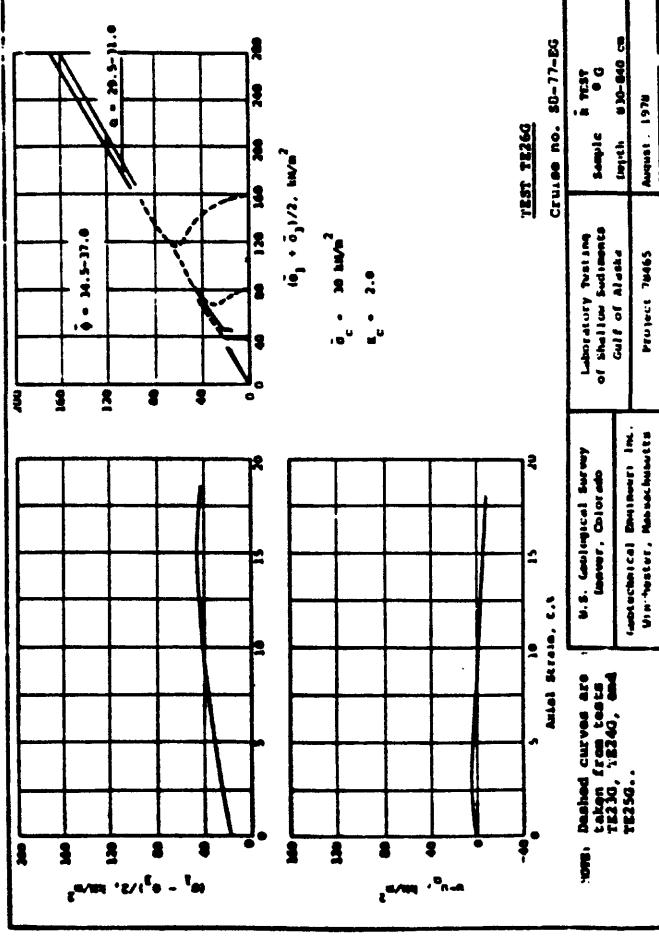
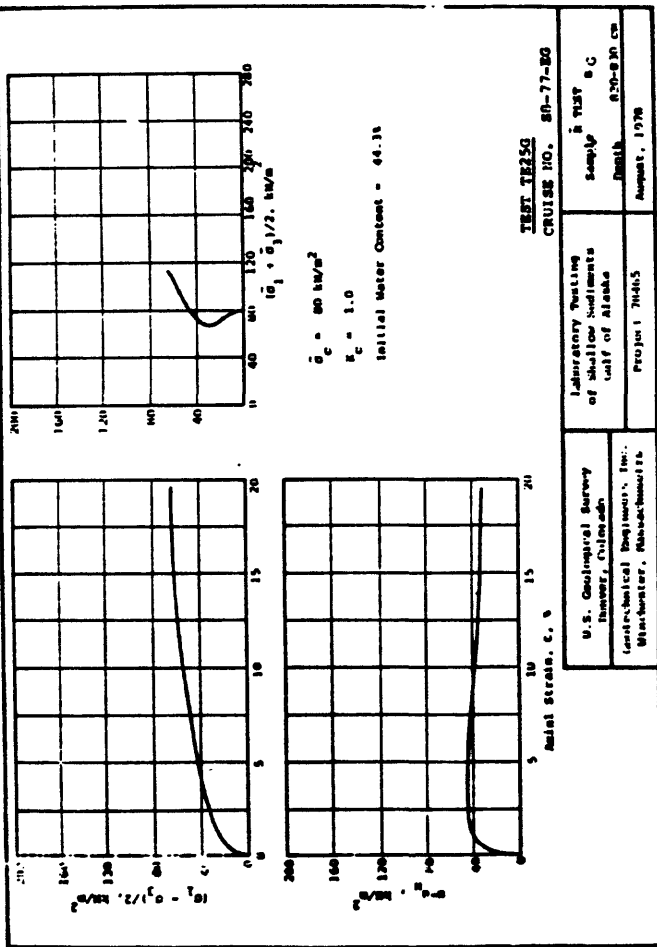
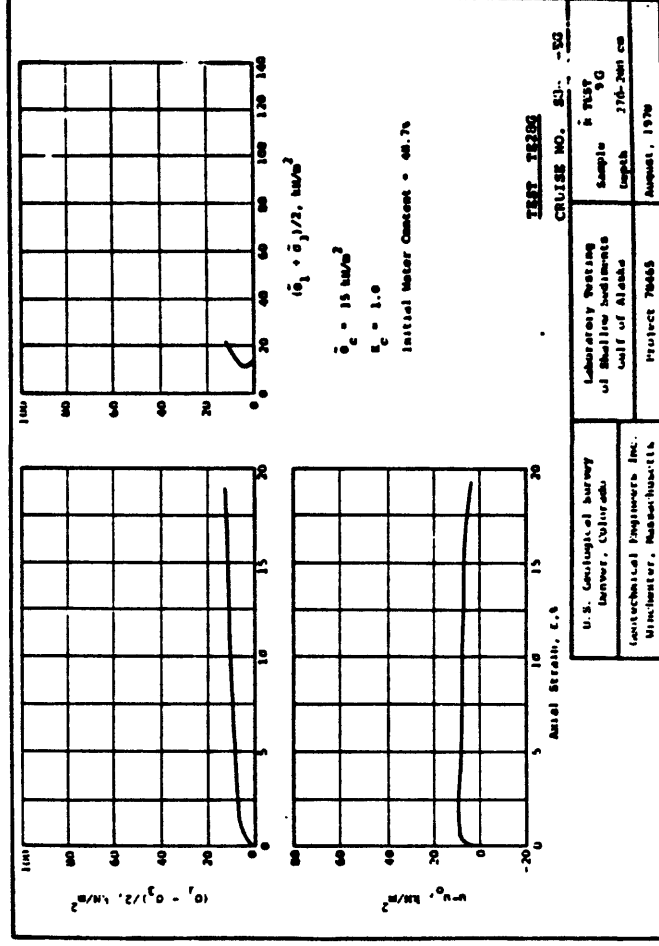
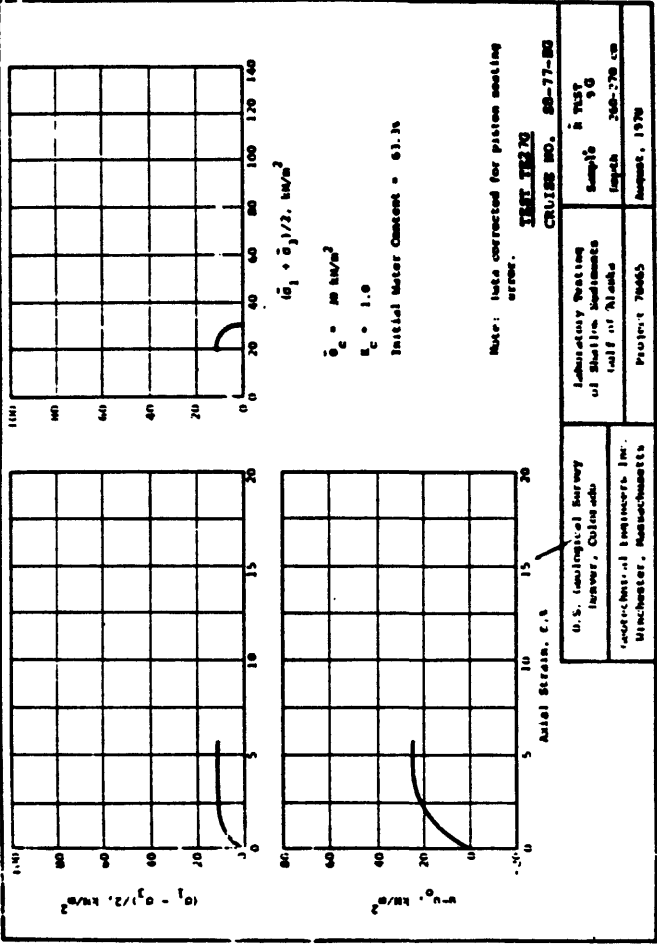


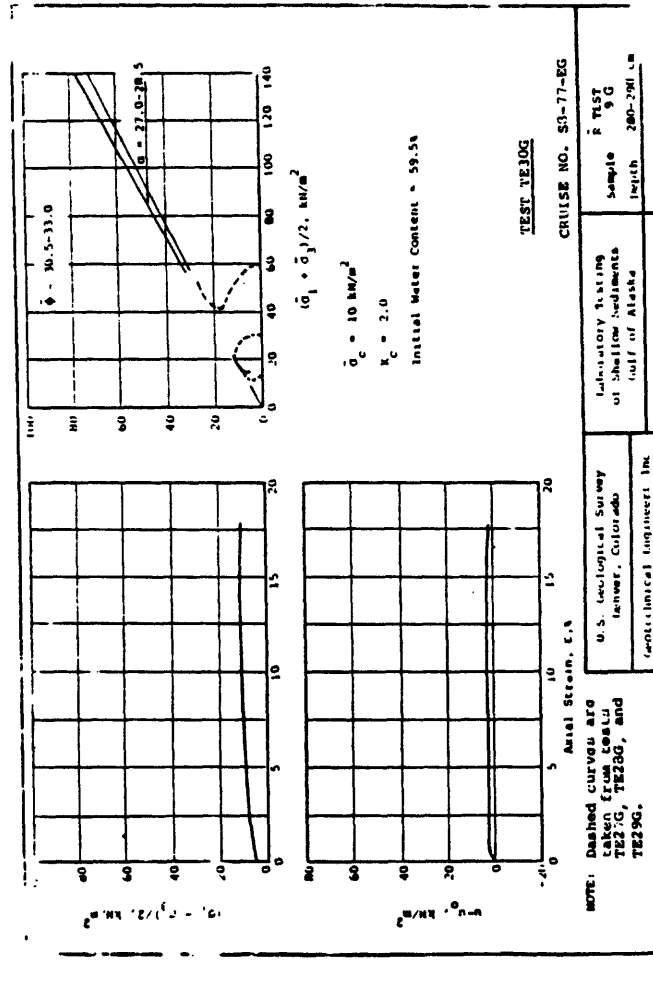
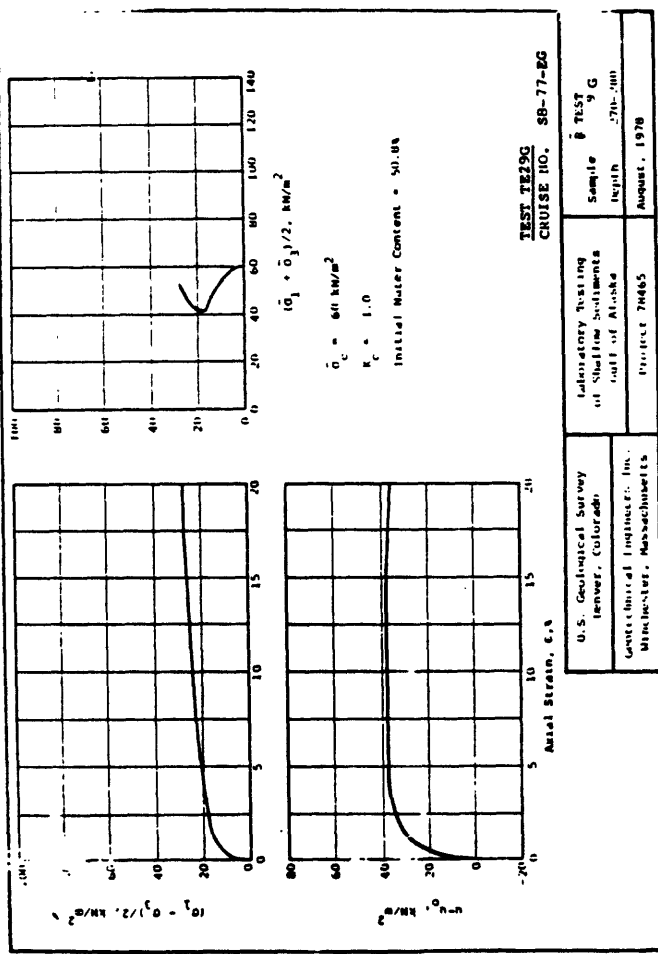
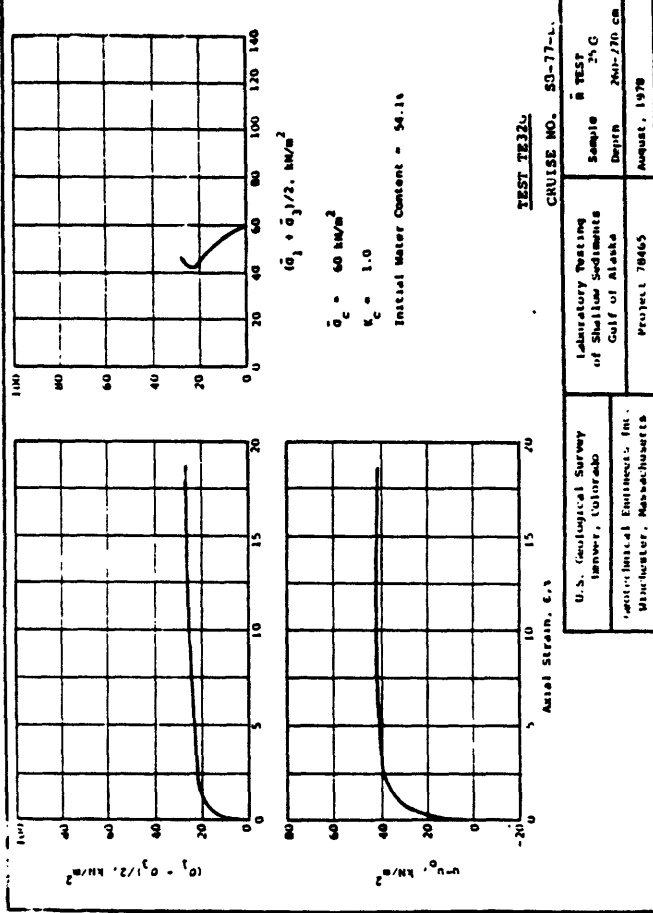
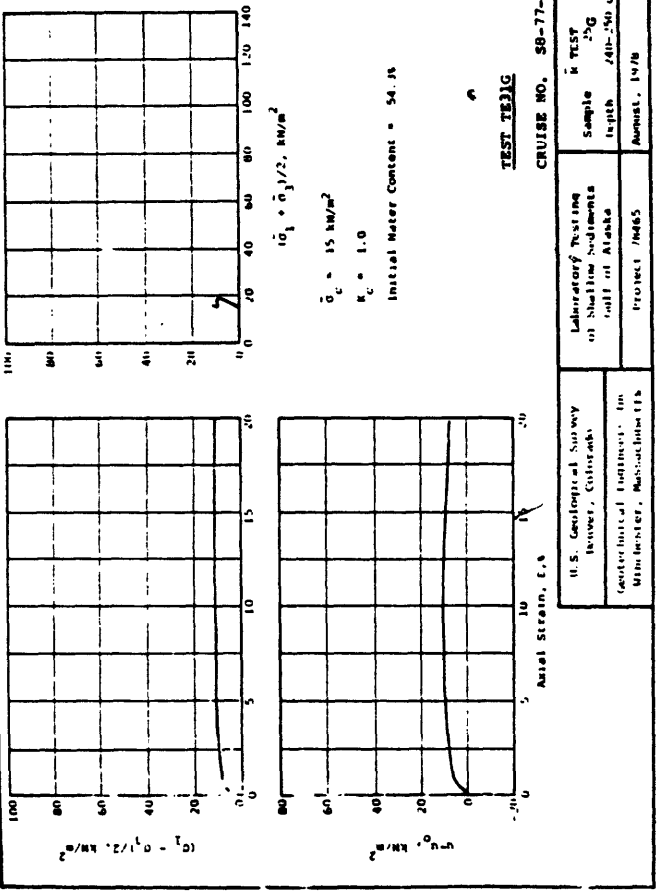


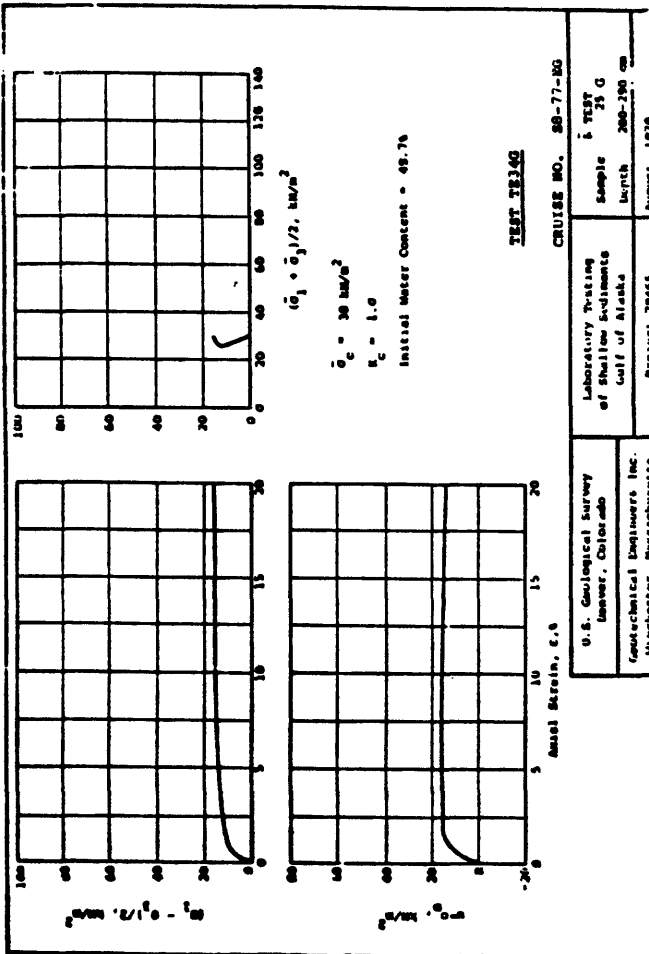
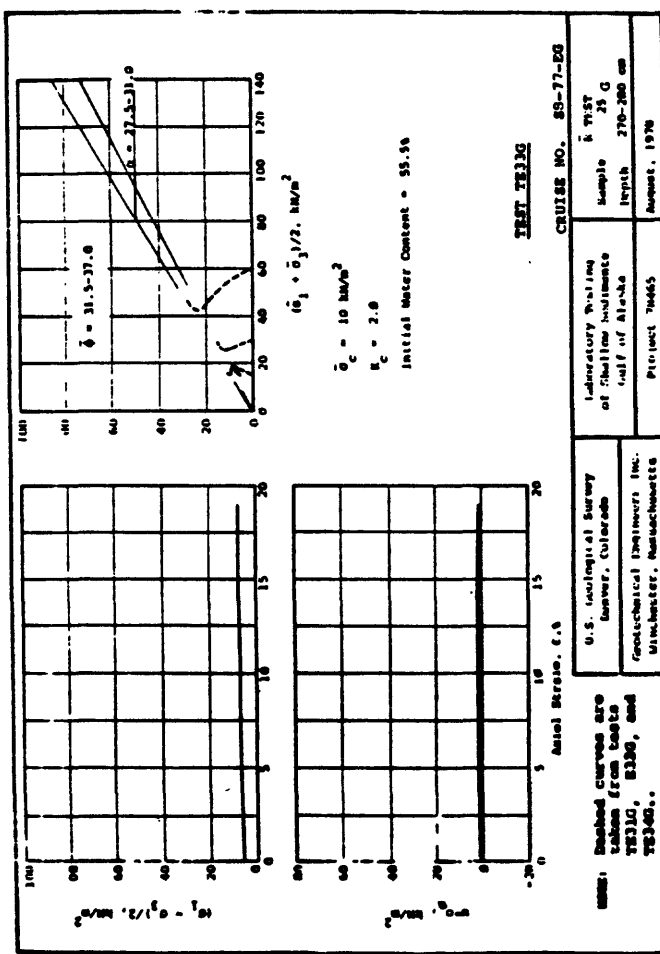
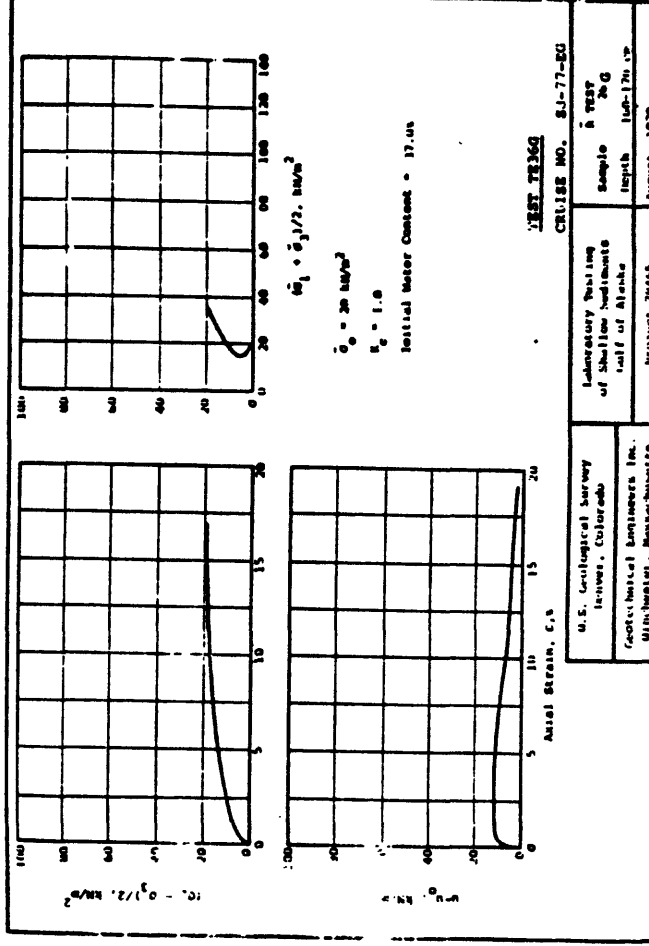
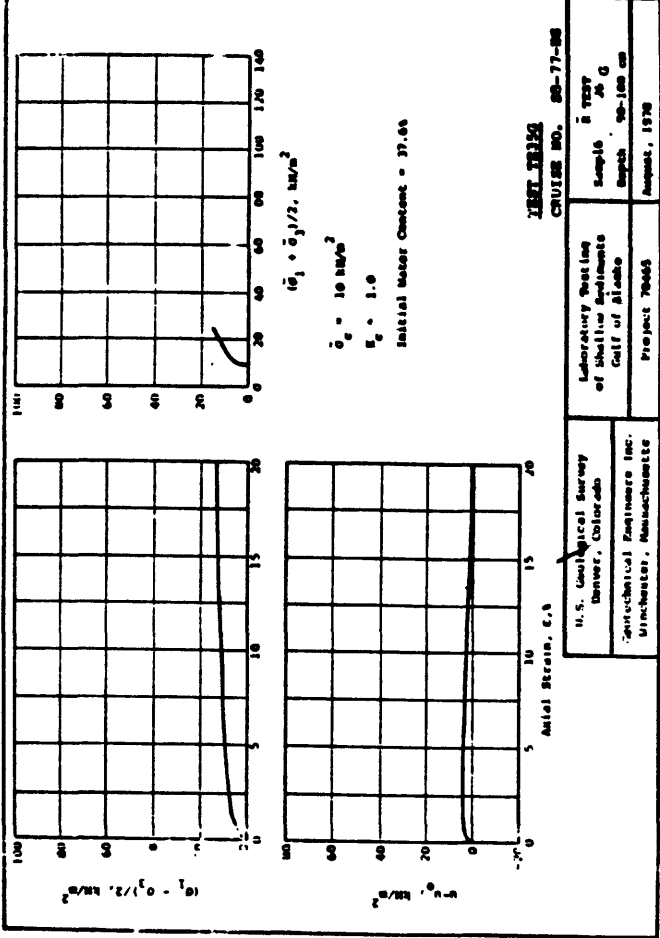


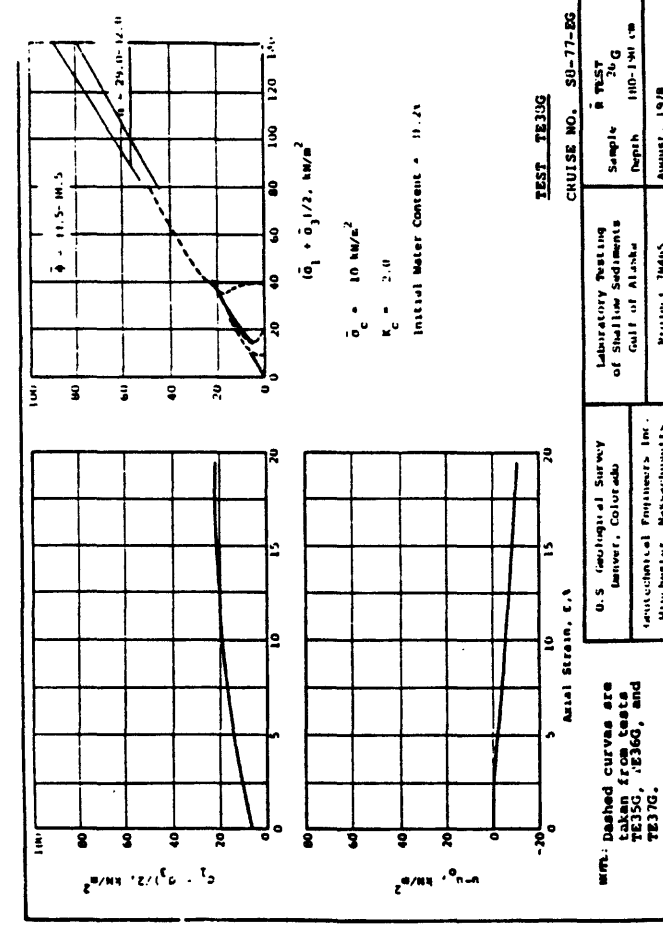
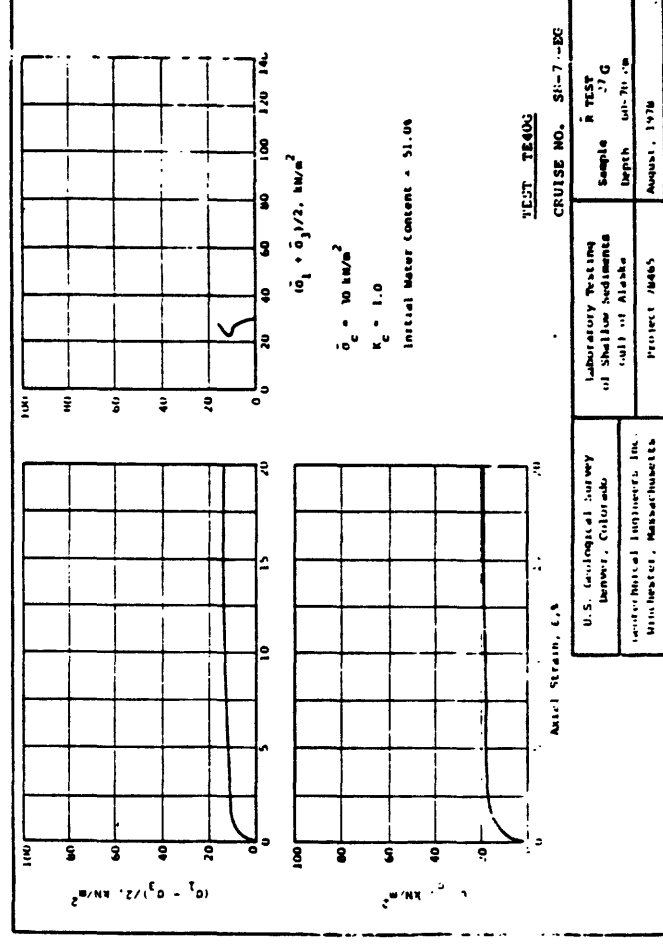
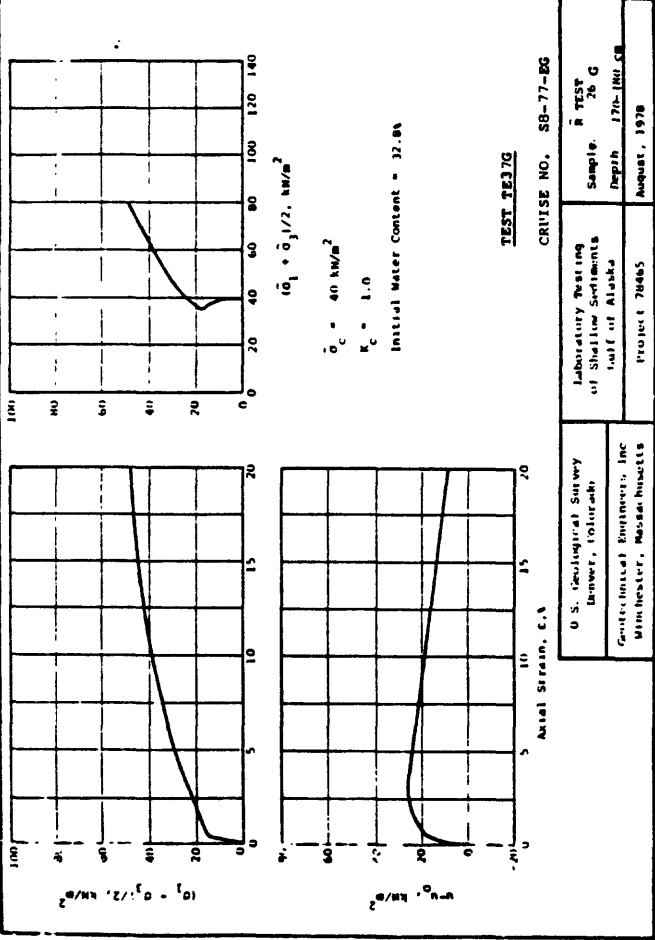
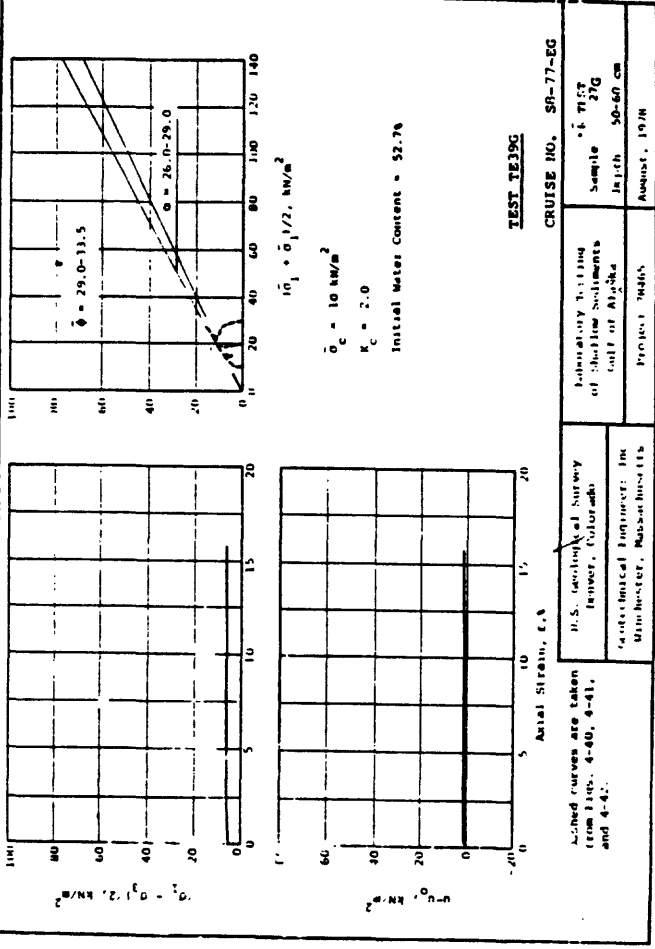


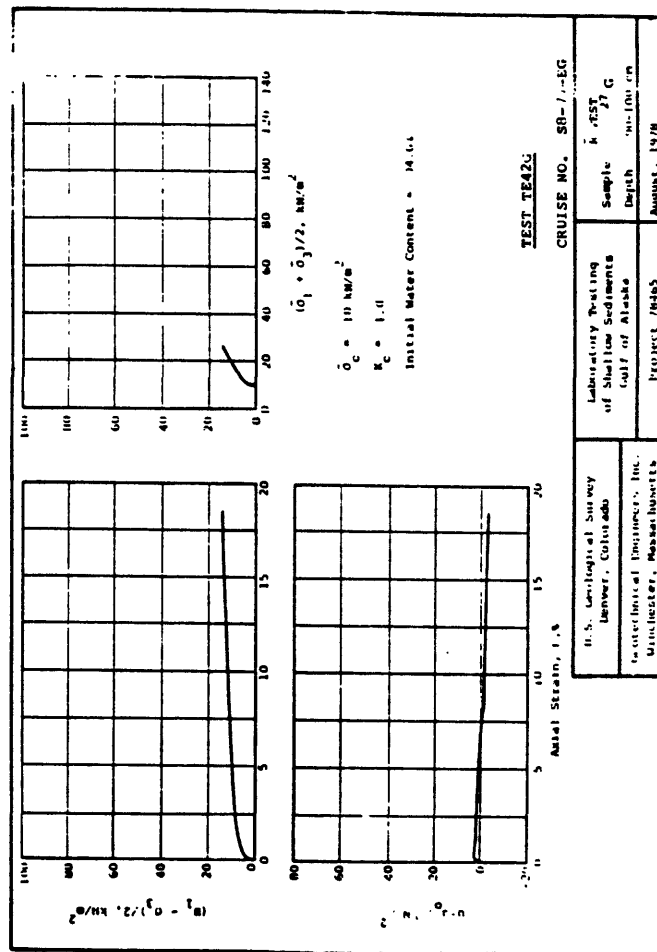
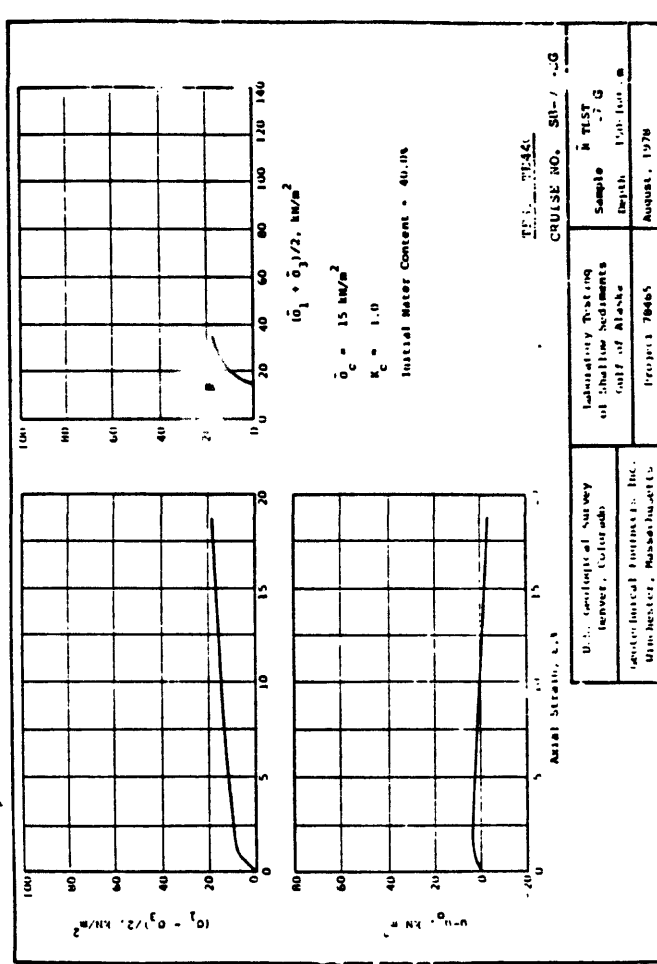
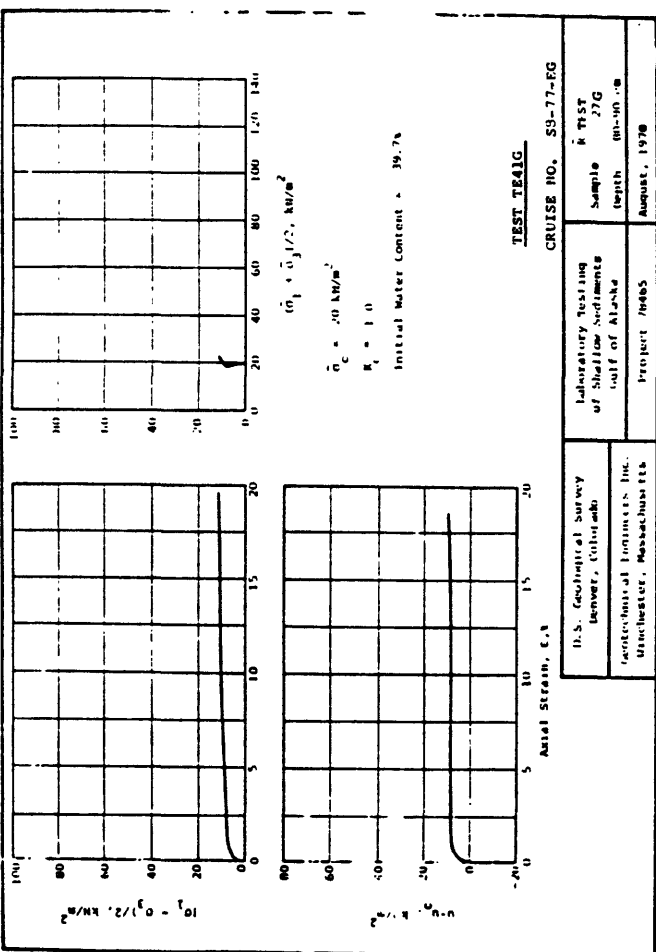
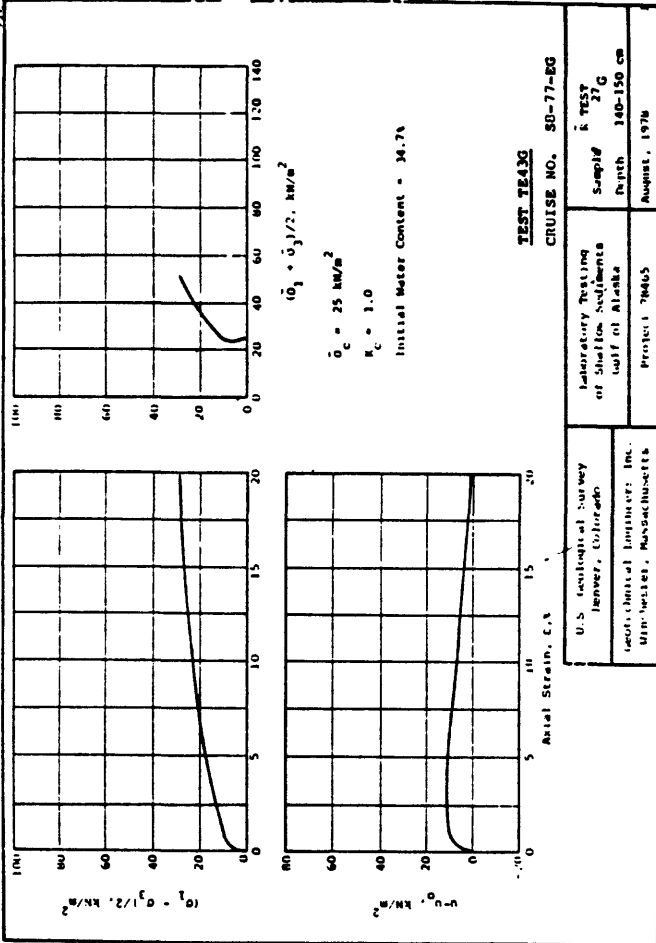


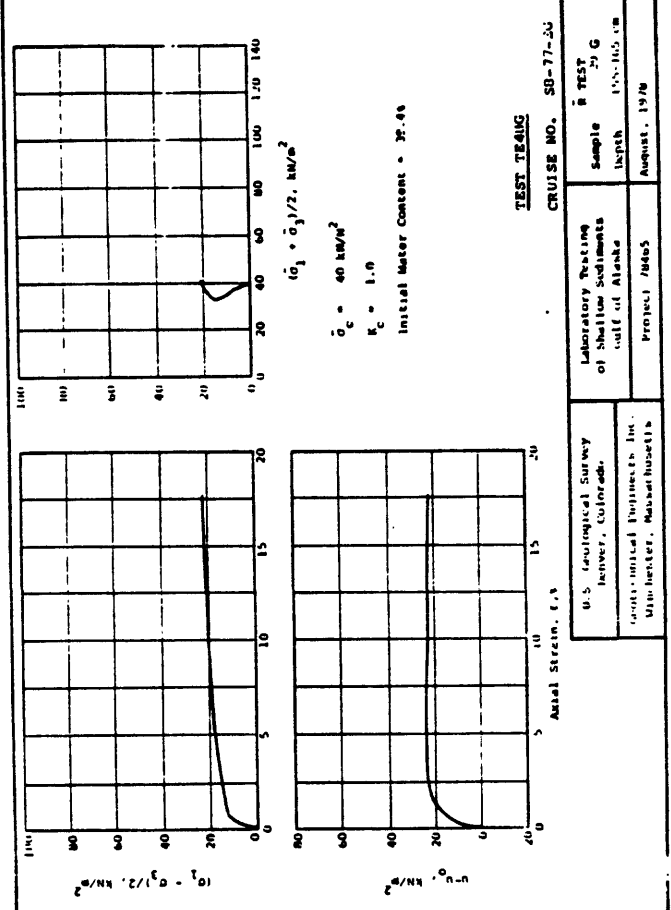
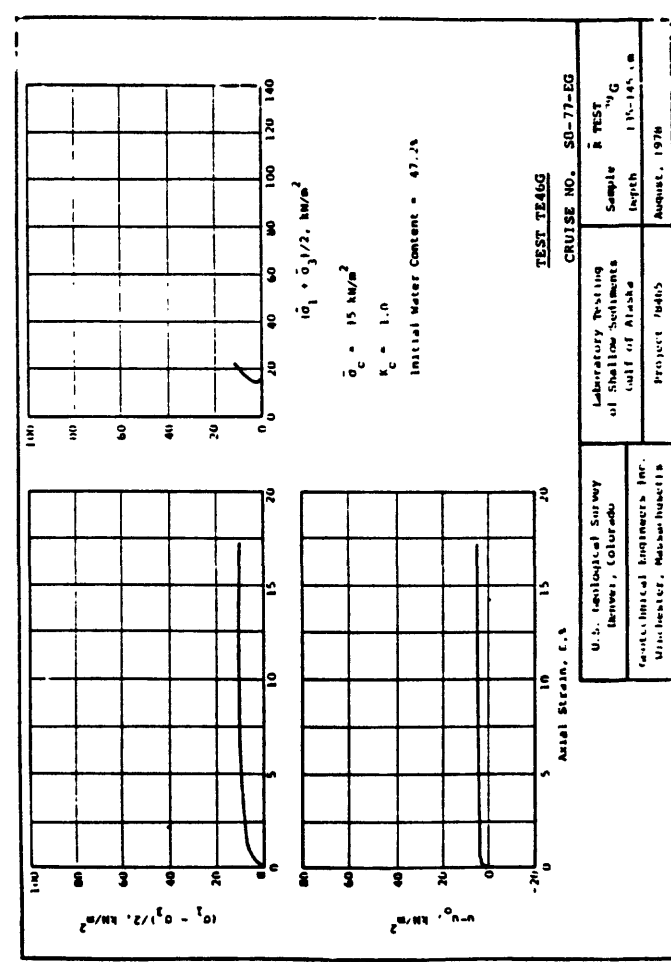
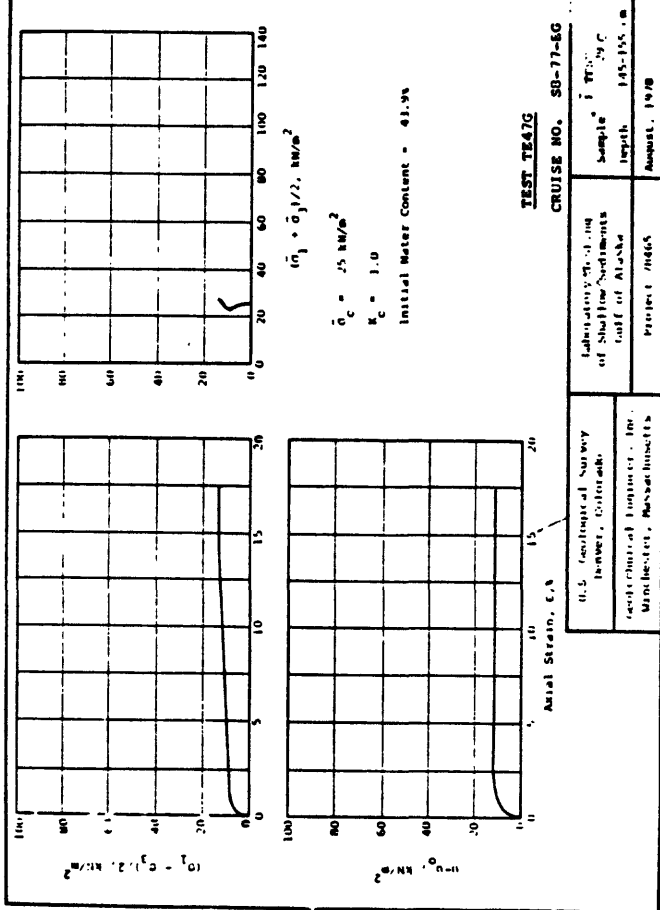
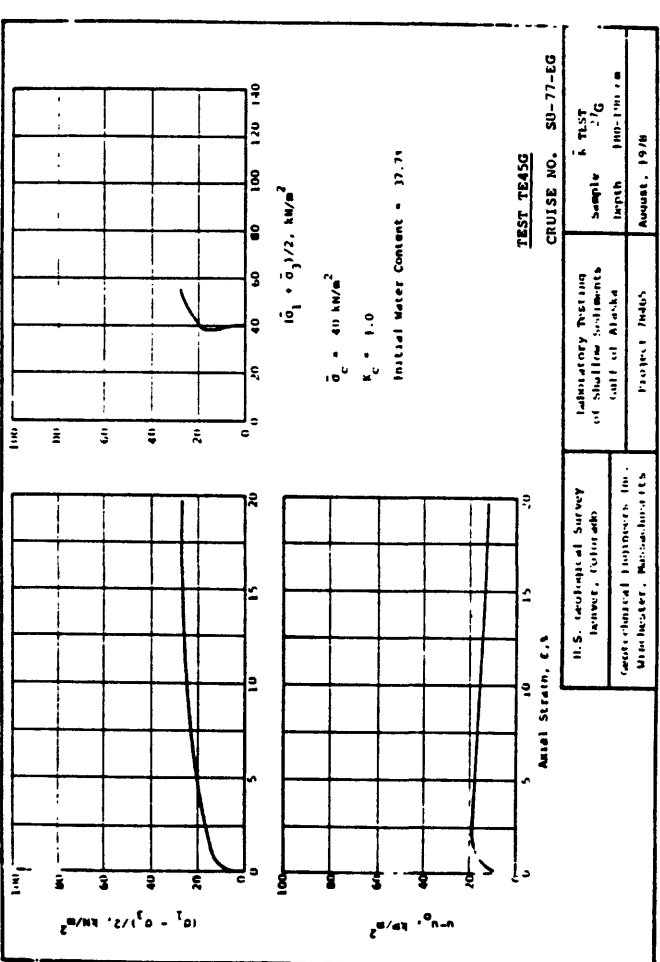


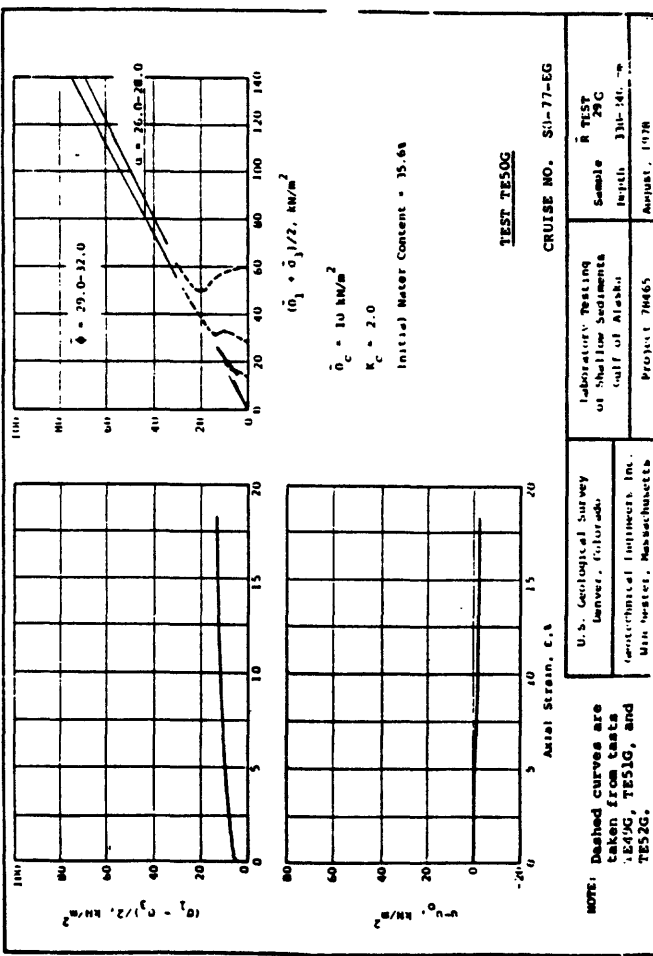
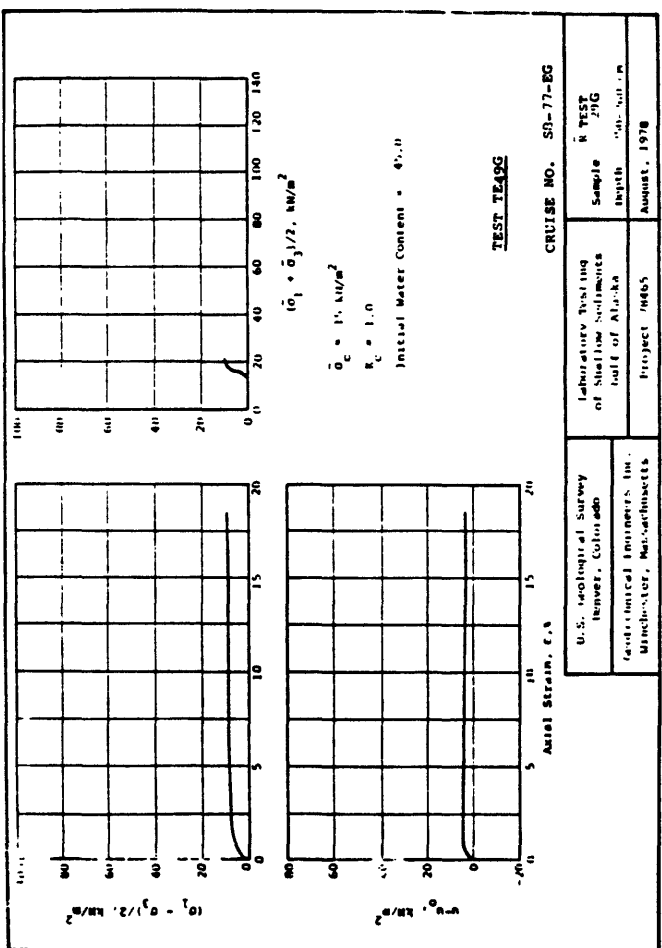
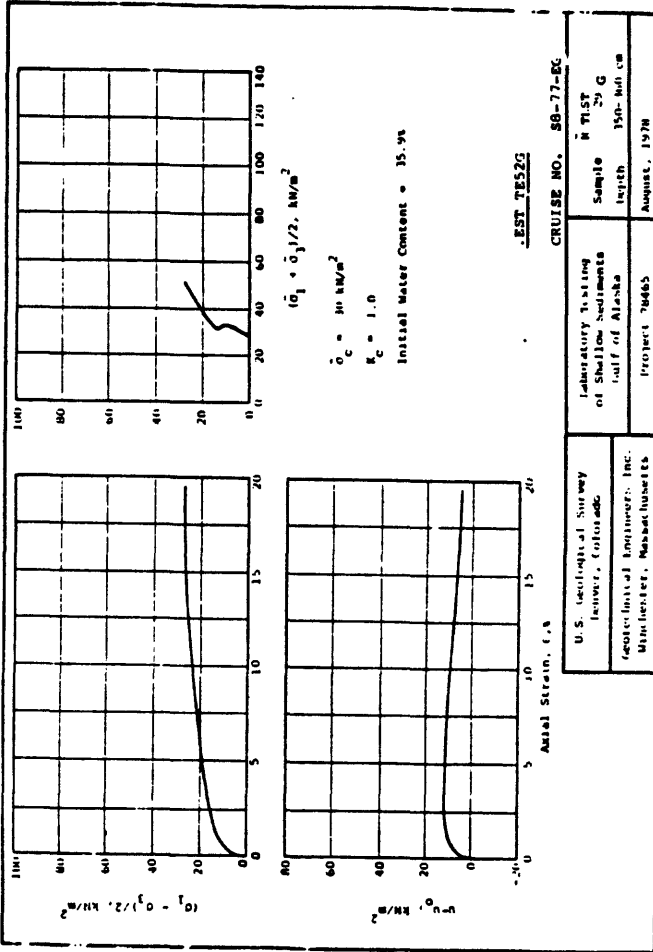
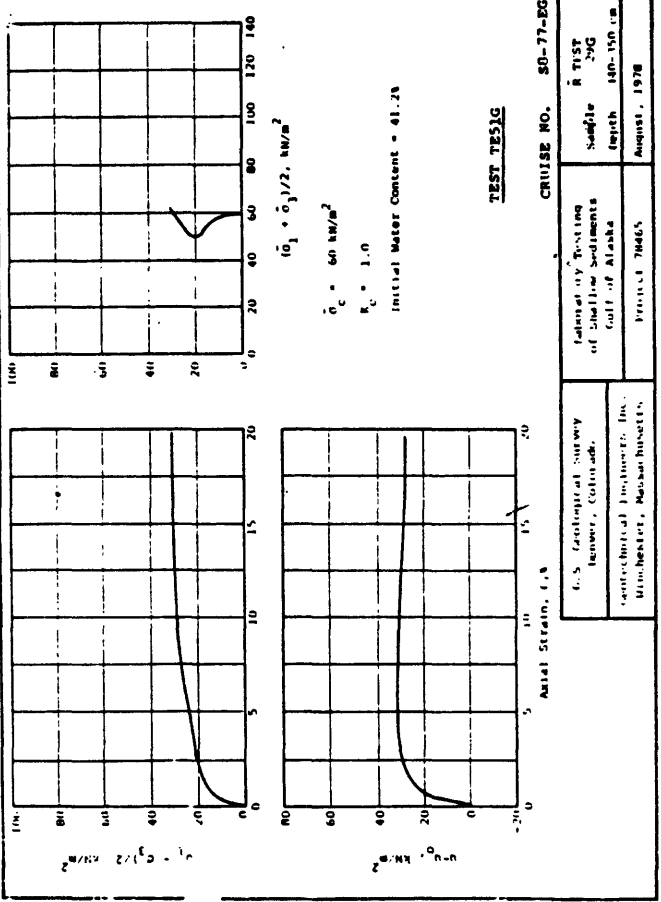




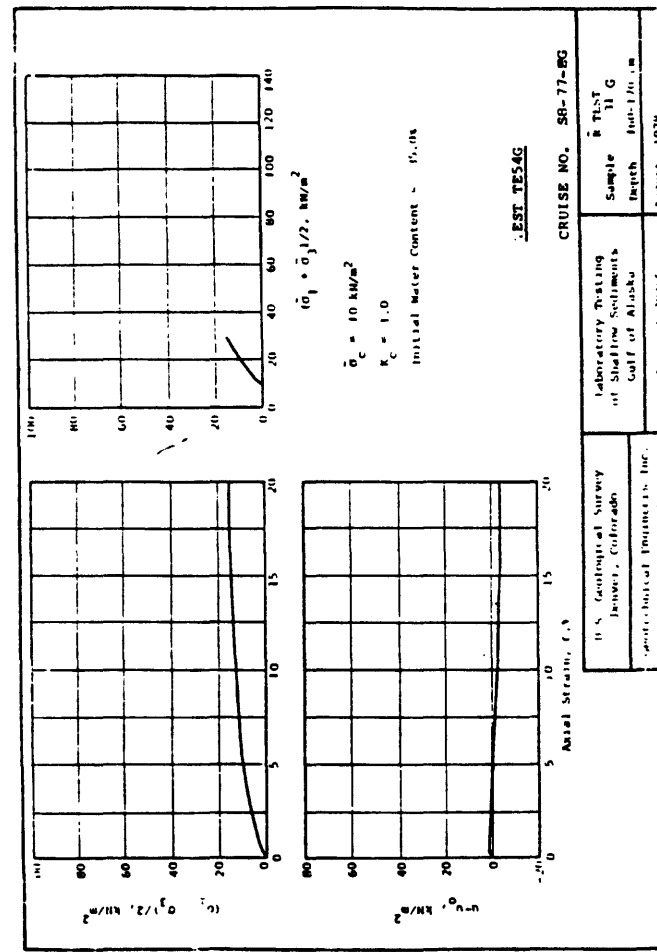
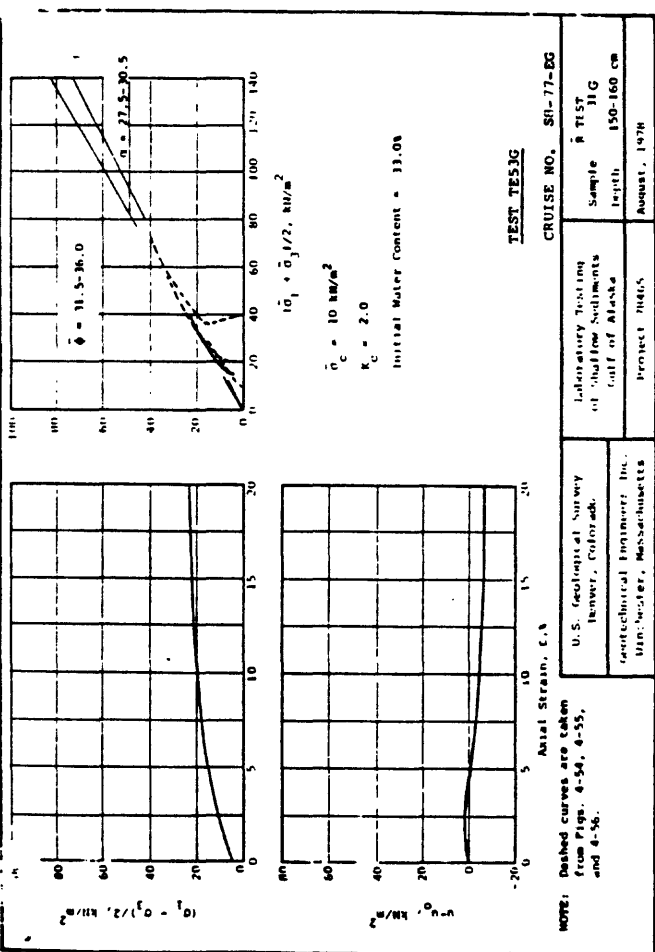
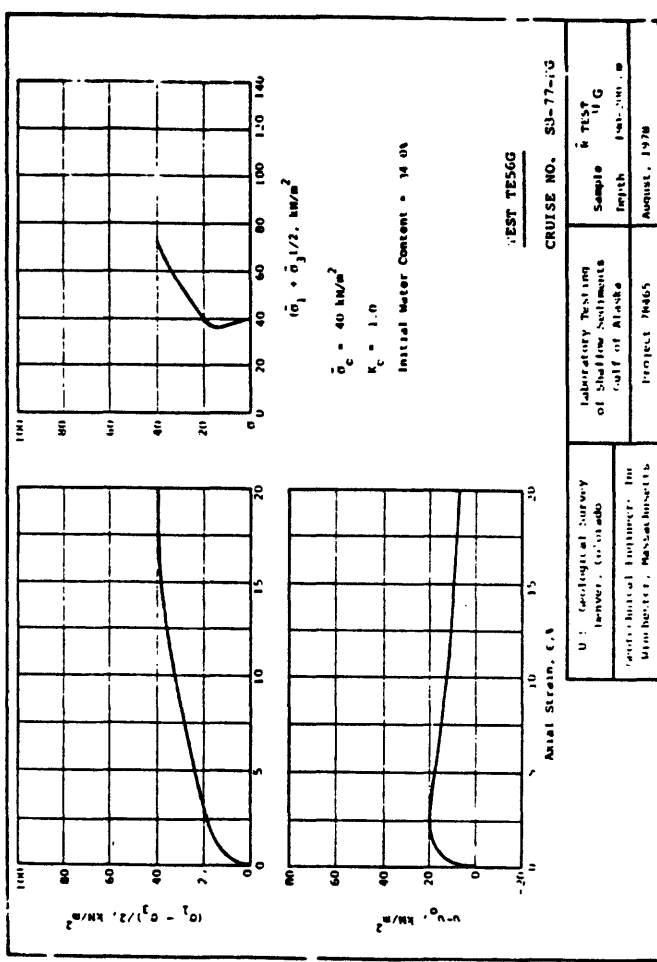
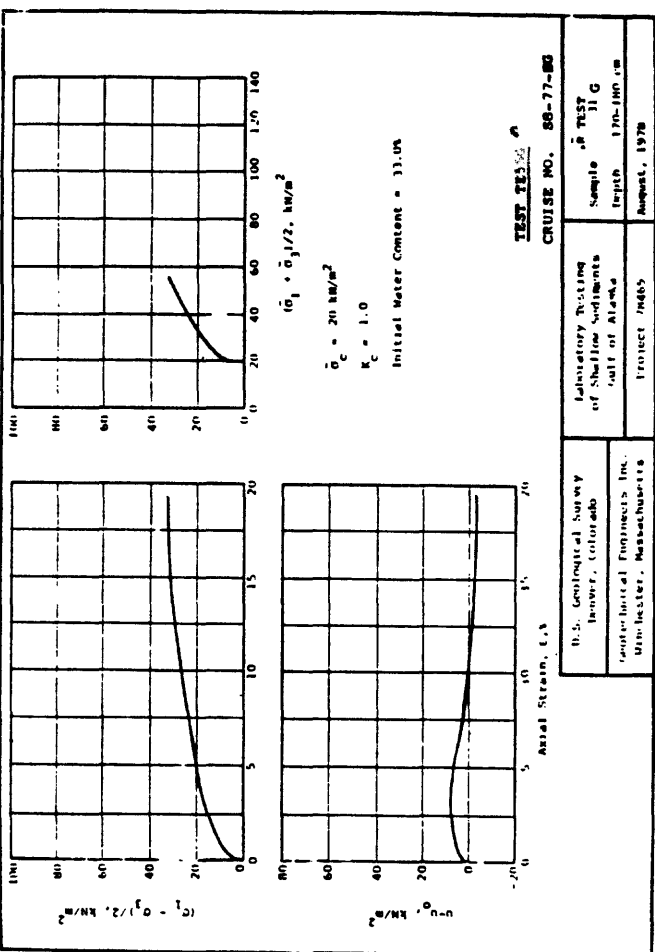


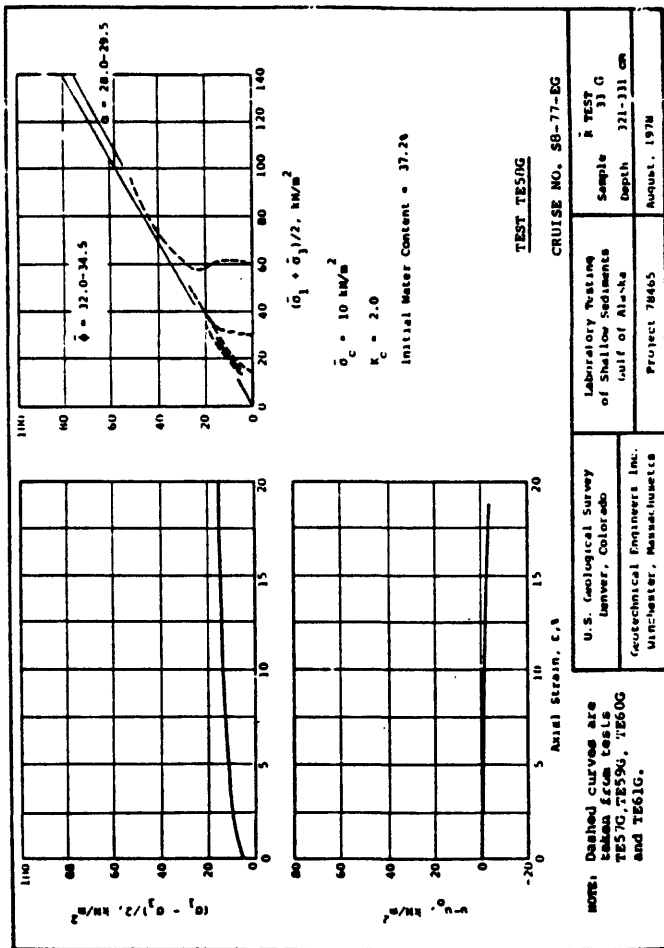
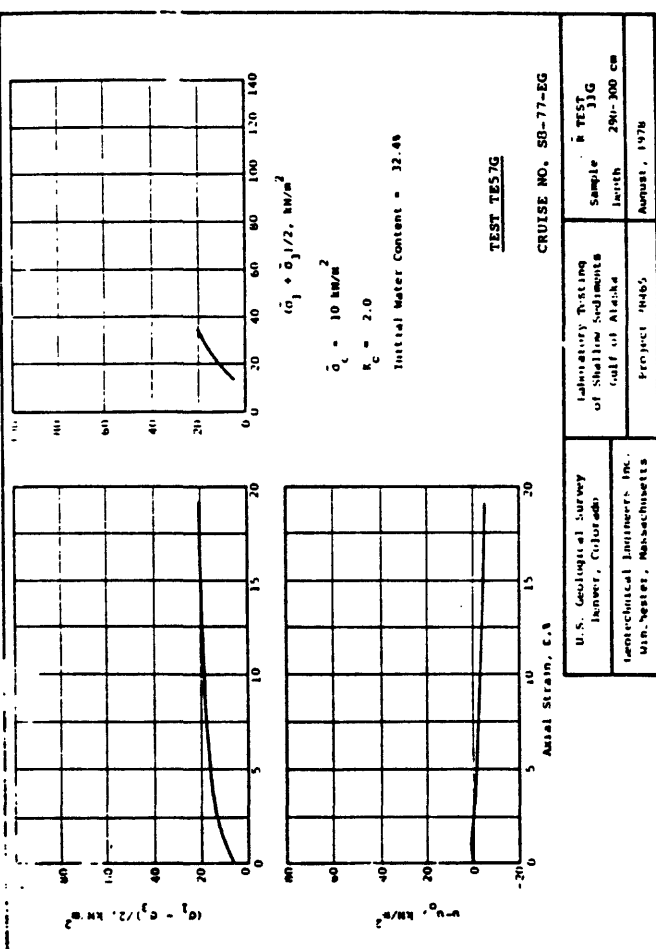
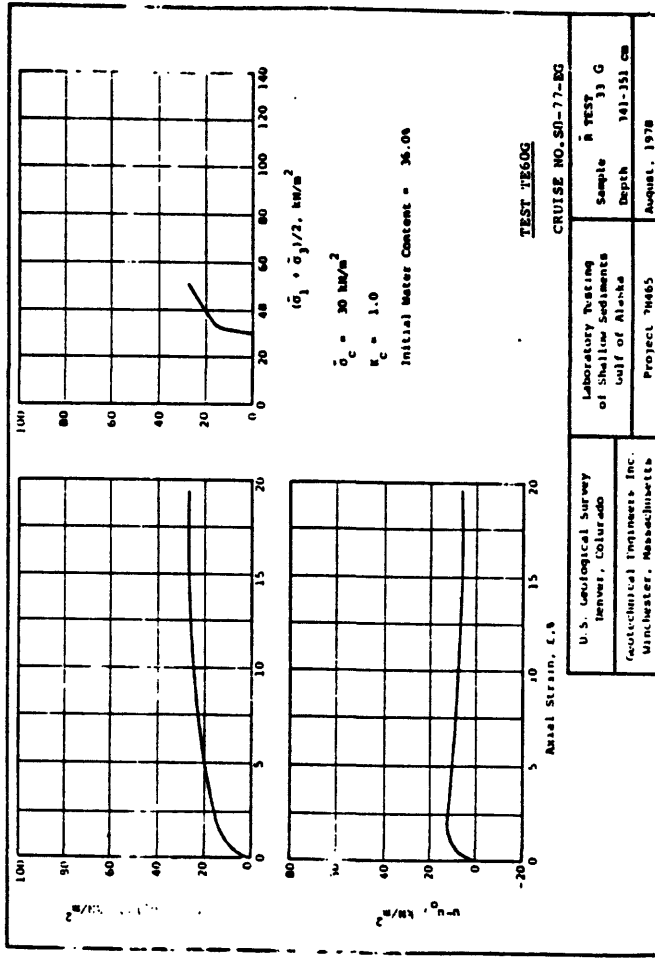
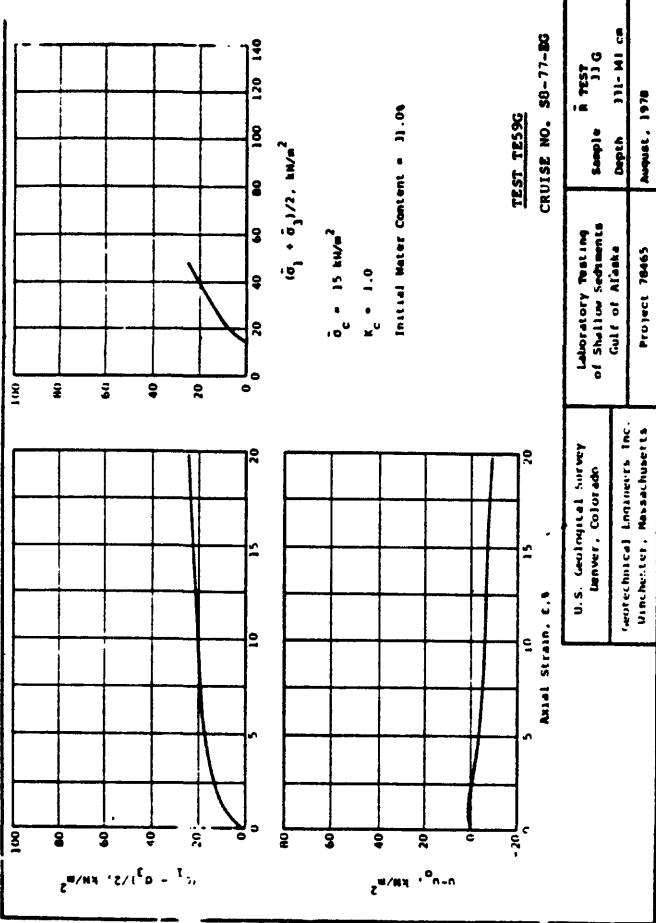


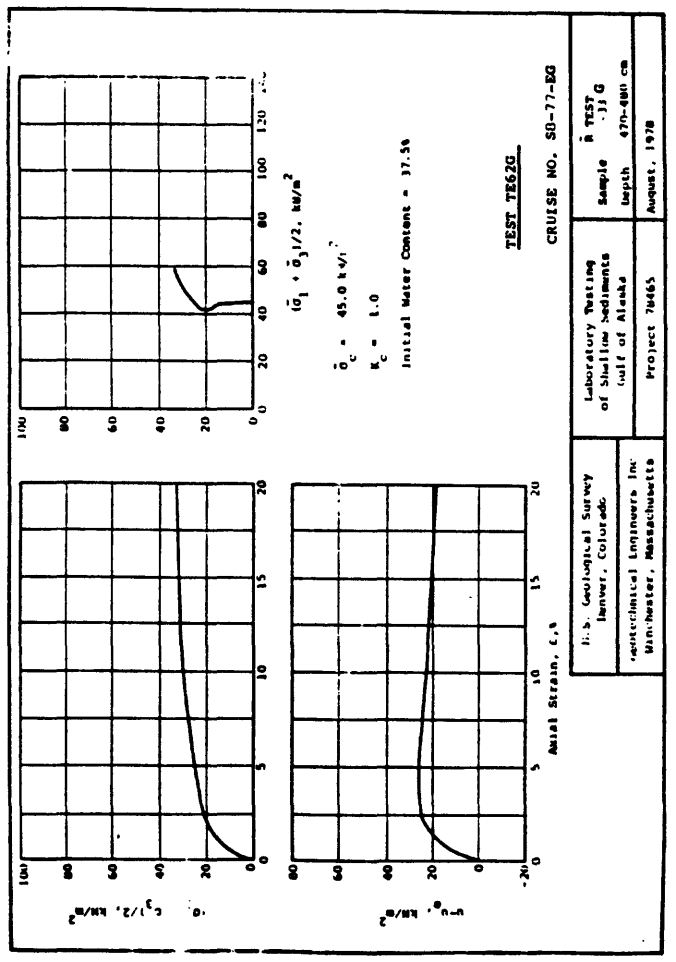
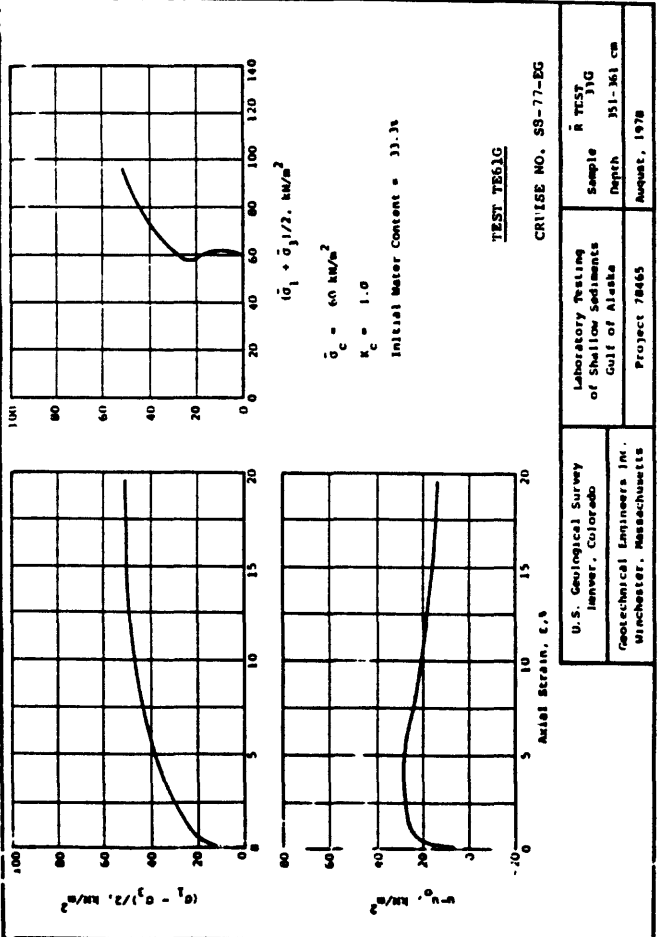
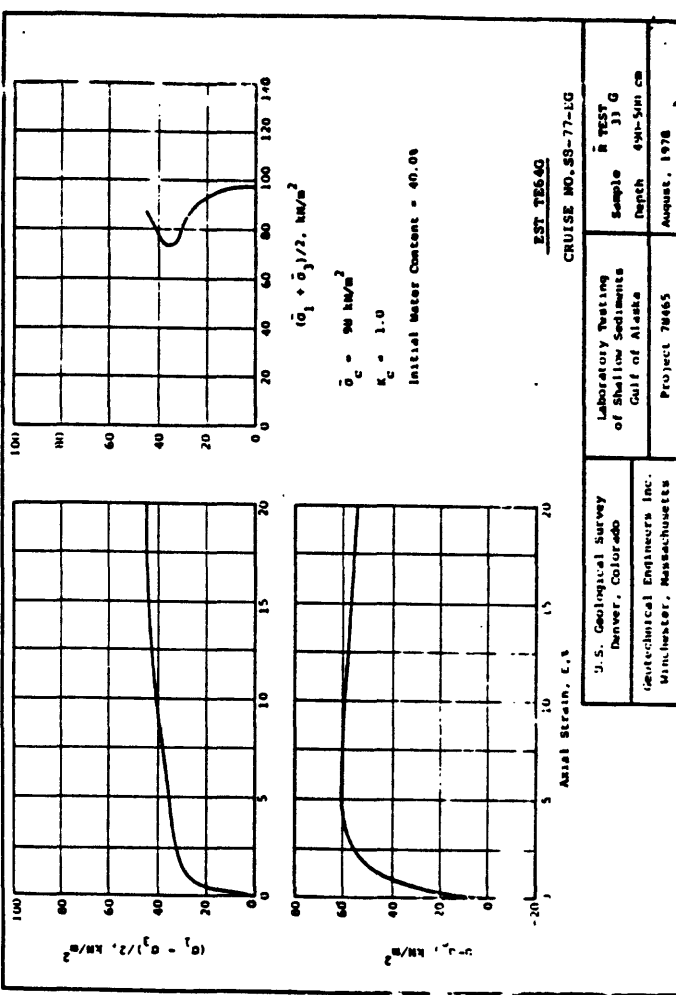
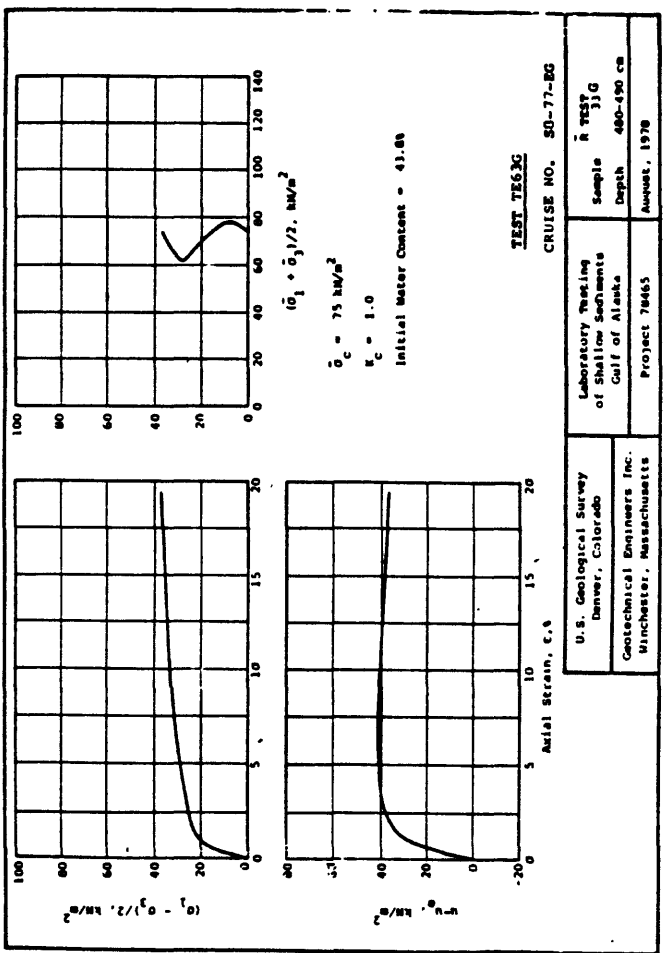


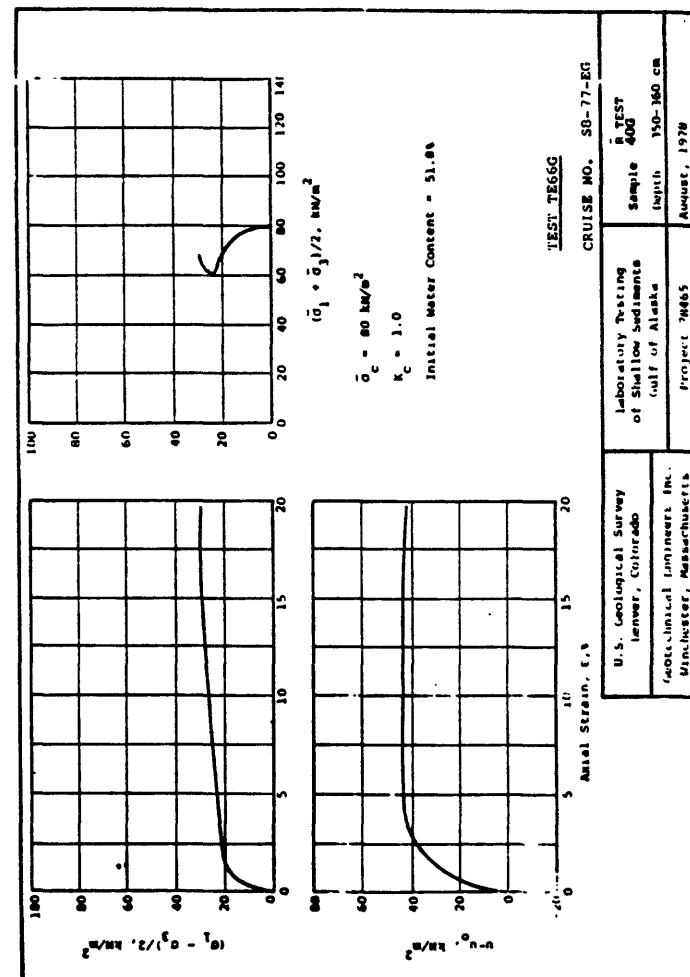
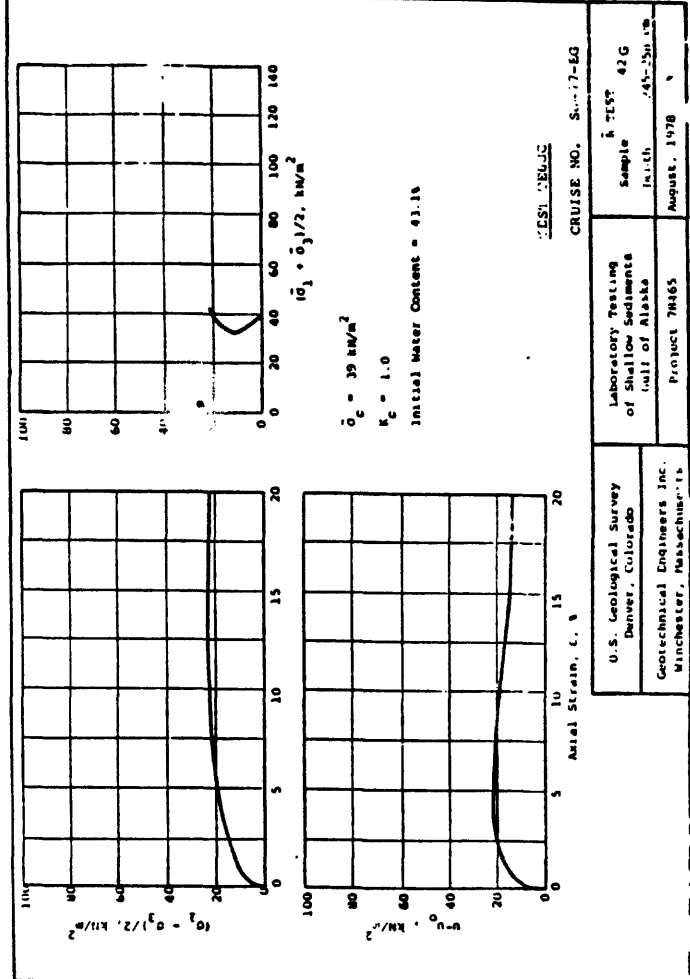
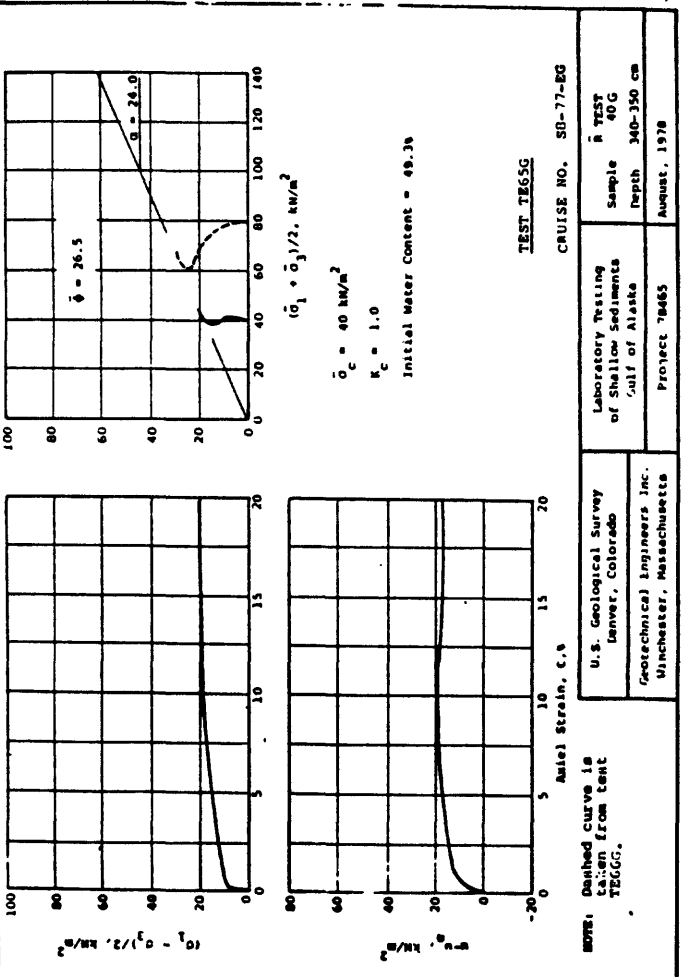
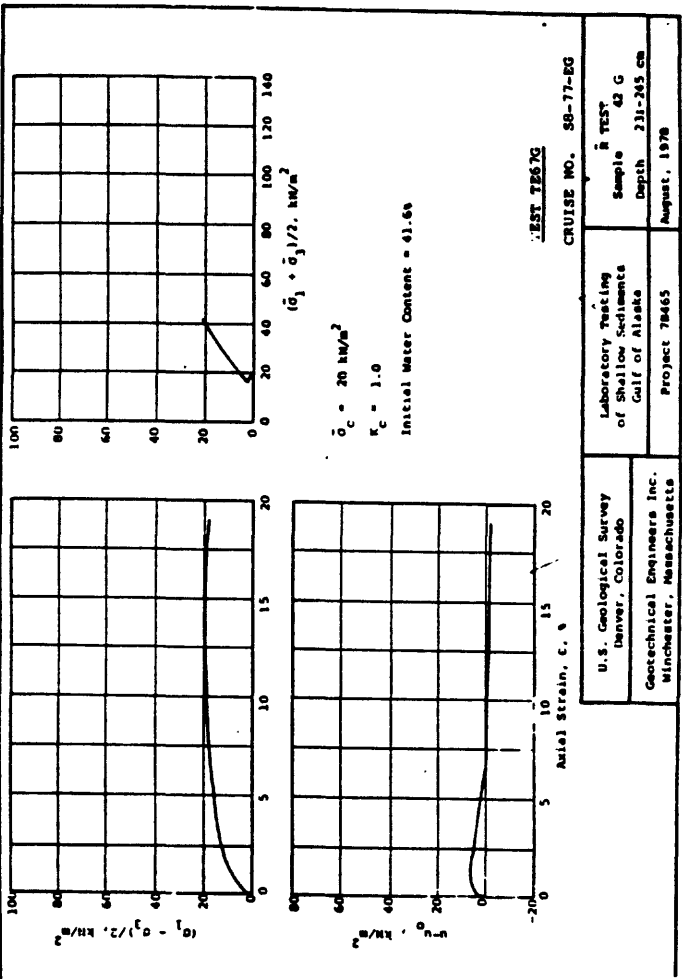


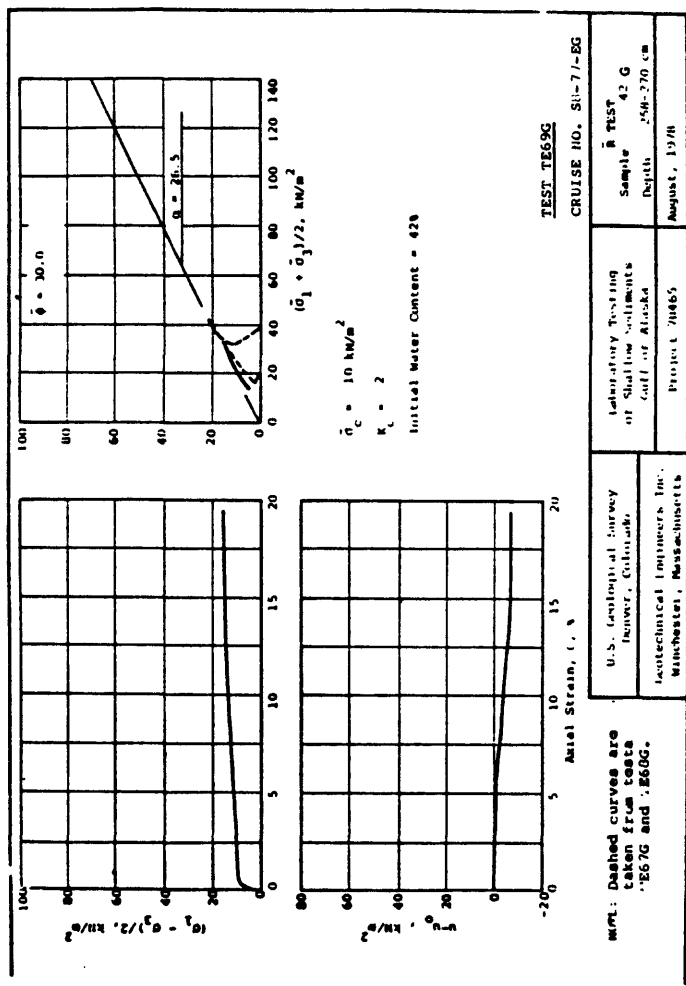
NOTE: Dashed curves are taken from data on TEST TE51G, TEST TE52G, and TEST TE49G.











NPL: Dashed curves are taken from tests TEC7G and TEC8G.

TEST TEC9G			
CRUISE NO. SII-71-EG			
U.S. Geological Survey Iowa City, Iowa, Laboratory Testing of Shallow Instruments Cult. of Alaska	Sample Depth Project Period	in TEST 42 G 250-270 cm TEC9G 1965 1965	
Technological Institute Inc. Wellesley, Massachusetts			

APPENDIX F. CONSOLIDATION AND TRIAXIAL TEST RESULTS-LAW ENGINEERING AND TESTING COMPANY (1980 cores)

This appendix presents the results of consolidation and triaxial testing performed by Law Engineering and Testing Company under Contract number 4-08-0001-19241 with the U.S. Geological Survey. Testing was performed under the direction of R.G. Hamadock, P.G. Swanson and P.W. Mayne. Core samples were from DC2-80-EG.

All tests in this group have been assigned a test number with L2 as the last two characters. The consolidation tests (first two characters are OE) are presented first and are ordered by test number. Results from a single test are presented on a page in the form of void ratio versus the vertical effective stress.

The static triaxial tests (first two characters are TE) are given second and ordered by test number. Results from one to as many as four tests are presented on the same sheet. The upper left plot is a stress path presented as a plot of maximum shear stress ( $q$ ) versus the normal effective stress on the plane of maximum shear ( $p'$ ). The stress paths of Appendix D are defined differently. The upper right plot is the maximum shearing stress versus the axial strain. The lower left plot is the measured excess pore water pressure plotted versus axial strain.

The cyclic triaxial tests (first two characters are TC) are given third and ordered by test number. Results from one to three tests are presented on two sheets. The first sheet includes  $p'$ - $q$  stress path, shear stress-axial strain and excess pore pressure-axial strain plots that are analogous to the plots given for static triaxial tests. However, the plots are given for only a few selected cycles to illustrate how the response changes as the number of cycles increases. Numbers on the plots correspond to cycle number.

The second sheet shows several parameters plotted versus cycle number. The upper left graph shows the cyclic stress level normalized by the static strength (obtained from a nearby sample-Method I of the main text) versus the number of cycles to achieve a given double amplitude strain level. Lines are drawn connecting points corresponding to the same strain level. The upper right graph shows the excess pore pressure generated as a function of the cycle number. The lower right graph shows the double amplitude axial strain as a function of cycle number.

LAW ENGINEERING  
TESTS

CONSOLIDATION TEST

TEST OEA12

CUMULATIVE STRAIN (%)  
0.100  
INITIAL VOID RATIO  
0.637  
INITIAL VERTICAL STRESS  
22  
INITIAL VOID RATIO  
0.637  
INITIAL WATER CONTENT  
41.4  
INITIAL SATURATION  
100.0  
INITIAL VACUUM  $\text{psia}^{-1}$   
10.20  
EFFECTIVE  
0.6  
OVERBURDEN PRESSURE  
5.6  
SAMPLE  
DC146EG  
IDENTIFICATION  
CONE NO.  
49 G  
DEPTH (ft)  
56.11

U.S. & MASHIM CO., INC.  
CONTRACT NO. 1600  
LETIC PROJECT NO. 6700

271

EFFECTIVE VERTICAL STRESS  $\text{psi}$   $\sigma_v'$   
1000  
500  
300  
200  
100  
50  
0

LAW ENGINEERING

LAW ENGINEERING  
TESTS

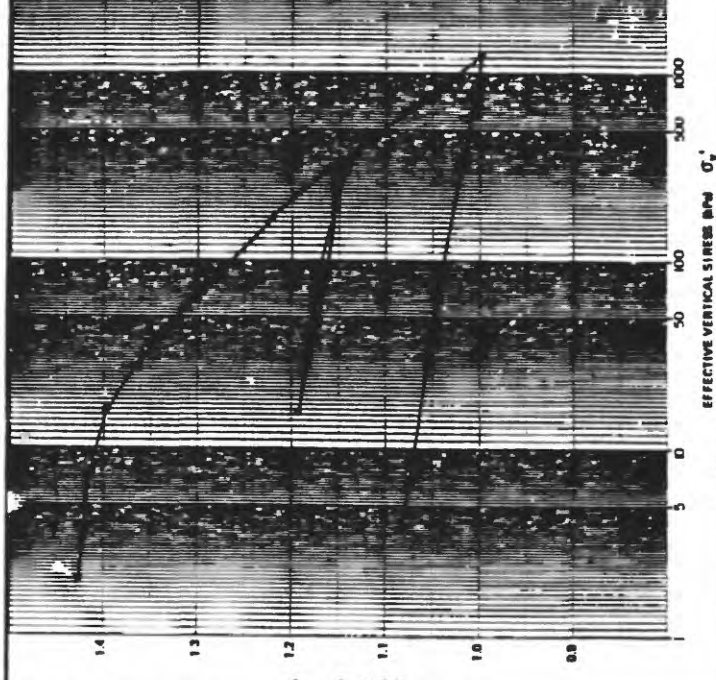
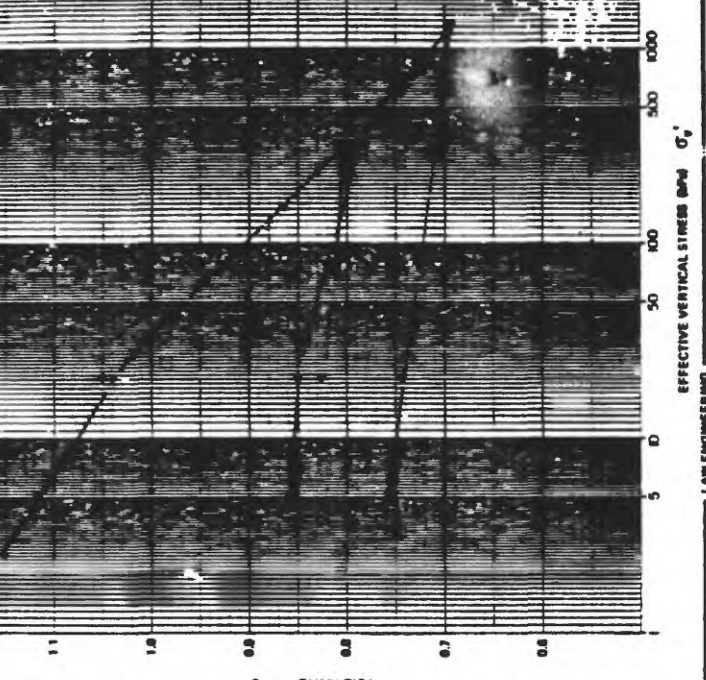
CONSOLIDATION TEST  
TEST OEA12

CUMULATIVE STRAIN (%)  
0.202  
INITIAL VERTICAL STRESS  
22  
INITIAL VOID RATIO  
0.637  
INITIAL WATER CONTENT  
41.4  
INITIAL SATURATION  
100.0  
INITIAL VACUUM  $\text{psia}^{-1}$   
10.20  
EFFECTIVE  
0.2  
OVERBURDEN PRESSURE  
SAMPLE  
DC246EG  
IDENTIFICATION  
CONE NO.  
49 G  
DEPTH (ft)  
74.50

U.S. & MASHIM CO., INC.  
CONTRACT NO. 1600  
LETIC PROJECT NO. 6700

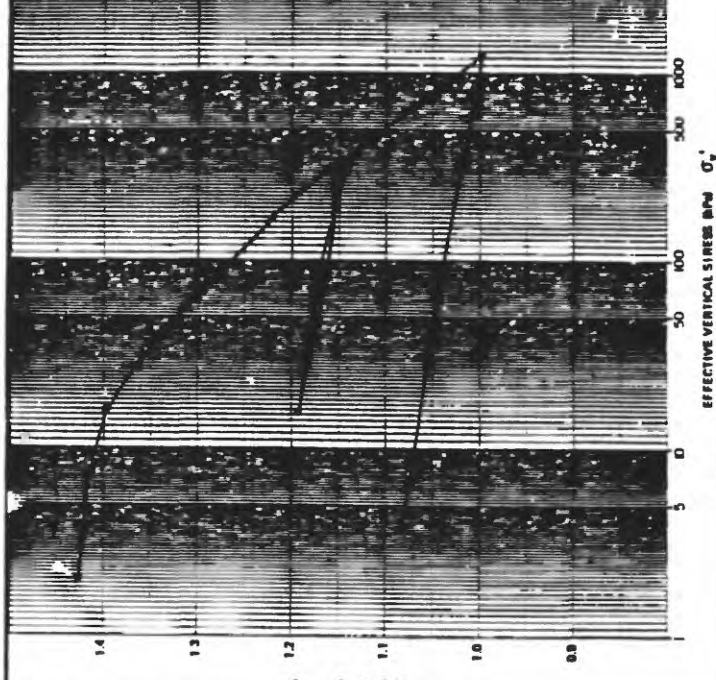
EFFECTIVE VERTICAL STRESS  $\text{psi}$   $\sigma_v'$   
1000  
500  
300  
200  
100  
50  
0

LAW ENGINEERING



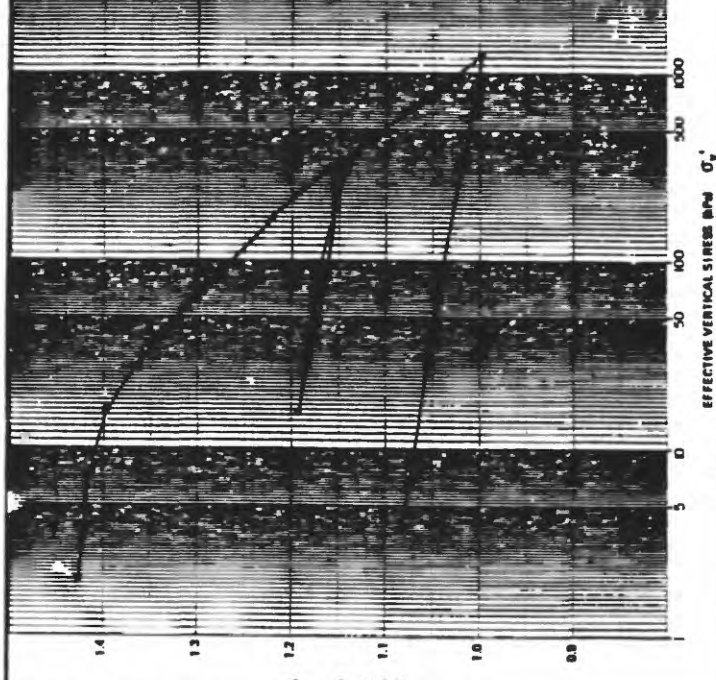
EFFECTIVE VERTICAL STRESS  $\text{psi}$   $\sigma_v'$   
1000  
500  
300  
200  
100  
50  
0

LAW ENGINEERING



EFFECTIVE VERTICAL STRESS  $\text{psi}$   $\sigma_v'$   
1000  
500  
300  
200  
100  
50  
0

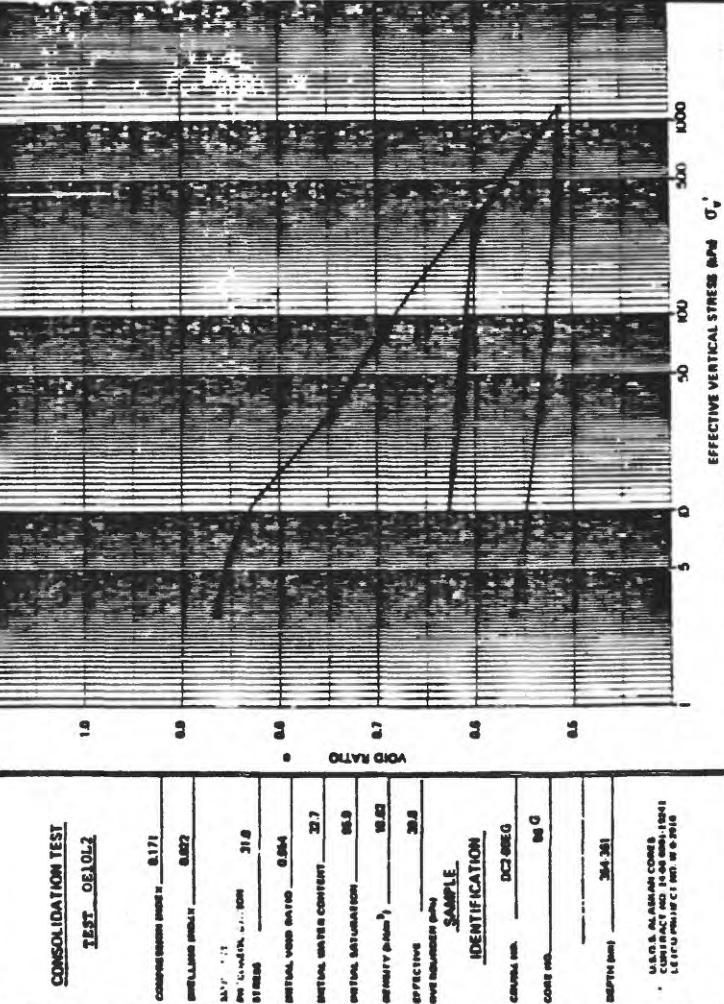
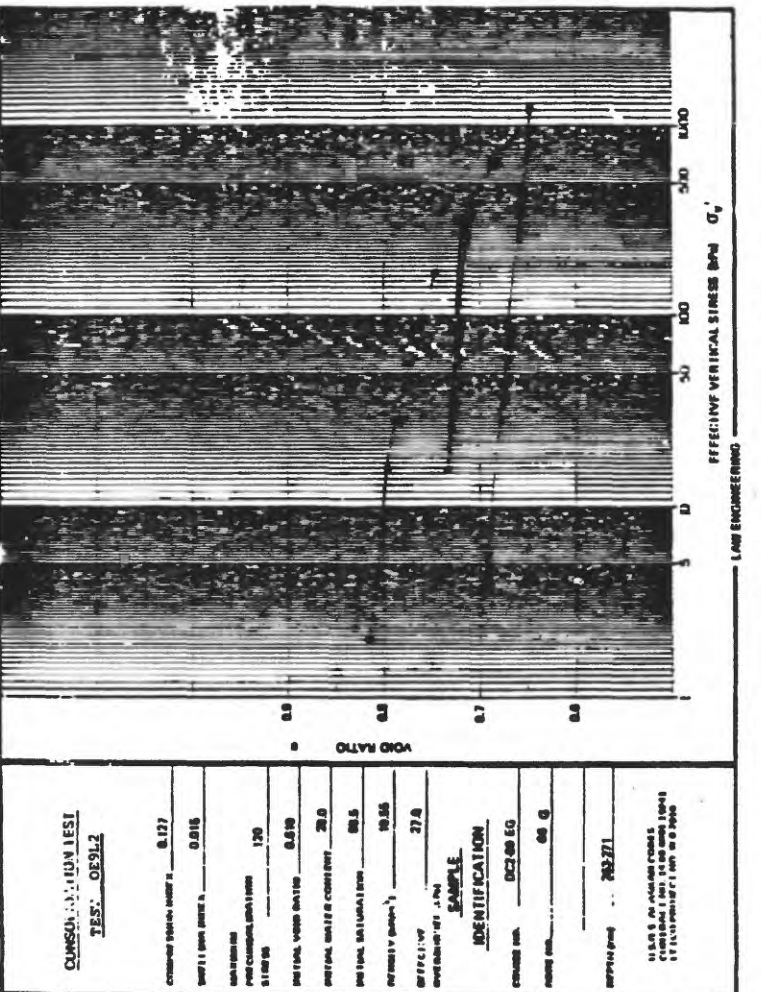
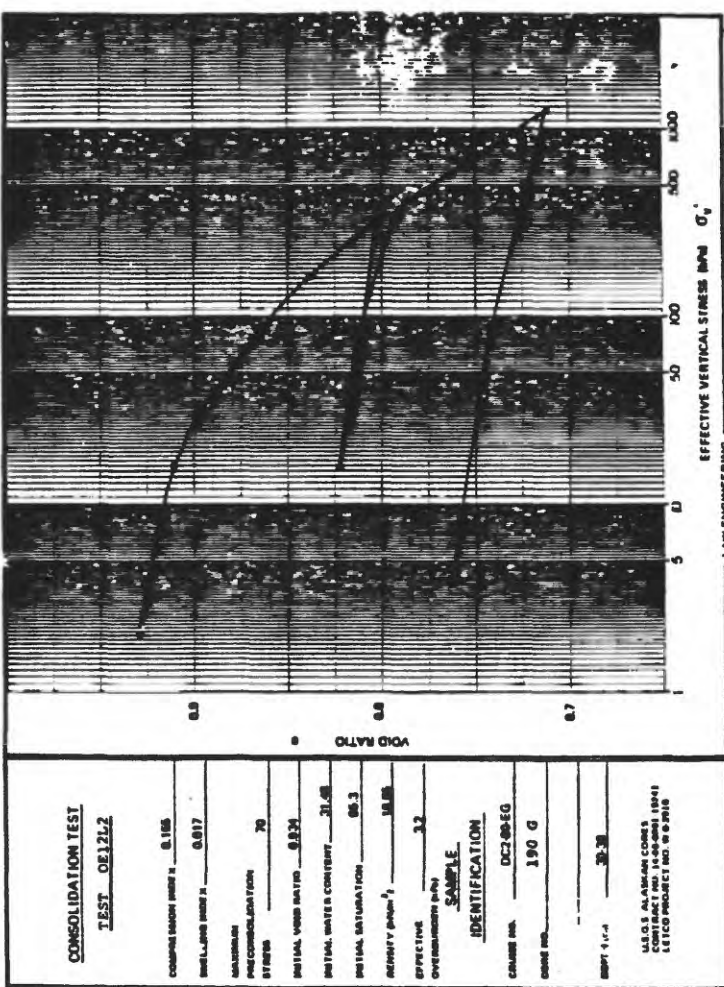
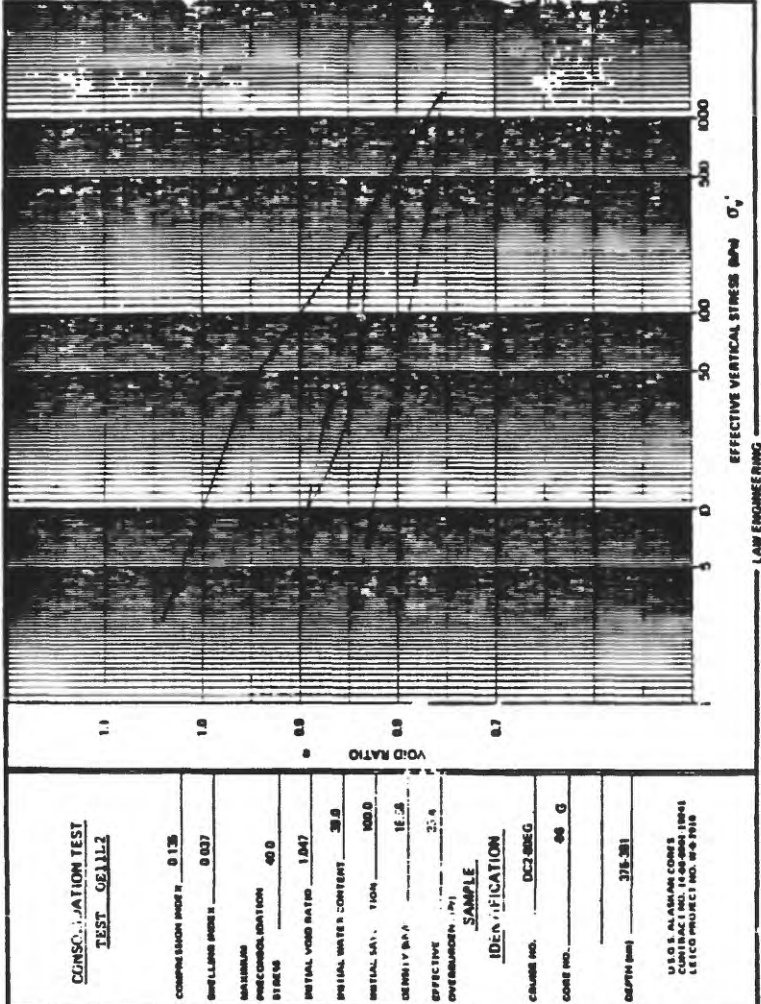
LAW ENGINEERING

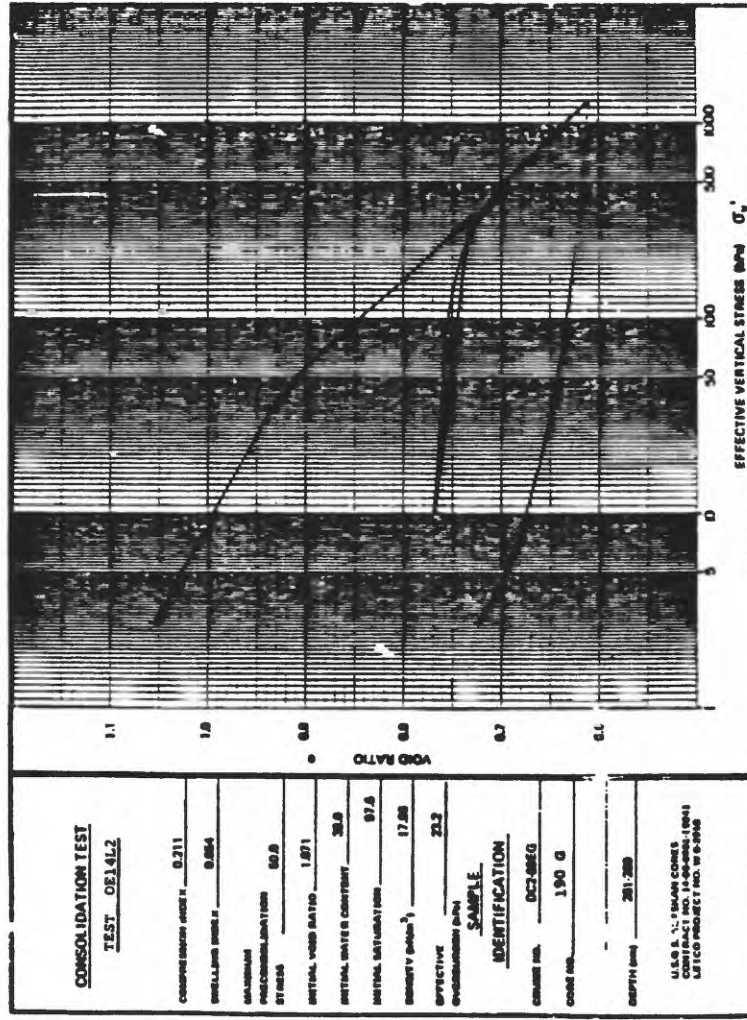
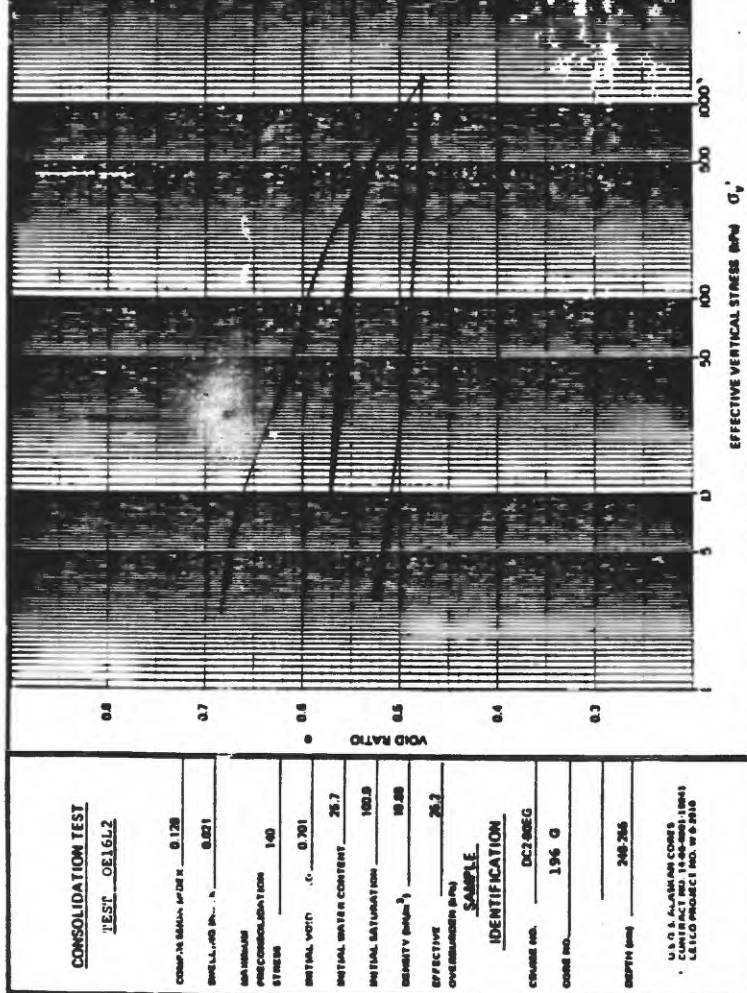
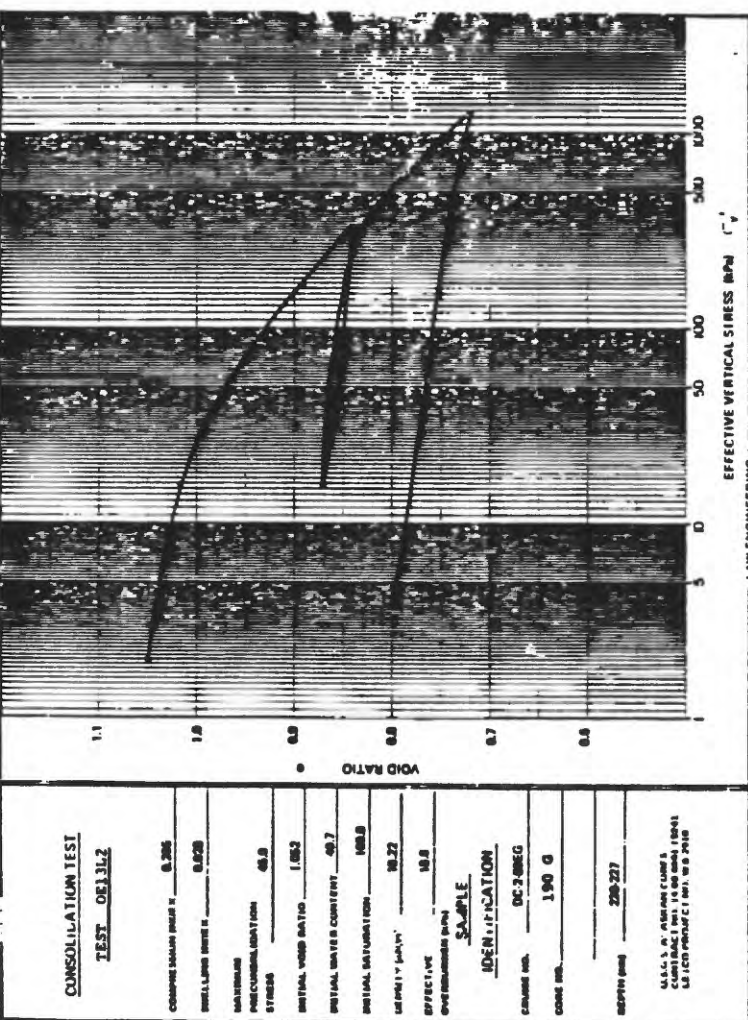
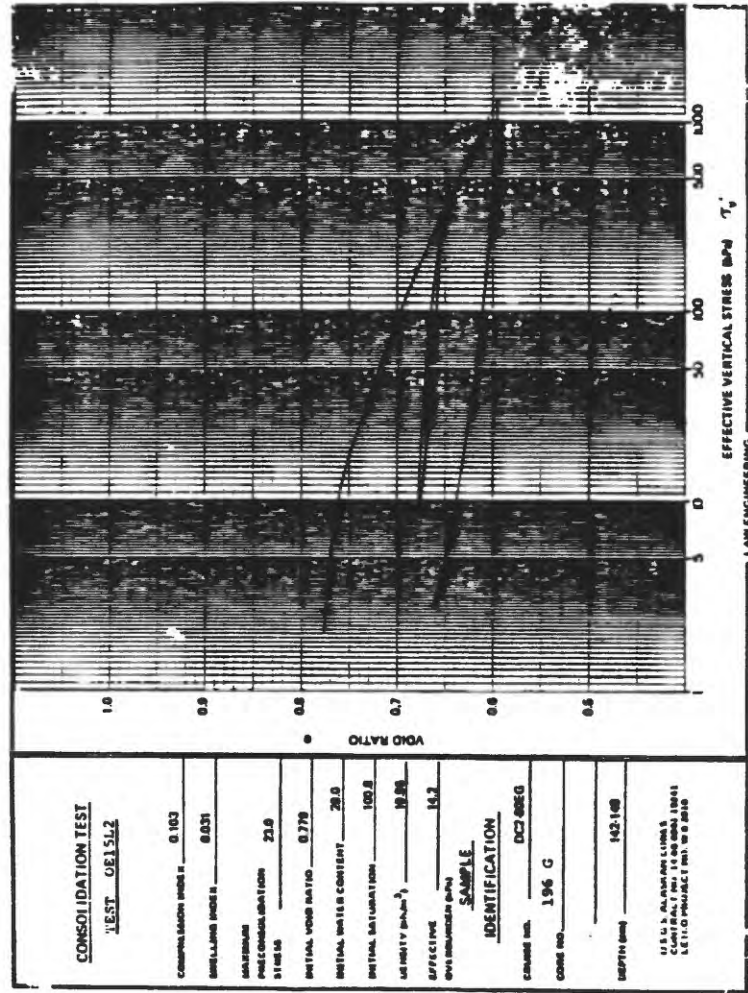


EFFECTIVE VERTICAL STRESS  $\text{psi}$   $\sigma_v'$   
1000  
500  
300  
200  
100  
50  
0

LAW ENGINEERING







CONSOLIDATION TEST

TEST\_OCT 74.2

COMPLIANCE INDEX =	0.60
INITIAL DRY UNIT W.	0.527
INITIAL DENSITY	12.0
INITIAL CONSOLIDATION STRESS	120.0
STRENGTH	0.602
INITIAL VOID RATIO	0.602
INITIAL WATER CONTENT	21.9
INITIAL SATURATION	0.4
TEST NO. (10 <sup>-6</sup> ft <sup>2</sup> )	20.20
EFFECTIVE STRESS	45.0
TEST NUMBER	195 Q
TEST NO.	0.5
TEST NO.	45449

U.S.A. STANDARDS CONTRACT NO. 100-64-1001

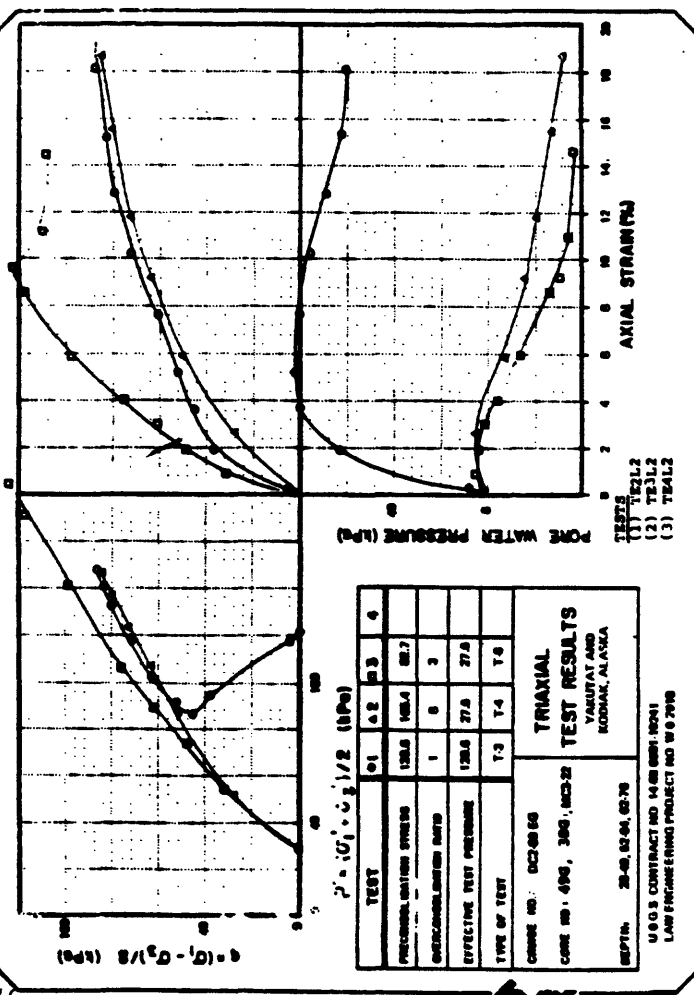
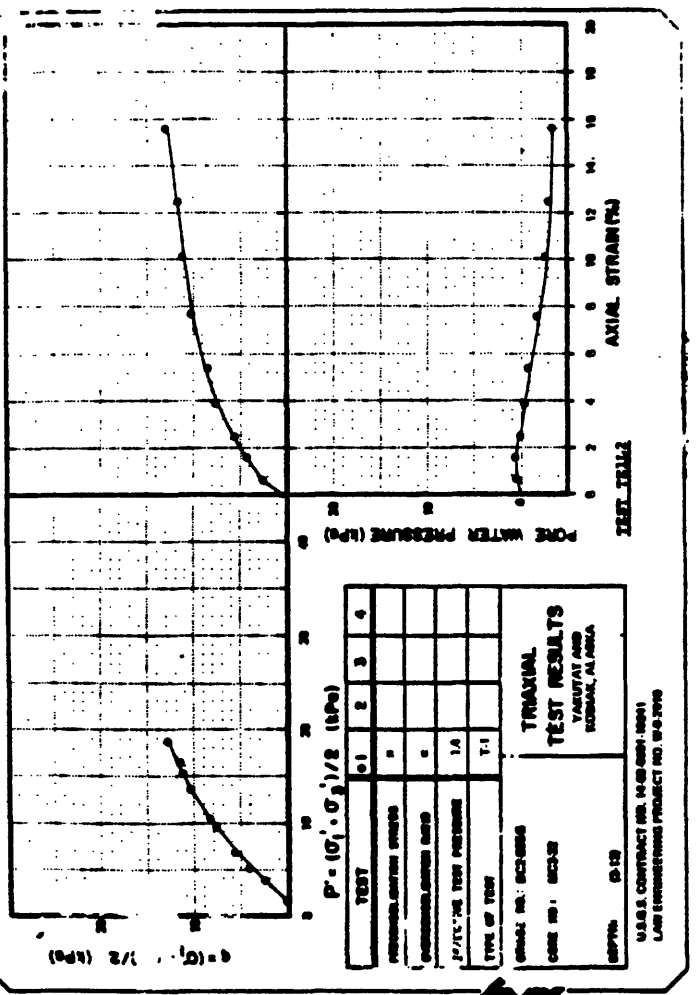
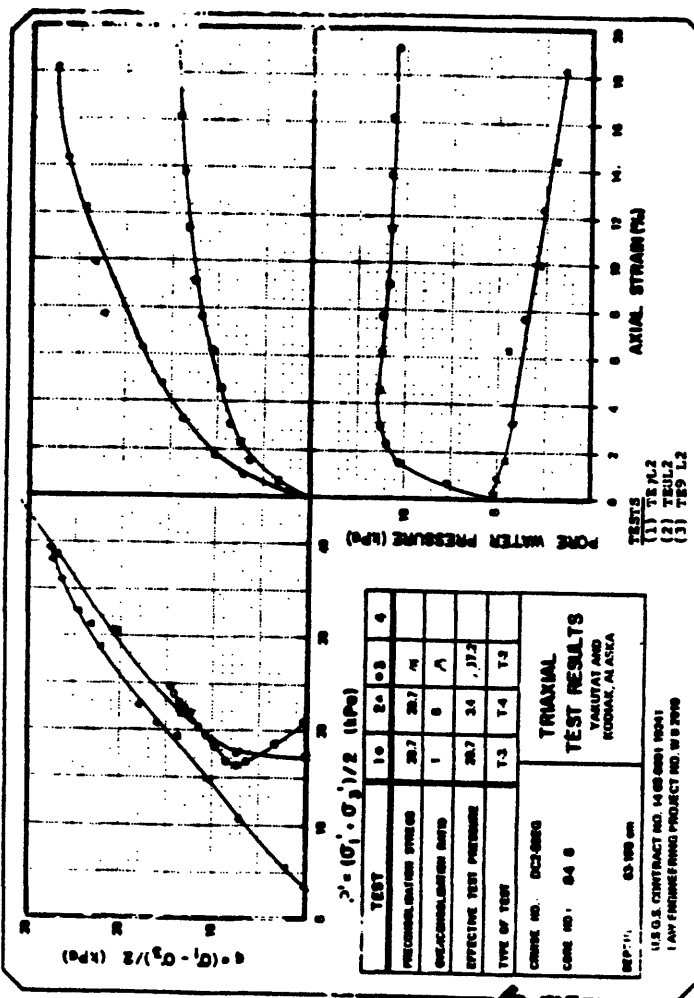
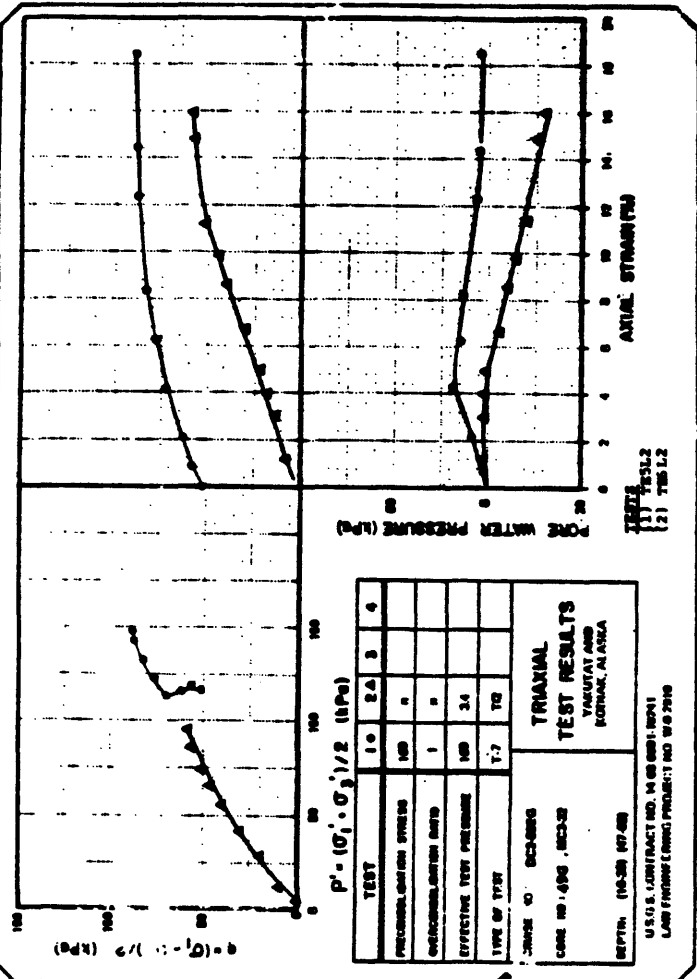
LEEDS & SEARS LTD. 9-2-1970

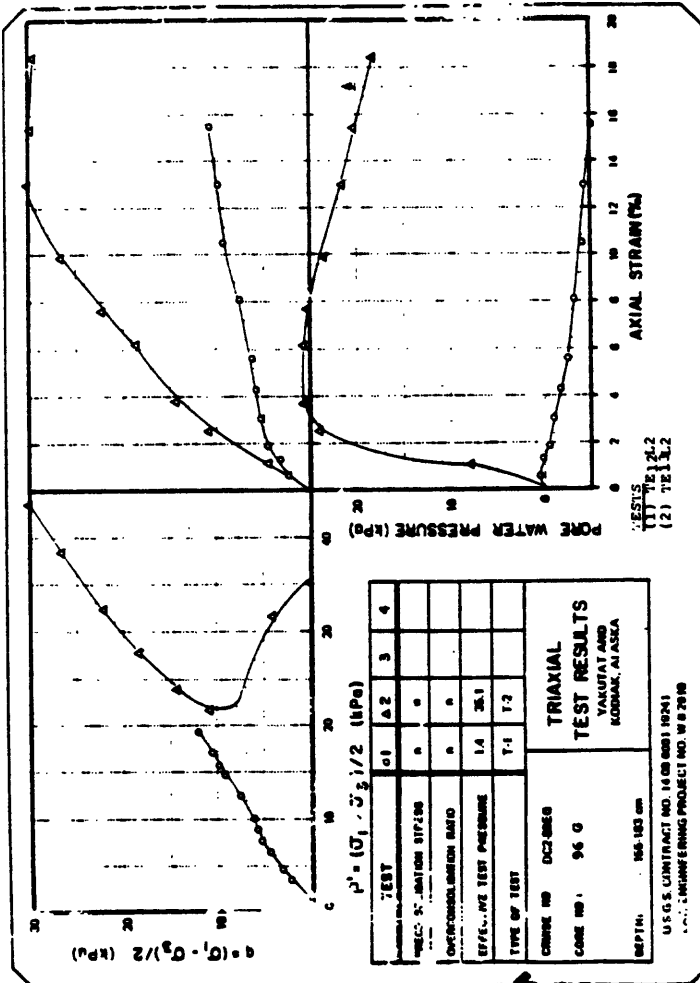
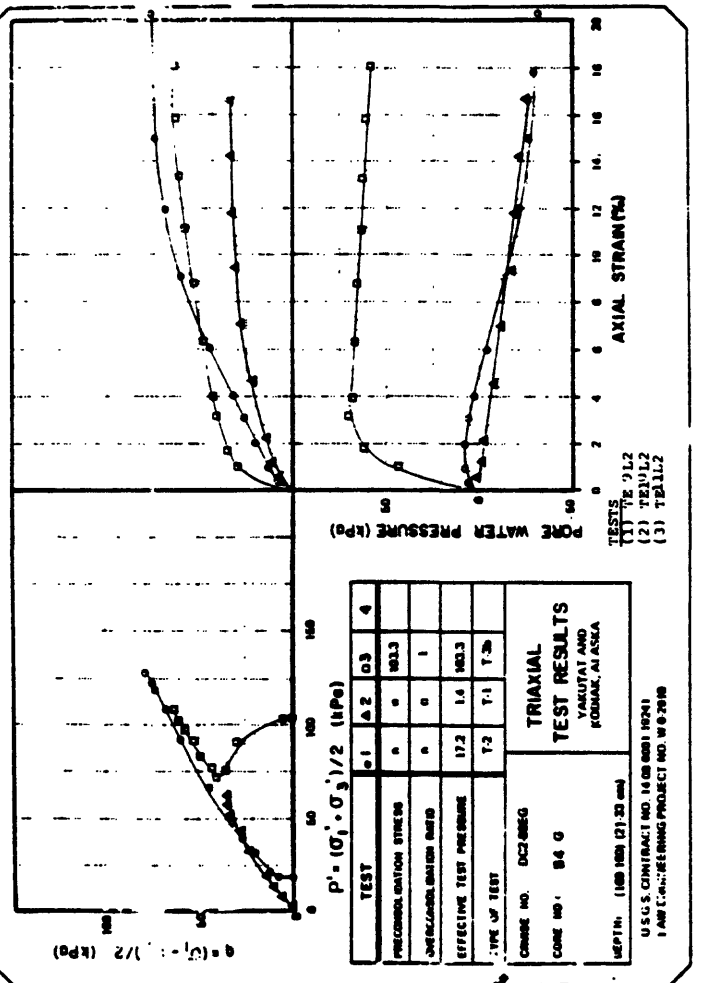
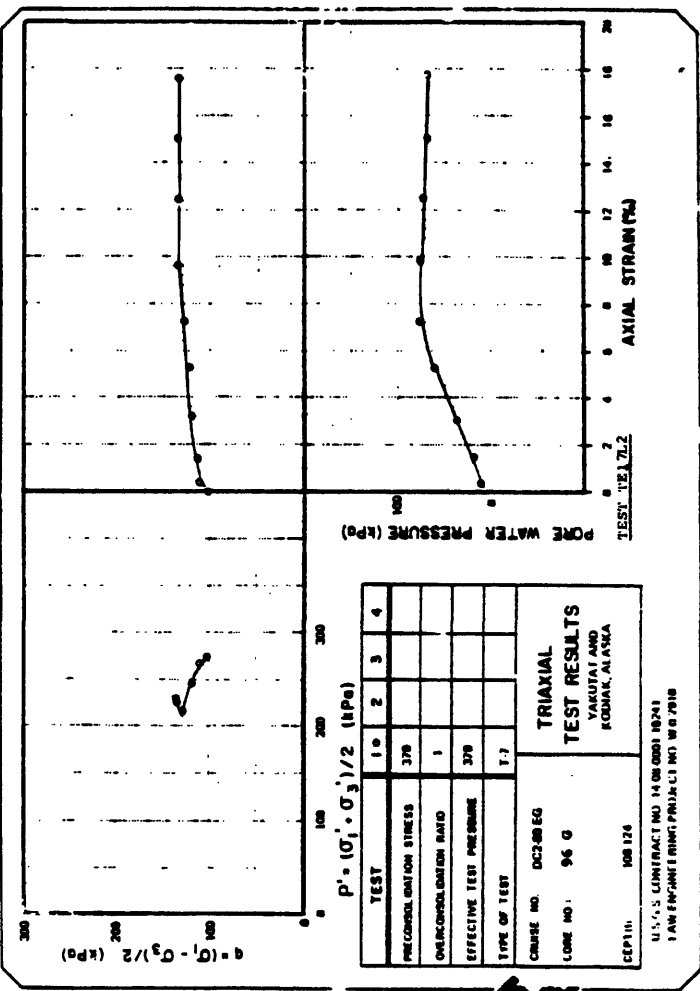
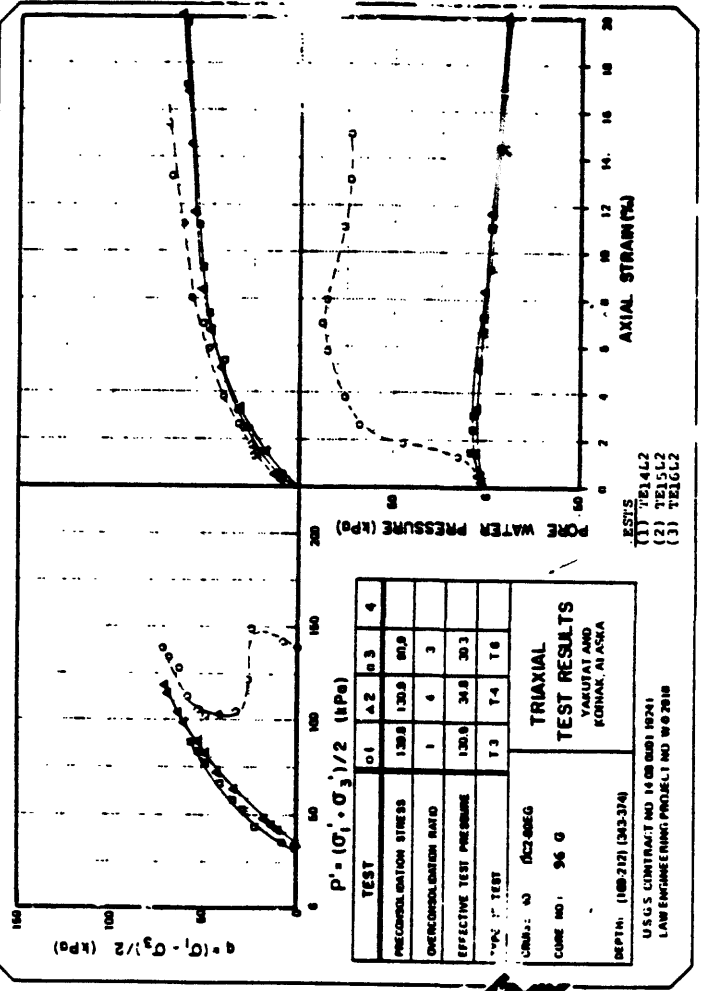
EFFECTIVE VERTICAL STRESS (KPA)  $\sigma'_v$

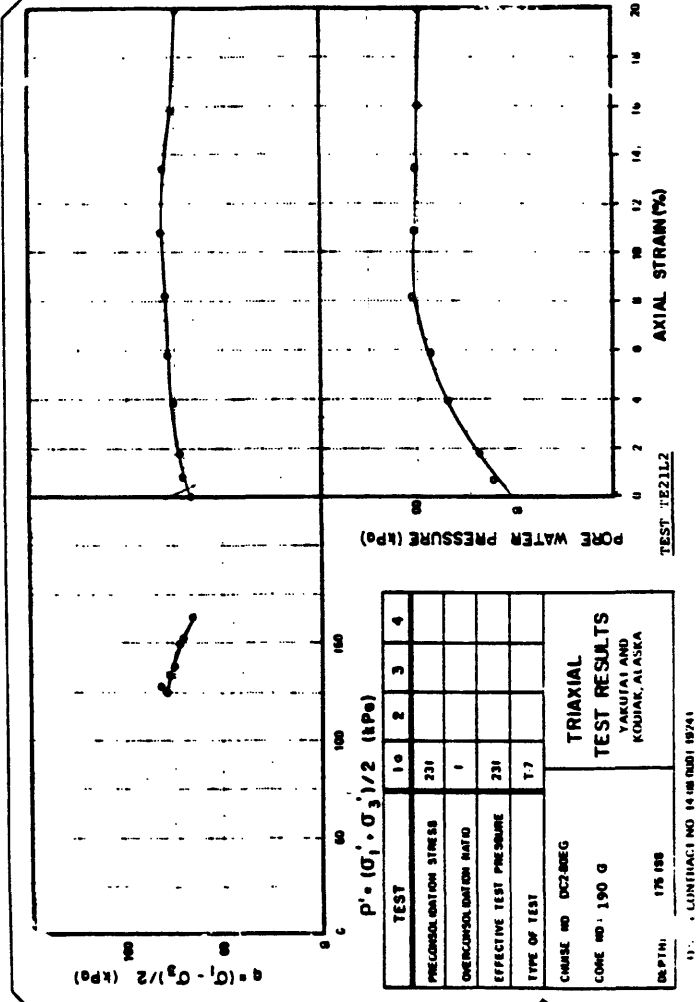
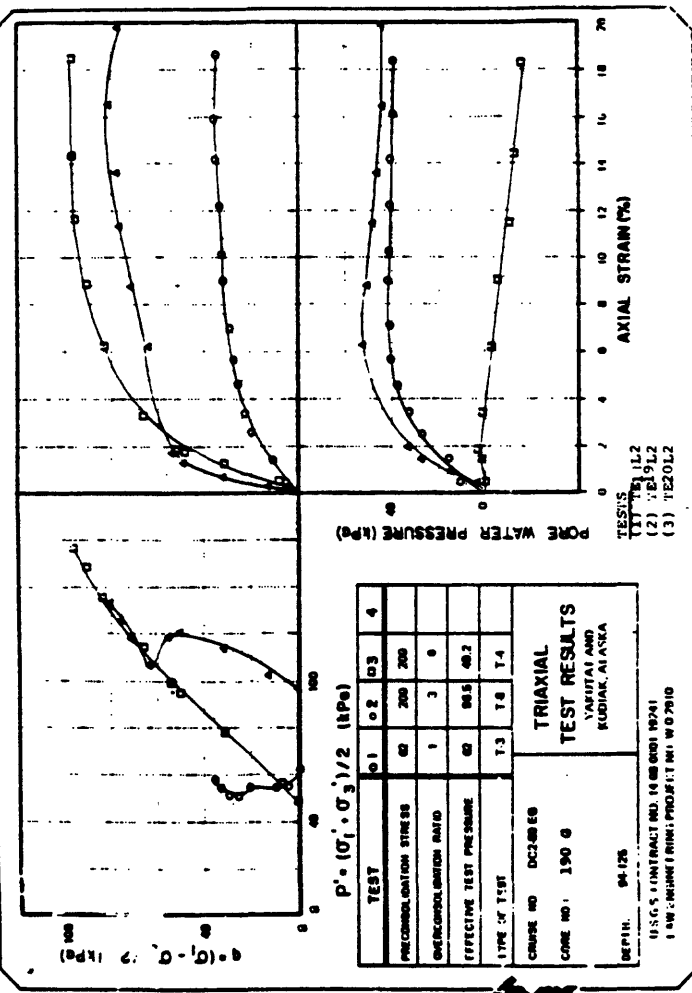
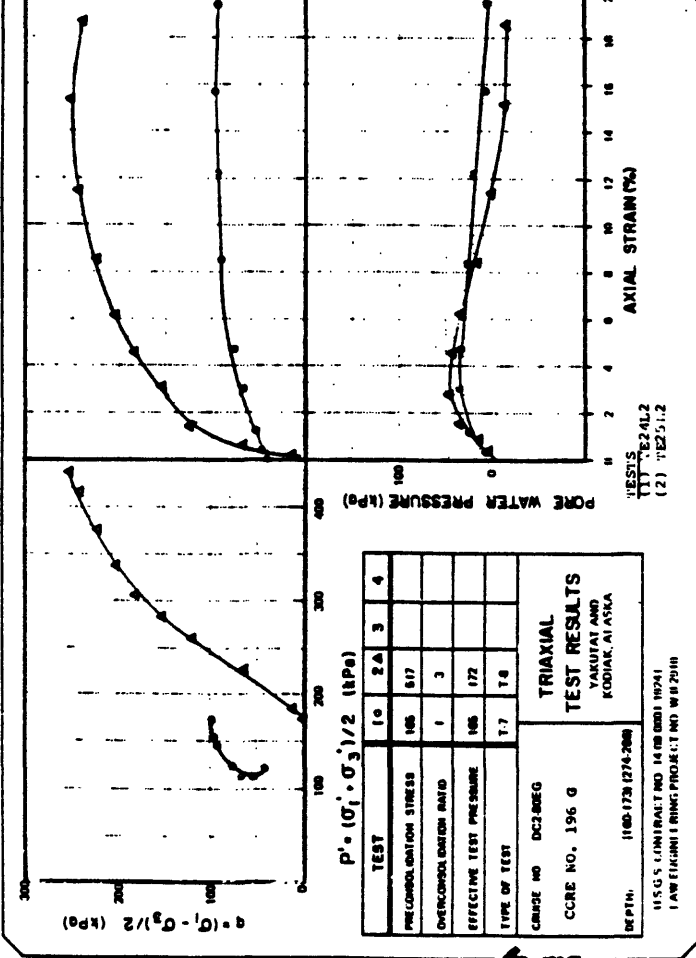
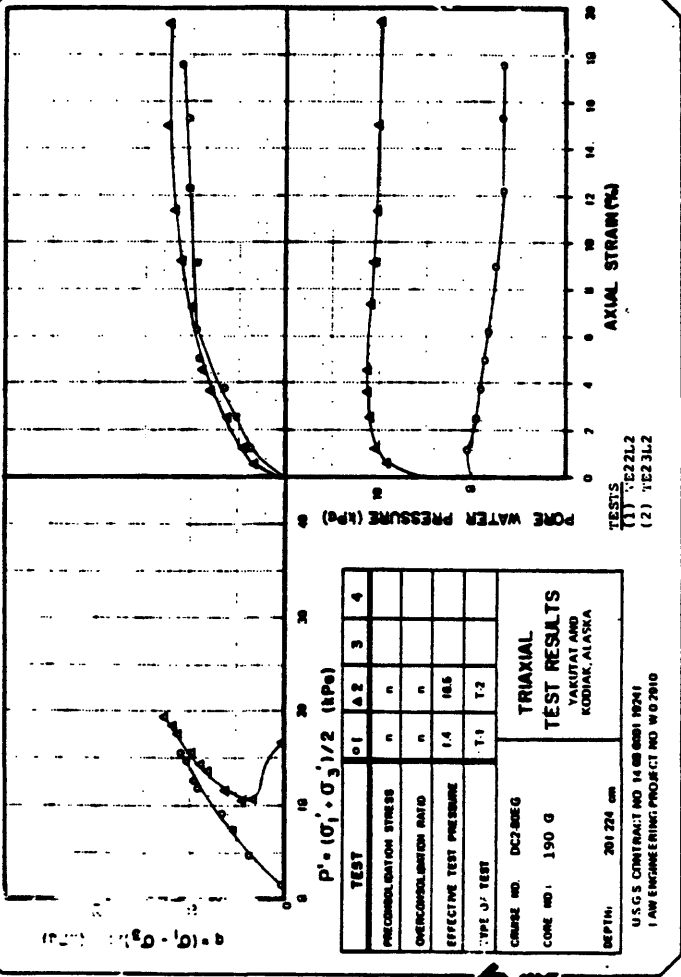
1000  
500  
100  
50  
10  
5

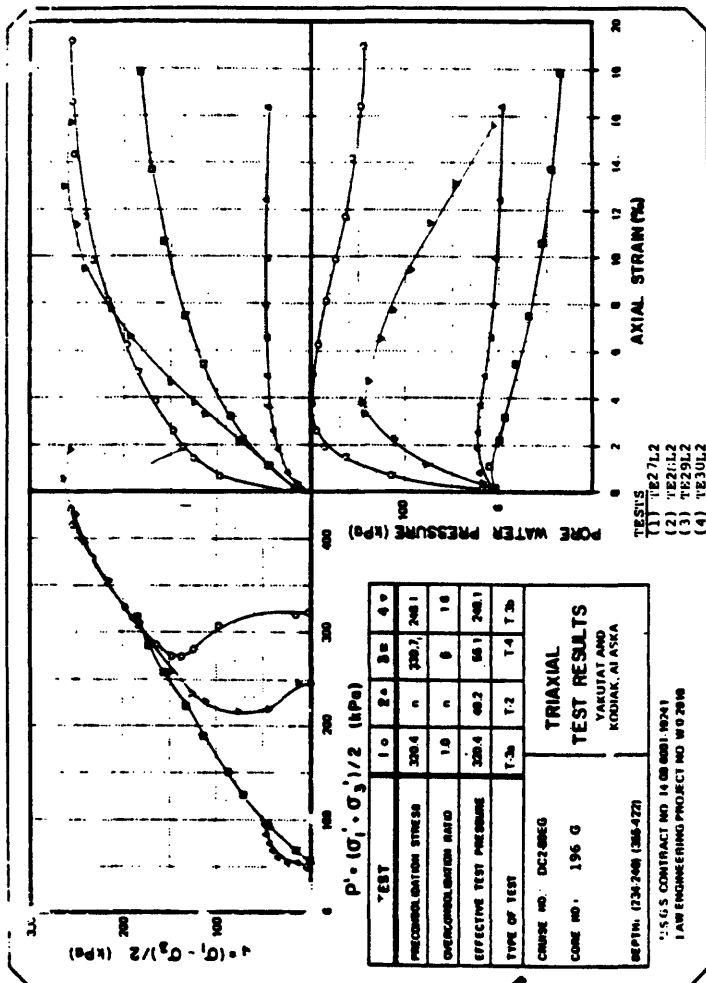
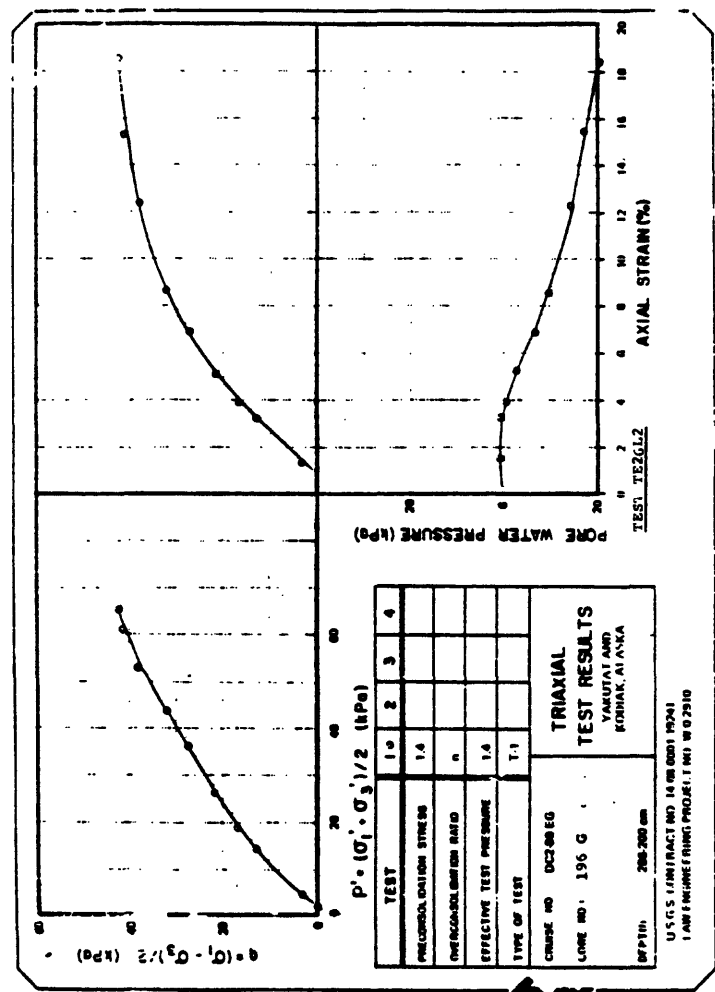
0

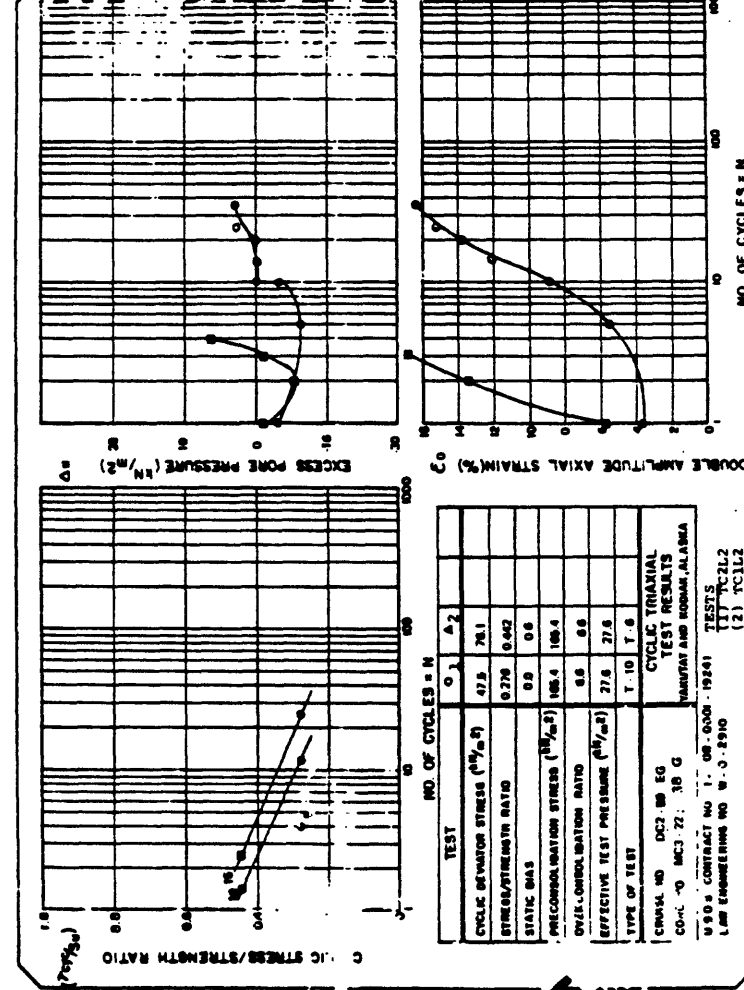
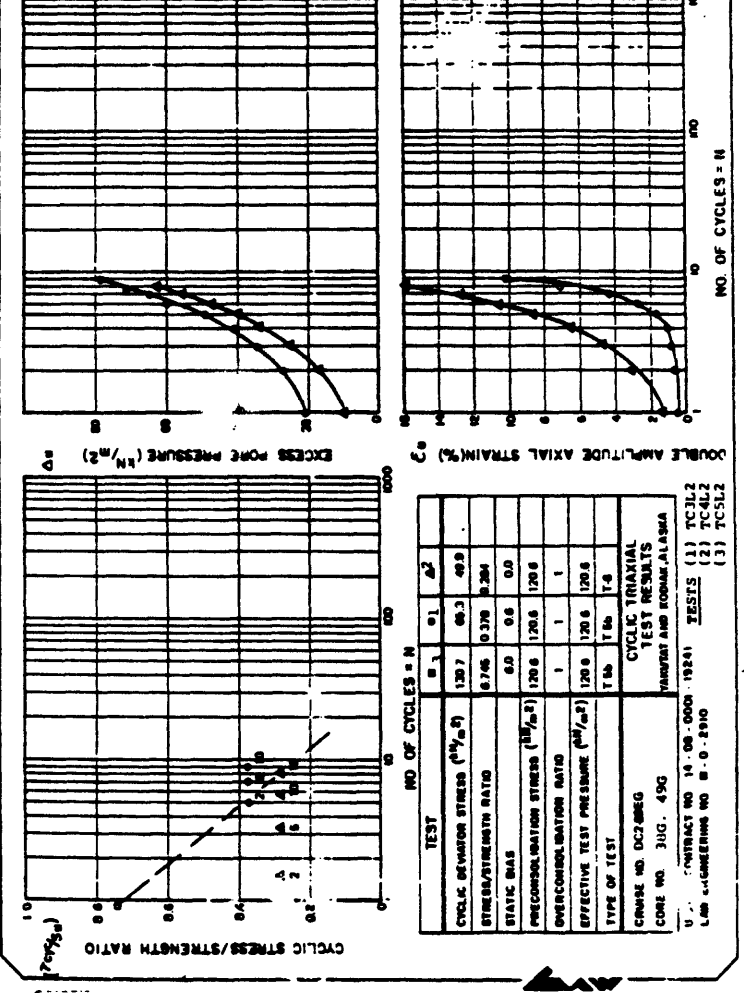
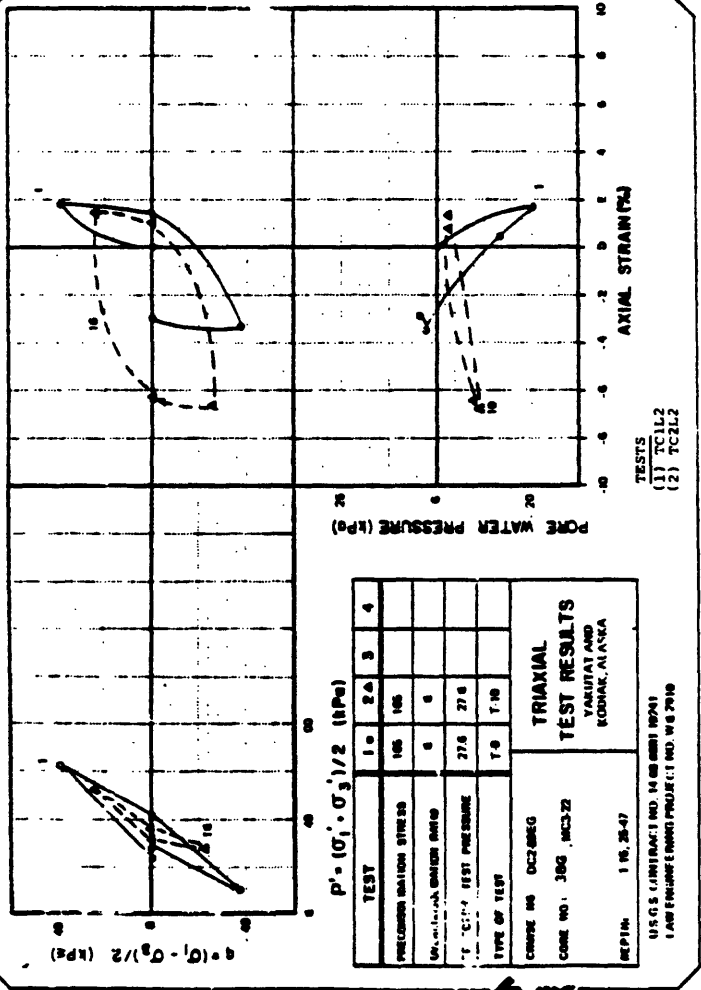
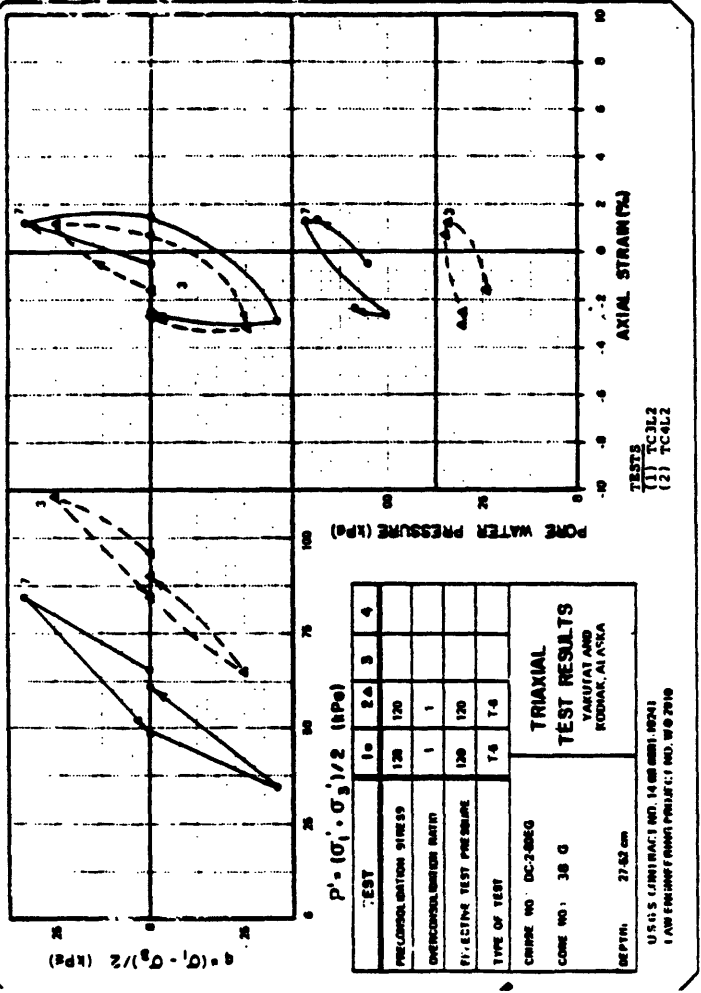
LAW ENGINEER INNO

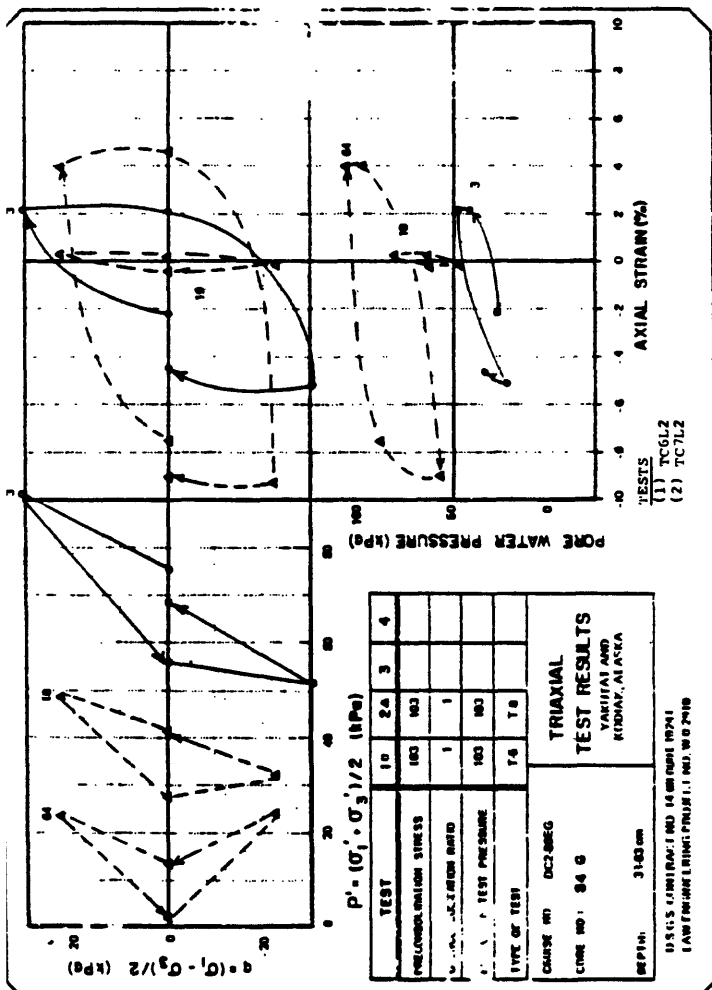




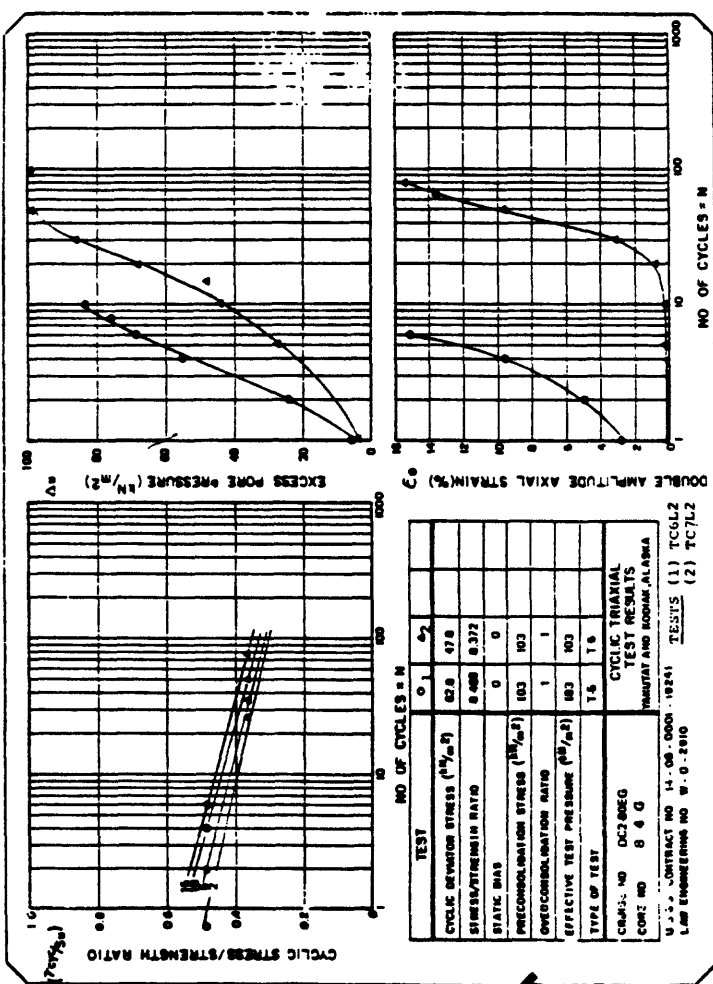


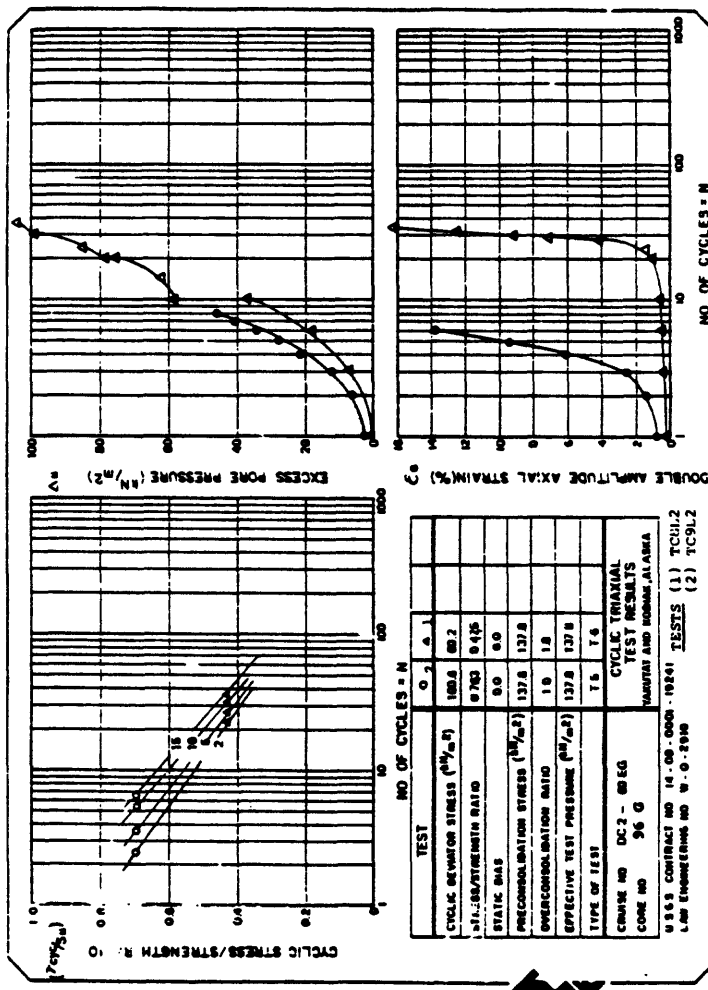
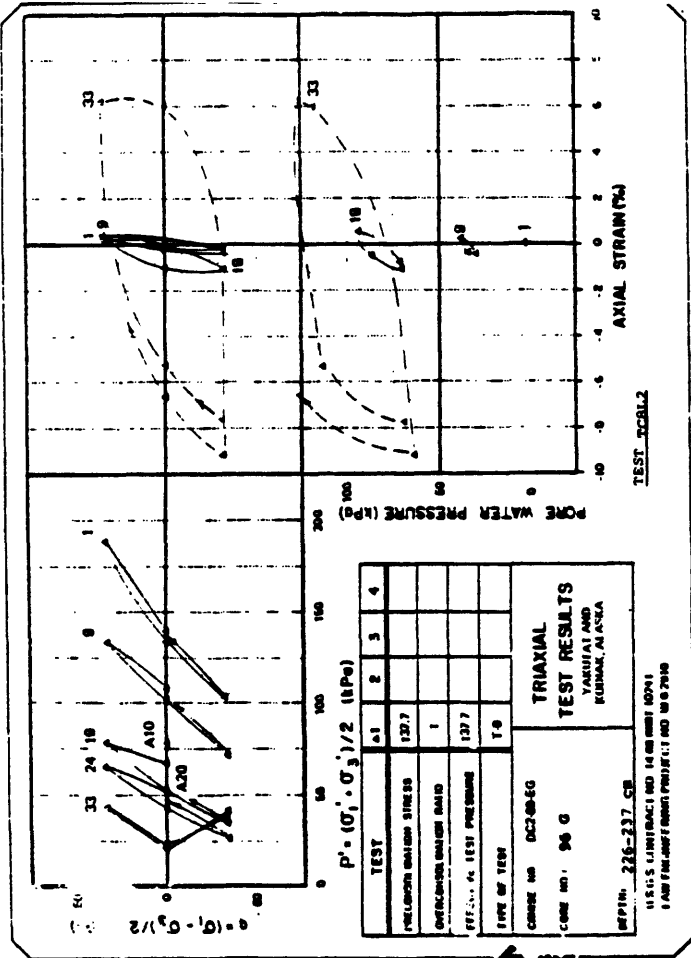
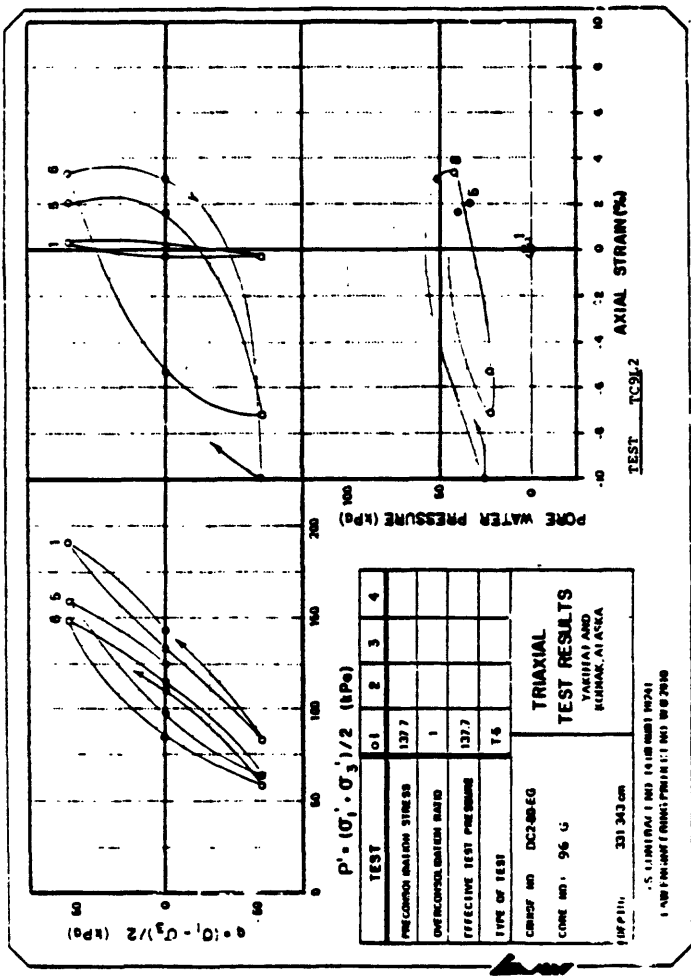


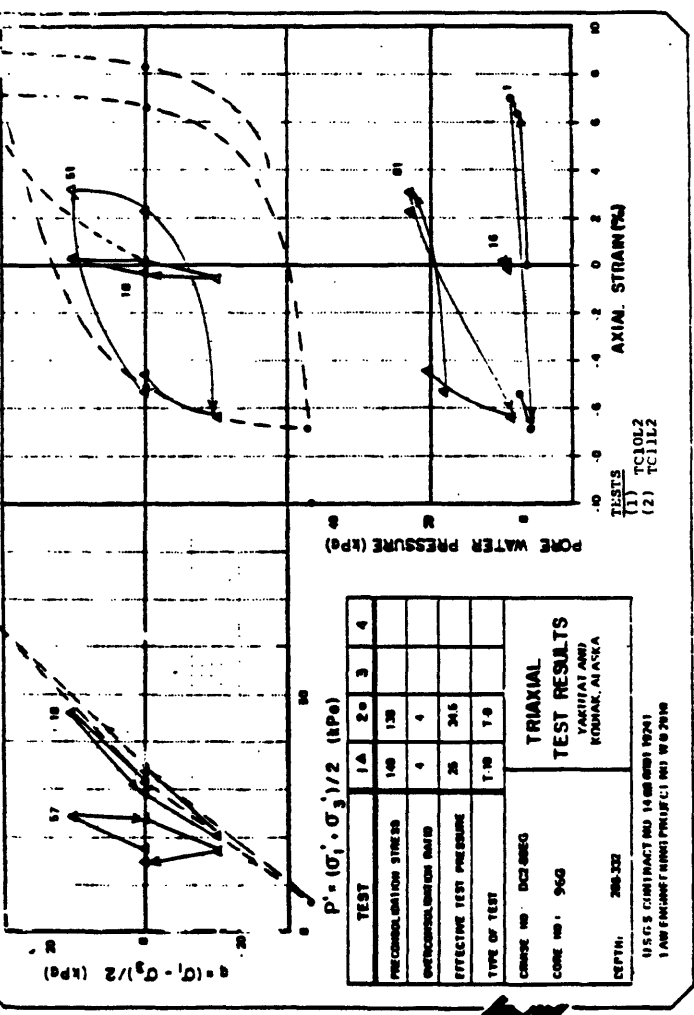
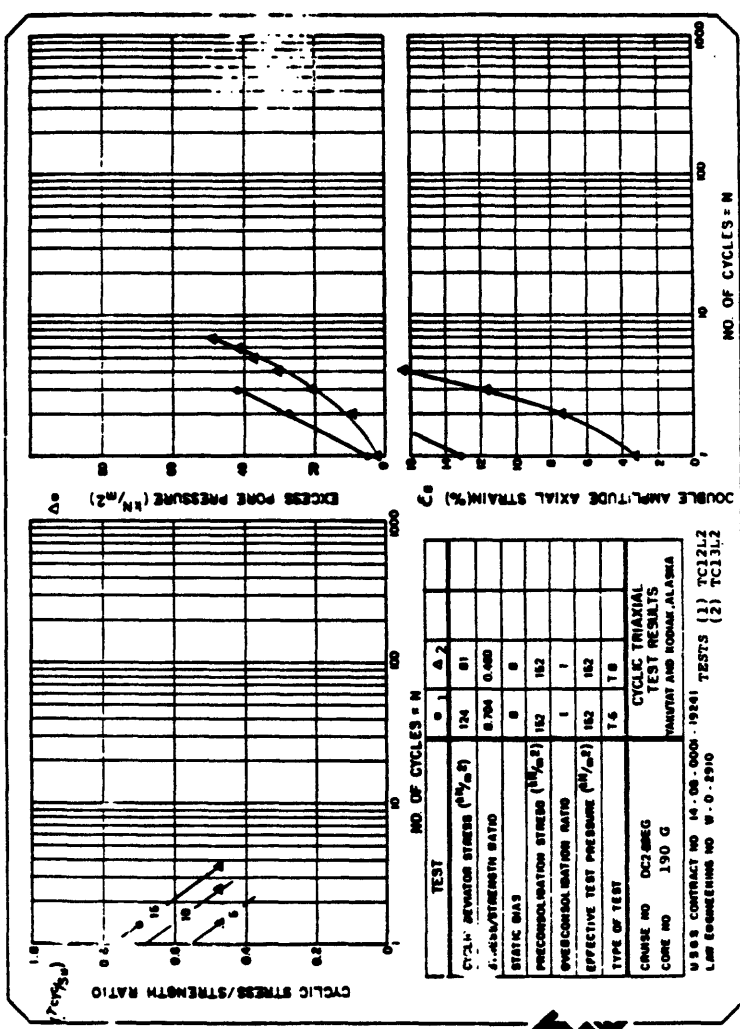
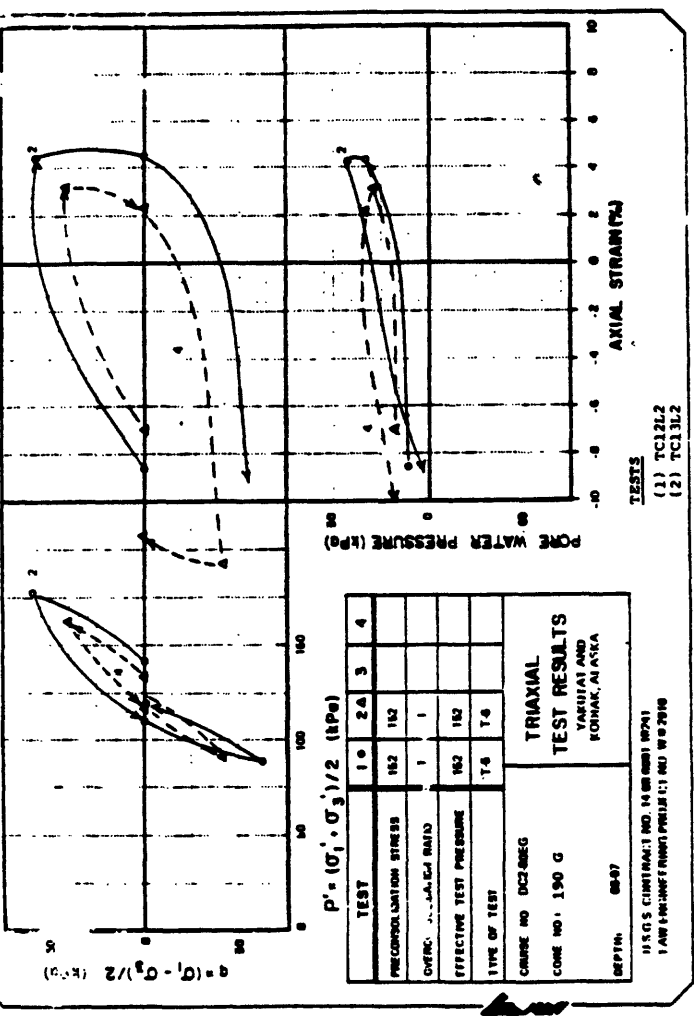


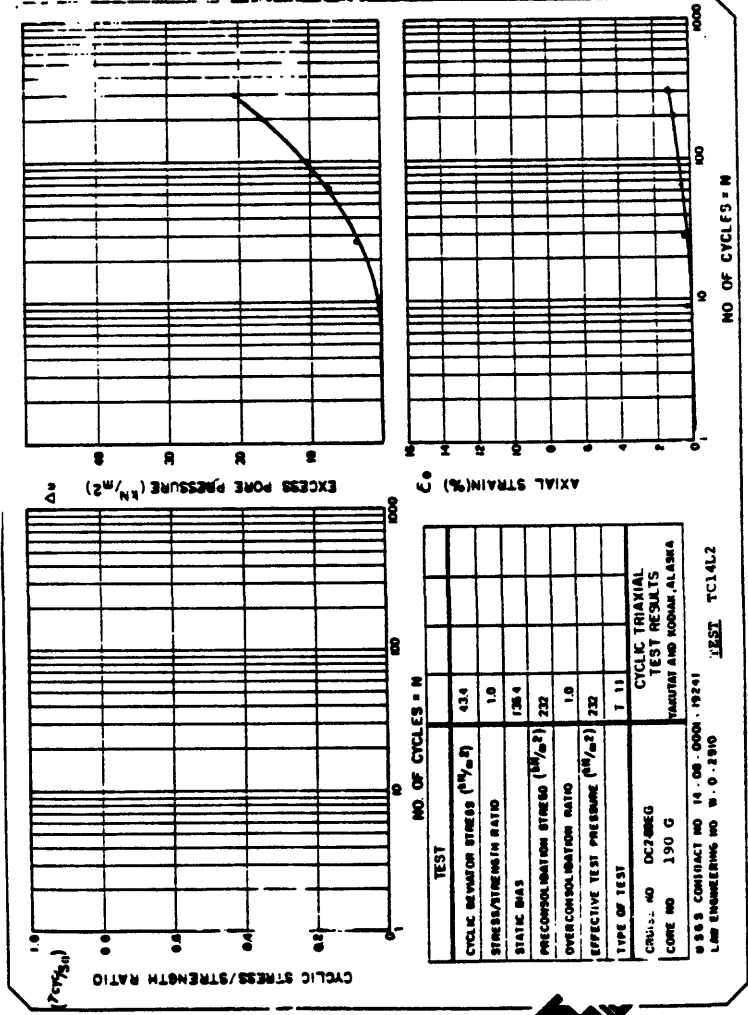
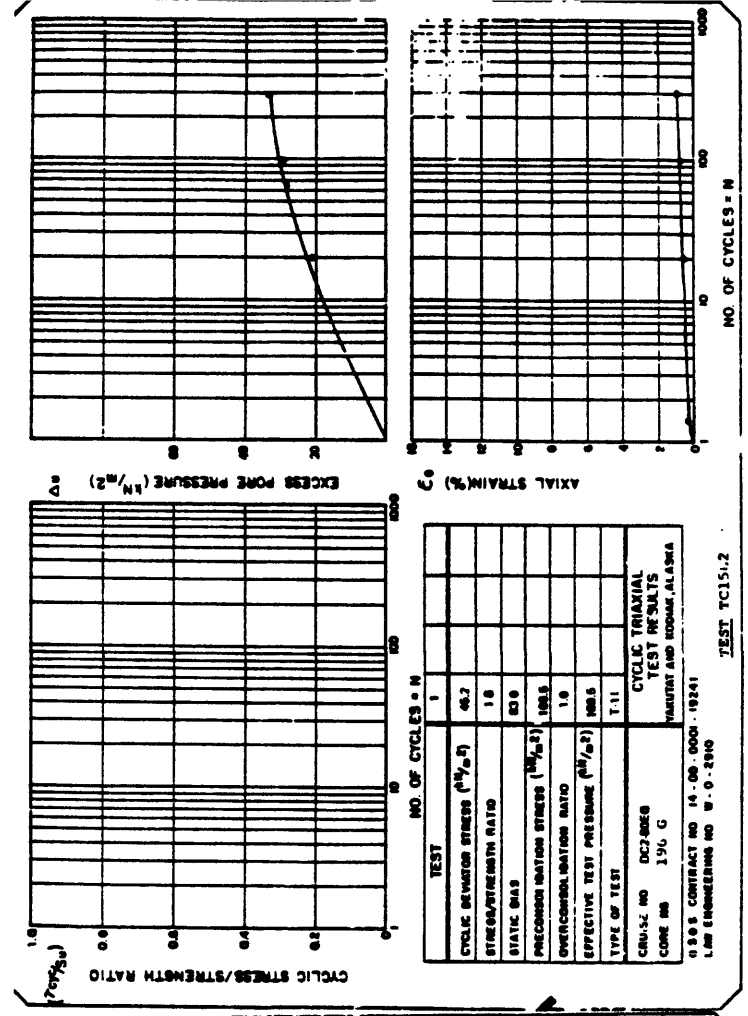
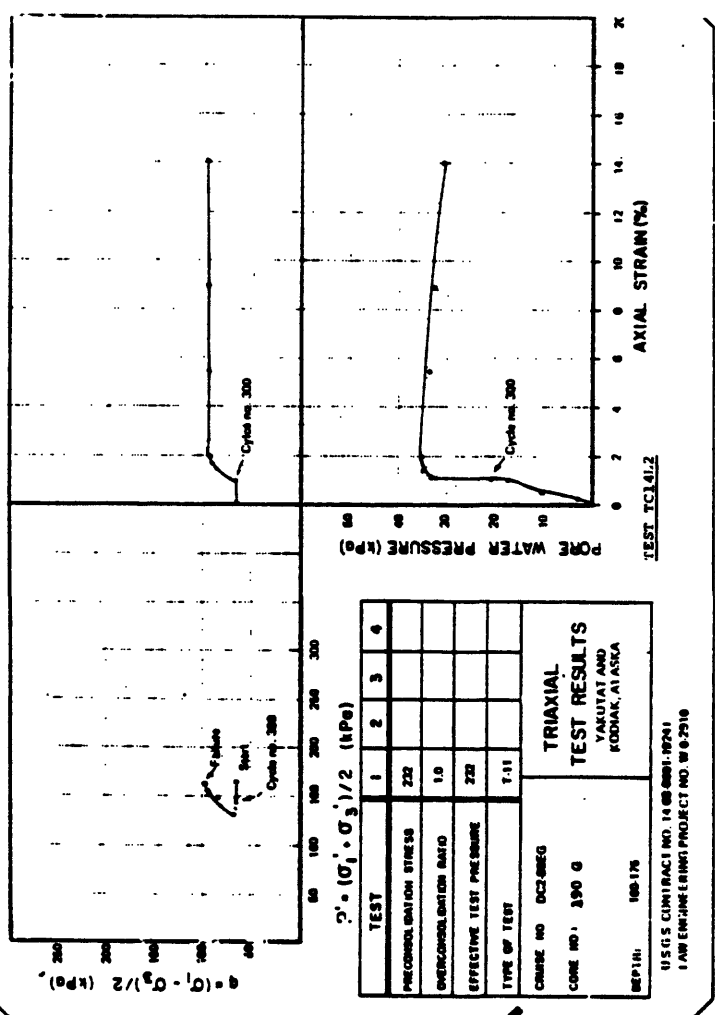
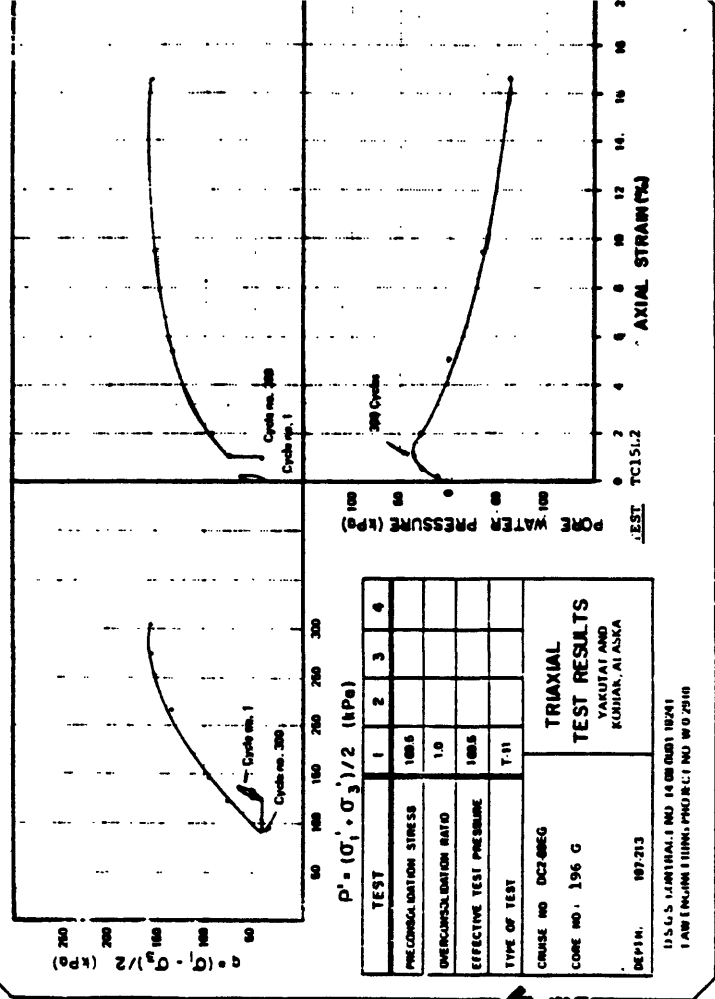


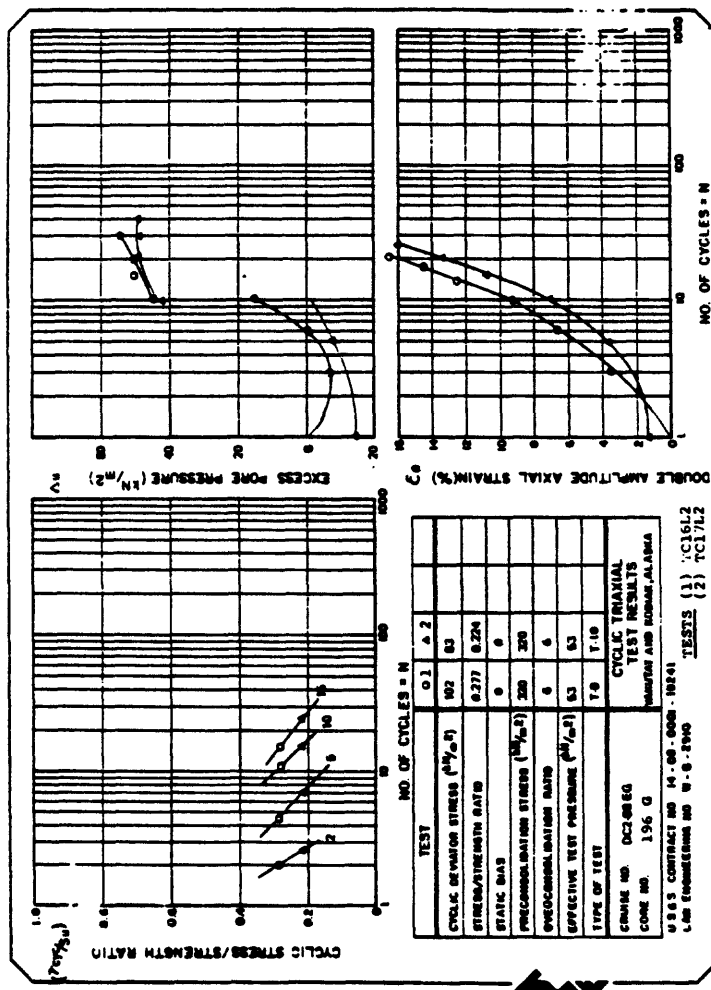
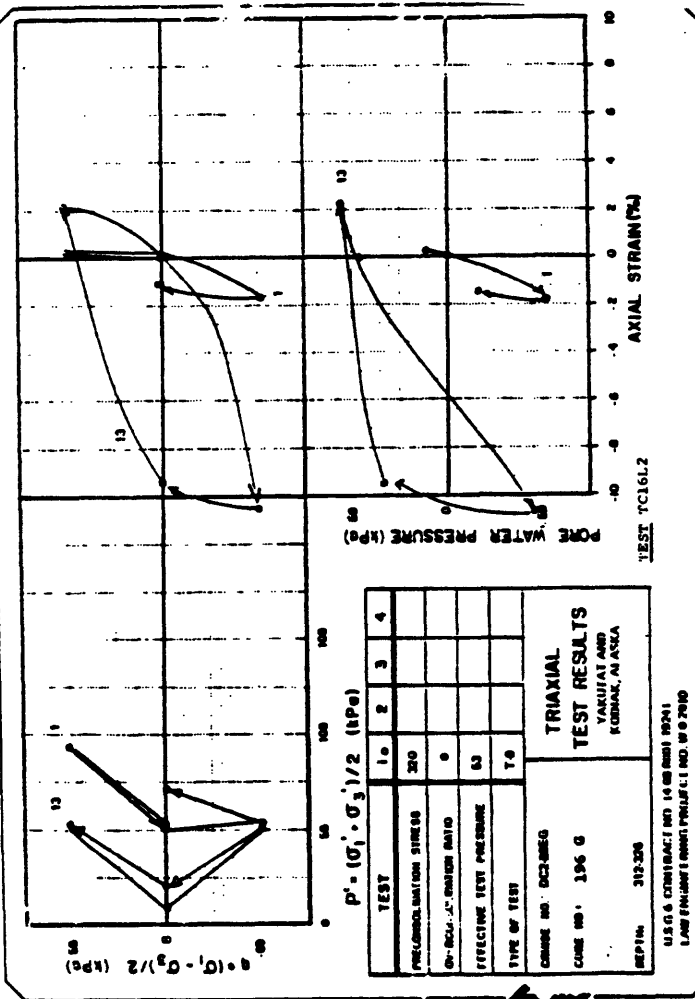
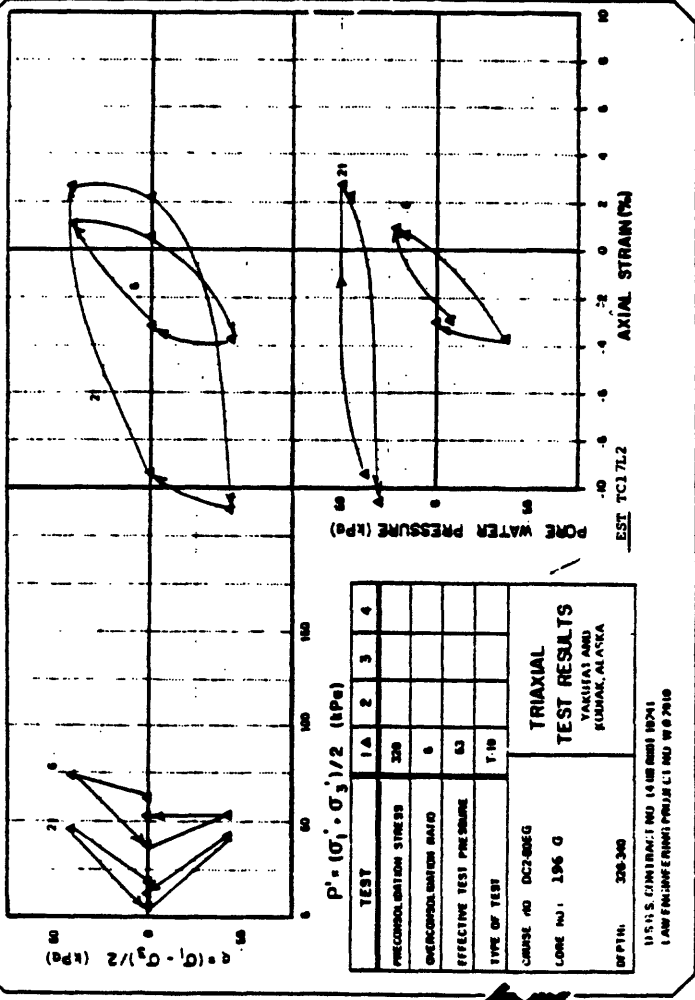
281

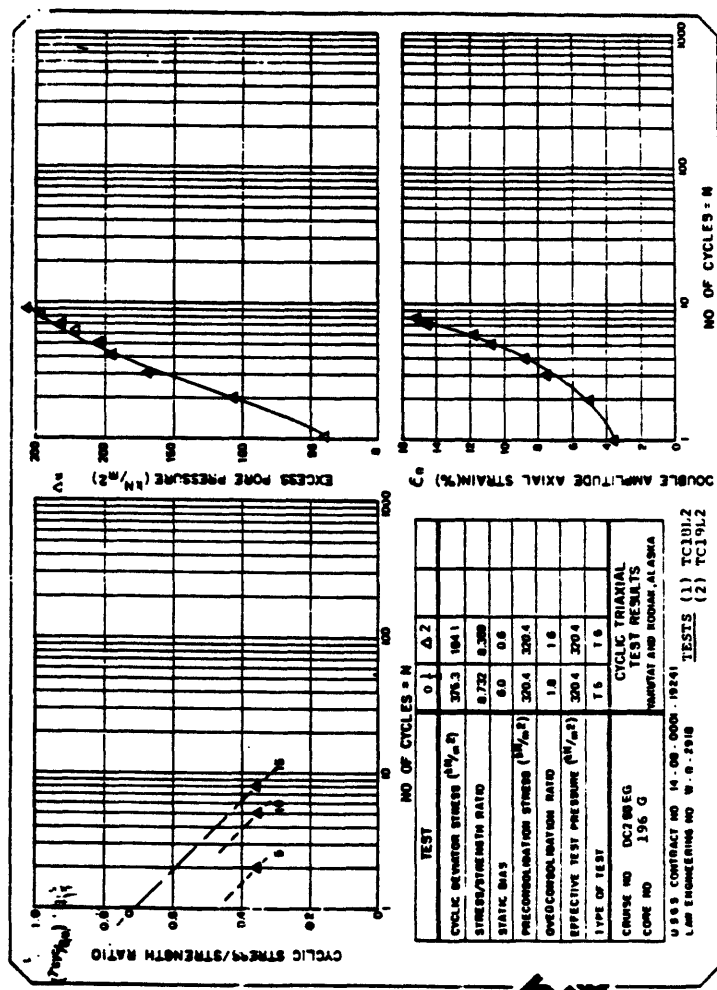
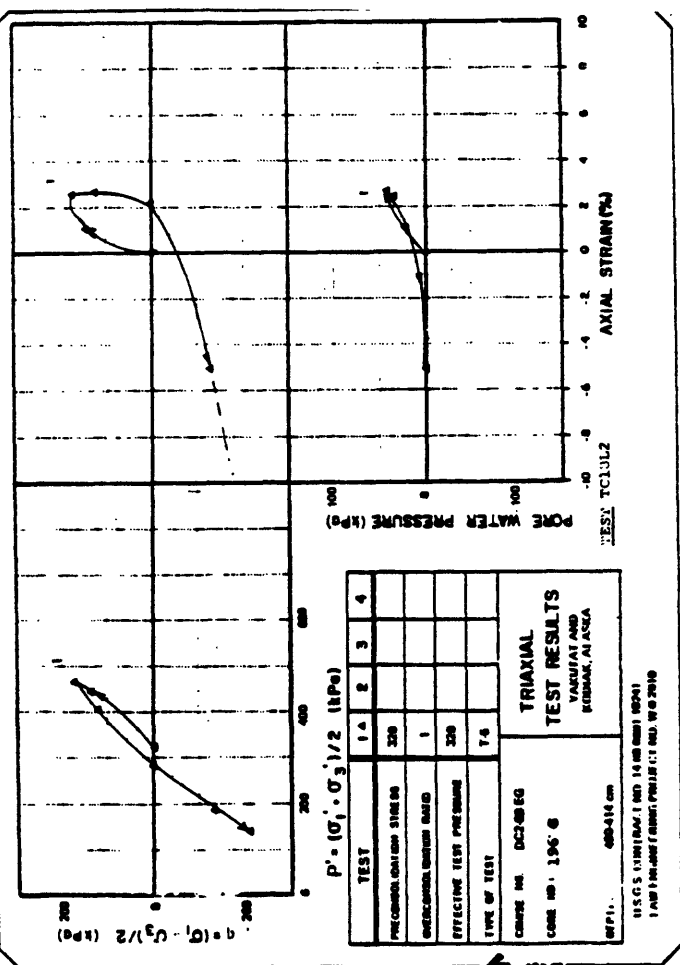
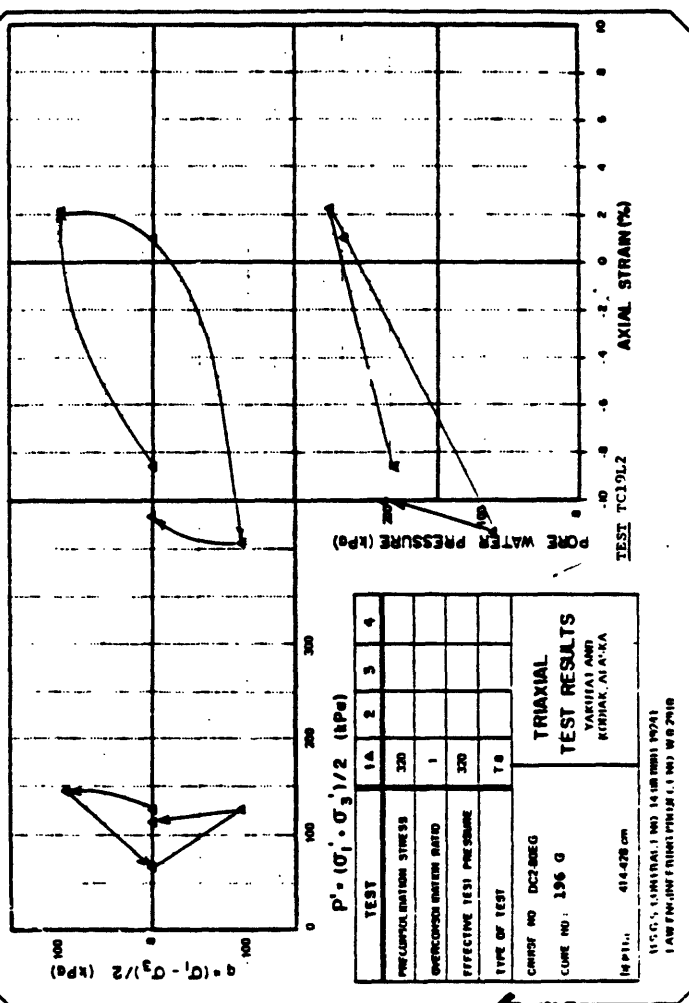












APPENDIX G. CONSOLIDATION AND TRIAXIAL TEST RESULTS-U.S. GEOLOGICAL SURVEY  
(1980 and 1981 cores)

This appendix presents the results of consolidation and triaxial testing performed at the U.S. Geological Survey's marine geotechnical laboratory. Core samples were from cruises DC2-80-EG and DC1-81-EG. Results were automatically recorded, reduced and plotted.

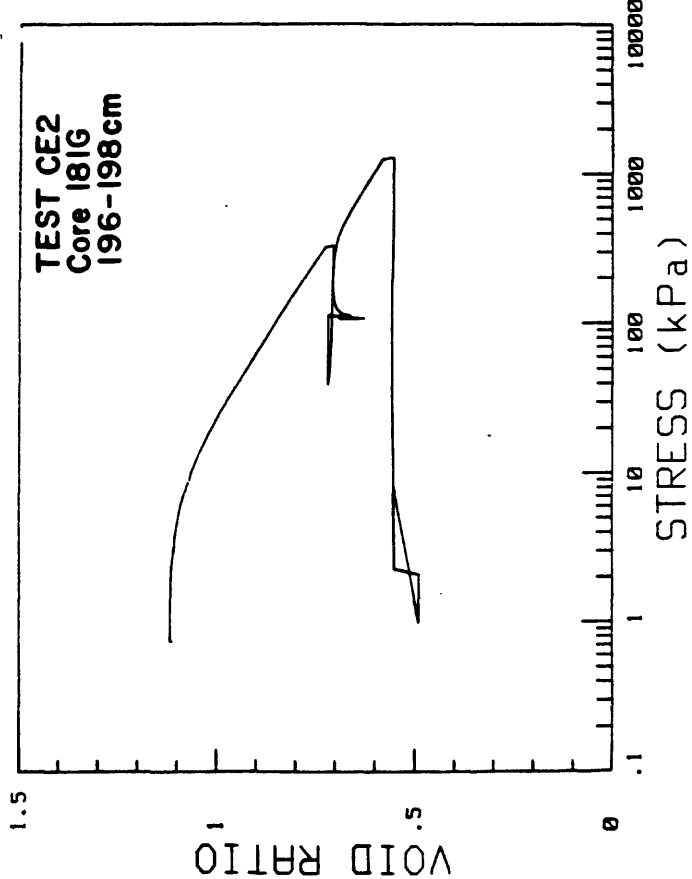
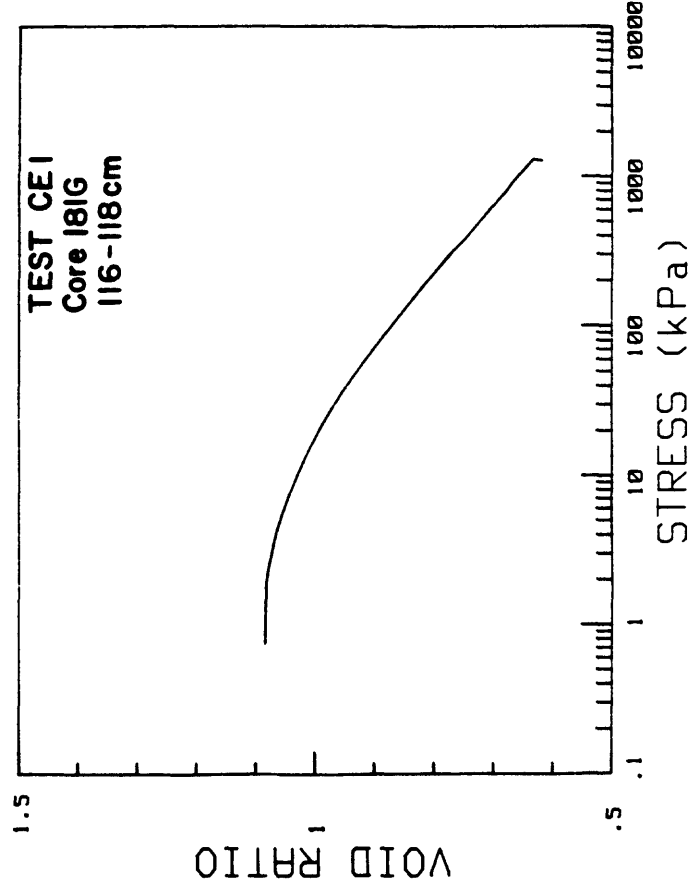
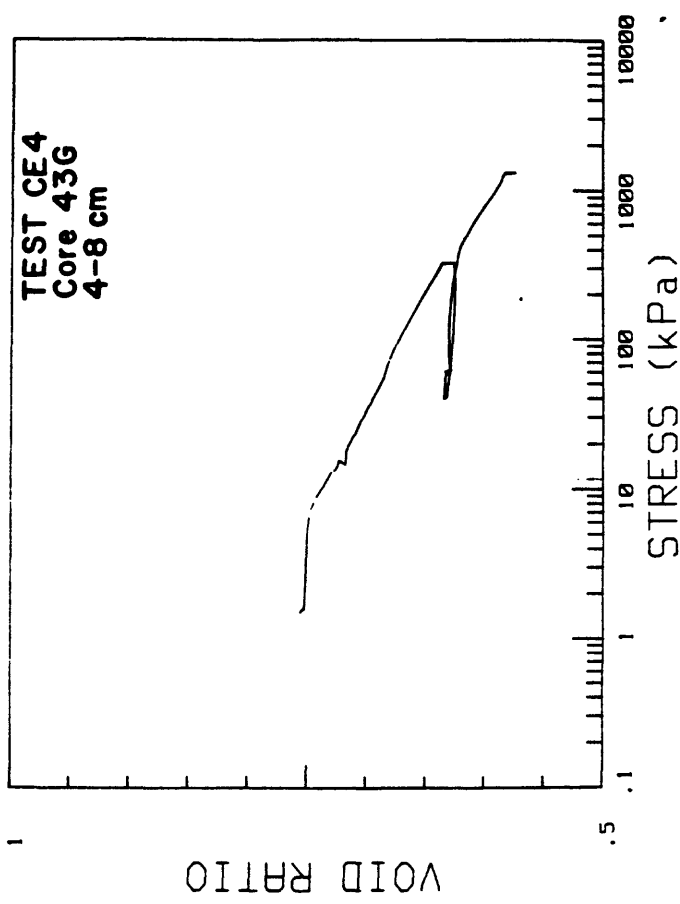
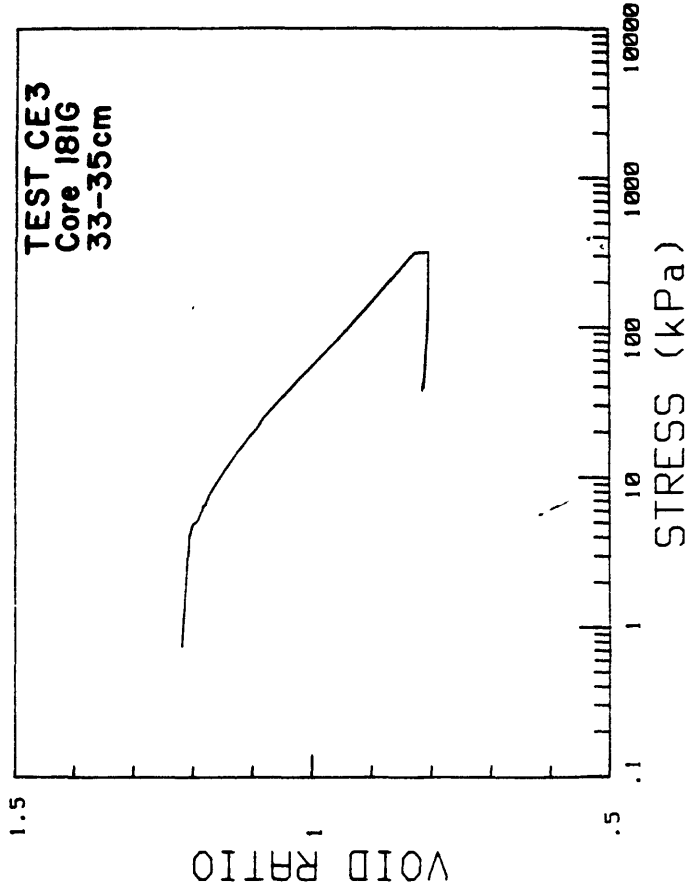
The tests in this group do not have trailing characters in their test numbers. The consolidation tests (first characters are CE for constant rate of strain, CRS, tests and OE for oedometer tests) are presented first and are ordered by test number. Results from a single test are presented on a single page in the form of void ratio and calculated coefficient of consolidation ( $c_v$ ) versus the vertical effective stress (identified as STRESS). Some of the plots for CRS tests are irregular as a result of transducer drift.

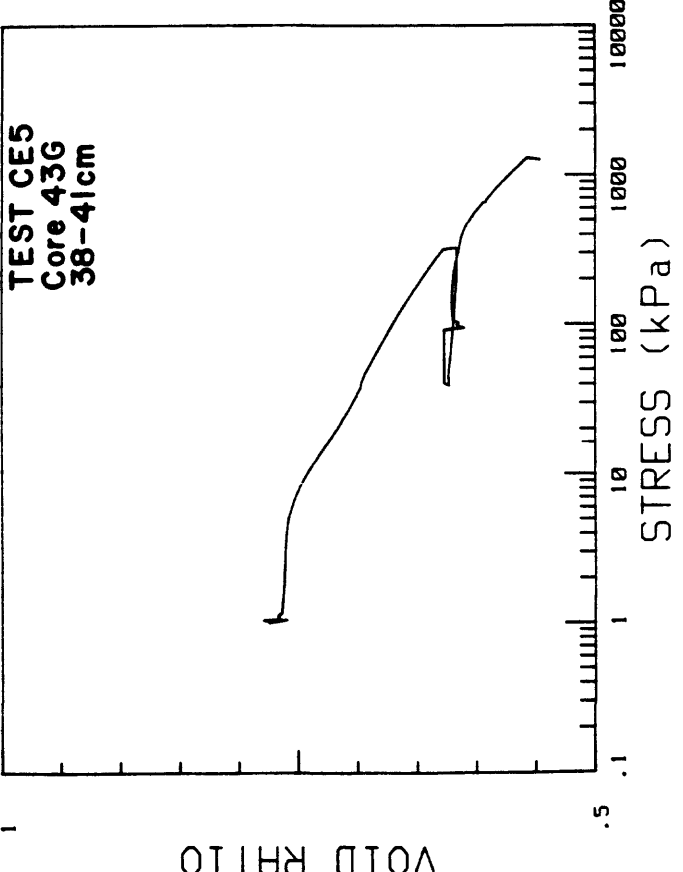
Static triaxial tests (first two characters are TE) are given second and ordered by test number. The upper left graph is a stress path presented as a plot of maximum shear stress ( $q$ ) versus the normal effective stress on the plane of maximum shear ( $p'$ ). The stress path plots of Appendix D are defined differently. The upper right plot is the maximum shearing stress versus strain. The lower right plot is the measured excess pore water pressure (DELT<sub>Au</sub>) versus axial strain. The title block gives SIG1c' and SIG3' which are the vertical and horizontal consolidation stresses, respectively. The induced OCR is the overconsolidation ratio forced on the sample in the triaxial cell. A value of 1.0 may or may not correspond to true overconsolidation because the triaxial cell consolidation stress may be less than the maximum past stress the sample experienced in place.

The cyclic triaxial tests (first two characters are TC) are given third and ordered by test number. Results from one test are presented on two sheets. The first sheet includes deviator stress (DEV STRESS or 2 times the shear stress)-axial strain and  $p'-q$  stress paths that are analogous to the graphs given for static triaxial tests. However, the plots are given for only a few selected cycles of loading to illustrate how the response changes as the number of cycles increases. Numbers on the plots correspond to cycle number.

The second sheet shows several parameters plotted versus cycle number. The upper left plot shows peak single amplitude strain (positive in compression) versus cycle number. Lower left and lower right plots show calculated damping and Young's modulus ( $E$ ) versus number of cycles, respectively. The upper right plot shows the minimum and maximum excess pore water pressure (DELU) measured during a cycle. In some plots a dashed line in both the strain and pore pressure plots shows an equilibrium value established between bursts of cyclic stress applications.

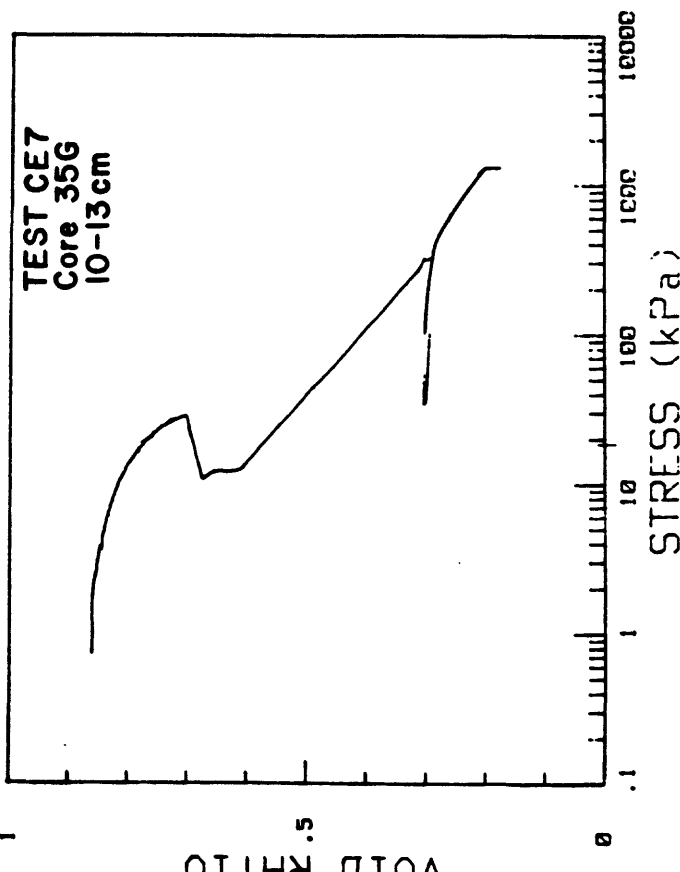
The title blocks for both figures show a static  $q_f$  or estimated static shearing strength. The value was obtained from a test on a nearby sample (Method I of the main text). The average maximum  $q$  (AVG MAX  $q$ ) is the average peak compressive shearing stress for all of the cycles. The percentage value that follows in parentheses represents the percentage of the estimated (Method I) static shearing strength. The "AVG MIN  $q$ " is the same as the average maximum  $q$  except it represents values in tension.





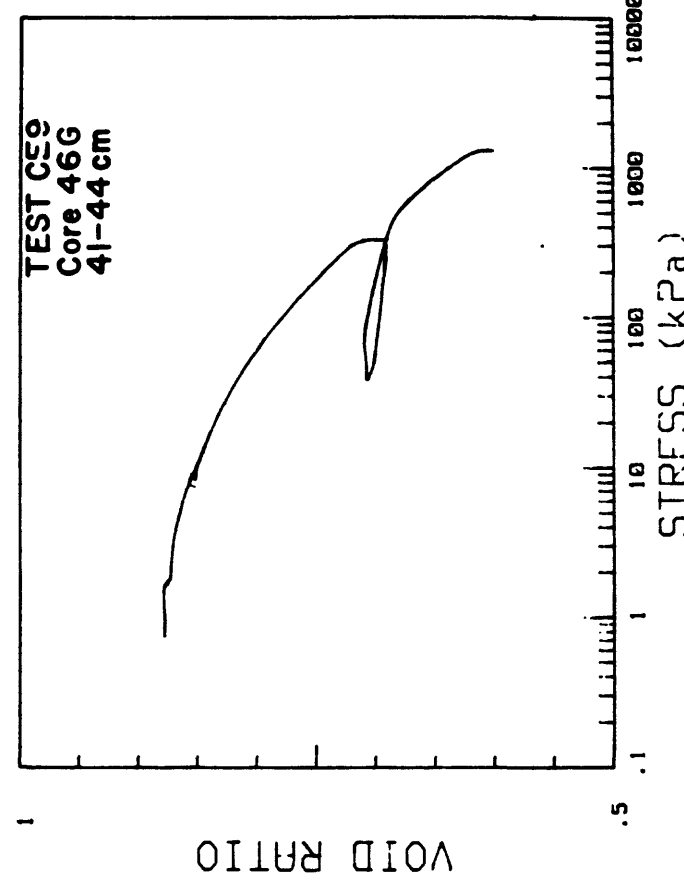
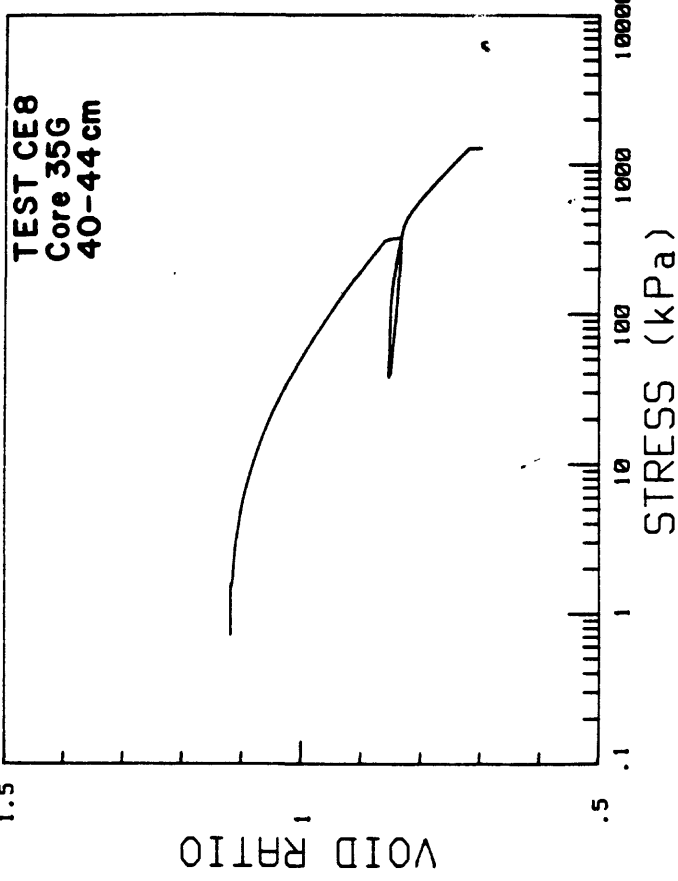
1.5  
1  
.5

VOID RATIO



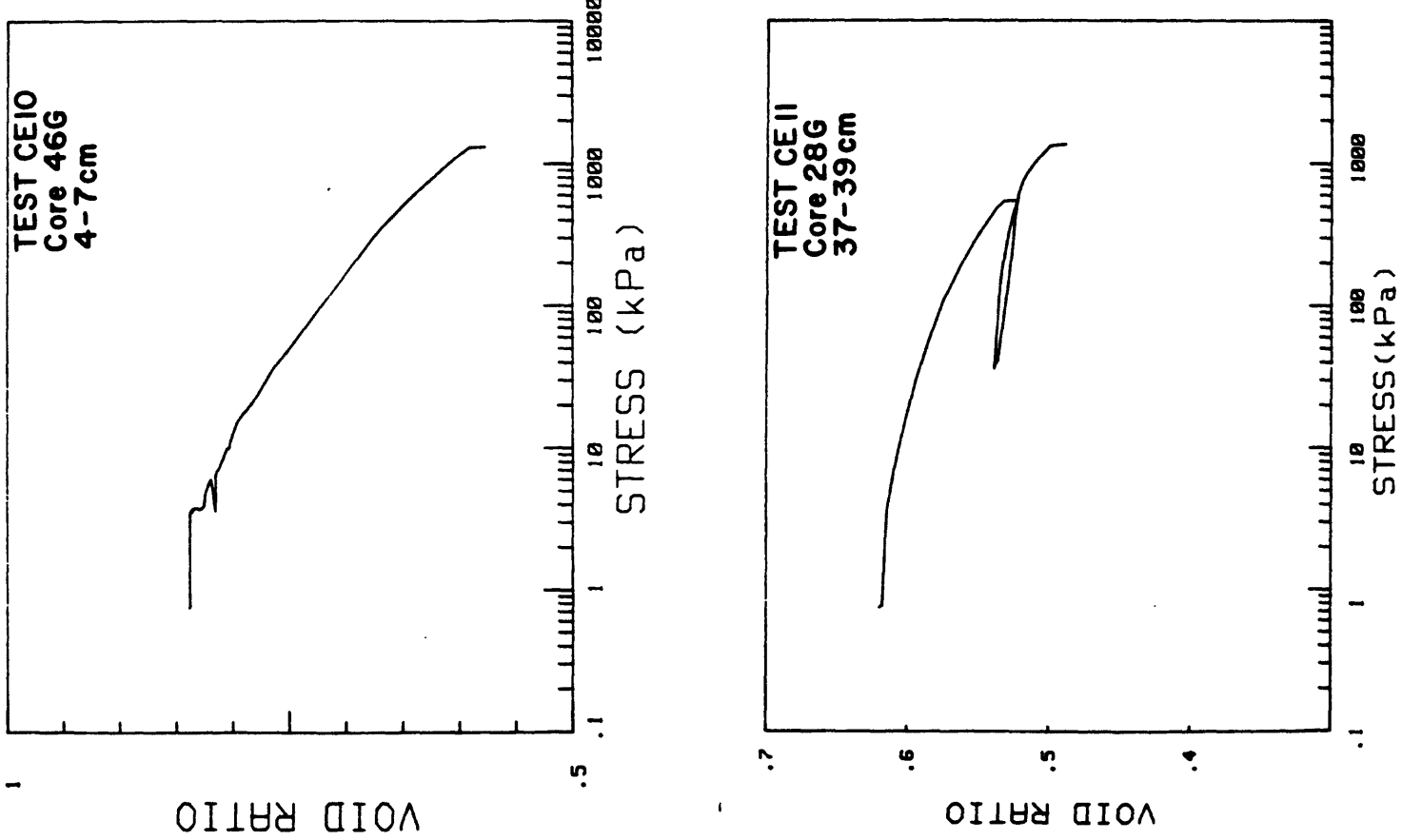
1  
.5  
0

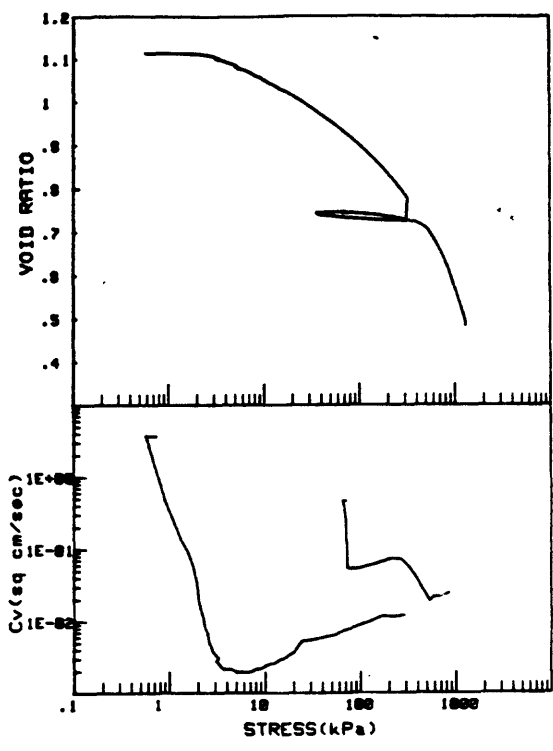
VOID RATIO



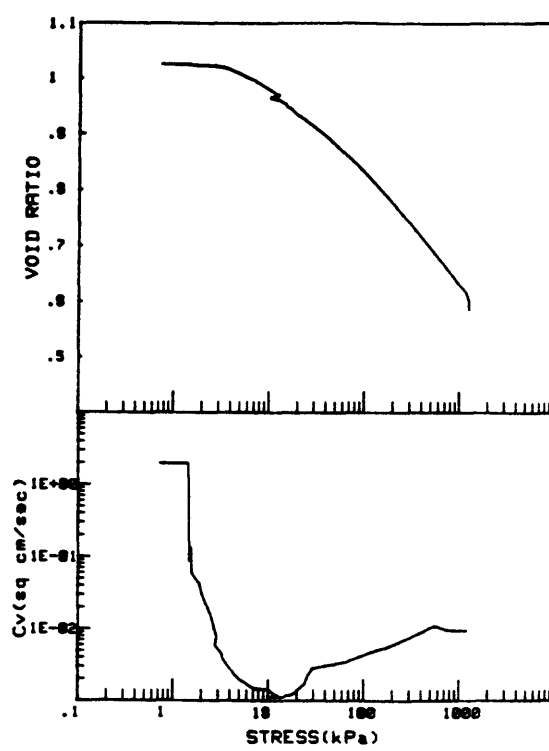
1  
.5  
0

VOID RATIO

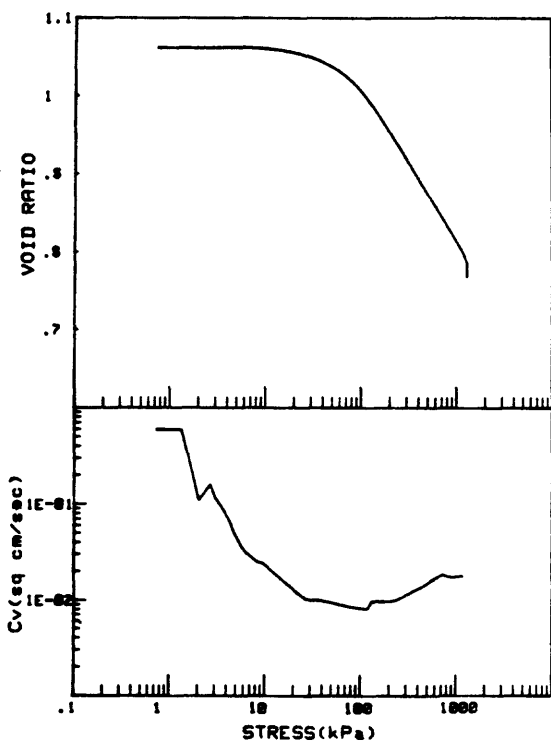




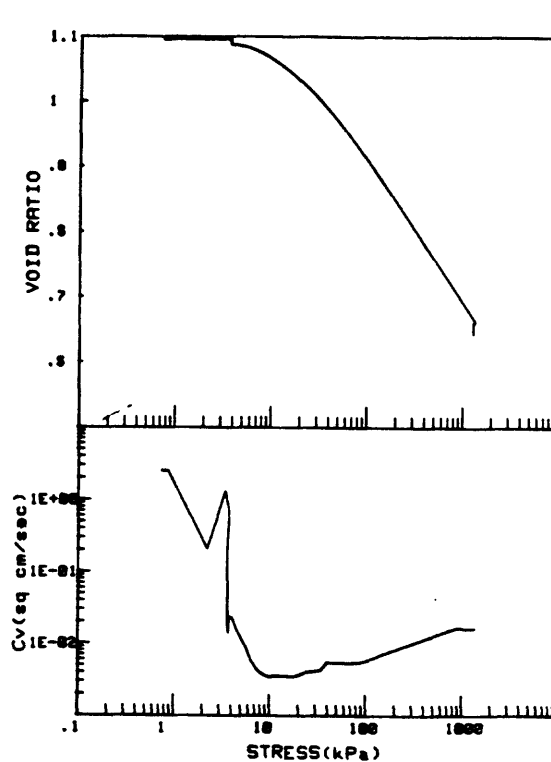
CRUISE DC1-B1-EG CORE NO. 827G2	INCREMENT (cm) TEST NO.	118-116 CE13



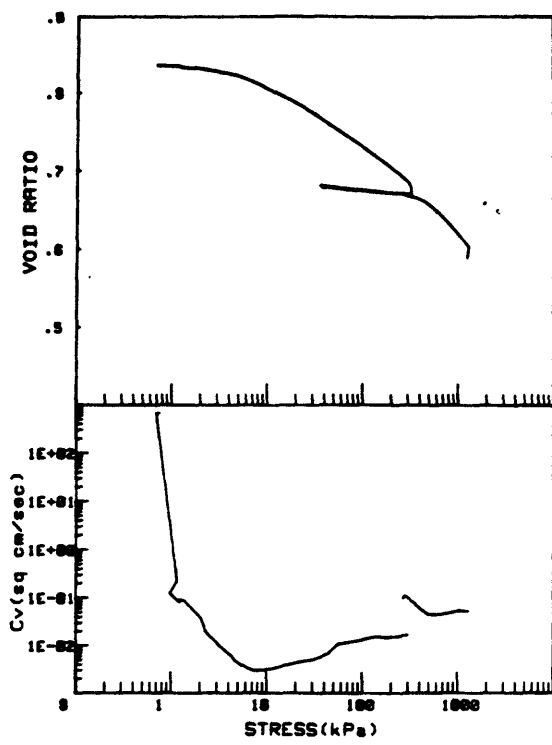
CRUISE DC1-B1-EG CORE NO. 827G2	INCREMENT (cm) TEST NO.	222-224 CE15



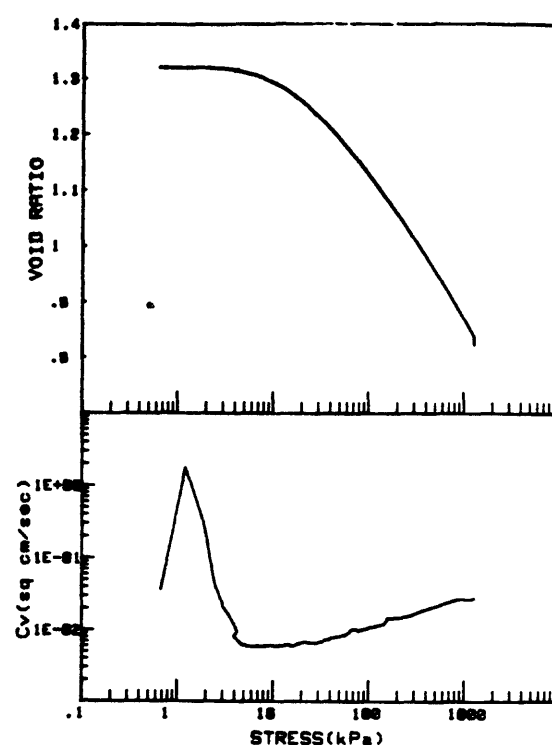
CRUISE DC1-B1-EG CORE NO. 827G2	INCREMENT (cm) TEST NO.	32-34 CE14



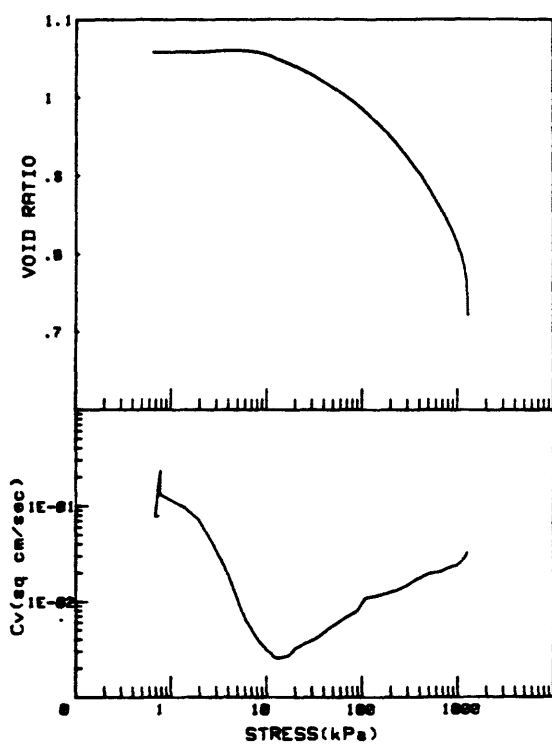
CRUISE DC1-B1-EG CORE NO. 827G2	INCREMENT (cm) TEST NO.	26-26 CE15



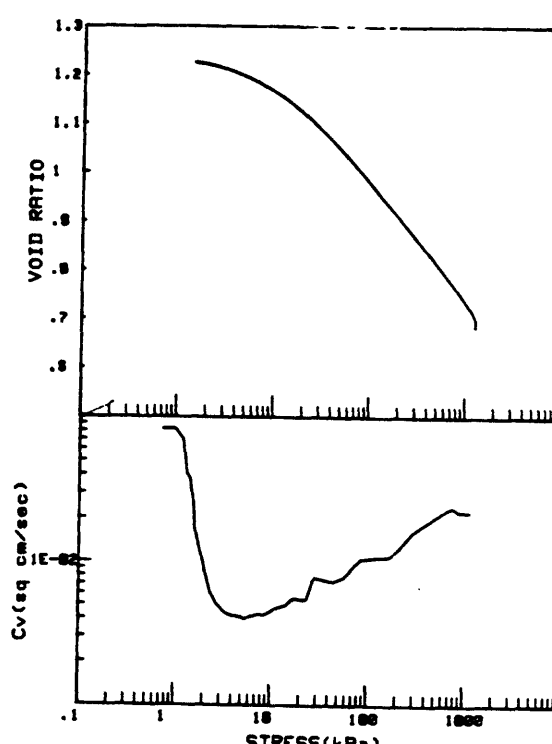
CRUISE DC1-B1-EG	INCREMENT (cm)	110-115
CORE NO. 818G2	TEST NO.	CE17



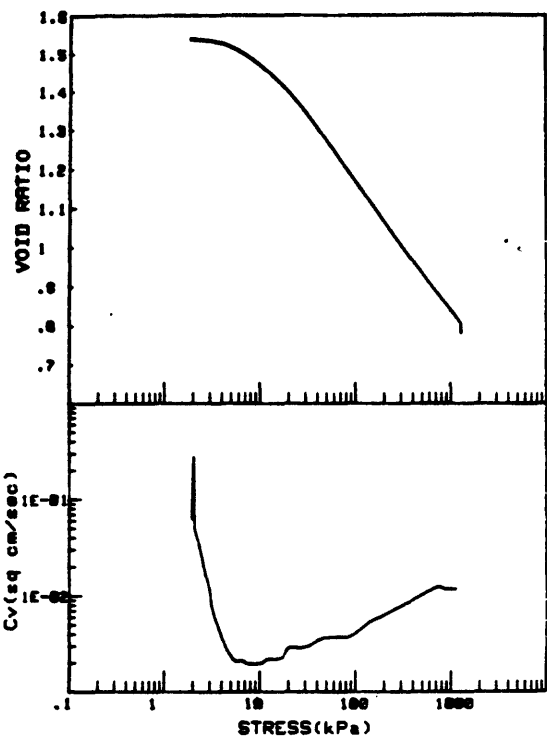
CRUISE DC1-B1-EG	INCREMENT (cm)	82-84
CORE NO. 818G2	TEST NO.	CE22



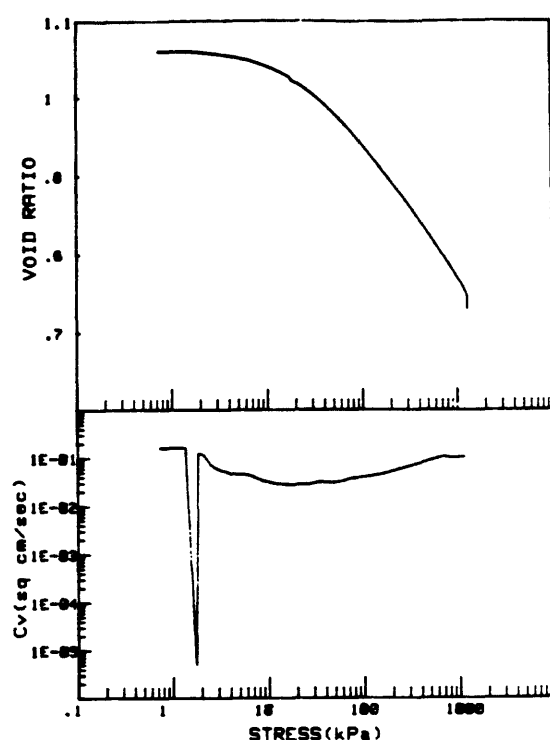
CRUISE DC1-B1-EG	INCREMENT (cm)	190-195
CORE NO. 818G2	TEST NO.	CE18



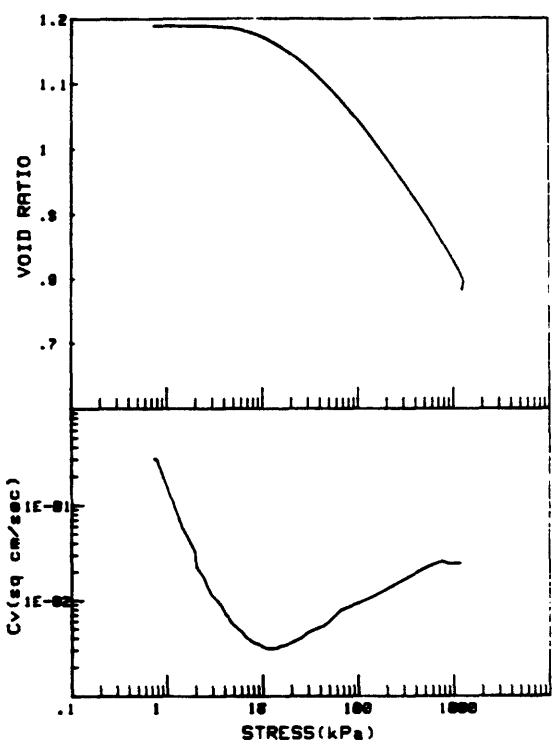
CRUISE DC1-B1-EG	INCREMENT (cm)	71-73
CORE NO. 828G2	TEST NO.	CE23



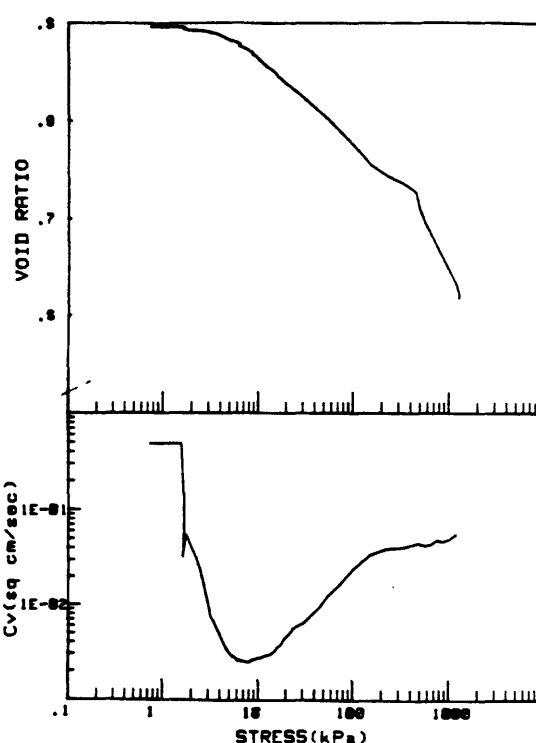
CRUISE DC1-81-EG	INCREMENT (cm)	47-48
CORE NO. 834G2	TEST NO.	CE24



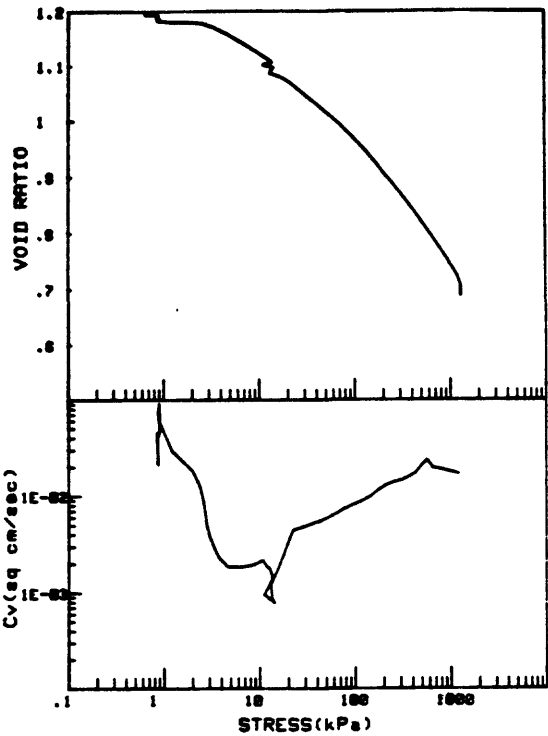
CRUISE DC2-88-EG	INCREMENT (cm)	148-149
CORE NO. 87G	TEST NO.	CE26



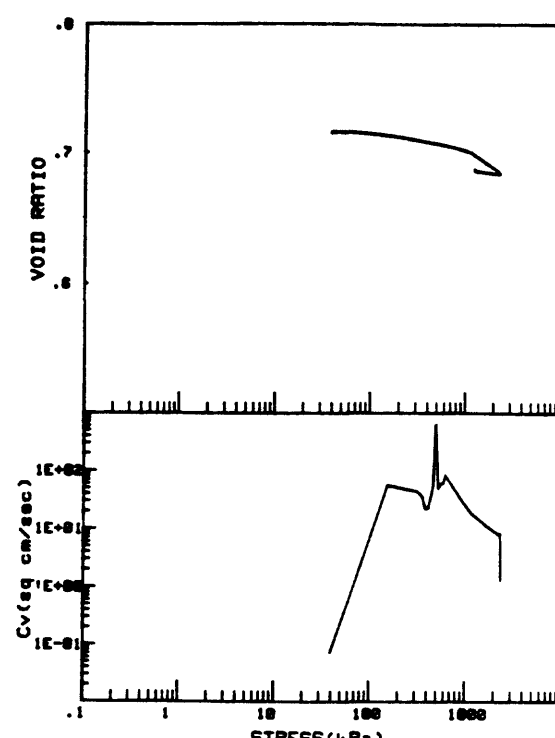
CRUISE DC1-81-EG	INCREMENT (cm)	153-155
CORE NO. 835G2	TEST NO.	CE25



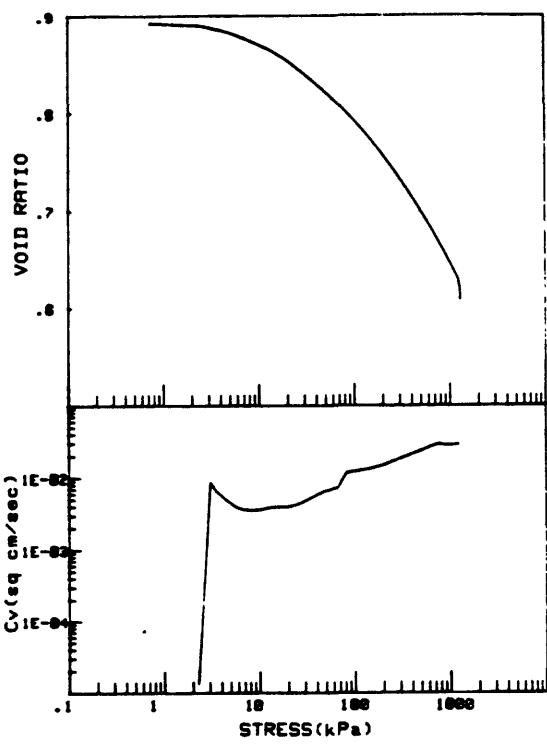
CRUISE DC1-81-EG	INCREMENT (cm)	210-212
CORE NO. 824R1	TEST NO.	CE27



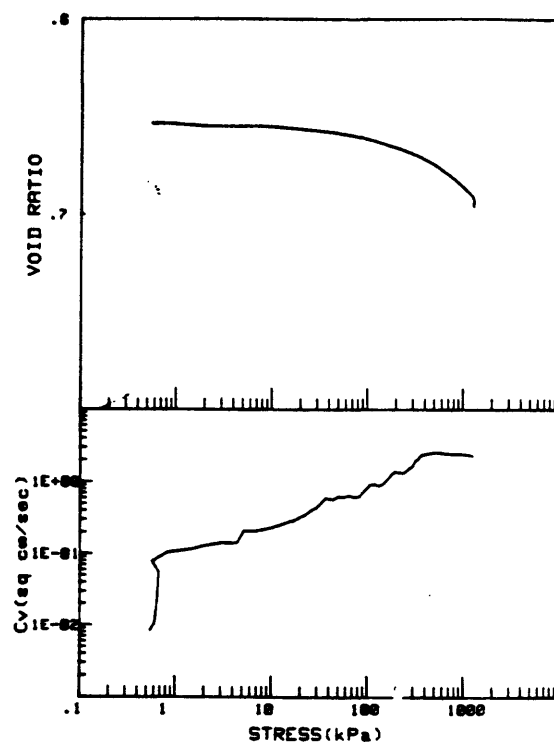
CRUISE DC1-81-EG	INCREMENT (ea)	188-188
CORE NO. 818G2	TEST NO.	CE28



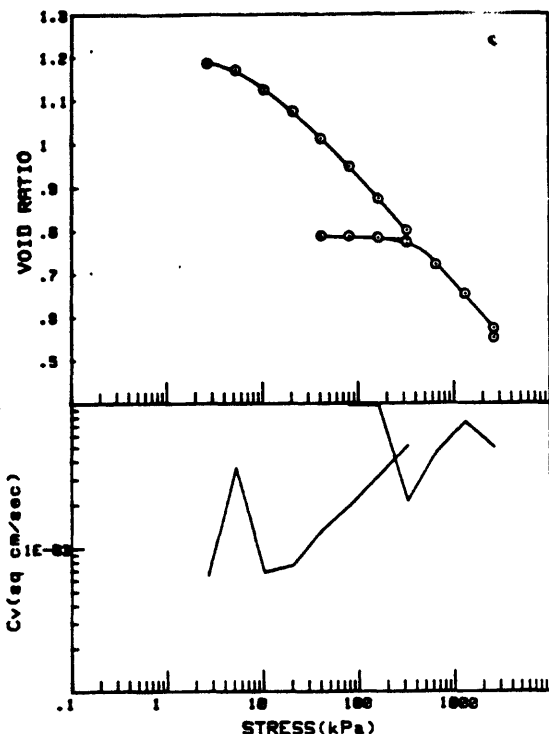
CRUISE DC1-81-EG	INCREMENT (ea)	200-211
CORE NO. 838P2	TEST NO.	CE32



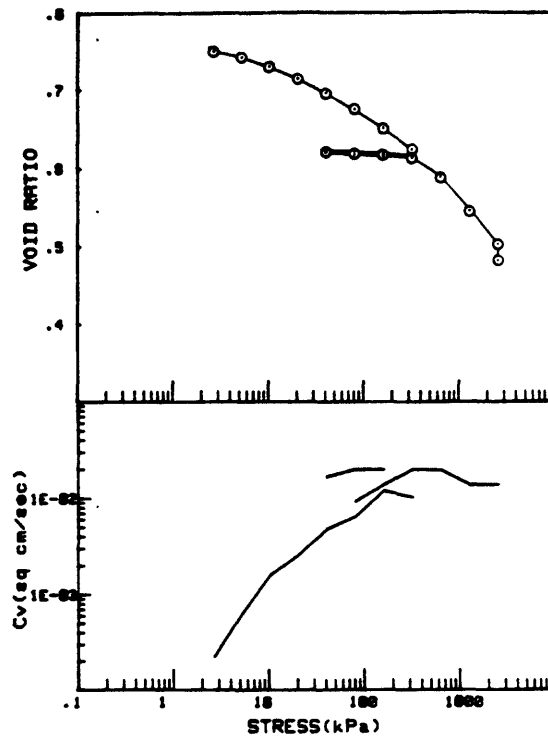
CRUISE DC1-81-EG	INCREMENT (ea)	78-78
CORE NO. 832G1	TEST NO.	CE31



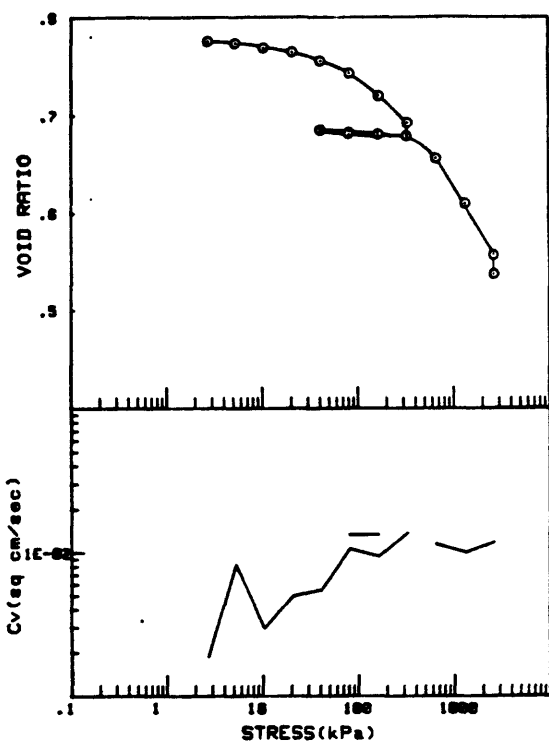
CRUISE DC1-81-EG	INCREMENT (ea)	152-157
CORE NO. 824P1	TEST NO.	CE33



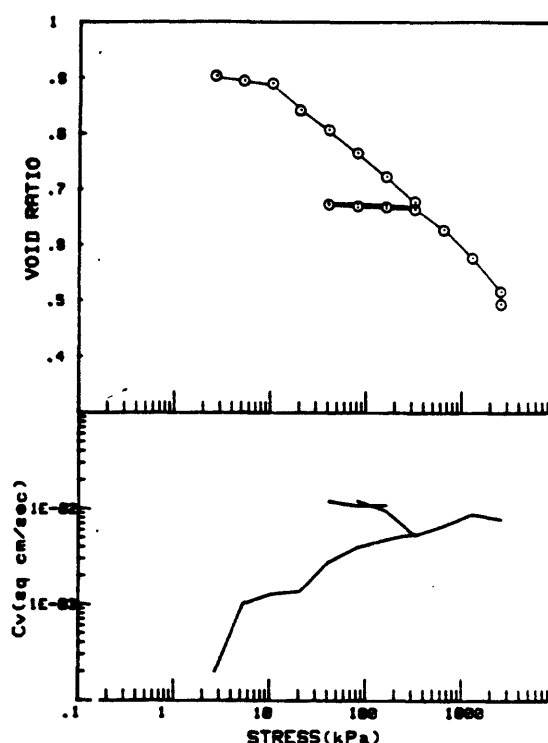
CRUISE DCI-81-EG	INCREMENT (cm)	122-124
CORE NO.	627G2	TEST NO.



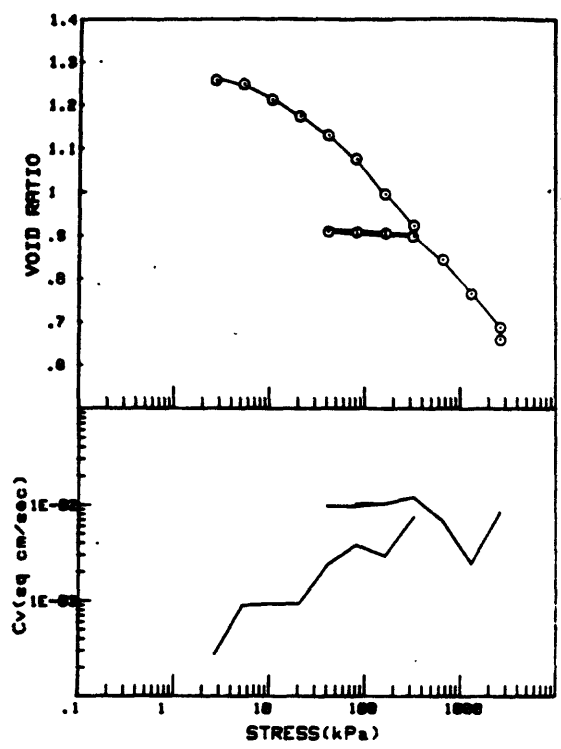
CRUISE DCI-81-EG	INCREMENT (cm)	148-144
CORE NO.	604G1	TEST NO.



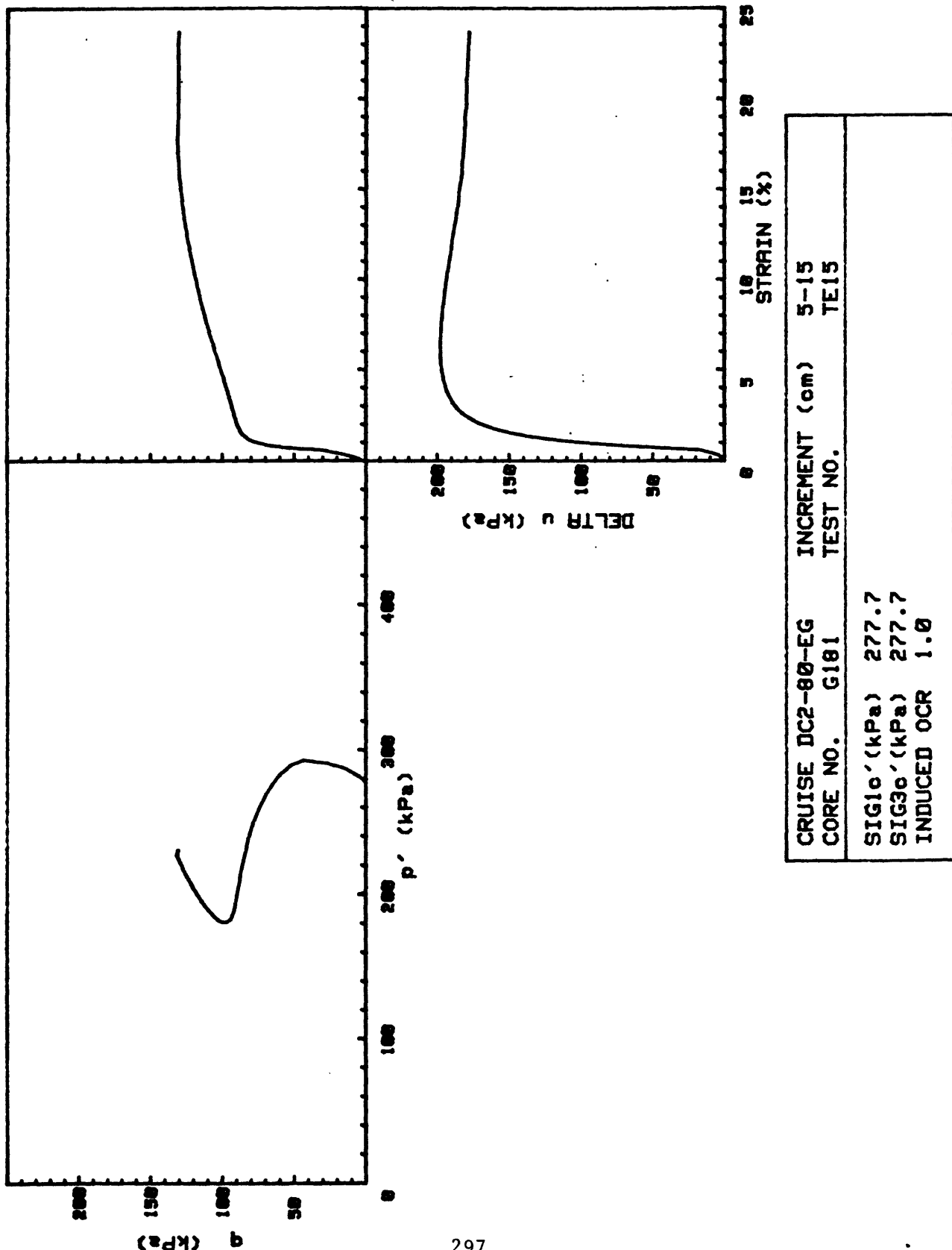
CRUISE DCI-81-EG	INCREMENT (cm)	168-168
CORE NO.	618G2	TEST NO.

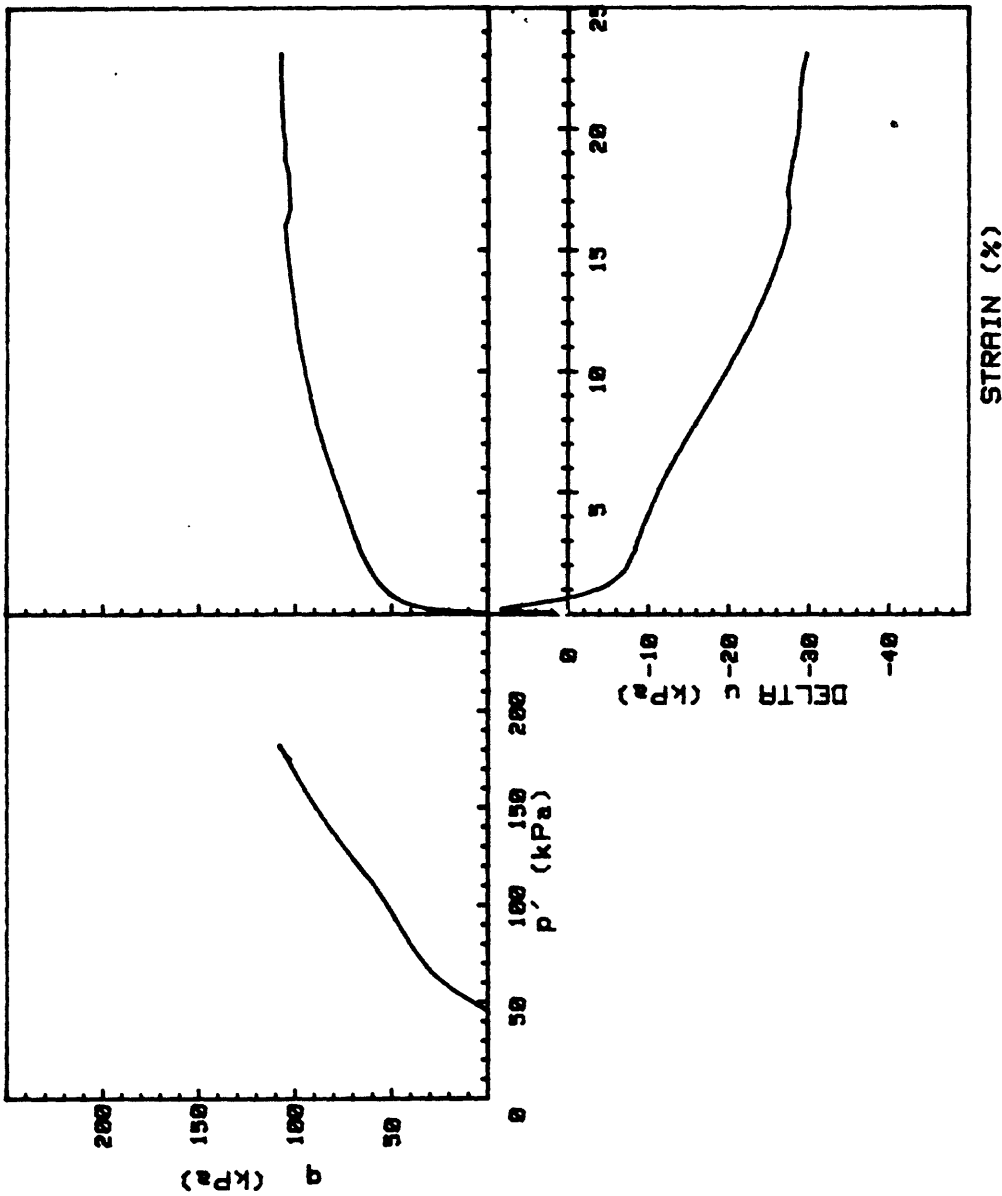


CRUISE DCI-81-EG	INCREMENT (cm)	186-288
CORE NO.	605G2	TEST NO.

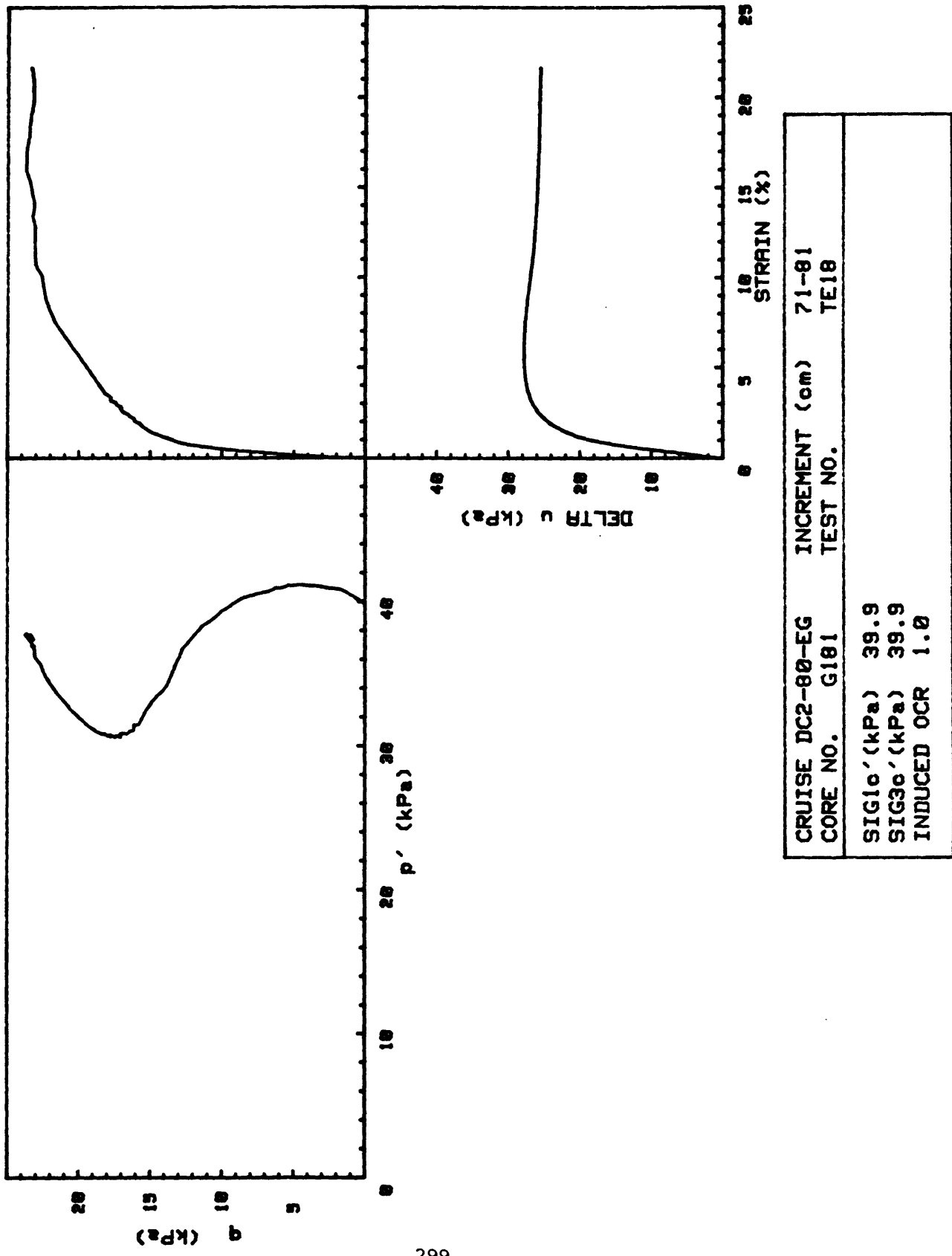


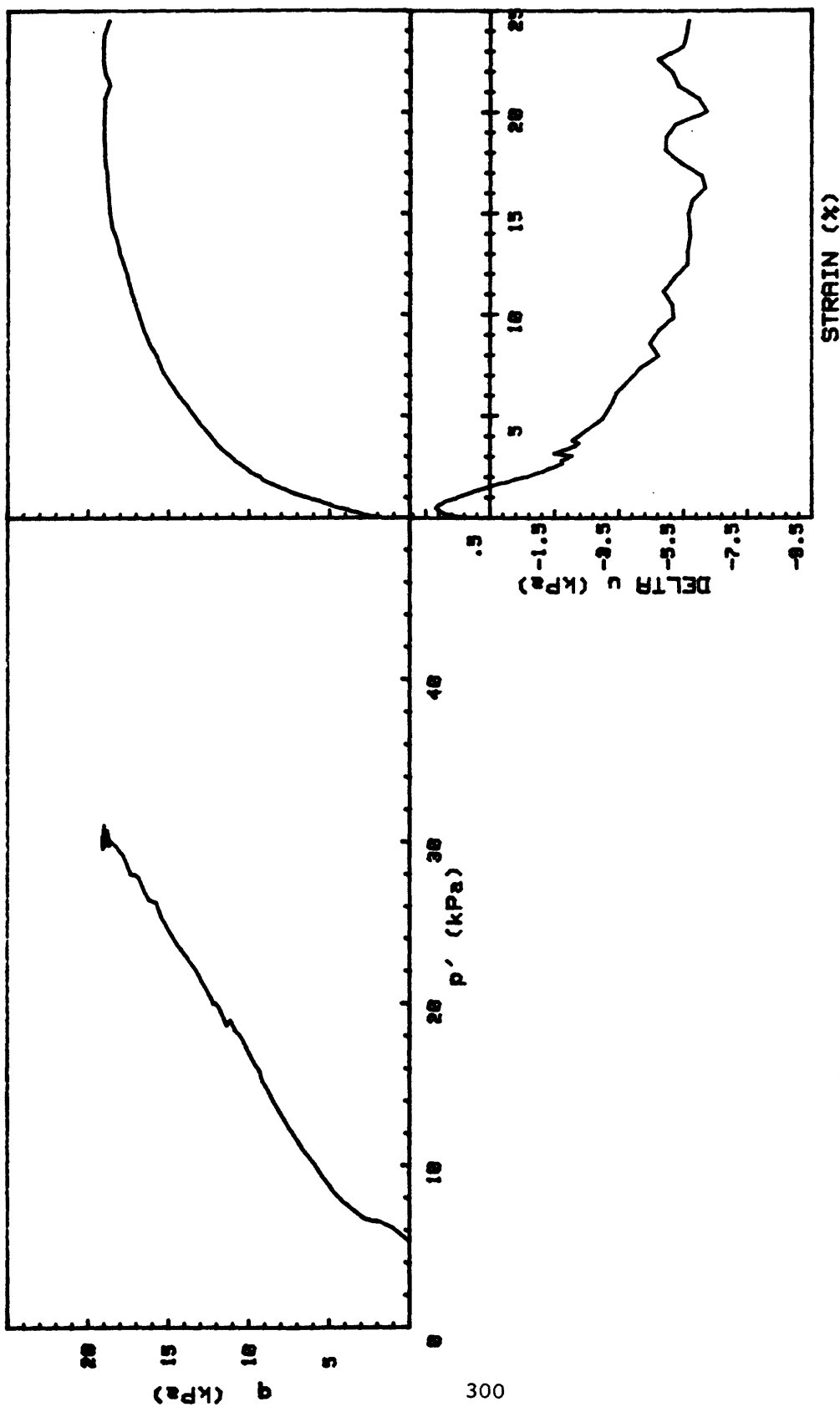
CRUISE DCI-81-EG INCREMENT (cm) 87-72  
CORE NO. 88561 TEST NO. 0E48



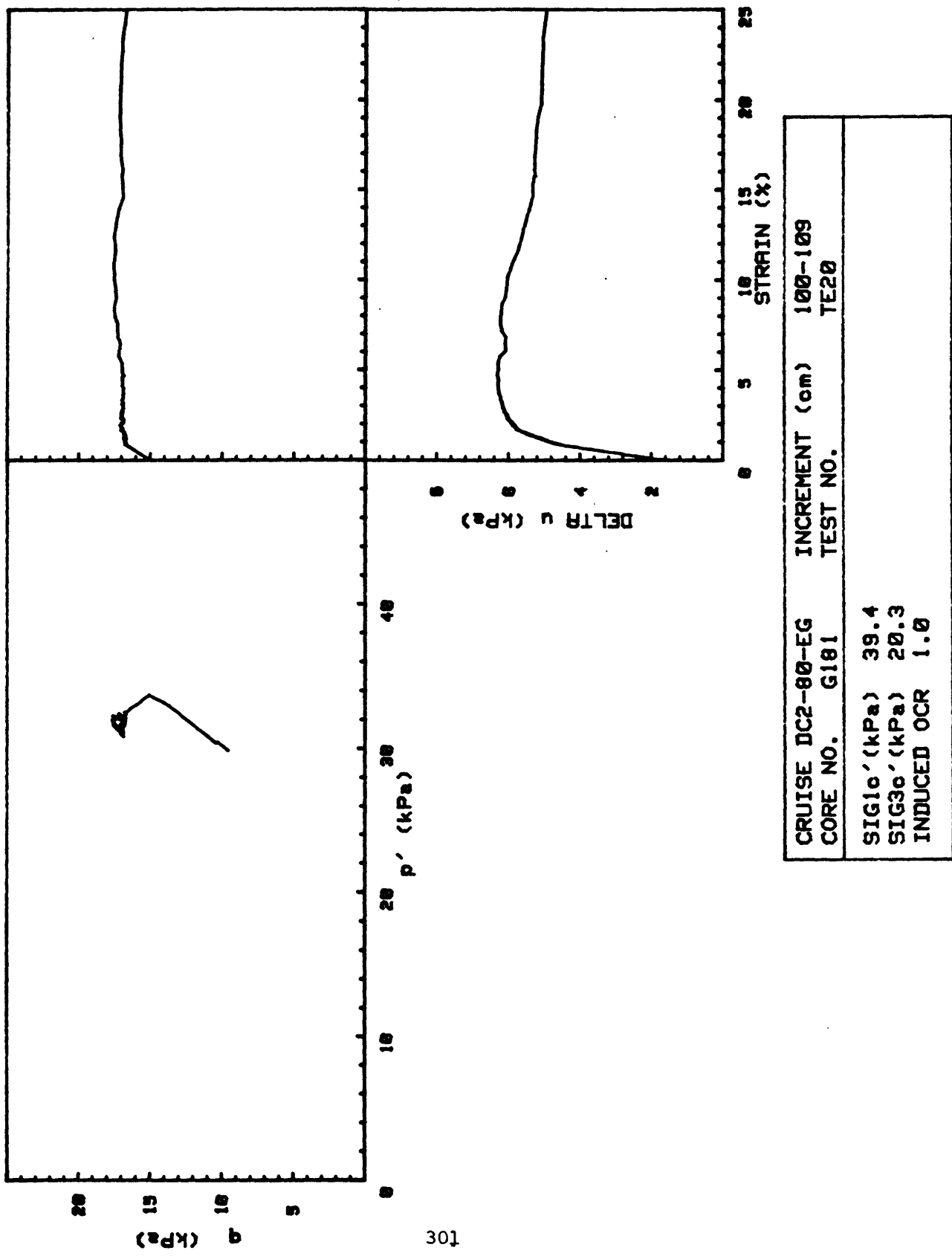


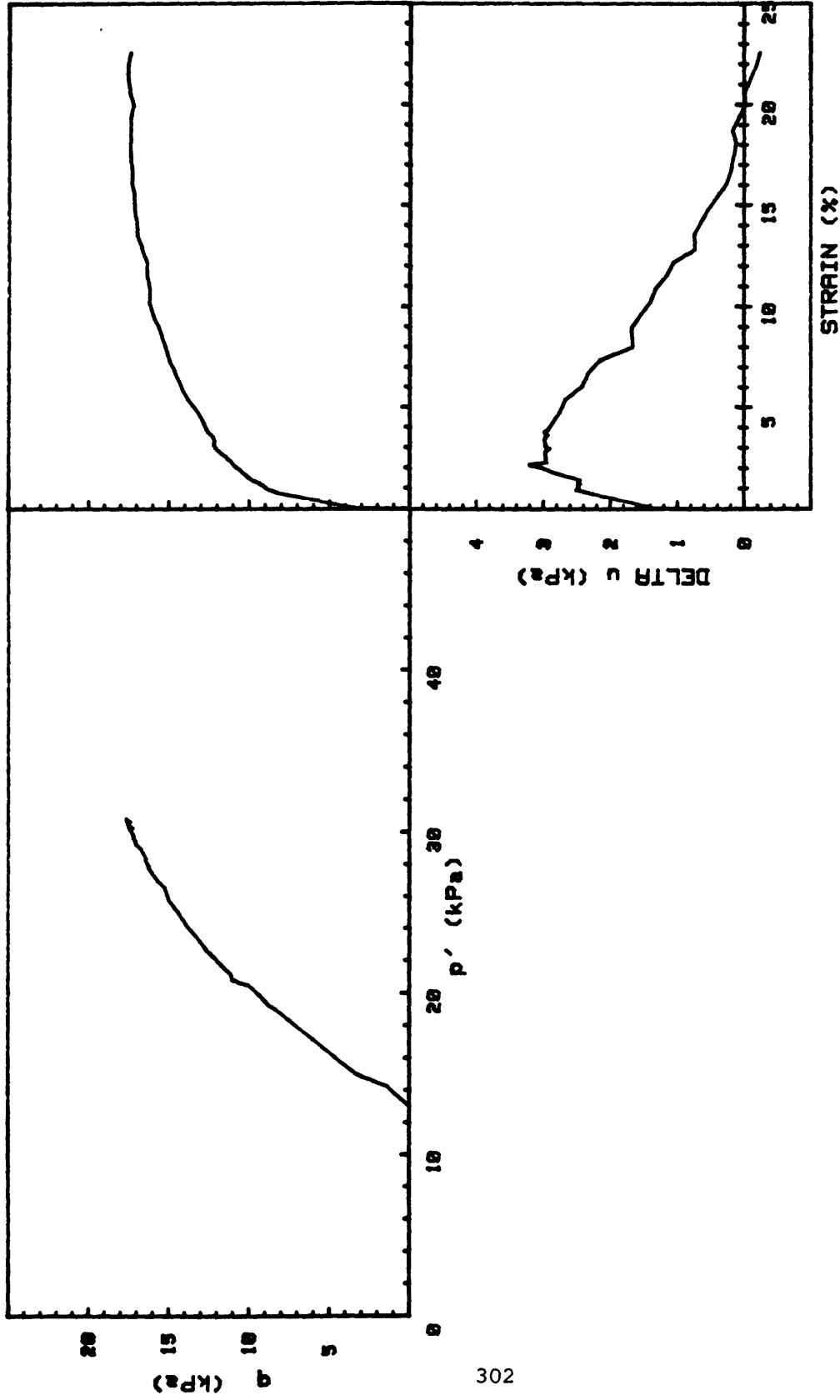
CRUISE	DC2-80-EG	INCREMENT (cm)	5-14
CORE NO.	G181	TEST NO.	TE16
SIG1 <sub>c'</sub> (kPa)	45.0		
SIG3 <sub>c'</sub> (kPa)	45.0		
INDUCED OCR	6.1		



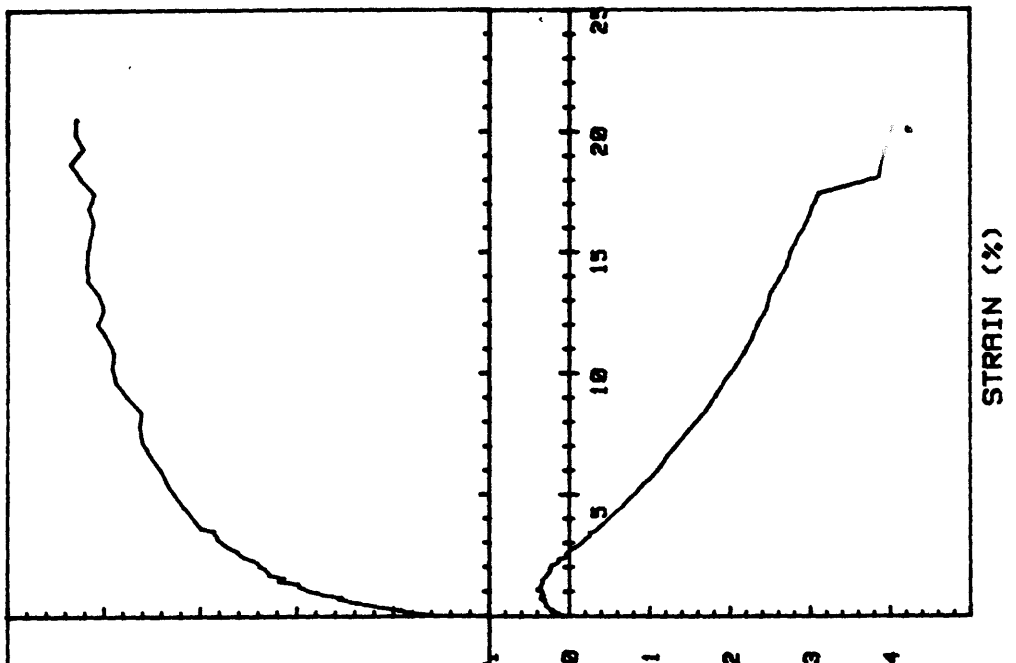


CRUISE DC2-80-EG	INCREMENT (cm)	71-80
CORE NO.	G181	TEST NO.
SIG1 <sub>o</sub> ' (kPa)	5.3	TE19
SIG3 <sub>o</sub> ' (kPa)	5.3	
INDUCED OCR	7.3	

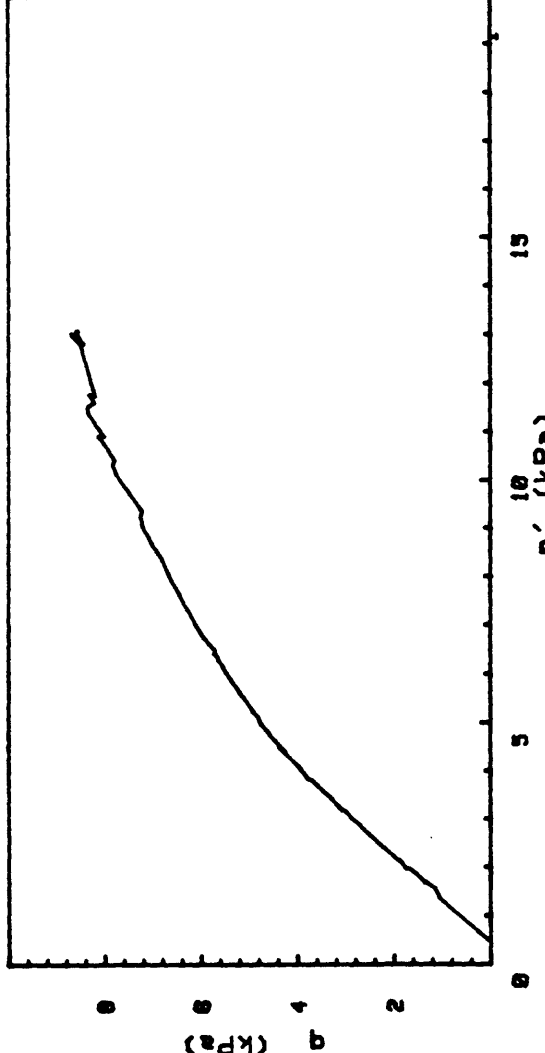


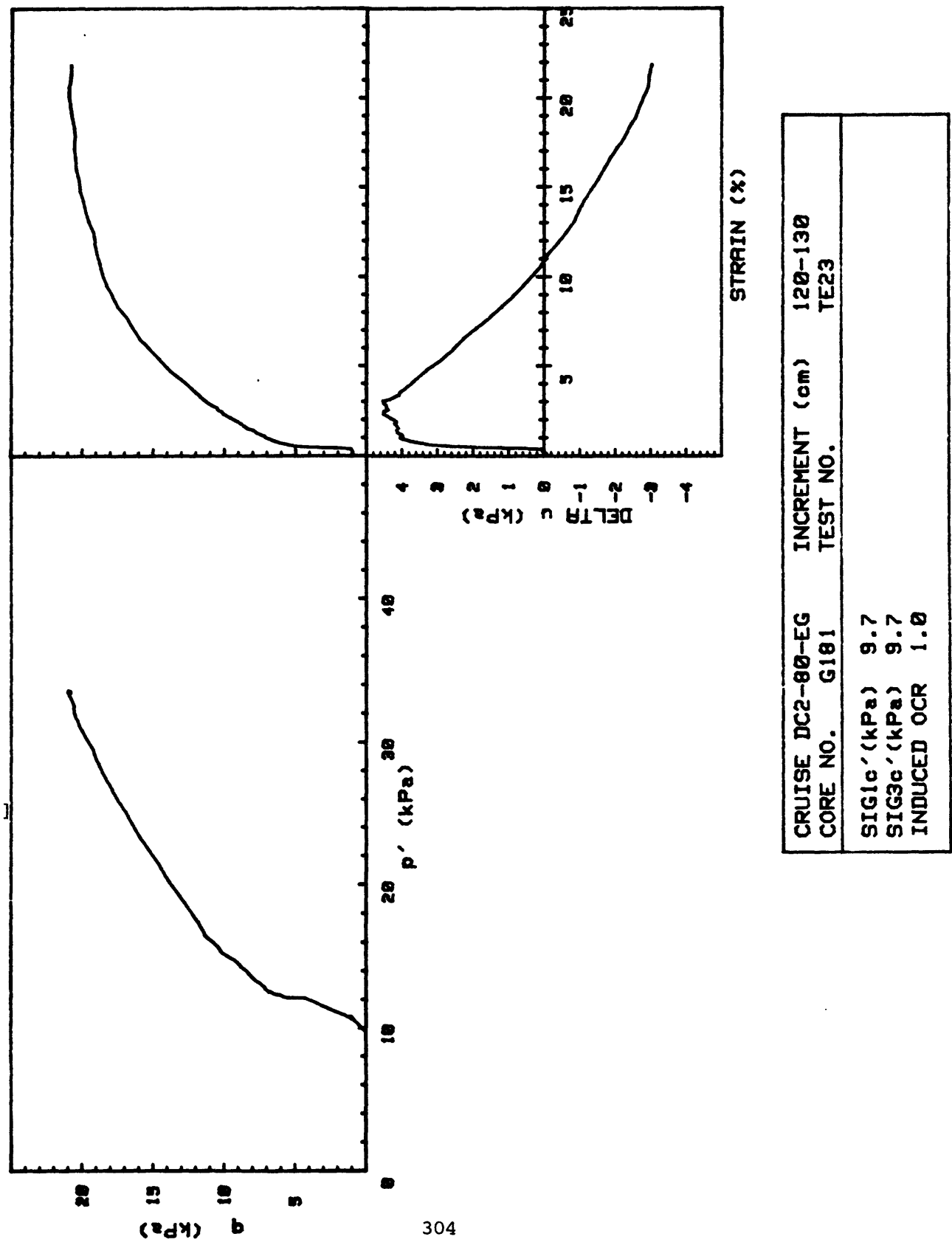


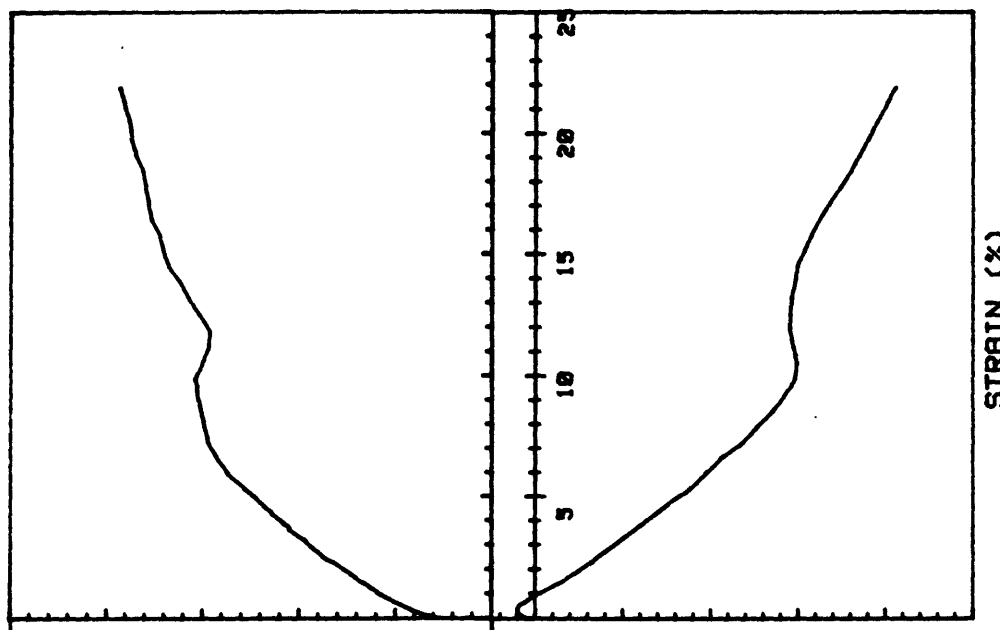
CRUISE DC2-80-EG		INCREMENT (cm)	100-110
CORE NO.	G181	TEST NO.	TE21
SIG1 $\sigma'$ (kPa)	13.1		
SIG3 $\sigma'$ (kPa)	13.1		
INDUCED OCR	3.0		



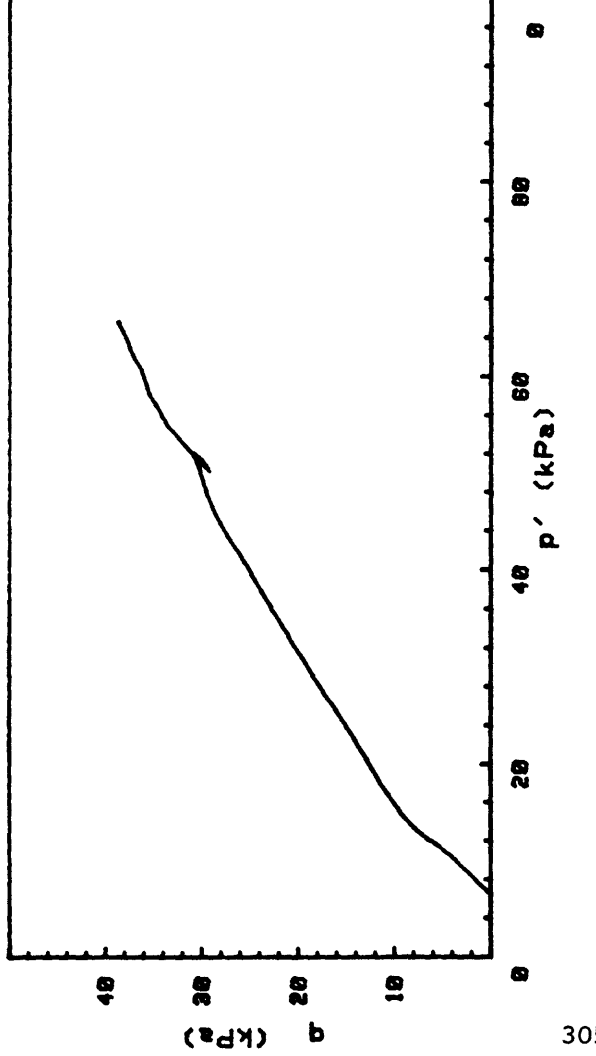
CRUISE DC2-80-EG	INCREMENT (cm)	120-130
CORE NO.	TEST NO.	
SIG1c' (kPa)	.5	
SIG3c' (kPa)	.5	
INDUCED OCR	1.0	

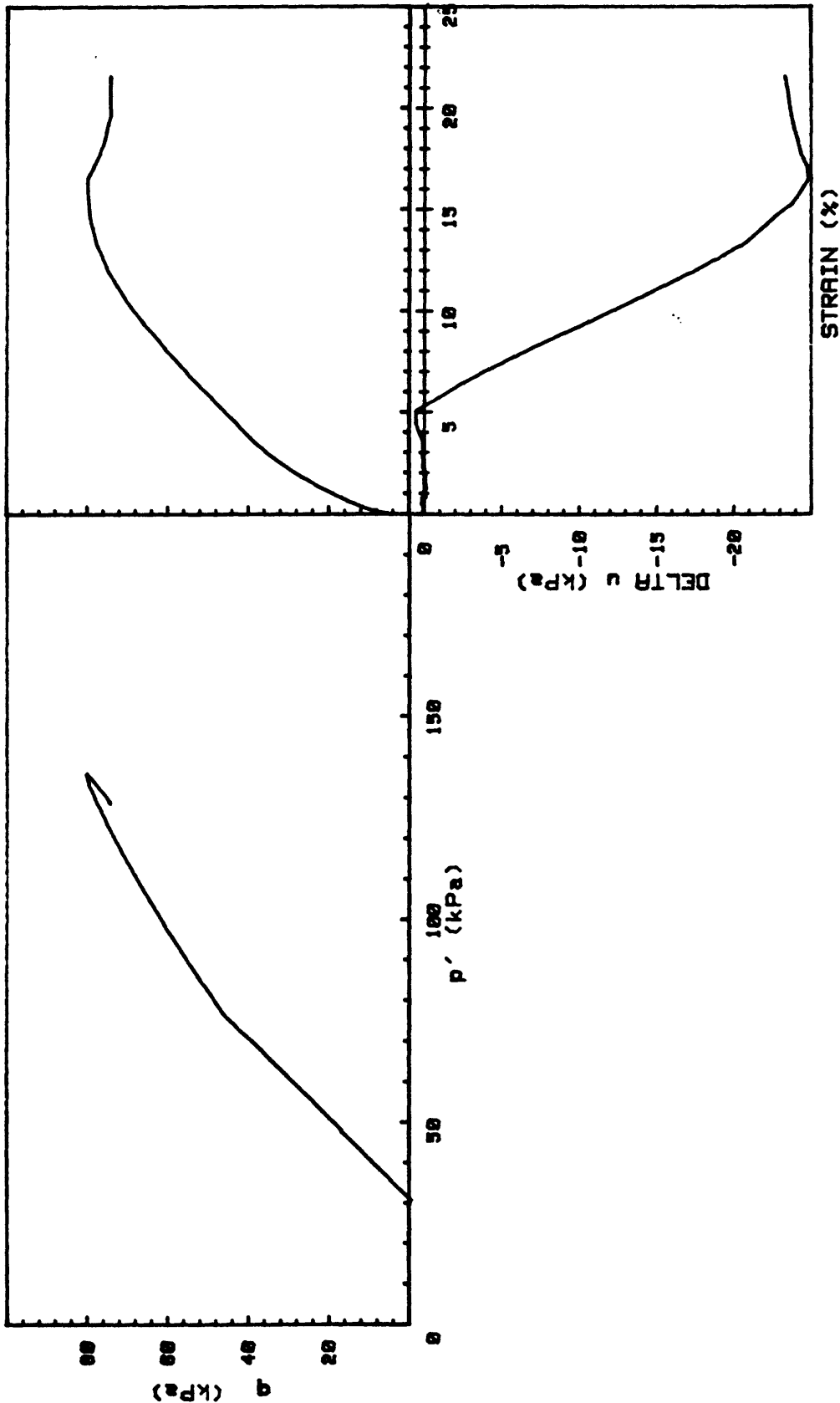




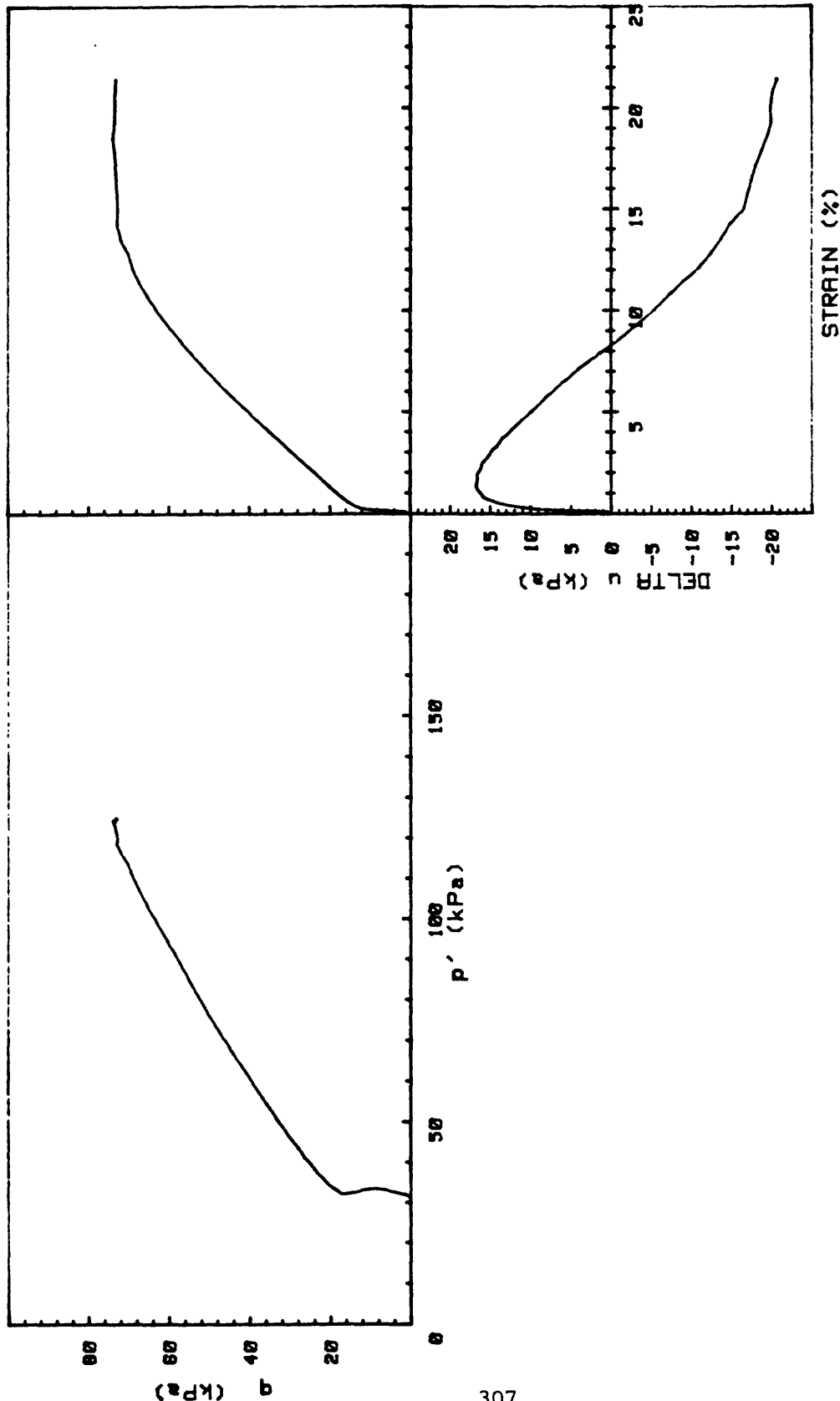


CRUISE DCC-80-EG		INCREMENT (cm)	8-17
CORE NO.	43G	TEST NO.	TE27
SIG1c' (kPa)	6.5		
SIG3c' (kPa)	6.5		
INDUCED OCR	5.0		

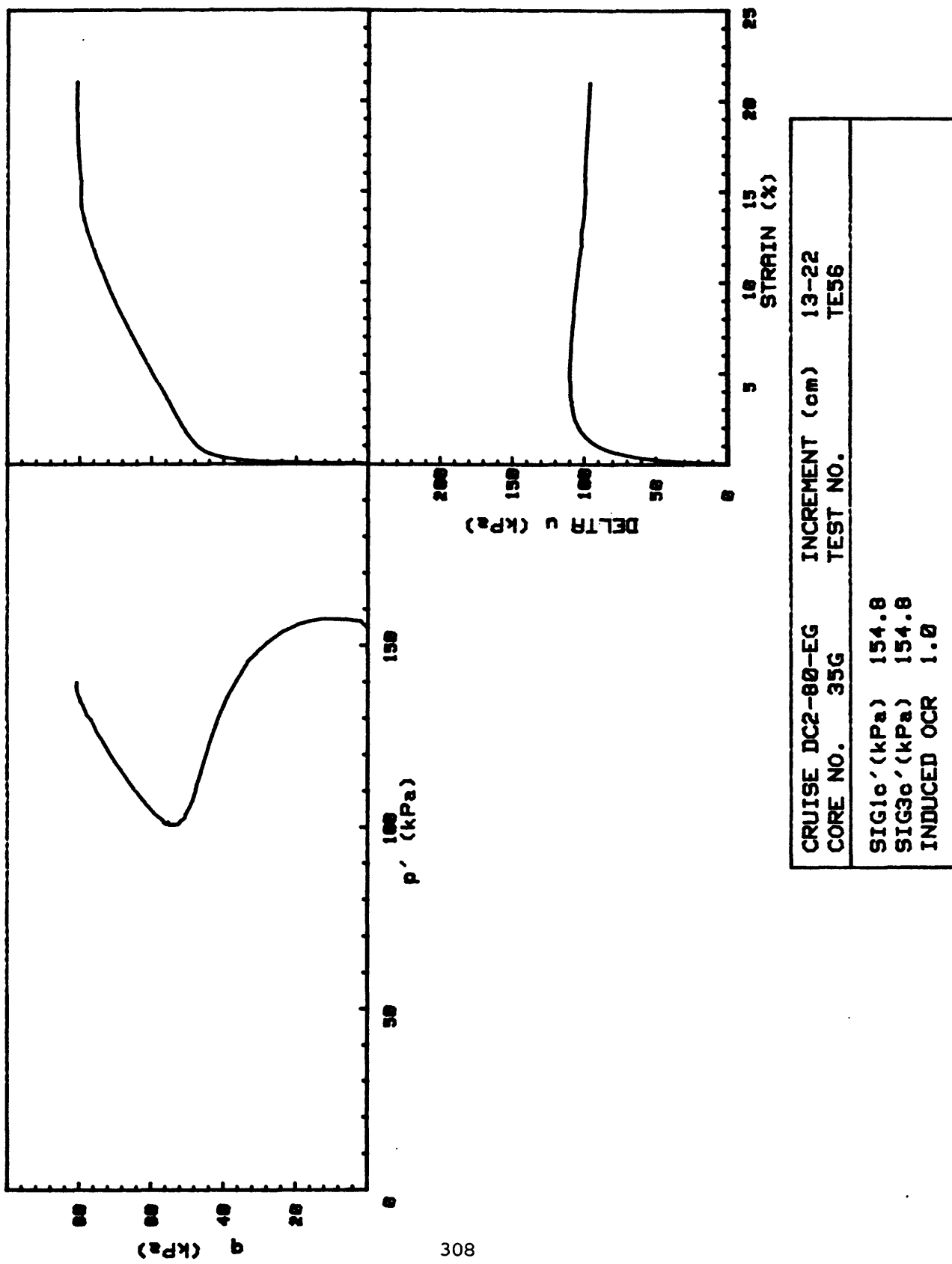


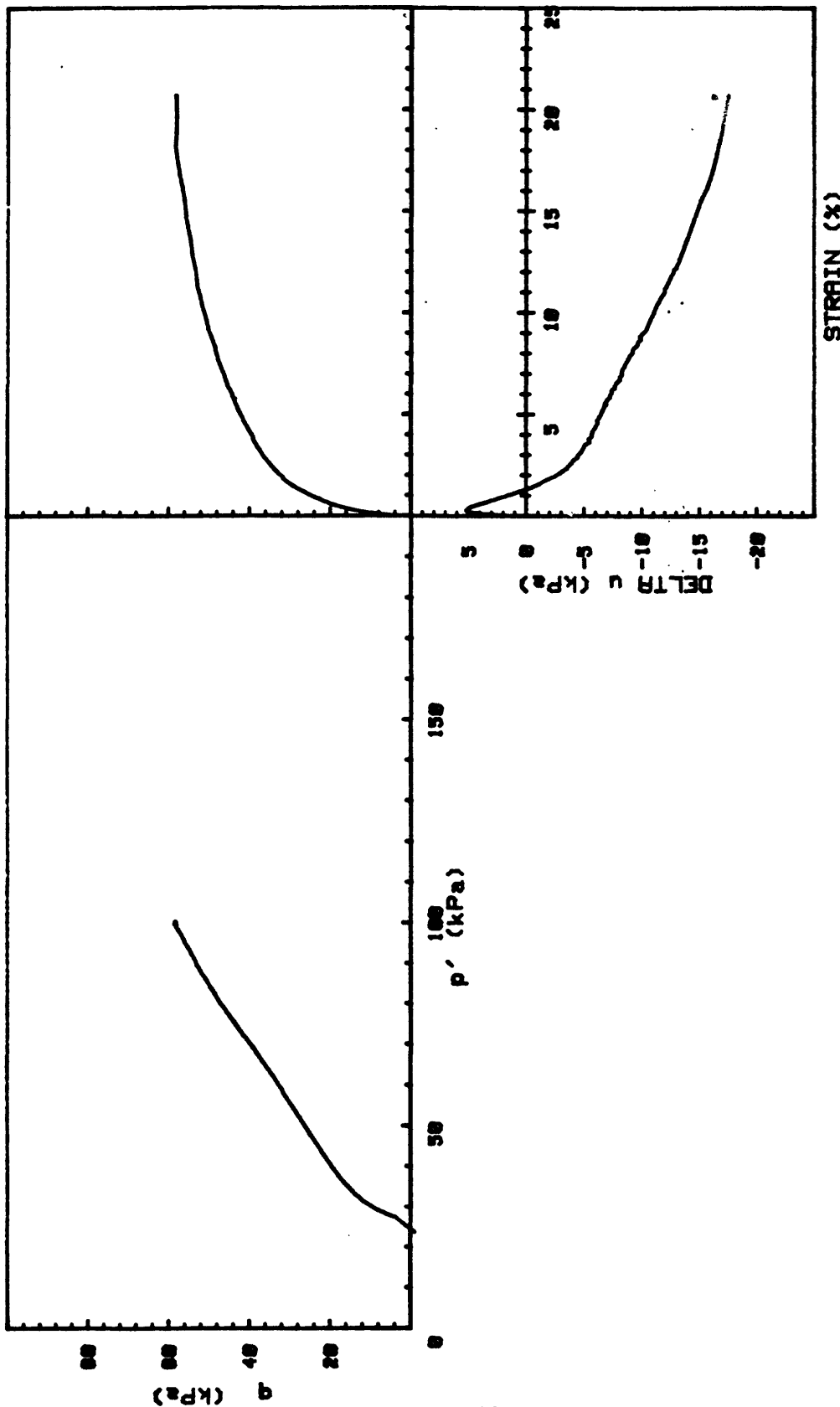


CRUISE DC2-80-EG		INCREMENT (cm)	18-27
CORE NO.	43G	TEST NO.	TE34
SIG1c' (kPa)	31.3		
SIG3c' (kPa)	31.3		
INDUCED OCR	1.0		

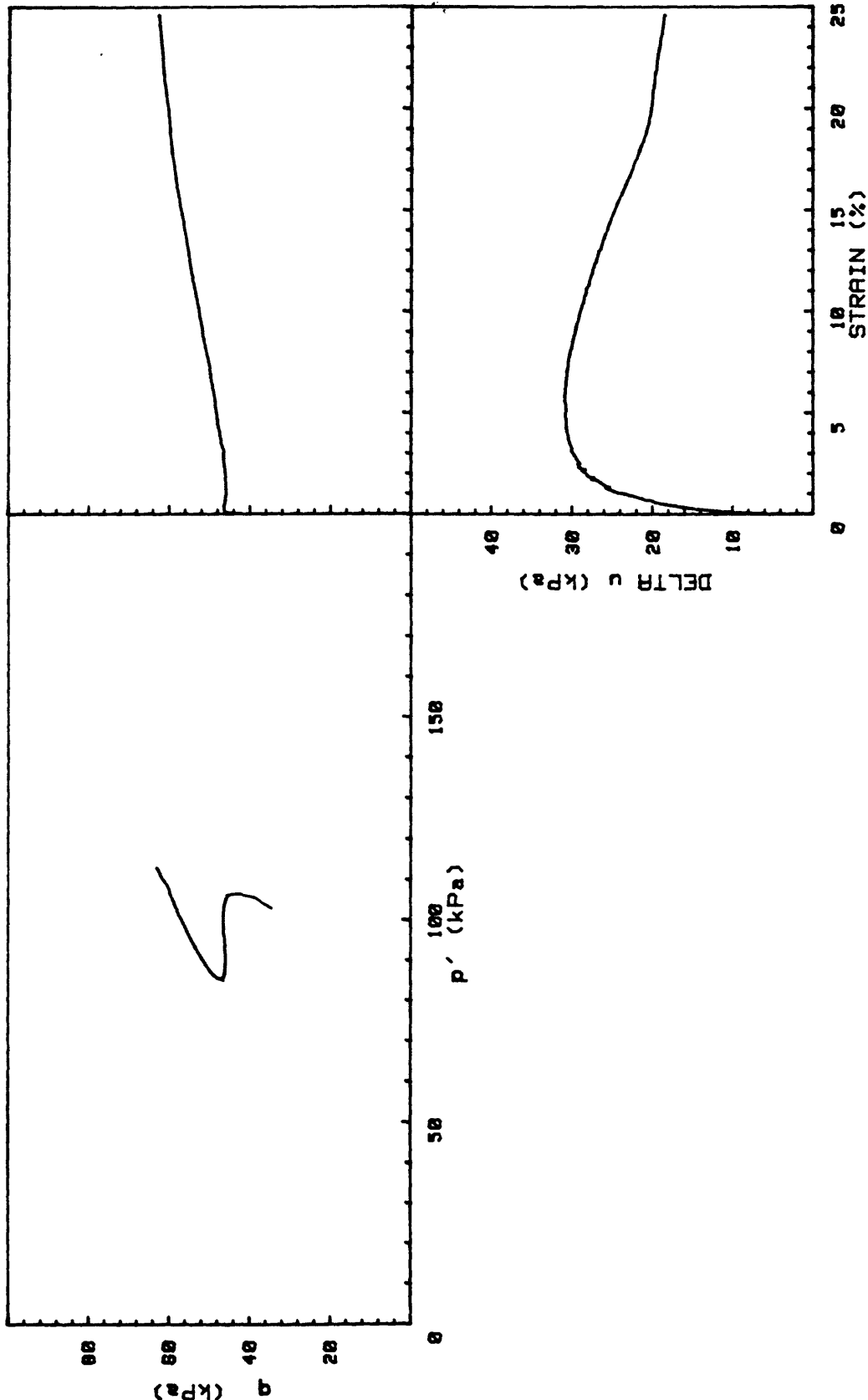


CRUISE	DC2-80-EG	INCREMENT	(cm)	18-27
CORE NO.	43G	TEST NO.	TE35	
SIG1c' (kPa)	31.1			
SIG3c' (kPa)	31.1			
INDUCED OCR	1.0			

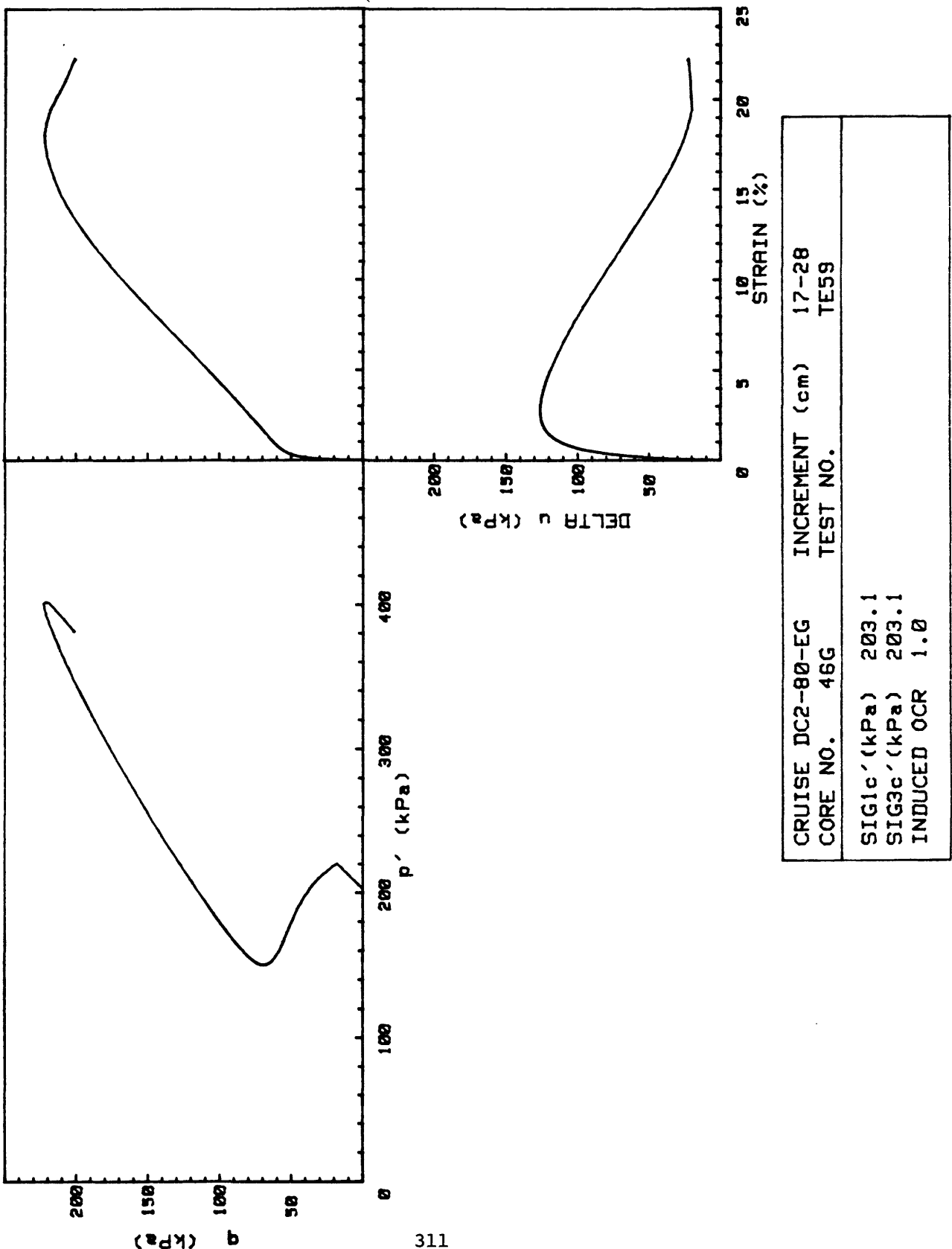


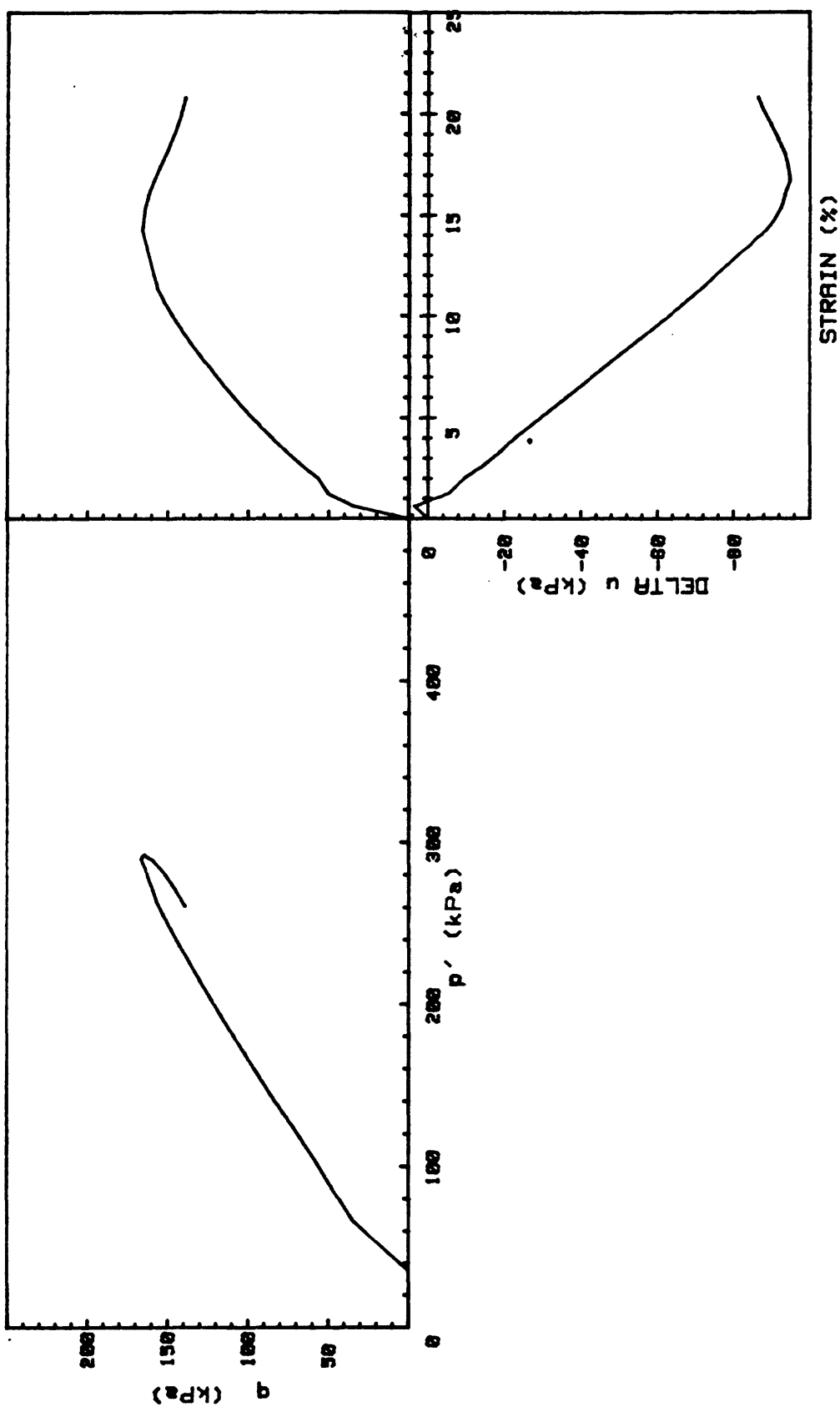


CRUISE DC2-80-EG	INCREMENT (cm)	13-25
CORE NO. 35G	TEST NO.	TE57
SIG1 <sub>c</sub> ' (kPa)	24.7	
SIG3 <sub>c</sub> ' (kPa)	24.7	
INDUCED OCR	6.0	

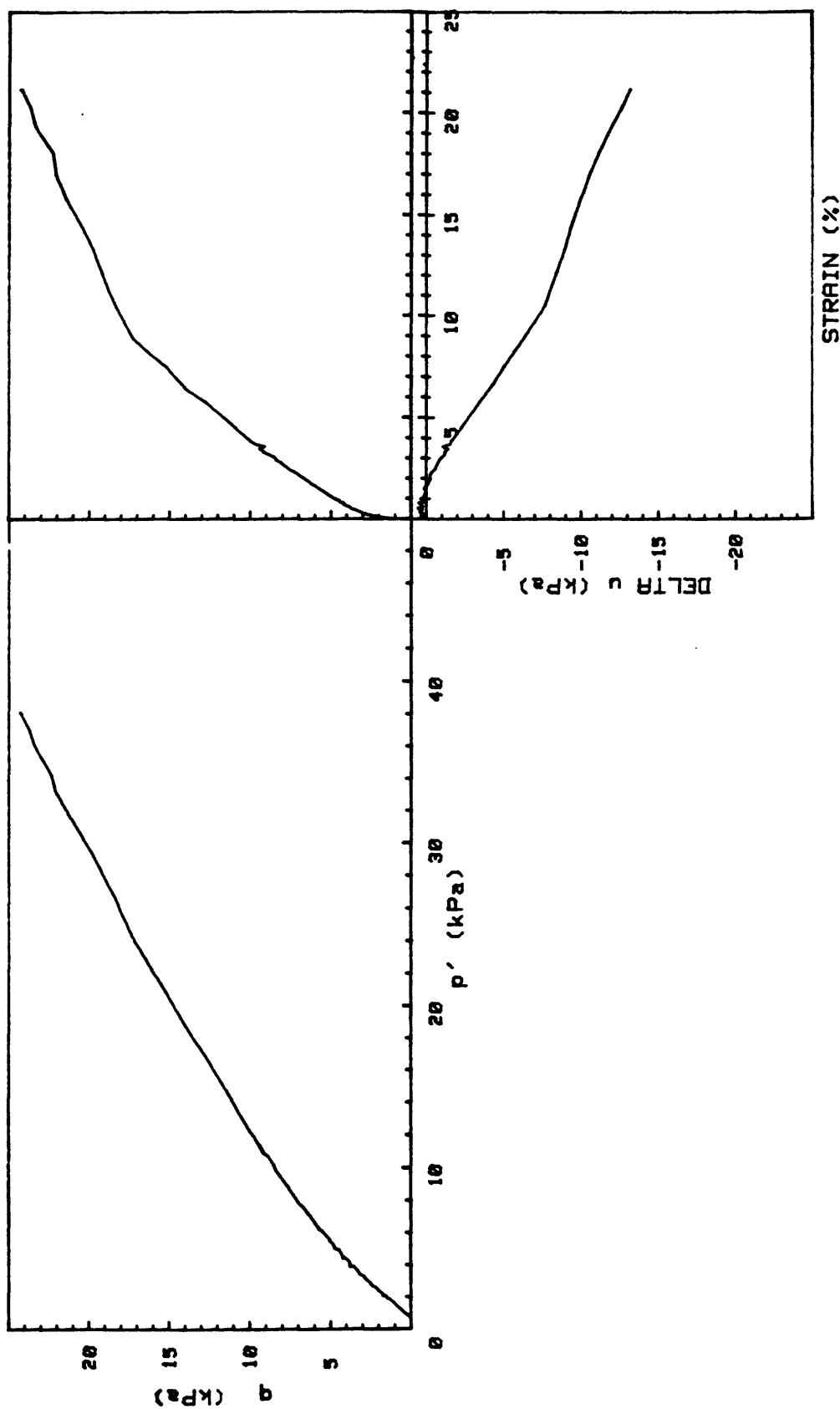


CRUISE	DC2-80-EG	INCREMENT	(cm)	25-32
CORE NO.	35G	TEST NO.	TE58	
SIG1c' (kPa)	137.6			
SIG3c' (kPa)	68.5			
INDUCED OCR	1.0			

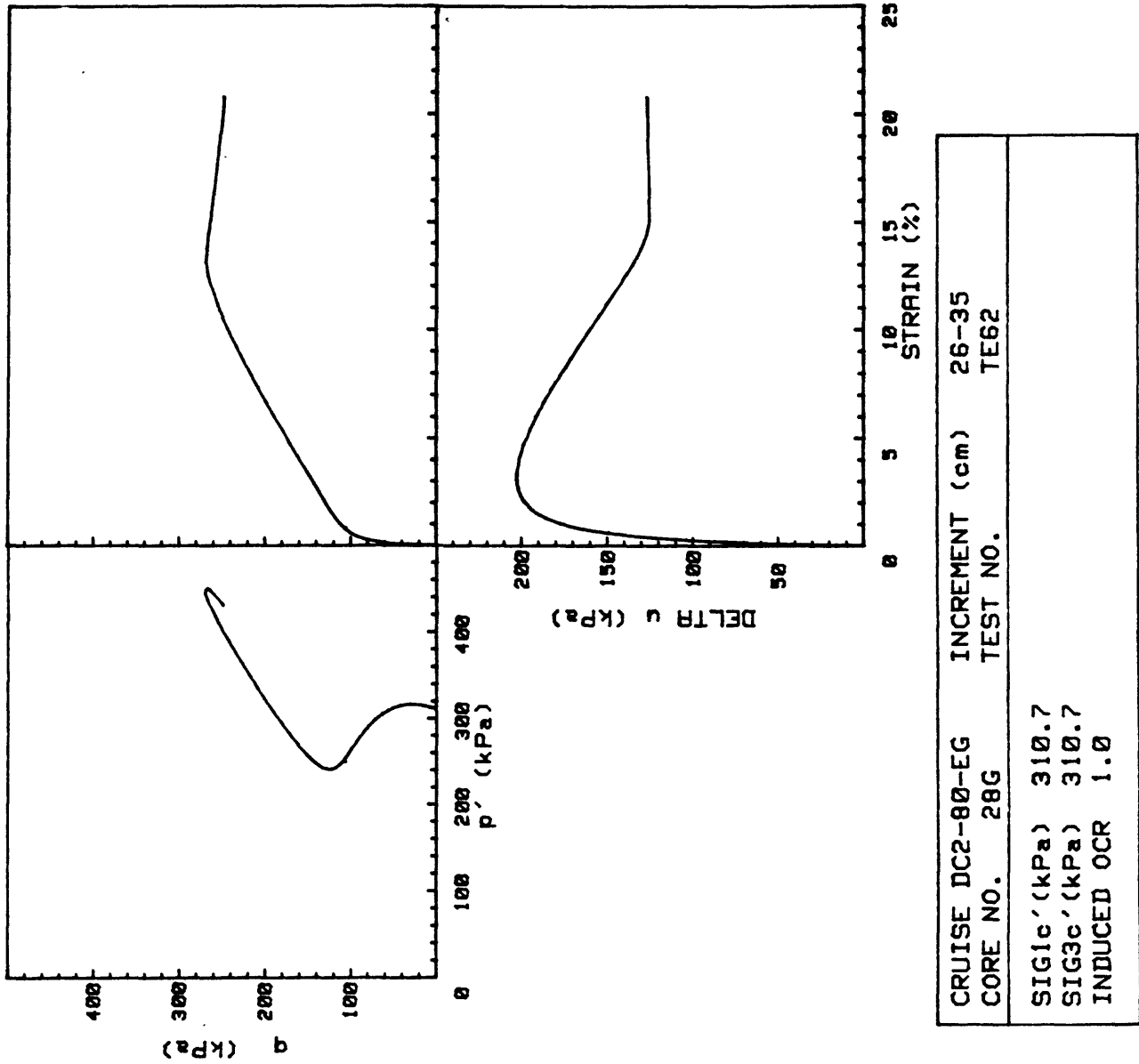


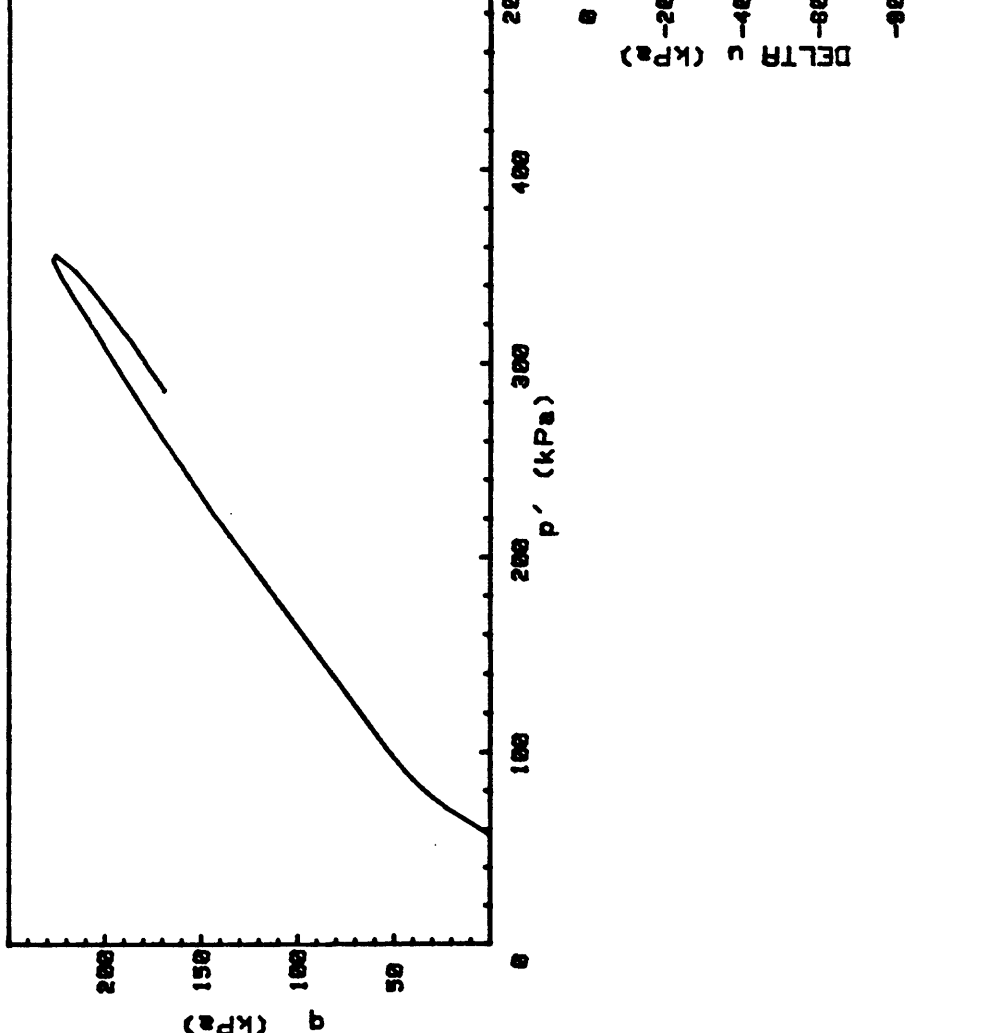
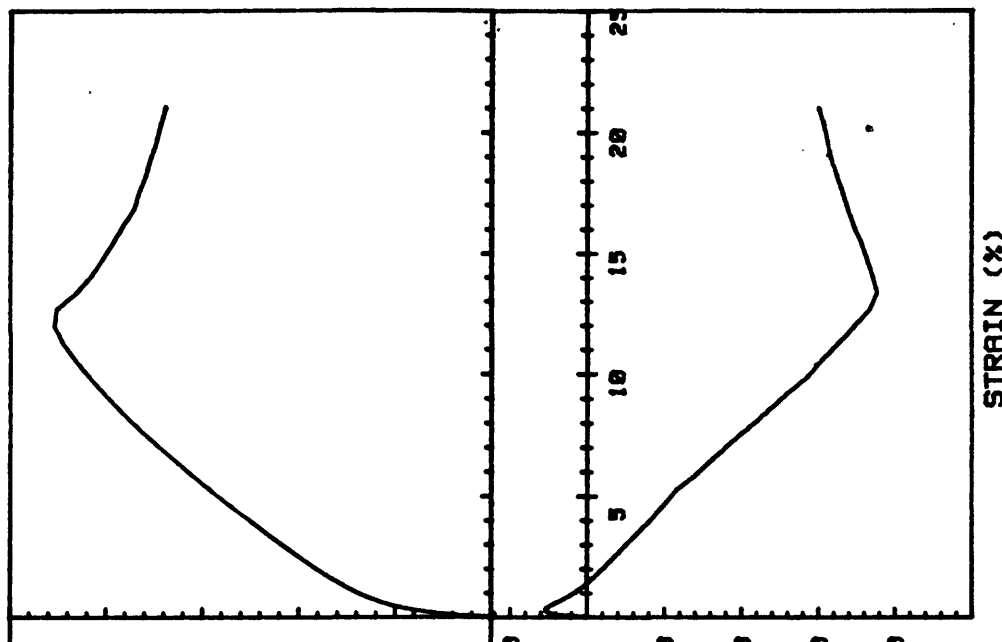


CRUISE DC2-80-EG	INCREMENT (cm)	28-37
CORE NO. 46G	TEST NO.	TE60
SIG1c' (kPa)	35.7	
SIG3c' (kPa)	35.7	
INDUCED OCR	6.0	

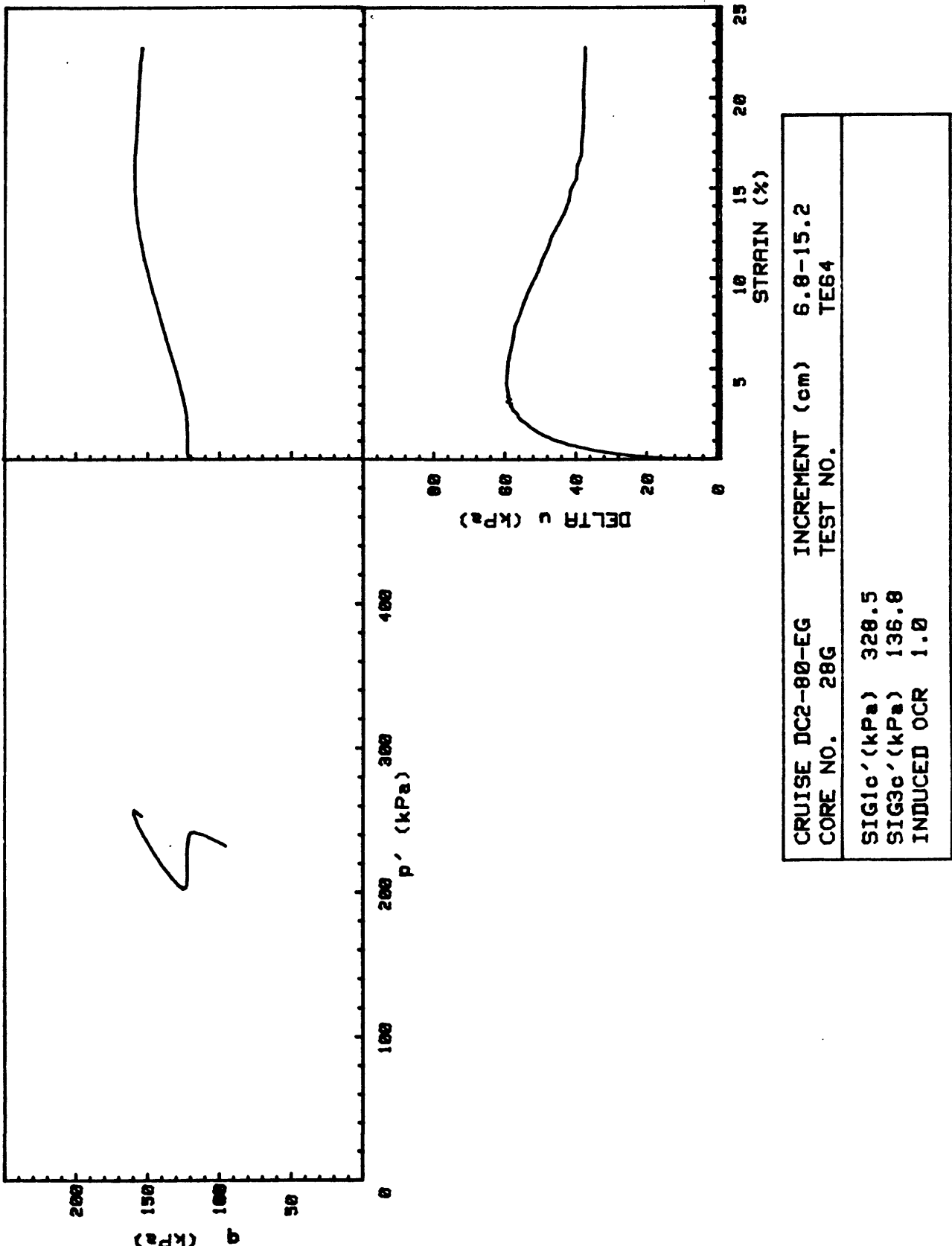


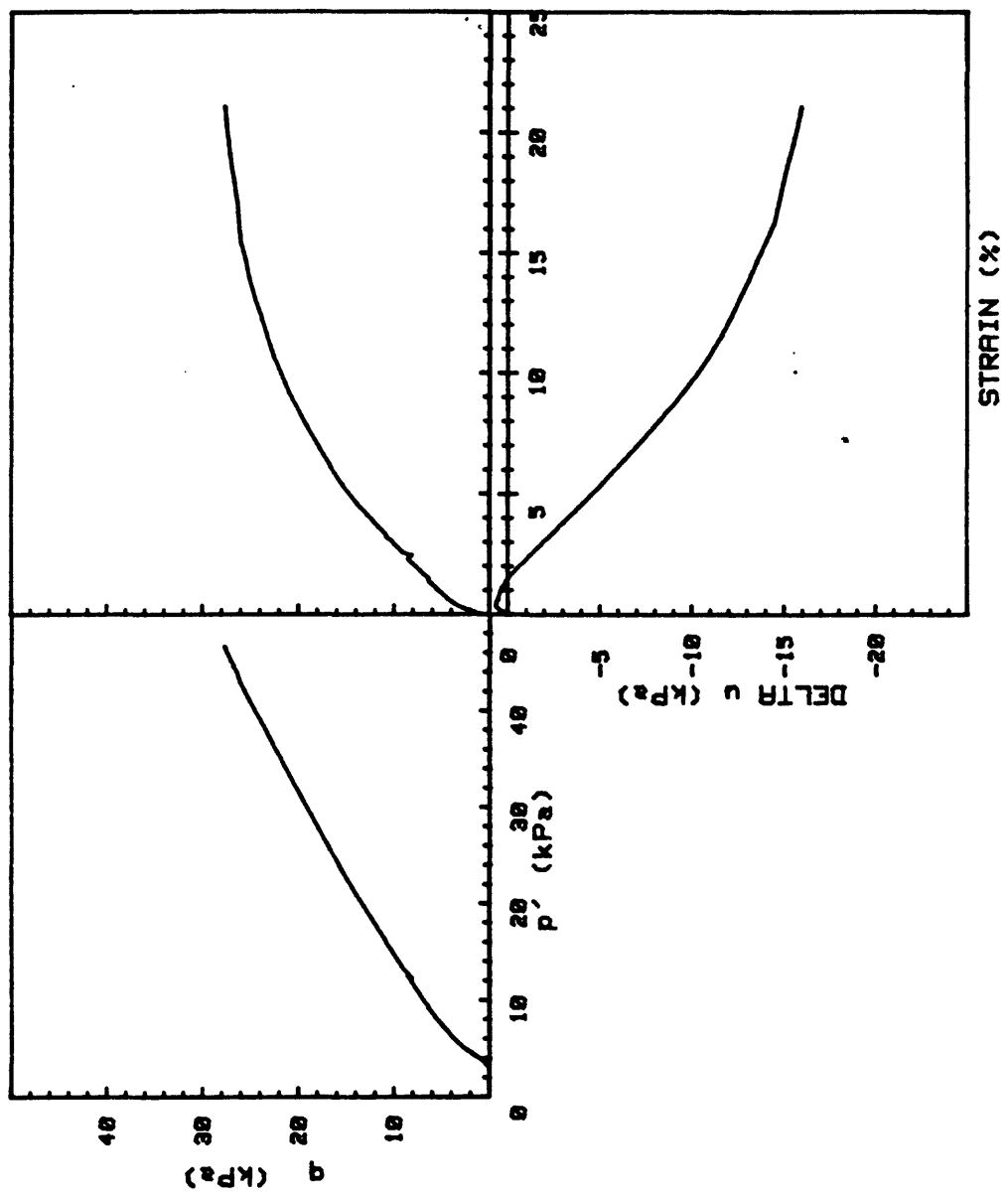
CRUISE DC2-80-EG	INCREMENT (cm)	28-37
CORE NO.	TEST NO.	TE61
46G		
SIG1c' (kPa)	.7	
SIG3c' (kPa)	.7	
INDUCED OCR	1.0	



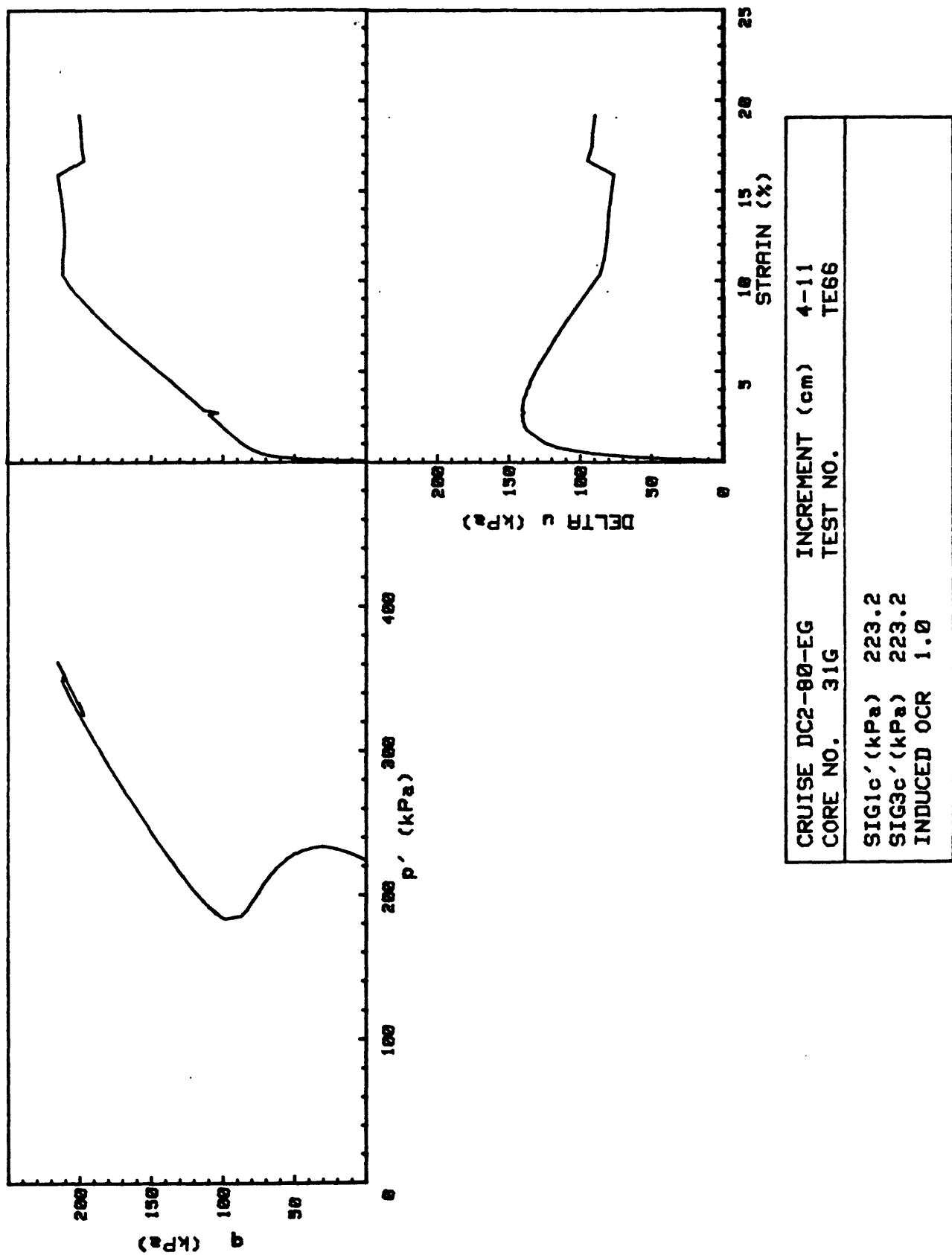


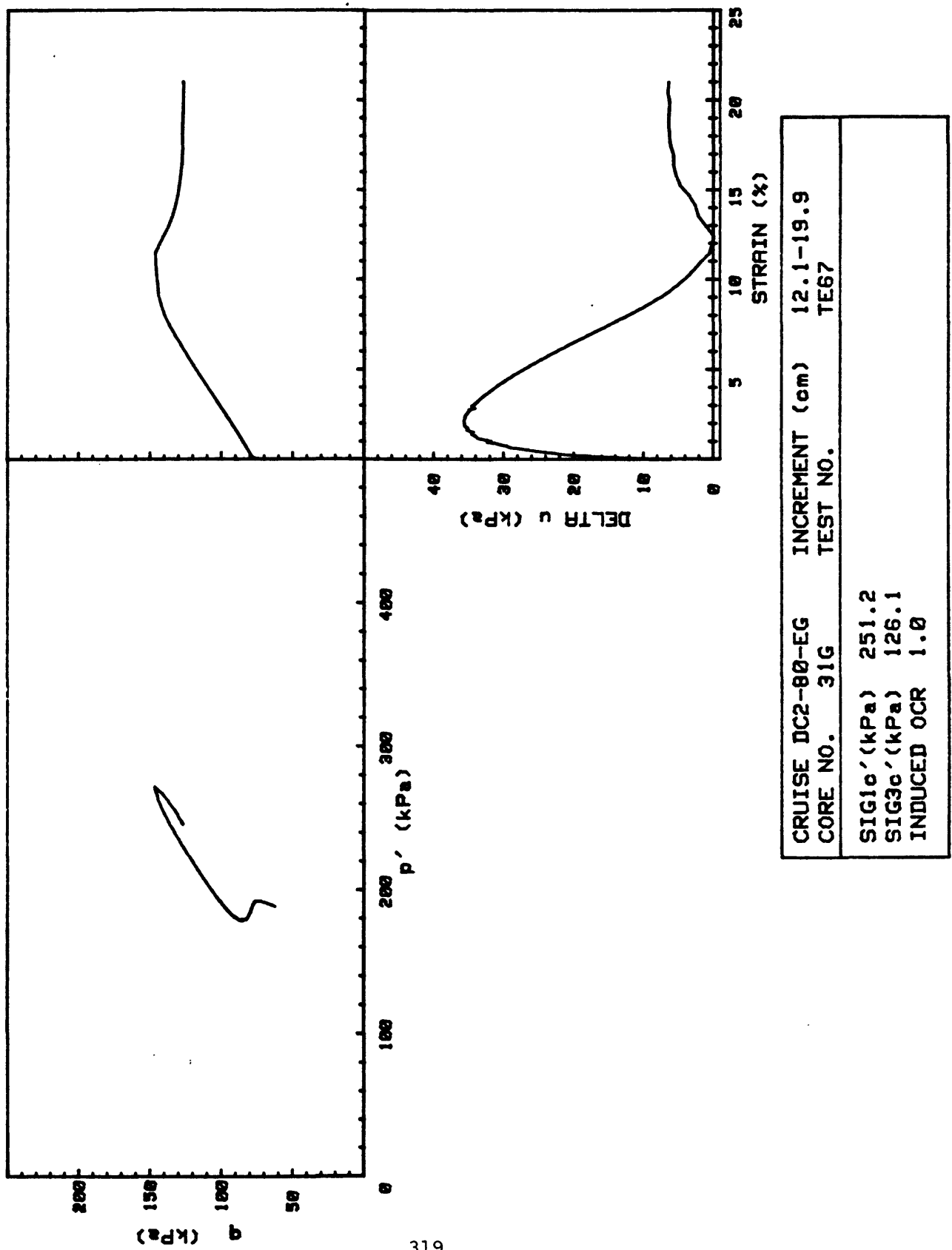
CRUISE DC-2-80 EG	INCREMENT (cm)	26.5-35.1
CORE NO.	TEST NO.	TE63
SIG1e' (kPa)	56.9	
SIG3c' (kPa)	56.9	
INDUCED OCR	6.0	

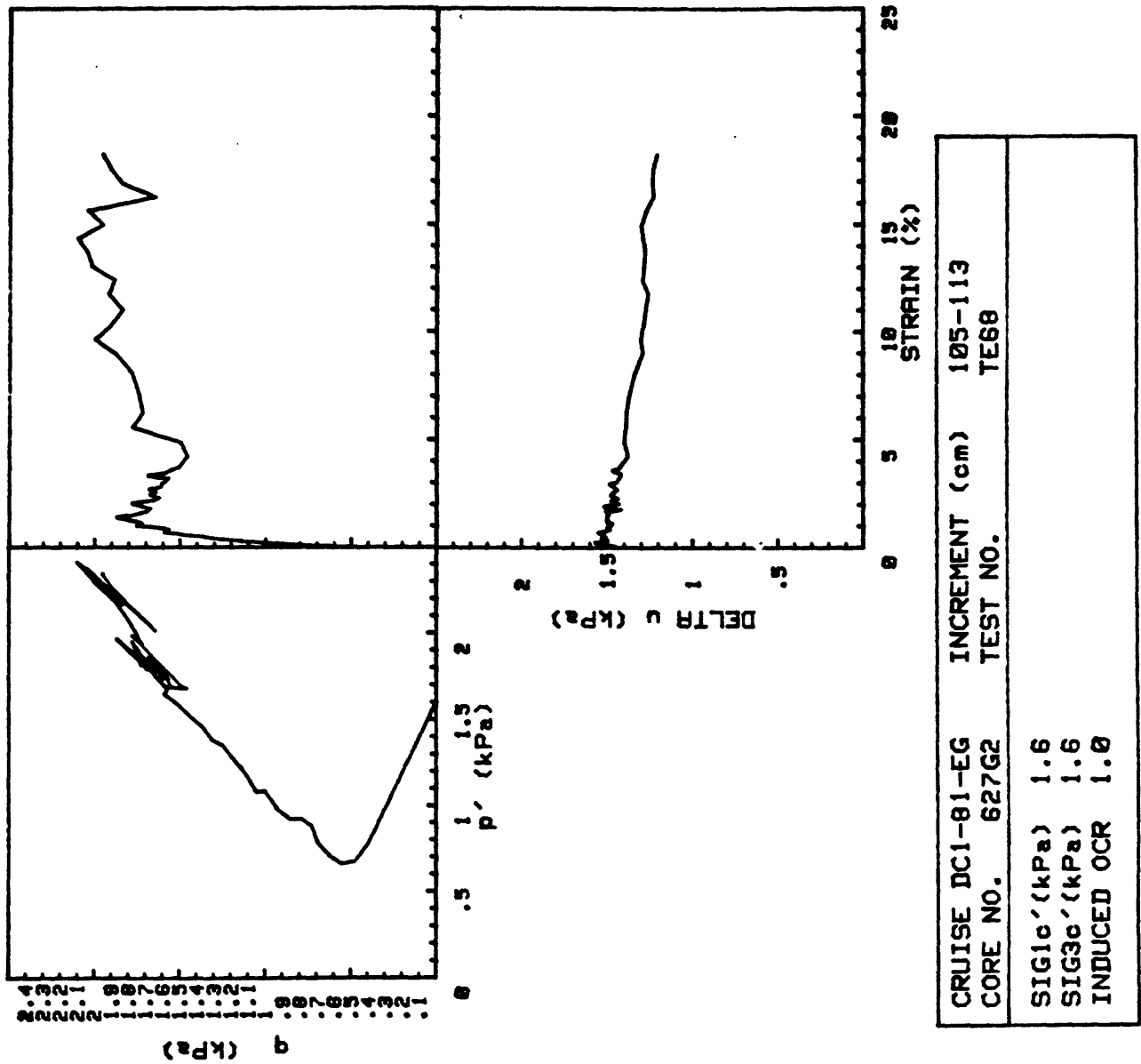


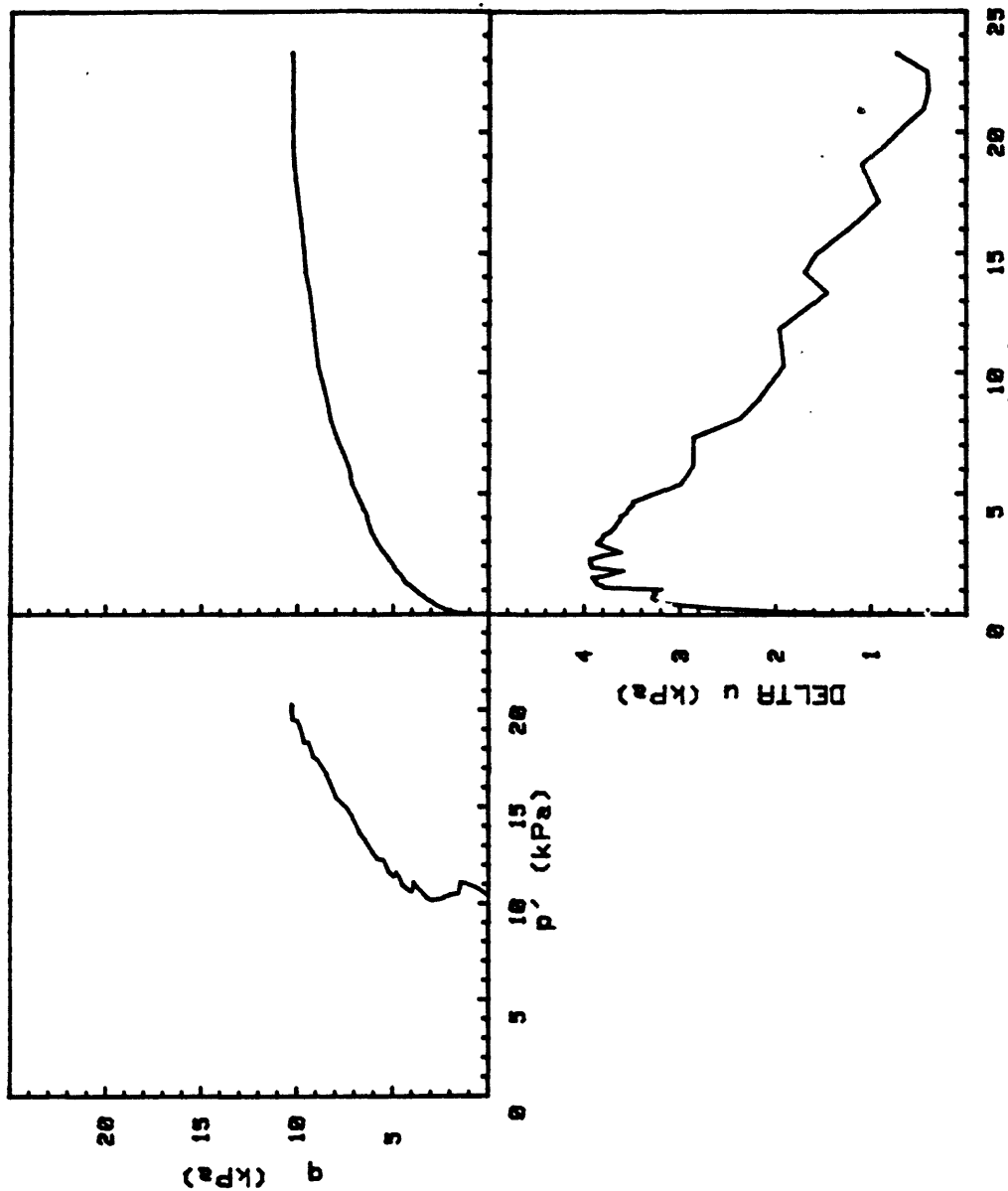


CRUISE DC2-80-EG	INCREMENT (cm)	4-11
CORE NO.	TEST NO.	TE65
SIG1c' (kPa)	3.0	
SIG3c' (kPa)	3.0	
INDUCED OCR	1.0	

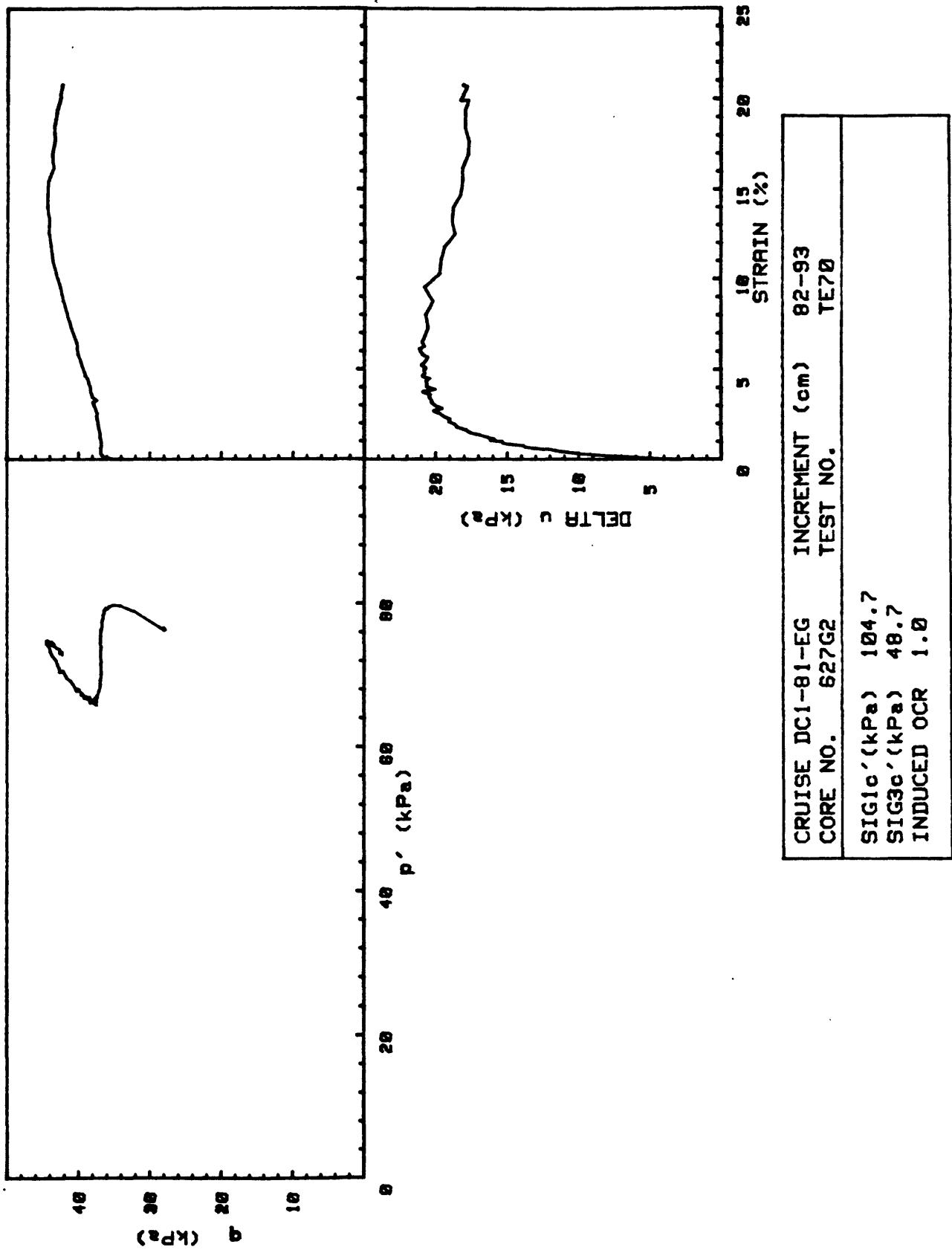


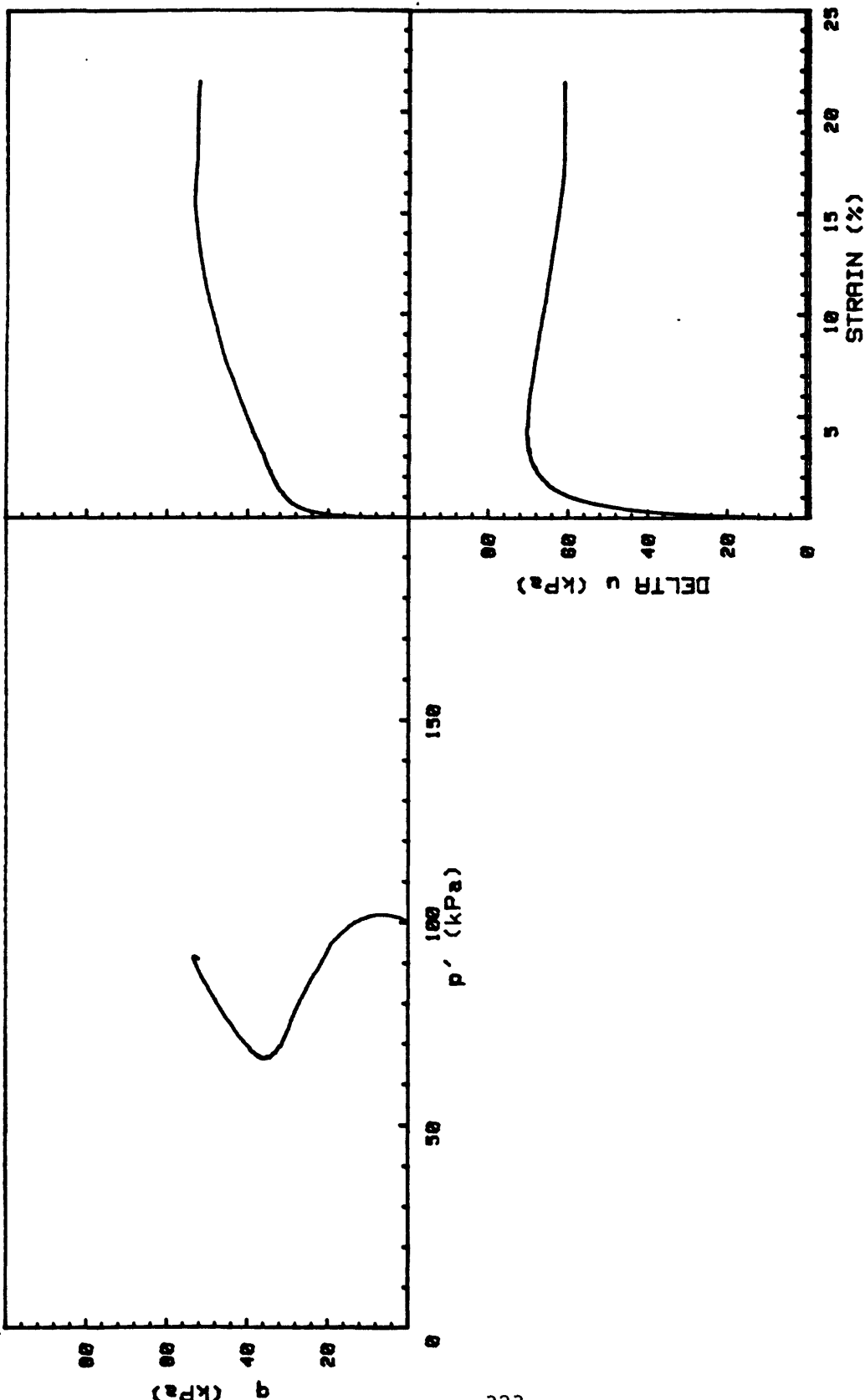




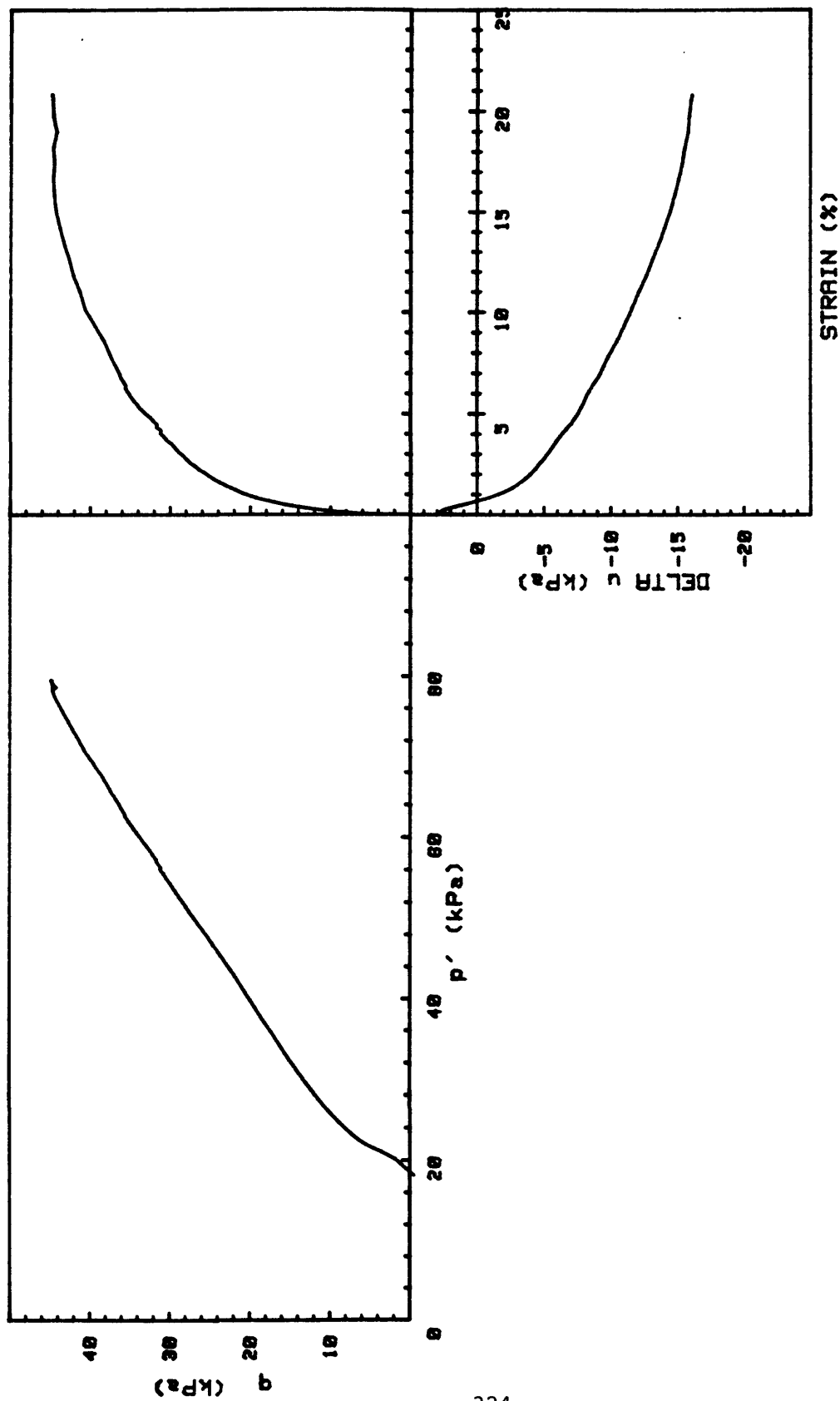


CRUISE DC1-81-EG	INCREMENT (cm)	105.5-113.7
CORE NO.	TEST NO.	TE69
SIG1c' (kPa)	10.4	
SIG3c' (kPa)	10.4	
INDUCED OCR	1.0	

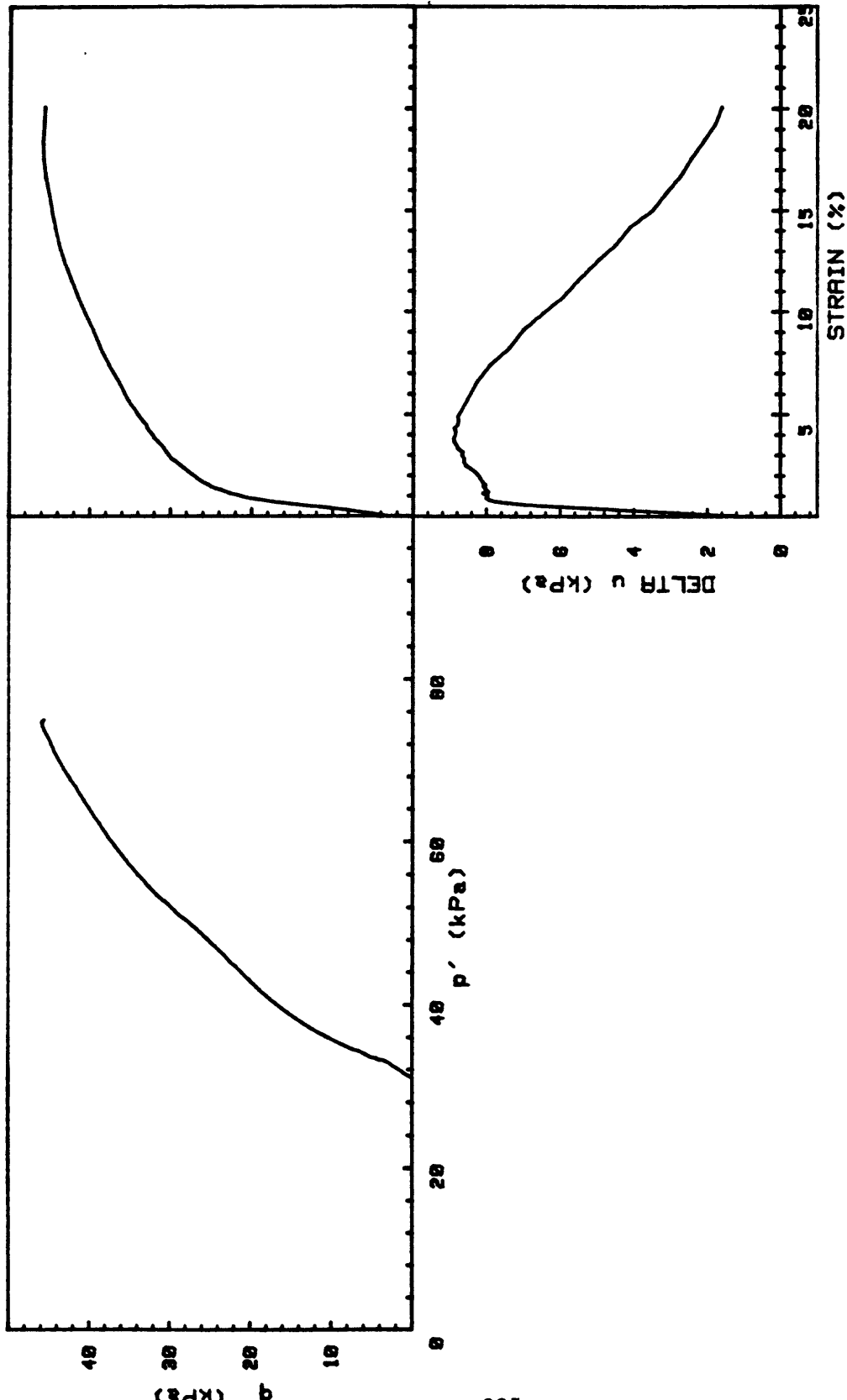




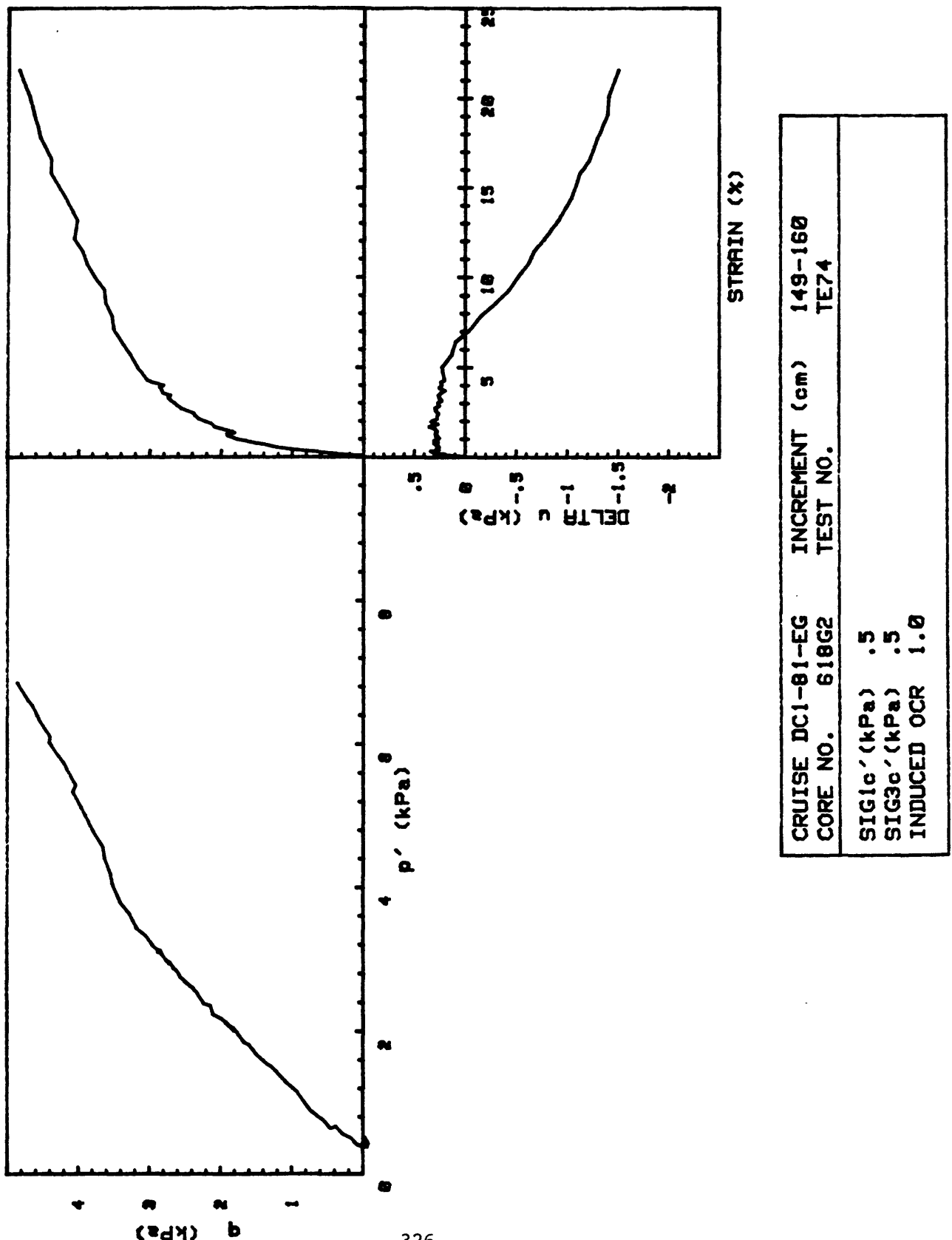
CRUISE NO.	DC1-81-EG	INCREMENT (cm)	82-93
SIG1e' (kPa)	100.1		
SIG3e' (kPa)	100.1		
INDUCED OCR	1.0	TEST NO.	TE71

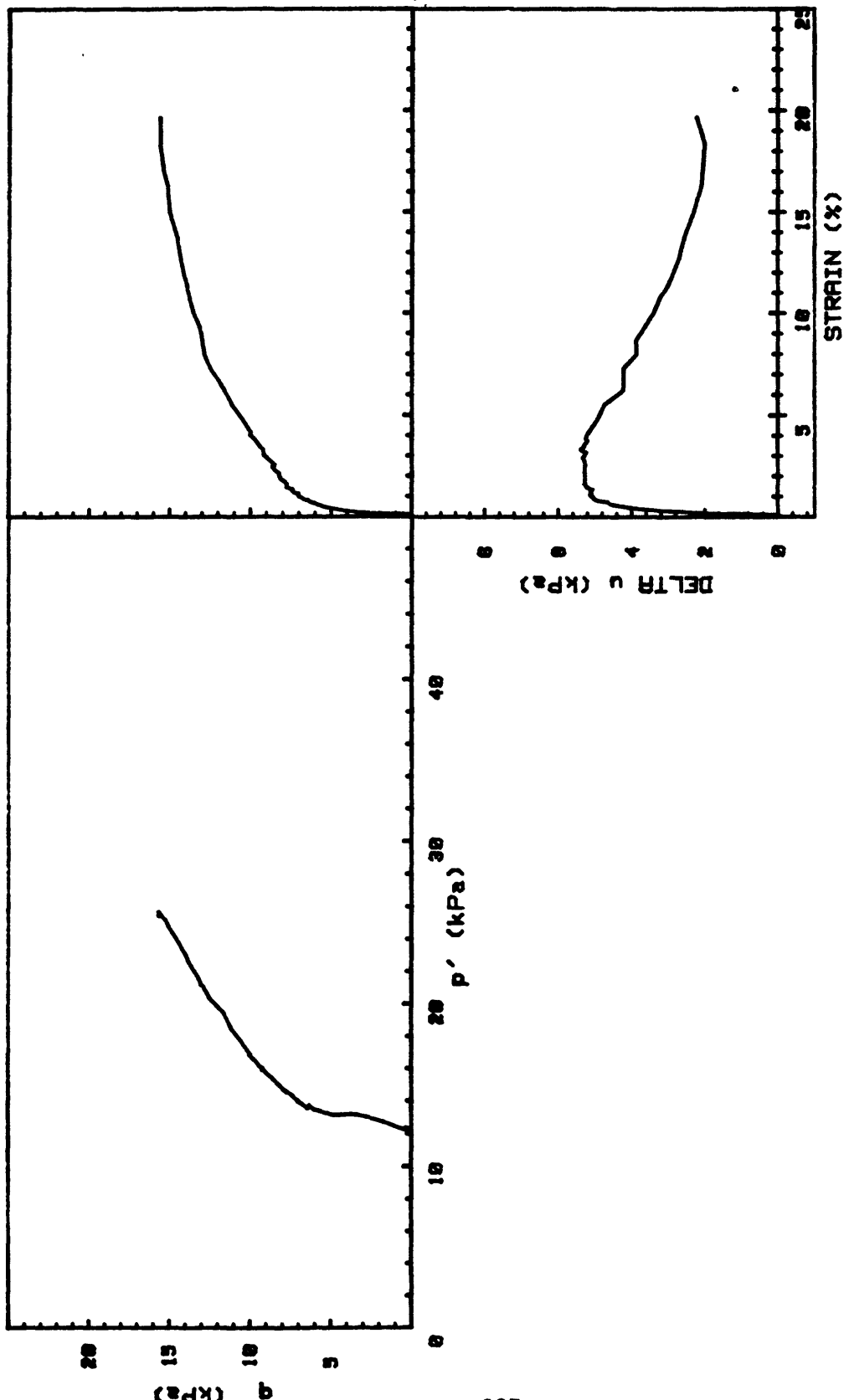


CRUISE DC1-81-EG	INCREMENT (cm)	71-82
CORE NO.	TEST NO.	TE72
SIG1c' (kPa)	10.6	
SIG3c' (kPa)	10.6	
INDUCED OCR	6.0	

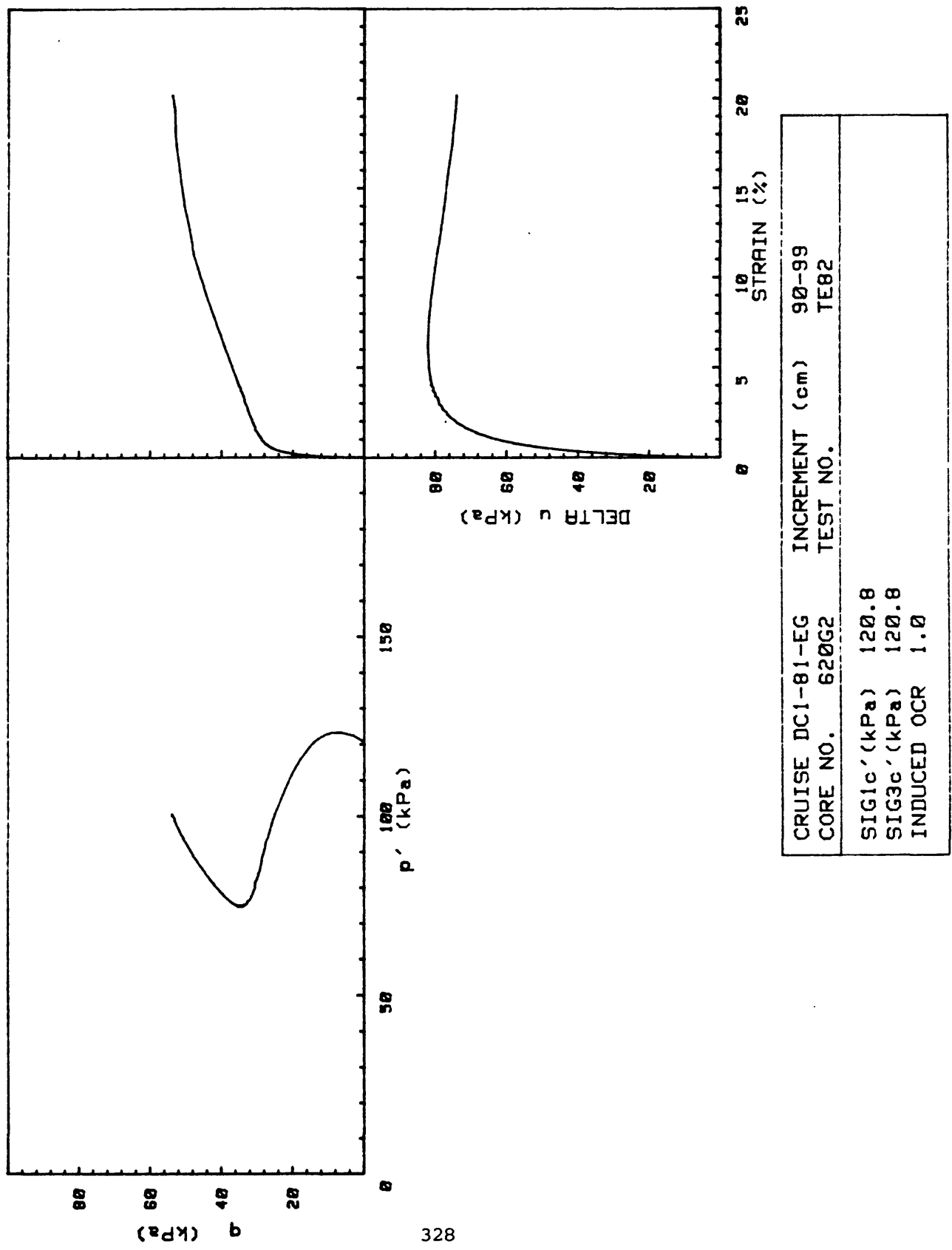


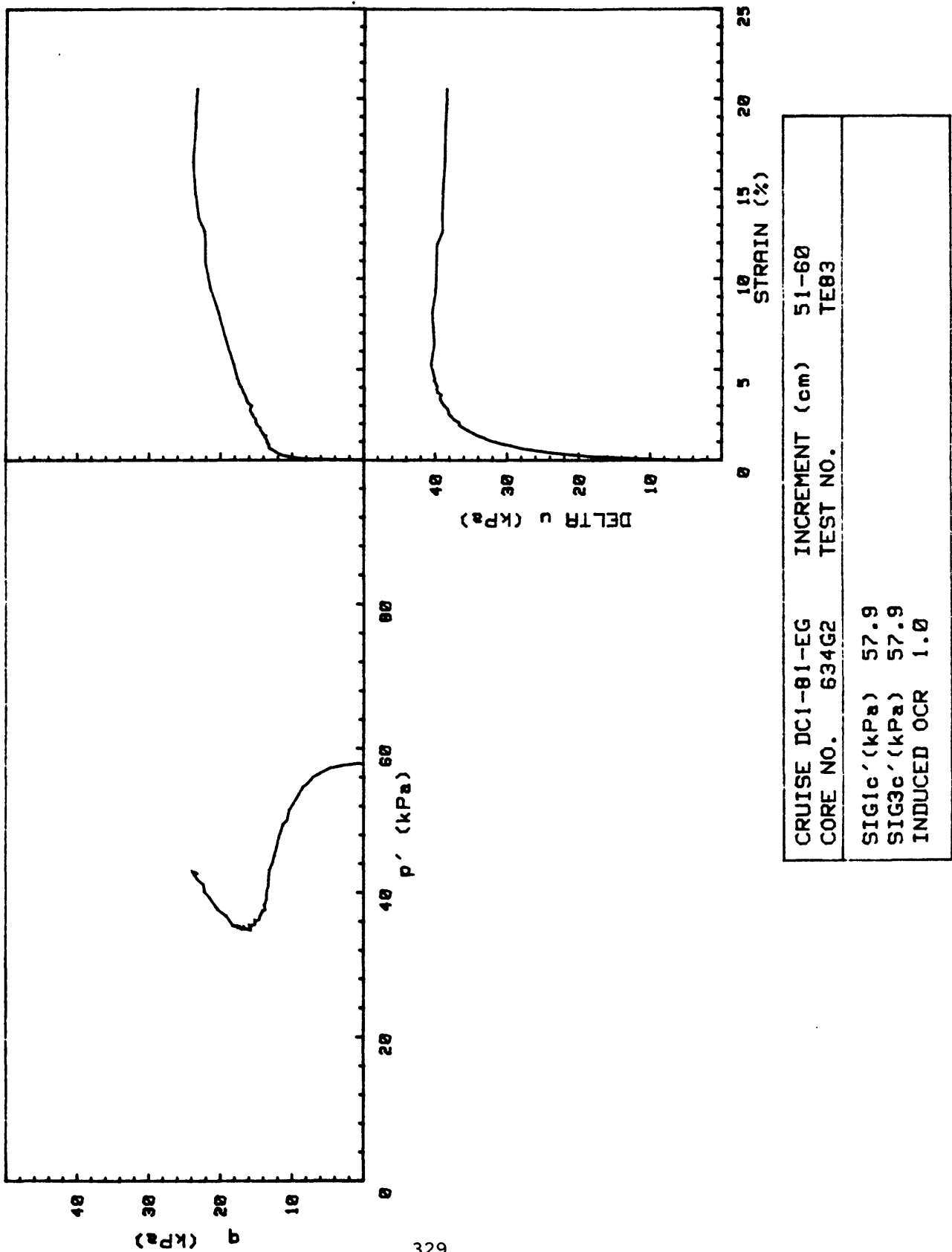
CRUISE DC1-81-EG	INCREMENT (cm)	71-82
CORE NO.	TEST NO.	TE73
SIG1c' (kPa)	31.0	
SIG3c' (kPa)	31.0	
INDUCED OCR	3.0	

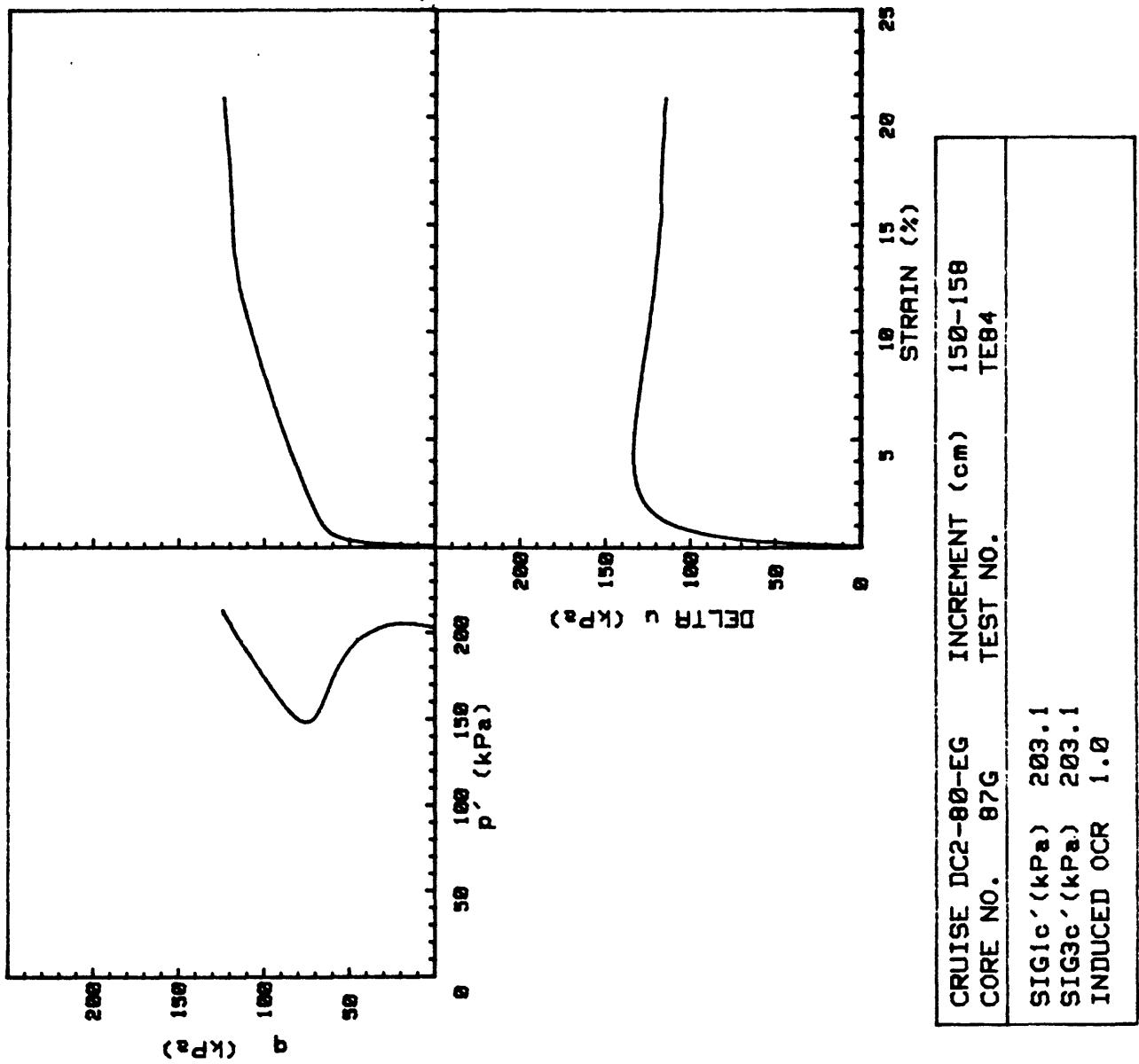


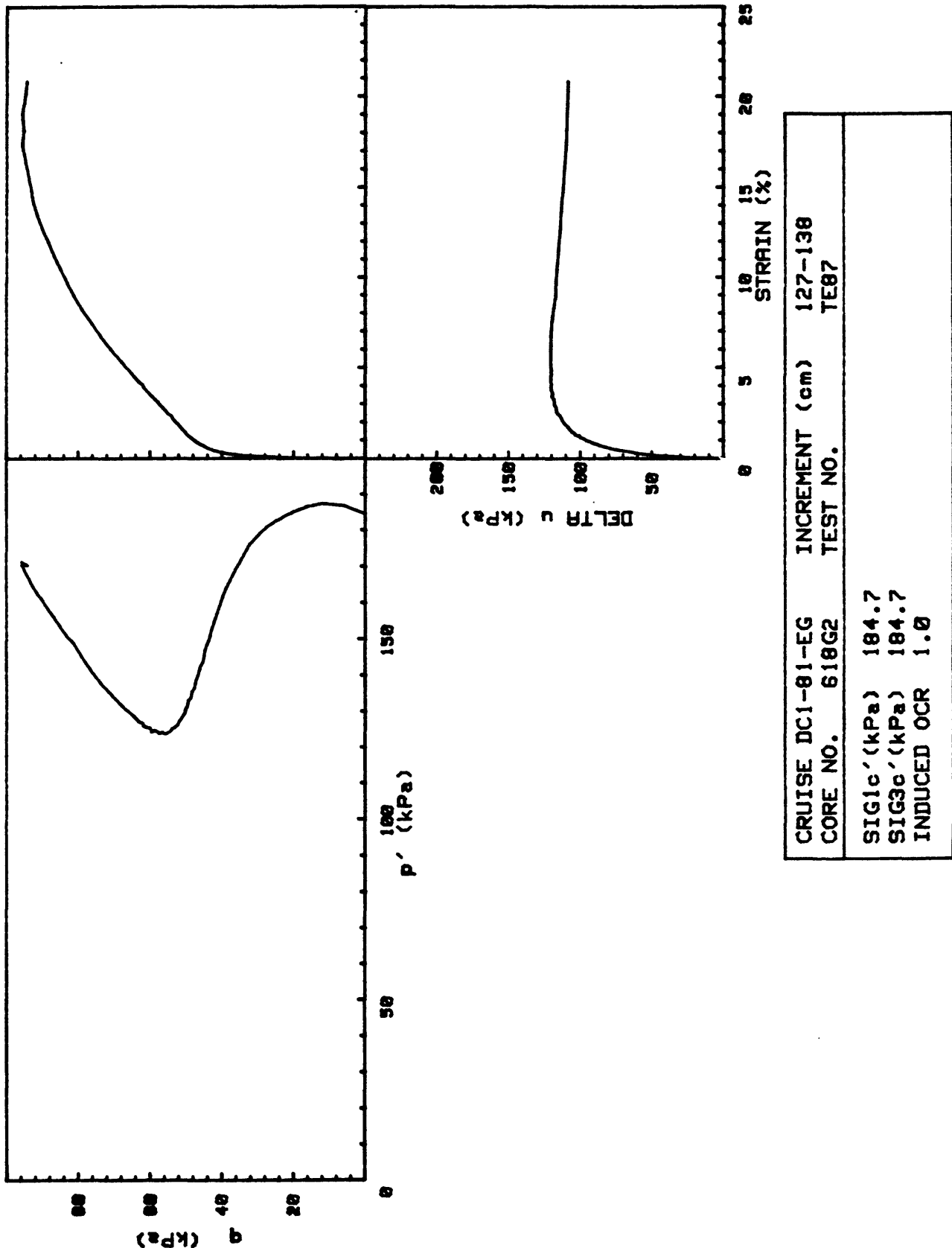


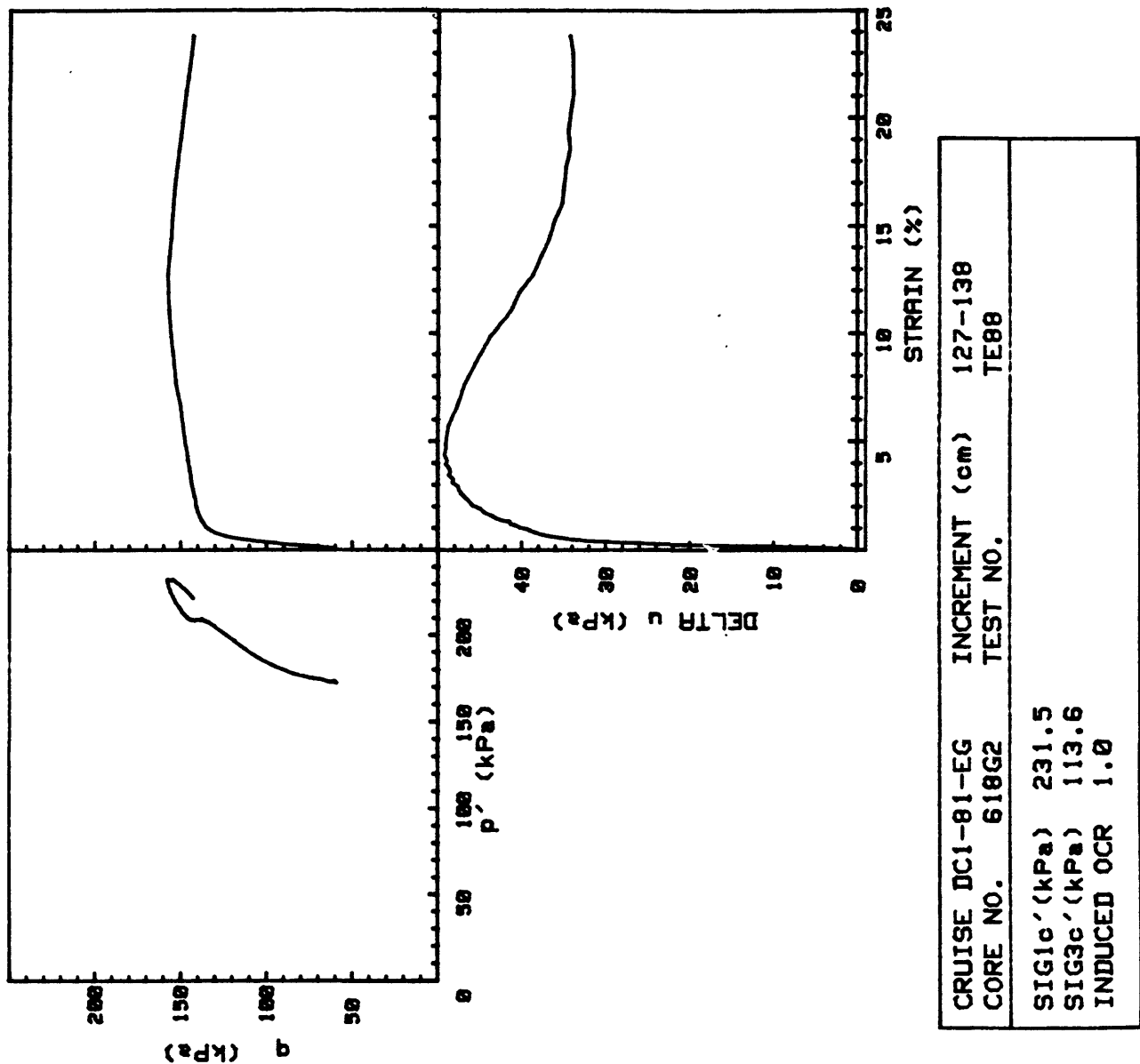
CRUISE DC1-81-EG	INCREMENT (cm)	149-160
CORE NO. 618G2	TEST NO.	TE75
SIG10' (kPa)	12.1	
SIG30' (kPa)	12.1	
INDUCED OCR	1.0	

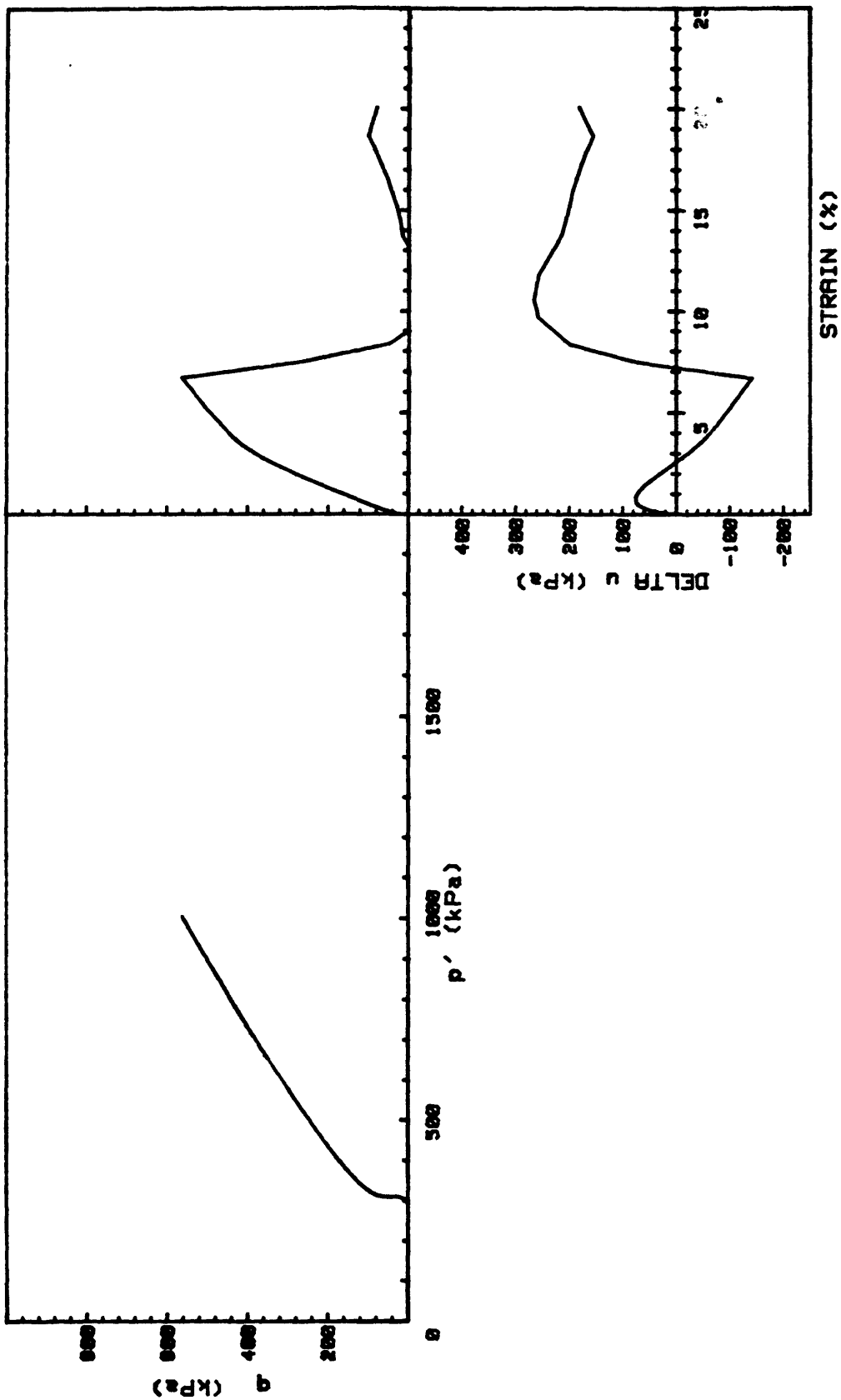




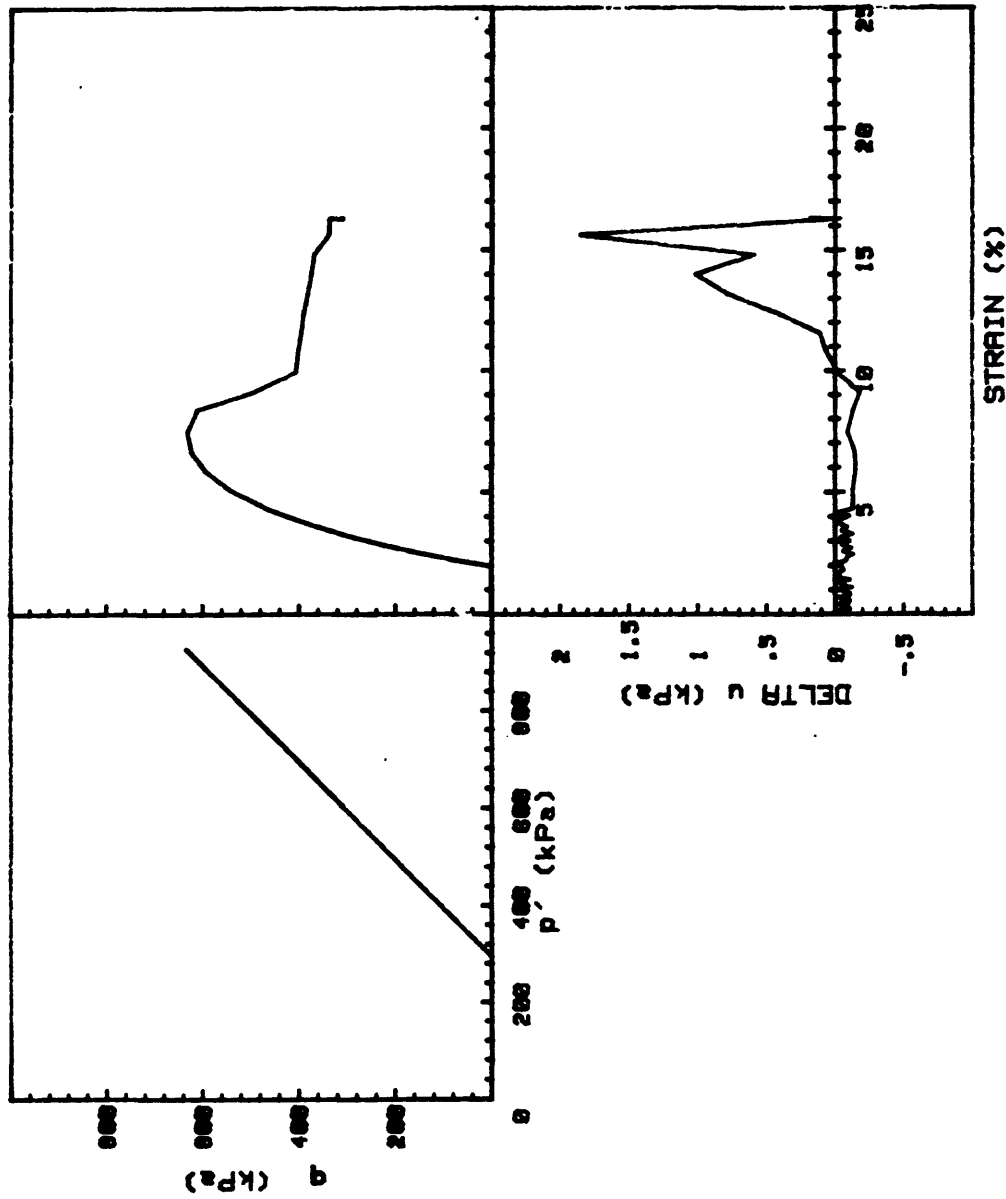




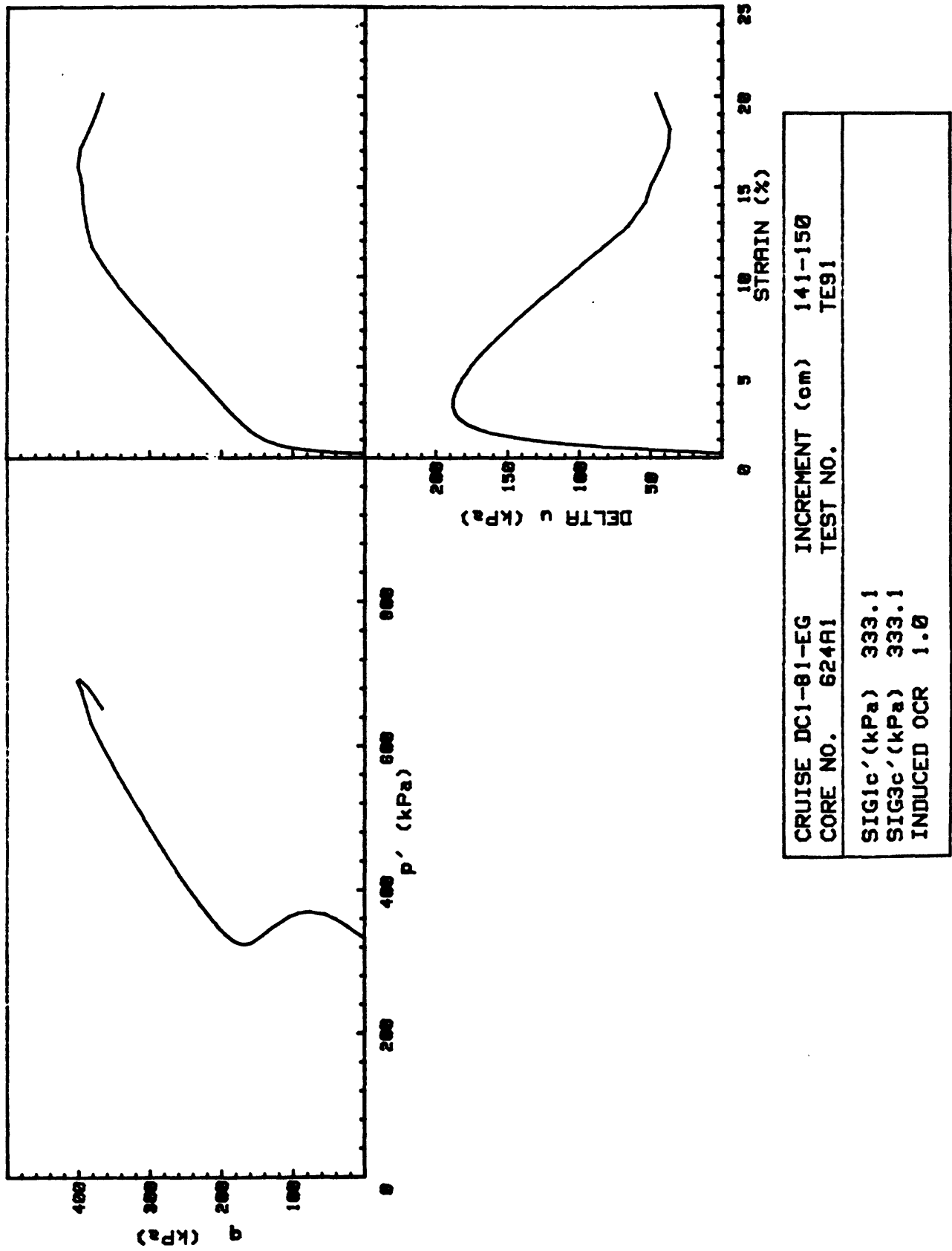


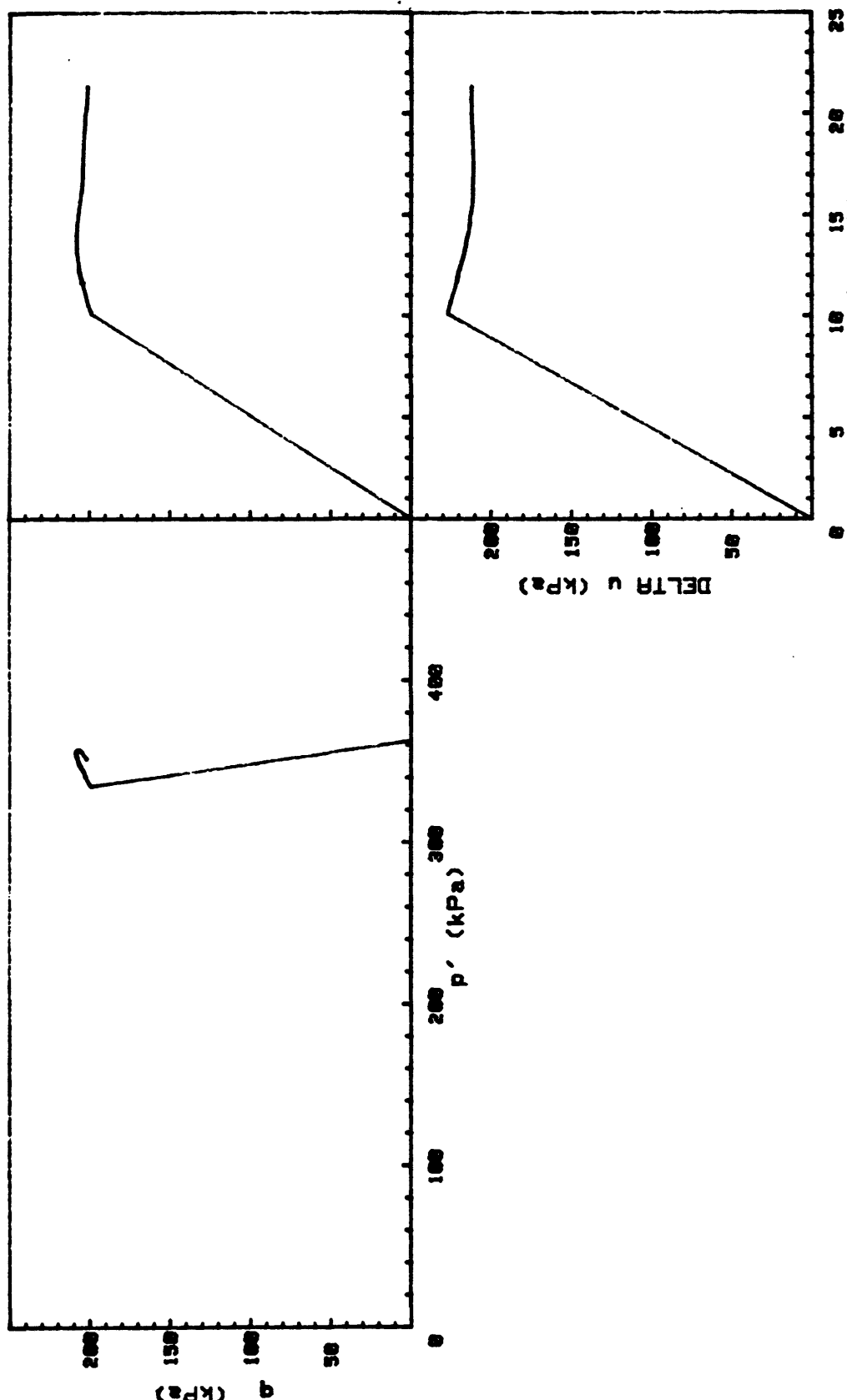


CRUISE	DC1-81-EG	INCREMENT	(cm)	220-230
CORE NO.	630A2	TEST NO.		TE89
SIG1c' (kPa)	299.9			
SIG3c' (kPa)	299.9			
INDUCED OCR	1.0			

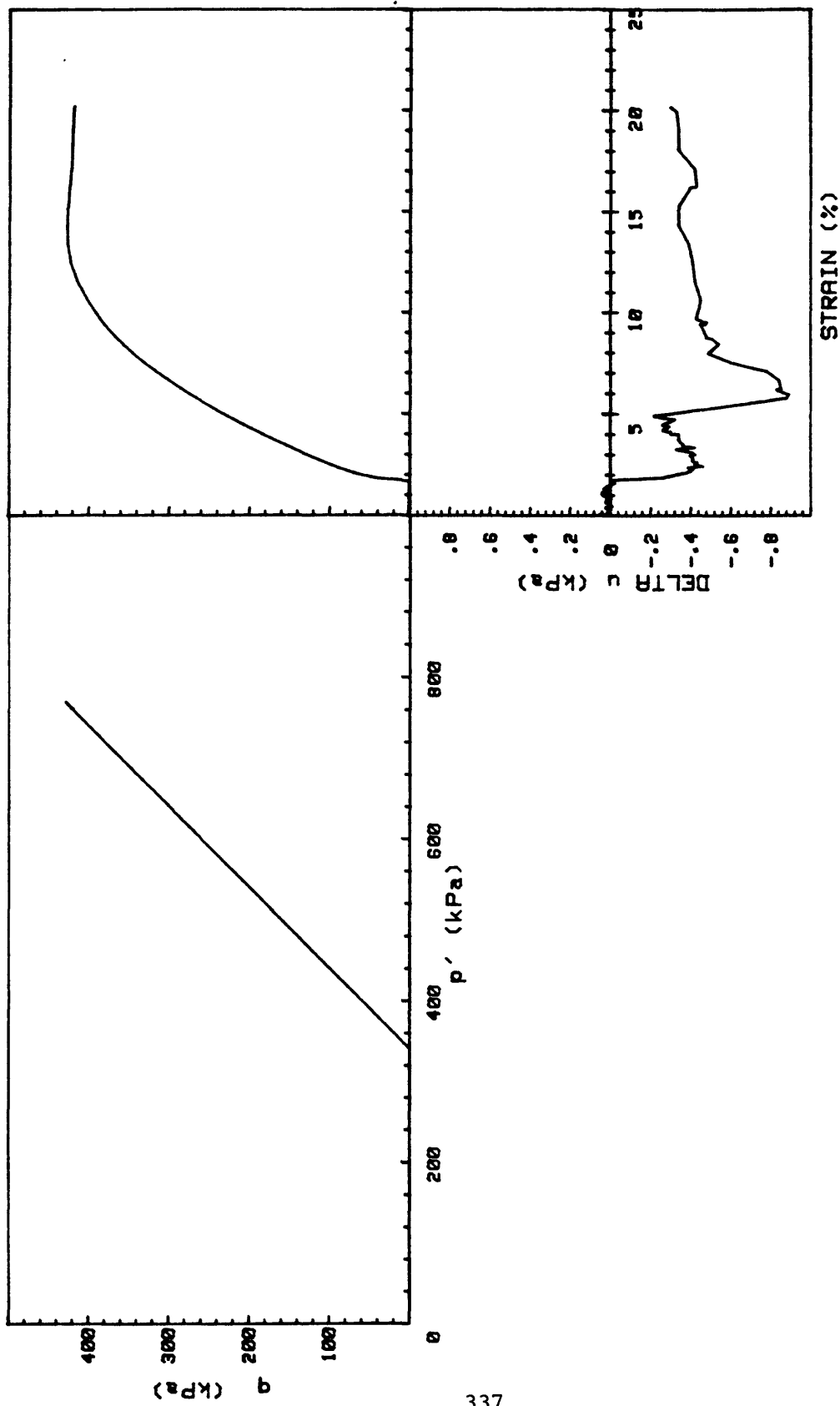


CRUISE DCI-81-EG	INCREMENT (cm)	220-229
CORE NO. 630R2	TEST NO.	TE90
SIG1 <sub>c</sub> ' (kPa)	295.5	
SIG3 <sub>c</sub> ' (kPa)	295.5	
INDUCED OCR	1.0	

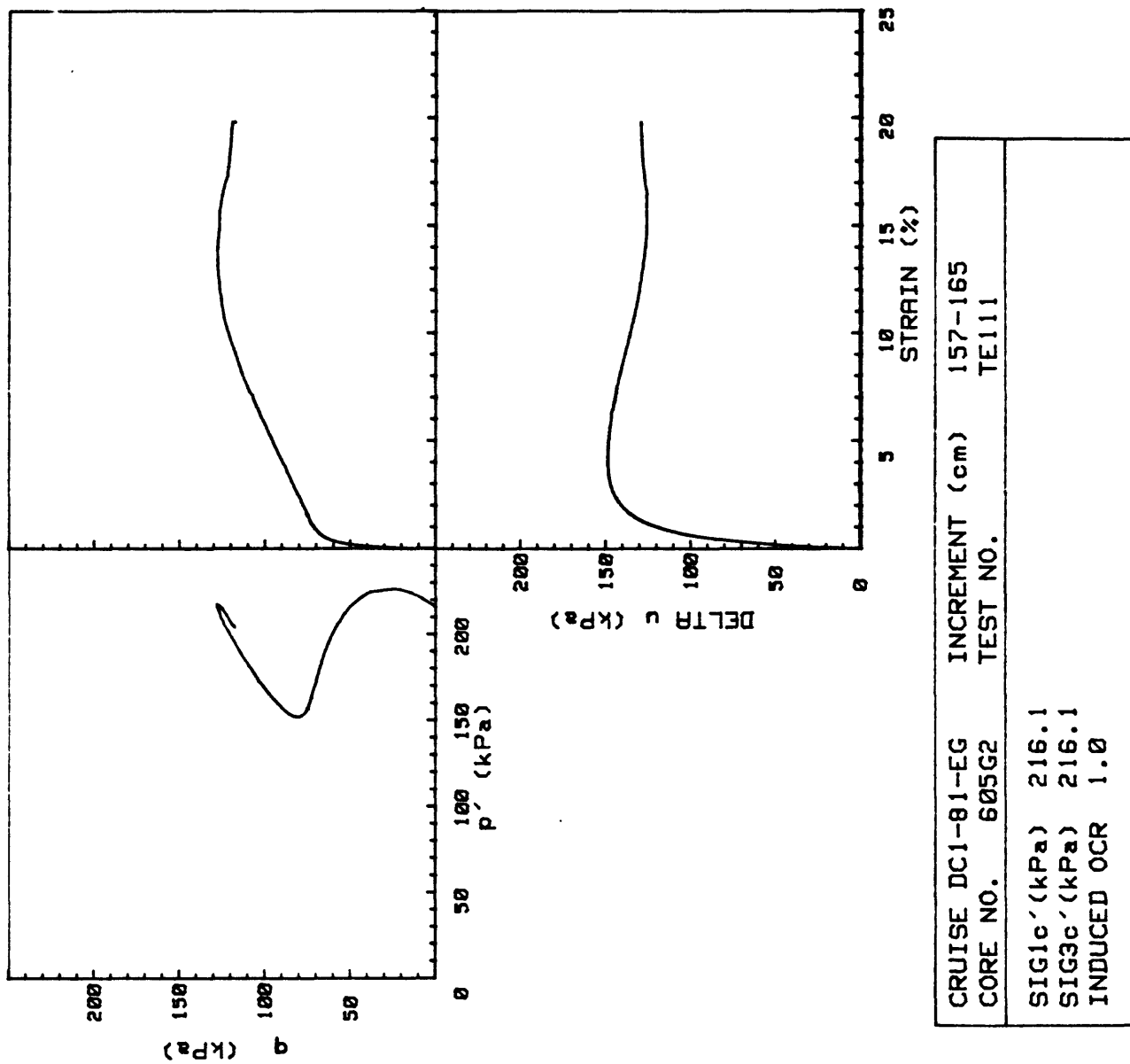


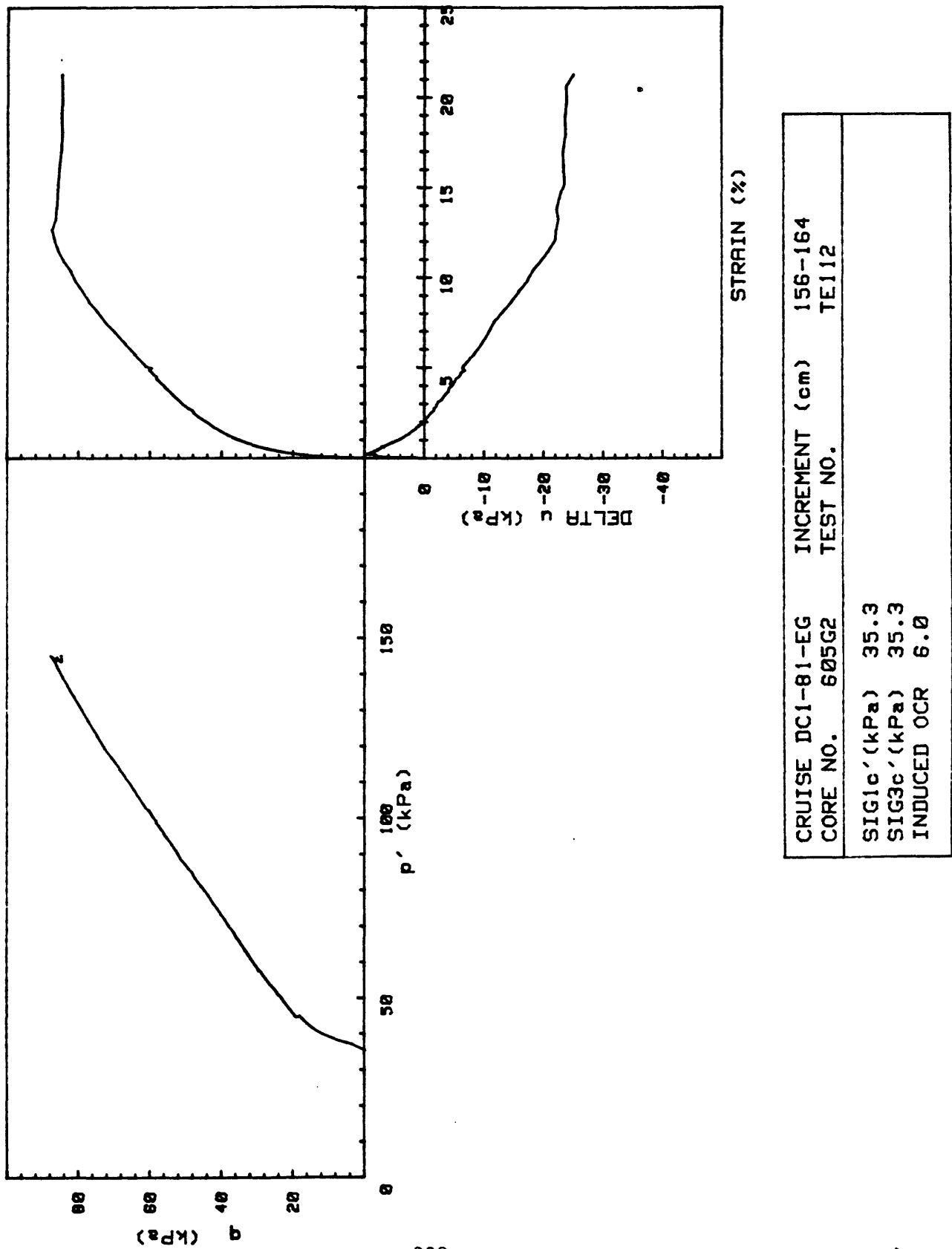


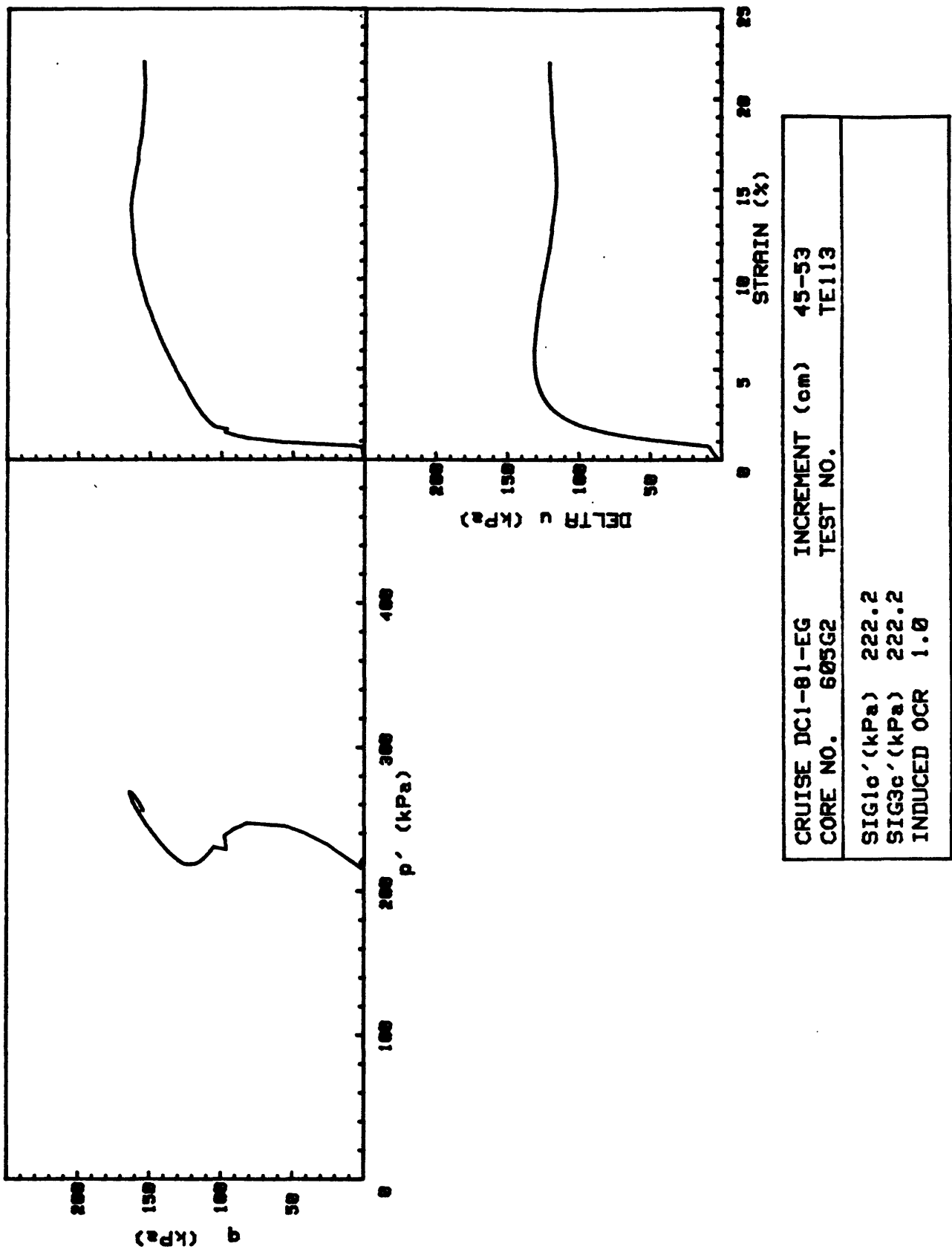
CRUISE DC1-81-EG	INCREMENT (cm)	80-89
CORE NO.	TEST NO.	TE92
SIG1e' (kPa)	362.8	
SIG3e' (kPa)	362.8	
INDUCED OCR	1.0	

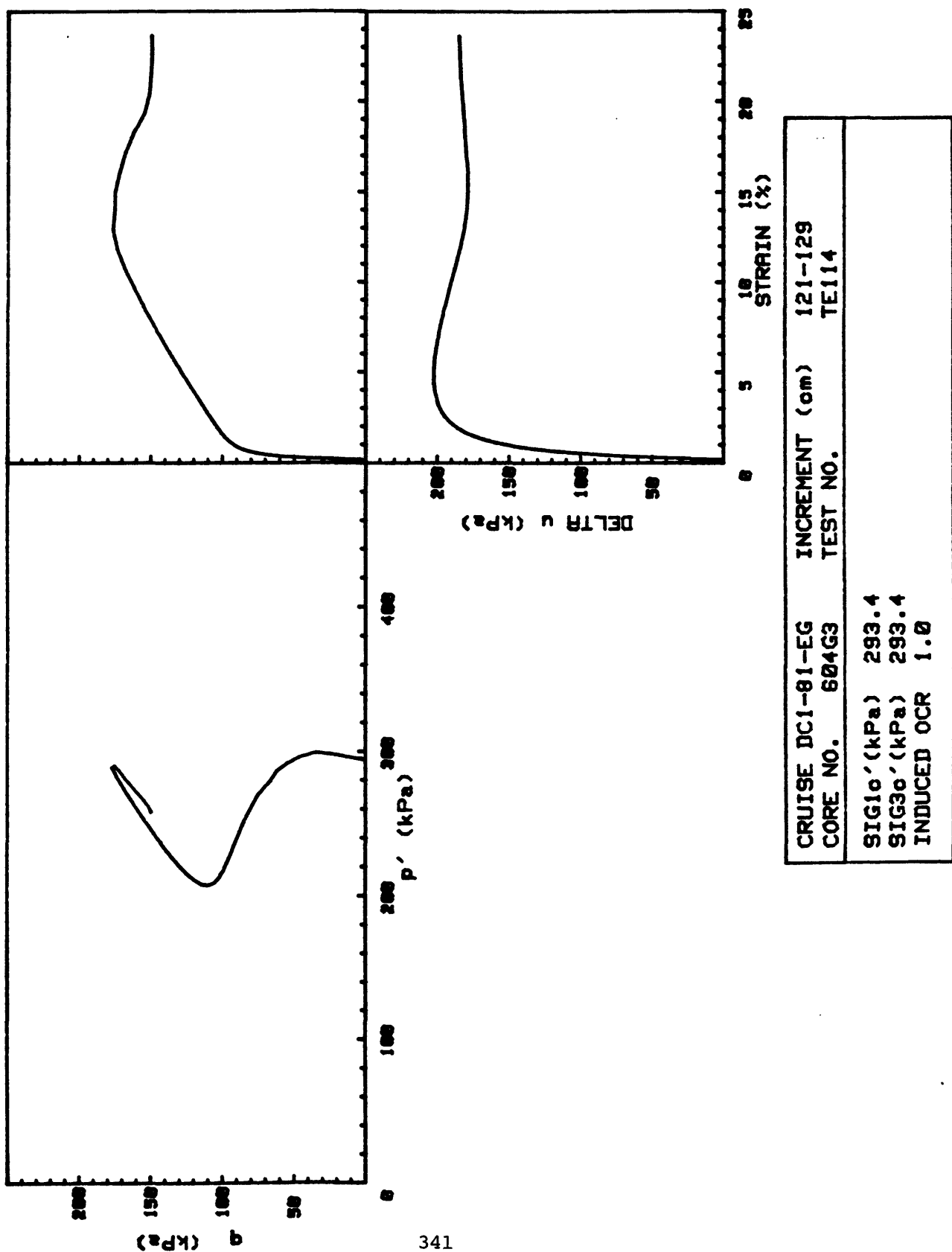


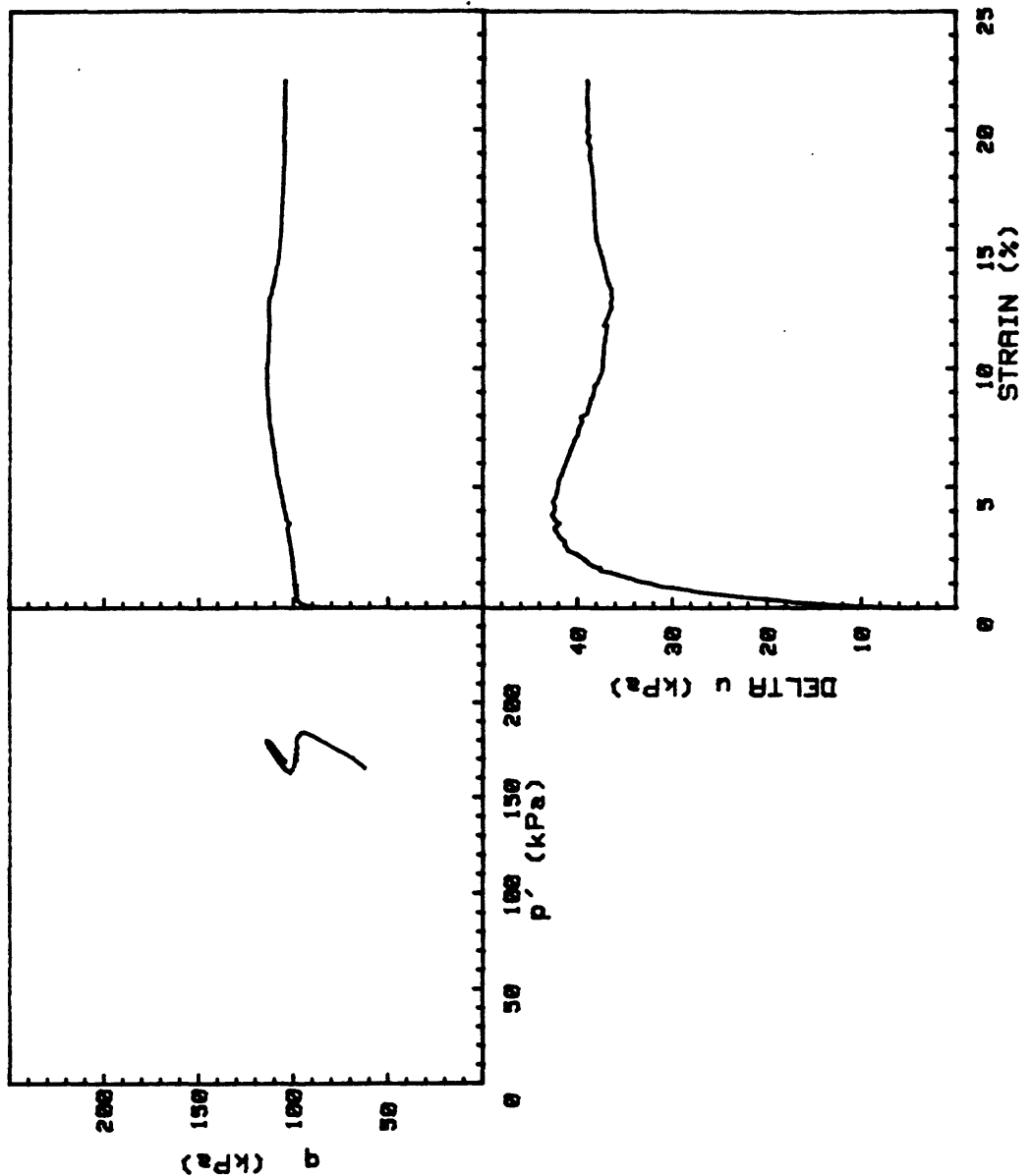
CRUISE NO.	DC1-81-EG	INCREMENT (cm)	162-168
624R1		TEST NO.	TE93
SIG1c' (kPa)	341.5		
SIG3c' (kPa)	341.5		
INDUCED OCR	1.0		



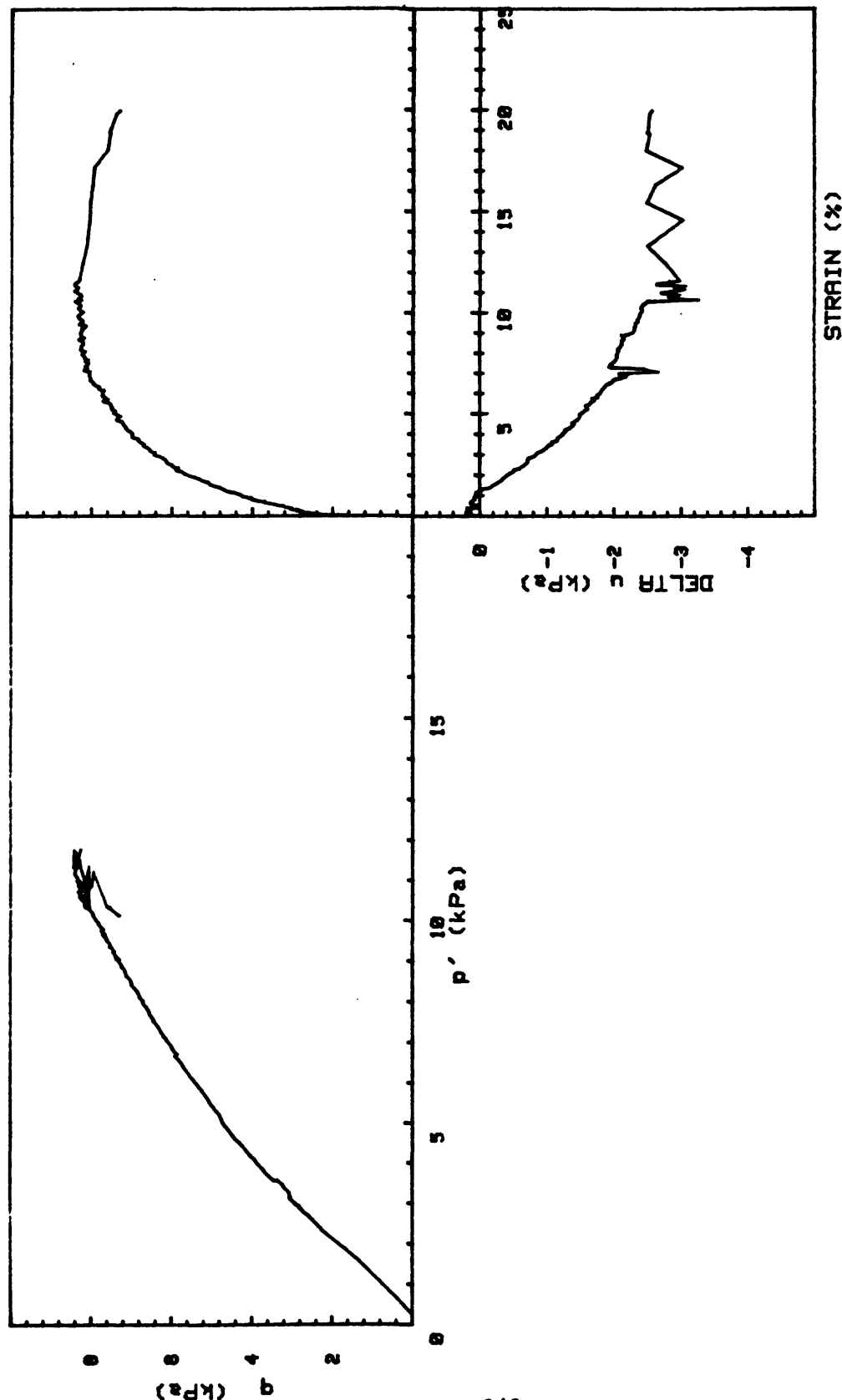




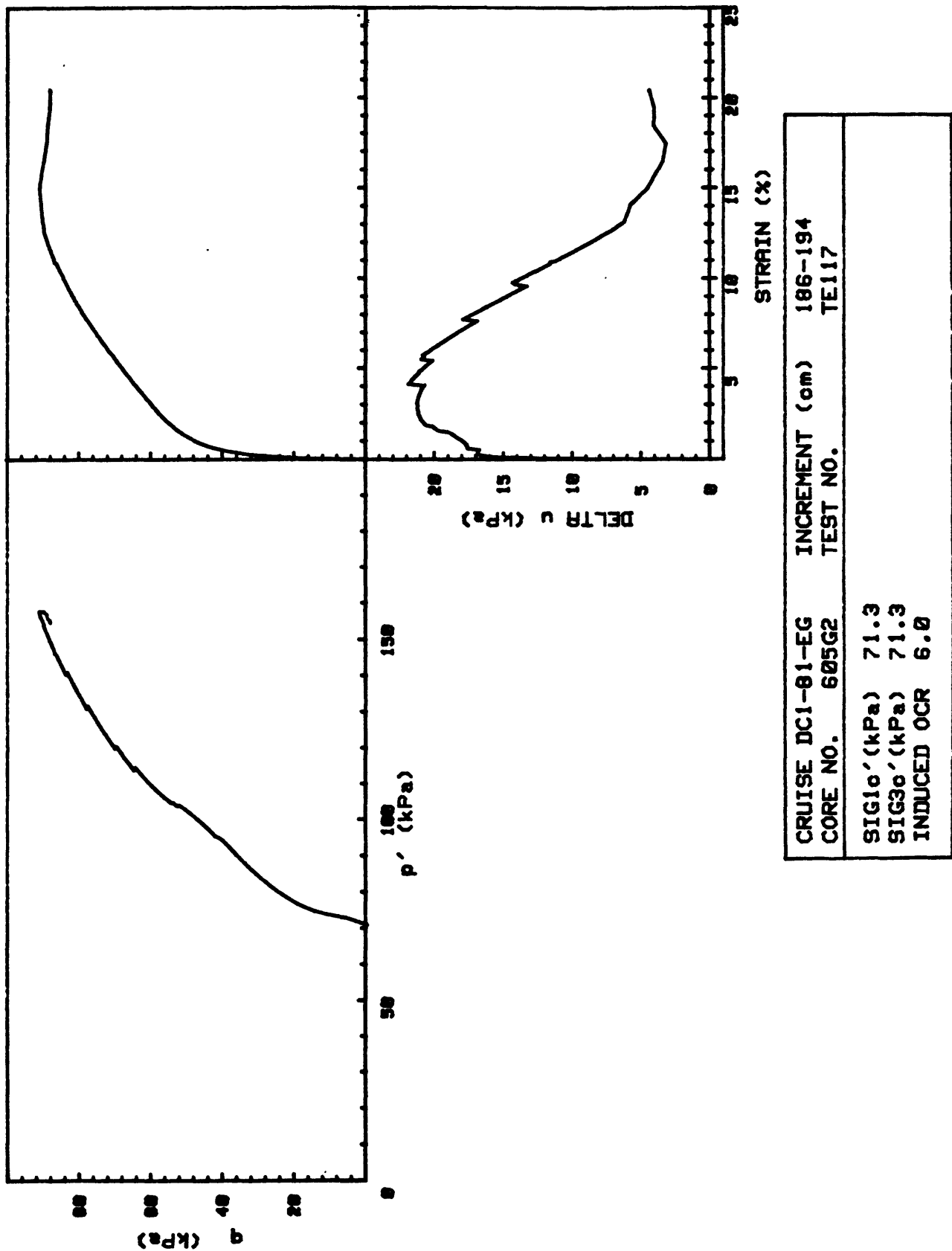


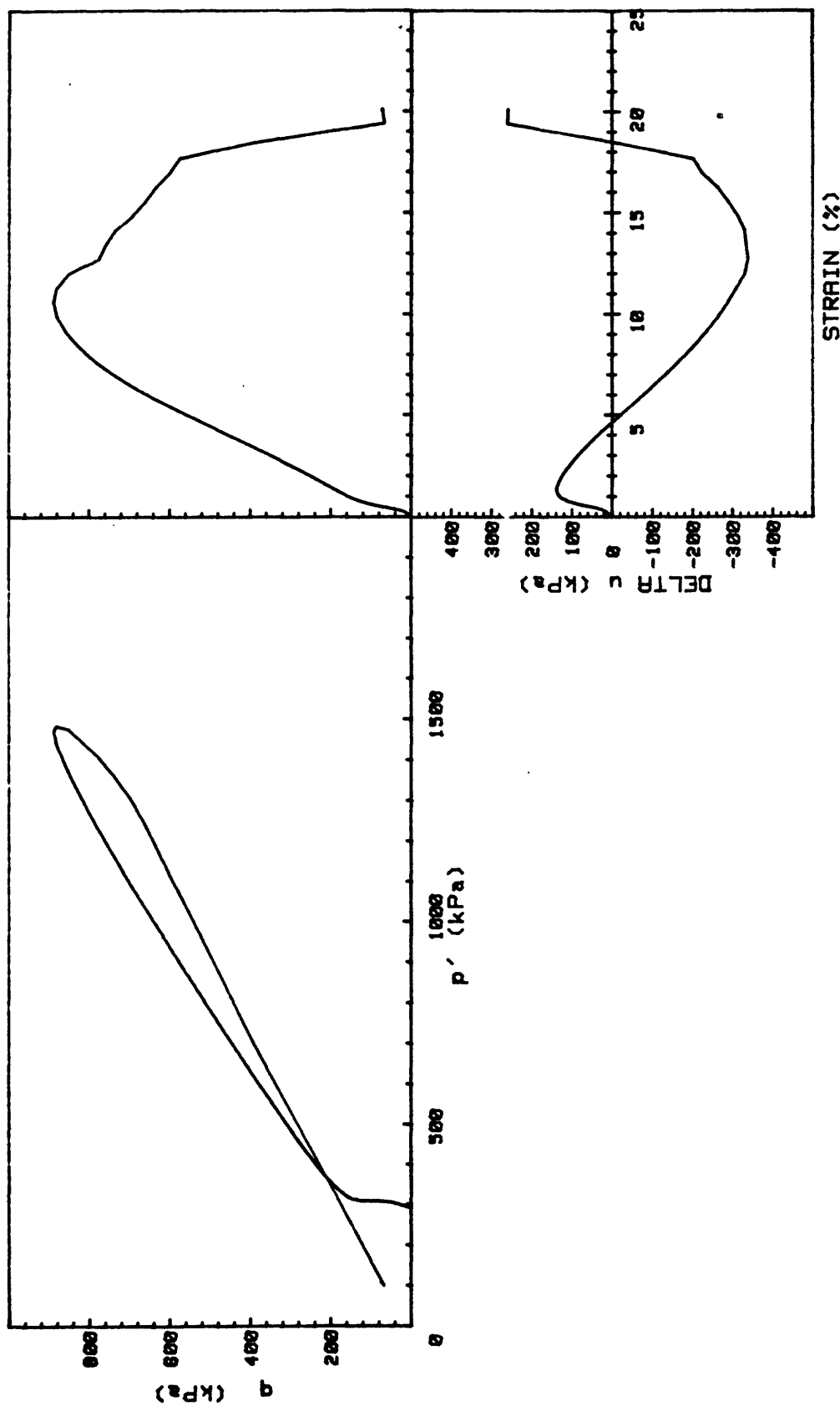


CRUISE DC1-81-EG	INCREMENT (cm)	176-184
CORE NO.	TEST NO.	TE115
SIG1c' (kPa)	227.9	
SIG3c' (kPa)	102.9	
INDUCED OCR	1.0	

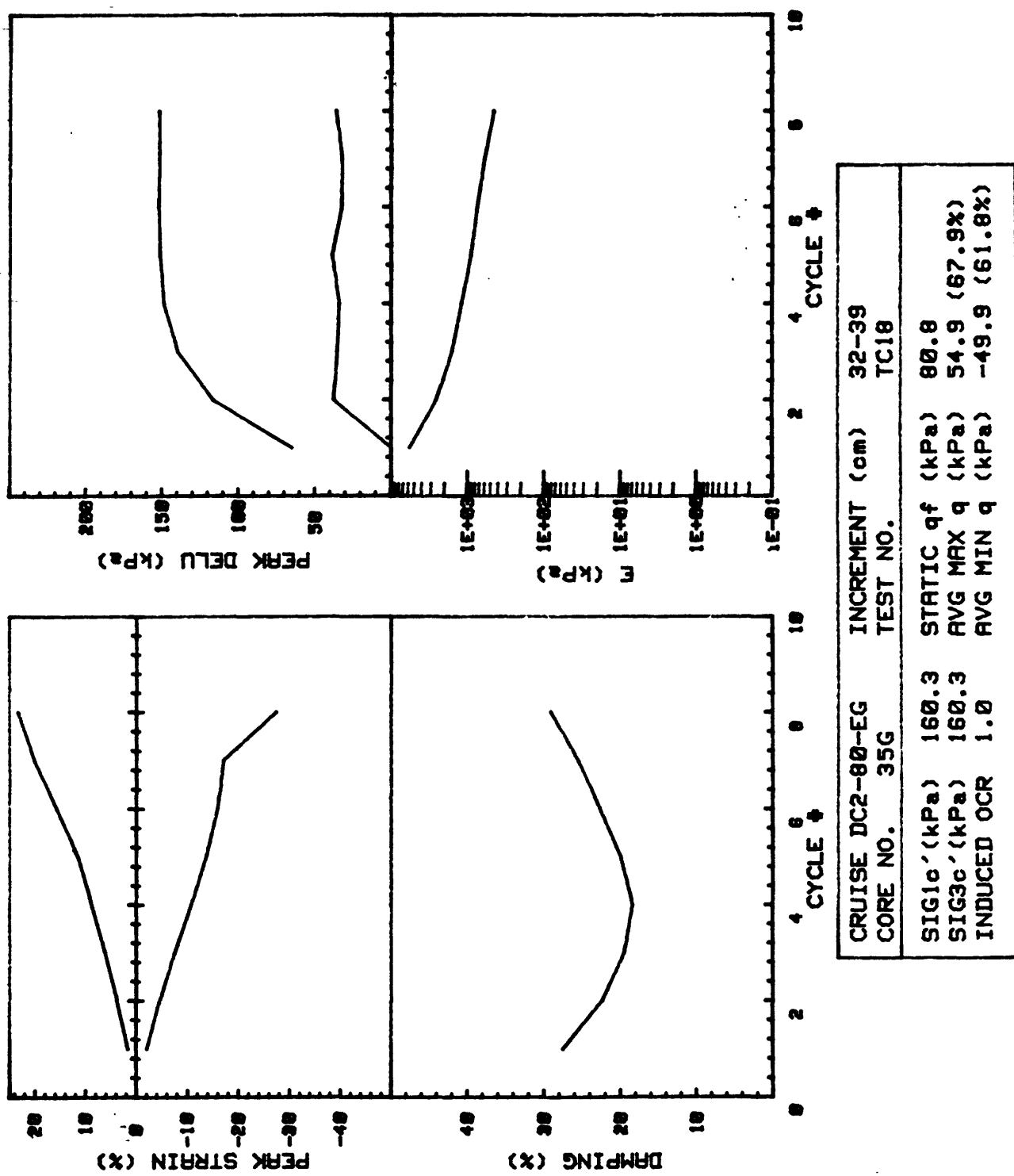


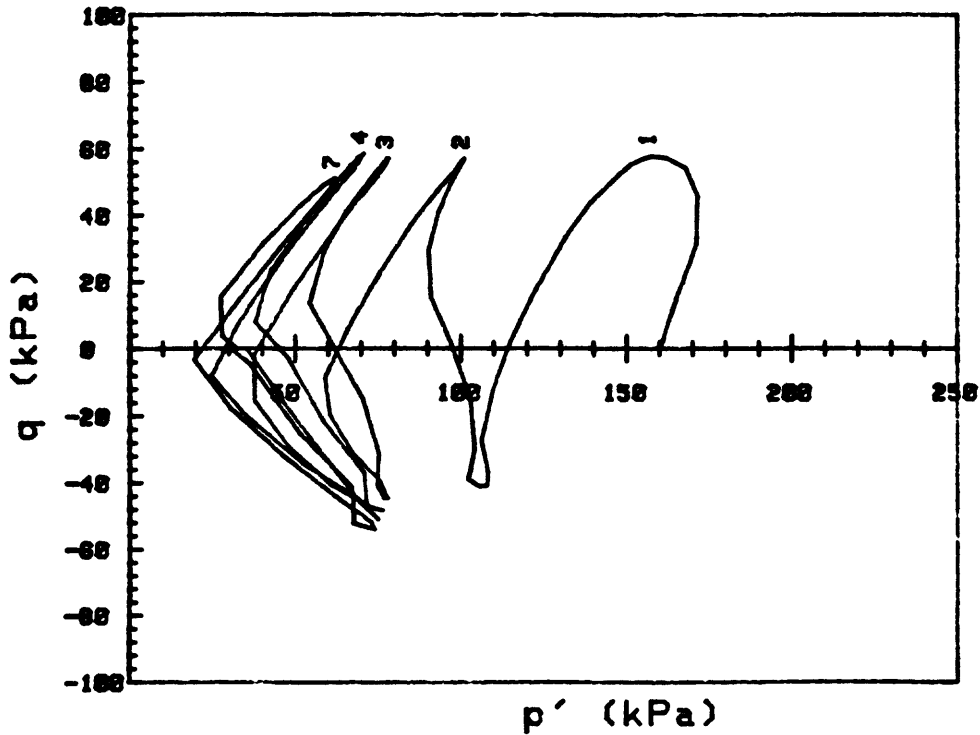
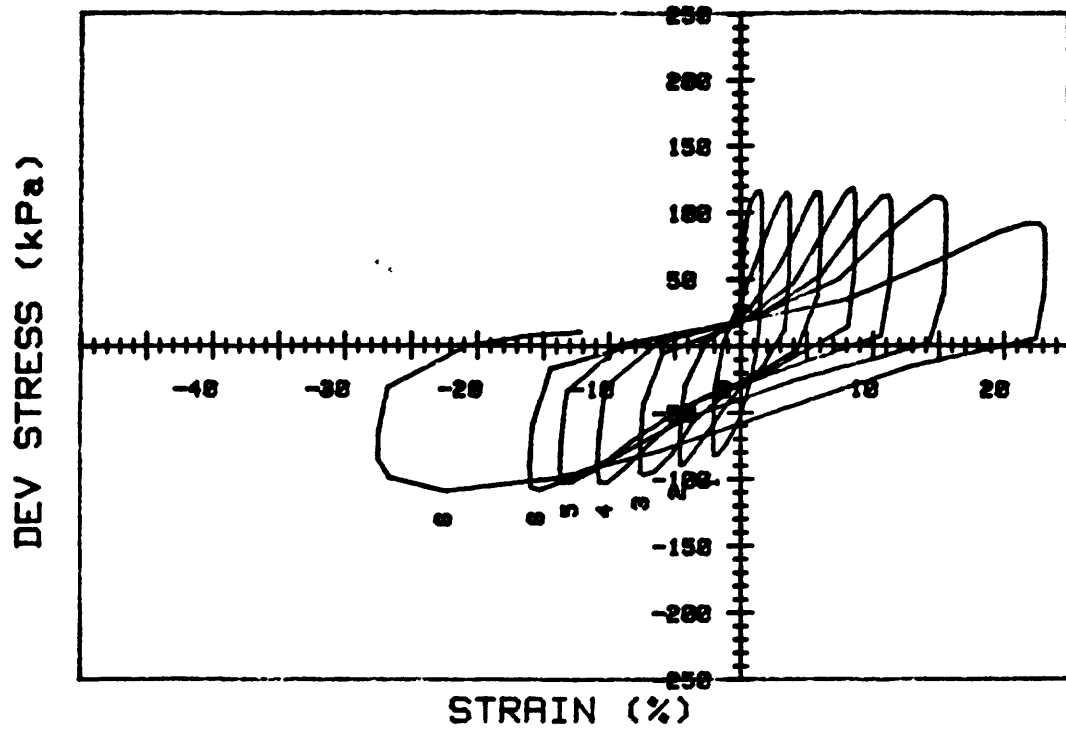
CRUISE DC1-81-EG	INCREMENT (cm)	141-149
CORE NO.	TEST NO.	TE116
SIG1c' (kPa)	.3	
SIG3c' (kPa)	.3	
INDUCED OCR	1.0	



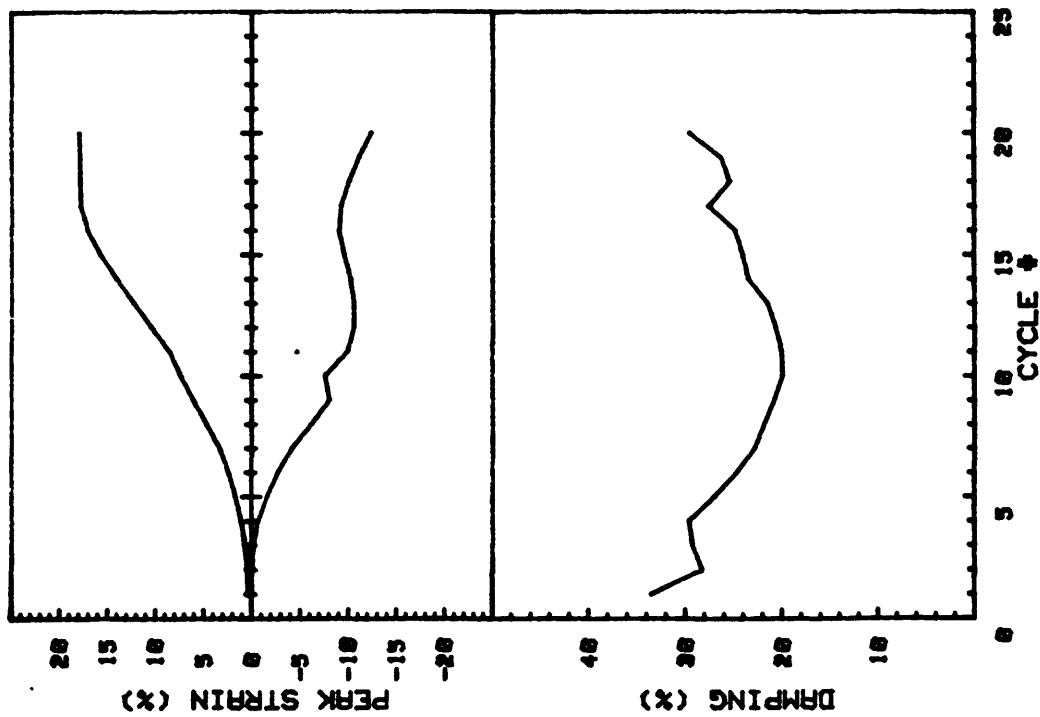
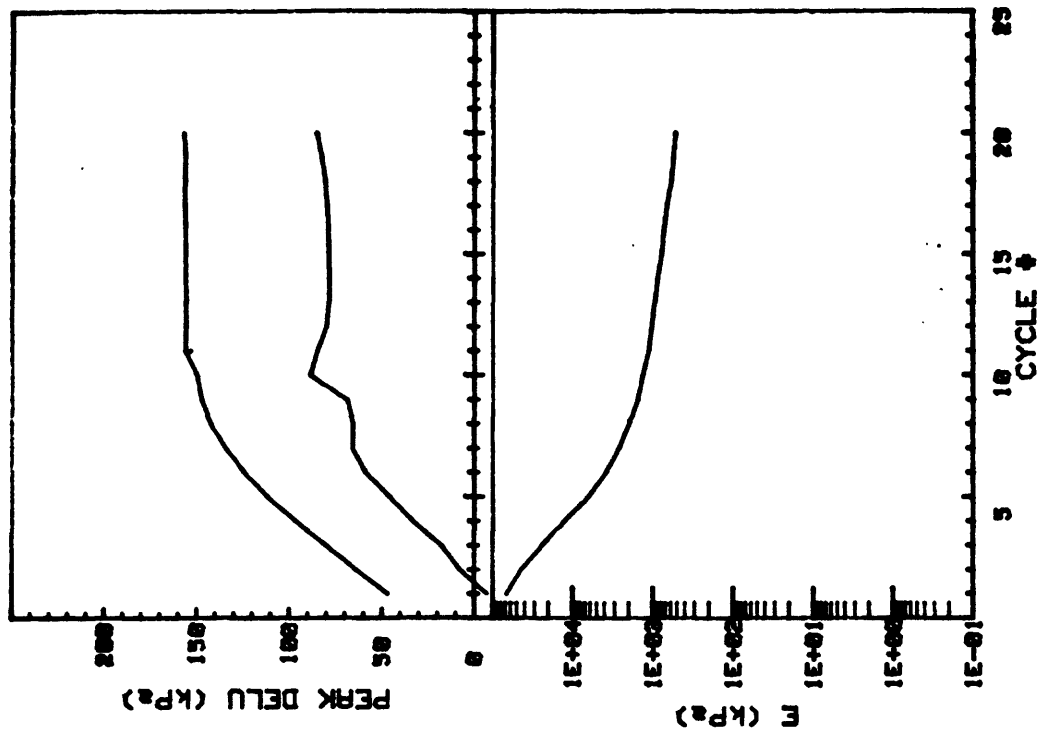


CRUISE DC1-81-EG	INCREMENT (cm)	170-180
CORE NO.	TEST NO.	TE118
SIG1c' (kPa)	293.3	
SIG3c' (kPa)	293.3	
INDUCED OCR	1.0	

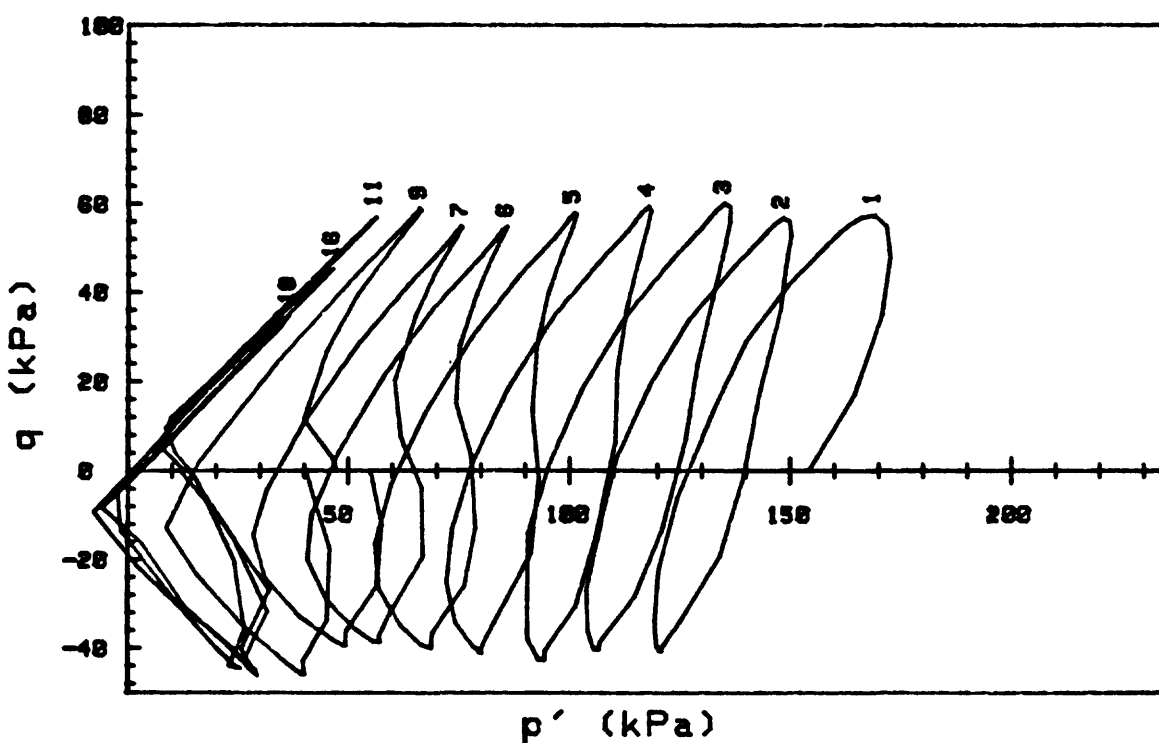
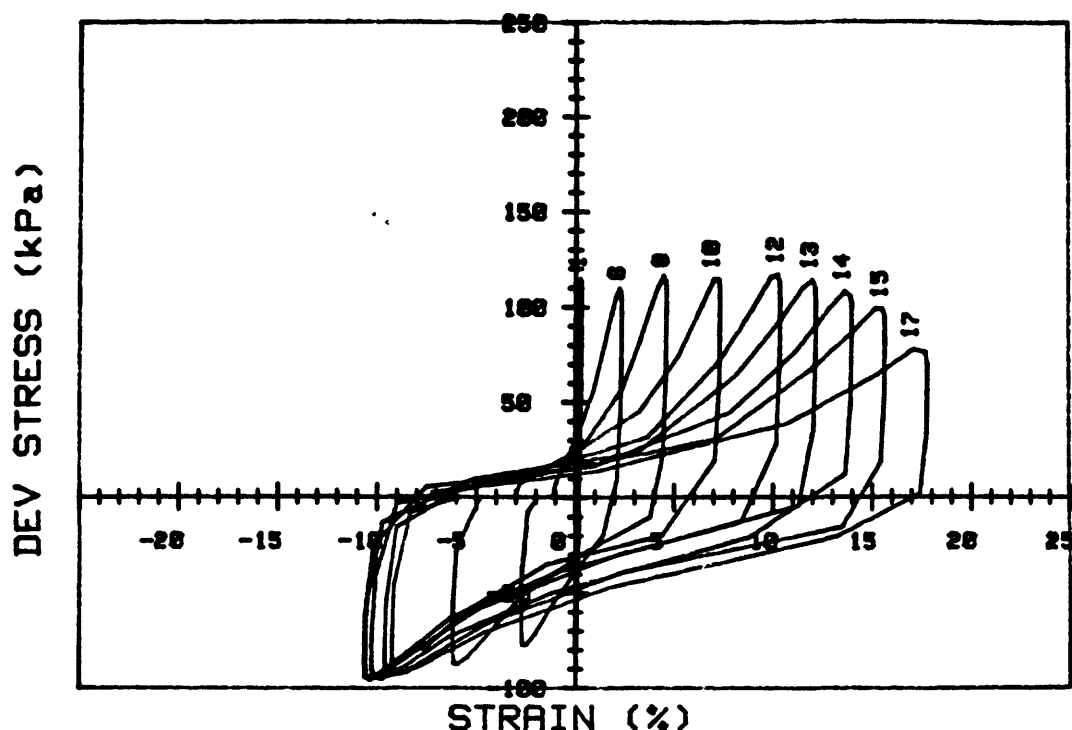




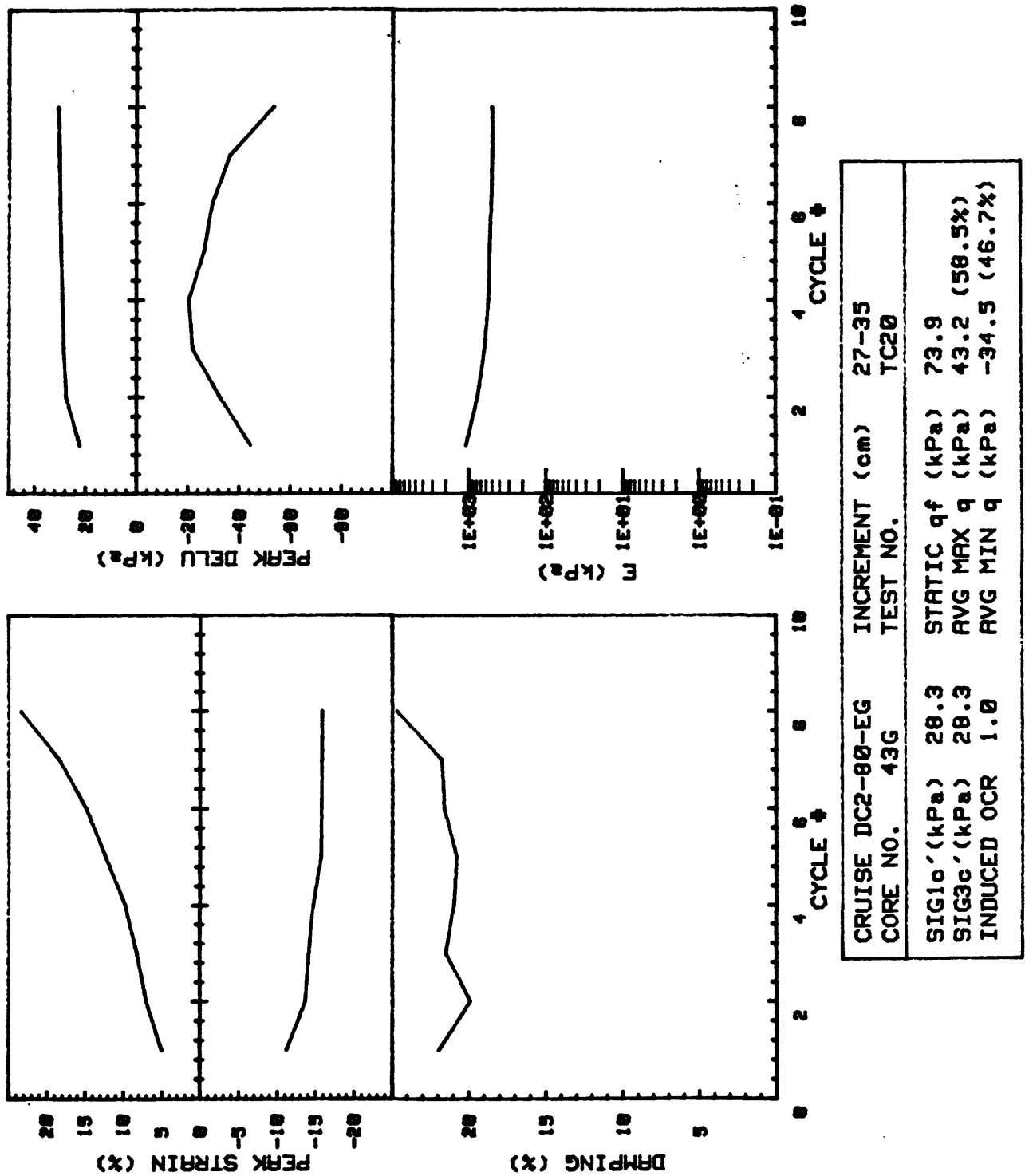
CRUISE DC2-80-EG CORE NO. 35G	INCREMENT (cm) TEST NO.	32-39 TC18	
SIG1 $\sigma'$ (kPa)	160.3	STATIC q <sub>f</sub> (kPa)	80.8
SIG3 $\sigma'$ (kPa)	160.3	Avg MAX q (kPa)	54.9 (67.9%)
INDUCED OCR	1.0	Avg MIN q (kPa)	-49.9 (61.8%)

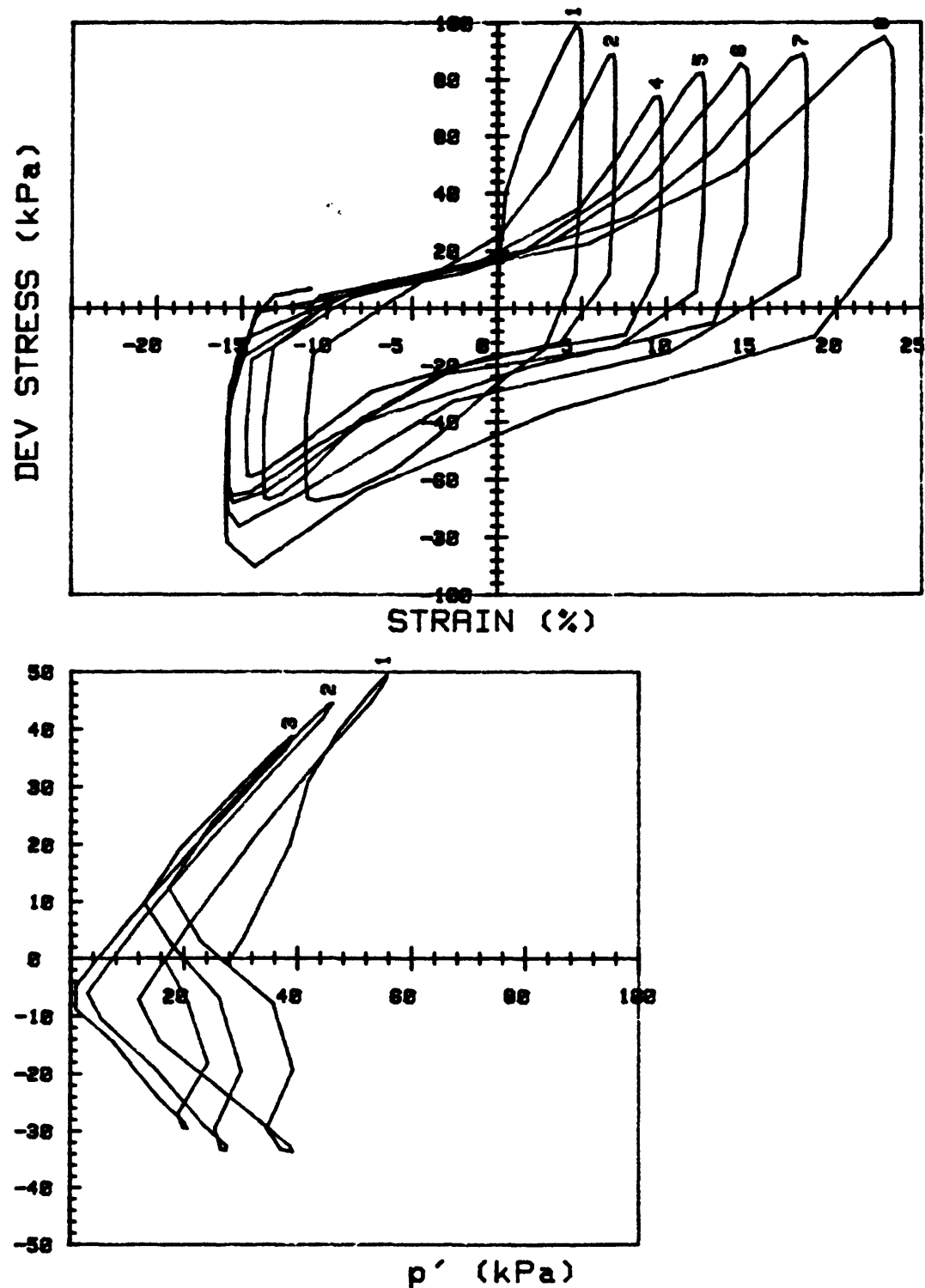


CRUISE DC2-80-EG		INCREMENT (cm)	32-39
CORE NO.	35G	TEST NO.	TC19
SIG1' (kPa)	154.6	STATIC q <sub>f</sub> (kPa)	80.8
SIG3' (kPa)	154.6	Avg MAX q (kPa)	51.6 (63.9%)
INDUCED OCR	1.0	Avg MIN q (kPa)	-43.5 (53.8%)

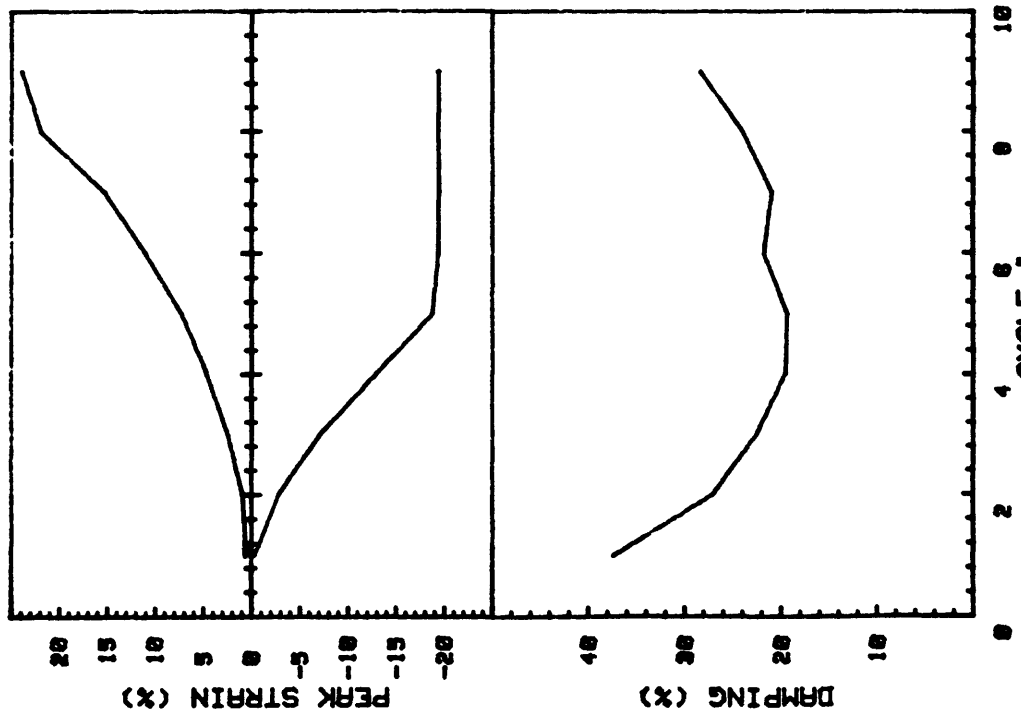
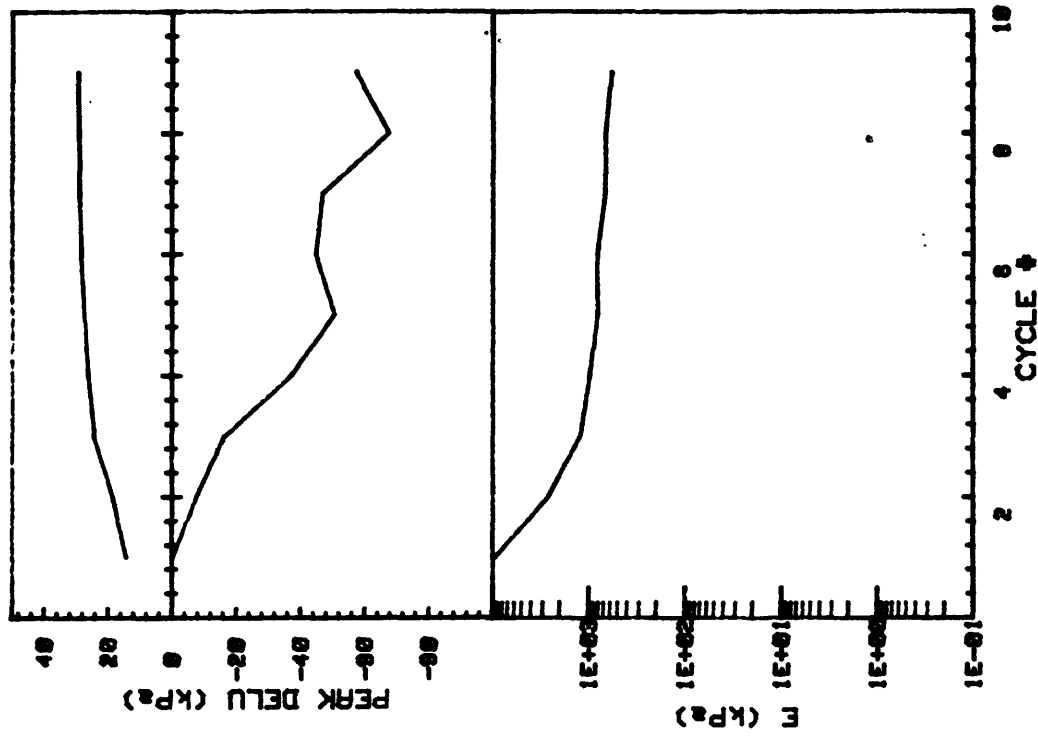


CRUISE DC2-80-EG CORE NO. 35G	INCREMENT (cm) TEST NO.	32-39 TC19
SIG1c' (kPa)	154.6	STATIC qf (kPa) 80.8
SIG3c' (kPa)	154.6	AVG MAX q (kPa) 51.6 (63.9%)
INDUCED OCR	1.0	AVG MIN q (kPa) -43.5 (53.8%)

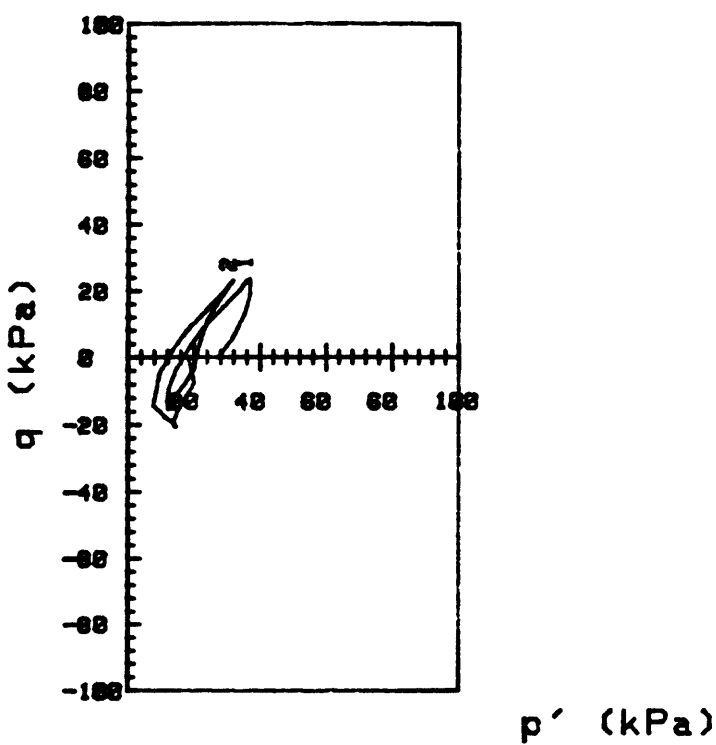
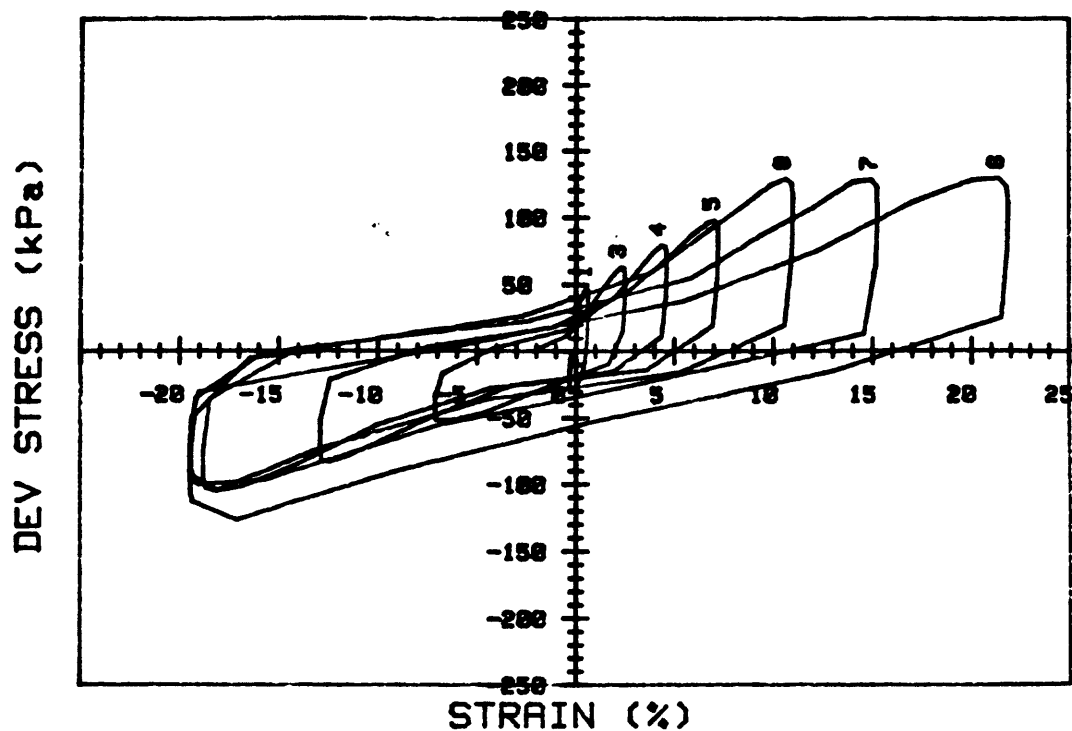




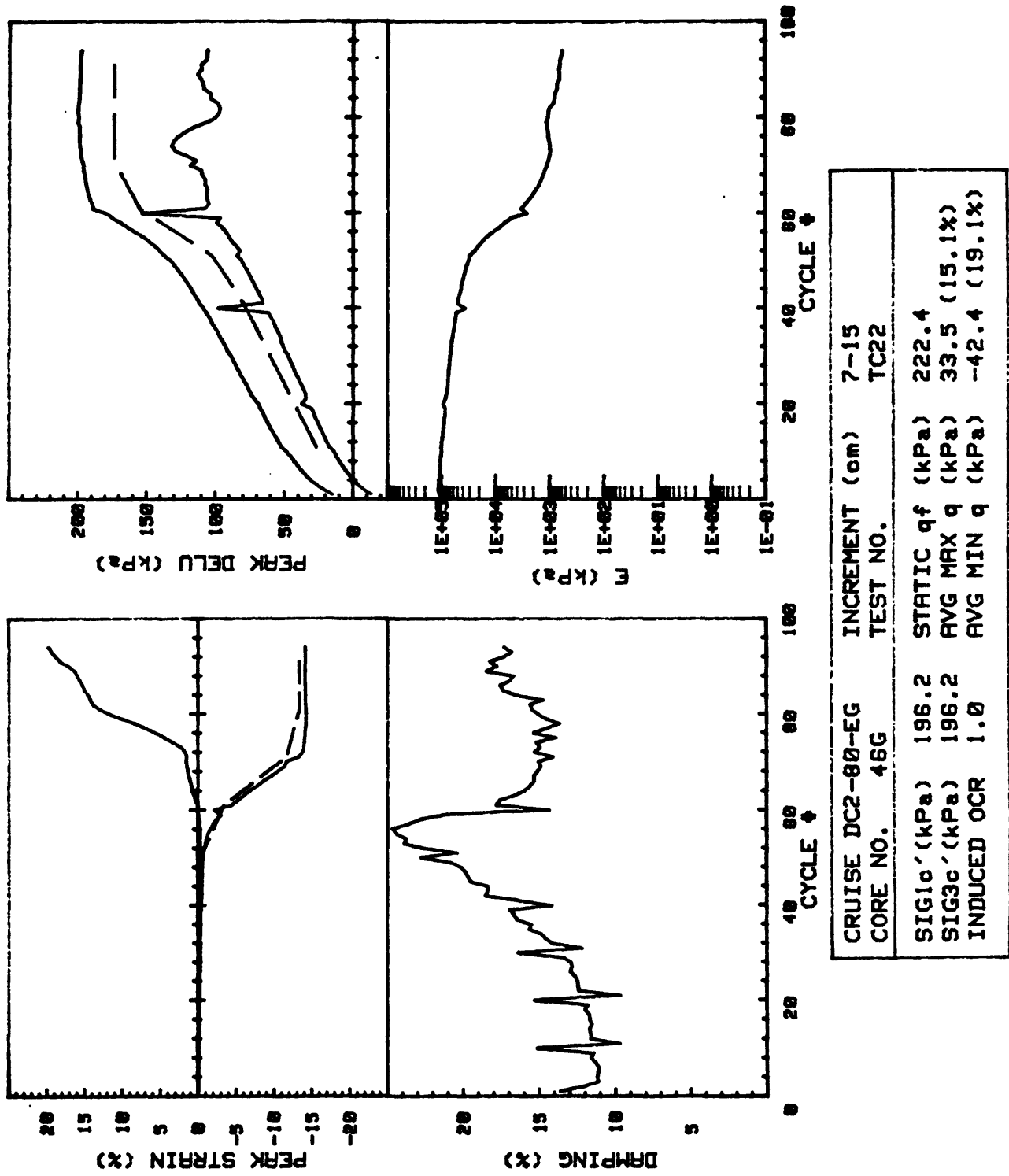
CRUISE DC2-80-EG CORE NO. 43G	INCREMENT (cm) TEST NO.	27-35 TC20	
SIG1c'(kPa)	28.3	STATIC q <sub>f</sub> (kPa)	73.9
SIG3c'(kPa)	28.3	AVG MAX q (kPa)	43.2 (58.5%)
INDUCED OCR	1.0	AVG MIN q (kPa)	-34.5 (46.7%)

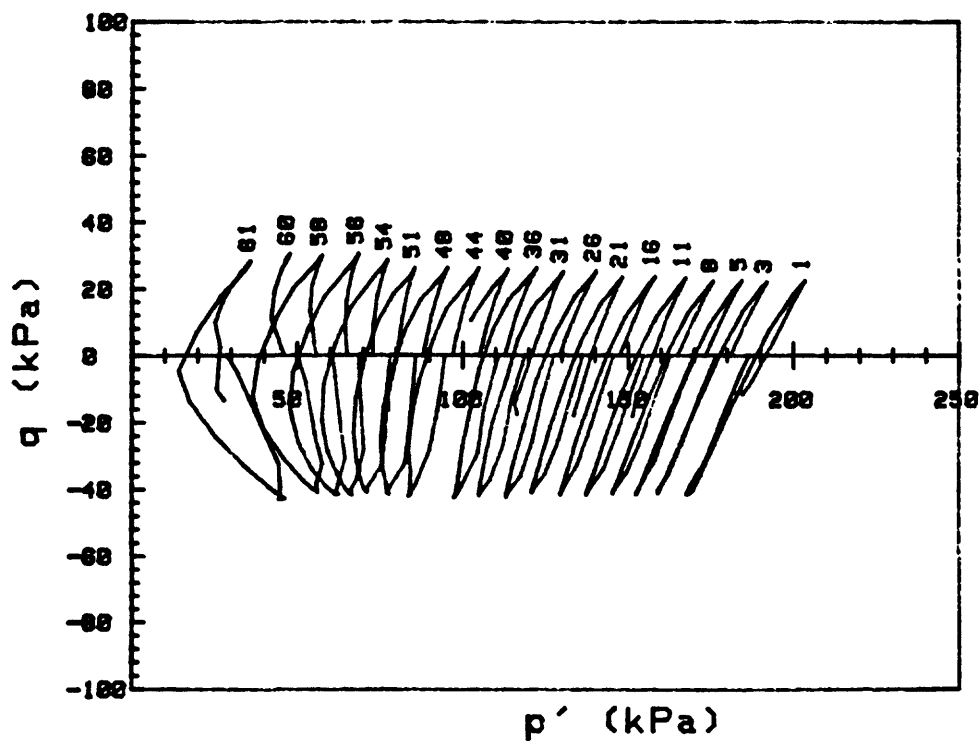
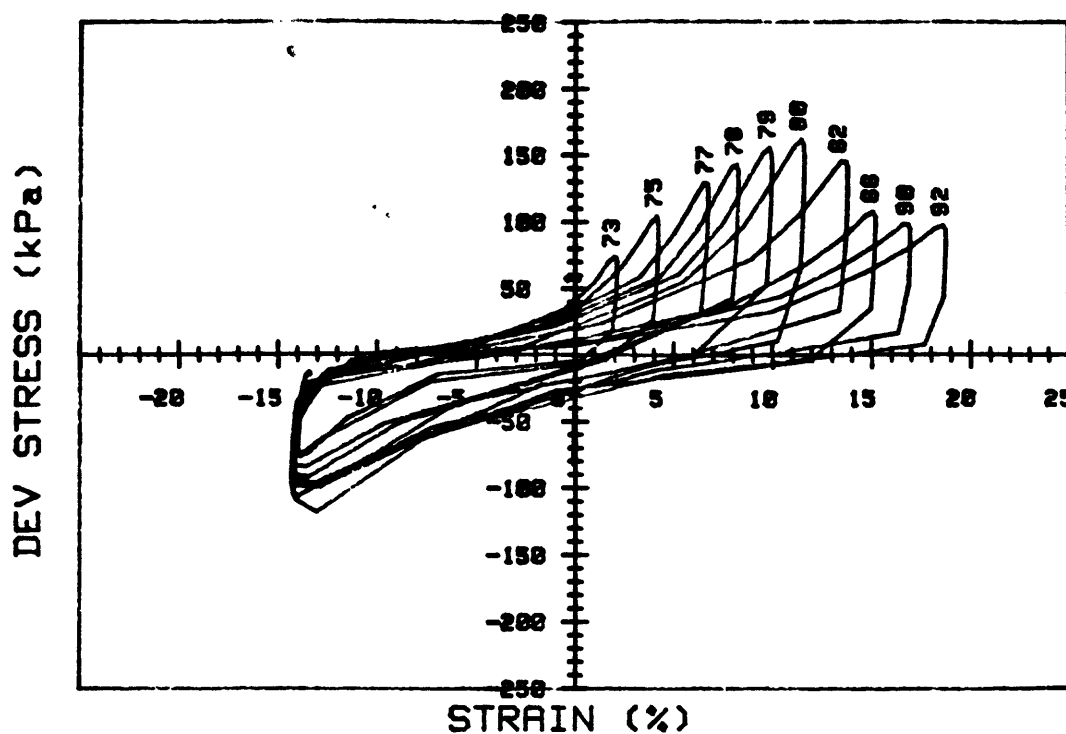


CRUISE CORE NO.	DC2-80-EG 43G	INCREMENT TEST NO.	27-35 TC2!
SIG1o' (kPa)	27.2	STATIC qf	(kPa) 73.9
SIG3o' (kPa)	27.2	Avg MAX q	(kPa) 45.7 (61.8%)
INDUCED OCR	1.0	Avg MIN q	(kPa) -42.0 (56.8%)

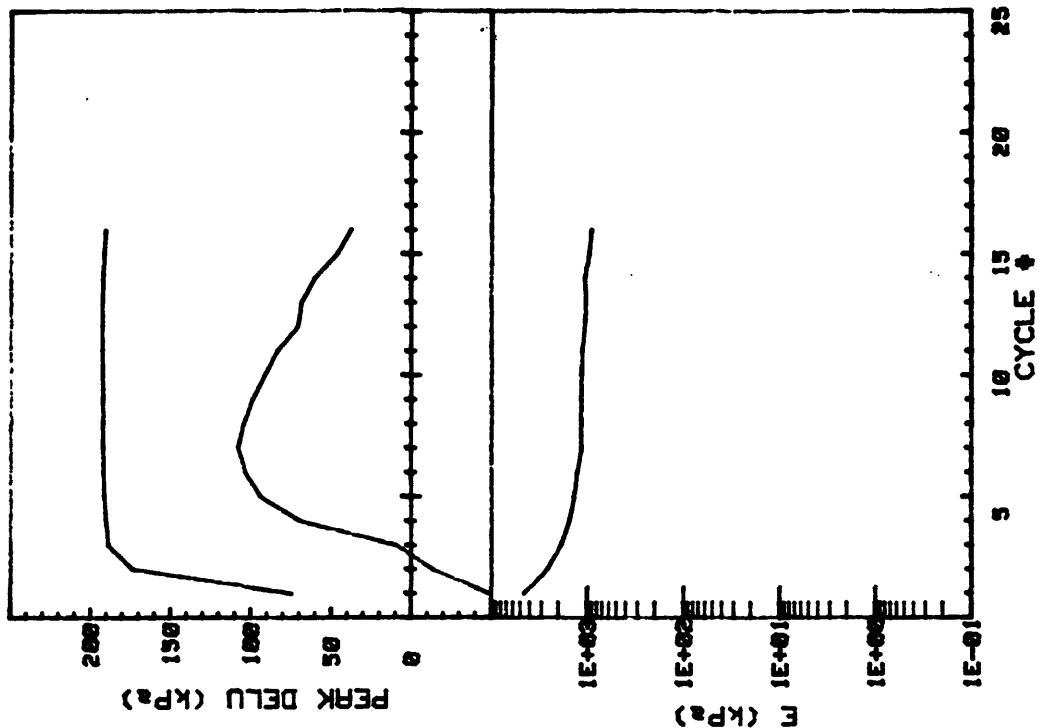


CRUISE DC2-80-EG	INCREMENT (cm)	27-35	
CORE NO. 43G	TEST NO.	TC21	
SIG1c'(kPa)	27.2	STATIC q <sub>f</sub> (kPa)	73.9
SIG3c'(kPa)	27.2	AVG MAX q (kPa)	45.7 (61.0%)
INDUCED OCR	1.0	AVG MIN q (kPa)	-42.0 (56.8%)

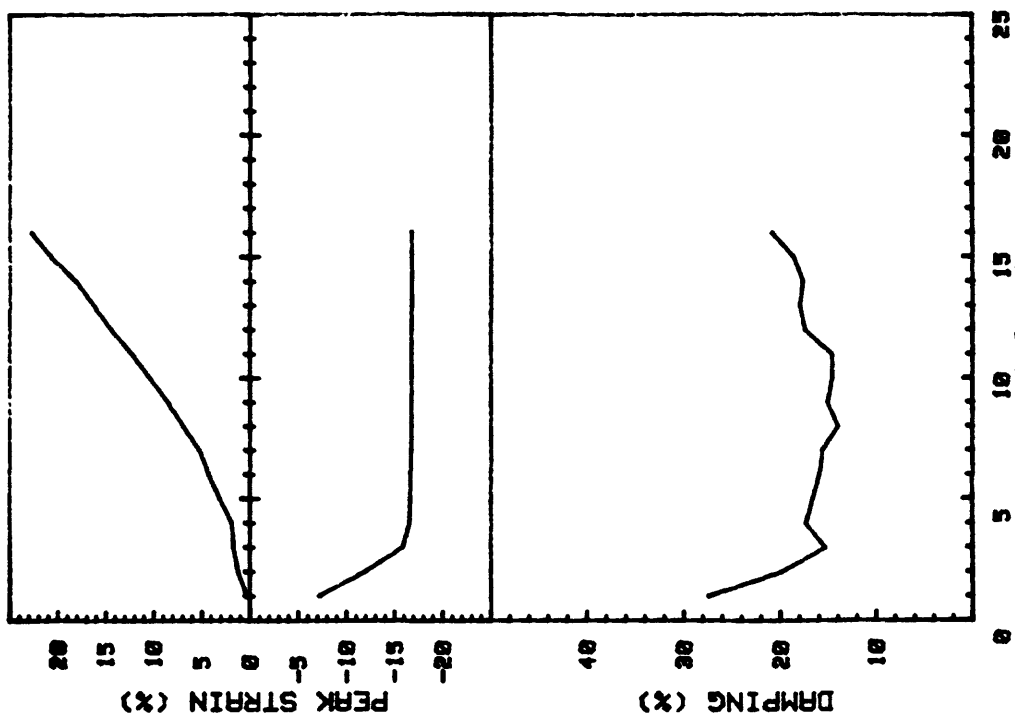


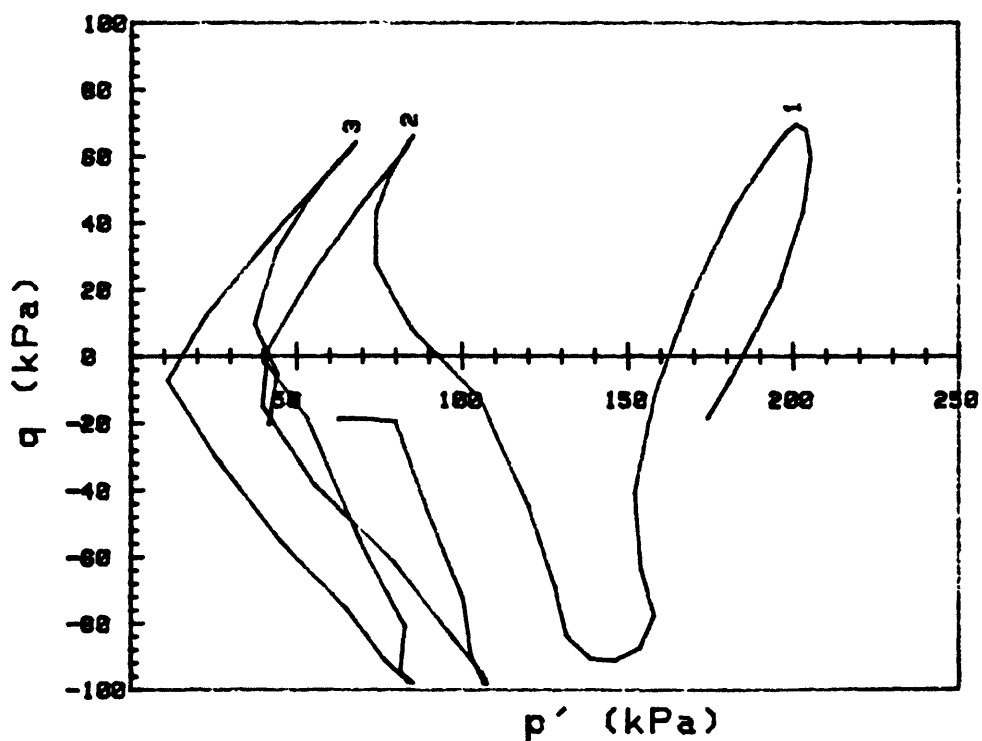
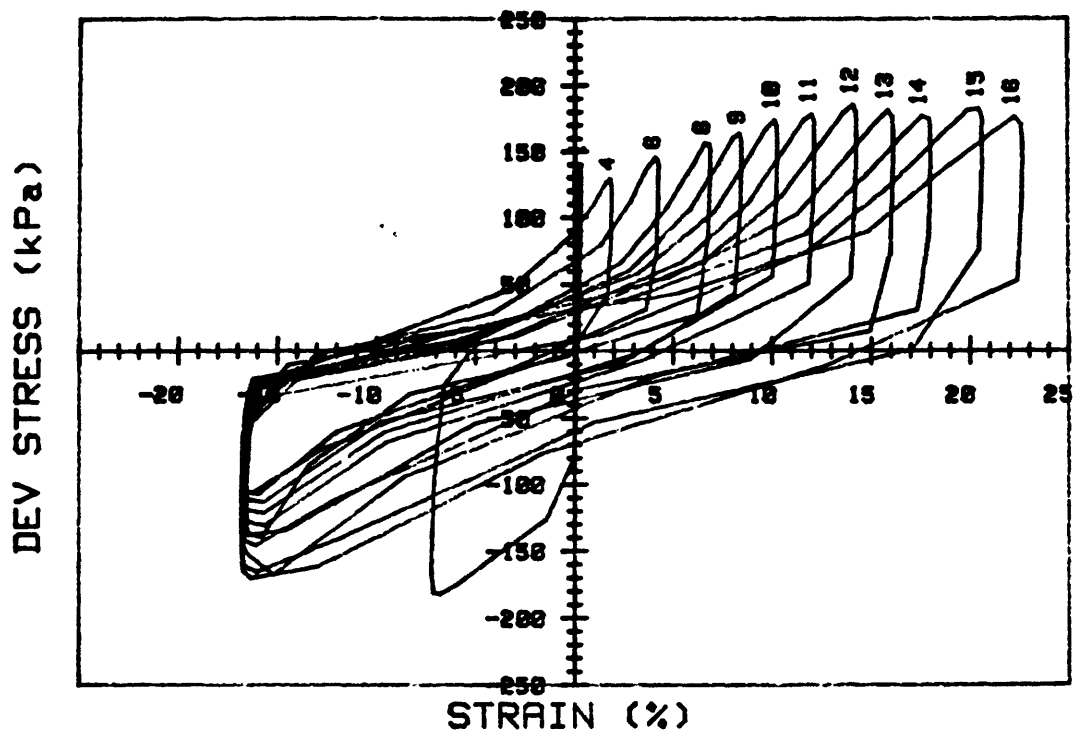


CRUISE DC2-80-EG	INCREMENT (cm)	7-15	
CORE NO. 46G	TEST NO.	TC22	
SIG1 $c'$ (kPa)	196.2	STATIC $q_f$ (kPa)	222.4
SIG3 $c'$ (kPa)	196.2	AVG MAX $q$ (kPa)	33.5 (15.1%)
INDUCED OCR	1.0	AVG MIN $q$ (kPa)	-42.4 (19.1%)

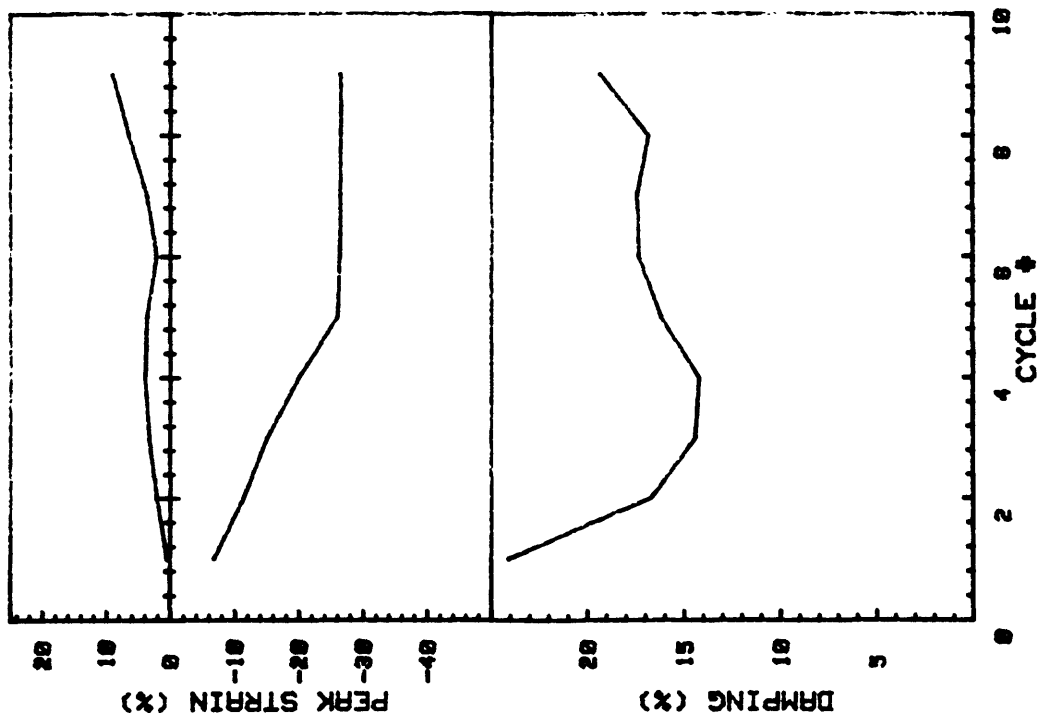
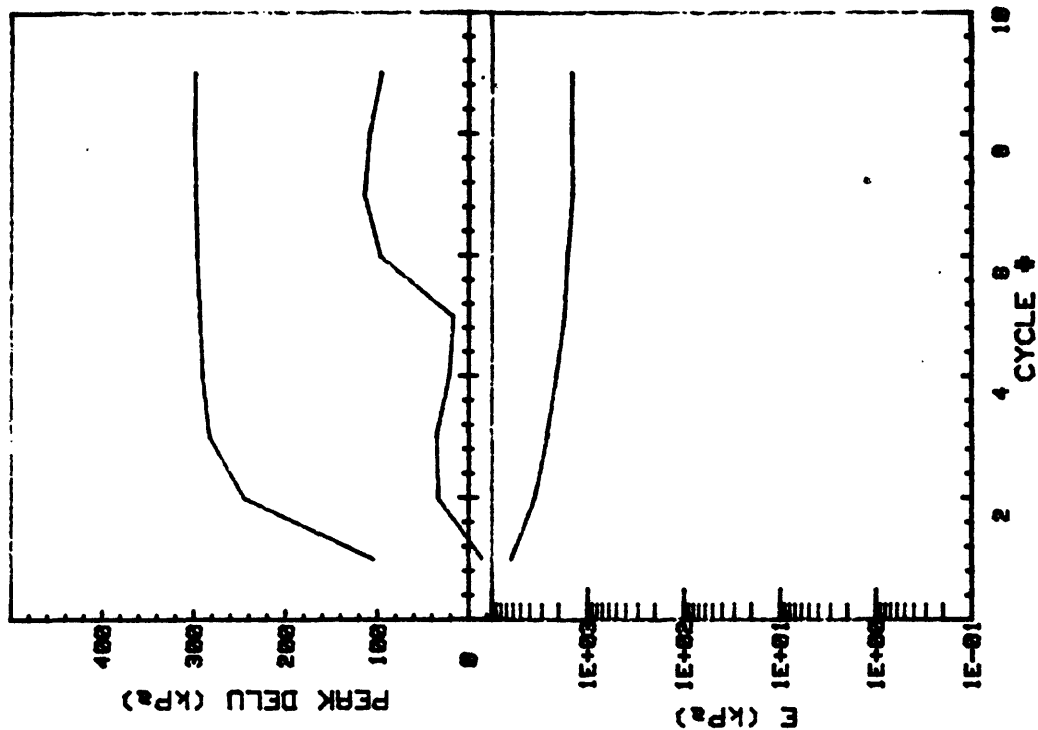


CRUISE DC2-80-EG	INCREMENT (cm)	7-15
CORE NO.	TEST NO.	TC23
SIG1c' (kPa)	192.6	STATIC q <sub>f</sub> (kPa)
SIG3c' (kPa)	192.6	Avg MAX q (kPa)
INDUCED OCR	1.0	Avg MIN q (kPa)
		-71.8 (32.3%)

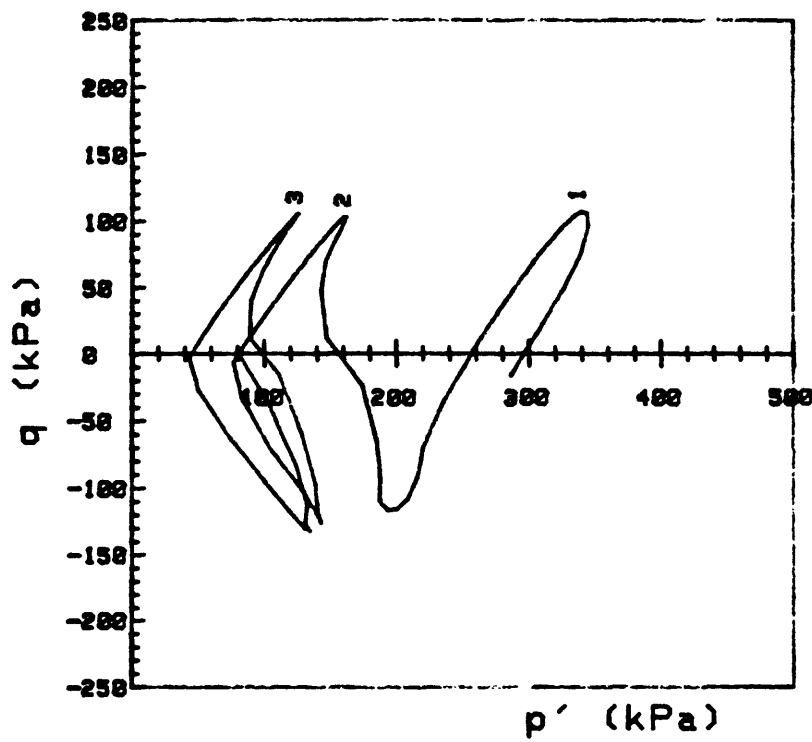
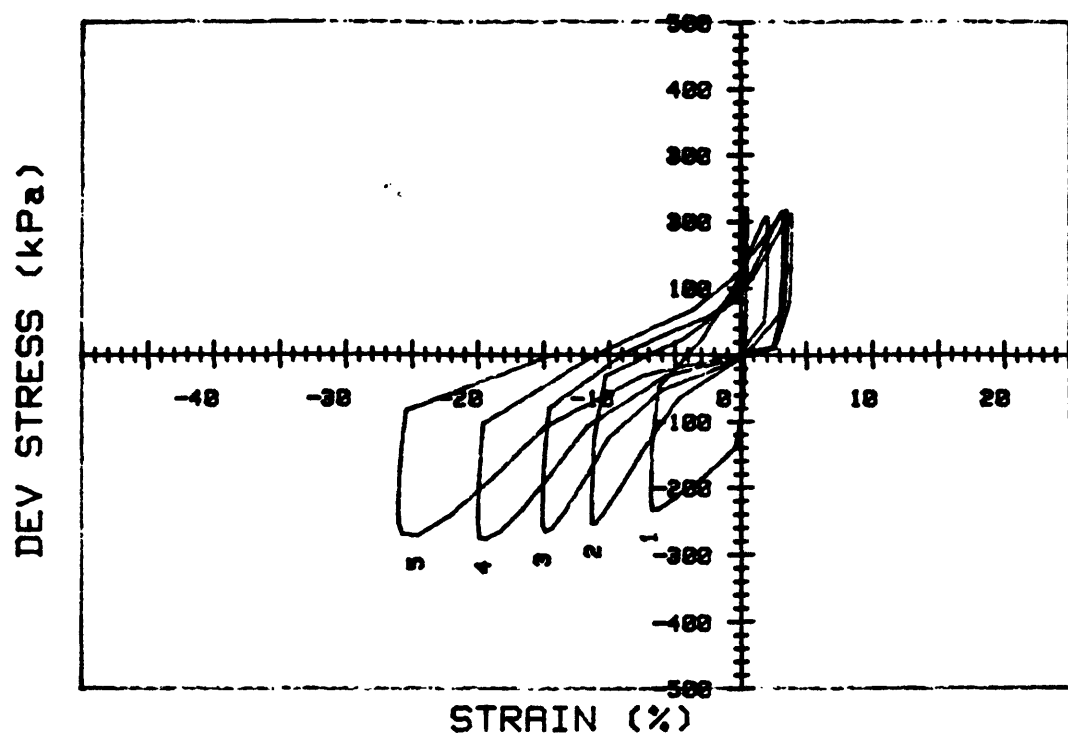




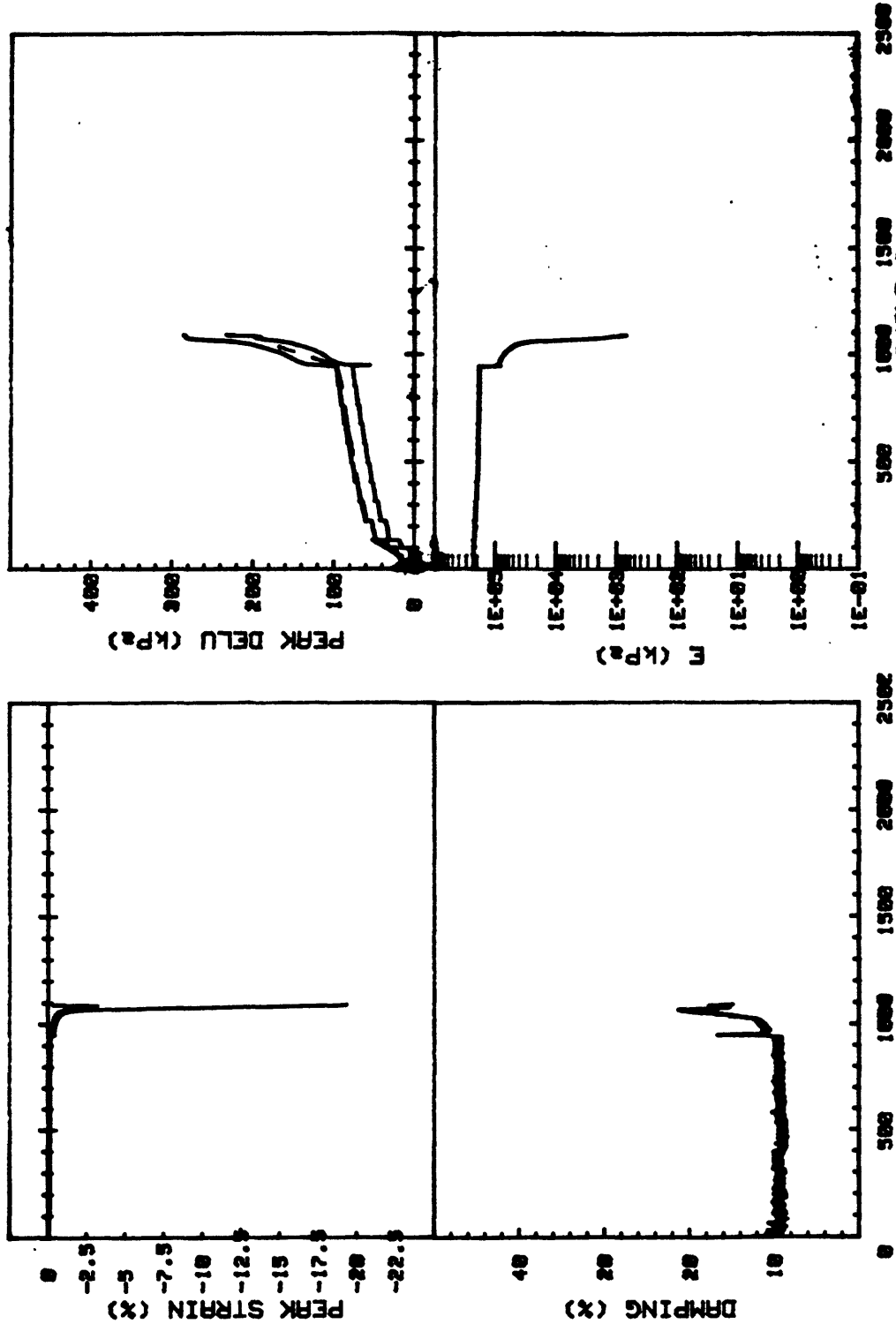
CRUISE DC2-80-EG CORE NO. 46G	INCREMENT (cm) TEST NO.	7-15 TC23	
SIG1c' (kPa)	192.6	STATIC $q_f$ (kPa)	222.4
SIG3c' (kPa)	192.6	AVG MAX $q$ (kPa)	79.0 (35.5%)
INDUCED OCR	1.0	AVG MIN $q$ (kPa)	-71.8 (32.3%)



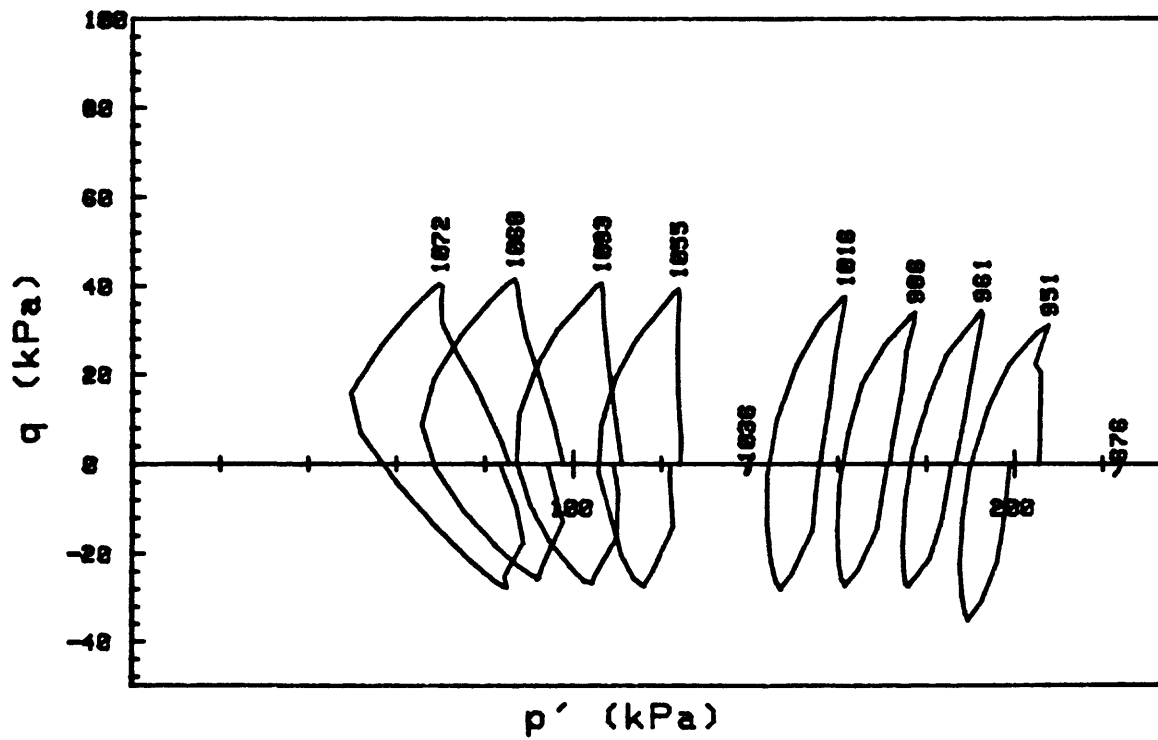
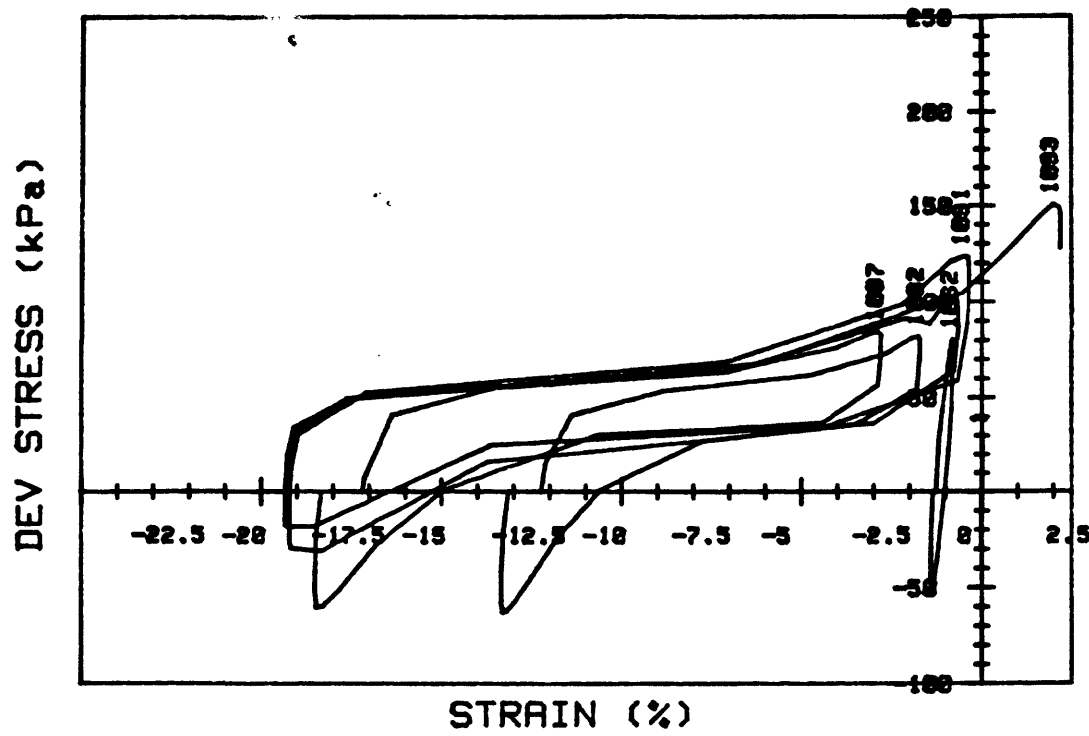
CRUISE DC2-80-EG		INCREMENT (cm)	15-22
CORE NO.	28G	TEST NO.	TC24
SIG1c' (kPa)	302.6	STATIC q <sub>f</sub> (kPa)	268.9
SIG3c' (kPa)	302.6	AVG MAX q (kPa)	115.6 (43.0%)
INDUCED OCR	1.0	AVG MIN q (kPa)	-100.5 (37.4%)



CRUISE DC2-80-EG	INCREMENT (cm)	15-22	
CORE NO. 28G	TEST NO.	TC24	
SIG1c'(kPa)	302.6	STATIC qf (kPa)	268.9
SIG3c'(kPa)	302.6	AVG MAX q (kPa)	115.6 (43.0%)
INDUCED OCR	1.0	AVG MIN q (kPa)	-100.5 (37.4%)

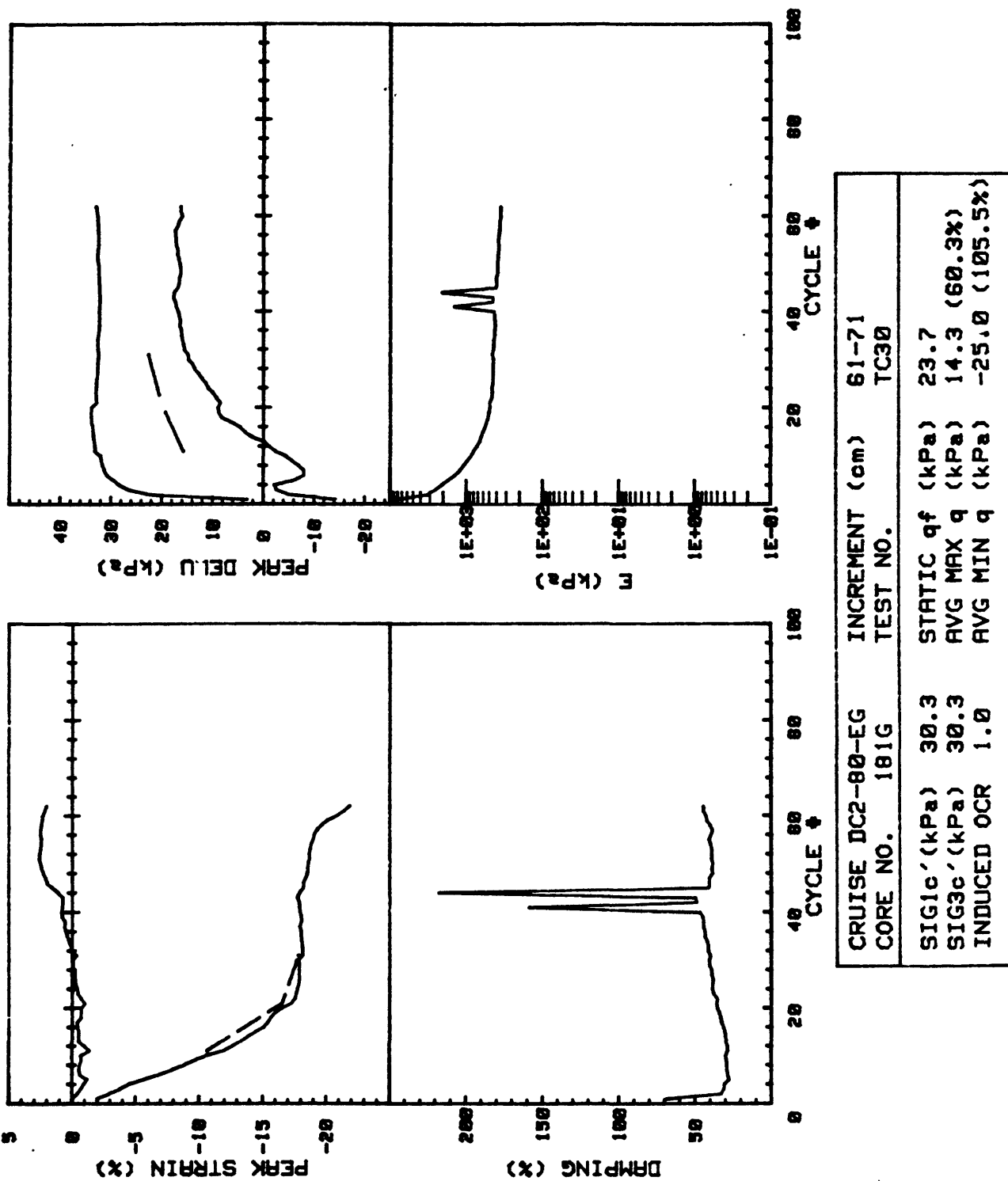


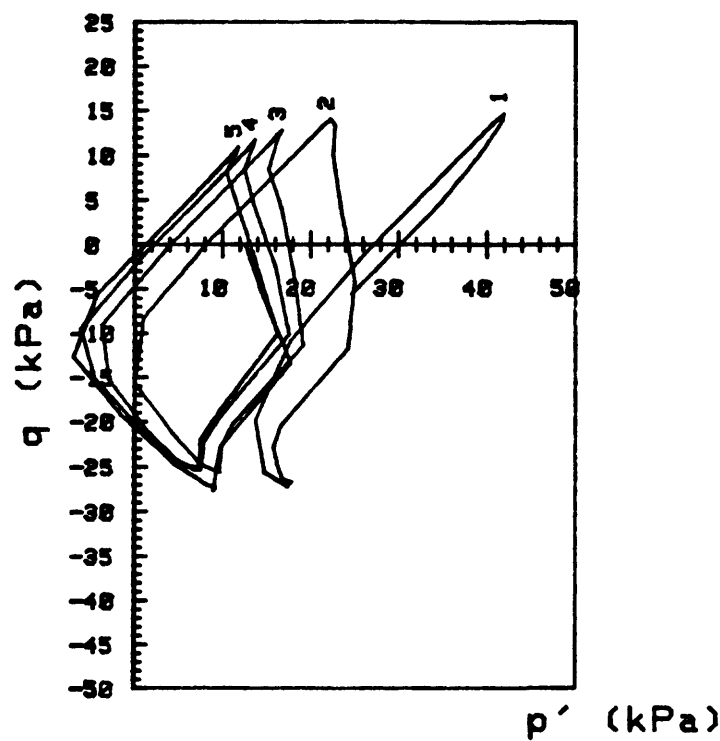
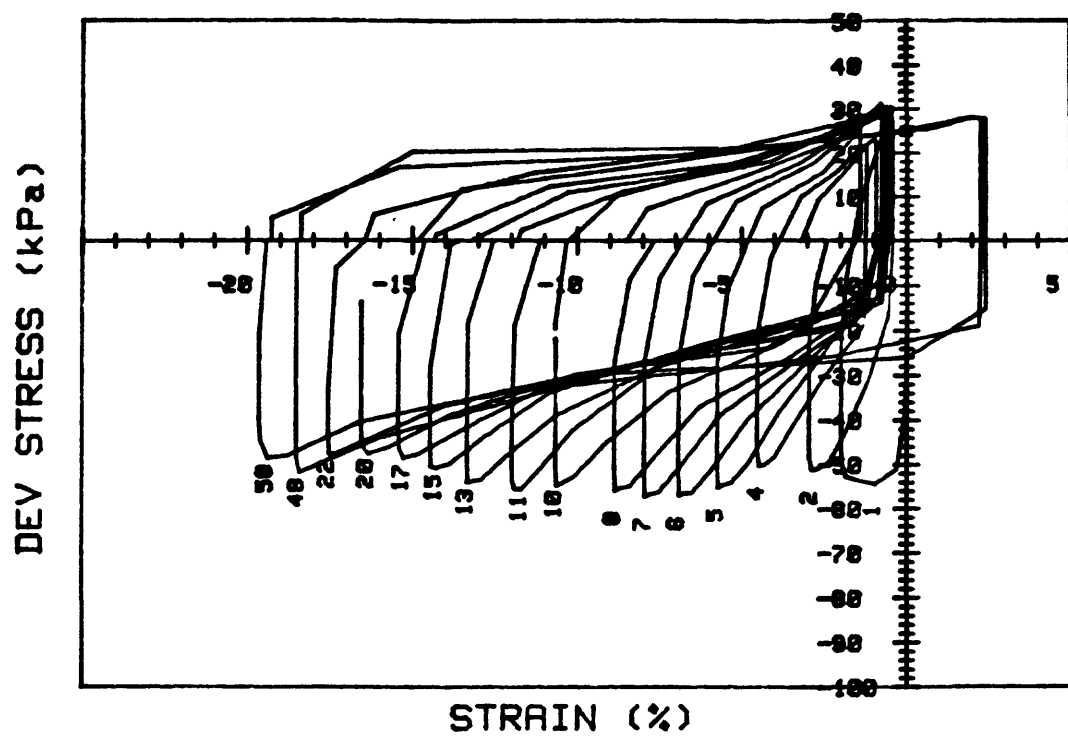
CRUISE	DC2-80-EG	INCREMENT (cm)	15-22.4
CORE NO.	28G	TEST NO.	TC25
SIG1 <sub>0</sub> ' (kPa)	297.9	STATIC q <sub>f</sub> (kPa)	270.0
SIG3 <sub>0</sub> ' (kPa)	297.9	AVG MAX q (kPa)	21.1 (7.8%)
INDUCED OCR	1.0	AVG MIN q (kPa)	-16.6 (6.1%)



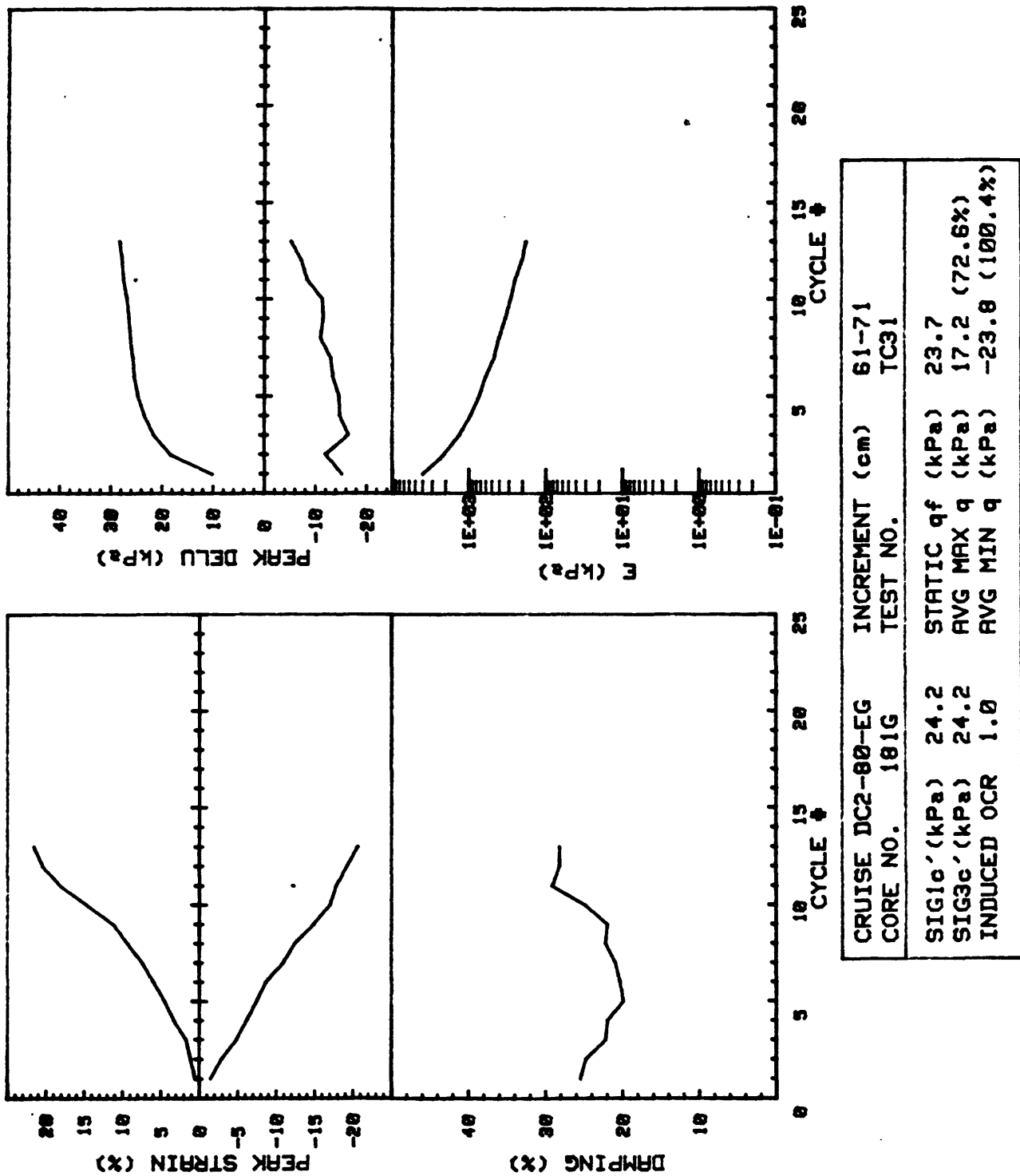
CRUISE DC2-80-EG	INCREMENT (cm)	15-22.4
CORE NO. 28G	TEST NO.	TC25

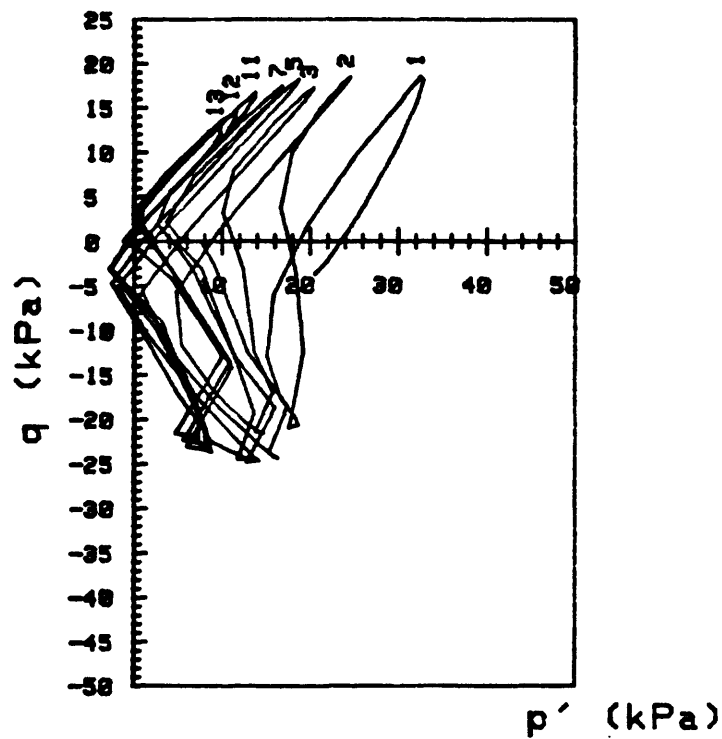
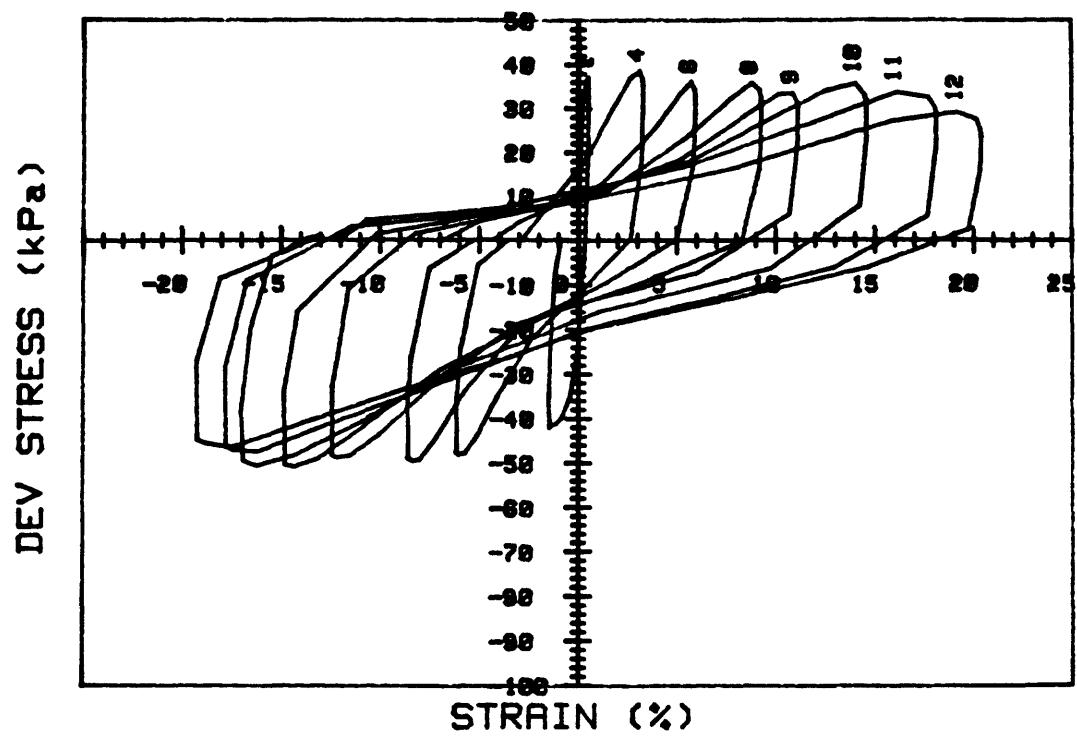
SIG1c'(kPa)	297.9	STATIC q <sub>f</sub> (kPa)	270.0
SIG3c'(kPa)	297.9	AVG MAX q (kPa)	21.1 (7.8%)
INDUCED OCR	1.0	AVG MIN q (kPa)	-16.6 (6.1%)



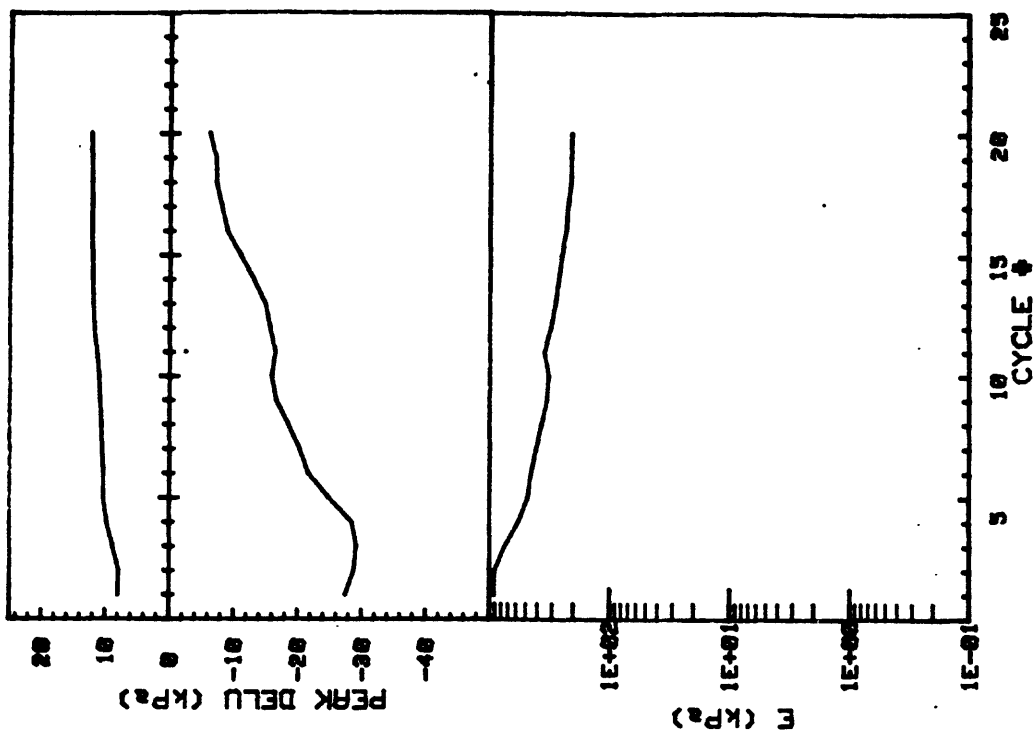


CRUISE DC2-80-EG CORE NO. 181G	INCREMENT (cm) TEST NO.	61-71 TC30
SIG1c'(kPa)	STATIC qf (kPa)	23.7
SIG3c'(kPa)	AVG MAX q (kPa)	14.3 (60.3%)
INDUCED OCR	AVG MIN q (kPa)	-25.0 (105.5%)

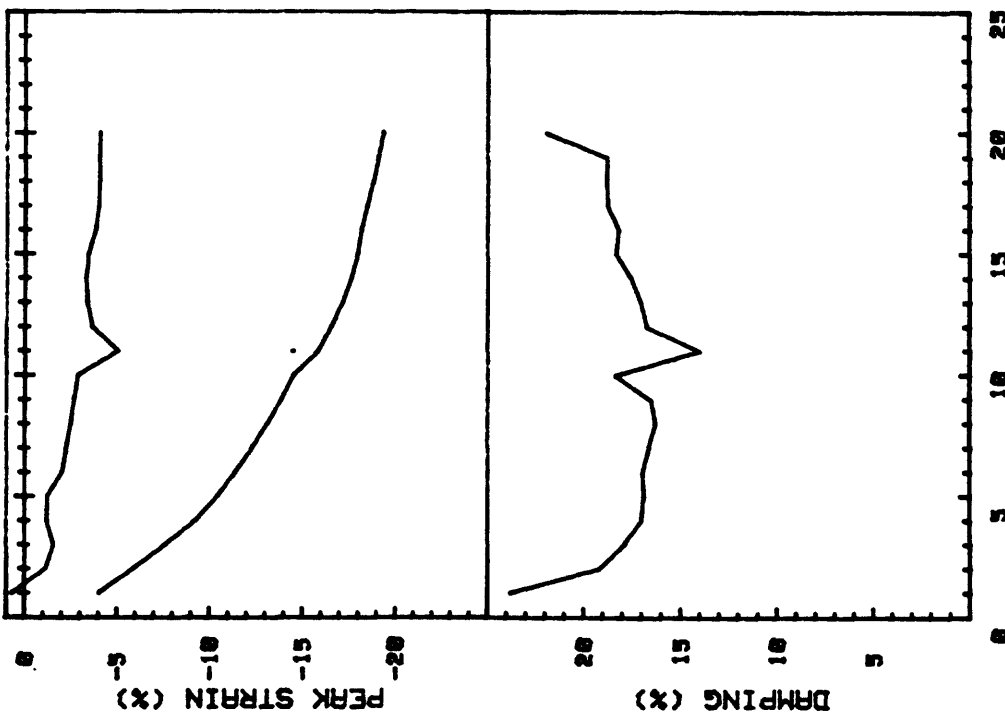


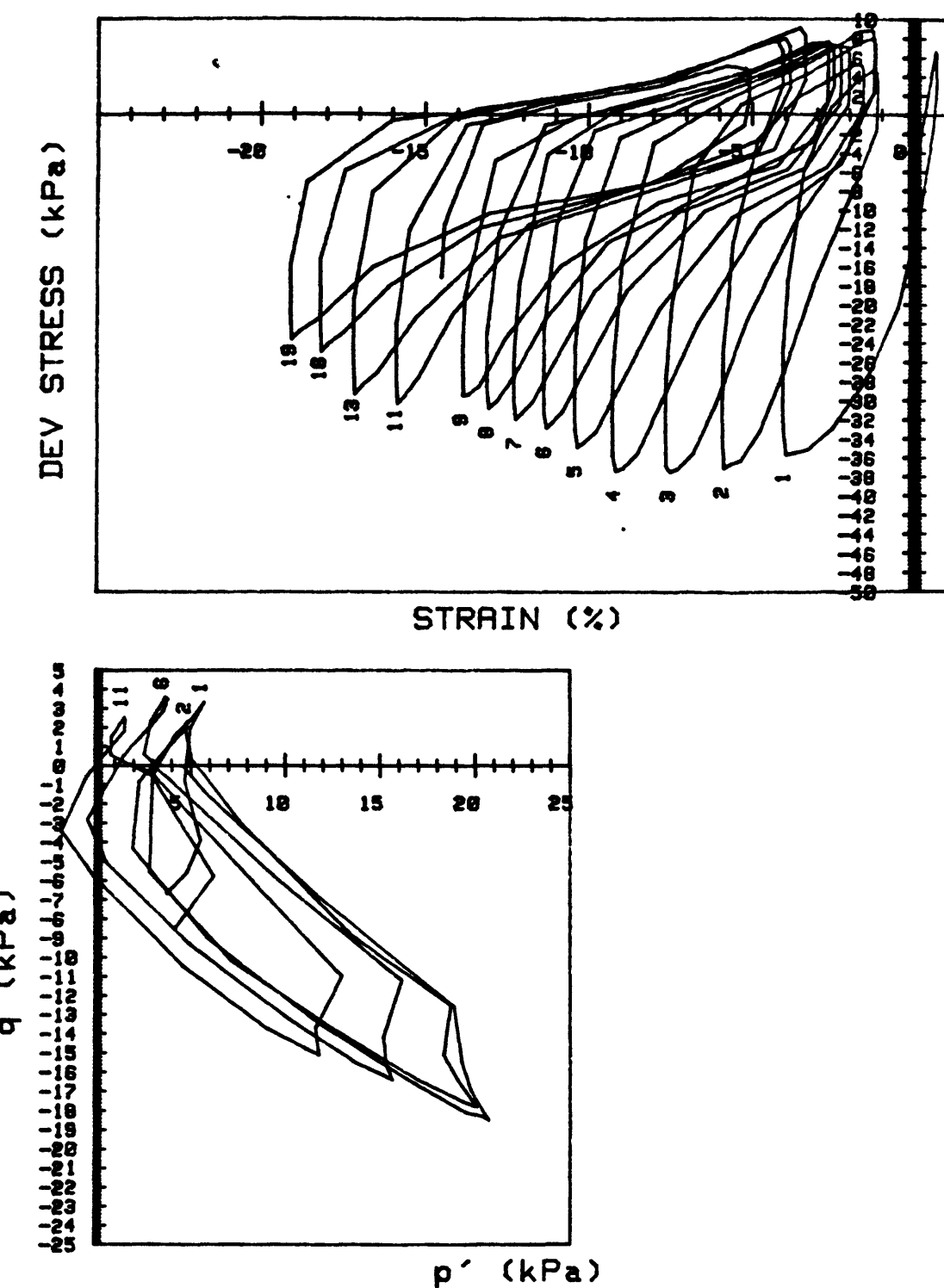


CRUISE DC2-80-EG CORE NO. 181G	INCREMENT (cm) TEST NO.	61-71 TC31	
SIG1c'(kPa)	24.2	STATIC q <sub>f</sub> (kPa)	23.7
SIG3c'(kPa)	24.2	AVG MAX q (kPa)	17.2 (72.6%)
INDUCED OCR	1.0	AVG MIN q (kPa)	-23.8 (100.4%)

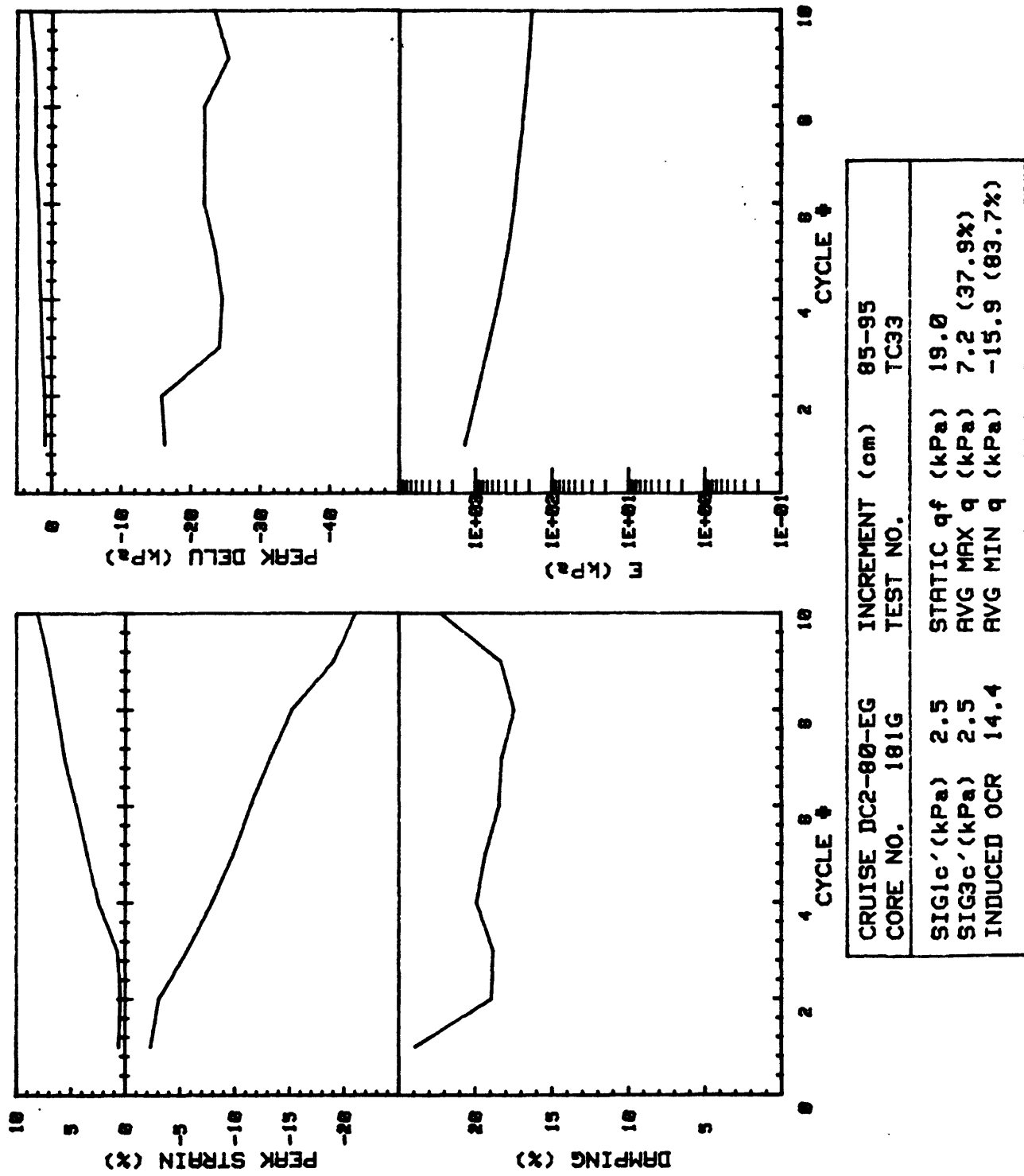


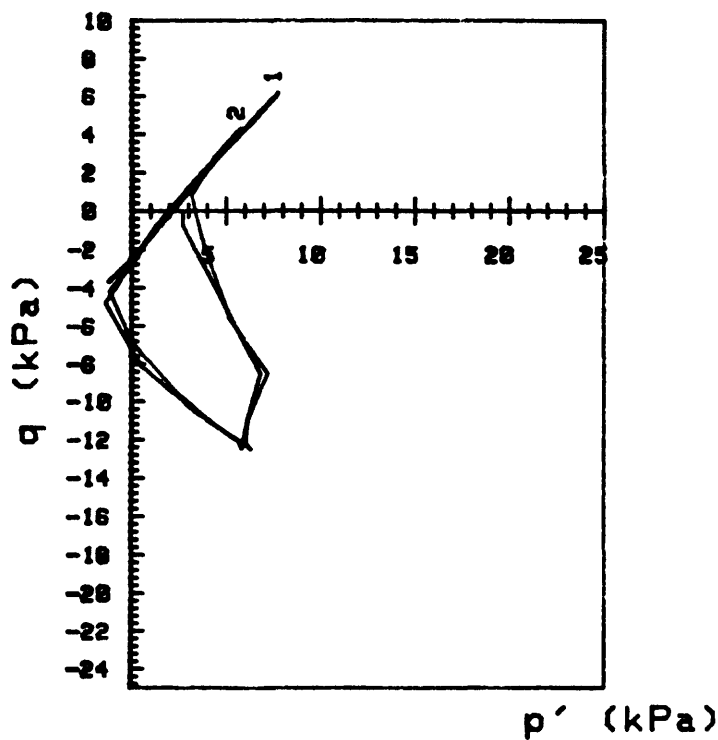
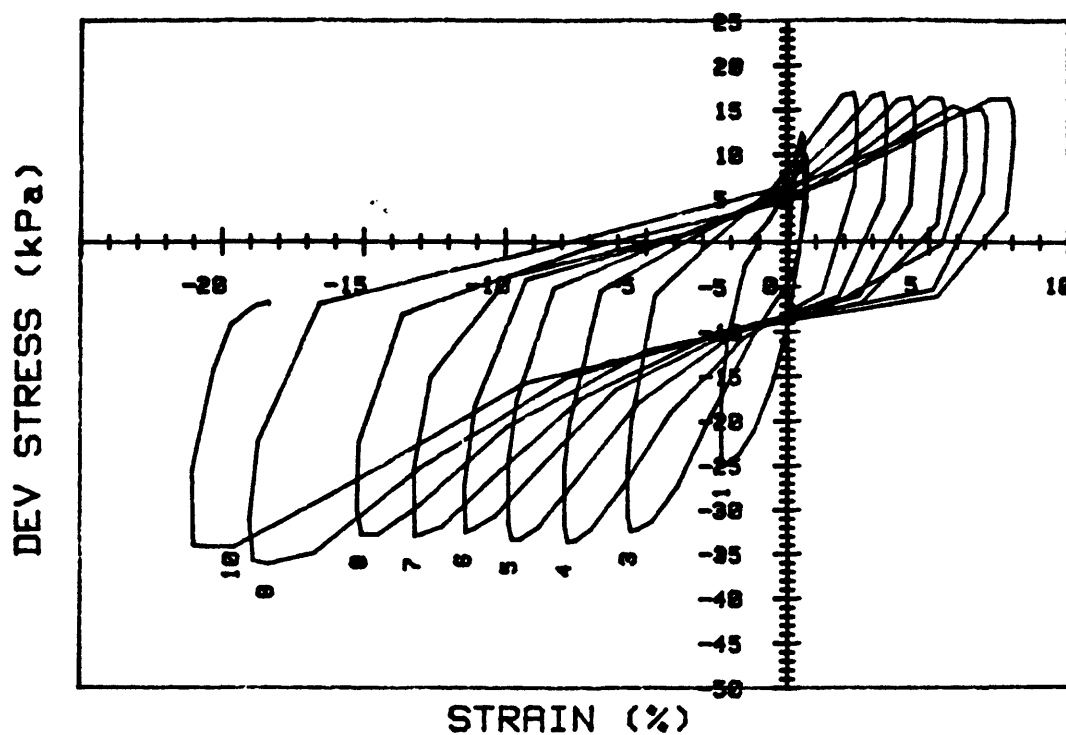
CRUISE DC2-80-EG		INCREMENT (cm)	85-95
CORE NO.	TEST NO.		TC32
SIG1' (kPa)	10.4	STATIC $q_f$ (kPa)	19.0
SIG3c' (kPa)	10.4	Avg MAX $q$ (kPa)	3.7 (19.5%)
INDUCED OCR	3.5	Avg MIN $q$ (kPa)	-15.0 (78.9%)



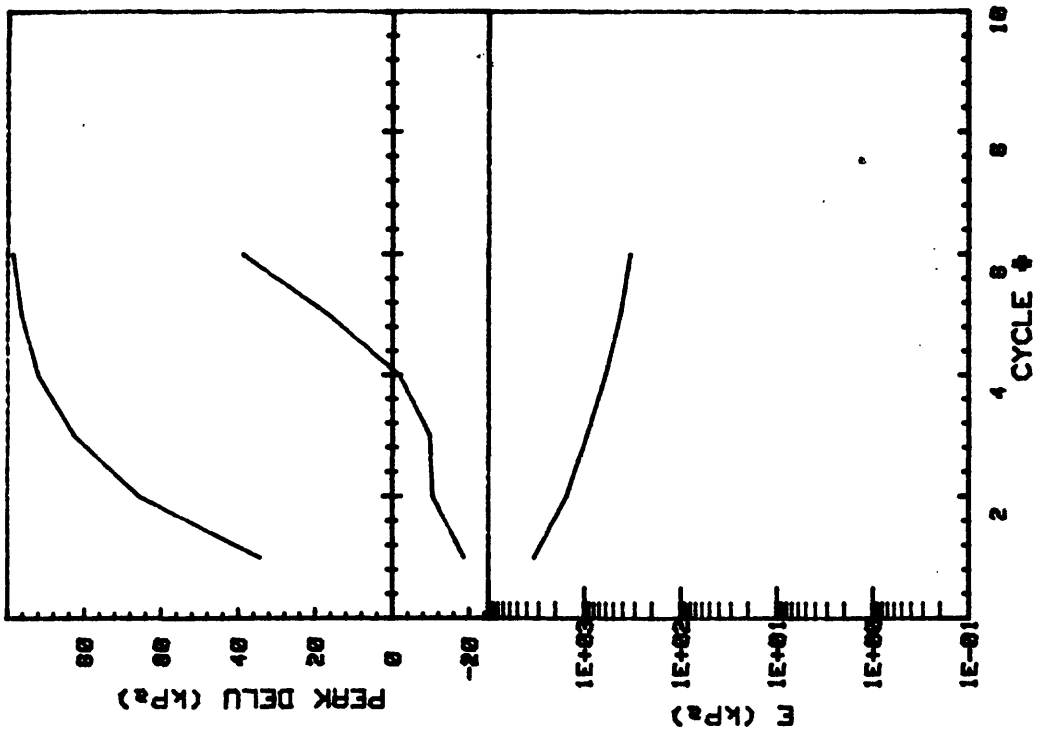


CRUISE DC2-80-EG	INCREMENT (cm)	85-95	
CORE NO. 181G	TEST NO.	TC32	
SIG1c'(kPa)	10.4	STATIC q <sub>f</sub> (kPa)	19.0
SIG3c'(kPa)	10.4	AVG MAX q (kPa)	3.7 (19.5%)
INDUCED OCR	3.5	AVG MIN q (kPa)	-15.0 (78.9%)

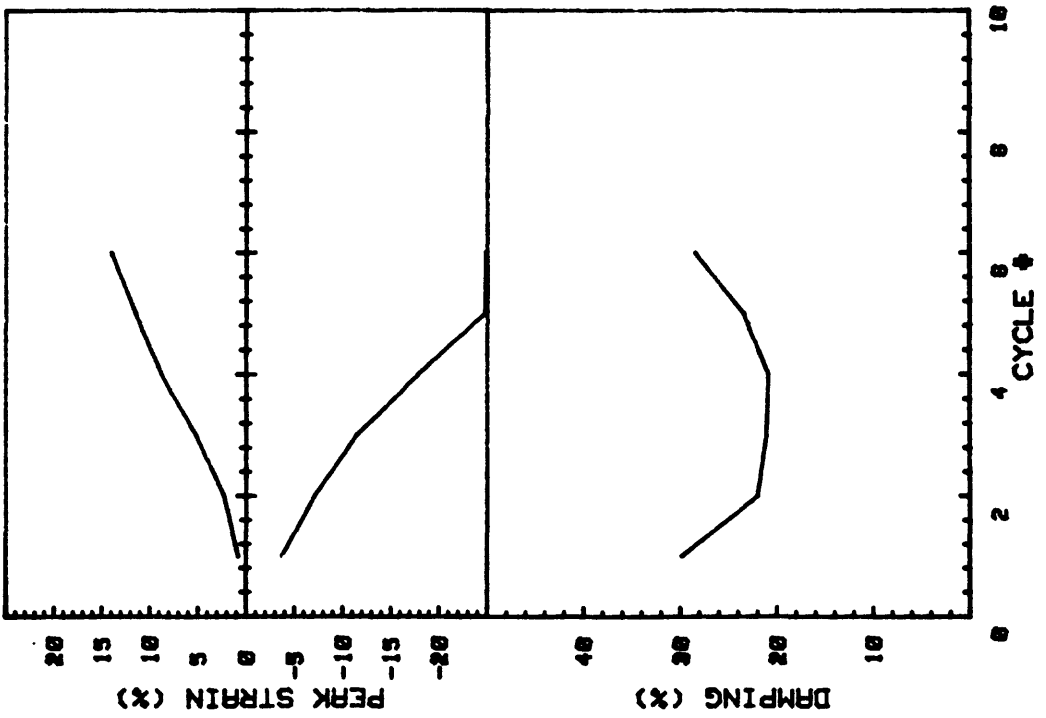


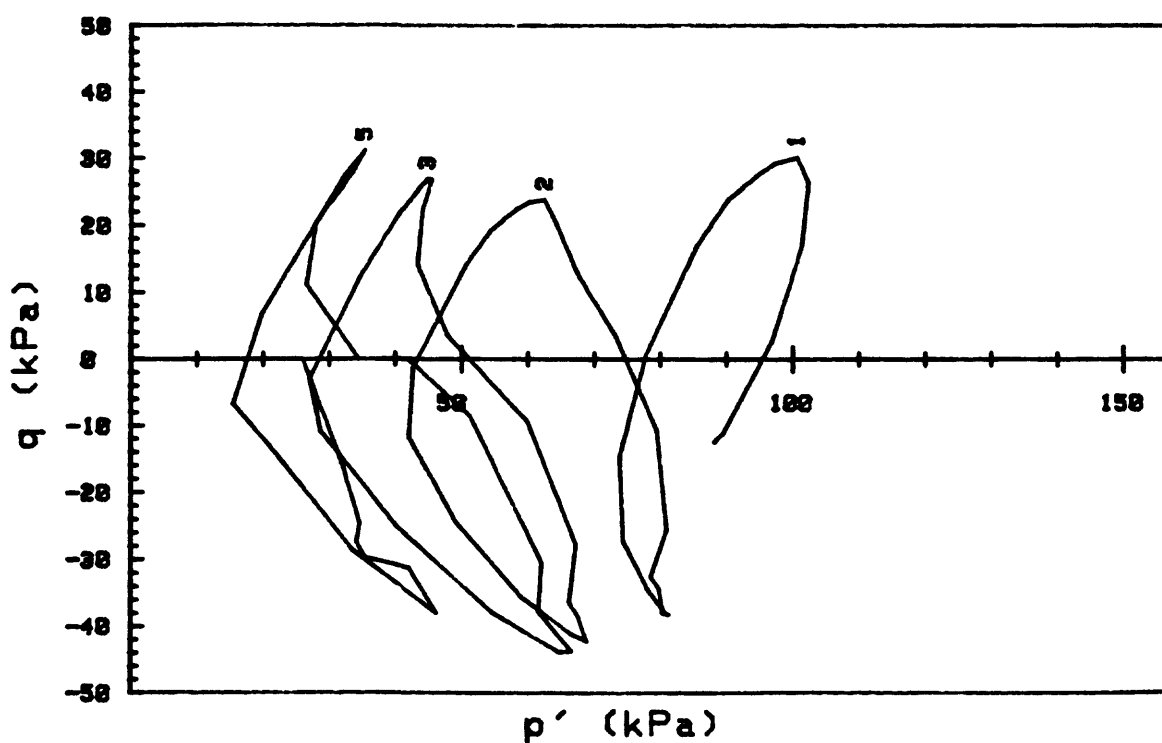
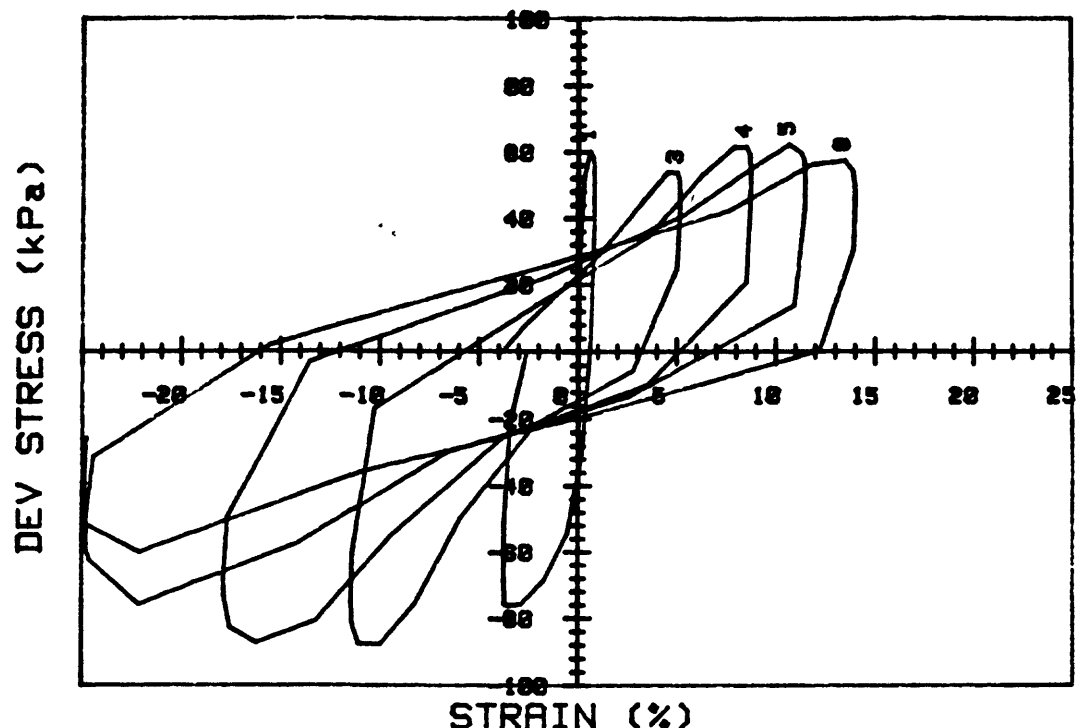


CRUISE DC2-80-EG	INCREMENT (cm)	85-95
CORE NO. 181G	TEST NO.	TC33
SIG1c'(kPa) 2.5	STATIC q <sub>f</sub> (kPa)	19.0
SIG3c'(kPa) 2.5	AVG MAX q (kPa)	7.2 (37.9%)
INDUCED OCR 14.4	AVG MIN q (kPa)	-15.9 (83.7%)

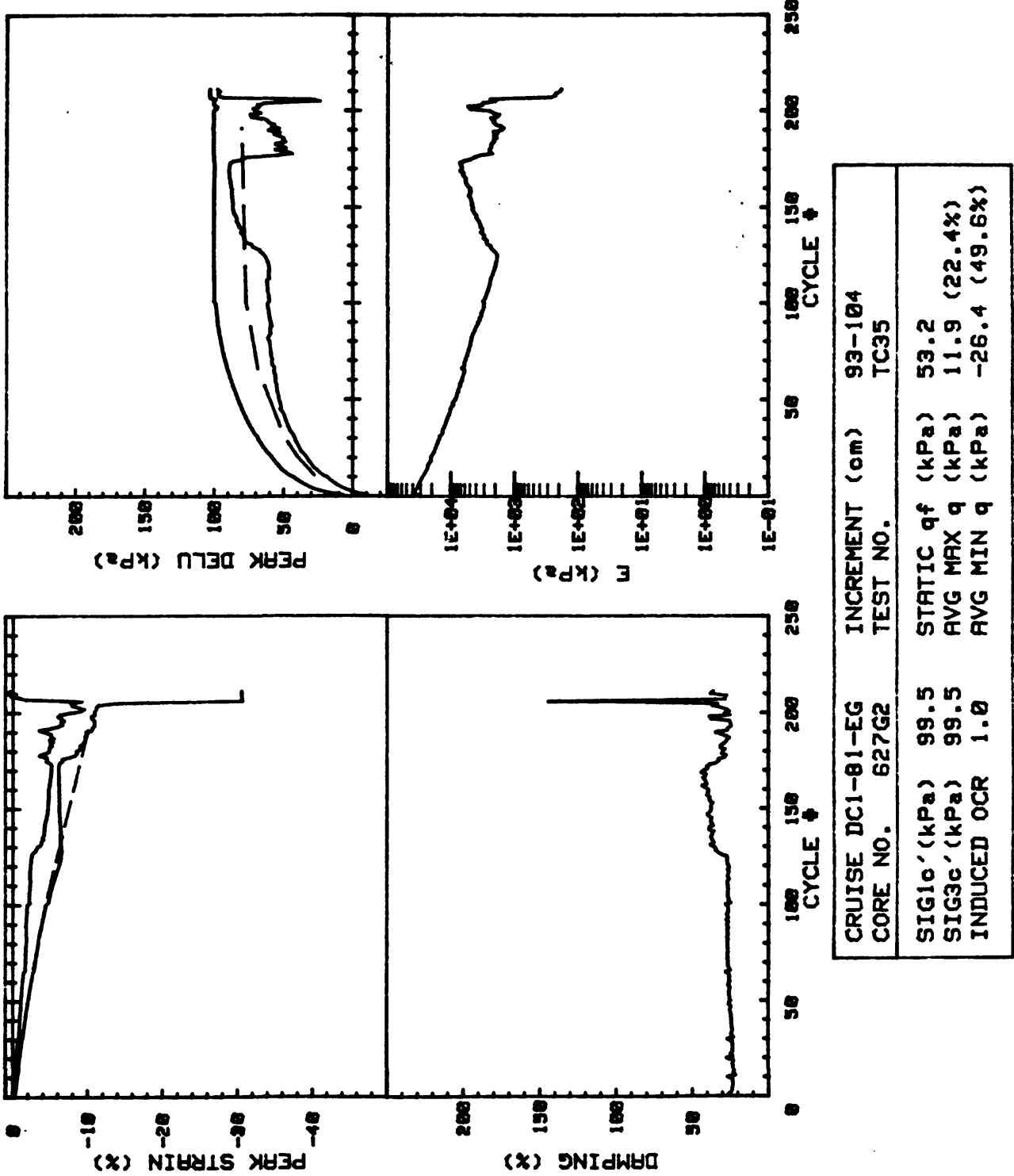


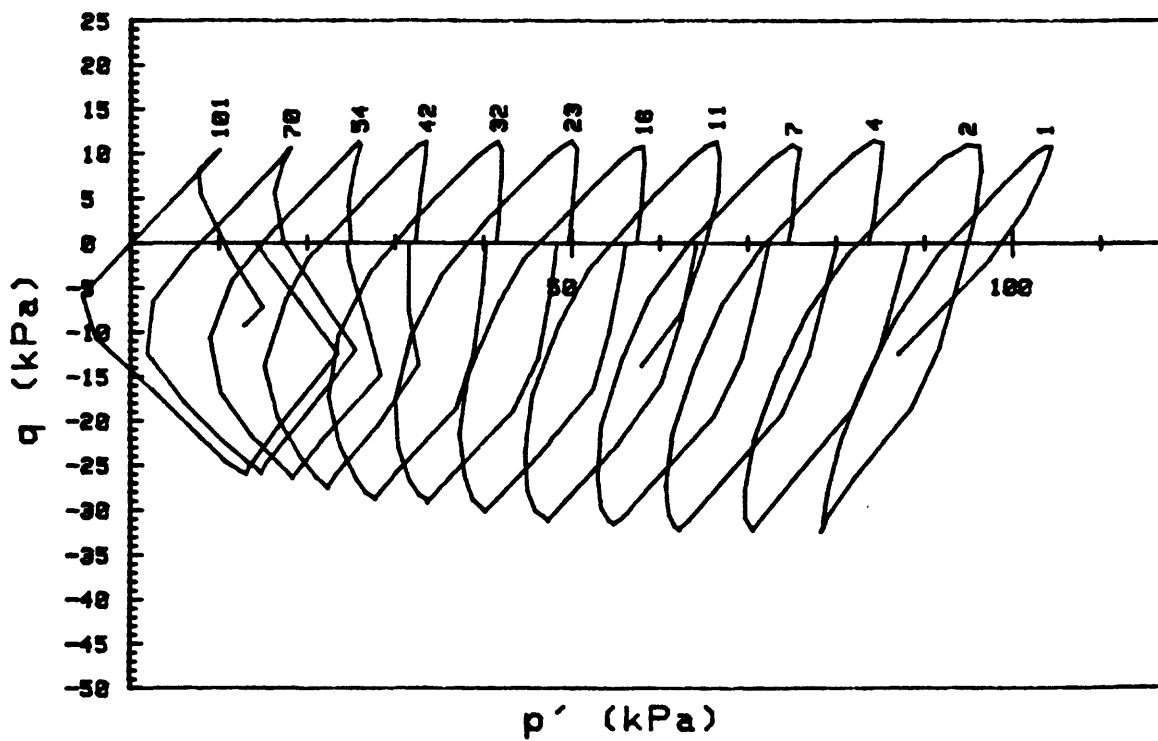
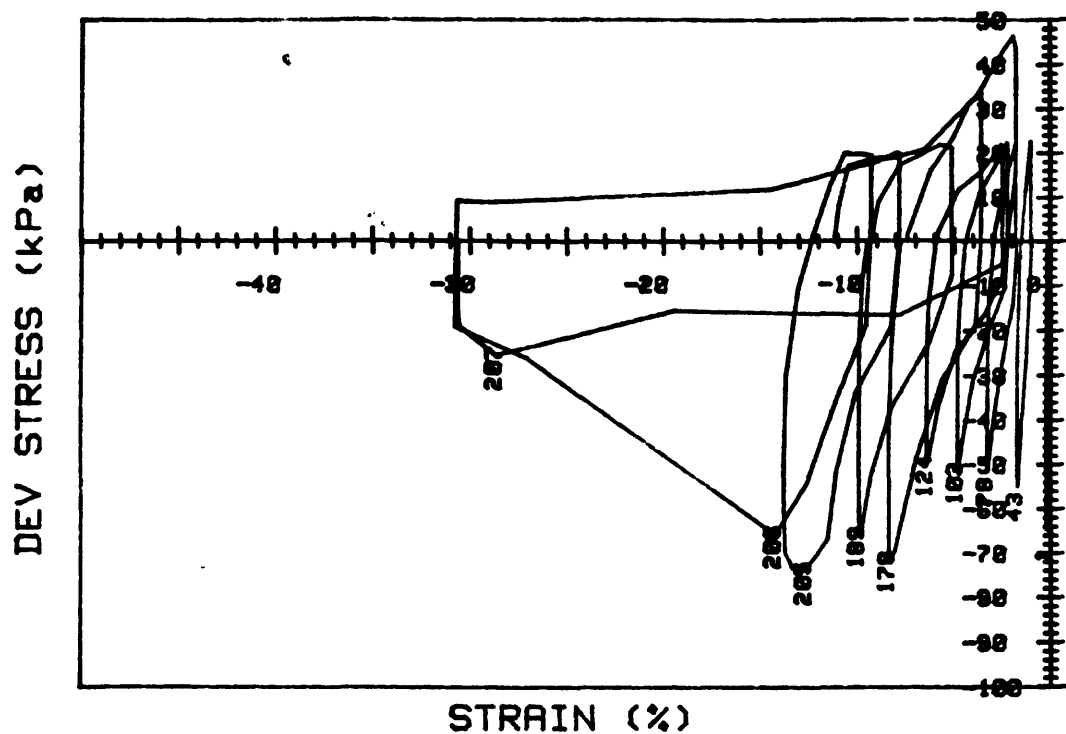
CRUISE DC1-81-EG CORE NO.	INCREMENT (cm)	93-104 TEST NO.
SIG1' (kPa)	100.7	STATIC q <sub>f</sub> (kPa)
SIG3e' (kPa)	100.7	Avg MAX q (kPa)
INDUCED OCR	1.0	Avg MIN q (kPa)



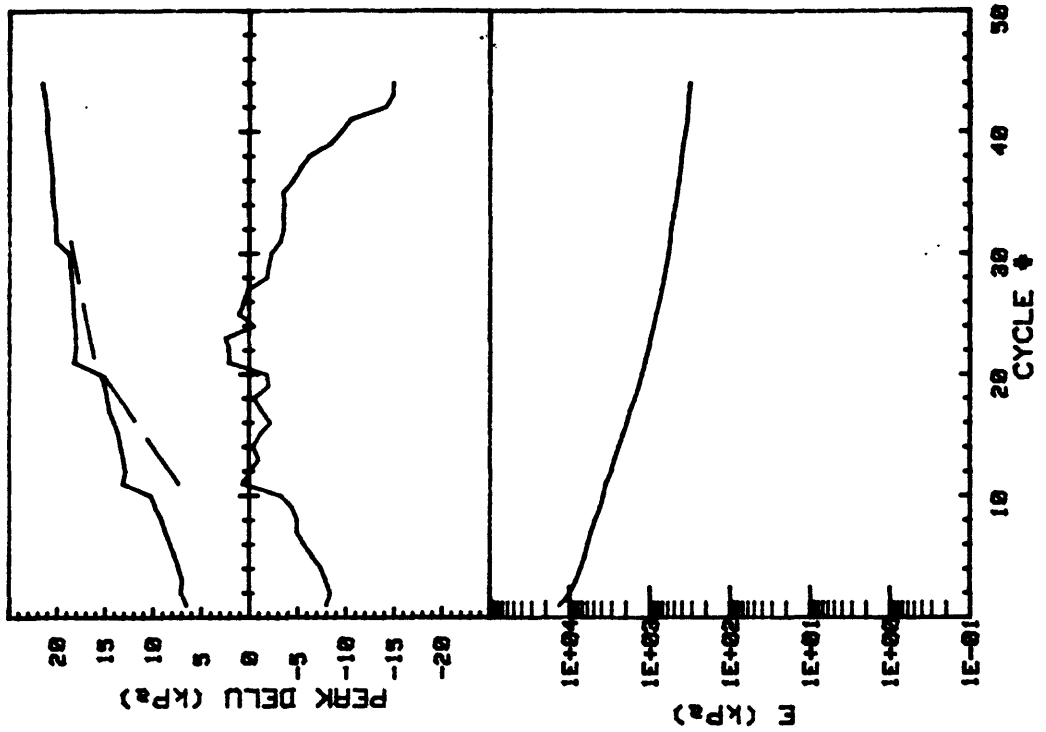


CRUISE DC1-81-EG	INCREMENT (cm)	93-104
CORE NO. 627G2	TEST NO.	TC34
SIG1c'(kPa) 100.7	STATIC q <sub>f</sub> (kPa)	53.2
SIG3c'(kPa) 100.7	AVG MAX q (kPa)	28.6 (53.8%)
INDUCED OCR 1.0	AVG MIN q (kPa)	-39.4 (74.1%)

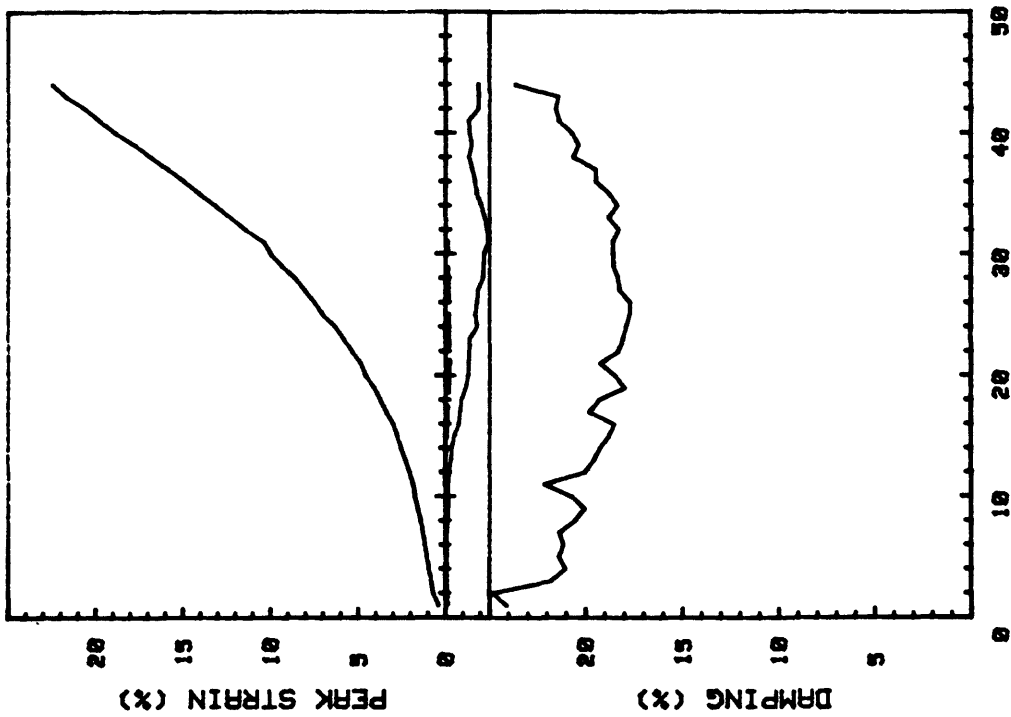


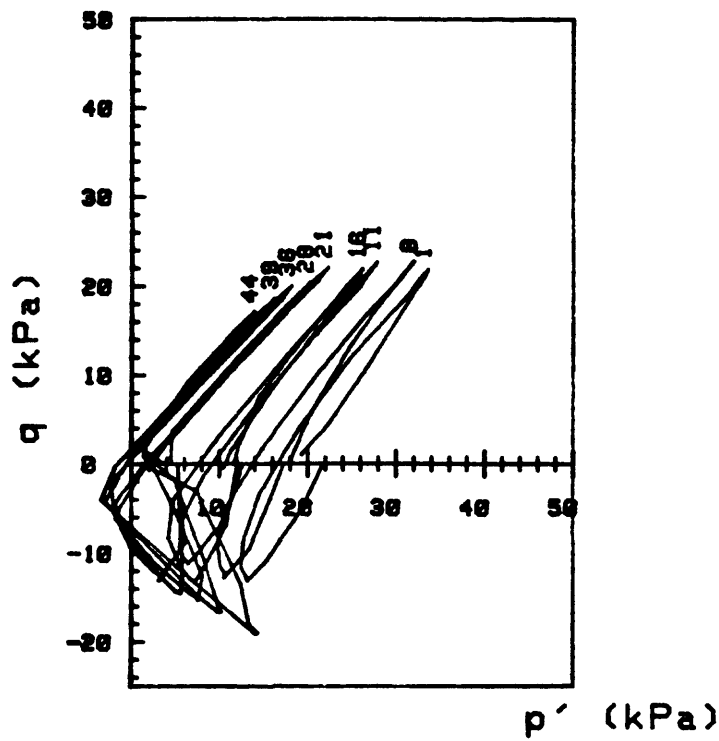
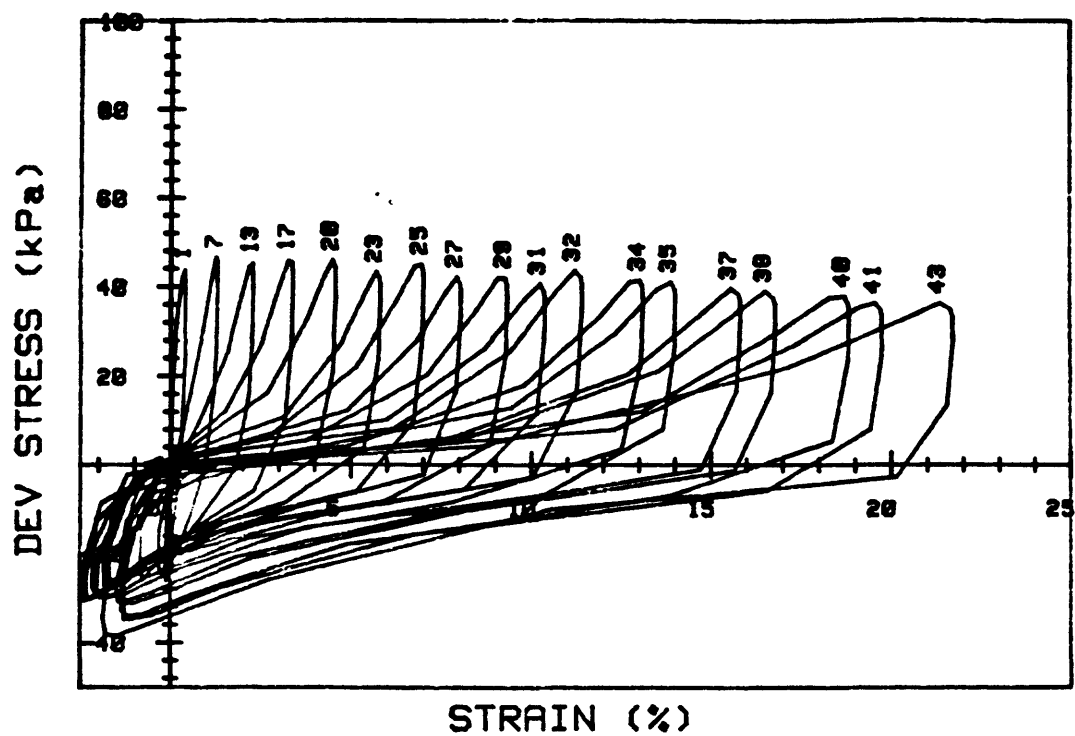


CRUISE DC1-81-EG	INCREMENT (cm)	93-104
CORE NO. 627G2	TEST NO.	TC35
SIG1 $c'$ (kPa) 99.5	STATIC $q_f$ (kPa)	53.2
SIG3 $c'$ (kPa) 99.5	AVG MAX $q$ (kPa)	11.9 (22.4%)
INDUCED OCR 1.0	AVG MIN $q$ (kPa)	-26.4 (49.6%)

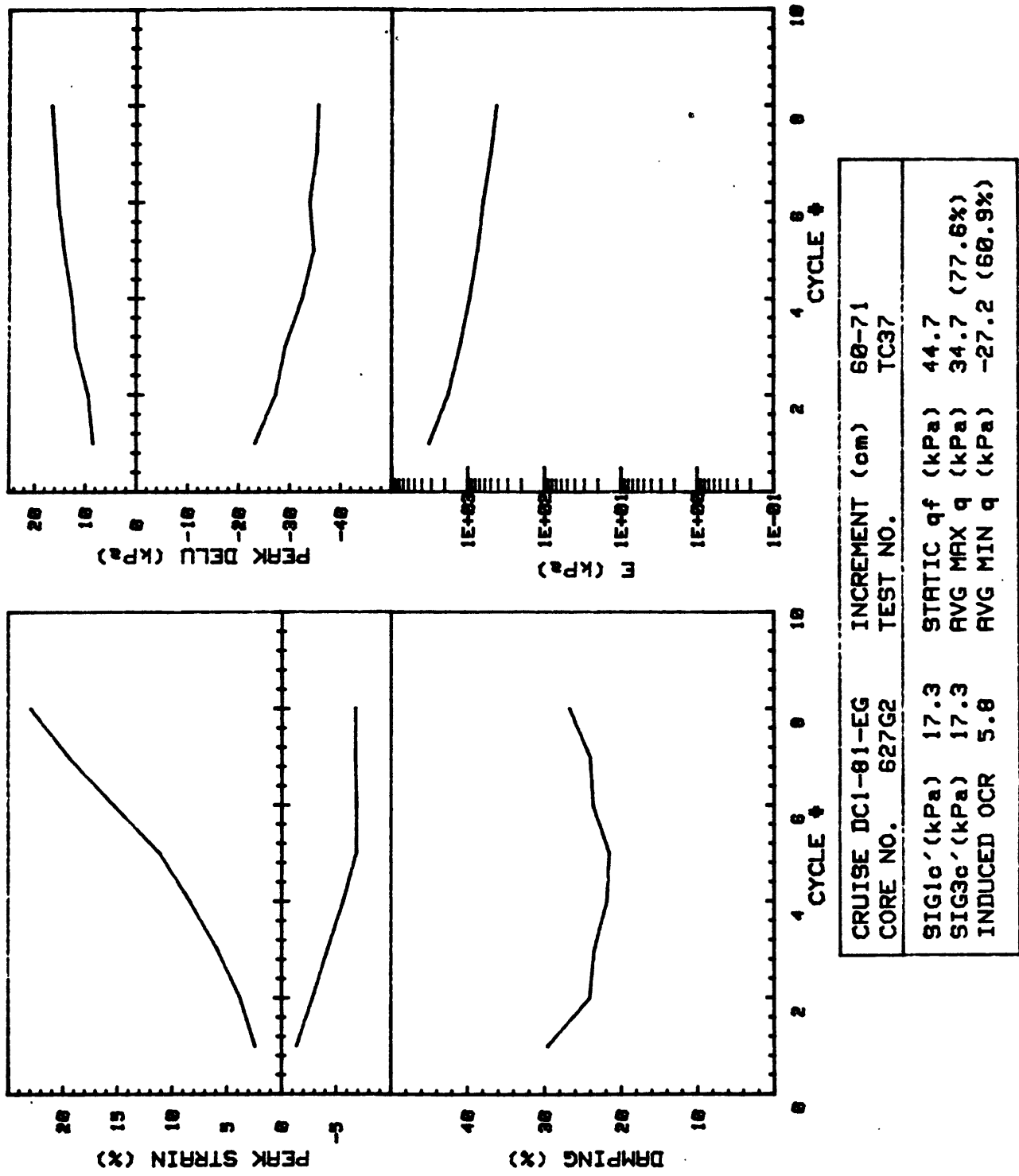


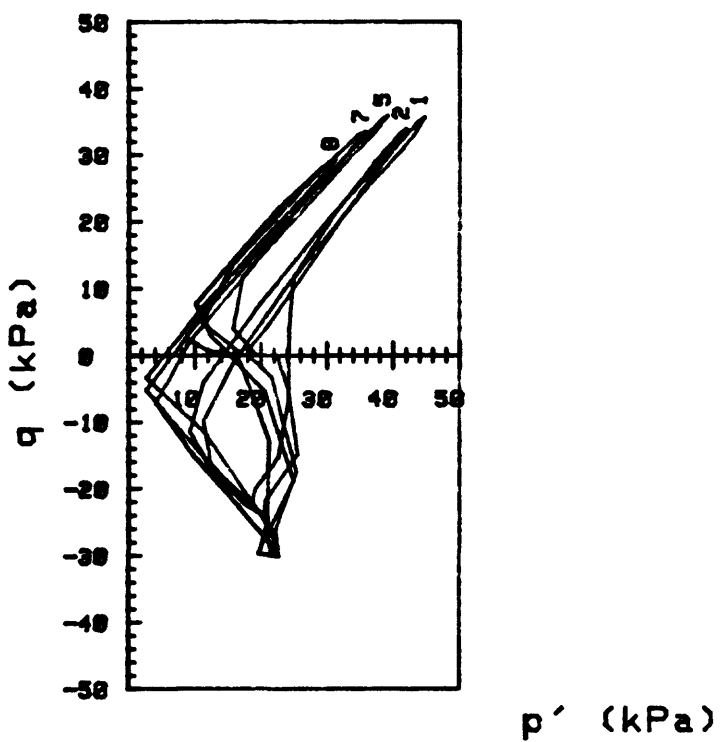
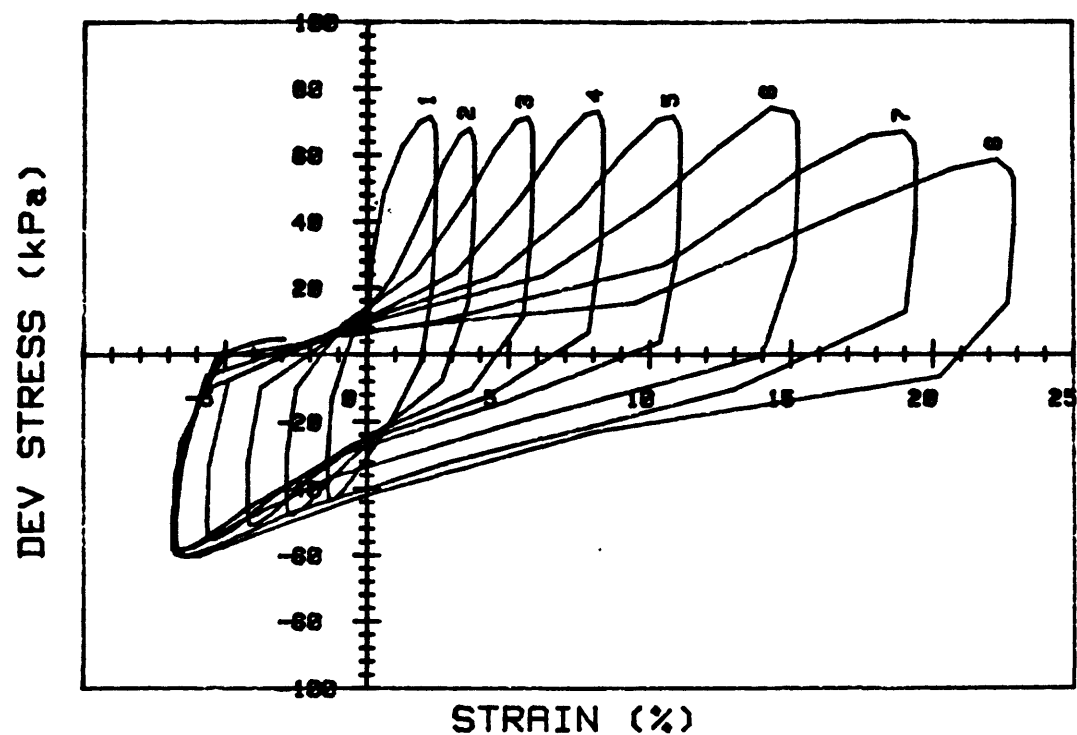
CRUISE DC1-81-EG		INCREMENT (cm)	60-71
CORE NO. 627G2		TEST NO.	TC36
SIG1c' (kPa)	18.3	STATIC $q_f$ (kPa)	44.7
SIG3c' (kPa)	18.3	Avg MAX $q$ (kPa)	21.5 (48.1%)
INDUCED OCR	5.5	Avg MIN $q$ (kPa)	-14.0 (31.3%)



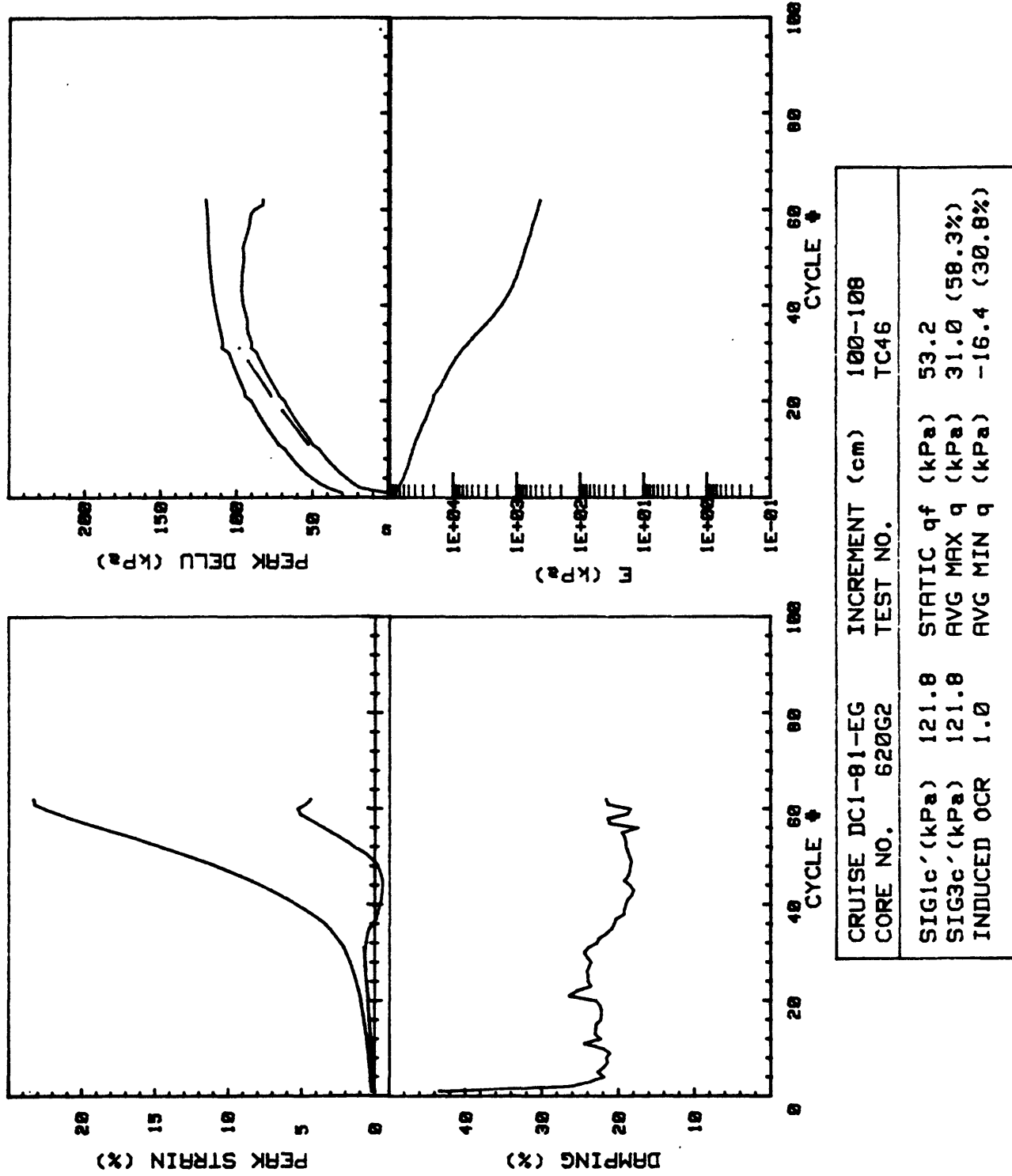


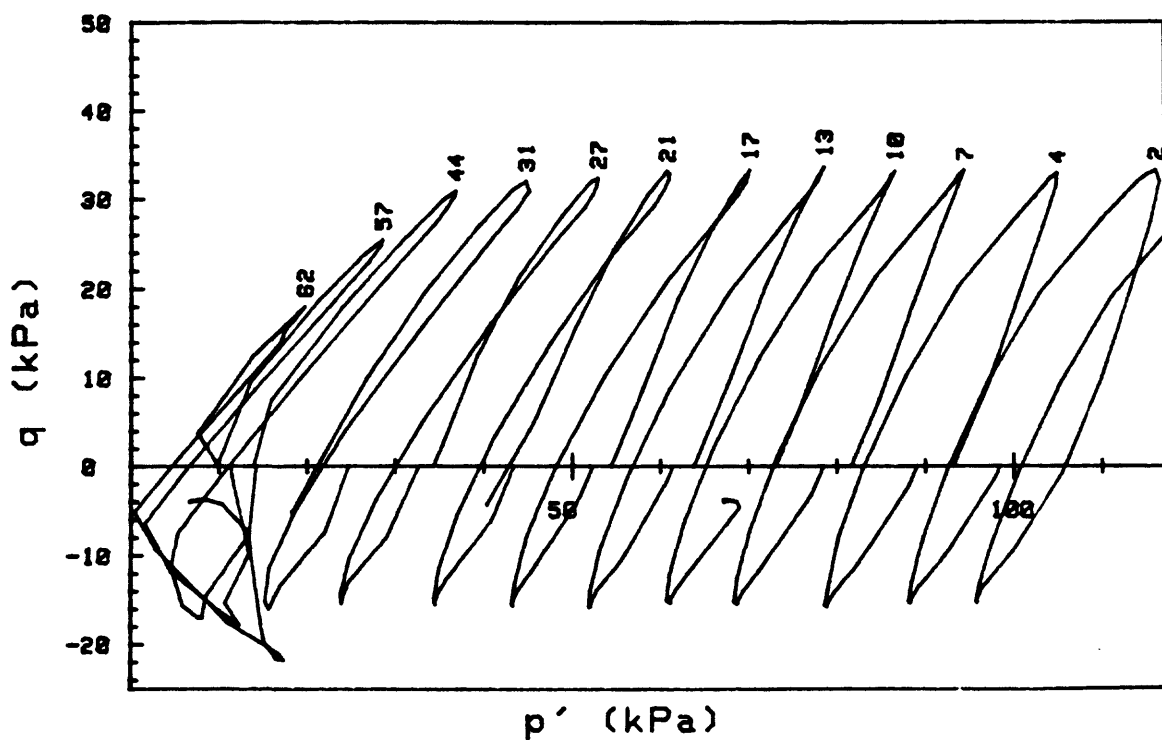
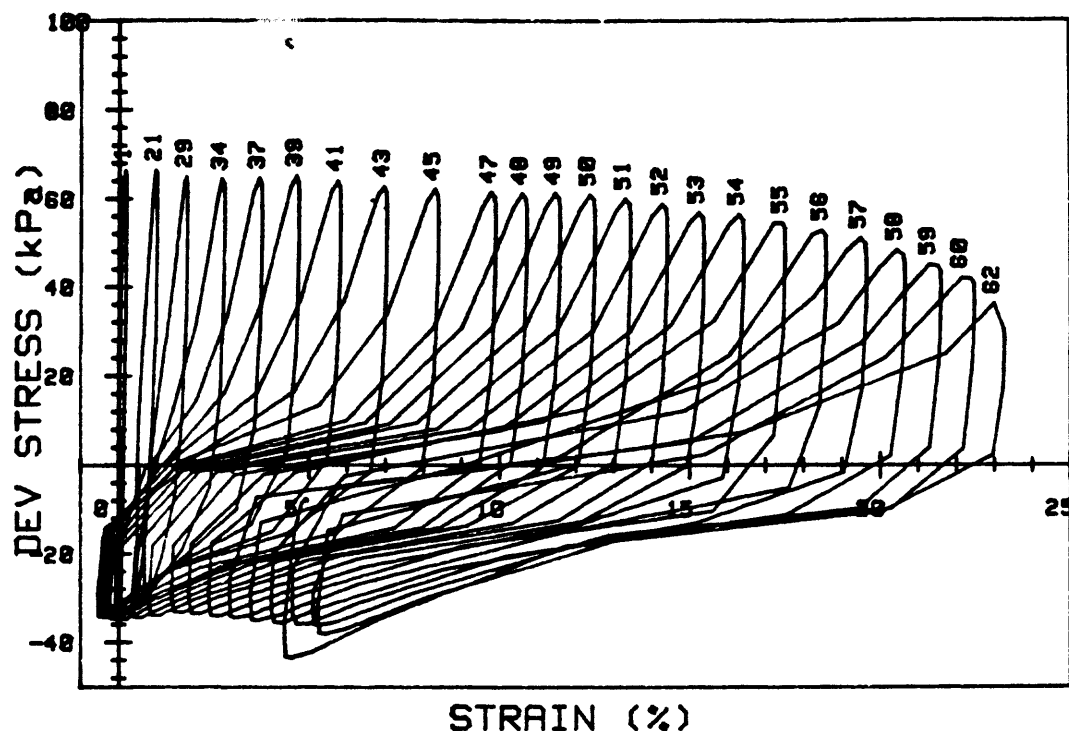
CRUISE DC1-B1-EG CORE NO. 627G2	INCREMENT (cm) TEST NO.	60-71 TC36
SIG1 $c'$ (kPa)	18.3	STATIC $q_f$ (kPa) 44.7
SIG3 $c'$ (kPa)	18.3	AVG MAX $q$ (kPa) 21.5 (48.1%)
INDUCED OCR	5.5	AVG MIN $q$ (kPa) -14.0 (31.3%)



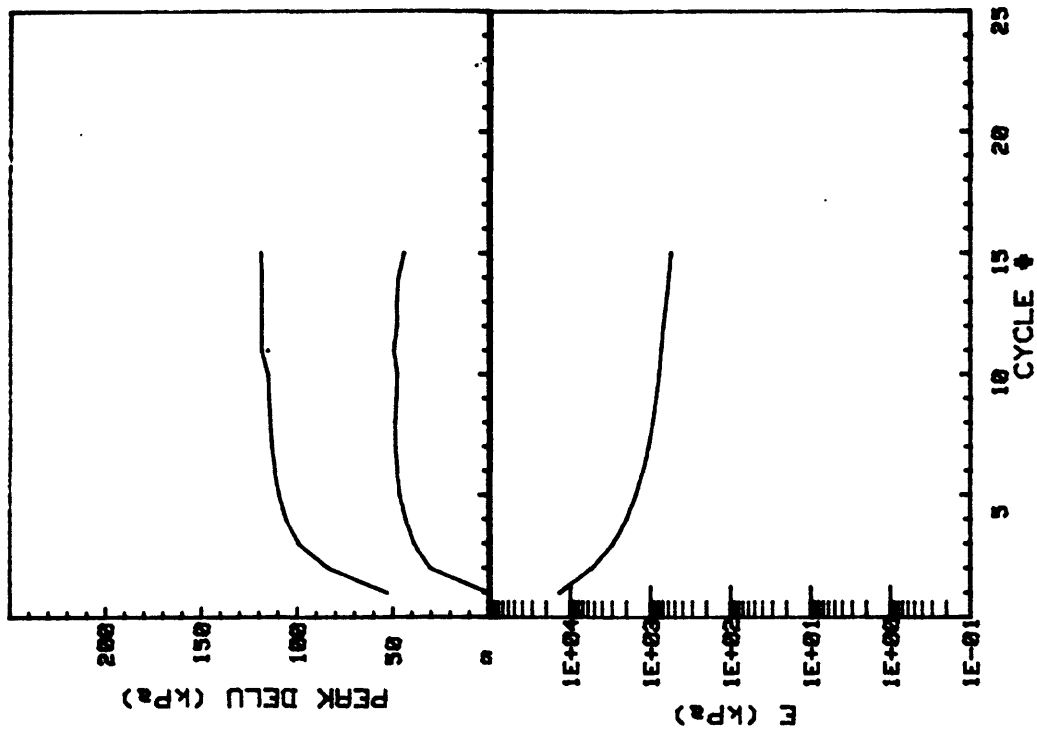


CRUISE DC1-81-EG	INCREMENT (cm)	60-71	
CORE NO. 627G2	TEST NO.	TC37	
SIG1c'(kPa)	17.3	STATIC q <sub>f</sub> (kPa)	44.7
SIG3c'(kPa)	17.3	AVG MAX q (kPa)	34.7 (77.6%)
INDUCED OCR	5.8	AVG MIN q (kPa)	-27.2 (60.9%)

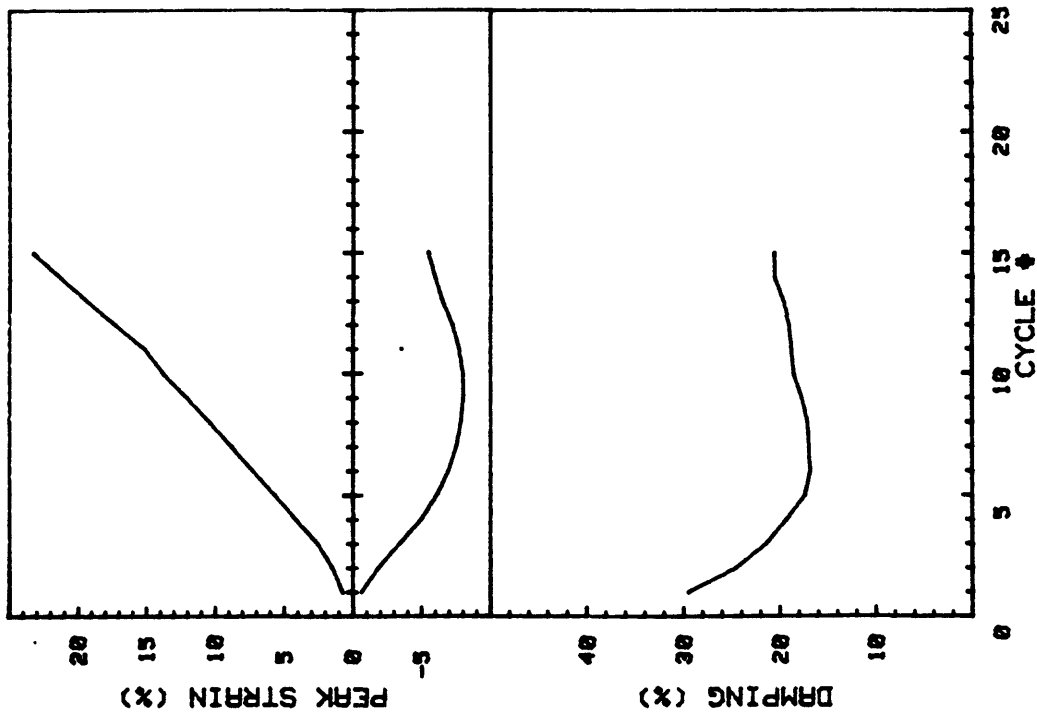


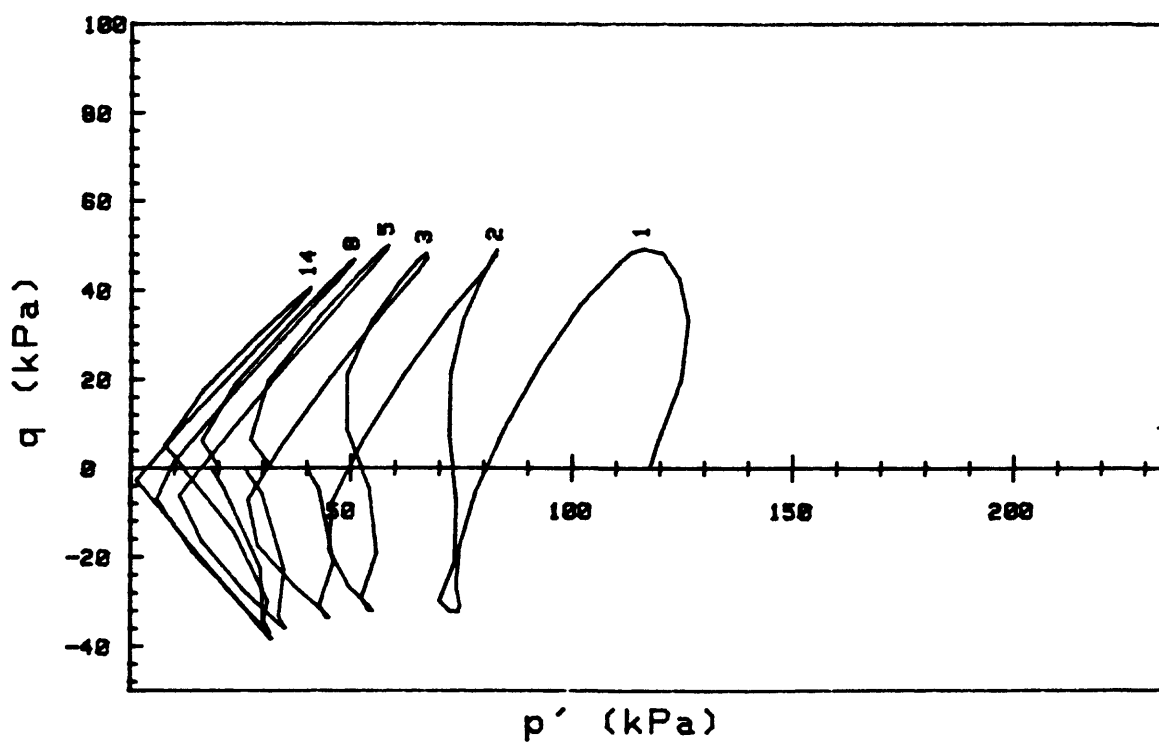
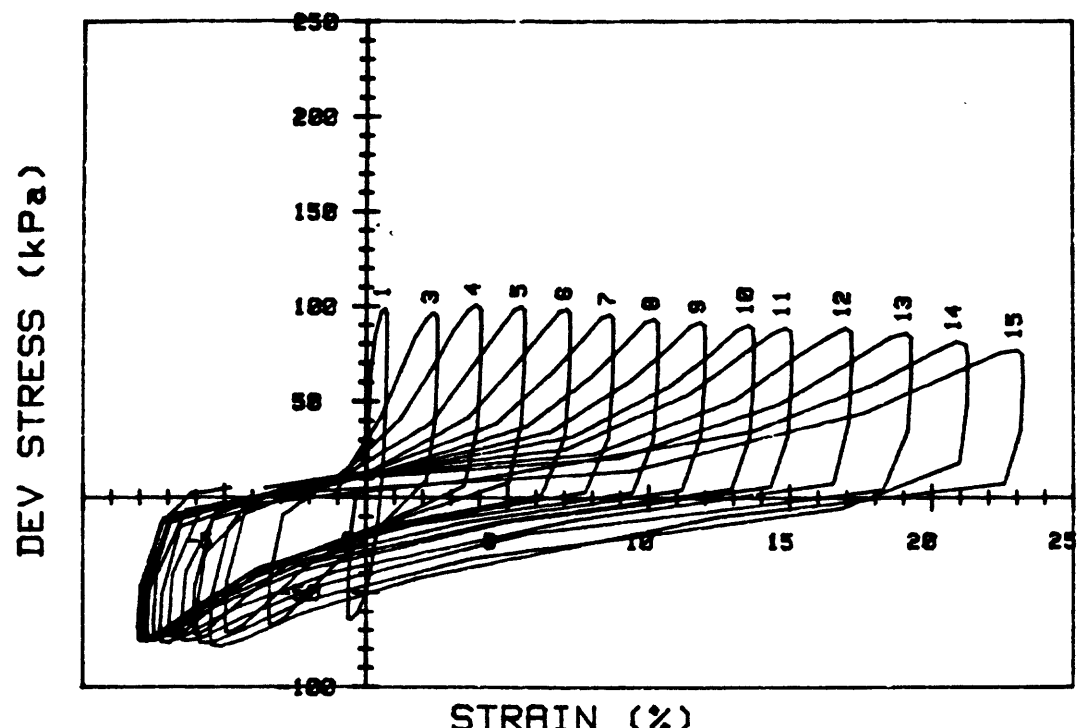


CRUISE DC1-81-EG CORE NO. 620G2	INCREMENT (cm) TEST NO.	100-108 TC46
SIG1c'(kPa)	121.8	STATIC q <sub>f</sub> (kPa) 53.2
SIG3c'(kPa)	121.8	AVG MAX q (kPa) 31.0 (58.3%)
INDUCED OCR	1.0	AVG MIN q (kPa) -16.4 (30.8%)

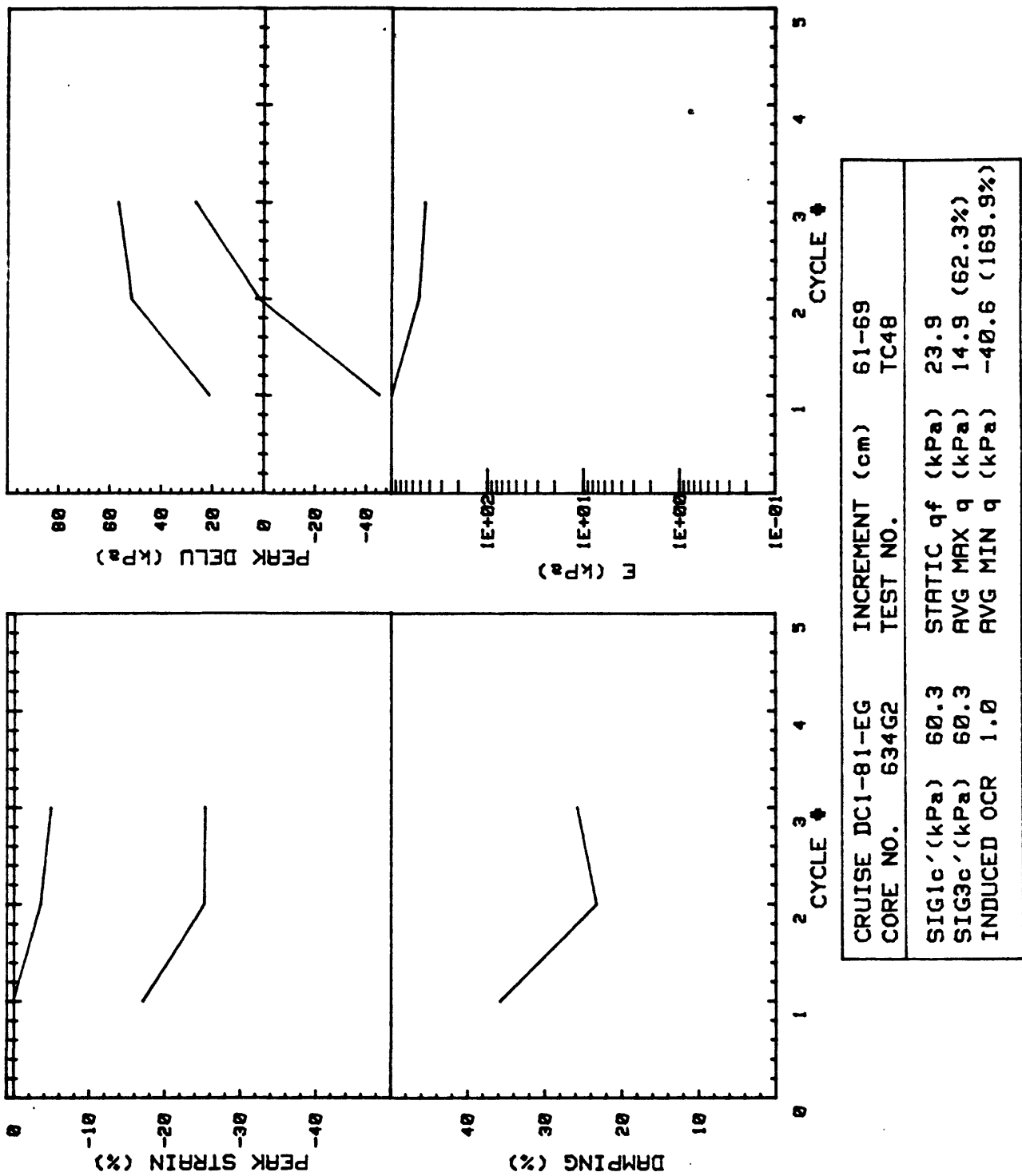


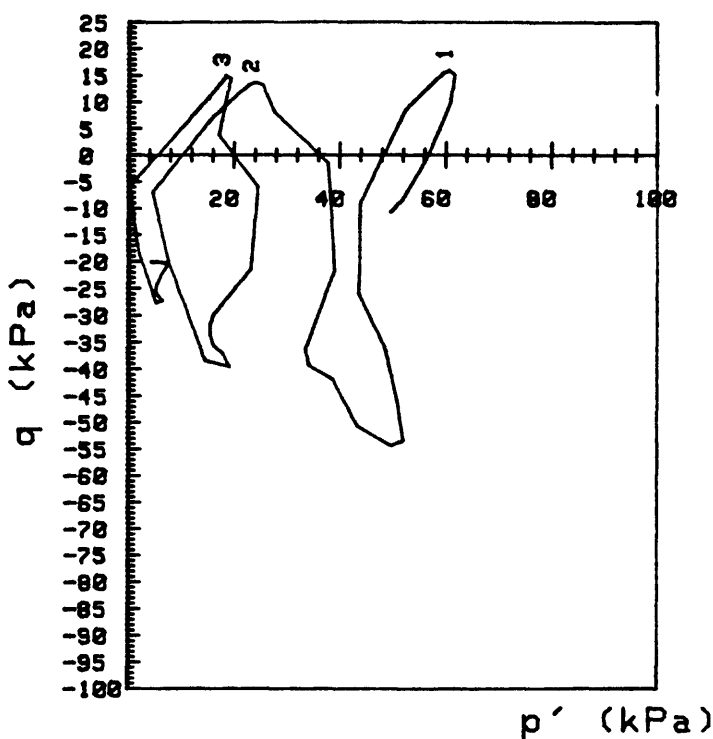
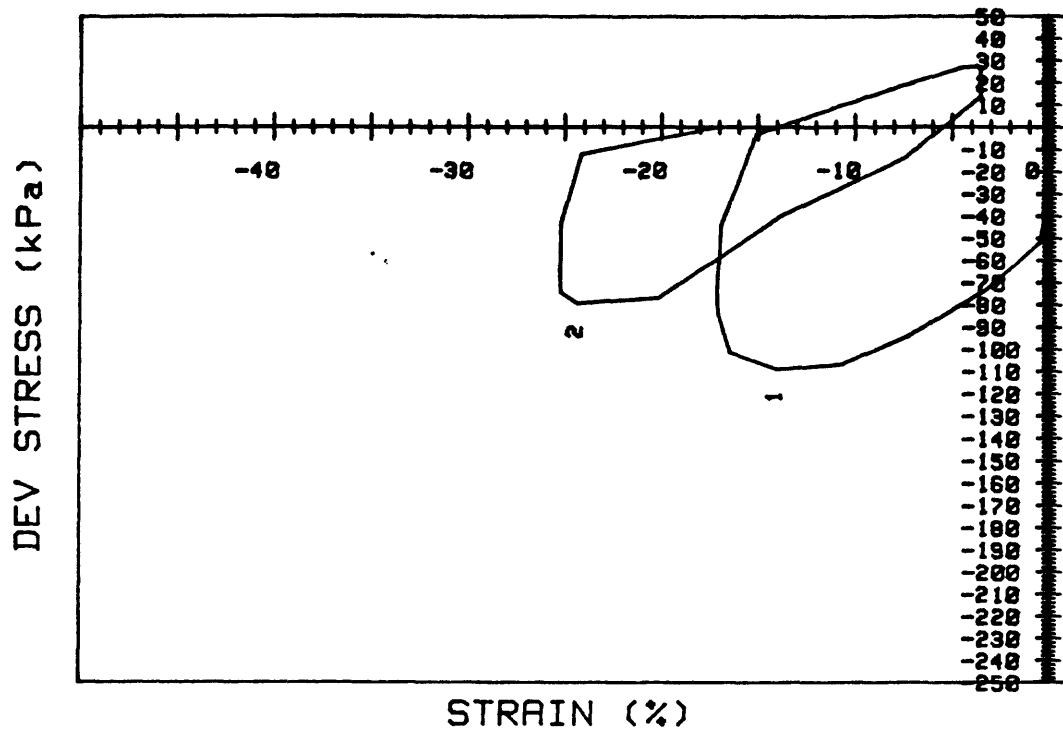
CRUISE DC1-81-EG CORE NO. 620G2		
	INCREMENT (cm)	TEST NO.
SIG1' (kPa)	117.6	STATIC q <sub>f</sub> (kPa)
SIG3c' (kPa)	117.6	Avg MAX q (kPa)
INDUCED OCR	1.0	Avg MIN q (kPa)
		53.2 (86.7%)
		46.1 (86.7%)
		-36.4 (68.4%)



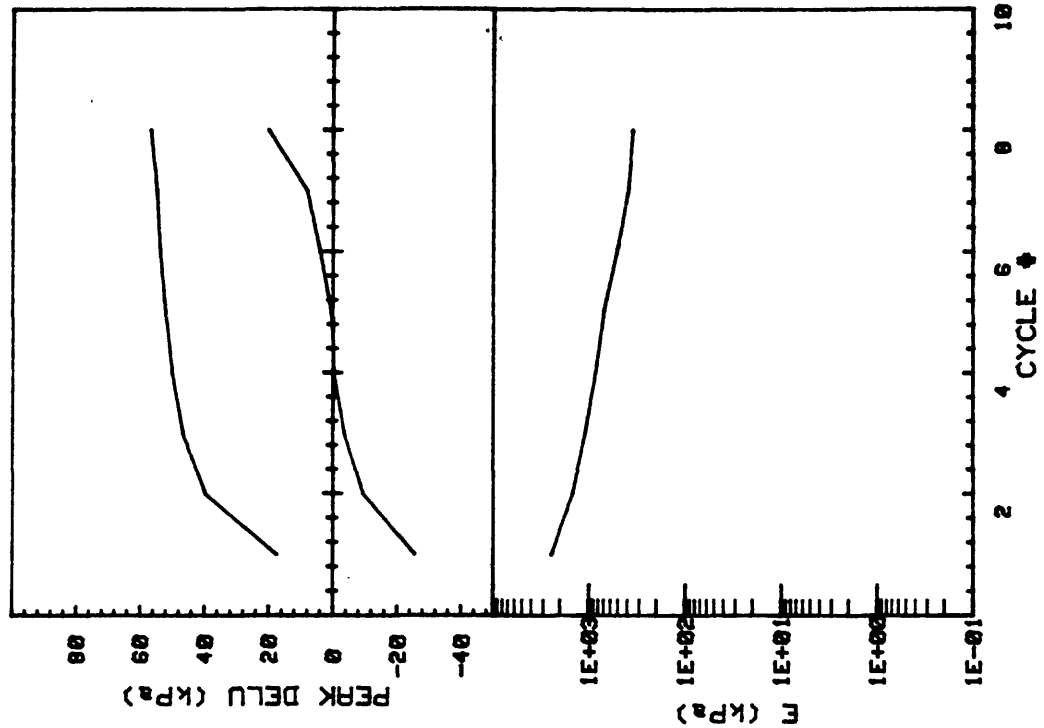


CRUISE DC1-81-EG CORE NO. 620G2	INCREMENT (cm) TEST NO.	100-108 TC47
SIG1c'(kPa)	117.6	STATIC q <sub>f</sub> (kPa) 53.2
SIG3c'(kPa)	117.6	AVG MAX q (kPa) 46.1 (86.7%)
INDUCED OCR	1.0	AVG MIN q (kPa) -3E.4 (68.4%)

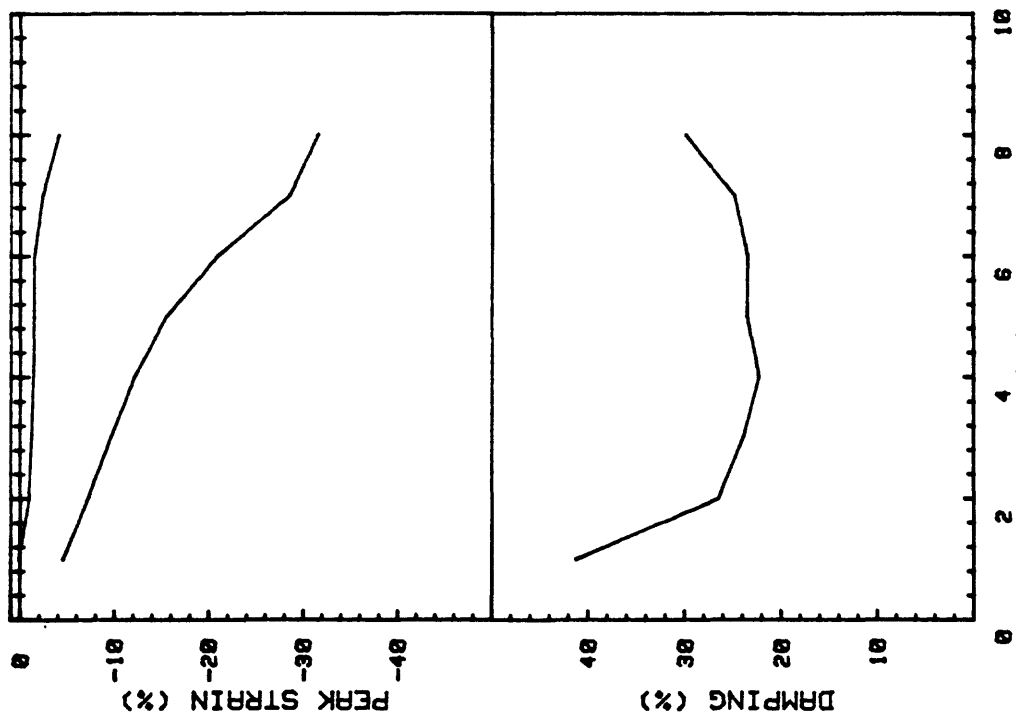


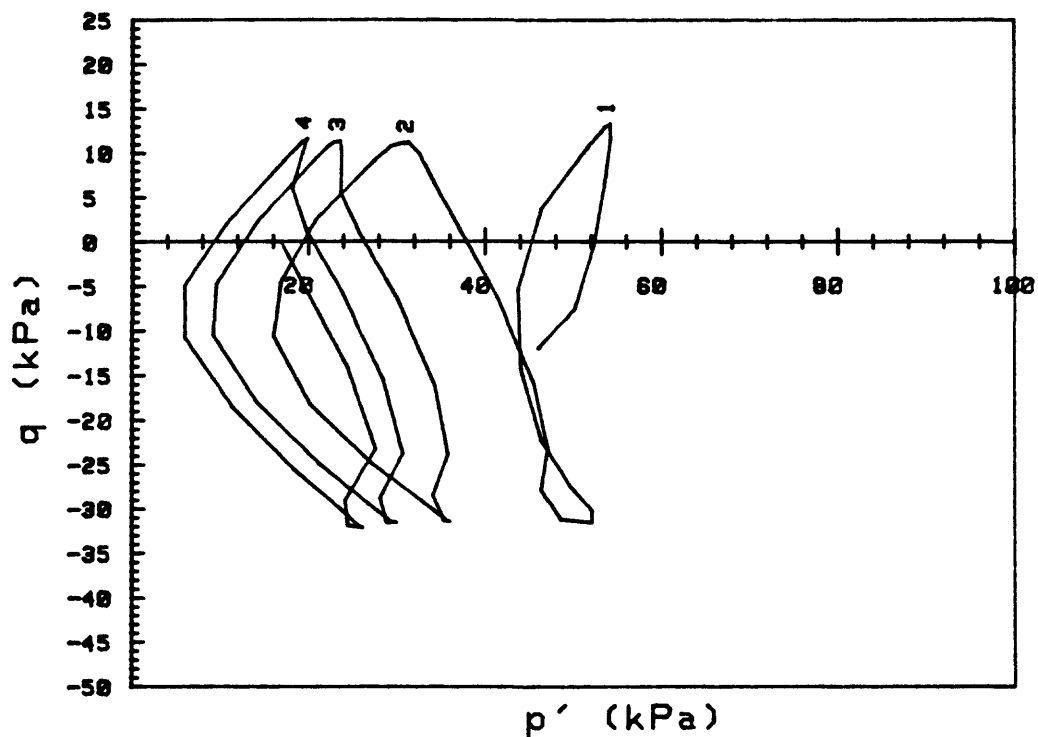
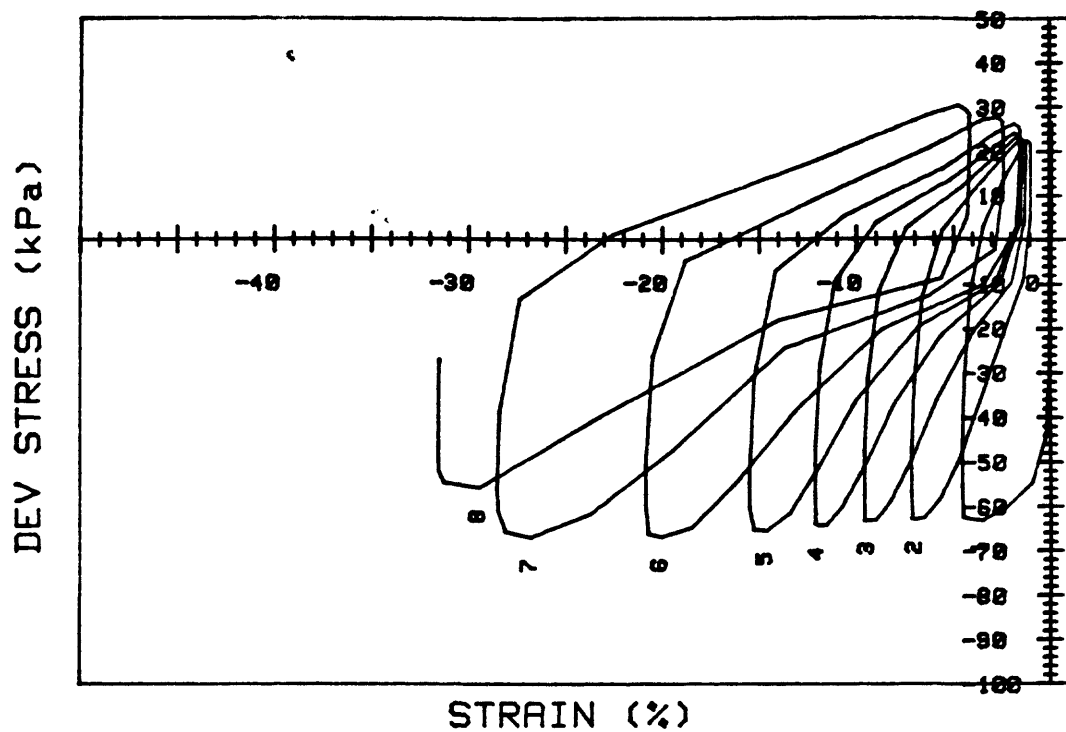


CRUISE DC1-81-EG	INCREMENT (cm)	61-69
CORE NO. 634G2	TEST NO.	TC48
SIG1c'(kPa) 60.3	STATIC qf (kPa)	23.9
SIG3c'(kPa) 60.3	AVG MAX q (kPa)	14.9 (62.3%)
INDUCED OCR 1.0	AVG MIN q (kPa)	-40.6 (169.9%)

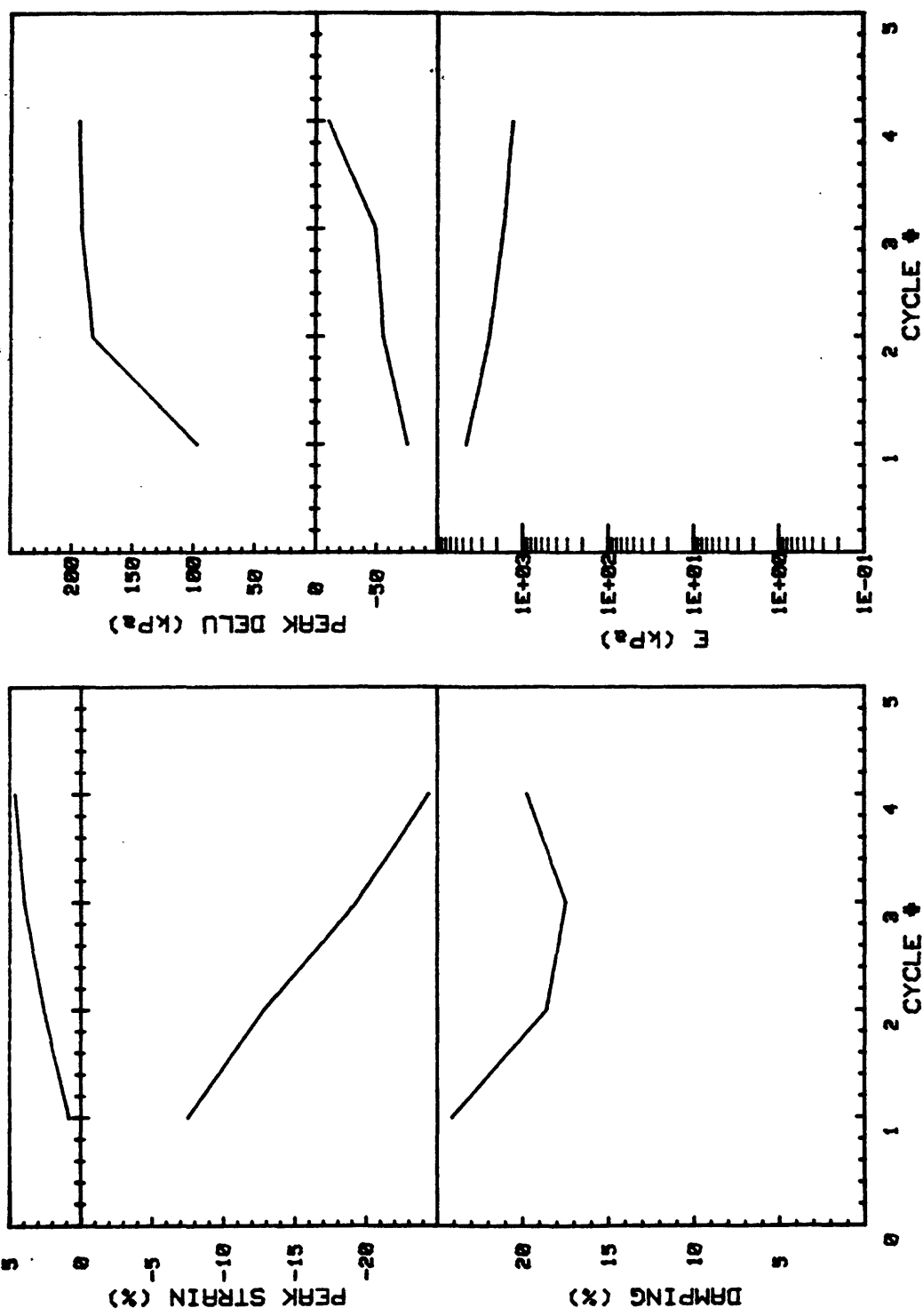


CRUISE DC1-81-EG	INCREMENT (cm)	61-68
CORE NO.	TEST NO.	TC49
SIG1c' (kPa)	STATIC q <sub>f</sub> (kPa)	23.9
SIG3c' (kPa)	Avg MAX q (kPa)	12.7 (53.1%)
INDUCED OCR	Avg MIN q (kPa)	-31.8 (-133.1%)

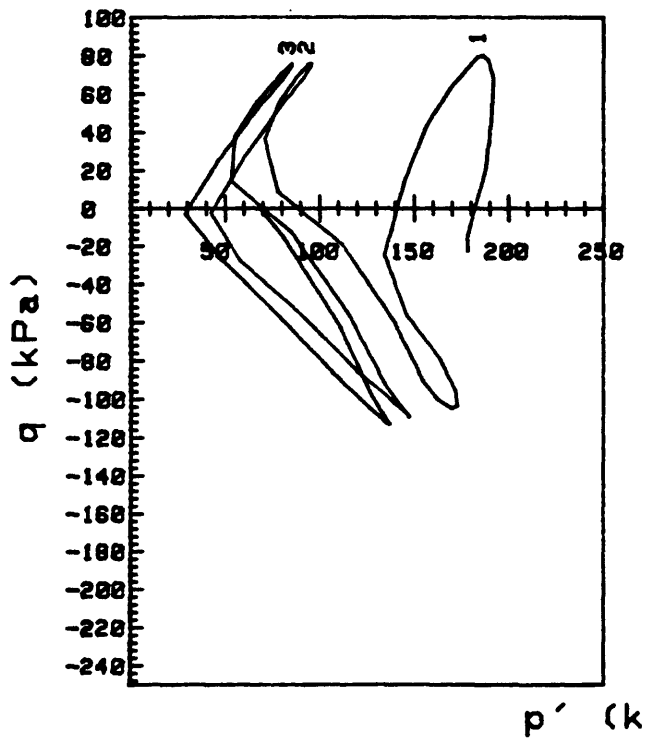
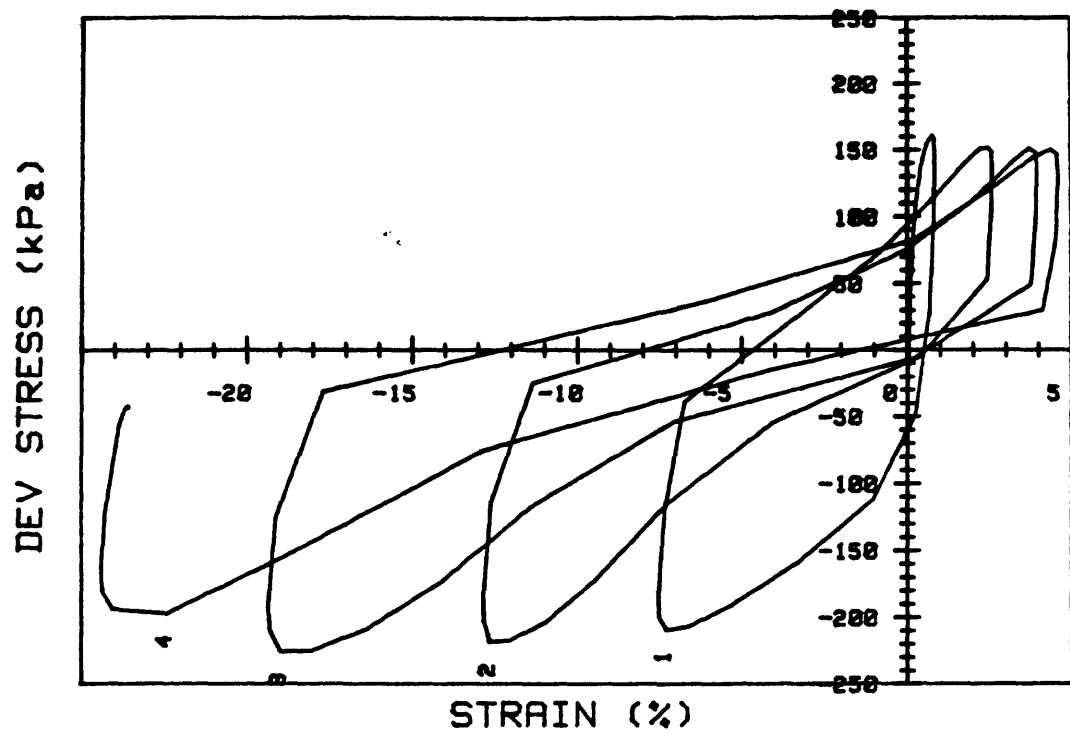




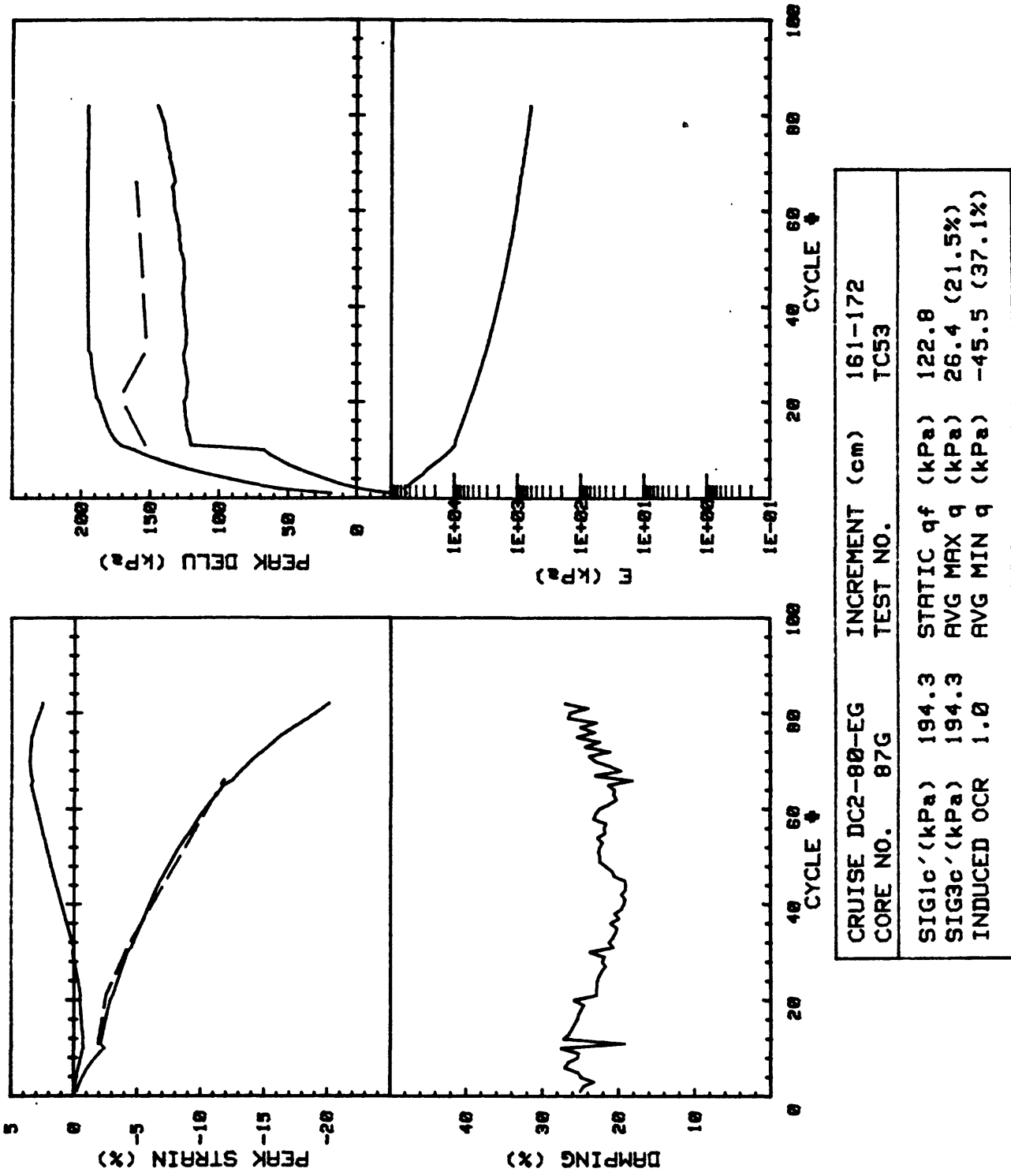
CRUISE DC1-81-EG	INCREMENT (cm)	61-68
CORE NO. 634G2	TEST NO.	TC49
SIG1c'(kPa) 58.1	STATIC q <sub>f</sub> (kPa)	23.9
SIG3c'(kPa) 58.1	AVG MAX q (kPa)	12.7 (53.1%)
INDUCED OCR 1.0	AVG MIN q (kPa)	-31.8 (133.1%)

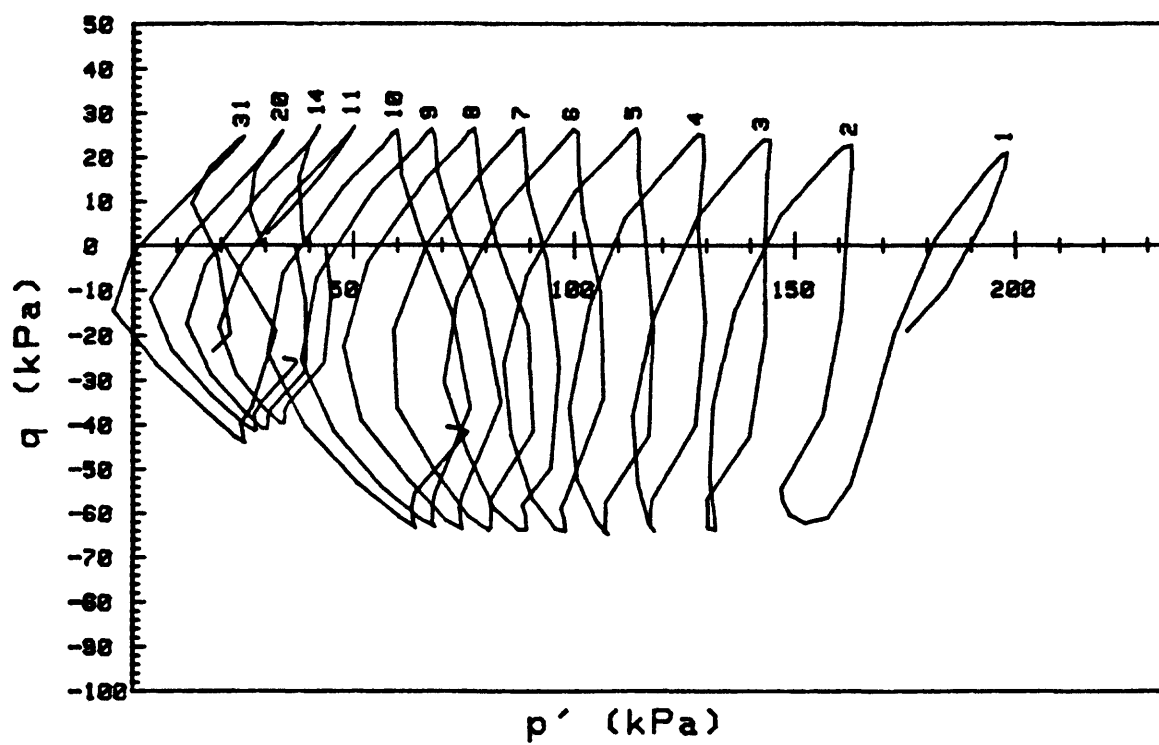
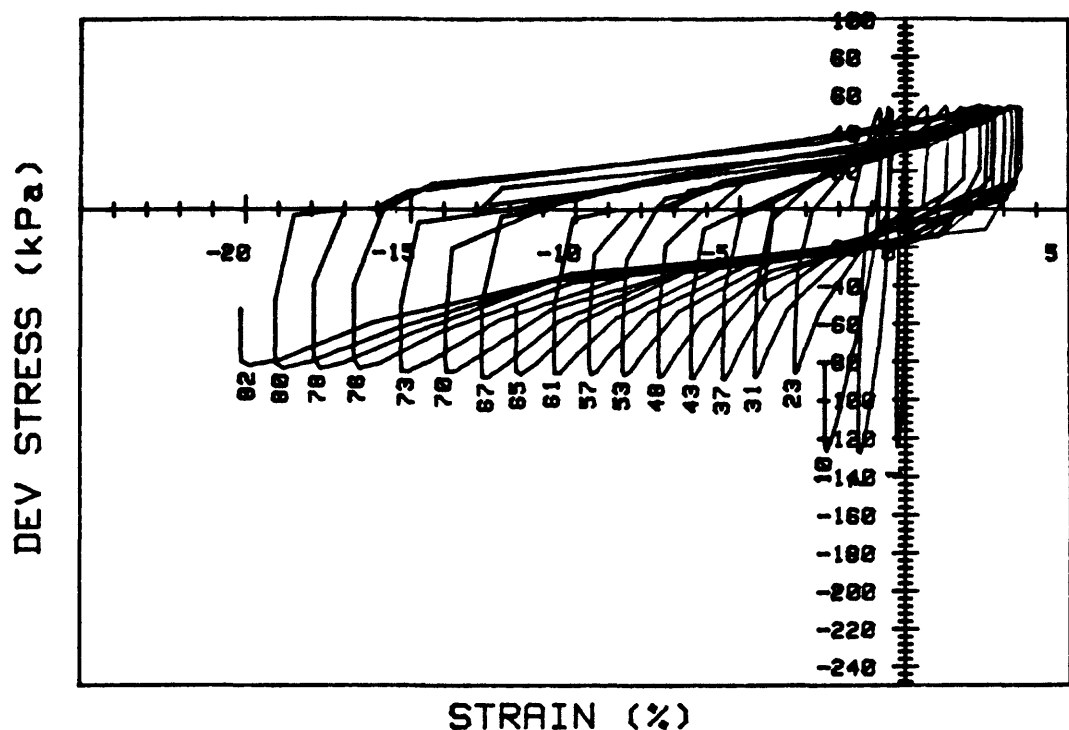


CRUISE DC2-80-EG		INCREMENT (cm)	161-172
CORE NO.	TEST NO.		TC52
SIG1c' (kPa)	200.9	STATIC q <sub>f</sub> (kPa)	122.8
SIG3c' (kPa)	200.9	AVG MAX q (kPa)	76.8 (62.5%)
INDUCED OCR	1.0	AVG MIN q (kPa)	-106.3 (86.6%)

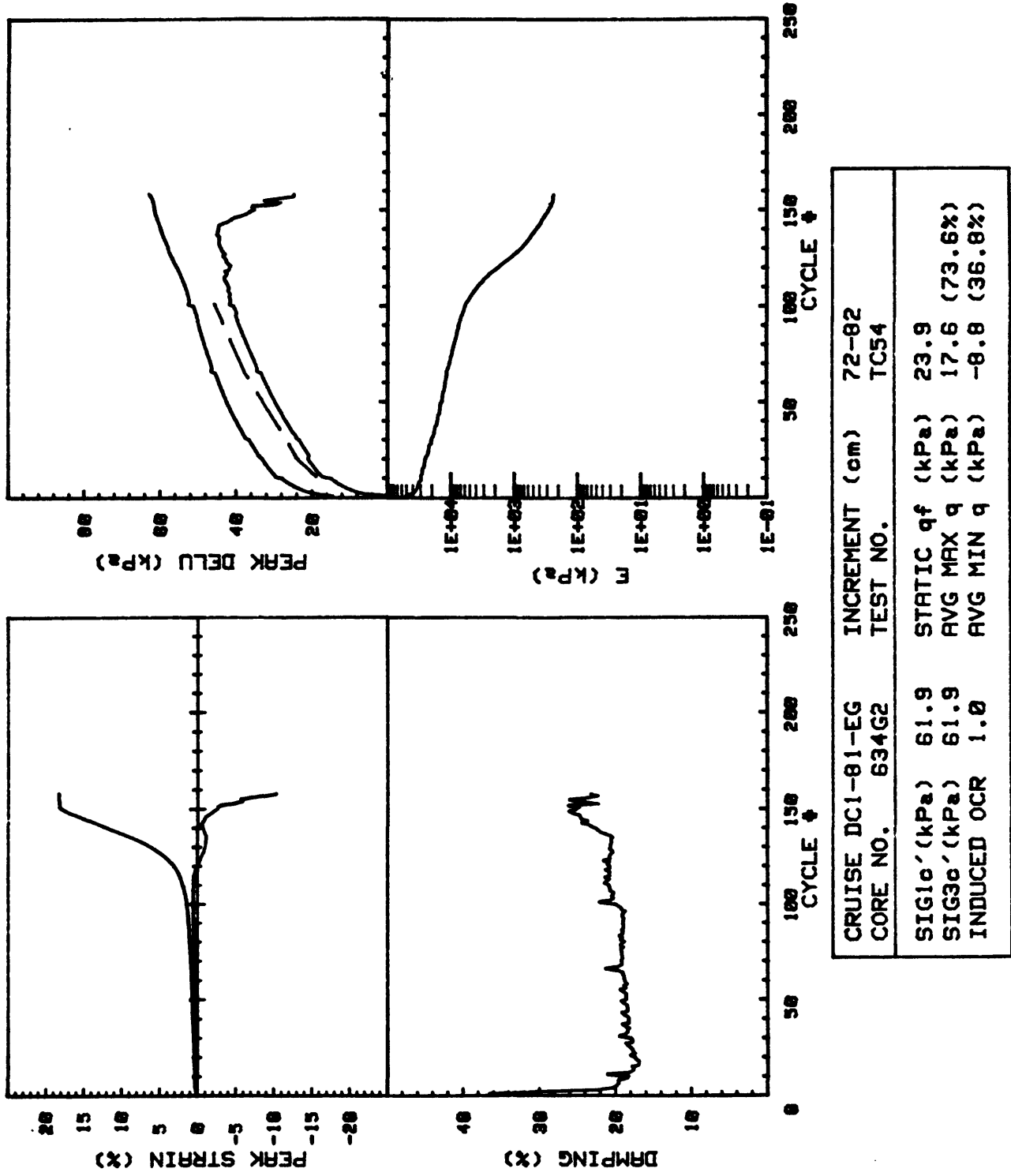


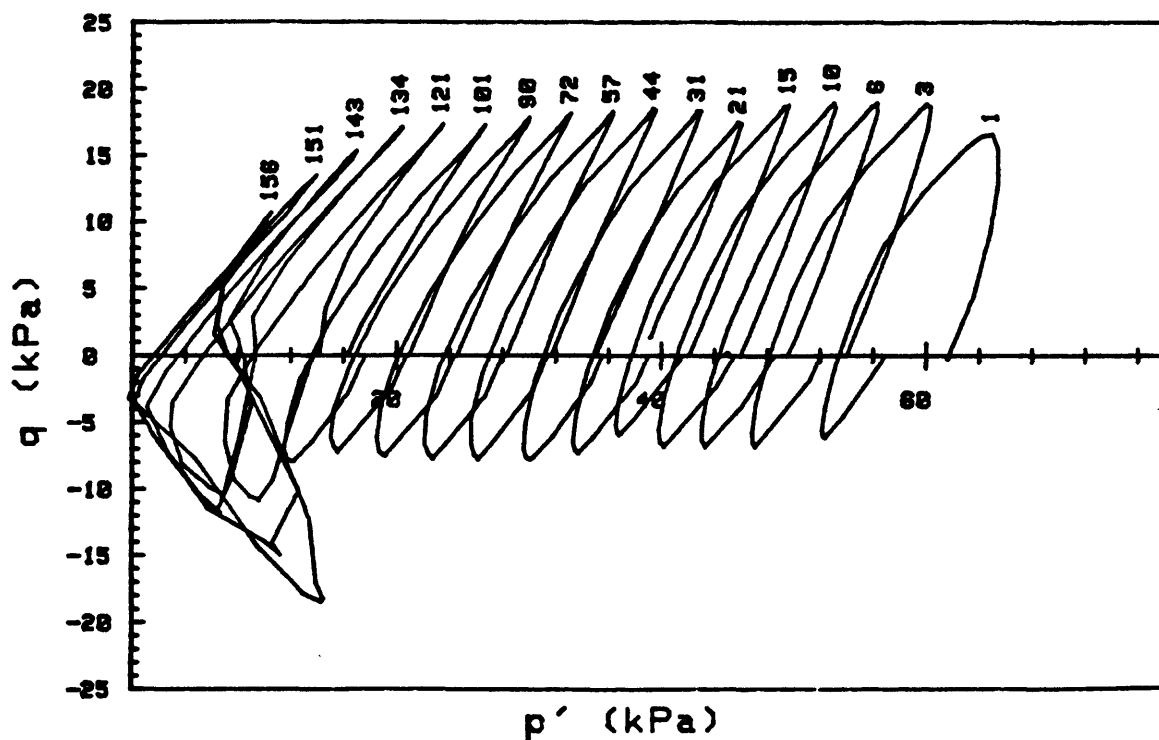
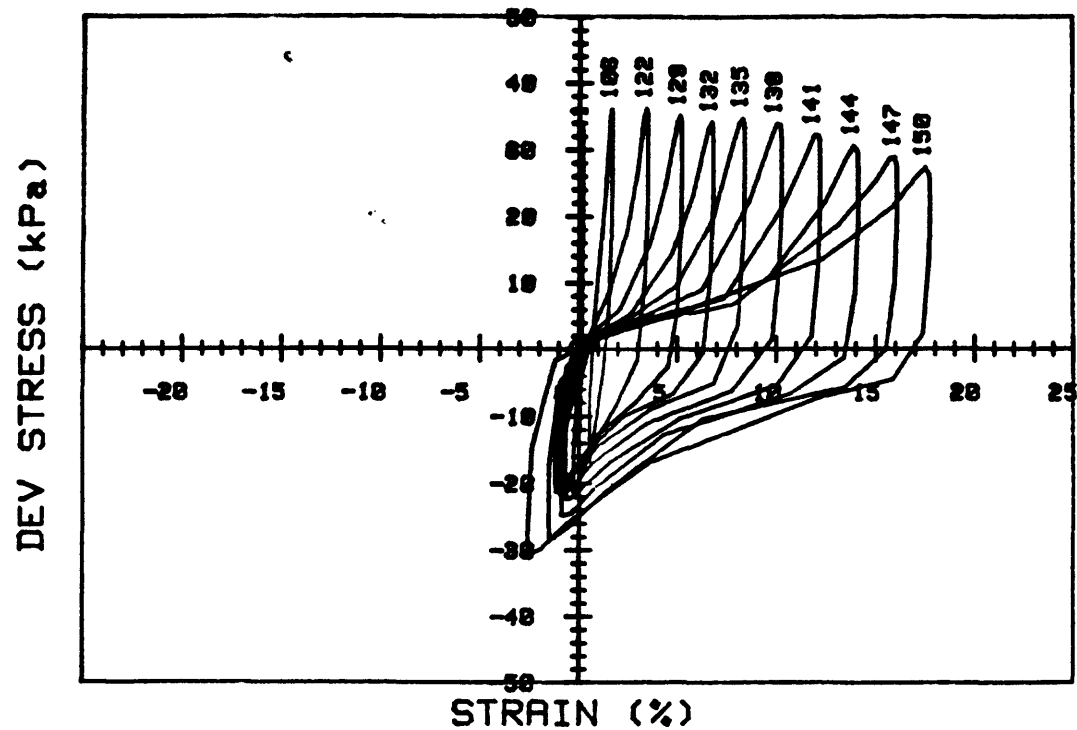
CRUISE DC2-80-EG CORE NO. 87G	INCREMENT (cm) TEST NO.	161-172 TC52
SIG1c' (kPa)	200.9	STATIC qf (kPa) 122.8
SIG3c' (kPa)	200.9	Avg MAX q (kPa) 76.8 (62.5%)
INDUCED OCR	1.0	Avg MIN q (kPa) -106.3 (86.6%)



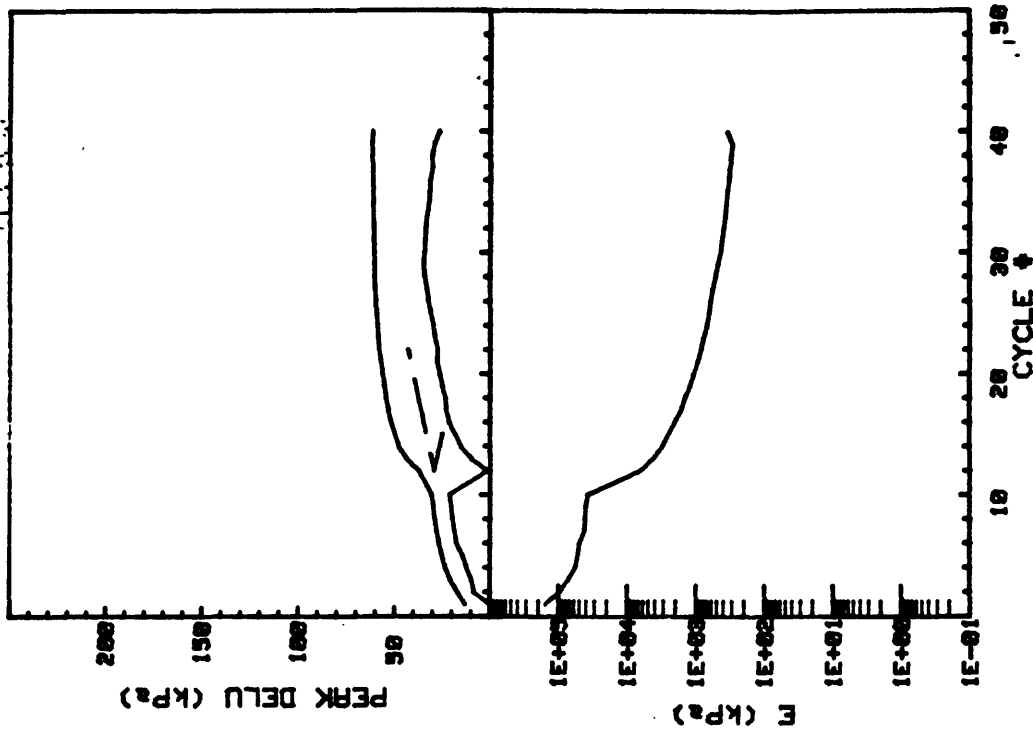


CRUISE DC2-80-EG	INCREMENT (cm)	161-172	
CORE NO. 87G	TEST NO.	TC53	
SIG1c'(kPa)	194.3	STATIC q <sub>f</sub> (kPa)	122.8
SIG3c'(kPa)	194.3	AVG MAX q (kPa)	26.4 (21.5%)
INDUCED OCR	1.0	AVG MIN q (kPa)	-45.5 (37.1%)

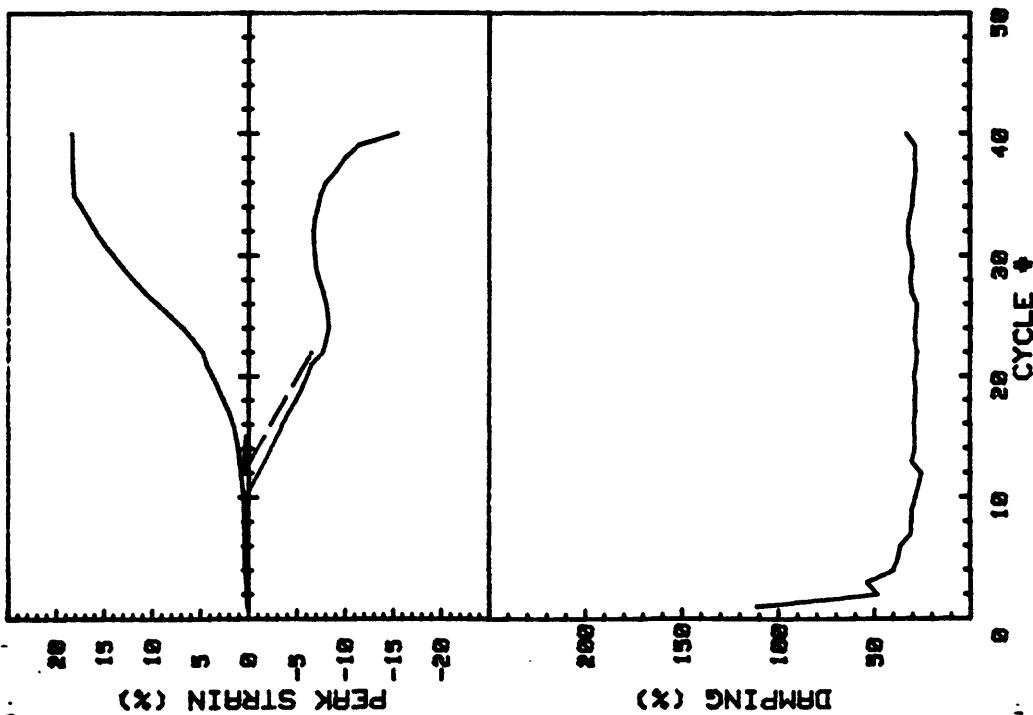




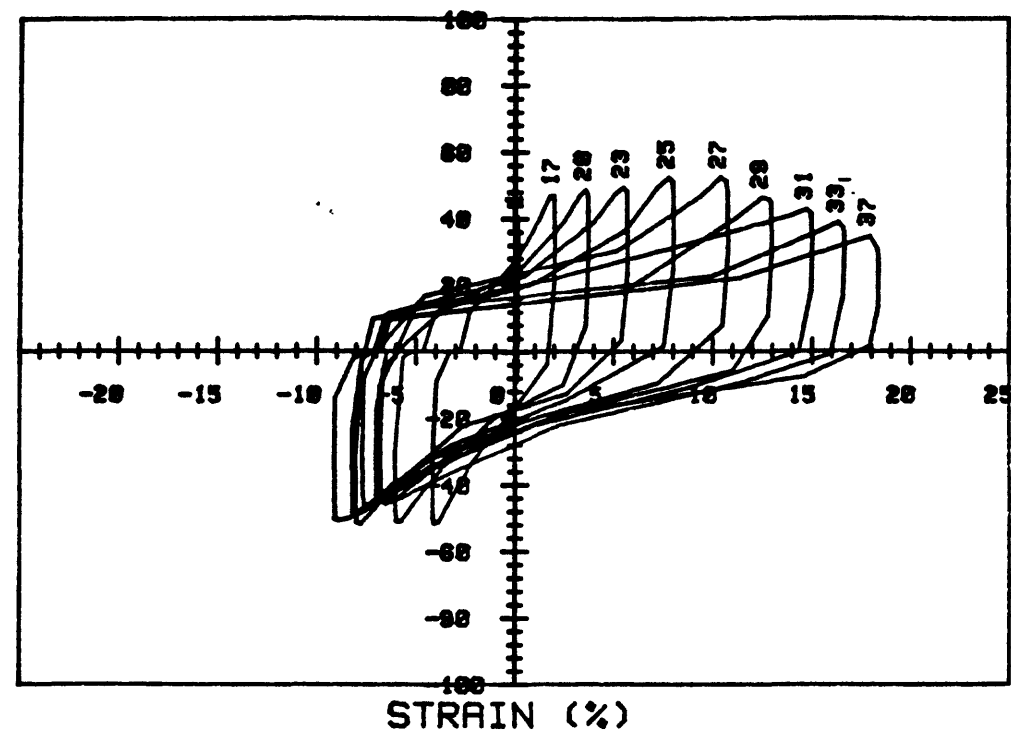
CRUISE DC1-81-EG CORE NO. 634G2	INCREMENT (cm) TEST NO.	72-82 TC54
SIG1c'(kPa)	61.9	STATIC q <sub>f</sub> (kPa) 23.9
SIG3c'(kPa)	61.9	AVG MAX q (kPa) 17.6 (73.6%)
INDUCED OCR	1.0	AVG MIN q (kPa) -8.8 (36.8%)



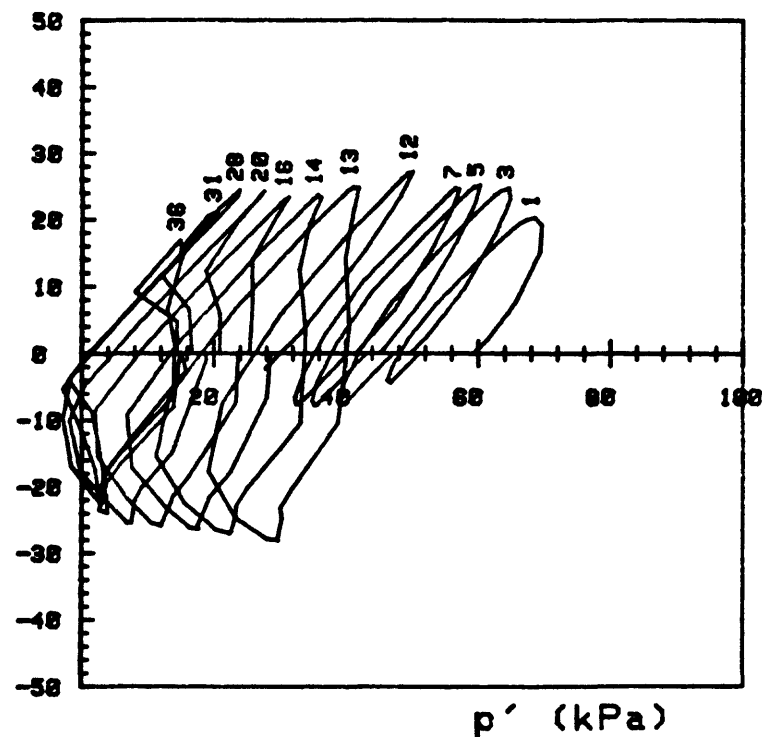
CRUISE DCI-81-EG		INCREMENT (cm)	72-82
CORE NO.	634G2	TEST NO.	TC55
SIG1c' (kPa)	59.3	STATIC q <sub>f</sub> (kPa)	23.9
SIG3c' (kPa)	59.3	Avg MAX q (kPa)	22.2 (92.9%)
INDUCED OCR	1.0	Avg MIN q (kPa)	-19.9 (83.3%)

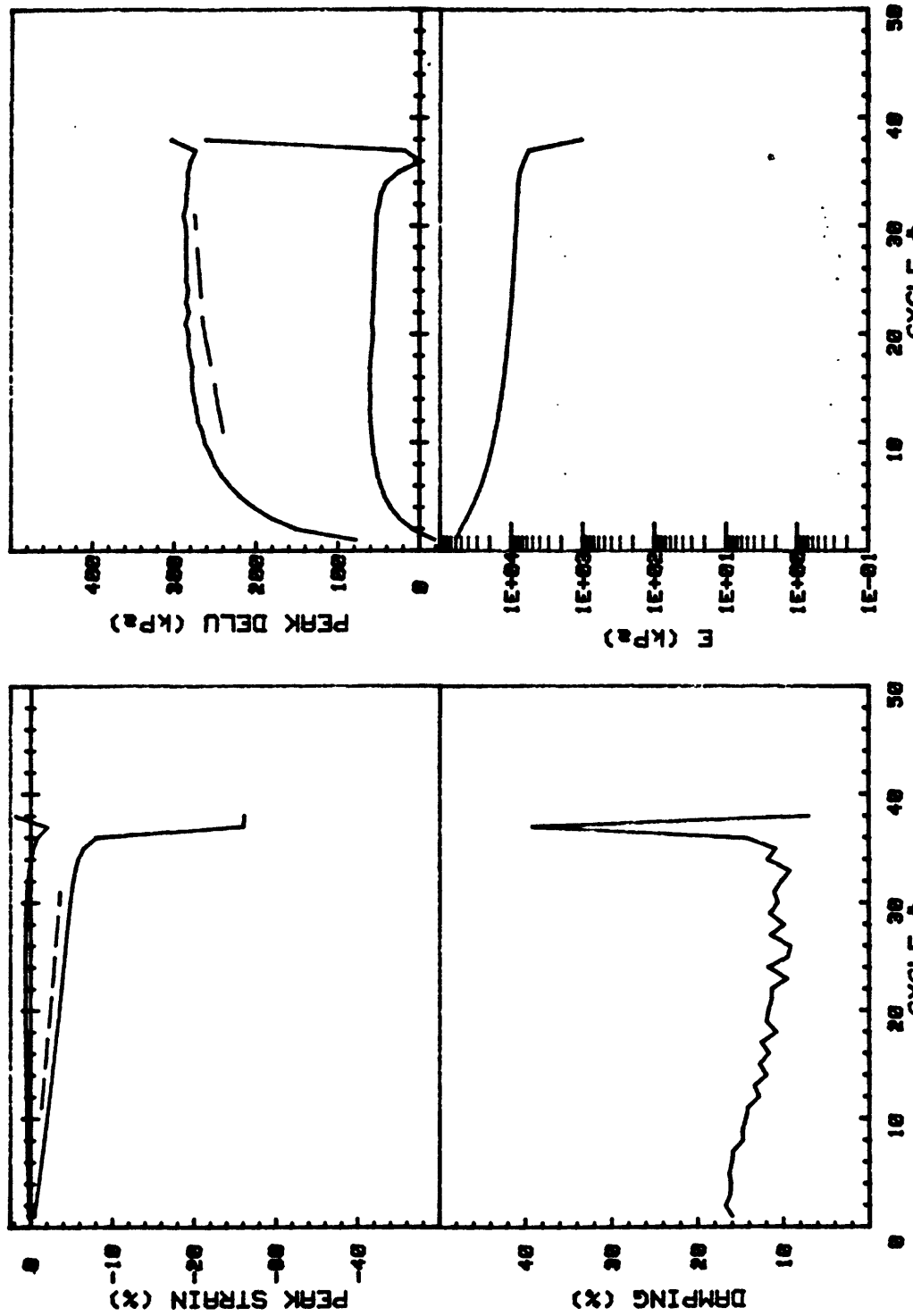


DEV STRESS (kPa)

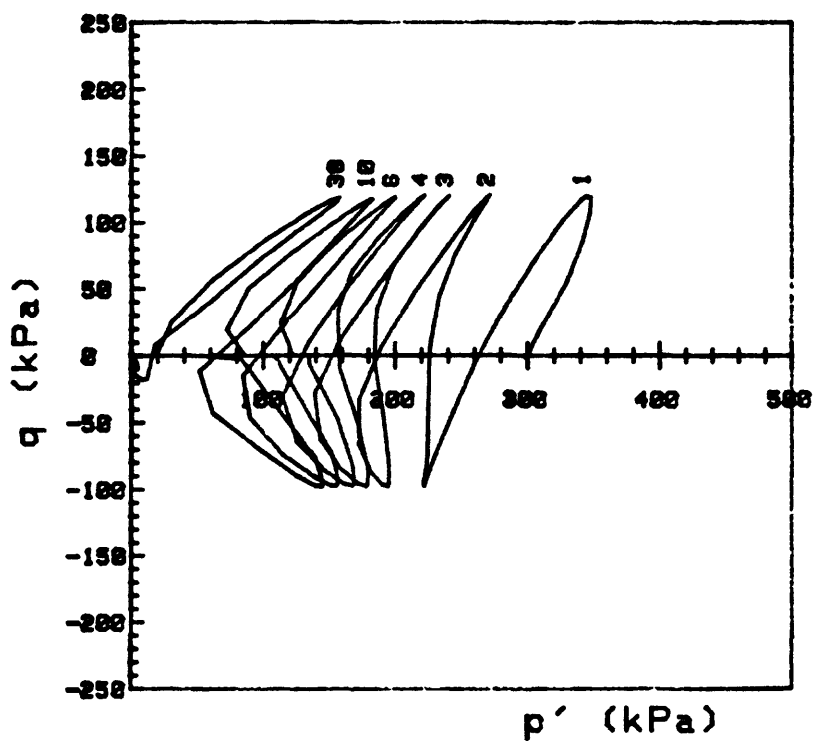
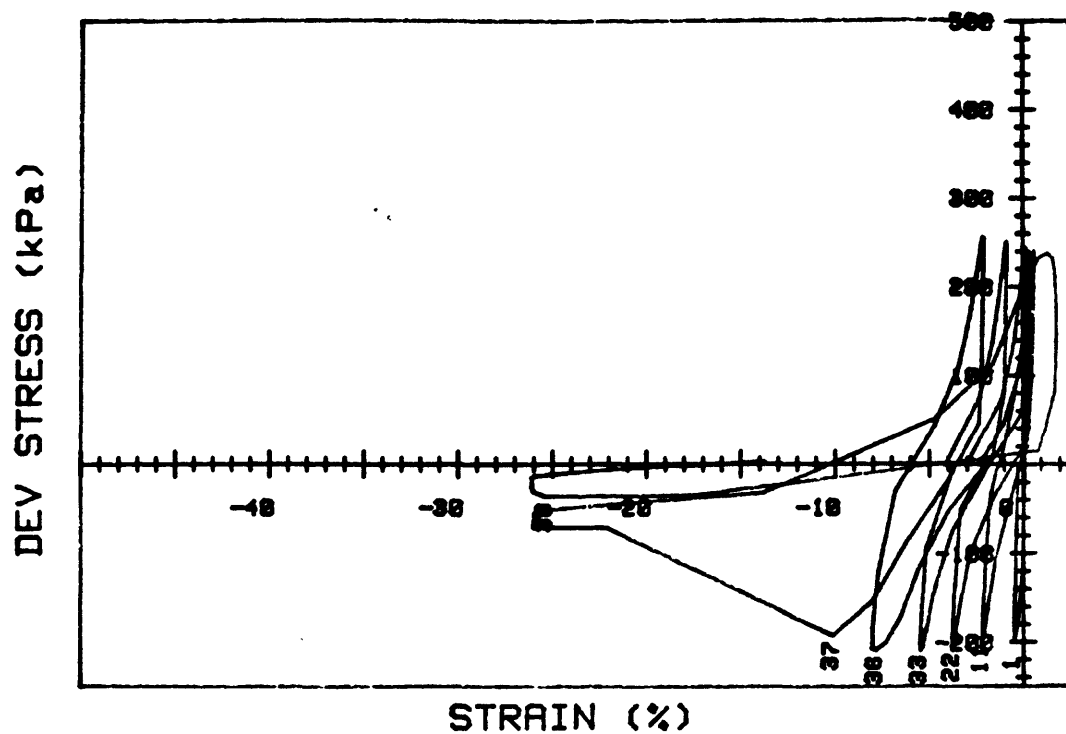


q (kPa)

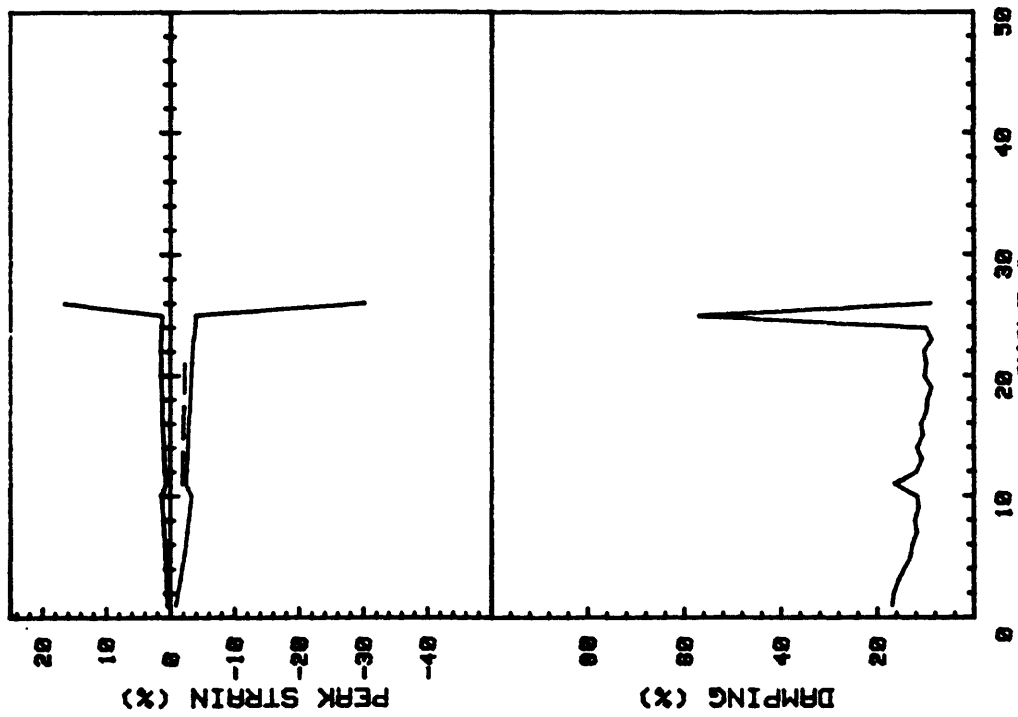
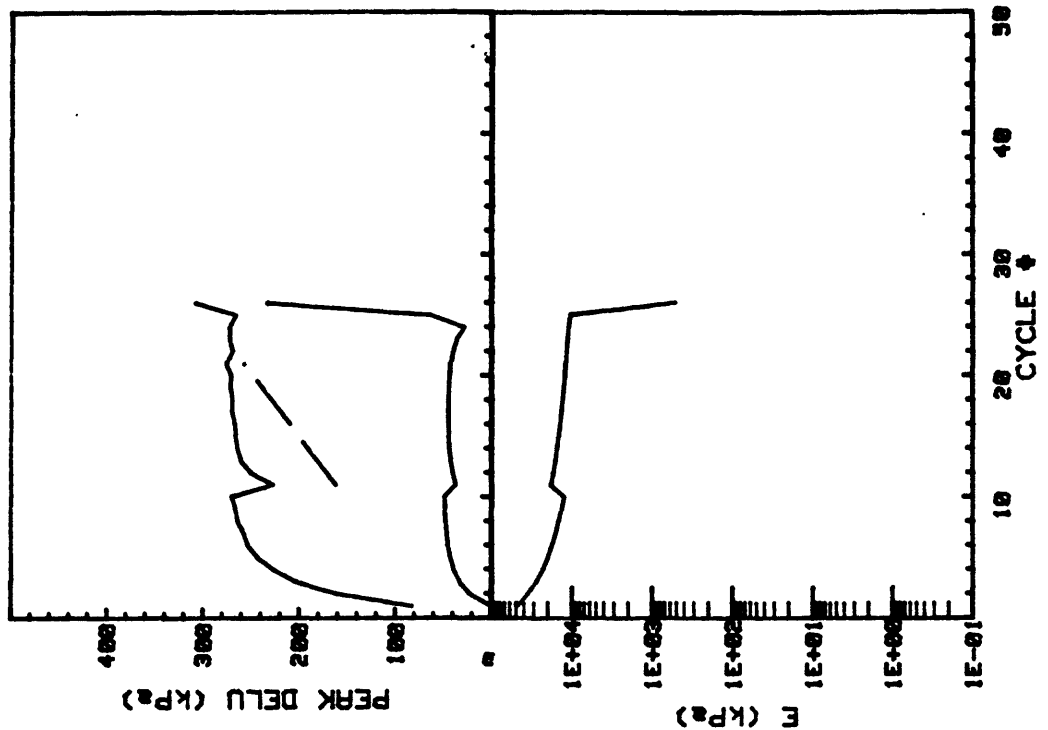
CRUISE DC1-B1-EG  
CORE NO. 634G2INCREMENT (cm)  
TEST NO.72-82  
TC55SIG1c'(kPa) 59.3  
SIG3c'(kPa) 59.3  
INDUCED OCR 1.0STATIC q<sub>f</sub> (kPa) 23.9  
AVG MAX q (kPa) 22.2 (92.9%)  
AVG MIN q (kPa) -19.9 (83.3%)



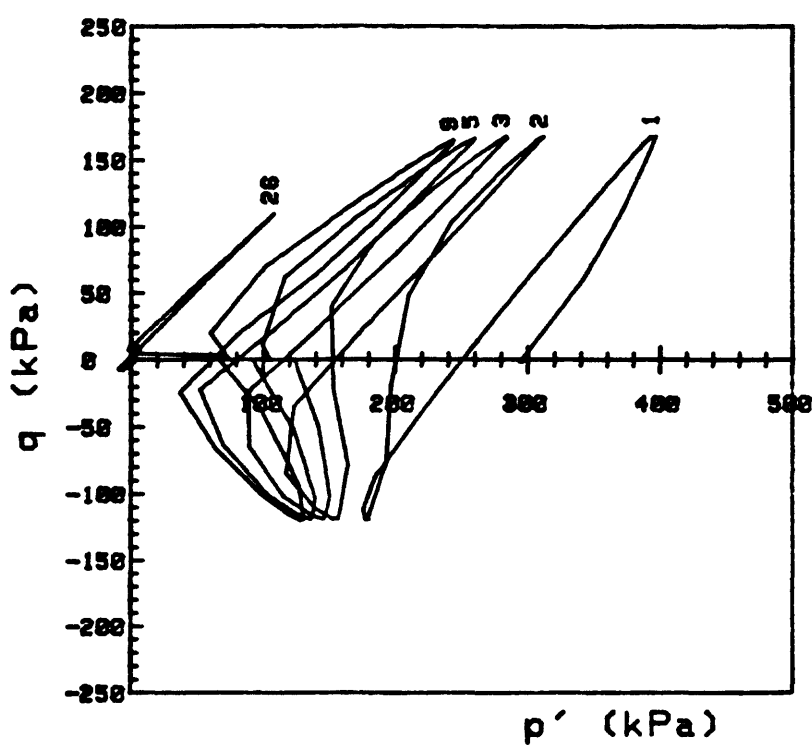
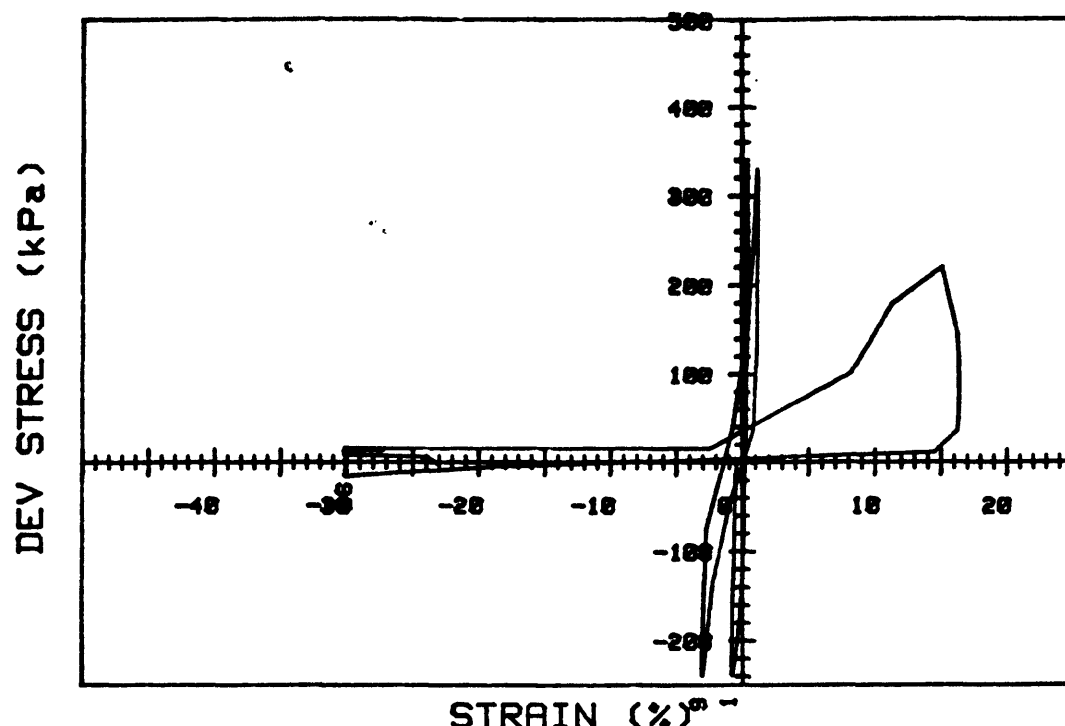
CRUISE DC1-81-EG		INCREMENT (cm)	153-161
CORE NO.	TEST NO.		TC56
SIG1o' (kPa)	301.0	STATIC q <sub>f</sub> (kPa)	562.0
SIG3o' (kPa)	301.0	Avg MAX q (kPa)	120.2 (21.4%)
INDUCED OCR	1.0	Avg MIN q (kPa)	-98.8 (17.6%)



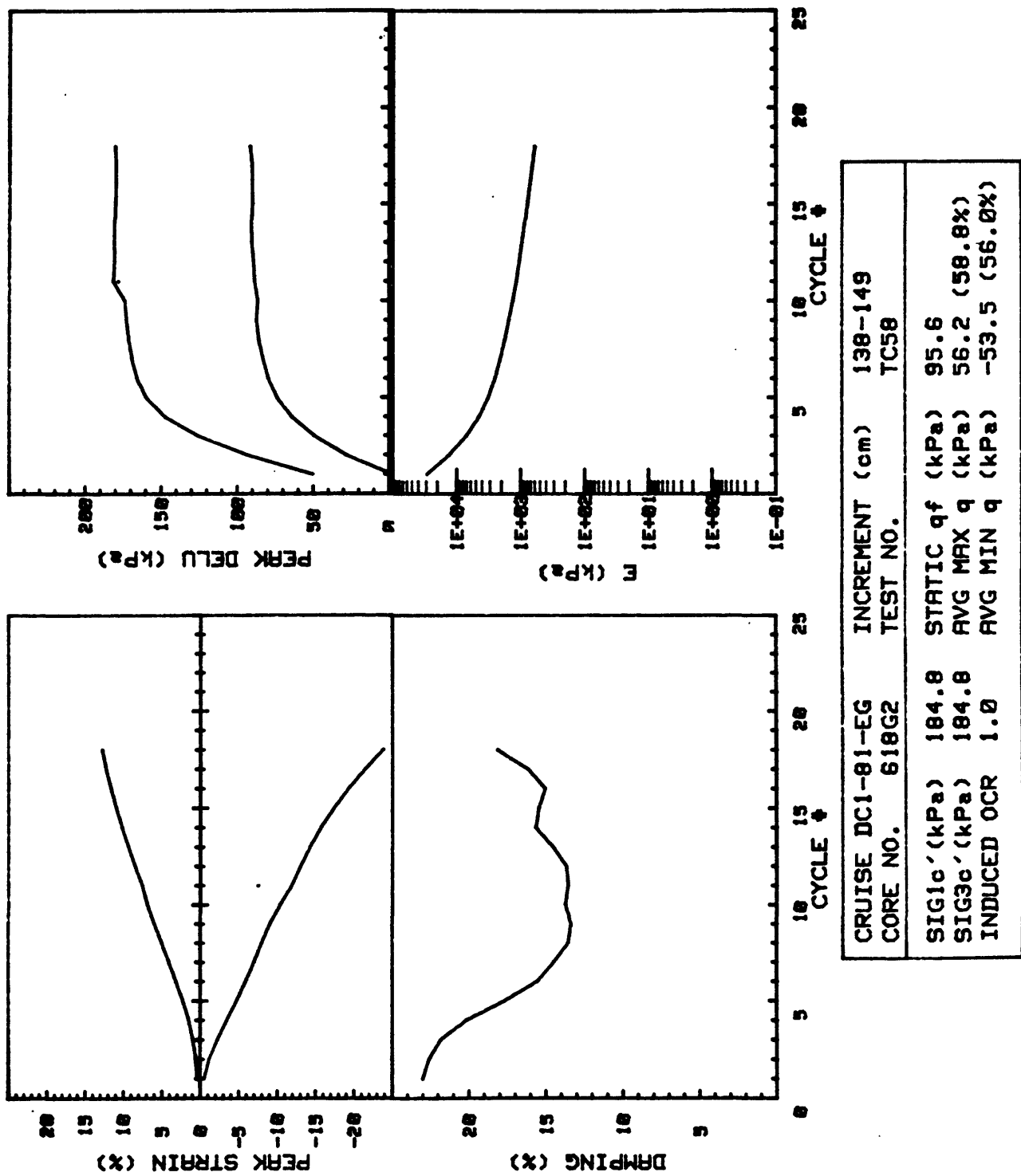
CRUISE DC1-81-EG	INCREMENT (cm)	153-161
CORE NO. 630R2	TEST NO.	TC56
SIG1c'(kPa) 301.0	STATIC qf (kPa)	562.0
SIG3c'(kPa) 301.0	AVG MAX q (kPa)	120.2 (21.4%)
INDUCED OCR 1.0	AVG MIN q (kPa)	-90.8 (17.6%)

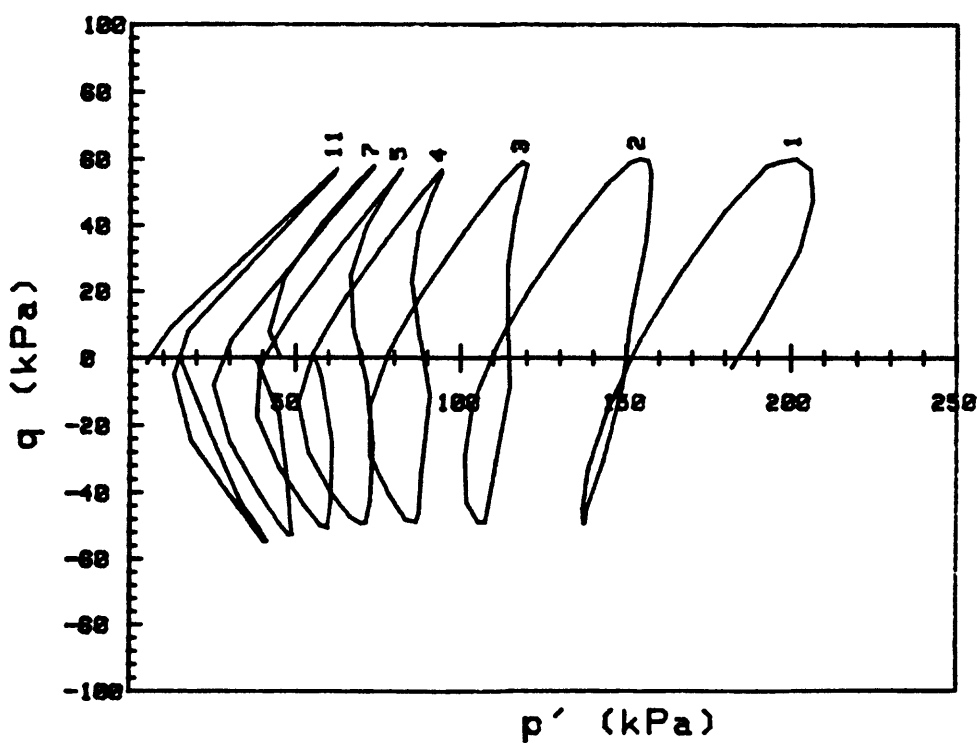
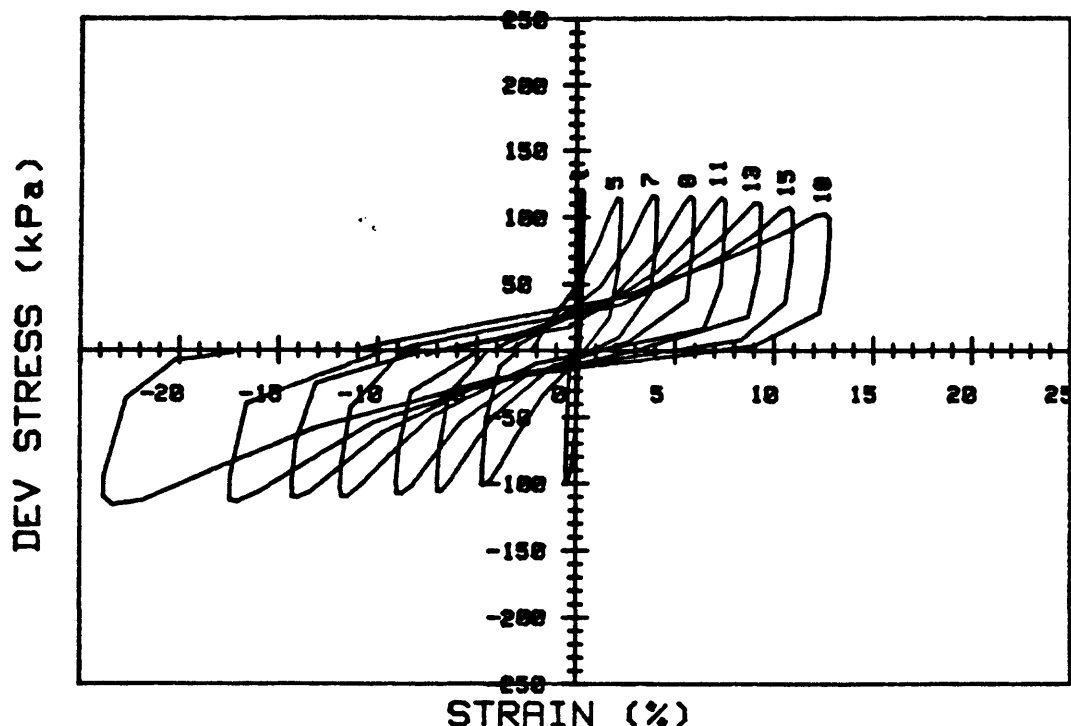


CRUISE	DC1-81-EG	INCREMENT (cm)	153-160.5
CORE NO.	630R2	TEST NO.	TC57
SIG1c' (kPa)	297.9	STATIC q <sub>f</sub> (kPa)	562.0
SIG3c' (kPa)	297.9	AVG MAX q (kPa)	162.9 (29.0%)
INDUCED OCR	1.0	AVG MIN q (kPa)	-115.1 (20.5%)

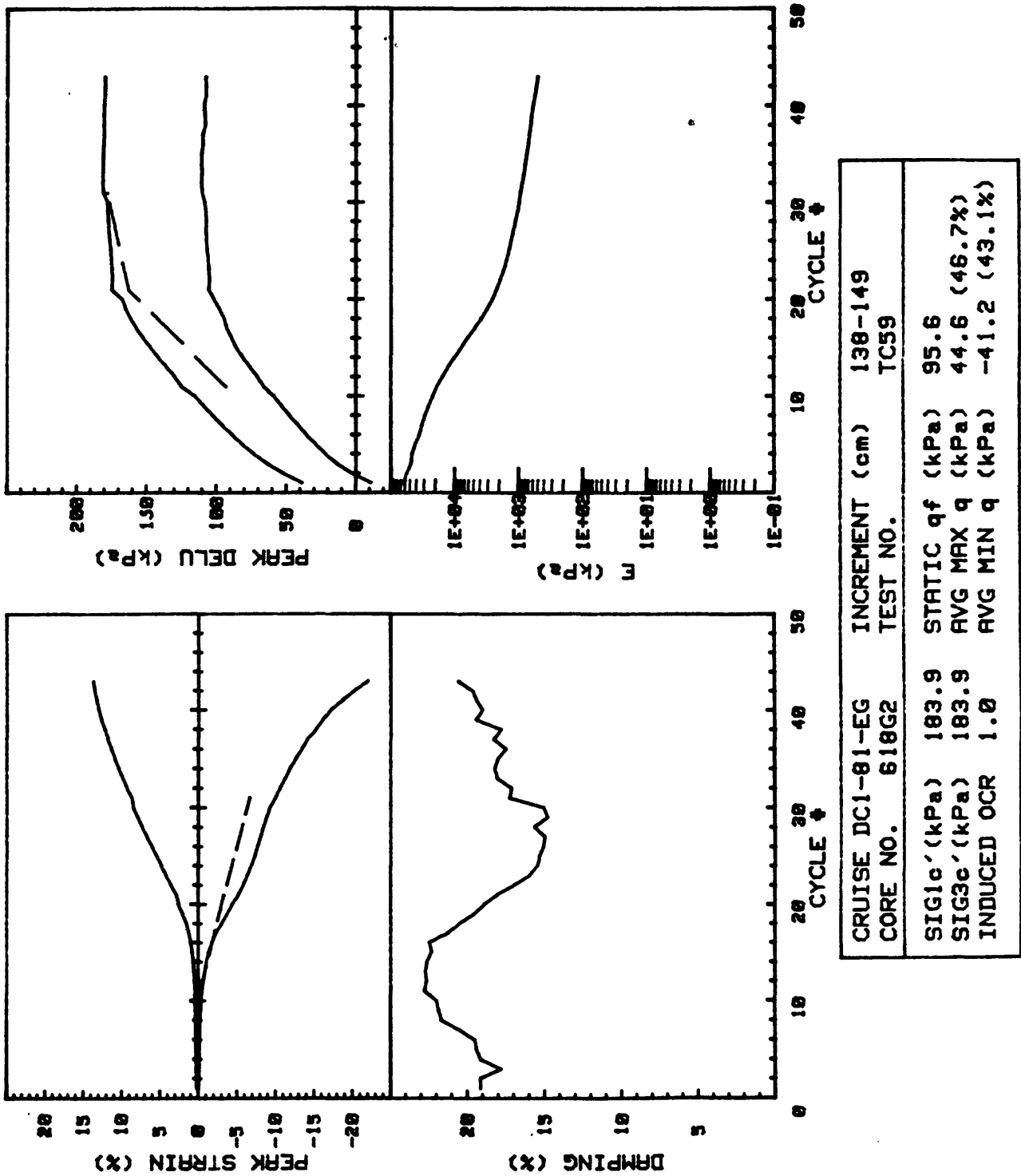


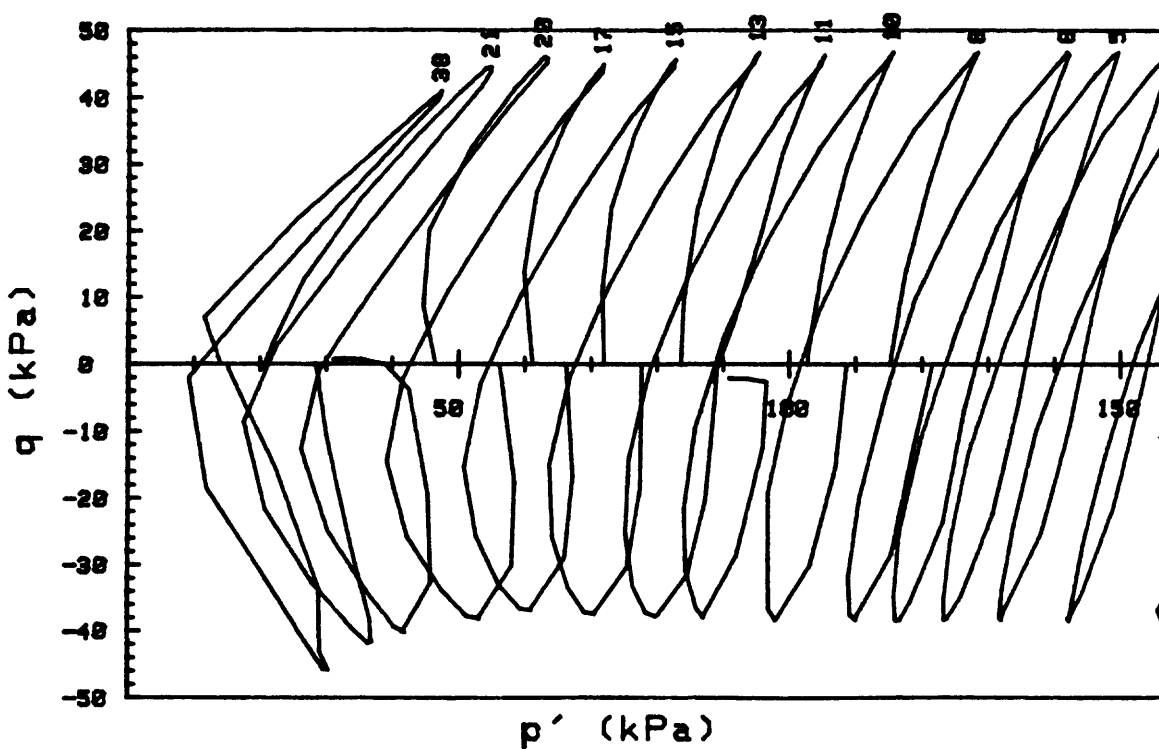
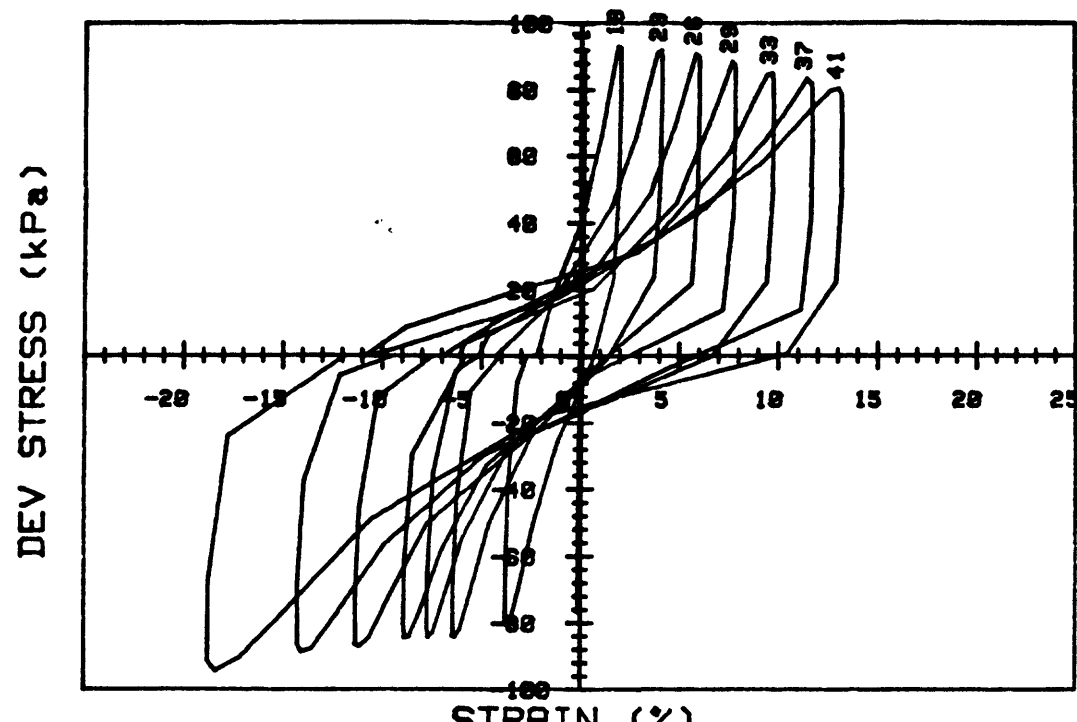
CRUISE DC1-81-EG CORE NO. 630A2	INCREMENT (cm) TEST NO.	153-160.5 TC57	
SIG1c' (kPa)	297.9	STATIC $q_f$ (kPa)	562.0
SIG3c' (kPa)	297.9	Avg MAX q (kPa)	162.9 (29.0%)
INDUCED OCR	1.0	Avg MIN q (kPa)	-115.1 (20.5%)



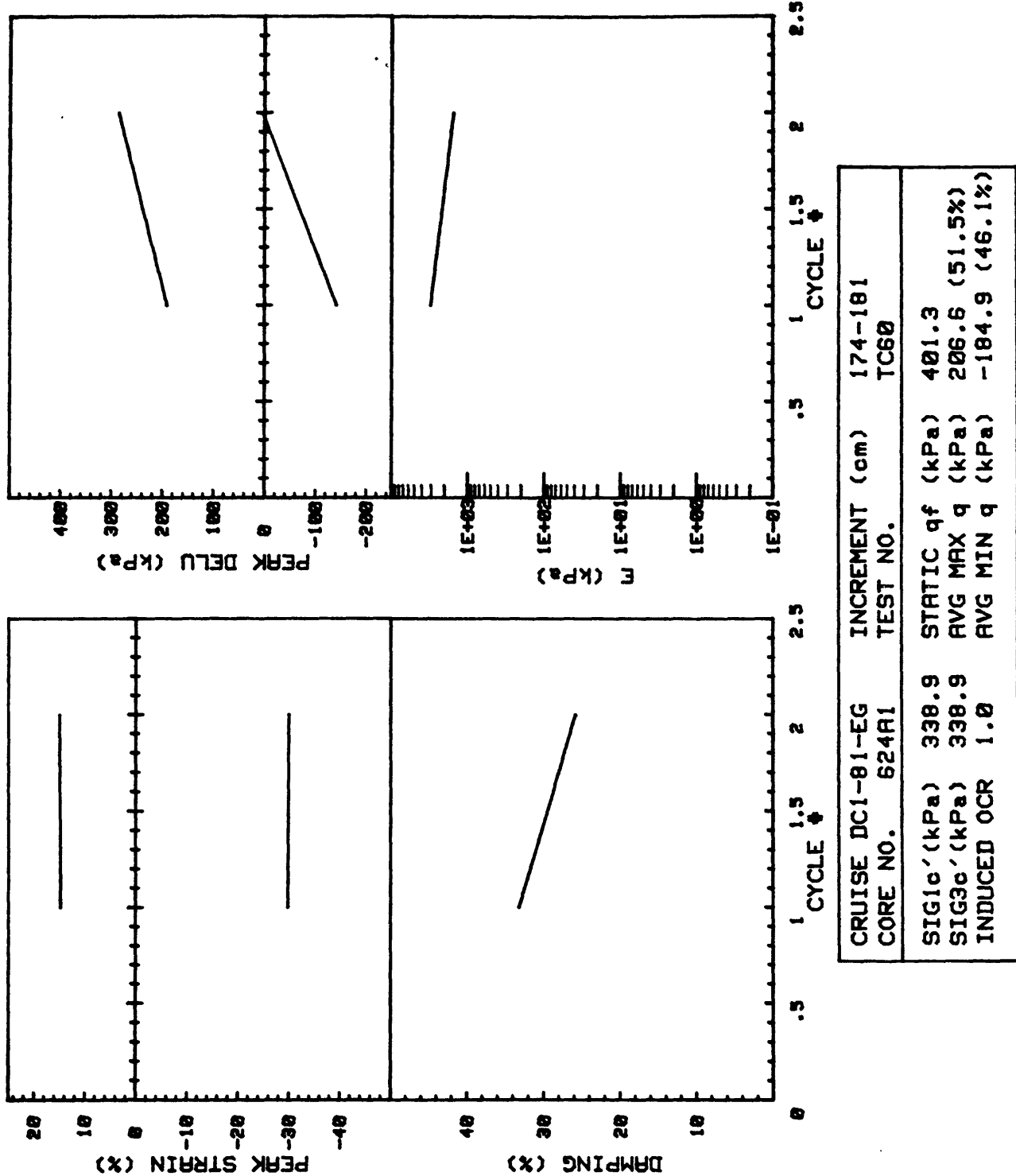


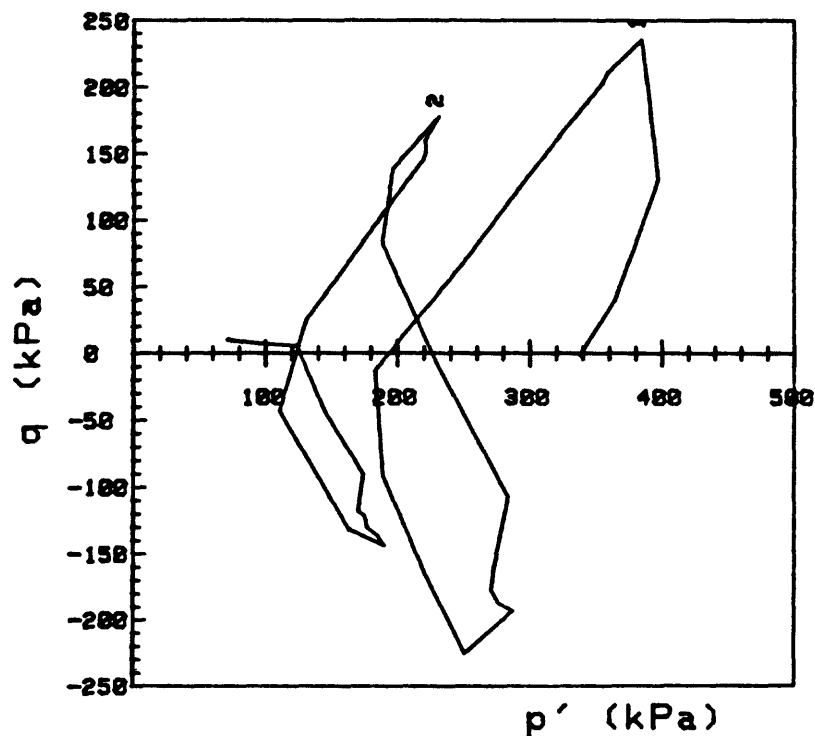
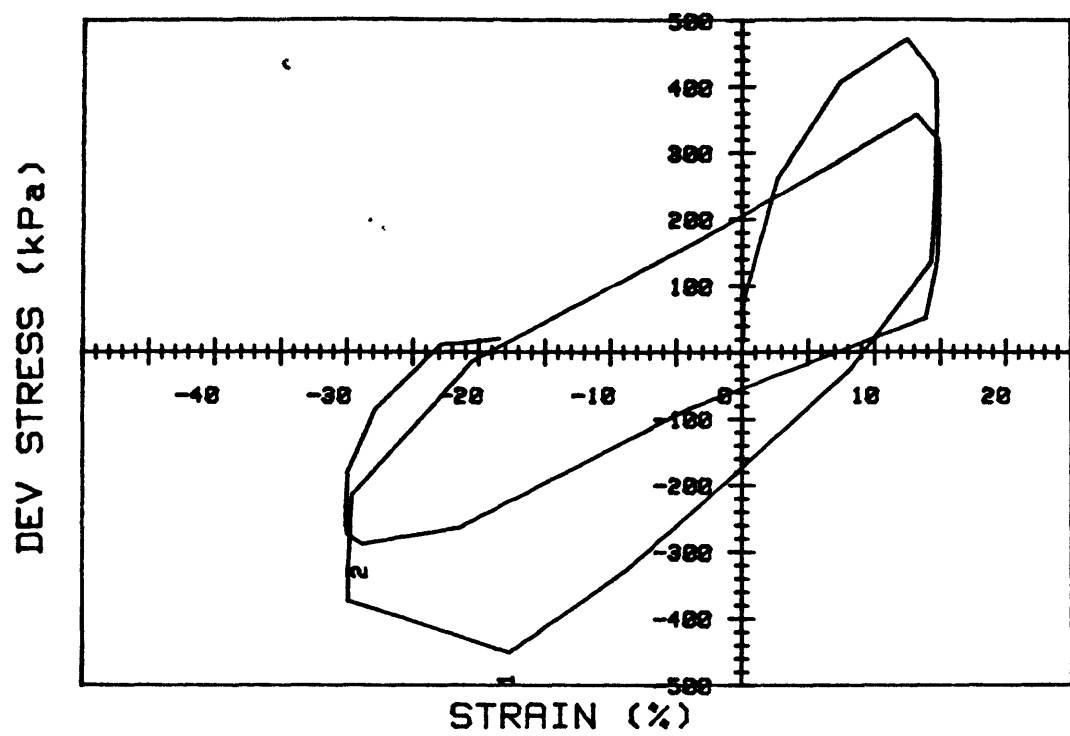
CRUISE DC1-B1-EG	INCREMENT (cm)	138-149
CORE NO. 618G2	TEST NO.	TC58
SIG1c'(kPa) 184.8	STATIC qf (kPa)	95.6
SIG3c'(kPa) 184.8	AVG MAX q (kPa)	56.2 (58.8%)
INDUCED OCR 1.0	AVG MIN q (kPa)	-53.5 (56.0%)



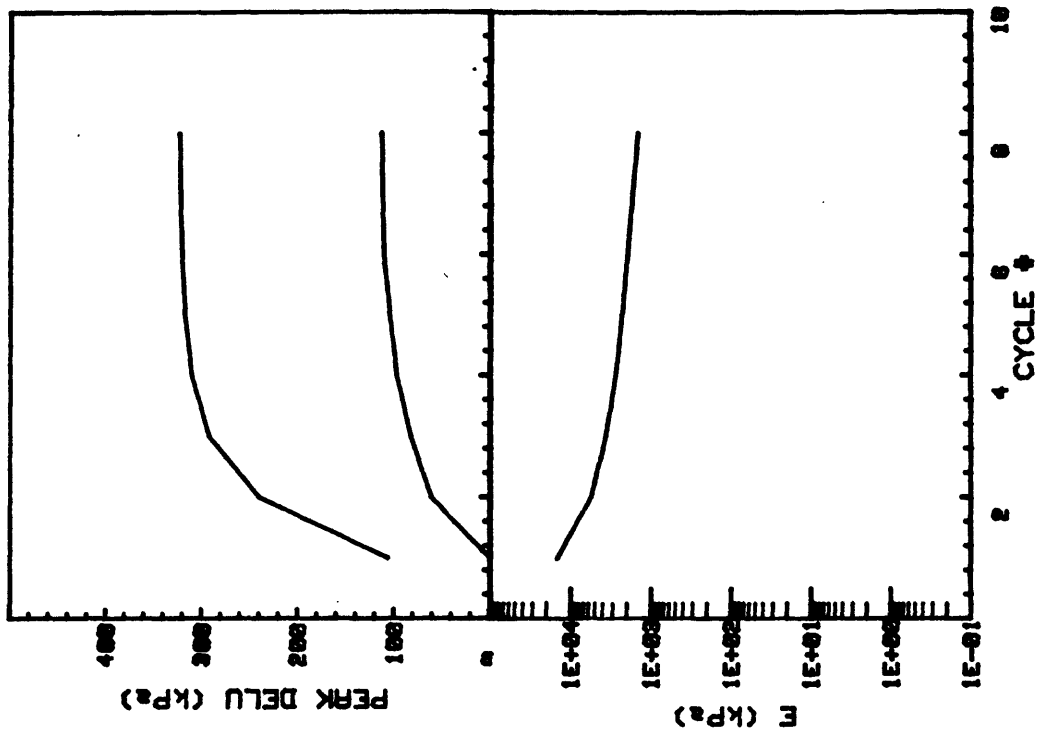


CRUISE DC1-81-EG CORE NO. 618G2	INCREMENT (cm) TEST NO.	138-149 TC59
SIG1c' (kPa) 183.9 SIG3c' (kPa) 183.9 INDUCED OCR 1.0	STATIC q <sub>f</sub> (kPa) AVG MAX q (kPa) AVG MIN q (kPa)	95.6 44.6 (46.7%) -41.2 (43.1%)

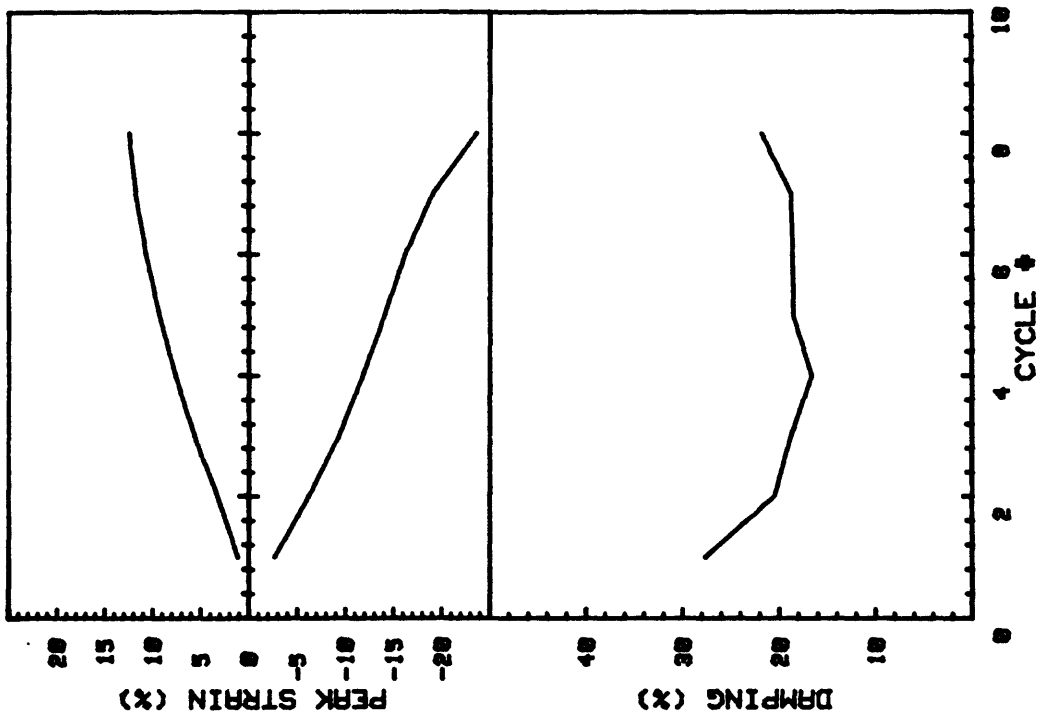


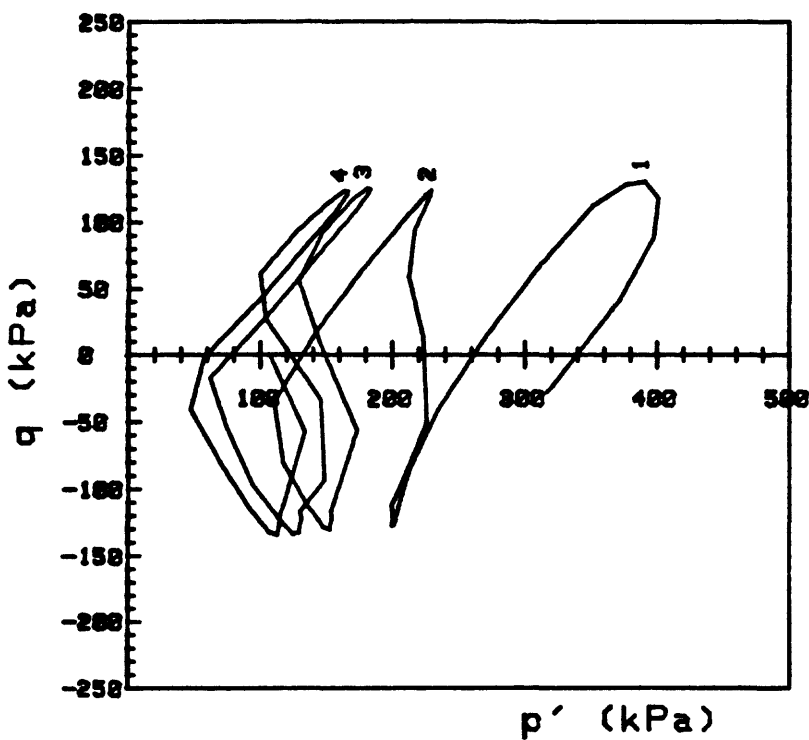
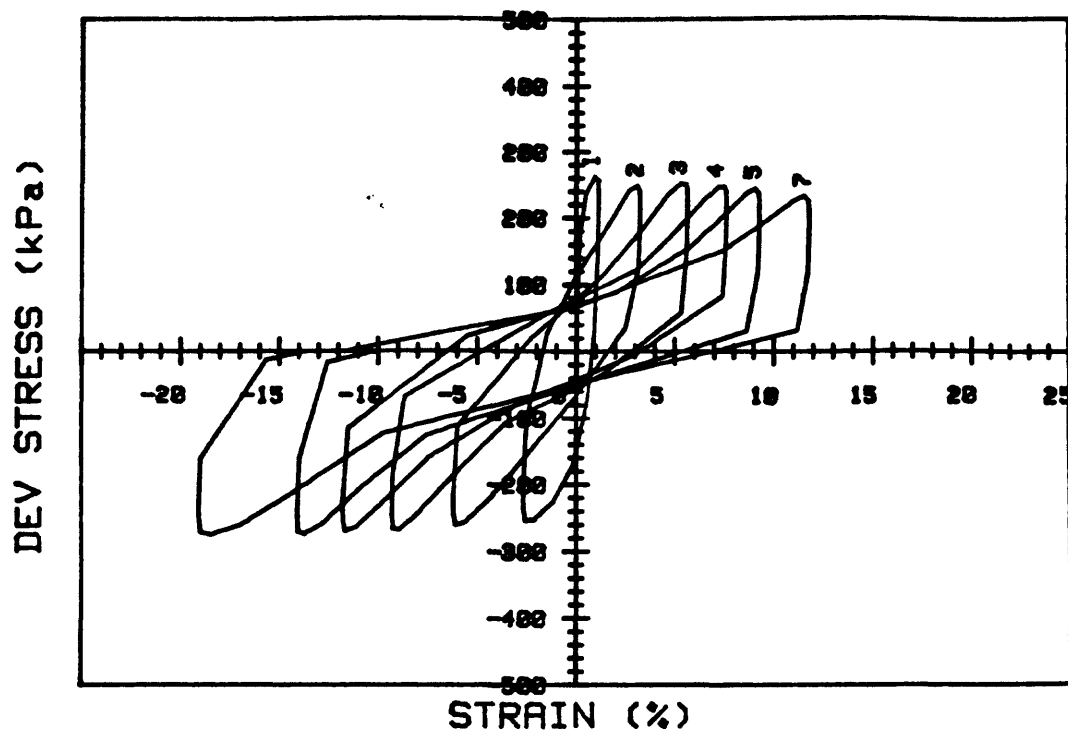


CRUISE DC1-81-EG	INCREMENT (cm)	174-181
CORE NO. 624A1	TEST NO.	TC60
SIG1c'(kPa) 338.9	STATIC qf (kPa)	401.3
SIG3c'(kPa) 338.9	AVG MAX q (kPa)	206.6 (51.5%)
INDUCED OCR 1.0	AVG MIN q (kPa)	-184.9 (46.1%)

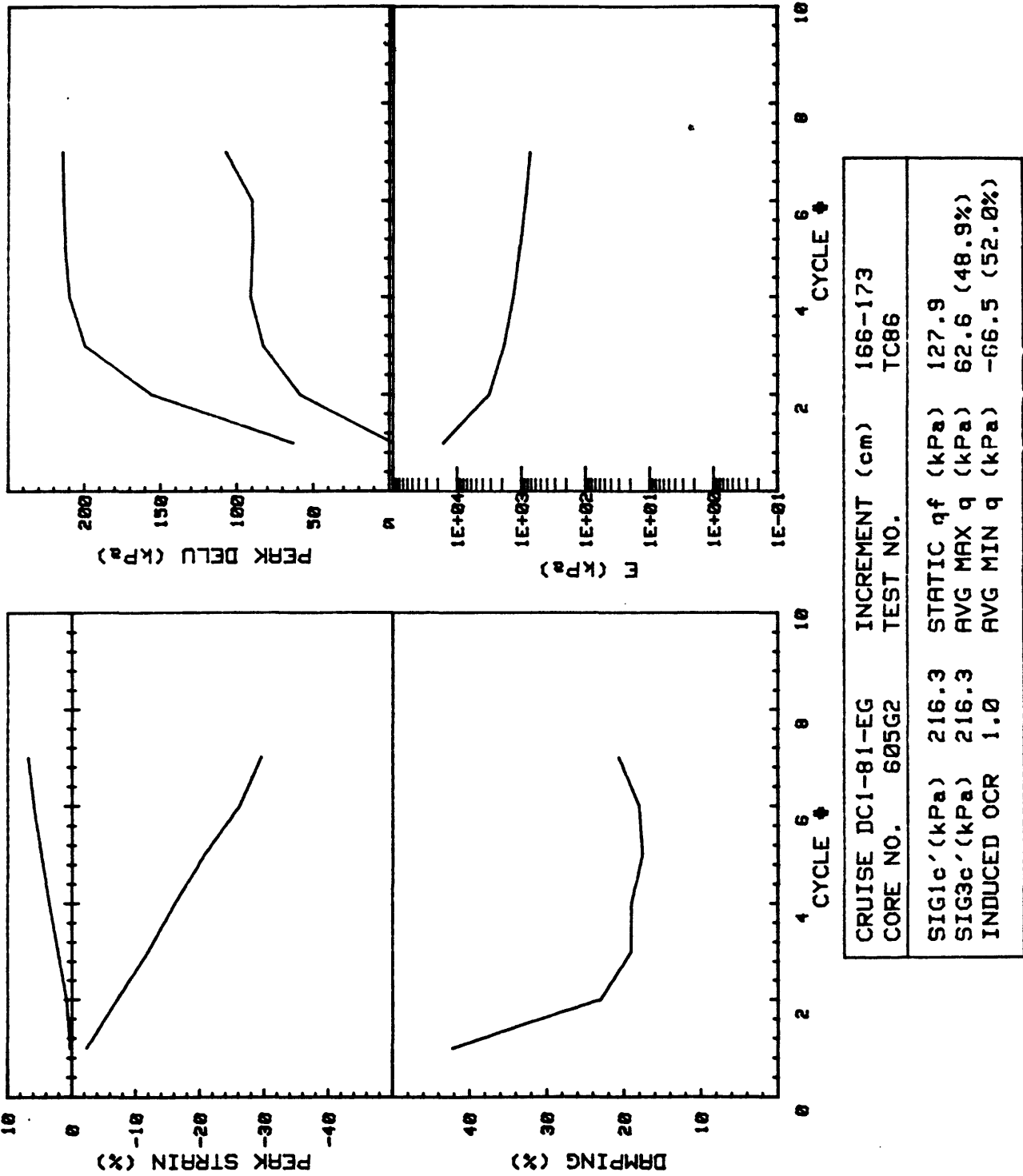


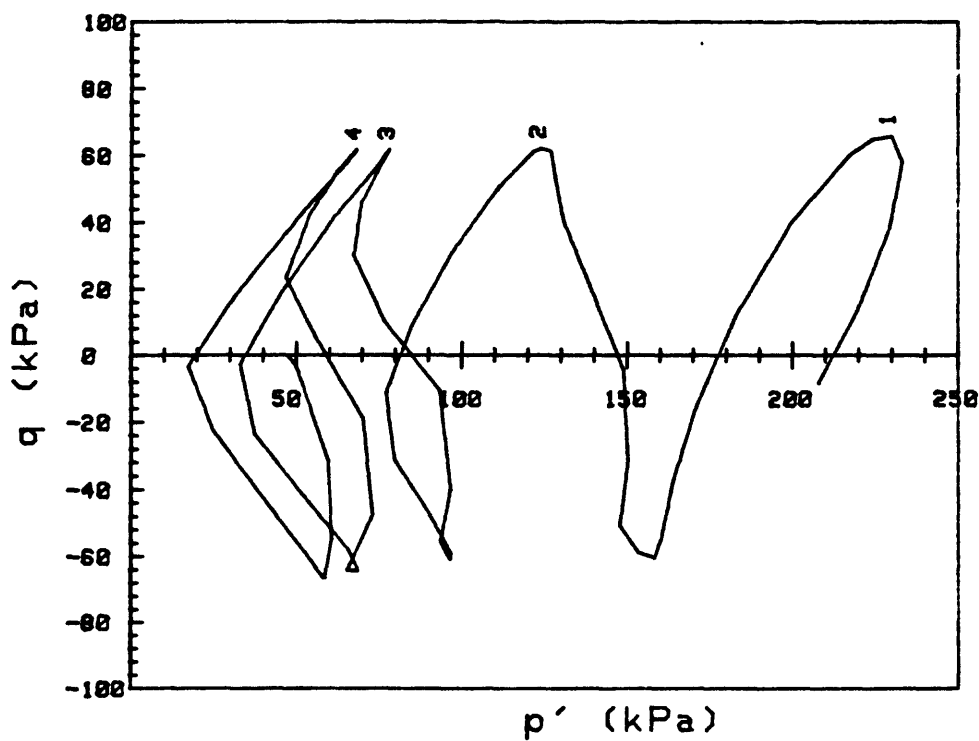
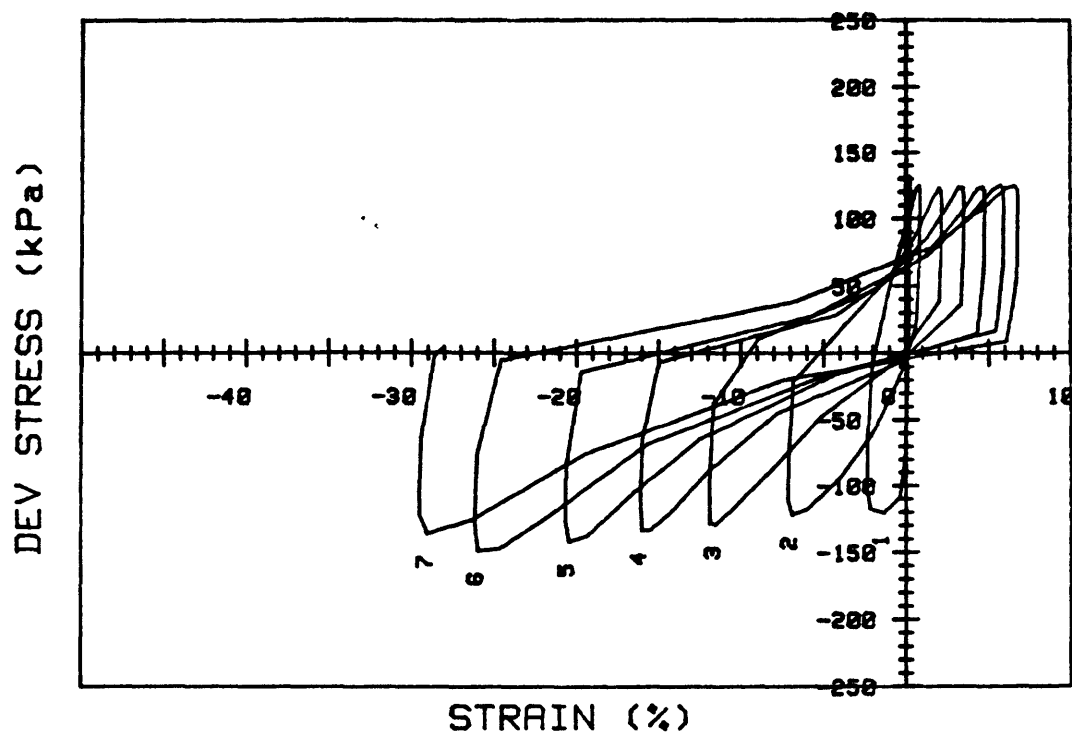
CRUISE DC1-81-EG		INCREMENT (cm)	174-181
CORE NO.	624R1	TEST NO.	TC61
SIG1 <sub>c</sub> (kPa)	344.7	STATIC q <sub>f</sub> (kPa)	401.3
SIG3 <sub>c</sub> (kPa)	344.7	Avg MAX q (kPa)	121.8 (30.4%)
INDUCED OCR	1.0	Avg MIN q (kPa)	-134.6 (33.5%)



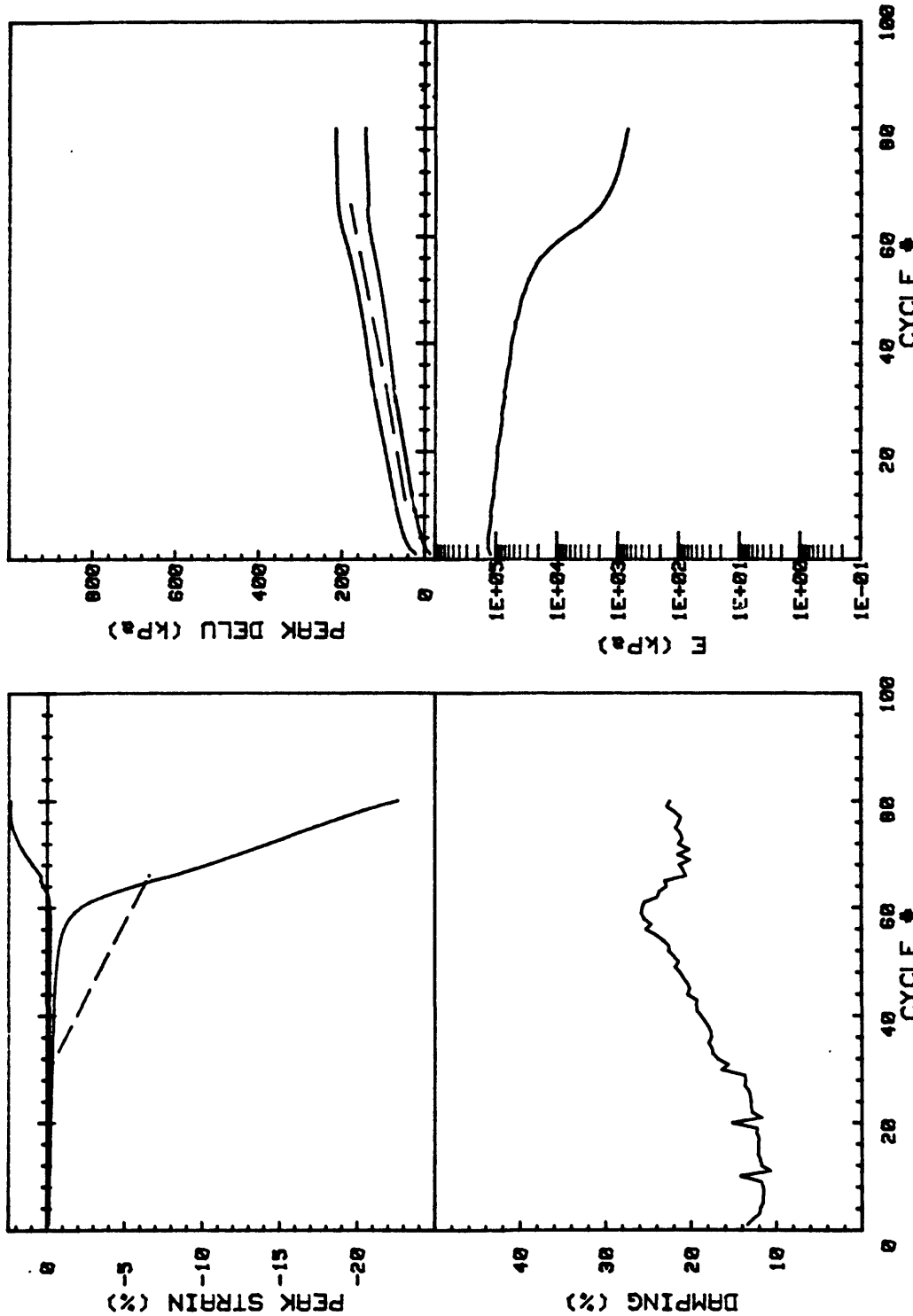


CRUISE DC1-81-EG CORE NO. 624R1	INCREMENT (cm) TEST NO.	174-181 TC61	
SIG1c'(kPa)	344.7	STATIC qf (kPa)	401.3
SIG3c'(kPa)	344.7	AVG MAX q (kPa)	121.8 (30.4%)
INDUCED OCR	1.0	AVG MIN q (kPa)	-134.6 (33.5%)

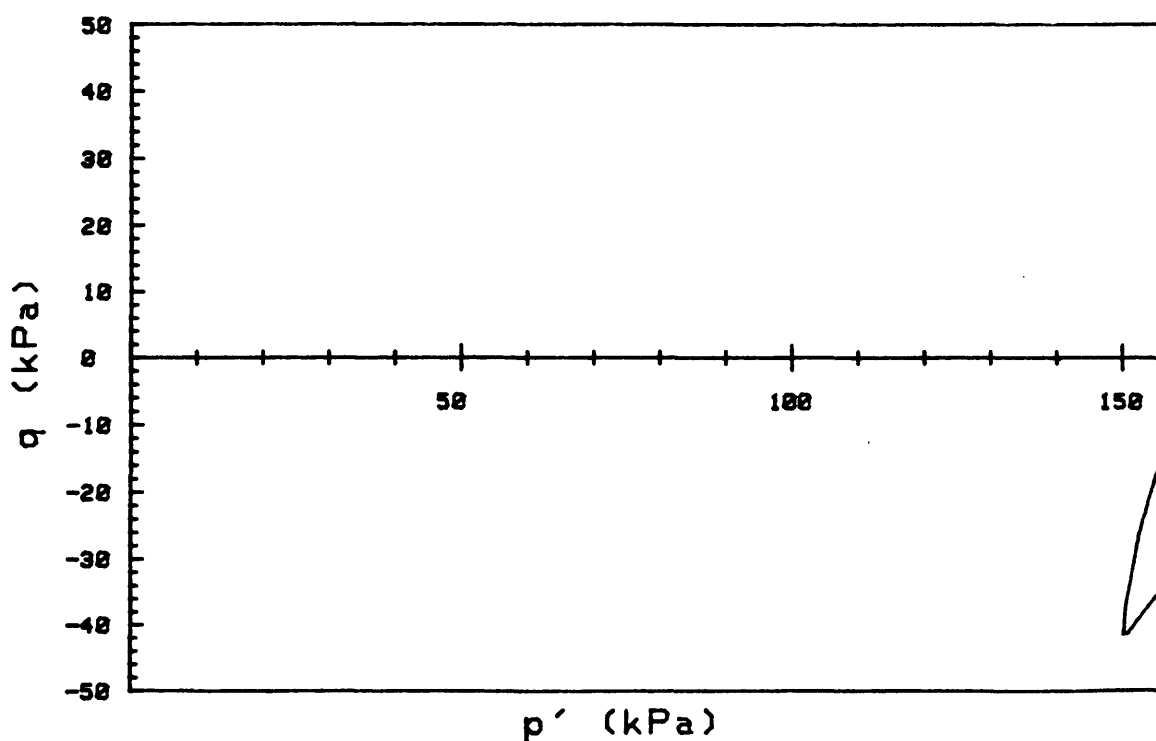
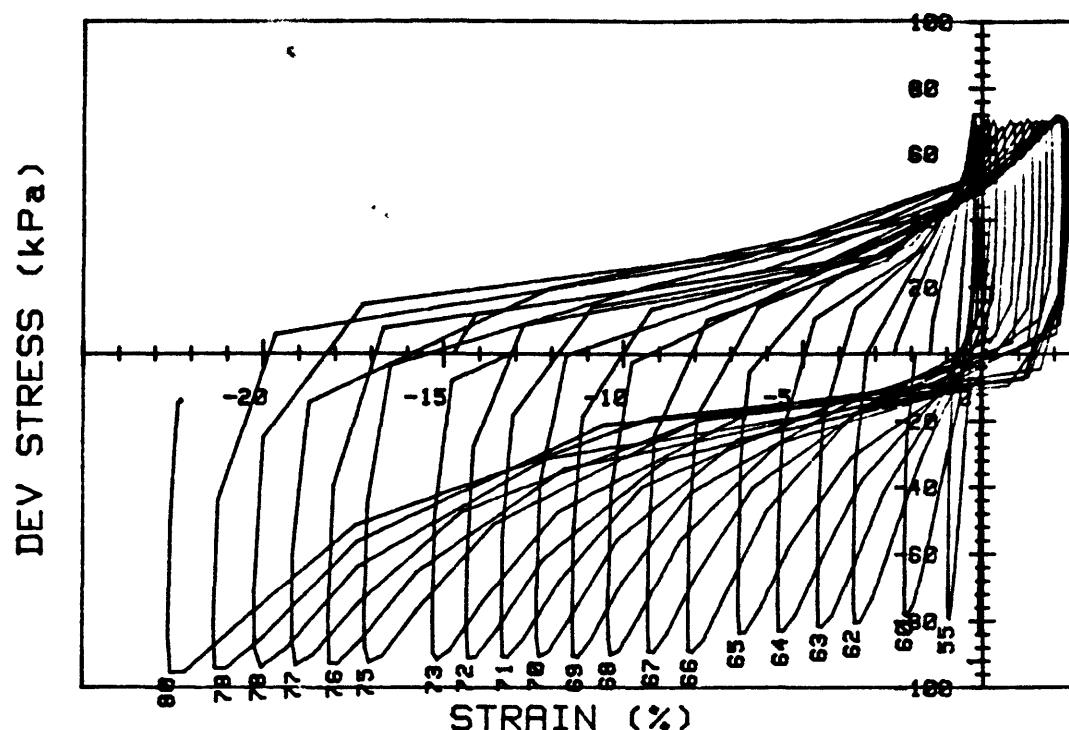




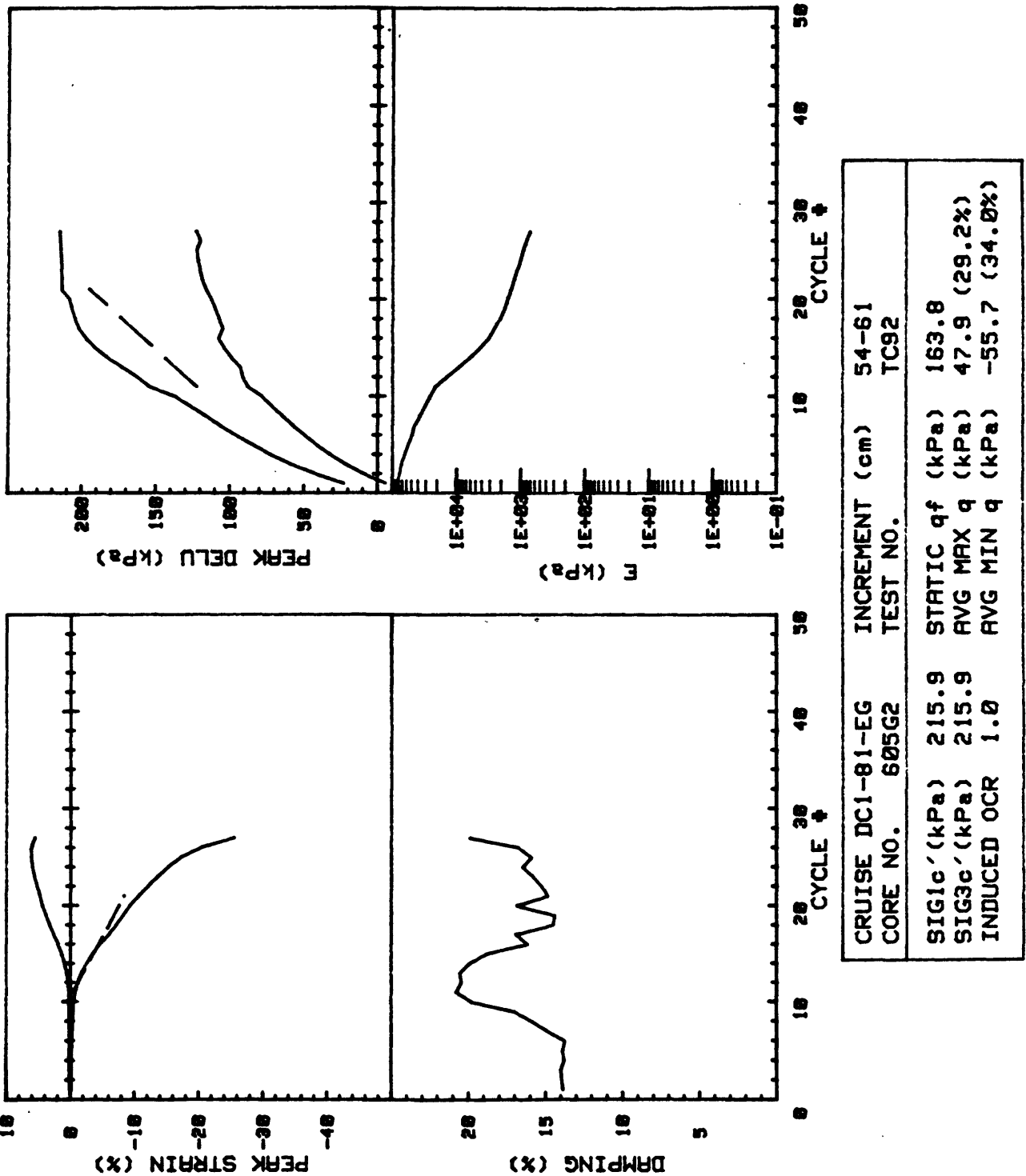
CRUISE DC1-81-EG CORE NO. 605G2	INCREMENT (cm) TEST NO.	166-173 TC86	
SIG1c'(kPa)	216.3	STATIC q <sub>f</sub> (kPa)	127.9
SIG3c'(kPa)	216.3	AVG MAX q (kPa)	62.6 (48.9%)
INDUCED OCR	1.0	AVG MIN q (kPa)	-66.5 (52.0%)

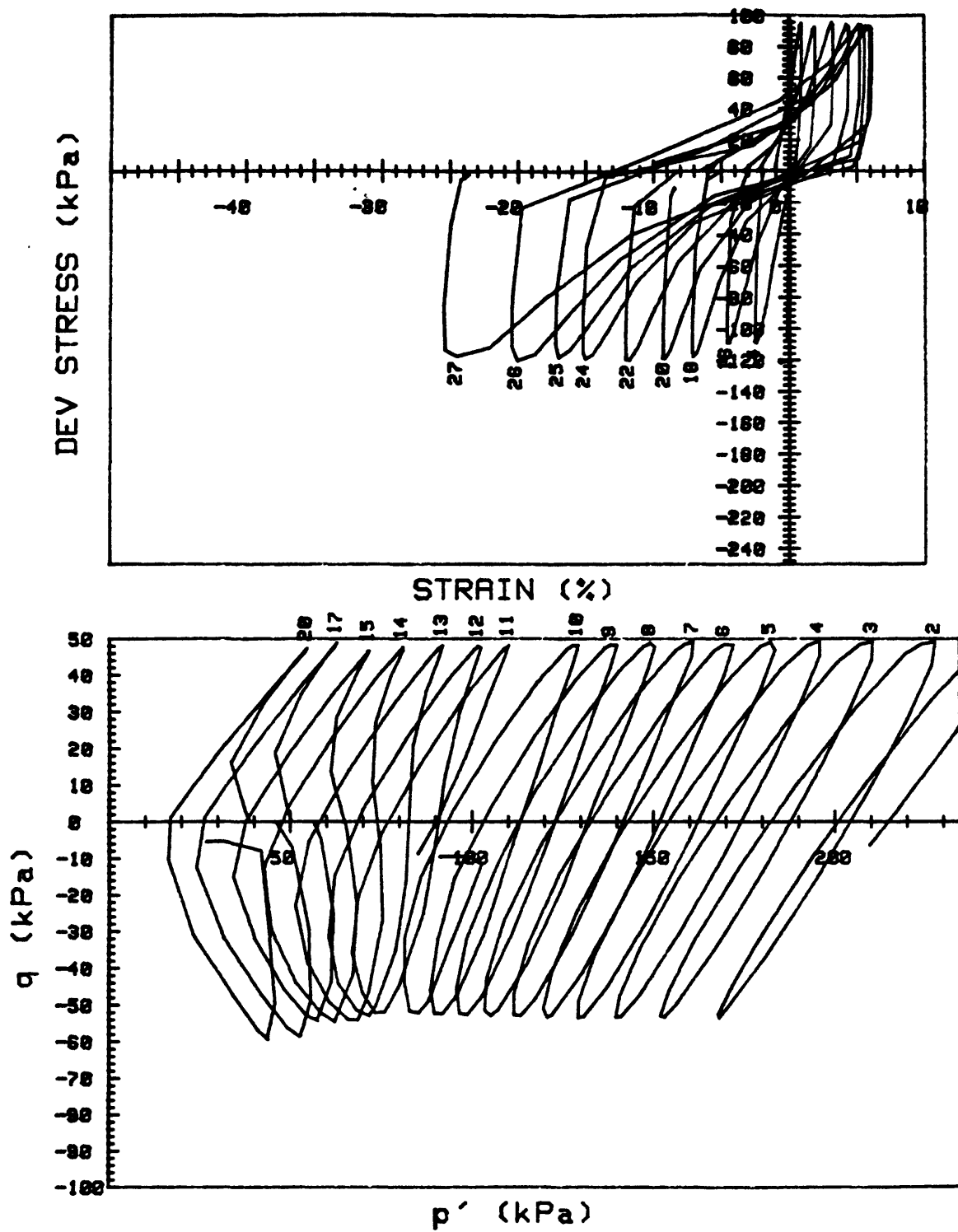


CRUISE DC1-81-EG		INCREMENT (cm)	166-173
CORE NO.	605G2	TEST NO.	TC87
SIG1 <sub>c'</sub> (kPa)	215.1	STATIC q <sub>f</sub> (kPa)	127.9
SIG3 <sub>c'</sub> (kPa)	215.1	AVG MAX q (kPa)	35.5 (27.8%)
INDUCED OCR	1.0	AVG MIN q (kPa)	-41.8 (32.7%)

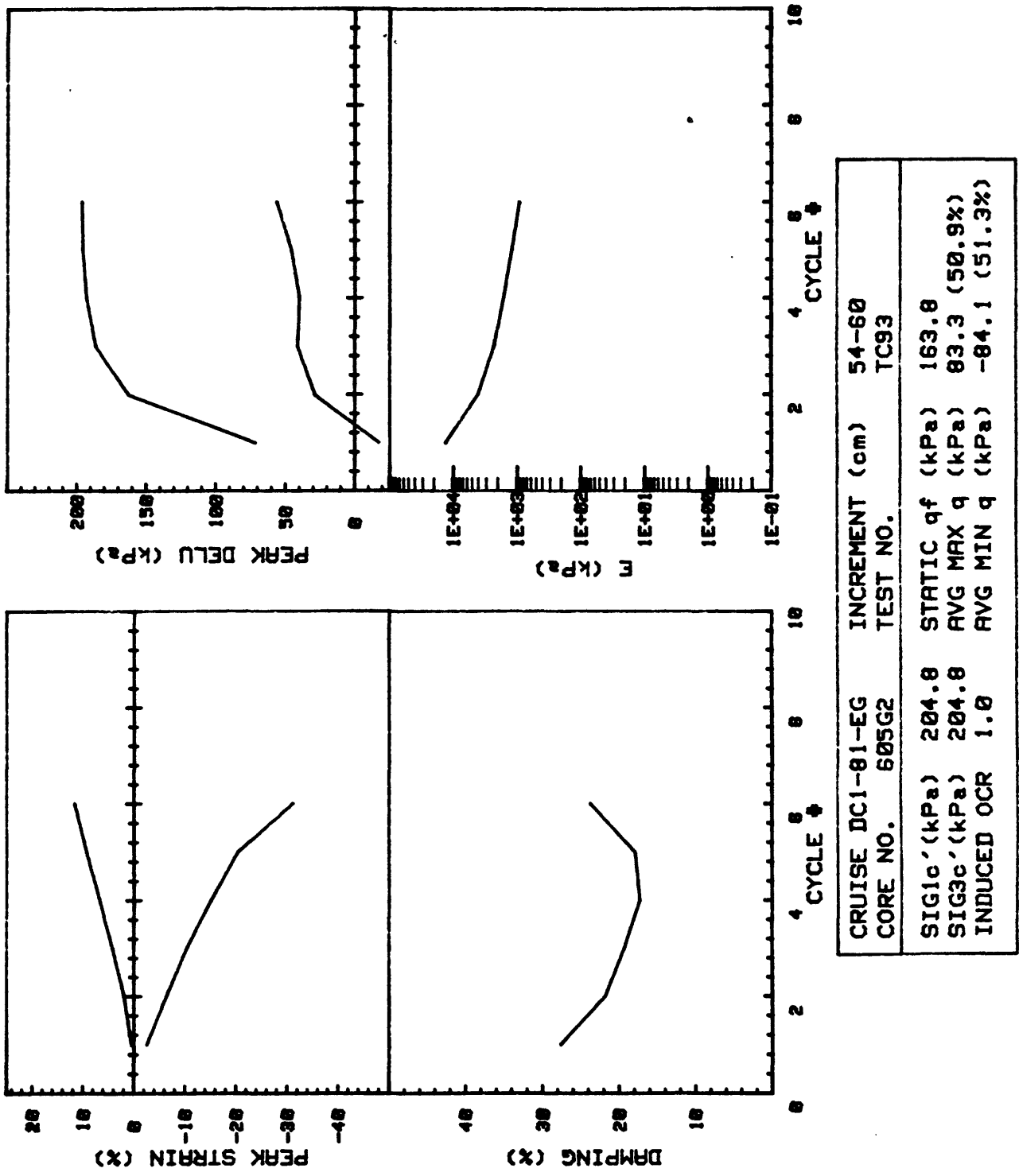


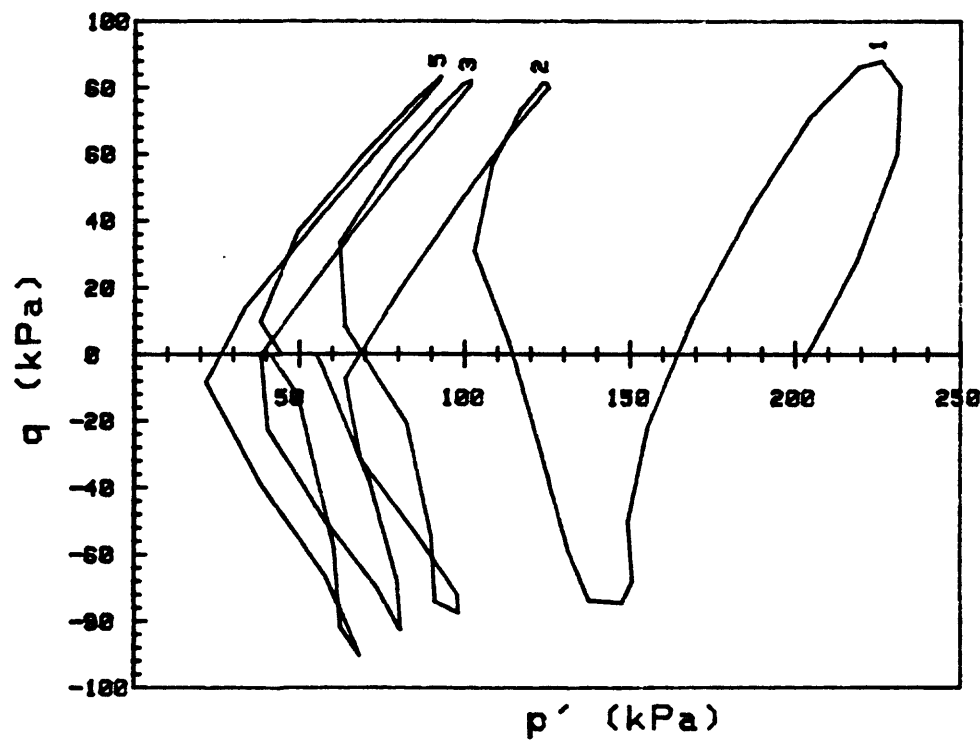
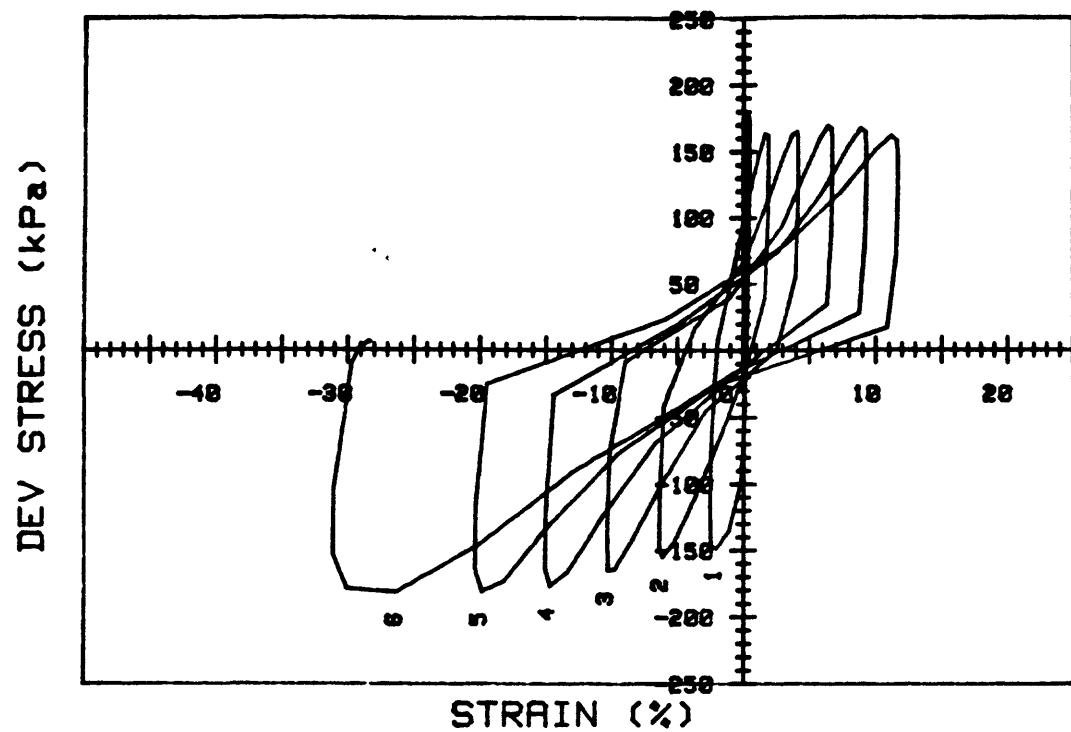
CRUISE DC1-81-EG	INCREMENT (cm)	166-173
CORE NO. 605G2	TEST NO.	TC87
SIG1c'(kPa) 215.1	STATIC q <sub>f</sub> (kPa)	127.9
SIG3c'(kPa) 215.1	AVG MAX q (kPa)	35.5 (27.8%)
INDUCED OCR 1.0	AVG MIN q (kPa)	-41.8 (32.7%)



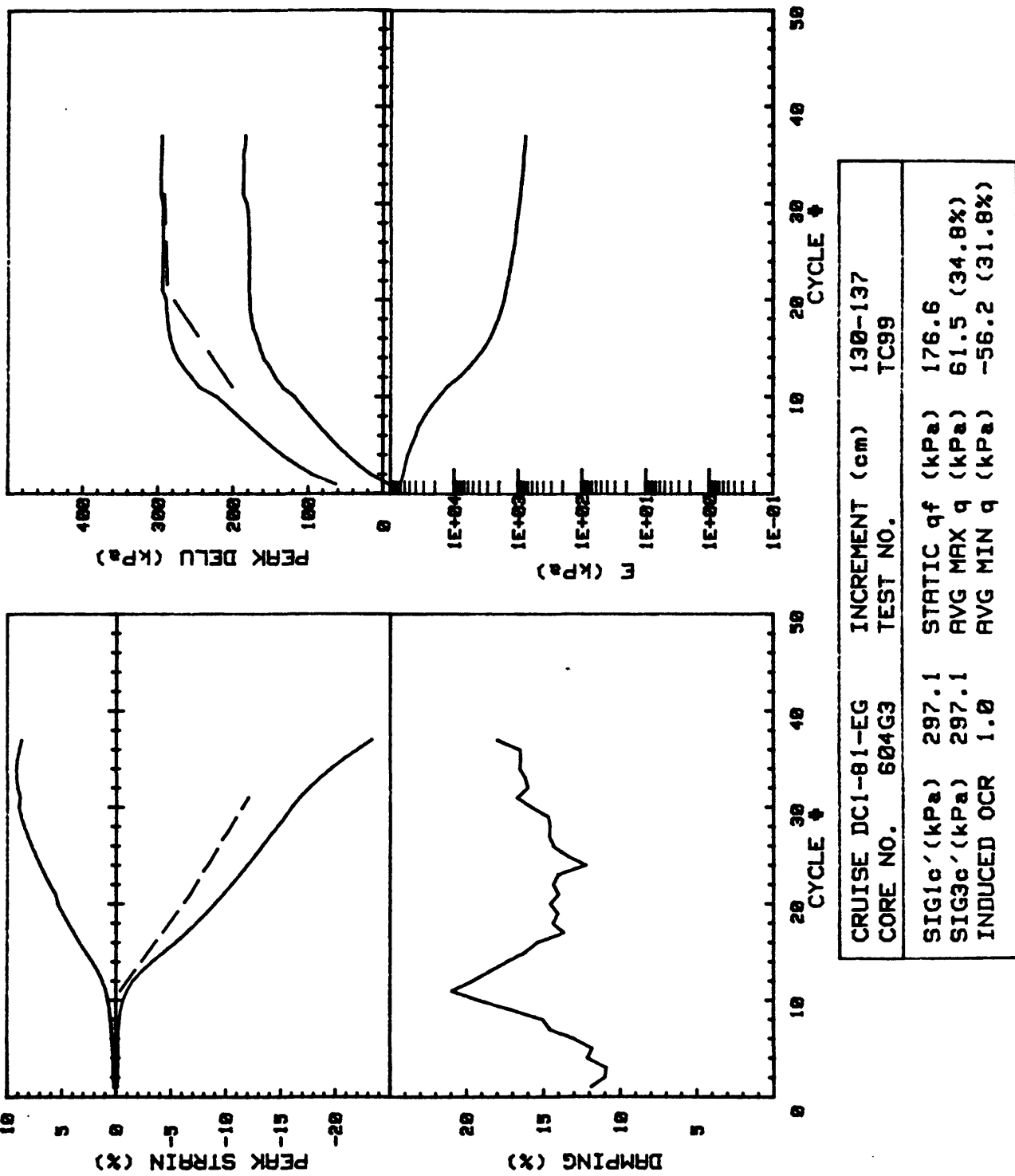


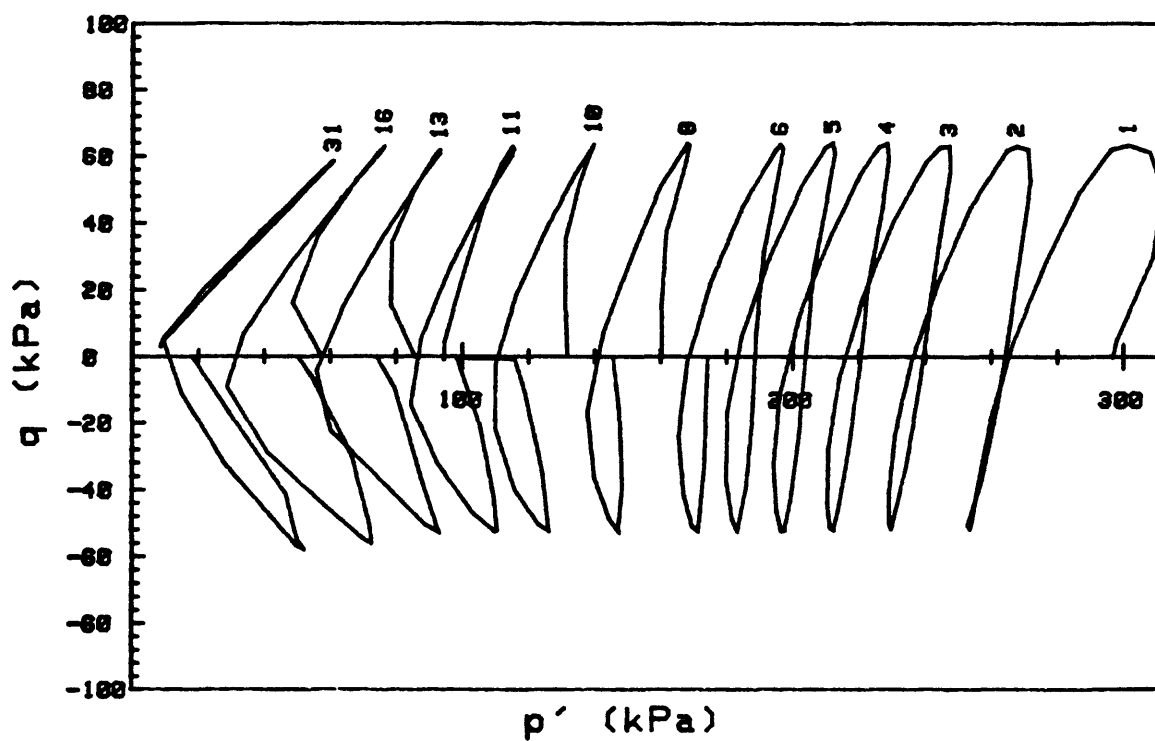
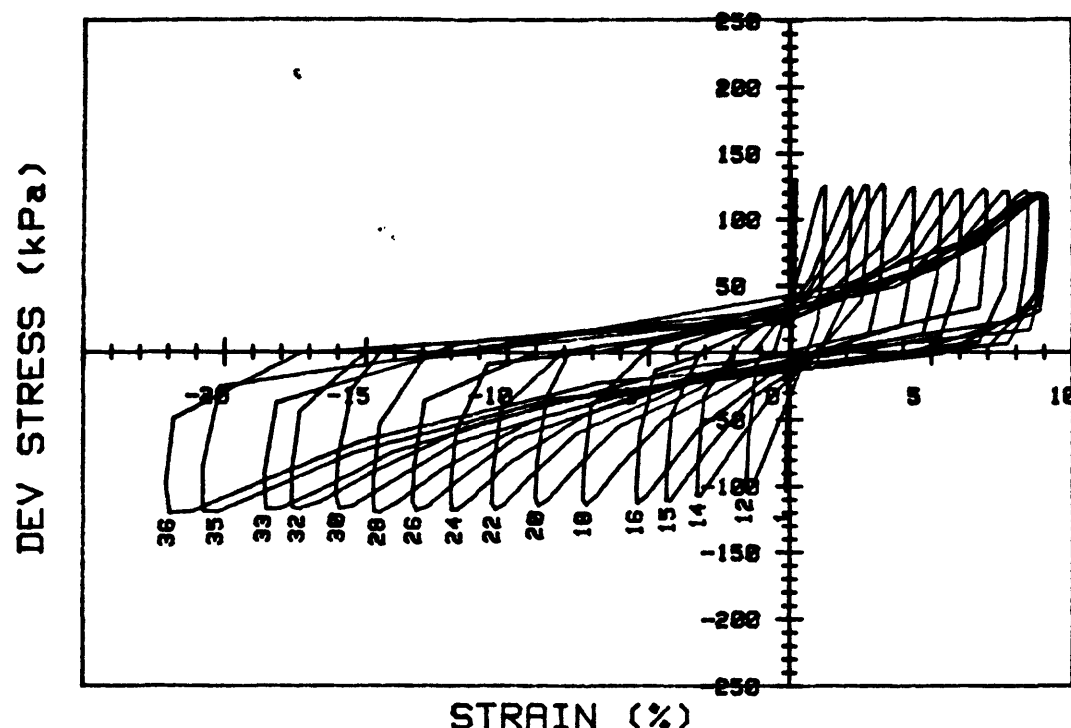
CRUISE DC1-81-EG	INCREMENT (cm)	54-61
CORE NO. 605G2	TEST NO.	TC92
SIG1c'(kPa) 215.9	STATIC q <sub>f</sub> (kPa)	163.8
SIG3c'(kPa) 215.9	AVG MAX q (kPa)	47.9 (29.2%)
INDUCED OCR 1.0	AVG MIN q (kPa)	-55.7 (34.0%)



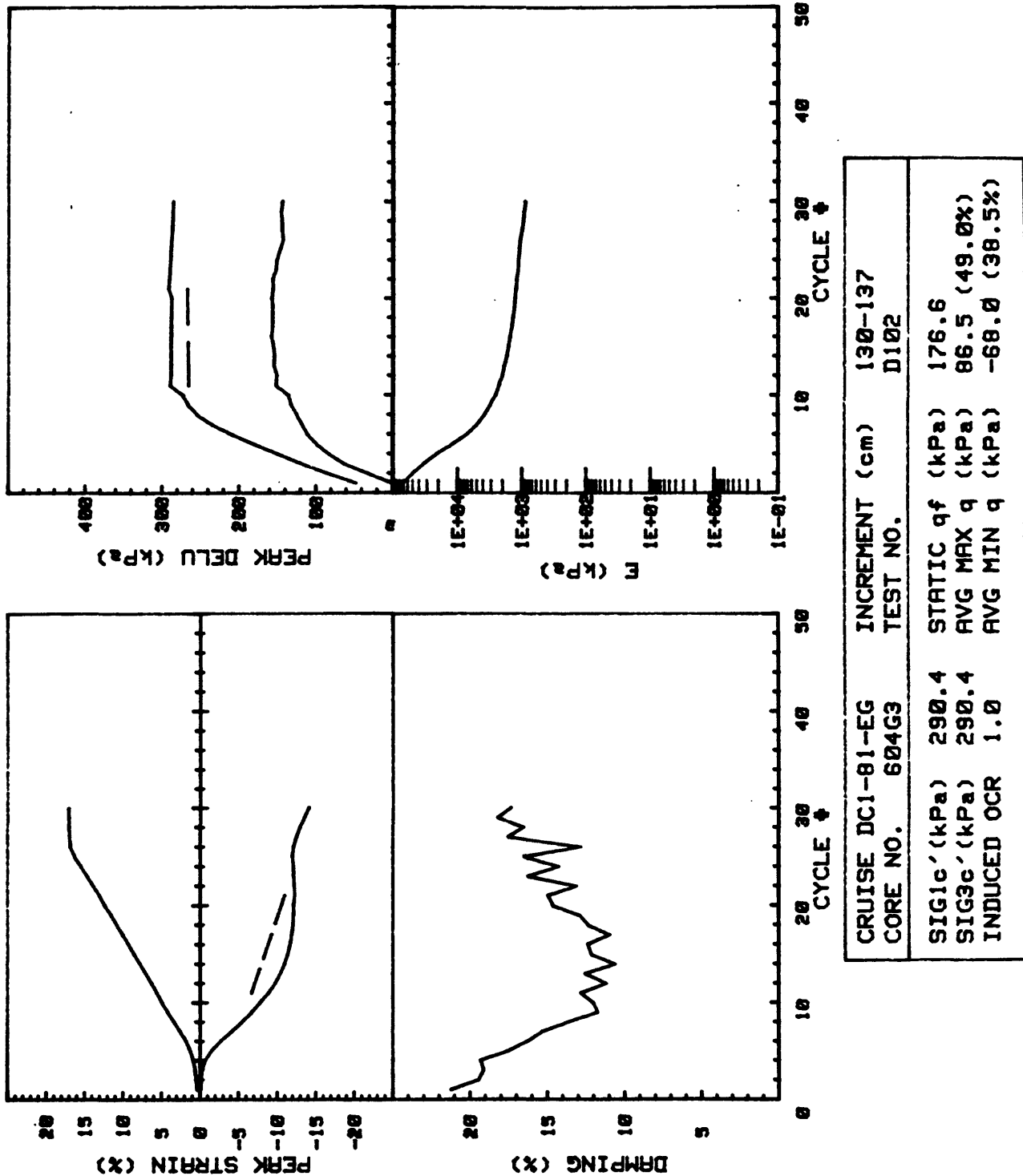


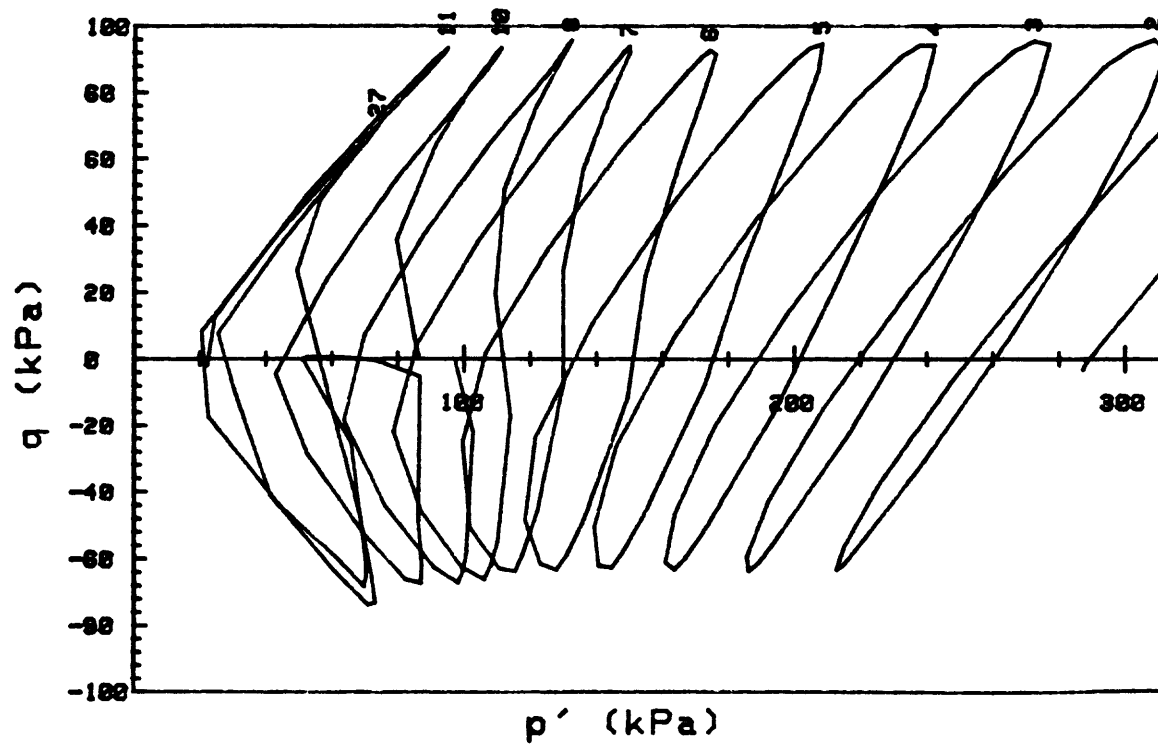
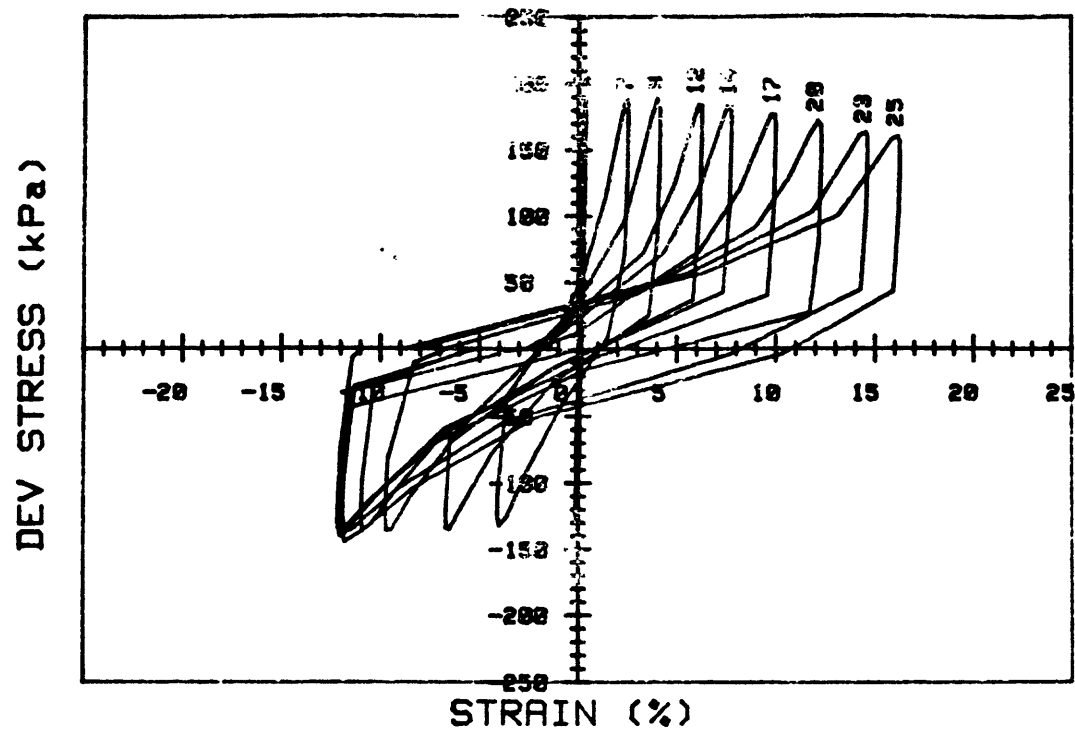
CRUISE DC1-81-EG	INCREMENT (cm)	54-60
CORE NO. 605G2	TEST NO.	TC93
SIG1c'(kPa) 204.8	STATIC q <sub>f</sub> (kPa)	163.8
SIG3c'(kPa) 204.8	AVG MAX q (kPa)	83.3 (50.9%)
INDUCED OCR 1.0	AVG MIN q (kPa)	-84.1 (51.3%)





CRUISE DC1-81-EG CORE NO. 604G3	INCREMENT (cm) TEST NO.	130-137 TC99	
SIG1c'(kPa)	297.1	STATIC q <sub>f</sub> (kPa)	176.6
SIG3c'(kPa)	297.1	AVG MAX q (kPa)	61.5 (34.8%)
INDUCED OCR	1.0	AVG MIN q (kPa)	-56.2 (31.8%)





CRUISE DC1-81-EG	INCREMENT (cm)	130-137
CORE NO. 604G3	TEST NO.	D102

SIG1c'(kPa)	290.4	STATIC q <sub>f</sub> (kPa)	176.6
SIG3c'(kPa)	290.4	AVG MAX q (kPa)	86.5 (49.0%)
INDUCED OCR	1.0	AVG MIN q (kPa)	-68.0 (38.5%)